PHOTOGRAPH THIS SHEET

A134185

DTIC ACCESSION NUMBER

II

LEVEL

1

INVENTORY

Proceedings of the 10th Annual Conference on Manual Control. Held at the Air Force Institute of Technology. 9-11 Apr. 1974

DOCUMENT IDENTIFICATION

DISTRIBUTION STATEMENT A
Approved for public release;
Distribution Unlimited

DISTRIBUTION STATEMENT

ACCESSION FOR	
NTIS	GRA&I
DTIC	TAB
UNANNOUNCED	
JUSTIFICATION	
BY	
DISTRIBUTION /	
AVAILABILITY CODES	
DIST	AVAIL AND/OR SPECIAL
A/3	

DISTRIBUTION STAMP

DTIC
ELECTE
S NOV 22 1983 D
D

DATE ACCESSIONED

DTIC COPY INSPECTED

83 11 21 014

DATE RECEIVED IN DTIC

PHOTOGRAPH THIS SHEET AND RETURN TO DTIC-DDA-2

DTIC FORM OCT 79 70A

DOCUMENT PROCESSING SHEET

proceedings of the Xth annual Conference on Manual Control

9-11 april 1974
wright-patterson afb, ohio

air force institute of technology
air force flight dynamics laboratory

NOTICE

When Government drawings, specifications, or other data are used for any purpose other than in connection with a definitely related Government procurement operation, the United States Government thereby incurs no responsibility nor any obligation whatsoever; and the fact that the government may have formulated, furnished, or in any way supplied the said drawings, specifications, or other data, is not to be regarded by implication or otherwise as in any manner licensing the holder or any other person or corporation, or conveying any rights or permission to manufacture, use, or sell any patented invention that may in any way be related thereto.

Copies of this report should not be returned unless return is required by security considerations, contractual obligations, or notice on a specific document.

AIR FORCE/56780/20 September 1974 — 350

BLANK PAGES
IN THIS
DOCUMENT
WERE NOT
FILMED

SECURITY CLASSIFICATION OF THIS PAGE (When Data Entered)

REPORT DOCUMENTATION PAGE		READ INSTRUCTIONS BEFORE COMPLETING FORM
1. REPORT NUMBER	2. GOVT ACCESSION NO.	3. RECIPIENT'S CATALOG NUMBER
4. TITLE (and Subtitle) Proceedings of the Xth Annual Conference on Manual Control		5. TYPE OF REPORT & PERIOD COVERED 9-11 April 1974 6. PERFORMING ORG. REPORT NUMBER
7. AUTHOR(s)		8. CONTRACT OR GRANT NUMBER(s)
9. PERFORMING ORGANIZATION NAME AND ADDRESS		10. PROGRAM ELEMENT, PROJECT, TASK AREA & WORK UNIT NUMBERS 1986
11. CONTROLLING OFFICE NAME AND ADDRESS AF Wright Aeronautical Laboratories Flight Dynamics Laboratory (AFWAL/FIGC) Wright-Patterson AFB, OH 45433		12. REPORT DATE Apr 74 13. NUMBER OF PAGES 753
14. MONITORING AGENCY NAME & ADDRESS (if different from Controlling Office)		15. SECURITY CLASS. (of this report) Unclassified 15a. DECLASSIFICATION/DOWNGRADING SCHEDULE

16. DISTRIBUTION STATEMENT (of this Report)

Approved for Public Release; Distribution Unlimited

17. DISTRIBUTION STATEMENT (of the abstract entered in Block 20, if different from Report)

18. SUPPLEMENTARY NOTES

19. KEY WORDS (Continue on reverse side if necessary and identify by block number)

Manual Control
Stability Control
Human Operators
Control Analysis

20. ABSTRACT (Continue on reverse side if necessary and identify by block number)

This volume presents recent developments in the field of manual control theory and applications as presented at the Tenth Annual Conference on Manual Control. Formal sessions at this three day meeting delt with modeling theory, man-machine integration, and application-simulation. The session on future trends in research and applications in manual control was conducted as a panel with informal and spontaneous comments from the panel and conference attendees.

DD FORM 1 JAN 73 1473 EDITION OF 1 NOV 65 IS OBSOLETE

SECURITY CLASSIFICATION OF THIS PAGE (When Data Entered)

PREFACE

On April 9, 10 and 11, 1974, the Tenth Annual Conference on Manual Control Systems was held at the Air Force Institute of Technology. It brought together more than one hundred engineers and scientists interested in research and development of manual control systems, those systems in which the human operator plays a significant role in control and stabilization. As reflected in the volume of papers that follow, the discussions ranged from analytic approaches to system analysis and system identification to empirical studies of human operator performance in a variety of practical tasks. Although the predominate theme focuses on application to aircraft control and handling qualities, papers were also presented concerning human control of automobiles.

The reader of this volume may also be interested in earlier volumes in this series. They are referenced below.

First Annual NASA-University Conference on Manual Control, The University of Michigan, December 1964. (Proceedings not printed.)

Second Annual NASA-University Conference on Manual Control, MIT, Feb 28 to March 2, 1966, NASA SP-128.

Third Annual NASA-University Conference on Manual Control, University of Southern California, March 1 - 3, 1967, NASA SP-144.

Fourth Annual NASA-University Conference on Manual Control, The University of Michigan, March 21-23, 1968, NASA SP-192.

Fifth Annual NASA-University Conference on Manual Control, MIT, March 27 - 29, 1969, NASA SP-215.

Sixth Annual Conference on Manual Control, Wright-Patterson AFB, April 7 - 9, 1970.

Seventh Annual Conference on Manual Control, University of Southern California, June 2 - 4, 1971, NASA SP-281.

Eighth Annual Conference on Manual Control, University of Michigan, Ann Arbor, Michigan, May 17 - 19, 1972.

Ninth Annual Conference on Manual Control, Massachusetts Institute of Technology, May 23 - 25, 1973.

Note: The Proceedings of the Sixth, Eighth, and Tenth Conference were published by the Air Force; address, requests to: AFFDL/FGD, Wright-Patterson Air Force Base, Ohio 45433.

TABLE OF CONTENTS

DECISION BEHAVIOR WITH CHANGING SIGNAL STRENGTH

Renwick E. Curry and Eliezer G. Gai
Massachusetts Institute of Technology
Cambridge, Massachusetts

and

David C. Nagel
National Aeronautics and Space Administration
Ames Research Center
Moffett Field, California

ABSTRACT

The Theory of Signal Detectability (TSD) has nearly replaced classical notions of the threshold because of its ability to separate sensory and decision processes in weak signal detection and recognition paradigms. The primary emphasis of recent work has concentrated on the sensory rather than the decision aspects and almost all work has been exclusively at one signal strength. We propose a model to describe behavior at different signal strengths based on subjective rather than objective distributions. The model predicts ensemble performance at a constant objective likelihood ratio (LR) criterion (even though subjective distributions are the basis for determining cutoff criteria) unless the observer adopts a subjective Neyman-Pearson objective. Results from an experiment in visual discrimination show that some observers in fact operate at a constant objective LR's as signal strength is varied randomly over a wide range. The objective LR's of the other subjects changed dramatically with signal strength, but this behavior is consistent with the use of a subjective Neyman-Pearson decision rule and the linear relation between subjective and objective log LR's found in studies of subjective probability.

INTRODUCTION

In this paper we consider in some detail the decision aspects of the Theory of Signal Detectability (TSD) that has found wide application in the psychophysics of the past several decades, particularly as a model for psychophysical detection and recognition tasks. Although the theory was first detailed by Swets, Tanner and Birdsall (1955), Green and Swets (1966) provide the most detailed discussion of the concept and applications of the general model. As with the majority of expositions of TSD, we consider here the case of two alternative stimulus classes, which in the theory are represented as hypotheses. Each presentation of a stimulus is assumed to map to a unidimensional sensory continuum; the continuum is divided into intervals and (neglecting boundary or criterion variability) a realization of the stimulus anywhere within that interval leads to a unique response.

TSD, in common with the more modern of the threshold theories, has allowed the experimental separation of the sensory and response elements of psychophysics. In the present context, the sensory elements are derived from the ensemble distributions of the realizations for each stimulus. It is the normalized distance between these distributions (commonly referred to as the signal strength or signal-to-noise ratio (SNR)), that determines the sensory capabilities, whereas the response elements are defined by the points separating the intervals on the continuum.

In the formal application of TSD as a normative and descriptive theory, the sensory continuum has been identified with the likelihood ratio (LR), or a monotonic function of the LR (see Green and Swets, 1966).

Early experiments (e.g. Egan, Schulman and Greenberg, 1959; Tanner, Swets and Green, 1956) were performed to investigate the manipulation of the response criterion levels. Results were generally as predicted by the theory, although real observers tended to be somewhat more conservative than the normative theory would have it, and research efforts then concentrated on the sensory rather than the decison aspects of the model, in large measure. With this change of emphasis, the concept of the likelihood ratio decision axis seemed overrestrictive and unnecessary. This fact, coupled with some logical inconsistencies, especially the non-monotonic behavior of LR for the unequal-variance Gaussian distributions, led to new theories which did not rely on the LR (Wickelgren, 1968) and which began to fall more in line with the Thurstonian view (see Lee, 1969 for a comparison of TSD and Thurstonian scaling).

The demise of the LR concept, however, created a void in one important element of the sensory continuum threshold models; namely, what sort of decision or choice behavior does one expect for the stimulus situations where signal strength is allowed to vary from trial to trial? Indeed, the theory has never been fully examined under these stringent conditions. As treated in developments to follow, the task of the decision maker is to determine which one of two hypotheses is true from one available observation. To make decisions in an optimal manner, the following objectives might be considered (e.g. see Green, 1960):

1. Maximize percent correct
2. Maximize expected value
3. Maximize P(Hit) - $\beta \cdot$P(False Alarm)
4. Maximize a posteriori probability

5. Maximize P(Hit) at fixed P(False Alarm), commonly known as the Neyman-Pearson objective.

As shown by Green and Swets, the optimal strategy for all of the above objectives at a given SNR is to base decisions on the LR, viz. respond "H_0" if the LR is less than some value, otherwise repond "H_1", where (H_0,H_1) are the two alternative hypotheses. This poses obvious difficulties if one is trying to determine the objective of a decision maker for which only the inputs and outputs can be observed, since many objective functions can lead to the same criterion value at a fixed signal strength.

The next logical step to obtain an identification of the objective of a normative decision maker is to change the distributions from which the observations are drawn, i.e. the SNR. This is conceptually of limiting value, however, for a perusal of LR criterion levels shows that only the Neyman-Pearson objective predicts a change in LR criterion level with SNR. All other LR criteria levels remain constant regardless of the objective being extremalized or changes in signal strength.

To our knowledge only Kinchla and Smyzer (1967) have performed experiments where different detectibilities were an important aspect of the design, although certain of those interested in trial-to-trial adaptive effects in psychophysical experiments have used zero- or half-strength trials in an attempt to measure the effects of certain kinds of response bias (Atkinson and Kinchla, 1965; Ahumada, 1972). In these latter cases, however, TSD was not the model being examined. Where Kinchla and Smyzer emphasize the sensory and perceptual mechanisms, we concentrate on the

decision aspects of the model. First, we review the expected performance for the normative decison model for various decision objectives. At any given SNR, all the objectives proposed in this paper yield the same strategy based on a LR decision rule, as has been noted before (Green and Swets, 1966). We show, furthermore, that for the objectives considered, the LR criterion level remains constant as the SNR is varied unless the Neyman-Pearson objective is employed by the "observer".

We propose a model for decision behavior in which the observer is presumed to perform the optimal processing using subjective rather than objective distributions, as is usually the case. This approach is analagous to the "misperception", as opposed to the "misaggregation", explanation of the conservatism in decision makers' behavior (Rapoport and Wallsten, 1972). Bayes' Rule is used correctly, but on subjective rather than objective distributions. Wheeler and Beach (1968) and Peterson, DuCharme and Edwards (1968) measured subjective distributions and found better predictions of probability updating or revisions with these than if they had used the theoretical or objective distributions. Results of a visual discrimination experiment are presented that are consistent with the notion that people make decisions on the basis of subjective distributions that do not coincide with the true or objective stimulus distributions. Two possible explanations for the experimental results are discussed in terms of the general decision model presented here, one that involves the use of a subjective Neyman-Pearson decision strategy and another that implys the breakdown of the Subjective Expected Utility (SEU) principle. One unequivocal finding is that for experimental situations in which signal strength is allowed to vary from trial-to-trial, decisions are not made on the basis of a constant likelihood ratio criterion.

A MODEL FOR DECISION BEHAVIOR WITH CHANGING SIGNAL STRENGTHS

In this section we develop a descriptive model for decision behavior of observers in a detection or recognition task. The first hypothesis is the familiar one for the continuous sensory threshold models.

Assumptions of the model

A1. There exists a unidimensional psychological continuum, $\mathbb{X}$, on which the realization of any stimulus is described by a point, x. The distributions of these realizations over the ensemble of stimulus presentations of m stimulus pairs $\{S_i, \bar{S}_i,\ i=1,\cdots,m\}$ are represented by the conditional probability density functions $\{p(x|S_i), p(x|\bar{S}_i)\ i = 1,\cdots,m\}$.

The log likelihood ratio (LLR) for these ensemble distributions is:

$$\lambda_i(x) = \ln \frac{p(x|S_i)}{p(x|\bar{S}_i)} \quad i = 1,\cdots,m \qquad (1)$$

A2. We assume the existence of subjective uncertainties which are represented here by the intermediate construct of subjective probability densities $\{p^s(x\ S_i), p^s(x\ \bar{S}_i),\ i=1,\cdots,m\}$ with the corresponding LLR:

$$\lambda_i^s(x) = \ln \frac{p^s(x|S_i)}{p^s(x|\bar{S}_i)} \quad i = 1,\cdots,m \qquad (2)$$

A3. A total of n ordered category responses $\{R_j,\ j=1,\cdots,n\}$ are available, and for the i^{th} stimulus pair, its j^{th} response is chosen if:

$$\lambda_{i,j-1}^s \leq \lambda_i^s(x) \leq \lambda_{i,j}^s \rightarrow R_j \qquad (3)$$

where $\lambda_{i,j}^s$ is the criterion level at or below which $\lambda_i^s(x)$ leads to a response R_1 or R_2 ... or R_n for stimulus pair i.

A4. The observer changes his criterion levels in response to different stimuli in order to satisfy a decision objective in the same manner as would an objective decision maker, but subjective, rather than objective distributions are used in this process.

As mentioned before, the first assumption concerning the mapping of a stimulus to the psychological continuum is the basic one for all sensory continuum models. It is important to realize that the variability in responses over the ensemble of trials is attributed to the ensemble distributions of these points (neglecting any criterion variability). In subsequent discussions, we will refer to these as the objective distributions, since knowledge of these distributions is necessary for a decision maker to optimize performance. The objective distributions are typically considered to be determined by external experimental constraints (e.g. choice of signals), sensory processing (e.g. the "critical band" processing concept in audition), and/or memory processing.

The observer's ultimate representations of these distributions is explicitly recognized here as being different from the objective distributions (A2). The traditional statements of TSD assume that it is the objective distributions that are learned by the observer in a psychophysical experiment during the training periods. We do not make that restriction here, and point to the work of Lee (1963) in which he showed distinct differences between inferred values of subjective and objective LLR for externally distributed stimuli. In particular, Lee found that the subjective LLR can be monotonic for unequal-variance Gaussian distributions when the objective LLR is not. To the extent that this holds true for

internally distributed stimuli, using subjective rather than objective LR's for response determination (A3) removes the bothersome aspect of nonmonotonic LR's that are characteristic of conventional TSD.

Assumption A4 has a substantial impact on the prediction of observed performance over the ensemble of trials. If an observer is presumed to be extremalizing any objective function other than the Neyman-Pearson, the value of subjective LR at the criterion point should remain constant over all stimulus strengths. There is a large class of subjective and objective distributions which would admit a one-to-one mapping from subjective LR to objective LR; experimental evidence suggests that this is usually satisfied in practice (e.g. Wheeler and Beach, 1968; Peterson, et al.,1968). In particular, distributions which lead to a monotone nondecreasing $\lambda^s(x)$ and <u>any</u> $\lambda(x)$ will have such a property.

ENSEMBLE PERFORMANCE

In this section we derive the analytical expressions for model parameters in terms of measures of performance over the ensemble of trials for equal-variance stimulus pairs. These relationships are used in estimating parameters from observed data.

Objective distributions

The objective distributions describe the variability on the psychological continuum from trial to trial. Each stimulus is presumed to give rise to a distribution $p(x|\cdot)$ and it is further assumed that each realization is independent of all others.

Denote by $P_{H,i,j}$ and $P_{FA,i,j}$ the "hit" and "false alarm" probabilities for stimulus pair i with respect to criterion level j, i.e:

$$P_{H,i,j} = P(R_1 \text{ or } R_2 \text{ or } \cdots \text{ or } R_j | S_i) = P(\lambda_i^s(x) \geq \lambda_{i,j}^s | S_i)$$
$$P_{FA,i,j} = P(R_1 \text{ or } R_2 \text{ or } \cdots \text{ or } R_j | \bar{S}_i) = P(\lambda_i^s(x) \geq \lambda_{i,j}^s | \bar{S}_i) \quad (4)$$

When the underlying objective distributions are Gaussian, these expressions reduce to a particularly simple form:

$$P_{H,i,j} = \Phi(z_{H,i,j})$$
$$P_{FA,i,j} = \Phi(z_{FA,i,j}) \quad (5)$$

$$z_{H,i,j} = \frac{\lambda_{i,j}}{d_i'} + \frac{d_i'}{2}$$
$$z_{FA,i,j} = \frac{\lambda_{i,j}}{d_i'} - \frac{d_i'}{2} \quad (6)$$

where Φ is the distribution funnction for unit normal variables, and the z's are the correpsonding unit deviates. The LLR criterion levels, $\lambda_{i,j}$ are those observed from an objective decision maker operating on two equal-variance Gaussian distributions with a SNR of d_i'. These values can be estimated from the observed proportion of hits and false alarms at each SNR. It is the model of the decisions based on subjective LLR that constrains the objective LLR criterion levels between SNR levels and prevents these $\lambda_{i,j}$ from being completely free parameters. Figure 1 contains theoretical curves of constant d' (ROC curves) and curves of constant λ (isobias curves). Thus if an observer were operating at constant (objective) LLR, the points on the P(Hit)-P(FA) plane would lie along the corresponding constant-λ curves as d' is varied from 0 to ∞.

Subjective Distributions.

Constant Subjective LR. As described above, many of the decision

objectives lead to constant LR criterion levels as the distributions (SNR's) are changed. Assumption A4 leads to the conclusion that the observer will use constant subjective LR criteria over all SNR's. To the extent that a given subjective LR corresponds to a unique value of objective LR, this behavior over the ensemble of trials will be identical to an observer using constant objective LR criteria on the objective distributions. More specifically, if the objective LLR is functionally related to subjective LLR by:

$$\lambda(x) = g\left(\lambda^s(x)\right) \tag{7}$$

and if $g(\cdot)$ is a one-to-one mapping, then a constant subjective LLR for criterion level, j,

$$\lambda^s_{i,j} \equiv \tilde{\lambda}^s_j \qquad \text{all } i \tag{8}$$

leads to a constant objective LLR,

$$\lambda_{i,j} = \tilde{\lambda}_j = g(\tilde{\lambda}^s_j) \quad \text{all } i \tag{9}$$

This condition will hold under a wide class of objective and subjective distributions, although the empirical evidence suggests that a simple linear relation in (7) is a good approximation in many situations (Rapoport and Wallsten, 1972). Thus, the expressions for observed unit deviates (6) become,

$$\begin{aligned} z_{H,i,j} &= \frac{g(\tilde{\lambda}^s_j)}{d_i'} + \frac{d_i'}{2} \\ z_{FA,i,j} &= \frac{g(\tilde{\lambda}^s_j)}{d_i'} + \frac{d_i'}{2} \end{aligned} \tag{10}$$

Neyman-Pearson Objective. The development for subjective Neyman-Pearson decisions requires a more detailed structure than that for constant subjective LR. In addition to the assumption of Gaussian objective distributions, we further assume that:

a. the subjective distributions are normal, and

b. $\lambda^s(x) = b \cdot \lambda(x)$ (11)

The constant, b, relating subjective LLR to objective LLR is the so-called accuracy ratio; the validity of this expression as a first approximation has been verified under a wide range of experimental conditions (Rapoport and Wallsten, 1972).

The ensemble performance of an observer using a subjective Neyman-Pearson rule for the jth criterion level will be constrained by constant (subjective) probability of false alarm, or, equivalently,

$$z^s_{FA,j} = \text{const} = \frac{\lambda^s_{i,j}}{d'^s_i} - \frac{d'^s_i}{2} \tag{12}$$

where the superscript, s, denotes subjective values. For zero-mean normal distributions it is well known that (Green and Swets, 1966):

$$\lambda(x) = d' \cdot x \tag{13}$$

which leads to an expression for subjective-SNR, d'^s,

$$d'^s \cdot x = \lambda^s(x) = b \cdot \lambda(x) = b \cdot d' \cdot x$$

and thus, $$d'^s = b \cdot d' \tag{14}$$

Substituting (14) and (13) into (12), solving for $\tilde{\lambda}_{i,j}$, in turn, and substituting the result into (6) provides an expression for the unit

deviates over the ensemble of trials.

$$z_{H,i,j} = z^{s}_{FA,j} + \frac{d_i'}{2} \cdot (1+b)$$

$$z_{FA,i,j} = z^{s}_{FA,j} - \frac{d_i'}{2} \cdot (1-b) \qquad (15)$$

In recognition and discrimination tasks, the distinction between "noise" and "signal plus noise" becomes arbitrary and so operation at a constant probability of hit may be expected. The corresponding expressions are,

$$z_{H,i,j} = z^{s}_{H,j} + \frac{d_i'}{2} \cdot (1-b)$$

$$z_{FA,i,j} = z^{s}_{H,j} - \frac{d_i'}{2} \cdot (1+b) \qquad (16)$$

This family of curves describing the ensemble performance has a particularly simple form in the unit-deviate plane (Figure 2); the loci of observations lie on straight lines with slope of $(1+b)/(b-1)$ or $(b-1)/(1+b)$, and

reduce to the expected result when the objective and subjective distributions are equal ($b=1$). The corresponding loci in the P(Hit)-P(False Alarm) plane are shown in Figure 3 for representative values of b. The most striking characteristic is that for any $b<1$ the limiting values as $d' \to \infty$ of the observed probability of false alarm is zero; when the probability of hit is subjectively constant, its (objective) limiting value is 1.

Degrees of Freedom: Positive or Negative?

With the introduction of the subjective basis for decisions and

subsequent analysis for ensemble performance, one might wonder whether there are so many parameters that the model loses any significance it might have had. In reality, we have only added one new parameter and placed new interpretations on old parameters. Thus the model is quite parsimonious as can be seen in the accompanying table (Table 1) which was prepared for m pairs of equal-variance Gaussian stimuli (m-SNR's)

and an n-category rating scale. As an example, using 2 and 3 SNR's with a 4 category scale yields 6 and 11 degrees of freedom, respectively.

VISUAL DISCRIMINATION WITH RANDOMLY VARYING SNR

Method

Apparatus. A visual discrimination task was presented on a 17-inch CRT in the form of pairs of quarter-inch circles. Ten pairs of circles, at five distances from a cursor, constituted the entire stimulus set, shown in Figure 4. The observers' task was to indicate whether the pair of circles was to the right or left of a vertical line passing

through the small vertical cursor near the bottom of the screen. This provided five SNR's since the discrimination is easier for circles closer to the cursor than for those farther away. Subjects indicated their response by pushing one of 3 buttons corresponding to "think left", "don't know", and "think right". An odd number of categories was used to avoid the central criterion; we have results similar to those reproted here with an even number of categories.

Subjects. Six graduate students participated as observers on a voluntary basis in four half-hour sessions.

Procedure. A standard set of instructions were read to the subjects

describing the experimental setup, informing them of equiprobable right and left presentations and the scoring method displayed to them at the end of each session. Three points were given for a correct response, minus three points for an incorrect response, and zero for "don't know". A stimulus (e.g. a pair of circles) appeared for 4 seconds and the screen was then blanked for a 2-second response interval. Feedback after each trial was not given.

After 10 minutes of practice, subjects began the first of four half hour sessions of 300 presentations of the stimuli in random order. The data for all sessions were pooled, resulting in an average of 120 presentations per stimulus or 240 presentations per SNR for each subject.

Results.

Maximum likelihood estimates of model parameters were made for each subject in several ways. First the two LLR criterion levels ($\tilde{\lambda}_1, \tilde{\lambda}_2$) and equal-variance d' values were estimated for each SNR. (Table 2). Three of these parameter sets were not attempted because of extreme observations (e.g. no errors) at the highest SNR. A χ^2 goodness of fit test did not indicate a rejection of the equal-variance Gaussian hypothesis for any of the 27 parameter sets even though d' values ranged from .15 to 3.89.

A more sophisticated routine (Curry, 1974) was used to obtain the ML estimates of the global model, i.e., the simultaneous estimation of 5 d' values and the two (or three) parameters describing the decision rule. Not all combinations of decision strategies were evaluated since inspection of the raw data on the P(Hit)-P(False Alarm) plane ruled out many as being unreasonable. However, a constant LR strategy was

tried for each subjedt to provide information regarding this hypothesis. We have included the results for a mixed strategy, where the first criterion level is assumed to be a constant LR criterion while the second criterion level is obtained via application of a subjective Neyman-Pearson rule.

The χ^2 values of the ML estimates for the various decision strategies are summarized in Table 3. The degrees of freedom are not the same because data were ppoled to obtain cells with expected frequencies

greater than 4. We feel that this constitutes a powerful test of the model, since one and only one strategy was not rejected by the χ^2 test for five of the six subjects. Examination of Table 3 (or figures 9 and 10 which follow) shows that the data are best explained by mixed decision strategies for subjects 5 and 6, i.e. a constant LR criterion for one threshold and a subjective Neyman-Pearson criterion for the other threshold yield the minimum χ^2 value. This, we feel, is due to the assumed linear relation between subjective and objective likelihood ratios, rather than a difference in strategies. The primary reason for this is the sensitivity of P(Hit)-P(False Alarm) values to LLR at low d' (see Figure 9, where a small change in the theoretical LLR would dramatically change the predicted data point at the lowest d').

Thus a slight relaxation of the linear constraint would significantly imporve the descriptive power of the model without affecting its usefulness. Deviations from linearity should be allowed in future applications because first, any calculated accuracy ratio is sensitive

to sampling variations at small levels of LLR, and second, many subjects exhibit systematic nonlinear trends, with a decrease in accuracy ratio at higher LLR being typical (Peterson, et al., 1968).

The ROC curves in Figures 5 through 10 are the theoretical predictions from the Maximum Likelihood estimates yielding the smallest χ^2 value.

DISCUSSION

The strongest conclusion to be drawn from the experimental results is that subjects operate with (objective) LR criterion levels that vary with SNR. Data similar in nature were tabulated in Kinchla and Smyzer (1967) and we have plotted it in the P(H)-P(FA) plane in Figure 11 as further evidence of this behavior.

There are several explanations for these results. We feel that the response mode (an odd number of categories) can be ruled out since we have obtained similar results with an even number of categories, and the Kinchla and Smyzer data were generated from binary responses. There may be some decision strategy other than the Neyman-Pearson rule that we have not considered which requires a shift in LR criterion with SNR. For example, the criterion levels might be fixed on the sensory continuum. This hypothesis is, however, inconsistent with the data.

The possibility of a drift in perceptual memory as a source of the criterion shift was suggested by Kinchla and Smyzer for the auditory

task (Figure 11b); they did not discuss the criterion shifts that apparently exist for the visual task (Figure 11a). A memory function was not required for the experiments reported here, and it seems unlikely that the LLR criterion shift has a sensory basis. Thus the LLR change would appear to be related to decision processes, and this appears to be an alternative explanation to the results reported by Kinchla and Smyzer as well.

The most viable alternative to the subjective Neyman-Pearson rule as an explanation of the observations is a breakdown of the Subjectively Expected Utility (SEU) theory. Of the three major assumptions comprising the SEU model (Tversky, 1967) the independence of utilities and subjective probabilities is critical in this situation. When the independence principle is valid, the subjective LLR criterion level is determined by:

$$\tilde{\lambda}_j^s = \ln \frac{U_{00} - U_{01}}{U_{11} - U_{10}} \qquad (17)$$

where U_{ij} is the utility of responding hypothesis i when hypothesis j is actually true. It is difficult to completely eliminate the change in utilities as the source of variation without experimental evidence to the contrary. Although the payoff matrix has been manipulated to alter criterion levels (Green and Swets, 1966) we are not aware of any utility measurements in a psychophysical setting even at one SNR, and results for multiple SNRs would be required here.

In spite of this lack of data, we feel that the change of utilities with SNR (i.e. the breakdown of the SEU model) is a less satisfactory explanation than the subjective Neyman-Pearson rule for the following

reasons. Wallsten (1970), in explaining when the SEU model has been found to be valid, summarized the experimental efforts by suggesting that the SEU model is more appropriate in "simple" rather than "complex" decision situations. Although the line of demarcation between "simple" and "complex" decisions must necessarily be a fuzzy one, the decisions reported here must surely lie toward the "simple" end of the continuum. Furthermore, unusual changes in utilities would be necessary to explain the observed results. An examination of the objective LLR criterion levels from the Maximum Likelihood estimation procedure shows non-monotonic behavior of criterion level with SNR, and even changes of sign. Although this is consistent with a Neyman-Pearson rule, the utilities would have to change in a manner such that:

(1) a "right" (or "left") response is preferred at the longer distances,

(2) the utilities change to strengthen this preference for "right" or "left" at intermediate distances, and

(3) the utilities change again to bias responses in the opposite direction at nearer distances.

In summary, we have examined the decision behavior with multiple signal-to-noise ratio stimuli and proposed a quantitative model in which subjective (rather than objective) distributions play a key role. The model predicts that the ensemble performance of an observer should lie along a constant (objective) LR curve unless he is using the Neyman-Pearson objective. The experimental evidence from a visual discrimination task certainly shows that the LR criterion level can change with SNR. The most plausible alternative explanation to a subjective Neyman-Pearson

rule is the breakdown of the SEU model. The experimental evidence suggests that this is unlikely in the "simple" decision setting used here, and moreover the required utility changes would be most unusual to explain the observations. The constant subjective LR and subjective Neyman-Pearson rules describe the data well on the local and global levels.

REFERENCES

AHUMADA, A. Sequential response bias adjustment in signal detection. Unpublished manuscript

ATKINSON, R. C., & KINCHLA, R. A. A learning model for forced-choice detection experiments. British Journal of Mathematical and Statistical Psychology, 1965, 18, 183-206

CURRY, R. E. A general multinomial maximum likelihood program for behavioral models. In preparation

EGAN, J. P., SCHULMAN, A. I., & GREENBERG, G. Z. Operating characteristics determined by binary decisions and by ratings. Journal of the Acoustical Society of America, 1959, 31, 768-773

GREEN, D. M. Psychoacoustics and detection theory. Journal of the Acoustical Society of America, 1960, 32, 1189-1203

GREEN, D. M., & SWETS, J. A. Signal detection theory and psychophysics. New York: Wiley, 1966

KINCHLA, R. A.,& SMYZER, F. A diffusion model of perceptual memory. Perception and Psychophysics, 1967, 2, 219-229

LEE, W. Choosing among confusably distributed stimuli with specified likelihood ratios. Perception and Motor Skills, 1963, 16, 445-467

PETERSON, C. R., DuCHARME, W. M., & EDWARDS, W. Sampling distributions and probability revisions. Journal of Experimental Psychology, 1968, 76,236-243

RAPOPORT, A., & WALLSTEN, T. S. Individual decision behavior. Annual Review of Psychology, 1972

SWETS, J. A., TANNER, W. P., & BIRDSALL, T. G. The evidence for a decision-making theory of visual detection. University of Michigan: Electronics Defense Group, Technical Report No. 40, 1955

SWETS, J. A., TANNER, W. P., & BIRDSALL, T. G. Decision processes in perception. Psychological Review, 1961, 68, 301-340

TANNER, W. P., SWETS, J. A., & GREEN, D. M. Some general properties of the hearing mechanism. University of Michigan: Electronics Defense Group, Technical Report No. 30, 1956

TVERSKY, A. Additivity, utility, and subjective probability. Journal of Mathematical Psychology, 1967, 4, 175-201

WALLSTEN, T. S. Subjects' probability estimates and subjectively expected utility theory. University of North Carolina: Psychometric Research Laboratory Report No. 85, 1970

WHEELER, G., & BEACH, L. R. Subjective sampling distributions and conservatism. Organizational Behavior and Human Performance, 1968, 3, 36-46

WICKELGREN, W. Unidimensional strength theory and component analysis of noise in absolute and comparative judgement. Journal of Mathematical Psychology, 1968, 5, 102-122

Table 1

Parameter Summary for m Pairs of Equal-Variance

Gaussian Stimuli (m SNRs)

Model	Parameters to be Estimated (number)	Degrees of Freedom[a]
Constant Objective LLR	d_i' (m), $\tilde{\lambda}_j$ (n-1)	(2m-1)(n-1) - m
Objective Neyman-Pearson	d_i' (m), $z^s_{FA,j}$ (n-1)	(2m-1)(n-1) - m
Constant Subjective LLR	d_i' (m), $g(\tilde{\lambda}^s_j)$ (n-1)	(2m-1)(n-1) - m
Subjective Neyman-Pearson	d_i' (m) , b, $z^s_{FA,j}$ (n-1)	(2m-1)(n-1) - (m+1)
Mixed Strategy	d_i' (m) , b, $z^s_{FA,j}$ or $g(\tilde{\lambda}^s_j)$ (n-1)	(2m-1)(n-1) - (m+1)

[a]Degrees of freedom are the number of independent equations, 2m(n-1), minus the number of parameters.

Table 2

Maximum Likelihood Estimates of LLR and d' at Each SNR

Subject	SNR	$\tilde{\lambda}_1$	$\tilde{\lambda}_2$	d'	χ^2 [a]
	1	-.73	.14	.43	.12
	2	-.94	.18	.59	.79
1	3	-1.09	.22	1.12	3.74
	4	-1.00	-.05	2.00	1.27
	5	--	--	--	--
	1	-.28	.21	.18	1.16
	2	-.88	.61	.72	.26
2	3	-1.19	.66	1.48	1.13
	4	-1.28	.04	2.32	.01
	5	--	--	--	--
	1	-.36	-.01	.23	3.83
	2	-.62	-.09	.36	.08
3	3	-1.28	-.20	.95	.22
	4	-1.78	-.04	1.63	.18
	5	-3.46	1.06	3.89	2.17
	1	-.39	.07	.36	.18
	2	-.43	.15	.52	.30
4	3	-.59	.52	1.10	.01
	4	-.35	.93	1.49	.03
	5	1.06	2.30	3.00	.37

Table 2 (continued)

Subject	SNR	$\tilde{\lambda}_1$	$\tilde{\lambda}_2$	d'	χ^2
	1	-.15	.01	.15	2.67
	2	-.18	.06	.30	.26
5	3	-.24	.25	.65	.07
	4	-.17	.56	1.14	1.15
	5	.26	1.34	2.56	1.74
	1	-.32	.18	.58	3.24
	2	-.36	.32	.93	.53
6	3	-.21	.38	1.07	.04
	4	.07	.85	1.69	.11
	5	--	--	--	--

[a] All chi square values have one degree of freedom (χ^2>3.84 with Pr=.05)

Table 3

χ^2 Goodness of Fit Tests of ML Estimates (5 SNRs)

Subject	χ^2(df)			
	Constant LLR	Objective Neyman-Pearson	Subjective Neyman-Pearson	Mixed Strategies
1	6.3(7)	29.8(6)** [a]	19.6(5)**	---
2	11.0(8)	33.3(11)**	20.9(8)**	---
3	39.8(10)**	---	16.7(9)	27.7(8)**
4	70.0(13)**	39.6(12)**	28.3(11)**	28.7(11)**
5	68.2(13)**	---	---	20.8(12)
6	21.2(9)**	---	19.9(9)*	12.1(9)

[a] *p<.05 **p<.01

FIGURE CAPTIONS

Figure 1 Theoretical curves in the P(hit)-P(FA) plane for equal-variance normal distributions. Solid lines are isosensitivity curves ($d' = .5, 1., 2.$). Dotted lines are isobias curves ($|\lambda| = .1, .5, 1.$). Positive values of λ in the upper half-plane, increasing toward the top. Negative values of λ in the left half-plane, decreasing toward the left.

Figure 2 Theoretical curves of unit deviates for observed P(hit)-P(FA) when the observer uses a subjective Neyman-Pearson decision rule. The subjective distributions are assumed normal, and b is the ratio of subjective to objective LLR.

Figure 3 Theoretical curves of P(Hit)-P(FA) using subjective Neyman-Pearson decision rules. The straight dashed lines are for $b = 1$ (subjective LLR equals objective LLR) ; the other loci are for $b = .75$ and $.25$.

Figure 4 Stimuli for the visual discrimination task showing both hypotheses (left and right) and the five SNRs (distances from the cursor). Not drawn to scale.

Figure 5 P(Hit)-P(FA) for observer 1 with constant LLR decision rules ($\lambda = -.93, .17$). Theoretical curves are the ML estimates yielding minimum χ^2 values.

Figure 6 P(Hit)-P(FA) for observer 2 with constant LLR rules ($\lambda = -.86, .58$)

Figure 7 P(Hit)-P(FA) for observer 3 with subjective Neyman-Pearson decision rules ($b = .29$).

Figure 8 P(Hit)-P(FA) for observer 4 with subjective Neyman-Pearson decision rules ($b = .66$).

Figure Captions (Continued)

Figure 9 P(Hit)-P(FA) for observer 5 with constant LLR and subjective Neyman-Pearson decision rules (λ = -.22, b = .25).

Figure 10 P(Hit)-P(FA) for observer 6 with constant LLR and subjective Neyman-Pearson decision rules (λ = -.26, b = .22)

Figure 11 P(Hit)-P(FA) performance in perceptual memory tasks (data from Kinchla and Smyzer, 1967). a) Visual b) Auditory

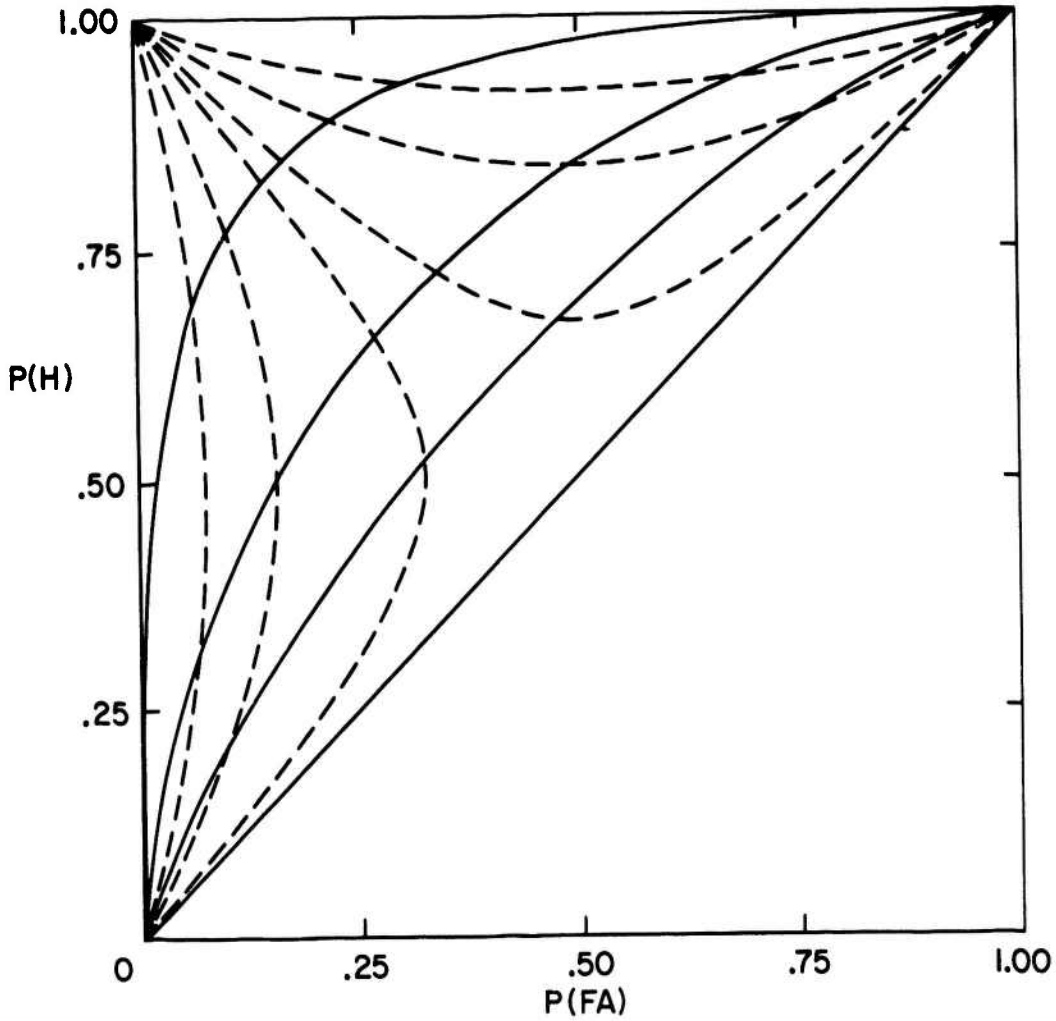

FIGURE 1

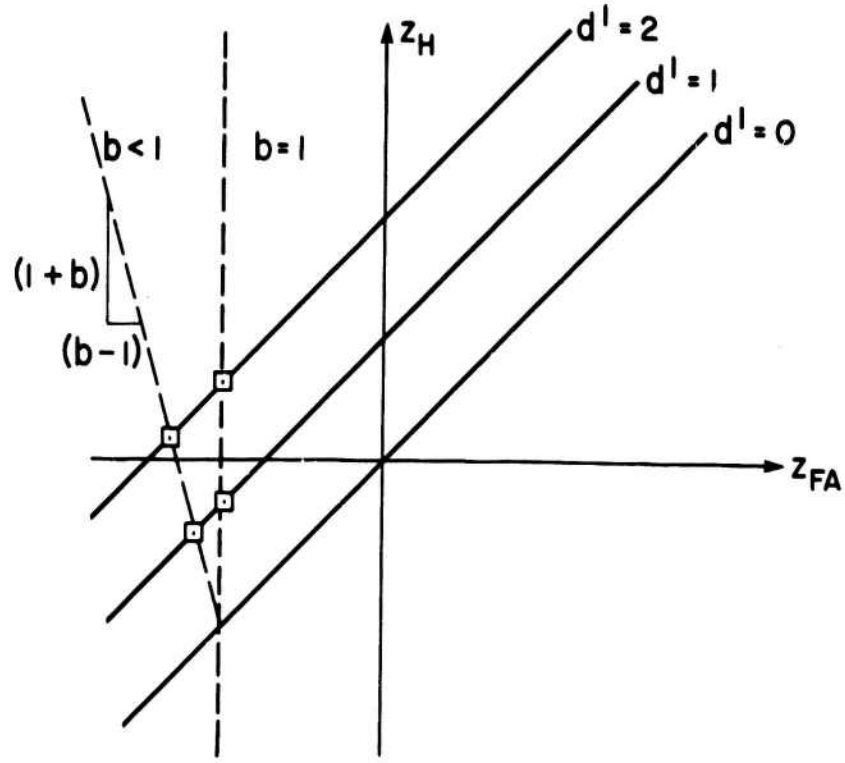

FIGURE 2

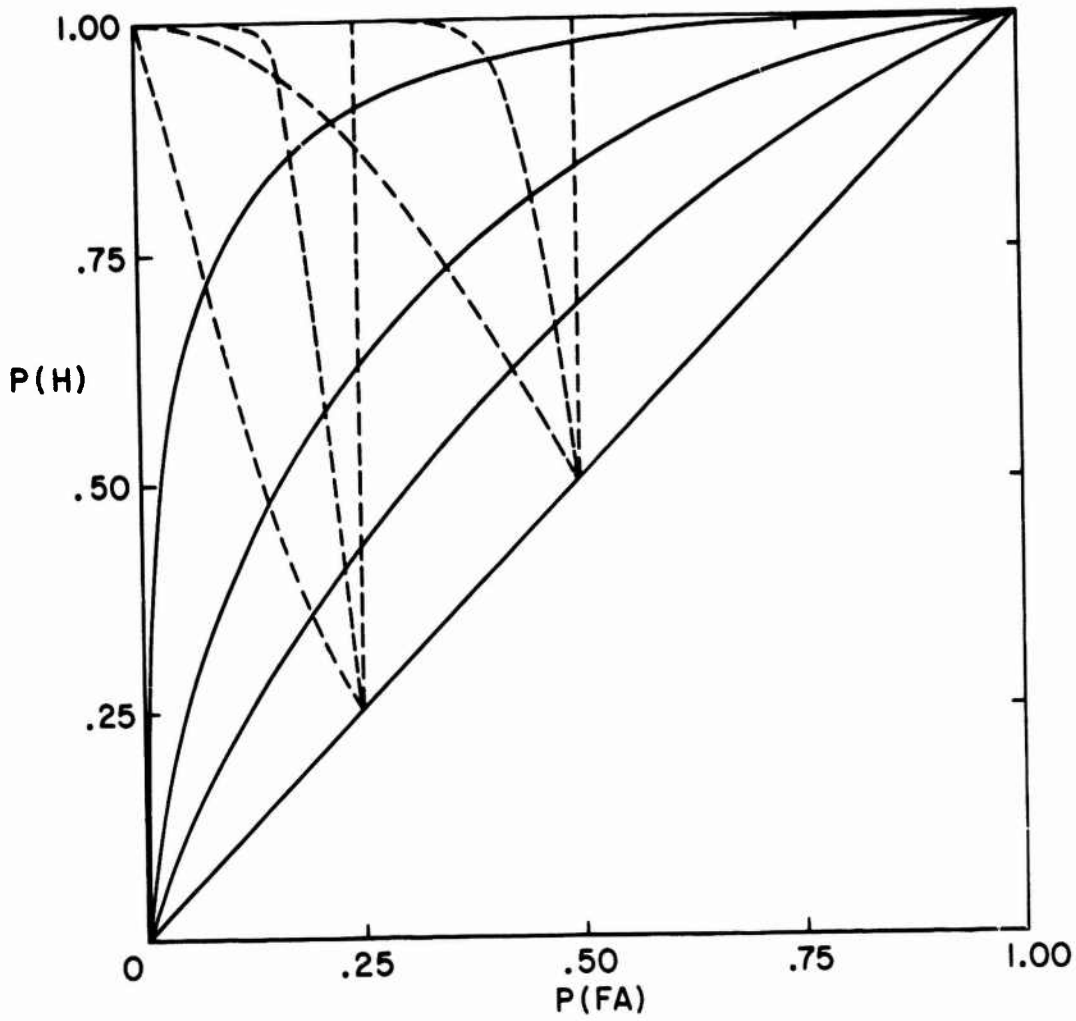

FIGURE 3

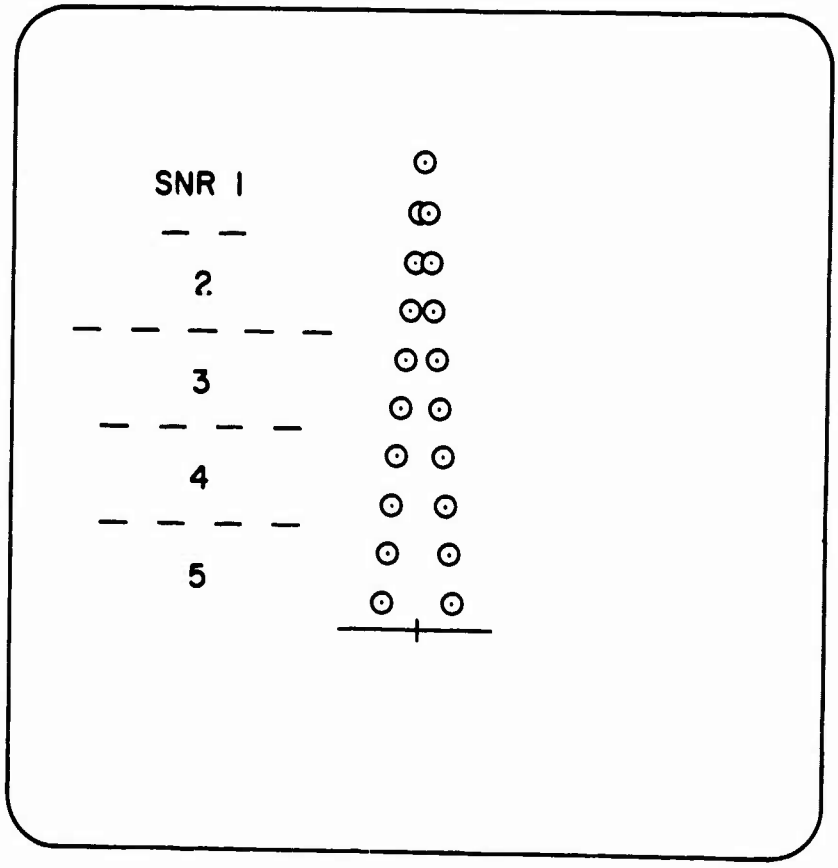

FIGURE 4

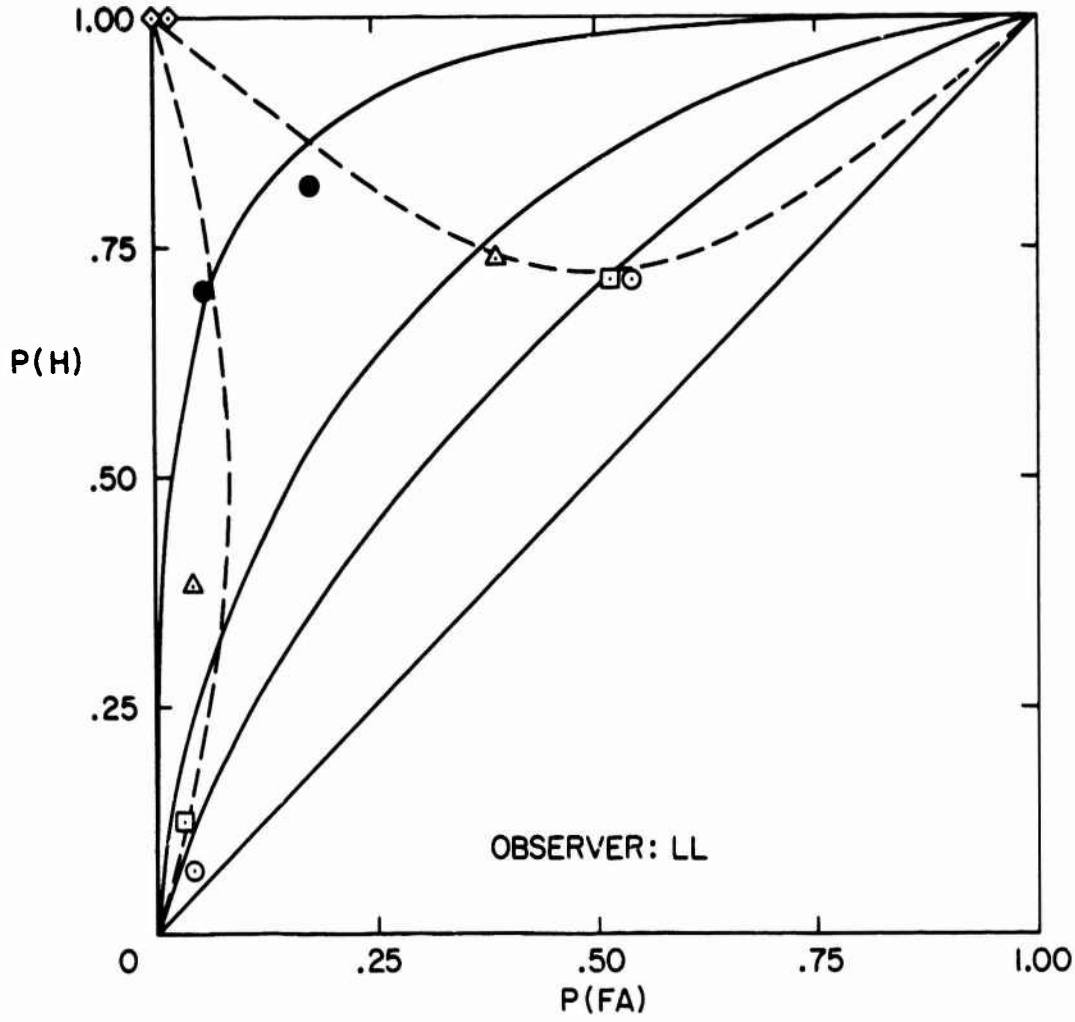

FIGURE 5

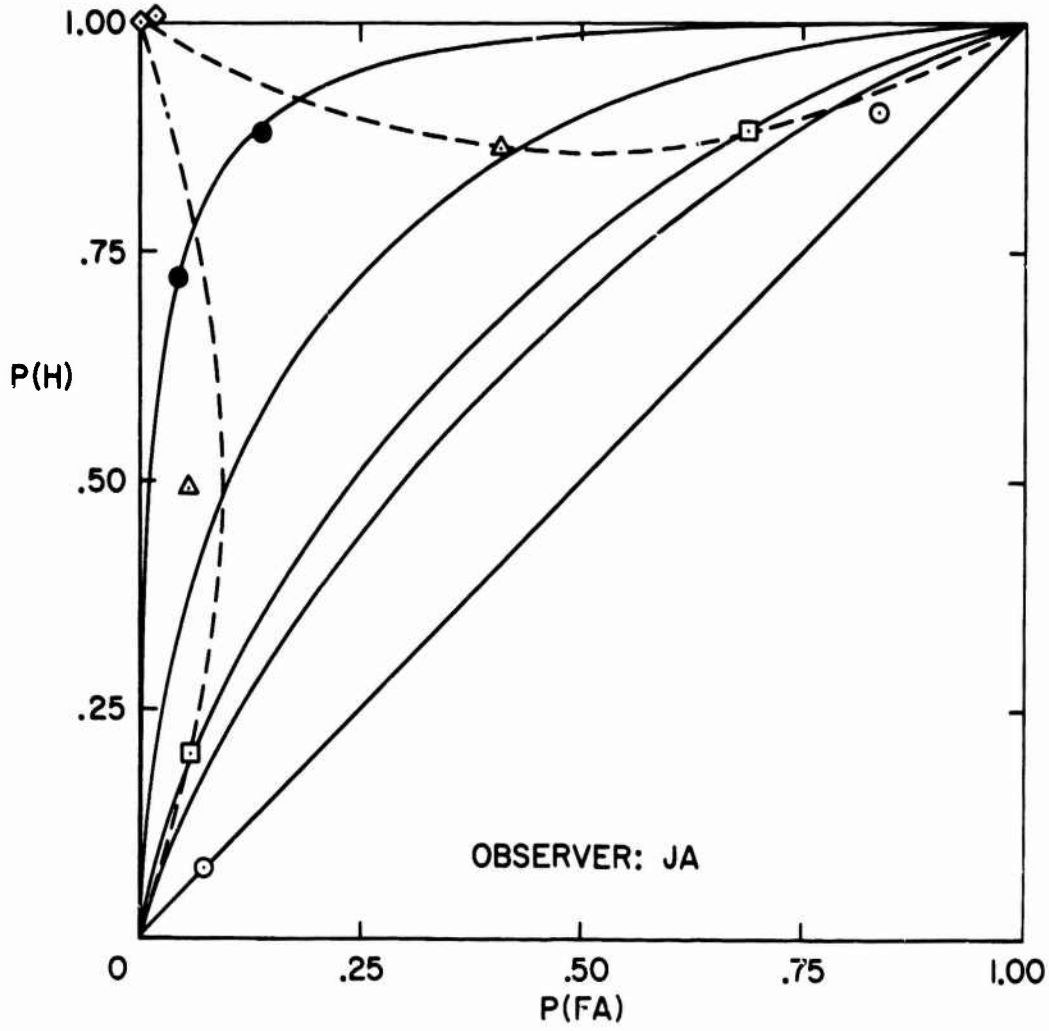

FIGURE 6

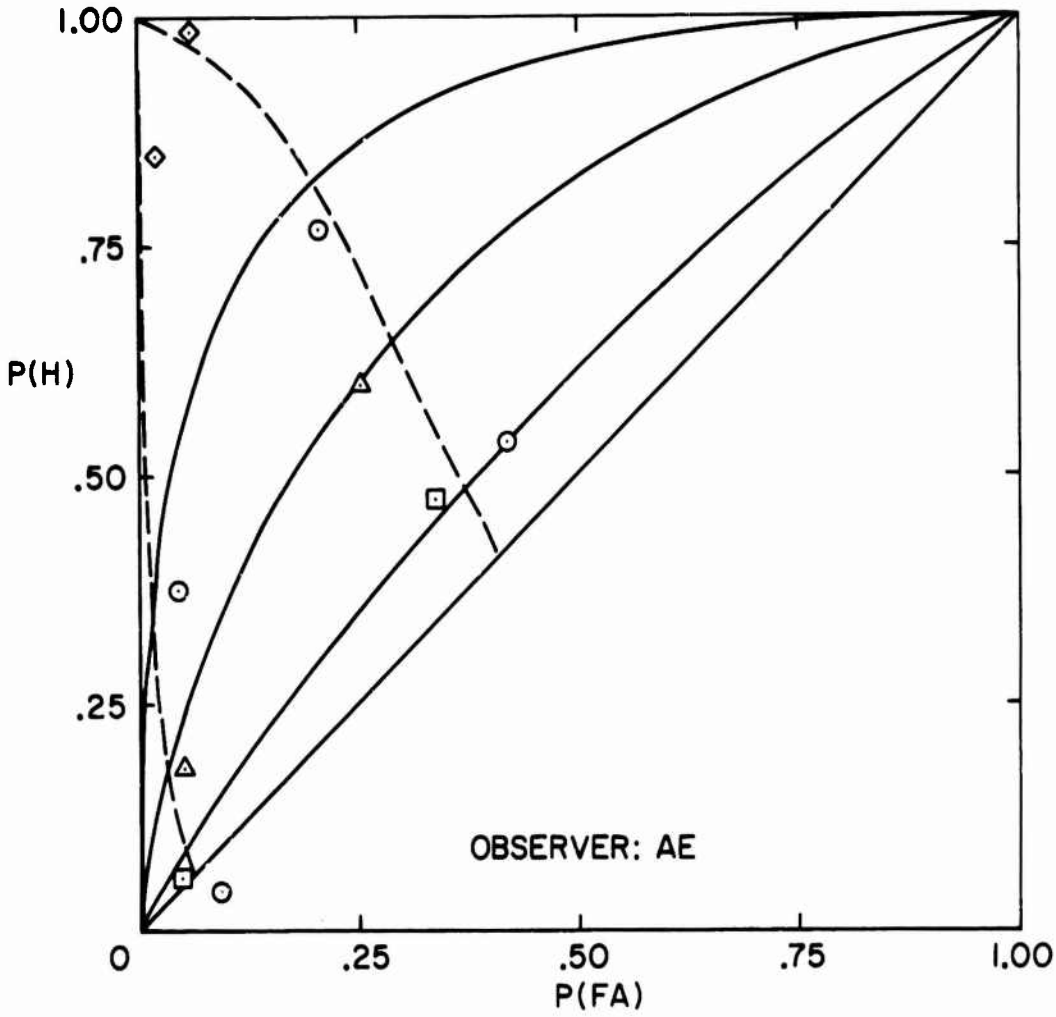

FIGURE 7

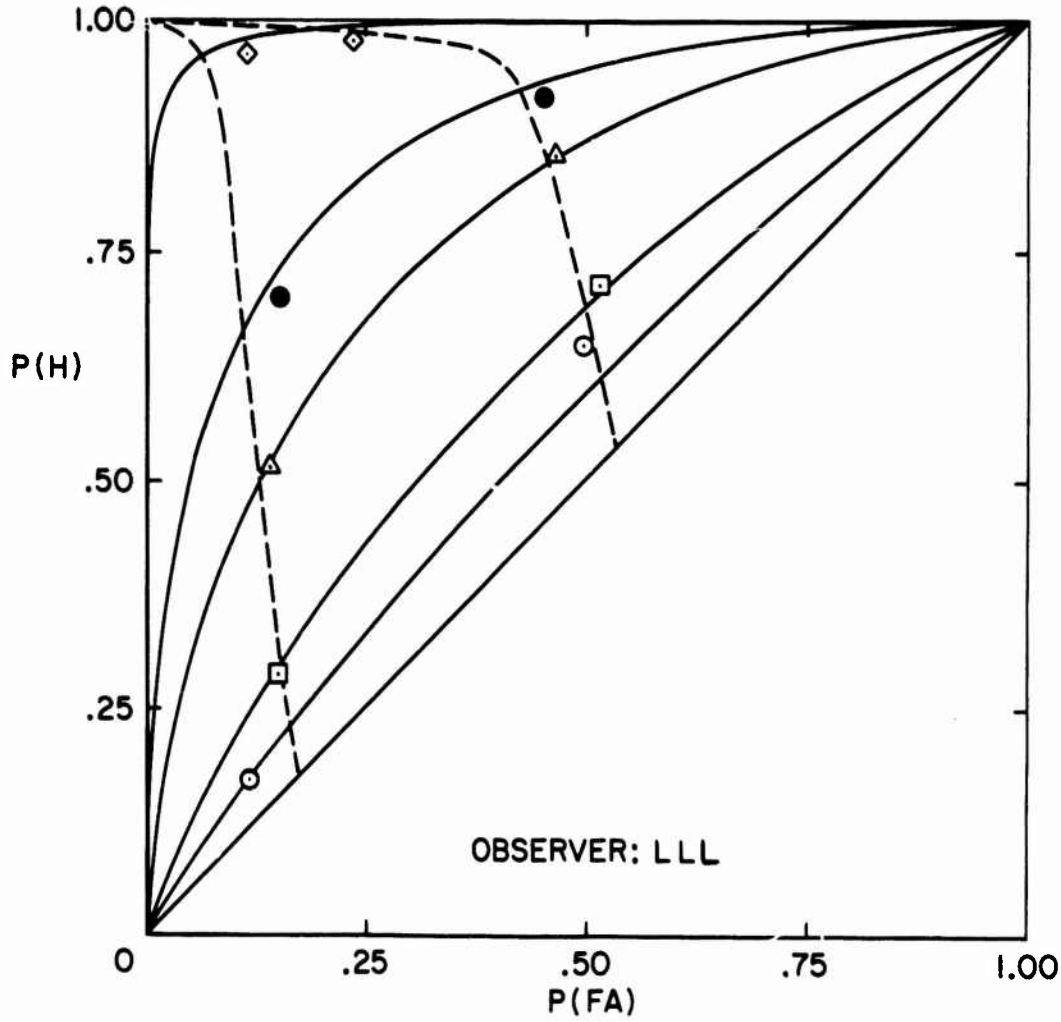

FIGURE 8

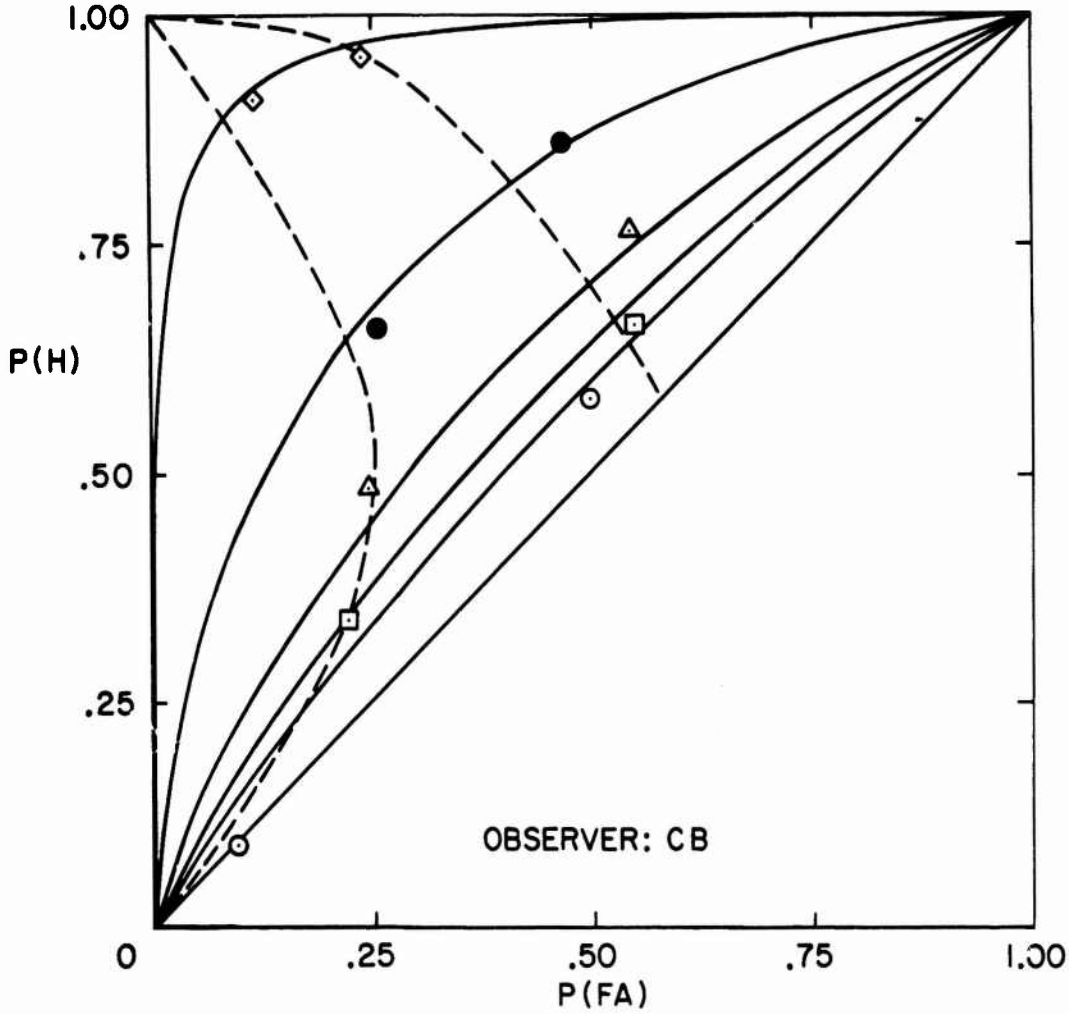

FIGURE 9

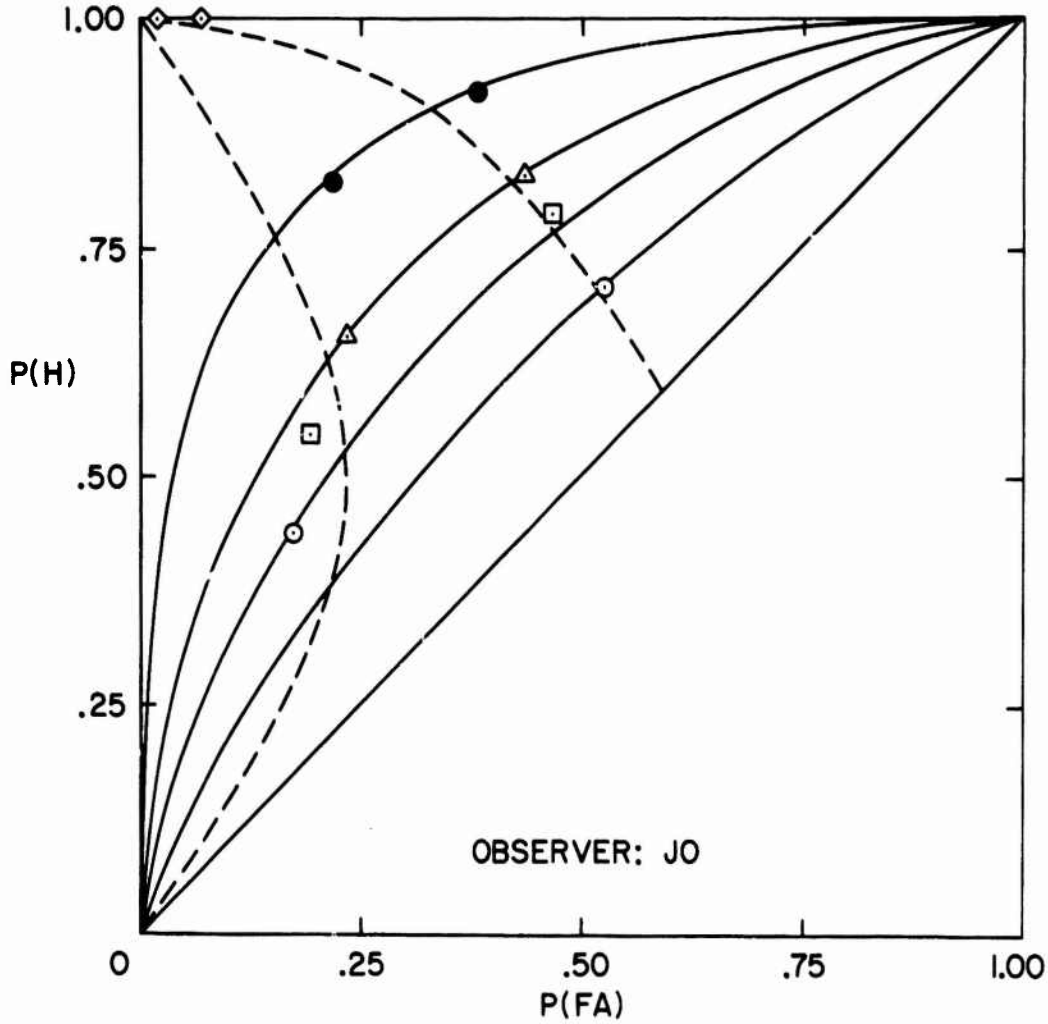

FIGURE 10

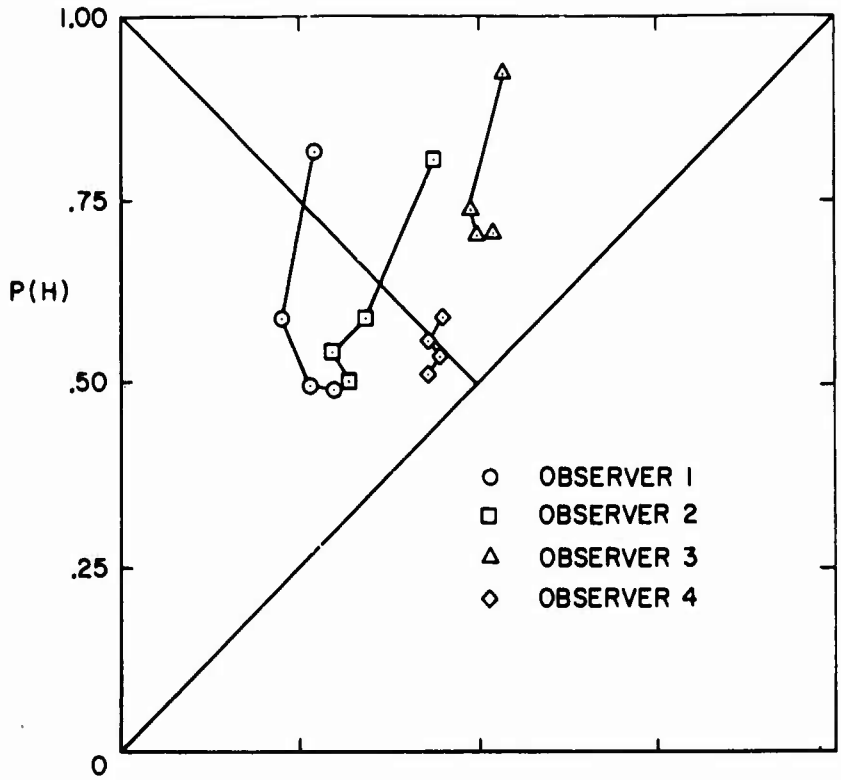
1.00
.75
P(H)
.50
.25
0
OBSERVER 1
OBSERVER 2
OBSERVER 3
OBSERVER 4

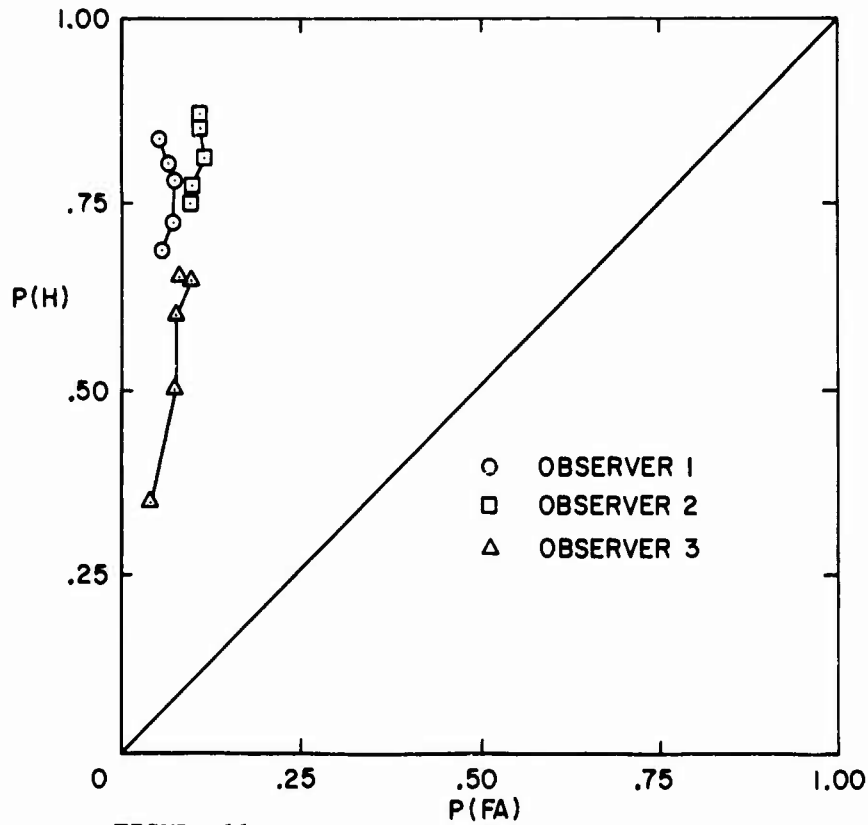
1.00
.75
P(H)
.50
.25
0
.25
.50
.75
1.00
P(FA)
OBSERVER 1
OBSERVER 2
OBSERVER 3

FIGURE 11

A METHOD FOR UNBIASED PARAMETER ESTIMATION BY MEANS OF THE EQUATION ERROR INPUT COVARIANCE

by

S.J. MERHAV and E. GABAY
Department of Aeronautical Engineering
Technion - Israel Institute of Technology,
Haifa, Israel.

ABSTRACT

A new method for obtaining a unique and unbiased estimate of an r-dimensional parameter vector in open or closed loop linear systems in the presence of noise is described. The method is based on the "equation error" and is presented in continuous time. Instead of the classical least squares approach, the equation error is correlated with the input and the covariance is equated to zero. The resulting single linear equation in the r unknown parameters provides a necessary condition for their unique identification. From it, r - 1 additional independent equations are generated. The resulting r linear equations provide the unbiased estimate of the parameter vector. The method does not require the identification of the noise statistics and no precise knowledge of the form and order of the system is required. Implementation is indicated in hybrid analog-digital form. The method is illustrated by numerical examples.

1. INTRODUCTION

Most current methods for identifying linear dynamical systems are based on least squares estimation [1]. The fundamental idea is to generate an error between a "model" and the system to be identified and to minimize a quadratic function of this error with respect to a parameter vector, the solution of which constitutes the "least squares estimate". The attractive property of this approach, as manifested in the "equation error" method [2], is that the error is linearly related to the parameter vector. This property guarantees that the least squares estimate is unique. In other methods, such as the parallel model error [1], this relation is not linear and, in general, the parameter estimate is not unique. However, a severe disadvantage of the least squares approach is, that in the presence of noise at the system input or output, the estimate of the parameter vector becomes biased [3]. This bias can become extremely large even for apparently low noise levels, especially if the system to be identified is of comparatively high order [4]. Identification becomes particularly difficult if the system operates in a closed loop in which the circulation of noise components creates "correlated residuals" leading to bias. In recent years several methods have been developed which remove this noise-due bias. The best known of these are the "generalized least squares" [5] and the "instrumental variable" method [6]. Essentially, these are extensions of the classical least squares method. Examples to which they have been applied demonstrate that the bias can be eliminated. This, however, is achieved at the expense of two factors:

1. Considerable complication of the algorithm and increase in computation time.

2. Loss of the fundamental property of uniqueness of the estimate which exists in classical least squares [1].

In this paper, a new method for parameter estimation is described. It is based on the "equation error" and as such it retains the fundamental linear relationship with the parameter vector. However, instead of minimizing a quadratic measure of this error, it is correlated with the system input. Equating the equation error - input - covariance to zero, yields a necessary condition from which complete identification of the parameter vector of a system in a closed loop and in the presence of noise is achieved. The method, called "Equation-Error-Input-Covariance" method (EEIC) has the following properties:

1. Unbiased estimate both in open and closed loop.
2. The estimate is unique.
3. Identification of the noise statistics is not required.
4. The assumed model may be of higher order than the real system. The excess parameters are forced to zero so that both form, order and parameters are simultaneously identified.
5. On-line identification is possible if a recursive algorithm is applied.

2. NOTATION AND BACKGROUND

Let S_n^m be a linear single-input-single-output time invariant system. m and n are the highest powers in the numerator and denominator respectively. These are defined by:

$$\left.\begin{aligned} N(p,\underline{b}) &= \sum_{i=o}^{m} b_i p^i \\ D(p,\underline{a}) &= 1 + \sum_{j=1}^{n} a_j p^j \end{aligned}\right\} \qquad (1)$$

$p^i \triangleq d^i/dt^i$. S_n^m may be a closed loop system in which $G(p)$ is the dynamic element to be identified and $L(p)$ is the loop closure. $x(t)$ is a random stationary input and $y(t)$ is the corresponding system output. Let $H(p)\{Col[p^o,p^1,\ldots,p^h]\}$ and $H(p)\{Col[p^o,p^1,\ldots,p^\ell]\}$ be vectors of linear operators on $x(t)$ and $y(t)$ respectively. As shown in [7], $\ell > n$ and $h > m$ is permitted with the formulation of Eq. (1). This has the advantage that no precise a priori assumptions regarding the form and order of S_n^m are required. The role of the linear operator $H(p)$ is usually to avoid pure differentiations [2] but its specific task in this paper will become clear later. Let $\underline{\alpha}$ and $\underline{\beta}$ be parameters corresponding to $\underline{a}$ and $\underline{b}$. On forming:

$$\left.\begin{aligned} R(p,\underline{\beta}) &\triangleq H(p) \sum_{i=o}^{h} \beta_i p^i \\ Q(p,\underline{\alpha}) &\triangleq H(p)\,(1 + \sum_{j=1}^{\ell} \alpha_j p^j) \end{aligned}\right\} \qquad (2)$$

the noiseless "equation error" [2] $e(t)$ is given by

$$e(t) = Q(p,\underline{\alpha})y(t) - R(p,\underline{\beta})x(t) \qquad (3)$$

In practical systems the output $y(t)$ is usually contaminated by noise $n_i(t)$ which is zero mean and is uncorrelated with $x(t)$. A block diagram is given in Fig. 1.

The input-output relations in terms of Laplace transforms are:

$$y(s) = T(s)x(s)+n(s) \qquad (4)$$

where

$$T(s) = \frac{G(s)}{1 + L(s)G(s)} = S_n^m \tag{5}$$

and

$$n(s) = \frac{n_1(s)}{1 + L(s)G(s)} \tag{6}$$

The filtered state variables in accordance with Eq. (3) are

$$\left.\begin{aligned} x_i &\triangleq H(p)p^i x, \quad i = 0, 1, \ldots, h \\ y_j + n_j &\triangleq H(p)p^j(y+n), \quad j = 0, 1, \ldots, \ell \end{aligned}\right\} \tag{7}$$

The complete filtered $r = \ell + h + 1$ dimensional state vector is defined by:

$$\underline{w} + \underline{n} \triangleq \mathrm{Col}\{(y_1+n_1), \ldots, (y_\ell+n_\ell), x_o, x_1, \ldots, x_h\} \tag{8}$$

With these notations the equation error is given by:

$$e = y_o+n_o+ \sum_{j=1}^{\ell} \alpha_j(y_j+n_j) - \sum_{i=o}^{h} \beta_i x_i = y_o+n_o +(\underline{w}+\underline{n})^T \underline{\Gamma} \tag{9}$$

where $\underline{\Gamma}$ is a $\ell+h+1 = r$ dimensional parameter vector given by

$$\underline{\Gamma} \triangleq \mathrm{Col}(\alpha_1, .., \alpha_\ell, -\beta_o, \ldots, -\beta_h) \tag{10}$$

and $y_o = y$, $n_o = n$. For $n(t) \equiv 0$, if all components of $\underline{w}$ are linearly independent, $e(t) \equiv 0$ is necessary and sufficient for the complete identification of $\underline{c} \triangleq \mathrm{Col}\ (\underline{a}, \underline{b})$. On minimizing the cost function $I = (1/2)E(e^2)$, where $E(e^2)$ is the expectation of an ensemble of functions $e^2(t)$, the solution of the least squares estimate of $\underline{\Gamma}$, $\hat{\underline{\Gamma}}$ is found to be [3],

$$\hat{\underline{\Gamma}} = -(\bar{A} + \bar{A}_n)^{-1}(\bar{\underline{u}} + \bar{\underline{u}}_n) \tag{11}$$

where:

$$\left.\begin{aligned} \bar{A} &\triangleq E(\underline{w}\,\underline{w}^T) \\ \bar{A}_n &\triangleq E(\underline{n}\,\underline{n}^T) \\ \underline{\bar{u}} &\triangleq E(y_o\underline{w}) \\ \underline{\bar{u}}_n &\triangleq E(n_o\underline{n}) \end{aligned}\right\} \qquad (12)$$

The true unbiased least squares estimate $\hat{\underline{\Gamma}}_o$ of $\underline{c} \triangleq \mathrm{Col}(\underline{a},\underline{b})$ is:

$$\hat{\underline{\Gamma}}_o = -\bar{A}^{-1}\,\underline{\bar{u}} \qquad (13)$$

A major problem in process parameter estimation is the elimination of the bias $\underline{\hat{b}} = \underline{\hat{\Gamma}} - \underline{\hat{\Gamma}}_o$. Methods which achieve this are referenced in [1]. The best known, [5], [6] retain some of the fundamental properties of least squares but in general, convergence to the unique estimate $\hat{\underline{\Gamma}}_o = -\bar{A}^{-1}\,\underline{\bar{u}}$ cannot be proven. In this paper a new method, called the "Equation Error - Input Covariance" (EEIC) method is presented. Its basic property is that it provides a unique and unbiased parameter estimate of $\underline{c}$. Unlike the above mentioned extended least squares methods in which the bias is eliminated by auxiliary procedures, its existence is prevented at the outset by virtue of the basic principle involved.

3. THE EEIC METHOD

In accordance with Eqs. (3) - (6) the equation error is given by:

$$e(t) = T(p)Q(p,\underline{\alpha})x(t) - R(p,\underline{\beta})x(t) + Q(p,\underline{\alpha})n(t) \qquad (14)$$

Multiplying $e(t)$ by $x(t)$ and taking the expectation of the product, one has:

$$E[x(t)e(t)] = E\{x^2(t)[T(p)Q(p,\underline{\alpha}) - R(p,\underline{\beta})]\} + E[x(t)n(t)Q(p,\underline{\alpha})] =$$

$$= [T(p)Q(p,\underline{\alpha}) - R(p,\underline{\beta})]E[x^2(t)] + Q(p,\underline{\alpha})E[x(t)n(t)] \qquad (15)$$

Since $n(t)$ and $x(t)$ are assumed to be uncorrelated (Sec. 2), the second term in Eq. (15) vanishes. Since $E[x^2(t)] \neq 0$, the first term in Eq. (15) can vanish if, and only if

$$T(p)Q(p,\underline{\alpha}) - R(p,\underline{\beta}) \equiv 0 \tag{16}$$

Since $y(t)/x(t) \underline{\Delta} T(p)$, it follows from Eq. (3), that this is the condition for the vanishing of the "noiseless" equation error $e(t)$.

In accordance with Eqs. (1) and (10), Eq. (16) is fulfilled if, and only if, $\underline{\alpha} = \underline{a}$ and $\underline{\beta} = -\underline{b}$ so that from Eq. (15) the condition necessary for the complete identification of $\underline{c} \underline{\Delta} \text{Col}\ (\underline{a},\underline{b})$ is:

$$E[x(t)e(t)] = 0 \tag{17}$$

Eq. (17) is one equation in the r unknowns which constitute the r-dimensional parameter vector $\underline{\Gamma}$. Substituting $e(t)$ from Eq. (9) and by virtue of Eq. (15) disregarding the noise terms, one has:

$$E[x(y_o + \underline{w}^T\underline{\Gamma})] = 0 \tag{18}$$

or:

$$E[x\ w_1]\Gamma_1 + E[x\ w_2]\Gamma_2 + \ldots + E[x\ w_r]\Gamma_r = -E[x\ y_o] \tag{19}$$

Consequently the solution for $\underline{\Gamma}$ lies on the r-dimensional hyperplane defined by Eq. (19). In order to determine the point which is the solution $\underline{\Gamma} = \hat{\underline{\Gamma}}_o$, Eq. (19) must be supplemented by additional $r - 1$ independent linear equations in $\Gamma_1, \ldots, \Gamma_r$. The generation of these additional $r - 1$ equations is a straightforward matter if one recalls that the linear operator $H(p)$ in Eqs. (2) and therefore in Eq. (3), is, in principle arbitrary. One can, therefore, form a linearly independent set, $H_1(p)$, $H_2(p), \ldots H_r(p)$ which operate on the system output $y(t)$ and in accordance with Eqs. (7), (8) set up the corresponding set of equations as follows:

$$\left.\begin{aligned}
E[x\,w_{11}]\Gamma_1 + E[x\,w_{12}]\Gamma_2 \;+,\ldots,+\; E[x\,w_{1r}]\Gamma_1 &= -\,E[x\,y_{10}] \\
E[x\,w_{21}]\Gamma_1 + E[x\,w_{22}]\Gamma_2 \;+,\ldots,+\; E[x\,w_{2r}]\Gamma_2 &= -\,E[x\,y_{20}] \\
\cdot \qquad\quad \cdot \qquad\qquad\quad \cdot \qquad\quad \cdot & \\
\cdot \qquad\quad \cdot \qquad\qquad\quad \cdot \qquad\quad \cdot & \\
\cdot \qquad\quad \cdot \qquad\qquad\quad \cdot \qquad\quad \cdot & \\
E[x\,w_{r1}]\Gamma_1 + E[x\,w_{r2}]\Gamma_2 \;+,\ldots,+\; E[x\,w_{rr}]\Gamma_r &= -\,E[x\,y_{ro}]
\end{aligned}\right\} \qquad (20)$$

Or in compact form:

$$\{E(xw)\}\underline{\Gamma} = -\,E\{x\,\underline{y}_o\} \qquad (21)$$

If the set $H_1(p),\ldots.H_r(p)$ is properly chosen in accordance with $x(t)$ and $T(p)$, the covariance matrix $E\{(xw)\}$ has an inverse and the solution of $\underline{\Gamma}$ is unique and is given by:

$$\underline{\Gamma} = \hat{\underline{\Gamma}}_o = -\,\{E(xw)\}^{-1}E\{x\,\underline{y}_o\} \qquad (22)$$

The elements w_{ij} in Eq. (20) are specifically given as follows in terms of Laplace transforms:

$$\left.\begin{aligned}
w_i &= y_o s^i H(s); \qquad i = 0,1,\ldots,\ell \\
&= x_o s^i H(s); \qquad i = \ell+1,\ \ell+2,\ldots,r
\end{aligned}\right\} \qquad (23)$$

With the set $H_j(s)$, $j = 1,2,\ldots, r$ one has:

$$\left.\begin{aligned}
w_{ij} &= y_o s^i H_j(s); \quad i = 0,1,\ldots,\ell \\
&= x_o s^i H_j(s); \quad i = \ell+1,\ \ell+2,\ldots,r
\end{aligned}\right\} \qquad (24)$$

In order to compute the expectations in Eq. (20), the following property of the cross-correlation function $E[x(t)w_i(t+\tau)] = R_{xw_i}(\tau)$ is made use of:

$$R_{xw_i}(\tau) = \frac{d^i}{d\tau^i}R_{xw_c}(\tau) = \frac{d^i}{d\tau^i}R_{xy_o}(\tau) \qquad (25)$$

A convenient operator for $H_j(s)$ is a pure time delay

$$H_j(s) = e^{-j\tau_o s}; \qquad j = 1,2,\ldots,r \tag{26}$$

This results in:

$$R_{xw_{ij}}(\tau) = \frac{d^i}{d\tau^i} R_{xy_o}(\tau - j\tau_o); \qquad j = 1,2,\ldots,r \tag{27}$$

which means that $R_{xw_{ij}}(\tau)$ is $R_{xw_i}(\tau)$ shifted in the negative direction of τ by $j\tau_o$. For the covariances one has:

$$\left.\begin{aligned} E(xw_{ij}) = R_{xw_{ij}}(0) &= \left[\frac{d^i}{d\tau^i} R_{xy_o}(\tau)\right]_{\tau=j\tau_o}; && i = 0,1,\ldots,\ell \\ &= \left[\frac{d^i}{d\tau^i} R_{xx}(\tau)\right]_{\tau=j\tau_o}; && i = \ell+1,\ldots,r \\ & && j = 0,1,2,\ldots,r-1 \\ & && \tau \geq 0 \end{aligned}\right\} \tag{28}$$

Provided that the derivatives at $\tau = j\tau_o$ exist for all j. These expressions are abbreviated as follows:

$$\left.\begin{aligned} \left[\frac{d}{d\tau^i} R_{xy_o}(\tau)\right]_{\tau=j\tau_o} &= R^{(i)}_{xy_o}(\tau)_{\tau=j\tau_o}; && i = 0,1,\ldots,\ell \\ &= R^{(i)}_{xx}(\tau)_{\tau=j\tau_o}; && i = \ell+1,\ldots,r \\ & && j = 0,1,2,\ldots,r-1 \\ & && \tau \geq 0 \end{aligned}\right\} \tag{29}$$

The choice of $H_j(s)e^{-j\tau_o s}$ has two advantages:

1. It has the power to generate a set of independent equations (2) over a wide range of frequencies.
2. In exploring the method numerically all the elements in the matrix $\{E(xw)\}$ of Eq. (21) are easily determined from the single expression of the cross-correlation $R_{xy_o}(\tau)$ and autocorrelation $R_{xx}(\tau)$.

Dropping the indices in Eqs. (29), Eq. (20) takes the form:

$$\left.\begin{aligned}
&R^{(1)}(0)\Gamma_1 + R^{(2)}(0)\Gamma_2 + \ldots\ldots, + R^{(r)}(0)\Gamma_r &&= -R(0)\\
&R^{(1)}(\tau_o)\Gamma_1 + R^{(2)}(\tau_o)\Gamma_2 + \ldots\ldots, + R^{(r)}(\tau_o)\Gamma_r &&= -R(\tau_o)\\
&\quad\cdot \qquad\qquad \cdot \qquad\qquad\quad \cdot &&\quad\cdot\\
&\quad\cdot \qquad\qquad \cdot \qquad\qquad\quad \cdot &&\quad\cdot\\
&\quad\cdot \qquad\qquad \cdot \qquad\qquad\quad \cdot &&\quad\cdot\\
&R^{(1)}[(r-1)\tau_o]\Gamma_1 + R^{(2)}[(r-1)\tau_o]\Gamma_2 + \ldots, + R^{(r)}[(r-1)\tau_o]\Gamma_r &&= -R[(r-1)\tau_o]
\end{aligned}\right\} \quad (30)$$

Since $j\tau_o$ $(j = 0,1,2,\ldots,r-1)$ are positive time shifts of the origin, only the region $\tau > 0$ is of interest. In compact form, the unbiased estimate then takes the form:

$$\underline{\Gamma} = \hat{\underline{\Gamma}}_o = -\{R\}^{-1}\underline{R} \quad (31)$$

The definitions of the matrix $\{R\}$ and the vector $\underline{R}$ are self evident from Eq. (30).

3. IMPLEMENTATION OF THE EEIC METHOD

In the actual implementation, the set of linear operators $H_1(p)$, $H_2(p),\ldots,H_r(p)$ is applied to the input $x(t)$ and not to the system output $y(t)$. This modification considerably simplifies the realization of the computer program. Denoting the set of corresponding responses by $x_1, x_2,\ldots,x_r$, the following set of equations results:

$$\left.\begin{aligned}
&E(x_1w_1)\Gamma_1 + E(x_1w_2)\Gamma_2 + \ldots, + E(x_1w_r)\Gamma_r &&= -E(x_1y_o)\\
&E(x_2w_1)\Gamma_1 + E(x_2w_2)\Gamma_2 + \ldots, + E(x_2w_r)\Gamma_r &&= -E(x_2y_o)\\
&\quad\cdot \qquad\qquad \cdot \qquad\qquad\quad \cdot &&\quad\cdot\\
&\quad\cdot \qquad\qquad \cdot \qquad\qquad\quad \cdot &&\quad\cdot\\
&\quad\cdot \qquad\qquad \cdot \qquad\qquad\quad \cdot &&\quad\cdot\\
&E(x_rw_1)\Gamma_1 + E(x_rw_2)\Gamma_2 + \ldots, + E(x_rw_r)\Gamma_r &&= -E(x_ry_o)
\end{aligned}\right\} \quad (32)$$

Using pure time delays, the responses are $x_k = xe^{-(k-1)\tau s_o}$, $k = 1,2,...r$. It is easily verified that a set of equations equal to Eq. (30) is obtained since Eqs. (20) and Eq. (32) are completely equivalent. An outline of a hybrid analog digital computer realization is shown in Fig. 2. The differentiations are conveniently performed in the analog part and the delays and multiplications, in the digital part. In practice, these differentiations are not pure but will take the form $s^i/K(s)$, where $K(s)$ is a polynomial in s of order $q \geq r$. The required modifications of the cross correlations in Eqs. (28) and (29) are straightforward and they do not alter the results of Sec. 3. It is important to note, however, that due to $K(s)$, the continuity of $[R^{(i)}_{xy_o}(\tau)]_{\tau=o}$ is guaranteed for all i. With the time delays operating on the input $x(t)$, Eq. (15) is modified as follows: e.g., for the j-th equation one has:

$$E[x(t-j\tau_c)e(t)] = [T(p)Q(p,\underline{\alpha}) - R(p,\underline{\beta})]R_{xx}(j\tau_o) + Q(p,\underline{\alpha})E[x(t-j\tau_o)n(t)] \qquad (33)$$

The second term again is zero. As for the first term, it sustains the validity of condition (16) except for isolated points at which $R_{xx}(j\tau_o)$ may be zero. The $r(r+1)$ products $x_j w_i$ and $x_j y_o$ are stored, averaged and processed for the solution of $\hat{\underline{\Gamma}}_o$ in accordance with Eq. (22). In practice, in particular if "on-line" identification is required, the solution of $\hat{\underline{\Gamma}}_o$ is obtained by a recursive average process (see Appendix) and not by Eq. (22).

The parameters of $G(s)$ are readily determined from the closed loop parameter vector of $T(s)$, $\hat{\underline{\Gamma}}_o = \text{Col}\,(\alpha_1, \alpha_2,..,\alpha_\ell, -\beta_o, -\beta_1,..,-\beta_h)$. The vanishing of the excess parameters $\alpha_{m+1},...,\alpha_\ell$ and $\beta_{m+1},..,\beta_h$ is guaranteed by Eq. (16) and by auxiliary procedures of pole-zero cancellation discussed in [7].

From Eq. (5) one has:

$$G(s) = \frac{T(s)}{1 - L(s)T(s)} \tag{33}$$

Denoting $G(s) = N'(s)/D'(s)$, and recalling that $n > m$, then for e.g. $L(s) = 1$ it is easily verified that the corresponding parameter vector $\underline{\Gamma}' = \text{Col}(\alpha_1', \alpha_2', \ldots, \alpha_n', -\beta_o', -\beta_1', \ldots, -\beta_m')$ of $N'(s)/D'(s)$ is:

$$\left.\begin{aligned}
\alpha_1' &= \frac{\alpha_1 - \beta_1}{1 - \beta_o} \\
&\vdots \\
\alpha_m' &= \frac{\alpha_m - \beta_m}{1 - \beta_o} \\
\alpha_{m+1}' &= \frac{\alpha_{m+1}}{1 - \beta_o} \\
\beta_o' &= \frac{\beta_o}{1 - \beta_o} \\
&\vdots \\
\beta_m' &= \frac{\beta_m}{1 - \beta_o}
\end{aligned}\right\} \tag{34}$$

The appropriate solution of $\underline{\Gamma}'$ can easily be determined for any form of $L(s)$. If $x(t)$ is a disturbance operating on $L(s)$, the EEIC method is equally effective and the slight modifications required in the computations are straightforward.

4. NUMERICAL EXAMPLES

Example 1

A simple numerical example based on time delays in accordance with Eq. (30) serves to illustrate the method. The system S_1^o and the input spectrum

are chosen as :

$$T(s) = S_1^o = \frac{b_o}{1 + a_1 s} = \frac{6.25}{1 + 1.25s} = \frac{5}{0.8 + s} \tag{35}$$

$$\Phi_{xx}(s) = \frac{1}{(1 + s)(1 - s)} \tag{36}$$

The input-output cross-spectrum is:

$$\Phi_{xy_o}(s) = \Phi_{xx}(s)T(s) = \frac{5}{(1+s)(1-s)(0.8+s)} \tag{37}$$

The corresponding cross correlation function is:

$$\left.\begin{aligned} R_{xy_o}(\tau) &= -12.5\, e^{-\tau} + 13.9e^{-0.8\tau} && \tau \geq 0 \\ &= 1.39e^{\tau} && \tau \leq 0 \end{aligned}\right\} \tag{38}$$

The input autocorrelation function is:

$$R_{xx}(|\tau|) = 0.5e^{-|\tau|} \tag{39}$$

The equation error is

$$e = y_o + y_1\alpha_1 - x\beta_o \tag{40}$$

The EEIC is given by

$$E(ex) = E(xy_o) + E(xy_1)\alpha_1 - E(x^2)\beta_o = 0 \tag{41}$$

In accordance with Eq. (30) we have:

$$\left.\begin{aligned} R^{(1)}_{xy_o}(0)\alpha_1 - R_{xx}(0)\beta_o &= -R_{xy_o}(0) \\ R^{(1)}_{xy_o}(\tau_o)\alpha_1 - R_{xx}(\tau_o)\beta_o &= -R_{xy_o}(\tau_o) \end{aligned}\right\} \tag{42}$$

The required covariances are readily determined from Eqs. (38) and (39). Choosing $\tau_o = 0.5$ sec, Eqs. (42) become:

$$\left.\begin{aligned} 1.4\alpha_1 - 0.5\beta_o &= -1.39 \\ 0.15\alpha_1 - 0.305\beta_o &= -1.72 \end{aligned}\right\} \tag{43}$$

which yield the exact estimates: $\beta_o = 6.25$; $\alpha_1 = 1.25$. The determinant of Eqs. (42) is $\det\{R\} = -0.352$. This quite large value indicates that the

matrix

$$\{R\} = \begin{pmatrix} 1.4 & -0.5 \\ 0.15 & -0.305 \end{pmatrix} \tag{44}$$

is far from being singular thus demonstrating the effectivity of the time-delay operators.

Let the assumed form now be $\beta_o/(1 + \alpha_1 s + \alpha_2 s^2)$. The equation error now is:

$$e = y_o + y_1\alpha_1 + y_2\alpha_2 - x\beta_o \tag{45}$$

and the set of equations in accordance with Eq. (30) is:

$$\left.\begin{aligned} R^{(2)}_{xy_o}(0)\alpha_2 + R^{(1)}_{xy_o}(0)\alpha_1 - R_{xx}(0)\beta_o &= - R_{xy_o}(0) \\ R^{(2)}_{xy}(\tau_o)\alpha_2 + R^{(1)}_{xy_o}(\tau_o)\alpha_1 - R_{xx}(\tau_o)\beta_o &= - R_{xy_o}(\tau_o) \\ R^{(2)}_{xy_o}(2\tau_o)\alpha_2 + R^{(1)}_{xy_o}(2\tau_o)\alpha_1 - R_{xx}(2\tau_o)\beta_o &= - R_{xy_o}(2\tau_o) \end{aligned}\right\} \tag{46}$$

Choosing again $\tau_o = 0.5$ sec. Eqs. (46) become:

$$\left.\begin{aligned} - 3.6\alpha_2 + 1.4\alpha_1 - 0.5\beta_o &= - 1.39 \\ - 1.52\alpha_2 + 0.15\alpha_1 - 0.303\beta_o &= - 1.72 \\ - 0.6\alpha_2 - 0.38\alpha_1 - 0.184\beta_o &= - 1.62 \end{aligned}\right\} \tag{47}$$

The determinant of Eqs. (47) is $\det\{R\} = - 0.035$ and their solution is: $\alpha_2 = 0$; $\alpha_1 = 1.25$; $\beta_o = 6.25$. This result indicates that the method can handle "higher order models" i.e. models in which the powers of the numerator and denominator are higher than in the real system, S^m_n. The excess parameter estimate α_2 which is zero, demonstrates that the form and order of $T(s) = S^m_n$ can be identified along with the parameters.

Example 2

The second example illustrates the identification of a zero and a pole.

$$T(s) = S_1^1 = \frac{b_o + b_1 s}{1 + a_1 s} = \frac{6.25 + 2.5s}{1 + 1.25s} = 2\,\frac{2.5 + s}{0.8 + s} \tag{48}$$

$$\Phi_{xx}(s) = \frac{1}{(1+s)(1-s)(2+s)(2-s)} \tag{49}$$

The input-output cross-spectrum is:

$$\Phi_{xy_o}(s) = \Phi_{xx}(s)T(s) = \frac{2(2.5 + s)}{(1+s)(2+s)(1-s)(2-s)(0.8+s)} \tag{50}$$

The corresponding cross correlation function is:

$$R_{xy_o}(\tau) = -2.5e^{-\tau} + 0.07e^{-2\tau} + 2.82e^{-0.8\tau}; \qquad \tau \geq 0 \tag{51}$$

The input autocorrelation function is:

$$R_{xx}(|\tau|) = \frac{1}{6}\,e^{-|\tau|} - \frac{1}{12}\,e^{-2|\tau|} \tag{52}$$

The equation error is:

$$e = y_o + y_1\alpha_1 - x_o\beta_o - x_1\beta_1 \tag{53}$$

The EEIC is given by:

$$E(ex) = E(xy_o) + E(xy_1)\alpha_1 - E(x^2)\beta_o - E(xx_1)\beta_1 = 0 \tag{53}$$

In accordance with Eq. (30) we have:

$$\left.\begin{aligned} R^{(1)}_{xy_o}(0)\alpha_1 - R_{xx}(0)\beta_o - R^{(1)}_{xx}(0)\beta_1 &= -R_{xy_o}(0) \\ R^{(1)}_{xy_o}(\tau_o)\alpha_1 - R_{xx}(\tau_o)\beta_o - R^{(1)}_{xx}(\tau_o)\beta_1 &= -R_{xy_o}(\tau_o) \\ R^{(1)}_{xy_o}(2\tau_o)\alpha_1 - R_{xx}(2\tau_o)\beta_o - R^{(1)}_{xx}(2\tau_o)\beta_1 &= -R_{xy_o}(2\tau_o) \end{aligned}\right\} \tag{54}$$

Choosing $\tau_o = 0.5$ sec as before, the resulting set of equations is:

$$\left.\begin{aligned} 0.1\alpha_1 - 0.0833\beta_o - 0\beta_1 &= -0.39 \\ -0.051\alpha_1 - 0.07\beta_o + 0.04\beta_1 &= -0.4 \\ -0.114\alpha_1 - 0.05\beta_o + 0.039\beta_1 &= -0.354 \end{aligned}\right\} \quad (55)$$

The determinant is $\det\{R\} \cong -10^{-4}$ and the solution is: $\beta_o = 6.25$; $\beta_1 = 2.5$; $\alpha_1 = 1.25$.

It should be noted that in this example $x(s)$ (Eq. (49)), has been chosen so that $R_{xx}(\tau)$ at $\tau = 0$ is continuous. This guarantees the existence of $R_{xx}^{(1)}(0)$ in (54). In practice this is guaranteed by the state filter $K(s)$.

CONCLUSIONS

It has been shown that by correlating the system input with the equation error an effective and relatively general algorithm is obtained for the unbiased estimation of parameters both in open and closed loop. By properly formulating the equation error, it has also been demonstrated that the order and form of the system to be identified must not be precisely known. If a sufficiently high order model can be afforded in the computer program, the excess parameters are estimated as zero so that the order and form are identified along with the parameters. The method is amenable to hybrid or to pure digital computing facilities. In the development of the actual computer software a recursive algorithm will be employed so that on-line identification can be achieved. Rapidity of convergence of the parameter estimate and its variance and extensions to multivariable systems are subjects for further work.

APPENDIX

RECURSIVE ON-LINE IMPLEMENTATION.

The solution of the parameter vector estimate as given by Eq. (31) is:

$$\hat{\underline{\Gamma}}_o = - \{R\}^{-1}\underline{R} \tag{A1}$$

where the elements of $\{R\}$ are the cross correlations

$$\{R\} = \{R_{ij}\} = \{R_{x_i w_j}(0)\} = \{R_{x w_j}(\tau_i)\} \tag{A2}$$

$$i = 0,1,\ldots,r$$

$$j = 1,2,\ldots,r$$

and the elements of $\underline{R}$ are:

$$\underline{R} = (\underline{R}_j) = (R_{x_j y_o}(0)) = (R_{x y_o}(\tau_j) \quad j = o,1,\ldots,r \tag{A3}$$

For on-line implementation a hybrid computer may be used, where the time delay is performed in the digital part and the cross correlations are computed by:

$$R^k_{xy}(\tau) = \frac{1}{k} \sum_{i=1}^{k} x(iT - \tau)y(iT) \tag{A4}$$

T is the sampling interval and k the number of samples. Eq. (A4) may be be written in a recursive form which enables real time processing.

$$R^{k+1}_{xy}(\tau) = \frac{1}{k+1} \sum_{i=1}^{k+1} x(iT - \tau)y(iT) =$$

$$= \frac{1}{k+1} \sum_{i=1}^{k} x(iT-\tau)y(iT) + \frac{1}{k+1} x[(k+1)T-\tau]y[(k+1)T]$$

$$= R^k_{xy}(\tau) - \frac{R^k_{xy}(\tau) - x[(k+1)T-\tau]y[(k+1)T]}{k+1} \tag{A5}$$

Eq. (A5) may be rewritten as follows:

$$R^{k+1}_{xy}(\tau) = R^k_{xy}(\tau) + \Delta R^{k+1}_{xy}(\tau) \tag{A6}$$

where:

$$\Delta R_{xy}^{k+1}(\tau) = -\frac{R_{xy}^{k}(\tau) - x[(k+1)t-\tau]y[(k+1)T]}{k+1} \tag{A7}$$

Thus every sample (consisting of $x(t_k)$, $y_o(t_k)$, $w_i(t_k)$ $i = 1,2,\ldots,r$) updates the elements of $\{R\}$ and $\underline{R}$ recursively

$$\{R^{k+1}\} = \{R^{k}\} + \{\Delta R^{k+1}\} \tag{A8}$$

$$\underline{R}^{k+1} = \underline{R}^{k} + \Delta\underline{R}^{k+1} \tag{A9}$$

The elements of $\{\Delta R\}$ and $\Delta\underline{R}$ (Eqs. A2-A3) are computed using Eqs. (A6-A7). Substituting Eqs. (A8-A9) into (A1) we obtain:

$$\hat{\underline{\Gamma}}^{k+1} = -(\{R^{k}\} + \{\Delta\underline{R}^{k+1}\})^{-1}(\underline{R}^{k} + \Delta\underline{R}^{k+1}) \tag{A10}$$

Using the well known matrix inversion lemma

$$(\{R^{k}\} + \{\Delta R^{k+1}\})^{-1} = \{R^{k}\}^{-1} - \{R^{k}\}^{-1}\{\Delta R^{k+1}\}[I + \{R^{k}\}^{-1}\{\Delta R^{k+1}\}]^{-1}\{R^{k}\}^{-1} =$$

$$= \{R^{k}\}^{-1} + \{\delta R^{k+1}\} \tag{A11}$$

where

$$\{\delta R^{k+1}\} = -\{R^{k}\}^{-1}\{\Delta R^{k+1}\}[I + \{R^{k}\}^{-1}\{\Delta R^{k+1}\}]^{-1}\{R^{k}\}^{-1} \tag{A12}$$

Substituting in Eq. (A10)

$$\hat{\underline{\Gamma}}^{k+1} = -[\{R^{k}\}^{-1} + \{\delta R^{k+1}\}](\underline{R}^{k} + \Delta\underline{R}^{k+1}) =$$

$$= -\{R^{k}\}^{-1}\underline{R}^{k} - [\{R^{k}\}^{-1}\Delta\underline{R}^{k+1} + \{\delta R^{k+1}\}(\underline{R}^{k} + \Delta\underline{R}^{k+1})] \tag{A13}$$

Denoting

$$\Delta\hat{\underline{\Gamma}}^{k+1} = -[\{R^{k}\}^{-1}\Delta\underline{R}^{k+1} + \{\delta R^{k+1}\}(\underline{R}^{k} + \Delta\underline{R}^{k+1})] \tag{A14}$$

and since

$$\hat{\underline{\Gamma}}^{k} = -\{R^{k}\}^{-1}\underline{R}^{k} \tag{A15}$$

Eq. (A13) becomes

$$\hat{\underline{\Gamma}}^{k+1} = \hat{\underline{\Gamma}}^{k} + \Delta\hat{\underline{\Gamma}}^{k+1} \tag{A16}$$

To provide the initial value of $\{R^{k}\}^{-1}$ the initial measurements, say the first ten measurements, should be processed using Eqs. (A4, A15) obtaining $\{\underline{R}^{10}\}$, $\underline{R}^{10}$, $\hat{\underline{\Gamma}}^{10}$. With these, the recursive process (Eqs. A8, 11, 14, 16) can be started (with k=10).

REFERENCES

[1] Astrom, K.J. and Eykhoff P., "System Identification - a Survey", Automatica, Vol.7, 1971, pp.123-162.

[2] Lion P.M., "Rapid Identification of Linear and Nonlinear Systems", Proc. JACC, Washington, 1966, pp.605-616.

[3] Eykhoff P., "Process Parameter and State Estimation",Automatica,Vol.4, 1968, pp.205-233.

[4] Stankovic S.S. and Kouwenberg, N.G.M., "Some Aspects of Human Operator Identification in Real Time",Proc. 3rd IFAC Symposium on Identification and System Parameter Estimation", Pt. 1, the Hague, June 1973, pp.247-250.

[5] Clarke, D.W., "Generalized Least Squares Estimation of the Parameters of a Dynamic Model", IFAC Symp. on Identification in Automatic Control Systems, Prague, 1967, Paper 3.17.

[6] Wong, K.Y. and Polak, E., "Identification of Linear Discrete Systems using the Instrumental Variable Method", IEEE Trans. AC-12, 1967, pp.707-718.

[7] Merhav, S.J., and Gabay, E., "On Simultaneous Structure and Parameter Identification of Linear Dynamical Systems", to be published in IEEE Trans. on Automatic Control, June 1974.

[8] Young P.C., "An Instrumental Variable Method for Real Time Identification of a Noisy Process", Automatica, Vol. 6., 1970, pp.271-287.

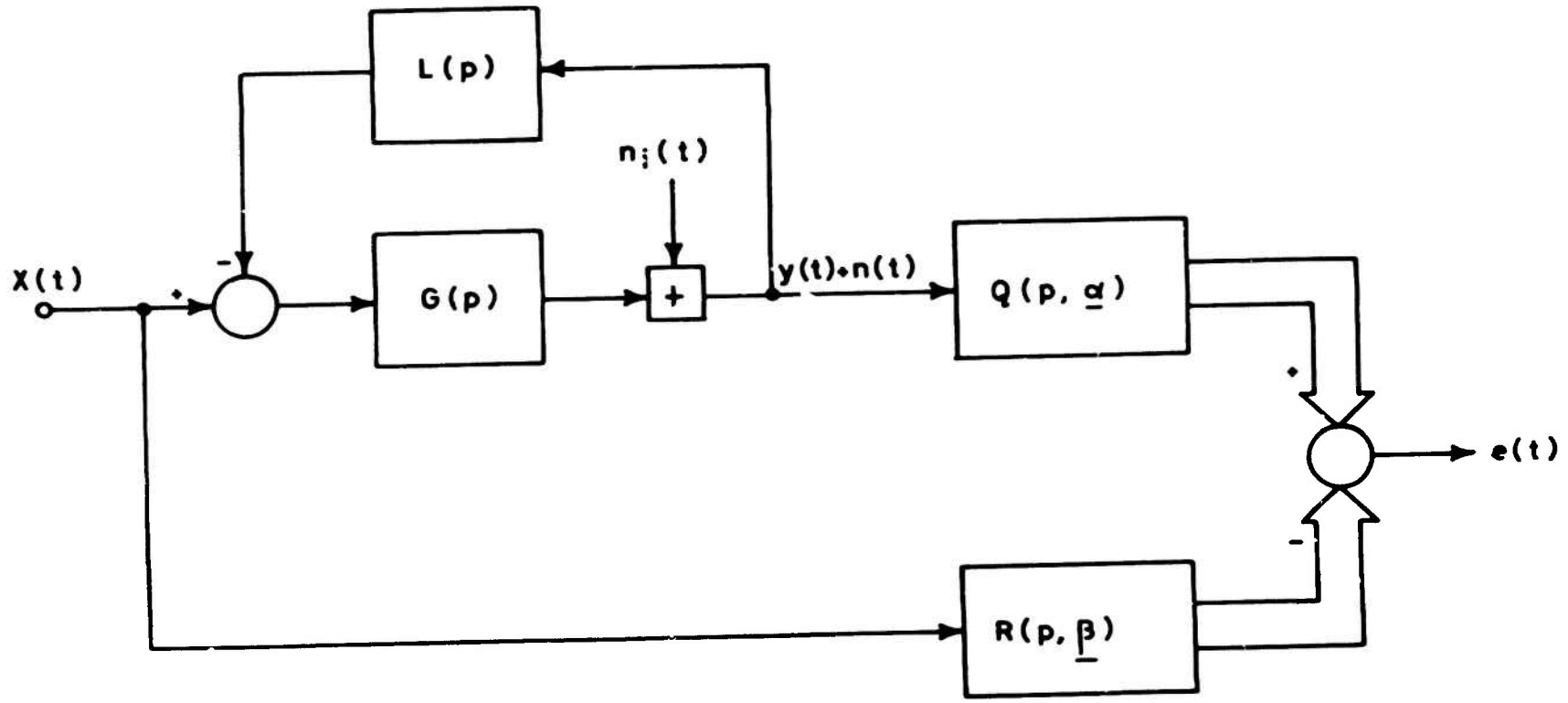

FIGURE 1 - GENERATION OF THE EQUATION ERROR OF A CLOSED LOOP SYSTEM WITH NOISE.

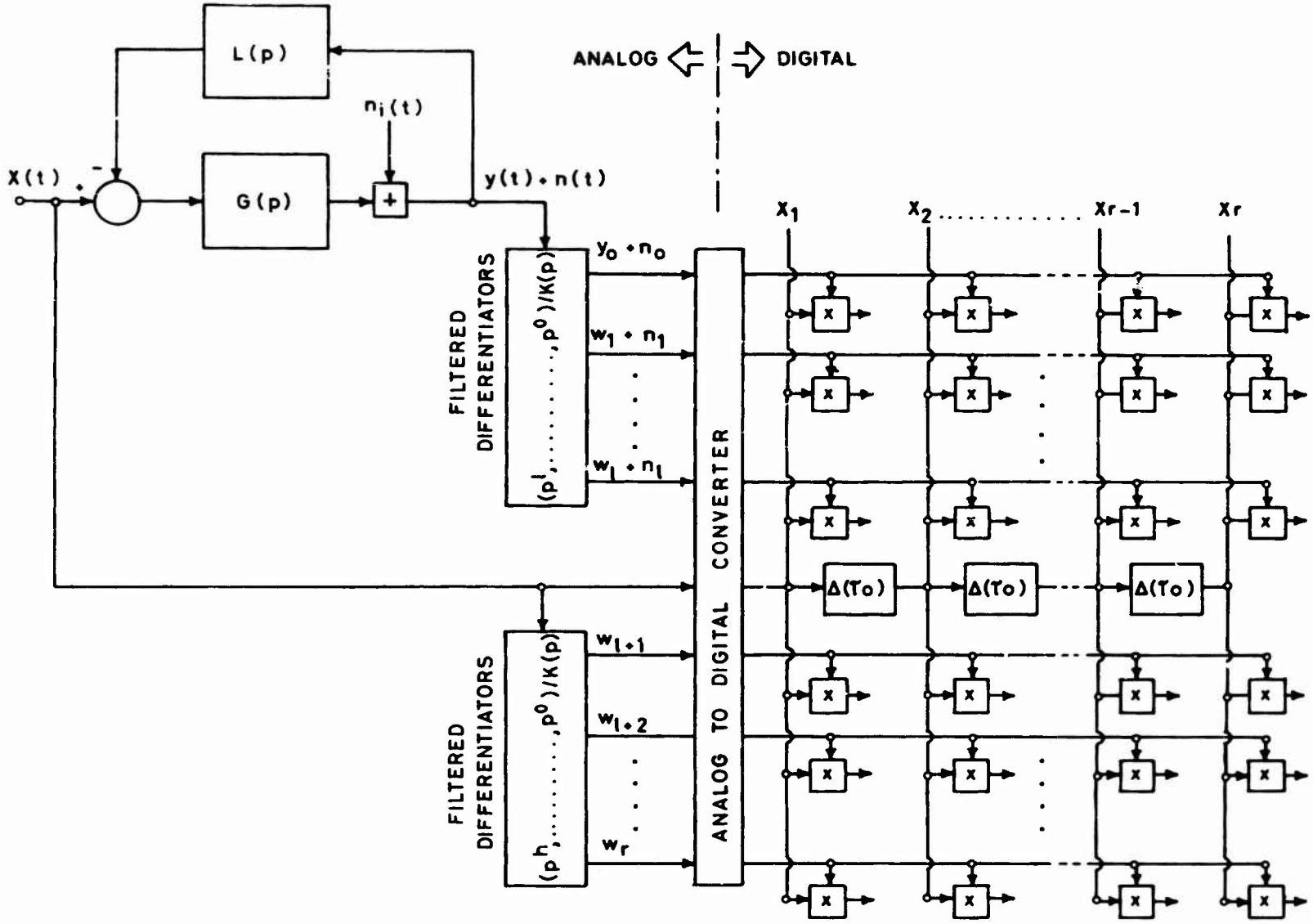

FIGURE 2 - IMPLEMENTATION OF THE BASIC EEIC METHOD IN HYBRID ANALOG-DIGITAL FORM

74-28,209#3

MEASUREMENTS AND MODELING ON THE NATURE OF PHYSIOLOGICAL TREMOR

Günter Rau
Forschungsinstitut für Anthropotechnik (FAT)
(Research Institute for Humon Engineering)
Meckenheim, F.R. Germany

ABSTRACT

Fine-motor unsteadiness limits the accuracy of perceptual-motor control as described e.g. by Magdaleno et al. at the 1973 Annual Manual. At least a portion of these minute limb movements are referred to as normal tremor. New measurements on forefinger tremor and a resulting simplified tremor model are presented and discussed.

In our experiments forefinger tremor showed a sharp peak in the frequency spectrum of the acceleration at 20 - 25 Hz which is clearly seperated from the peaks of hand tremor (10 Hz) and forearm tremor (1-3 Hz). At the same time the "EMG pulsations" at the correspondi ng forefinger extensor muscle showed a broad spectrum with a flat maximum at about 15 Hz. When we added an extra mass (up to 90 g) the peak of the acceleration spectrum was shifted towards lower frequencies while the EMG spectrum remained unchanged. Our results indicate that this type of tremor can be described by a linear mechanical model without a neuromuscular reflex loop which moy well play a role in other types of tremor as e.g. force tremor.

A. INTRODUCTION

It has long been known that posture, as well as voluntary movements even in healthy subjects, are associated with physiological tremor. These small rhythmical involuntary fluctuations in position of various body parts impair the accuracy of fine motor performonce. For example, in control tasks using a smoll finger stick or in the use of hand field glasses [1], the resolution is limited by tremor oscillations. Other examples are mentioned by Allen, Magdaleno and Jex [2] and other authors [3]. However, every possible means which can be employed to reduce the influence of tremor movements depend on knowledge of its frequency distribution. Therefore, it is important to analyse the tremor frequency spectrum, and also to get some insight into the origin of the oscillations. These tasks can be assisted by modeling different possible system configurations.

1. Servo-loop hypothesis : In previous studies, the postural tremor is reported to show its predominant frequency at about 10 cycles per second. Lippold [4, 5] concluded from his experiments on finger tremor that physiological tremor in the 8-12 Hz band is due to oscillation in the reflex servo-loop. Also other authors have been in favour of the reflex loop hypothesis [6, 7]. However, it seems to be clear now that it is impossible to define a uniform or unique tremor frequency. On the basis of peaks in the tremor frequency spectrum it is possible to make distinctions between finger tremor (20 - 25 Hz), hand tremor (8 - 10 Hz), and forearm tremor (1 - 3 Hz) [8, 9]. The disagreement in the above results moy be explained by differences in the experimental situation. For example,

Lippold's measurements at the finger tip comprised mainly hand tremor movements masking the finger tremor with its much lower amplitude values. Two reasons are responsible for this strong masking of finger tremor : (1) the detection of finger displacement instead of the acceleration, results in smaller amplitudes of the frequency peak relative to higher amplitudes in the lower frequency band of hand tremor ; and (2) the positioning of the hand on the table in a manner which allows, at least, a portion of hand tremor movements to be superimposed on finger movements.

2. Mechanical filter hypothesis : In contrast to the servo mechanism hypothesis, tremor could be described as a feature of an underdamped, second-order, linear system according to the mechanical properties (mass, spring, damping) of a limb-muscle system [8, 9, 10, 11]. This system is activated through forces developed by the muscles involved. These muscle forces may be estimated by recording EMG activities. This is possible because at least for small changes in the force an approximately linear relationship between EMG activity and the exerted muscle force can be assumed [12, 13]. The mechanical filter hypothesis predicts the tremor peak frequency to decrease with added weights without a shift in the lower frequencies of the EMG spectrum.

Based on these considerations we studied finger tremor in order to discriminate between the servo-loop and mechanical filter.

B. EXPERIMENTS ON FINGER TREMOR

1. Methods : The hand was rested in a relaxed position on a special support [10, 11] with the index finger extended as shown by figure 1. This support was designed to eliminate hand movement.

The forearm was held in a pronated position and supported at the elbow region. An accelerometer (weight 4g) was attached to the end phalanx of the index finger picking up the flexion-extension movement selectively. The acceleration frequency spectrum was obtained by means of a filter bank as described by Alewijnse and Koster [14].

The EMG signals were picked up with a pair of surface electrodes (8 mm diameter, 40 mm interdistance) from the distal part of the M. extensor indicis, and then amplified (flat between 15-1000 Hz [10]). Signals were processed further by double-wave rectification and low-pass filtering (24 dB/oct., about 30 Hz cut off frequency) ; the result being an envelope of the EMG signal. The frequency spectrum of the EMG envelope was analyzed by using the same filter bank as for the acceleration processing.

Additional weights were attached around the first phalanx in the form of small pieces of lead.

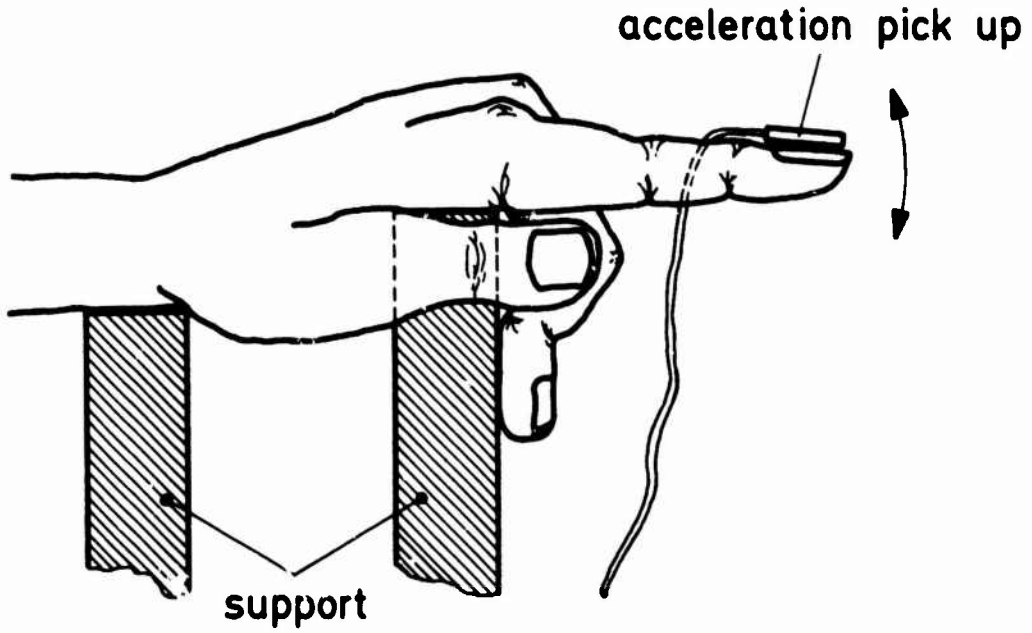

Figure 1 : Arrangement for finger tremor measurements

2. Results : The acceleration amplitude of the forefinger's oscillations is shown (figure 2a) as a function of frequency for two different example masses. When the forefinger was loaded with 16 g, the frequency spectrum showed a peak at 20 Hz. This peak was shifted down to 9 Hz when the extra mass was increased to 87 g.

The EMG envelope spectrum is shown by figure 2b. Here, too, a peak frequency is observed, but the peak is not very sharp ; the spectrum is much broader than that of the acceleration. Different weights up to about 100 g did not cause any shift of the flat maximum ; there is no change in the form of the noiselike spectrum which could be related to changes in the acceleration spectrum of figure 2a.

Similar results were obtained with various masses [10]and different subjects as well as when a different method for spectrum analysis was applied [15].

3. Discussion and filter modeling : The acceleration spectra showed sharp peaks and are in good agreement with results reported in the literature [8, 10, 15]. The EMG spectra were much broader and showed no changes when a mass was added.

Thinking in terms of a mechanical filter the following concept has to be tested. The frequency spectrum of the EMG envelope may be taken as a representation of the muscle forces as already mentioned. The mechanical resonant system is driven by varying muscle forces which have a broad frequency spectrum, and it filters out a narrow band of the

a

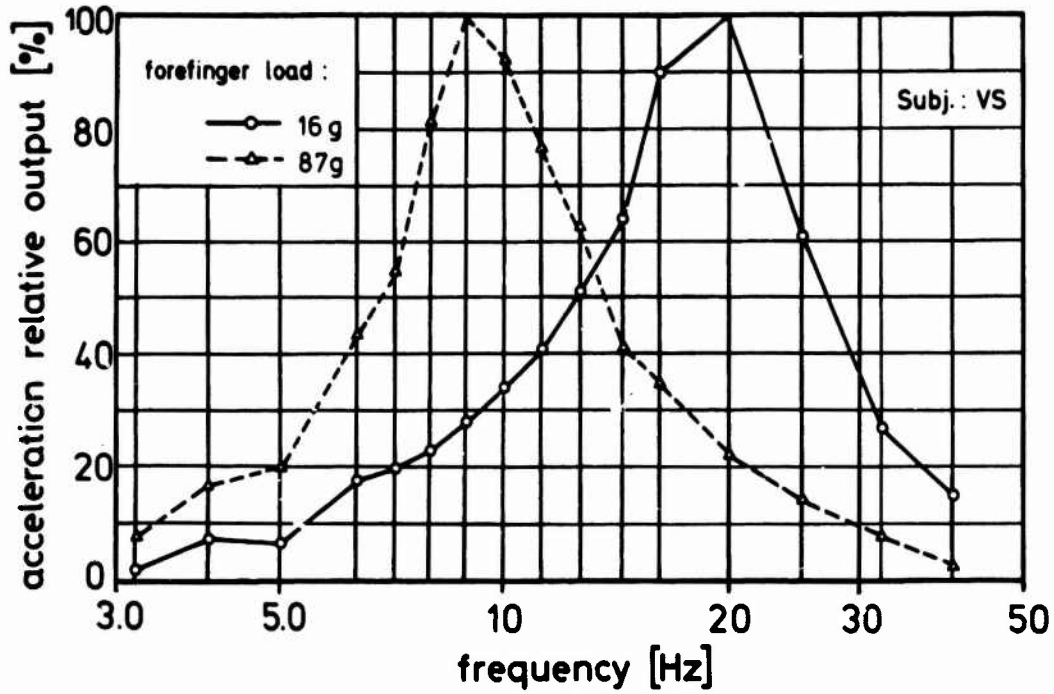

b

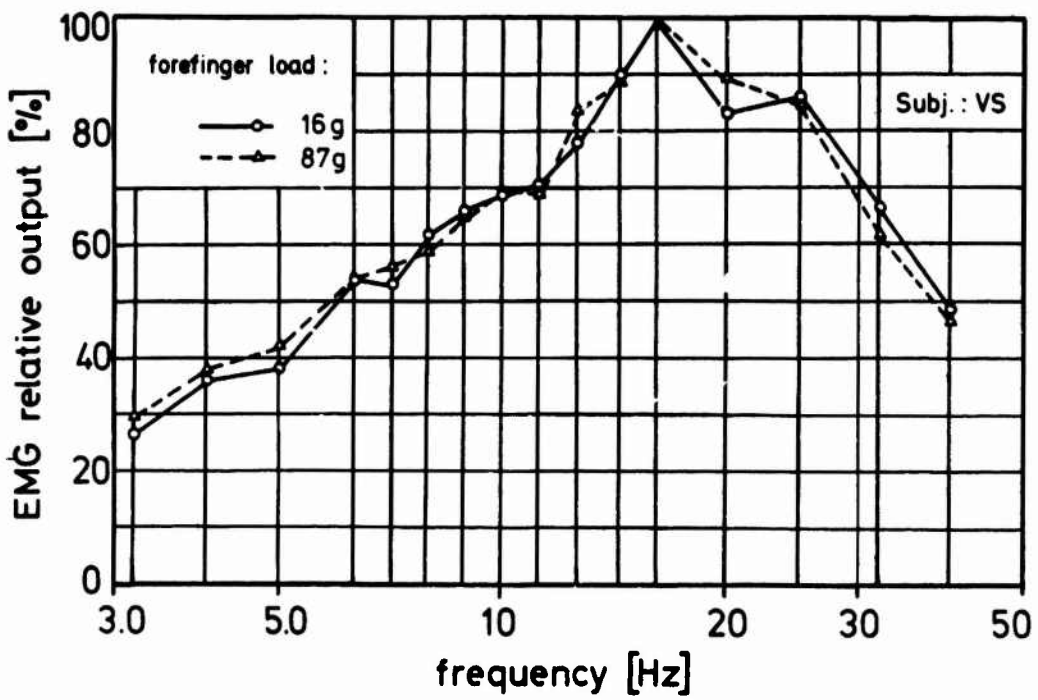

Figure 2 : Finger tremor with two different masses
a) amplitude spectrum of the acceleration
b) amplitude spectrum of the EMG activity

whole input driving spectrum. The spectrum of the acceleration can, therefore, be expected to primarily indicate the porperties of the mechanical filter. A comparison of the spectra of figure 2a and 2b reveals no equivocal relationship between the driving force and the filter response.

This concept is also in agreement with results reported and discussed by Hamoen [16] concerning hand tremor oscillations. The results of Fox and Randall [9] obtained by detecting the forearm tremor and the envelope of the biceps EMG are essentially the same, thus supporting the mechanical filter concept.

Using a second-order linear filter equation to describe the acceleration spectrum of forefinger movements, it is possible to estimate the shift of the peak frcquency caused by increasing the mass. Taking the effective mass of the finger to be M_o, the peak frequency is

$$f_o = \frac{1}{2\pi} \sqrt{\frac{c_o}{M_o}} \qquad (1)$$

while c_o is the stiffness of the system. Assuming the stiffness c_o to be independent of the added mass, we get

$$f_{res} = \sim \frac{1}{\sqrt{M_o + m}} \qquad (2)$$

This means that with additional masses attached to the finger, the frequency will decrease with the square root of the total mass.

Assuming that the moved mass of our subject's finger system is about $M_o = 10$ g, we can start with the peak frequency of 25 Hz where no mass is added except the transducer; and calculate the shift corresponding to the mass m_1. By applying (1) recurrently, we can use the ratio

$$\frac{f_1}{f_2} = \sqrt{\frac{M_o + m_2}{M_o + m_1}} \qquad (3)$$

for calculation of the resonance frequencies.

The table below shows that the results of this approximation are in good agreement with the measurements [10]:

Table

mass g	f peak Hz measured	f peak Hz predicted
4	25	25
16	19	18.5
45	12.6	12.5
87	9	9.5

Figure 3 shows the relation between mass and resonance frequency represented by a line starting from zero as predicted by the model. Various data points of resonance frequencies of finger oscillations were entered. These data points were derived from our experiments [10] and those of other investigators. Measurements of physiological tremor [8, 10] and measurements of die-away oscillations following a sharp tap to the finger [12] were included.

Each set of values entered fell on a line parallel to the theoretical line of the model. Effective finger mass values were of course not given in the literature, since they can not easily be measured directly. However, it is reasonable to assume these masses differ with different subjects. Effective finger mass assumptions can be made in such a way that the values are situated very close to the theoretical line. In fact, this procedure is an indirect method for estimating the effective finger mass.

The agreement between data and the model tend to support the mechanical filter hypothesis. In addition, the assumption of the system's stiffness to be a constant is supported.

Our experiments involved masses up to 100 g. As recently reported Koster and van Schuur [15] extended their measurements to extra masses up to 184 g. The shift of the acceleration peak frequency in their extended range of masses can also be described very well by the filter model. But in that range the spectrum of the EMG envelope gradually exhibited a peak at the tremor frequency. Similarly, Lippold [4, 5] reported EMG pulsations synchronously with the die-away oscillations follwing a tap to the finger. How could these phenomena be explained in accordance with the filter model ?

4. Muscle spindle feedback : During normal tremor oscillations, the maximum amplitude of the finger tip is about 0.2 mm [4]. The muscle spindles which are acting in the reflex loop as the sensors seem to have a threshold for small amplitudes [17], i.e. changes in muscle lenght must exceed a minimum value to cause an excitation of the muscle spindles. It can be assumend that the tendon organs have higher thresholds compared to

those of the sensitive muscle spindle endings [17]. Therefore, only the muscle spindle endings will be taken into consideration here. On the basis of measured data, a test can be made of the proposition that the length of the muscle spindles (during normal tremor amplitudes) can be changedsubthreshold, while during the marked changes in length following a tap on the finger, this threshold could be exceeded.

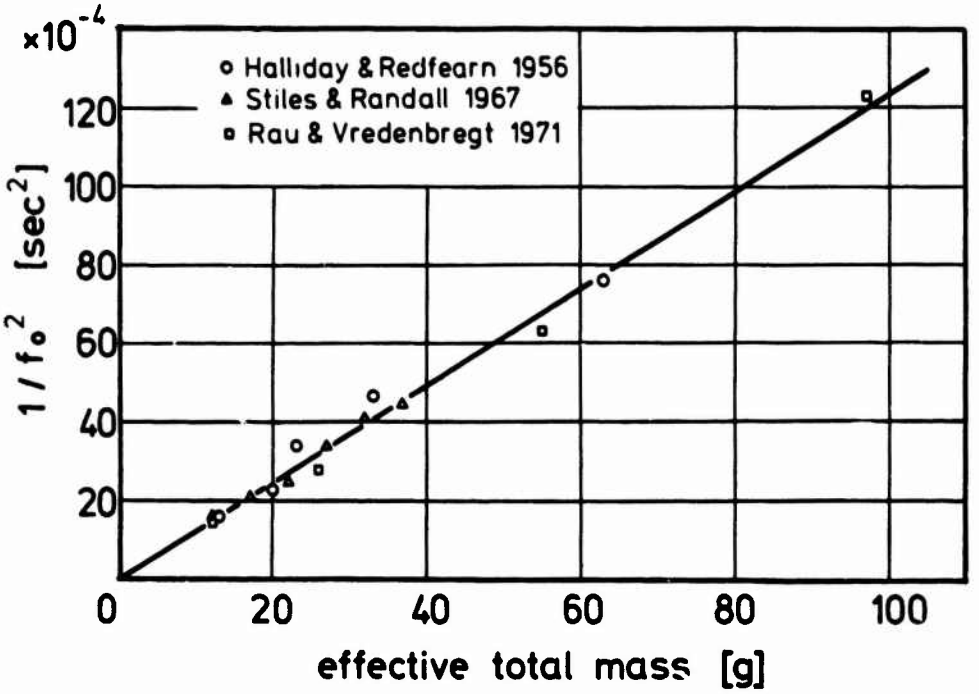

Figure 3 : Relationship between peak frequency f_o and moved total mass. The line is given by the 2nd order filter model, data points are derived from measurements [6, 8, 10]. Assumptions for finger masses M_o : Halliday & Redfearn : 13 g ; Stiles & Randall : 12 g ; Rau & Vredenbregt : 10 g.

In the following discussion, the finger system is approximated by the model given schematically in figure 4. The length of a rigid forefinger is assumend to be 10 cm, and the tendon connected to the finger 1 cm distant from the axis of rotation (metacarpal joint). Further, it can be assumed that tendon stiffness is many times that of muscle tissue. Therefore, a displacement of the finger tip will cause a change only in muscle length.

On the basis of these assumptions, during normal tremor a finger tip displacement of 0.2 mm causes a change in muscle length of about 0.02 mm. For a totol muscle length of about 200 mm the relative change in length is 0.02/200 = 1/10 000. The amplitudes of the finger tip displacement observed as a response to a tap was about 1.5 mm [4], causing a change in muscle length of 0.15 mm. Thus the relative change is 0.15/200 = 1/1 330. The results are illustrated in figure 5.

The most sensitive parts of the muscle spindle receptor are the primary endings. For example, changes in the length of the muscle spindle of 0.05 mm or somewhat less, lead

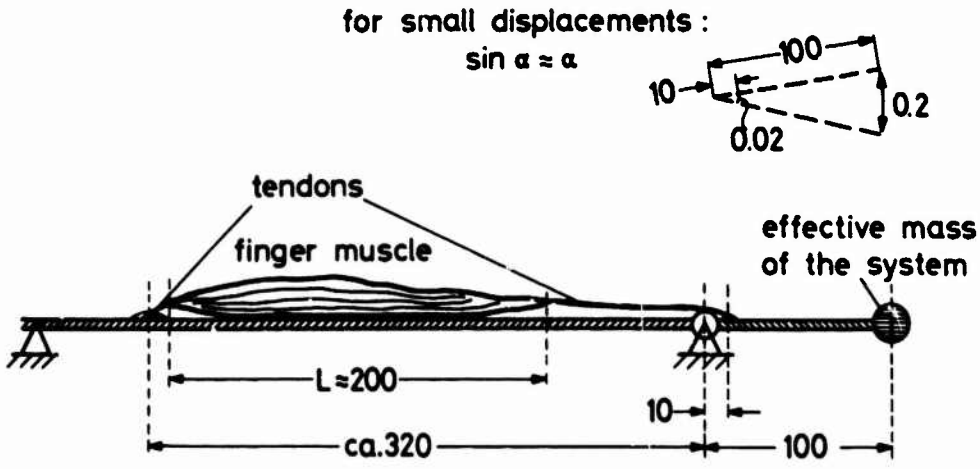

Figure 4 : Simplified model of a finger (figures are scaled in mm)

to changes in the spindle firing rate [17]. In the situation as given by the proposed model it is difficult to estimate the factual length change of the spindles when the surrounding muscle tissue is stretched ! In addition, the finger muscle is very long with respect to its extension. It can be expected that a dynamic extension of the whole muscle at a tremor-like frequency (e.g. 25 Hz) will result in only a partial stretch of the primary endings of the spindle.

Experiments with the soleus muscle of the cat [17]have shown : when a sinussoidal length variation was applied to the tendon at a frequency of 100 Hz the lowest amplitude threshold of the most sensitive primary ending showed to be about 0.005 mm. This corresponds to a relative change in muscle length of 1/10 000 (fig. 5). In the experimental situation the sensitivity of the primary endings was already enhanced by a mechanical prestretch of the muscle.

It can be further assumed that the amplitude threshold of the spindle is also about the same magnitude in the range of tremor oscillations. In the literature no comparable electrophysiological measurements on humon subjects are available which would permit a determination of the threshold of muscle spindles relative to total muscle length changes. Therefore, the results of the cat experiments are used to give some indication of the order of magnitude in sensitivities in judging the situation of finger tremor.

Comparing the cat soleus threshold reported by Mathews [17] with the finger movement amplitudes estimated in the model (figure 4), one can presume that the amplitude of normal tremor may be too small to excite the muscle spindles in the human finger muscle. In contrast, the amplitudes of die-away oscillations in response to a tap on the finger could exceed the threshold of the muscle spindles. Also, during oscillations with additional masses above 100 g the finger movement amplitudes were increased markedly [15].

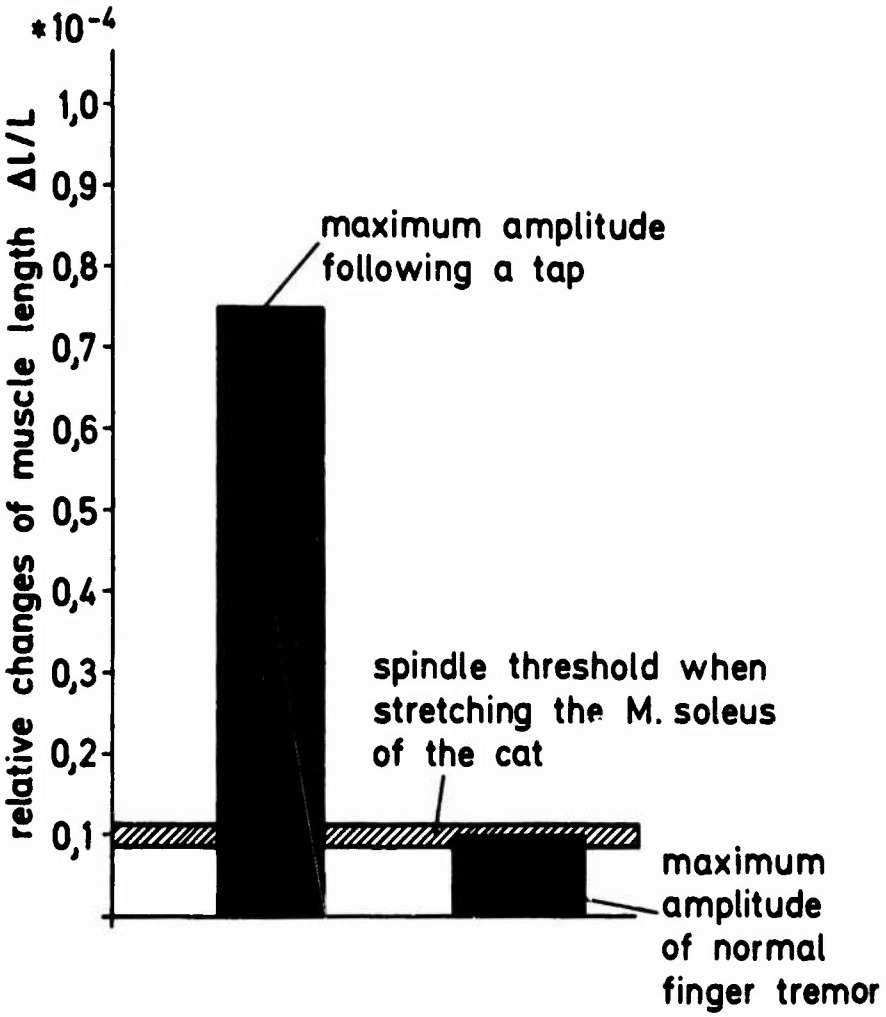

Figure 5 : Estimated changes of relative muscle lengths

Consequently, it should not be expected that in normal finger tremor the frequency is determined by the reflex loop, since it can be considered to be an open-loop circuit This is because feedback is missing due to the receptor being excited only subthreshold. The force driving the finger system is supplied by the resting activity of the muscle. This is in agreement with the observation that EMG activity was constant and showed no pulsations with the same rhythm as occurred in the movements. In the case of a tap to the finger the reflex loop would be closed, since the greater movement amplitudes can cause a spindle excitation. As expected, EMG pulsations with the same rhythm of the finger oscillations are observable, as shown by Lippold's investigations [4, 5]. But the EMG pulsations can not be considered as the cause of these finger movements, they are only a consequence.

C. TREMOR MODELS

In this section an attempt is made to describe models which incorporate all the above mentioned results and which enable one to make predictions with respect to other types of tremor.

Three separate models are illustrated schematically (figure 6). With small modifications these modells can be combined into one. They were simulated on an analog computer.

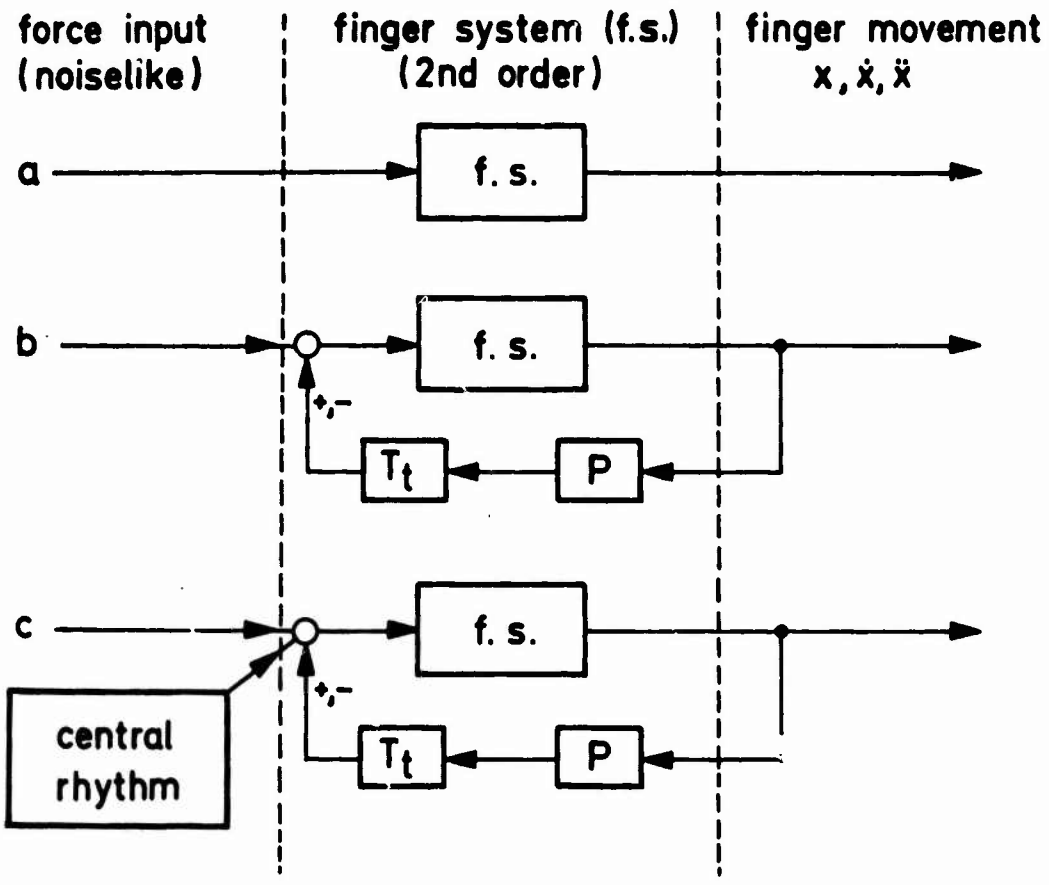

Figure 6 : Models describing 3 different types of tremor : (a) 2nd order filter, (b) Reflex-loop model, (c) Central rhythm model

1. Linear mechanical filter : This model is shown in figure6 a. The shift of the peak frequency (f_o) as illustrated in figure 2a was previously discussed in section B3. Figure 7 shows the spectra of the acceleration, the velocity and the displacement for different values of the mass. These results are similar to those described in figure 2a. Notice that the variations in peak amplitudes are not to be seen in figure 2a because of the normalization to 100 %. However, the tremor amplitudes are worthwhile studying in the future because they can provide indications about increases in input force as well as changes in the mechanical properties of the oscillating system.

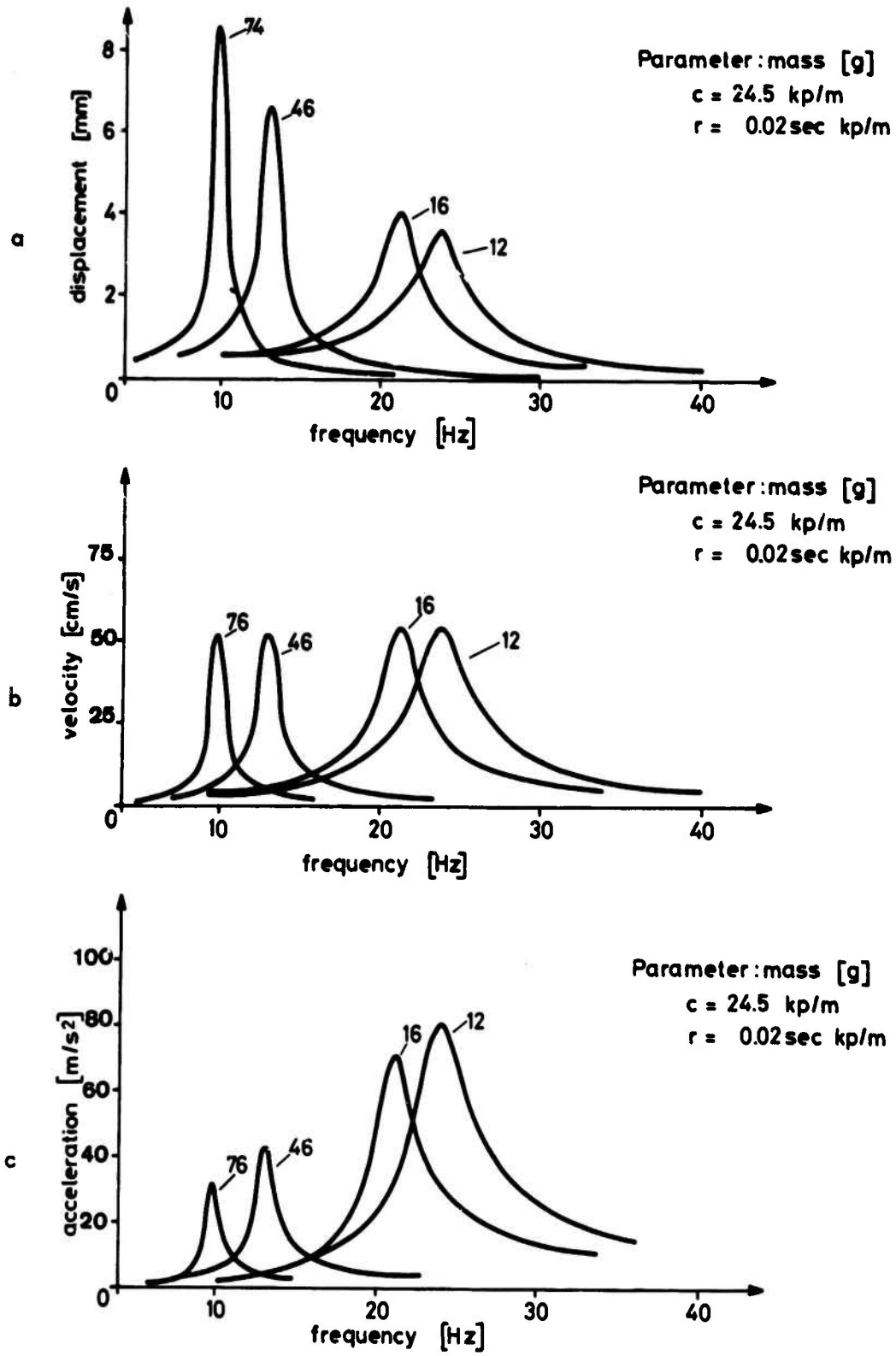

Figure 7 : Resonance curves of a linear 2nd order filter (spring, mass, damping) with the mass as a parameter (a) displacement spectrum (b) velocity spectrum (c) acceleration spectrum

2. Reflex-loop model : The length and the tension of a skeletal muscle is at least partly controlled by the reflex loop of the stretch reflex. As anticipated with greater oscillation amplitudes, the muscle spindles are excited superthreshold, when the loop becomes closed as indicated in figure 6b. From control systems theory it is well known that such a closed loop can have the tendency to oscillate or even to become unstable if a given delay time exists and the loop gain exceeds a limiting value. The finite signal velocity of nerve transmission and the synapse time constants cause a real delay time of the reflex loop of about 30 msec. This estimate is derived from electrophysiological data [18]. At a tremor frequency of 10 Hz [4, 5]the delay time would have to be about 100 msec if the reflex loop were responsible for the oscillations. Subsequently, a simple simulation of the finger system including the reflex loop was tested with the two delay times : 30 msec and 100 msec.

The feedback signal detected by the muscle spindle contains not only information of the displacement but also of the velocity (and possibly also of the acceleration). Thus, a whole set of different cases of positive and negative feedback configurations had to be investigated. Combinations of displacement, velocity or acceleration as feedback signals were not studied. The results of these experiments can be summarized as follows : No stable oscillations occurred without the peak frequency varying with the additional mass. These results contradict the hypothesis that the reflex loop may be the origin of normal tremor oscillations at a uniform frequency of 10 Hz.

An additional property of the reflex-loop model was observed when the oscillation frequency was shifted close to that given by the delay time ; this shift can be accomplished either by changing the mass or the proportional feedback gain. When this was done, the system became unstable and the amplitudes would have increased indefinitely if the amplifiers of the analog computer had no limit. Because of this non-liniarity a further shift in the frequency through an increase in mass was not to be detected, while an increase in the input force amplitude still caused an increase of the movement amplitude. The output signal was still nearly sinussoidal.- Are there similar tremor phenomena to be seen in human limbs ?

3. Experiments on force tremor : To answer that question I made experiments on isometric contraction (flexion and extension) of the hand. The isometric contraction, or rather, static contraction in respect to movement is similar to a contraction for moving an indefinitely large mass. The subject was asked to sustain a moderately large force. Force variations after eliminating the DC level and the EMG activities at the flexor and extensor muscle groups were recorded simultaneously as shown in figure 8.

One can see force oscillations which are of the same frequency as the fluctuations in the EMG envelope at the agonist muscles. At the antagonist muscles only a very low activity is to be detected, it is almost slack. During flexion the result is basically the same as during extension. The oscillation frequency in both situations was about 12 Hz and was seen to be very stable and independent from the sustained contraction force in a wide range. The oscillation amplitudes increased with increasing forces.

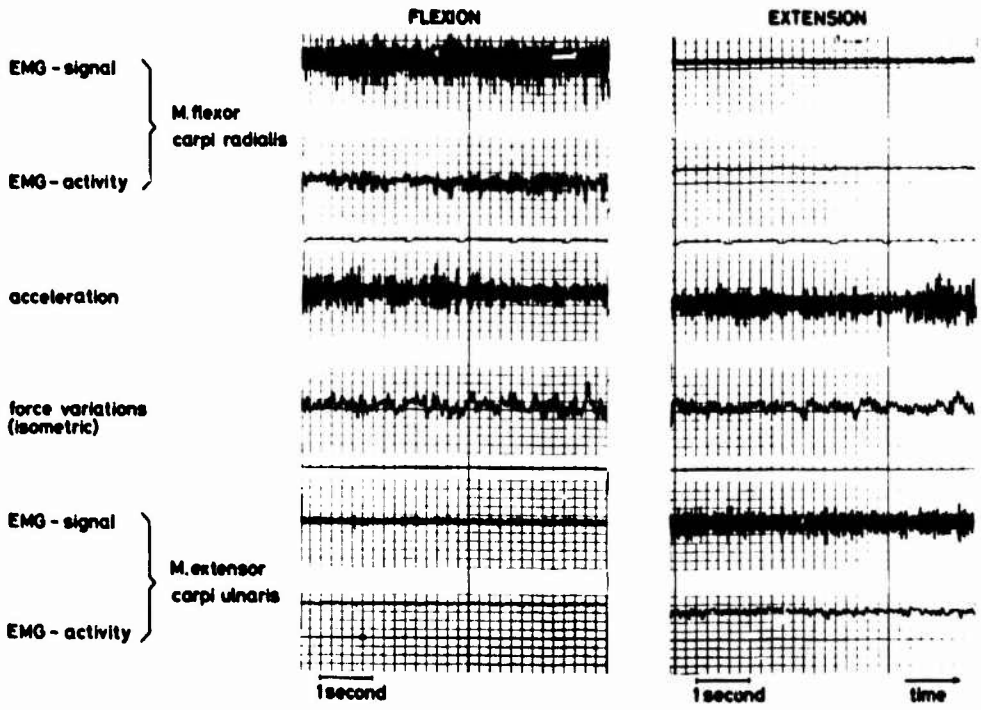

Figure 8 : Record of isometric flexion and extension at the wrist

This type of tremor is different to the type of normal or postural tremor and may be called "force tremor". Here a reflex loop plays a role because the EMG and exerted forces showed oscillations of the same frequency. It can be assumed that the stretch reflex is responsible for this phenomena. The results cannot be due to a reflex system combining the agonist and antagonist muscle groups since the antagonist showed nearly resting activities indicated by the small EMG signal as shown in figure 8. Similar results can be observed when the forearm is loaded by a big mass and the EMG activity of the biceps muscle is compared to accelerations in forearm oscillation movements ; the frequency of this tremor also showed to be about 11 Hz. Additional similar results are reported by Magdaleno et al. [2] for finger oscillations : the frequency of the forefinger was about 12 Hz. Different exerted forces caused changes in amplitude while no marked changes in frequency are to be seen.

4. Central rhythm model : A further type of tremor can be due to rhythmical excitations with its origin in the central nervous system as observed e.g. with Parkinson tremors [19] . Our simulation tests of the model illustrated in figure 6c showed that the oscillation frequency of the finger model is determined by the rhythmical force changes at the input independent of the mass. This is in agreement with measurements on hand tremor of Parkinson patients [20] ; which show that the sharp peak in the

acceleration spectrum coincided with the peak in the EMG spectrum and an extra mass caused only a very small shift of these peaks.

D. CONSEQUENCES AND APPLICATIONS

1. Consequences : The measurements and the model studies give strong evidence for different types of tremors depending on their origins. Distinctions can be made between these types, (a) by changing the mechanical properties of the moving system, and (b) by using the surface EMG as an indication of the muscle activities and thus indirectly of the muscle forces. A prerequesite for a reliable tremor measurement is a well defined positioning of the moving limb. As a future goal, measuring techniques for the quantitative evaluation of amplitudes has to be worked out. A better quantification would also permit detection of the bandwidth of resonance curves. This gives an indication of the mechanical parameters of the moving system such as damping. For each experimental situation it should be determined whether the displacement, the velocity or the acceleration, or even all of them simultaneously, should be recorded [21].

Still an unsolved problem remains with the assumption that stiffness in the mechanical filter model may be constant. It is known [22, 23, 24] that an increase in muscle force also increases the stiffness of the muscle. When the finger was loaded with an extra mass the EMG activity increased. This means an increase in force and, therefore, an increase in stiffness had to be expected. To avoid this problem, Stiles and Randall [8] instructed their subjects to keep the EMG activity constant by providing them with visual feedback while adding different loads. The aim was to keep the stiffness of the muscle independent of the load. In fact, the same relation between frequency and mass as defined by equation (2) was found.

2. Applications : In each design of an arm, hand, or finger control the tremor phenomena have to be taken into consideration, especially when fine control movements have to be performed. For example, a well defined positioning support of the arm and possibly of the hand can prevent the arm and hand tremor movements from disturbing or limiting fine control with a finger stick. Similarly, an isometric control may be used only with small sustained forces. Otherwise no fine control would be possible because of the occurrence of force tremor oscillations.

Before selecting deflection resistance for a control (mass, spring, damping as a function of the displacement) one has to test the behaviour of the whole system including the moved limb. For example, a big mass of the control could shift the resonance peak of the displacement spectrum too much towards lower frequencies ; while an appropriate spring stiffness could cause a desired shift to higher frequencies as can be seen from equation (1).

Evaluation of tremor amplitudes can be utilized in two other fields of ergonomics. (1) As reported in the literature [25] changes in the amplitudes of physiological tremor are correlated with mental laad and drug influences. Therefore, an index of mental work load could be obtained. (2) Tremor is reported to be a very specific feature of different subjects [25]. On the basis of tremor amplitudes it seems possible to select persons who

are especially suited for fine motor performances. However, these applications still have to be preceeded by improvement in the repeatability of results by better methods and techniques in quantitative tremor analysis as a diagnostic tool.

REFERENCES

[1] Schober, H.A.W., and Miller, U.M., "Measurement of Muscle Tremor Associated with Hand-Held Field Glasses", J. Opt. Soc. 55, 1520-1527 (1965).

[2] Allen, R.W., Magdaleno, R.E. and Jex, H.R., "Modeling and Measuring limb fine-motor unsteadiness", 9th Ann. Conf. on Manual Control, MIT, Cambridge (1973).

[3] Sälzer, M., Schreiber, H.J. and Rohmert, W., "Tremor und Arbeitssicherheit - Eine Dokumentation und Systematisierung der Literatur", Bundesanstalt für Arbeitsschutz und Unfallforschung, Dortmund (F.R.Germany), Forschgsber. Nr. 103 (1973).

[4] Lippold, O.C.J., "Oscillation in the stretch reflex arc and the origin of the rhythmical, 8-12 c/s component of physiological tremor", J. Physiol. 206, 359-382 (1970).

[5] Lippold, O.C.J. "Physiological Tremor", Sc. American 224, 65-73 (1971).

[6] Halliday, A.M. and Redfearn, J.W.T., "An analysis of the frequencies of finger tremor in healthy subjects", J. Physiol. 134, 600-611 (1956).

[7] Lippold, O.C.J., Redfearn, J.W.T. and Vučo, J. "The rhythmical activity of groups of motor units in the voluntary contraction of muscle", J. Physiol. 137, 473-487 (1957).

[8] Stiles, R.N. and Randall, J.E. "Mechanical factors in human tremor frequency", J. Appl. Physiol. 23, 324-330 (1967).

[9] Fox, J.R. and Randall, J.E., "Relationship between forearm tremor and the biceps electromyogram", J. Appl. Physiol. 29, 103-108 (1970).

[10] Rau, G. and Vredenbregt, J., "Finger tremor and electromyographic activity", Annual Progr. Rep. 5, 174-178 (1970), Inst. f. Perception Research, Eindhoven.

[11] Rau, G., "Einige Modellüberlegungen zur Natur des normalen Fingertremors", Anthropotechn. Mittlg. 3/73 (1973), Inst. f. Anthropotechnik, Meckenheim.

[12] Bouisset, S., "EMG and Muscle Force in Normal Motor Activities", in : New Developments in Electromyography and Clinical Neurophysiology" (J.E.Desmedt, ed.), Vol. 1, pp. 547-583 (Karger, Basel 1973).

[13] Vredenbregt, J. and Rau, G., "Surface Electromyography in Relation to Force, Muscle Length and Endurance", in : New Developments in Electromyography and Clinical Neurophysiology (J.E. Desmedt, ed.), Vol. 1, pp. 607-622 (Karger, Basel 1973).

[14] Alewijnse, M.A. and Koster, W.G., "Measurement of Tremor", Institute for Perception Research, Eindhoven, Ann. Progr. Rep. 5, 208-214 (1970).

[15] Koster, W.G. and van Schuur, R., "On the origin of physiological tremor", Institute for Perception Research, Eindhoven, Ann. Progr. Rep. 7, 80-87 (1972).

[16] Hamoen, A.M., "Über das Wesen des physiologischen Tremors der Hand", Psychiat. Neurol. Neurochir. 65, 109-116 (1962).

[17] Mathews P.B.C., "Mammalian muscle receptors and their central actions", Edw: Arnold (Publ.) Ltd., London 1972.

[18] Clarke, A.M., Michie, P.T. and Glue, L.C.T., "Human phasic reflex to parameters of a mechanical stimulus : an index of muscle-spindle sensitivity", Med. and Biol. Engng. 11, 597-602 (1973).

[19] Pallock, L.J. and Davis, L. "Muscle tone in parkinsonian states", Archs. Neurol. Psychiat. (Chicago), 23, 303-319 (1930).

[20] Koster, W.G. and van Schuur, R., "A note on parkinsonian tremor", Inst. f. Percept. Res., Eindhoven, Ann. Progr. Rep. 7, 88-91 (1972).

[21] Sälzer, M., "Methodenvergleich verschiedener Tremoraufnehmer", Int. z. angew. Physiol. 30, 292-301 (1972).

[22] Wilkie, D.R., "The mechanical properties of muscle", Brit. Med. Bull. 12, 177-182 (1956).

[23] Granit, R., "Neuromuscular interaction in the postural tone of the cat's isometric soleus muscle", J. Physiol. 143, 387-402 (1958).

[24] Vredenbregt, J. and Koster, W.G., "A method for measuring the passive force-length relationship of the human biceps muscle in vivo", Inst. f. Percept. Res., Eindhoven, Internal Report 83 (1966).

[25] Sälzer, M., "Untersuchung über die Reproduzierbarkeit von Hand-Tremormessungen", Europ. J. Appl. Physiol. 32, 71-80 (1973).

74-28,209 #4

DETERMINATION OF IN-FLIGHT PILOT PARAMETERS USING A NEWTON-RAPHSON MINIMIZATION TECHNIQUE

Daniel L. Kugel
AF Flight Dynamics Laboratory, Wright-Patterson AFB, Ohio

Abstract — This paper describes the application of a modified Newton-Raphson parameter identification program to a post-simulation analysis of a large delta-wing aircraft similar to a Concorde supersonic transport. Pilot parameters are determined by minimizing the weighted mean square difference between the computed model responses and the measured responses of the total pilot-vehicle system. Pilot remnant is calculated using a power spectral density approach. These results are compared to presimulation analysis results obtained using an automated digital scheme and to those which were measured by an on-board analog computer. This study illustrates the utility of modern parameter identification techniques to post-simulation analysis.

I. Introduction

The mathematical modeling of pilot response in a particular task is of continuing interest in the fields of aircraft development and handling qualities evaluation. A model which can accurately represent a pilot's response is of great benefit and can be used to predict pilot rating and aircraft performance. A modeling effort such as this was applied to a recent study using the Total In-Flight Simulator (TIFS) to investigate the landing approach handling qualities of a large delta-wing aircraft. [1].

The TIFS is a variable stability research aircraft which permits the duplication of motion effects in the cockpit, as well as visual and instrument cues. Crosswinds and turbulence can be introduced electronically into the evaluation task. These signals are recorded to provide deterministic environmental disturbances which can be used later in the analysis program. All aircraft states and pilot response data are also recorded on a digital tape.

Prior to conducting this experiment a presimulation analysis of handling qualities was performed using Pitch Paper Pilot [2]. This analysis provided the predicted parameters of a pilot model for pitch control [3]. During the flight, an analog computer known as a Describing Function Analyzer (DFA) was used to measure the Bode response, (amplitude and phase) of the human operator at each frequency component of the input forcing function. The predicted and measured pilot parameters were then computed. The recorded data for the in-flight simulation provided a data base from which a technique could be developed to extract pilot model parameters from flight test data records by application of parameter identification techniques.

This paper will describe the models of the aircraft, the flight control system, and the pilot used in the post-simulation analysis. A description of the modified Newton-Raphson parameter identification routine used to extract the pilot parameters will also be discussed. The results will then be presented and compared with the results using the Describing Function Analyzer and Pitch Paper Pilot.

II. System and Disturbance Models

The total pilot-vehicle system for the approach and landing task of a large delta-wing aircraft can be represented by Figure 1.

Aircraft Dynamics

The longitudinal dynamics of the supersonic transport were programmed on the TIFS simulator using linearized, three-degree-of-freedom, small perturbation equations of motion. For parameter identification purposes the longitudinal responses were simplified by using a short period approximation to help limit the size of the overall model. This was a fairly good approximation since only a small section of data was being analyzed at any one time (40 seconds) and since approach speed was held relatively constant.

The aircraft short period linear equations used in this analysis were of the form

$$\dot{x} = Ax + Bd$$

For the short period approximation

$$x = [\theta, \alpha, q]^T$$

where

θ pitch angle (rad)

α angle of attack (rad)

q pitch rate (red/sec)

The aircraft can be represented by the following first order linear differential equations:

$$\dot{\theta} = q$$

$$\dot{q} = (M_q + M_{\dot{\alpha}})q + (M_{\dot{\alpha}}Z_\alpha + M_\alpha)\alpha + (M_{\dot{\alpha}}Z_{\delta_e} + M_{\delta_e})\delta_e + (M_{\dot{\alpha}}Z_\alpha + M_\alpha)\alpha_{gust}$$

$$\dot{\alpha} = q + Z_\alpha\alpha + Z_{\delta_e}\delta_e + Z_\alpha\alpha_{gust}$$

From the above equation it can be seen that

$$B = [0, (M_{\dot{\alpha}}Z_\alpha + M_\alpha), Z_\alpha]^T$$

and

$$d = \text{disturbance vector} = \alpha_{gust}$$

The disturbance used was a sum of five sinusoids whose frequency content was equally spaced when plotted on a logarithmic axis [4]. The power

distribution resembled that of a Dryden spectra for an angle of attack gust, α_{gust}, of 1.272 degrees, whose associated vertical gust, Wg, was 6.0 ft/sec. The disturbance had the form

$$\alpha_{gust}(\omega) = \sum_{n=0}^{4} A_n \sin \omega_n t$$

Figure 2 shows the power distribution of this disturbance [5].

Control - Feel System

The control system for this analysis duplicated that programmed on the TIFS [1]. Coupled with the control system was a second order feel system which provided control feel to the wheel and rudder pedals. The total control-feel system can be modeled by a fourth order linear differential equation. This system is shown in Figure 3. Combining these two second order systems produces the following transfer function:

$$\frac{\delta_a}{\delta_p} = \frac{a_4}{s^4 + a_1 s^3 + a_2 s^2 + a_3 s + a_4}$$

Using three dummy states, this equation can be transferred into four first order linear differential equations of the form

$$\dot{x} = Ax$$

These equations are

$$\dot{\delta}_e = \delta_{e_2}$$

$$\dot{\delta}_{e_2} = \delta_{e_3}$$

$$\dot{\delta}_{a_3} = \delta_{e_4}$$

$$\dot{\delta}_{a_4} = -a_4\delta_e - a_3\delta_{e_2} - a_2\delta_{e_3} - a_1\delta_{e_4} + a_4\delta_p$$

Human Operator

The model chosen for the human operator is a quasi-linear pilot describing function of the form

$$Y_p(s) = K_p e^{-\tau s}(T_L s + 1)\frac{K_n}{(T_L s + 1)\left[\frac{s^2}{\omega_n^2} + \frac{2\xi_n s}{\omega_n} + 1\right]}$$

[6], [7] and [8],

where the remnant term is defined to be that portion of the actual pilot's response not accounted for by the linear model.

The linear describing function, $Y_p(s)$, can be written in form

$$\dot{x} = Ax$$

by representing the pure time delay by a first order Padé approximation. The block diagram of Figure 4 represents the human operator model. Using the Padé approximation

$$e^{-\tau s} = \frac{-(s - 2/\tau)}{(s + 2/\tau)}$$

and

$$K = K_p K_n$$

then the human operator can be represented by four first order linear differential equations

$$\dot{y}_1 = \frac{1}{T_I}\theta + \frac{T_L}{T_I}q - \frac{1}{T_I}y_1$$

$$\dot{y}_2 = K\omega_n^2 y_1 - 2\xi_n\omega_n y_2 - \omega_n^2\delta'$$

$$\dot{y}_3 = (-2/\tau)y_3 + (4/\tau)\delta'$$

$$\dot{\delta}' = y_2$$

Total Pitch Tracking Model

The total pitch tracking model can be represented in the state vector form by

$$\dot{x} = Ax + Bd$$

where

$$x = (\theta, \alpha, q, \delta_a, \delta_{e_2}, \delta_{a_3}, \delta_{e_4}, y_1, y_2, y_3, \delta')^T$$

and A is a partitioned matrix of the form given in Figure 5. The vectors B and d are the same as before.

III. Newton-Raphson Minimization

A linear system can be represented by

$$\dot{x} = Ax + Bd$$

and a set of output expressions

$$y = Fx + Gu + b$$

and

$$z = y + n$$

In the above equations

x	state vector
y	calculated response vector
z	measured response vector
d	disturbance vector
b	constant bias vector
n	noise vector
A	airframe/gust correlation vector
F	state transition matrix
G	gust transition vector

A cost function which is proportional to the mean square error can be represented by

$$J = \sum_{i=1}^{NM} (z_i - y_i)^T D_1 (z_i - y_i)$$

where NM is the number of samples and D_1 is a weighting matrix for the difference in response [9]. This weighing matrix should equal the inverse of the appropriate error covariance matrix [10].

Because the aircraft, feel system, and control system dynamics are known quantities (programmed on the TIFS simulator [1], only the parameters of the human operator are identified. These pilot parameters make up an unknown parameter vector, c, which relates to the system states and system responses as

$$\dot{x}(t) = f[x(t), c, u(t)]$$
$$y(t) = g[x(t), c] + \eta$$

For this experiment

$$c = [1/T_I, T_L/T_I, -\omega_n^2, K_p\omega_n^2, 2\xi_n\omega_n, 2/\tau]^T$$

The estimate for these parameters can ba found by

$$\hat{c} = \text{ARG MIN } (J)$$

where ARG MIN means the vector c which minimizes the cost function J.

The calculated response vector y can bs linearised with respect to the unknown parameter vector c such that

$$y_i = y_{i_o} + \nabla_c y_i \, (c - c_o)$$

where

y_{i_o}	nominal response calculated by using c_o
$\nabla_c y_i$	gradient of y with respect to c
c_o	nominal c vector

The optimal estimate for the unknown parameter vector is the vector c which minimizes J, and hence the mean square response error. This estimate can be found by applying the following equation iteratively to update the calculated nominal response and its gradient with respect to the vector of unknown parameters.

$$\hat{c} = c_o + \left[\sum_{i=1}^{NM} (\nabla_c y_i)^T D_1 (\nabla_c y_i)\right]^{-1} \left[\sum_{i=1}^{NM} (\nabla_c y_i)^T D_1 (z_i - y_{i_o})\right]$$

A priori estimates of the unknown parameters can be incorporated into the cost function using probability theory [9], [10]. This is done by maximizing the unconditional probability of z. The optimum parameter vector, $\hat{c}$, will result if a cost function containing the sum of the mean square response error and the mean square difference of c and its a priori value is minimized.

$$c = \underset{c}{\text{ARG MIN}} \sum_{i=1}^{NM} (z_i - y_i)^T M_1^{-1} (z_i - y_i) + (c - c_o)^T M_2^{-1} (c - c_o)$$

where

η	noise vector
c_o	nominal parameter vector
M_1	$E\{\eta\eta^T\}$
M_2	$E\{(c - c_o)(c - c_o)^T\}$

where E is the expectation operator. This occurs provided the weighting matrices used are equal to the appropriate inverse error covariance matrices. (The abova information taken from [9]).

IV. Program Operation

The analysis using the Newton-Raphson method [9] was conducted on a Control Data Cyber-74 computer. The program takes 56,000 words of central memory to compile and execute. For a data record length containing 400 data points of 11 state variables, the program takes approximately 350 seconds of central processor time and 25 seconds of peripheral processor time. The program has the capability of printing out the values of the gradient and RMS error of each state and the value of the cost function at each iteration. After convergence, the program prints out the final A, B, F, and G matrices, and the bias vector b. Also printed out are the pilot parameters, an error covariance matrix of the estimated results and their approximate standard deviation. After convergence is reached, new time histories, using the estimated matrices, are calculated.

V. Results

Predictions (Paper Pilot)

Tha results of the presimulation analysis using Paper Pilot [11], with a pure time delay of $\tau = 0.2$ seconds and a first order neuromuscular lag of $T_I = 0.1$ second, predicted a pilot lead of $T_L = 3.89$ seconds and a pilot gain of $K_p = 0.691$. These parameters were obtained by optimizing the pilot parameters to minimize a cost functional based on the root mean square tracking error and the pilot lead [2].

Frequency Techniques (DFA)

During the flight test of the TIFS simulator, the DFA calculated, on-line, the finite Fourier transform of the various system signals. The real and imaginary parts of the Fourier transform were then used in simple off-line calculations to yield system response and performance data. The resulting describing function measurements can be seen in Table 1.

Newton-Raphson Method

Using the aircraft and pilot response data, which were recorded during the experiment, the Newton-Raphson minimization routine was used to extract pilot parameters based on the theory previously discussed.

During the digitization of this data, a 3-second section of data was improperly digitized midway through the run. As a result, the 100 seconds of data was divided into a two 40 second data records and each processed separately. During the identification analysis, the natural frequency and damping of the second order neuromuscular dynamics were set at ω_n = 16.5 radians/sec and ξ_n = 0.12 [6].

The identified pilot parameters in Table 2 were obtained using the Newton-Raphson technique.

It should be noted that this method can yield biased estimates if the mean of the distribution of θ is non-zero. This bias can be reduced by using the longest data records possible. The Newton-Raphson program also has the capability of estimating the bias terms of each of the states.

The above describing functions have been plotted in Bode form for comparison purposes. These plots appear in Figure 6.

Remnant

A determination of remnant was made by calculating the power spectral density [12] of the difference signal formed by subtracting the pilot output of the model from the actual recorded pilot command to the elevator. Figure 7 shows the power spectral density plots of the recorded elevator command of the pilot, the modeled elevator command, and the calculated remnant.

As can be seen from a close examination of the power spectral density functions of the pilot model, the model produces an output which has power at each of the five input frequencies. The spectral density functions of the actual recorded pilot output, however, has power at frequencies other than those of the input. These extraneous powers are defined as remnant powers. The small spikes in the power spectral density plots could result from nonlinear or nonstationary operation of the pilot or from the fact that the approach and landing tasks required the control of some side tasks and as a result was not truly a single loop compensatory task. The large spike in each of the remnant plots is attributed to "pilot pumping". Pumping is performed by the pilot to obtain dynamic information about the aircraft as it enters ground effects. The pumping frequency observed from in-flight records was always greater than 1.0 radians/sec. This oscillatory input to the elevator would show up as a pilot generated input and could therefore not be accounted for by the linear describing function. Making a sinusoidal approximation to the pilot pumping the remnant term will appear relatively flat and look more like a typical remnant spectra.

VI. Development Status

To date, the Newton-Raphson method as applied to pilot modeling has only been used with the longitudinal dynamics of a large transport aircraft simulation. By including the lateral directional dynamics and a roll pilot model, a two axis tracking situation could be made. Also, an analytical expression for pilot rating, such as is used in Paper Pilot [3], or in the Naal-Smith method [14], could be incorporated to give not only identified pilot parameters, but also to relate these parameters to a useful handling qualities criterion.

Finally, the Newton-Raphson method could be used in manual control situations for other than aircraft situations, such as automobile control in response to highway gusts [15], or the behavior of a helmsman steering a ship [16].

Further use and refinement of this technique could provide a valuable tool in the area of handling qualities and human operator modeling.

BIBLIOGRAPHY

[1]. Wassarman, Richard, et al, "In-Flight Simulation of Minimum Longitudinal Stability for Large Delta-Wing Transports in Landing Approach and Touchdown", Vol I and II, AFFDL-TR-72-143, Wright-Patterson AFB, Ohio, February 1973.

[2]. Andarson, R. O., Connors, Alonzo J., and Dillow, James D., "Paper Pilot Ponders Pitch", AFFDL/FGC-TM-70-1, Wright-Patterson AFB, Ohio, Novembar 1970.

[3]. Stone, John R., "Pradiction and Measurament of an In-Flight Pilot Modal for Supersonic Transport", AFFDL/FGD-TM-74-22, Wright-Patterson AFB, Ohio, January 1974.

[4]. Patera, R. A. and Allen, R. W., "Oparational Manual for Deacribing Function Analyzer", W-P-406-2, Systems Tachnology, Inc., Hawthorna, California, 1970.

[5]. Taper, Gary L., "An Assessment of the 'Paper Pilot' - An Analytical Approach to the Specification and Evaluation of Flying Qualities", AFFDL-TR-71-174, Wright-Pattarson AFB, Ohio, Juna 1972.

[6]. McRuer, Duane and Krendal, Ezra, "Human Pilot Dynamics in Compensatory Syatams", AFFDL-TR-65-15, Wright-Patterson AFB, Ohio, July 1965.

[7]. McRuar, Duane T., et al, "New Approaches to Human-Pilot/Vahicle Dynamics Analysis, AFFDL-TR-67-150. Wright-Patterson AFB, Ohio, February 1968.

[8]. Bekay, George A., "An Investigation of Samplad-Data Models of the Human Oparator in a Control System", ASD-TR-62-36, Wright-Patterson AFB, Ohio, May 1962.

[9]. Taylor, Lawrenca W., et al, "Systems Idantification Using a Modifiad Newton-Raphson Mathod - A Fortran Program", NASA-TN-D-6734, Langley Research Cantar, May 1972.

[10]. Iliff, Kenneth W. and Taylor, Lawranca W., Jr., "Determination of Stability Derivatives from Flight Data Using a Newton-Raphson Minimization Tachnique", NASA-TN-D-6579, Langlay Research Center, May 1972.

[11]. Stone, John R., "Papar Pilot Ponders Suparsonic Transports", Ninth Annual Conferanca on Manual Control, Seasion II, Massachusetts Instituta of Technology, May 1973.

[12]. Ralston, Anthony and Wilf, Herbert S., Mathematical Method for Digital Computars, Chaptar 19, John Wiley and Sons, Inc., New York, 1960.

[13]. Anderson, Ronald O., "A New Approach to the Specification and Evaluation of Flying Qualities", AFFDL-TR-69-12C, Wright-Pattarson AFB, Ohio, June 1970.

[14]. Mayhew, David R., "A Digital Computer Program for the Calculation of Parametars Necessary to Satisfy tha Closed Loop Criteria of T. P. Neal", AFFDL/FGC-TM-73-110, Wright-Patterson AFB, Ohio, August 1973.

[15]. Weir, D. H. and Hoh, R. H., "Driver/Vehicle Responsa and Performance in tha Presence of Aerodynamic Disturbancas", Fourteenth Joint Annual Control Conference, Ohio State University, June 1973.

[16]. Valdhuyzen, W., and Stassen, H. G., "Modelling the Behavior of the Helsman Staering a Ship", Ninth Annual Conferanca on Manual Control, Session VIII, Massachusetts Institute of Technology, May 1973.

PITCH TRACKING MODEL

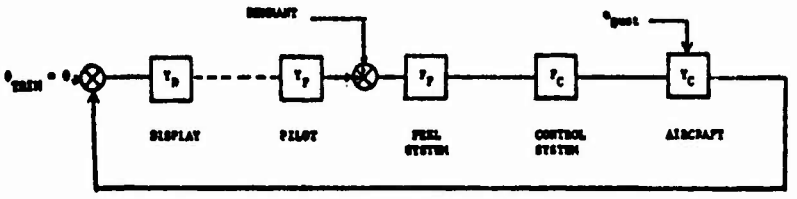

FIGURE 1

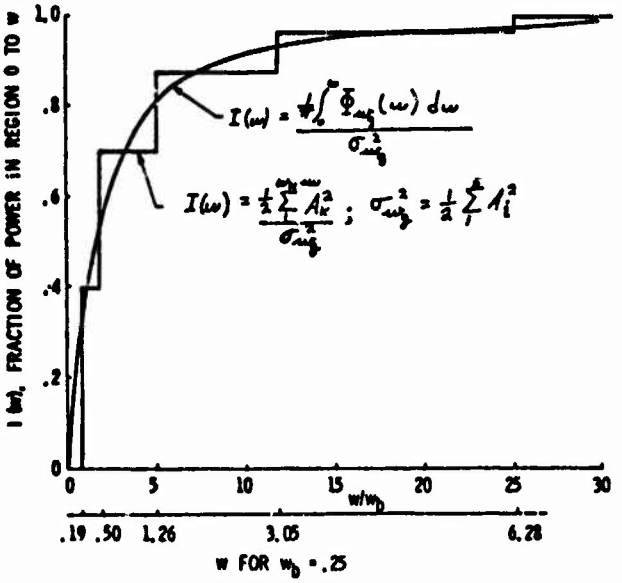

FIGURE 2

CONTROL AND FEEL SYSTEM

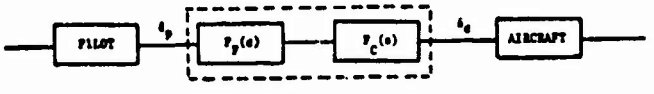

FIGURE 3

HUMAN OPERATOR MODEL

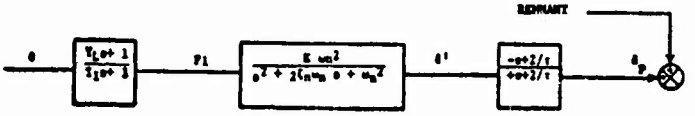

FIGURE 4

TOTAL PITCH TRACKING MODEL

$$A = \begin{array}{|c|c|c|} \hline \text{AIRCRAFT DYNAMICS} & 0 & 0 \\ \hline 0 & \text{CONTROL AND FEEL SYSTEM} & 0 \\ \hline \text{EQUALIZATION COEFFICIENTS } T_L, T_I & 0 & \text{HUMAN OPERATOR } K_p, \tau, \omega_k, \zeta_n \\ \hline \end{array}$$

FIGURE 5

ω (rad/sec)	0.18	0.50	1.25	3.01	6.28
AMPLITUDE(dB)	-1.7	3.3	12.9	21.4	25.8
PHASE(deg)	-86.5	-150.4	-194.0	-168.6	-225.6

TABLE 1

	K_p	T_L	T_I	τ
RUN 1 T = 1 - 41 sec	0.702	1.605	0.102	0.333
RUN 2 T = 63 - 103 sec	0.475	2.528	0.104	0.336

TABLE 2

IN-FLIGHT PILOT MODEL PREDICTIONS AND MEASUREMENTS FOR AN SST IN POWER APPROACH

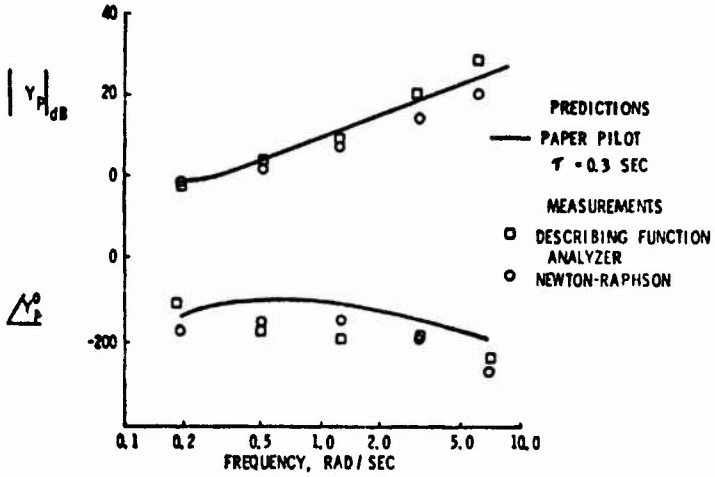

FIGURE 6

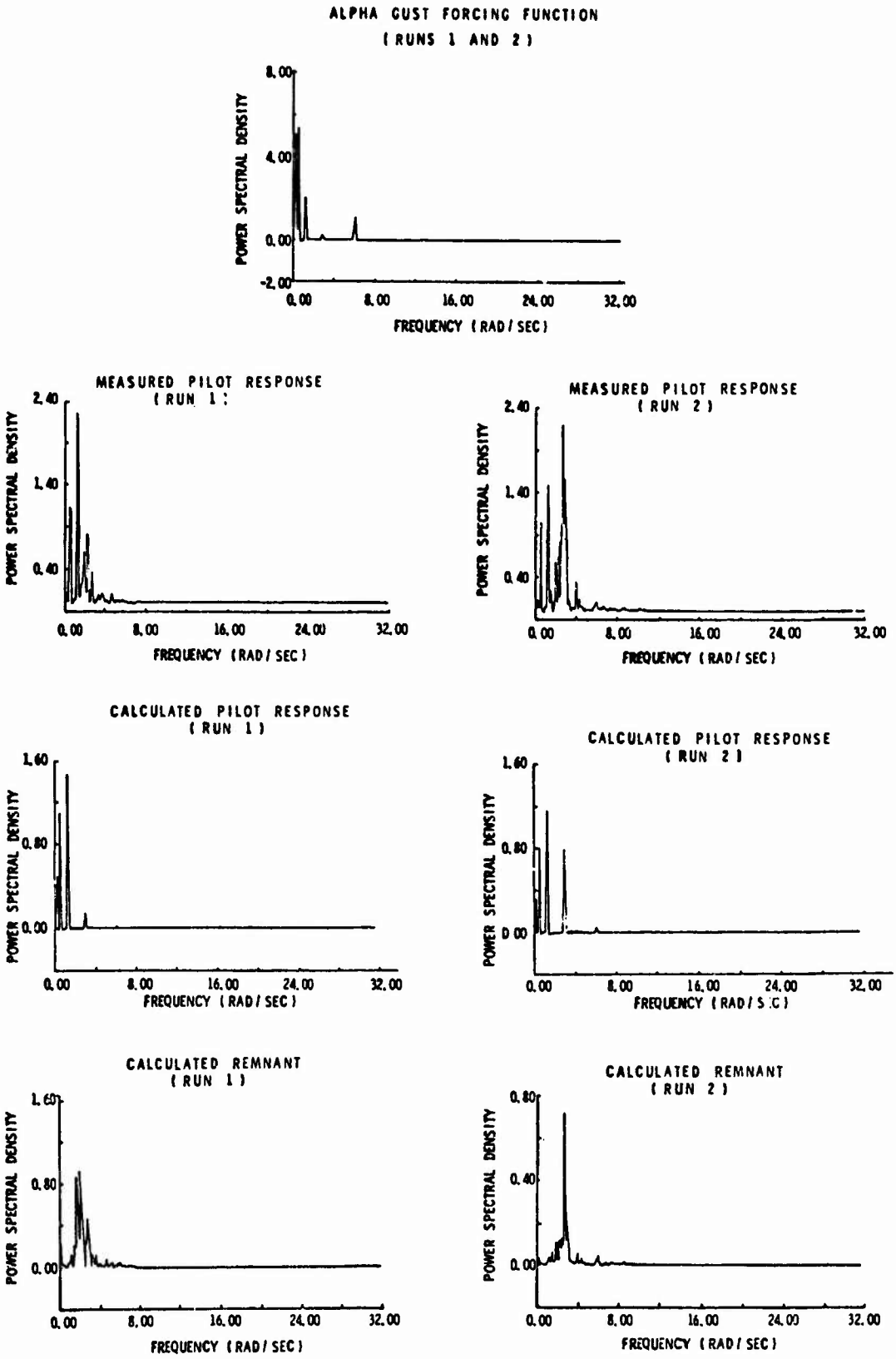
ALPHA GUST FORCING FUNCTION
(RUNS 1 AND 2)
POWER SPECTRAL DENSITY
8.00
4.00
0.00
-2.00
0.00
8.00
16.00
24.00
32.00
FREQUENCY (RAD / SEC)
MEASURED PILOT RESPONSE
(RUN 1)
POWER SPECTRAL DENSITY
2.40
1.40
0.40
0.00
8.00
16.00
24.00
32.00
FREQUENCY (RAD / SEC)
MEASURED PILOT RESPONSE
(RUN 2)
POWER SPECTRAL DENSITY
2.40
1.40
0.40
0.00
8.00
16.00
24.00
32.00
FREQUENCY (RAD / SEC)
CALCULATED PILOT RESPONSE
(RUN 1)
POWER SPECTRAL DENSITY
1.60
0.80
0.00
0.00
8.00
16.00
24.00
32.00
FREQUENCY (RAD / SEC)
CALCULATED PILOT RESPONSE
(RUN 2)
POWER SPECTRAL DENSITY
1.60
0.80
0.00
0.00
8.00
16.00
24.00
32.00
FREQUENCY (RAD / SEC)
CALCULATED REMNANT
(RUN 1)
POWER SPECTRAL DENSITY
1.60
0.80
0.00
0.00
8.00
16.00
24.00
32.00
FREQUENCY (RAD / SEC)
CALCULATED REMNANT
(RUN 2)
POWER SPECTRAL DENSITY
0.80
0.40
0.00
0.00
8.00
16.00
24.00
32.00
FREQUENCY (RAD / SEC)

FIGURE 7

MEASUREMENT OF MUSCLE STIFFNESS DURING A TWITCH CONTRACTION

Gerald L. Gottlieb and Gyan C. Agarwal
Department of Biomedical Engineering
Presbyterian - St. Luke's Hospital
and
College of Engineering
University of Illinois at Chicago Circle

This work was supported in part by the
National Science Foundation

Tenth Annual Conference on Manual Control
April 9-11, 1974
Wright Patterson Air Force Base
Dayton, Ohio

INTRODUCTION

There are a variety of approaches to describing the human motor control system. One is to describe its individual components; sensors, controllers and and effectors, in order to assemble them into a realistic model. In this paper we shall consider the effector organ, skeletal muscle, and one series of experiments for identifying and measuring muscle's parameters.

For purposes of exposition, it is helpful to consider a simple visco-elastic model of muscle illustrated in Figure 1[1,2]. Such a model makes two points. In response to deforming mechanical forces, muscle acts like a visco-elastic structure, albeit a more complex one, and muscle is also a force generator which is filtered by its own internal visco-elasticity.

One of the major advances in muscle physiology was the recognition that any force measured externally from a muscle's attachments, except perhaps during fused tetany, is not the force actively generated by that muscle's intrinsic contractile mechanism[1]. The difference between those two forces arises as a direct consequence of the mechanical filtering[3]. One goal of research into muscle mechanisms has been to deduce the character of this internal force. Figure 2 diagramatically shows that force as well as the externally measured force when muscle is stimulated to a single twitch contraction[4].

Part of the difficulty in studying this intrinsic force (which of course cannot be directly measured) is that the properties of the mechanical filter are not accurately known. However, it is well established that the visco-elastic properties of muscle are not invariant, but are in fact a function of the same mechanisms which generate and control active contraction. A muscle which is contracting is much stiffer than one which is relaxed[2,5].

Knowledge of how the muscle visco-elasticity varies with contraction is presently limited to steady state conditions. During tonic contraction, both

the elastic and the viscous stiffness are proportional to the degree of contraction[5]. This study is an attempt to investigate the state of muscle viscoelasticity during a transient muscle contraction.

METHODS

The subjects (3 normal adult males) were seated with their right foot strapped to a rigid device which prevented movement of the foot and also measured torque about the ankle joint.

The transient contraction was produced by an electrical shock of 1.5 msec duration delivered percutaneously to the posterior tibial nerve and causing a twitch contraction of the triceps surae.

Muscle stiffness was measured by delivering a tap to the achilles tendon. The force measured in the hammer head and its displacement were assumed to be directly proportional to the stretching force and to the degree of stretch imposed upon the muscle.

Fifty-five twitches were elicited, about six seconds apart. Once during each twitch a tap would be delivered to the tendon and the hammer force and displacement recorded for 50 msec. The first five taps were delivered prior to the twitch and the last 50 at increasing intervals after the start of the twitch. Figure 3 shows the 55 records of hammer force and displacement for one such experiment.

The computation of stiffness was made by taking the difference in hammer force at 75% and 25% of its peak and dividing it by the difference in hammer displacement at corresponding instants in time. These instants were determined on the first hammer blow and used for the succeeding fifty-four. This gave the ratio of force change to length change over an interval of from 6 to 10 msec. The tic marks on each trace of Figure 3 indicate the points actually used for the computation.

RESULTS

Figure 4 shows the change in relative stiffness over a 400 msec interval. On the same time scale, the muscle twitch is also shown. All the data is normalized to fill the range of the graph. The peak stiffness represents an approximate doubling of the base line level. Figure 5 shows another experiment in which the subject attempted to maintain a constant level of muscle contraction during the stimuli.

DISCUSSION

The data of Figure 4 show that muscle stiffness, as we have defined and measured it, varies along a time course that is similar to, but slightly faster than the muscle twitch. The resemblance between the shape of the stiffness curve in Figure 4 and the intrinsic tension curve in Figure 2 is most striking.

The stiffness in Figure 5 also varies as we would expect if it were produced by the same mechanism responsible for active contraction. In that experiment the muscle was initially contracted. Under such conditions, a twitch produces a brief period, the so-called silent period, in which muscle activity is reduced by means of reflex mechanisms. In such a case we expect that the contractile process shuts off briefly even though the external tension remains above the initial level. The increase in stiffness near the end of contraction is due to reactivation of the muscle.

Although such data are promising, a number of cautionary remarks about its interpretation should be made. An obvious, but not very troublesome shortcoming is that our computation of stiffness does not distinguish between viscous and elastic components (and in more realistic models than Figure 1 there may be several of each). This does not invalidate the qualitative implications of the data. For more quantitative information, a more complex approach (such as finding the best solution to a differential equation) is needed. For a preliminary investigation

however, it was felt that sophisticated mathematical techniques were premature.

A more basic problem is that our measure for stiffness is only valid under the assumption that the active force does not change significantly during the interval over which the measurement for stiffness is made. That this assumption is very much open to question can be deduced from Figure 2, especially during the initial rising phase of the active state.

The third problem is in relating variables measured at the hammer to actual changes in muscle length and tension. We have assumed a linear relation over the operating range in these experiments.

It is worth noting however that this very simple and innocuous experiment shows promise of permitting the study of aspects of muscle contraction for which there are currently no alternative techniques.

REFERENCES

1. A.V. Hill, "The heat of shortening and the dynamic constants of muscle", Proc. Royal Society, Series B, Vol. 126, pp. 136-195, 1938.

2. D.R. Wilkie, "The relation between force and velocity in human muscle", J. Physiology, Vol. 110, pp. 249-280, 1950.

3. A.S. Bahler, J.T. Fales and K.L. Zierler, "The active state of mammalian skeletal muscle", J. General Physiology, Vol. 50, pp. 2239-2253, 1967.

4. L. Macpherson and D.R. Wilkie, "The duration of the active state in a muscle twitch", J. Physiology, Vol. 124, pp. 292-299, 1954.

5. G.C. Agarwal, B.M. Berman and L. Stark, "Studies in postural control systems. Part I: Torque Disturbance Input", IEEE Trans. on Systems Science and Cybernetics, Vol. 6, pp. 116-121, 1970.

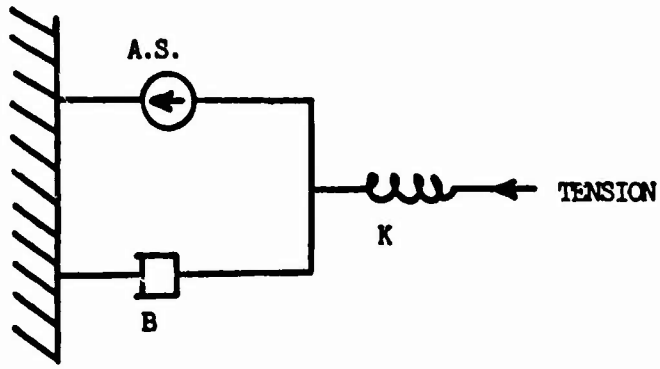

Figure 1. A model for active muscle where the parallel elastic element has been neglected. The contractile element consists of a force generator (A.S.) in parallel with viscous damping (B).

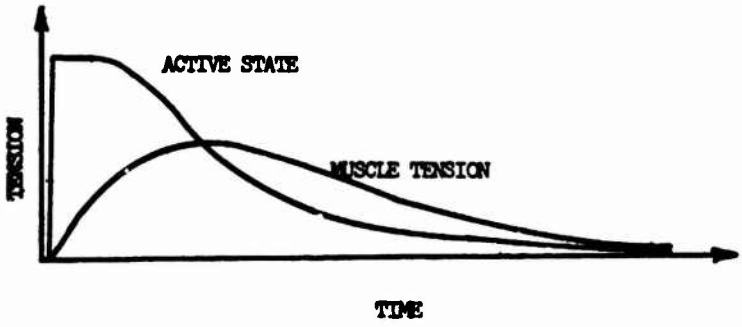

Figure 2. A facsimile for the active state (intrinsic tension) and isometric tension of an isolated frog sartorius muscle responding to an electrical stimulus (From (4)).

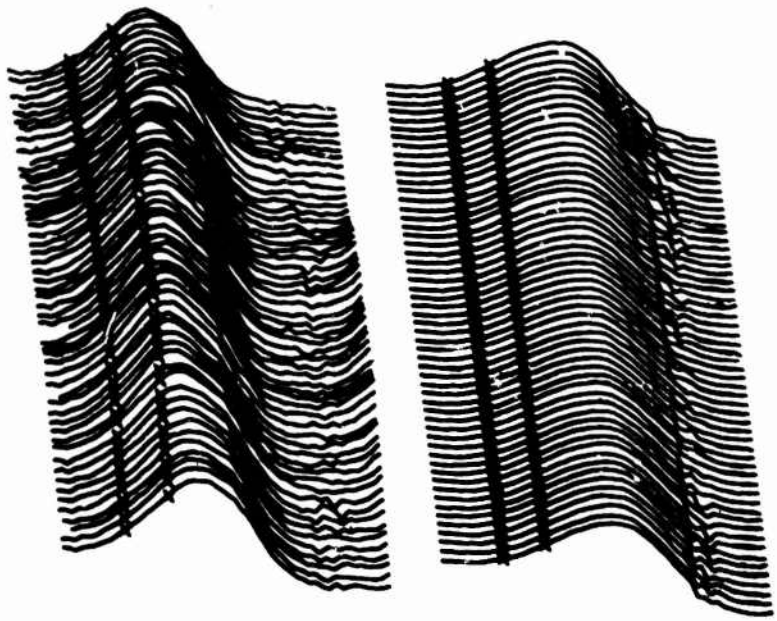

Figure 3. Records of hammer force (left) and hammer displacement (right) for one experiment. The length of each record is 50 msecs. The tic marks at 10 and 16 msecs indicate values used to compute stiffness in Figure 4.

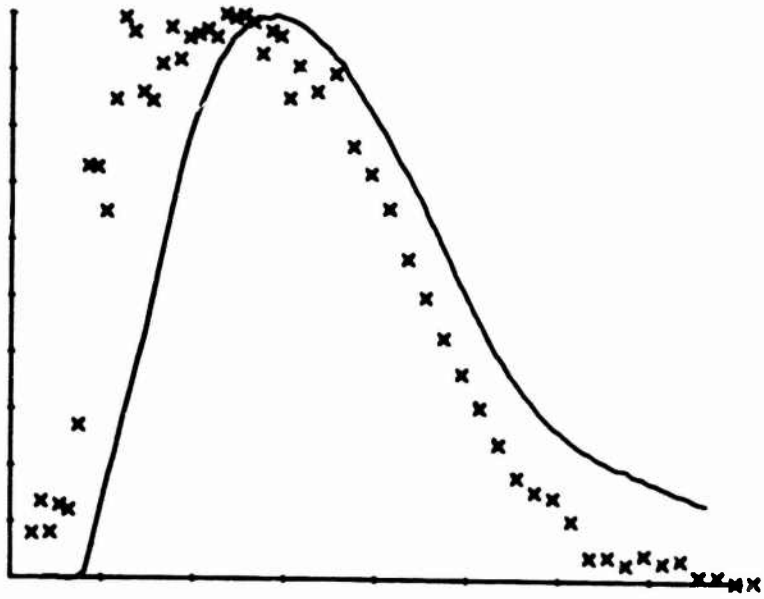

Figure 4. Variation in stiffness (x marks) during a twitch contraction (continuous line) with triceps surae muscle relaxed before the electrical input. The abscissa is time from 0 to 400 msec. The ordinates are uncalibrated. The relative change in stiffness is a factor of two.

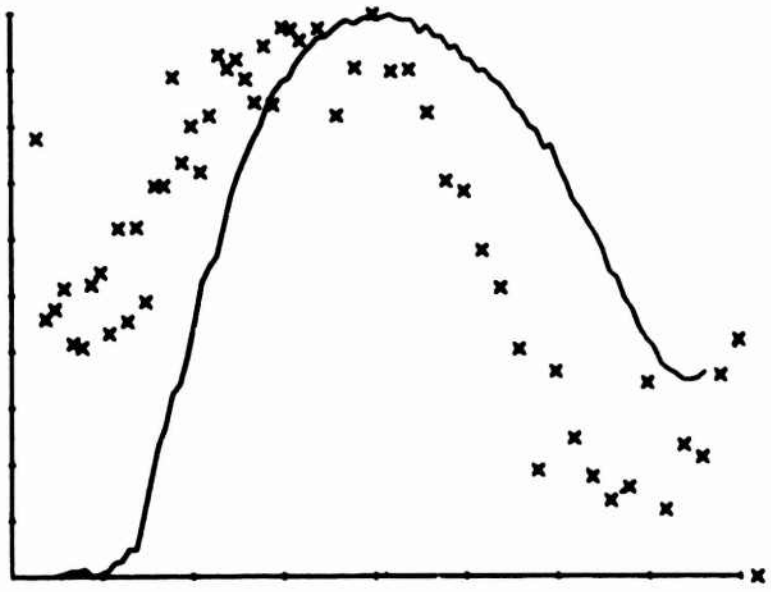

Figure 5. Variation in stiffness (x marks) during a twitch contraction (continuous line) with *triceps surae* muscle contraction at the time of electrical input. The abscissa is time from 0 to 400 msec.

DETECTION OF A CHANGE IN PLANT DYNAMICS IN A MAN-MACHINE SYSTEM

R. J. Niemela
U.S. Army Avionics Laboratory
Fort Monmouth, N.J.

E. S. Krendel
University of Pennsylvania
Philadelphia, Pennsylvania

ABSTRACT

Description of man's adaptive behavior in a closed-loop system requires a model of the means by which the human operator detects the change in operating conditions. This paper describes the detection portion of a concise model of human operator adaptation in manually tracking a step change in polarity of double integral plant dynamics.

The general form of the detection boundaries in error state space was postulated based on examination of man-machine error trajectory responses. This form was verified and the actual boundaries determined by experimental data.

INTRODUCTION

A prime reason for including the human operator as an active element in a man-machine system is to make use of his adaptive capabilities. However, system designers are restricted in the employment of these capabilities by an incomplete understanding of man's adaptive characteristics and the manner in which they interact with the system parameters. A concise mathematical description of man's adaptive behavior similar to the quasi-linear model developed for steady-state tracking would be a great asset to man-machine system design.

Previous research efforts [Sadoff (1962), Young (1964), Elkind and Miller (1967), Phatak and Bekey (1968), and Gilstad and Fu (1970)] have applied a diversity of analysis and modeling techniques to the problem of human operator adaptation to sudden changes in plant dynamics. These previous efforts resulted in several general conclusions although no comprehensive models have emerged for human operator adaptation to a step change in plant dynamics. A thorough survey of the topic is presented in a tutorial article by Young (1969).

APPROACH

Human operator adaptation to a step change in plant dynamics can be represented by a variable structure system model (Niemela 1973). The current paper describes the detection aspect of this model. Due to the incomplete understanding of human operator adaptation the current effort investigated the following task : human operator adaptation in a one-dimensional, compensatory, visual input tracking task with a step change in plant dynamics.

In the main experiment, the subjects were well trained in the task shown in Figure 1. The input was low-pass filtered "white noise" with equivalent statistical bandwidth* 1.5 radians/second. System error was displayed by the lateral displacement of a dot from a reference line on a raster scan cathode ray tube. The control stick was a lightly damped single axis sidearm controller. During the course of a two-minute tracking task, the polarity of the double integral plant dynamics was suddenly reversed. The subjects were instructed to minimize error at all times during the course of the trails.

*The bandwidth of the input is specified in terms of "equivalent statistical bandwidth" defined as

$$\omega_e = \frac{[\int_0^\infty \phi_{ii}(\omega)d\omega]^2}{\int_0^\infty \phi_{ii}^2(\omega)d\omega}$$

where $\phi_{ii}(\omega)$ is the power spectrum of the input. This quantity has been found to be an appropriate measure of input "randomness" for man-machine investigations (McRuer et al. 1965, Elkind 1964).

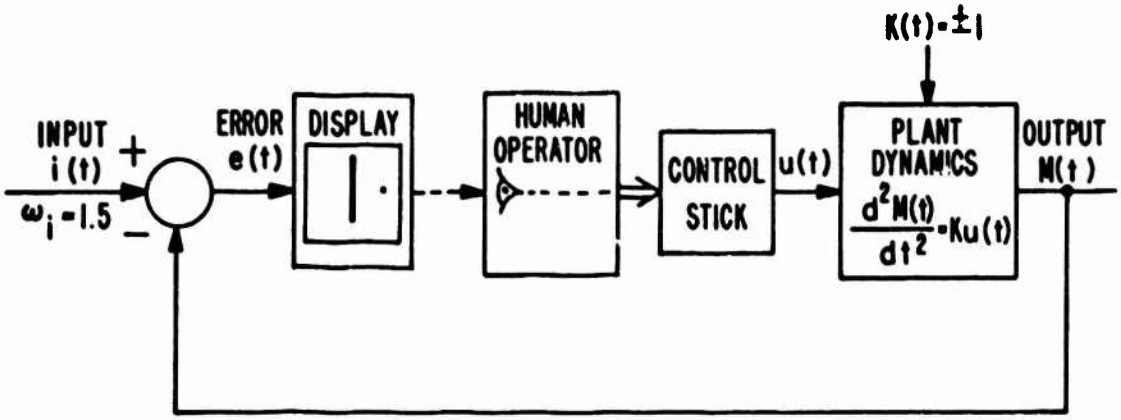

Figure 1. Elements of Man-Machine Investigation

The error and error rate are the difference between the input and system output and their first time derivatives:

$$e(t) = i(t) - m(t)$$

$$\dot{e}(t) = \dot{i}(t) - \dot{m}(t)$$

Upon completion of the experiment, error and error rate for time just before and immediately after the change in plant dynamics were played back on an X-Y plotter. Examination of the error trajectories revealed that during steady-state tracking, the error trajectory was confined to a region relatively close to the origin. Immediately after the change in plant dynamics, the error increased rapidly until the subject detected the change and recovered control. Figure 2 is a typical error trajectory obtained for the double integral set of dynamics. Examination of the data produced in this manner revealed several dominant features of the error trajectories: error rate peak and error at that instant, maximum error, and the second error rate peak and error at that instant.

Trajectories similar to that shown in Figure 2 and its inverted mirror image appeared with approximately equal frequency. For ease of analysis and discussion, those trajectories in the second and third quadrants were normalized to appear in the first and forth quadrant. It was found that the well-trained subject generated error time histories with essentially no overshoot in response to a step change in double integral plant dynamics. This observation is supported by averages of error time histories compiled by Elkind and Miller (1967) for a variety of plant dynamics.

THE DETECTION PROCESS

The manner in which the human operator detects the change in plant dynamics is of prime importance : this detection process determines the state of the system from which the human operator must recover control.

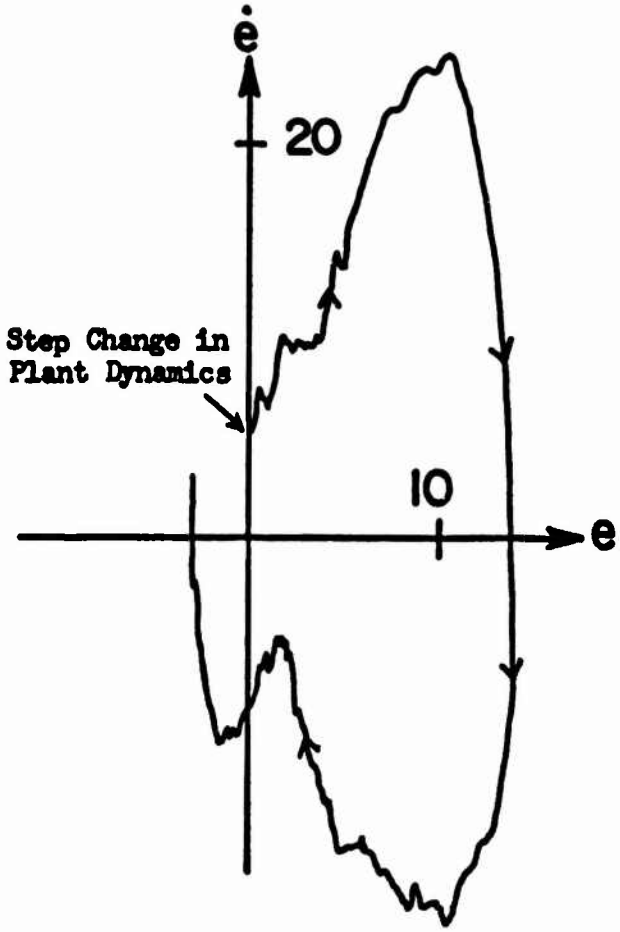

Figure 2. Typical Error Trajectory Response

Numerical data is presented in units of volts and/or volts/sec. Conversion to display deflection units can be accomplished with the factor .625 cm/volt.

Detection by the human operator was manifested by an abrupt reversal of the manipulator resulting in an error rate peak. It is evident that the subject perceived the change in plant dynamics before this error rate peak but his reaction time delayed his response.

Those trajectories in the data set which displayed a very small excursion of the error trajectory from the origin were of particular interest. Examination of several of these error trajectories indicated that the human operator did not perceive a change in dynamics with sizeable errors if the velocity is toward the origin. Futhermore, it appeared that detection was accomplished if both the error and error rate were sufficiently large in magnitude and identical in sign. The general form and logical representation of the detection boundaries implied from the above observation are shown in Figure 3. In this model, a change in plant dynamics is detected if the error trajectory enters the crosshatched region.

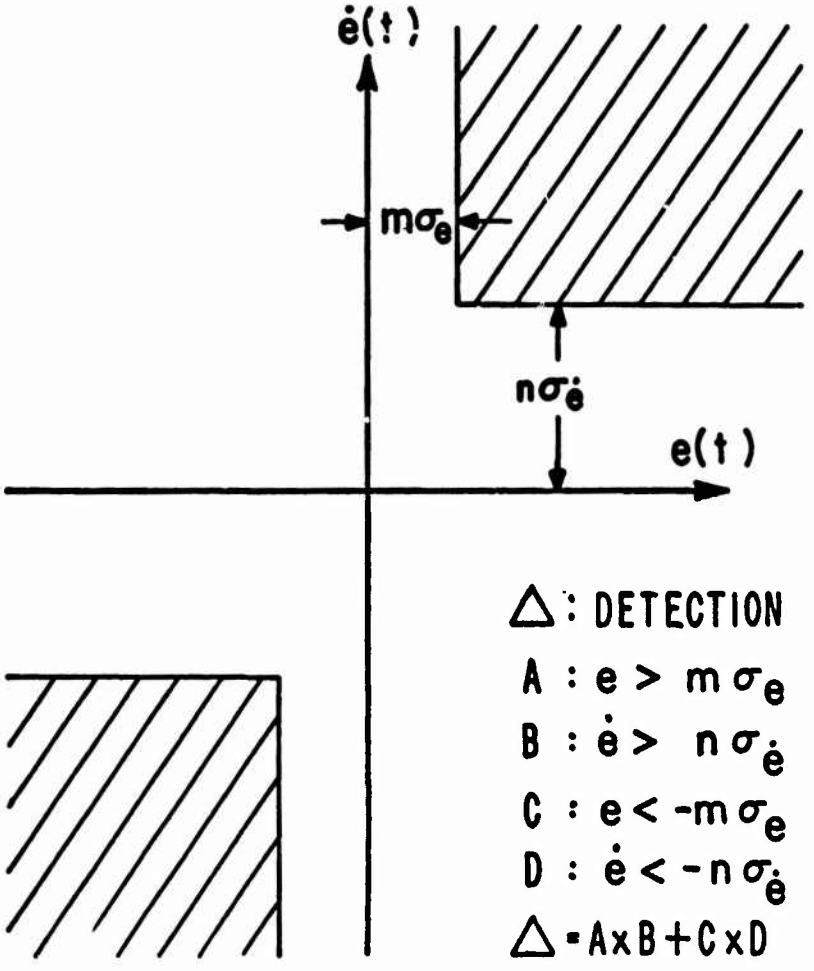

Figure 3. General Form of Detection Boundaries

Recognizing that the human operator detects a change in plant dynamics based on a combination of error and error rate, the manner in which this detection is made was determined through construction of a supplemental experiment.

Elkind and Miller (1967) have shown that if the subject were alerted by a 1 kHz audio tone the instant the plant dynamics changed, a statistically significant reduction in the average peak error resulted in the postransition transient than if the subject had to deduce the failure based on the error alone. Elkind and Miller found a reduction in average peak error from 6.83 to 3.93. This reduction was significant at the 0.05 level.

It was postulated that if the subject were alerted when the error trajectory intersected computer generated boundaries, the location of the human operator's detection boundaries could be determined by examining the average peak error for each set of boundaries. For those boundaries which gave no improvement over the nonalerted case, the alerting signal was redundant information to the subject. For those boundaries which gave significant improvement in average peak error, the alerting signal aided the subject in the detection process.

Two methods of alerting the subject were investigated in preexperiment trials - visual and audio. The visual means consisted of a small white bar which was displayed to alert the subject. It was found that this indication was distracting to the subject as has been noted in other experiments involving visual alarms (Poole 1966). A 1 kHz audio signal similar to that employed in Elkind and Miller's investigation was introduced. Mowbray and Gebhard (1961) found that the human operator's response to audio alarms is quicker than visual alarms. This characteristic of audio alarms is fortunate in the context of the supplemental experiment. It was desired to have the subject aware the instant the error trajectory crossed a particular boundary.

Prior to the experiment, the subject was told that an audio tone would be provided to alert him of a change in plant dynamics. He was further instructed that the mechanism for providing the "audio alert" would not operate in an identical manner from one trial to the next. Similar to the procedure in the main experiment, the subject was instructed to minimize tracking error at all times in the course of a trial.

Table I contains the values of the absolute peak errors as the detection boundaries were varied. The detection boundary location was specified by the lower left corner of the region in terms of multiples of the steady-state RMS error and RMS error rate.

Trial \ Treatment	1	2	3	4	5	6
1	8.0	7.5	12.5	15.5	12.9	11.5
2	4.5	12.0	15.8	12.8	15.9	9.5
3	4.8	3.5	8.5	15.0	11.5	12.3
4	9.8	10.0	12.7	10.2	12.1	9.5
5	6.1	13.0	11.6	8.0	10.5	9.5
6	7.9	8.5	11.9	14.2	9.5	14.5
7	8.5	11.6	14.5		11.5	14.0
8	3.0	7.5	11.9			
9	4.0	9.0	9.9			
10	4.5	8.2				
Mean Absolute Peak Error	6.11	9.08	12.1	12.6	12.0	11.5

Treatment Number	Detection Region Corner Location in State Space (Expressed in Multiples of RMS Error and RMS Error Rate)
1	(0, 0)
2	(1, 1)
3	(2, 2)
4	(3, 3)
5	(3, 1)
6	(00, 00)

Table I. Tabulation of Peak Error versus Alerting Boundaries

Six sets of alerting boundaries were considered and multiple comparisons between sets of boundaries were performed to determine those boundaries which aided the subject and those that did not. Table II contains the elements of the Analysis of Variance for the supplemental experiment.

Define,

Y_{ij} : Absolute peak error for i^{th} treatment and j^{th} trial.

$Y_{.k} = \sum_{i=1}^{nj} Y_{ik}$: Sum of absolute error peaks within treatments.

$Y_{..} = \sum_{i=1}^{n_j} \sum_{j=1}^{k} Y_{ij}$: Sum of absolute error peaks across treatments and trials.

Source of Variation	Sum of Squares (S.S.)	Degrees of Freedom (υ)	Mean Square (S.S./υ)
Columns $\sum_{j=1}^{k} \frac{Y_{.j}^2}{n_j} - \frac{Y_{..}^2}{N}$	282	5	56.5
Errors $\sum_{i=1}^{n_j} \sum_{j=1}^{k} Y_{ij}^2 - \sum_{j=1}^{k} \frac{Y_{.j}^2}{n_j}$	250	43	5.82
Total $\sum_{i=1}^{nj} \sum_{j=1}^{k} Y_{ij}^2 - \frac{Y_{..}^2}{N}$	532	48	

Table II. Elements of the ANOVA

Since the ratio $F = \frac{(M.S.)\ \text{columns}}{(M.S.)\ \text{error}} = 9.71$ is greater than 3.48 (F for 5 x 43 @ 1% level), the null hypothesis that all the means are equal can be rejected at the 0.01 level.

Sheffé's (1959) multiple comparison test was employed, since it can accommodate an unequal number of trials. Application of Sheffé's method to the present experiment was adopted from discussions by McNemar (1969) and Edwards (1965) and summarized on the following page.

Define the following variables:

Σx_i : Sum of absolute peak errors for i^{th} treatment

k : Number of treatments

n_i : Number of trials in i^{th} treatment

a_j : Coefficient of weighted average of the j^{th} treatment

S'^2 : Error mean squared

Any two sets of the k treatments can be contrasted through use of the ratio defined as:

$$F = \frac{D^2}{S'^2 \sum_{j=1}^{k} n_j a_j^2}$$

where,

$$D = \sum_{j=1}^{k} a_j \Sigma x_j$$

subject to the condition,

$$\sum_{j=1}^{k} n_j a_j = 0$$

The calculated value of F is tested against the quantity $(k-1)F'$: F' is for $(k-1)$ by $(\sum_{j=1}^{k} n_j - k)$ degrees of freedom at the desired level.

For the current case $k = 6$, $\sum_{j=1}^{k} n_j = 49$ $F_{0.05} = 12.1$

Table III presents the contrasts employed to determine the approximate location of the detection boundary. The elements of the table are the values of a_j for each particular contrast.

Contrast	X_1= 61.1 n_1= 10	X_2= 90.8 n_2= 10	X_3= 109.3 n_3= 9	X_4= 75.4 n_4= 6	X_5= 83.9 n_5= 7	X_6= 80.8 n_6= 7	F
1 vs. 2	1	-1					7.58
1 vs. 3	9/19		-10/19				29.6 >12.1
1 vs. 4	6/16			-10/16			26.8 >12.1
1 vs. 5	7/17				-10/17		24.4 >12.1
1 vs. 6	7/17					-10/17	21.0 >12.1
2 vs. 3		9/19	-10/19				7.65
2 vs. 4		6/16		-10/16			7.85
2 vs. 5		7/17			-10/17		5.97
2 vs. 6		7/17				-10/17	4.30
4 vs. 6				7/13		-6/13	0.582
1 vs. 3,4, 5,6	-1/10	1/50	1/45	1/30	1/35	1/35	38.9 >12.1
2 vs. 3,4, 5,6		-1/10	1/36	1/24	1/28	1/28	11.3 >9.95
1&2 vs. 3, 4,5,6	-1/20	-1/20	1/36	1/24	1/28	1/28	40.2 > 12.1

Table III. Multiple Comparison Tests

Based on the contrast of means which were determined to be significant, Table IV was constructed. All the contrasts were significant at the 0.05 level with the exception of [2 vs. 3,4,5,6], which is significant at the 0.1 level. The bars group means which were found to have a significant contrast.

Contrast \ Treatment	1	2	3	4	5	6
1 vs. 3	⌊—⌋		⌊—⌋			
1 vs. 4	⌊—⌋			⌊—⌋		
1 vs. 5	⌊—⌋				⌊—⌋	
1 vs. 6	⌊—⌋					⌊—⌋
1 vs. 3,4,5,6	⌊—⌋		⌊——	——	——	——⌋
2 vs. 3,4,5,6		⌊——	——	——	——	——⌋
1 & 2 vs. 3,4,5,6	⌊——	——	——	——	——	——⌋

Table IV. Summary of Multiple Comparisons

The alerting boundaries which reduced average peak error are associated with the treatments on one side of the human operator's detection boundary. Similarly, the alerting boundaries which had no effect on average peak error are associated with treatments on the other side of the detection boundary. The location of the human operator's detection boundary lies, therefore, between the two sets of boundaries. From Table IV, it is concluded that Treatment 1 and 2 are on one side of the boundary and Treatment 3, 4, 5, and 6 are associated with the other side of the boundary.

Alerting boundaries for cases 3, 4, 5, and 6 (Figure 4) did not

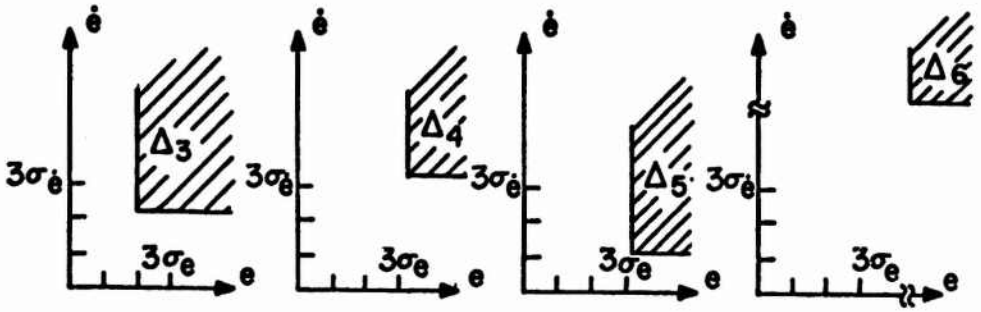

Figure 4. Definition of Alerting Boundaries for Treatments 3, 4, 5, 6

significantly reduce average peak error. Thus, it is reasonable to expect that the boundary formed by the logical union of their alerting boundaries (Figure 5) would not significantly reduce average peak error.

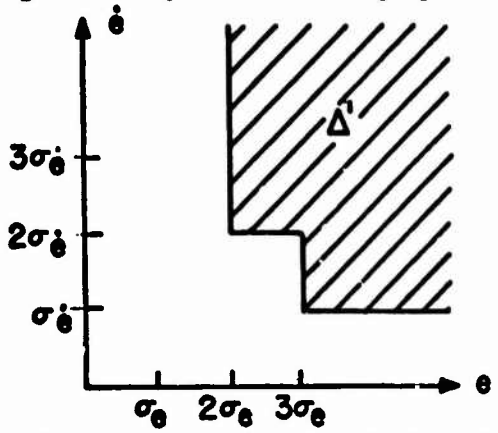

Figure 5. Union of Alerting Boundaries which did not Reduce Average Peak Error

By defining

Δ_i : alerting boundary associated with the i^{th} treatment

It is seen from Figure 5 that

$$\Delta' = \Delta_3 + \Delta_4 + \Delta_5 + \Delta_6$$

Similary, since alerting boundaries for Treatments 1 and 2 (Figure 6) did significantly reduce average peak error, the boundary formed by the union of those two alerting boundaries (Figure 7) would reduce average peak error.

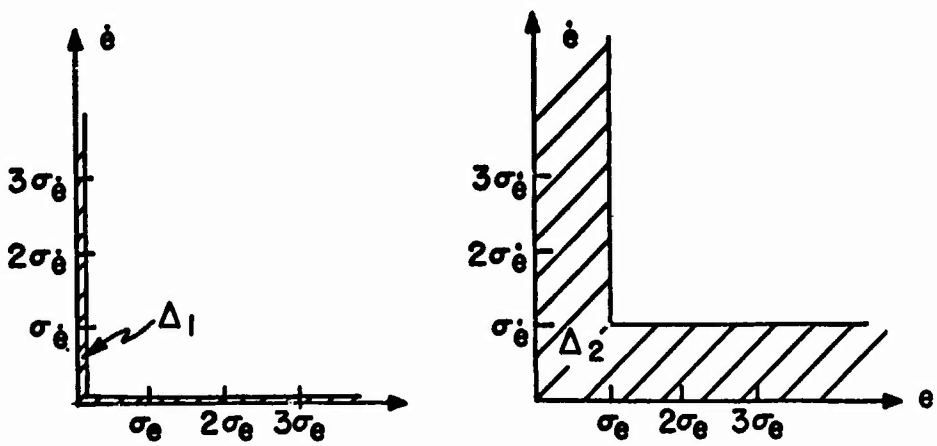

Figure 6. Definition of Alerting Boundaries for Treatments 1, 2

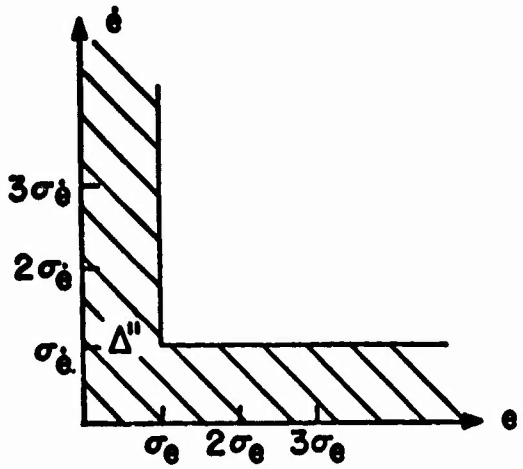

Figure 7. Union of Alerting Boundaries which did Reduce Average Peak Error

Therefore,

$$\Delta'' = \Delta_1 + \Delta_2$$

Hence, the human operator's detection region lies between these two sets of alerting boundaries (Figure 8).

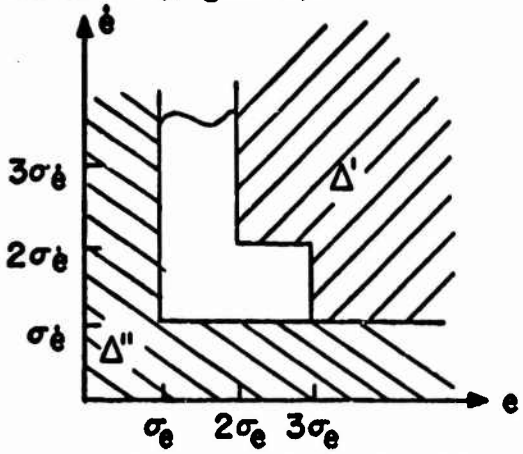

Figure 8. Approximate Location of Human Operator's Detection Boundary

CONCLUSIONS

This paper has defined a model of human operator detection of a change in plant dynamics. The general form of the detection boundaries was developed based on examination of man-machine data. The form of these boundaries was verified and the location determined through an analysis of variance and multiple comparison tests of the man-machine data.

The location and form of the detection boundaries defined in Figure 8 does not imply that they are rectangular, hyperbolic, or any other mathematical form. Subsequent research may, however, refine the location and give a more concise representation of its form.

The variables employed by the detection model could be monitored in a real world man-machine system to provide an explicit indication to the human operator of critical changes. In this manner, it may be possible to improve the safety and reliability of systems in which man and machine operate in concert.

BIBLIOGRAPHY

Elkind, J.I.: "A Survey of the Development of Models for the Human Controller, "Guidance and Control - II, ed. R.C. Langford and C.J. Mundo, (Progress in Astronautics and Aeronautics, Vol. 13), New York: Academic Press, June 1964.

Elkind, J.I. and Miller, D.C.: Adaptive Characteristics of the Human Controller of Time-Varying Systems, Air Force Flight Dynamics Laboratory Technical Report, TR-66-60, 1967.

Edwards, A.L.: Experimental Design in Psychological Research, New York: Holt, Rinehart and Winston, 1965.

Gilstad, D.W. and Fu, K.S., 1970, "A Two-Dimensional Adaptive Model of a Human Operator in a Time Varying Control System," School of Electrical Engineering, Purdue University, Lafayette, Indiana, Tech. Rep. TR-EE 70-10 June 1970.

McNemar, Q.: Psychological Statistics, New York: John Wiley & Sons, 1969.

McRuer, D.T. Graham, D. Krendel, E.S. and Reisener, W.: Human Pilot Dynamics in Compensatory Systems, Air Force Flight Dynamics Laboratory, TR-65-15, July 1965.

Mowbray, G.H. and Gebhard, J.W.: "Man's Senses as Informational Channels," Selected Papers on Human Factors in the Design and Use of Control System, H. Wallace Sinaiko ed., New York: Dover, 1961.

Niemela, R.J.: Variable Structure System Model of an Adaptive Man-Machine Process, Ph.D. dissertation, University of Pennsylvania, 1973.

Phatak, A.V. and Bekey, G.A.: "Model of the Adaptive Behavior of the Human Operator in Response to a Sudden Change in the Control Situation," Proceeding of Fourth Annual NASA-University Conference on Manual Control, NASA-SP-192, 1968.

Poole, H.H.: Fundamentals of Display Systems, Washington: Spartan Books, 1966.

Sadoff, M.: A Study of a Pilot's Ability to Control During Simulated Stability Augmentation System Failures, NASA TN D-1552, 1962.

Scheffé, H.: The Analysis of Variance, New York: John Wiley and Sons, 1959.

Young, L.R.: "On Adaptive Manual Control," IEEE Transactions on Man-Machine Systems, 10:4, December 1969.

MULTI-AXIS PILOT-VEHICLE DYNAMICS

Edward D. Onstott

Vehicle Dynamics and
Control Research

Northrop Corporation,
Aircraft Division
Hawthorne, California

ABSTRACT

A method for directly computing sampled data, time sharing, thresholds, and other nonlinear characteristics of the human pilot has been developed and applied to the two axis example of VTOL precision hover. The task is generated by a model of pilot induced disturbances including crossfeed and remnant. After the model was optimized, a fixed base flight simulation was performed. The agreement between the previously computed analytical and the experimental data shows close correspondence in all system variable statistics, distribution of sampling periods, frequency content, and ground path characteristics. Direct methods were used to identify and estimate two independent sources of inadvertent crossfeed, and a semi-direct, or Archimedean method of estimating pilot remnant models was also developed. By avoiding linearization of the pilot model, many effects related to the time sharing operation of the human controller have been studied analytically. Current applications include problems of weapon delivery and loss of control.

INTRODUCTION

Historically, the development of mathematical models of the human controller has been based upon linear continuous operators, such as the Laplace transform. This formulation lends itself to ready analysis of piloted system stability and frequency response, and the great progress made using this approach has lead to the development of pilot-vehicle modeling as a widely employed and established discipline. A large bibliography now exists, and the dynamic properties of single axis time-invariant human control are recorded in detail. If one considers the problem of continuous linear systems driven by Gaussian processes, additional performance information

can be obtained, since the input and output power spectra are related. For a zero mean process, the integral of the output spectrum is simply the mean square of the time history. In this way, time domain information can be obtained for problems where root mean square (rms) performance must be optimized.

Under contract to AFFDL* Northrop took this approach to define methods for predicting and evaluating flying quaiities in turbulence. These studies are reported in References 1, 2, and 3, and concern attitude stabilization in bank angle, pitch angle, and heading as single axis tasks. The method was used in a purely predictive manner by optimizing the gains for a standard gain, lead, time delay pilot model. Figure 1, reproduced from Reference 1, shows the comparison between moving base flight simulation data and the model predictions that had previously been submitted to the Air Force Project Monitor, Mr. Frank L. George. The task is bank angle stabilization and each point represents a different aircraft.

A larger study to validate this methodology led to a favorable evaluation of the method's accuracy. These statistical data are given in Figure 2, from Reference 2, and include 64 F-5 and A-7 flight conditions and failure states. Subsequent to this research, these techniques were used in support of several Northrop development projects, and the advantages of getting time domain information out of the pilot-vehicle analysis was clearly demonstrated.

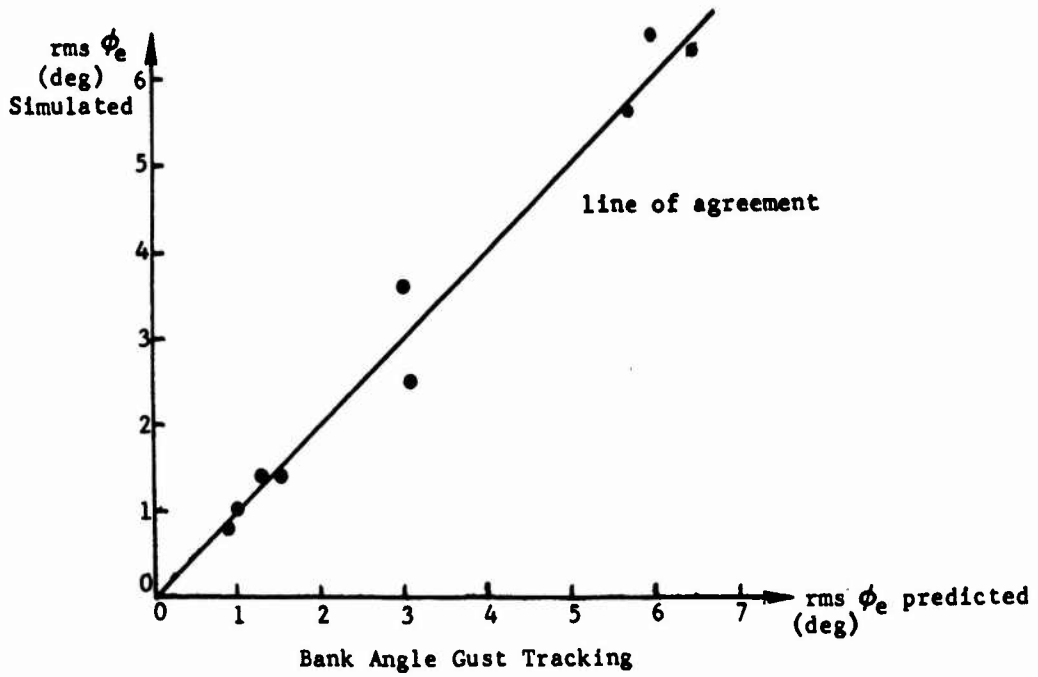

Figure 1. Agreement of Predictions with Simulation

*This research was largely carried out under contracts F33615-71-C-1077 and F33615-70-C-1156 for the Air Force Flight Dynamics Laboratory.

CONFIGURATIONS AVERAGED	AVERAGE % ERROR OF PREDICTIONS	% RANGE OF PREDICTIONS
Bank Angle Gust Tracking Normal Modes Only	13.35	205
Bank Angle Gust Tracking Normal and Failure Modes	29.89	389

Figure 2. Accuracy of Turbulence Prediction

Continuing this program of obtaining time domain information as directly as possible from the piloted system models, a more general and versatile handling qualities technology has been produced. Validating examples have been obtained and one of them - the VTOL hover problem - is described below along with a general account of this new approach.

Although linear continuous analysis has been useful for design and evaluation applications, it has not led to sufficiently comprehensive studies of large scale problems such as time-varying weapon delivery, and loss of control at high angles of attack. In order to study these examples, the total system model must contain the following features:

- Nonlinear and time-varying aircraft dynamics
- Nonlinear and time-vatying pilot dynamics
- Multi-axis as well as multiloop pilot operation including exact modeling of time sharing, sampling, changing criteria, and threshold effects
- Purely predictive adjustment using standard optimization
- Easy computational methods which permit the modeling of large systems with gross nonlinearities.

These requirements have now been largely met using the following two techniques:

- Direct digital simulation as a handling qualities method
- Dynamic (as contrasted to statistical) multi-axis pilot models that employ attention and control shifting criteria called urgency functions.

The VTOL hover problem discussed below will serve to illustrate these concepts.

DIRECT DIGITAL SIMULATION AS A HANDLING QUALITIES METHOD

Since the Fourier transform only partitions the set of autocorrelation functions into classes, each of which is represented by a single power spectrum, it is not a one-to-one mapping of dynamical problems into the class of power spectra. In other words, time-varying problems, discrete time points, and most nonlinearities are not preserved by the Laplace or any other linear transform, even if characterized by a continuous operator. Thus for such problems, the concept of eigenvalues loses its meaning and one is forced to find useful parameters in the time domain where these system properties naturally exist. The way to do this is by directly generating the time series corresponding to the dynamics of interest and performing analysis on the records produced. This approach has been extensively used to analyze the nonlinearities of limits, thresholds, hysteresis, and other questions of controls design, and the techniques for doing this kind of computation are generally known.

Although digital simulation has its share of traps and pitfalls, the method of Z-transforms and difference equations has proved to be practical; the entire system can be modeled directly with no linearizing assumptions on either the pilot or the aircraft with its control system. Furthermore, digital simulation programs have been produced that are very rapidly adapted to new problems, and readily available computers ensure accuracy and speed, both of which are necessary for general usage of the method. The specific application of digital simulation to handling qualities problems is a technology of its own and has undergone a rapid development at Northrop during the last two years, but the most dramatic success of digital simulation has been in the study of directly (as contrasted to statistically) modeled multi-axis piloted control.

To sum up, digital simulation as a handling qualities method

- is inexpensive and easily applied,
- allows the exact modeling of the system and the task,
- provides a method for applying a faithful multi-axis pilot model to handling qualities problems.

Digital simulation technology has been available for some time. What is needed is the multi-axis pilot model.

THE MULTI-AXIS HUMAN CONTROLLER

As mentioned above, a great deal is known about the dynamics of the human pilot performing continuous linear tasks on a single axis, including multiloop tasks. Much work has gone into developing models that match the amplitude and phase characteristics of the pilot's output at the controller, and many aspects of the internal structure of the human have been analyzed. These "ultra-precise" models are of use in solving many human factors problems about the interface between pilot and controller, but for the basic objective of determining the total system dynamics, it is usually sufficient to employ simple models that consist of gain K_p, lead T_L, time delay τ, and possible lag T_I:

$$Y_p = K_p \frac{(T_L s + 1)}{(T_I s + 1)} e^{-\tau s} \qquad (1)$$

The more exact pilot models can certainly be employed, but for most purposes the above simple model gives good statistical results.

There have been three main approaches previously taken in attempts to extend single axis model theory to multi-axis tasks. All of these recognize that the human must operate as a time shared device when faced with difficult control tasks on several independent axes. This intermittent operation degrades the performance of each axis from what the pilot would achieve in continuous control. As might be expected, these three approaches are 1) decrease the model gain from the optimum for continuous control, 2) increase the time delay to account for the periods of inattention, and 3) inject filtered noise to imitate the spectral content of the shifting pilot control. In many cases these methods have matched data already obtained from flight simulation, but they have never been used to predict, before the experiment, the statistics of any broad class of aircraft dynamics.

The problem with these three approaches is this: the human pilot is quite discriminating about when he will abandon the control of one task to take over the control of another. This leads to a sampling criterion that is functionally dependent on the total system variables. In no way can this be regarded as a purely random, or a regular sampling. Thus a multi-axis pilot model must contain an algorithm that determines when control shifting takes place, and the model must be computed in a way that preserves this information. Recently, Northrop developed a multi-axis pilot model which does just that, the urgency function model.

By using the method of digital simulation, the exact functional criterion, by which a pilot decides his control, can be directly computed without the gross distortions of linearization. The development of the form of these urgency criteria has now advanced to the point where they can be determined from 1) the system dynamics, 2) the task, and 3) the appropriate human factor information about the pilot.

Let x_i be the state variables of one axis of a two axis task, and let the other axis be represented by y_i. Then the control criterion is satisfied identically with the inequality

$$U_x(x_1) \geq U_y(y_1) \tag{2}$$

where U_x and U_y are the urgency functions of the x and the y axes. These functions are always nonlinear in the state variables, but fall into several precise classes. Some of these classes have been well explored, and a full tabulation of the urgency functions will appear later.

The multi-axis urgency function model thus consists of simple linear dynamics, equation (1), along with the control criterion of (2). Whichever axis has the larger urgency function gets the corrective control attention. The adjustment of the linear coefficients can usually be obtained (the hover problem was an exception) by an easy search starting with the optimum single axis coefficients. Almost always, the optimum multi-axis coefficients differ significantly from these values, especially in multiloop control on the two axes.

Before the VTOL example can be presented, there is another topic essential to the understanding of multi-axis control: pilot induced noise. In the continuous single axis case this noise is defined to be the linearly uncorrelated part of the pilot's output and is called remnant. It consists of white noise mechanically filtered by the muscle actuation system and arm-controller dynamics. Physically, this represents a blend of three sources of error in the pilot's response: observation noise, internal processing error, and actuation noise. For multi-axis tasks there is another source, inadvertent crossfeed.

If one obtains an x-y plot of lateral and longitudinal stick for a two axis tracking task, the results show not only the split control (the lines going mainly up and down, and left to right like a small town street map) but also inadvertent control inputs. In a task where there is zero mean control deflection, the pattern is similar to Figure 3 obtained from a Northrop simulator.

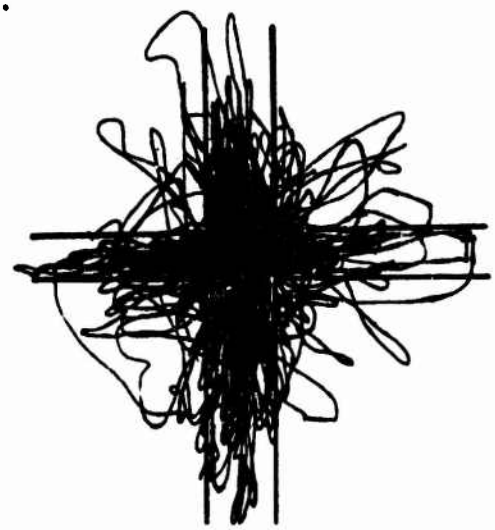

Figure 3. Cross Plot of Lateral and Longitudinal Stick

If one ignores the small amount of time the trace is outside the cross drawn on the figure, it is apparent that the controller motions are distributed about an ideal motion which would coincide with the axes. This inadvertent crossfeed noise has two sources as shown in Figure 4, and using the method of digital simulation is modeled as shown in Figure 5.

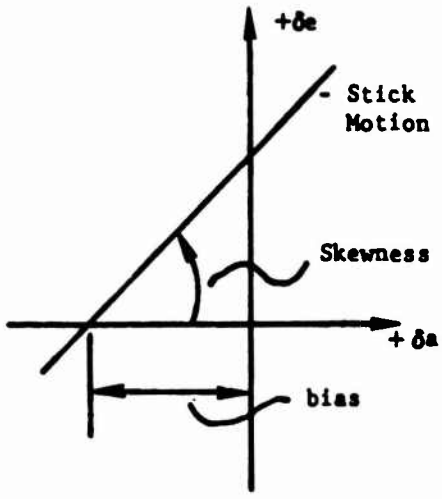

Figure 4. Sources of Crossfeed

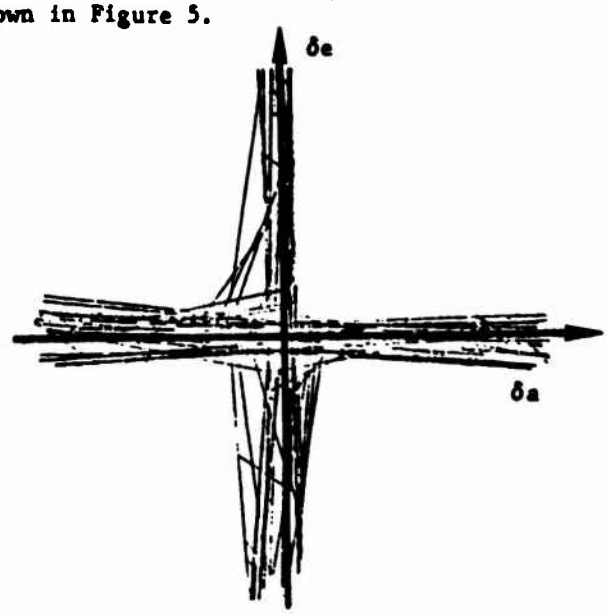

Figure 5. Multi-axis Pilot Model Stick Output

By using previously obtained x-y stick plots for various tasks, the amount of the crossfeed, bias and skewness, can be estimated with sufficient accuracy. If the system under study is driven by a large input such as a command tracking task or aerodynamic disturbance, the effect of these error sources may be small. However, in difficult tracking tasks where the principal disturbance is the pilot himself, the remnant and the crossfeed have overwhelming influence on the system performance.

Now that the two multi-axis sources of pilot induced noise have been joined to the urgency function pilot model described above, the VTOL hover problem can be discussed.

A SELF-GENERATED TWO-AXIS VTOL HOVER TASK

In order to demonstrate the operation of all features of the urgency function pilot model, a problem was selected that is perhaps the most difficult case of any yet encountered or contemplated. The analysis of this problem proceeded by estimating the remnant and the crossfeed, and optimizing the linear coefficients and the urgency functions for a standard time delay of .3 seconds. The analysis showed the importance of all aspects of the model, and once completed, a flight simulation was performed.

The vehicle is essentially a fourth order integration of each (lateral and longitudinal) axis. The task is to hover as close to the origin as possible in still air; there are no external disturbances. Thus the task for the pilot is two-axis multiloop control disturbed only by remnant, crossfeed, and urgency function switching.

A block diagram of the digital simulation of this problem is given in Figure 6.

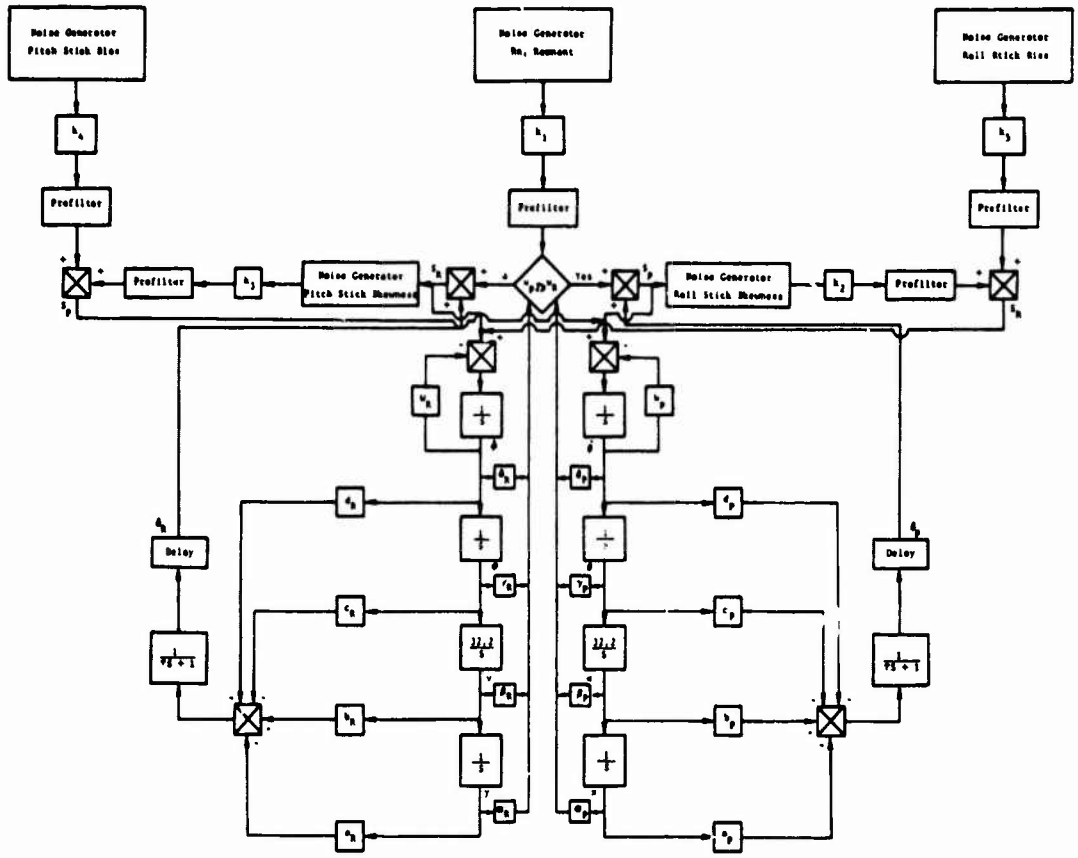

Figure 6. Urgency Function Multi-axis Model of VTOL Hover

Explicitly, the linear parts of the pilot models consist of inner loop attitude control and outer loop position control. The urgency functions take position, velocity, attitude, and attitude rate into account. These control laws are as follows, where the subscript "P" indicates longitudinal quantities, and "R" lateral:

$$Y_{P\theta} = \frac{\left(d_P s + c_P\right)}{\left(T_I s + 1\right)} e^{-.3s} \qquad \text{(inner loop)}$$

$$\text{longitudinal} \qquad Y_{Px} = \frac{\left(b_P s + a_P\right)}{\left(T_I s + 1\right)} e^{-.3s} \qquad \text{(outer loop)} \qquad (3)$$

$$U_P = U_P\left(\delta_P \dot{\theta},\ \gamma_P \theta,\ \beta_P u,\ \alpha_P x\right)$$

$$Y_{R\phi} = \frac{\left(d_R s + c_R\right)}{\left(T_I s + 1\right)} e^{-.3s} \qquad \text{(inner loop)}$$

$$\text{lateral} \qquad Y_{Ry} = \frac{\left(b_R s + a_R\right)}{\left(T_I s + 1\right)} e^{-.3s} \qquad \text{(outer loop)} \qquad (4)$$

$$U_R = U_R\left(\delta_R \dot{\phi},\ \gamma_R \phi,\ \beta_R v,\ \alpha_R y\right)$$

Before the experimental results are given, there are a few aspects of the model performance that should be discussed. The adjustment of the coefficients for this study is by far the most difficult case yet encountered, and turned out to be sensitive to both the form and the values of the urgency functions. The correct form of U_P and U_R were derived without much trouble, but a parameter search had to be made for the coefficients. Once stable hovering was achieved - which incidently is not possible with regular or random sampling - a manual gradient method was used to simultaneously adjust both the linear and the urgency coefficients. This was done by using an on-line graphical computer terminal. The model was optimized for minimum rms position error. For non-optimum urgency function forms, the vehicle would orbit the origin a few times then spiral outwards unstable; for non-optimum urgency coefficients, the hovering was stable, led to rapid switching, and had other unrealistic features of the ground path traces. The remnant level was adjusted from previous analysis and simulation; the novel method for doing the remnant calibrations will be discussed later.

The experimental work was undertaken after the analysis of this hover problem was complete. The model had been optimized, and many other attempts to improve its performance by varying the urgency functions did not succeed.

The simulation facility was a fixed base arrangement using a side-arm controller, a dual beam oscilloscope display, and analog computation. The gain on the display was increased to the point that pilot induced noise served to drive the pilot-vehicle system. This required high gains in the equipment, and considerable effort was made to maintain good signal to noise ratios and prevent cross-talk on the patchboard. The display consisted of an illuminated dot representing ground position, and an illuminated line that gave attitude information as shown in Figure 7.

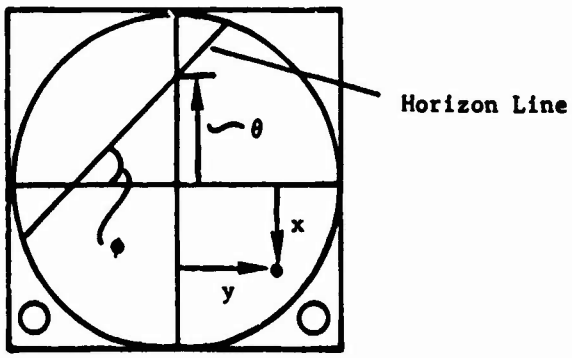

Figure 7. VTOL Hover Simulation Display

The subject, a former Navy test pilot, determined the optimum control sensitivities and was asymptotically trained. Data were taken for a total of twenty trials of 100 seconds duration. The data from the simulation are tightly clustered and show only a slight learning trend during the final ten trials. A comparison between the model and the simulation ground paths is shown in Figure 8, each drawn to the same scale.

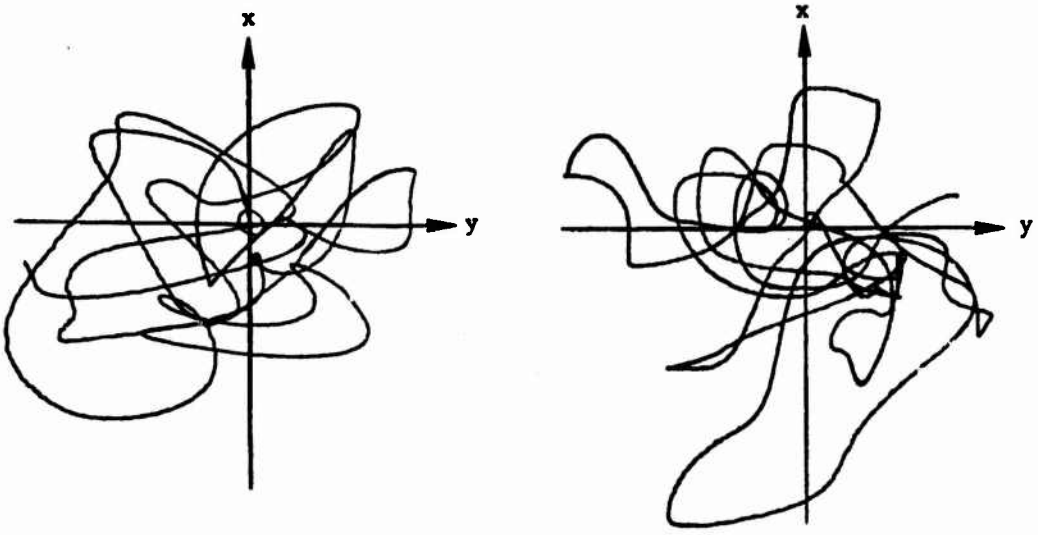

Urgency Pilot Model

Flight Simulation

Figure 8. Ground Paths of Model and Simulation

These ground path traces show many similar qualitative features, absent in the non-optimum model, such as the sharp points and tight turns where the pilot nearly stops the translation of the airplane in order to initiate a better velocity vector. The similar size and shape of the loops indicates similar spectral content. Figure 9 shows a segment of the time history of pitch angle as generated by the model and by the simulation.

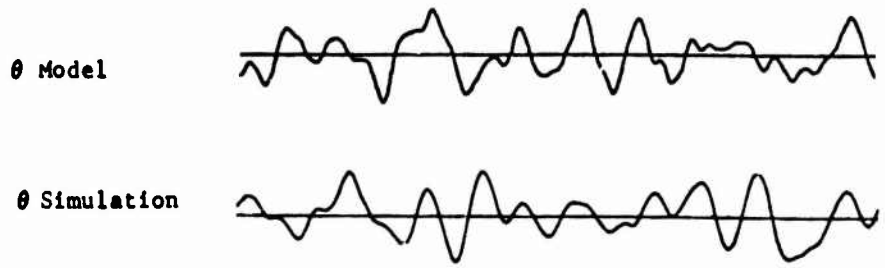

Figure 9. Theta Time Histories from Model and Simulation

The switching times produced by the model and by estimation from the strip chart recording of the lateral and longitudinal stick are compared in the following histograms, Figure 10, which show the mean sample period to be between 1.5 and 2.0 seconds. These statistics are combined from lateral and longitudinal data since the dynamics of the two axes are identical.

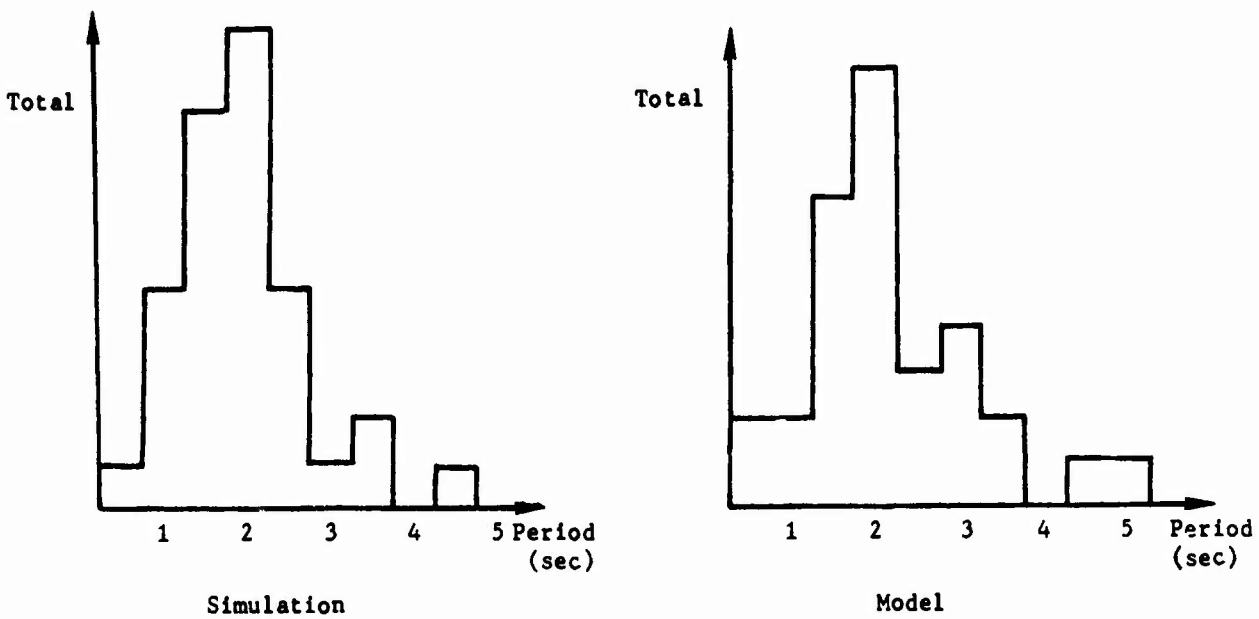

Figure 10. Histograms of Pilot Switching

The most telling comparison of the urgency function model and the flight simulation is in the statistics. These are shown in Figure 11.

	Flight Simulation Data	2-axis Model Predictions
X (ft)	.221	.225
Y (ft)	.217	.172
U (ft/sec)	.065	.084
V (ft/sec)	.074	.082
θ (deg)	.057	.153
ϕ (deg)	.120	.151
$\dot{\theta}$ (deg/sec)	.198	.256
$\dot{\phi}$ (deg/sec)	.440	.261

Figure 11. Comparison of Model and Simulation Statistics

This agreement of the model and the simulation completes the comparisons for the VTOL example. In retrospect, there seems to be no area where the model has failed to be accurate in statistical, spectral, or qualitative features. Currently more general, or representative VTOL system models are being investigated, but the model has required no further modifications. The next generalization of this problem is the time varying problem of VTOL

handling qualities during transition. By using the digital simulation approach along with the urgency function multi-axis pilot model, this time-varying problem can be approached in its full generality.

ANOTHER MULTI-AXIS EXAMPLE

In order to obtain further examples and validations, data from several two-axis tracking tasks were surveyed and analyzed. The problem given here is found in the AFIT thesis "Extension of Pilot Describing Functions to Multiple Compensatory Tracking Tasks" by James E. Wanamaker and William A. Sower, Reference 4.

The problem consists of a main longitudinal command tracking task and a lateral stabilization task with unstable dynamics. Three sets of main dynamics are considered along with command tracking tasks of two different bandwidths, thus giving six cases in all. An urgency function two-axis pilot model was optimized for each of these tasks, and the resulting system has the form shown in Figure 12.

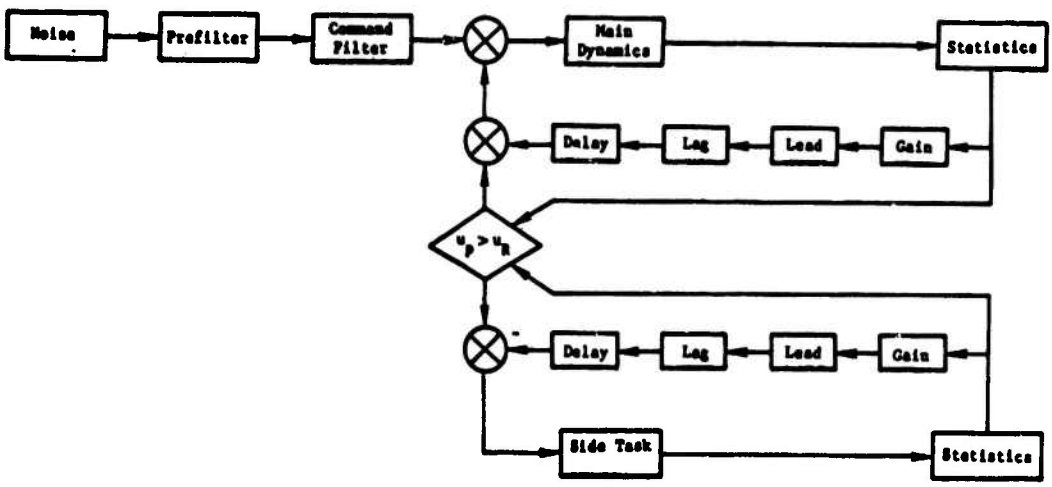

Figure 12. Urgency Function System Model

The comparison of the urgency function model with the Wanamaker-Sower data is given in Figures 13 through 18.

Longitudinal dynamics: K/s

Lateral dynamics: K/(s+1.5)

Command: $K/(s+1.5)^2$

	Subject 1	Subject 2	Northrop 2-axis model
σ/σ_c (RMS)	.6249	.6156	.6159
Mean Sample (sec)	1.22	1.17	1.11
Error Bandwidth (rad/sec)	4.87	3.54	4.6

Figure 13.

Longitudinal dynamics: K/(s-1)

Lateral dynamics: K/(s-1.5)

Command: $K/(s+1.5)^2$

	Subject 1	Subject 2	Northrop 2-axis model
σ/σ_c (RMS)	.8454	.8839	.8598
Mean Sample (sec)	1.077	1.008	1.041
Error Bandwidth (rad/sec)	4.3	3.1	4.1

Figure 14.

Longitudinal dynamics: K/s^2

Lateral dynamics: K/(s-4.5)

Command: $K/(s+1.5)^2$

	Subject 1	Subject 2	Northrop 2-axis model
σ/σ_c (RMS)	.8201	1.0556	.8991
Mean Sample (sec)	1.551	1.944	1.923
Error Bandwidth (rad/sec)	7.04	5.13	4.9

Figure 15.

Longitudinal dynamics: K/s

Lateral dynamics: K/(s-1.5)

Command: $K/(s+.5)^2$

	Subject 1	Subject 2	Subject 3	Northrop 2-axis model
σ/σ_c (RMS)	.2029	.2781	.2465	.2335
Mean Sample (sec)	1.093	1.1515	.8939	1.031
Error Bandwidth (rad/sec)	3.83	3.32	3.62	3.8

Figure 16.

Longitudinal dynamics: $K/(s-1)$

Lateral dynamics: $K/(s-1.5)$

Command: $K/(s+.5)^2$

	Subject 1	Subject 2	Subject 3	Northrop 2-axis model
σ/σ_c (RMS)	.2742	.3696	.3697	.4161
Mean Sample (sec)	.9309	.9271	.9277	1.110
Error Bandwidth (rad/sec)	3.83	3.61	3.71	4.20

Figure 17.

Longitudinal dynamics: K/s^2

Lateral dynamics: $K/(s-.5)$

Command: $K/(s+.5)^2$

	Subject 1	Subject 2	Subject 3	Northrop 2-axis model
σ/σ_c (RMS)	.3195	.4553	.5406	.3825
Mean Sample (sec)	1.238	1.285	1.1006	1.32
Error Bandwidth (rad/sec)	6.22	5.92	3.66	3.8

Figure 18.

Examples of time histories of the tracking command and the response of the two-axis model is given in Figure 19.

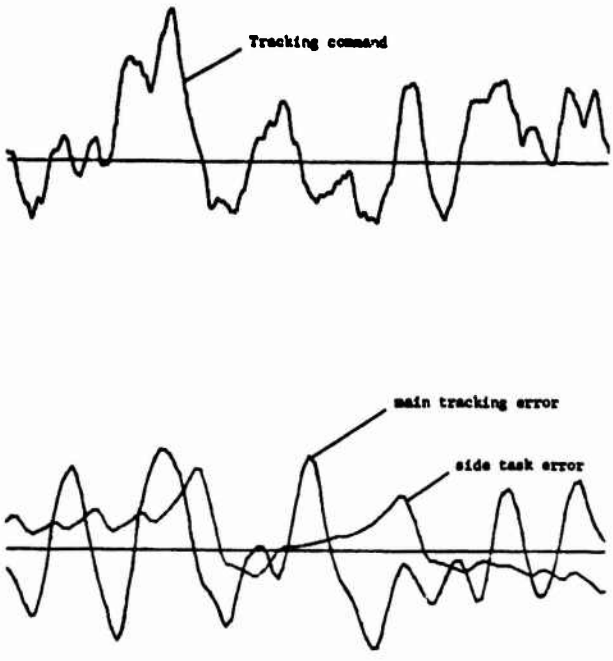

Figure 19. Time Histories of Model Response

A summary of these six cases is given in Figure 20 which compares the model with the Wanamaker-Sower simulation data.

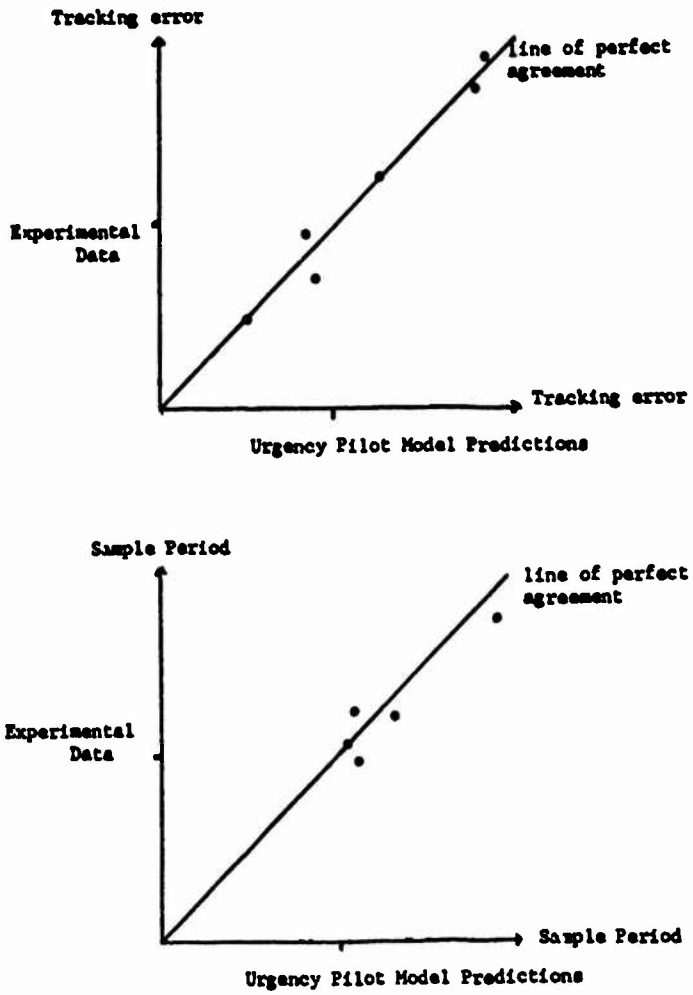

Figure 20. Comparison of Urgency Model with Simulation Data

Currently, these results are being enlarged by including extentions of the Wanamaker-Sower research as contained in an AFIT thesis by Machuca and Lind which studies lateral and longitudinal F-4 dynamics. Many cases of this kind have been already analyzed using the urgency function multi-axis pilot model, and further Northrop simulation is now in progress.

REMNANT MODELING AND CALIBRATION

Remnant is defined for continuous tracking to be the linearly uncorrelated part of the pilots output. Spectrally, it is white noise attenuated through the mechanical filtering of the arm and controller dynamics. Since many tasks are primarily disturbed by the pilot himself, it is essential to have a way of determining by the most simple and direct method possible 1) whether the assumed spectral shape of the remnant is appropriate, and 2) what amplitude the remnant should be given in the model. In order to do this for the VTOL hover problem, a method for calibrating remnant was developed that can be readily used in any control situation. It also provides a rough check on the correctness of the spectral shape in terms of the statistical performance of the piloted system.

The method is essentially Archimedean, and the way it was developed is as follows: If a pilot's actual remnant were an accessible quantity, the remnant amplitude could be altered. Thus one could determine the unknown remnant level by simply turning it down until the system error vanishes; the amount of reduction would be equal to the original remnant. A second glance at this reveals that one doesn't need to turn the pilot's remnant down, since the slope of the line and the point of the unaltered performance will suffice to determine the intercept at zero tracking error. At this point it becomes apparent that the pilot's remnant can be increased experimentally by adding noise of the right spectral shape to his output and by measuring the change in tracking performance the slope can be found. This method is diagrammed in Figure 21.

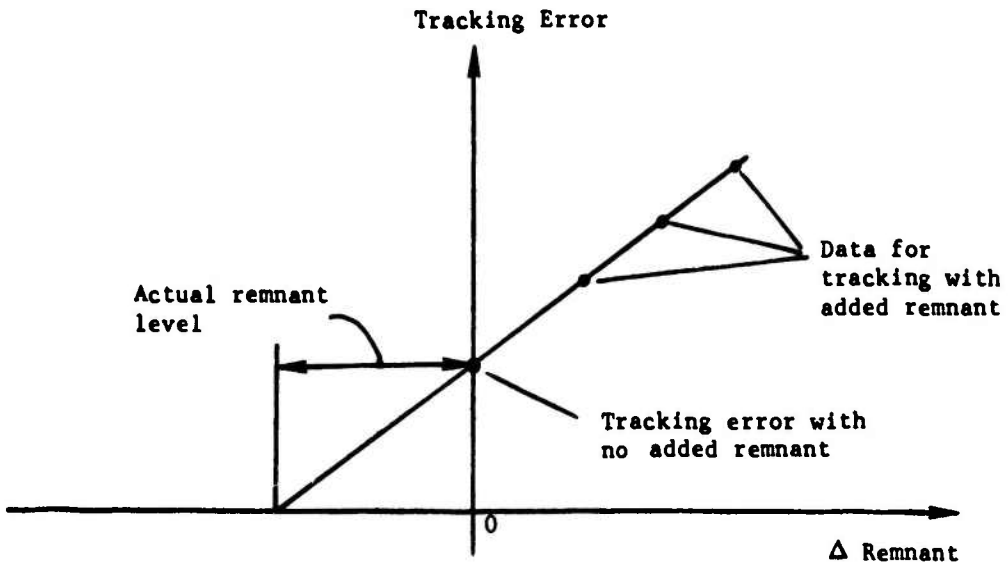

Figure 21. Remnant Model Calibration Method

This method has been employed to calibrate the remnant levels for not only the VTOL hover task detailed above, but two-axis attitude stabilization tasks as well. Figure 22 shows the experiemntal data for an attitude stabilization task with incremented remnant. Each data point represents a 100 second simulation.

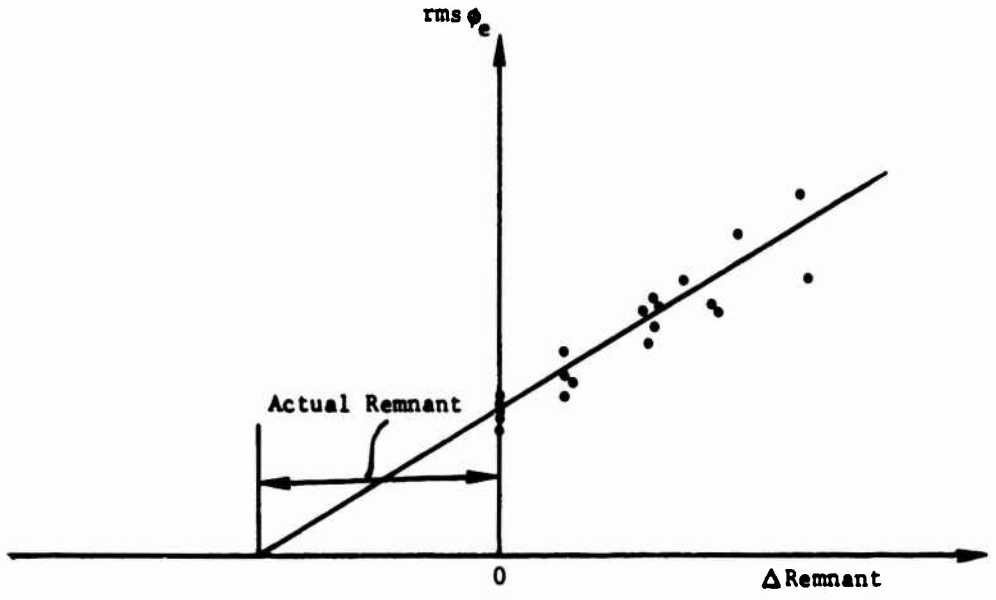

Figure 22. Experimental Remnant Calibration Data

The white noise used for this simulation of remnant was filtered by a 40db/decade filter with a time constant of .1 seconds. In this case the model was statistically appropriate since the data form a straight line through the base point where no artificial remnant is added. (To see this consider a 100 Hz component of mis-modeled remnant. This would displace the incremented remnant data to the right, and a kink would show in the data.)

Although this method of modeling remnant with noise injection is useful, newer methods have been developed at Northrop and are now going into use. If one considers the physical sources of remnant, there are three contributions. The first, observation error, is modeled by using available human factor data to randomize the information going to the pilot model. This corresponds to various threshold and discrimination limits of the human in a given control environment. The second, internal human data processing, is modeled by perturbing the constants (gain, lead, and delay) of the linear model. The final source of remnant is human actuation noise. Here again human factor data are used to estimate the accuracy of control positioning and the actuation noise is modeled by randomization.

In this way, the fundamental program of replacing statistical models of the human controller by dynamic models becomes complete.

APPLICATIONS AND FURTHER RESEARCH

Since these methods of digital simulation and multi-axis pilot models allow large scale maneuvers to be studied as the closed loop nonlinear and time-varying problems that they are, there are a large number of applications which can be undertaken. The following is just a sample of the scope of problems now possible. Northrop is currently working on several major examples, and further work will include as diverse a collection as possible.

WEAPON DELIVERY

Both air-to-air and air-to-ground problems can be studied. In dive bombing, for example, the analysis includes target acquisition, roll-in, acquisition of the glide slope, tracking using the weapon sight, intense but briefly unstable attitude rate stabilization prior to weapon release, and pull up. The entire maneuver can be digitally "flown" many times in the presence of the realistic environment of low level turbulence and pilot induced system noise, and the statistics of impact error produced.

CARRIER LANDING APPROACH

The aerodynamics of carrier approach are not well represented by constant coefficient linear uncoupled dynamics. Furthermore, the landing task in the presence of low level turbulence and carrier roll and heave, make the use of the exact nonlinear models of the problem necessary. Much has been learned from linear methods about the form of the control strategy that the pilot must use, and the study of the behavior of the multi-axis pilot model can utilize this information to produce a comprehensive analysis of the entire maneuver.

VTOL HANDLING QUALITIES

The hover problem discussed above is just an illustration of the application of multi-axis pilot models to the study of VTOL handling qualities. The most interesting problem is to investigate the handling qualities of the nonlinear vehicle from hover through transition.

COORDINATION OF ANALYSIS AND FLIGHT SIMULATION

The multi-axis pilot model technologies developed at Northrop will not replace piloted flight simulation, but in fact can be used to greatly improve its efficiency. Not only will consistent analytical and experimental results give greater credibility to both, but the ability to screen away needless experiments by analysis will also improve the overall efficiency of aircraft evaluation and design.

LOSS OF CONTROL AT HIGH ANGLES OF ATTACK

Once aerodynamic descriptions of this flight condition are determined, the nonlinear and time-varying modeling capabilities of the Northrop methods can be immediately applied. The multi-axis pilot models required will be similar to the ones developed for attitude stabilization. As an example,

and a frightening one at that, consider Figure 23. This is the time history of one axis of a two-axis attitude stabilization problem. The system remained well-behaved for 120 seconds at which time a resonance effect coupled through the pilot model caused a sudden divergence of the system in .3 seconds.

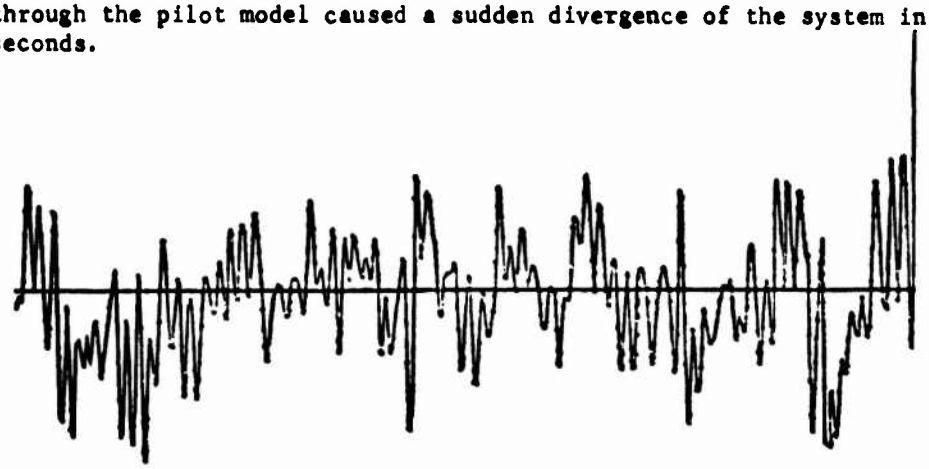

Figure 23. Sudden Loss of Control in a Two-Axis Task

Analysis and experimentation to determine more about this kind of system divergence is now in progress.

HANDLING QUALITIES SPECIFICATION

The ultimate objective of handling qualities specification is to ensure acceptable performance of piloted aircraft. Most often the only way to determine criteria is to hunt for physical aircraft characteristics that correlate strongly with desired system response. Historically, this has proved to be valuable for a large class of operational aircraft. Documents such as MIL-F-8785B "Military Specification of Flying Qualities of Piloted Aircraft" and the Background and Users Guide have been invaluable not only for aircraft evaluation, but also as a guide to preliminary design and the entire process of achieving a final system configuration. However, the advent of high authority control systems, control configured technologies, and the great premium on high performance vehicles gives much greater freedom to the range of basic airframe designs and control configurations. Consequently, many new kinds of systems are under development that may not be expected to fit the pattern of past aircraft and their associated parameter correlations with good pilot ratings.

In order to fill this broadened specification requirement, newer technologies that take into account the total pilot-vehicle system must be utilized. The use of linear pilot model theory in problems of pilot induced ocsillations (PIO) certainly demonstrates the importance of such analysis, but the possibilities now go significantly further. By directly modeling the specific missions that a system is designed to perform, as well as the general performance during all phases of operation, it is possible to obtain a comprehensive analytical assessment of the piloted flying qualities. Once the methods of linear pilot theory, digital

simulation, and urgency function multi-axis pilot models are generally used and experience is gained in their application, the realization of more definitive handling qualities criteria will follow.

FINAL REMARKS

The above discussion is but a survey account of Northrop research into urgency function pilot models and digital simulation as a handling qualities method. However, the examples presented above do illustrate the way in which the entire system can be modeled and evaluated. There is a wealth of additional information that has been generated during the last several years indicating many areas of pilot dynamics and task interaction. Some of these properties appear to be candidates for specification, and others indicate that substantial gains in piloted performance can be achieved in multi-axis optimization of many systems where the associated single axis tasks are well behaved.

The coupling of lateral and longitudinal tasks through the pilot as well as the nonlinear airframe in problems of landing approach, weapon delivery, and control at high angles of attack warrant an extensive investigation of nonlinear pilot-vehicle technologies. Northrop is vigorously supporting this direction of handling qualities research, and hopes that this account will stimulate similar work elsewhere; there are many important problems within reach.

REFERENCES

1. Onstott, E. D., and Salmon, E. P., Airplane Flying Qualities in Turbulence, AFFDL-TR-70-143 Air Force Flight Dynamics Laboratory, Wright-Patterson Air Force Base, Ohio Feb. 1971.

2. Onstott, E. D. et al, Prediction and Evaluation of Flying Qualities in Turbulence, AFFDL-TR-71-162 Air Force Flight Dynamics Laboratory, Wright-Patterson Air Force Base, Ohio Feb. 1972.

3. Onstott, E. D., Prediction and Evaluation of Flying Qualities in Turbulence, AFFDL-TR-72-92, Proceedings of the Eight Annual Conference on Manual Control.

4. Wanamaker, James E., and Sower, Wiliam, A., Extension of Pilot Describing Functions to Multiple Compensatory Tracking Tasks, Air Force Institute of Technology thesis GE/EE/69-18, Dayton, Ohio, 1969.

14-28,209#8

COMPARISON OF SEVEN PERFORMANCE MEASURES IN A TIME-DELAYED MANIPULATION TASK*

John W. Hill
Stanford Research Institute
Menlo Park, California 94025

ABSTRACT

Real-time performance data was collected during a pick-up task carried out with Rancho master-slave manipulator using a minicomputer-based data taker. Motions on all seven master and all seven slave joints as well as instantaneous electrical power consumed were continuously monitored. In addition to the usual task-time measurements, computer algorithms to integrate the energy consumed and to count and time the number of moves were implemented. In addition to these measures, several derived measures as the fraction of time moving (MRATIO) and mean time per move (MBAR) were obtained in an off-line analysis. A major goal of these experiments is to compare the seven different measures of performance to determine which are best for evaluating particular experimental conditions. Preliminary results of the time delay experiment indicate that two new measures, MRATIO and MBAR, are almost an order of magnitude more sensitive than task time, the conventional measure, in determining performance changes with transmission delays in the range from 0.0 to 1.0 second. Taking advantage of the operator's move-and-wait strategy, we also show how the energy consumed in carrying out a task can be reduced by a factor of three in the one-second transmission-delay case.

---

*This work was supported by the National Aeronautics and Space Administration under Contract NAS2-7507 to SRI.

BACKGROUND

In communication systems with transmission delay, such as those used in exploration of the moon or the planets, direct control by human operators becomes a very slow and laborious process. The problem is that the operator cannot see the results of an action until some later time determined by the transmission delay. During this period, the environment may have changed, or a movement may have overshot the target. The operator is thus forced into a move-and-wait situation in which his moves are cautious and are punctuated with periods of waiting to see the results of his actions. Physical fatigue and frustration may compound the problem.

In experiments with a two-degree-of-freedom master-slave manipulator, Sheridan and Ferrell (1963) and Ferrell (1965) found that open-loop task measurements made with no transmission delay could be used to predict performance times with 1.0-, 2.1-, and 3.2-second time delays using a simple model. Experimenting with a six-degree-of-freedom manipulator, Blackmer et al. (1968) found only fair correspondence between task times with no transmission delay and those with 1-, 3-, and 6-second delays using the Ferrell (1965) model. With a six-degree-of-freedom manipulator, Black (1970) showed a high correlation between task time and the number of moves with a 3.5-second delay.

The preliminary study summarized in this paper* was carried out to explore manipulation with a wide range of transmission delays. Shorter delays than those used in the previous studies (0.0, 0.3, and 1.0 seconds)

---

*A more complete description of the work reported here is given in a technical report (Hill, McGovern, and Sword, 1974).

were included to study the transition from continuous to the interrupted "move-and-wait" strategy. Delays longer than those used in previous studies (10 seconds) were included to determine the magnitude of the attentive or steadying problems that would develop. Main departures of this work from the previous experiments are (1) that no particular movement strategy was imposed on the subjects, and (2) that an automated, rather than subjective, method of counting and timing moves was used.

A COMPLEX MOVE-AND-WAIT STRATEGY

A time history of master moves and the subsequent slave moves is illustrated in Figure 1. A move is defined as the period of time between the beginning of a master move and the beginning of the subsequent master move. Each master move is considered to occur in three phases (Sheridan and Ferrell, 1963): move time, wait time, and reaction time, as defined below.

- M_m--Duration of master move.
- M_w--Time from end of master move to end of slave move.
- M_r--Time while master reacts to the consequences of his move and decides upon a subsequent move.

When a simple move-and-wait strategy is being used, the total task time can be expressed in terms of these times, using the following formula:

$$\text{Task Time} = \sum_{i=1}^{N} \left(M_{mi} + M_{wi} + M_{ri} \right) ,$$

where N is the total number of moves required to complete the task.

A complete description of the situation, however, requires the specification of both the system transmission delay and the slave movement times defined below that correspond to the previous master move times.

- T_d--Round trip transmission delay
- S_r--Slave reaction time
- S_m--Duration of slave move
- S_w--Same as M_r.

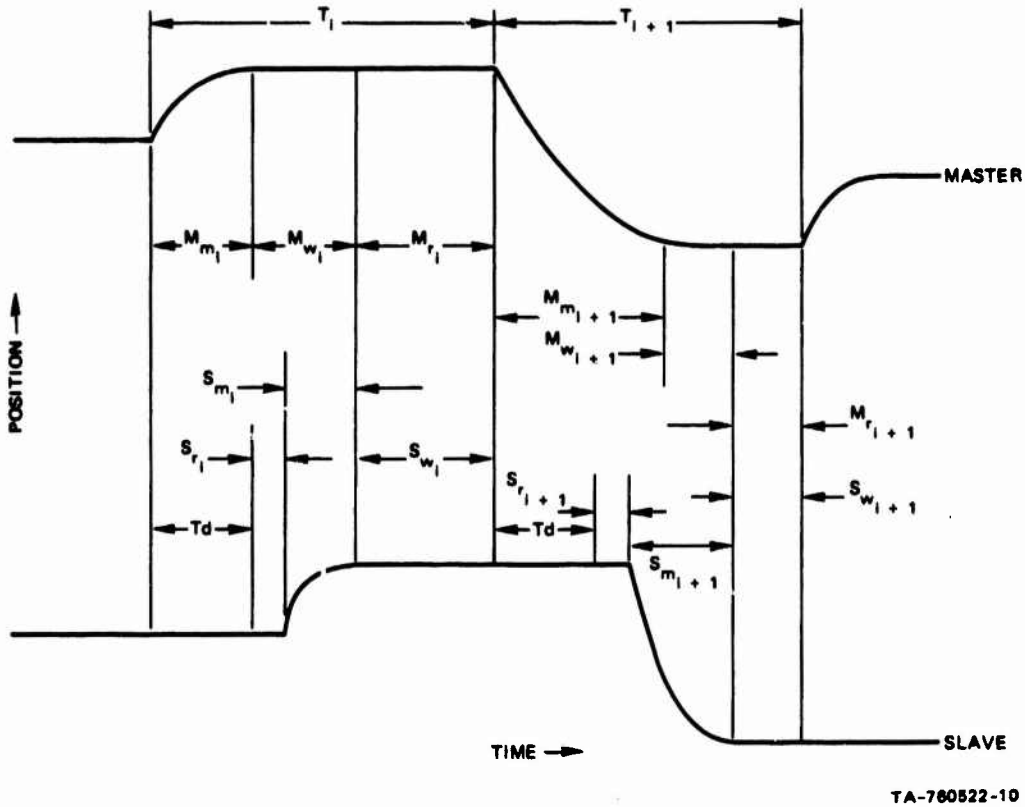

FIGURE 1 TIME HISTORY OF THE i^{th} AND THE $i + 1^{st}$ MOVES FOR A MOVE-AND-WAIT SITUATION

If the master follows a true move-and-wait strategy and does not move again until the slave has finished moving (simple move-and-wait strategy), the relationship shown in Figure 1 exists among the above quantities.

To investigate these quantities and their relationship, the transmission delay simulation of the supervisory control system described by Hill and Sword '1973) was used. Preliminary investigations with delays between zero and five seconds indicated a considerable deviation from Sheridan and Ferrell's (1963) result; the simple move-and-wait strategy is not always followed. The longer the time delay, the more frequently complex moves are made before the result of the main move is evident. With a five-second time delay, for example, two or three moves are frequently given before their results are seen, as if the operator were impatient to see his results. In other cases, he overreaches his target and makes a second move while the first move is in progress. Examples of both simple and complex moves are indicated in the chart recording of Figure 2, obtained with the chart recorder monitor described by Hill and Sword (1973).

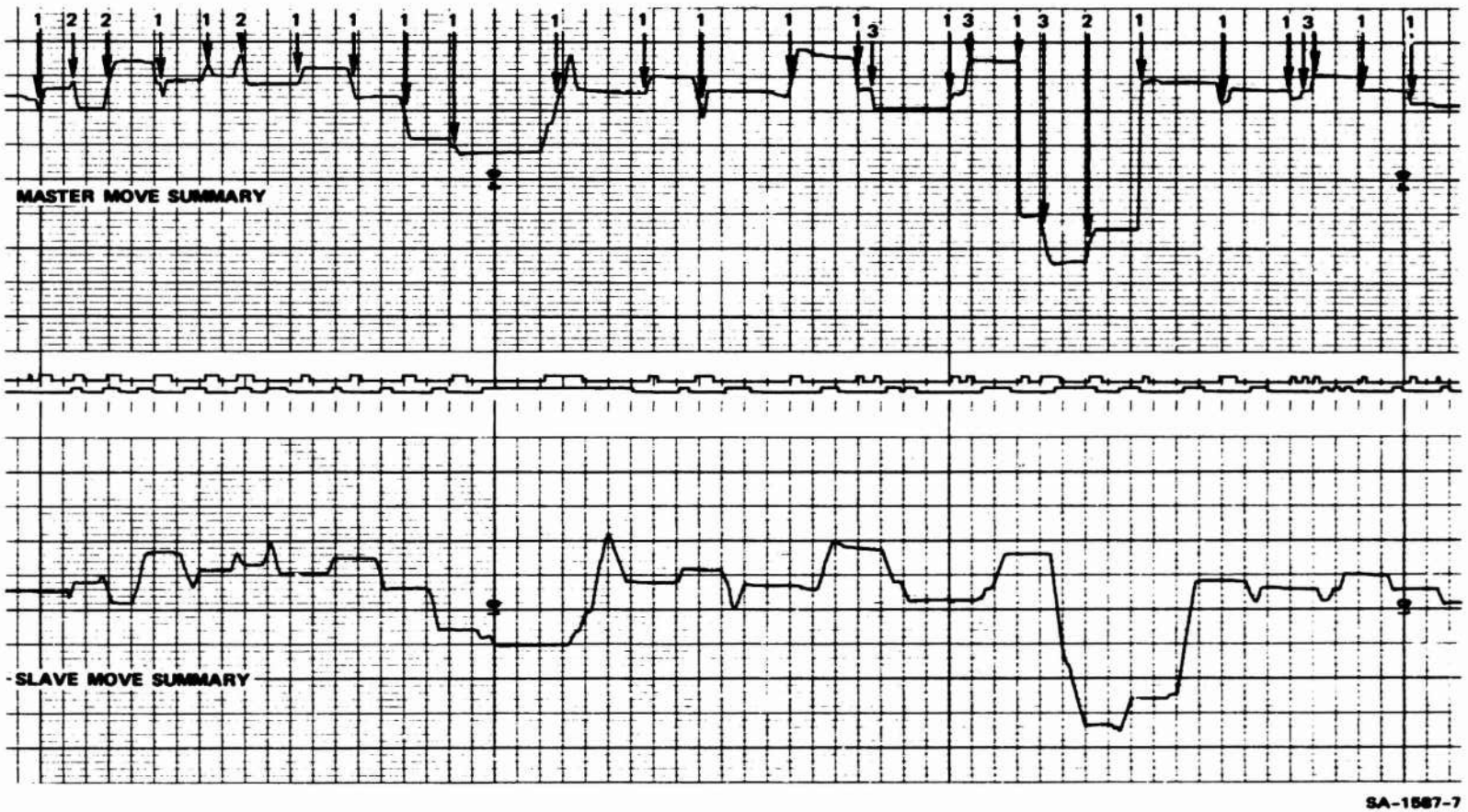

FIGURE 2 RECORD OF MASTER AND SLAVE MOVES WITH THREE-SECOND TIME DELAY

Master moves denoted by arrows are labeled according to slave motion: 1 indicates move while slave stationary (simple move-and-wait), 2 indicates move while slave moving (move-while-moving), and 3 indicates an additional move before result of first move seen (complex move-and-wait). (One time division = 2.5 seconds.)

MINI-COMPUTER-BASED PERFORMANCE MONITOR

A mini-computer-based performance monitor package was created to study (1) the complex move-and-wait strategy, and (2) the movement and waiting times with different transmission delays. A series of computer programs are used to measure and tabulate the movement and waiting times with considerably greater accuracy and reliability than is possible for a human observer with a stop watch.

The performance monitor package consists of an on-line program for data logging and several off-line programs for numerical analysis. During the experimental runs, a high-speed disk memory logs on-line data. After the experiment is completed the data are copied to magnetic tape for permanent storage. Different off-line programs are used to search the log and to extract the desired performance indices.

The on-line performance logger detects the beginning and end of moves by using derivatives of the individual joint angles. In total, 14 derivatives (seven master- and seven slave-joint angles) are updated and digitally filtered every 1/30th of a second. If any of the master or slave joints exceeds a predetermined threshold for motion during a 1/30-second period, a note of the fact is made in separate master- and slave-move detection queues. These queues (software shift registers) record whether or not a move was detected during 12 successive 1/30-second intervals. From these intermediate data, decisions are made to determine whether a master or slave move has begun or ended. The criteria for detecting the beginnings and ends of moves that have proved successful are defined below:

- Move criterion. A move begins when the velocity threshold is exceeded during the current 1/30-second interval and will be exceeded on five of the next 12 intervals.
- Done criterion. A move is done when the velocity threshold is not exceeded during the current interval and will not be exceeded more than once in the next 12 intervals.

Two total task measurements are also obtained. The on-line program counts the number of 1/30-second intervals taken to complete a task and logs the total at the end to permit the calculation of task duration. Additionally, it accumulates the current delivered by the 24-volt servo power supply every 1/30th of a second and logs the total at the end of the run to permit calculation of the total energy consumed.

One off-line program searches the data-log to calculate the following seven different measures for each test run:

M-MOVES	Number of master moves
S-MOVES	Number of slave moves
ENERGY	Total task energy consumed
TIME	Total task time
MTIME	Total time during which the master was moving
MRATIO	MTIME/TIME, or the fraction of task time the master was moving
MBAR	MTIME/M-MOVES, or the mean time per move.

A second program can be used to determine the distribution of movement times from a particular set of test runs. Any of the master- or slave-movement times defined in Figure 1 can be analyzed. Details of the on-line and off-line analysis procedures are given by Hill and Sword (1974).

The experiment is arranged in a 3 × 5 × 2 factorial design, as shown in Figure 3. Each cell in the design represents a performance characteristic measured on two subjects in eleven repetitions of the task.

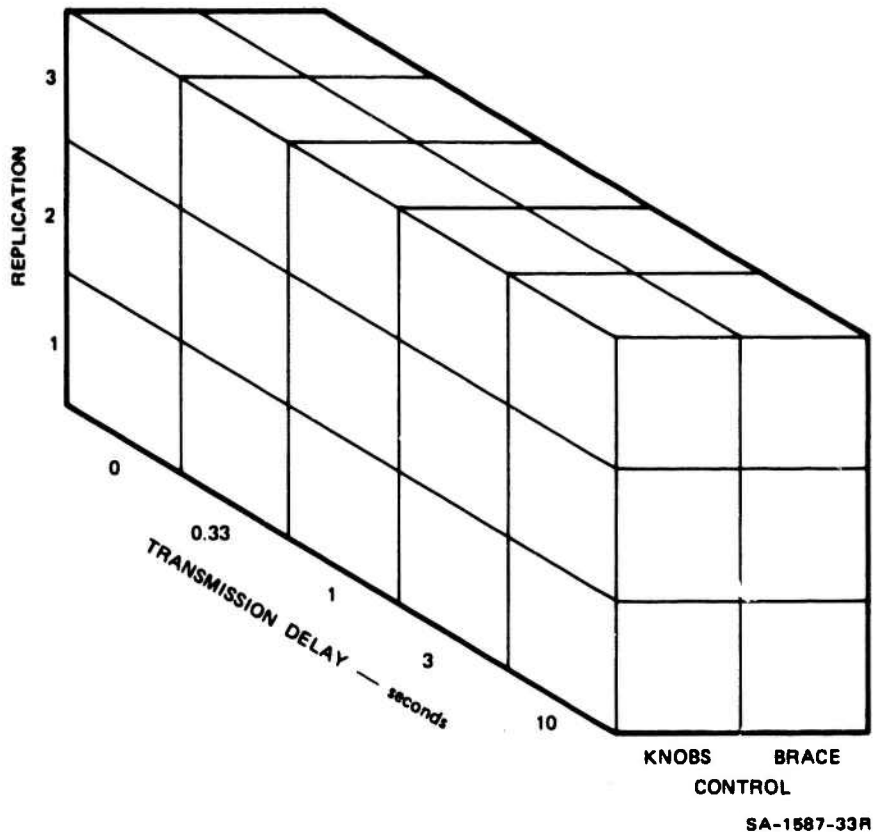

FIGURE 3 DESIGN OF THE PILOT TIME DELAY EXPERIMENT

The experiment variables are (1) manual control mode, (2) transmission delay, and (3) replication, as indicated in Figure 3. The manual control mode is varied by use of either the Rancho master brace or a bank of six potentiometers. Transmission delays from zero to ten seconds are provided in both control conditions, and in all replications by using the 30-Hz delay line simulation (Hill and Sword, 1973). Direct viewing was used, and audio cues were provided in all experimental cases.

Apparatus

The Rancho arm and computer-augmented control system described by Hill and Sword (1973) in Section II of Reference 1 were used for this experiment. The control modes were solely manual, master-slave modes.

No sensory feedback other than direct vision was provided to the operator. The task was to pick up a block randomly placed within the arm workspace and deposit it in a small container.

Subjects

Two male subjects, LM and SM, were used for this experiment. Both had had considerable experience in using the manual control modes for a pickup task. However, neither subject had ever attempted the task with a transmission delay.

Procedure

The on-line performance logger is started by the experimenter when the end effector passes through a plane one foot above the table top on the way down to grasp the object. The experimenter detects the plane crossing by observing a pointer attached to a string running over a pulley on the ceiling attached to the end effector. The task is complete when the object is grasped and deposited in the receptacle about one foot away, and the end effector moves up above the plane. Simultaneously, the experimenter stops the performance logger by typing a letter on the control teletype. The difficulty of both the pickup and drop tasks is about 3.5 bits.

In a single replication, each subject performed 10 runs consisting of 11 repetitions each. Five runs, each corresponding to one of the transmission delays, were performed, using each of the two control modes. This sequence was repeated three times for each subject (three replications). In all, each subject made 330 individual pickups.

RESULTS

The average number of master moves per pickup as a function of transmission delay is shown in Figure 4.

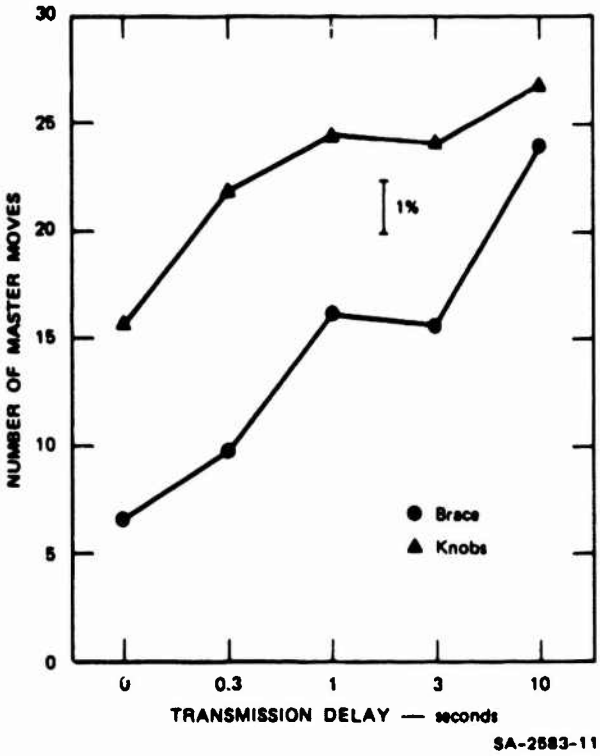

FIGURE 4 NUMBER OF MASTER MOVES IN TIME DELAY EXPERIMENT

The increasing number of moves suggests that in the zero- to one-second time-delay region, the control strategy is being continuously changed from continuous control to the move-and-wait strategy. Between the one- to three-second delay region, the number of moves is constant, suggesting a constant move-and-wait strategy; and at 10-seconds' delay, problems of holding the brace stationary for such a long time cause an increasing, perhaps unintentional, number of brace moves. In going from

three to ten seconds, the number of knob-generated moves does not increase as much as the number of brace-generated moves. If the time delay were increased much beyond ten seconds, the knobs would become the preferred control mode. The constant number of moves in the one- to three-second range agrees with the results of Sheridan and Ferrell (1963), and Ferrell (1965), who explored only this range. Outside this range, however, different explanations must hold.

Two other measures, task time and the time spent moving the master, are both shown for comparison in Figure 5. Whereas the task time increases

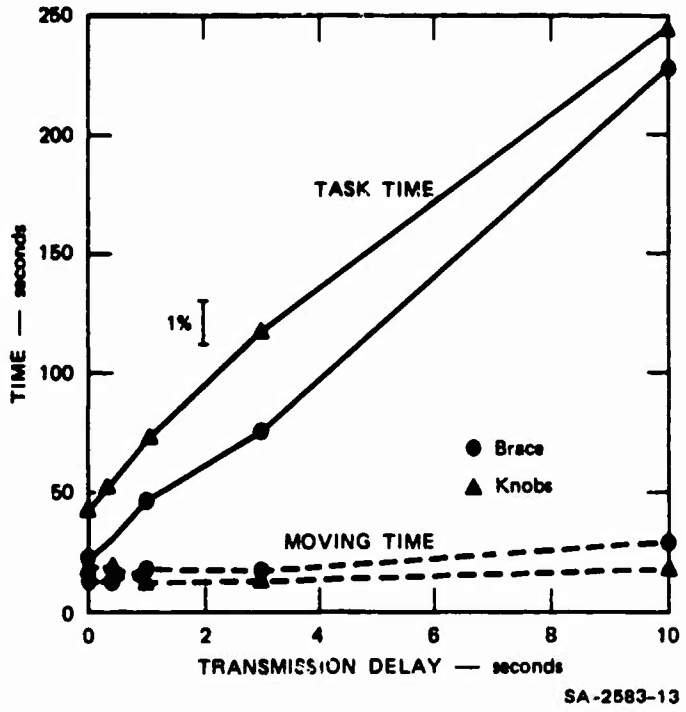

FIGURE 5 TASK TIME AND MOVING TIME IN THE TIME DELAY EXPERIMENT

almost directly with the time delay, the moving time is nearly constant at about 20 seconds, independent of time delay. The task time with the control brace can be simply modeled as a fixed time of 20 seconds plus 20 additional seconds for every second of transmission delay:

$$TIME_b = 20 + 20 \text{ (transmission delay)} \quad . \qquad (1)$$

The additional time (or cost) for using the simpler control source (knobs instead of brace) is roughly 25 seconds, giving:

$$TIME_k = 45 + 20 \text{ (transmission delay)} \quad . \qquad (2)$$

An expanded plot of the relatively constant moving time is given in Figure 6. It can be seen that there is a statistically significant cross-over of moving times between 0.3- and 1.0-second-transmission delay, and

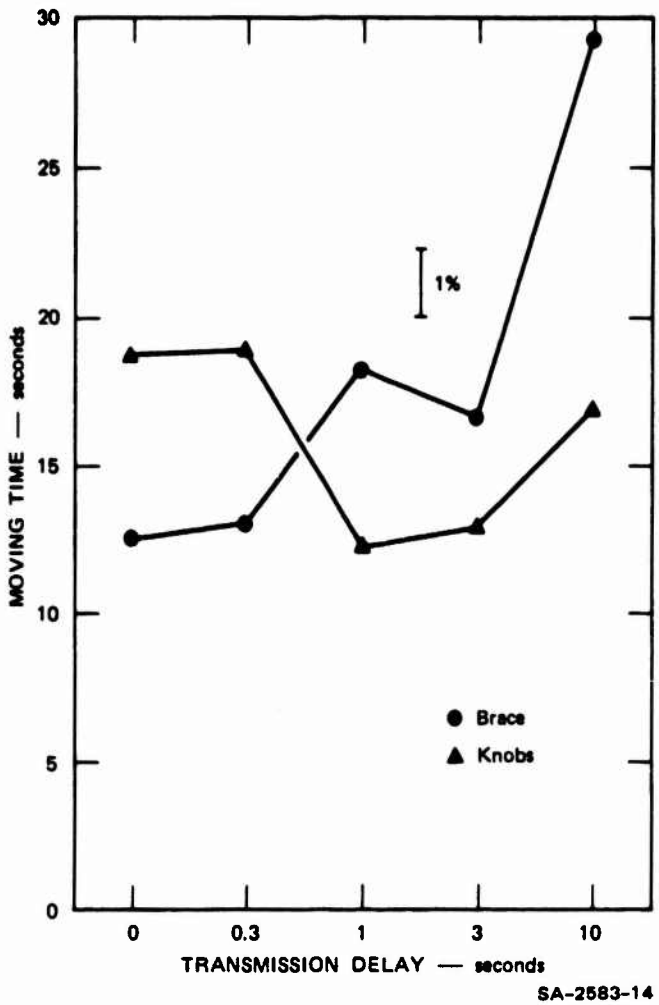

FIGURE 6 TOTAL MOVING TIME IN THE TIME DELAY EXPERIMENT

very large increase in brace-moving time with the 10-second delay. While the percentage changes in moving time are small compared to the other performance measures, the statistically significant crossover between 0.3- and 1.0-second delay (with less moving time for the brace at small delays, and less moving time for knobs at large delays), may be the result of a changeover from the continuous to the move-and-wait strategy in this range of time delays.

When the moving time is divided by the task time, we have the proportion of time moving; or by multiplying by 100, the percentage of time moving. This ratio, which turns out to be an exceedingly stable measure of performance, is shown for this experiment in Figure 7. In addition

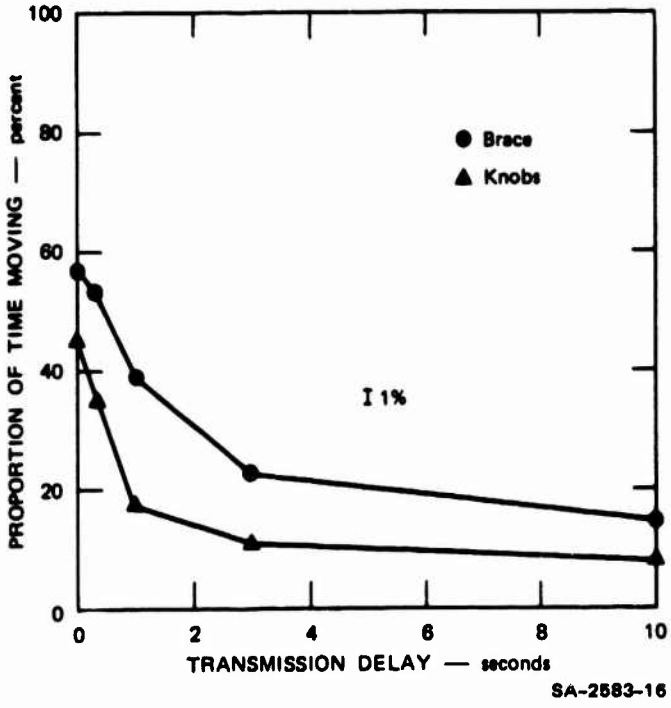

FIGURE 7 PERCENTAGE OF TIME MOVING IN THE TIME DELAY EXPERIMENT

to the low variance of this measurement, two surprising results are indicated in Figure 7. Looking at the intercept at zero time delays, we see that only about half of the time is spent moving in this condition.

Previously it has been assumed that in the zero time-delay condition the master brace was continuously moving. The low percentage of time moving (57 percent), together with the fact that there are about five brace moves during the task with zero time delay, tells us that there are several waits and that the waits are nearly as long as the moves. There are several possible alternative reasons for the apparent pauses (move-and-wait strategy) measured at zero-transmission delay. One reason may be inadequacy of the on-line performance logger. In this case, the velocity threshold used to determine whether the master is moving may be too high. Another explanation may be that the master was moved quickly and the slowly responding slave was still moving. In this second case, the operator would be waiting for the slave to come to rest before making another move. A third explanation may be that control with the brace is somewhat more difficult than has been thought, and that there is a time necessary at major-move points during the task, when the operator actually hesitates while deciding which joints to move next to produce the desired action.

Another surprising feature of the moving ratio of Figure 6 is that as the transmission delay increases, the curves do not approach their asymptotes as the reciprocal of the delay. The reciprocal relation would be predicted by the simple move-and-wait strategy of Sheridan and Ferrell (1963). The failure to hold with this relation is roughly a factor of two in the moving time ratios shown in Figure 7.

The reductions in the moving ratio with short transmission delays, in three replications of the experiment shown in Figure 8, suggest that the second of the above-mentioned three reasons explains the low moving ratios observed. Since the moving ratio decreases with practice, and the

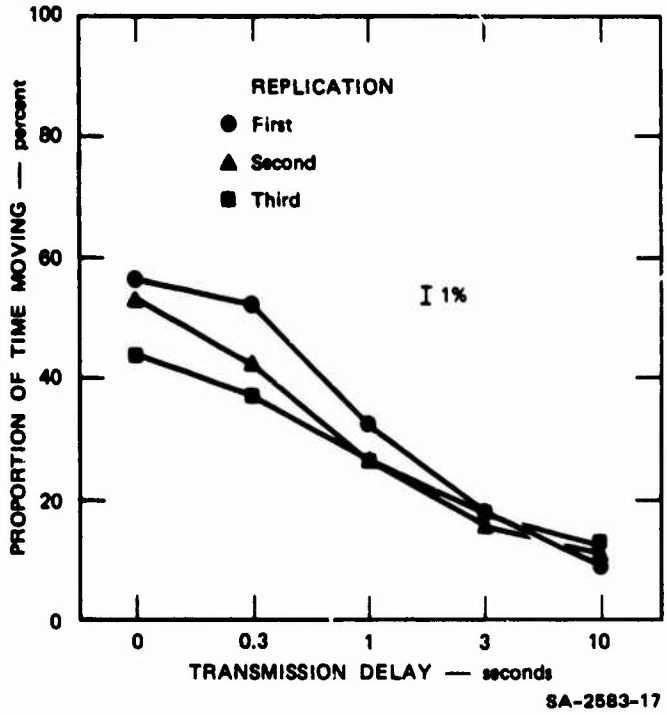

FIGURE 8 PERCENTAGE OF TIME MOVING FOR THE THREE REPLICATIONS OF THE EXPERIMENT

task time also decreases with practice, the first and third explanations are ruled out. The hypothesis that the long wait times are due to the operator's waiting for the slave to catch up with the master can be tested by further processing of the data taken.

The mean move-time results shown in Figure 9 suggest that the time required to make a single move with the knobs is half that of the control brace, independent of time delay. As was shown previously in Figure 4, however, a larger number of control movements are made with the knobs than the brace. Multiplying movement time by the number of control moves gives the relatively constant total moving time of Figure 6.

For both brace and knobs, the mean time per move decreases as the transmission delay is increased to one second, is constant with one- and three-second delays, and finally begins to increase slightly with ten

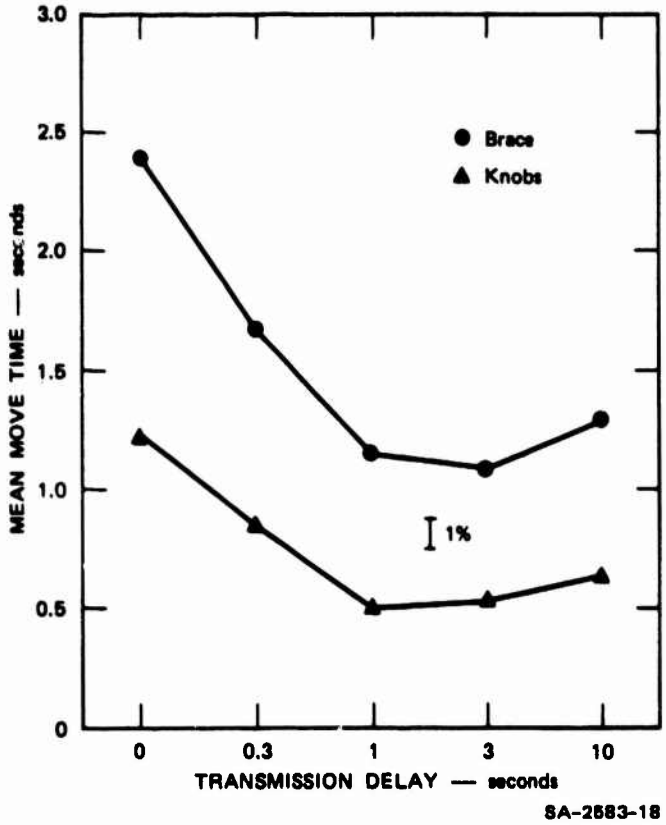

FIGURE 9 MEAN MOVE TIME IN THE TIME DELAY EXPERIMENT

seconds' delay. These changes are very similar to those seen in the number of master moves shown in Figure 7. For both curves, the changes seen over the first second of transmission delay reflect the increasing use of the move-and-wait strategy, and the constancy for delays of one second or longer reflects a fairly consistent move-and-wait strategy.

Energy Consumed and a Scheme for Reducing It

The energy consumed by the slave arm in carrying out the pickup task is shown in Figure 10. The energy consumption with increasing time delay is linear for both knob and brace control, and is very similar to the task-time results shown in Figure 3. The crossover between brace and

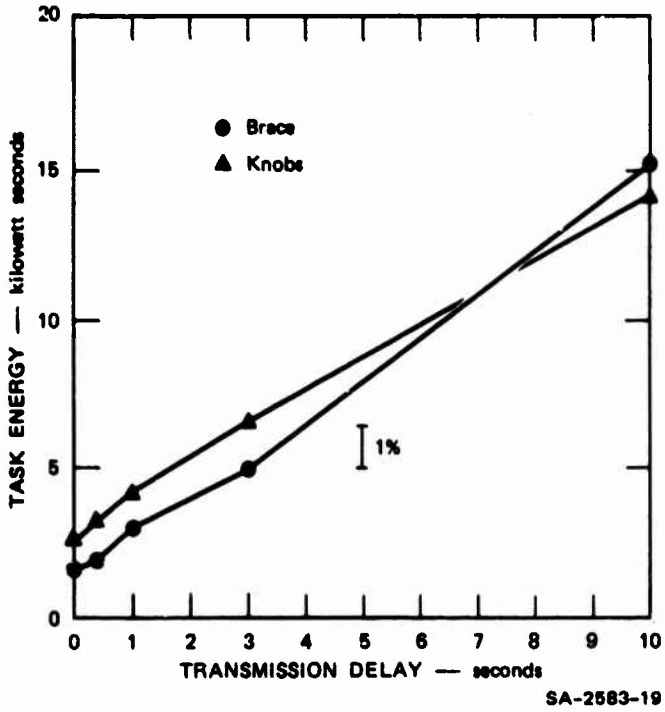

FIGURE 10 ELECTRICAL ENERGY CONSUMED IN THE TIME DELAY EXPERIMENT

knobs at the 10.0-second delay in Figure 9 is not statistically significant, and the energy consumed (in kilowatt seconds) for brace and knob control can be modeled as

$$\text{Energy}_b = 2 + 1.2\ (\text{transmission delay}) \quad . \tag{4}$$

$$\text{Energy}_k = 3 + 1.2\ (\text{transmission delay}) \quad . \tag{5}$$

The price for using the simpler control source (the knobs) is an additional kilowatt second.

Combining the relationship of the task time to transmission delay [Eqs. (1) and (2)] with the very similar relationship of energy to transmission delay [Eqs. (4) and (5)], we may express task energy in terms of task time for brace and knob control as

$$\text{Energy}_b = 0.8 + 0.06 \text{ (task time)} \quad . \tag{6}$$

$$\text{Energy}_k = 0.3 + 0.06 \text{ (task time)} \quad . \tag{7}$$

With the simple master-slave control scheme used in the laboratory, more energy is consumed in carrying out the same task as the transmission delay becomes greater. By using our knowledge that the total moving time for the task is relatively constant, even though the task time increases greatly with transmission delay (the difference between the task and moving time of Figure 3), we may design a remote control system that only requires a fixed amount of energy for a task, no matter what the delay. This can be accomplished by simply cutting off the power at the slave arm whenever it is at rest. Such a modification, taking advantage of the move-and-wait strategy to conserve power, could be implemented with individual threshold circuits on each joint, each circuit capable of turning off the servoamplifier whenever the error was less than a preset level.

DISTRIBUTION OF MOVEMENT TIMES

Using the off-line histogram program, we measured and tabulated the durations of the moving times. Ten distributions were obtained, one for each of the five time delays and each of the two control modes, by combining the data of the two subjects and the three replications of the experiment. These results are shown in Figures 11 and 12. The total number of moves under each curve and the mean moving time for each curve is given in Table 1.

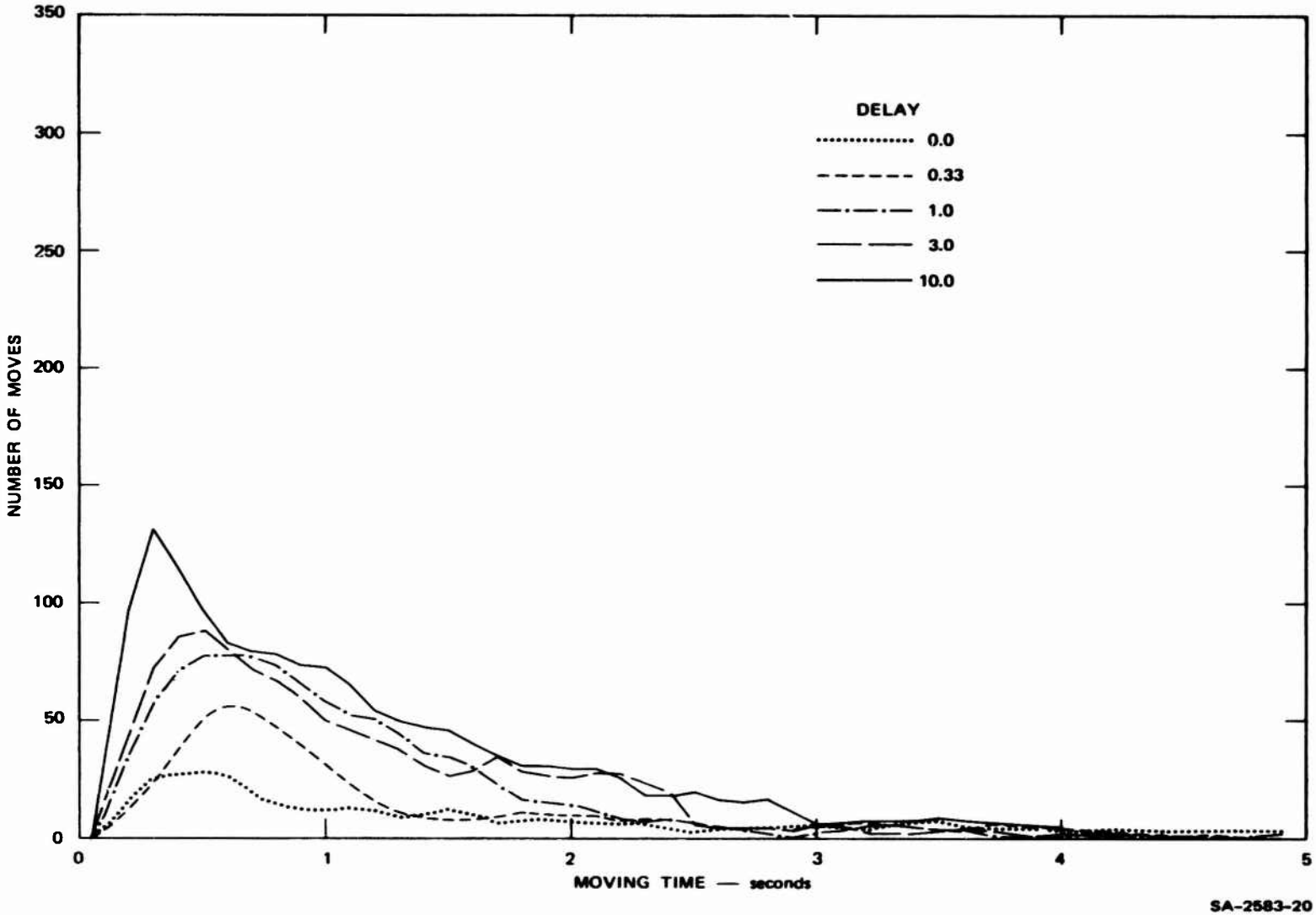

FIGURE 11 DISTRIBUTION OF MOVING TIMES WITH BRACE CONTROL

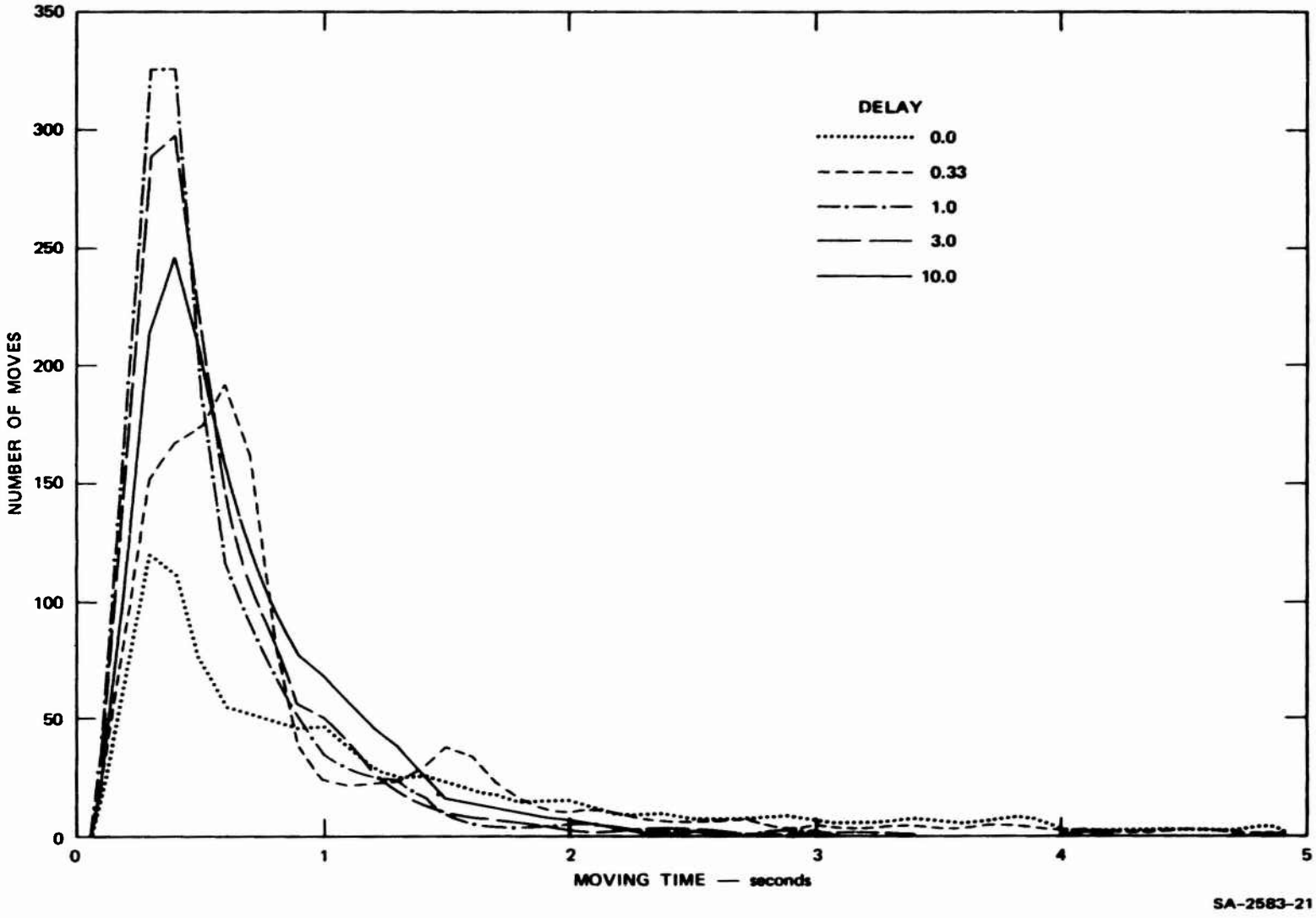

FIGURE 12 DISTRIBUTION OF MOVING TIMES WITH KNOB CONTROL

Table 1

TOTAL NUMBER OF MOVES AND MEAN MOVING TIME
FOR THE PILOT TIME DELAY EXPERIMENT

Control	Delay	Moves	Mean Move Time
Brace	0.0	427	1.938
	0.33	643	1.542
	1.0	1044	1.135
	3.0	1056	1.059
	10.0	1581	1.224
Knobs	0.0	1033	1.188
	0.33	1448	0.861
	1.0	1570	0.505
	3.0	1607	0.532
	10.0	1567	0.630

Several changes are obvious from the curves and data of Table 1. As the transmission delay increases, so does the number of moves of duration shorter than 0.5 second, with both knob and brace control. On the other hand, the number of moves longer than 2.0 seconds decreases with knob control, but increases with brace control, as the transmission delay increases. These differences may be due to the great increase in total moves (270 percent) with brace, and small increase with knobs (52 percent), as the transmission delay goes from 0.0 to 10.0 seconds.

A surprising feature of the brace-moving time distributions is the constancy of the shape of the distribution with increasing time delay. It has been assumed previously that going from continuous to delayed conditions caused the operator to change from continuous moving to abrupt, short moves and ensuing waits. The results of Figure 11, however, show that the moving times are very similar for continuous and time-delayed operation. There is a large proportion of long moves (two seconds or more) for all time delays.

The distribution of knob moves better fits the stereotyped change from continuous to move-and-wait strategy. These distributions (see Figure 12) can be visually broken down into the sum of two distributions, one peaking between 0.4 and 0.5 seconds, and a second continuous, long-tailed distribution similar to that of the brace distribution of Figure 11. As the time delay increases, the area under the peaked distribution greatly increases, while the amplitude of the long-tailed distribution greatly decreases.

COMPARISON OF SEVEN DIFFERENT PERFORMANCE MEASURES

An analysis of variance was made on each of the performance measures to determine their ability to distinguish between the four experimental variables: test subjects, replications, means of control, and time delays. The results of these analyses, summarized in Table 2, show that a large number of the variables and their interactions are statistically significant.

In addition to being a test of the null hypothesis for each variable, the F-ratios given in Table 2 are figures of merit for determining which of the seven measures best indicates changes from a particular variable or combination of variables. For a good performance measure, we want (1) large changes (large variance) in the measure with an experimental variable; and (2) small changes (small variance) in repeated measurements with the same conditions. The F-ratio is the ratio of the variance attributed to an experimental variable divided by the variance in repeated measurements. Thus, the larger the F-ratio, the better a measure distinguishes between experimental variables.

With the F-ratio used as a figure of merit, the largest F-ratio for each of the 15 sources of variation given in Table 2 is marked with a rectangular box. Surveying the seven performance measures indicates that only five rank largest in some source of variation; and of these, only three claim the great majority of the largest F-ratios. The three most important measures, in decreasing rank, are

- Moving ratio
- Total moving time
- Task time.

Table 2

SUMMARY OF SEVEN ANALYSES OF VARIANCE OF THE SEVEN MEASURES TAKEN IN THE PRELIMINARY TIME DELAY EXPERIMENT

Missing entries have F-values less than that given in the rightmost column and are not significant at the 0.01 level.

Source of Variation	df	M-MOVES	S-MOVES	ENERGY	TIME	MTIME	MRATIO	MBAR	$F_{0.01}$
Subjects (S)	1	7.71	--	--	11.50	--	8.97	--	6.63
Replication (R)	2	21.84	14.44	--	21.23	48.88	48.72	37.64	4.61
Control (C)	1	194.03	156.32	--	33.95	18.27	722.25	658.30	6.63
Delay (D)	4	65.99	54.12	194.43	282.21	29.65	897.38	213.34	3.32
S x R	2	--	--	--	--	--	--	--	4.61
S x C	1	--	--	--	--	--	--	--	6.63
S x D	4	--	--	--	4.99	--	5.14	--	3.32
R x C	2	4.83	--	7.58	5.71	5.85	16.76	9.93	4.61
R x D	8	--	--	--	5.71	3.43	16.17	17.83	2.51
C x D	4	6.61	--	--	--	35.66	25.96	13.34	3.32
S x R x C	2	--	--	--	--	--	8.65	--	4.61
S x R x D	8	--	--	--	--	--	--	--	2.51
S x C x D	4	--	--	5.52	5.82	--	--	--	3.32
R x C x D	8	--	2.95	--	--	4.43	4.38	11.23	2.51
S x R x C x D	8	2.87	--	--	--	--	--	--	2.51
Within repetitions	600								

These results indicate that different measurements should be made, depending on which experimental conditions it is desirable to compare. For example, differences between subjects are best measured with task time (TIME); and differences between control source are best measured with moving time (MTIME), or mean movement time (MBAR).

Another way of ranking the experimental variables is by the total variance attributed to each. This ratio lumps the test conditions and their interactions into one figure of merit and indicates for the experiment as a whole which measurement is best. The resulting variance ratios, given in Table 3, indicate that the MRATIO is clearly the best measurement, and that MBAR and TIME are the second best. For the experiment as a whole, MRATIO, the fraction of time moving, is by far the most sensitive measurement.

Table 3

TOTAL EXPERIMENTAL VARIANCE
DIVIDED BY ERROR VARIANCE

Variable	Variance Ratio
M-MOVES	12.06
S-MOVES	8.31
ENERGY	14.97
TIME	23.00
MTIME	8.03
MRATIO	81.09
MBAR	28.63

CORRELATIONS BETWEEN THE SEVEN PERFORMANCE MEASURES

Frequently two or more measures change nearly identically with the experimental variables. For example, the task time and the energy consumed both vary similarly for the different time delays and control sources. To determine the relation between the seven performance measures the pairwise correlation* coefficients based on all 660 measured values of each variable were computed. The results are shown in Table 4 as an array of correlation coefficients. Some interesting relations between variables shown in the correlation coefficients are mentioned below.

- The number of master and slave moves (M-MOVES and S-MOVES) are, as we might expect, highly correlated ($r = 0.961$); and we may consider that either of these two variables measures changes in the other. We recommend selecting the number of master moves as a performance measure and not being concerned with the number of slave moves.

- Task time and energy consumed are also highly correlated ($r = 0.913$), and we may similarly choose either of these variables as representative of the changes measured by the other. As time has been measured in these experiments as a matter of course, and is easy to measure without sophisticated equipment, we think time is a better measure of performance than energy. It is possible to express energy in terms of time, using the equations given previously in the discussion of energy.

- The last three variables, MTIME, MRATIO, and MBAR, correlate poorly with each other and with the other variables in the experiment.

---

*Pearson correlations, $r = \sigma_{xy}/\sigma_x \sigma_y$.

The total moving time, MTIME, does not correlate statistically with MRATIO or MBAR ($p > 0.01$), which indicates that the total moving time measures a performance characteristic that is independent of these other two variables.

This analysis shows that the number of performance measures can be reduced because of high correlations between some of the measures. Both the number of slave moves and the energy consumed may be omitted because of their high similarity to other measures. Taking the two measures

Table 4

CORRELATION COEFFICIENTS BETWEEN VARIABLES IN THE PRELIMINARY TIME DELAY EXPERIMENT

Coefficients not significant at the 0.01 level are designated by 0.

Variable	S-MOVES	ENERGY	TIME	MTIME	MRATIO	MBAR
M-MOVES	0.961	0.645	0.721	0.663	-0.525	-0.521
S-MOVES	--	0.645	0.707	0.607	-0.514	-0.491
ENERGY	--	--	0.913	0.532	-0.548	-0.240
TIME	--	--	--	0.530	-0.598	-0.289
MTIME	--	--	--	--	0	0
MRATIO	--	--	--	--	--	0.716

M-MOVES and TIME together with any one of the remaining three (MTIME, MRATIO, and MBAR), we may reproduce any of the others. This is true because of the relations between the variables as they are defined on the first page of this section. Because of its low variation, the choice of MRATIO (MTIME divided by TIME) as the third variable to complement M-MOVES and TIME seems a natural choice. As a consequence, three measurements, M-MOVES, TIME, and MRATIO are recommended as a complete description of time-delayed performance.

CHOICE OF MEASURES FOR FUTURE EXPERIMENTS WITH A TRANSMISSION DELAY

Though the range of delays used in this experiment varied from 0.0 to 10.0 seconds, the main purpose in analyzing it was to determine the ranges and usefulness of several performance measures in the transmission delay range from 0.0 to 1.0 second. These results will be used to design the main transmission-delay experiment, which will have a finer gradation of delay within this range.

To compare the seven different performance measures in the delay range from 0.0 to 1.0 second, certain measurements obtained with the control brace for two subjects are given in Table 5. The table presents in successive columns measurements taken with no delay and with 1.0 second delay; the percentage change of the measurements in going from 0.0 to 1.0 second delay; and the change measured in standard deviations in going from 0.0 to 1.0 second delay. A desirable feature of a performance measure is a large percentage change in going from one case to another. A more valuable feature, however, particularly for statistical comparison and hypothesis testing, is the change measured in standard deviations.

On the basis of the previous correlation analysis and the change in standard deviations from Table 5, the following conclusions may be made regarding measurements to be taken on the main transmission-delay experiment.

- M-MOVES is a better measure than S-MOVES (both are highly correlated), because of the greater change in standard deviations.
- TIME is a better measure than ENERGY (both are highly correlated), for the above reason.
- Neither TIME nor ENERGY is a really good statistical measure of performance, because of their low change in standard deviations over this delay range. TIME should be included in the analysis for comparison with results of past experiments.
- Of the last three new measures, MRATIO and MBAR are most reliable of all, showing larger changes (measured in standard deviations) than any of the other variables.
- MBAR, the mean move time, is by far the best measure, showing an overall change of more than two to one (the highest, except for M-MOVES), and by far the most reliable, with a change of 26 standard deviations.

Table 5

COMPARISON OF SEVEN DIFFERENT MEASURES OF PERFORMANCE WITH THE CONTROL BRACE AT ZERO AND ONE SECOND DELAY

Variable	$\Delta T = 0$	$\Delta T = 1$	Percentage Change	Change in Standard Deviations
M-MOVES	6.47	16.22	150	10.4
S-MOVES	5.47	13.53	147	8.9
ENERGY (kW-s)	1.56	3.05	95	2.8
TIME (s)	22.56	46.76	107	3.4
MTIME (s)	12.49	18.22	45	6.4
MRATIO	0.56	0.39	-31	-22.1
MBAR (s)	2.40	1.14	-52	-26.3

BIBLIOGRAPHY

Black, J. D., Jr., "Factorial Study of Remote Manipulation with Transmission Time Delay," Report DSR 70283-16, Engineering Projects Laboratory, Department of Mechanical Engineering, Massachusetts Institute of Technology (December 1970).

Blackmer, R. H., et al., "Remote Manipulators and Mass Transfer Study," Technical Report AFAPL-TR-68-75 (AD 843767 from NTIS), Air Force Aero Propulsion Laboratory, Wright-Patterson Air Force Base, Ohio (November 1968).

Ferrell, W. R., "Remote Manipulation with Transmission Delay," IEEE Transactions, Vol. HFE-6, pp. 24-32 (September 1965).

Hill, J. W., and A. J. Sword, "Studies to Design and Develop Improved Remote Manipulator Systems," NASA Contractor Report CR-2238, National Aeronautical and Space Administration, Washington, D.C. (April 1973).

Hill, J. W., D. McGovern, and A. J. Sword, "Study to Design and Develop Improved Remote Manipulator System," Final Report, Contract NAS2-7507, SRI, Menlo Park, California (May 1974).

Sheridan, T. B., and W. R. Ferrell, "Remote Manipulative Control with Transmission Delay," IEEE Transactions, Vol. HFE-4, pp. 25-29 (September 1963).

HUMAN OPERATOR WORKLOAD FOR VARIOUS CONTROL SITUATIONS

Wewerinke, P.H.

National Aerospace Laboratory NLR
Amsterdam, the Netherlands

ABSTRACT

This paper presents the results of an exploratory experiment which was conducted to investigate human response characteristics in control situations of widely varying difficulty. The experiment was aimed at a better understanding of the human operator limitations in terms of control effort as included in the optimal control model which is briefly discussed in the next section.

Based on the experimental results a workload index is presented which is consistent with those suggested by others in the past and an extended version of the workload index given by Levison et al (Ref. 3).

As will be shown the "predicted" workload correlates excellently with subjective ratings and seems to have a useful generality.

1 INTRODUCTION

The ever increasing complexity of man-machine systems necessitates a better understanding of the relevant human functions in order to base design problems on more rational principles. The study which is the subject of this paper concentrates on the human controller's function. This function is often important and even crucial in many man-machine situations.

Apart from human performance, which is for a given control situation directly related to system performance, it is also necessary to consider the effort the human has to exert to achieve that performance. Even this restricted concept of control effort has so far hardly obtained the attention which it deserves in many manual control problems.

In this paper an experimental program is reported which was conducted to explore human response characteristics in various control task situations. Experimental results were obtained in terms of subjective ratings and model parameters of the (fitted) optimal control model which is briefly discussed in the next section. In terms of these parameters a workload model is defined. The computed model "predictions" are compared with the subjective ratings. Also trade-offs between performance and effort are considered.

2 OPTIMAL CONTROL MODEL AND TASK INTERFERENCE MODEL

This section contains the principal features of the optimal control model of the human as a feedback controller developed by Kleinman et al (Ref. 1). Although the model is discussed extensively elsewere, it will be described briefly in this section for completeness sake.

The model is based on optimization and estimation theory and can be used for multivariable linear control systems. The basic assumption is that the well-trained, well-motivated human operator behaves "optimally" in some sense, subject to his inherent limitations and constraints and his control task.

2.1 System and task description

It is assumed that the system dynamics can be represented by the linear(ized), time-invariant equations of motion

$$\dot{\underline{x}} = \underline{A}\,\underline{x} + \underline{B}\,\underline{u} + \underline{E}\,\underline{w} \qquad (1)$$

where $\underline{x}$ is the vector of system states
$\underline{u}$ the vector of pilot control outputs
$\underline{w}$ the vector of linear independent Gaussian white noises.

The system outputs consist of the displayed variables and are assumed to be linear combinations of the state and control variables

$$\underline{y} = \underline{C}\,\underline{x} + \underline{D}\,\underline{u} \tag{2}$$

Primarily the perception of these variables ($\underline{y}_p$) is subject to the human's psychophysiological limitations.

The control task is specified in terms of a performance criterion that the human is to optimize. This criterion is incorporated in a cost functional, conditioned on the observations $\underline{y}_p$, which is minimal for the optimal control input

$$J(u) = E\left\{ \underline{y}'\underline{Q}\,\underline{y} + \underline{u}'\underline{R}\,\underline{u} + \dot{\underline{u}}'\underline{G}\,\dot{\underline{u}} \right\} \tag{3}$$

For relatively simple control tasks (single axis), good approximations to experimental measurements have been obtained (also in the present program) with a cost functional consisting simply of a weighted sum of system error variance and control rate variance. This cost on control rate results in a first order lag (time constant T_N) being introduced in the optimal controller.

2.2 Human limitations

The psychophysical limitations inherent in the human which are included in the model are represented by

$$\underline{y}_p(t) = \underline{y}(t-\tau) + \underline{v}_y(t-\tau) \tag{4}$$

indicating that the human perceives a noisy, delayed version of the displayed variables. $\underline{v}_y$ is a vector of white Gaussian observation noises, the autocovariance of each observation noise component appears to vary proportionally with mean squared signal level

$$V_{y_i} = \pi P_{y_i} E\left\{ y_i^2 \right\} \tag{5}$$

where P_{y_i} is the "noise/signal" ratio and has units of normalized power (positive frequencies) per rad/sec.

In order to model certain control situations adequately, it is necessary to include a motor noise term $\underline{v}_u$ in addition to the observation noise.

Also the motor noise vector is assumed to consist of independent, zero-mean, Gaussian white noises. The element of the autocovariance $\underline{V}_u$ is assumed to be

$$V_{u_i} = \pi P_{u_i} E\left\{u_{c_i}^2\right\} \tag{6}$$

2.3 Model structure

The model consists of a cascade combination of a Kalman filter, a least-mean-squared predictor and a set of gains, acting on the best estimate of the system states.

2.4 A model for task interference and workload

Levison et al (Ref. 3) define a workload index as the fraction of the controller's capacity that is required to perform a given task to some specified level of performance. The concept of this index is based on the assumption that the human operator possesses a fixed amount of (channel) capacity to be shared among his tasks It is straightforwardly derived from their model for task interference. This model is based on the assumptions that

- multiple tasks are performed in parallel
- the human operator has a fixed amount of "information-processing" capacity ("channels") to distribute among his various tasks
- each information-processing channel is perturbed by a white, Gaussian noise process which is linearly uncorrelated with all other noise processes and system variables. The noise levels are proportional to signal variance.

The model implies that the power spectral density level of the equivalent observation noise process (all sources of randomness of the human operator are reflected to his input) is inversely proportional to the fraction of capacity that is required to perform a given control task (m)

$$P_m = \frac{P_o}{f_m} \tag{7}$$

where the observation noise ratio P_o corresponds to "full capacity". The workload index is defined as

$$WI = \frac{P_o}{P_c} \qquad (8)$$

where P_c is the noise ratio corresponding to the required level of system performance.

The generality of the aforementioned model is limited because the workload index is highly task-dependent and "calibration" experiments will be necessary to determine the human operator's "full" capacity in a given control situation. Next the fraction of this "total" capacity can be determined in multiple-tasks situations. As such, the workload index serves only as a means for comparing the relative load imposed on the human operator by various tasks.

In order to derive an absolute workload metric which can be used to predict the load imposed on the human operator in new control situations, it is necessary to determine

- how the total capacity is related to the human operator's environment, specifically, the task variables.
- the relationship between the actual effort the human operator exerts and the demand of the task.

The primary goal of the experimental program discussed in the next section, was to provide data for a variety of control situations to build and validate an absolute workload model.

3 EXPERIMENTS

3.1 Experimental conditions

In order to include all possibly important characteristics of pilot behaviour in control situations of (our) interest, a variety of single-axis control tasks were performed by four well-trained, highly motivated subjects (experienced fighter pilots). The controlled elements are summarized in table 1. As shown in the table, the choice of the tasks were mainly determined by two characteristics: pilot equalization and the sensitivity of task performance to the effort exerted by the human operator. The latter was considered to be an important aspect of the given problem and a means to achieve sufficient variation in task difficulty to

obtain statistically significant differences in the experimental data: scores of system parameters of interest, frequency domain measures (describing function and remnant data), and subjective information by means of the rating scales given in table 2. Three scales were presented to the subjects, a non-adjectival rating scale and two scales (controllability and demand on the pilot) adapted from reference 4.

The task was to regulate against a disturbance input. The inputs were summed sinusoids to provide signals that were random appearing and whose spectra approximated white noise filtered by a second order filter with a pole at 2 rad/sec and a mean-squared value of 1.2 cm^2 on the display for the position control task. For the rate- and acceleration control tasks the disturbance spectra approximated white noise processed by a first order filter with a pole at 1 rad/sec entering the system as a velocity disturbance with a mean-squared value of 1 cm^2/sec^2. The system output was displayed on a CRT. The display format was a cross. The distance of the eye to the CRT was such that 1 cm on the display corresponded to 1 deg visual arc. The subjects manupulated a force-sensitive hand control.

3.2 Experimental results.

The experimental results are presented in terms of scores and frequency domain measurements (describing function and equivalent observation noise). The inter- and intra-subject variability was sufficiently small to obtain meaningful measures that were representative of subject behaviour in general by averaging the measures of the subjects and the replications (four subjects, three runs/subject).

Both the measured scores and the frequency domain measurements were matched with the model results by adjusting the following model parameters:
the relative weighting on control rate variance (uniquely related to the lag factor T_N), the time delay, the observation noise ratios, associated with both position and rate of the display indicator, and (if necessary) the motor noise ratio. The model parameters obtained are given in table 3.
Table 3 reveals that the time delay τ is essentially constant for all the tasks. Also the lag factor T_N exhibits a relatively small variation. As distinct from results reported in reference 5 different observation noise ratios to be associ-

ated with position and rate informations were necessary to obtain a good match to the measured remnant spectra. For the acceleration control tasks the values of the position noise ratios are somewhat arbitrary because both scores and frequency domain measurements are hardly changed by an increase of this noise ratio of -10 dB to -20 dB. For the acceleration tasks a substantial motor noise level had to be included.

The scores obtained from the experiments and from the model are shown in table 4. As can be seen from this table the model scores agree very well with the measured scores. The frequency domain measures in terms of describing functions and normalized observation noise spectra are given in figures 1-6. As can be seen from these figures the agreement between experimental frequency domain measures, and the measures obtained from the model is good.

The subjective ratings were normalized so that the ratings of every subject had a mean of zero and a standard deviation of unity (z-scores). Next, the ratings of the subjects were averaged. The correlation between the ratings of the effort scale and the data of the demand scale was very high (linear correlation coefficient of .99). Hence, only the ratings of the (non adjectival) effort scale (table 5) are considered in the following discussion.

The aforementioned results have shown that

- for a variety of control situations the available measures of human operator behaviour can accurately be duplicated by the optimal control model by primarily a variation in the pertinent noise ratios
- The values of the noise ratios are task dependent
- The effort involved in achieving the pertinent noise ratios is clearly task dependent.

The last observation can be demonstrated comparing the K with the K/s configuration. The control effort according to the subjective ratings was for both tasks the same, yet the observation noise levels are substantially lower for the position control task. Evidently, it was easier for the subjects to realize these low noise ratios for the position control task than in the rate control situation.

4 HUMAN OPERATOR WORKLOAD MODEL

Based on the foregoing observations a control effort index is proposed in accordance with work done by other researchers and consistent with some notions of attention and effort of the experimental psychology (Refs. 6 and 7).

The index is based on the following notions:

- Human operators behaviour is partly determined by mechanisms that control the choice of stimuli, by which is meant both selectively attending to some stimuli in preference to others and investing more or less attention per source of information. This can be identified with voluntary attention, reflecting that the subject attends to the stimuli because of their relevance for performing the task and not only because of their arousal function.
- Also the aspect of involuntary attention has to be included in the index. This can be related to the level of arousal and is largely dictated by the properties of the stimuli. Processing novel and surprising stimuli involves more effort than in the situation of more familiar stimuli.

The formes aspect (voluntary attention) is incorporated in the control effort index in terms of signal to noise ratio of the various sources of information. This can be identified with the amount of attention as suggested by Levison et al. The latter aspect (involuntary attention) is included in terms of sensitivity of task performance (mean squared error or error rate) to the momentary attention paid by the subject as indicated by the pertinent signal to noise ratios.

Thus, the workload index can be represented as

$$W = \frac{S}{P} \tag{9}$$

with

$$S = \frac{\dfrac{\partial \sigma_x^2}{\sigma_x^2}}{\dfrac{\partial P}{P}} \tag{10a}$$

where σ_x^2 is now taken as the relevant performance index (variance) of quantity x

An alternate expression for S is

$$S = \frac{\partial \sigma_x^{2}(dB)}{\partial P\ (dB)} \tag{10b}$$

In control situations where more than one source of information is of interest (position information, rate information, etc.) the workload index is defined as the sum of the separate portions.

For the six control situations previously discussed the sensitivity parameter S was straightforwardly computed for the model parameters of table 3. The result is shown in table 6. Before going into a discussion of this table the relationship between the "predicted" workload and the subjective ratings is shown in figure 7. The relationship is surprisingly linear (r = .99!).

Returning to table 6 it can be seen that the effort involved in controlling the K-dynamics is primarily related to position information (which is well known). Most of the load imposed on controlling the K/s dynamics is related to rate information. Practically all the effort involved in the acceleration control tasks is connected to processing rate information (which was expected). The position of workload related to attending to position information is negligibly small. For the acceleration control situations where motor noise had to be included the partial derivative, $\frac{\partial \sigma_{\dot{m}}^2}{\partial P_{\dot{m}}}$, implied a constant motor noise ratio. The effect of motor noise on the workload index is implicit. The same is true for the other model parameters (time delay and lag factor).

It is interesting to consider the relationship between system performance and workload. For the position control task this is shown in figure 8.
Both position noise ratio and rate noise ratio are independently varied. The arrows indicate the levels of load imposed on processing position, respectively rate information. Figure 9 shows the same trade-off for the rate control task. As might be expected, exerting little effort gives a relatively large improvement in performance. Below a certain level of performance the effect of more effort is very small. One would expect the optimum trade-off at the "knee" of the curve. The experimental result confirms this. The same discussion is applicable to the acceleration control task. For this situation the pertinent relationship is visualized in Figure 10.

Important the predictive power of the model, in the case of new control situations.
The following procedure is suggested.

1. take a time delay of .20 sec and adjust the relative weighting on control rate to yield a lag time constant of approximately .1 sec.
2. Neglect motor noise or predict motor noise on the basis of the relationship between scores and motor noise ratio.
3. Starting with nominal values of observation noise ratios compute the trade-off between system performance and workload.
   In case the system performance is specified the workload is determined.
   Otherwise both system performance and workload can be established as suggested in Figs. 8-10.

5 CONCLUDING REMARKS

Also the present experiments have demonstrated that the optimal control model provides a useful tool to describe human operator behaviour in a variety of control situations.

The workload index suggested in this paper correlates surprisingly well with subjective ratings. By means of trade-off studies between system performance and pilot workload, the effect of task variables of interest in new control situations can be studied.

More control situations (also multiple control tasks) have to be considered to be able to extend the generality of the proposed workload index.

6 REFERENCES

1	Kleinman, D.L. Baron, S.	Manned Vehicle System Analysis by Means of Modern Control Theory. NASA CR-1753, June 1971.
2	Levison, W.H., Baron, S. and Kleinman, D.L.	A Model for Human Controller Remnant. IEEE Trans. MMS, Vol. MMS-10, No. 4, December 1969.
3	Levison, W.H., Elkind, J.I. and Ward, J.L.	Studies of Multivariable Manual Control Systems: A model for Task Interference. NASA CR-1746, May 1971.
4	McDonnell, J.D.	Pilot Rating Techniques for the Estimation and Evaluation of Handling Qualities. AFFDL TR 68-76, December 1968.
5	Levison, W.H.	The Effects of Display Gain and Signal Bandwidth on Human Controller Remnant. AMRL-TR-70-93, March 1971.
6	Kahneman, D.	Attention and Effort. Prentice-Hall Inc. 1973.
7	Berlyne, D.E.	Conflict, Arousal and Curiosity. McGraw-Hill, New York, 1960.

Pilot Equalization			
Lag	K		
"pure gain"	K/s	K/s-3	
Lead	K/s^2	K/s(s-.5)	K/s(s-1)
	increased sensitivity of tasks performance to "effort"		

Table 1 Controlled elements

Name:

Task:

Using the scale below, indicate the degree of effort you spend on performing the task

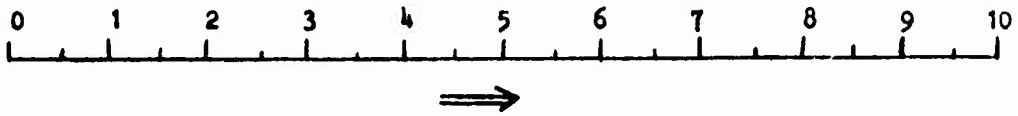

Rating scale for Control-lability and Precision

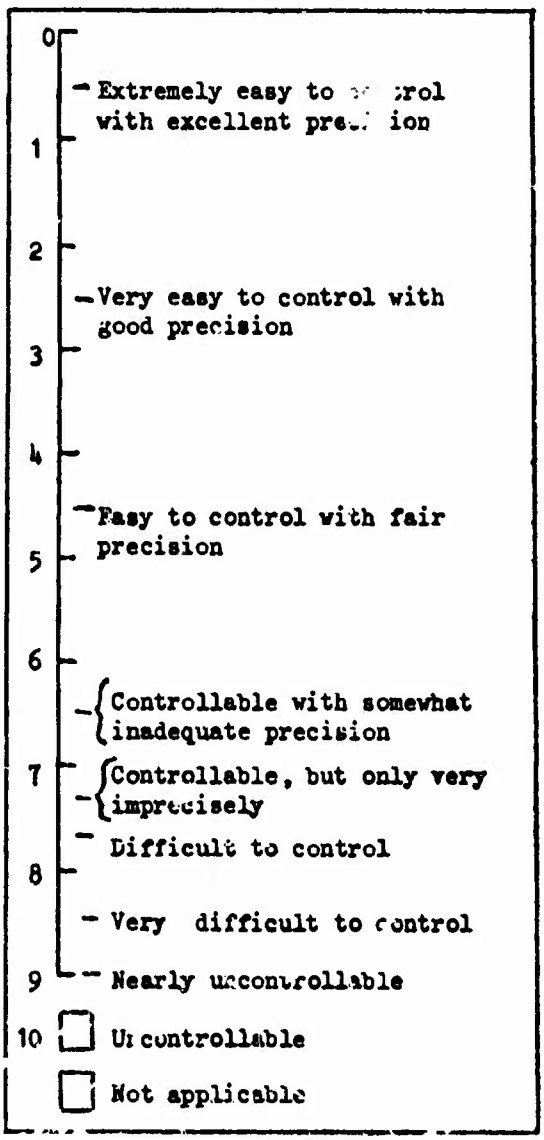

Rating Scale for Demands on Pilot

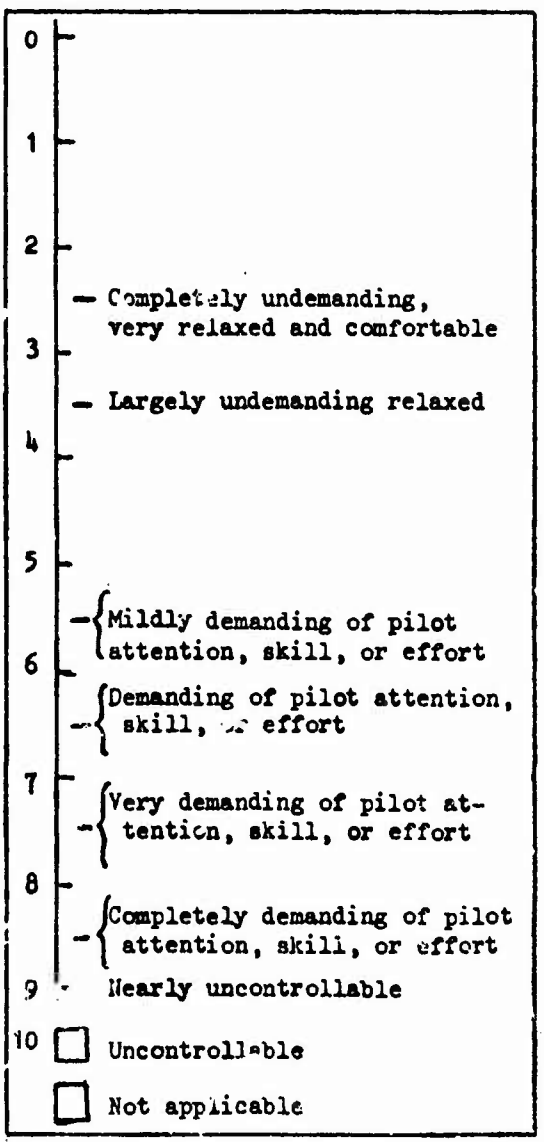

Controlled element	Time Delay τ (sec)	Lag Factor T_N (sec)	Observation noise ratio (dB)		Motor noise ratio (dB)
			P_m	$P_{\dot{m}}$	
K	.20	.07	-23.6	-26.0	-
K/s	.21	.13	-15.0	-21.2	-
K/s-3	.21	.09	-15.9	-25.0	-
K/s^2	.22	.11	-11.0	-27.1	-18.7
K/s(s-.5)	.22	.11	-20.0	-29.1	-18.8
K/s(s-1)	.22	.11	-20.0	-30.3	-19.0

Table 3 Model parameters

Controlled element	Score	σ_m^2 (cm^2)	$\sigma_{\dot{m}}^2$ (cm^2/sec^2)	σ_c^2 (N^2)
K	measured	.16		1.1
	model	.18	19.4	.9
K/s	measured	.072	.87	.33
	model	.073	.82	.31
K/s-3	measured	.54	5.0	.30
	model	.51	5.2	.30
K/s^2	measured	.29	2.0	.41
	model	.29	1.9	.41
K/s(s-.5)	measured	.49	3.4	.76
	model	.45	3.2	.75
K/s/(s-1)	measured	.98	6.9	1.7
	model	.97	6.4	1.6

Table 4 Scores obtained from experiment and model.

Controlled element	Subjective rating effort scale	
	mean	st.dev.
K	-1.40	.72
K/s	-1.18	.57
K/s-3	.49	.53
K/s^2	-.76	.73
K/s(s-.5)	.11	.59
K/s(s-1)	.55	.73

Table 5 Normalized subjective ratings.
Averaged over subjects and replications

Controlled element	S_m	P_m	$\frac{S_m}{P_m}$	$S_{\dot{m}}$	$P_{\dot{m}}$	$\frac{S_{\dot{m}}}{P_{\dot{m}}}$	W
K	.07	.004	17.5	.02	.0025	8.0	25.5
K/s	.11	.032	3.5	.18	.0079	23.0	26.5
K/s-3	.17	.025	7	1.0	.0032	325	332
K/s^2	-	-		.20	.002	102	102
K/s(s-.5)	-	-		.34	.0012	265	265
K/s(s-1)	-	-		.36	.001	360	360

Table 6 Computed workload for the various controlled elements.

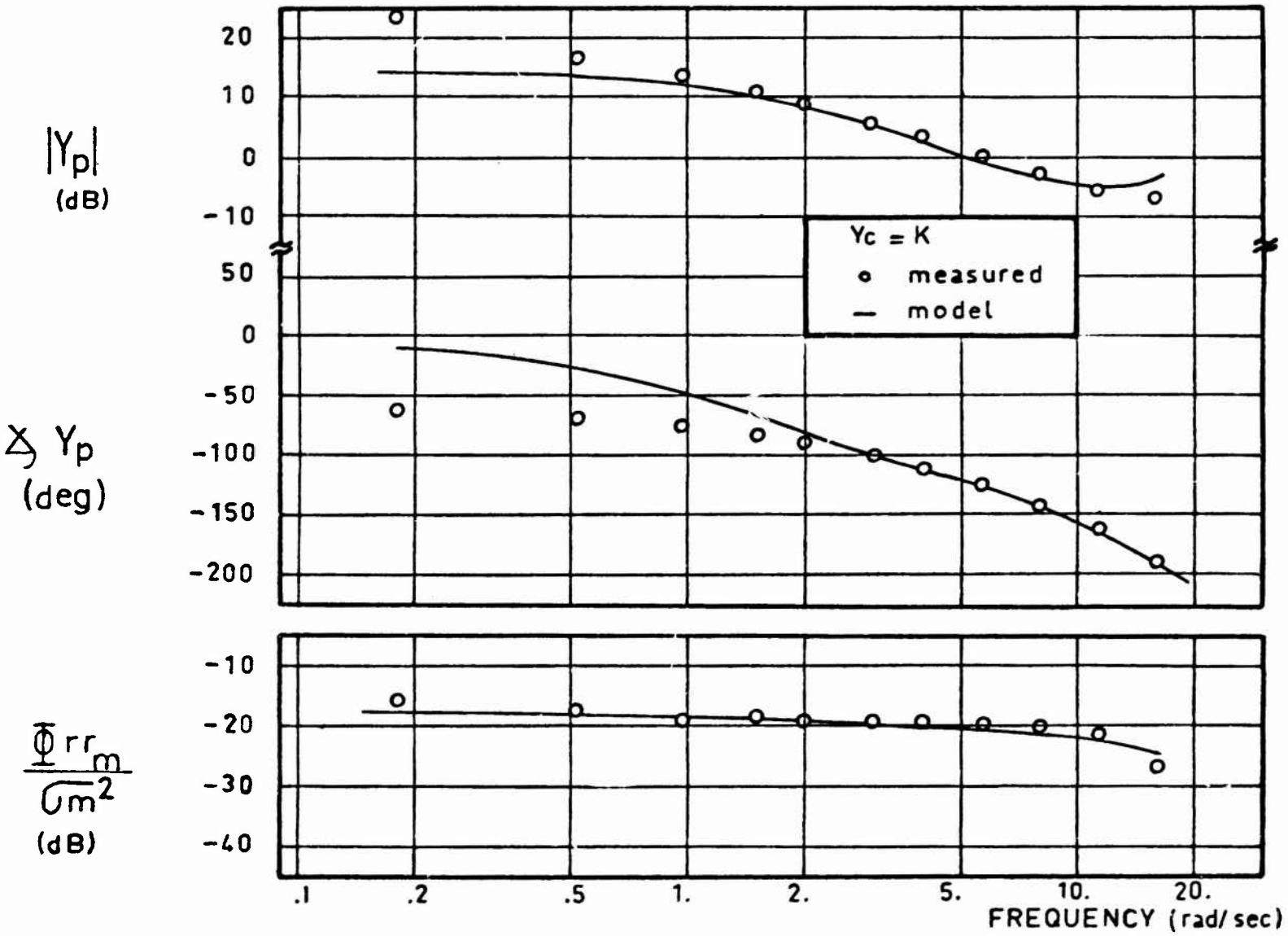

Fig. 1 Frequency domain measures - $Y_c = K$
Average of 4 subjects, 3 trials/subject

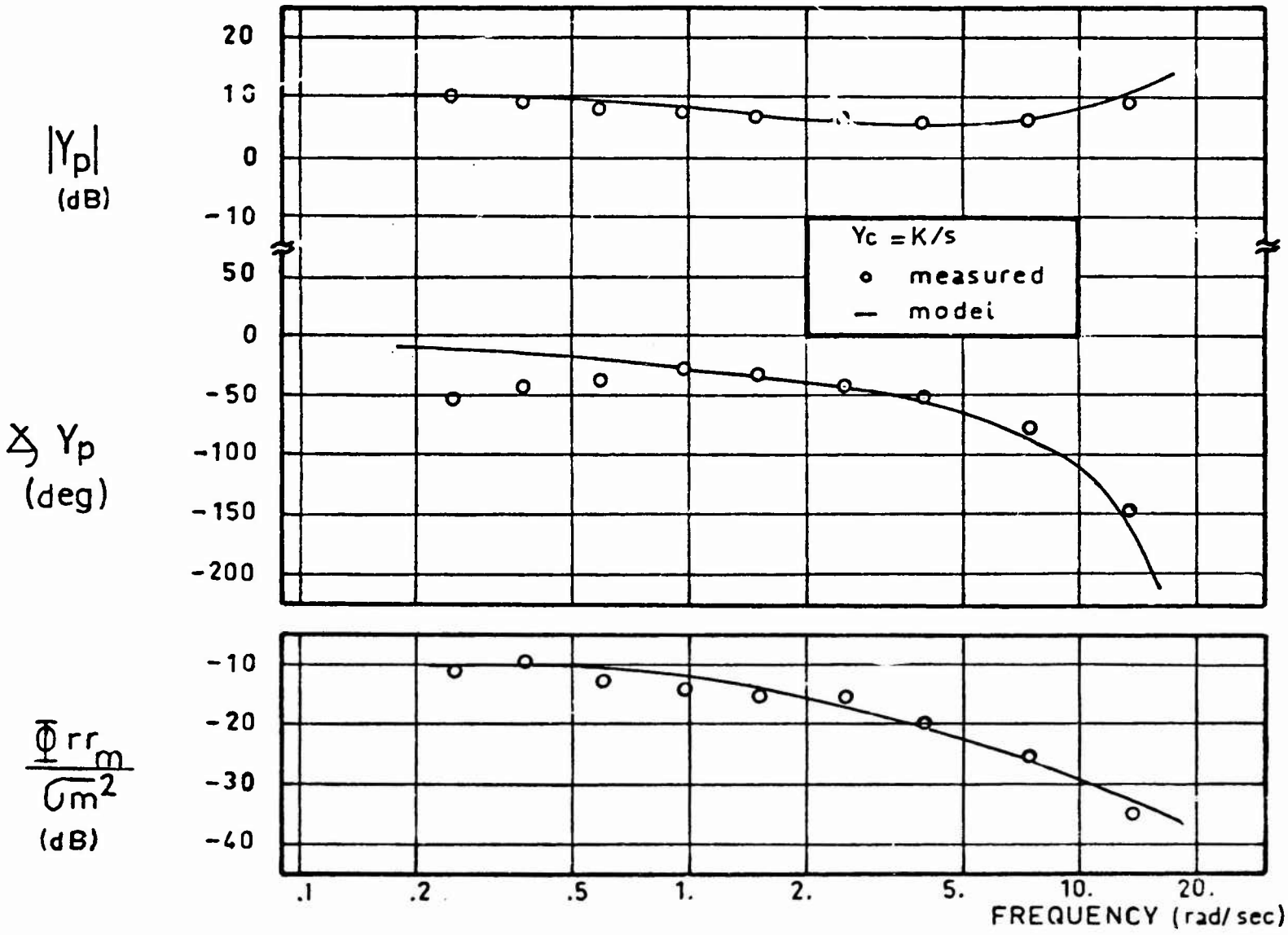

Fig. 2 Frequency domain measures - Y_c = K/s
Average of 4 subjects, 3 trials/subject

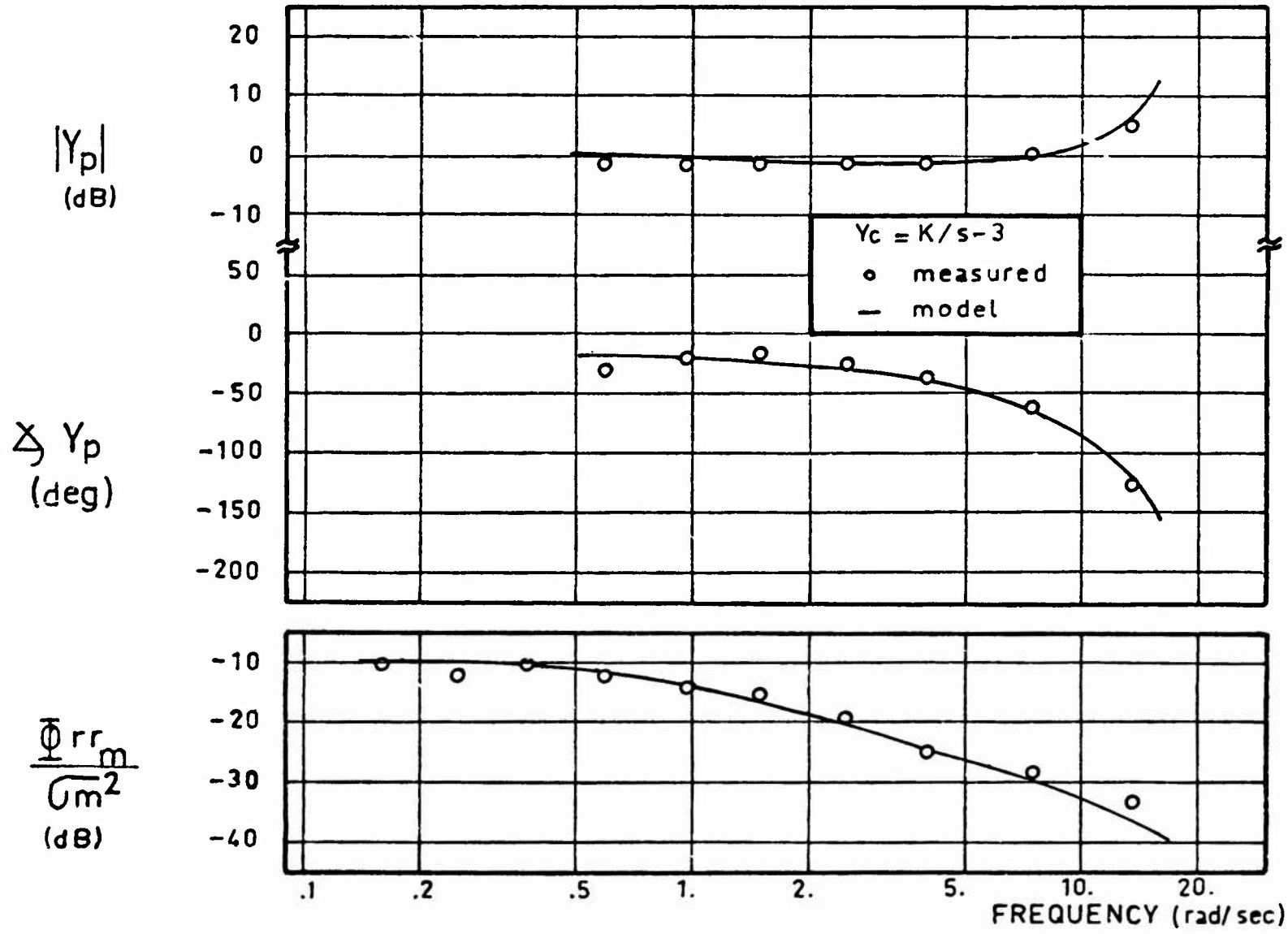

Fig. 3 Frequency domain measures - Y_c = K/s-3
Average of 4 subjects, 3 trials/subject

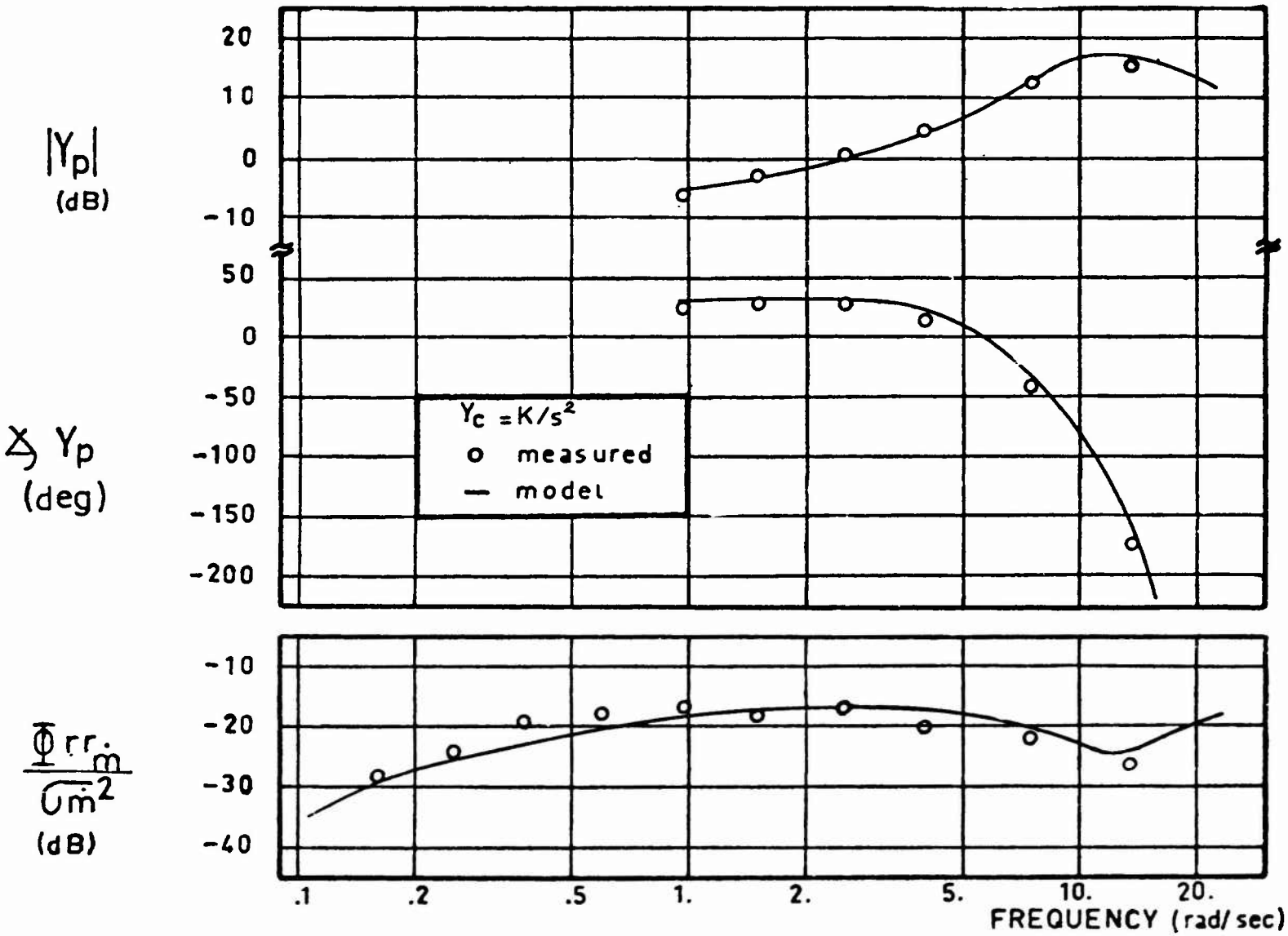

Fig. 4 Frequency domain measures - $Y_c = K/s^2$
Average of 4 subjects, 3 trials/subject

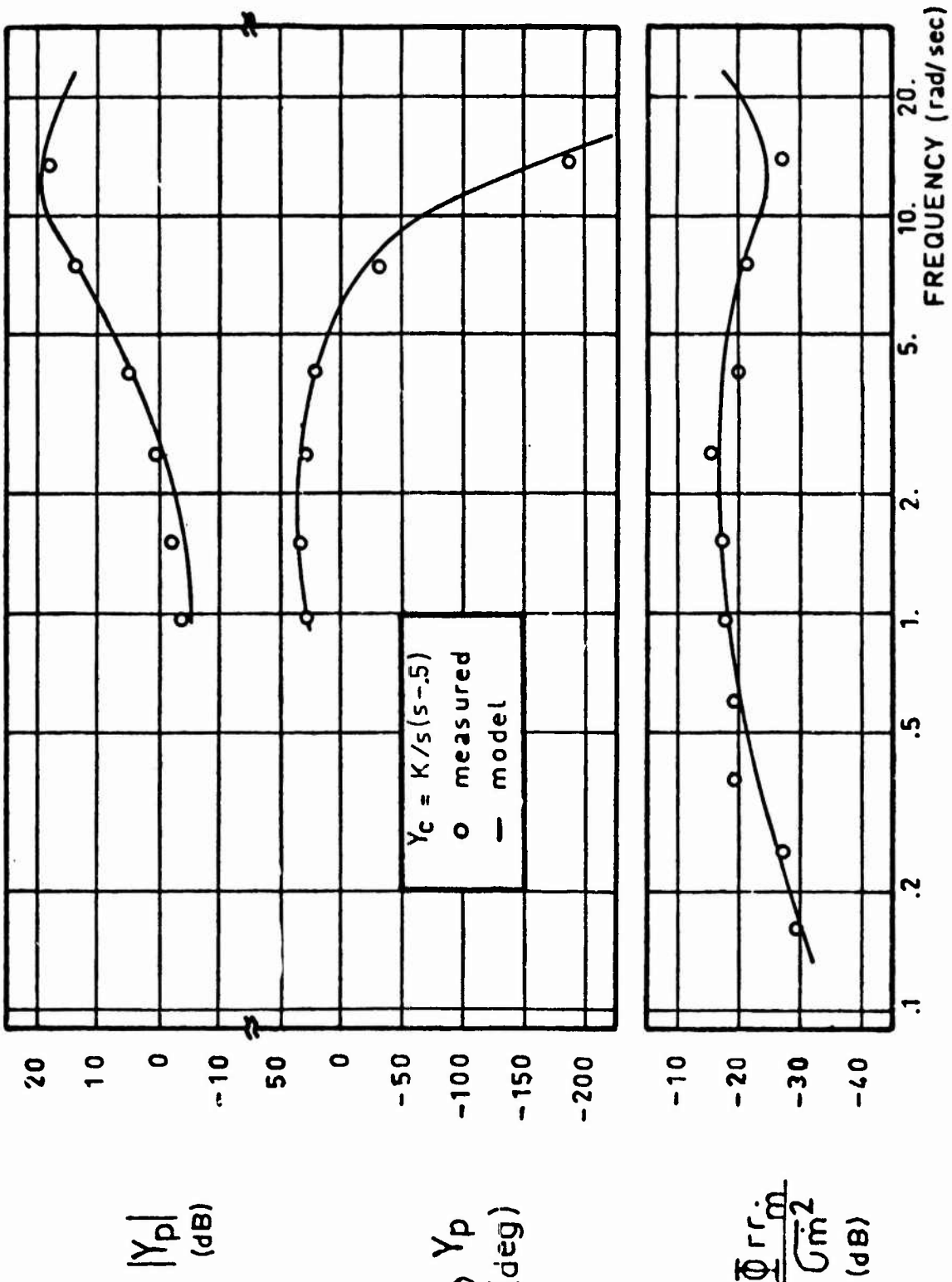

Fig. 5 Frequency domain measures - Y_c = K/s(s-.5)
Average of 4 subjects, 3 trials/subject

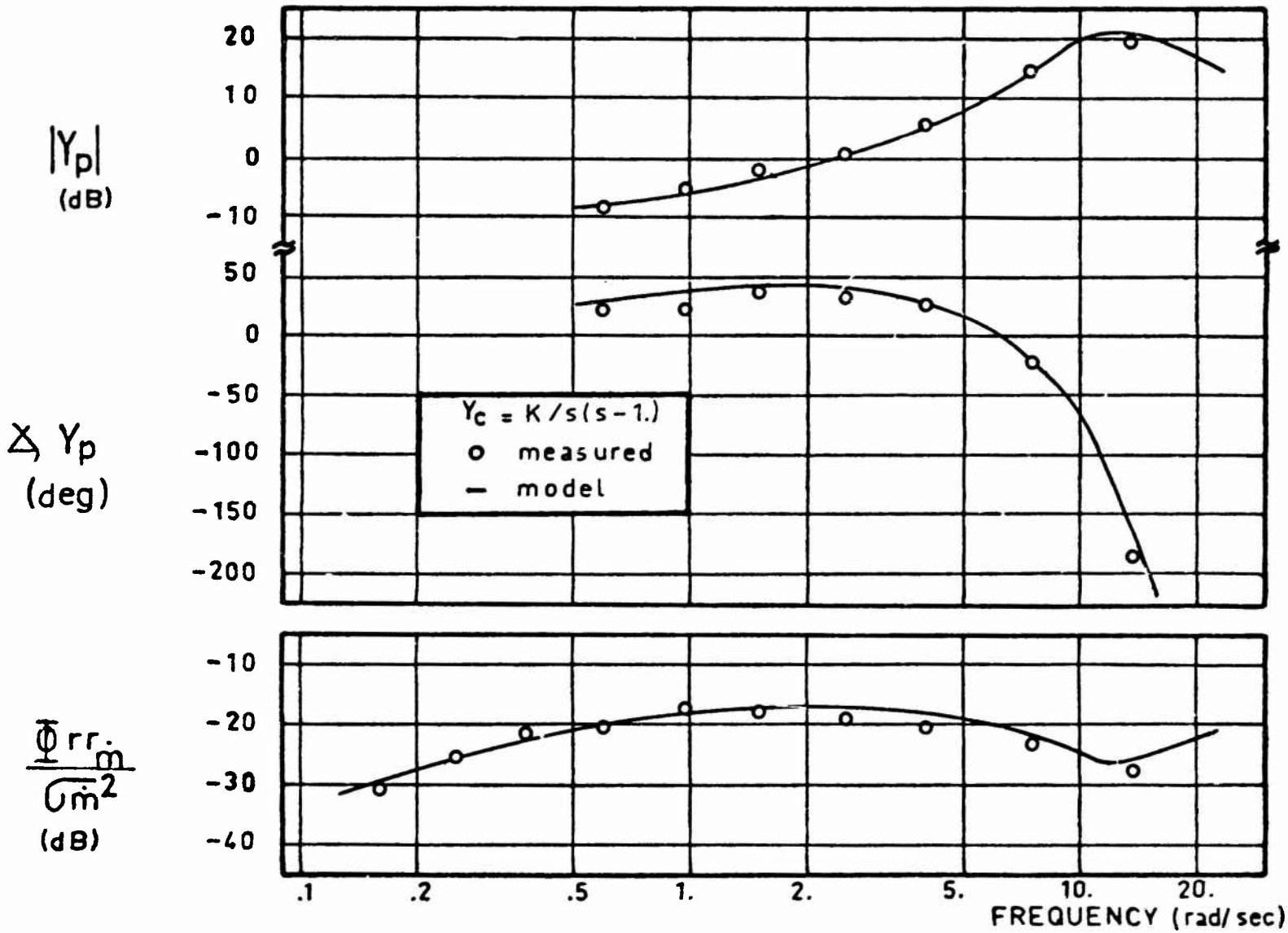

Fig. 6 Frequency domain measures - $Y_c = K/s(s-1)$
Average of 4 subjects, 3 trials/subject

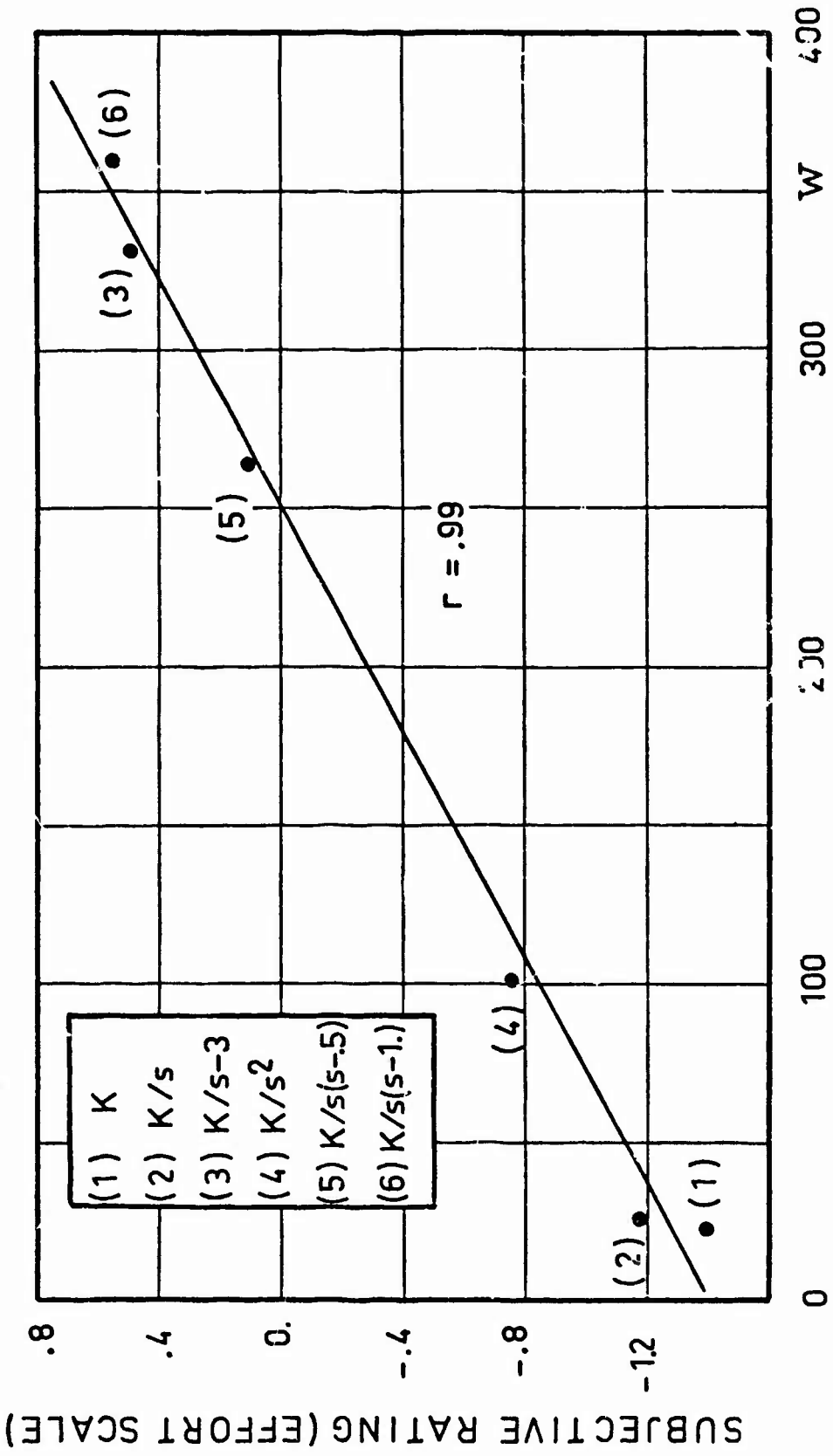

Fig. 7 The relationship between subjective ratings and computed workload.

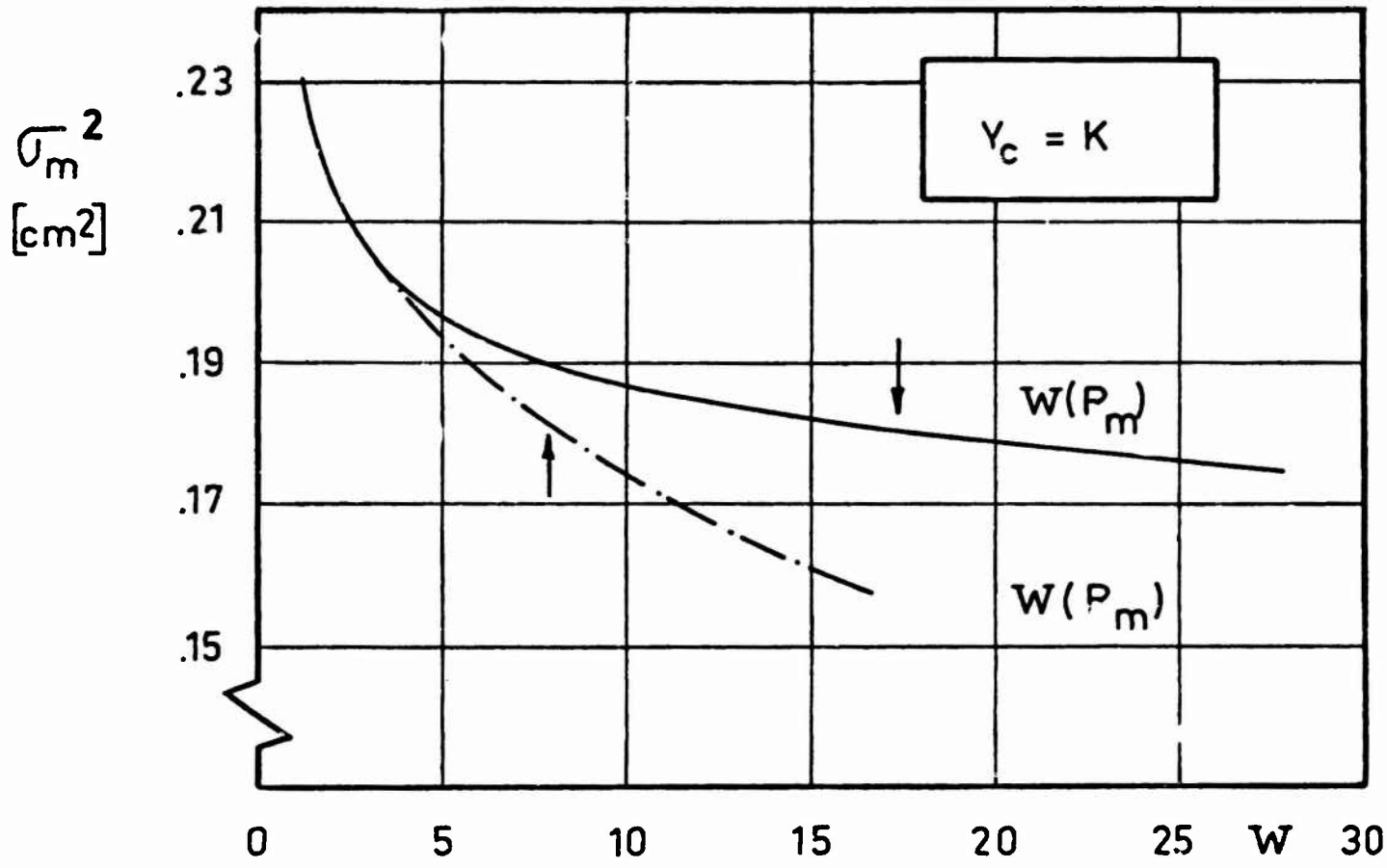

Fig. 8 The relationship between system performance and workload $Y_c = K$

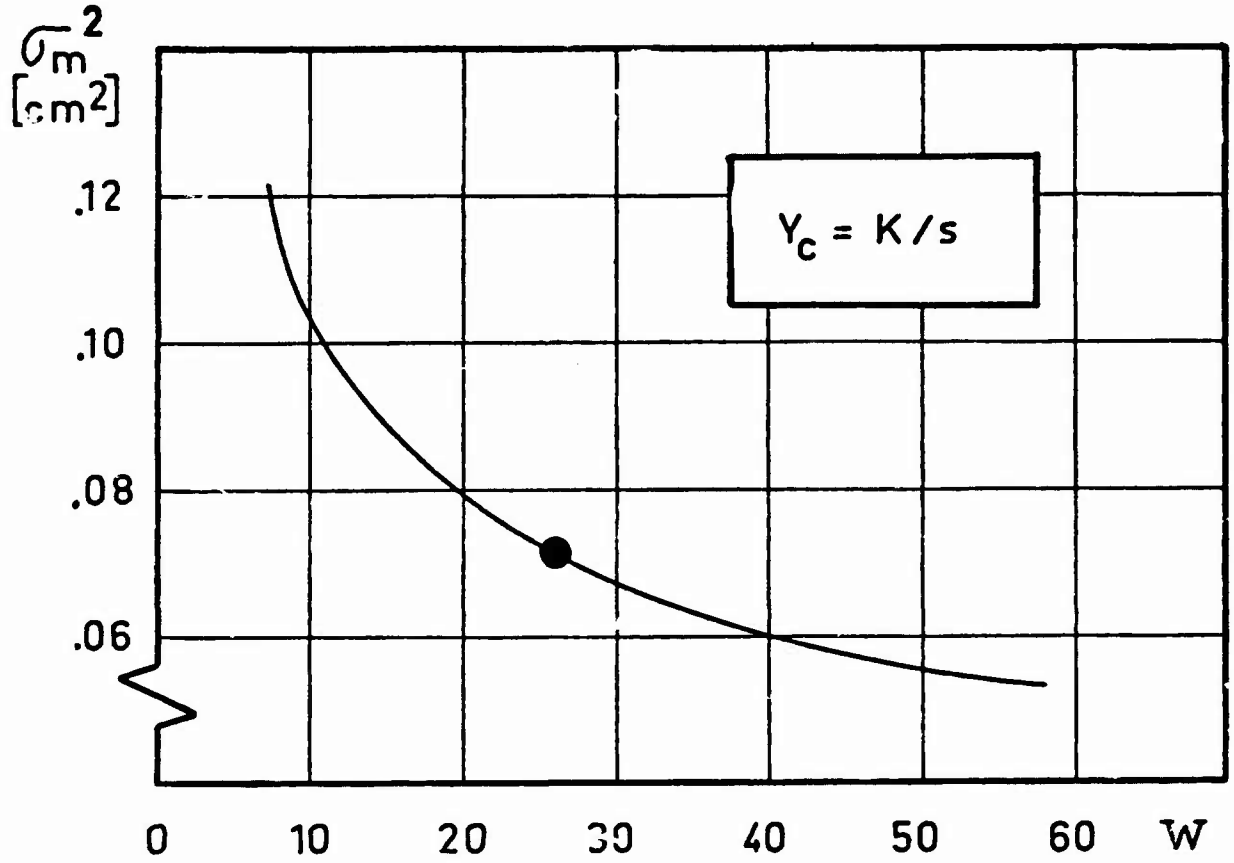

Fig. 9 The relationship between system performance and workload Y_c = K/s

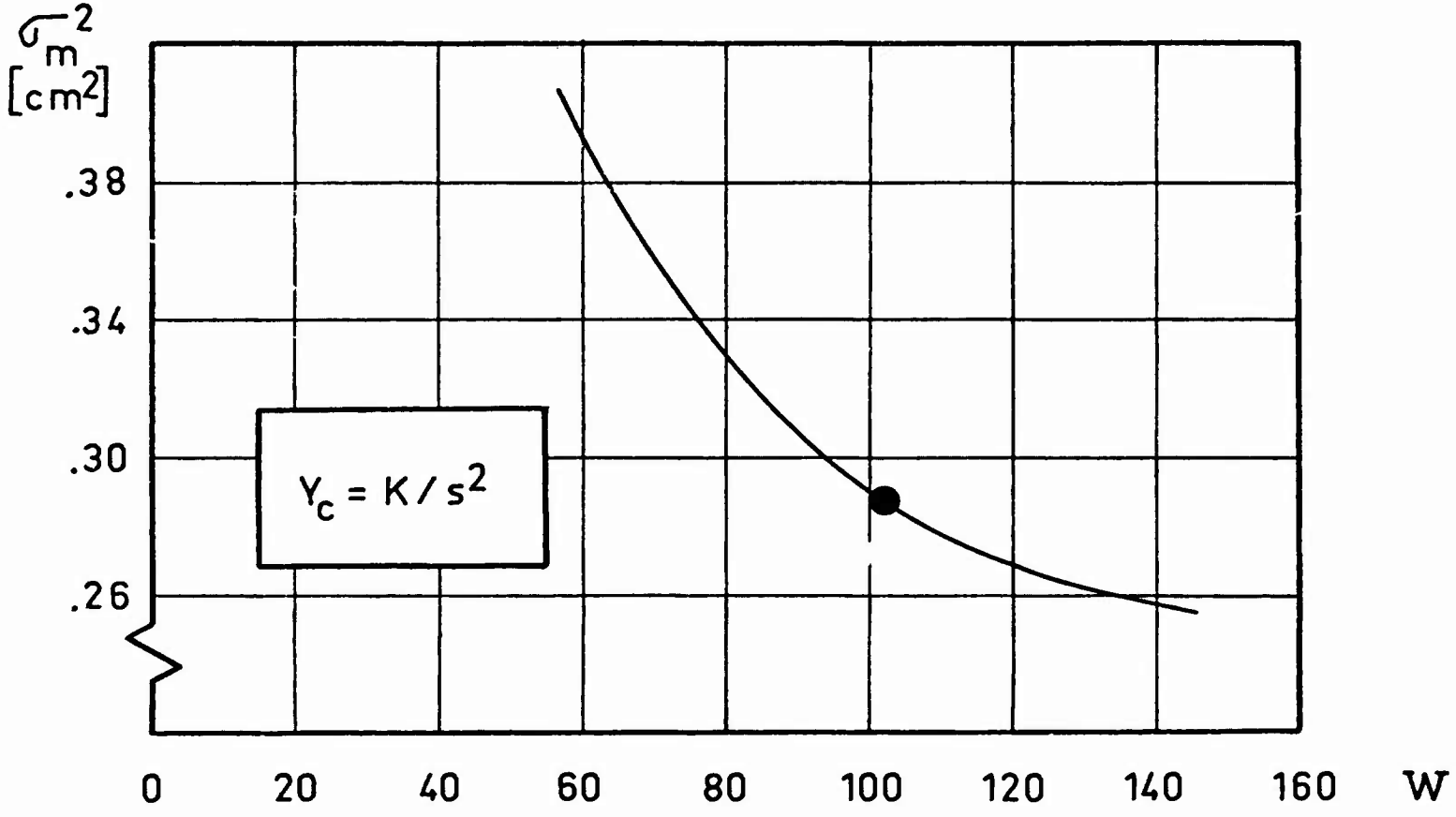

Fig. 10 The relationship between system performance and workload $Y_c = K/s^2$

AN ANALYSIS OF THE NEAL-SMITH LONGITUDINAL FLYING QUALITIES CRITERIA USING A DIGITAL COMPUTER PROGRAM

David R. Mayhew

USAF Flight Dynamics Laboratory
Flight Control Division

Presented at the Tenth Annual Conference on
Manual Control, April 1974

ABSTRACT

A digital computer program has been written which calculates the pilot parameters necessary to satisfy the Neal-Smith flying qualities criteria proposed in Reference 1. With the use of this program, an evaluation is made of the effect on flying qualities of variations in bandwidth frequency and maximum allowable droop in the closed loop pitch amplitude ratio.

INTRODUCTION

A closed loop handling qualities criteria was proposed for the pitch tracking task in Reference 1 in which pilot generated gain and lead or lag was applied to the open loop flight control system (FCS) and airframe transfer function of pitch angle to stick force in such a manner as to satisfy certain requirements on a Nichols Chart of closed loop amplitude and phase. The block diagram for the pitch tracking task is shown in Figure 1.

To satisfy the criteria in Reference 1, a plot of amplitude vs phase for the open loop transfer function $\theta/\theta_e(s)$ is superposed on a Nichols Chart and the values of K_p, τ_{p_1}, and τ_{p_2} are adjusted to make the point on the plot corresponding to a stipulated "bandwidth", frequency fall on the closed loop phase curve of $\phi_c = -90°$. (The values of bandwidth frequency suggested in Reference 1 for fighter airplanes were 3.0 and 3.5 radians per second, depending on the aircraft speed.) Simultaneously, the minimum closed loop amplitude for frequencies below the bandwidth frequency is held to -3 dB. This amplitude is referred to as "droop". Figure 2 depicts a typical closed loop Bode plot, showing droop, resonance, and bandwidth.

When these two criteria are met, the maximum closed loop amplitude, or resonant peak, is obtained from the Nichols Chart and this value, along with the degrees of pilot lead or lag required to meet the criteria, determine the level of flying qualities for the aircraft being considered. The effect of closed loop resonance and pilot lead or lag on levels of flying qualities is shown in Figure 3, along with typical pilot comments to be expected in each portion of the plot. Essentially the magnitude of the resonant peak is a measure of the tendency of the aircraft to bobble, oscillate, or PIO on target. The lead or lag compensation is a measure of the pilot workload.

The basis for establishing the closed loop criteria was a series of variable stability T-33 flights in which the primary task was pitch attitude tracking representative of up-and-away tasks associated with air-to-air combat. The tasks were performed at 250 and 350 knot airspeeds.

Because the data correlation in Reference 1 was performed by a tedious graphical process of overlaying open loop amplitude vs phase plots on Nichols Charts, it was not possible to fully assess the effects of bandwidth and droop on data correlation. It was, however, found that good correlation was obtained when a bandwidth frequency of 3.0 radians per second was used with the 250 knot data and 3.5 radians per second was used with the 350 knot data. The droop amplitude value was set at -3 dB.

Subsequent to the study in Reference 1, a digital computer program was written which calculates the pilot generated gain, lead, and lag necessary to satisfy the criteria for any input values of bandwidth frequency and droop, and for any set of aircraft plus FCS dynamics. In addition, the program computes the closed loop resonance and the frequencies at which droop and resonance occur. The program is documented in Reference 2.

With the use of this program, it is now possible to vary the nominal bandwidth and droop values used in the criteria, and note their effect on the location of the Figure 3 plot of resonance vs lead/lag compensation. This not only permits a better correlation with a given data base, but allows us to examine the concept of the pilot as an optimum controller (Reference 3); i.e., he might select other than nominal values of bandwidth and droop if he could significantly lower the resonance, thereby improving his performance, or reduce the lead/lag compensation necessary, thereby reducing his workload.

BANDWIDTH

Figures 4 through 22 depict closed loop resonance vs pilot generated lead/lag for several configurations from Reference 1, as a function of different values of bandwidth frequency and droop used to satisfy the Neal-Smith criteria. The values of droop are presented as amplitude instead of log magnitude. On this scale, .79 is approximately -2 dB, .71 is approximately -3 dB, .63 is approximately -4 dB, etc. We will speak of lower values of amplitude representing increasing droop.

The bandwidth frequency, defined as that frequency at which the closed loop phase first exceeds -90°, is a measure of how aggressively the pilot wishes to perform the tracking task. If he detects a tracking error, it is a measure of how rapidly he wishes to correct the error.

It is obvious that in many cases a small variation in bandwidth can have a drastic effect on resonance and/or pilot generated phase compensation. It follows that the proper selection of bandwidth for the evaluation of handling qualities is critical. This fact is recognized in Reference 4 where the value of bandwidth is made a function of aircraft class, flight phase category, and level of flying qualities, as defined in Reference 5.

Figures 4 through 16 represent several cases from Reference 1 in which the pilot ratings and comments seem to correlate rather well with the proposed boundaries of Figure 3. Since a bandwidth of 3.0 radians/sec was selected for the 250 knot configurations and 3.5 radians/sec was selected for the 350 knot cases, it is probable that the pilot was trying to achieve a bandwidth somewhere between these two values for most configurations in Reference 1. In several cases, a dramatic decrease in resonance and thus an improvement in flying qualities would result if the pilot were willing to decrease his bandwidth from 3.0 to 2.5. This is especially true in configurations 1E, 4D, 4B, and 4C. It seems remarkable that the pilot is apparently unwilling to do this.

Figures 17 through 19 depict configurations for which pilot ratings and complaints of oscillatory or PIO tendencies appear more severe than would be predicted. It may be that the pilot is striving for a higher bandwidth than that used to correlate the data.

DROOP

The amount of droop in the closed loop amplitude vs frequency plot is indicative of the uniformity of response to inputs of varying frequency. A configuration having a large amount of droop would, for example, require an increasing amount of back pressure on the stick to hold a pitch rate after initially responding to a step input.

Configurations 6A, 4A, and 5A, shown in Figures 20 through 22, are characterized in Reference 1 as having significantly better ratings and less problems with oscillatory or PIO tendencies than would be predicted. Configuration 6A has the most pronounced decrease in resonance for an increase in droop of any configuration examined, and it appears that the pilot is accepting a slight increase in droop over the nominal -3 dB to significantly reduce the oscillatory tendencies of the aircraft.

Configurations 4A and 5A both require lag compensation. A very tentative hypothesis might be that the pilot will increase the droop (and possibly lower the bandwidth slightly) when, by so doing, he not only lowers the peak resonance but also decreases his workload by decreasing the magnitude of the phase compensation. Note that in the case of lead compensation, increasing the droop has the effect of increasing the lead compensation and hence the pilot workload. In support of this very tenuous hypothesis, data is presented from Reference 6 in Figures 23 through 29. The data was the result of a fixed base simulation of flying qualities in an attitude holding task, and the pilot ratings were based on the old Cooper scale. Because of the differences in the simulations in Reference 1 and Reference 6, no attempt will be made to validate the boundaries on Figure 3 using this data base. However, a comparison of the lead and lag cases shows that, assuming a bandwidth of approximately 3.0 and a droop amplitude around .71, the pilot ratings for the lag compensation cases appear better than predicted, whereas the lead compensation ratings seem to be in consonance with, or worse than, predicted.

DATA BASE

The data examined from Reference 1, although not comprehensive, are considered to be representative of cases which satisfied the proposed boundaries of Figure 3, as well as cases in which the ratings were either worse than or better than predicted. Excluded from presentation in this paper were those cases for which ratings were worse than predicted for reasons not pertaining to the present analysis. Specifically, the anomaly in cases 3A, 3B, 8A, 8B, 13 and 14 appears to be better explained in terms of the high pitch-acceleration sensitivity of these configurations, as explicated in Reference 1, than by the hypotheses proposed here.

The data from Reference 6 presented here in support of a hypothesis represents all the data examined in a random sample from this data base. It is felt that enough cases were examined to lend credence to the qualitative nature of the conclusions drawn from the data.

CONCLUSIONS

The primary purpose of this paper has been to illustrate a data analysis using a digital program for varying the parameters in the Neal-Smith criteria. Because of the limited data base and the subjective nature and variability of pilot ratings, any conclusions drawn from the analysis regarding the data base have to be regarded as very tentative. With this admonishment, the following conclusions are offered.

1. The analysis presented here points up the extreme sensitivity of predicted pilot workload and oscillatory or PIO tendencies in pitch (in terms of the parameters in Figure 3) to bandwidth frequency. The proper selection of bandwidth for the task, flight conditions, and class of airplane is seen to be crucial to the successful application of the closed loop criteria in Reference 1.

2. It appears that, for the tracking task in Reference 1, the pilot is unwilling to lower his bandwidth for poor configurations, even when substantial reduction in closed loop resonance and/or workload would result.

3. There appears to be some tendency for the pilot to rate the aircraft better than predicted for a combination of some or all of the following factors.

   a. Lag compensation is required. This generally means that increasing the droop, in addition to lowering the closed loop resonance, will decrease the magnitude of phase compensation required.

   b. The sensitivity of closed loop resonance to changes in droop is relatively high.

   c. The predicted rating of the configuration, using nominal values of bandwidth and droop, is Level 3 or near the Level 3 boundary.

4. It is felt that a variation of parameter analysis such as presented here is a useful, even necessary supplement to the closed loop criteria of Reference 1. Not only does it facilitate a determination of the proper values of bandwidth and droop for application of the criteria, but it provides insight into anomalies in the data.

REFERENCES

1. Neal, T.P. and R.E. Smith, "An In-Flight Investigation to Develop Control System Design Criteria for Fighter Airplanes", AFFDL TR 70-74, December 1970

2. Mayhew, D.R., "A Digital Computer Program for the Calculation of Parameters Necessary to Satisfy the Closed Loop Criteria of T.P. Neal", AFFDL FGC TM 73-110, August 1973

3. Anderson, R.O., "A New Approach to the Specification and Evaluation of Flying Qualities", AFFDL TR 69-120, November 1969

4. Chalk, C.R., et al, "Revisions to MIL-F-8785B(ASG) Proposed by Cornell Aeronautical Laboratory Under Contract F33615-71-C-1254", AFFDL TR 72-41, March 1974

5. Anon, "Military Specification - Flying Qualities of Piloted Airplanes", MIL-F-8785B(ASG), August 1969

6. Chalk, C.R., "Fixed-Base Simulator Investigation of the Effects of L_α and True Speed on Pilot Opinion of Longitudinal Flying Qualities", ASD TDR 63-399, November 1963

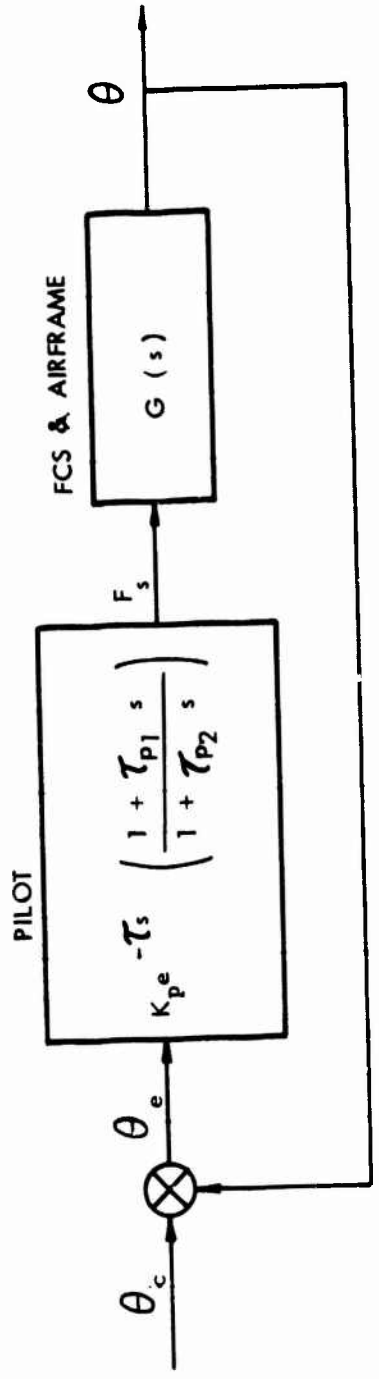

FIGURE 1. CLOSED LOOP PITCH TRACKING MODEL

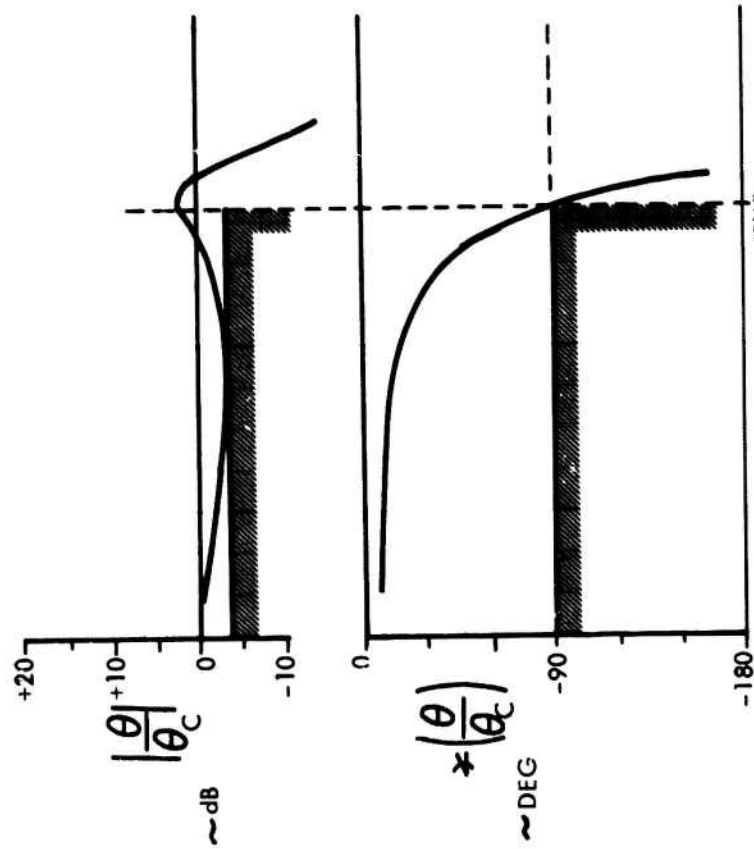

FIGURE 2. CLOSED LOOP BODE PLOT

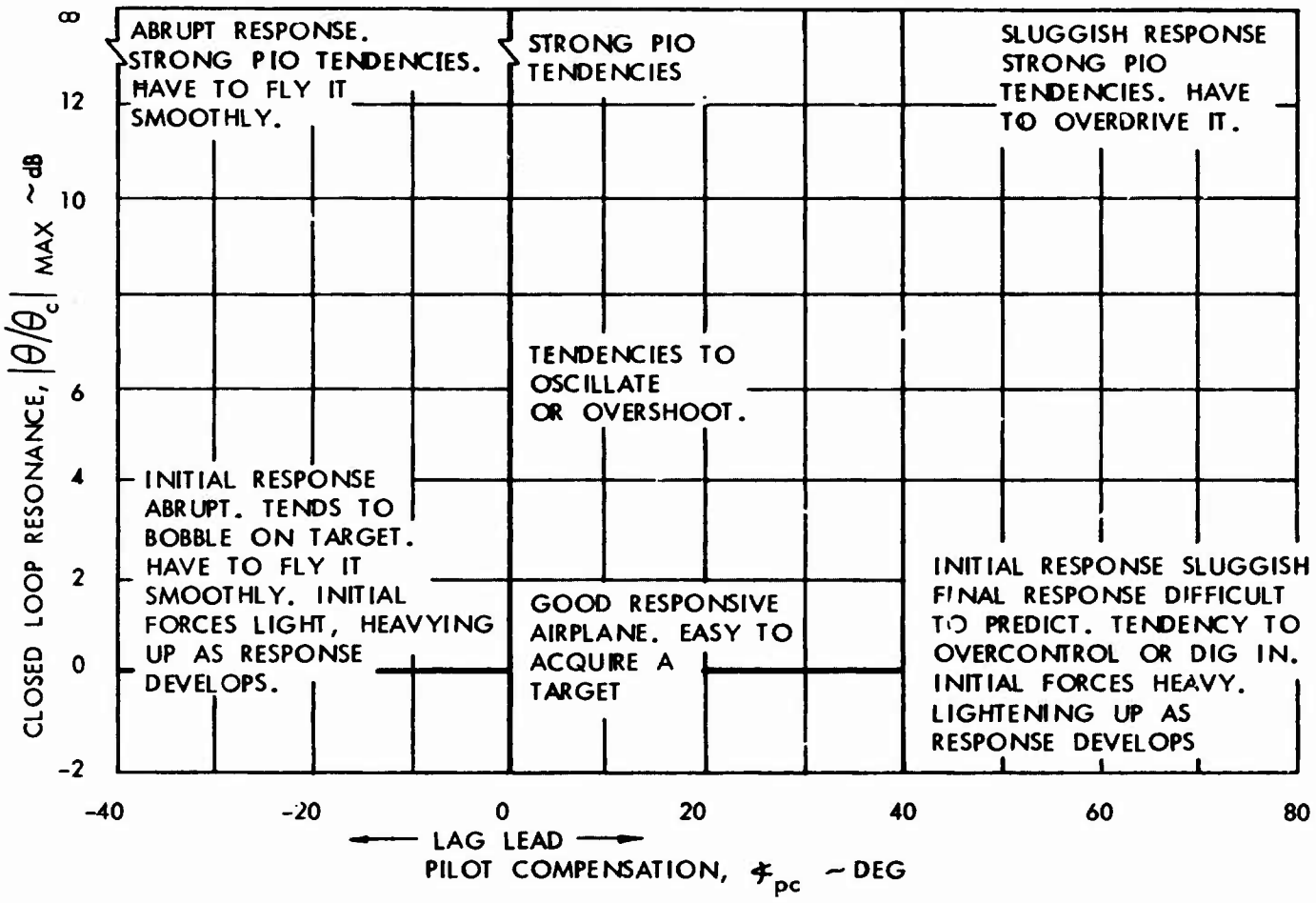

FIGURE 3. FLYING QUALITIES AS A FUNCTION OF CLOSED LOOP RESONANCE AND PILOT COMPENSATION

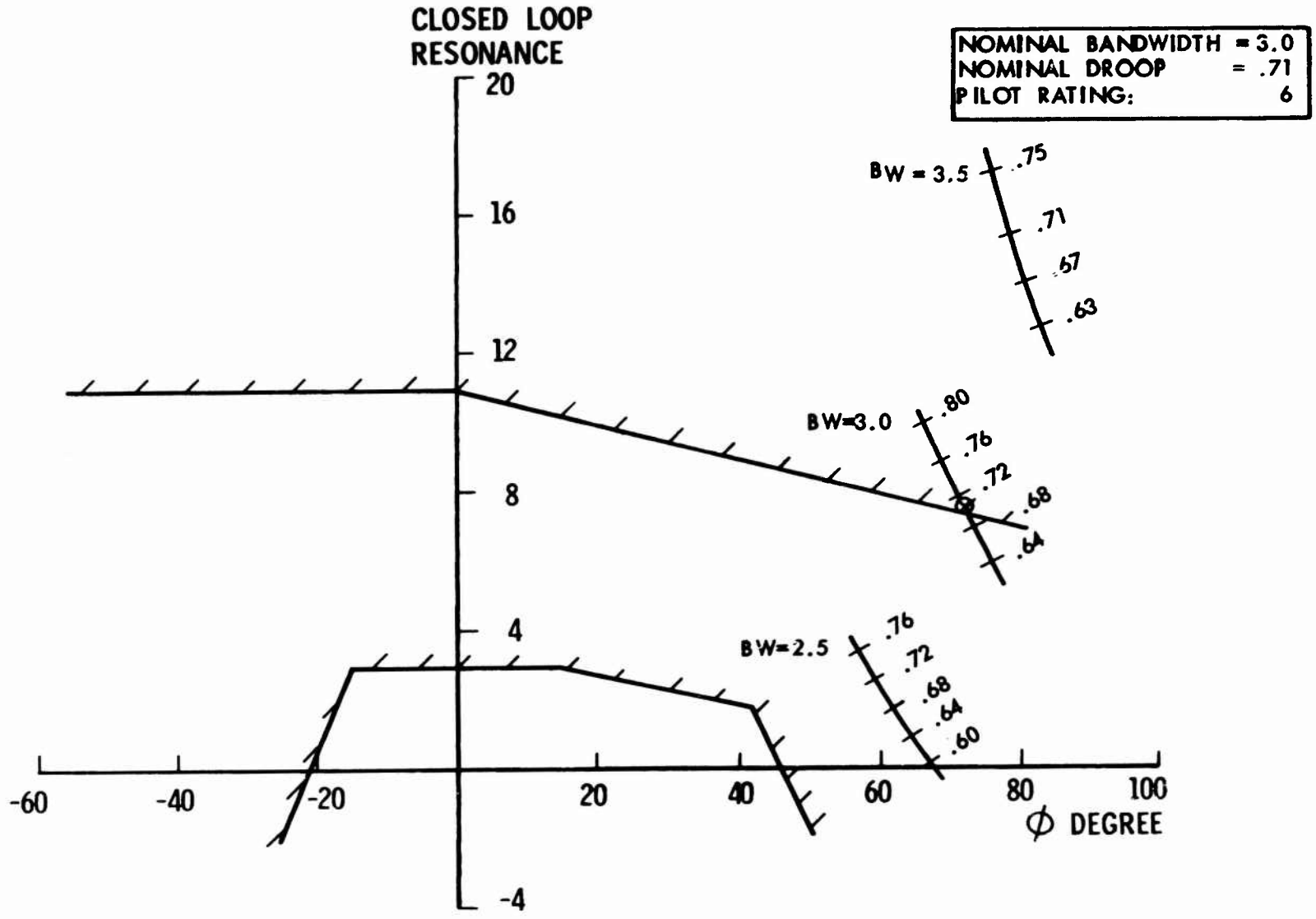

FIGURE 4. EFFECT OF BANDWIDTH AND DROOP; REFERENCE 1 DATA, CONFIGURATION 1E

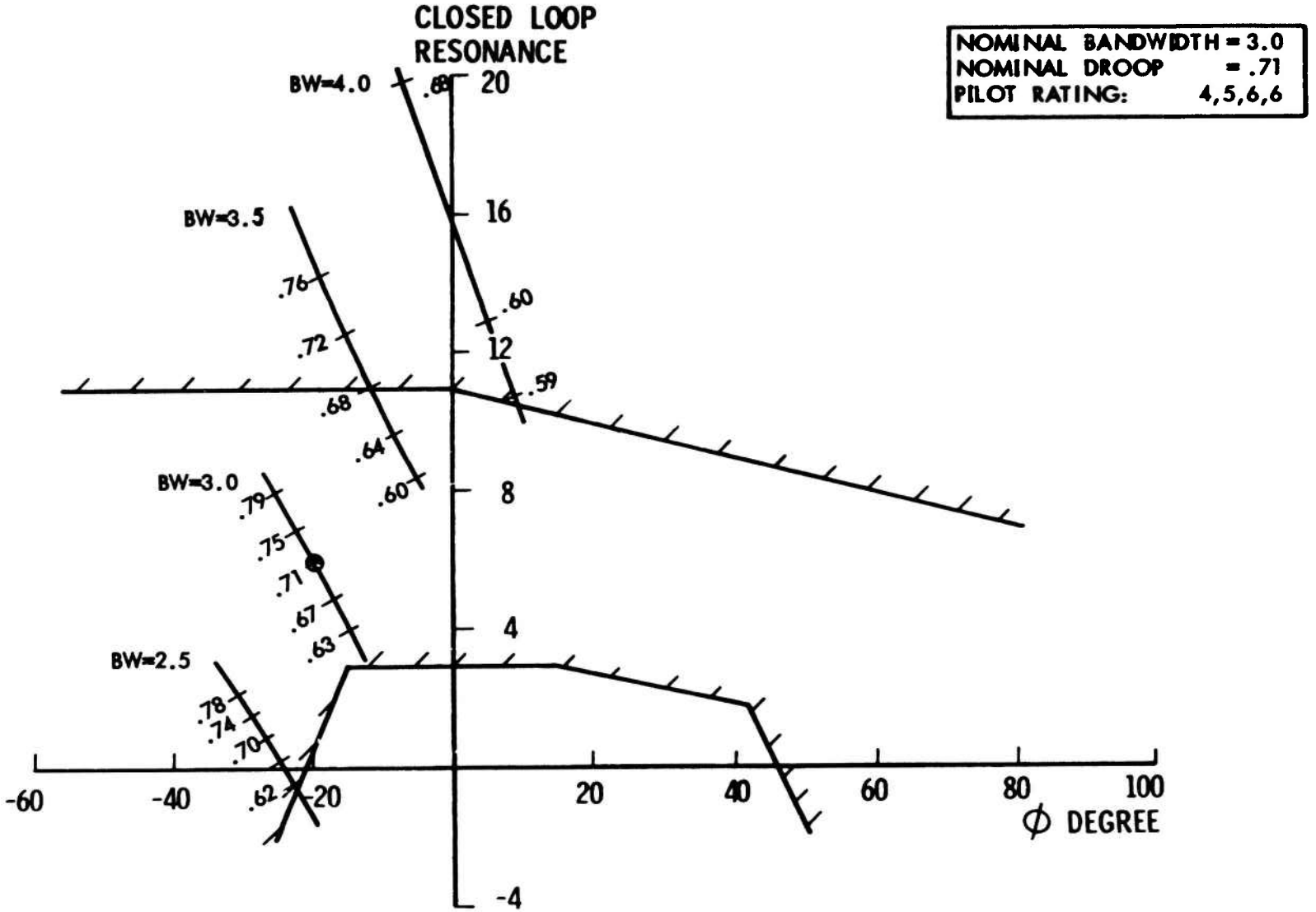

FIGURE 5. EFFECT OF BANDWIDTH AND DROOP; REFERENCE 1 DATA, CONFIGURATION 2B

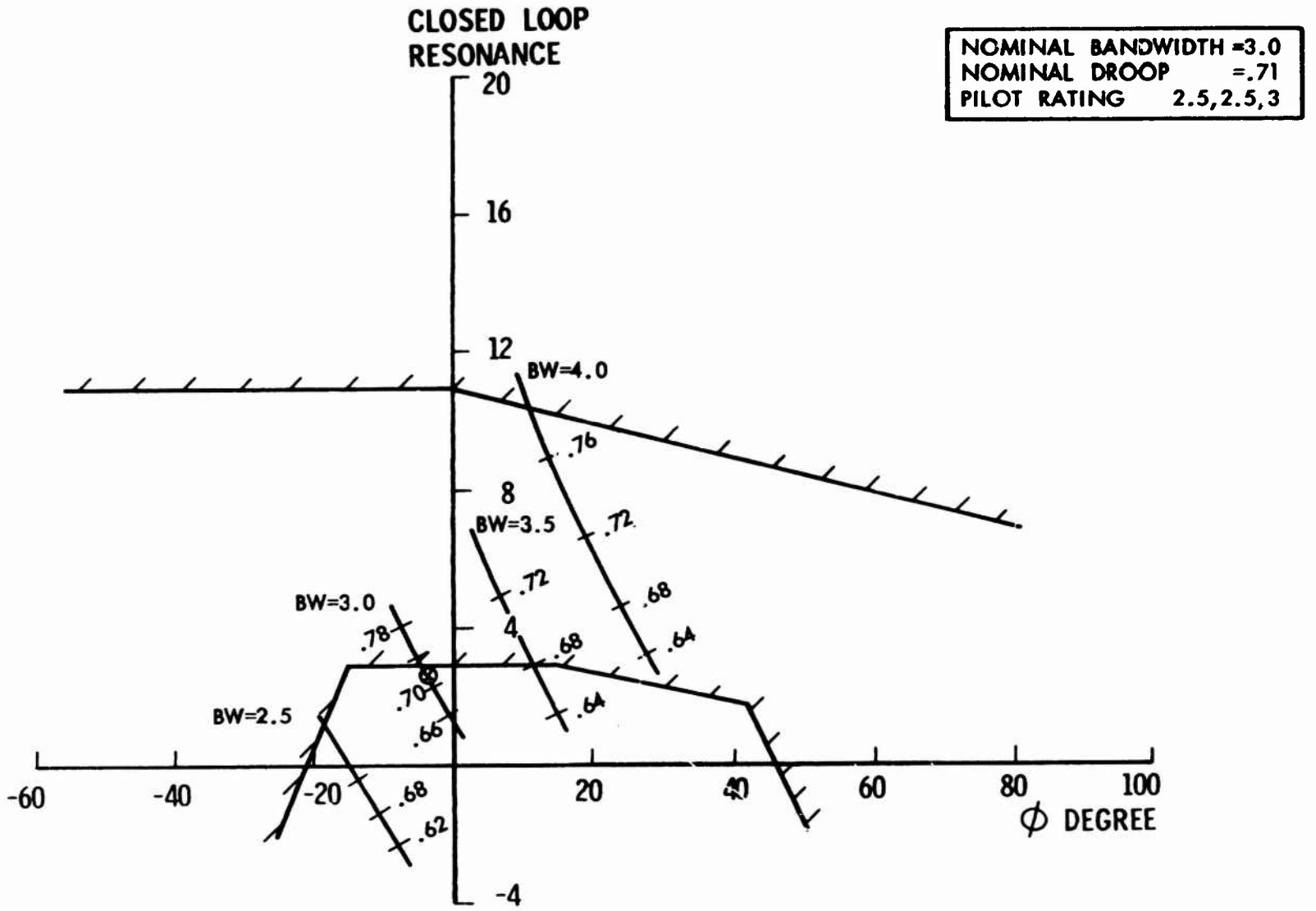

FIGURE 6. EFFECT OF BANDWIDTH AND DROOP; REFERENCE 1 DATA, CONFIGURATION 2D

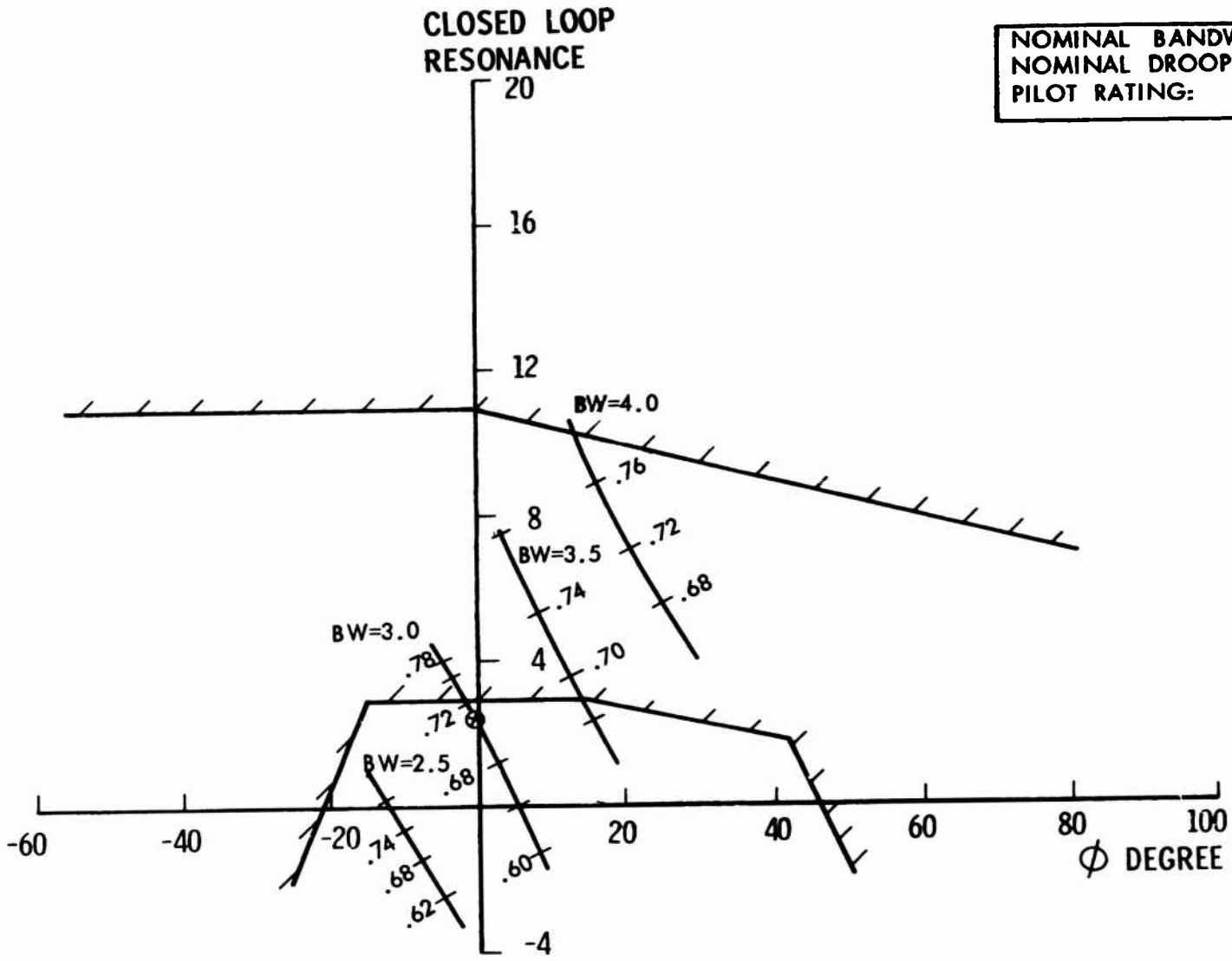

FIGURE 7. EFFECT OF BANDWIDTH AND DROOP; REFERENCE 1 DATA, CONFIGURATION 3C

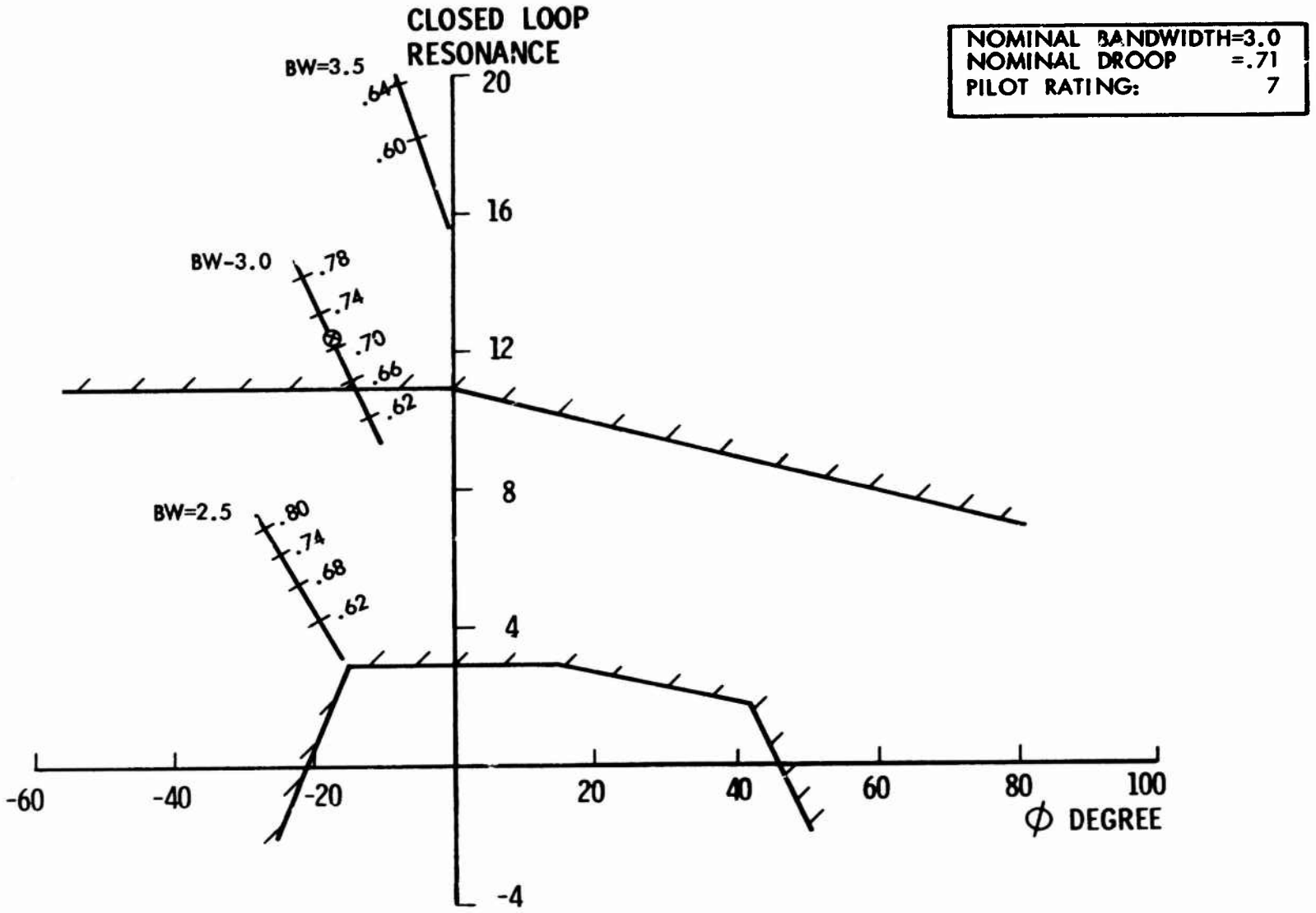

FIGURE 8. EFFECT OF BANDWIDTH AND DROOP; REFERENCE 1 DATA, CONFIGURATION 4B

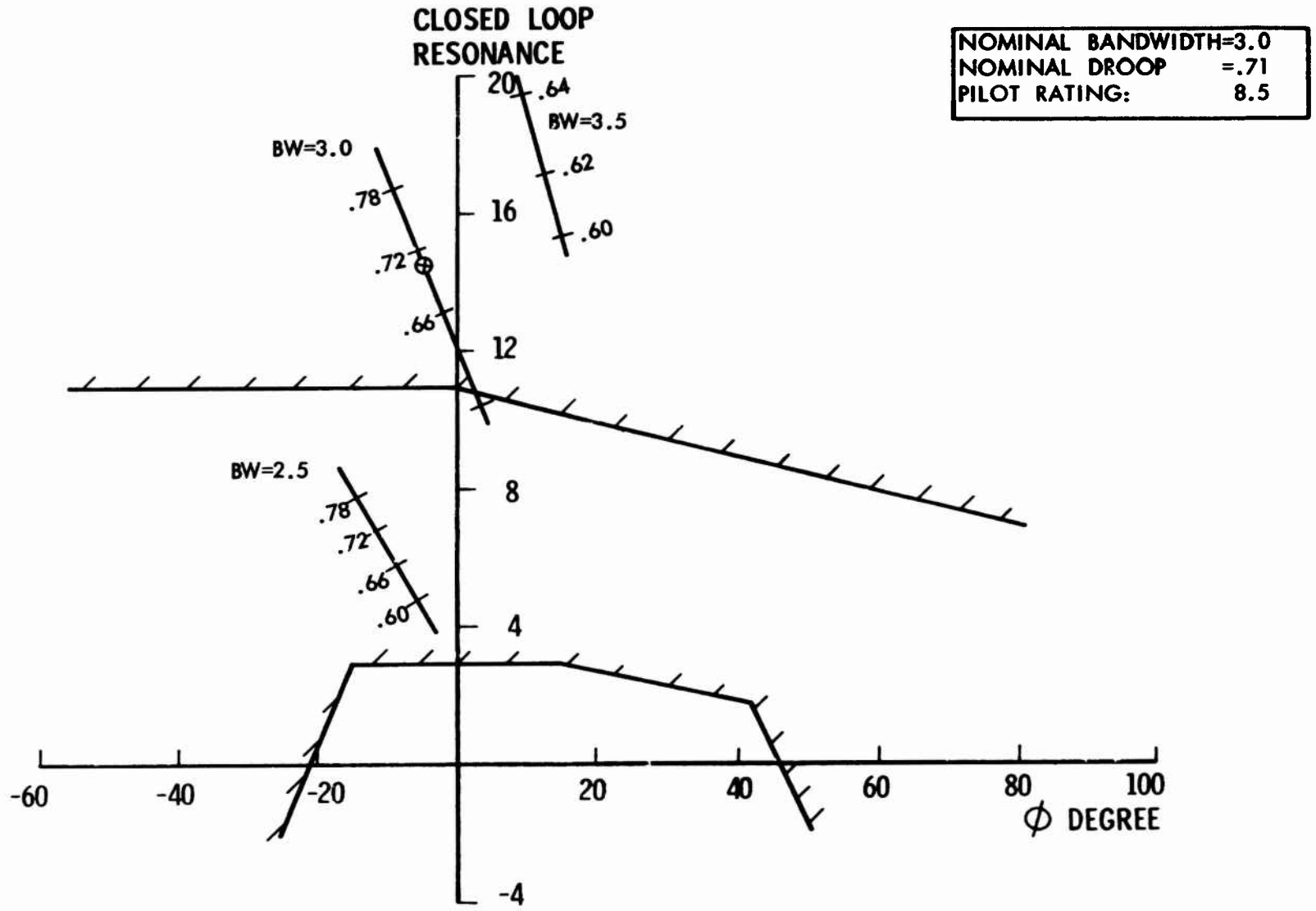

FIGURE 9. EFFECT OF BANDWIDTH AND DROOP; REFERENCE 1 DATA, CONFIGURATION 4C

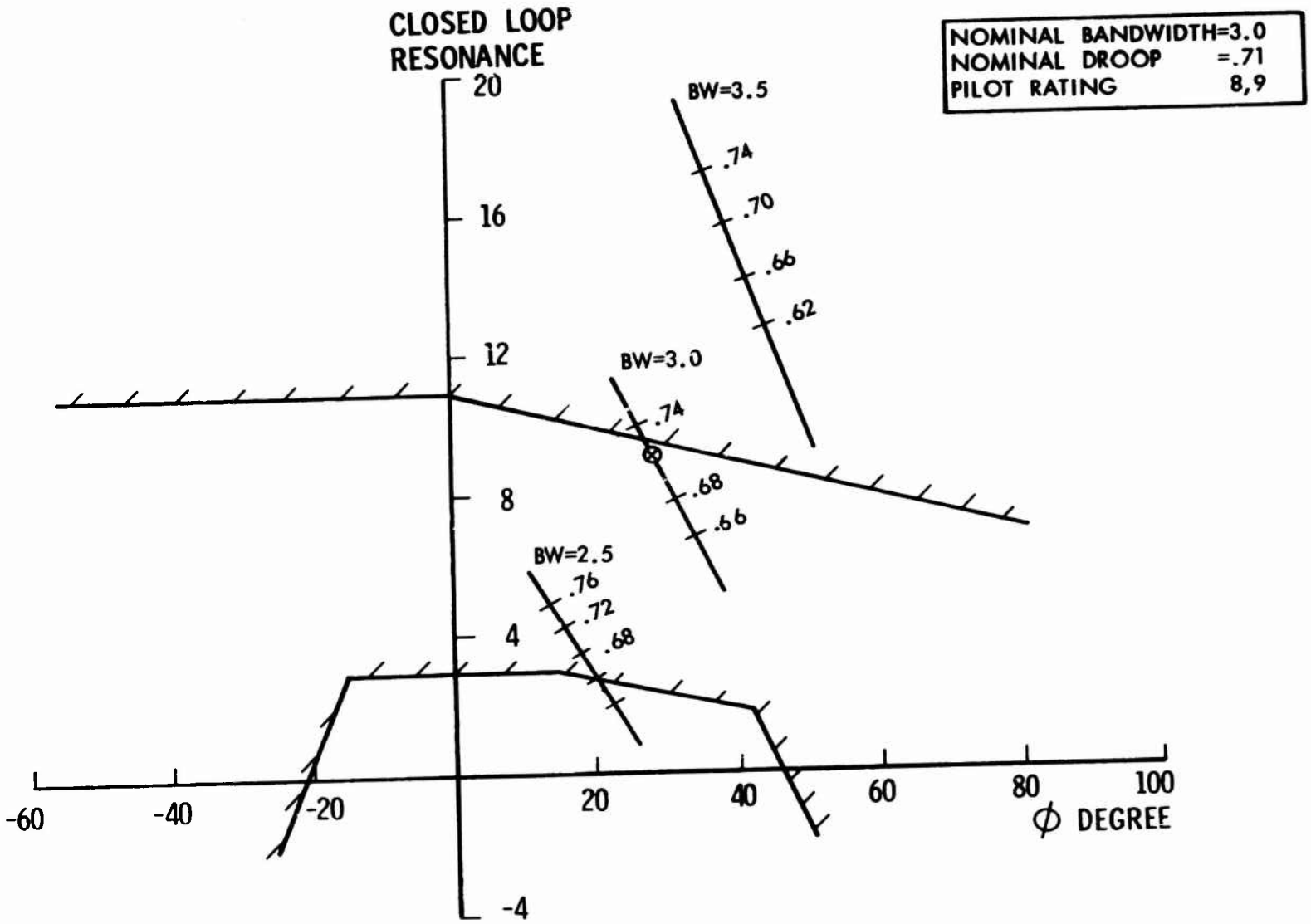

FIGURE 10. EFFECT OF BANDWIDTH AND DROOP; REFERENCE 1 DATA, CONFIGURATION 4D

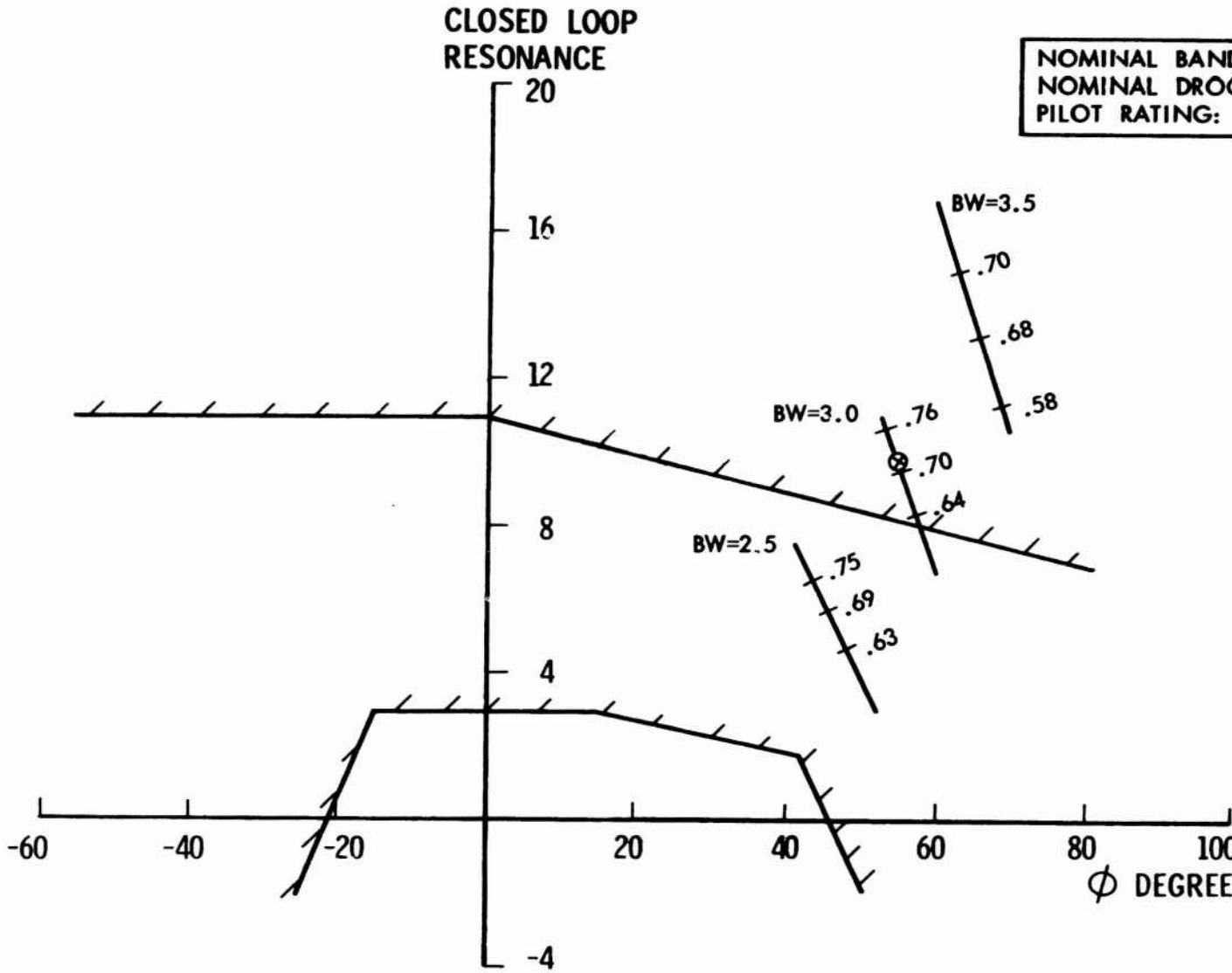

FIGURE 11. EFFECT OF BANDWIDTH AND DROOP; REFERENCE 1 DATA, CONFIGURATION 4E

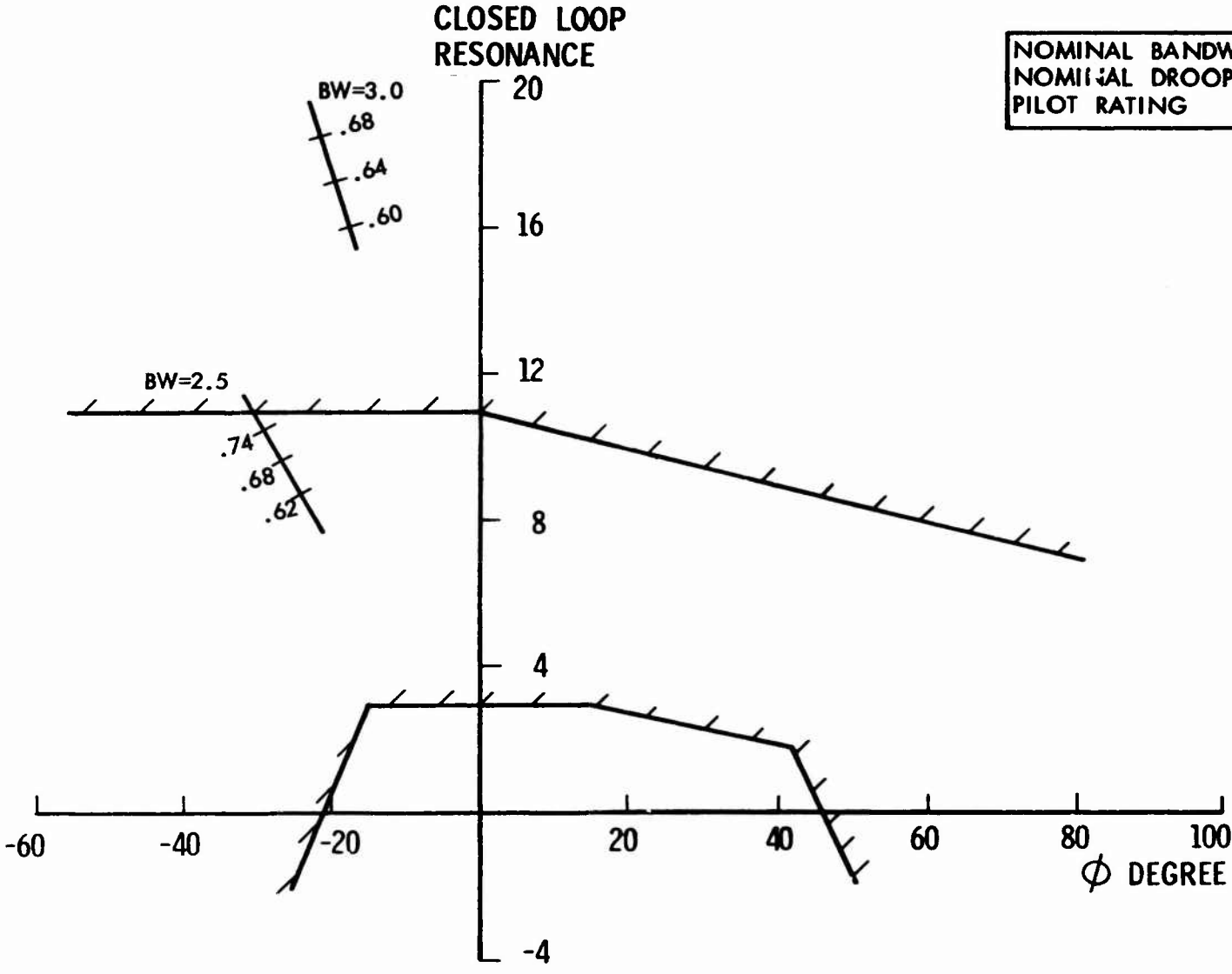

FIGURE 12. EFFECT OF BANDWIDTH AND DROOP; REFERENCE 1 DATA, CONFIGURATION 5B

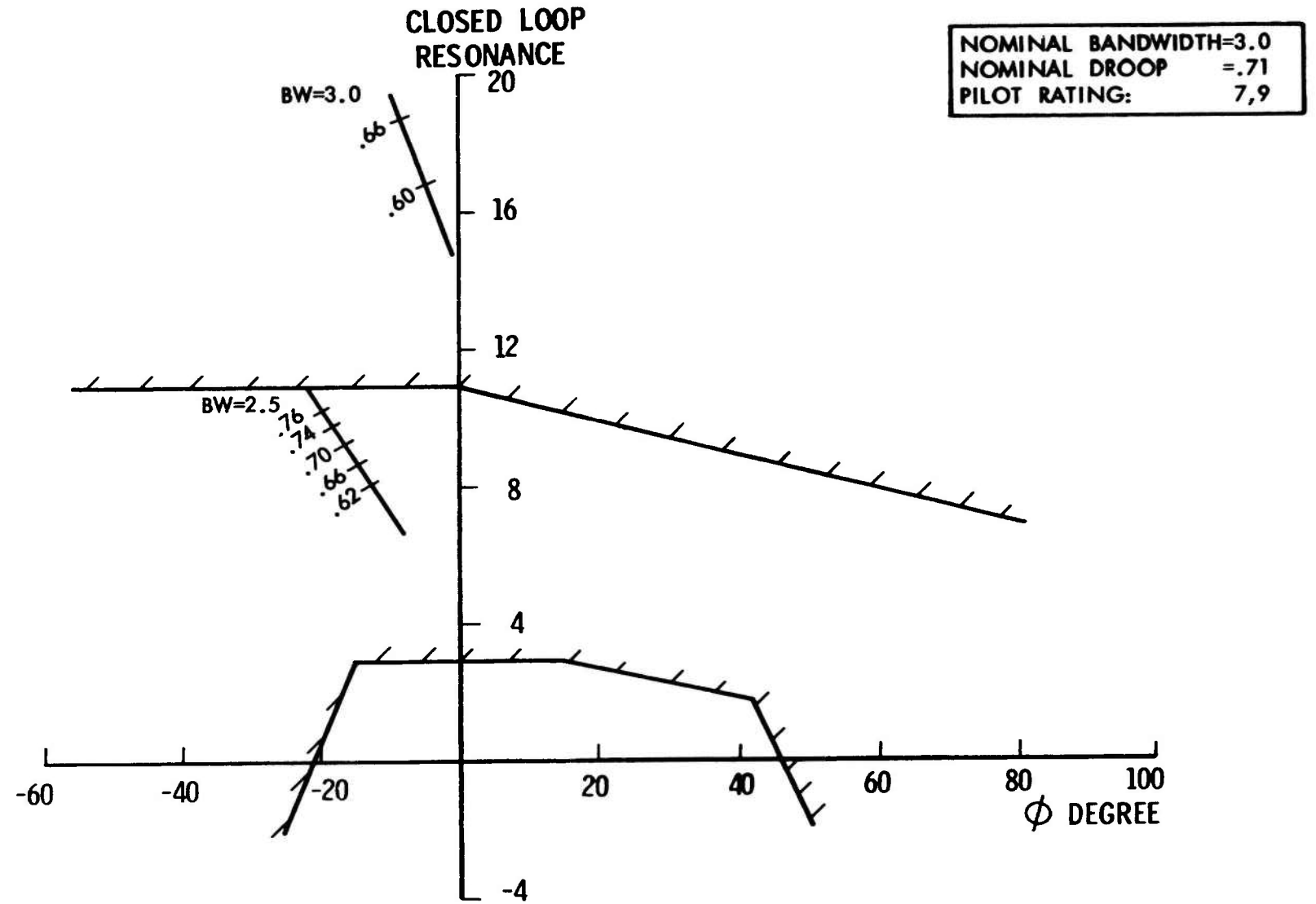

FIGURE 13. EFFECT OF BANDWIDTH AND DROOP; REFERENCE 1 DATA, CONFIGURATION 5C

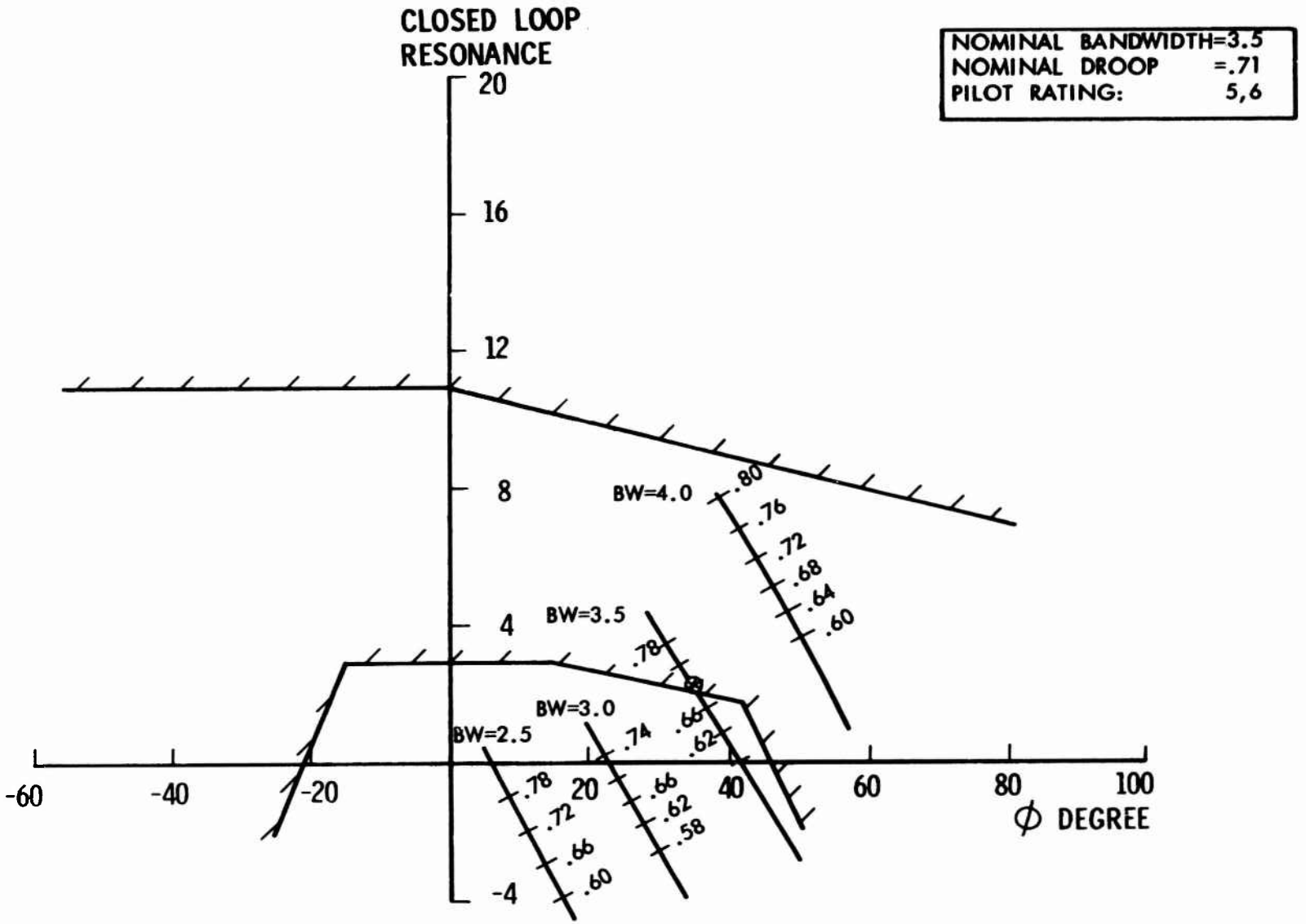

FIGURE 14. EFFECT OF BANDWIDTH AND DROOP; REFERENCE 1 DATA, CONFIGURATION 7E

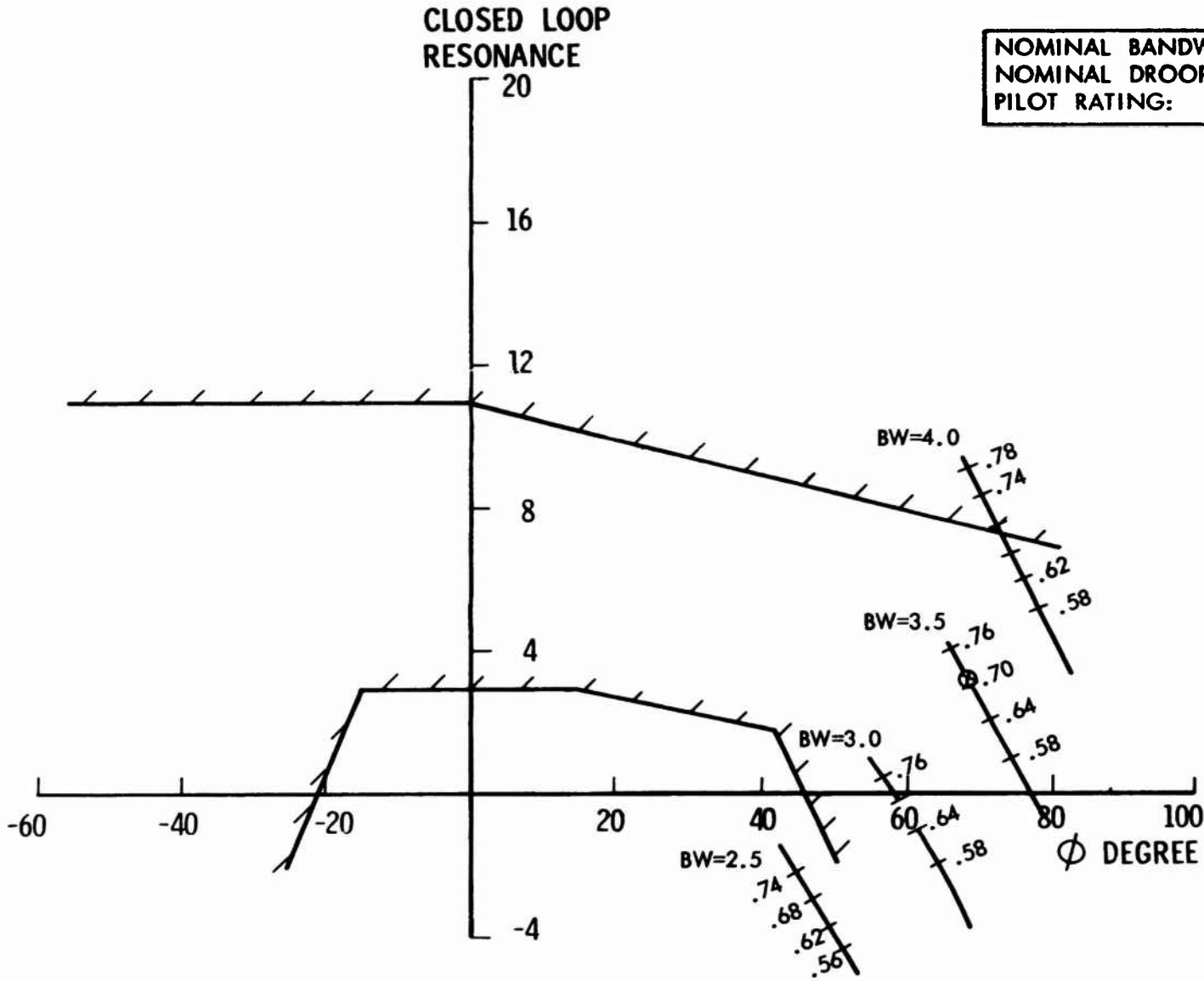

FIGURE 15. EFFECT OF BANDWIDTH AND DROOP; REFERENCE 1 DATA, CONFIGURATION 7G

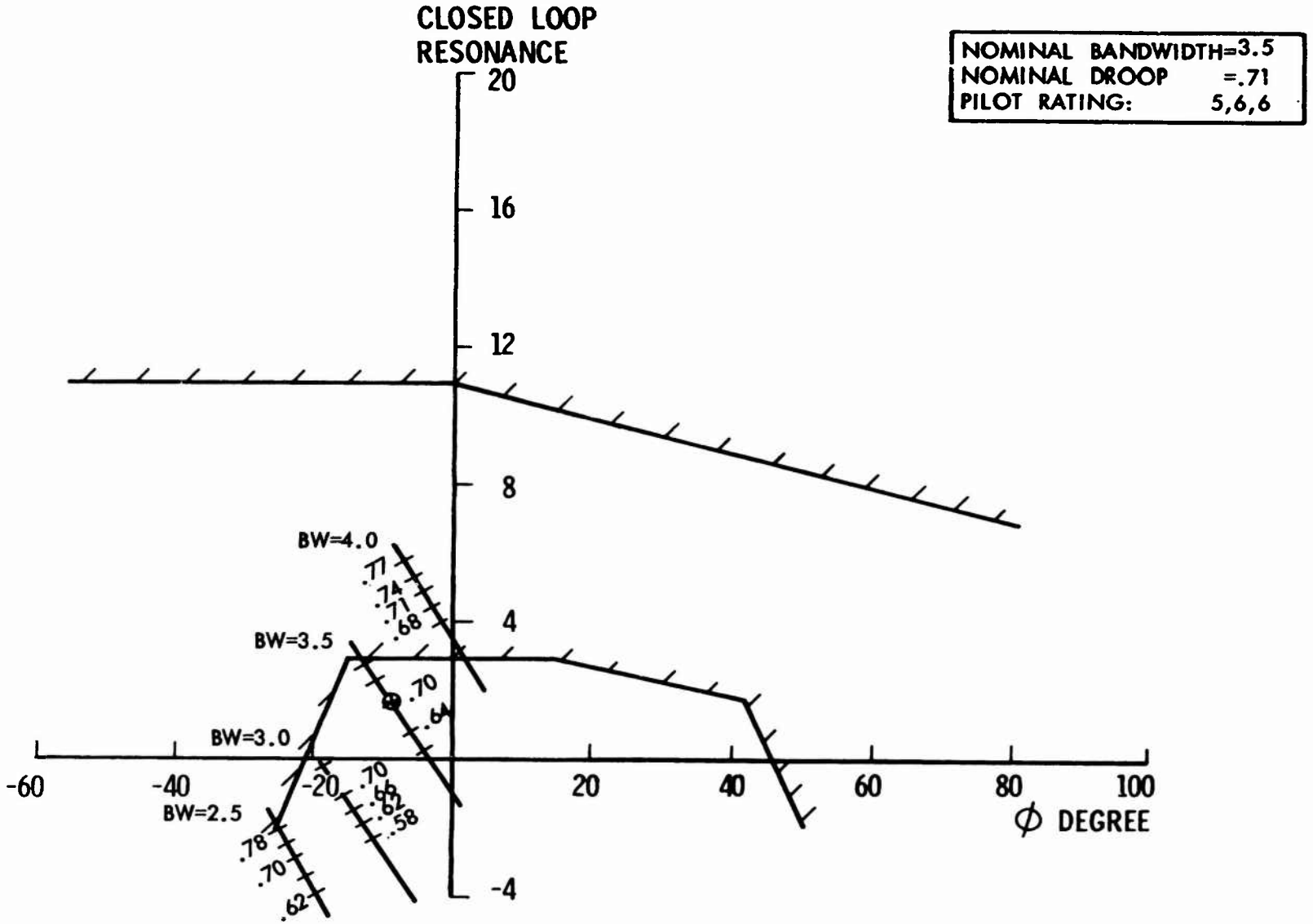

FIGURE 16. EFFECT OF BANDWIDTH AND DROOP; REFERENCE 1 DATA, CONFIGURATION 12

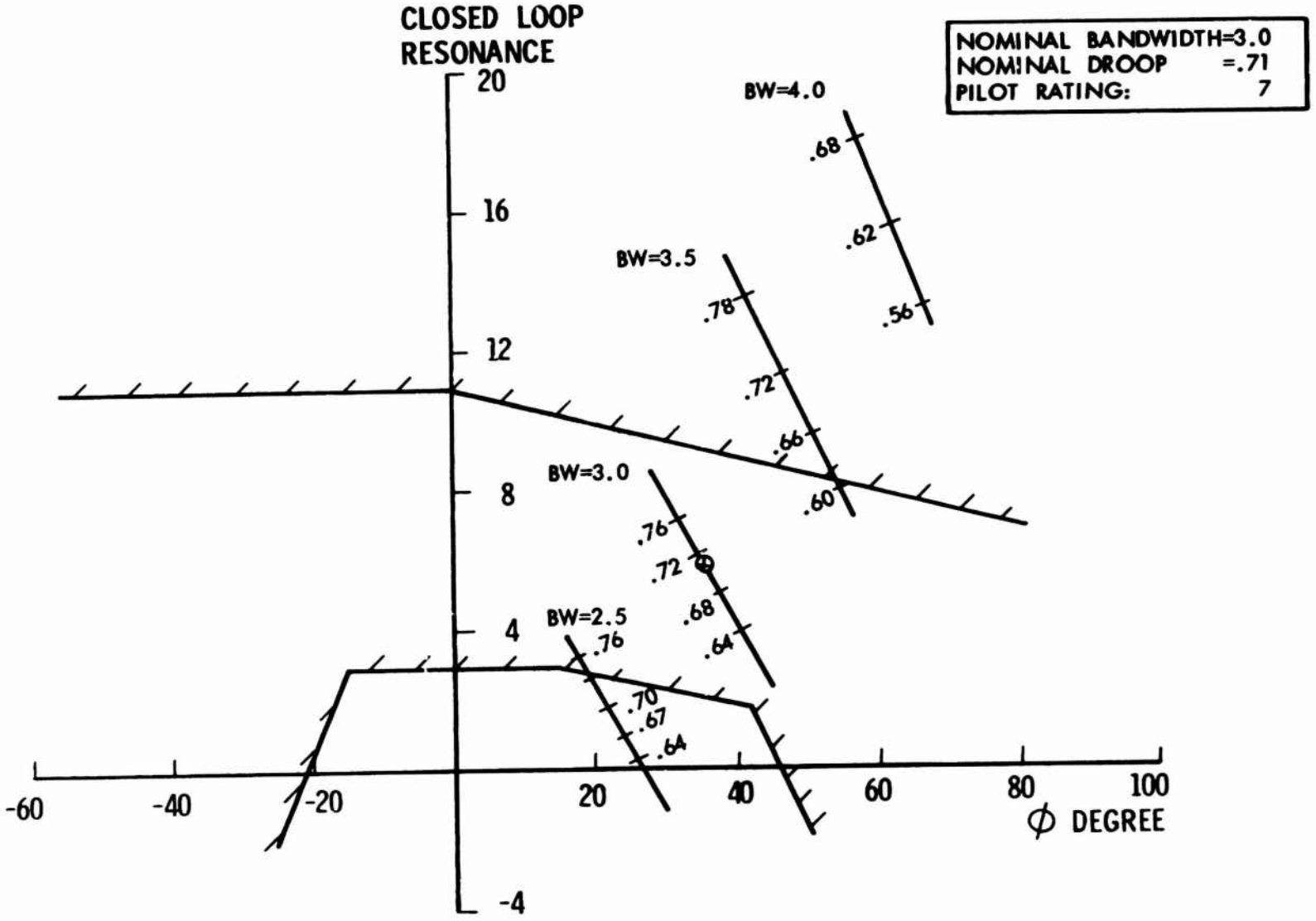

FIGURE 17. EFFECT OF BANDWIDTH AND DROOP; REFERENCE 1 DATA, CONFIGURATION 2G

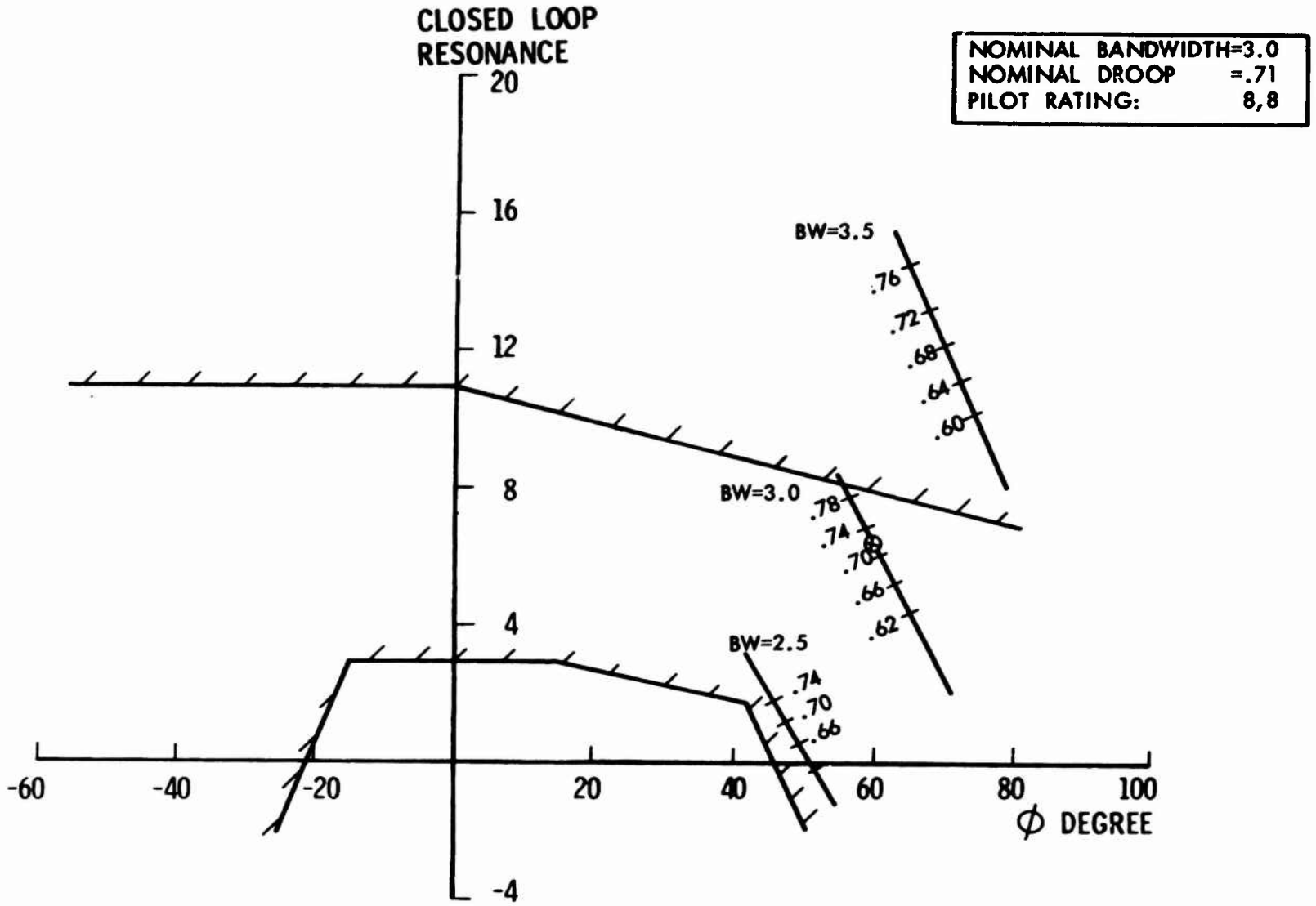

FIGURE 18. EFFECT OF BANDWIDTH AND DROOP; REFERENCE 1 DATA, CONFIGURATION 21

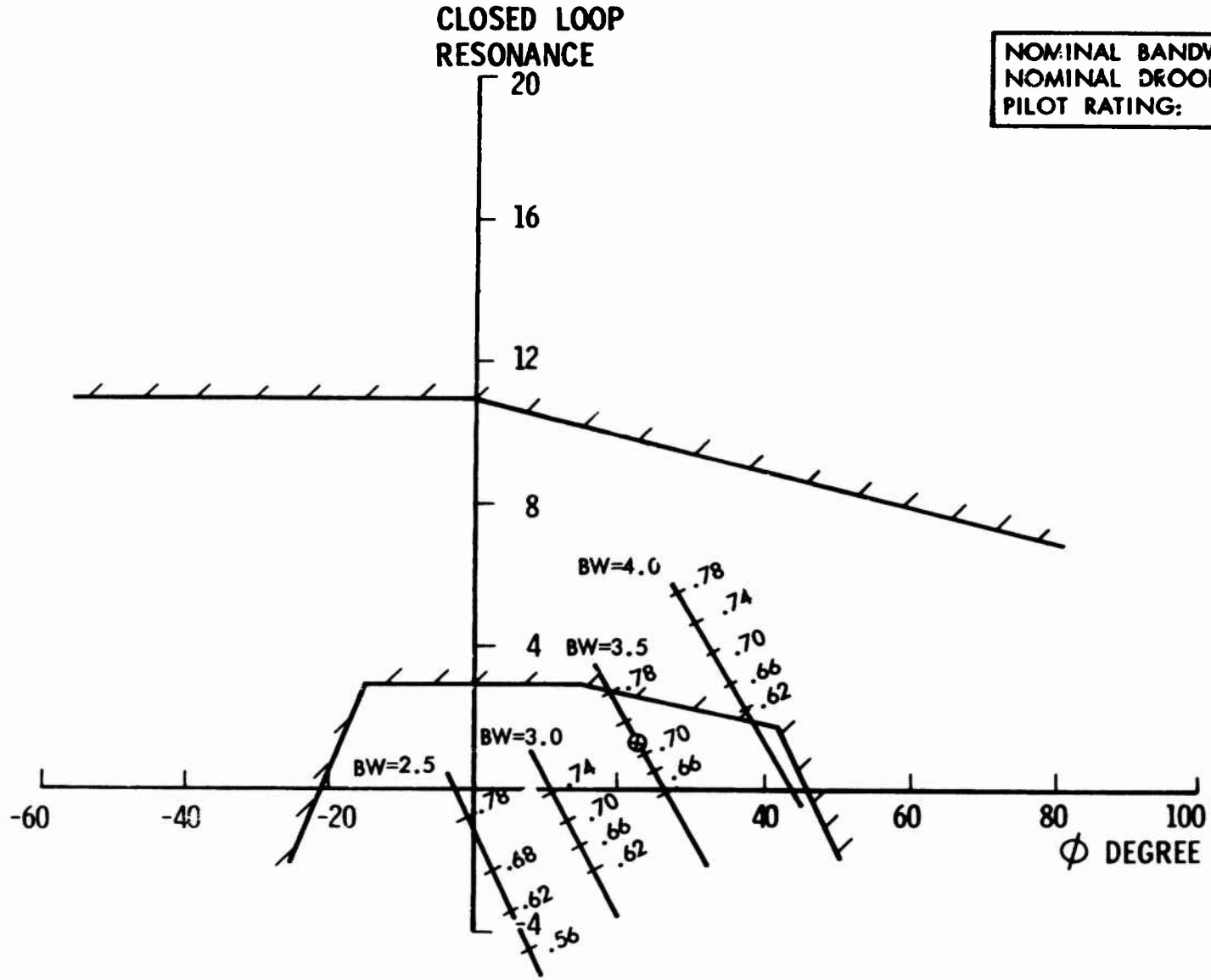

FIGURE 19. EFFECT OF BANDWIDTH AND DROOP; REFERENCE 1 DATA, CONFIGURATION 7D

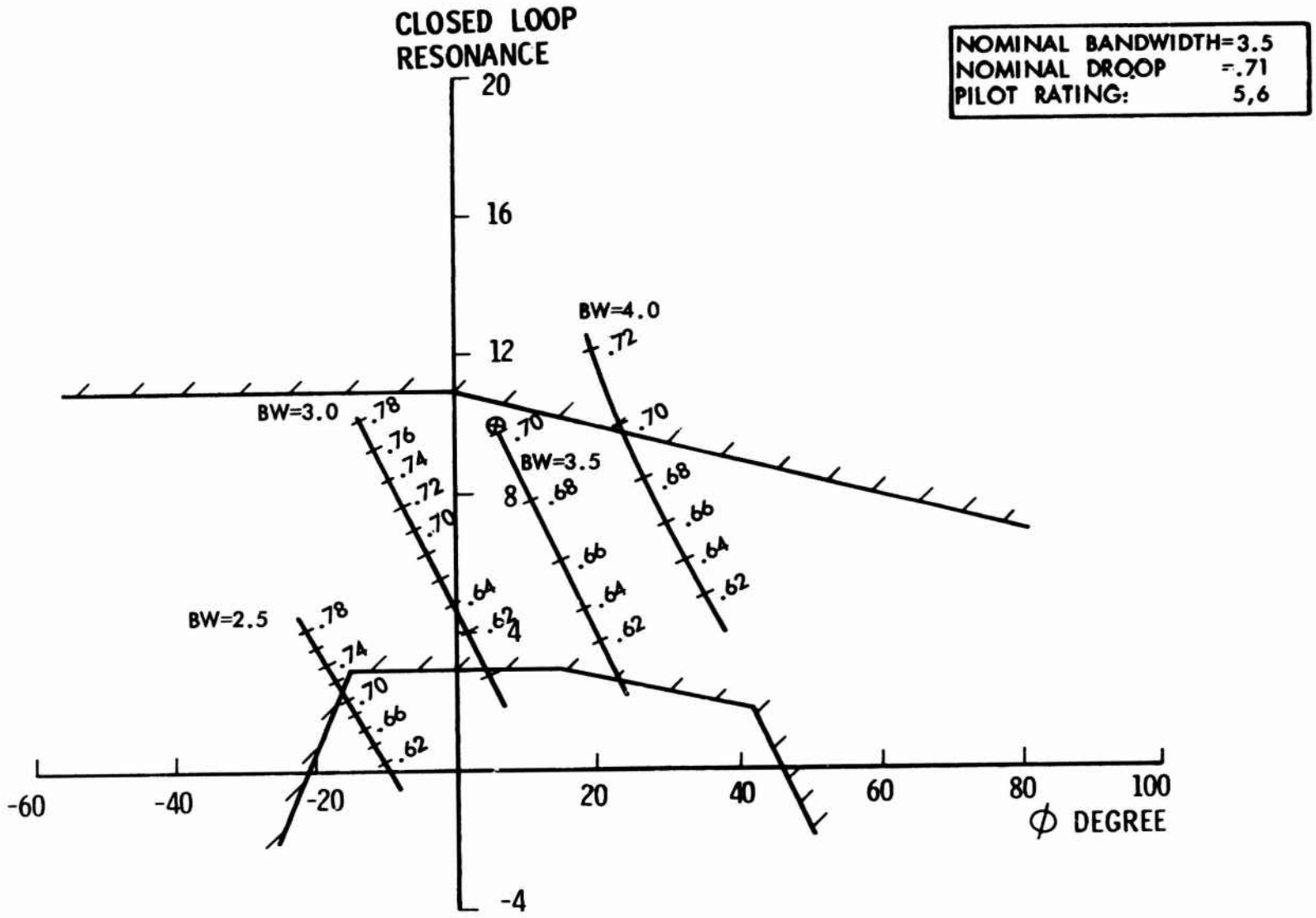

FIGURE 20. EFFECT OF BANDWIDTH AND DROOP; REFERENCE 1 DATA, CONFIGURATION 6A

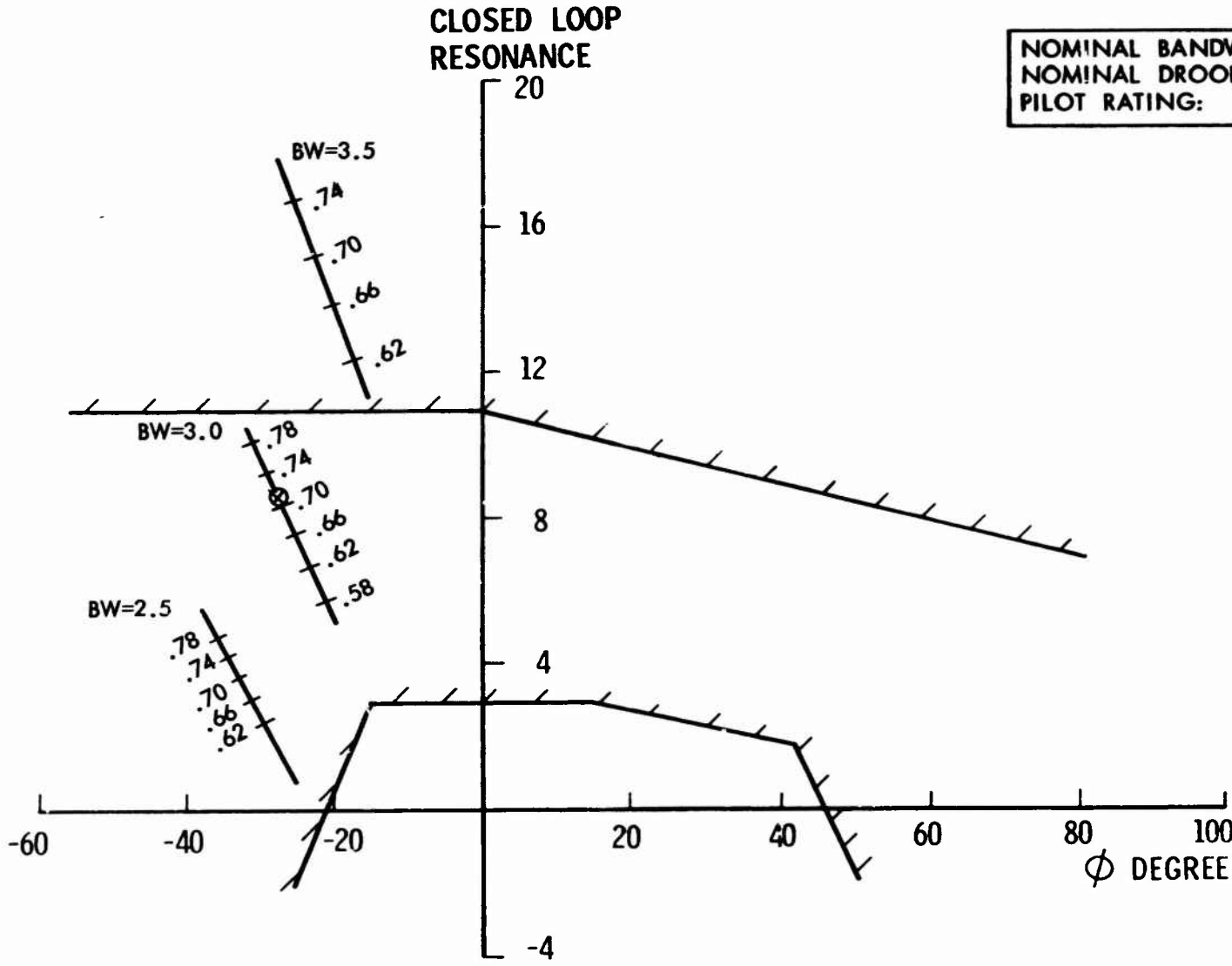

FIGURE 21. EFFECT OF BANDWIDTH AND DROOP; REFERENCE 1 DATA, CONFIGURATION 4A

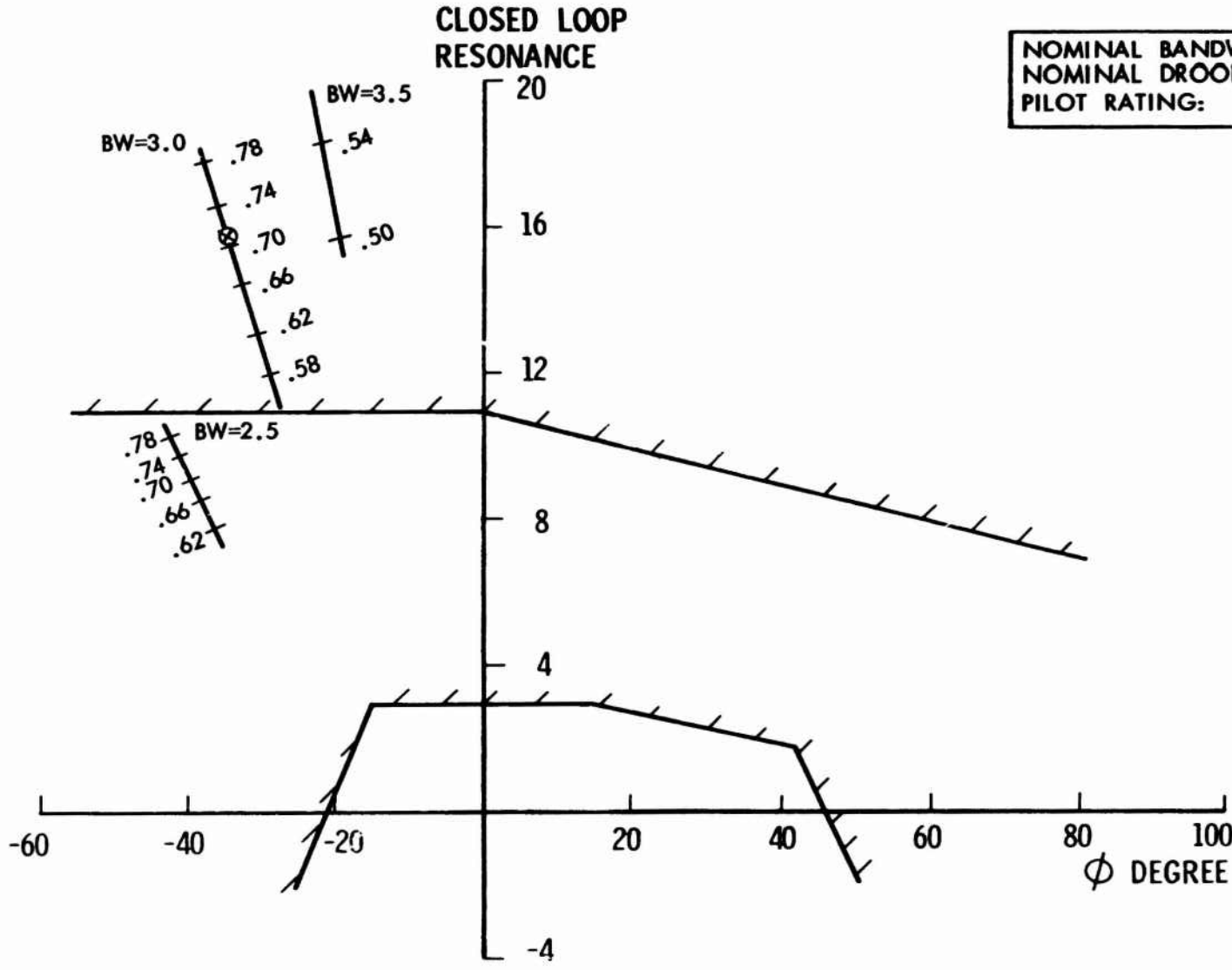

FIGURE 22. EFFECT OF BANDWIDTH AND DROOP; REFERENCE 1 DATA, CONFIGURATION 5A

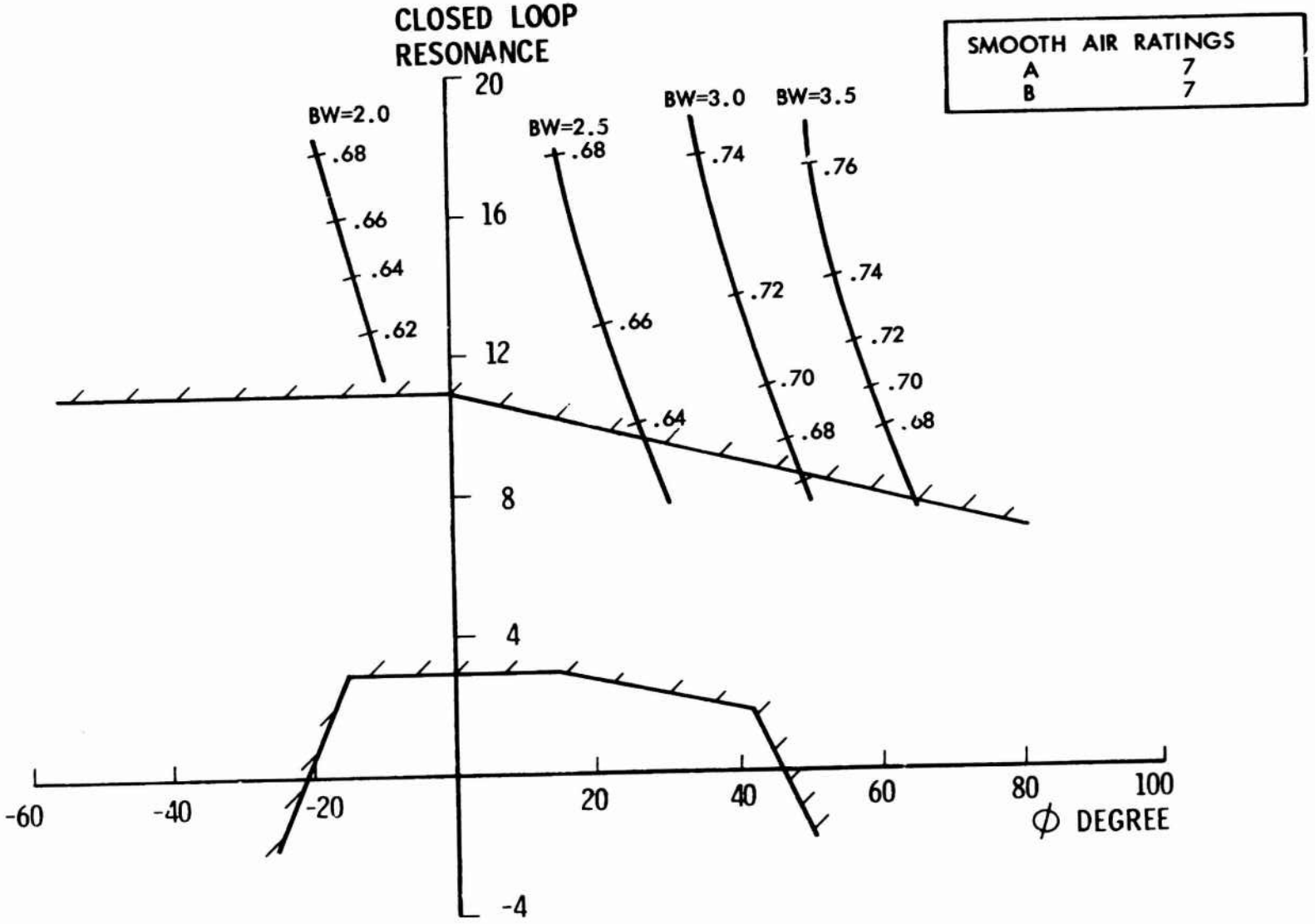

FIGURE 23. EFFECT OF BANDWIDTH AND DROOP; REFERENCE 6 DATA, CASE 034

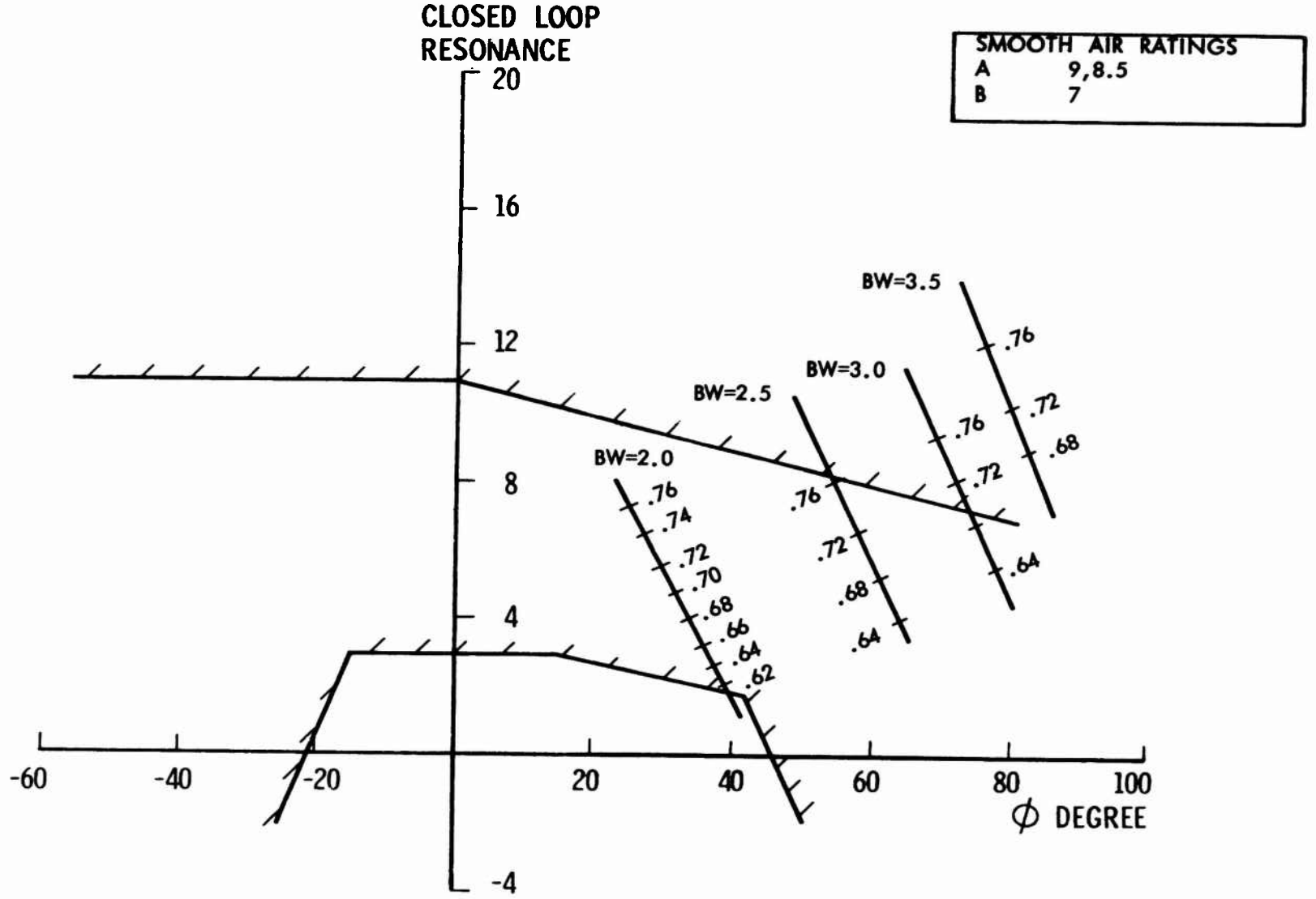

FIGURE 24. EFFECT OF BANDWIDTH AND DROOP; REFERENCE 6 DATA, CASE 044

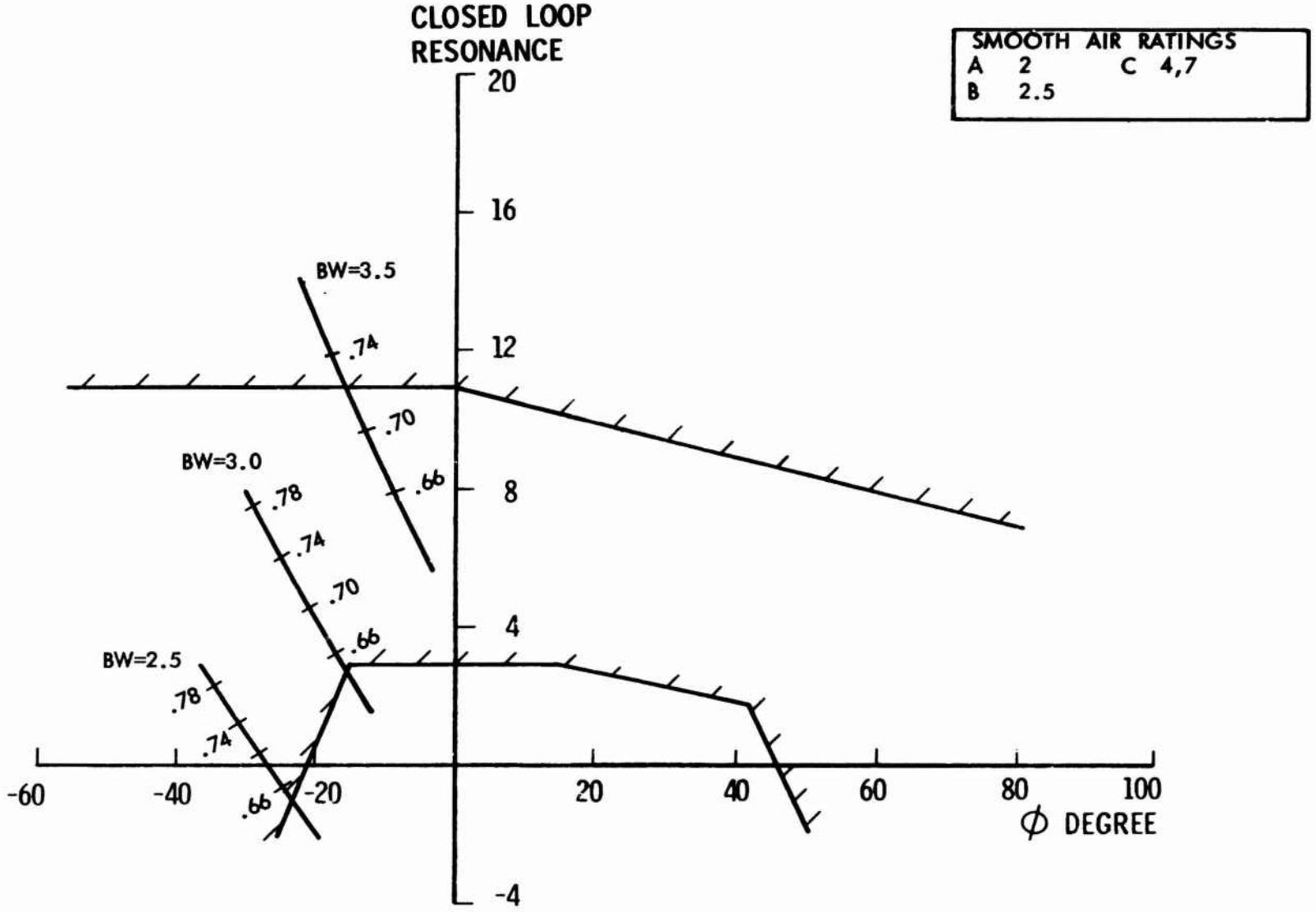

FIGURE 25. EFFECT OF BANDWIDTH AND DROOP; REFERENCE 6 DATA, CASE 131

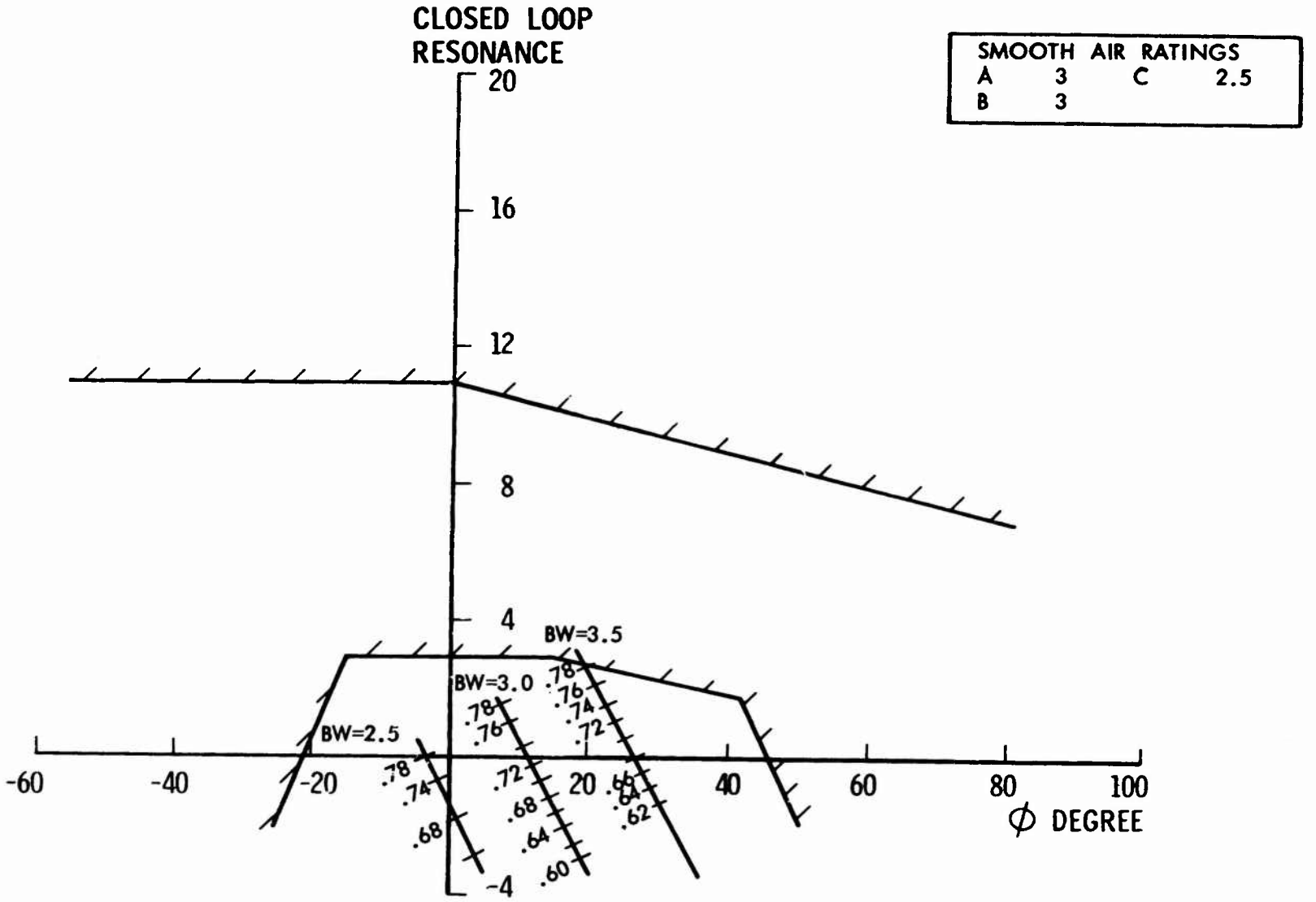

FIGURE 26. EFFECT OF BANDWIDTH AND DROOP; REFERENCE 6 DATA, CASE 141

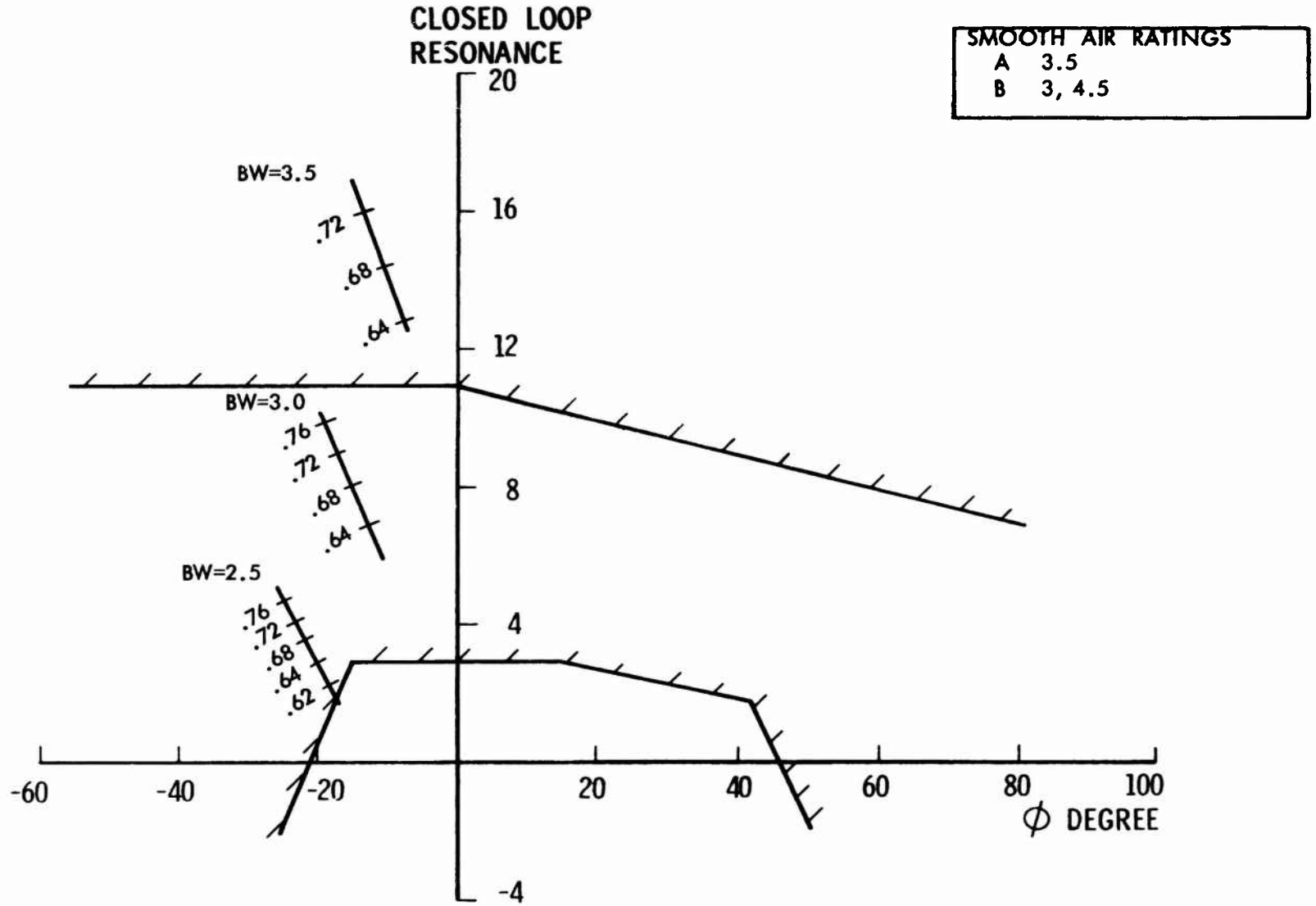

FIGURE 27. EFFECT OF BANDWIDTH AND DROOP; REFERENCE 6 DATA, CONFIGURATION 142

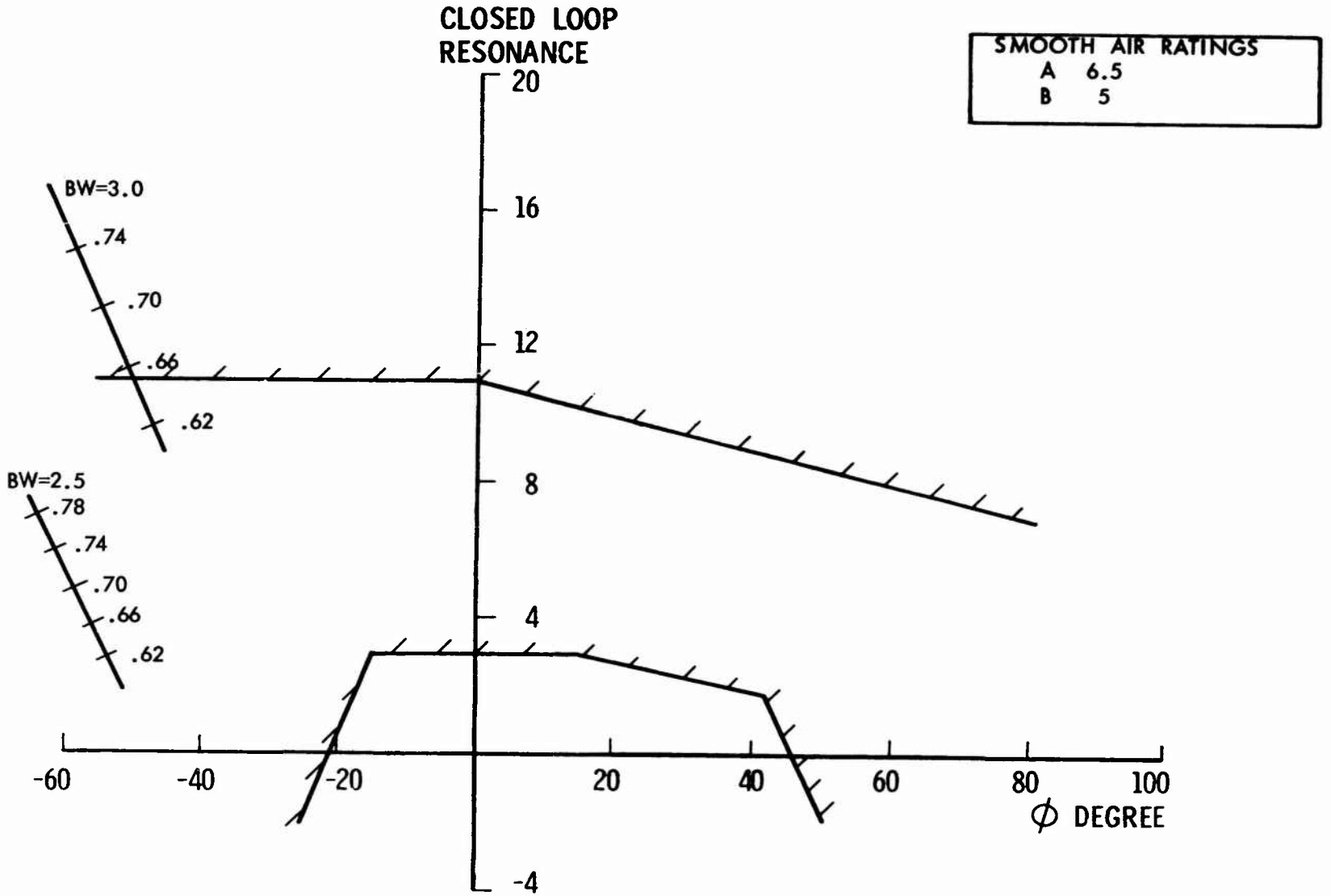

FIGURE 28. EFFECT OF BANDWIDTH AND DROOP; REFERENCE 6 DATA, CASE 322

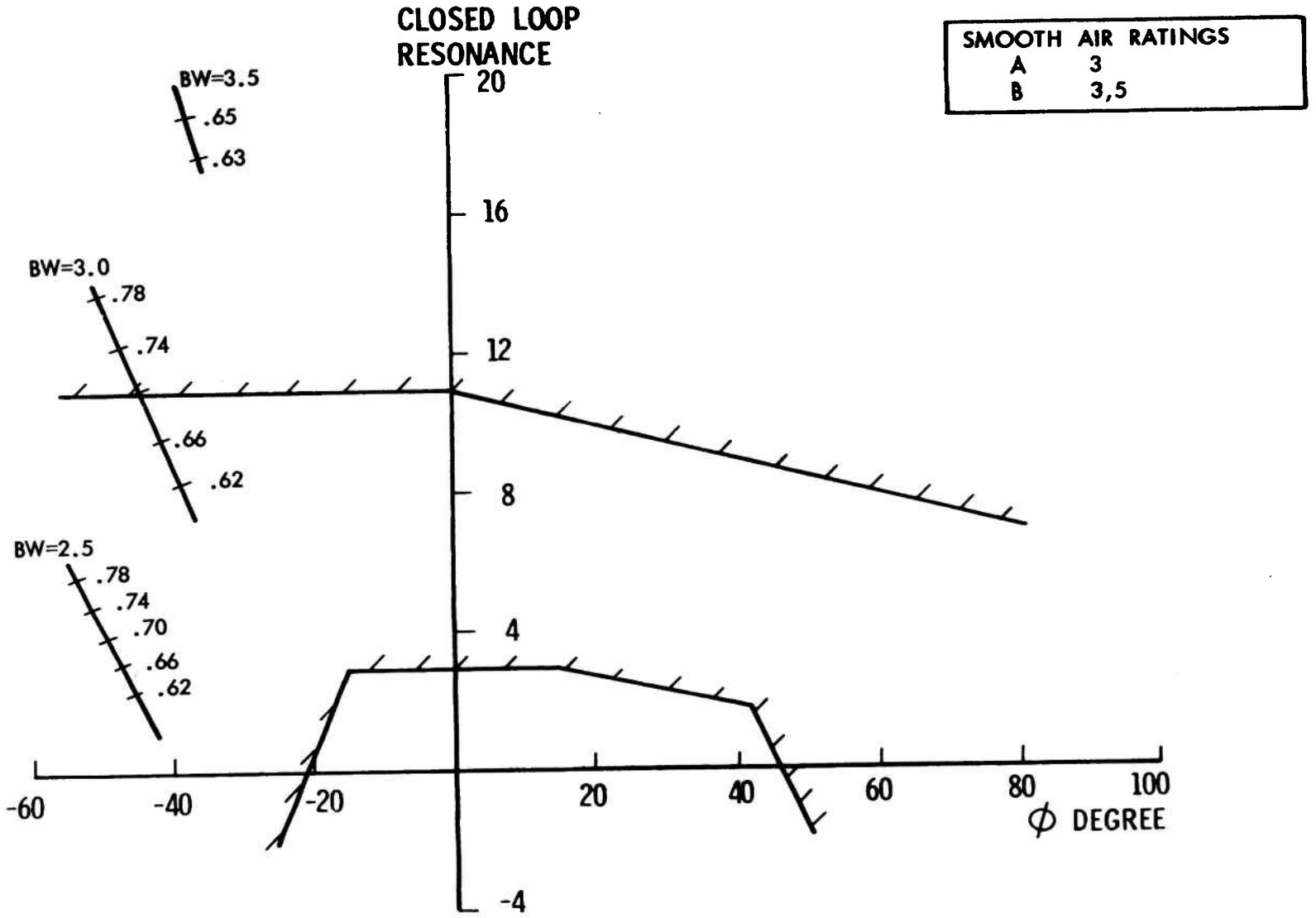

FIGURE 29. EFFECT OF BANDWIDTH AND DROOP; REFERENCE 6 DATA, CASE 332

TRACKING WITH HEAD POSITION USING AN ELECTRO-OPTICAL MONITOR

by

Bernard A. Chouet and Laurence R. Young

Man-Vehicle Laboratory
Massachusetts Institute of Technology

Abstract

An electro-optical head position monitoring system was designed and built and is used in single axis and three-axis "hands off" control tasks. The monitor consists of a transparent plexiglass body-fixed helmet, provided with a set of eight silicon photo-detectors sensing pitch, roll and yaw motions of the head. Two light-emitting diodes, attached to the pilot's helmet liner, provide the AC modulated near infrared radiation. Head control is compared with conventional manual control for single axis and three axis tracking tasks. Both performance curves and describing functions are presented.

1. INTRODUCTION

The use of head position as a control effector has been suggested and implemented for a variety of applications for which conventional manual control is impossible or undesirable. This paper describes a new photoelectric head monitor system and its integration in a closed-loop tracking situation with the three-axis moving base simulator in the M.I.T. Man-Vehicle Laboratory.

The head monitor serves a dual purpose. As a sensor of head rotation in three axes, it allows study of the dynamics of head movement. It also is used as a measure of three-axis head rotations for control purposes. The applications of such a system include "hands-off" attitude stabilization for astronaut extravehicular activity or control of systems under high acceleration conditions.

2. THE HEAD MONITORING SYSTEM

The concept of using head position as a control for man's attitude was investigated by Von Renner in our laboratory in 1970[10]. By measuring the electromyograms from sets of neck muscles with surface electrodes, he was able to control the position of a rotating chair in the yaw axis. The subject commanded chair velocity by simply turning his head to the left or right. However, the existence of a large rotation dead-band ($\pm 45°$) and the complexity of the signal conditioning circuits limited the feasibility of that system as a whole.

Many other approaches to head movement measurement have been tried[1,5,6,9] including acoustic, electro-magnetic, gyroscopic and optical configurations. The important considerations in the design of a head position sensor were flexibility, reliability, maintainability, linearity and human compatibility. By human compatibility we include the following:

- -The monitor should not interfere with visual functions
- -The monitor should not interfere with normal head movements
- -Attachments on the head should be minimized
- -A lockout device should permit free head movements unrelated to control.

An electro-optical system was designed to be compatible with these constraints. The monitor consists of an astronaut helmet, similar to the Apollo design. This piece is attached to a shoulder fixture and the head is free to move within it.

A set of eight silicon photodetectors is fitted in the helmet wall (Figure 1a) and two Light-Emitting Diodes (LEDs) are attached to the pilot's helmet liner (Figure 1b). The electronics for signal processing are in a separate box. The helmet, made of transparent plexiglass, was designed and built

specifically for the purpose of head position monitoring. Maximum neck mobility and anthropometric characteristics of the head typical of the astronaut population were considered as design factors[3,10]

As shown in Figure 1b, the instrumentation mounted on the pilot's head is limited to the two LEDs. One LED is attached to the helmet liner on the top of the head, aligned with the head vertical axis, and is used for the measurement of pitch and roll. The second LED is set on the back of the head and used for the measurement of yaw head movements. Each LED has an emission beam angle of 175° between half-power points. The radiation spectrum is centered at 9300 Å. Each photodetector has a directional sensitivity covering a solid angle of 180°. Pitch and roll head motions are sensed by a set of two detectors per axis. Direction of motion is determined by phase sensitive demodulation of the detector pair at the 1 kHz frequency of LED oscillation. The yaw axis has a similar arrangement, although it includes an additional two sensors to insure a monitor output saturation level when the pilot executes large turning motions. The helmet limits head rotations to +20° in pitch and roll. Head movement is unlimited in yaw; however, the monitoring range extends to only ±60°; (when used in yaw position control, the monitor is provided sufficient feedback gain so that the pilot need not perform large head movements).

The system operates on a ±15 volt 500 milliampere power supply. The two TIXL26 LEDs, mounted in series, are AC driven at 1 kHz by a Colpitts oscillator. Eight TIL65 phototransistors are used for detecting head motion. Each axis processing circuit consists of a preamplifier, ring demodulator and an output isolation operational amplier. The three demodulator reference signals are provided by the Colpitts oscillator which drives the LEDs. The monitor output for each axis is a DC voltage which varies within the range +15 volt. The system time constant is 2 milliseconds and contains a measured 1.2% ripple. The electronics are shielded from electromagnetic interference. Optical shielding of the helmet from ambient light was not necessary for the simulator environment. However, laboratory experiments showed that a 500 Å layer of vacuum deposited aluminum was sufficient to cut transmittance of all wavelengths down to 30% without significantly reducing the ability to see through the visor. A detailed description of the electronic and geometrical characteristics of the monitor is given by Chouet[2]. A view of the monitoring equipment is shown in Figure 1c.

3. SYSTEM OUTPUT DECOUPLING

The geometry of the monitoring system, with the yaw detectors placed above the center of head rotation, leads to a coupling between the roll and yaw axes. Furthermore, most natural yaw head

movements involve a small amount of roll as well. Decoupling of the pitch, roll and yaw commands was realized with a real time PDP-8 computer operating on the monitor output. The decoupling scheme can be expressed by Equation 1:

$$\Delta \begin{Bmatrix} \psi_c \\ \theta_c \\ \phi_c \end{Bmatrix} = \begin{bmatrix} 1 & a_{\psi\theta} & a_{\psi\phi} \\ a_{\theta\psi} & 1 & a_{\theta\phi} \\ a_{\phi\psi} & a_{\phi\theta} & 1 \end{bmatrix} \begin{Bmatrix} v_\psi \\ v_\theta \\ v_\phi \end{Bmatrix} \tag{1}$$

or in a condensed vectorial form:

$$\Delta n_c = A v_n \tag{2}$$

The angles ψ_c, θ_c, and ϕ_c represent the command vector for yaw, pitch and roll axes respectively, whereas v_ψ, v_θ, and v_ϕ are the measured monitor output voltages for those axes. Δ indicates a change in the command vector from the nominal angles. (Normally, the nominal angles are established for the head upright and look-straight ahead).

The six coefficients a_{ij} of the decoupling matrix A must be established individually for each pilot wearing the monitor. As an example, in the case of pure pitch motions, we would want the command roll and yaw to be zero.

$$\begin{aligned} v_\psi(\theta,\ \psi = 0,\ \phi = 0) &+ a_{\psi\theta} v_\theta[\theta(t)] \simeq 0 \\ v_\phi(\theta,\ \psi = 0,\ \phi = 0) &+ a_{\phi\theta} v_\theta[\theta(t)] \simeq 0 \end{aligned} \tag{3}$$

To accomplish this, we define the cross-coupling cost function:

$$J_{\psi\theta} = \frac{1}{T}\int_0^T [v_\psi(\theta(t)) + a_{\psi\theta} v_\theta(\theta(t))]^2 dt$$

$$= \frac{1}{T}\int_0^T v_\psi^2\, dt + \frac{2a_{\psi\theta}}{T}\int_0^T v_\psi v_\theta dt + \frac{a_{\psi\theta}^2}{T}\int_0^T v_\theta^2\, dt \tag{4}$$

Minimizing the cost function with respect to $a_{\psi\theta}$ gives:

$$\frac{\partial J_{\psi\theta}}{\partial a_{\psi\theta}} = \frac{2}{T}\int_0^T v_\psi v_\theta dt + \frac{2a_{\psi\theta}}{T}\int_0^T v_\theta^2 dt = 0 \tag{5}$$

Hence:

$$a_{\psi\theta} = -\frac{\int_0^T v_\psi v_\theta dt}{\int_0^T v_\theta^2 dt} \tag{6}$$

And similarly, to minimize the effect of pitch motion on roll detection, we calculate the coefficient:

$$a_{\phi\theta} = -\frac{\int_0^T v_\psi v_\theta dt}{\int_0^T v_\theta^2 dt} \qquad (7)$$

The same procedure applied to pure roll and pure yaw motions leads to similar computations. The six coefficients are summarized below:

ROLL	YAW	PITCH
$a_{\psi\phi} = -\frac{\int_0^T v_\phi v_\phi dt}{\int_0^T v_\phi^2 dt}$	$a_{\theta\psi} = -\frac{\int_0^T v_\theta v_\psi dt}{\int_0^T v_\psi^2 dt}$	$a_{\psi\theta} = -\frac{\int_0^T v_\psi v_\theta dt}{\int_0^T v_\theta^2 dt}$
$a_{\theta\phi} = -\frac{\int_0^T v_\theta v_\phi dt}{\int_0^T v_\phi^2 dt}$	$a_{\phi\psi} = -\frac{\int_0^T v_\phi v_\psi dt}{\int_0^T v_\psi^2 dt}$	$a_{\phi\theta} = -\frac{\int_0^T v_\phi v_\theta dt}{\int_0^T v_\theta^2 dt}$

The head motion used for the computation of the coefficients was a natural, approximately sinusoidal, swing of the head about the axis to be decoupled. Several cycles were taken to obtain a good average value for each factor. The basic interval of computation was thirty seconds, one value of each of the two coefficients involved being updated every five seconds. Convergence was then estimated and with satisfactory results the final values were stored in the computer memory for later use in the experiment. The accuracy of each decoupling coefficient depends on the regularity and also the amplitude of the subject's head motions during the computation procedure. The error involved in the linearization process was small, however, and is depicted in the average value of the decoupling efficacy, as defined in the next section.

	$a_{\theta\psi}$	$a_{\phi\psi}$	$a_{\theta\phi}$	$a_{\psi\phi}$	$a_{\psi\theta}$	$a_{\phi\theta}$
Average Decoupling Efficacy in % (3 subjects)	97.2	89.4	97.6	79.3	98.4	99.3

The tightest coupling of head movement was, as expected, between yaw and roll head movements. Subjects' relative inability to make a pure yaw or roll head movement, combined with the geometric factors of detector placement to make the decoupling problem most severe about these axes. However, even in the worst case (coefficient $a_{\psi\phi}$) the residual coupling between the roll and yaw axes did not affect the subjects' performance. Typical sensitivities were 0.44 volts/deg. in yaw, 0.59 volts/deg. in roll and 0.72 volts/deg in pitch. Linearity is about 2% of the full scale in pitch and roll and 6% of full scale in yaw.

4. THE EXPERIMENTS

Three subjects were used in the experiments. Two of them (SY

and JD) had control experience in dynamics of various order, including one case (JD) flying a light airplane. The third subject (DC) had no experience with control systems, simulators or any vehicle.

The experiments were performed using the three-axis motion simulator (modified Link GAT-1) of the Man-Vehicle Laboratory. Tracking with head and manual control were compared for each separate axis in compensatory tasks. The ability to control the attitude of the vehicle was then tested for both manual and head control in three axis control tasks.

The dynamics of the trainer in yaw, roll and pitch were modified to approximate a rate control. The compensated dynamics of the trainer in each axis were then:

$$G(s) = \frac{1}{s}\left[\frac{1}{0.1s + 1}\right] \approx \frac{1}{s} \qquad \text{degree/volt}$$

The monitor assembly was fixed to the back of the vehicle seat and arranged to fit each pilot. The subjects themselves were strapped to the seat and the head was free to move with respect to the body, within the limits of the helmet. Thus, we roughly simulated the situation encountered by an astronaut in space, where the head can move freely with respect to the shoulders inside the space helmet.

The trainer and monitor were linked to a hybrid PDP-8/GPS Corp. 290T computer system. Compensation circuits were wired on the analog section. The vehicle faced a 13 foot radius curved screen on which its motions were displayed by a one inch wide arrow projected from the roof of the trainer. For compensatory tracking tasks, a fixed target was set on the screen, consisting of two red strips, spaced one inch apart. The subjects were provided with a lockout switch to shut the system off in case of an emergency. The switch was never used.

Single-Axis Compensatory Tracking Tasks

The ability to control the vehicle position was first tested for compensatory tracking tasks. A block diagram of the head control is shown in Figure 2. Two sets of pseudo-random input disturbances were used. Each was a zero-mean rectangular spectrum composed of 16 sinusoids. Bandwidths were 0.295 Hz and 1.55 Hz. Each control axis was tested separately. While one motion was being studied, the two other vehicle axes were locked out by a position control to avoid any bias due to rotational cross-coupling. The head monitor outputs were scaled at $\pm$ 10 volts, the computer generated decoupled command signals in the range of $\pm$ 2.5 volts. In manual control, the actuator was a three-axis single arm spring restrained stick, characterized by $\pm$ 7 volt maximum output levels. The range of disturbance amplitudes was also limited to $\pm$ 7 volts. On the yaw axis, the result was a maximum rotation, in the absence of control of about three full revolutions, with typical maximum angular velocities of 15 to 20°/sec. Pitch motions were within the trainer limits of 16° up and 10° down, with maximum

velocities of 20°/sec. Maximum roll motion was set to ± 12.5°, restricted by the trainer limits, and peak roll velocities were similar to those in pitch.

The subjects were only instructed to maintain the vehicle's position with respect to the visual reference on the screen, by head or stick movements. Their comments were recorded and suggestions for adjustment of the helmet were implemented. All tracking runs were of three minutes duration, with a five minute rest between each of them. Before the tests started, the subjects were given several practice runs to familiarize themselves with the system. Data were then taken for the next series of experiments. Chart records were obtained of the random input, head command signals, vehicle position output, Integrated Squared Input (ISI) and Integrated Squared Vehicle Position Error (ISVPE). The ratios of ISVPE to ISI provided us with performance indices to compare individual runs and intrasubject performance. Similarly, the two other monitor outputs were squared and integrated over the entire length of a run and then divided by the ISI. These ratios were used to define the decoupling efficacy of the computer program; (a ratio of zero represents an efficacy of one hundred percent, whereas a ratio of one or higher represents an efficacy of zero percent). In parallel with the decoupling task and the computation of the integrated squared signals, as well as performance indices, the program could be used to include various thresholds in the monitor output characteristics.

The vehicle velocity output and the five chart recorder signals were also recorded on FM magnetic tape for later describing function analysis. A sample of chart recorder signals is shown in Figure 3 for the yaw position control in the case of the low frequency disturbance input. Subject performance curves, shown in Figure 4a-f, were established as a function of the open loop gain (the product of monitor gain, computer scaling and control gain, with trainer gain unity). The corresponding mean Maximum Peak to Peak Head Motion (MPPHM) necessary for the control is also shown on the graphs. For comparison, performance curves of the three subjects in manual control are given in Figure 5a-f, over a similar range of open loop gains. (No direct comparison of gains in deg/deg has been made. Notice the insensitivity of performance to gain for stick control, and, to a much lesser extent, for head control). The Performance Indices (PI) at the optimum gain, for each subject are summarized in Table 1.

Table 1. Compensatory Tracking Tasks: Summary of Results

Head Control

Subject	PI-Low Frequency			PI-High Frequency		
	Yaw	Pitch	Roll	Yaw	Pitch	Roll
JD	0.075	0.104	0.342	0.083	0.086	0.980
SY	0.085	0.049	0.299	0.156	0.078	1.300
DC	0.131	0.071	0.810	0.181	0.096	1.500

Manual Control

Subject	PI-Low Frequency			PI-High Frequency		
	Yaw	Pitch	Roll	Yaw	Pitch	Roll
JD	0.044	0.043	0.029	0.058	0.049	0.107
SY	0.033	0.046	0.191	0.123	0.064	0.434
DC	0.209	0.068	0.143	0.379	0.103	0.289

Close scrutiny of the Table 1 figures, as well as comparison of the performance curves of each control in each axis, reveals marked similarities between the two systems. Comparatively poorer results were obtained in head control about the roll axis. In normal daily activity, voluntary head movements are primarily in the yaw and pitch planes. The absence of any need to maintain any specific roll orientation of visual fields limits most roll head movements to postural reactions keeping the head upright, and to quasi static tilts, as for example, those needed to orient the head with respect to the lines of print in a tilted book. It is hardly surprising, therefore, that unpracticed subjects found greater difficulty in using voluntary control of roll head position than for motion about the other axes. Furthermore, the location of the suspension point below the neck in this experiment contributed possible biomechanical cross-coupling between linear acceleration and head movement control for pitch and roll (the trainer pitch and roll axes were three feet below the subject's head). The sign of the inertial reaction of the head to a roll or pitch acceleration is in the correct direction for stabilization, however, and no systematic study of the influence of the cross-coupling was undertaken. Except for the roll axis, the head motion control compared favorably with manual control. The human compatibility of head movement control, especially in yaw, was noted. Optimal performances were obtained for ranges of head angles of $\pm$ 15° to $\pm$ 25° in yaw, $\pm$ 11° to $\pm$ 17° in roll, and $\pm$ 6° to $\pm$ 13° in pitch. The subjects did not complain about visual interaction. It is probable that single axis hand motions are more precise than head motions when the error to be compensated becomes small.

Describing Functions

The human operator's describing functions for manual and head

control in closed-loop compensatory tracking tasks were obtained using a Fast Fourier Transform (FFT) program. Samples were taken from the data stored on magnetic tape during the previous experiments and processed on the PDP-8 digital computer. To avoid initial transient artifacts, the sampling of the pilot's input and output (i.e. the trainer position error (ψ_e, θ_e, ϕ_e) and the control head or manual signal (n_c)) was made only in the middle portion of the run. Low frequency disturbance experiment data were taken every 0.25 second for 128 seconds. For the high frequency disturbance runs, the sampling period was 0.0625 seconds for 32 seconds of record. Only the specific frequency components of the random input were considered in calculating the describing function $Y_p(j\omega)$. All the graphs were established for the approximate moving base vehicle dynamics $Y_c(s) = K/s$ for the three axes in both head and manual control. These graphs are presented in Figures 6a-f. Over plots of $|1/Y_c|$ are drawn on each describing function. The crossover frequencies, indicated by the intersection of the $|1/Y_c|$ and the $|Y_p|$ curves, are presented in Table 2[7]. For the yaw axis the slightly better performance with stick control seen in Table 1, is not reflected in a difference in crossover frequency. The higher crossover frequencies in pitch and roll manual control, compared to yaw are consistent with the additional motion cues available through graviceptor stimulation[4,8]. The lower crossover frequency seen for roll head control, compared to roll stick control is reflected in the higher PI, as discussed above.

Table 2. Crossover Frequencies

	Head Control	Manual Control
Yaw	3.0 rad/sec	3.0 rad/sec
Pitch	4.6 rad/sec	5.5 rad/sec
Roll	3.0 rad/sec	5.0 rad/sec

Three-axis Control

Precision, speed, stability, smoothness and human compatibility of both manual and head piloting were compared in a three axis task. The block diagram for this experiment is the same as in Figure 2 with the disturbance removed; instead, a step is applied to the reference. Four targets were established on the screen. Reaching each of these required the use of the three degrees of rotational freedom of the trainer. The target disposition is given in Table 3, with rotation in the order of yaw, pitch and roll.

Table 3. Target Positions

Position	Yaw	Pitch	Roll
Target "0"	0°	0°	0°
Target "1"	150° left	11° up	12° left
Target "2"	53° left	13° up	3° left
Target "3"	90° left	10° down	12° right

As for compensatory tracking tasks, each target was made of two red strips clearly visible on the white background of the screen, and the projected spot, a vertical arrow, was to be set in between these markers.

The pilots were required to minimize the traveling time between the targets on the screen and to stabilize their position within the target limits (± 45 arc min) for at least fifteen seconds. Stability was estimated visually by the experimenter and clearance to leave for the next spot was communicated to the pilot when the result was judged satisfactory. The subjects were left free to practice with the system as long as they desired, (about ten minutes) and the feedback gains were varied until near optimal conditions were reached. The three head monitor control outputs were decoupled and ± 1° rotation thresholds were inserted in the commands to help the subjects in zeroing their head position. Typical time plots of the trainer trajectory are shown in Figure 7a-b. As seen on these plots, head control led naturally to simultaneous motions about the three axes. By looking in the right direction, the subjects were taking the shortest path from one target to the next. As they kept their head aimed at their destination, the position error between head and helmet gradually decreased following the trainer motion. A few corrections were then made in the vicinity of the target to lock into the required position. Starting from one spot and locking into another generally took ten to fifteen seconds. No significant differences were noted between the subjects, and all of them were able to stabilize on each target as long as needed. With the stick, however, the motions were clearly sequential. Knowing their destination, the subjects generally estimated which axis required the largest displacement and started moving about that particular axis first. A new estimation was then made, followed by another decoupled move, and so on; in Figure 7b for example, we see that the subject started from target "0" with a yaw, then made a pitch and finished with a roll. This behavior resulted in a longer path between the targets, but the total amount of time spent traveling and stabilizing was about the same as for head control, at least for two subjects, one pilot being unable to stabilize on target "2".

CONCLUSION

From an engineering point of view, the head monitoring system performed well, was very reliable, and proved flexible enough to accommodate each pilot. The subjects found it comfortable, although some complained about the loss of freedom in their head position. Non-linearities within the monitor's output were minimal. The subjects showed somewhat better tracking performance in single axis manual control than with the head control. In a three axis configuration, the head control led to more efficient synchronized motion than the manual control. To this advantage is added the fact that this type of control leaves the hands free.

REFERENCES

[1] Briggs, P., and Hofmann, L., "The Application of Human Operator Describing Function Theory to the Prediction of Tracking Performance in the CHEYENNE SWIVELING GUNNER'S STATION", Fifth Annual NASA-University Conference on Manual Control, M.I.T., March, 1969.

[2] Chouet, B., "An Electro-Optical Attitude Control System for Astronaut Space Activities", M.I.T., Department of Aeronautics and Astronautics, S.M. Thesis, June 1972.

[3] "Compendium of Human Responses to the Aerospace Environment", Vol. I and III, NASA CR-1205(I),(III), November 1968.

[4] Dinsdale, P.B., "Relative Effects of Roll and Yaw Motion Cues in Manual Control", M.I.T., Department of Aeronautics and Astronautics, S.M. Thesis, September 1968.

[5] Henke, A.H., "An Investigation of Head Tracking Performance using a Helmet Mounted Sight and Display System", Sixth Annual Conference on Manual Control, Wright Patterson AFB, April 1970.

[6] Howland, H.R., "An Angular Head-Position Indicator", B.S. E.E., M.I.T., June 1962.

[7] McRuer, D.T., Graham, D., and Krendel, E.S., "Manual Control of Single Loop Systems", J. Franklin Institute, Vol. 283, Nos. 1 and 2, 145-168, 1967.

[8] Shirley, R.S., and Young, L.R., "Effect of Roll-Motion Cues on Human Operator's Behavior in Compensatory Systems with Disturbance Inputs", IEEE Transactions on Man-Machine Systems, Vol. MMS-9, No. 4, December 1968.

[9] Sweeney, J., "Human Performance with a Helmet Mounted Display and Head Position Sensing System", Fifth Annual NASA-University Conference on Manual Control, M.I.T., March 1969.

[10] Von Renner, L.C., "Extravehicular Attitude Control by Use of Head Motions", M.I.T., Department of Aeronautics and Astronautics, S.M. Thesis, June 1970.

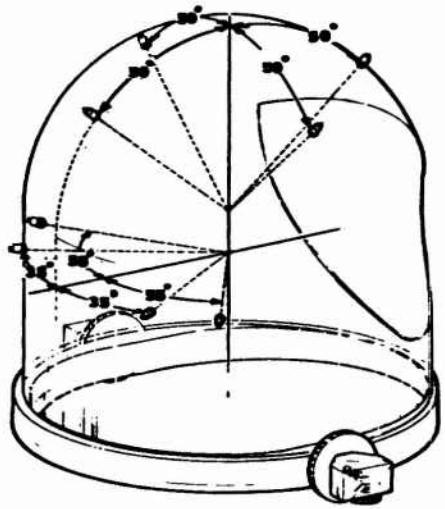

(a) Helmet and Disposition of the Eight Photodetectors

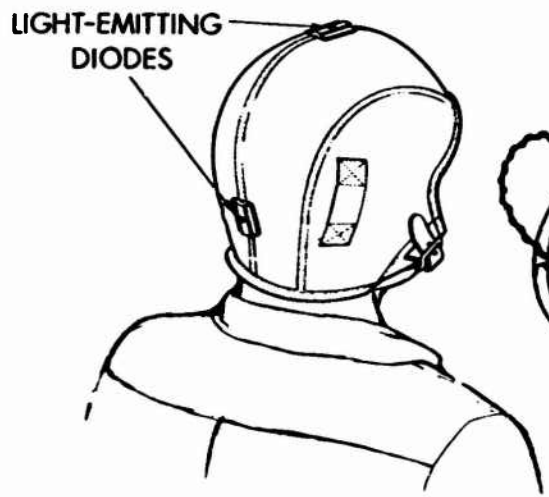

(b) Helmet Liner with the two LEDS

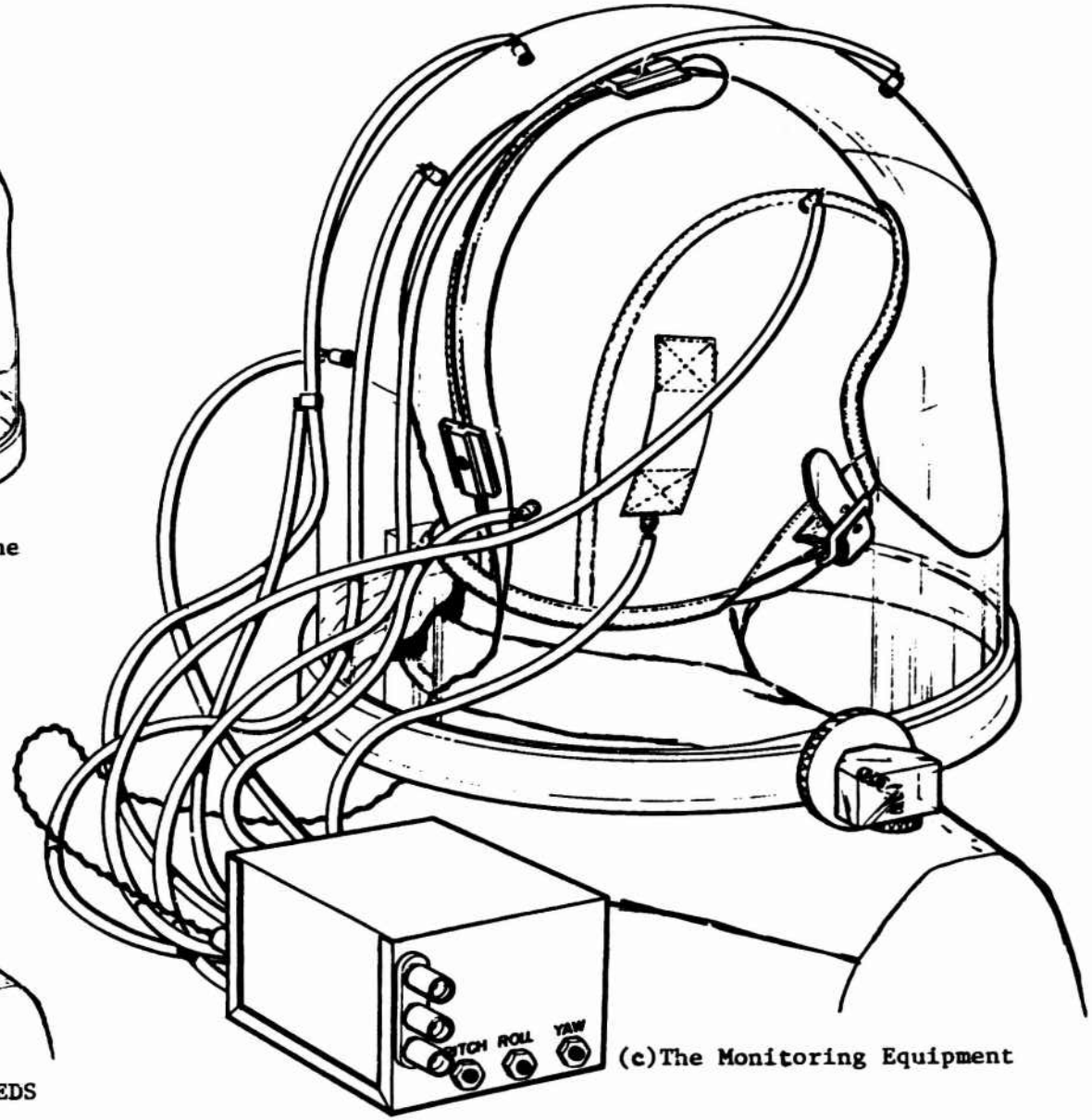

(c)The Monitoring Equipment

Figure 1

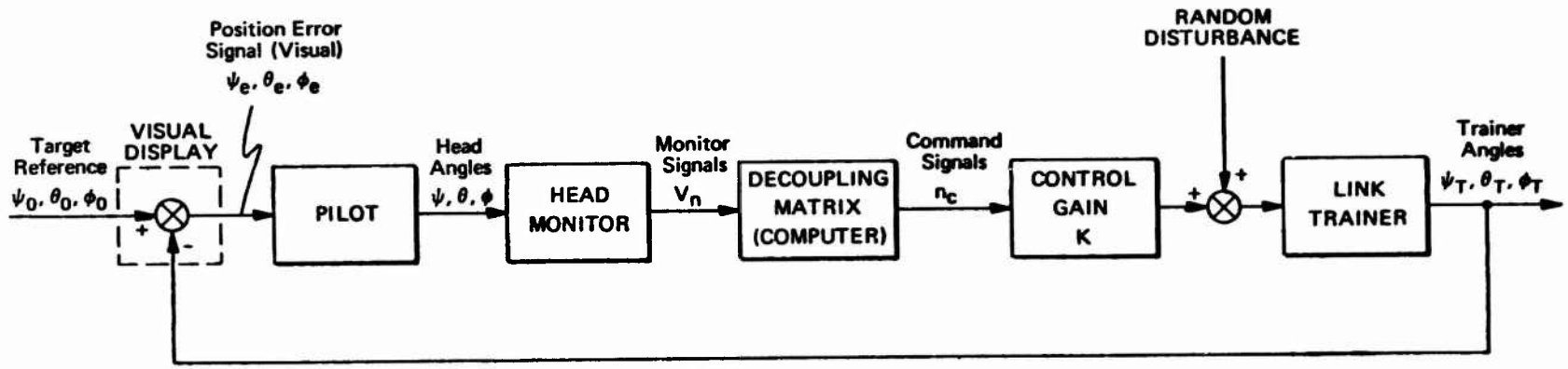

Figure 2 - Block Diagram of the Head Control Experiment

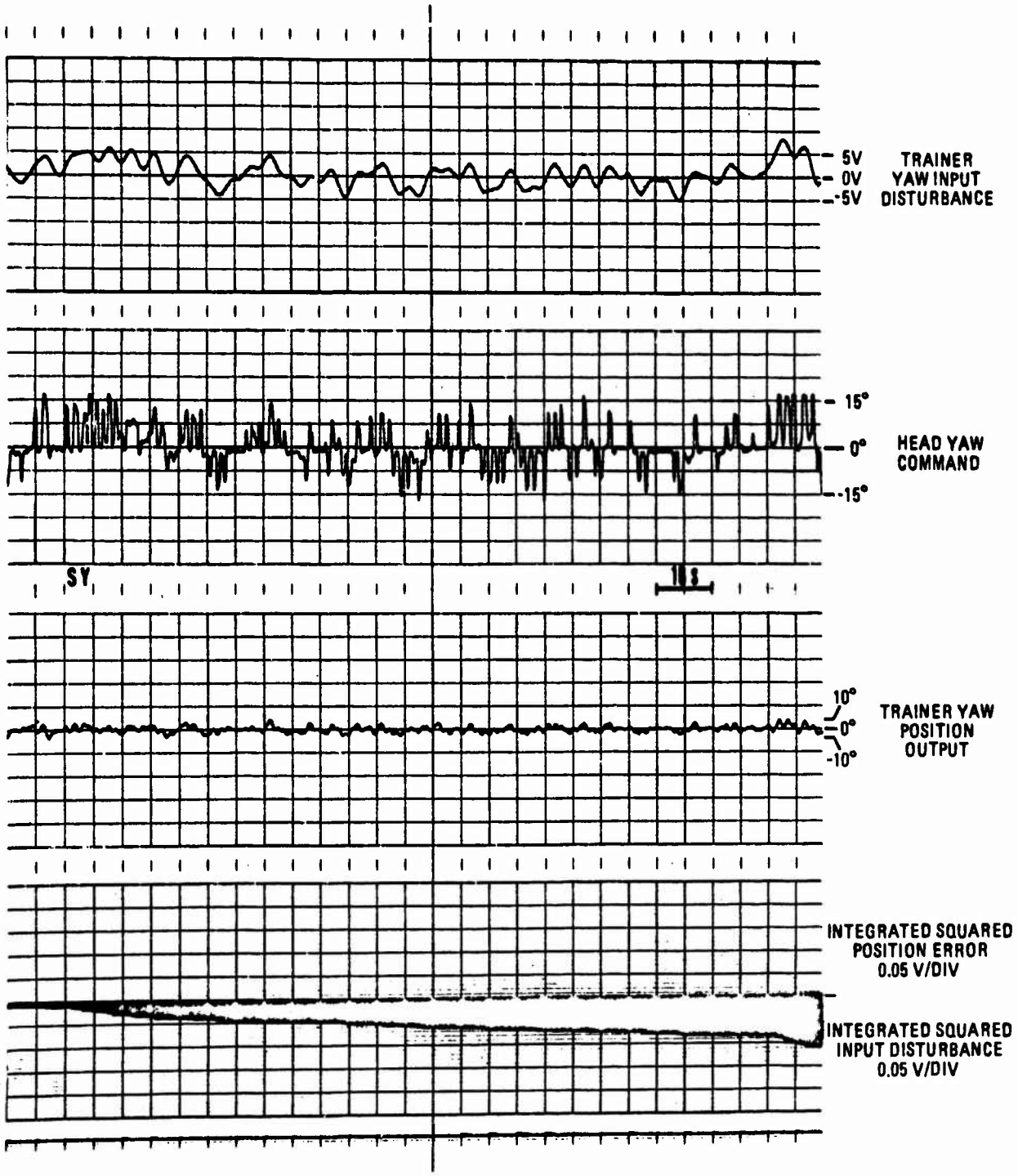

Figure 3 - Typical Yaw Motions with Head Control: Low Frequency Disturbance, Subject SY, Open-Loop Gain 0.66 Volt/Degree

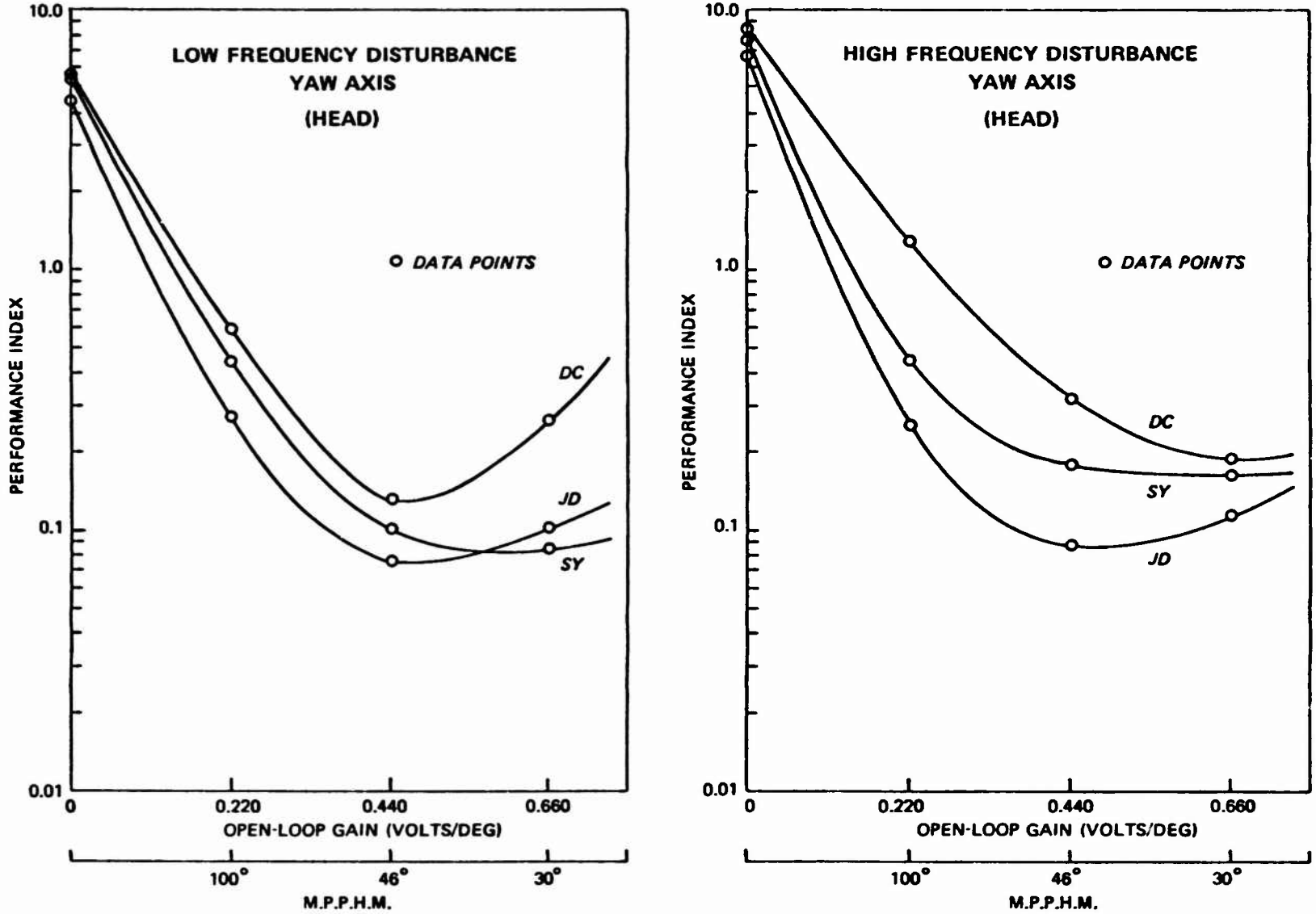

Figure 4 a & b - Head Control Performance Curves (Yaw Axis)

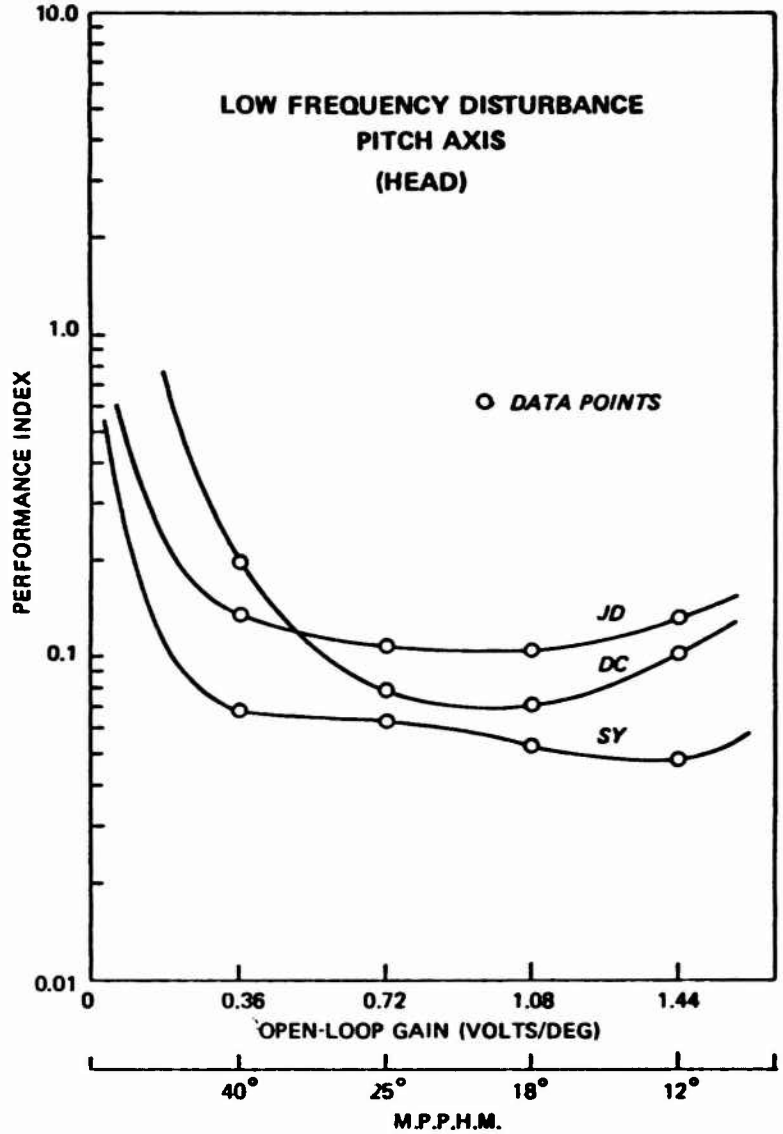

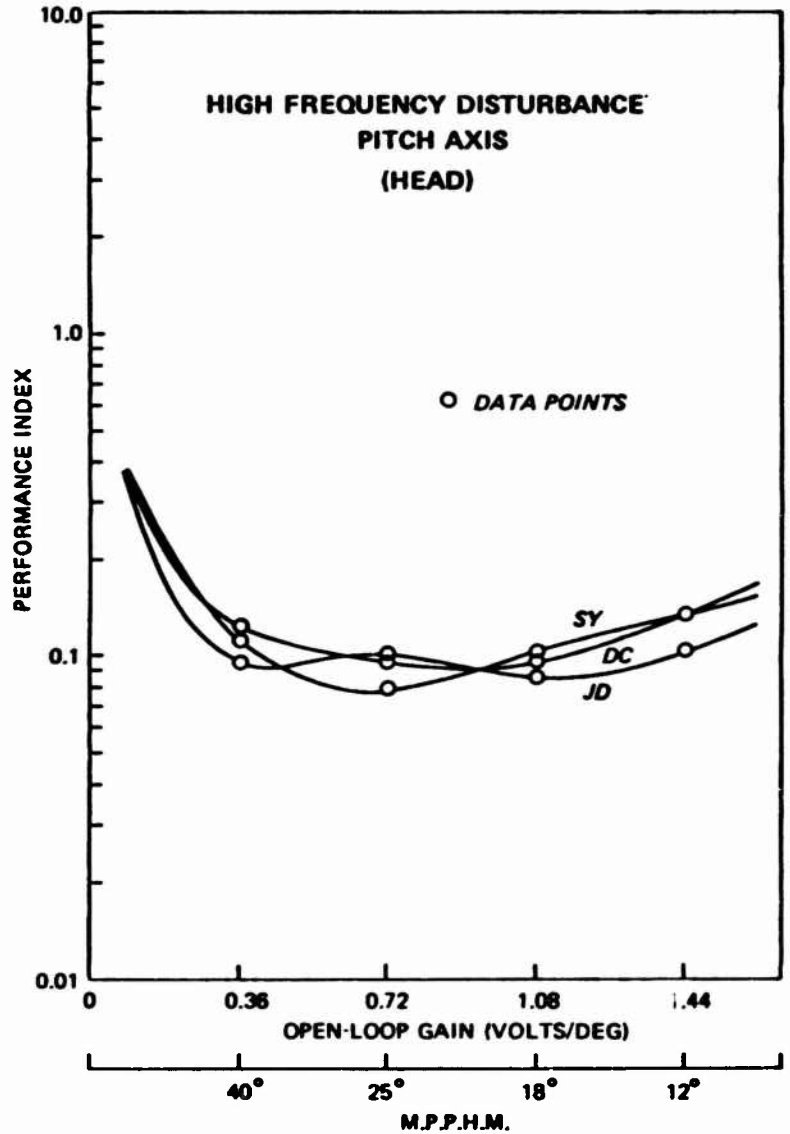

Figure 4 c & d - Head Control Performance Curves (Pitch Axis)

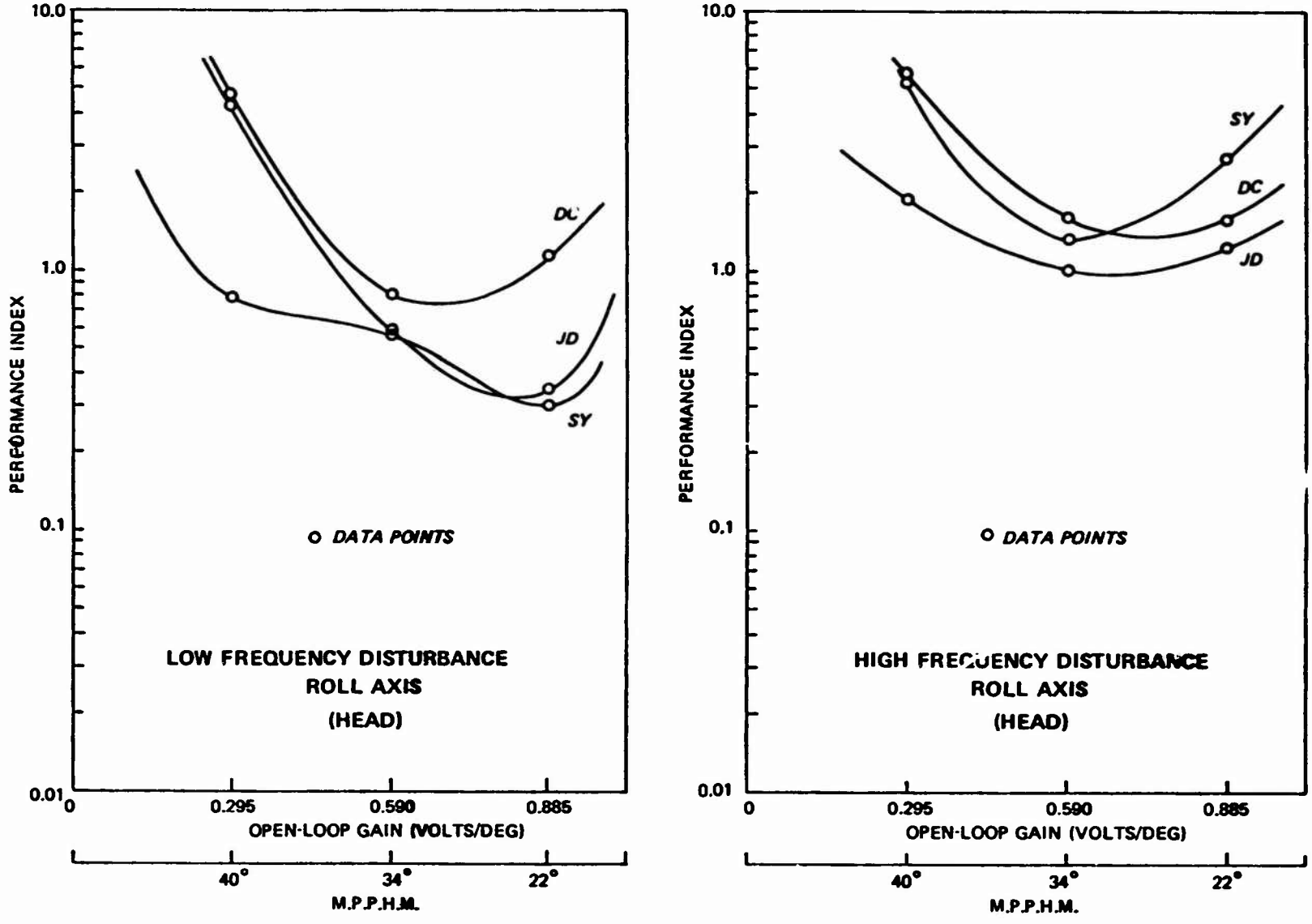

Figure 4 e & f - Head Control Performance Curves (Roll Axis)

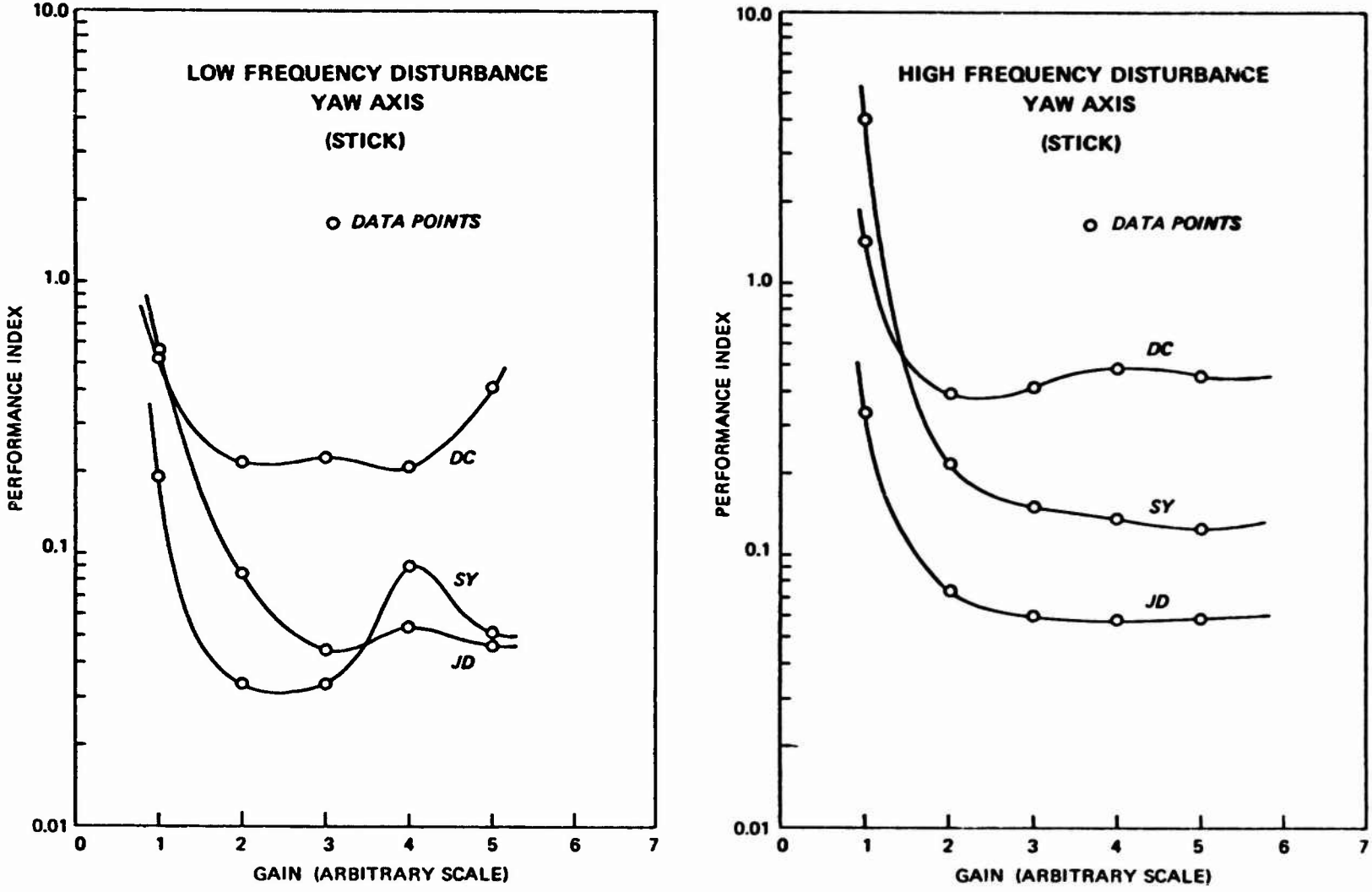

Figure 5 a & b - Manual Control Performance Curves (Yaw Axis)

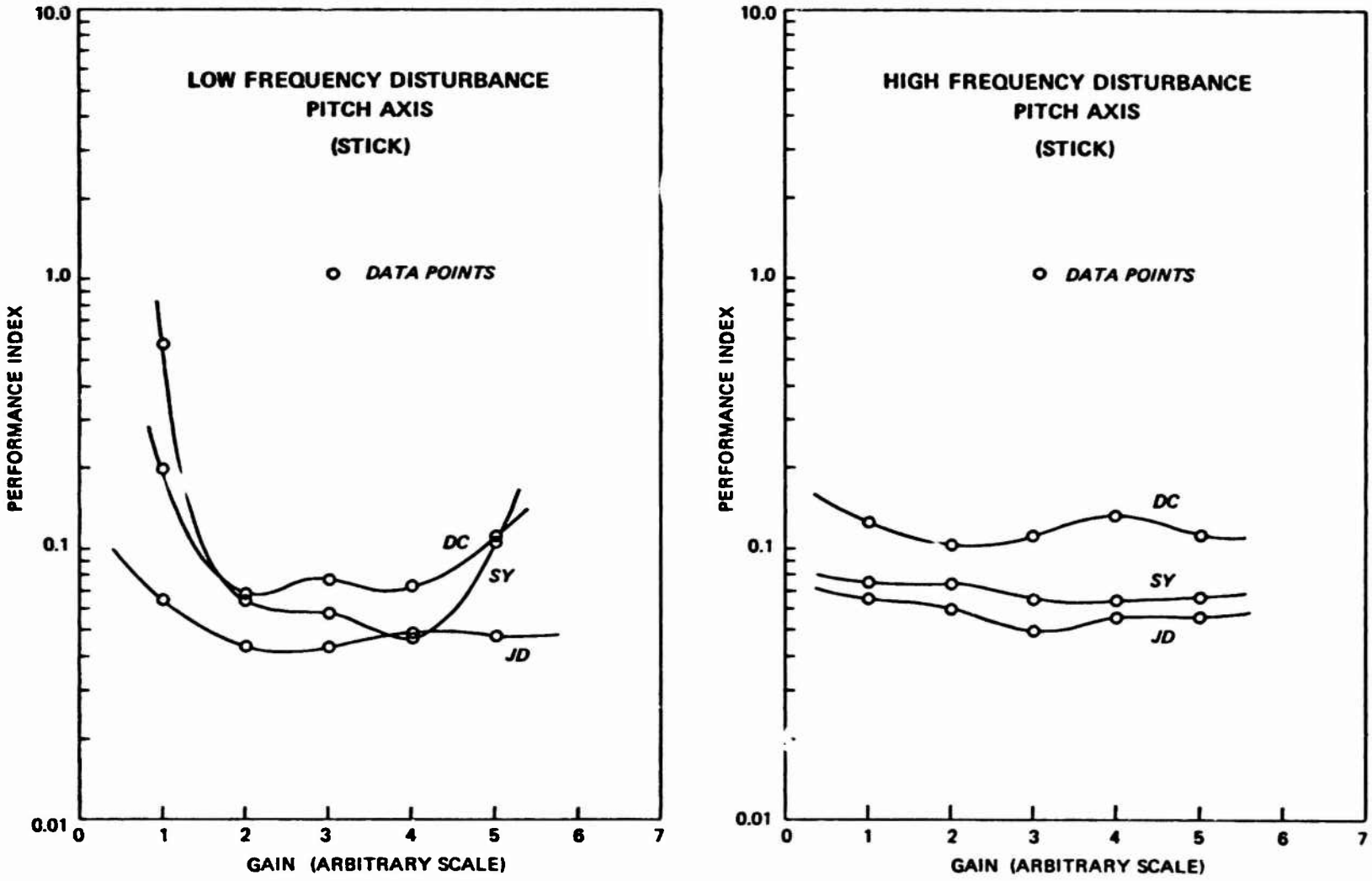

Figure 5 c & d - Manual Control Performance Curves (Pitch Axis)

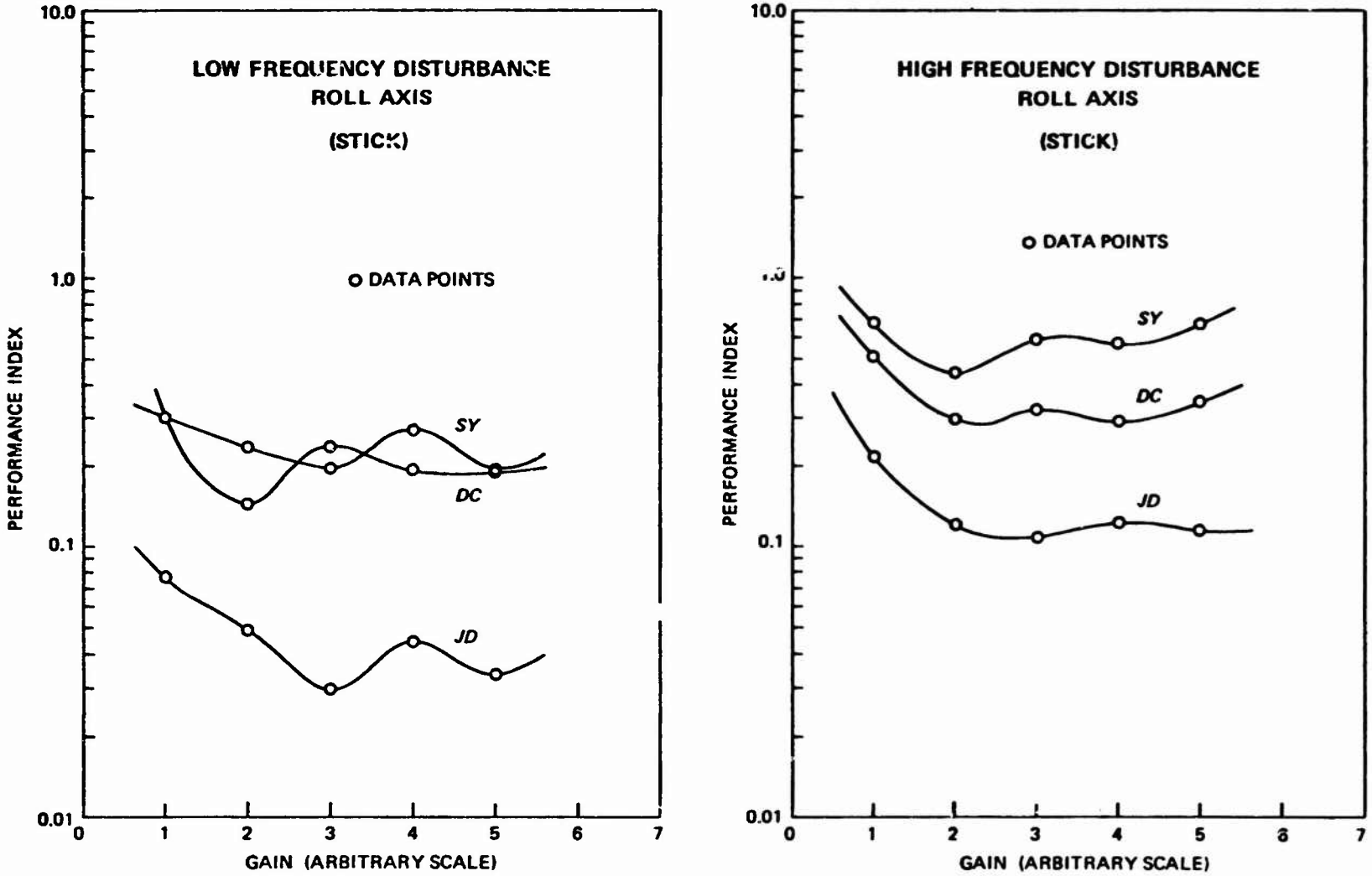

Figure 5 e & f - Manual Control Performance Curves (Roll Axis)

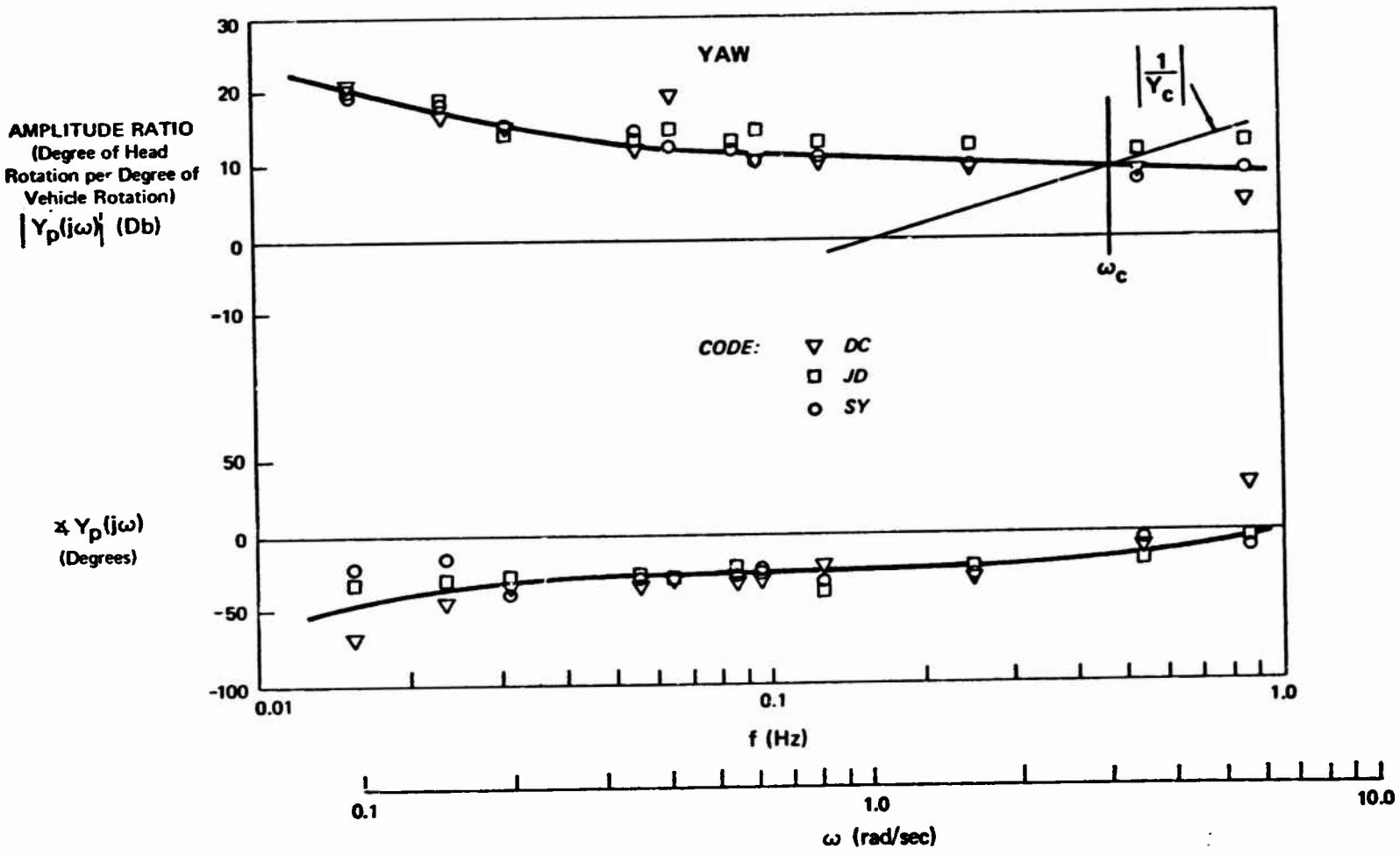

Figure 6a - Describing Functions for Head and Stick Control with Visual and Motion Cues. Plant Dynamics $Y_c(s) = K/s$. (Head Yaw Control)

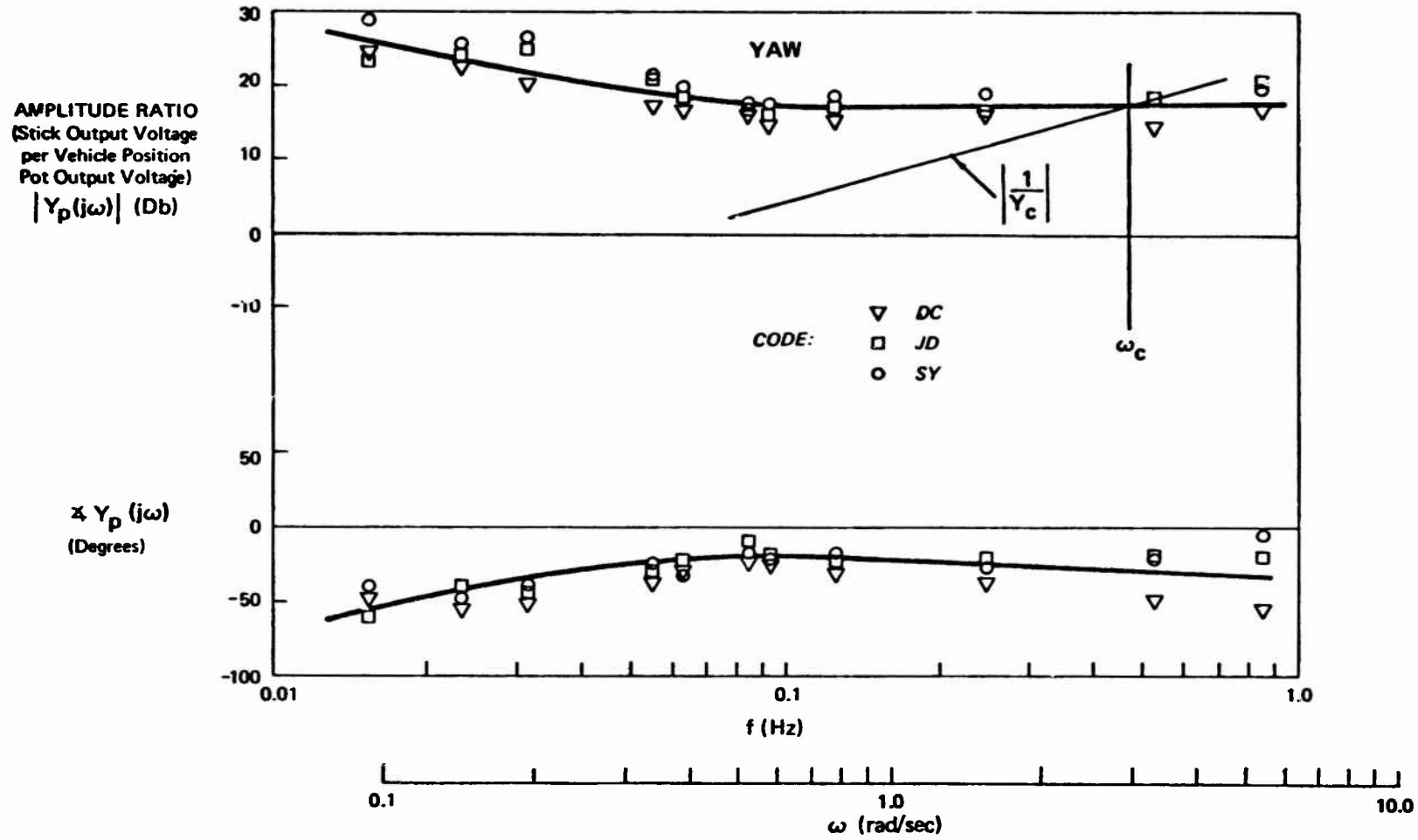

Figure 6b - Describing Functions for Head and Stick Control with Visual and Motion Cues. Plant Dynamics $Y_c(s) = K/s$. (Stick Yaw Control)

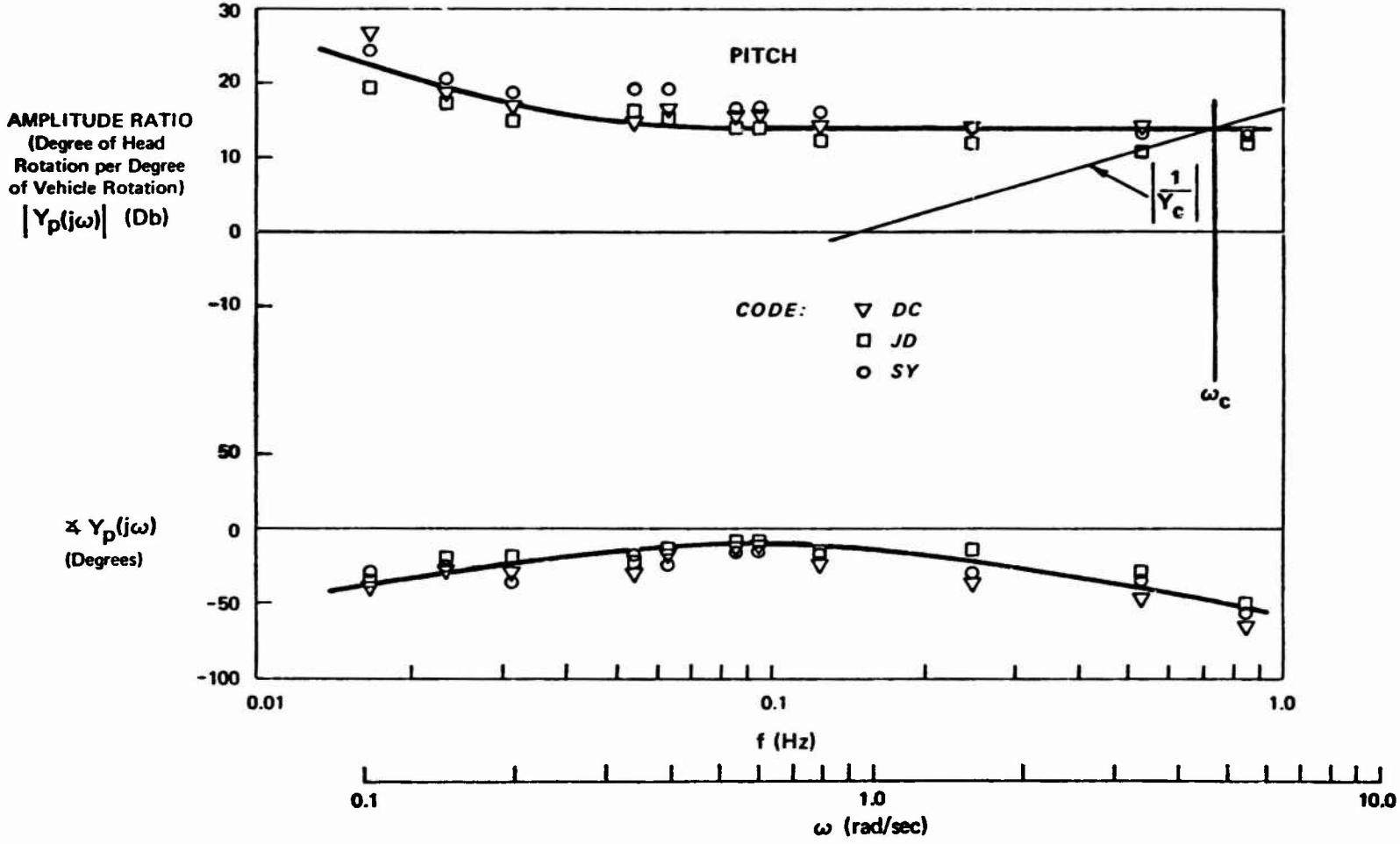

Figure 6c - Describing Functions for Head and Stick Control with Visual and Motion Cues. Plant Dynamics $Y_c(s) = K/s$. (Head Pitch Control)

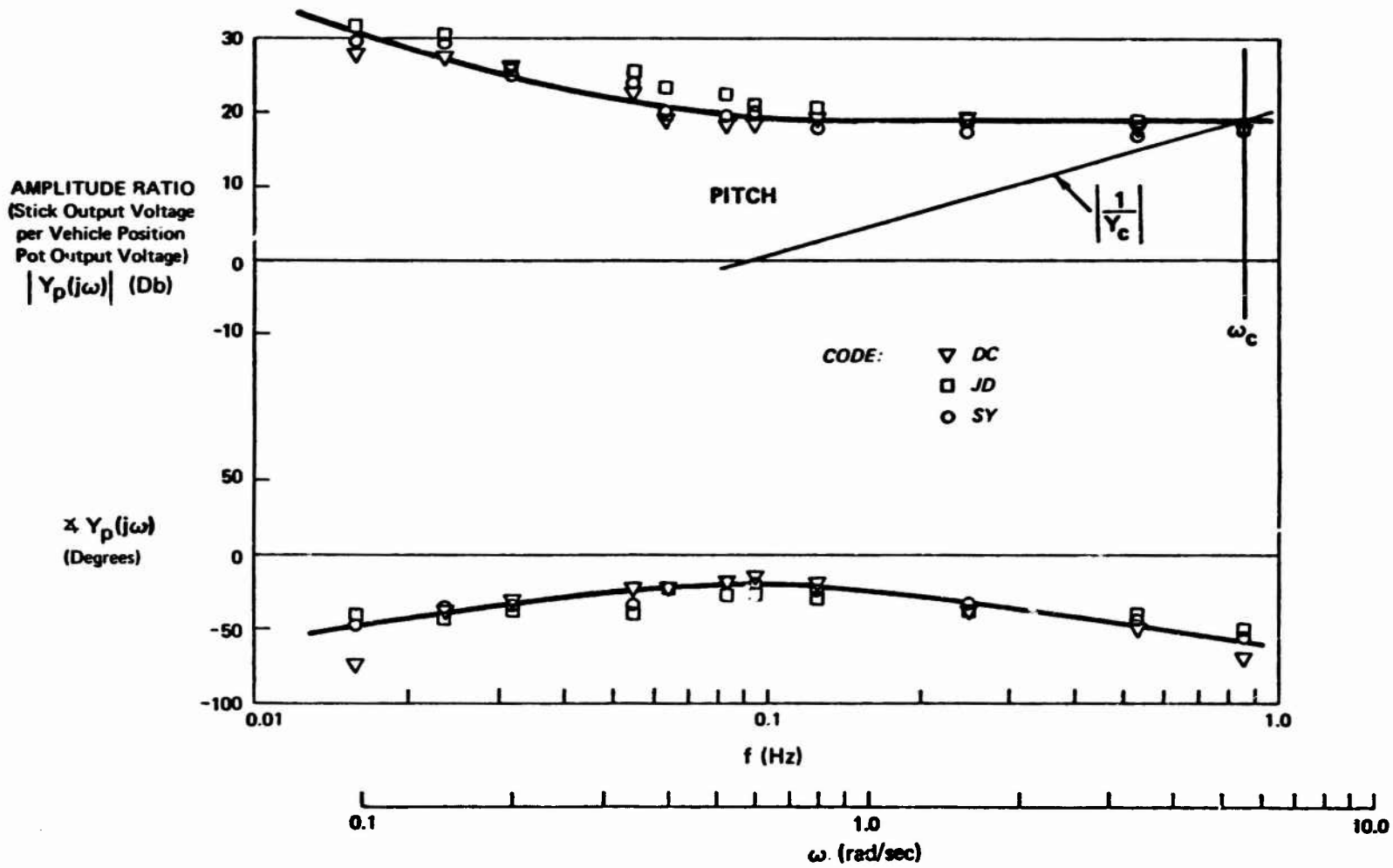

Figure 6d - Describing Functions for Head and Stick Control with Visual and Motion Cues. Plant Dynamics $Y_c(s) = K/s$. (Stick Pitch Control)

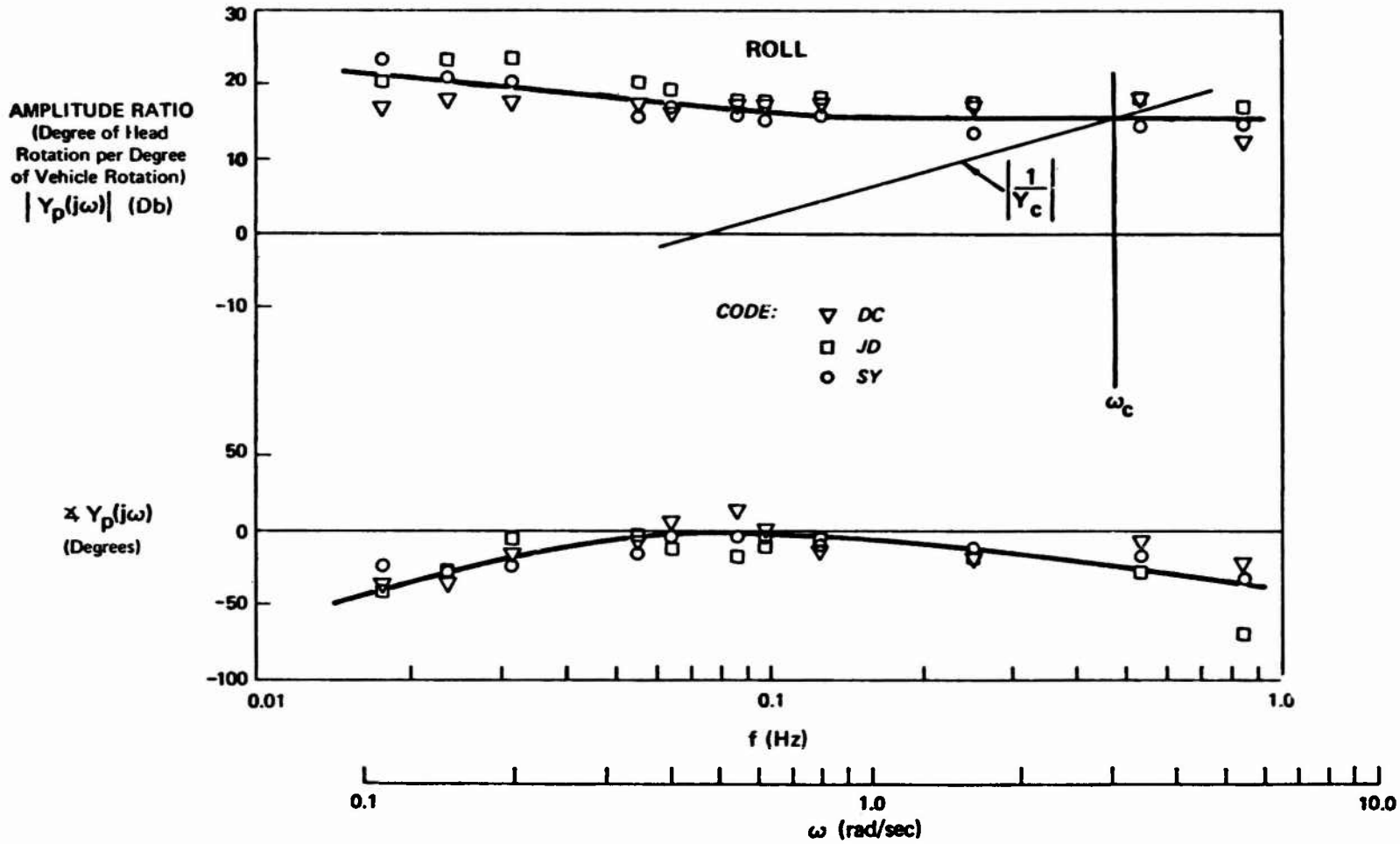

Figure 6e - Describing Functions for Head and Stick Control with Visual and Motion Cues. Plant Dynamics $Y_c(s) = K/s$. (Head Roll Control)

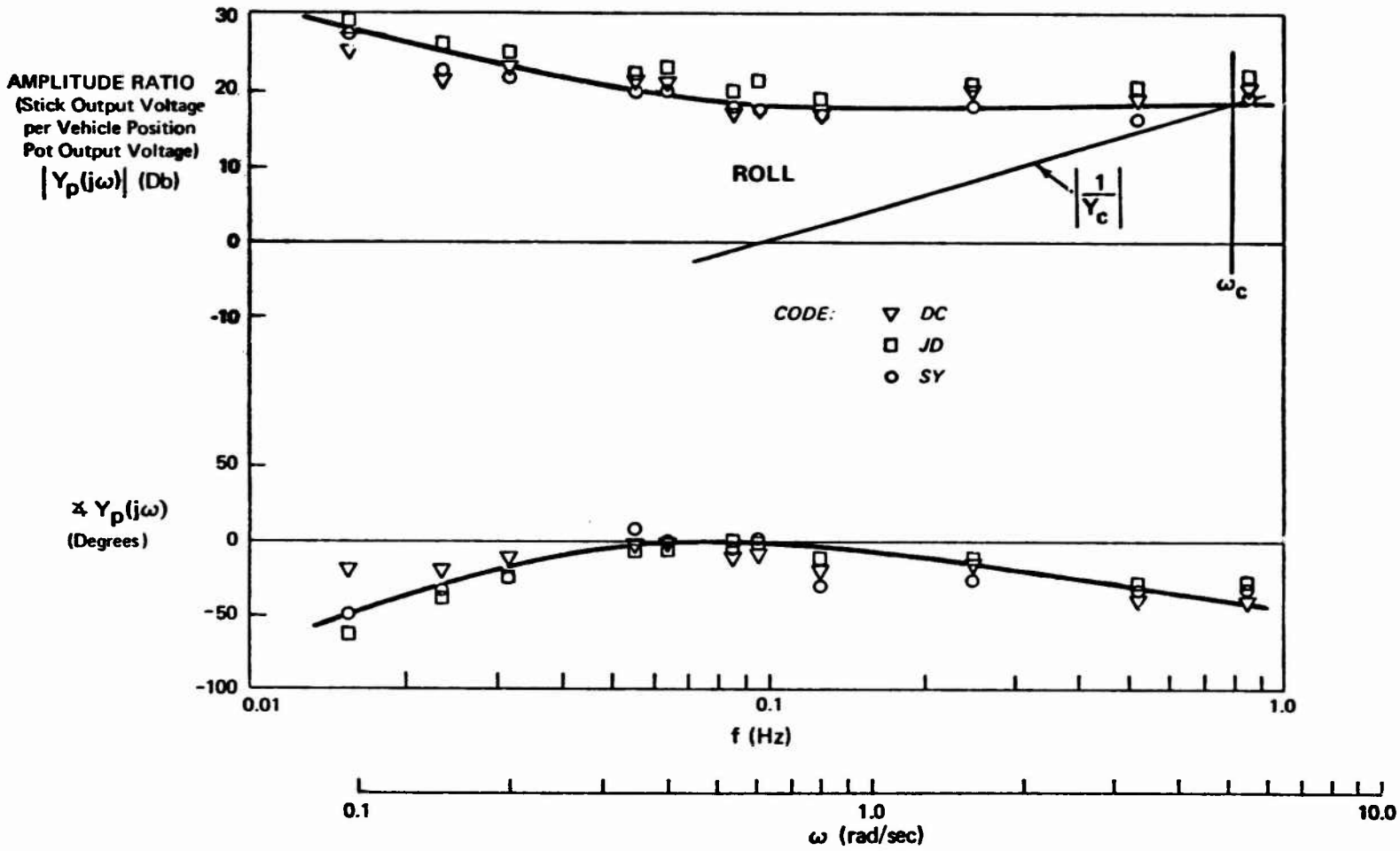

Figure 6f: Describing Functions for Head and Stick Control with Visual and Motion Cues. Plant Dynamics $Y_c(s) = K/s$. (Stick Roll Control)

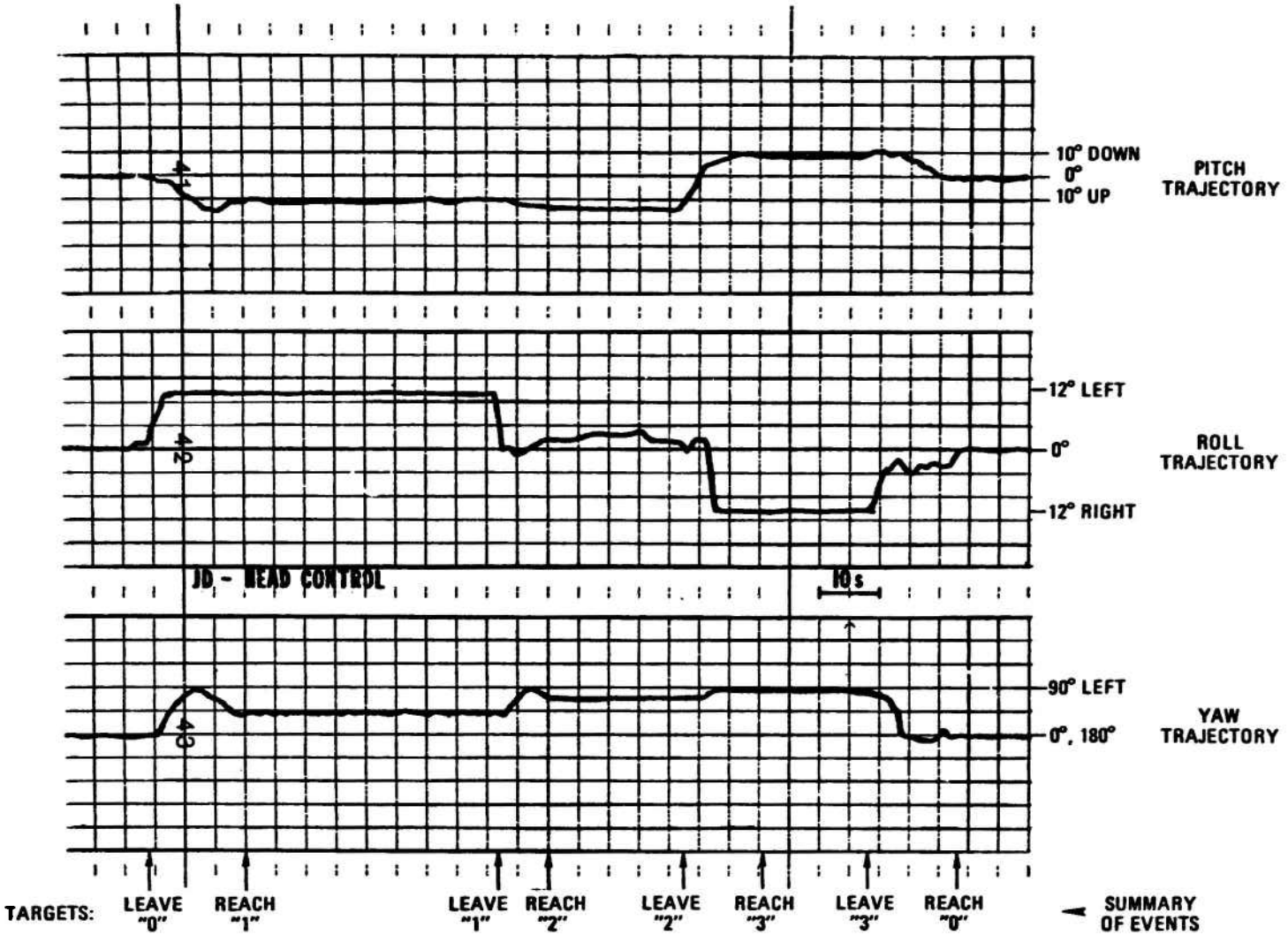

Figure 7a - Three Axis Trajectories, Head Control (Yaw Trajectory Indicates Sine of the Yaw Angle)

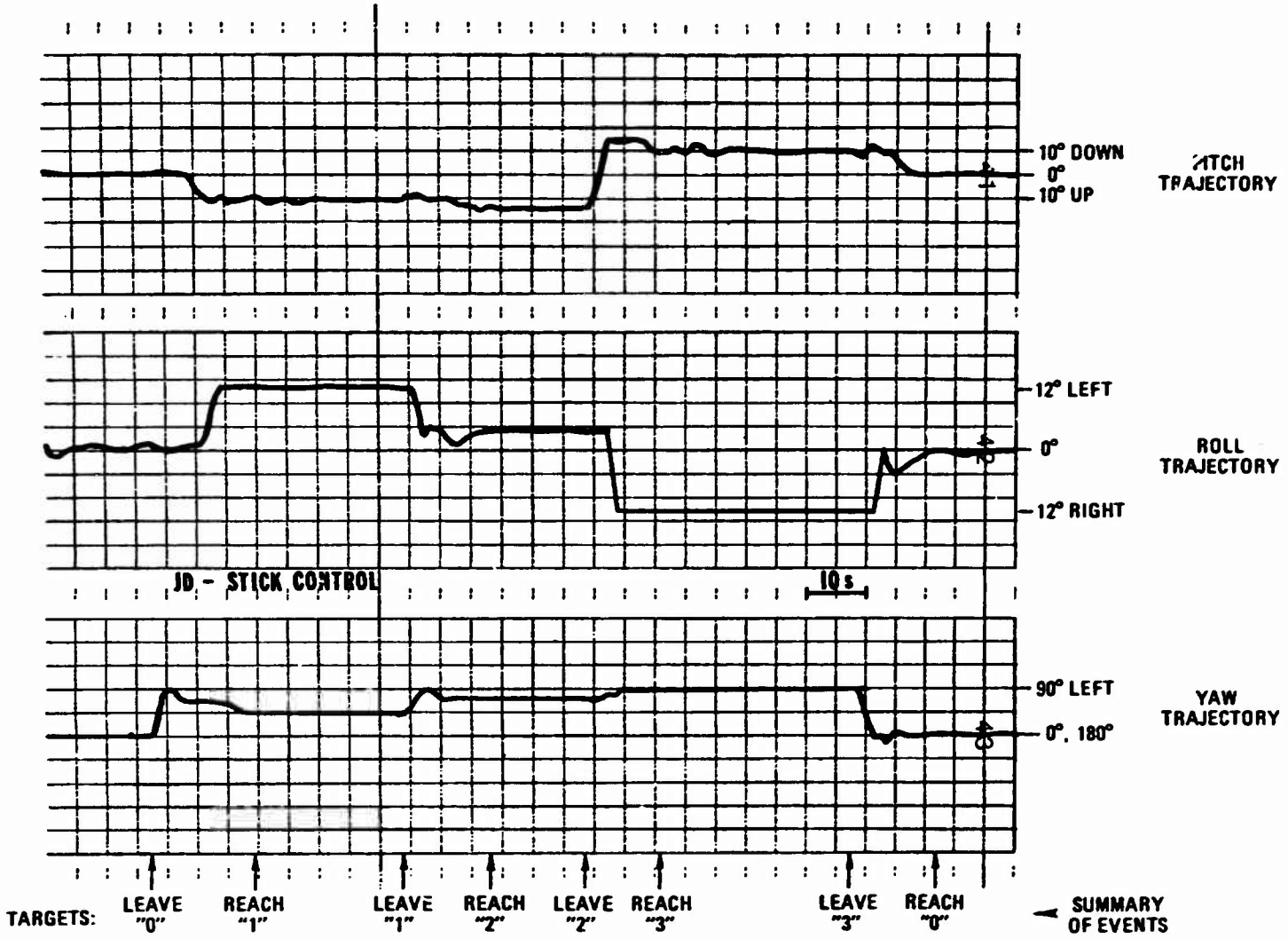

Figure 7b - Three Axis Trajectories, Stick Control (Yaw Trajectory Indicates Sine of the Yaw Angle)

GENERAL APPROACH TO GENERATING SENSORY FEEDBACK INFORMATION FROM UPPER EXTREMITY PROSTHETIC TERMINAL DEVICE

M. Solomonow, A. Freedy, J. Lyman
Biotechnology Laboratory
School of Engineering and Applied Science
University of California, Los Angeles

ABSTRACT

Present artificial arms do not provide sensory feedback information such as pressure and temperature, elbow and wrist angular position, etc.

This paper will be concerned with closing the loop between the amputee, his prosthesis, and the environment, by providing a basic general pattern for generating sensory feedback information.

A model of a neuromuscular receptor in the feedback loop of the peripheral neuromuscular system was constructed from experimental data. Functional analysis of the model resulted in undertaking efforts at three levels; development of a pressure sensitive electro-mechanical transducer, electronic simulation of neural sensory element discharge patterns, and the interface network of the system with the amputee.

Methods of implementation, including skin stimulation as well as various subcutaneous stimulations, are discussed.

INTRODUCTION

Lack of sensation from the terminal device of upper extremity prostheses is a factor that may lead some amputees to abandon their prostheses shortly after fitting, or to use them primarily for cosmetic purposes.

It is logical that the addition of some kind of subconscious direct sensory feedback to the amputee will result in improved overall adaptation, performance and control. Direct subconscious sensation will bring about reduction in training time, an increase in controllability of the prostheses trajectories, a reduction of required visual supervision, and will produce the psychological effect of making the prosthesis become more "human." The mental burden of operating the prosthesis will be reduced to a subconscious level, especially if EMG command signals are used to generate control.

Several attempts have been made in the past to provide sensory features to upper extremity prostheses. The most recent successful attempt was made by Clippinger, et al. (1973) at Duke University, in a pilot study. Implant procedures were used to relay signals extracted from strain gages on mechanically controlled prostheses to the median nerve in a proportional manner. Two encouraging results were obtained from this experiment: First, the central nervous system is capable of being stimulated externally by a peripheral nerve in a manner that forms a mental image of force at

the terminal device that is proportional to the actual force. Second, implant procedures of stimulating sensory nerve fibers subcutaneously proved to be successful.

In light of the evidence, it seems that the foundation for further work is established. However, several engineering problems, mainly involving external transducer and electronic design, still require solution.

This paper presents a system for the sensory feedback loop of a prosthetic terminal device which is capable of sensing grasp pressure. The relevant characteristics of the neuromuscular sensory feedback system provide conceptual guidance to this approach. Electronic simulation of a biological neural element discharge pattern is used to stimulate selected skin areas, while sensory input is provided by pressure sensitive transducers.

MODEL OF A NEUROMUSCULAR SENSORY RECEPTOR

The neuromuscular system could be described in engineering terminology as a closed loop control system. The neural motor activity and muscle dynamics (contraction/elongation) form the forward loop, with the muscle spindle receptor as the feedback element monitoring elongation and its rates. The α motoneurons of the spinal cord constitute the summation point and error signal generator (Figure 1).

In order to reconstruct the feedback loop, it is necessary to define the characteristics of the muscle spindle.

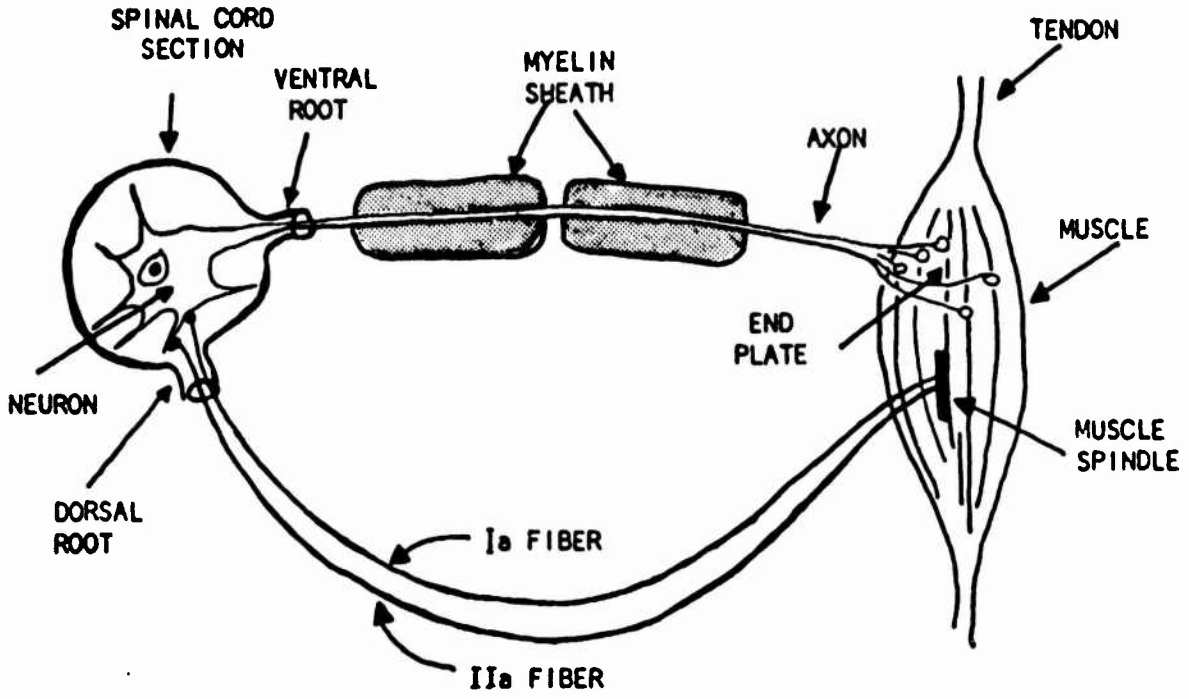

THE NEUROMUSCULAR SYSTEM: PHYSIOLOGY

FIGURE 1 (a)

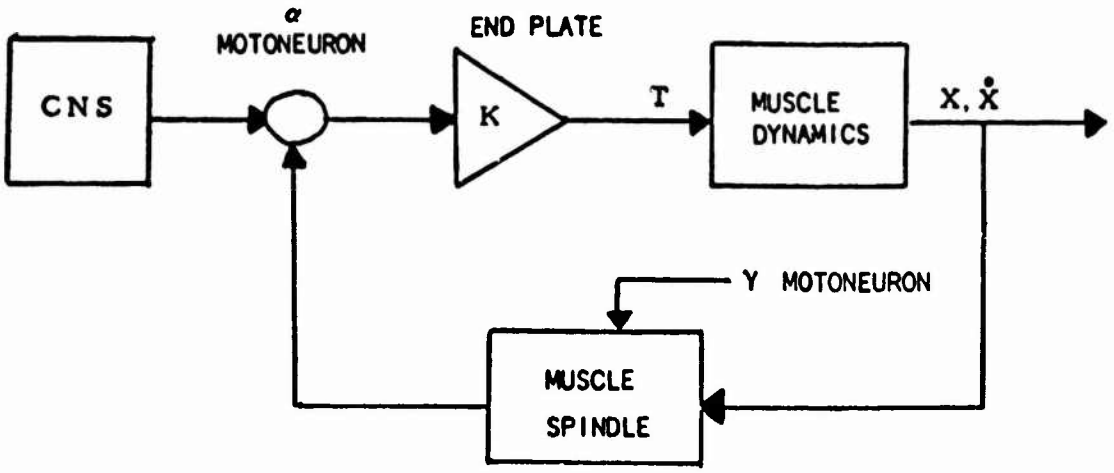

THE NEUROMUSCULAR SYSTEM: ENGINEERING MODEL

FIGURE 1 (b)

Earlier work (Solomonow, 1972) defined some of the characteristic behavior of the spindle impulse firing upon muscle elongation. The frequency of the impulses was directly related to the elongation (X), and to its rate ($\dot{X}$). Several typical recordings from the afferents of the muscle spindle are given in Figure 2. The final steady state discharge frequency indicates the elongation, while the initial transient frequency increase indicates the rate of elongation.

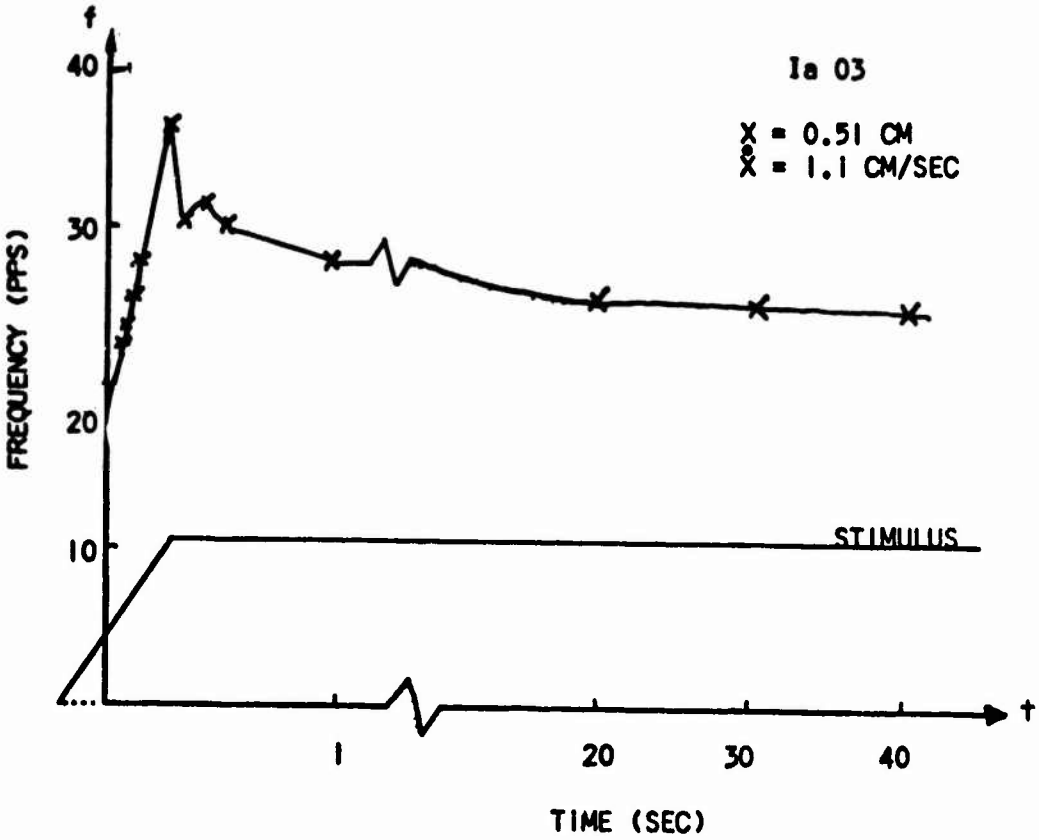

TYPICAL DISCHARGE PATTERN OF THE MUSCLE SPINDLE

FIGURE 2 (a)

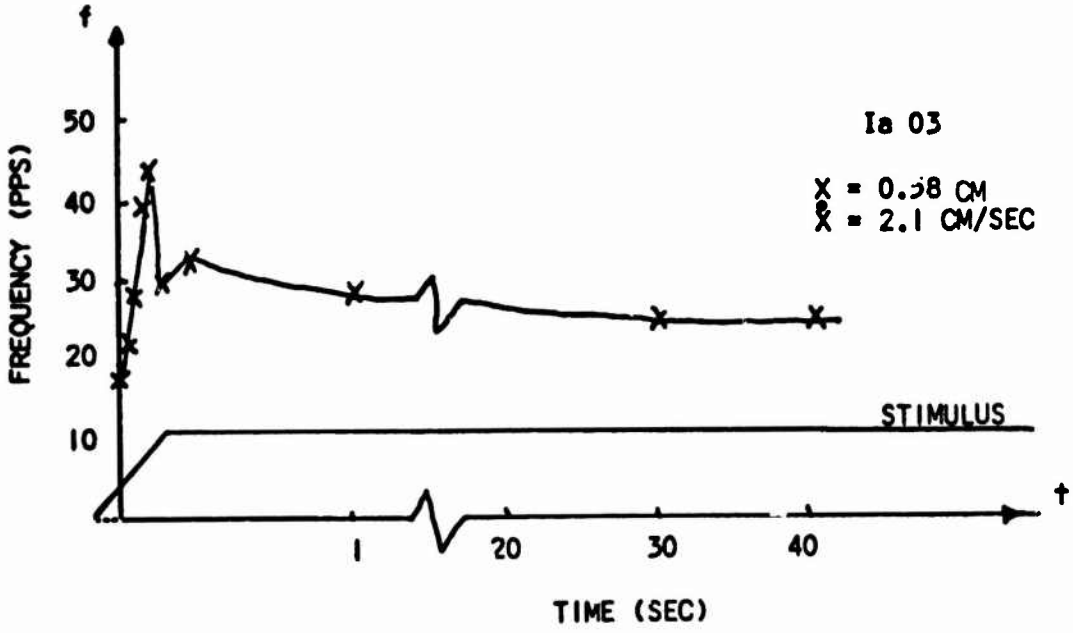

FIGURE 2 (b)

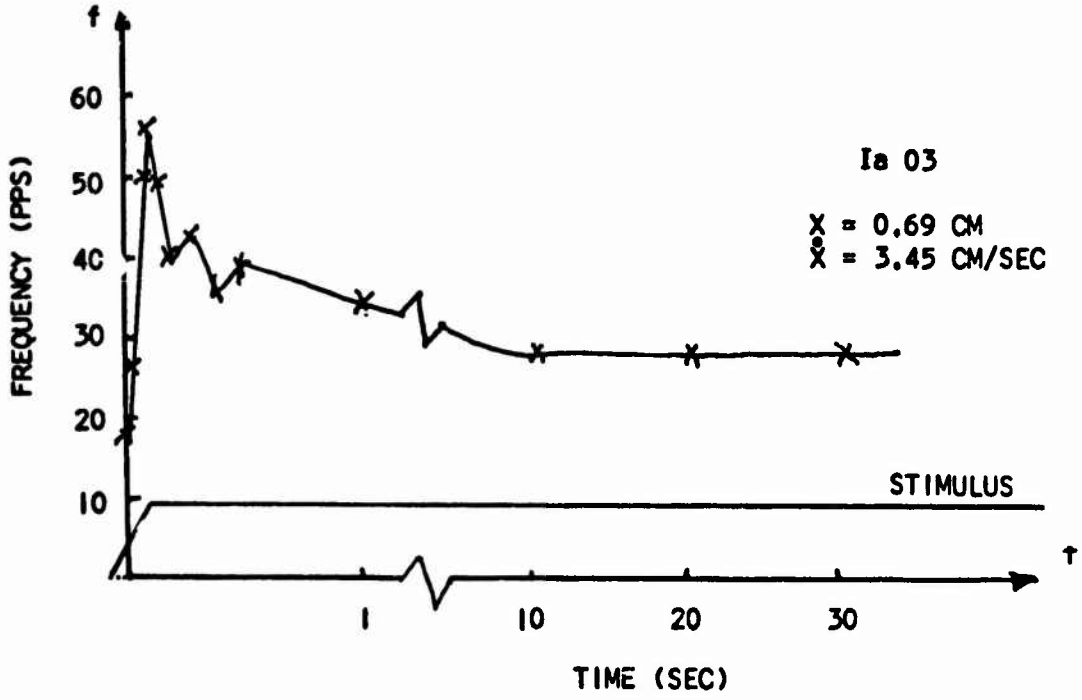

FIGURE 2 (c)

Changes in frequency of the transition discharge with changes in rate of extension are uniform in behavior. The top curve of Figure 3 shows the peak frequencies at the end of the transition period for 1.5 cm. elongation at different rates of stretching. In addition, the frequencies for two other levels of elongation are given. At 1.5 cm. elongation, the frequencies appear to reach a limit at the highest rate of extension. Otherwise, the frequency increases regularly as the rate of extension increases for all lengths and rates.

THE DYNAMIC FREQUENCY

At the end of the transition period, the frequency response will oscillate for a few milliseconds and quickly reach a steady value. During the first second or two, the frequency will continue to decay slowly, stabilizing about a fixed frequency value a minute later. The impulses will continue to fire at this frequency for prolonged periods of time without perturbation. Plotting the dynamic frequency against levels of elongation results in a straight line of slow positive slope, as shown in Figure 4. When varying the rates of extension between .2 and 4.7 cm/sec. for a constant level of extension, no change in dynamic frequency is observed. This behavior implies that the dynamic frequency is independent of the rate of extension being determined by the level of elongation.

To conclude, the muscle spindle is a mechano-electric transducer which is capable of generating impulses. The impulses translate elongation and its rates (X, $\dot{X}$) into meaningful electric signals

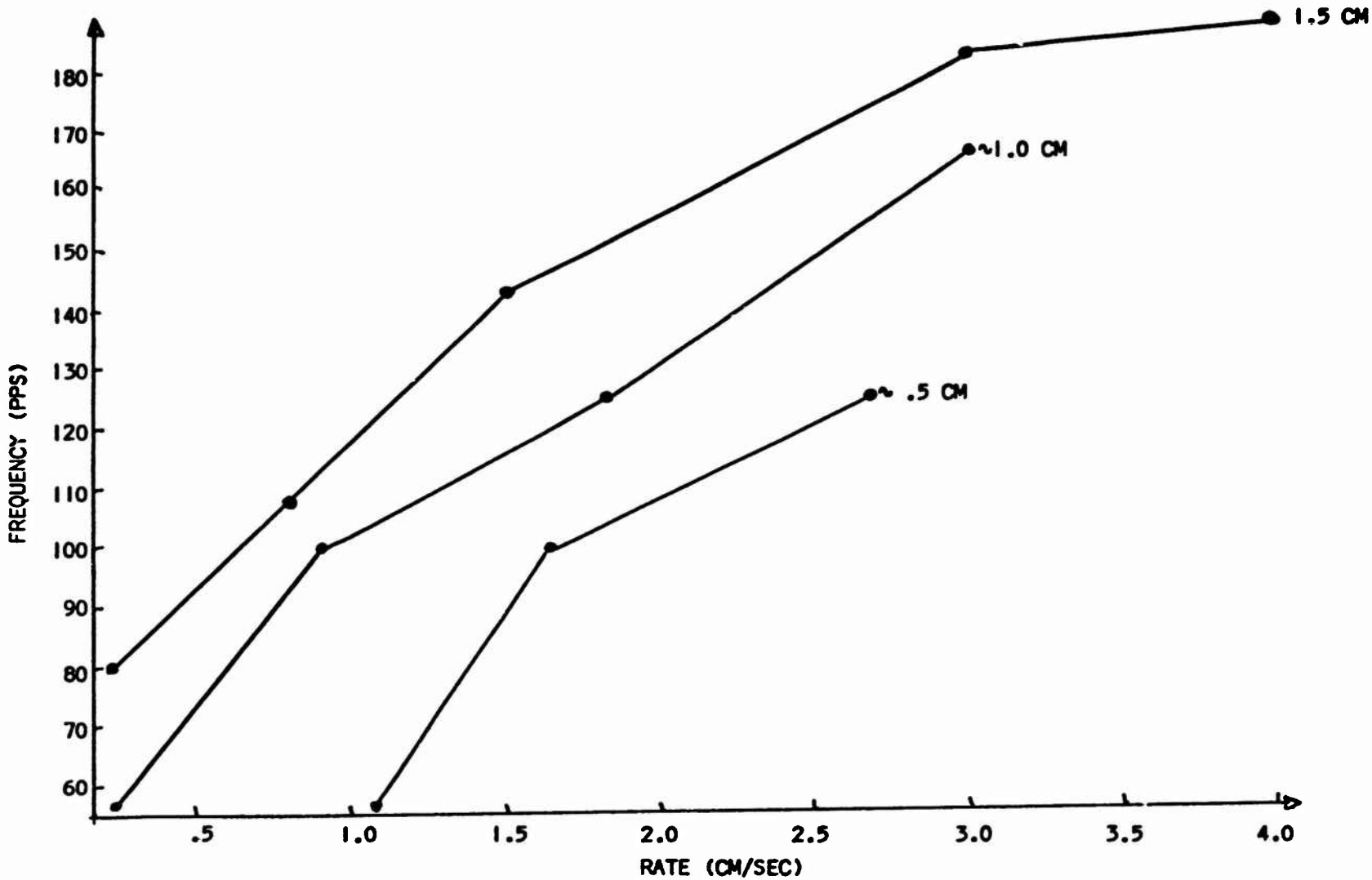

TRANSITION DISCHARGE FREQUENCY AT THREE LEVELS OF EXTENSION DURING STRETCHING AT DIFFERENT RATES

FIGURE 3

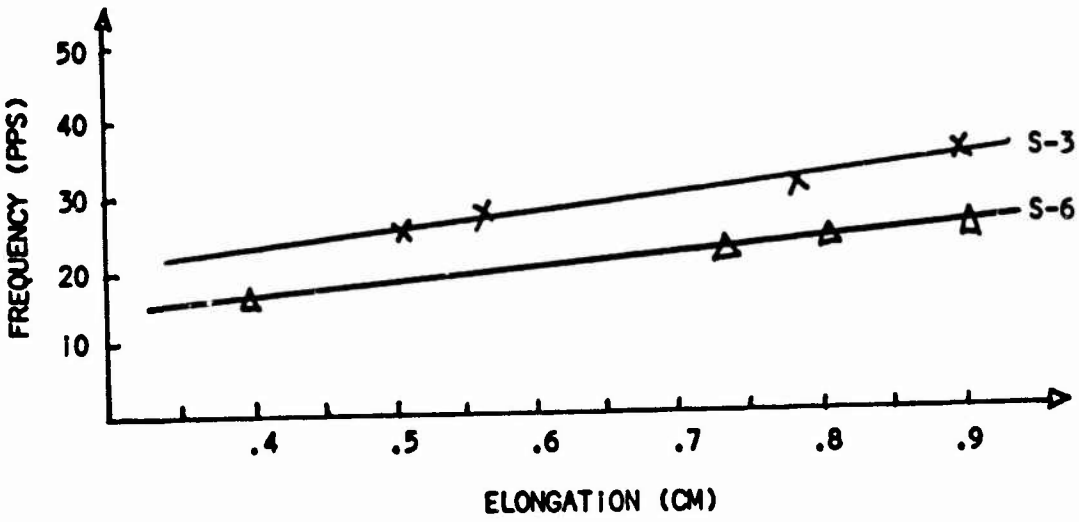

DYNAMIC FREQUENCY INCREASES LINEARLY WITH ELONGATION

FIGURE 4

transmitted to the CNS with frequency and rate of change of frequency (f, $\dot{f}$), as the variable parameters. The feedback element could be redrawn to include the characteristic behavior of the spindle, and the transformation of X, $\dot{X}$ into f, $\dot{f}$.

RECONSTRUCTION OF THE SENSORY FEEDBACK SECTION

The muscle spindle properties discussed above can be simulated for purposes of sensory feedback in cases of peripheral amputation, leprosy, etc.

Examination of the spindle structure in Figure 5 reveals some of the characteristics that are necessary in the reproduction of sensory feedback. The spindle consists of elastic elements embedded in the muscle bulk. It serves two purposes:

1. Monitoring the mechanical state of the muscle, i.e., elongation/contraction and their rates (X, $\dot{X}$), which indirectly are indicators of the associated pressures.
2. Initiation of neuro-electric signals in the form of variable frequency impulses with the impulse frequency as the controlling variable.

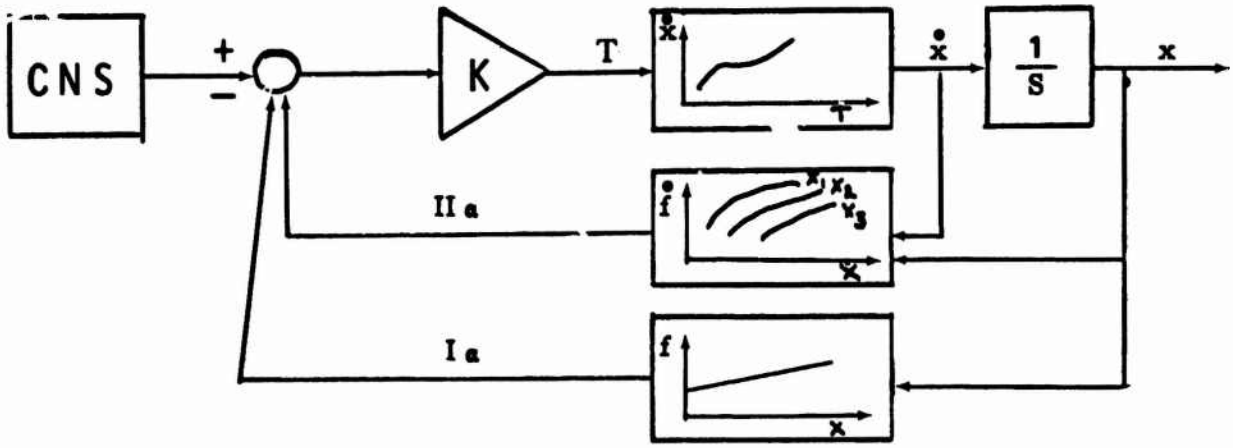

THE MUSCLE SPINDLE'S CHARACTERISTICS

FIGURE 5

In the neuromuscular system, the neuro-electric signals are interfaced via the dorsal roots to the peripheral levels of the central nervous system (CNS), and whenever relevant to its higher centers.

It becomes necessary then, for reproduction purposes, to construct three distinct subsystems, i.e., a device which is capable of monitoring elastic deformation and its rates, an information transformation network to duplicate the variable frequency format of the muscle spindle discharge, and an interface system transmitting the information to the amputee. The information transformation network is intended to be controlled by the deformation monitoring device. A reconstructed control diagram including the above elements is shown in Figure 6.

Several methods of relaying the artificial neuroelectric signal to the CNS exist. Discussions of these methods appear in later sections of this paper.

The monitoring device, situated either at the terminal device of the prosthesis or at any of the degrees of freedom, could be made to monitor a variety of parameters, viz., pressure, temperature, angular position of wrist, elbow, etc. In the past, attempts were made to monitor pressure and temperature from the terminal device making use of strain gages and thermocouples, respectively. Angular position of wrist and elbow could be monitored by a variety of commercially available potentiometers. The information transformation system is the basic component of this feedback system, regardless of the controlling sensing device or the interface system. Variables such as pressure, temperature and position can be converted by the information

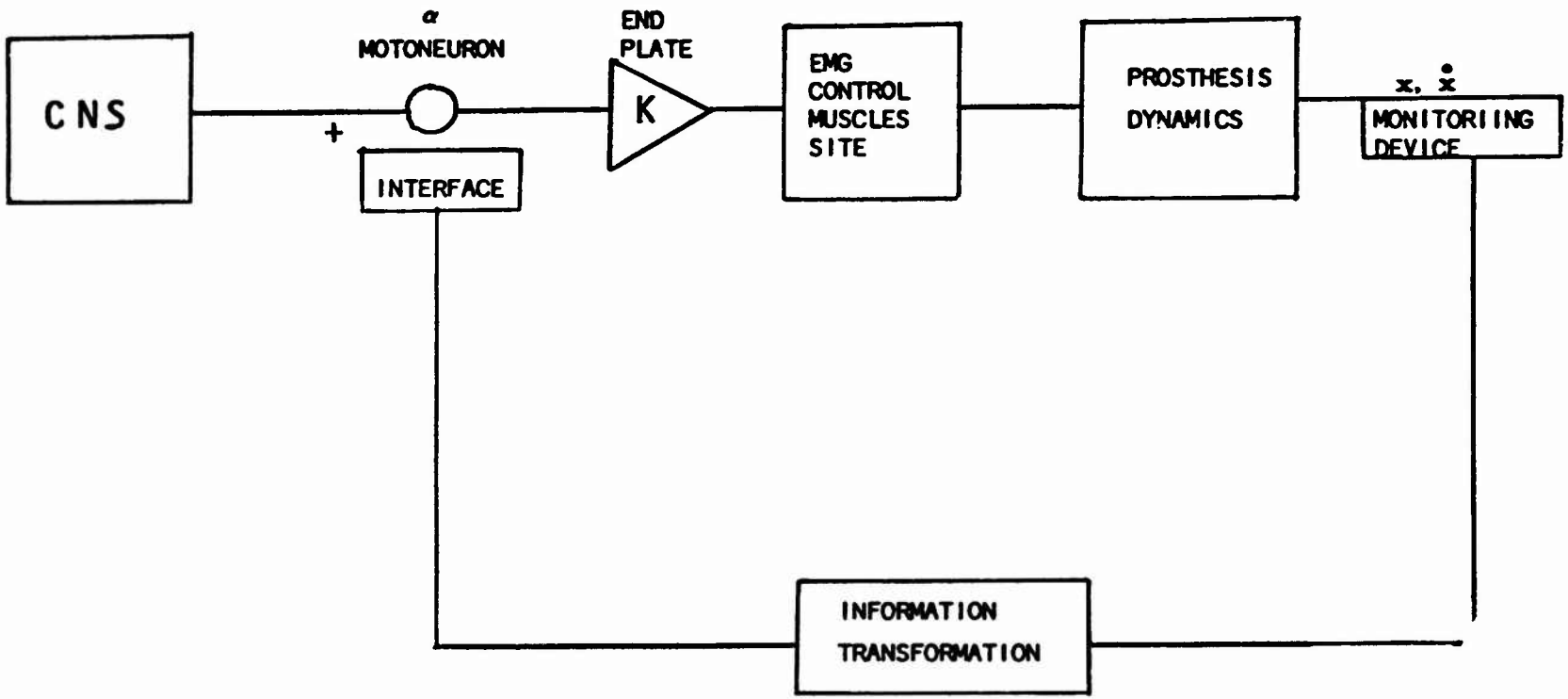

RECONSTRUCTED CONTROL DIAGRAM OF THE NEUROMUSCULAR SYSTEM

FIGURE 6

transformation system into artificial neural pulses of changing frequency of the range 0 - 120 pps. The strength of the pulses is dependent on the method of the interface. For example, a subcutaneous neural interface will require compliance with the strength-duration relationships observed in nerve axons (Katz, 1966), while skin stimulation requires compliance with Weber-Fechner and Stevens' Laws, as well as findings reported by Prior (1972), with strengths of over 100V.

It becomes apparent, then, that the information transformation system is to contain a means for adjusting both pulse width and amplitude, depending on the stimulation method used.

The interface of the system with the amputee is of major importance, especially with respect to the following human factors:

1. The information transmitted to the amputee should be on a subconscious level in order to decrease the mental burden and supervision tasks.
2. The information should be reliable and approximately instantaneous.
3. High resolution factors should be achieved, so that the operator will be able to distinguish minor changes in the state of his prosthesis.
4. The method of interface should be safe; no skin, nerve, or muscle should undergo deterioration due to the technique applied.
5. Easy removal and application procedure should be arranged, along with continuous comfort while applied.

6. The location of the interface on the body should have strong correlation to the site where the information was monitored.

In the past, several methods of interfacing information, such as auditory methods, skin vibration, cineplasty, skin pinch, and air pressure on the skin, were attempted without success due to deficiencies in the above requirements (Clippinger, 1973). It becomes obvious, therefore, that future solutions to the interface problem should resort to closely duplicating the natural physiological method of relaying sensory information, i.e., nerve stimulation or electrical skin stimulation, whenever invasive implant procedures are not feasible.

Electrical skin stimulation experiments using metal electrodes (silver, stainless steel, etc.) show that this method of interface has the adverse features of pain, along with interference with EMG signal detection, whenever used with myoelectrically controlled prosthesis. The first feature can be solved by using recently developed conductive rubber electrodes, or by applying generous amounts of skin paste. Locating the interface away from the area where EMG is detected will eliminate interference; nevertheless, it may become difficult for the amputee to associate hand pressure, for example, with stimulation in areas remote from his artificial hand (the remote locations might be in the abdomen or the opposite hand). The use of concentric electrodes partially decreases EMG interference, but this is not the best solution to the problem.

A general procedure in generating sensory feedback, including various approaches of monitoring and interfacing, is shown in Figure 7.

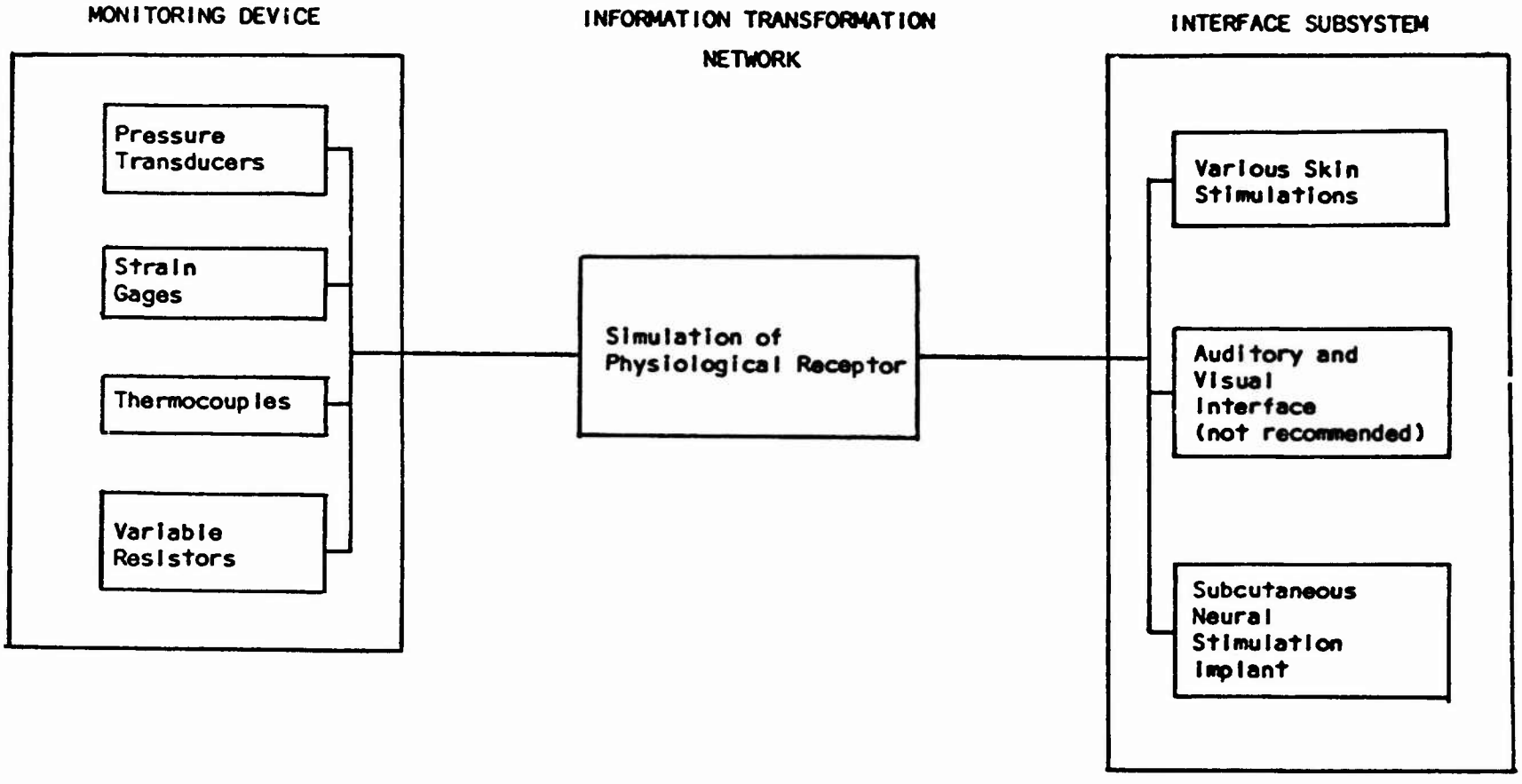

THE SENSORY FEEDBACK SYSTEM

FIGURE 7

THE PRESSURE TRANSDUCER

Several experimental units of pressure sensitive elements were constructed at the Biotechnology Laboratory. Rubber foam pieces were dipped in carbon powder and injected with liquid latex. Both materials were found to contribute to the capacitance-resistance characteristics of the transducer when used in various amounts. Resistances ranging from 2 to 15 KΩ could be established for combinations of carbon powder-liquid latex. Generally the resistance was observed to increase with increasing amounts of liquid latex. Typical deformation-resistance behavior of the transducer is shown in Figure 8.

The unit was coated with a room temperature vulcanizing compound (RTV) in order to isolate it from the environment, to regulate the pressure range, and to regulate the response time. Several types of RTV were used to coat various units, resulting in different unit response characteristics. The type of RTV used and the thickness of the coating influenced response; a thick coating yielded a transducer which sustained larger ranges of pressure, along with better recovery time. The last parameter is an important one, since fast recovery time permits perception of more rapid changes of pressure.

Evaluation of the type of transducer we have described has suggested the following advantages:

1. The possibility of shaping the element in a fingertip like form, and therefore implementing it directly at the fingertips of a prosthetic hand (see Figure 9).

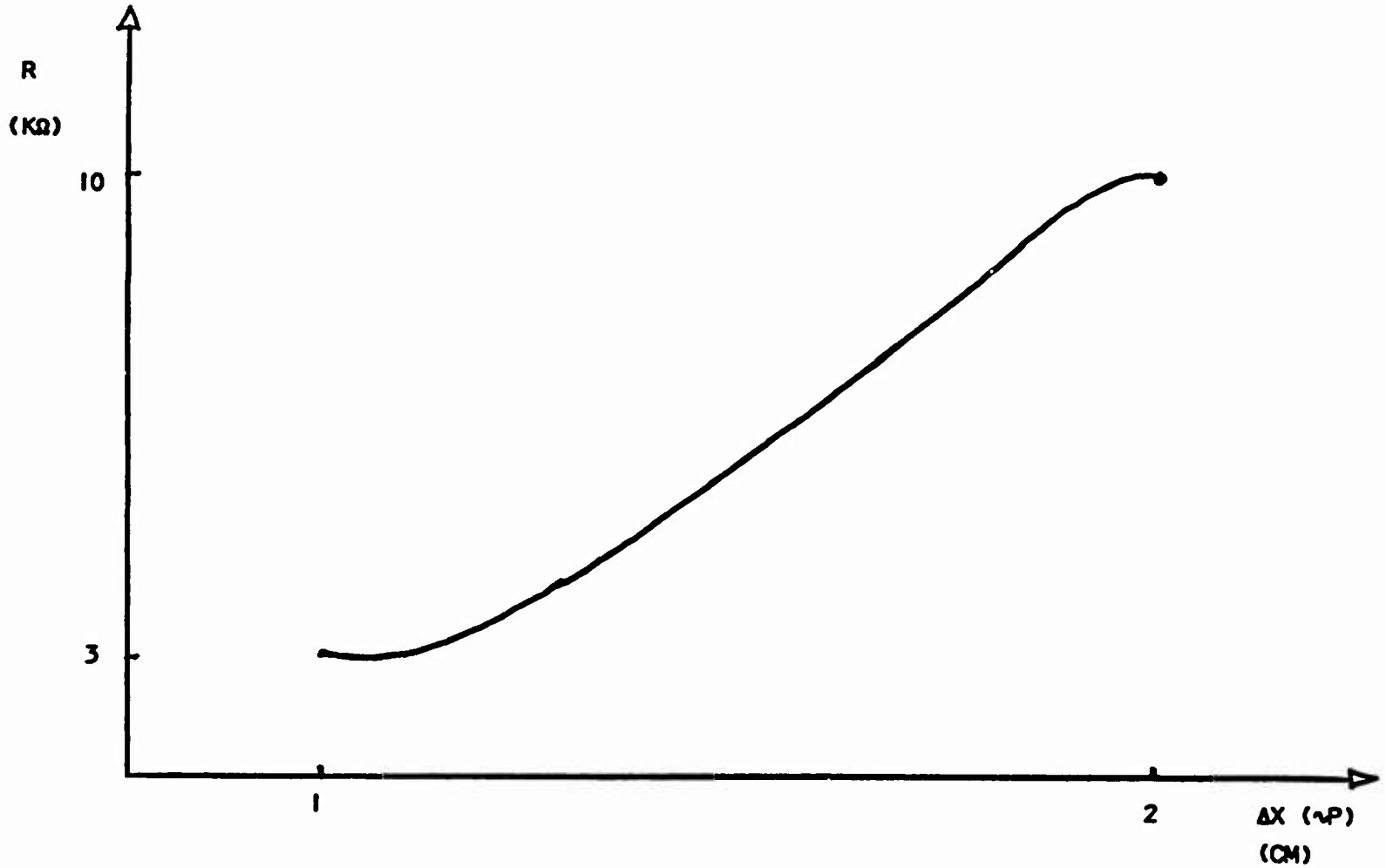

DEFORMATION-RESISTANCE CHARACTERISTICS OF THE PRESSURE TRANSDUCER

FIGURE 8

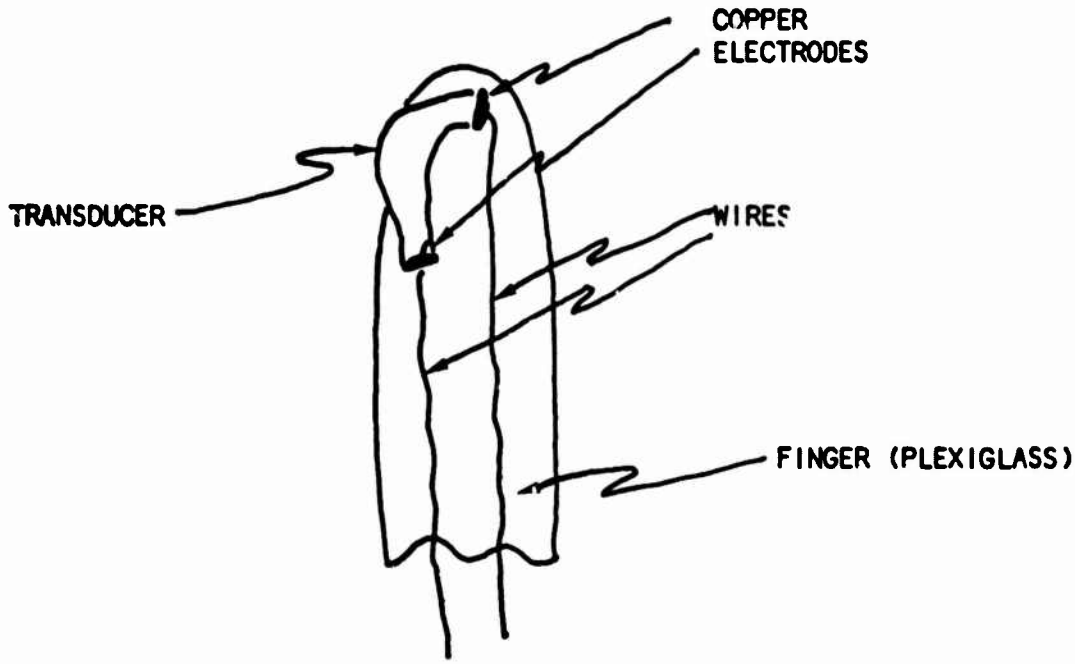

THE FINGERTIP PRESSURE TRANSDUCER

FIGURE 9

2. Durability; the external coating of the RTV can be made in any shape, and stands up well to temperature, friction, impact, etc.
3. Large ranges of deformation pressures are feasible, depending on the size of the element and the type of thickness of the

RTV coating. Fine pressure ranges are desired especially, in order to allow sensitivity in fine activity tasks.

INFORMATION TRANSFORMATION ELECTRONIC SYSTEM

The defined function of this system is to transform pressure information into physiologically meaningful coded signals. At present, the output of this system is dependent on the interface with the amputee. From our model and from experienced evolved from this field in recent years (Reswick, 1972) it is well known that both skin and nerve fibers can be stimulated by pulses of variable frequencies in the range between 10-100 pps. Thus a reasonable requirement is that the system design contain a basic portion transforming the analog pressure information into pulses over the range of 10-100 pps. The chosen interface with the amputee will determine the intermediate buffer network suitable for skin or nerve stimulation.

The system constructed at the Biotechnology Laboratory consists of the following components: pulse generator, frequency controller, and pulse width controller. The schematic is described in Figure 10.

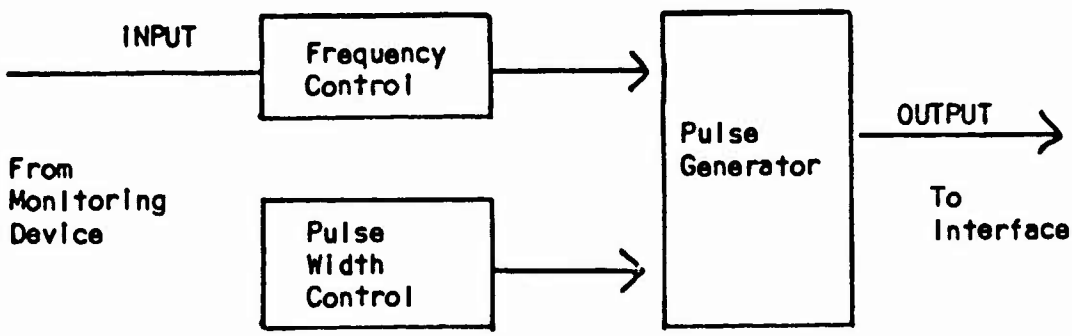

INFORMATION TRANSFORMATION NETWORK

FIGURE 10

The block diagram in Figure 10 can be simply realized by a single semiconductor and several passive components, as shown in Figure 11.

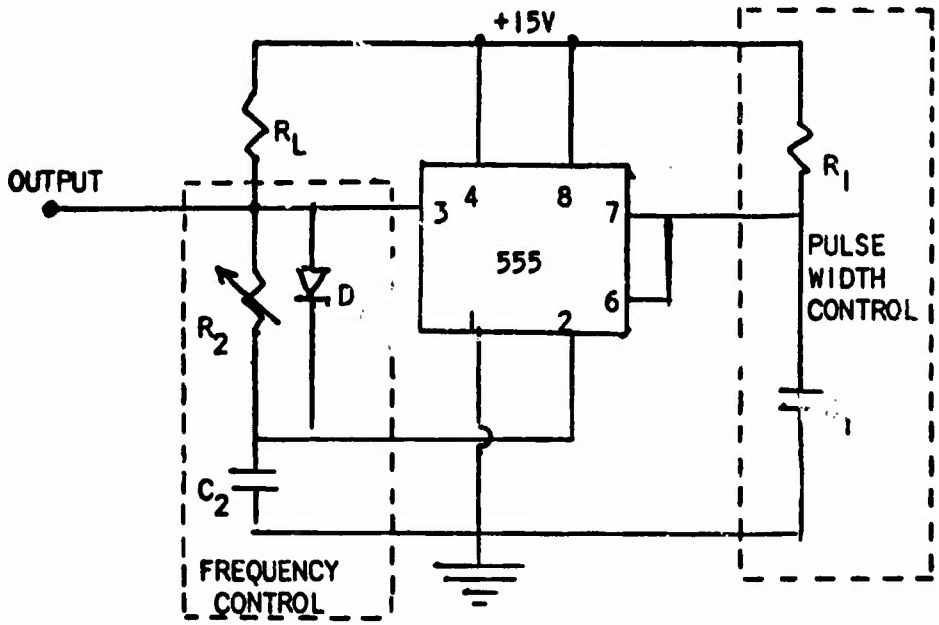

SCHEMATIC DIAGRAM OF INFORMATION TRANSFORMATION NETWORK

FIGURE 11

The pressure transducer developed was substituted for R_2 as the frequency controlling element.

The system is simple, and could be easily miniaturized for implementation in the socket or the forearm portions of the prosthesis; a power supply could be included.

For purposes of skin stimulation, a transformer was introduced at the output of the pulse generator to increase the strength of the pulses from 15V to 200V, with a potentiometer output for adjusting the pulse characteristics for individual comfort, as shown in Figure 12.

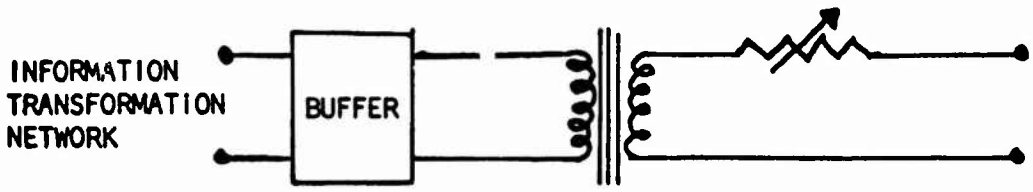

SKIN STIMULATION ADAPTOR

FIGURE 12

THE INTERFACE

Conductive sponge rubber skin electrodes were designed and constructed at the Biotechnology Laboratory in a concentric fashion. A circular 1-inch outer diameter plexiglas plate was used to house the concentric electrodes. A hole was drilled in the center of the rod where a cylindrical piece of conductive sponge mounted on a copper electrode was inserted. Another cylindrical electrode was mounted on a copper electrode and inserted 1/2-inch away from the center, as shown in Figures 13 and 14.

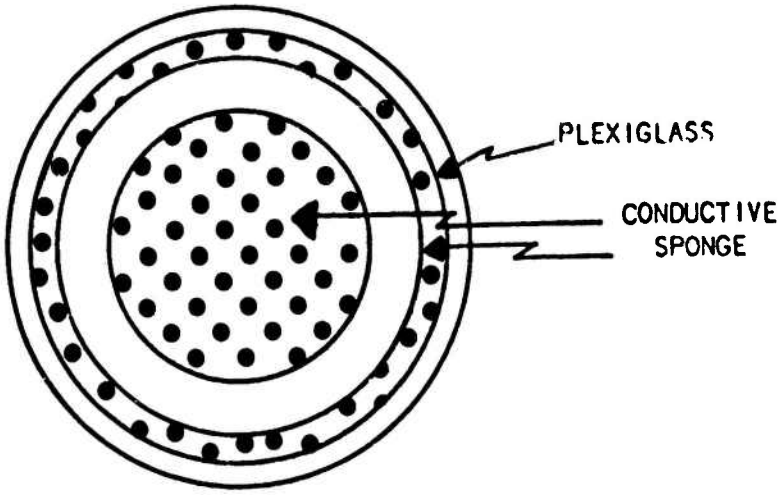

BOTTOM VIEW OF THE INTERFACE

FIGURE 13

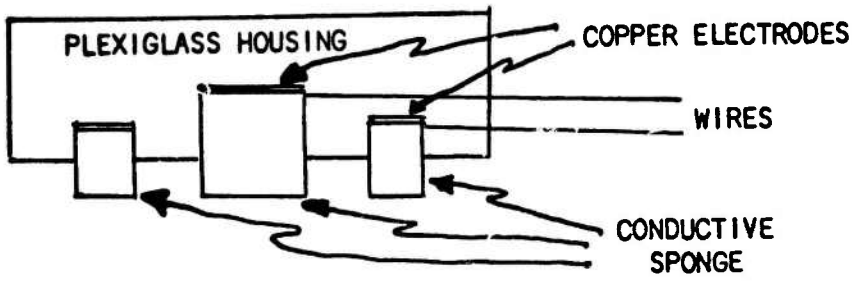

SIDE VIEW OF THE INTERFACE

FIGURE 14

The conductive sponge elements were exposed .1-inch below the plexiglas housing for contact with the skin. A wire was drawn from each copper electrode and connected to the outputs of the information transformation system.

The interface illustrated in Figures 13 and 14 is placed on the waistline of the amputee on the side of the amputation. It is held in place by connecting the plexiglass housing to the waist strap of the undergarment. Electrode skin paste is sparingly applied to the electrode to insure good contact. The waistline location was chosen to be purposely away from the arm and shoulder area where EMG control recordings were done, in order to prevent interference with the myoelectric signals.

DISCUSSION

Preliminary testing and evaluation of the system for several pressure ranges resulted in a clear vibration sensation on the skin, with good resolution up to 120 pps, with complete comfort. Several important points were revealed during the experiment:

a. Except for a slight initial sting, the major part of the pain component observed in metal electrodes was not present.

b. As pressure applied to the electrodes against the skin was increased, no sting or discomfort was detected at any phase.

c. Several electrode sizes of the same structure and design features were used, revealing that more comfort is observed as the diameter of the electrode increases.

The physical phenomenon behind this observation lies in the decreased current density generated by the concentric electrodes. Since the field just outside the center electrode is proportional to the radius of the electrode, large diameters result in reduced electric field and the associated current density. Smaller current densities effectively reduce the sting/pain effect, and result in increased comfort. Also, as the pressure on the electrodes against the skin increases, more surface contact area is available for the current to flow through. This also results in increased comfort.

Skin stimulation of the forearm required several seconds before sensation was detected, while stimulation of fingertip or abdomen resulted in immediate sensation. Direct placement of the electrodes above nerves and muscles yielded more pronounced vibration sensation due to the stimulation of the organs. The above observations indicate the variations in sensitivity of different locations of the body.

In conclusion, the above findings point out that further work is required in order to define the relationships of comfortable sensation to electrode size, contact pressure on the skin, and appropriate location of the electrodes on the body. Further work should also be done to define the waveform for which skin stimulation results in maximal reduction of discomfort. Interpretation of the stimulus does not seem to be a serious problem at this time.

REFERENCES

Agarwal, G., G. Gottlieb and L. Stark, "Models of Muscle Proprioceptive Receptors," Proceedings of the Fourth Annual Conference on Manual Control, University of Michigan, Ann Arbor, Michigan, 1968

Clippinger, F., Unpublished Communication, Duke University, Durham-Raleigh, North Carolina, 1973

Katz, B., Nerve, Muscle and Synapse, McGraw-Hill, 1966

Prior, R., "Study of Electrocutaneous Parameters Relevant to Dynamic Tactual Communication Systems," Ph.D. Dissertation, University of California at Los Angeles, 1972

Reswick, J., Personal Communication, Neuromuscular Engineering Section, Rancho Los Amigos Hospital, Downey, California, 1972

Solomonow, M., "The Response of the Mammalian Muscle Spindle to Muscular Perturbations," M.S. Thesis, California State University at Los Angeles, 1972

Stassen, H. G., A. Meyer and A. Van Lunteren, "On Possibilities of Tactile Information Transmission," Proceedings of the Sixth Annual Conference on Manual Control, Wright-Patterson Air Force Base, Ohio, 1970

14-28,209 #13

A PERFORMANCE MEASUREMENT MODEL FOR NON-LINEAR MAN-MACHINE CONTROL PROBLEMS*

E. M. Connelly
D. G. Loental

Quest Research Corporation
6845 Elm Street, Suite 407
McLean, Virginia 22101

ABSTRACT

This paper presents a method of deriving system performance models by applying a processing model to demonstration data. The approach is an empirical one in which data representing various levels of performance are examined and a performance model is automatically constructed. The technique employs a transition model which divides the problem space into discrete cells and measures performance based on how the system transfers from cell to cell. This processing model is applicable to many problems because it is based on output demonstration data rather than a description of the actual control task.

This performance measurement model is a computer program which has been applied to flight data produced by operators using the F-106 simulator located at AMRL/HES, Wright-Patterson Air Force Base, Ohio. The paper includes descriptions of the processing models and the resulting performance measures developed from the F-106 simulator data.

INTRODUCTION

Performance of manned systems is limited by our ability to measure system and component subsystem performance in a reliable and sensitive manner. Without adequate performance measures, there is no way to produce and test system designs, plan and execute training systems, or evaluate operational systems. Methods of developing these performance measures can be characterized by the way in which performance criteria are obtained. Ideally, performance criteria would be established by mathematical techniques to ensure a firm theoretical basis. For example, if a problem requires that an aircraft climb to a specified altitude while conserving fuel during the climb, the criterion, i.e., minimization of fuel, can be precisely defined. Frequently, however, problems can not be solved

*This work was supported by 6570th Aerospace Medical Research Laboratory, Air Force Systems Command, United States Air Force, Wright-Patterson Air Force Base, Ohio.

analytically, but demonstrations of superior as well as less than superior performances are available. In this situation, we find that man can demonstrate good (and also poor) performance even though he is unable to describe how he achieves that performance or what criteria he uses. Decision-making (policy), flying performance, and athletic performance are a few of the areas in this category.

This paper documents an empirical approach to the development of system performance measures whereby flight data from demonstrations of various performance levels are systematically processed to obtain the desired system performance information. This approach is based on the rationale that:

1. Demonstrated performances can at least be sorted according to the independent measure of performance. This is true even if the independent measure is a terminal one that indicates the value of the performance only at weapons launch, and

2. Operator's actions which produce superior results can be modeled and examined to show how superior results are achieved.

Thus, the method is designed to:

1. Identify critical tasks,
2. Identify measures of performance,
3. Identify control techniques associated with superior performance,
4. Establish performance criteria, and
5. Establish system design criteria.

Three types of models are used to represent system performance. As shown in Figure 1, the three models are:

1. An operator/pilot operating with the simulated system,
2. Model of the operator/pilot operating with a simulated system, and
3. A system performance model.

Performance demonstration data, such as flight trajectories and values of an independent performance variable (a performance score), are obtained from model 1 (above). In the F-106 attack problem, for example, the terminal steering error and error rate (at missile launch) are used as the independent performance variables. Performance runs are divided into groups according

SYSTEM PERFORMANCE MODEL

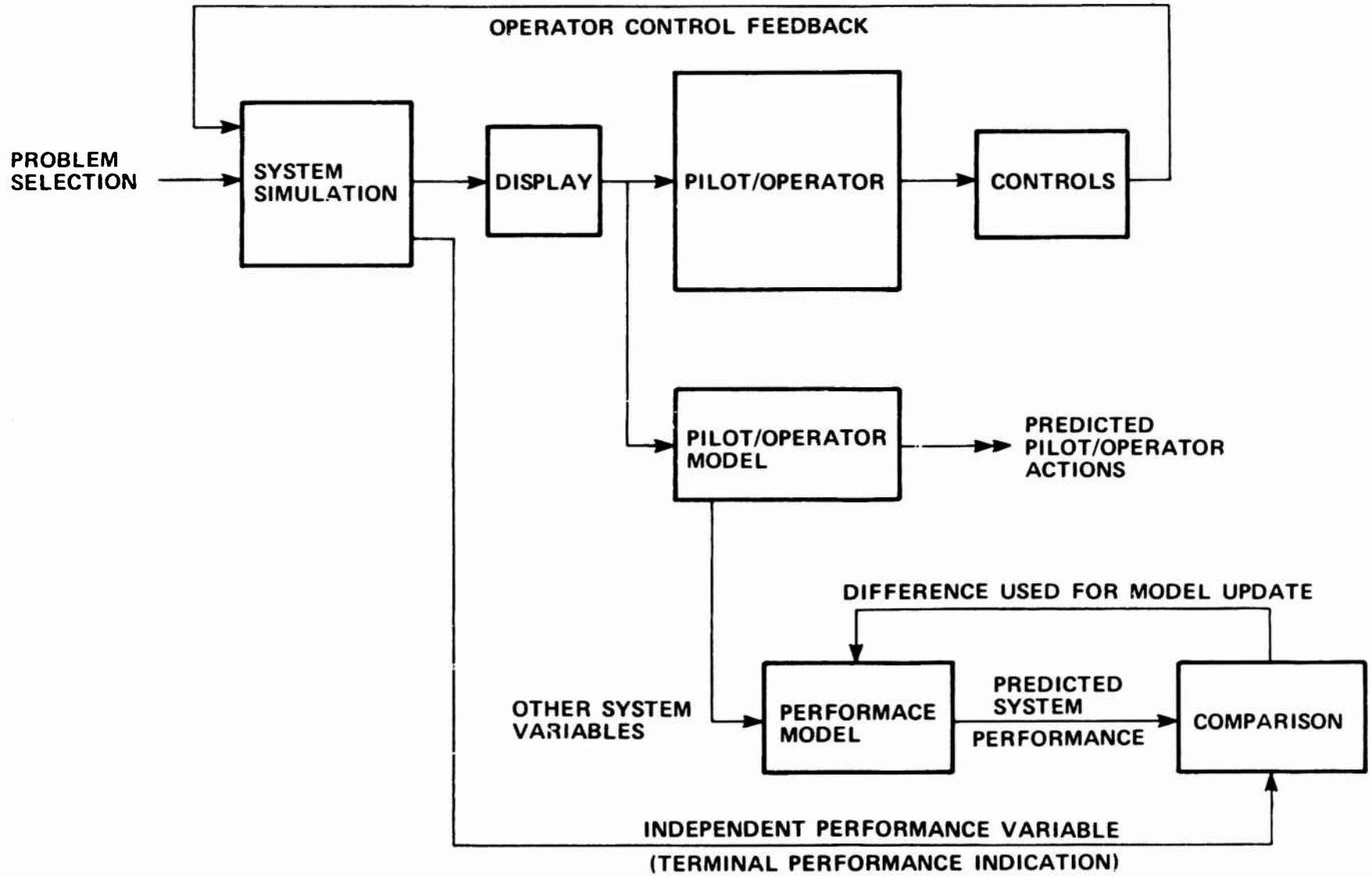

FIGURE 1 SYSTEM PERFORMANCE MODELS

to the independent performance variables. Also, the problem situation space is divided into regions so that representative pilot control policies (model 2 above) for each performance group in each problem situation can be examined. Finally a performance model (3 above) can be constructed by relating pilot control patterns in each situation to the independent variable.

The F-106 attack mission simulation has three phases:

1. Spotlight (prelock-on)
2. Lock-on (attempts)
3. Attack (post lock-on)

In the spotlight mode, the pilot controls the aircraft to reduce steering error. In the lock-on phase, he not only controls the aircraft but must also adjust his antenna azimuth and range gate controls to obtain lock-on. Finally, in post lock-on, he controls steering errors and pulls the arming trigger prior to weapons launch. Each of the three phases can be performed with greater than 20 seconds to missile launch (no time stress) or with less than 20 seconds (time stress). Thus, there are six problem situations. While the pilot controls steering error as a primary task, analysis of the performance demonstrations shows that he performs this task in a different way in each problem situation. The performance measurement tool described in this paper utilizes a transition matrix representation of pilot control policy and provides a means for (1) identifying those portions of the control policy useful in performance discrimination, and (2) identifying the effects of secondary tasks and time stress.

Data included in this paper are extracted from the final report of Contract No. F33615-73-C-4121 which contains a more complete description of the experiment and results.

PERFORMANCE MEASUREMENT DEVELOPMENT METHOD

Performance Measure System

The development of performance measures from demonstration data requires a systematic means for processing the data so that standard computerized routines can be used to develop the measures and to support analysis of the operator control policies. While a standardized process is desirable, each different type of operator control task utilizes different criterion functions and, therefore, require different types of measures. The performance measurement development method described here accepts information specific to the problem at hand, such as recommended criterion functions, and employs a standardized processing method to generate the performance measures.

Figure 2 is a block diagram of the system used to process the data. The problem input variables, from a system simulation, are directed to a set of Boolean functions which ask questions about the variable values. These questions are selected to extract information believed to be important to performance measurement and to allow convenient analysis of the input data. For example, the error state space is quantized into regions and the transition patterns from one region to another are examined to develop the performance metrics required. The Boolean variables contain two types of information:

1. Information extracted from the input variables, and
2. Information concerning functions, criteria and other

data believed to be important to performance measurement in this particular problem.

Since the inputs to the Boolean functions are functions of time, the outputs are Boolean time sequences. These are:

1. Boolean variables believed to be related to performance, and
2. Boolean situation variables identifying the existence of

each problem situation.

Problem situation variables allow consideration of each situation separately. For instance, in the problem at hand, the problem situation variables identify prelock, attempted lock-on, post lock, etc., so that performance and operator control characteristics in each situation can be determined.

As shown in Figure 2, pattern detectors are used to extract information on patterns which are likely to provide good performance discrimination. Candidate performance measures are developed from these patterns, compared with the independent performance variable and adjusted, ordered, selected or rejected, based on the degree of the agreement with the independent performance variable. Once agreement is obtained between the predicted performance variable and the independent performance variable, the performance measurement development process is terminated and the performance measurement test and validation process is initiated. The validation process consists of two steps.

1. Introduce problem variables from new data into the system and generate predicted performance variables which are compared against the independent performance variable values. No adjustment is made in the performance measure function when testing against the new data.

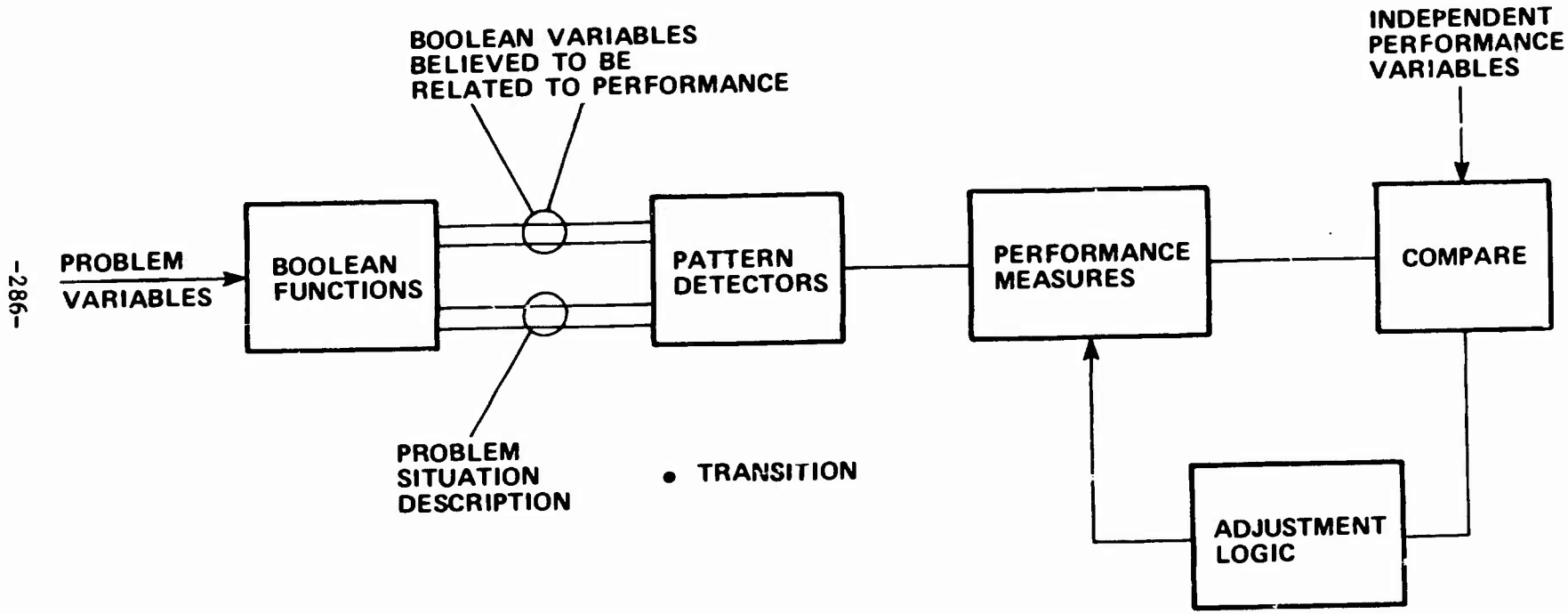

FIGURE 2

PERFORMANCE MEASUREMENT SYSTEM

2. Examine the structure of the performance measures which appear to have validity based on the data tests. This examination is required to determine what factors led to the generation of effective performance measures and evaluate whether these are "reasonable" factors.

Once acceptable performance measures have been developed, the associated transition patterns can be examined to determine what pilot control factors are associated with superior performance and not associated with less than superior performance. Also, the transition patterns are examined to determine how operator performance in each category is modified under time stress and/or secondary problem tasks.

Transition Analysis Method

As shown in Figure 3, one set of Boolean functions divides the steering error and the steering error rate phase plane into 15 regions or cells. These Boolean functions automatically determine the present location (cell) of the demonstration data, which facilitates the state transition computation.

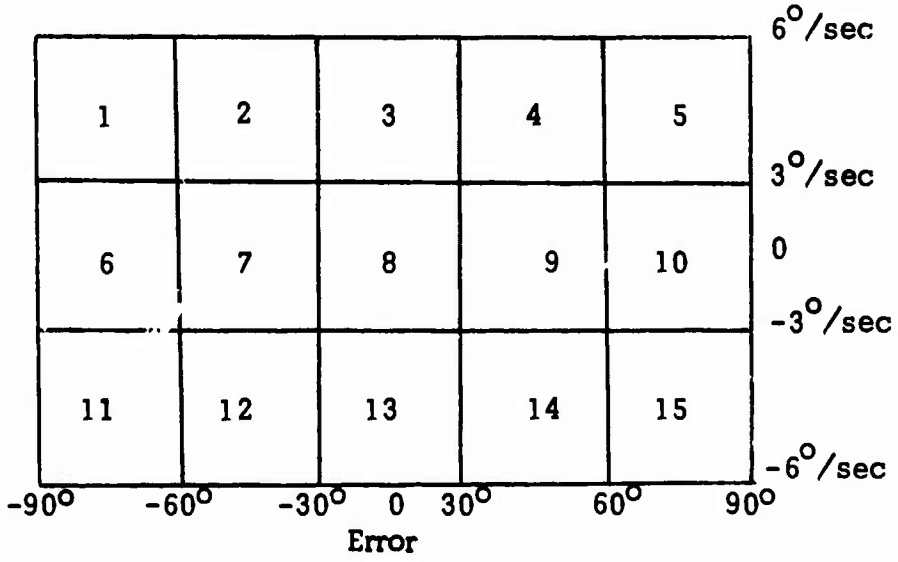

Figure 3 Transition States

Several matrices are used in the transition analysis of operator performance. One matrix is the transition matrix which is a 15 x 15 matrix whose elements are the probabilities of transfer from cell i to cell j on a given trial, i.e., from sample to sample. This matrix is constructed by counting the number of times the system is in each cell and makes each transition. If the resulting transition matrix represents a regular Markov

process, the state of the system after N transitions, starting from an initial state (cell) distribution represented by π_0, is given by

$$\pi_N = \pi_0 T^N \tag{1}$$

As N approaches infinity, there is a limiting distribution α given by

$$\lim_{N \to \infty} \pi_N = \alpha \tag{2}$$

α is the ensemble state distribution existing after a large number of trials. The limiting distribution can be regarded as the steady state distribution, such that

$$\alpha T = \alpha \tag{3}$$

A second matrix useful in analysis of operator control policies by transition matrices is defined by Equation 4 and is the weighted transition matrix, such that each element is given by:

$$D_{ij} = T_{ij}\, \alpha_i \tag{4}$$

This matrix, referred to as the D matrix, is obtained by multiplying each row of the transition matrix by the probability the ensemble will be in the corresponding state. The elements of the D matrix correspond to the probabilities that a particular transition (transtate) is used in a given control effort. Elements of the D matrix are used to generate a performance matrix according to:

$$P = \sum_i \sum_j D_{ij}\, TSM_{ij} \tag{5}$$

where TSM is a transtate score matrix whose element values correspond to the relative importance of each transtate to performance.

The objective of applying transition analysis to model operator control policies is to determine how the superior operators achieve superior results and to derive system performance measures. Specific questions of interest are:

1. What techniques do operators use in providing excellent control?
2. Are the control policies symmetrical?
3. Can we determine where performance differences occur in the state space?

4. Can we determine how the control policy changes with different problem situations within a performance level?

5. Can we determine policy changes or policy differences across performance levels, i.e., how do control policies developed by good operators (superior operators) differ from those developed by intermediate or poor operators in the same problem situation?

6. Do the trends within a performance level apply across performance levels?

PROBLEM DESCRIPTION

The experimental setup consisted of an operators control stick housing the radar lock-on controls, and a display system interfaced with an IBM 360 coded to simulate an F-106 aircraft in a co-planar attack. Aircraft heading control is the primary task and the operator's input for this task consists of lateral motions of the control stick. Radar lock-on tasks, (azimuth and range gate control) provide secondary tasks. The essential elements of the operator's display are shown in Figure 4. Roll (ϕ) is the angle between the wings and artifical horizon. Steering error is displayed by the steering circle displacement radius from the display center. Radar azimuth and range gate position are also indicated on the display.

The pilot/operator's flying task is to control aircraft roll so that the steering error circle moves to the center of the display and remains as close to that zero steering error position as possible. Radar lock-on requires two operations, adjusting the antenna azimuth so it is pointing to the target and adjusting the range gate to bracket the target. Operator control of radar lock-on was considered as a secondary task and lock-on performance itself was not measured.

The flying task can be described with the aid of Figure 5. Roll angle and steering error are displayed to the operator and he attempts to reduce the steering error by adjusting the control stick. Roll rate is equal to a constant times the control stick position. Automatic turn coordination is assumed and thus aircraft turning rate is a TAN function of roll angle. The difference between desired heading and actual is the aircraft heading error, ψ_e, which is displayed. Reference heading ψ_R is computed using lead pursuit equations so that the pilot is not required to lead the target but instead to null the steering error.

SIMULATOR DISPLAY

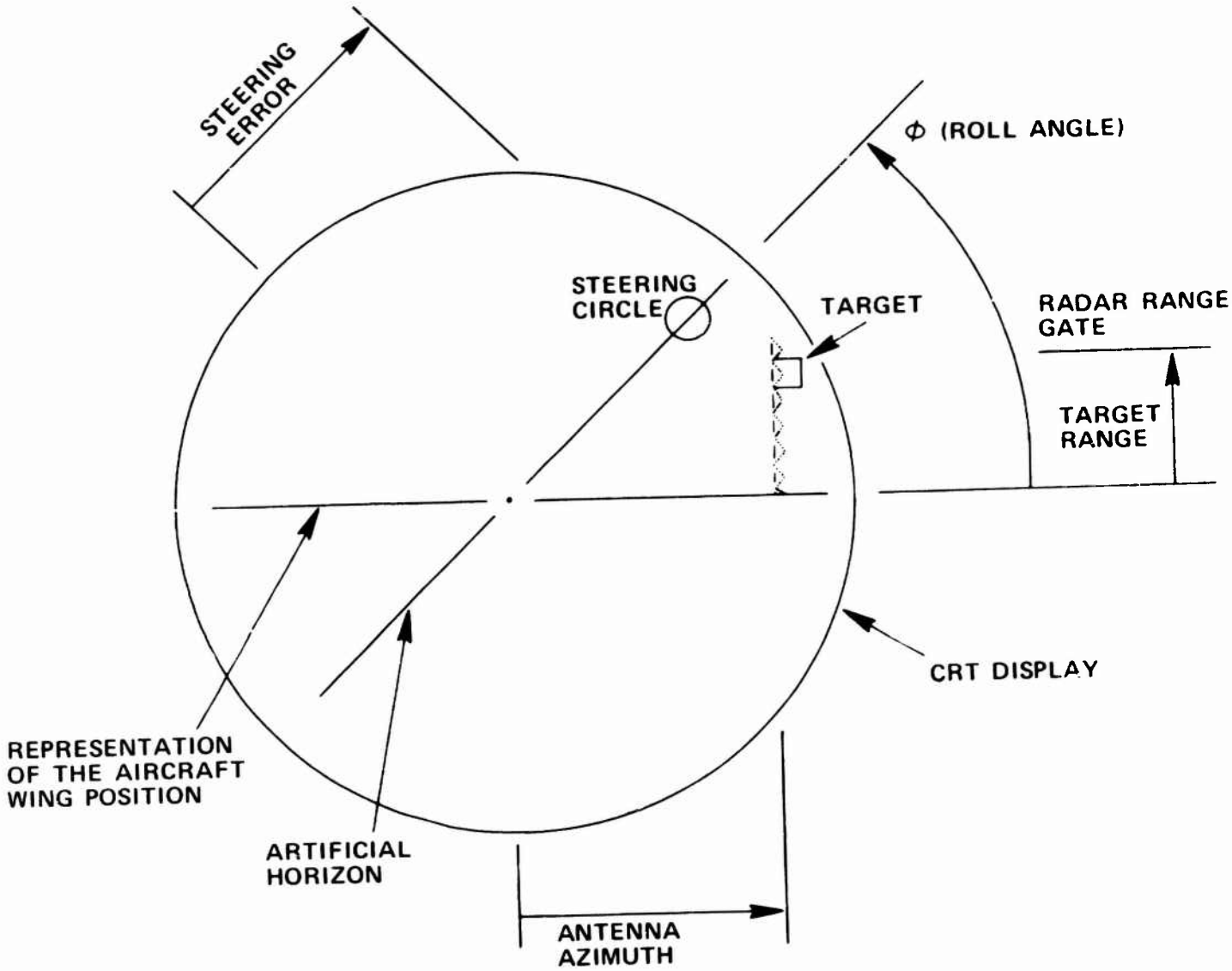

FIGURE 4
SIMULATOR DISPLAY

BLOCK DIAGRAM CONTROL PROBLEM

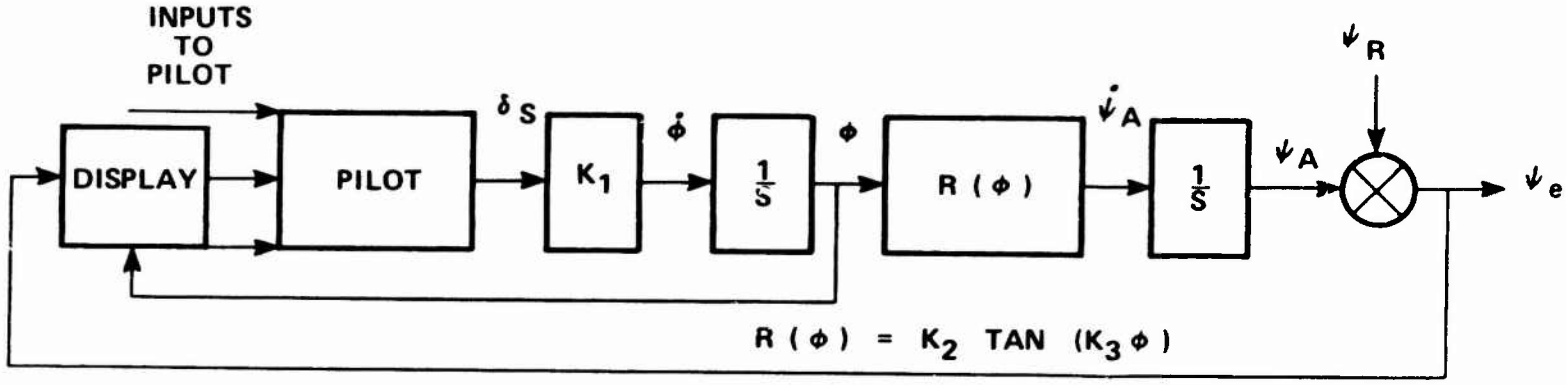

FIGURE 5

BLOCK DIAGRAM CONTROL PROBLEM

Three types of problems were presented to the operators. Problem A allows considerable time prior to lock-on and provides the operator an opportunity to demonstrate his control technique without time stress and secondary tasks. Problem B and C require rapid control of the aircraft steering error and radar lock-on.

SUMMARY OF EXPERIMENTAL DATA

The terminal scores (heading error and error rate at missile launch) for each of the 87 demonstrations are plotted in Figure 6. It is seen that all runs for operators 1 and 2 fall within the region from 0 to X_1 on the abscissa and from 0 to Y_1 on the ordinate. These two operators consistently achieve excellent performance. Another region, identified as the area between X_1 and X_2 on the abscissa and Y_1 and Y_2 on the ordinate, was selected to include 100% of the runs of operator 4. A third region was selected to include a clustering of run data which had errors less than 30° and turning rates less than 3° per second, as indicated by bounds X_3, Y_3. The fourth region includes the remaining data. All demonstrated performances are grouped according to the region in which the terminal performance belongs, i.e., operator identity was not used to group demonstration data.

Typical Trajectories

Figures 7 through 12 are plots of problem trajectories obtained from simulator data which show ψ_e steering error versus $\dot{\psi}$ heading rate. It should be noted that the aircraft turning rate is not necessarily the same as the rate of change of steering error since the steering error is not necessarily constant for constant aircraft heading. In these problems, however, the target velocities are constant and thus, the computed intercept point is constant. As a result, the reference heading is also constant. Figure 7 shows the trajectory of run 111 during the spotlight or prelock-on phase of problem A. The technique used by operator 1 is to roll the aircraft rapidly to the maximum roll angle (75°) and subsequently, when the steering error is approximately 10°, he rolls the aircraft to a near wings level attitude. This produces a slight overshoot causing approximately a 4° error. The trajectory occuring during lock-on is not recorded because the lock-on takes only a few seconds and the lock-on effort does not induce additional errors. Figure 8 shows the post lock-on trajectory for the same run on a different scale. Note that the post lock-on control characteristic yields a small oscillation about the error axis with a rate limit of approximately $\pm.2^{\circ}$ per second and an error drift from +1 to -.2 degrees. At 2° error, a jump occurs to a 4.2° error, as shown by the dotted line. This is believed to be a

OPERATOR SCORE DATA

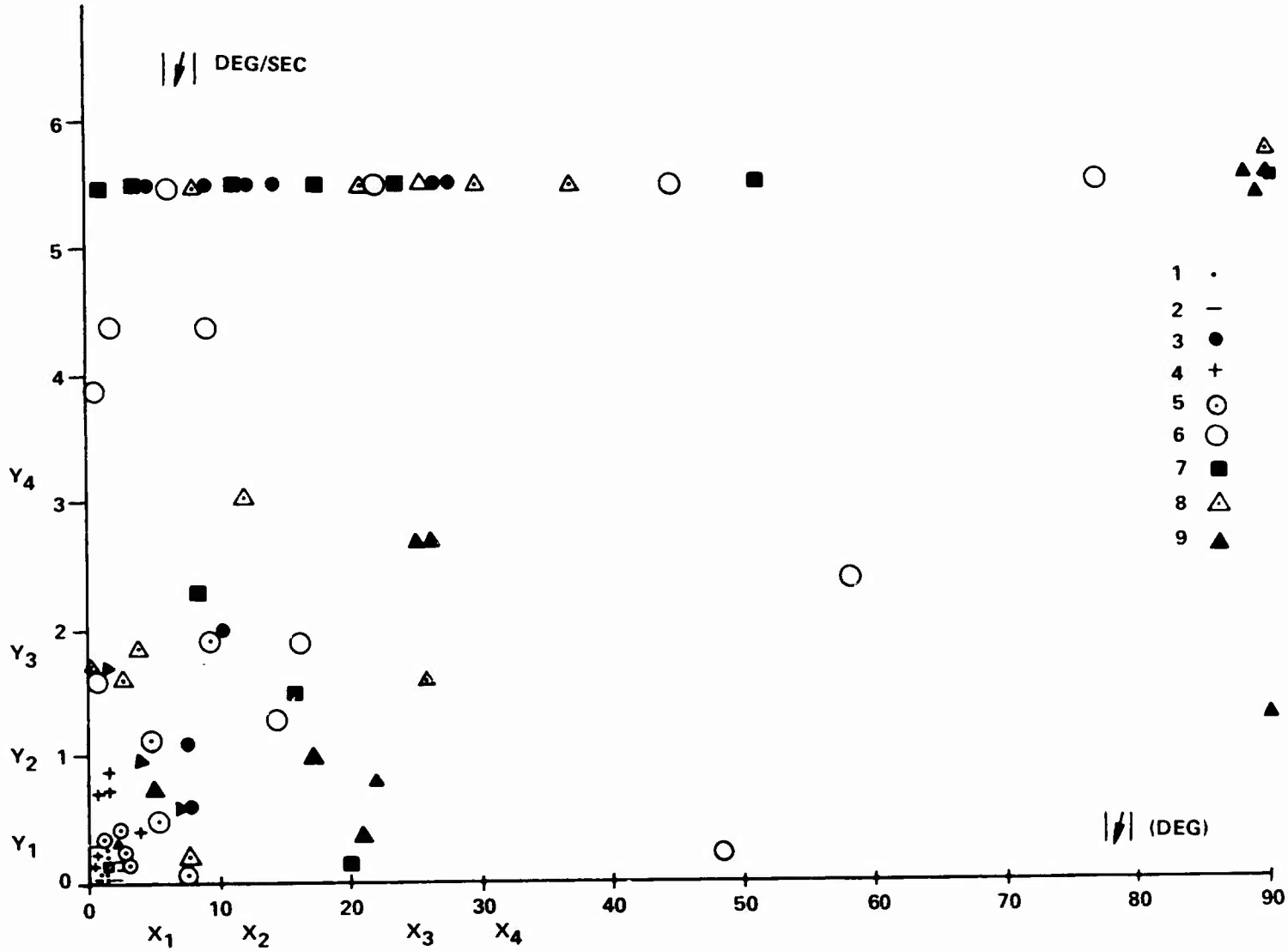

FIGURE 6 OPERATOR SCORE DATA

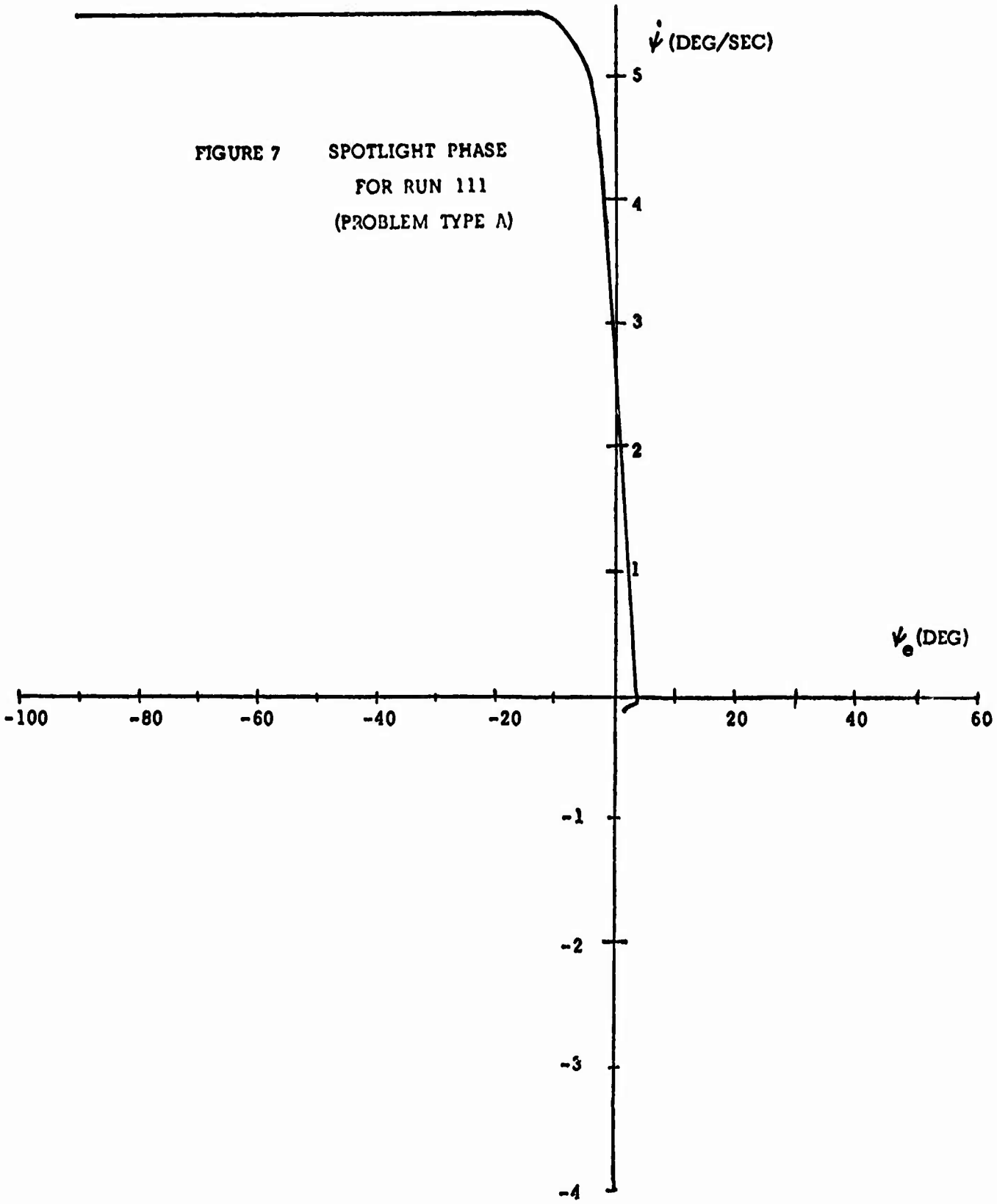

FIGURE 7 SPOTLIGHT PHASE FOR RUN 111 (PROBLEM TYPE A)

FIGURE 8 POST LOCK-ON PHASE FOR RUN 111 (PROBLEM TYPE A)

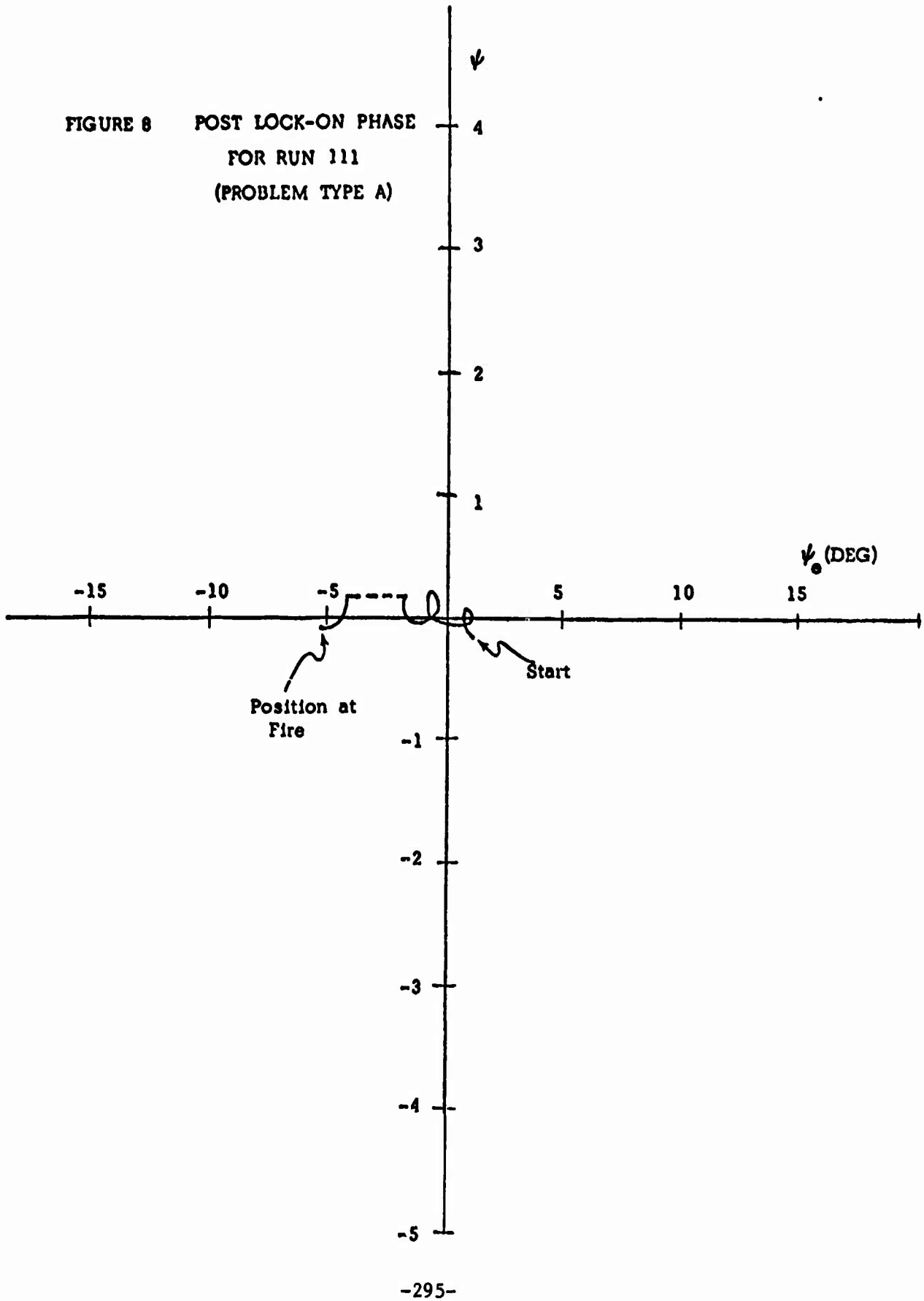

discontinuity in the simulator and occurred at an unfortunate time, i.e., just prior to time of fire. The operator's score should have been closer to -2^{o} instead of -5^{o}. This run demonstrates very good control because the error was reduced rapidly during the spotlight phase, little steering error was introduced during the radar lock-on phase, and a small error and small error rate was maintained during the attack phase (post lock-on).

Figure 9 presents the trajectories produced by operator 1 on his first attempt at problem B. In this problem, the target is initially within radar lock-on range and offset, so the operator must make a sharp turn to obtain lock-on. Note that he rolls rapidly to the roll saturation limit of 75^{o} but rolls out late at approximately 2^{o} steering error which produces a large overshoot. In spite of this overshoot, he covers nicely, producing an oscillatory response with a decreasing steering error. Recall that problem B has initial conditions set so that the problem is initially within radar lock-on range. The technique used is to roll to a 75^{o} roll angle hard limit (the 75^{o} hard limit is built into the simulation) and adjust his antenna azimuth and range gate to obtain lock-on while the aircraft is against that hard limit. This technique is very useful in the simulator but unrealistic since the aircraft has no hard limit.

Figure 10 presents the trajectories obtained by operator 1 on his second attempt on problem B. He uses essentially the same control technique and achieves the same result as he did on his first trial.

Trajectories for operator 1's first and second attempts on problem C are given in Figure 11. Since the target is initially within radar lock-on range, the operator attempts lock-on almost immediately and thus the spotlight phase exists for only a few seconds. Figure 11 shows trajectories for the lock-on phase for both the first and second runs. On the first run the pilot is able to achieve lock-on while introducing the steering error of only 4^{o} and requiring only 3.5 seconds. In his second attempt a larger error of 10^{o} is introduced, but radar lock-on is obtained quickly (3.0 seconds). Recovery from the steering errors introduced during lock-on is shown in Figure 12. Both trajectories show a rapid convergence of the steering error to an oscillatory response bounded by $\pm 4^{o}$ error and $\pm 4^{o}$/sec error rate. These trajectories are typical of those obtained from excellent and good operators and indicate the type of response obtained.

FIGURE 9 POST LOCK-ON PHASE
FOR RUN 1121
(PROBLEM TYPE B)

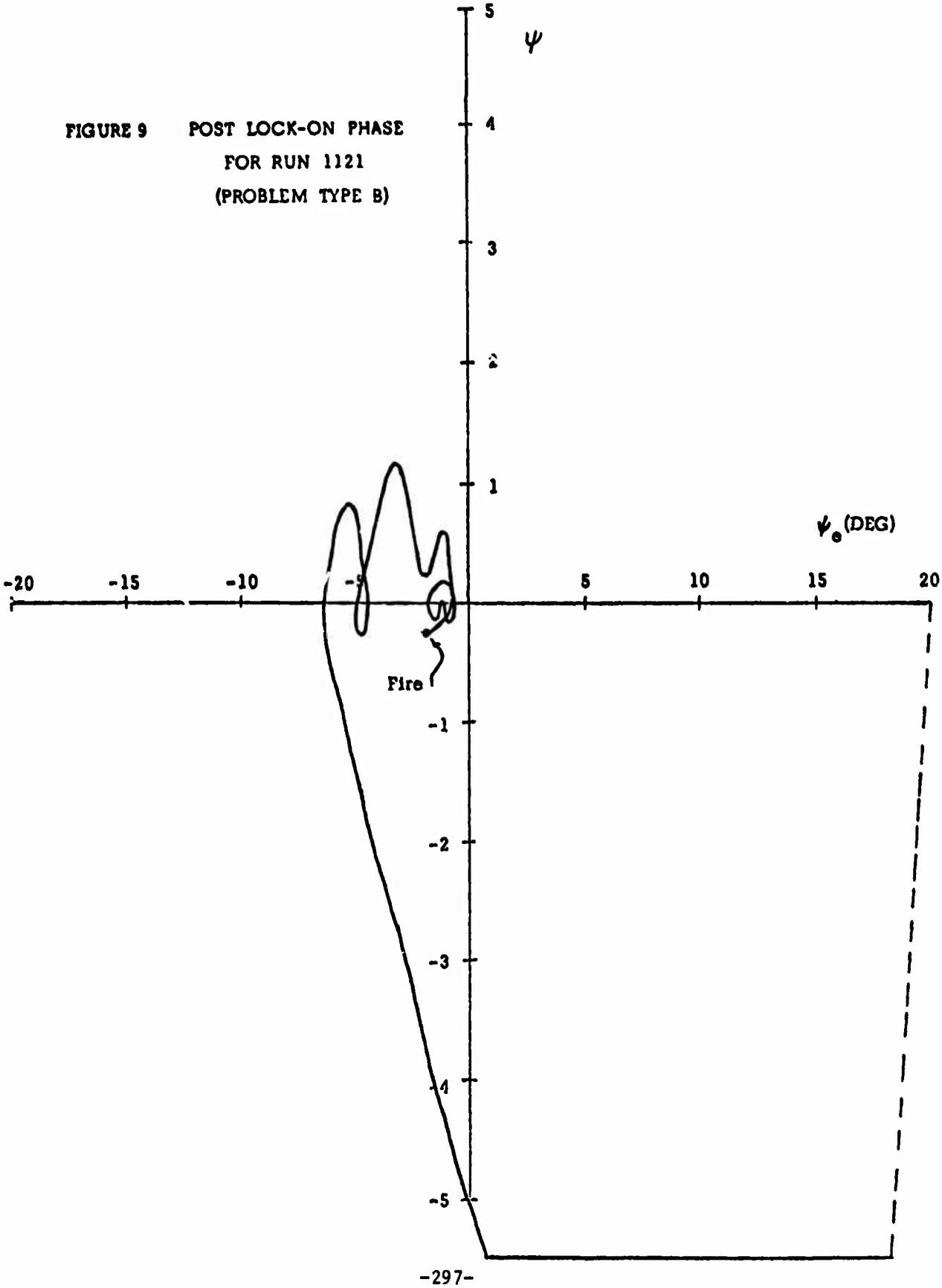

FIGURE 10 POST LOCK-ON PHASE FOR RUN 1122 (PROBLEM TYPE B)

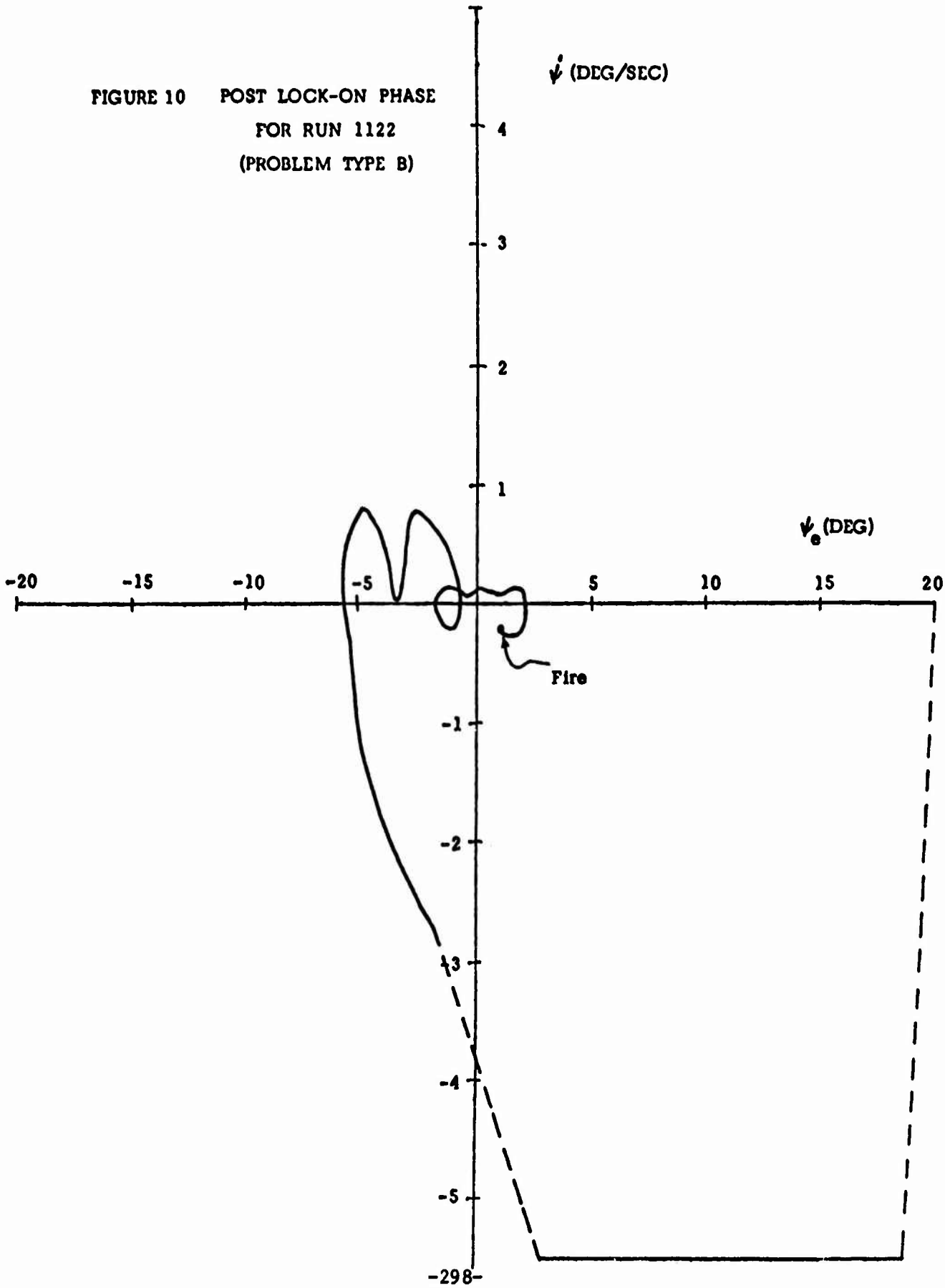

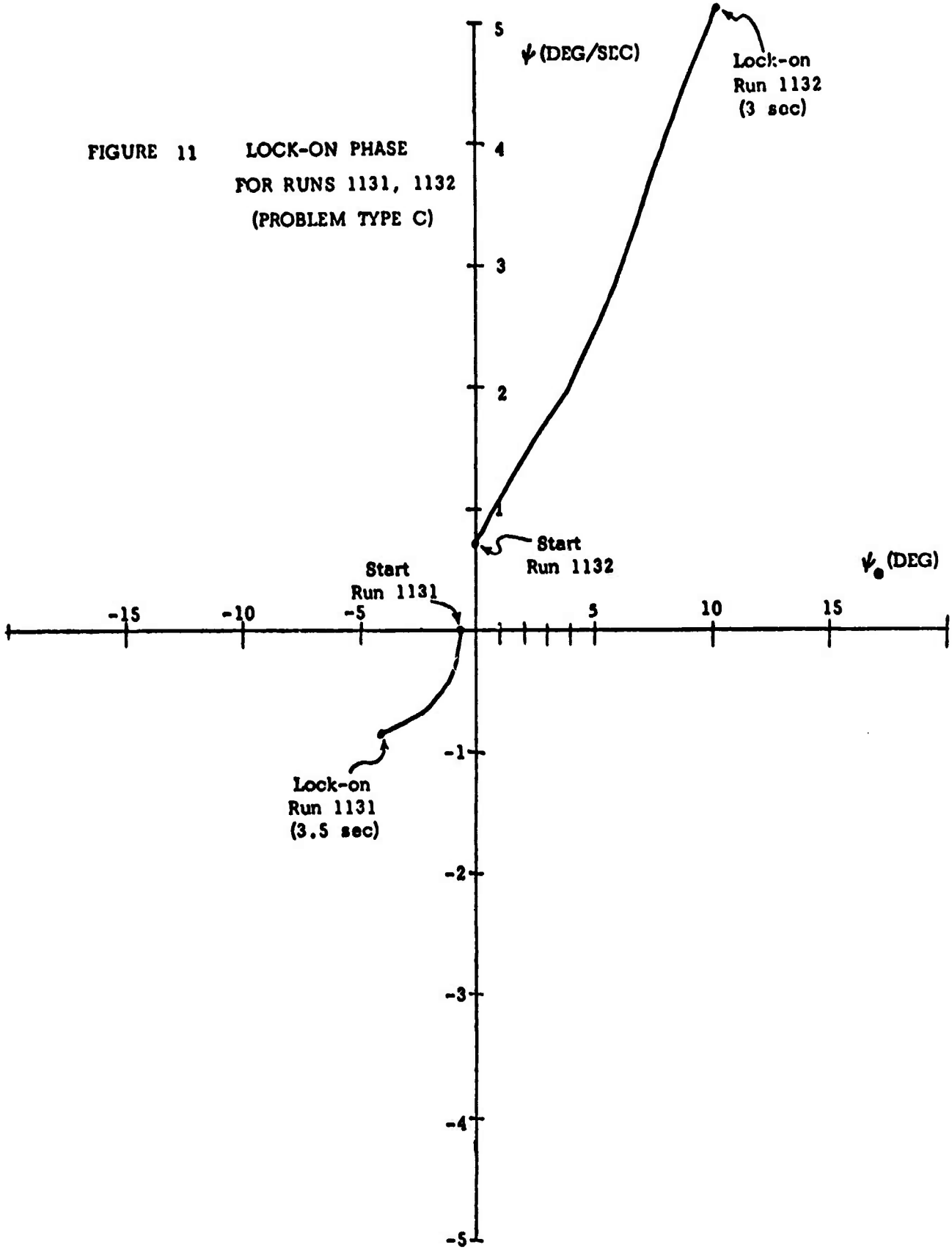

FIGURE 11 LOCK-ON PHASE FOR RUNS 1131, 1132 (PROBLEM TYPE C)

FIGURE 12 POST LOCK-ON PHASE FOR RUN 1121, 1132 (PROBLEM TYPE C)

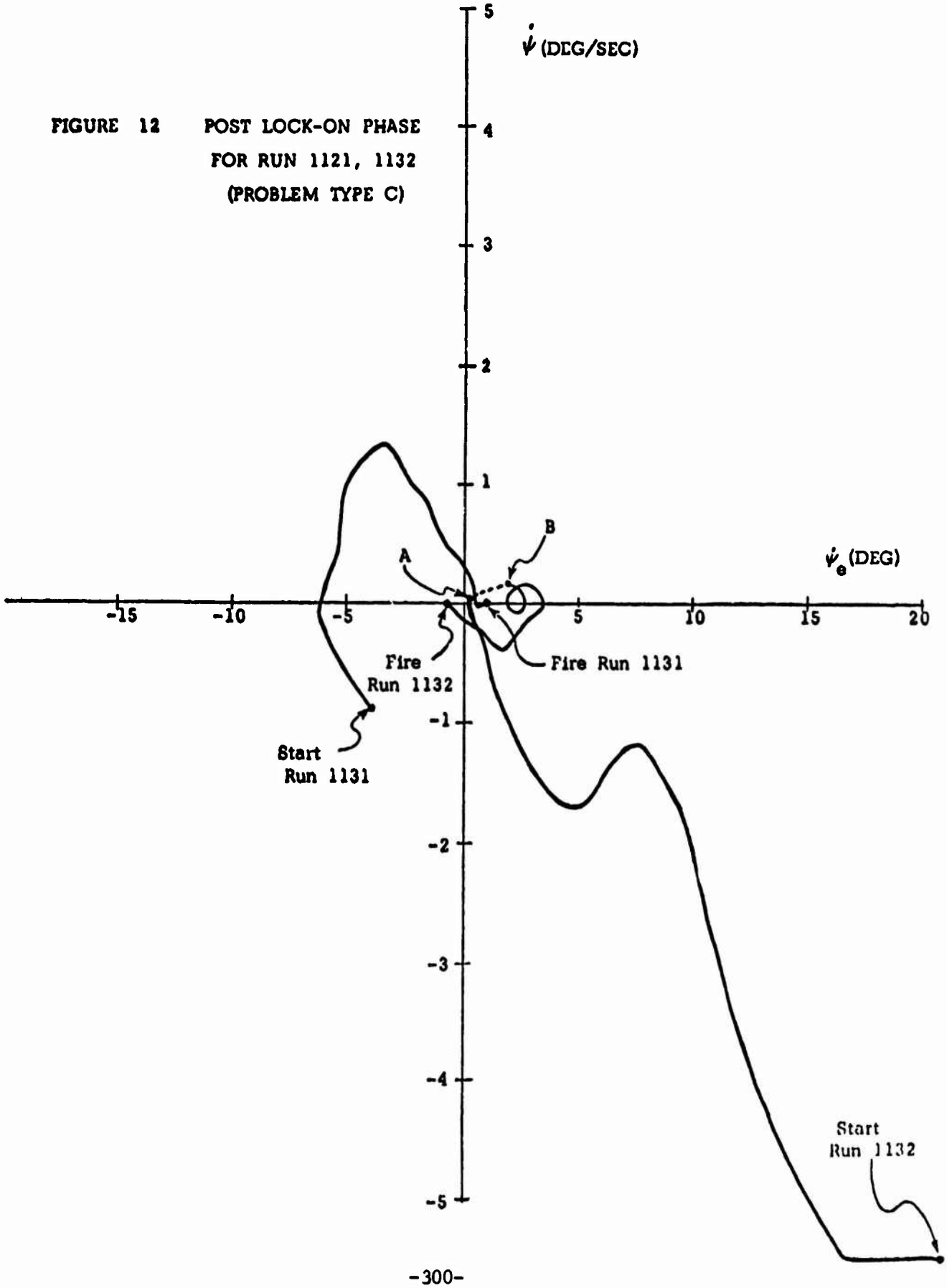

ANALYSIS OF OPERATOR CONTROL POLICIES

The transition matrix and limiting state distribution vector representing each performance level provide information on how superior operators achieve superior performance and what transitions discriminate performance. Characteristics of interest include:

1. Probability of remaining in state 8 on a single iteration, given that the system is in state 8. Note, state 8 is the desired terminal cell, as shown in Figure 3.
2. Probability of transferring to state 8 on a single iteration.
3. Probability of (an ensemble) being in state 8.
4. Mean number of iterations required to return to state 8 after leaving it.
5. Favored entry states into state 8.
6. Symmetry of important transitions.

For the F-106 attack problem, probabilities representing factors 1 and 3 for each performance level and problem state are of special interest and are listed in Figures13 and 14 respectively. Other data are included in the program final report.

Problem situation (PS) 0 exists at prelock-on-attempts with greater than 20 seconds to missile launch (no time stress). Situations 2 and 3 occur when the pilot is attempting lock-on, with situation 3 being under time stress (20 seconds to go). PS 4 and 5 are post lock-on where accurate steering control is important and State 5 exists when the problem has less than 20 seconds to go (time stress).

Referring to Figure 13 is seen that a high probability (exceeding .90) exists for performance level (PL) 1 subjects in problem situations 0, 4 and 5. In PS 2, the operator is attempting lock-on and, as a result, has a lower (.83) probability of staying in state 8. Note that no data is available for PL 1 performance in PS 3 because in no case were skilled operators still attempting lock-on with 20 seconds to go. This means that superior operators were always able to obtain lock-on prior to the terminal portion of the mission. The lower probability of staying in state 8 while attempting lock-on reflects the influence of the secondary tasks (radar lock-on) on the flying performance. This suggests that even though the steering error was small and the wings were near level, the radar lock-on task interfered with the pilot's ability to fly the aircraft, even where it was only necessary to maintain a wings level attitude.

PROBABILITY OF STAYING IN STATE 8

	1	2	3	4
0	.91	.58	.54	.51
2	.83	.67	.56	.53
3	ND	.50	.43	ND
4	.94	.80	.80	.87
5	.96	.67	.65	.83

FIGURE 13

PROBABILITY OF BEING IN STATE 8

	1	2	3	4
0	.49	.13	.12	.06
2	0	.07	.13	.06
3	ND	0	.02	0
4	.72	.63	.80	.55
5	.71	.53	.44	.21

FIGURE 14

A similar analysis can be applied to the probability of being in state 8 (as shown in Figure 14). The first performance category shows a 0.49 probability of being in state 8 prior to lock-on attempt, a 0.0 probability of being in state 8 during lock-on, and 0.72 and 0.71 probabilities of being in post lock-on states 4 and 5 respectively. The 0.49 probability associated with prelock-on for the excellent operators indicates that the sequence of states used in achieving superior performance allows approximately .5 probability of being in the desired state. This serves as a norm against which other performances can be judged. The near consistency of the probability of being in state 8 for PS 4 and 5 show that good operators do not allow time stress to significantly degrade their performance.

The probabilities of remaining in state 8 (Figure 13), given that the system is in state 8 for performance levels 2, 3 and 4, tend to be in the 0.5-0.6 range until after lock-on is achieved. During post lock-on and prior to time stress (PS 4), a relatively high (0.8) probability of remaining in state 8 is achieved; however, in performance categories 2 and 3 it is seen that the probability of remaining in state 8 drops to .67 and .65 respectively due to the effect of time stress. The corresponding probabilities for performance category 4 are surprisingly high and, as indicated previously, possibly reflect that some operators were able to achieve state 8 and maintain it, thus producing a high probability of staying in state 8. However, upon leaving state 8, they were unable to return in a timely manner and, produced a low score.

The entry for PS 3 for PL 4 does not contain any data because these operators never achieved state 8. This should be distinguished from the corresponding lack of data for level 1 performance where the superior operators are simply not attempting lock-on during the terminal portion of the problem. Thus, the poor operators in PL 4 were attempting lock-on during the terminal portion of the problem but were not able to achieve state 8, whereas the superior operators, except for one sample, had always achieved lock-on prior to that time.

The effect of attempting lock-on is also indicated clearly by the data shown in Figure 14, where for PS 3 we have near zero probabilities of being in state 8 for performance levels 2, 3 and 4. This indicates a lack of accurate aircraft control while attempting radar lock-on. Also, post lock-on without time stress (Situation 4) shows a marked increase in the probability of being in state 8. However, it is seen that there is a significant reduction in that probability under time stress (Situation 5).

As expected, the ordering of the probabilities of being in state 8 are in complete agreement with the terminal performance metric (i.e., the steering error and error rate at missile launch). It appears that several factors affect performance of manned systems and of these the ability to maintain stable aircraft control and properly correct for small errors (i.e., remaining in the desired state 8) are of critical importance, as demonstrated by the data in Figure 14.

PERFORMANCE MEASURES

The performance measurement system used consists of two operations:

1. Training the performance measurement processor, and
2. Producing performance measurement scores.

The training process employs a search of the transition matrices associated with each performance level to find the importance of each transition (transtate) to performance measurement. This process generates a transtate score matrix indicating the relative significance of the associated transitions to performance measurement. Thus, the training process identifies which transitions are consistently employed by operators providing excellent performance and which transitions are consistently used by operators with other levels of performance. The numerical value of each element of the transition score matrix is adjusted during the training phase based on the independent performance variable. Thus, when a transition score matrix is produced by the training phase, a performance score can be obtained from any transition matrix by observing the value of each transition. For example, it is possible to train the transition score matrix based on the flight data associated with one problem situation, say initial prelock-on attempt, where the operator is not time stressed nor attempting to perform a secondary task. The transition score matrix developed from this data can be applied to transition matrices produced by any problem situation. This allows evaluation of performance, i.e., control policies, in one problem situation based on transition ratings developed from a different problem situation. Furthermore, comparison of transtate score matrices developed for different problem situations can be compared to determine how differences in operator flight control problem requirements affect the way performance discrimination can be measured.

Two transtate score matrices were developed, corresponding to the following problem situations:

1. PS 0 (prelock-on attempt, no time stress), and
2. PS 5 (post lock-on, time stress).

The first condition is one in which the operators have no time stress, i.e., greater than 20 seconds to go, and need only control the aircraft heading since they are not attempting radar lock-on. In the second condition the operator is under time stress.

Figure 15 shows the score for each PL and each PS produced by a transition matrix as developed from Case 1. Since the score matrix was developed based on PS 0, it is not surprising that the performance scores in the figure for that situation are ordered, the highest associated with the performance level (1). Examining the scores developed for the high performance category (1), it is seen that the initial high score (63) is reduced to a low of 15 in problem situation 2, i.e., when the operator attempts radar lock-on. A relatively high performance is achieved in problem situation 4 (91) followed by a slight reduction in the score in the terminal phase when the operator is under time stress. This clearly indicates that operator flight control performance is poor while attempting radar lock-on and improves in post lock-on, but degrades slightly with a time stress. This evaluation is based on factors deemed important by analysis of all performance levels in PS 0 and therefore tends to emphasize or score highly those control characteristics related to aircraft flight performance category without time stress. Note that evaluation of each performance category in the final problem situation (5) is not ordered by this metric and, indeed, performance level 2 trials are rated lower than level 4 trials for this particular metric.

Performance evaluation based on Case 2 is shown in Figure 16. In this case, we see that the values associated with the terminal problem situation (5) are well ordered in accordance with the independent (terminal) performance variable (aircraft steering error and error rate at missile launch). Examination of the first column of the matrix, which corresponds to the performance predictions for the superior performance level, indicates the general trend of problem situations that was observed previously. The values of the first row of the figure indicate the lack of monotonic ordering in that the second level group is rated lower than that of the third and fourth. This evaluation, of course, is based on those factors deemed important in the terminal problem phase during a time stress situation. It suggests that if the operators of the second category had used, in the final terminal situation, the control policy demonstrated in the first problem situation, that group would of been rated last. It is of interest, therefore, to examine the differences in transition matrices and transition score matrices that would explain the performance characteristics shown in Figure 15 and 16.

	E_{10}	E_{20}	E_{30}	E_{40}
0	63.1	56.6	41.7	29.8
2	15.2	46.9	50.8	35.2
3	(ND)	2.8	26.7	10.6
4	91.3	86.5	32.2	77.1
5	83.4	49.7	70.8	63.5

FIGURE 15

PERFORMANCE MEASURES BASED ON PS 0 PERFORMANCE

	E_{10}	E_{20}	E_{30}	E_{40}
0	56.9	20.4	30.8	31.6
2	70.1	28.5	26.4	33.2
3	(ND)	45.1	26.7	21.8
4	73.0	62.5	72.2	57.0
5	69.8	62.3	44.0	24.0

FIGURE 16

PERFORMANCE MEASURES BASED ON PS 5 PERFORMANCE

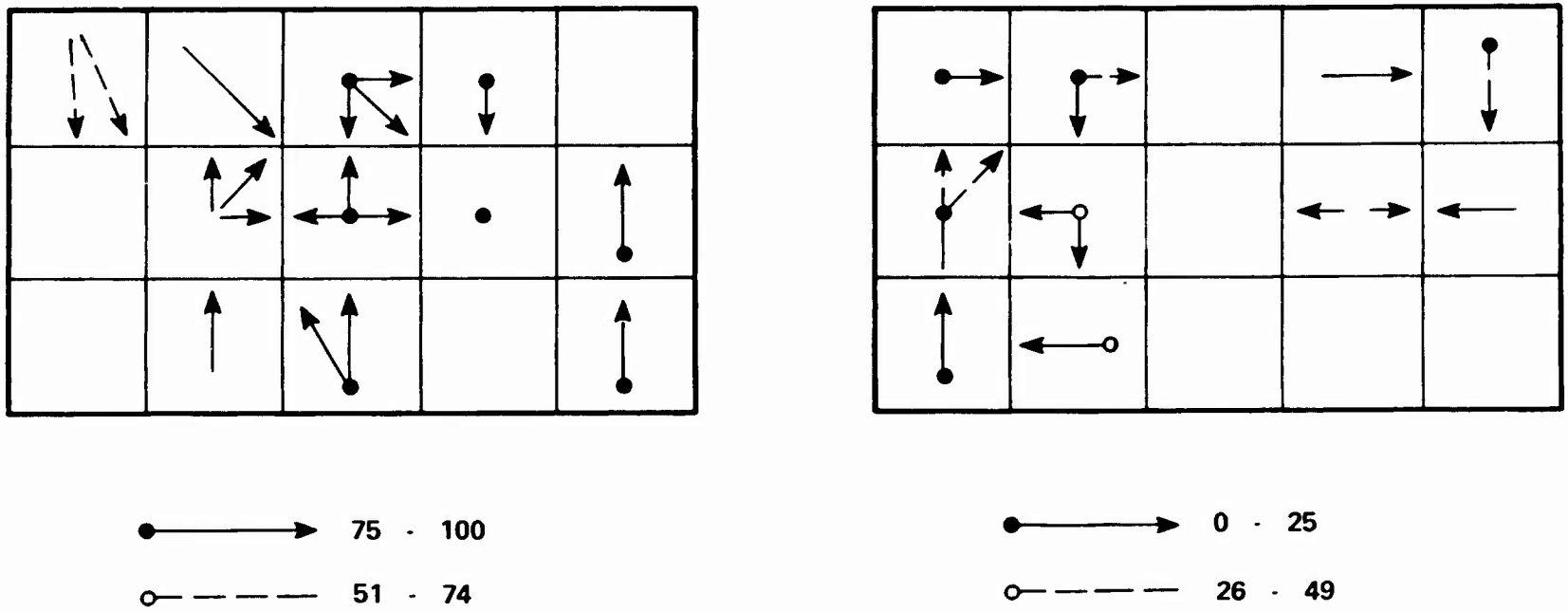

FIGURE 17

TRANSITIONS FOR PERFORMANCE DISCRIMINATION
BASED ON PS 0 PERFORMANCE

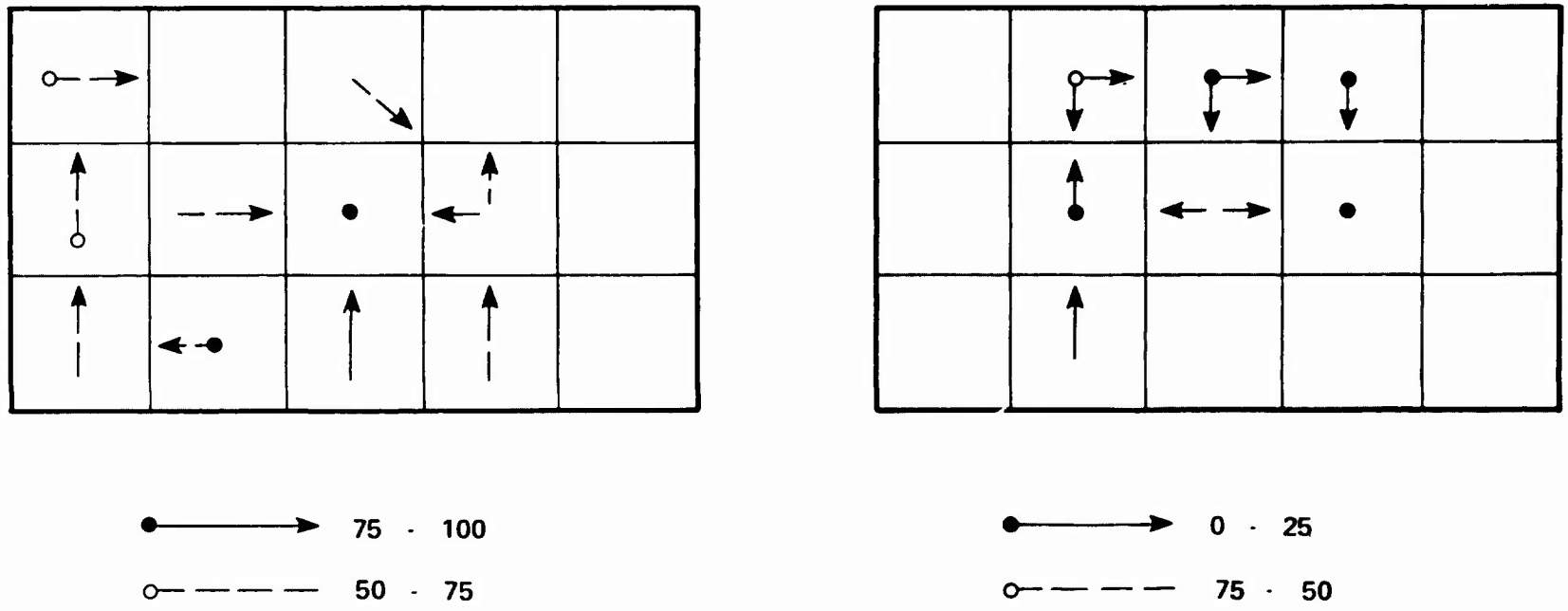

FIGURE 18

TRANSITIONS FOR PERFORMANCE DISCRIMINATION
BASED ON PS 5 PERFORMANCE

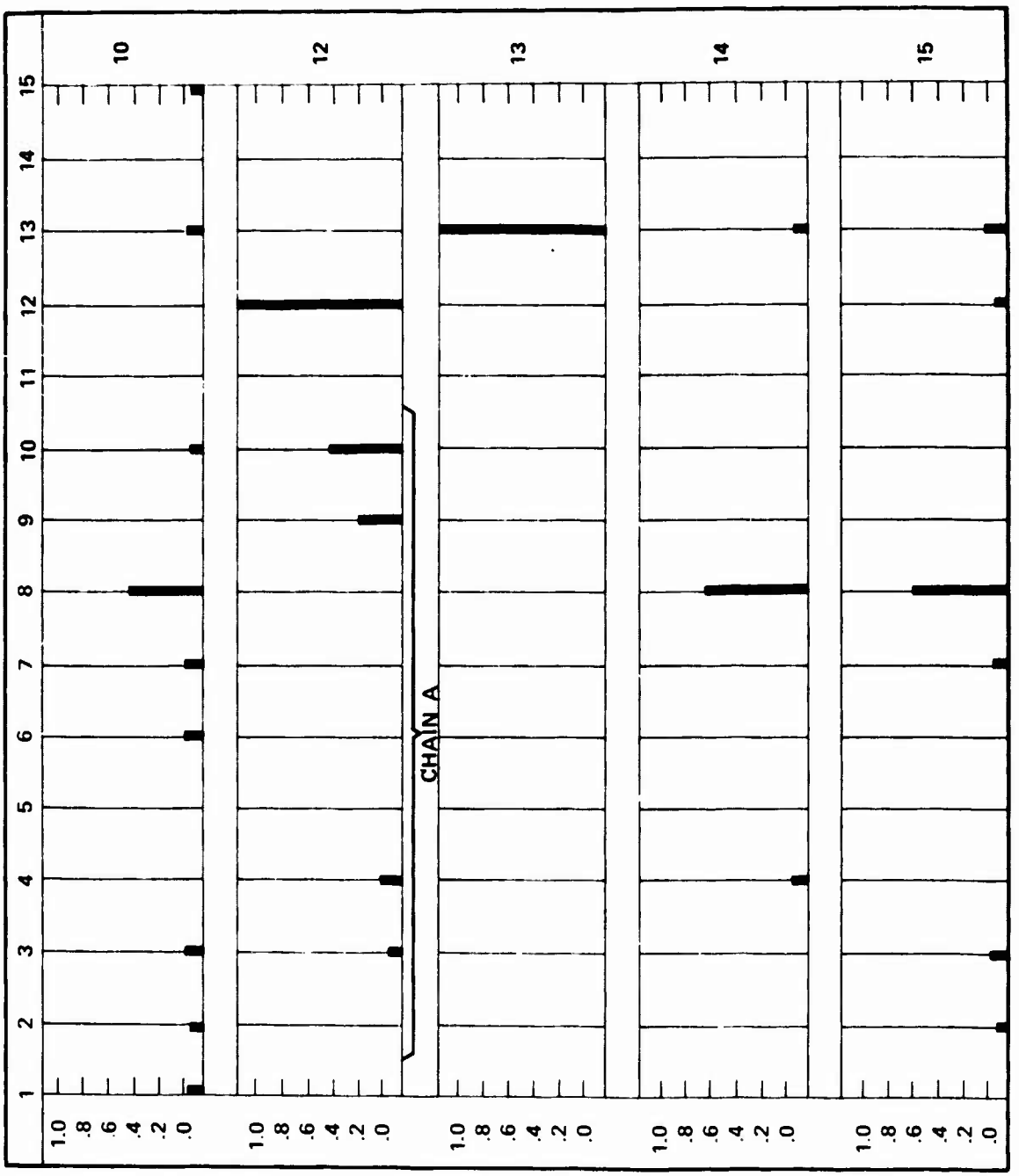

FIGURE 19

PL 1 STATE DISTRIBUTIONS

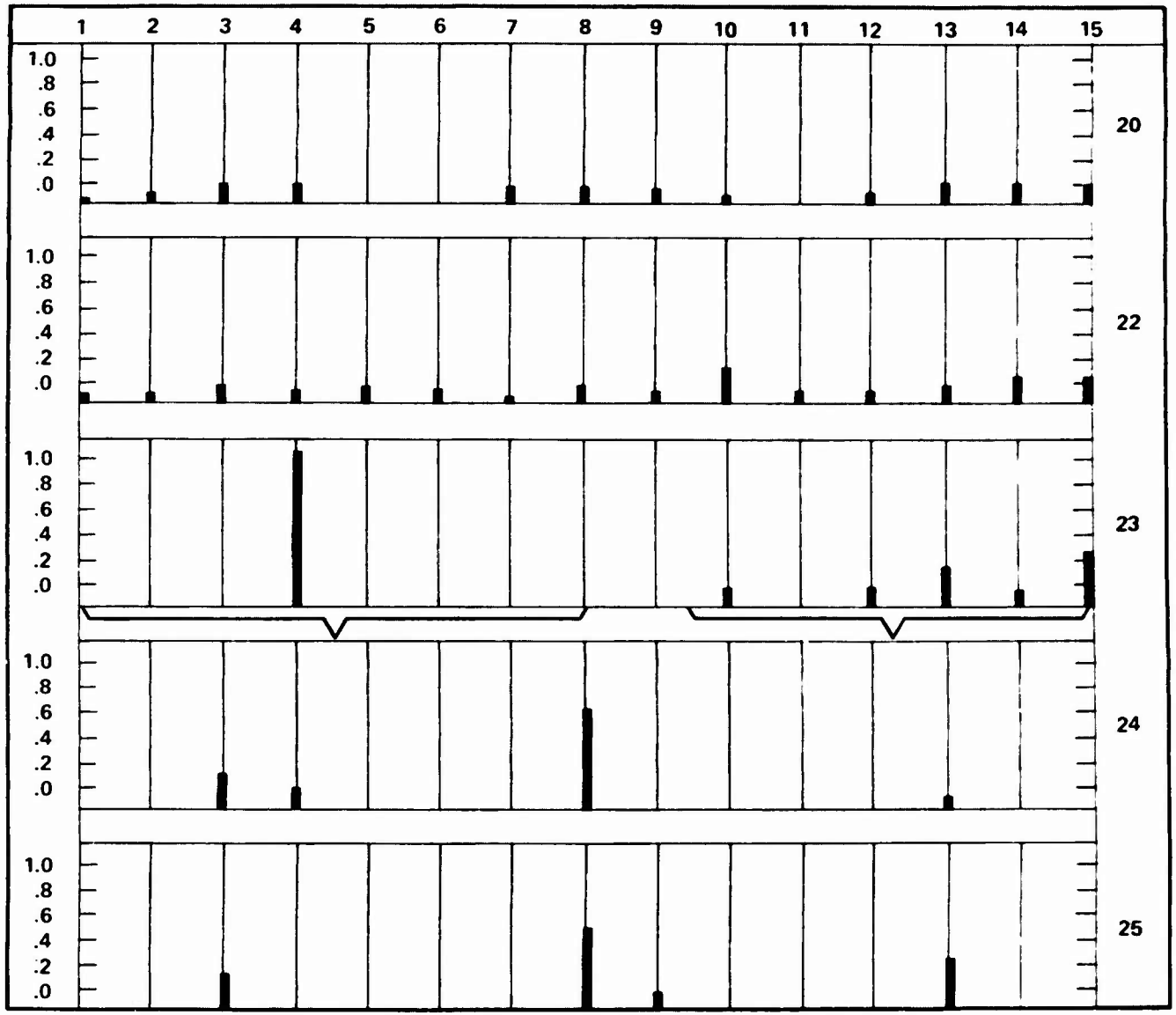

FIGURE 20

PL 2 STATE DISTRIBUTIONS

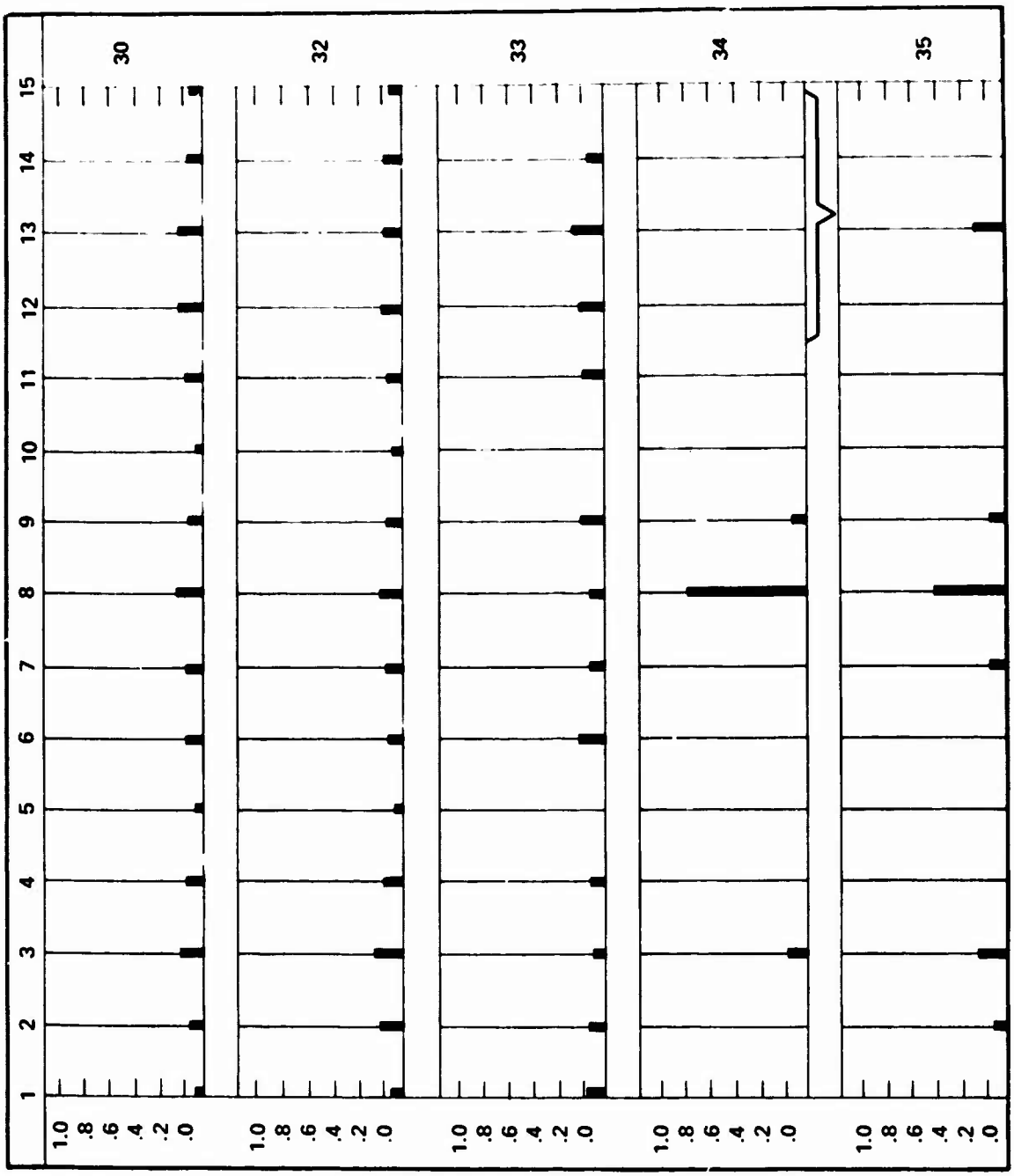

FIGURE 21

PL 3 STATE DISTRIBUTIONS

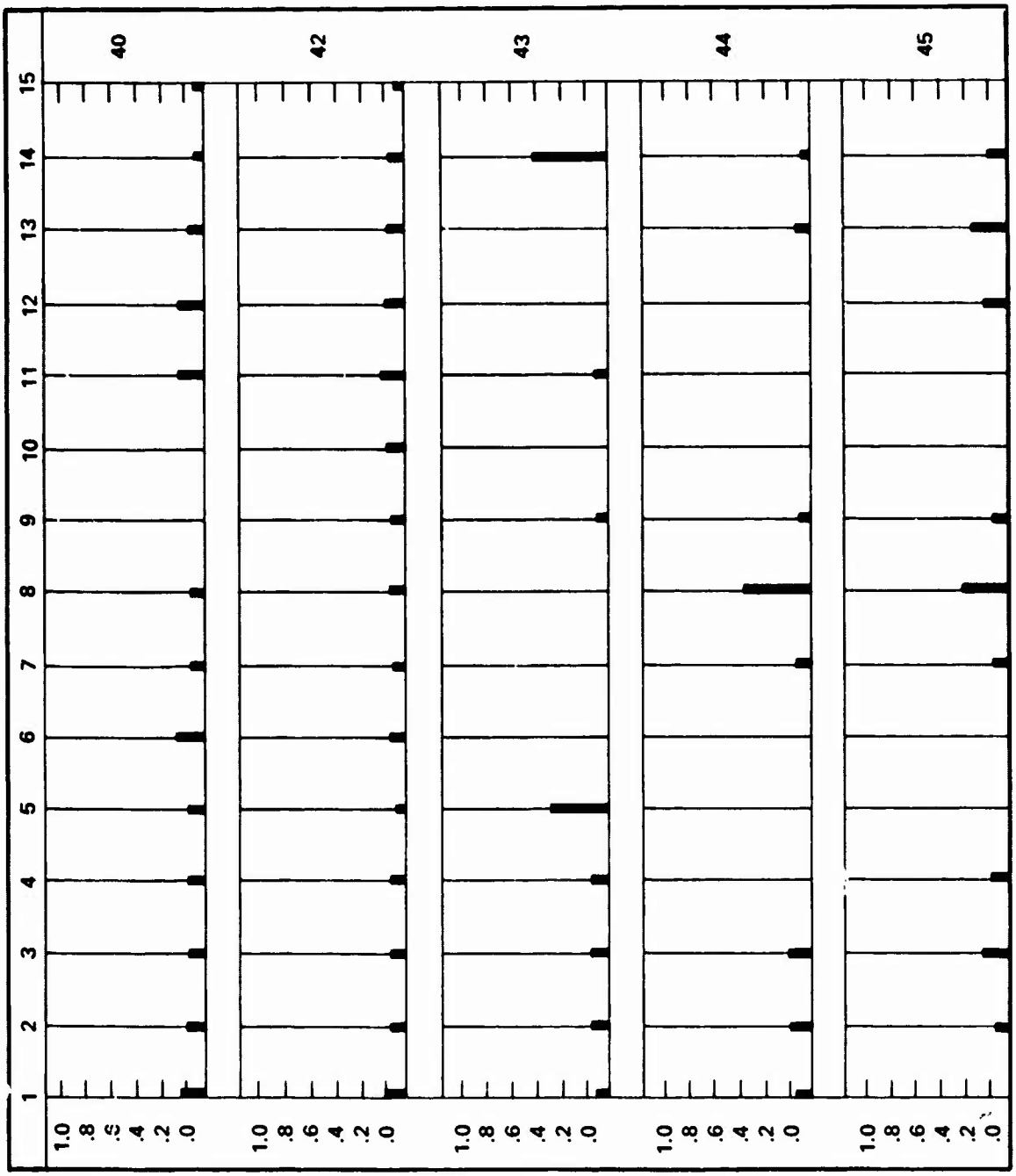

FIGURE 22

PL 4 STATE DISTRIBUTIONS

The transtate score matrix elements identify which transitions are consistently related with high performance and which transitions are consistently related to low performance. These are the transitions that are used to discriminate among performance levels. Figure 17 shows the transitions associated with high and low performance for Case I in graphical form. In the left portion of the figure, the solid dots and solid lines indicate the transitions associated with score values of 75 to 100, while the open circles and dotted lines represent those transitions associated with incremental score values of 51 through 74. The right portion of the figure uses a similar coding but uses the solid line and dot representation to indicate low scores rather than high scores. It is seen that transitions associated with high performance tend to conform with the slow response transitions. That is, slow rate of change of error seems to be favored. A surprising factor is that transitions from state 8 to 7, 3 and 9 are used to identify identify high performance policies. The solid dot in the center of state 8, which represents the "transition" of remaining in state 8, is associated with a high performance level as expected. Transitions associated with low performance tend to move the system towards high rates of change, that is, transitions to states 1, 2, 5, 11 and 12.

A companion transition diagram for Case II representing states used for performance discrimination in problem situation 5 is given in Figure 18. In this case we see that transitions from state 8 to its neighbors have been eliminated as a criterion for identifying high performance. In addition, we see a tendency for higher rates to be favored by the high performance system. Likewise, we see that low performances are revealed by transitions from state 8. Thus we conclude that performance discrimination under stress and no stress require a different set of measures. Several transition analyses are included in the final report on the program but were not included here for briefness.

Another way of analyzing operator performance is based on the distribution of states remaining variant under a single transition. As noted previously, if the transition matrix represents a regular process, the state distribution that remains invariant under a single transition is the limiting distribution. The variant distributions for performance levels 1 through 4 are shown in Figures 19 through 22 respectively. Referring to Figure 19, we have the state distributions for each of the five problem situations analyzed. The first situation is prelock-on and shows there is approximately a 50 percent probability of being in state 8 and a probability of .1 or less for the remaining states. This indicates that skilled

operators are able to move through the sequence of states leading to state 8 and remain or quickly return there. This control characteristic contributes to the high probability of being in the desired state. As shown in the figure, the transition characteristic for PS 2 yields two chains. One chain (A) includes states 1 through 10, while the other (B) includes states 12 through 15. These are absorbing chains with an absorbing state (12) in chain B, so that once state 12 is reached the system remains there. This reflects a case of limited data where an operator moved to state 12 while attempting lock-on and remained there during lock-on, which occurred very rapidly. The other chain transition probabilities yield a high probability of being in states 9 and 10 during lock-on, which reflects a relatively low error drift rate. Only one sample value was found in PS 3. That is, in only one instance did any one of the superior operators attempt radar lock-on with 20 seconds to go in the problem period. This probably occurred as the operator was attempting lock-on and the time decreased to 20 seconds to go just as he achieved the lock-on, giving us only one sample in that problem situation. Thus, that particular bar chart has no significance.

The post lock conditions, 4 and 5, indicate a high probability of being in the desired state (8) with a slight degradation in performance under time stress, as indicated by the diagram for situation 5.

Performance level 2 control policies are illustrated by the invarient distribution characteristics shown in Figure 20. In contrast with the performance demonstrated by the PL 1 operators, PL 2 operators show no definite tendency to maintain a high probability of being in state 8 in PS 0. Instead, there is a uniform probability of being in each state with voids or near voids in states 5, 6, 10 and 11. A similar situation exists as the operator attempts lock-on without time stress. Performance does not seem significantly different, perhaps because performance was not very good before the operator attempted radar lock-on and therefore, there is little room for degradation of performance during lock-on attempts. In problem situation 3 (attempted lock-on with time stress), the process is broken into two chains, one consisting of state 4 and the other comprising states 10 through 15. However, limited data in this problem situation prohibits meaningful analysis. Distributions for PS 4 and 5 show that the operators in this classification can do a reasonably good job in maintaining control of the aircraft prior to time stress but tend to deviate from state 8, moving significantly in problem situation 5. Note that deviations include states 3 and 13, which indicate that the operators are trying to correct for small errors with large roll angles and thus, are moving out of state 8 with large error rates. This is a common problem in terminal control tasks where the operators are aware of time limitations.

Figure 21 shows the distribution of states for PL 3 operators and indicates control difficulty in problem situations 0, 2 and 3. In these cases, a substantial amount of data is available for radar lock-on attempts (situations 2 and 3) since the operators had great difficulty in achieving radar lock-on either because the aircraft was not maintained in a suitable attitude for radar lock-on or the operators were not skilled in adjusting antenna azimuth and range gate control in order to obtain radar lock-on. As a result, a substantial amount of time was devoted to attempting lock-on and these operators were often still attempting lock-on in the terminal problem phase. This control policy results in a relatively flat distribution in state 3, as shown in Figure 21. Post lock operations show that the operators can maintain a high probability of being in state 8 when there is not time stress and after radar lock-on is achieved. However, we see a severe degradation in performance with time stress in that the probability of being in state 8 decreases from .8 to approximately .5 as the problem moves to the terminal phase.

A very similar situation exists with the PL 4 operators' performance, as shown in Figure 22. In the situation 4, the probability of being in state 8 is .60,but the control policy yields a wide distribution of other states including 1, 2, 3, 4, 7, 9, 13 and 14. This indicates that when the system leaves state 8, the operators have difficulty returning in an efficient and timely manner and require great excursions throughout the state space in order to attempt to bring the system back to the origin. A significant degradation occurs under time stress for PL 4 operators where the favorable distribution in PS 4 is completely modified and the system now concentrates in states 2, 3, 4, 7, 8, 9, 12, 13, and 14, which are precisely those states required to represent a large limit cycle. Thus we see that the level 4 operators' performance degenerates into a large limit cycle under time stress.

CONCLUSIONS AND RECOMMENDATIONS

The performance measurement tools described in this paper allow analysis of operator control policy in each performance category and problem situation. It should be recognized that the subject operators used in this study were not skilled F-106 pilots and thus, conclusions related to performance characteristics may not reflect skilled pilot control characteristics.

Conclusions and recommendations from this study include:

1. The F-106 flight control problem, as presented by the F-106 simulator, can be flown reasonably well by experienced operators.

However, there is a tendency for undershoots caused by a premature roll to wings level. Some experienced operators use an overshoot to achieve a rapid response, but many operators, including those less experienced, tend toward the undershoot control policy. Operator tendency to overshoot may be caused by the non-linear relationship between the display variables, steering error and roll angle. This display should be modified by indicating the non-linear relationship to the operator or by modifying the display characteristics to remove this factor. Following the modification, the system should be retested.

3. Operators' flight control policies tend to become unstable when radar lock-on is attempted and when time-to-go is less than 20 seconds. Operator flight instability when attempting lock-on is understandable because the operator is concentrating on a task other than flying. It should be noted, however, that antenna azimuth and range gate controls are mounted on the flight control stick and any motion and/or force used for antenna control may affect flight control.

4. Time-to-go of less than 20 seconds is indicated by a shrinking circle on the display. Since the operator tends toward unstable control at this time, the value of that display function is questionable.

5. A system performance measure (performance model) is available as a function of the state transitions and state limiting distributions. Valid performance measures (i.e., those that discriminate performance levels) for each problem situation require different measure functions. Recognition of this difference is important because the operator control criteria is different in each PS and as a result performance measurement must be tailored to each task criterion.

6. Skilled operators demonstrated an asymmetrical control policy producing a preference for approaching the origin from one direction; however, the experiment was not designed to test for this policy characteristic. Additional experiments are required to ascertain if the asymmetrical control policy is typical of skilled pilots. It is important to determine if this policy is commonly used by skilled pilots since that fact could be exploited in air combat.

REFERENCES

1. "Program Documentation for the Manned Interceptor Simulation", January 1971, HES Report #71-2.
2. Connelly, E.M., Schuler, A.R., Bourne, F.J., Knoop, P.A., Application of Adaptive Mathematical Models to a T37 Pilot Performance Measurement Problem, 1971, AFHRL-TR-70-95, Air Force Human Resources Laboratory, Wright-Patterson Air Force Base, Ohio.
3. Connelly, E.M., Schuler, A.R., Knoop, P.A., Study of Adaptive Mathematical Models for Deriving Automated Pilot Performance Measurement Techniques, 1969, AFHRL-69-7, Volumes I & II, Air Force Human Resources Laboratory, Wright-Patterson Air Force Base, Ohio.

74-28,209#14

Influence of Head Position and Field on Visually Induced Motion Effects in Three Axes of Rotation*

L.R. Young and C.M. Oman
Man-Vehicle Laboratory
Massachusetts Institute of Technology
Cambridge, Massachusetts

ABSTRACT

The sensation of self-motion based on rotating visual fields was investigated in the pitch, roll and yaw axes using large visual field motion in a high performance aircraft simulator. The development of roll tilt angle and steady state yaw velocity, for constant speed roll and yaw stimuli respectively, were consistent with earlier reports. Steady pitch offset was also discovered, increasing with pitching field velocity up to 40 deg/second. The induced pitch angle was markedly stronger in the forward than in the backward sense.

Pitch and roll effects were found to depend strongly on head position. The tilt magnitudes were increased for the head 90° to the side, and for the head inverted, but were decreased for the head pitched 25° forward. These results support a hypothesis that the visually induced tilt is limited by conflict with otolith information, which fails to confirm this tilt. They are consistent with the observations by other investigators that uncertainty in orientation based on graviceptor cues increases as the major utricular plane is tilted out of the horizontal.

Peripheral field stimulation was shown to be the adequate stimulus for the self-motion rotation about all three axes. The upper visual field was found to be dominant in the generation of pitch sensation. Any moving visual scene containing sufficient moving visual borders, including a realistic picture of the earth (but not the blank sky), was able to generate the self motion.

*This work was supported under NASA Grant NGR 22-009-701.

The sensation of self-motion created by moving visual scenes was known for many years (Mach, 1973; Fischer and Kornmüller, 1930). It is used in flight simulators (Miller and Goodson, 1960) and for amusement, and has recently been associated with vestibular stimulation. The vestibular tie appears in both psychophysical and neurophysiological investigations. The association also bears on the etiology of motion sickness (Graybiel and Miller, 1968; Johnson, 1968; Money, 1970). The development of self rotation or circular-vection (CV) about the longitudinal (yaw) axis influences the perception of true body acceleration (Young et al, 1973). The influence of moving visual fields has been seen in single unit recordings in the vestibular nerve of goldfish (Klinke and Schmidt, 1970) and the vestibular nucleus of goldfish (Dichgans et al, 1973) and monkeys (Henn et al, 1974). Self motion effects have been studied in yaw, lateral tilt (Dichgans et al, 1972), and in linear motion (Pavard et al, 1974). The goal of the present study was to investigate the parameters of the adequate visual stimulation for pitch as well as for roll and yaw effects, and to test a theory of visual-vestibular interactions by assessing the influence of different head orientations on the visual effect. In particular, the theory holds that the extent of tilt of the apparent vertical based on visual cues, including moving scenes, is limited by conflict with information from the otoliths. As will be shown, head orientations away from the erect position place the utricular graviceptors in relatively less sensitive positions, which are consequently less effective in inhibiting the visual tilt illusion.

All of the principal experiments were carried out in one of the differential maneuvering simulators (DMS) at the NASA Langley Research Center*. Each simulator consists of a jet cockpit mounted on a platform inside a forty foot diameter projection sphere. In the present experiments, one subject sat in the cockpit, and the remaining subjects stood beside the cockpit at the edge of the platform. All were afforded a complete full field view of the sphere wall in the direction they were facing, with the exception of the subject in the cockpit, who had only an upper field view.

Visual scenes were projected on the interior of the sphere wall by a computer controlled projection system. This consisted of two servo-driven transparent plastic hemispheres

---

* Mr. Ralph Stone of NASA coordinated the experimental facility at Langley and arranged for our experiments. We are grateful to the NASA personnel, especially Mr. Billy Ashworth for coordinating the programming and simulator operation, and to Dr. C. Ormsby and Professor R. Curry of M.I.T.

on which the scenes to be projected were painted. A high intensity point light source mounted near the center of each hemisphere projected the scene onto the interior walls of the simulator sphere. The standard hemispheres used in these experiments projected a pattern of 464 randomly spaced and oriented black rectangles, 2-3° in subtended angle, against a white background. The black-white ratio was approximately 25%. For certain experiments, a realistic, colored earth-sky globe, and a black-white latitude-longitude globe were used.

A minimum of four subjects participated in each experiment. The cockpit subject indicated his perception of the vertical and of yaw rate with instruments provided for this purpose. All subjects reported their subjective sensations of rotation (circularvection, CV), tilt and linear motion (linearvection, LV) quantitatively on reporting forms. All subjects were previously trained to report angular velocity and tilt consistently.

Experiment 1: Yaw Circularvection

Method

A series of constant velocity yaw stimuli were presented randomly left and right at speeds of 5, 10, 20, 40, 60 and 120 degrees/second. Subjects reported CV strength in deg/sec, and latency to onset, using a stopwatch. Subjects were aware of the speeds available.

Results

The circularvection generally increased monotonically with field velocity, but was usually not saturated (the pattern did not appear stationary in space during perceived steady state self rotation). The latencies to onset of CV decreased with increasing field speed, as shown in Figure 1.

Discussion

The rapid decrease in time to onset of CV with increasing pattern speed is consistent with, but much more marked than that reported by Brandt et al (1973). The use of the lowest test speed, 5 deg/sec, in the current experiments makes the trend clearer than in the earlier experiments. The fact that the time to onset of CV decreases with field speed, whereas the time to steady state, as reported by Brandt et al, increases with stimulus speed, requires further investigation in light of the interpretation of latencies based on resolution of the visual vestibular conflict.

Experiment 2: Apparent Tilt in Pitch and Roll for various Head Positions

Method

The method for presenting rotating visual fields in the pitch and roll plane was the same as for yaw. Velocities of ± 5, 10, 20, 40, and 60 deg/sec were presented randomly for 40 seconds with a pause of 20 seconds between tests. The subjects were tested with their head in four positions: head erect, head forward, head tilted right ear down, and head inverted. Head erect is the normal upright position. In head forward position, the head was nodded 25° forward so as to put the dominant plane of the utricular otoliths in the earth horizontal plane. This head position was achieved approximately by instructing the subject to place a line between the external auditory meatus and the upper margin of the bony orbit in a horizontal plane. The head tilted right ear down position was intended to place a lateral axis of the head in a vertical plane. Subjects used the railing of the simulator platform for assistance as a convenient vertical reference in setting head position. For the head inverted experiments, subjects placed themselves supine on the platform with their head leaning backward over the edge of the platform. In reporting on subjective pitch and roll, all reports were referenced to the platform axis. For example, a subject viewing this in a head inverted position so that the visual field was moving toward the top of his head, would feel that he was pitching upward in this platform coordinate system. All pitching and rolling effects were much stronger for subjects positioned in the cockpit at the center of the sphere than for those standing on the platform. Therefore, for analysis of effects of different head positions on visually induced tilts, only those two subjects are considered who stood on the platform for all four head positions in pitch and roll.

Results

Figure 2 shows the reported steady state roll angle for each subject at each speed of roll stimulation with the visual field rolling to the right and to the left. Rotation of the visual field to the right as seen by the subject (clockwise) results in a steady state perception of subjective tilt to the left (roll left). For the head erect, the median tilt as well as that for each subject, showed the characteristic increase of apparent tilt with field speed up to a maximum level generally in the region of 40 deg/sec, although some subjects showed maximum response at 60 deg/sec. (By way of comparison, the tilt angle versus field speed used in the partial field experiment reported by Dichgans et al is also

shown in figure 2b and is seen to produce a lesser degree of induced tilt.) The four conditions of different head position are shown in figures 2a, b, c, and d, arranged in the order of predicted increase in subjective tilt. Note that in the head 25° forward position, the apparent tilt was reduced relative to the head erect. In contrast, as the head is moved to the right shoulder, the strength of the tilt illusion increases markedly at all speeds. Tilt angle was still greater in the head inverted position.

Most cases of roll apparent tilt were also accompanied by a sensation of linear translation (linearvection) to the left or right, except when the subject was positioned on the axis of rotation in the cockpit. In each case, the linear motion sensation could be attributed to the subject's head position away from the axis of rotation of the field.

A similar presentation of induced pitch angle for a visual pitching stimulus is shown in figures 3a-d. Figure 3b, for the head erect position, demonstrates that a pitch illusion similar to that found for the roll case is indeed present. The illusion of pitching increases with the speed of field rotation up to a plateau in the region of 40 deg/sec for the field moving down (pitch up). The most obvious difference between the pitch and roll situations is the presence of a marked asymmetry in pitch. All subjects experienced a much stronger sensation of pitching down than of pitching up for symmetric visual stimuli. Another important difference between the pitch and roll sensation is the presence of a substantial amount of linearvection in the vertical direction for pure pitch stimuli. The visual field pitching down resulted in a sensation of constant velocity vertical translation upward as well as pitch up, and conversely for the visual field moving upward.

Returning to figure 3a (the head forward position) one sees a marked reduction in the pitch sensation both for field pitching up and for field pitching down. The pitch sensation was almost entirely replaced by a sensation of pure linearvection in the upward or downward direction. As the head is tilted to right ear down position (figure 3c) the pitch sensation was increased relative to the head erect orientation. Finally, with the head in the inverted position, as seen in figure 3d, the magnitude of the pitch sensation was very markedly increased, resulting in subjective pitch of greater than 90° on occasion. It is also to be noted that in the head inverted position, the sensation of pitching up was much stronger than the sensation of pitching down. However recalling that pitch is indicated in "platform coordinates", one sees that the direction of the asymmetry in pitch remains the same with respect to the body (figure 3b); i.e. the induced sensation of tumbling forward was stronger than that of tumbling backward. Notice that the asymmetry does not entirely disappear for the case of the head on the right shoulder, where the visual stimulus for pitching up and down is symmetric.

To compare the effects of head position on pitch and roll tilt quantitatively, linear regression lines were calculated for those two subjects who completed all test conditions on the platform. These regression lines, representing the strength of the visually induced tilt, passed through the origin and formed a least mean squares fit to the induced tilt angles at 10, 20, and 40 deg/sec stimulation. Separate lines were calculated for each direction of stimulation. Figure 4 shows the slope of the regression line for roll tilt in the 0 to 40 deg/sec stimulus range for the four head positions considered. Pitching the head forward by 25° inhibited the strength of the induced tilt illusion by about 35%, whereas tilting the head to the right shoulder increased the strength of the illusion by approximately 35%.

The regression line slopes for the same two subjects for the pitch experiments are given in figure 5. For the head erect position the illusion of pitching down had an index 40% greater than that for pitching up. When the head was tilted 25° forward the asymmetry remained, but the strength of the apparent pitch was greatly reduced. Tilting the head 90° to the right increased the sensitivity of pitch illusion somewhat compared to the head erect position, while retaining the earlier asymmetry, in body axes, but not in head axes. For the head in the inverted position, the strength of the pitching response was enormously increased and the direction of the asymmetry in simulator axes is reversed.

Discussion

The experimental evidence summarized in figures 4 and 5 supports the hypothesis that the strength of the pitching and rolling illusions depends on head orientation with respect to the vertical.

For cases of continuous circularvection about a vertical axis, the otoliths play no apparent part in confirming or denying the visually induced sensation of continuous motion, since no change in orientation with respect to the vertical is implied. When the visually induced sensation is such as to produce a change in orientation with respect to the vertical, however, the subject would normally expect to receive otolith signals confirming this change in position. The fact that the head actually remains fixed in each of these experiments, and that such confirming otolith information is not forthcoming, may be thought of as creating a sensory conflict which limits the extent of the visually induced sensation (Guedry, 1968). Other indirect evidence (e.g. Schöne and Udo de Haes, 1968; Udo de Haes and Schöne, 1970; Benson, 1974; Guedry, 1968; Graybiel and Clark, 1962) for example supports the notion that otolith effectiveness in surpressing orientation information from other sensors is

maximum in the head erect position and minimized when the head is tilted to the side (Young, 1971). Although the fact is well established that graviceptor information, used to indicate perceived orientation, displays increasing systematic and random errors with head tilt, the explanation is not certain. It is possible that a central pattern recognition system processing the wide range of otolith and other graviceptor afferents is tuned to operate in the most common position for postural control of the standing, head erect man. Alternatively, the explanation could be based in large part on the mechanical processes in the labyrinth. This working hypothesis assumes that the utricular otolith is primarily responsible for the sensation of head tilt, and that the shear component of gravity is the adequate stimulus.* (Accelerations normal to the utricular plane lead to frequent misjudgements of direction (Malcolm and Melvill Jones, 1974; Melvill Jones and Young, 1974)). The head orientation for "best sensitivity" of the utricular otolith, and thus maximal inhibition of visually induced pitch and roll, should be

---

*The components of gravity along the axes directed forward along the "utricular plane" (x), laterally to the left in this plane (y), and normal to the plane, pointing upward, (z) are:

$$f_x = \cos\gamma \sin\theta - \sin\gamma \cos\phi \cos\theta$$
$$f_y = -\sin\phi \cos\theta$$
$$f_z = -\sin\gamma \sin\theta - \cos\gamma \cos\phi \cos\theta$$

where γ = angle of elevation of the utricular plane with respect to the head lateral plane (approx. 25°)
θ = pitch angle of the head about the horizontal axis (positive for pitch down)
ϕ = lateral tilt of the head about the head forward axis (positive for roll right ear down).

θ and ϕ are Euler angles. A given head orientation is defined by a rotation in θ followed by one in ϕ.

The sensitivity to pitch is given by

$$\cos\gamma \cos\theta + \sin\gamma \cos\phi \sin\theta$$

and for the special case of $\phi = 0$, it simplifies to

$$\cos(\theta - \gamma)$$

which is maximized for the head pitched forward by γ. Pitch sensitivity is 90% of maximum for the head erect.
For roll about an earth horizontal axis (rather than the head forward axis) the roll sensitivity is

$$\cos(\theta - \gamma) \cos\phi$$

which is also maximized for the head pitched γ degrees forward, and decreases to a minimum for the head rolled 90 degrees to the right or left.

with the head pitched 25° forward from the normal head erect position. This position places the dominant plane of the utricular maculae in the horizontal plane and maximizes the change in gravitational component in this plane resulting from head movements. Tilting the head to the right 90° should place the utricular plane vertical, and make the utricular otoliths minimally sensitive to changes in body position. As is well known from psychophysical studies, the utility of statolith information with the head inverted is also poor. (The shear sensitivity model alone does not account for this fact. Additional assumptions concerning the ambiguity of sacculus information may be of help in interpretation (Ormsby, 1974)). The data for both pitch and roll supported the hypothesis that the otolith information is used to limit the magnitude of tilt based upon visual input, and that the effectiveness of this otolith information decreases in a predictable fashion as the head is moved away from its maximal sensitivity orientation of 25° pitched forward.

The observation that the direction of the pitch asymmetry remains fixed in body axis eliminates the possibility that it is associated with the direction of "down". Retinal or utricular directional asymmetries might be considered as the source, however. The results of experiment 4 support a visual origin of the pitch asymmetry. All speculation is complicated by the observation that this asymmetry seems to remain even with the head tilted 90° to the right, so that the visual field motion is in the head lateral plane. One possibility is that the coordinate system of importance is that of body axes (rather than head axes) since a principal role of visual and vestibular motion sensing is postural stabilization of the body, even with the head bent.

It might be argued that the usually induced tilt effects for the head tilted experiments could have been confounded by the Aubert or Müller effects of errors in tilt estimation with varying head positions. The non-visual orientation estimations were, in fact, measured for all subjects later, and were all A-effects (underestimation) of 15 to 30° for the head tilted right and left ear down. For the experiments under discussion, however, all indications of apparent tilt were made relative to an initial subjective orientation judged with tilted head and no moving visual scene. The present data therefore, concerns the visually induced tilt effects alone. Dichgans et al (1974) explore the relationship between subjective tilt based on head tilt and rotating visual field.

Experiment 3: Effects of Visual Field Placement on Induced Tilt

Method

A variety of masks were used in the pitch and roll experiments to determine the effects of different portions of the visual field upon the tilt effect. Brandt et al (1973) showed that the peripheral visual field is dominant in producing yaw circularvection, and Held et al (1974) demonstrated the increasing importance of peripheral field stimulation on the induced tilt in roll, showing sensitivity to stimuli increasing with angular distance from the fovea. Whereas those investigations explored principally the radial characteristics of the visual field, the current experiments investigated the differential effects of the upper and lower visual field in an attempt to discover a relationship to the asymmetry in the pitching response previously discussed. The experiment consisted of four test fields. All tests were performed with the head erect and the pitch and roll stimulation presented at $\pm$ 5, 10, 20, 40 and 60°/second. The control was the full field stimulus of experiments 1 and 2. The peripheral stimulus was obtained by use of a hand held cardboard mask blocking the central 60 degrees of the field. The upper visual field and the lower visual field stimuli were achieved by having each subject block his lower or upper field with a cardboard mask held at eye level.

Results

No obvious difference in the roll tilt effect is seen among the various conditions. For the two subjects completing all tests standing on the platform, the 0 - 40°/sec regression line slopes calculated as described earlier and shown in figure 6 showed no evident changes in sensitivity among these conditions.

The effect of visual field placement on the pitch sensation, however, was strikingly different. A dimunition of the size of the visual field decreased the strength of the pitch sensation. In figure 7a, for the case where the subjects could see the lower visual field only, all subjects standing on the platform had a marked reduction of pitch sensation in both directions relative to the full field. This field consistently produced strong vertical linearvection. When the upper field only was exposed, a stronger sensation of pitching down than of pitching up was evident, although neither was of the strength seen for the full field (figure 7b). With the peripheral field only exposed (figure 7c) the

pitch sensation was slightly reduced compared to that for the full field. The regression line slopes for the two subjects completing all visual field tests on the platform are given in figure 8. Notice that the marked pitch down dominance is present for the full field and even more so for the upper field only, but disappeared for the lower field only, where pitching up and down are both reduced.

Discussion

The fact that blanking the central 60 degrees of the visual field does not greatly reduce the pitch or roll effect is consistent with earlier results demonstrating the importance of peripheral stimulation for this effect. The differing effect of the upper and lower visual fields on subjective pitch is not as readily explainable. A possible explanation lies in the differences in the natural whole field motion normally seen, and its relation to different body movements. The lower visual field, below the horizon for the head erect, contains many near objects, some as close as the ground below one's feet. These objects all move downward in the visual field during forward locomotion, at an angular velocity inversely proportional to distance. Whole field motion downward in the lower field is therefore often correctly associated with linearvection. The upper visual field, more often contains objects at great distance; clouds or tall buildings, for example. Distant objects would not all move in the visual field during one's translatory motion, but they would during angular changes such as pitch and roll. It is therefore plausible that motion of the upper field only would lead to primarily a pitch sensation, whereas motion of the lower visual field primarily induces linearvection only. Furthermore, when falling forward from an erect position, the horizon line moves into the upper visual field, whereas it moves into the lower visual field for a backward fall. Following this line of reasoning, then, it is conceivable that the upper visual field is dominant in the determination of forward pitch, and conversely for the lower visual field.

Experiment 4: Dominance of Horizontal over Vertical Circularvection

Method

Continuous circularvection in the horizontal plane implies no steady state conflict with information stemming from the vestibular system, whereas any visually induced rotation in the vertical plane implies a conflict with gravireceptor signals. It would be expected, therefore, on the basis of limitation of the visually induced motion effects by vestibular conflict, that rotation in the horizontal plane would dominate over rotation in the vertical plane. The original experiments were performed on seven subjects viewing the rotating stripe display in the Tönnies' optokinetic nystagmus device in Zurich. (The details of the stimulus are described in Young and Henn, 1974.) The initial visual field movement was about a vertical axis, rotating 30°/sec. After CV was reported, the axis of rotation was tilted in 5° increments in roll, so that it had successively larger horizontal components. Each step lasted at least 30 seconds. Observations were made with roll in the direction of the yaw circularvection and in the opposite direction. Four other subjects were exposed to a similar stimulus presentation in the DMS at Langley, using 20°/sec field velocity. In each case subjects were required to report on the occurrence of apparent rotary motion, linearvection, and the first occurrence of any self-motion in the vertical plane, be it tilt or linearvection.

Results

For axes tilted by 5-10° from the vertical, the sensation remained one of pure horizontal circularvection, and the linear motion of the field was then perceived as a vertical component of the visual field, independent of the yaw circularvection. At fields rotating about an axis tilted by more than 20° from the vertical, all subjects perceived a change in their own orientation in the vertical plane. This was variously interpreted as a combination of pitch and/or vertical translation combined with the yaw circularvection to give the sensation of a climbing or diving turn. The median tilt angle required to generate the pitching sensation was 20° with a range from 10° to 60° for the subject. No difference was seen between the results in the smaller structured 30°/sec field, tested in Zurich, and the larger, 20°/sec, random pattern tested at Langley.

Discussion

The dominance of horizontal circularvection for fields which rotate about an axis up to 10° to 20° from the vertical is further evidence for the interpretation that moving visual

fields are interpreted in terms of subjective orientation in a manner which minimizes the dynamic conflict with vestibular information. Fields rotating about a vertical axis induce a steady horizontal circularvection which is consistent with a steady state null signal from the semicircular canals (indicating constant angular velocity). Sensation of rotation about an off-vertical axis, on the other hand, would imply the expected appearance of (sinusoidal) time varying otolith signals confirming this change in orientation. Such otolith information is not forthcoming in the head fixed experiments, and therefore the perceived axis of rotation remains vertical for small off-vertical deviations of the actual field rotation axis.

Conclusions

The current experiments on visually induced rotation sensation in pitch, roll and yaw, when considered with an earlier study on the interaction of vestibular and visual stimuli in yaw, support an interpretation of visual-vestibular interaction in human spatial orientation. The extent to which conflicting sensory information can be treated as a linear combination of the effects of the individual stimuli is limited. Visually induced rotation effects, when not confirmed by rotational information from the semicircular canals, are initially rejected in favor of vestibular information, and only dominate in the steady state, when they are consistent with a null signal from the semicircular canals indicating constant velocity rotation. Some neurophysiological evidence for this interpretation has been found (Klinke and Schmidt, 1970; Dichgans et al, 1973; Henn et al, 1974) for visually induced rotation about a horizontal axis. In pitch or roll, any steady-state angular velocity sensation would imply a continuing conflict with the otolith information. The resulting sensation of limited steady tilt would resolve the conflict by biasing the steady otolith information, which can be considered to adapt over the several seconds required for the illusion to develop. This interpretation is supported by the observation that the visually induced pitch and roll magnitudes vary with head position in a manner predicted by the theoretical sensitivity of the utricular otoliths to tilt from those head positions.

An asymmetry in the visually induced pitch effect, favoring the pitch forward sensation was discovered, and related to the dominance of the upper visual field in producing the subjective tilt.

References

BENSON, A. 1974 In Handbook of Sensory Physiology, Vol.VI: Vestibular System (ed. H.H. Kornhuber) Springer, Berlin (in press).

BERTHOZ, A., PAVARD, B., YOUNG, L.R. 1974 Rolé de la vision péripherique et interactions visuo-vestibularies dans la perception exocentrique du mouvement lineare chez l'homme. Compte Rendu, Acad. Des Sciences (Paris) (in press).

BRANDT, TH., DICHGANS, J., KOENIG, E. 1973 Differential effects of central versus peripheral vision on egocentric and exocentric motion perception. Exp. Brain Res. 10:476-491

DICHGANS, J., DIENER, H.C., BRANDT, TH. 1974 Optokinetic-graviceptive interaction in different head positions. (in prep.)

DICHGANS, J., HELD, R., YOUNG, L.R., BRANDT, TH. 1972 Moving visual scenes influence the apparent direction of gravity. Science 178:1217-1219

DICHGANS, J., SCHMIDT, C.L., GRAF, W. 1973 Visual input improves the speedometer function of the vestibular nuclei in goldfish. Exp Brain Res 18:319-322.

FISCHER, M.H., KORNMULLER, A.E. 1930 Optokinetisch ausgelöste Bewegungwahrnehmungen und optokinetischer Nystagmus J Psychol Neurol (lpz.) 41:273.

GRAYBIEL, A., CLARK, B. 1962 Perception of the horizontal or vertical with head upright, on the side, and inverted under static conditions and during exposure to centripetal force. Aerospace Med 33:147-155.

GRAYBIEL, A., MILLER, E. 1968 The otolith organs as a primary etiological factor in motion sickness: with a note on "off-vertical" rotation. Fourth Symposium on the role of the Vestibular Organs in Space Exploration. NASA SP-187, 53-66.

GUEDRY, F., JR. 1968 Conflicting sensory orientation cues as a factor in motion sickness. Fourth Symposium on the Role of the Vestibular Organs in Space Exploration. NASA SP-187 45-51.

HELD, R., DICHGANS, J., BAUER, J. 1974 Characteristics of moving visual scenes influencing spatial orientation. Vision Res. (in press).

HENN, V., YOUNG, L.R., FINLEY, C. 1974 Vestibular nucleus units in alert monkeys are also influenced by moving visual fields. Brain Res (in press) (Also: Pflug. Archiv. Suppl. to Vol 343, R86,1973).

JOHNSON, W. 1968 Secondary etiological factors in the causation of motion sickness. Fourth Symposium on the Role of the Vestibular Organs in Space Exploration, NASA SP-187, 83-87.

KLINKE, R.
SCHMIDT, C.L. 1970 Efferent influence on the vestibular organ during active movement of the body. Fflugers Archiv ges. Phsyiol. 318:325-332.

MACH, E. 1875 Grundlinien der Leher von den Bewegungsempfindungen. Engelmann, Leipzig. Also F.S. Bonset, Amsterdam, 1967.

MALCOLM, R.,
MELVILL JONES, G. 1974 Erroneous perception of vertical motion by humans seated in the upright position. Acta Otolaryng. (in press).

MELVILL JONES, G.,
YOUNG, L.R. 1974 Thresholds and latencies to perception of vertical acceleration in man. (in prep)

MONEY, K., 1970 Motion Sickness, Physiol. Rev. 50:1

MILLER, J.W.,
GOODSON, J.E., 1960 Motion sickness in a helicopter simulator. Aerospace Med 31:204-212

ORMSBY, C.C. 1974 Model of human dynamic orientation, PH.D. Thesis, Department of Aeronautics and Astronautics, Massachusetts Institute of Technology, Cambridge, Massachusetts.

SCHONE, H.,
UDO DE HAES, H.A. 1968 Perception of gravity-vertical as a function of head and trunk position. Z verg. Physiol 60:440-444.

UDO DE HAES, H.A.,
SCHONE, H. 1970 The effectiveness of the statolith organs in human spatial orientation. Acta Otolaryng. 69:25-31.

YOUNG, L.R. 1971 Developments in modeling visual-vestibular interactions, AMRL-TR-71-14, Wright-Patterson Air Force Base, Ohio.

YOUNG, L.R.,
DICHGANS, J.,
MURPHY, R.
BRANDT, TH. 1973 Interaction of Optokinetic and Vestibular Stimuli in Motion Perception. Acta Otolaryng. (Stockh) 76:24-31.

YOUNG, L.R.,
HENN, V.S. 1974 Selective habituation of vestibular nystagmus by visual stimulation. Acta Otolaryng (Stockh) in press.

FIGURE LEGENDS

Figure 1 Latency to onset of yaw circularvection. Subjects, pooling data from both directions when available. O - individual reports. - means.

Figure 2 Roll tilt angle induced by full field rolling visual stimulus, as a function of pattern speed and head position. Solid lines connect median values for data points from individual subjects. Dichgans et al (1973) data, shown for comparison, used a 130° field, pooling tilt in both directions.

Figure 3 Pitch tilt angle induced by full field pitching visual stimulus. Individual data and median lines.

Figure 4 Sensitivity to visually induced roll as a function of head position - average of two subjects. Regression line slope units deg/deg/sec (see text).

Figure 5 Sensitivity to visually induced pitch as a function of head position.

Figure 6 Sensitivity to visually induced roll as a function of field size and placement.

Figure 7 Sensitivity to visually induced pitch as a function of field size and placement.

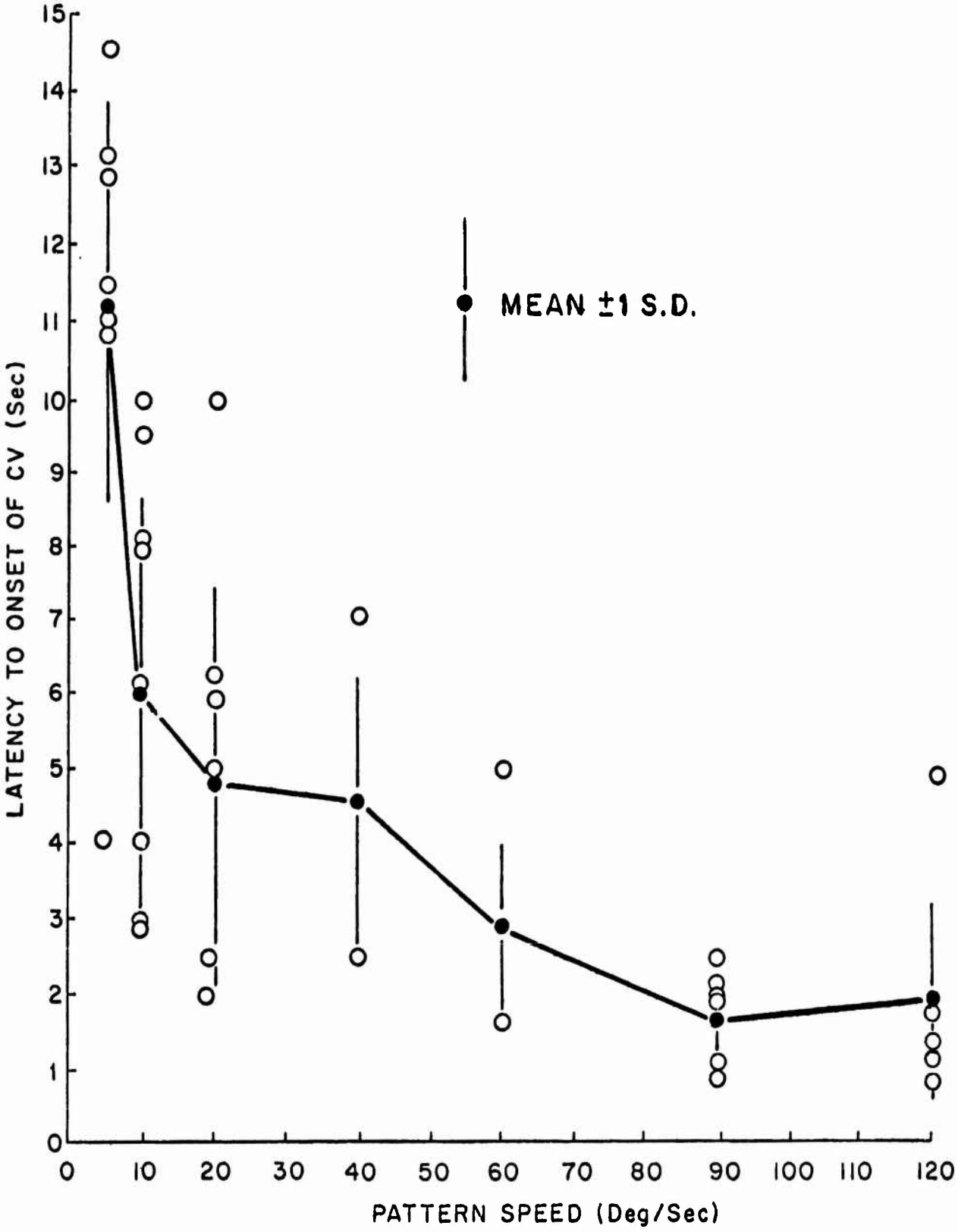
MEAN ±1 S.D.
LATENCY TO ONSET OF CV (Sec)
PATTERN SPEED (Deg/Sec)
0
1
2
3
4
5
6
7
8
9
10
11
12
13
14
15
0
10
20
30
40
50
60
70
80
90
100
110
120

Figure 1

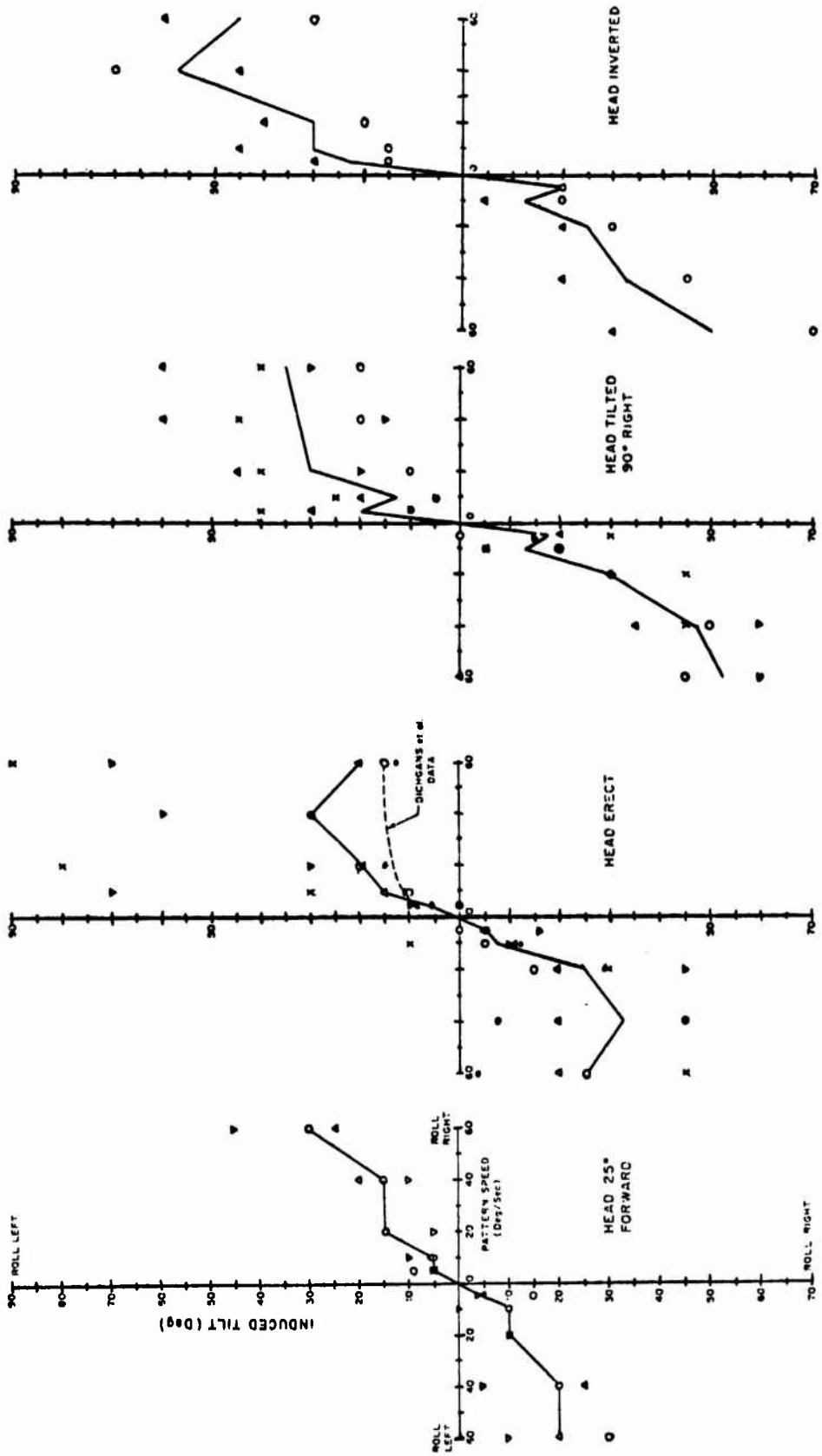
HEAD INVERTED
HEAD TILTED 90° RIGHT
HEAD ERECT
HEAD 25° FORWARD
SICHGANS et al DATA
INDUCED TILT (Deg)
PATTERN SPEED (Deg/Sec)
ROLL LEFT
ROLL RIGHT

Figure 2

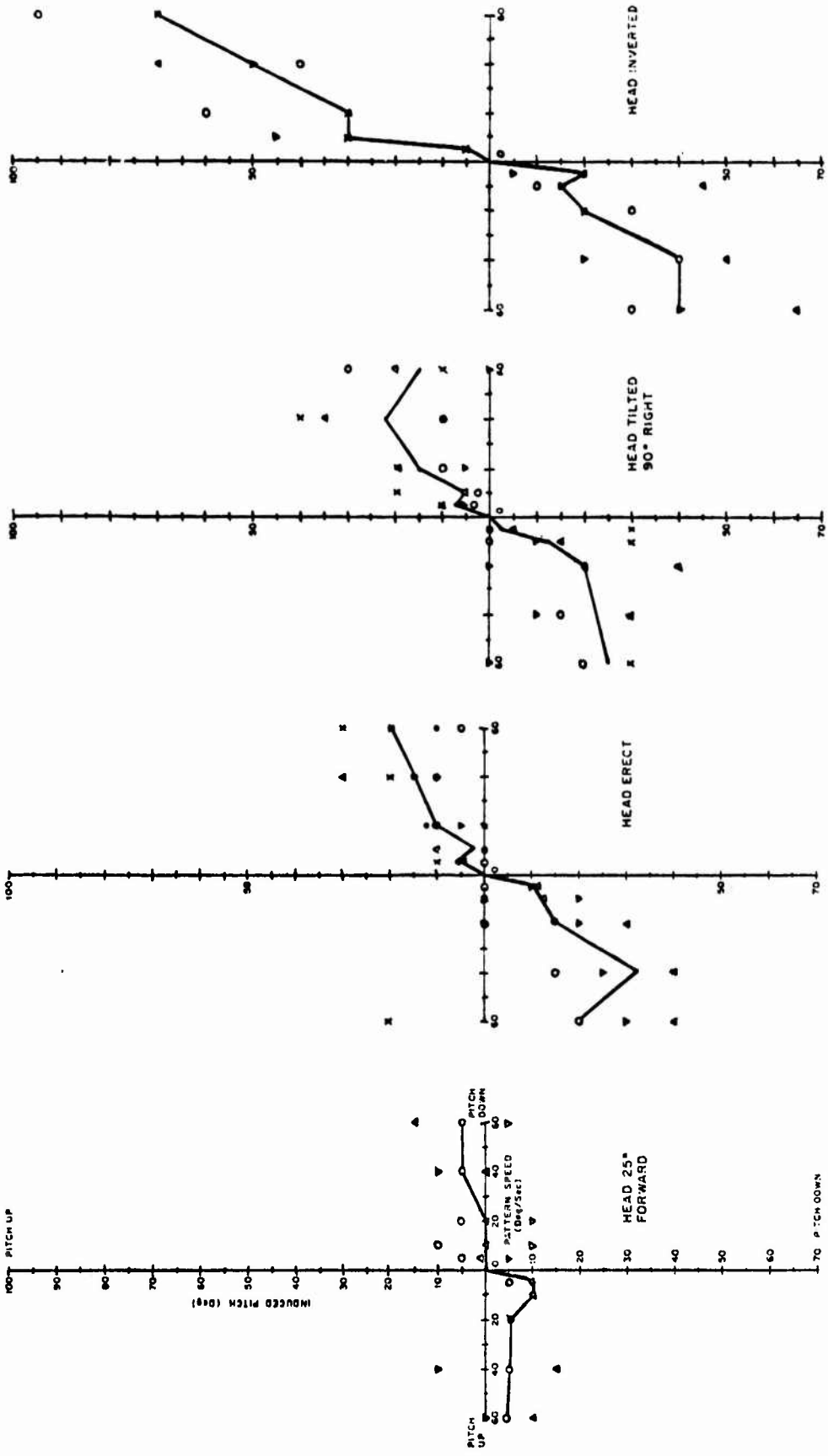
HEAD INVERTED
HEAD TILTED 90° RIGHT
HEAD ERECT
HEAD 25° FORWARD
INDUCED PITCH (DEG)
PITCH UP
PITCH DOWN
PATTERN SPEED (DEG/SEC)

Figure 3

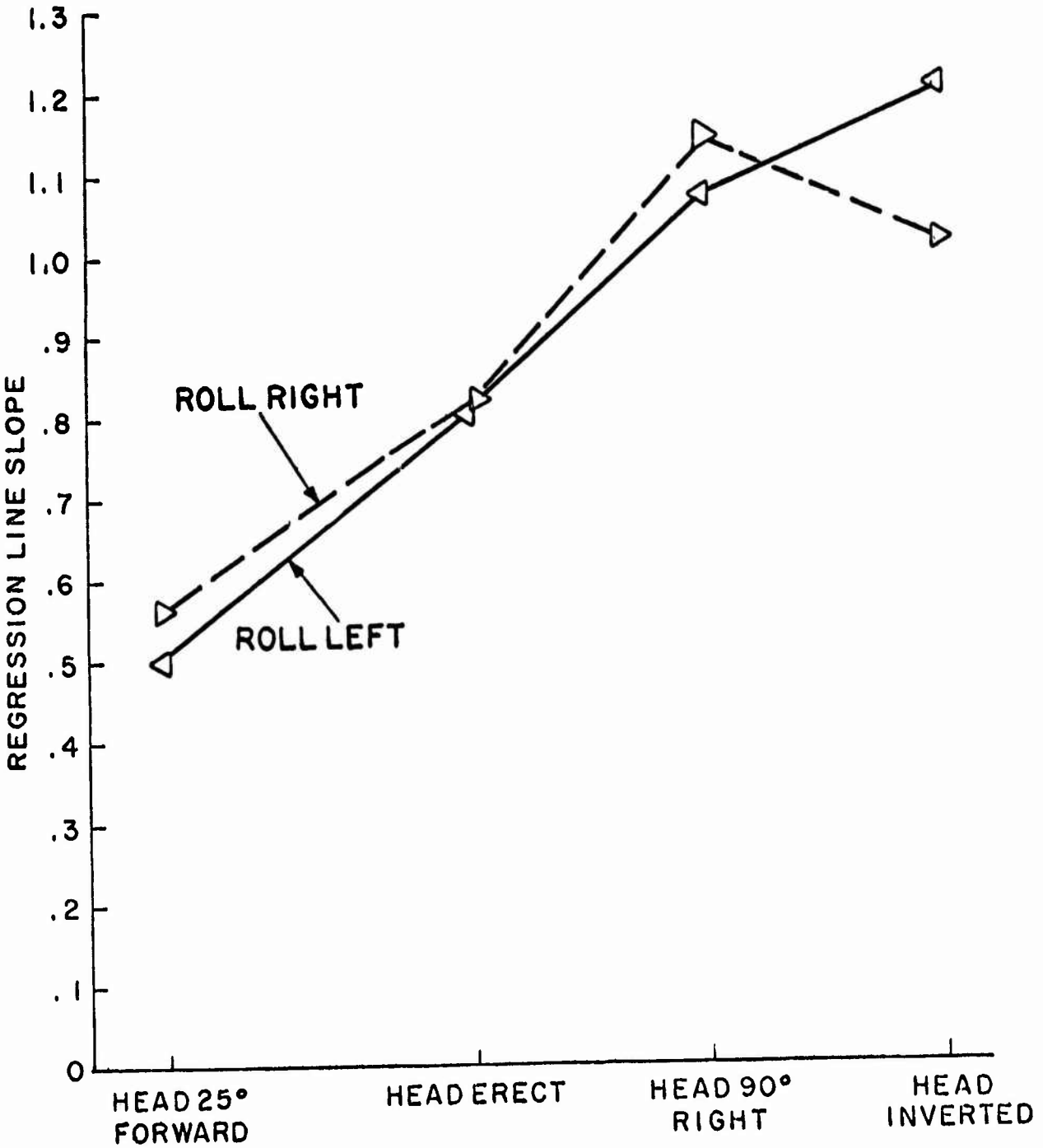
REGRESSION LINE SLOPE
1.3
1.2
1.1
1.0
.9
.8
.7
.6
.5
.4
.3
.2
.1
0
ROLL RIGHT
ROLL LEFT
HEAD 25° FORWARD
HEAD ERECT
HEAD 90° RIGHT
HEAD INVERTED

Figure 4

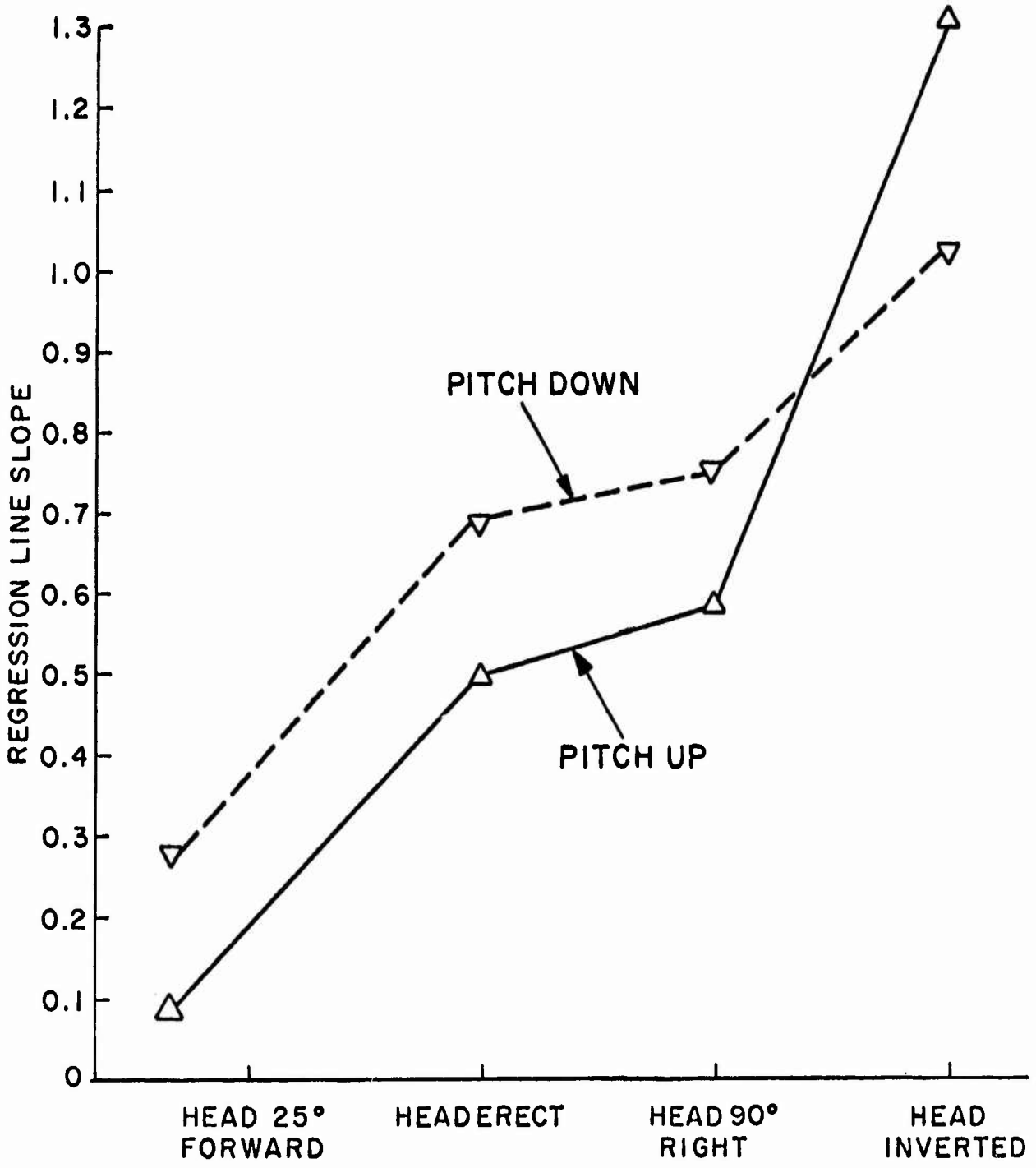
REGRESSION LINE SLOPE
1.3
1.2
1.1
1.0
0.9
0.8
0.7
0.6
0.5
0.4
0.3
0.2
0.1
0
PITCH DOWN
PITCH UP
HEAD 25° FORWARD
HEAD ERECT
HEAD 90° RIGHT
HEAD INVERTED

Figure 5

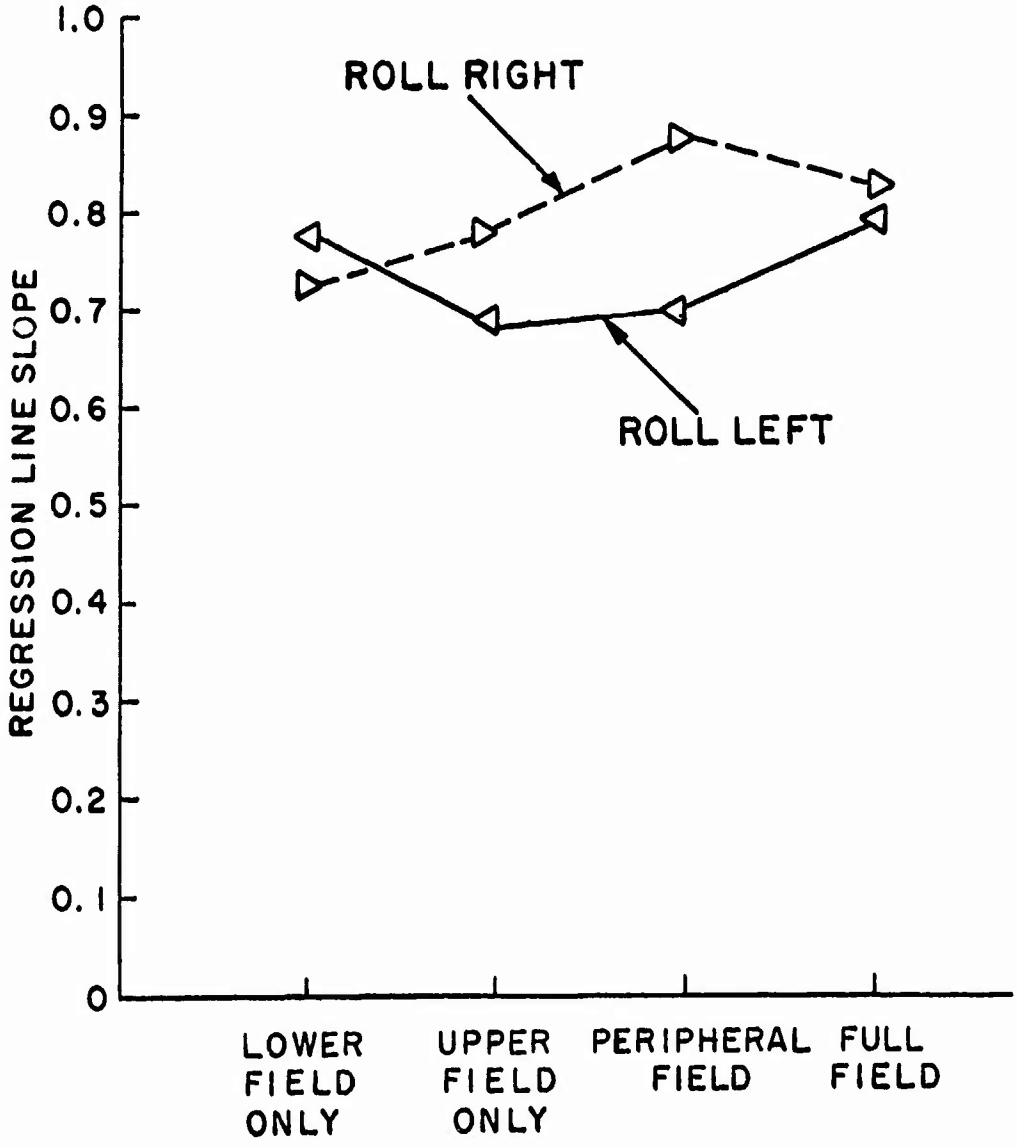
1.0
0.9
0.8
0.7
0.6
0.5
0.4
0.3
0.2
0.1
0
REGRESSION LINE SLOPE
ROLL RIGHT
ROLL LEFT
LOWER FIELD ONLY
UPPER FIELD ONLY
PERIPHERAL FIELD
FULL FIELD

Figure 6

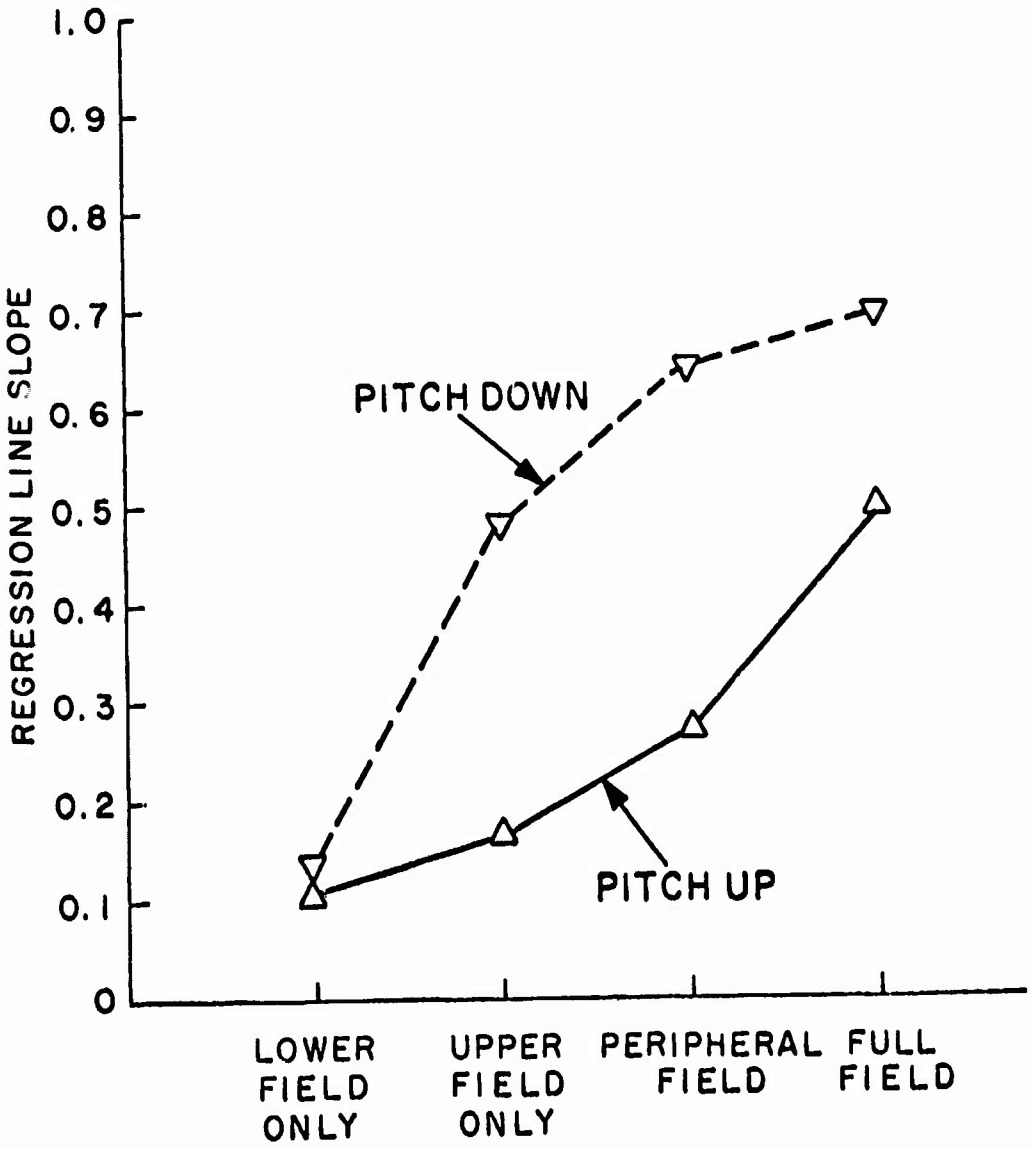
1.0
0.9
0.8
0.7
0.6
0.5
0.4
0.3
0.2
0.1
0
REGRESSION LINE SLOPE
PITCH DOWN
PITCH UP
LOWER FIELD ONLY
UPPER FIELD ONLY
PERIPHERAL FIELD
FULL FIELD

Figure 7

ALCOHOL EFFECTS ON DRIVING BEHAVIOR AND PERFORMANCE IN A CAR SIMULATOR*

R. Wade Allen, Henry R. Jex, Duane T. McRuer,
and Richard J. DiMarco†
Systems Technology, Inc., Hawthorne, California

ABSTRACT

A fixed-base simulation has been developed to test the effect of alcohol on driving performance. The simulation includes both lateral steering control and a discrete visual detection, recognition, and response task set up to provide the workload and division of attention typical of real world driving. Measurements of both driver control behavior and driver/vehicle performance were obtained for the steering task, and detection and recognition indexes and reaction time were measured on the discrete task. Preliminary results on scanning behavior as measured with an eye-point-of-regard monitor are also presented.

Data are given for eighteen drivers, ranging in age from 21-65, at BAC ≐ 0, 0.06, and 0.11. Alcohol causes larger lane and heading deviations, and increases detection and reaction times on the discrete task. Control-behavior measures show that the driver's control gain decreases but stability margins are maintained under alcohol, while driver remnant increases. Such effects could be due to indifference thresholds and/or intermittent attention in the control task.

Both continuous steering control and discrete peripheral "sign" response tasks were performed, singly and combined, to investigate the effects of divided attention. Performance on the steering control task was decreased when both tasks were done concurrently, but the sensitivity to alcohol effects was similar.

The driving simulation has proven an efficient tool for alcohol research. It has gained acceptance from subjects as a valid approximation of driving, and the various related measurements have proven to be reliable and sensitive to levels of intoxication.

---

*This work was sponsored under Contract DOT-HS-227-2-388 by NHTSA's Office of Driver Performance, with Dr. Leland Summers as Contract Technical Manager

†Senior Research Engineer, Principal Research Engineer, Technical Director, and Staff Engineer, Analytical, respectively.

INTRODUCTION

The epidemiological connection of alcohol with automobile accidents is fairly well established (e.g., Refs. 1 and 2). It has been found that the probability of involvement in serious crashes increases dramatically for blood alcohol concentration beyond 0.08 g/100 ml* (Ref. 3). A great deal of research has been devoted to identifying driving-relevant behavior impaired by alcohol. Past studies have employed a range of approaches including actual field test situations (e.g., Refs. 2 and 4), laboratory driving simulations (e.g., Refs. 5 and 6), and simpler laboratory tasks which measure psychomotor and/or cognitive skills (e.g., Refs. 7 and 8).

Although alcohol studies are hampered in general by procedural problems with dosage administration and measurement, and between-subject variability due to motivation and personality factors, some relatively generalizable results have surfaced from past research. First, the performance on divided attention tasks seems particularly sensitive to alcohol (Ref. 8-10). Further, in tasks requiring peripheral visual detection, alcohol seems to cause a "tunneling" effect such that peripheral information is either missed, ignored, or results in increased reaction times over sober performance (Refs. 9 and 11). Finally, although it has proven difficult to correlate the effects of alcohol on simple laboratory psychomotor tests with simulated and actual driving performance (Refs. 6 and 12), alcohol does consistently degrade driving performance both in terms of lateral (lane) position control (Refs. 6 and 13) and response to discrete events (Refs. 5, 13-14).

A great deal of effort has been devoted to determining the behavioral elements associated with discrete tasks, such as detection, information processing, etc., that are degraded by alcohol (Refs. 5, 10-11). This level of effort has not been carried through to the continuous control behavior portion of driving, however, which produces lane deviations that ultimately influence the probability of accident involvement.

---

*Blood alcohol levels are given here in conventional units of grams ethanol per 100 milliliters of blood, as measured by breath alcohol concentration, BAC (Ref. 23).

Research on driver control behavior has often been stymied in the past by the lack of appropriate behavioral models and efficient measurement techniques; however, recent advances in manual control technology have changed this situation. Guidance and control laws for driver/car steering have been developed and analyzed (Ref. 15), and validated with simulator and field test measurements (Refs. 16 and 17). Finally, efficient procedures have been developed which allow the driver's complex multiloop control behavior to be interpreted with simple describing function measurements (Ref. 18).

The purpose of this paper is to describe a simple, yet realistic and relevant, set of laboratory driving tasks and to present results from their use in a study of the basic effects of alcohol on driving. The driving tasks included both continuous steering control and discrete visual-motor response tasks requiring detection, scanning, and recognition. The two types of task were performed both separately and in combination in order to determine the effect of task interference on alcohol impairment. The other objective of this research was to determine if there is differential impairment between moderate and heavy drinkers, and these results are presented in a companion paper (Ref. 19).

SIMULATION AND MEASUREMENTS

Past research has shown divided attention tasks to be sensitive to alcohol impairment, and in fact typical driving situations involve a combination of both continuous control behavior and visual monitoring of discrete events, performed in parallel (Ref. 20). Accordingly, our simulation was set up to present the driver with both types of tasks as shown in Fig. 1, for which the scenario was driving on a rural road at night in stormy weather. The driver's control task was to drive down the center of a lane presented on a CRT display, while regulating against disturbances similar to those caused by wind gusts and/or road roughness. The discrete task consisted of peripheral "signs" which randomly flashed messages requiring response with the horn or brake. The details of the tasks and measures are as follows.

Steering Control Task

The control task scenario was similar to driving down a single lane road at night. The lane edges were drawn in perspective on the CRT with decreasing intensity in the distance. Heading and lane deviations of the car were represented properly by motions of the road relative to a fixed mask of a car hood, left fender, and windshield outline as shown in Fig. 1. An 8" × 10" CRT was used and the entire scene (mask and road) scaled down by 0.6 times in order to preserve the natural framing provided in a real car. A modified 1968 Mustang cab was used with the CRT mounted on the hood 24 in. in front of the driver. The steering wheel feel was set up to approximate the force feel characteristics of a power steering unit.

Two-degree-of-freedom equations were used for the car dynamics (Refs. 16 and 18) such that steering wheel inputs generate heading (ψ) and lateral (y) deviations which then drive the display. The dynamics used for this study were representative of an American sedan traveling at 30 mph and are summarized in Table 1. A disturbance signal was combined with the driver's steering signal as shown in Fig. 1, to simulate an equivalent wind gust input against which the driver had to regulate in order to maintain a center lane position. The disturbance was composed of a sum of five nonharmonically related sinusoids which appeared subjectively to be random.

The driver's steering behavior is modeled as quasi-linear response operations on ψ and y, plus an additive noise (remnant) as shown in Fig. 1. It is the parameters characterizing these two processes that we wish to measure in order to define the effect of alcohol on driver control behavior. The driver's dynamic response, Y_p^*, characterizes the portion of total steering control linearly correlated with heading and lateral deviations of the car. Since the perspective display is integrated and perceived as an entity, it is difficult to determine the manner in which ψ and y information is combined and processed. This problem is circumvented, however, with a recent development in multiloop car/driver measurement (Ref. 18). The technique results in an equivalent single-loop measurement of the driver's describing function, Y_p^* which combines the individual operation on functions of ψ and y. A typical form of Y_p^* is shown in Fig. 2. The magnitude of the low-frequency amplitude reflects the driver's sensitivity (gain) to path error

Figure 1

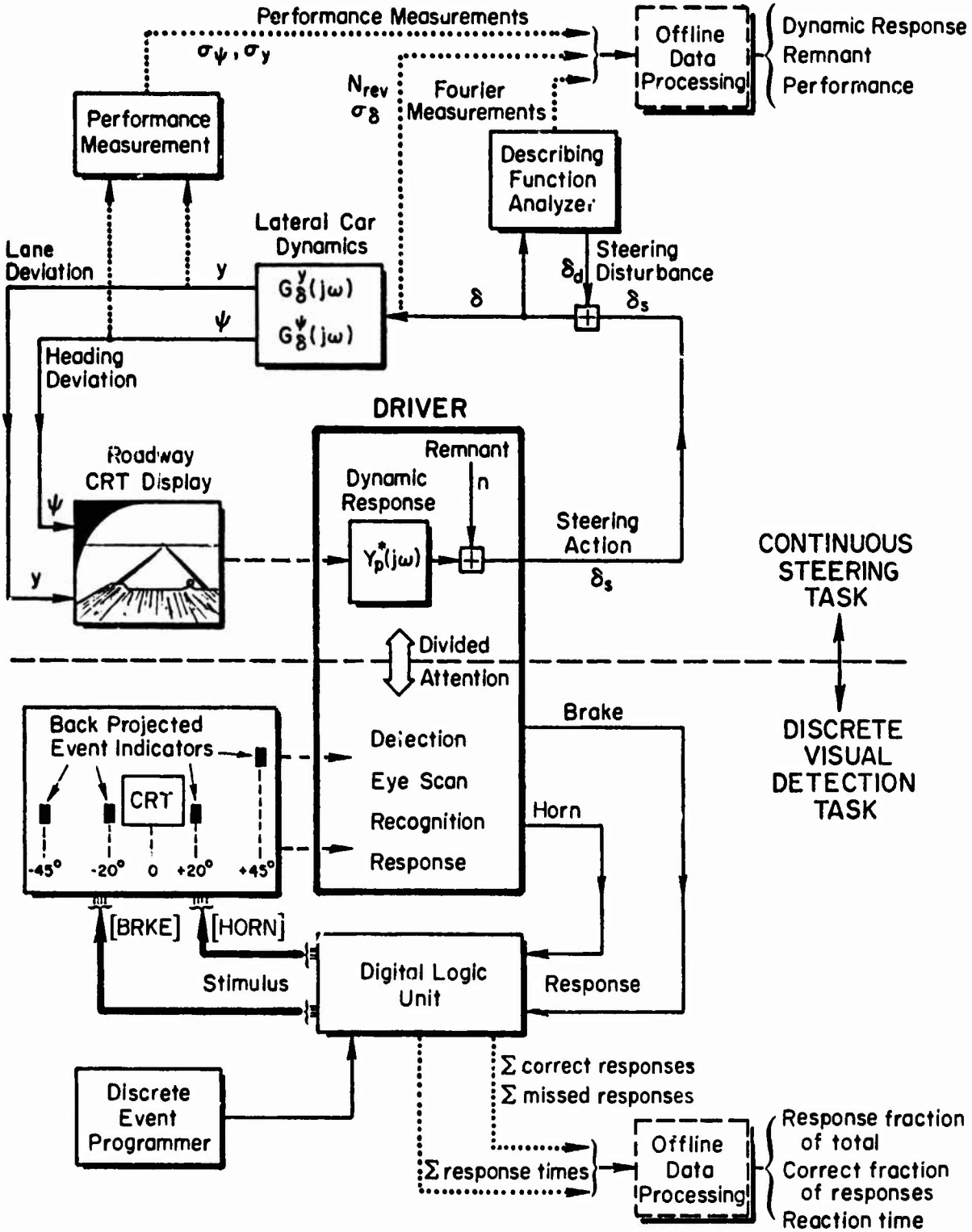

P-150

TABLE 1

CAR DYNAMICS AND DISTURBANCE INPUT

TRANSFER FUNCTIONS:

Path Control Dynamics

$$G_\delta^y = \frac{K_{ay}[s^2 + 2\zeta_y\omega_y s + \omega_y^2]}{s^2[s^2 + 2\zeta_1\omega_1 s + \omega_1^2]} = \frac{90.9[s^2 + 2(.36)(7.6)s + 7.6^2]}{s^2[s^2 + 2(.94)(5.6)s + 5.6^2]}$$

Heading Control Dynamics

$$G_\delta^\psi = \frac{19.5(s + T_r^{-1})}{s[s^2 + 2\zeta_1\omega_1 s + \omega_1^2]} = \frac{19.5(s + 6.1)}{s[s^2 + 2(.94)(5.6)s + 5.6^2]}$$

where ζ_1, ω_1 = damping and natural frequency of car heading response

T_r^{-1} = heading response zero

ζ_y, ω_y = damping and natural frequency of car lateral acceleration numerator

DISTURBANCE: $\delta_d = \sum_{k=1}^{5} A_k \cos(\omega_k t + \varphi_k)$

k	ω_k (rad/sec)	A_k STEERING WHEEL degrees
1	.19	6.36
2	.50	3.18
3	1.26	1.59
4	3.02	0.80
5	6.28	0.80
σ_{δ_d}		5.2

P-150

Figure 2

EQUIVALENT DRIVER DESCRIBING FUNCTION AMPLITUDE

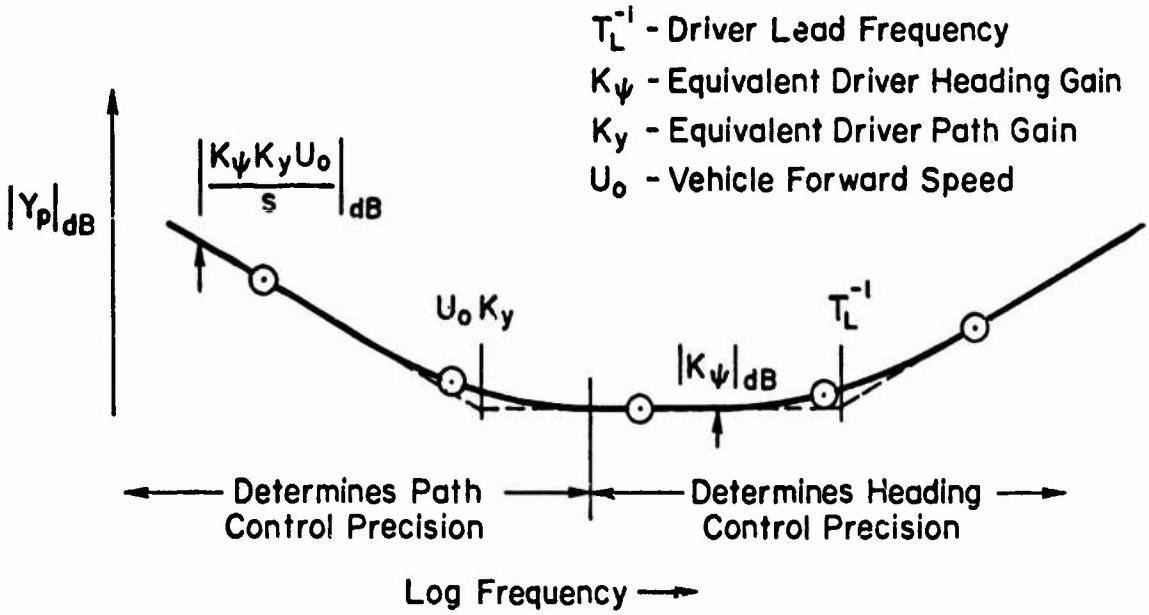

(K_y), while the mid- and high-frequency amplitude reflect heading sensitivity (K_ψ). The high-frequency break point represents lead (anticipation) generated by the driver to offset the lags in the vehicle heading response (Refs. 15 and 18). Generally, higher open-loop gains imply better closed-loop performance, up to the level at which stability margins are reduced to the point of diminishing returns, and oscillatory resonance sets in.

The above measurements were made using the STI Describing Function Analyzer (Ref. 21) as shown in Fig. 1. Associated performance measurements were also obtained with an analog computer and combined in further off-line data processing to yield a comprehensive set of performance and underlying driver control dynamic response measurements. The dynamic response measurements

included the equivalent driver describing function, $Y_p^*(jw)$; unity-gain and 180-deg-phase "crossover" frequencies (ω_c, ω_u) which are measures, respectively, of the actual and maximum achievable heading loop bandwidth; phase margin (φ_M), a measure of the heading loop closure stability margin; system rms performance measures of key signals such as steering wheel motion (δ_s), heading (ψ), and lane deviation (y); and overall linear coherency of the driver's steering action relative to the input disturbance ($\rho^2_{\delta_s}$) in which deviation from unity gives a measure of the remnant generated by the driver. A typical run lasted 120 seconds with the above measurements made over the last 100 sec.

Visual Detection Task

The visual detection task was set up to represent discrete events that the driver might encounter up ahead beside the road or through his rearview mirrors, and require response reflexes typical of driving. Back-projected one-inch indicator lights (IEE Series 0120) were mounted in the standard rearview mirror positions (roughly ±45 deg off center and at ±20 deg on either side of the CRT roadway display as shown in Fig. 1. Each indicator presented the messages [HORN] or [BRKE], requiring the subject to respond by depressing, respectively, the horn ring or brake pedal. The message was approximately 0.18" × 0.56" in size and the brackets were used to preclude the driver from recognizing the message content parafoveally. The message brightness was adjusted through trial and error to be just barely supra-threshold for parafoveal detection under sober conditions.

The indicator units were driven by a special purpose Digital Logic Unit (DLU) and event programmer which activated the messages in quasi-random sequences among the four indicators. Four different programs were used to minimize chances of learning the sequences. During a 100-second run, four messages were presented on each indicator (2 HORN, 2 BRKE), with the order of indicator and message randomized and counterbalanced during a run. The inter-message interval varied between one and five seconds and was also randomized. The DLU also accumulated the number of correct responses, the number of missed responses, and the reaction time of all responses. Each message was presented for (nominally) three seconds, and responses beyond this interval were counted

as misses. As a result of subsequent off-line processing, the accumulated data were reduced to measures of signals detected, signals correctly responded to, and average reaction time.

In order to gain insight into the eye scanning process for the present task setup, eye motions were recorded during selected runs using an STI EPR-2 eye-point-of-regard monitor (Ref. 22). This device provides a continuous indication of vertical and horizontal head and eye points-of-regard. It consists of a goniometer, held fixed relative to the subject's head by a rigid bite, and four light-sensitive sensors mounted on modified eyeglass frames. The goniometer measures head movement while the frame-mounted sensors measure eye movement relative to the head. EPR-2 electronics provide for individual adjustment and sensitivities of the goniometer and each of the sensors, and subsequent combining of goniometer and sensor outputs to provide eye point-of-regard with respect to an cab-fixed reference.

EXPERIMENTAL METHODS AND PROCEDURES

The subject population for the experiment consisted of 18 licensed drivers (17 males, 1 female) screened for normal intelligence (on the basis of results on a shortened version of the Shipley-Hartford Test, Ref. 24). Selected subjects were equally divided between moderate and heavy drinkers and were further selected to span the age range 21-65. This aspect of the study is discussed in detail in a companion paper (Ref. 19). The subjects were given training on the task during 2 sessions and performed the test battery (i.e., driving task only, sign task only, and combined driving and sign tasks) 5 to 9 times prior to the formal data sessions. Three subjects each from the moderate and heavy drinker categories were also selected to run single-blind placebo sessions in addition to their formal test sessions to determine whether other factors such as fatigue or learning might appreciably influence task performance during the formal data sessions. Subjects were tested in groups of two to four, usually including one placebo.

Formal data sessions were begun in the morning or early afternoon, and subjects were asked to refrain from eating immediately prior to reporting on the test day in order to obtain maximum alcohol absorption rates. Subjects were administered a warmup run and formal baseline tests prior to receiving

their first drink. During normal drinking sessions it was desired to test subjects at ascending and descending blood alcohol concentrations (BAC) of nominally 0.06 and peak levels of 0.11 (just beyond the legal limit for intoxication in many states). BAC was measured with a Mark II Gas Chromatograph Intoximeter. Heavy drinkers were also tested in additional sessions at higher BAC's, and this data is discussed in Ref. 19.

A lounge with games and reading material was provided for the subjects' relaxation during drinking and resting between tests in order to promote a modest social atmosphere. The drinks consisted of vodka or whiskey (for a few subjects who refused to drink vodka), diluted to 20 percent ethanol concentrations with a standard mixer. Alcohol dosage was adjusted for body weight to yield desired BAC's. Subjects were given two drinks calculated to give a nominal ascending BAC of 0.06 for testing. A third drink was then given to allow achievement of a maximum BAC on the order of 0.11. After testing at maximum BAC, subjects were given a meal, with no further drinks, and a final test was run at a nominal descending BAC of 0.06. A plot of the mean and standard deviation of BAC's achieved over all subjects as a function of time is given in Fig. 3. For placebo subjects a small amount of vodka was "floated" on top of a glass of their customary mix to give the illusion of a mixed drink.

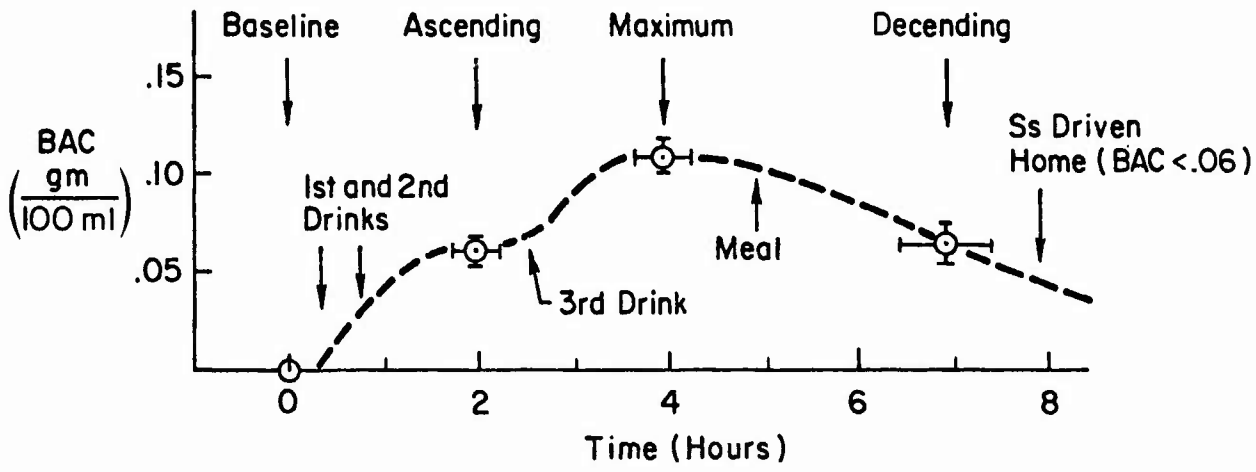

Figure 3. BAC as a Function of Time Averaged Over Subjects

RESULTS

Typical time traces of experimental trials conducted under sober and intoxicated conditions are shown in Fig. 4, and exhibit many of the experimental effects of alcohol on driving. For the continuous task it is apparent that both the heading and lane deviations of the car increase under alcohol. Also, the driver's steering actions seem to be less responsive with longer periods of constant wheel position under alcohol, although wheel motion does roughly correspond to the input disturbance as it should for regulation against the disturbance.

From a diagnostic standpoint, the EPR data allow the partitioning of the multiphasic discrete task response process into its components as quantified by the time interval allotted to each phase (initial delay to scan initiation, scan dwell, and time to respond following the initial scan). By such partitioning, the individual contributions of each phase to overall performance degradation can be assessed.

For the discrete task the EPR (eye-point-of-regard) trace shows that the driver did not continuously scan, but looked away from the road (CRT) in response to the appearance of sign messages, although under alcohol there are several cases of extra scans. This behavior is consistent with the stated primary nature of the control task and indicates the signs were detected parafoveally. Event "detection" is indicated by a scan in the correct direction.

Under sober conditions the scanning is made with single, rapid saccades (Fig. 4). Scans are initiated shortly after message onset and last 0.3-0.5 seconds, and there is no apparent interaction with steering wheel motions during the scanning and response processes. Under alcohol the scanning is much more sluggish, however, with multiple saccades and dwells on the order of 0.6-1.0 seconds which seems to correlate with a slight increase in the total response reaction time. There is also evidence of holds in the steering action under alcohol during the scanning and response process. Previous research (Ref. 25) including the sober data here has not shown this type of interference which may be a unique alcohol effect.

A preliminary review of EPR data from two subjects indicates that the typical response process, sober, can be broken down into: a 0.2-0.4 second initial delay between event onset (sign light-up) and the beginning of the

Figure 4

TIME TRACE OF COMBINED CONTINUOUS AND DISCRETE TASK OPERATION UNDER SOBER AND DRUNK CONDITIONS

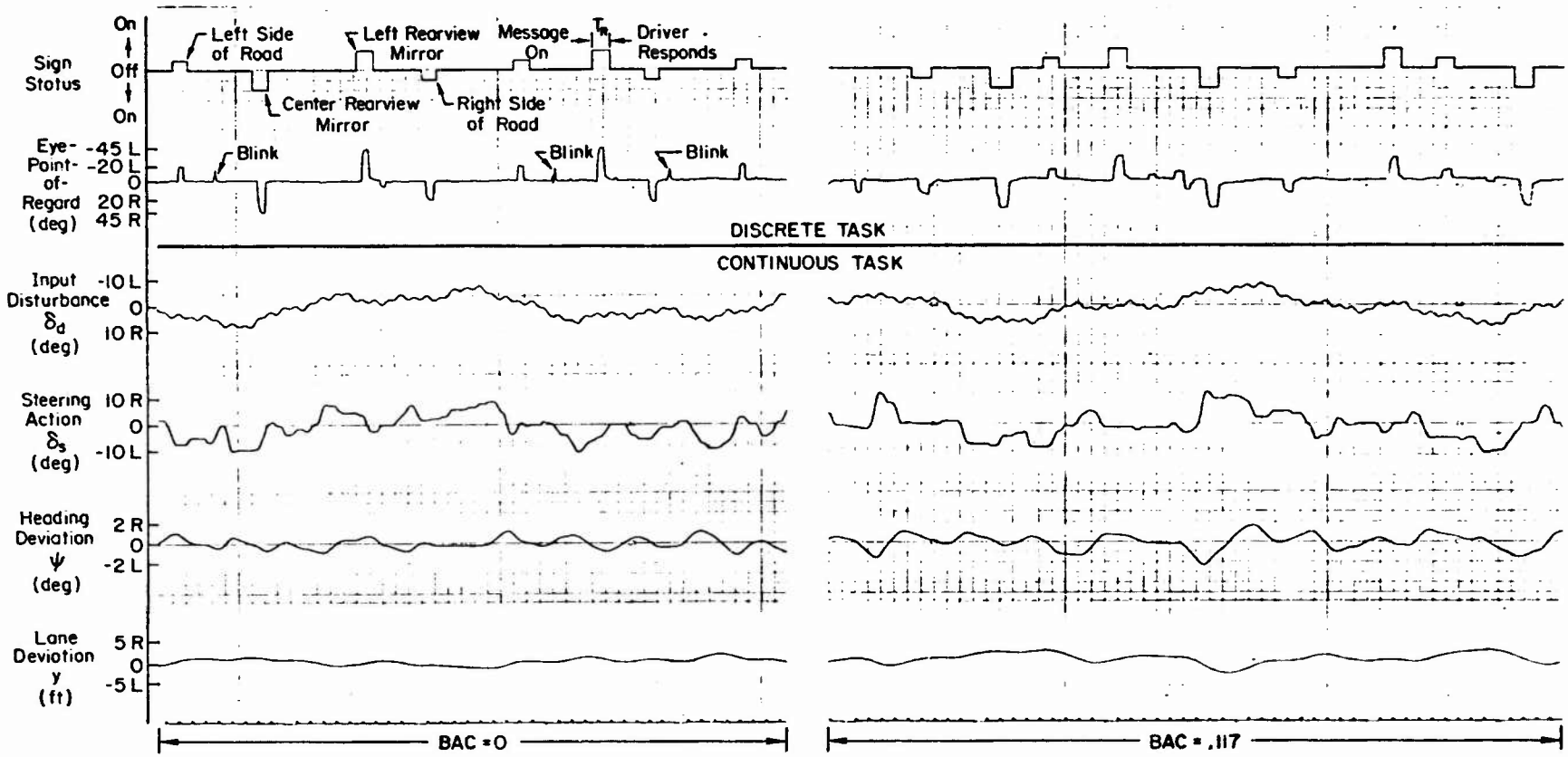

eye motion from the roadway to the sign; a 0.3-0.6 second dwell period during which the subject "recognizes" the sign; and a 0.1-0.3 second interval preceding response to the sign, after the eyes have returned to the roadway. With increasing BAC, typical initial delay and dwell increased, reaching values of 0.4-0.9 seconds and 0.7-1.1 seconds, respectively, at peak BAC, while the time to respond after scan diminished until both subjects would frequently respond before looking back to the roadway. Behavior for the discrete-task-only was markedly different. While typical detection delays were generally comparable to those observed for the combined task, typical scan dwell was always larger and the EPR usually returned to the road just after the response was made.

Under sober and intoxicated conditions, the response process was more consistent and showed much less evidence of random scanning (and no sober random scanning) when combined with the driving task. Other idiosyncratic behavior exposed by the EPR measurements included scanning from one roadway edge to the other rather than using a single fixation point for the continuous task reference and occasional failure to respond to signs after detection and apparent visual recognition (verifying subject's comments to that effect) while under the influence of alcohol.

While the above results are tentative, it is apparent that the EPR data can contribute considerable, and otherwise unavailable, insight to the scanning and response processes involved in driving and their deterioration under alcohol. Further analysis along these lines should be quite fruitful.

Analysis of the placebo data showed little effect on task performance during a given experimental session. Also analysis of the ascending vs. descending data at comparable BAC's failed to show any appreciable effect on performance. Consequently, the following discussion will be confined to results obtained at the baseline, ascending, and maximum levels of BAC (Fig. 3).

Performance data averaged across 18 subjects is plotted in Fig. 5. Steering activity and heading and lane deviations generally increase with BAC. The addition of the discrete task causes a constant increment in steering activity and heading deviations, while only the sensitivity of σ_y decrements to BAC is increased by the divided-attention nature of the combined task. The combined-task results show that path-following errors double (0.65 → 1.3 feet) when attentional demands are placed on the intoxicated

Figure 5

ALCOHOL EFFECTS ON DRIVING CONTROL PERFORMANCE AVERAGED OVER SUBJECTS

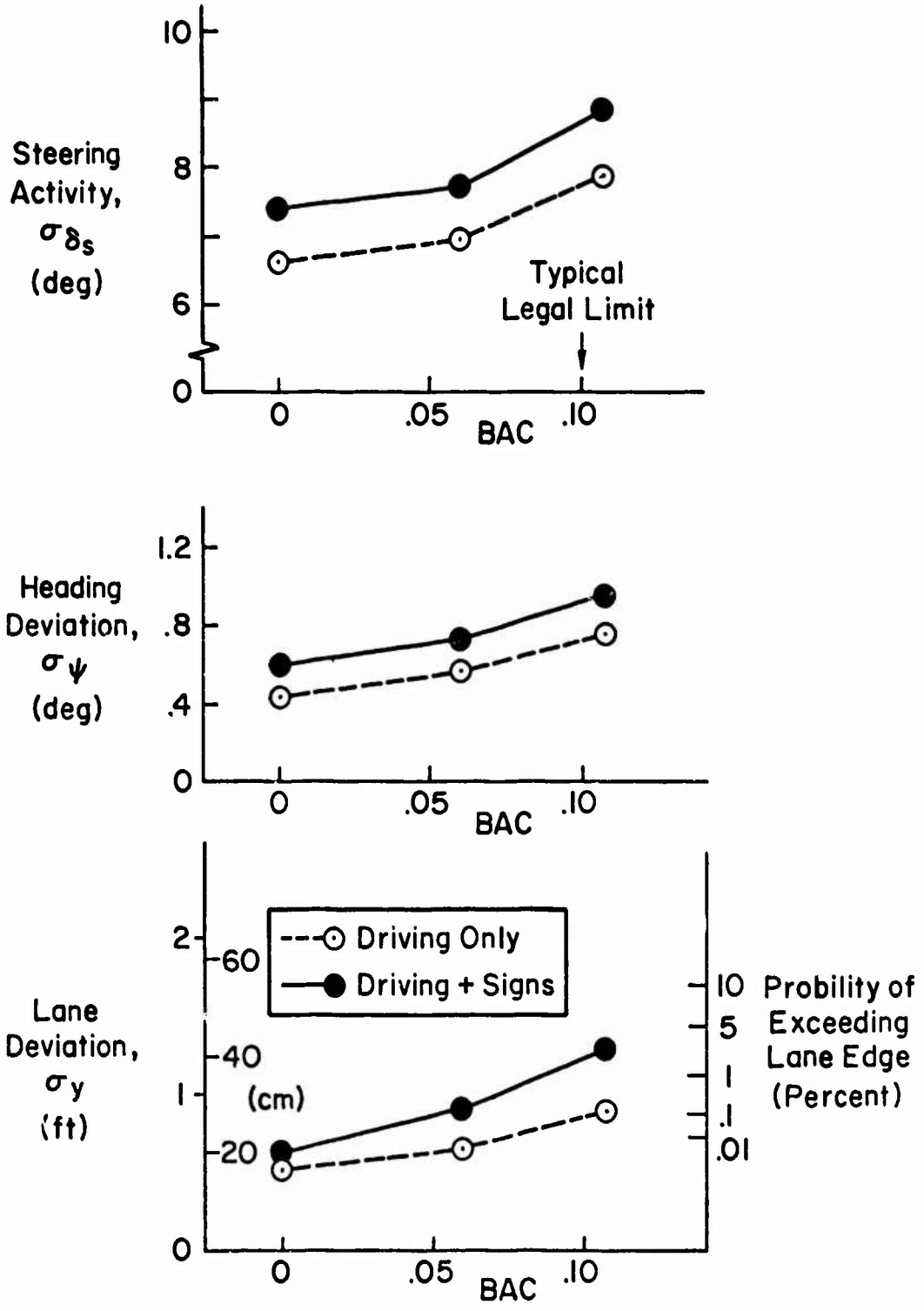

driver. The occasional peak deviations of a random path with this rms level will clearly extend a car past lane boundaries or off on the shoulder of a single lane road which increases the probability of accident involvement.

Driver control behavior responsible for the above performance effects is shown in Fig. 6. From the averaged describing function data it is obvious that the driver's sensitivity or gain is reduced when he is intoxicated. This is particularly true in the low-frequency region which mainly influences path following errors. The describing function phase data (Fig. 6a) are not particularly affected, so the change in the driver's dynamic response under alcohol is mainly a gain phenomenon. Furthermore, alcohol acts to increase driver remnant (Fig. 6b).

Both the remnant and describing function results might be explained by an increase in intermittency* and/or indifference threshold†. Alcohol may increase the driver's indifference threshold to lane deviations, a nonlinear behavior which would increase remnant while at the same time reducing measured gain. Also, as suggested by the time trace data in Fig. 4, the discrete-sign-task interference under alcohol seems to elicit intermittent steering actions, which could lead to further remnant increase and gain reductions as shown in Fig. 6.

In spite of the changes in dynamic response described above, alcohol does not seem to decrease the basic closed-loop stability of the driver/vehicle system, as shown in Fig. 7. The crossover frequencies and phase margin are computed from the equivalent single-loop driver/vehicle dynamics and relate mainly to the heading control loop. While the gain crossover frequency decreases under alcohol, which is consistent with the describing function data in Fig. 6, the phase margin stays relatively constant. In a similar vein, ω_u and ω_c change uniformly implying a constant gain margin. Also, with

---

*Indifference Threshold ≡ thresholds in a perceptual-motor control loop which are not specifically sensory or proprioceptive threshold; e.g., control inaction while the error is within some tolerance zones (Ref. 24).

†Attentional Intermittency ≡ switching of control attention frequently, and usually asynchronously, from task to task (or loop to loop); often (but not always) evidenced by eye-point-of-regard or control inactivity (e.g., Ref. 25).

Figure 6

EFFECTS OF ALCOHOL ON DRIVER CONTROL BEHAVIOR AVERAGED OVER SUBJECTS

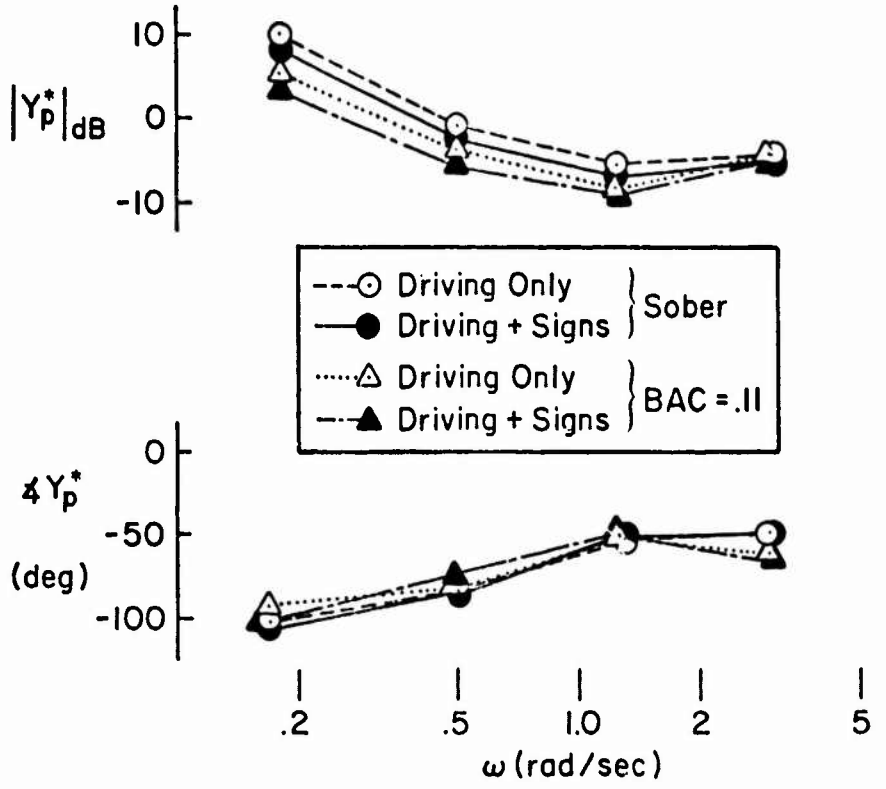

a) Equivalent Driver Describing Functions

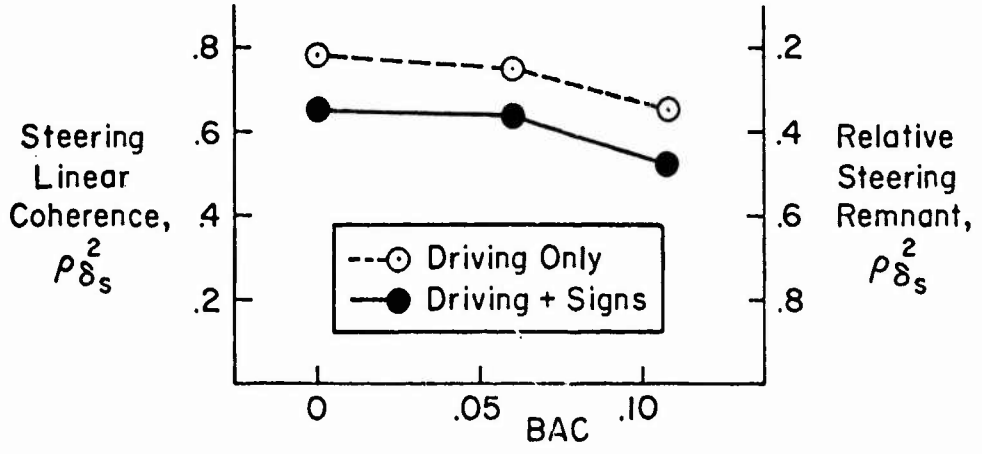

b) Remnant

Figure 7

DRIVER/VEHICLE DESCRIBING FUNCTIONS PARAMETERS AVERAGED ACROSS SUBJECTS

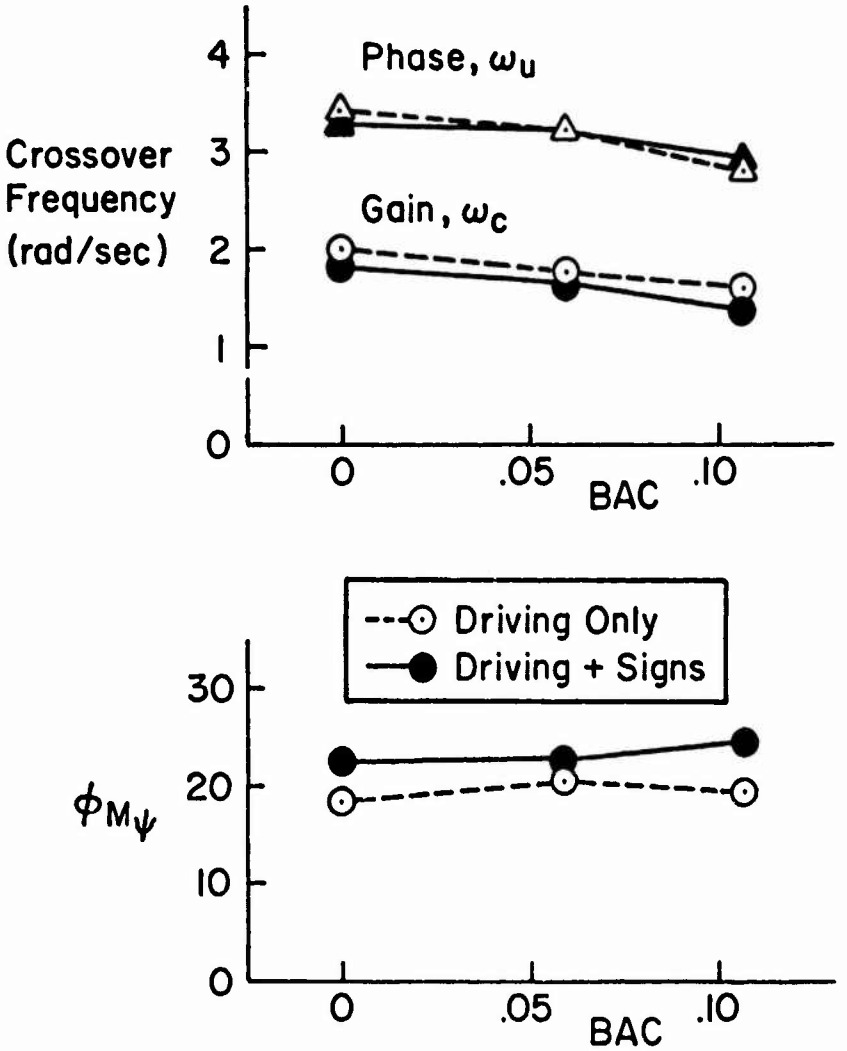

the added distraction of the sign task, the driver lowers his gain to further increase his stability margin. Finally, all the dynamic response and remnant data show similar effects between the single and combined tasks, implying little influence of divided attention on the driver's control behavior.

Performance on the discrete task is plotted in Fig. 8. The response ratio, N_R/N, is the fraction of signals responded to, and gives a measure of signal detectability. Dectection decreased with increasing BAC, and the added distraction of the control task seems to add an extra decrement at high blood alcohol levels. Signs were seldom incorrectly responded to (less than 3 percent at 0.1 BAC), so this was not a factor in task performance. The response times to the signs generally increased with BAC and was not influenced by the presence or absence of the control task. Finally, the reaction times measured here are quite similar to past simulator results (Ref. 5).

DISCUSSION

The results presented so far show a general deterioration in performance with increasing BAC in both the continuous and discrete tasks. The effects occur both when the tasks are performed singly and in combination; however, the divided attention aspect of the combined task does not seem to have affected the general sensitivity of the results to BAC, except for the path deviation. In order to further substantiate these findings, the key measurements were subjected to analysis of variance procedures, and the results are summarized in Table 2.

The BAC level effect was highly significant for all parameters as indicated in Table 2, except phase margin (φ_M), which was previously noted to remain relatively constant over the range of BAC's tested. The Task effect in Table 2 shows that performance of the steering task was significantly impaired by the presence of the discrete task; however, the reverse was not true. This is possibly because the discrete task interrupts the continuous nature of the steering task; whereas the discrete task is always performed on demand, so the detection process is not interferred with. The 3.0 sec "gate" on the signs probably motivated this behavior to a certain extent, which is realistic in the driving context where signs, unexpected obstacles, etc., must be reacted to before they are overrun. (At 30 mph, the car travels 132 ft in 3 seconds.)

Figure 8

ALCOHOL EFFECTS ON DISCRETE TASK PERFORMANCE AVERAGED OVER SUBJECTS

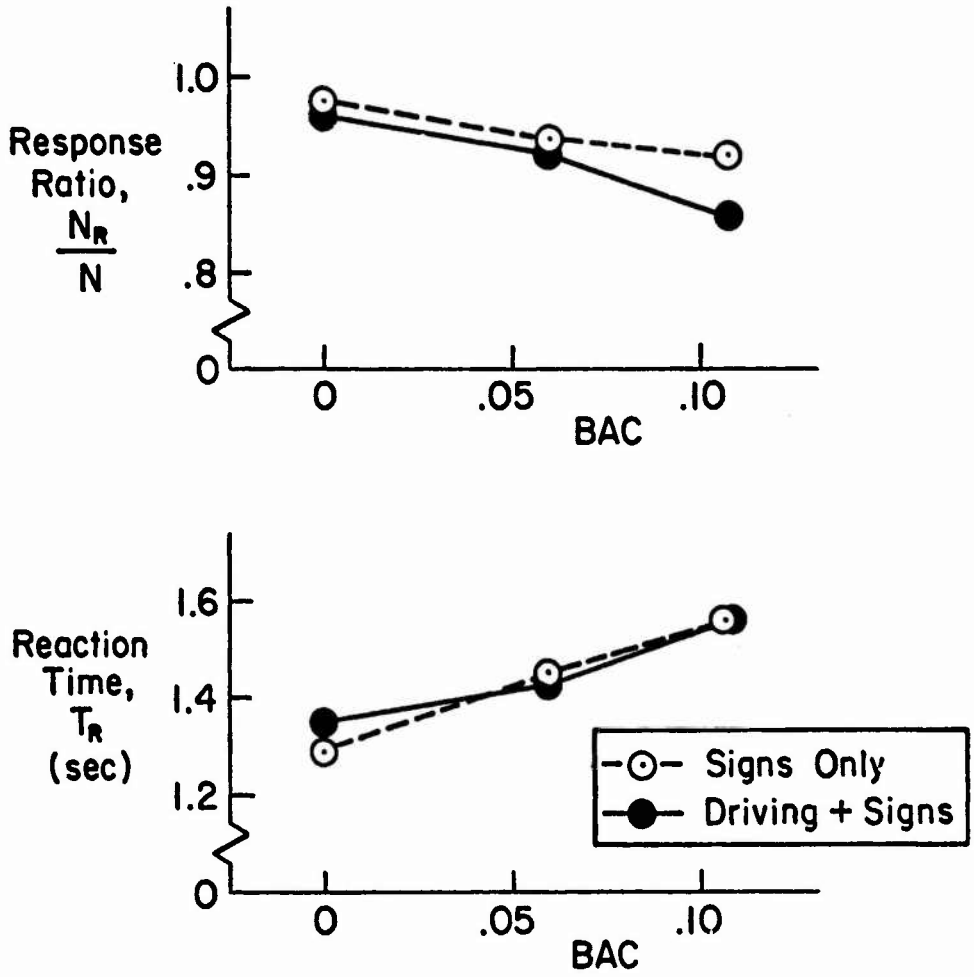

TABLE 2

ANOV SUMMARY OF KEY EXPERIMENTAL MEASUREMENTS†
(F-RATIOS AND LEVEL OF SIGNIFICANCE)

EFFECTS OF ↓ ON →	STEERING TASK MEASURES							DISCRETE TASK MEASURES		DEGREES OF FREEDOM
	STEERING		HEADING CONTROL			PATH CONTROL				
	δ_s	$\rho^2_{\delta_s}$	σ_ψ	ω_c	φ_M	σ_y	$\lvert Y^*_p \rvert_{\omega=.5}$	N_R/N	T_R	
BAC Level (Baseline; 0.06; 0.11)	14.2 ***	17.6 ***	31.0 ***	19.7 ***	0.56 NS	21.4 ***	16.9 ***	8.86 **	27.5 ***	2, 12
Task (Single vs. Divided Attention)	60.8 ***	44.0 ***	84.7 ***	12.4 **	7.64 *	30.1 ***	12.4 **	3.46 NS	0.36 NS	1, 12
BAC × Task (Divided Attention Interaction with Alcohol)	0.58 NS	0.78 NS	2.28 NS	0.61 NS	0.68 NS	14.64 ***	1.96 NS	1.01 NS	1.76 NS	2, 24

*** = 0.001 Level of Significance
** = 0.01 Level of Significance
* = 0.05 Level of Significance

†The experimental design included all combinations of BAC Level and Task. Subjects were also included as a variable in the analysis, and were further subdivided into groups by drinking habit and age, thus resulting in a nested design for the complete analysis. Subjects were considered a random variable and subject interactions were used for the F ratio denominators.

Finally, Table 2 bears out the previously-noted result that there is no significant interaction between BAC and Tasks other than for the lane deviation measurement. This one exception is quite important, however, since lane deviations influence the probability of accident involvement.

CONCLUDING REMARKS

A rather simple, yet directly driving-relevant, fixed-base laboratory driving simulator was developed which has elicited many of the anecdotal phenomena attributed to intoxicated drivers in past investigations. With a scenario of driving on a rural road on a stormy night, the simulation gained the acceptance of the 18 typical drinking driver subjects and has provided a reliable data base with many clearcut effects. The more important findings may be summarized as follows:

Driving Task

- Lane deviations increase with BAC level, which is explained by measures of lower driver control gain and increased remnant. Distraction of the sign response task further increased the impairment of path control by alcohol. These effects are consistent with increased indifference thresholds and/or control intermittency and significantly increase the probability of lane exceedances.

- Heading control gain also decreases under alcohol with a concomitant increase in heading deviations. Phase margin for the heading loop closure remains constant under alcohol, however, so that intoxication apparently does not decrease control stability.

Discrete Task

- The fraction of misses and the response time increase under alcohol, while incorrect responses are negligible under all conditions up to BAC = 0.11.

- The driving task does not interfere with the discrete task in either the detection or response processes, indicating the signs are acted upon on demand much as might be expected in a real driving situation in response to signals, unexpected obstacles, etc.

- EPR (eye-point-of-regard) measurements show that drivers do not continuously scan for signs. Scans are normally prompted by peripheral detection of a sign, although occasional unnecessary scans occur at higher BAC. Scanning is degraded in general under alcohol, and an observed increase in scan dwells may be partially responsible for increased reaction times and interference with the steering control task.

- The EPR measurements have given a great deal of insight into the detection and response processes in the discrete task and further analysis of the simultaneously recorded EPR, discrete response, and steering data would be fruitful.

This simulation was used successfully (in an experiment interleaved with this one) to investigate effects of different drinking habits (Moderate vs. Heavy) on the various measures of driving performance and behavior (Ref. 19), and additional data therein on heavy drinkers at 0, 0.11, and 0.16 BAC tends to support and extend the present findings.

REFERENCES

1. 1968 Alcohol and Highway Safety Report, U. S. Government Printing Office, Washington, D. C., 1968.

2. Perrine, M. W., Julian A. Waller, and Lawrence S. Harris, Alcohol and Highway Safety: Behavioral and Medical Aspects, Univ. of Vermont, Dept. of Psychology, Sept. 1971.

3. Hurst, P. M., "Estimating the Effectiveness of Blood Alcohol Limits," Behavioral Research in Highway Safety, Vol. 1, Summer (1970).

4. Coldwell, B. B., D. W. Penner, H. W. Smith, et al, "Effect of Ingestion of Distilled Spirits on Automobile Driving Skill," Quart. J. of Stud. Alcohol, Vol. 19, No. 4, 1958.

5. Moskowitz, H., The Effects of Alcohol on Performance in a Driving Simulator of Alcoholics and Social Drinkers, UCLA, Inst. of Transport. and Traffic Engrg., Rept. 7205, Dec. 1971.

6. Sugarman, Robert C., C. Paul Cozad, and Albert Zavala, Alcohol Induced Degradation of Performance on Simulated Driving Tasks, SAE Paper No. 730099, Jan. 1973.

7. Miles, Walter R., Alcohol and Human Efficiency, Experiments with Moderate Quantities and Dilute Solutions of Ethyl Alcohol on Human Subjects, Carnegie Institution of Washington, Publication No. 333, Mar. 1924.

8. Carpenter, John A., "Effects of Alcohol on Psychological Processes," Alcohol and Traffic Safety, ed. by B. H. Fox and J. H. Fox, U. S. Dept. of H.E.W., Bethesda, Md., 1963.

9. Hamilton, P., and A. Copeman, "The Effect of Alcohol and Noise on Components of a Tracking and Monitoring Task," Brit. J. Psychol., Vol. 61, No. 2, 1970, pp. 149-156.

10. Moskowitz, Herbert, and S. Sharma, "A Behavioral Mechanism of Alcohol-Related Accidents," First Annual Conference of the National Institutes of Alcohol Abuse and Alcoholism, Washington, D. C., June 26, 1971.

11. Huntley, M. S., Effects of Alcohol and Fixation-Task Demands upon Human Reaction Time to Achromatic Targets in the Horizontal Meridian of the Visual Field, (Doctoral dissertation, Univ. of Vermont), Ann Arbor, Mich., Univ. Microfilms, 1970, Vol. 31, No. 3026-B.

12. McLellan, D. R., "The Effects of Alcohol on Driving Skill," 12th Annual Symposium of the Amer. Assoc. for Automotive Medicine, Sacramento, Calif., 1968.

13. Loomis, T. A., and T. C. est, "The Influence of Alcohol on Automobile Driving Ability: An Experimental Study for the Evaluation of Certain Medicological Aspects," Quart. J. of Stud. Alcohol, Vol. 19, No. 4, 1958, pp. 30-64.

14. Case, Harry W., Slade Hulbert, and Herbert A. Moskowitz, Alcohol Level and Driving Performance, Univ. of Calif., UCLA-ENG-71-17, Apr. 1971.

15. Weir, D. H., and D. T. McRuer, "Dynamics of Driver Vehicle Steering Control," Automatica, Vol. 6, 1970, pp. 87-98.

16. Weir, David H., and Duane T. McRuer, "Measurement and Interpretation of Driver/Vehicle System Dynamic Response," Human Factors, Vol. 15, No. 4, Aug. 1973, pp. 367-378.

17. Weir, David H., et al, An Experimental and Analytical Investigation of the Effect of Bus-Induced Aerodynamic Disturbances on Adjacent Vehicle Control and Performance, Systems Technology, Inc., TR-1016-1, Nov. 1972.

18. McRuer, Duane T., et al, "Measurement of Driver/Vehicle Multiloop Response Properties with a Single Disturbance Input," Ninth Annual Conf. on Manual Control, Mass. Inst. of Tech., Cambridge, Mass., May 23-25, 1973.

19. Jex, Henry R., Richard J. DiMarco, and R. Wade Allen, "Impairment of Medium vs. Heavy Drinkers in Simulated Driving Tasks," to be presented at the Tenth Annual Conf. on Manual Control, AFIT, Apr. 1974.

20. Stephens, B. W., and R. M. Michaels, "Timesharing Between Two Driving Tasks," Public Roads, Vol. 33, No. 5, Dec. 1964, pp. 81-88.

21. Allen, R. Wade, and Henry R. Jex, "A Simple Fourier Analysis Technique for Measuring the Dynamic Response of Manual Control Systems," IEEE Trans., Vol. SMC-2, No. 5, Nov. 1972, pp. 638-643.

22. Klein, Richard H., and Henry R. Jex, "An Eye-Point-of-Regard System for Use in Scanning and Display Research, 15th Annual Tech. Symposium of the Society of Photo-Optical Instrumentation Engineers, Aug. 1970.

23. Alcohol and the Impaired Driver: A Manual on the Medicolegal Aspects of Chemical Tests for Intoxication, A.M.A., Chicago, Ill., 1970.

24. Buros, Oscar Krisen (ed.), The Seventh Mental Measurement Yearbook, Gryphon Press, Highland Park, N. J., 1972.

25. McRuer, D. T., and E. S. Krendel, Mathematical Models of Human Pilot Behavior, AGARD-AG-188, Jan. 1974, pp. 41-44.

26. Allen, R. W., W. F. Clement, H. R. Jex, Research on Display Scanning, Sampling, and Reconstruction Using Separate Main and Secondary Tracking Tasks, NASA CR-1569, July 1970.

27. McRuer, Duane T., and Ezra Krendel, Dynamic Response of Human Operators, WADC TR 56-524, Oct. 1957.

IMPAIRMENT OF MODERATE VERSUS HEAVY DRINKERS IN SIMULATED DRIVING TASKS*

Henry R. Jex, Richard J. DiMarco, and R. Wade Allen†
Systems Technology, Inc., Hawthorne, California

ABSTRACT

The objective of this program was to test, under carefully controlled and measured conditions at various blood alcohol concentrations, whether or not Heavy drinkers (i.e., those who ususally exceed 0.10 BAC when drinking) might have different driving impairment than Moderate drinkers (i.e., those who seldom reach 0.10 BAC when drinking). Two groups of ten drinking drivers, representing a typical distribution of age, education, and occupation were selected to have drinking habits near either extreme. The primary task was a steering control task in the presence of crosswind gust disturbances using a roadway perspective display in the STI Fixed-Base Car Simulator. A secondary discrete task included detection, interpretation, and response to simulated "signs" located at ±20 deg and ±45 deg in the peripheral fields. (The methods, setup, and comprehensive measurement schemes are described in a companion paper, Ref. 6). Two interleaved experiments were performed. In one, both Moderate and Heavy drinkers went to just over legal limits (Blood Alcohol Concentration, BAC ≐ 0.11 g/100 ml), and in the other the Heavy drinkers went up to BAC ≐ 0.16. The experiment design included a test battery of: steering only, discrete task only, and combined tasks; partial placebo sessions; and tests during sober (baseline), ascending, peak, and descending BAC phases. Also presented are some eye motion traces giving insight as to the nature of the discrete task decrements.

Results showed that Heavy drinkers were less impaired than Moderate drinkers at 0.11 BAC (near legal limits), in terms of larger heading and path errors, describing function gain decrements, increased remnant, more discrete task misses, and longer response times. However, the Heavy drinkers were somewhat more impaired at 0.16 BAC than the Moderate drinkers at their 0.11 BAC peak.

Based on lane deviation variance, the probability of lane exceedance of a standard sedan in a 12-foot lane was increased from 0.0001 when sober to 0.05 for the Moderate drinkers at 0.11 BAC, and for the Heavy drinkers to 0.01 at 0.11 BAC and to 0.10 at 0.16 BAC. A number of the observed effects of BAC (i.e., worse performance, lower driver sensitivity to lane and heading

---

*This work was sponsored under Contract DOT-HS-227-2-388 by NHTSA's Office of Driver Performance Research, with Dr. Leland Summers as Contract Technical Manager.

†Principal Research Engineer; Staff Engineer, Analytical; and Senior Research Engineer, respectively.

deviations, less control coherency, constant stability margins, and missing of discrete responses despite their accurate peripheral detection) are all consistent with an increase in the intoxicated driver's indifference thresholds and/or attentional intermittency.

INTRODUCTION

Objectives

The **underlying motivation** behind the present research has been clearly stated by the Office of Driver Performance Research of the National Highway Traffic Safety Administration (NHTSA) in Ref. 1, as follows:

> "The 1968 Alcohol and Highway Safety Report showed that alcohol related accidents account for 50% of the highway fatalities and that 80% of these fatalities have blood alcohol concentrations of 0.10% or higher. It has also been shown that the accident risk factor increases 6 and 20 fold for BAC levels of 0.10% and 0.15% (Ref. 2) respectively and the fatality risk factor is 9 and 35 fold for the same BAC levels (Ref. 3). It has also been found that heavy users of alcohol were over represented among those responsible for fatal and serious injury accidents and among those convicted of driving-while-intoxicated or other serious moving violations (Ref. 2). In fact it is generally concluded that problem drinkers who constitute a small portion of the population account for a very large part of the overall problem (1968 Alcohol and Highway Safety Report).
>
> Past and current research on alcohol and driving has shown that alcohol impairs driving and performance tests related to driving. However, the majority of this research was performed on college students who were social drinkers and did not differentiate between heavy or light drinkers. It is the intent of this procurement to determine if there is a difference between heavy versus light drinkers in their driving performance level and if there is a interaction between drinker type and alcohol dosage level."

NHTSA's **basic objectives** in this ongoing program are: 1) to determine, via laboratory driving tests, the primary causes of deterioration in driver performance under alcohol; and 2) to reveal performance indicators which might be used to differentiate "light" or "heavy" drinkers from the standpoint of applying selective countermeasures, and for revealing the most effective avenues for reducing the risk of subsequent crashes. The **specific purpose** of this investigation was to determine, via a simplified but relevant driving

simulation, if there is a difference in driving performance on the basis of an individual's drinking habits (Ref. 1). By using a simplified set of tests relevant to driving behavior, the task variables could be readily controlled, and the detailed characteristics of heavily drunk drivers could be safely and efficiently measured. The most promising of these tests and possible countermeasures could later be validated in the more risky (and expensive) field trials.

Research Approach

A relatively simple, fixed-base laboratory driving simulator and tasks and measures to test driving performance are described in detail in a companion paper (Ref. 6), which also presents some basic effects of Blood Alcohol Concentration (BAC)* and effects of divided attention, as noted below. Without repeating unnecessary details, we will comment here on the key considerations and features of our approach.

Drunk driving accidents usually occur at night, on rural (non-urban) streets, and involve one car driven into a collision (usually out of the lane) by a male driver (Refs. 4 and 5). The relevant driving tasks are of two general types operating in parallel: continuous **control tasks** (steering and speed) which intrinsically involve closed-loop operation of the car and driver (Ref. 6); and **discrete tasks** (e.g., brakes, horn, turn signals) which require responses to stimuli detected (often peripherally), recognized (usually by a visual scan), and responded to (in a practiced movement) all in an "open-loop" manner. When both types of task must be performed concurrently performance on one type can be affected by interference from the other due to divided attention. It was hypothesized that alcohol might more adversely affect performance on combined steering-plus-discrete driving tasks than either one alone. The overall experimental plan tested this hypothesis, and the results are reported in the companion paper (Ref. 6). For simplicity, and because they represent the more

*Blood alcohol concentration is given here, as customary, in grams ethanol per 100 ml blood, which approximates the volume percentage of ethanol in blood (whose specific gravity is about 1.05)(Ref. 4). The blood levels are inferred from measurement of breath alcohol concentration, for which the term "BAC" is used interchangeably.

realistic situation, only results for combined steering-plus-discrete tasks will be reported here.

Great care was expended on selection of a representative sample of subjects. Because the selection, training, drinking sessions, high BAC and placebo sessions were very costly per subject, the sample was limited to a total of twenty finalists (ten in each drinking category) from a set of some 50-80 "promising" candidates. We found that most "light" drinkers* could not reach the desired typical "legal limit" levels of 0.10 BAC without getting sick (under our somewhat intensive drinking regimen). Consequently, we had to raise the "light" category to "moderate" drinkers*, trying to find the lightest drinkers among those who would not get sick at 0.11 BAC. "Heavy" drinkers* were easy to find among the young, but were surprisingly hard to obtain in older ages, because we did not wish to test serious problem drinkers or alcoholics under rehabilitation. Various drinking habit questionnaires proved unreliable indicators of true alcohol capacity, so we conducted "screening drinking sessions" for the majority of candidates in order to verify and calibrate their alcohol capacity prior to more expensive training and test sessions.

These efforts to select subjects were further complicated by an effort to have in <u>each</u> drinking habit group: 1) a demographically representative and balanced spread of ages; 2) an average range of IQ and educational and driving experience; and 3) mostly male subjects (because females comprise only a few percent of the drunk driver fatalities, e.g., Ref. 5). These criteria were fairly well met.

The overall experiment was divided into two sets. The "main" experiment carried both Moderate and Heavy drinkers to a peak BAC = 0.11, just over the legal limit, and an extra "high BAC" session was run separately for the Heavy

---

*The type of drinker is defined here in terms of level of BAC reached in a typical drinking session:

Light:	BAC rarely exceeds 0.05.
Moderate:	BAC usually exceeds 0.05, may occasionally exceed 0.10, unlikely to ever reach 0.15.
Heavy:	BAC usually exceeds 0.10, and at least occasionally exceeds 0.15.

drinkers to take them toward their customary limits near BAC = 0.16+, with stops at BAC = 0.11 to tie in with the main experiment. The idea here was to compare Moderate and Heavy drinkers not only at the **same** (supra-legal) **BAC**, but also near **each group's customary limit**. This plan was successfully accomplished with interesting results, as will be shown later.

Previous experience with placebo sessions for each subject (Ref. 7) had shown little effect of time of day or fatigue, so we were reluctant to waste previous test time on non-drinking runs. Nevertheless, to establish similar placebo insensitivity of the current test battery, a partial set of single-blind placebo runs was made, with one subject per session having the placebo drinks to retain all of the social factors affecting performance through the session.

With this overview of our approach and rationale in mind, we will next briefly describe the subjects, apparatus, tests, measures, experimental design, and procedures.

EXPERIMENT SETUP, DESIGN AND PROCEDURES

Subjects

As explained in the Introduction, ten subjects in each drinking category were finally selected so as to achieve a demographically representative sample of mostly male licensed drivers of all ages, average intelligence, and average driving experience. (Data from one subject in each group in the main experiment and for two subjects in the high-BAC sessions were unusable.) Salient characteristics of the subjects are given in Table 1.

As a result of screening for drinking capability in a group drinking session, approximately 50 percent of the candidates failed to qualify for formal experiments. For the majority of those who did qualify, good calibrations of BAC vs. ethanol per drink were obtained, so it was possible to achieve fairly close levels of BAC for each subject in the final experiment. Even though we attempted to provide a multi-subject social ambience in an apartment-like living room, the drinking regimen was somewhat more intense, and the test atmosphere was somewhat more "tense" than a typical social drinking experience.

TABLE 1. DATA ON TEST SUBJECTS

a. "Moderate" Drinkers (Frequently to .05+ BAC, occasionally to .10 BAC)

SUBJECT*	AGE yrs	WEIGHT kgm	EDUCATION LEVEL†	DRIVING EXPERIENCE (yrs)	OCCUPATION
H	21	84	HS	7	(Unemployed)
J	22	76	Coll	6	Student
U	25	84	Coll	9	Mortuary salesman
R	32	67	Coll	16	Photographer
X	37	79	Coll	22	Data processing supervisor
D^f	43	55	Coll	26	Homemaker
P/	47	66	HS	28	Maintenance supervisor
V	47	77	HS	25	Real estate salesman
S	52	88	Coll	40	Driving instructor
N	65	82	HS	50	(Retired)

b. "Heavy" Drinkers (Frequently exceed .10 BAC; often to .15+ BAC)

SUBJECT*	AGE yrs	WEIGHT kgm	EDUCATION LEVEL†	DRIVING EXPERIENCE (yrs)	OCCUPATION
C	22	62	HS	6	Messenger
B	22	83	Coll	8	Student
A	23	74	HS	7	(Unemployed)
E	28	80	Coll	11	Student
K	37	82	HS	20	Truck driver
M	37	78	HS	20	Auto salesman
L/	42	79	HS	24	Auto salesman
W	42	98	Coll	27	Bar owner
Q	54	75	HS	36	Insurance agent
T	58	91	Coll	43	Realtor (retired)

*($)^f$ denotes female subjects; (/) denotes formal test data incomplete

†HS = High School; Coll = College

Perhaps because of this, subjects reported somewhat more than usual likelihood of feeling nauseated at their maximum BAC's.

Subjects were trained in the driving simulator for two half-day sessions in which they alternated runs with another subject. The simulated scenario was driving at 30 mph on a rural road at night in stormy weather — a difficult task at best — yet the subjects readily adapted to both the control and discrete tasks because they were based on well-practiced driving reflexes. The noticeable lack of motion cues was offset by a realistic (actual) car interior and controls, correct vehicle response dynamics, and a large-field-of-view moving roadway perspective. Consequently, the training required was similar to that required for any new car. All subjects accepted the simulator as a plausible approximation to a real car driving situation, and they produced behavior typical of actual car driving. (These attributes have been notably lacking in many earlier laboratory investigations of alcohol effects on driving.)

Subjects were motivated by an incentive pay formula which included: a base hourly rate through training and formal sessions; and a "get home" reward per run completion, which was increased with BAC. Approximately $4/hour was earned, on the average.

Apparatus

As noted earlier an appropriate scenario for drunk driving accidents is night driving on a rural road in stormy weather, which our tasks simulated (see Fig. 1). Reference 6 gives further details. The driver sat in an actual car cab with realistic steering, accelerator, brake, and turn signal controls. The road display was a slightly shrunken (0.6 scale) view over the car's hood towards a one-lane straight road fading into the distance. The dynamic perspective was drawn on a 25 cm (10 inch) CRT 60 cm from the subject's eyes at a refresh rate of 60 Hz, so that no blur, flicker, or jerk were apparent.

Peripheral, lightable "signs" were placed at the side and overhead rear-view mirror locations (±45 deg, respectively) and at ±20 deg alongside the CRT (corresponding to signs or events adjacent to the car lane ahead on the road). These signs had small 4-letter words (i.e., [HORN], [BRKE]) which were lit by a random program to command the driver to respond accordingly (i.e., tap the

Figure 1

BLOCK DIAGRAM OF TASKS AND MEASURES

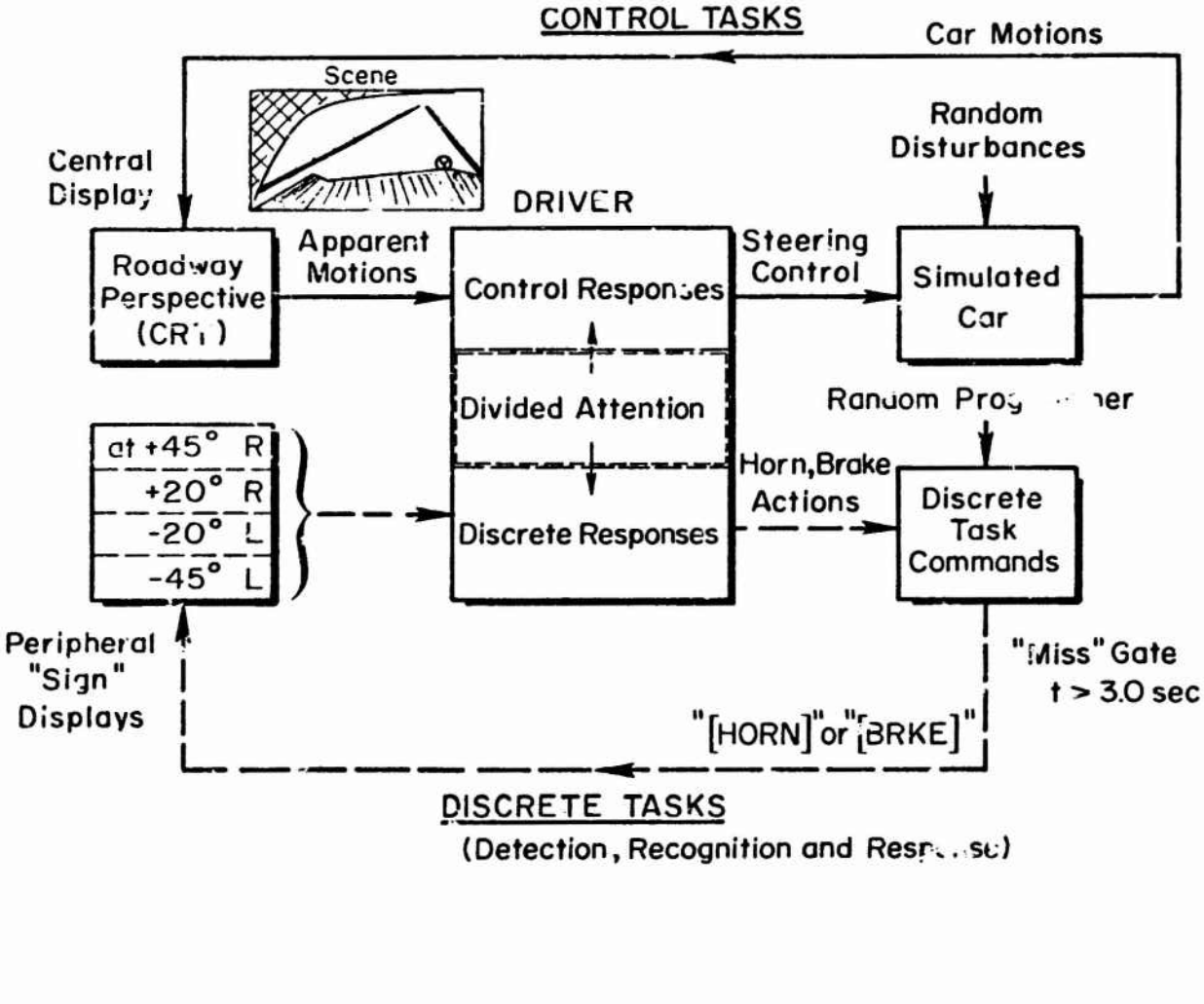

On-Line Measurement of :

Path and Heading Errors, Control Activity, ...

Describing Functions and Spectra

Steering Reversals
Signs Missed
Signs Correct
Eye and Head Motions

Data Reduction

Performance (RMS Errors)
Control Beh. Parometers

Detection ; Recognition Indices

Peripheral / Central Ratios etc.

horn ring or brake pedal). The letters were small enough (10 mm) and dimly lit so as to be just detectable parafoveally when turned on, but to require a fixation (scan) to read the discrete command. The two peripheral signs were adjusted brighter than the central pair to compensate for the cosine falloff of pupil aperture, thereby starting with **uniform detectability** across all lights at sober conditions (Ref. 12).

The dynamic response of the car-and-roadway perspective to steering control was simulated on an analog computer by two-degree-of-freedom (heading and lateral path displacement) equations of motions, set for a constant speed of 30 mph (50 km/hr). (Preliminary tests had shown that 60 mph was undrivable when intoxicated.) Unseen gust disturbances were simulated by a sum-of-five-sinusoids random forcing function. The task was subjectively like driving in strong crosswinds and was scored over a 100 sec period. Special analog and data logging equipment was developed to provide efficient on-line data reduction of path and heading errors, control activity, driver describing functions and spectra, and steering reversals. See Ref. 6 for details.

A sequence of 16 discrete sign commands was provided (4 each at 4 locations), ranging from 1-5 sec apart, with a 3 sec criterion for response time limit. The taped program was changed frequently to prevent learning of the pattern of events. A special Digital Logic Unit was developed for the discrete tasks to handle: programming, light operation, response scoring logic (misses, corrects, and response times), and data logging.

The highly compressed on-line data (roughly 30 numbers per run) were analyzed off-line by a previously developed STI program to yield a comprehensive array of performance and behavioral parameters such as: rms steering wheel activity, σ_{δ_s}; rms heading error, σ_ψ; rms path error, σ_y; crossover model fit parameters for the car/driver describing function, ω_c, ω_u, φ_M, τ_e (see Refs. 6 and 8); various open- and closed-loop describing functions, $Y_p(j\omega)$, spectra, and signal coherences, ρ^2 (remnant noise effects). This program also computes a number of discrete task measures such as: Detection Index, N_R/N (fraction of signs responded to); Recognition Index, N_C/N_R (fraction of non-missed responses which are correct); Response Time, T_R (from onset of sign to completion of response). The discrete task measures are computed for each

location and for various combinations, but only the overall averages are considered here because the peripheral and central pairs gave similar results.

For a number of runs, the STI Model EPR-2 Eye-Point-of-Regard System (Ref. 13) was used to monitor and tape record the driver's scanning behavior. This was the first known application of this device to a highly intoxicated human operator, but it worked surprisingly well and excellent data were recorded on 3 out of 4 subjects so instrumented.

Blood alcohol concentration was inferred from breath alcohol concentration, measured with an Intoximeters, Inc., Mark II Gas Chromatograph Intoximeter, which was calibrated daily against reference samples of 0.10 and 0.15 BAC. A minimum wait period of 15 minutes from the last drink was allowed for residual mouth alcohol to dissipate. The average of before- and after-run BAC's was used.

EXPERIMENTAL DESIGN

The rationale for the experimental design has been given in the Introduction. To meet the basic objectives, the main experiment contrasted the Moderate vs. Heavy drinkers at three equal levels of BAC up to just over the legal limit (0, $\doteq$ 0.06 BAC ascending, $\doteq$ 0.11 BAC maximum, $\doteq$ 0.06 BAC descending). A high-BAC session was given additionally to the heavy drinkers (0, $\doteq$ 0.11 BAC ascending, $\doteq$ 0.16 BAC maximum, $\doteq$ 0.11 BAC descending) to permit comparisons of alcohol effects at each group's maximum BAC (i.e., 0.11 BAC for Moderate vs. 0.16 BAC for Heavy drinkers).

The resulting matrix of experimental treatments is given in Fig. 2, along with a summary of other relevant conditions and tests. Each of the three types of test (Discrete, Control, and Combined Tasks) was given at each condition. Because the Moderate and Heavy groups intrinsically contain different people, the experimental design confounds Subjects with Drinking Habits, making it a nested design.

Unless a subject specifically requested otherwise (as did a few heavy whiskey drinkers), the standard drink was 80 proof vodka in orange juice for a roughly 20 percent ethanol drink, heavy in fructose for optimum absorption and elimination.

Figure 2

EXPERIMENTAL DESIGN

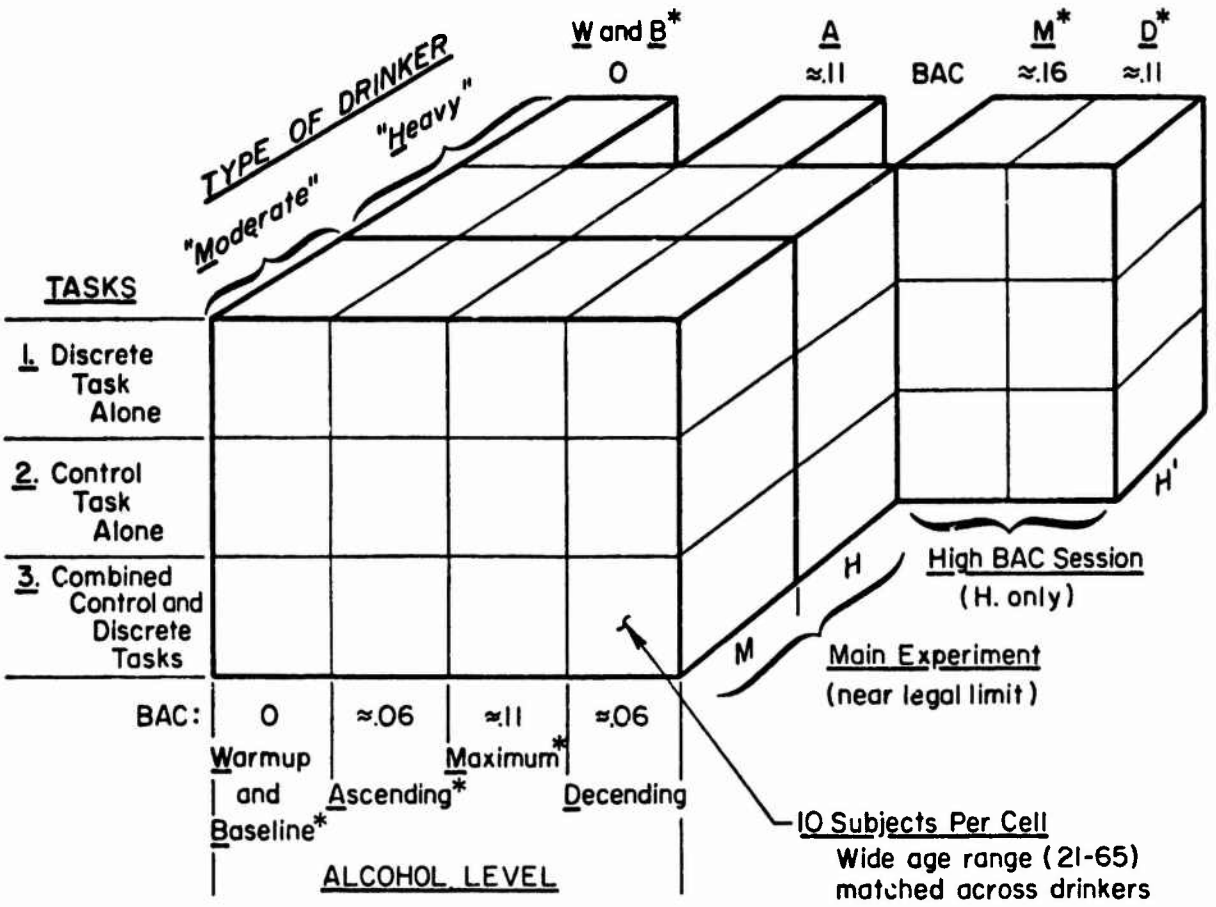

Drinks: Vodka in orange juice (20% ethanol, adjusted for weight)
3 drinks in ~3hrs; meal after maximum

Tests: BAC Measured via Gas Chomatograph Intoximeter
Driving Tests, per above (Eye motion records for 4Ss)
Clinical Sobriety Tests
Intoxication Ratings by Experimenters and Subjects

*Denotes cases used for statistical analyses herein

TABLE 2. EXPERIMENTAL PROTOCOLS

Session A. Orientation and Initial Training (4 hr)

- (Initial encounter) General briefing on overall program task description and instructions, first trials of test battery
- 2-5 additional rounds of test battery (control task only, discrete task only, and combined task)

Session B. Training (4 hr)

- Review task and instructions
- 3-4 repeat trials of test battery, until asymptotic

Sessions C, D, or E. Formal Experimental Session: Placebo, Drunk or High Drunk (8 hr)

- If AM, give light breakfast (toast and juice); if PM wait 2-3 hr from lunch
- Intoximeter check for 0 BAC
- Sober Warmup and Baseline runs — battery of driving* and clinical sobriety† tests
- Imbibe 2 vodka and orange juice drinks in 1-1/2 hr, alcohol quantity adjusted for body weight to give "Ascending" BAC level (0.06 for Main and 0.11 for Heavy Drinking Sessions)
- One Placebo‡ subject per session of 3-4 subjects
- Ascending BAC runs: driving (0.06+ for Main and 0.11+ for Heavy Sessions) and sobriety tests plus subjective questions§ and Intoximeter BAC
- Third drink, adjusted to give Maximum BAC level
- Peak BAC driving and sobriety runs: BAC = 0.11 for main and 0.16 for Heavy sessions; tests as above
- Light lunch or supper
- Descending BAC runs: at same BAC as Ascending tests

---

*Driving tests: Steering Task alone, Discrete Task alone, Combined Tasks; given in random order.

†Clinical sobriety tests: walking heel-to-toe; Rhomberg test (balance); positional nystagmus at periphery (PAN-1).

‡Placebo drink: 15 ml vodka floated on diluted orange juice mixer.

§Subjective questions: level of intoxication; capability of driving; degree of nausea and vertigo.

PROCEDURES

The protocols and sequencing of tests in each type of session are summarized in Table 2. Details of the drink administration and resulting BAC vs. time data are given in Ref. 6. Placebo drinks had 15 ml of vodka floated on the watered-down mixer to delay awareness of a non-intoxicating drink. During the Formal Experimental Sessions, from 2-4 subjects were present to lend a more sociable air to the drinking (when there were only 2 subjects an experimenter often joined their group conversationally). Despite every effort to prevent sickness (and the resulting loss of key data, as well as subject cooperation), a few cases did occur and some data cells are thereby missing on a few subjects.

RESULTS AND DISCUSSION

As noted in the Introduction, even though Control and Discrete Tasks were given along with the combined task, the present paper only discusses the combined task results, which are the most relevant for revealing differences between Medium and Heavy drinkers. Reference 6 analyzed the effects of separate vs. combined tasks in detail, for the main experiment only. The key results of that analysis apropos of our work are as follows:

- The discrete task interferes with the driving task when performed concurrently, the interference always being detrimental but small and causing differences in **degree** rather than **kind** of behavior.
- For most measures, the sensitivity to alcohol level is roughly parallel between driving tasks done singly vs. combined. Path deviations are more sensitive to BAC under combined tasks.
- Differences among placebo runs are not large or significant, meaning that time of day effects can be ignored.
- Ascending and descending BAC runs yield similar data at comparable BAC levels, thus either can be used.

So, we will consider only the **combined** control and discrete task data in this section. However, to simplify the presentation, the relatively straightforward discrete task results will be discussed first, saving the more complex control task results for last.

Before proceeding to the reduced data, let us first examine selected signals in a pair of time histories of tracking runs, sober and drunk (see Fig. 3). Points worth noting are as follows, starting at the top:

- The eye-point-of-regard fixations show that even when drunk the subject detects nearly all of the peripheral light onsets (as evidenced by a scan); however, some of the required responses are simply ignored.
- Once detected, the response is usually accurate, implying near-perfect recognition of the "sign" details.
- There are more blinks (b) sober than drunk.
- Longer scan latencies and dwells are seen at the high BAC condition, as well as some spurious scans.
- The steering and path errors both increase at high BAC, with some steering traces showing more "holds" than at sober conditions.
- The increased path error at high BAC is more of a wandering than oscillatory type, implying a looser steering control loop rather than any approach to oscillatory instability. (However, a few subjects showed occasional "weaving" of a neutral damped type.)

The parameters selected for analysis clearly reflect these qualitative observations.

Analysis of Variance

Before proceeding to the discussion of specific results, a summary is presented of an Analysis of Variance for the main experiment which covers Moderate vs. Heavy drinkers at alcohol levels up to the legal limit (BAC = 0, 0.06, 0.11; Moderate vs. Heavy drinkers with nine subjects per group). A partially-nested design was employed because a different set of subjects was necessary for the Moderate and Heavy drinking categories; otherwise there were full-factorial combinations of habit and BAC level, with nine subjects and one observation per cell. Subjects were considered a random variable, and Type of Drinker and BAC were included as fixed effects. Subjects were used as a systematic random variable in the ANOV so as to separate out any stratification in their own skill levels from the other sources under investigation (in effect, using each subject as his own experimental control).

Figure 3

TIME TRACES OF TYPICAL SOBER AND DRUNK DRIVING BEHAVIOR IN THE SIMULATOR

Legend: H = "Horn", B = "Brake", m = "miss", b = "blink"
Subject = E (young heavy drinker)

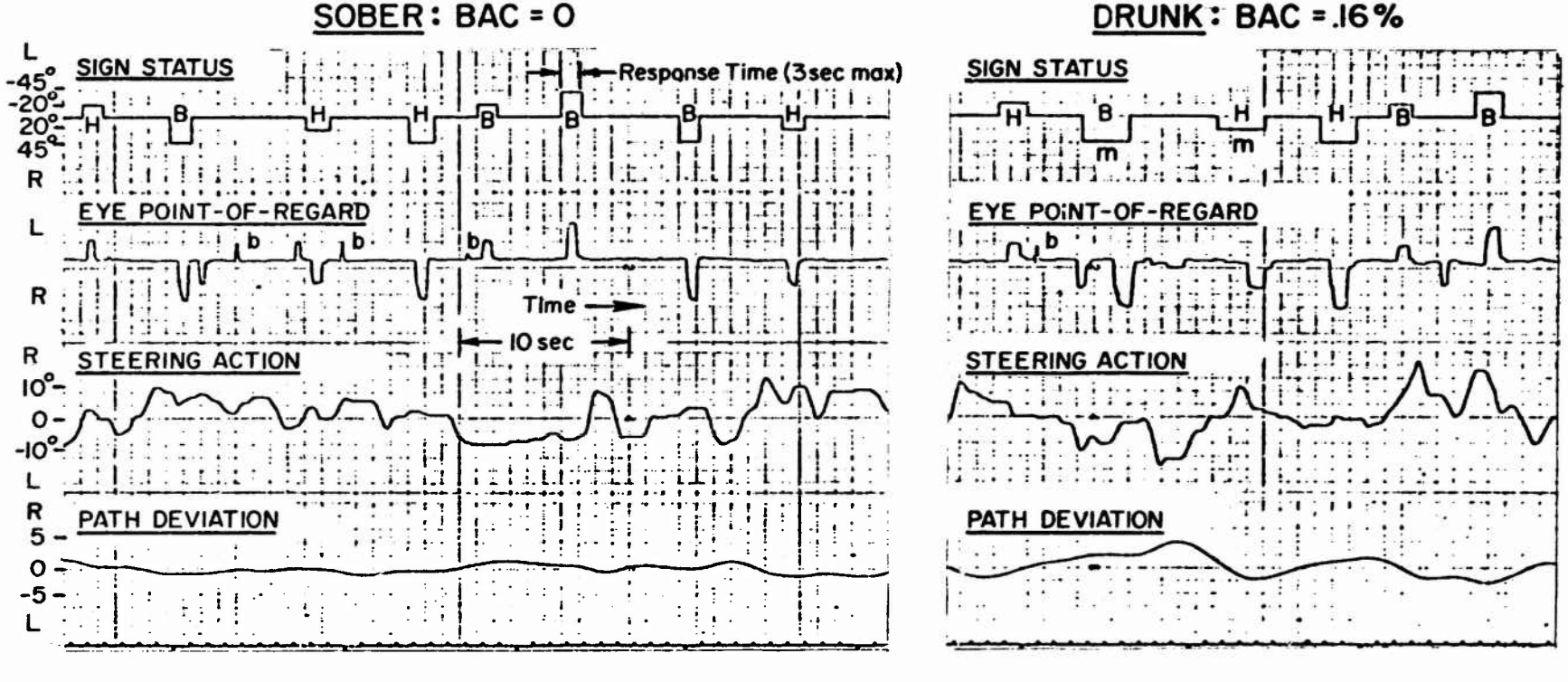

A summary of the resulting F-ratios for key measures of steering and discrete tasks, and their statistical reliability is given in Table 3. Taken across the board, this ANOV tells the following:

- The effects of BAC on both types of drinker are large and very reliable statistically.
- Averaged across all BAC up to legal limits, differences between the two drinker types are not statistically reliable.
- There are a number of parameters for which the effect of BAC was reliably different for the Moderate vs. Heavy drinkers.

Other implications of the ANOV will be used in the subsequent discussions.

Discrete Tasks

Key results from the discrete tasks are presented in Fig. 4, as a function of BAC for Moderate vs. Heavy drinkers in the main experiment and for Heavy drinkers in the high-BAC session. Cursory examinations of the data from central (±20 deg) vs. peripheral (±45 deg) locations showed only small differences, probably because the sober detectability was equalized for all angles. Thus, we will consider only the averaged data from all sign locations. Also, note that each pair of Heavy points near BAC = 0.11 lie close together, implying consistent behavior at a given BAC, because these data were measured in different sessions several days apart.

It is apparent that alcohol level does not impair discrete task performance as much as might be expected (though the impairment is very reliable, statistically), and that Moderate and Heavy drinkers appear to have different trends with BAC (although only "possibly significant" statistically). At BAC near legal limits, the Detection Index*, N_R/N (fraction of signs responded to within 3 seconds) shown in Fig. 4a, decreases about 20 percent for Moderates but negligibly for Heavies (this difference is possibly reliable; $t' = 1.4$ at 8 df, $\alpha = 0.1$). However, near their customary limits (Moderate at 0.11 BAC vs. Heavy

*In view of the evidence of peripheral detections from scanning data, N_R/N might more correctly be called the "Response Fraction."

TABLE 3. ANOV SUMMARY OF KEY EXPERIMENTAL MEASUREMENTS†
(Tables Give F-Ratios and Resulting Significance Levels)

EFFECTS OF ON → ↓	DOF† (N,D)	STEERING TASK MEASURES							DISCRETE TASK MEASURES	
		STEERING		HEADING CONTROL			PATH CONTROL			
		N_{rev}	$\rho^2_{\delta_s}$	σ_ψ	ω_c	φ_M	σ_y	$\lvert Y^*_p \rvert_{\omega = .5}$	N_R/N	T_R
BAC { 0 .06 .11	2,24	0.79 —	16.89 ***	28.99 ***	15.17 ***	0.54 —	28.46 ***	13.20 ***	5.90 **	18.95 ***
Type of Drinker { M H	1,12	1.12 —	0.59 —	0.25 —	0.61 —	0.18 —	0.39 —	0.16 —	2.26 —	1.71 —
BAC × Drinker	2,24	3.24 ?	6.91 **	2.24 —	3.22 ?	0.89 —	3.82 *	1.51 —	2.38 —	1.86 —

Values are F-ratios, symbols denote significance

DOF (N,D)	1,12	2,24	$\alpha <$	STATISTICAL RELIABILITY	
If F-ratio =	3.18	2.54	0.10	Possibly reliable	?
	4.75	3.40	0.05	Probably reliable	*
	9.33	5.61	0.01	Reliable	**
	18.6	9.34	0.001	Very reliable	***

†This analysis corresponds to a nested experimental design, with subjects nested within the drinker type categories. Subjects were further subdivided into age categories, however these results are not considered here. Subjects were considered a random variable and subject interaction terms were used as the F-ratio denominators.

Figure 4

DISCRETE TASK PERFORMANCE VS BAC AND HABITS

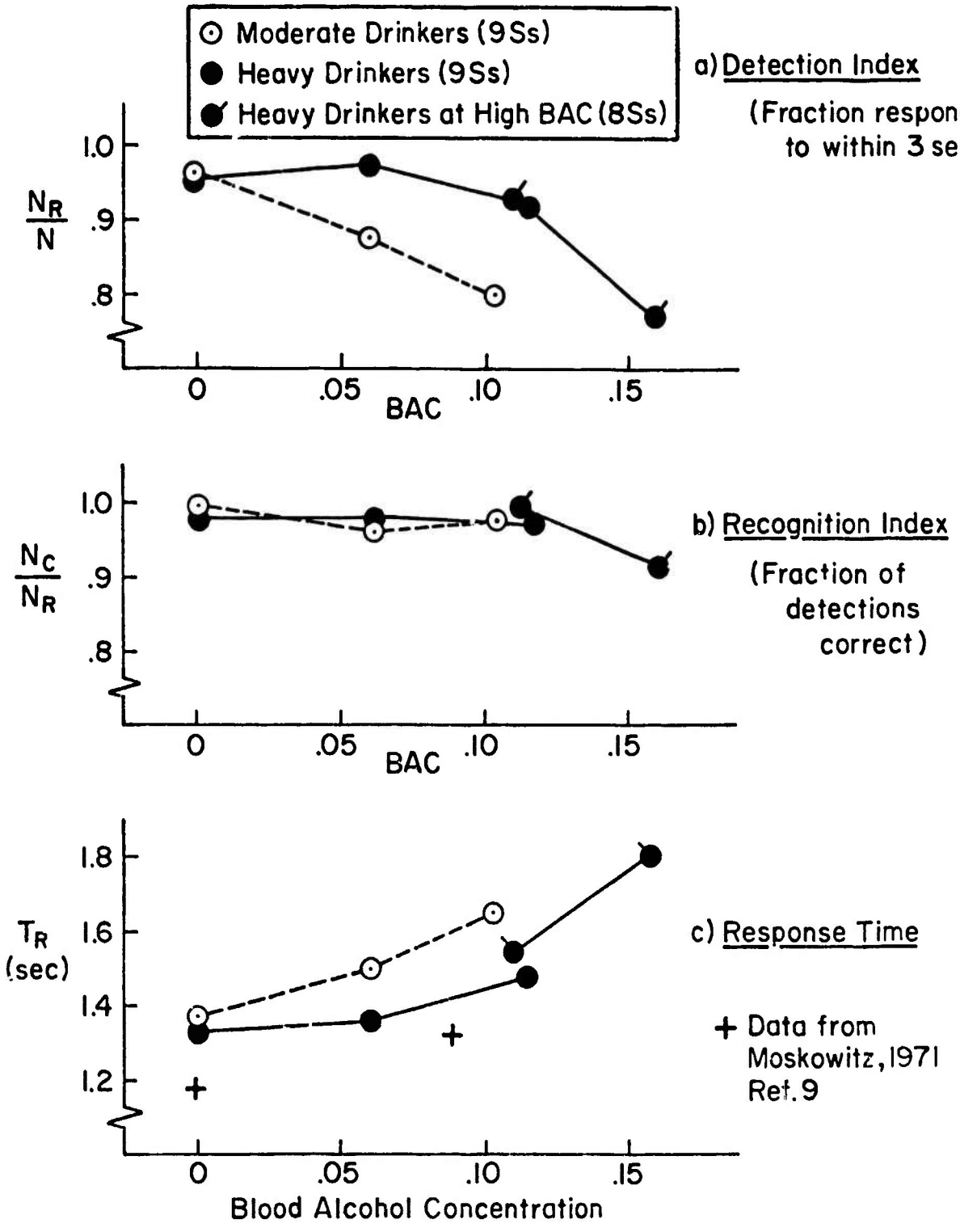

P-151

at 0.16 BAC), the Heavy drinkers' performance deteriorates to a slightly worse degree than does that of Moderate drinkers (not statistically reliable; $t' = 0.6$, 8 df; $\alpha > 0.1$).

The "Recognition Index," N_C/N_R (fraction correct of those not missed), shown in Fig. 4b, remains within a few percent of 1.00 for Moderate or Heavy drinkers up to BAC = 0.11, beyond which the Heavy drinkers show a small (6 percent) deterioration. This somewhat surprising result is consistent with the eye-point-of-regard data (discussed in connection with Fig. 3). Our interpretation is that most BAC-caused misses are due neither to lack of peripheral detection (all signs are fixated) nor to poor pattern recognition (because $N_C/N_R \doteq 1.0$); therefore, they must be due to the driver being excessively late, or even omitting the motor response — another manifestation of an "indifference threshold" effect noted in Ref. 6 and later herein.

This interpretation finds support in the Response Time data of Fig. 4c, where at legal limit BAC's, the Moderate drinkers show a 20 percent and the Heavy drinkers a 12 percent increase. Nearer their limit (BAC = 0.16) the Heavy drinkers show a 35 percent increase over their sober response time levels. As noted for the Detection Index, the response times of Heavy drinkers are impaired less than Moderates at near-legal limit BAC's, but are more impaired at BAC's nearer their drinking limits.

As the average response times increase from around 1.3 sec near 0 BAC to 1.5-1.8 sec at higher BAC's, some misses ($T_R > 3.0$ sec) will be expected from the longer-time "tails" of the T_R distributions, even though recognition remains nearly perfect. The trends in the M vs. H data for N_R/N and T_R in Fig. 4 are consistent with this explanation below 0.11 BAC, and should be further investigated using eye-point-of-regard data. As a tie-in with other related data, the open crosses in Fig. 4c are the response times from a roughly similar experiment conducted recently by H. Moskowitz at the UCLA Insitute of Traffic Engineering (Ref. 9). (In that experiment the subject, in a driving simulator, was asked to respond to a pair of colored lights mounted on the sun visor at ±15 deg off center by pressing up or down on one of a pair of turn-indicator-like switches.) Although the levels differ slightly, the trend with BAC is quite similar and indicates that our data are compatible with that from other investigators.

Steering Tasks

Performance Measures. Figure 5 presents the most important measures of overall steering task performance. Although the plots progress from the inner to outer loops (steering, heading, path), it is more instructive to consider them in reversed order. Just as for the discrete task data, the tie-in at the two Heavy drinker sessions near 0.11 BAC is excellent, indicating reliable data for the steering tasks.

Considering the path deviations of Fig. 5c first, it is apparent that alcohol seriously impairs the control performance of both Moderate and Heavy drinkers (ANOV: $\alpha < 0.001$). Furthermore, over the 0-0.11 BAC range, the differential effects of alcohol on Moderate vs. Heavy drinkers are statistically reliable ($\alpha < 0.05$).

On the right of Fig. 5c is noted the probability (computed on the basis of a Gaussian path-error distribution) that at any given time some portion of a standard size car 80 in. = 2m width may exceed a 12 ft (2.7 m) lane width. It is apparent that sober drivers will stay well within their lane, but drunk drivers may not. For Heavy drinkers this chance of lane exceedance goes from around 1 in 10,000 when sober to 1 in 100 near legal-limit BAC (0.11), and to 1 in 10 near their maximum levels (0.16 BAC). For Moderate drinkers the chance of lane exceedance grows more rapidly; from less than 1 in 10,000 when sober to around 1 in 20 when near legal limit (0.11 BAC). From another point of view, these results imply that, at near-legal limits of alcohol (0.11 BAC), experienced Heavy drinkers have on the order of one-fifth the lane exceedances as Moderate drinkers; but at levels of alcohol near each group's likely (nausea) limits the Heavy drinkers will have twice the number of lane exceedances of Moderate drinkers.

The heading deviations shown in Fig. 5b also increase drastically and reliably with BAC (ANOV: $\alpha < 0.001$). Again, Moderate drinkers show more sensitivity to BAC than Heavy drinkers (but the interaction is not quite statistically reliable), and here, too, Heavy drinkers perform better than Moderates at legal levels of BAC but significantly worse than Moderates at more customary limits ($t' = 2.2$, 8 df; $\alpha < 0.05$).

Figure 5

STEERING PERFORMANCE MEASURES VS BAC

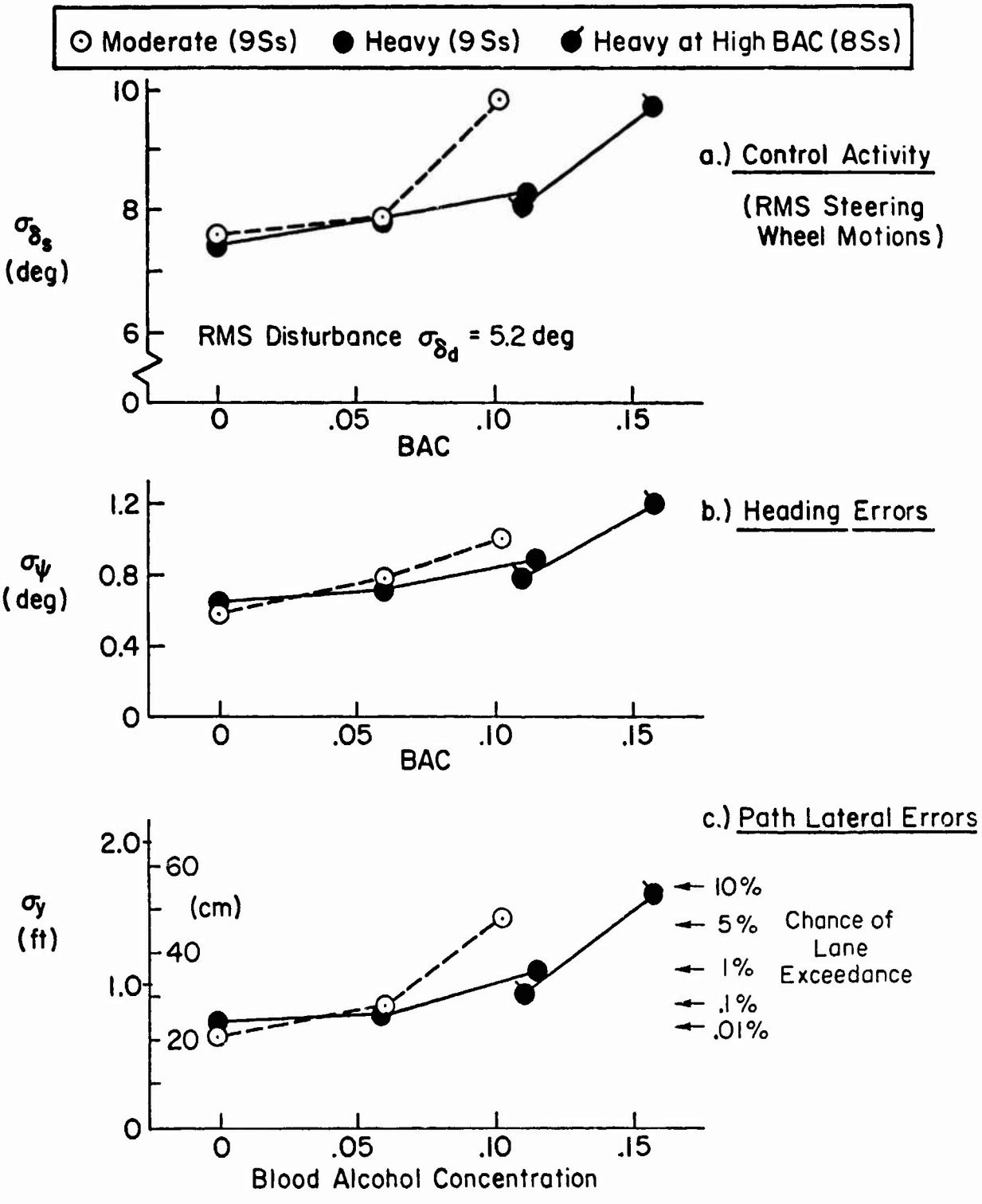

In both heading and path control the Moderate group performed slightly better when sober than the Heavy group. This difference is not statistically significant ($t' < 1.0$, $\alpha > 0.10$), but it masks any overall differences between the general performance of Moderate vs. Heavy drinkers at BAC < 0.06. It was observed that a number of Heavy drinkers performed better (in σ_y) at 0.06 BAC than when sober. (In the light of Figs. 4b and 4c, it might be more correct to say some Heavy drinkers performed slightly worse when sober than with a slight amount of alcohol.) This would tie in with anecdotal observations that some Heavy drinkers are "nervous" or "jumpy" when sober, and "calm down" at mild BAC levels. Detailed data on each individual are available to follow up on these leads, but we have not yet done so.

Lastly, consider the control activity performance σ_{δ_s}, given in Fig. 4a. If the driver perfectly cancelled the steering disturbance inputs, his score would be constant at $\sigma_d = 5.2$ degrees of steering wheel motion. In practice, he can cancel out low frequency disturbances (i.e., frequencies well below the unity-gain-crossover frequency, ω_c), but will lag and overshoot his corrections near ω_c, and will attenuate those above ω_c. In addition, any spurious steering actions such as "holds," "dither" or "limiting" will add remnant noise to the σ_{δ_s}. Since so many factors can influence σ_{δ_s} it serves mainly as an indicator of seriously excessive corrections; or if it drops, it indicates that the driver is not even attempting to correct most disturbances, and is in effect opening the heading control loop. Our results show that control activity always exceeded the disturbance-cancelling value, and was increased on the order of 20 percent at higher BAC's. As before, the Heavy drinkers show less sensitivity to BAC than Moderate drinkers at legal-limit levels, and comparable sensitivity at maximum BAC's.

Figure 6 shows additional performance measures of insightful value. At the top are shown the coherence data for steering activity and heading. "Relative remnant" (the fraction of noise in the total signal power) is measured by the complement of the coherence, as shown on the righthand scales. These data (with the ANOV of Table 3) imply that alcohol reliably increases relative steering remnant, but only at levels above 0.06 BAC for Moderate drinkers and above 0.11 BAC for Heavy drinkers. Overall, the effects of BAC on coherence are smaller than one might expect considering

Figure 6

CONTROL COHERENCY AND STEERING REVERSAL RATE VS BAC

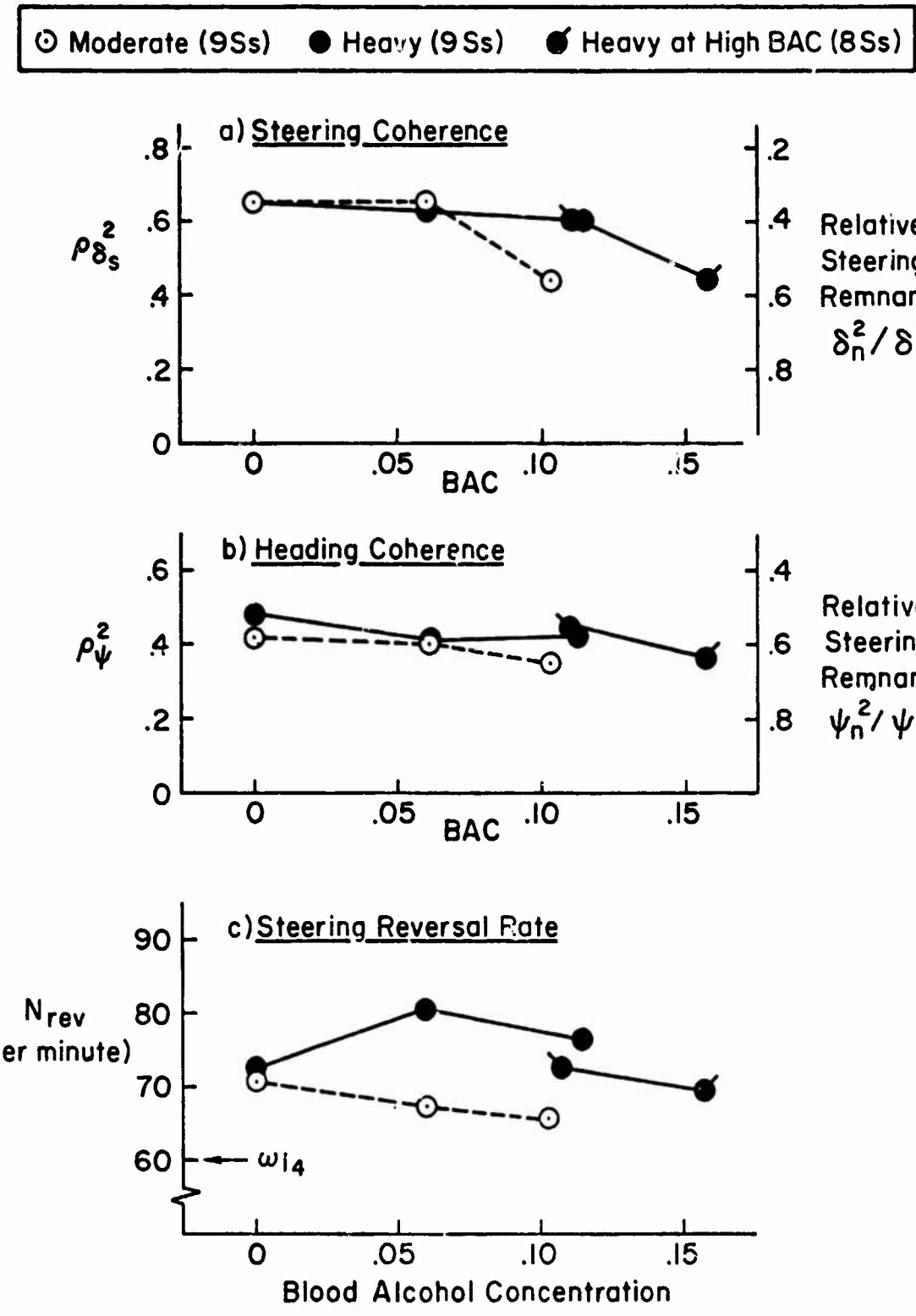

P-151

the more nonlinear appearance of the time traces. Apparently, this is explained by the fact that the increased remnant mainly reflects a constant proportion of increased linear errors.

We recorded steering wheel reversal rate, N_{rev}, (presented conventionally as + or -- reversals per minute for small reversals) for comparison with other investigators who use this measure of steering activity (e.g., Refs. 9 and 10) and these are shown in Fig. 6c. There is not much variation with BAC (note the suppressed origin scale), although there appears to be a slight rise in N_{rev} for Heavy drinkers at low BAC. (The ANOV implied no significant effects of BAC on Moderat vs. Heavy, but their differences at 0.11 BAC are possibly reliable.) Also shown is the nearest input frequency (ω_i = 6.28 rad/sec) which might possibly influence (stabilize) the steering reversal counts.

As a matter of interest, a rough estimate of the closed heading loop frequency was made, which turns out to be around ω_{CL} = 3.5 rad/sec. If the damping ratio is low (as the low phase-margin data presented later implies), then a spectral peak due to circulating remnant would occur at this frequency, and it might give rise to steering reversal rates of N_{rev} = 65-70 per minute, just in the range observed! This possibility is worthy of further investigation as a simple indicator of car/driver closed-loop bandwidth.

Driver Behavior Data (Describing Functions). As noted earlier, several factors can influence the overall measures of driver control performance, because these are intrinsically closed-loop measures wherein the output characteristics (e.g., path error) are a product of the input spectrum and level, the car/driver dynamics (measured via the frequency response describing functions), and the injected remnant (noise) contributions which circulate around the heading and path control loops (see Ref. 8 for the complex details). An essential ingredient in understanding the net effects of alcohol on performance is its effect on the driver's describing function, $Y_p(j\omega)$, with a realistic roadway dynamic perspective display to the perceptual system and with realistic car dynamic response properties in heading and path. Such describing function measurements have been made for every run and they clearly show the effects of alcohol. Reference 6 presents typical examples of $Y_p(j\omega)$ averaged over numerous subjects, and shows that a few key parameters suffice

to model their salient features. Some findings from Ref. 6 relevant to this discussion are the following:

- The driver's describing function can represent the sensitivity to both heading and path deviations, these being reflected in the gains, $|Y_p|$, at, respectively, high ($> \omega_c$) or low ($< \omega_c$) frequencies.

- Alcohol causes reductions in both heading and path gain, but mostly in path gain, best characterized by $|Y_p|$ at 0.19 rad/sec and/or 0.5 rad/sec, the latter being more reliable.

- Alcohol causes only small changes in phase lags below or near ω_c because decreases in neuromuscular subsystem bandwidth at higher frequencies are somewhat offset by their lower damping ratio (e.g., see also Ref. 11). As a result, the 180 deg phase crossover frequency, ω_u, is a better indicator than effective delay, τ_e, of the reduction in maximum driver bandwidth as limited by neuromuscular delays.

- Alcohol affects stability margins (phase or gain margins) surprisingly little when averaged across all types of subjects.

We will present some additional describing function data over Ref. 6 to extend these findings to higher BAC, and to investigate differences between drinking habits. Figure 7 gives the describing function parameters representing the driver's: bandwidths ($\omega_u \sim$ maximum bandwidth; $\omega_c \sim$ actual bandwidth — also to heading deviation sensitivity); stability margin, Φ_M (margin in phase lag relative to 180° = instability); and path error sensitivity (magnitude of $Y_p(j\omega)$ at 0.19 and 0.50 rad/sec).

At the top of Fig. 7 the bandwidths ω_u and ω_c both show a monotonic reduction with BAC which is very reliable statistically ($\alpha < 0.001$, Table 3). The Heavy-drinker data show that this trend extends to 0.16 BAC, with no sudden dropoff apparent. In fact, somewhat unexpectedly, ω_u tends to level off at 0.16 BAC, implying no drastic neuromuscular impairment at heading control frequencies. Moderate drivers start out at 0 BAC with slightly better bandwidths which decrease with BAC faster than for Heavy drinkers. This interaction is possibly reliable ($\alpha < 0.1$, Table 3), but the bandwidths averaged over 0-0.11 BAC are no different for Moderate and Heavy drinkers.

Figure 7

CONTROL-LOOP AND DESCRIBING FUNCTION PARAMETERS VS BAC

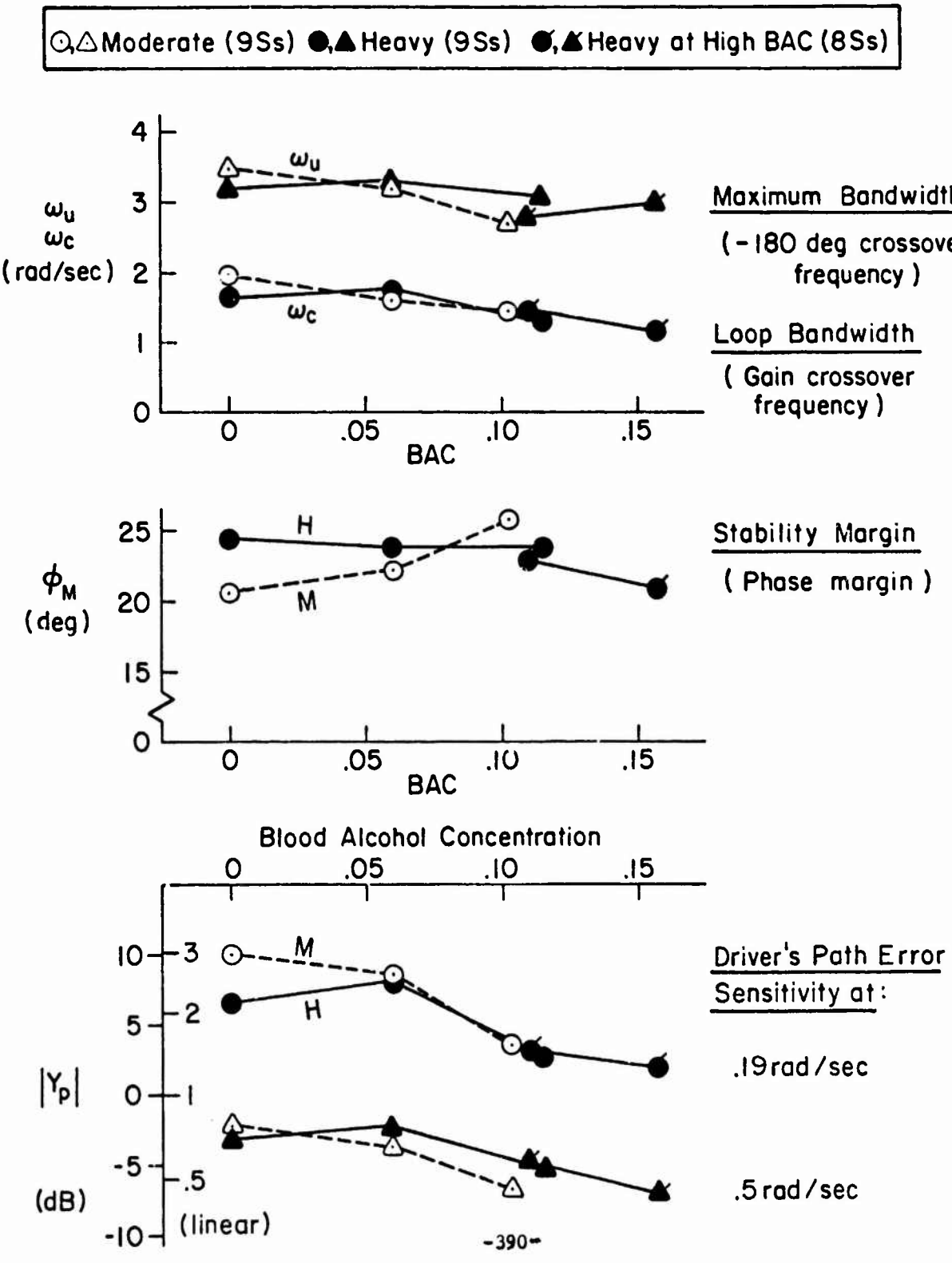

Figure 7b shows that the stability margins (φ_M) for Heavy drinkers fall off very slowly with alcohol, while those for Moderate drinkers actually seem to increase slightly up to 0.11 BAC (these effects are not statistically significant). Since the gain margin (roughly measured by the ratio of ω_c/ω_u) is slightly reduced for 0.11 BAC, while phase remains about constant, these gain and phase margin effects reflect a more conservative control strategy at high BAC.

Finally, the path-sensitivity data at the bottom of Fig. 7 show a strong and consistent reduction with increasing BAC, the reduction relative to sober BAC being slightly more for Moderate than Heavy drinkers (main BAC effect very reliable, $\alpha < 0.001$; interaction not so, per Table 3). Considering the linear ratio scale of Fig. 7c, it is apparent that, typically, the path sensitivity decreases, from 100 percent at 0 BAC to about 70 percent at 0.11 BAC and 50 percent at 0.16 BAC, with Heavy drinkers being less sensitive than Moderates.

An hypothesis is proposed in Ref. 6 that an increase of the driver's "indifference threshold"* and/or more "intermittency of attention"† could account for a number of the behavioral and performance effects of alcohol (e.g., lower gains, small phase effects, constant stability margins, more remnant, larger errors of a wandering rather than oscillatory type, etc.). The present results for Heavy drinkers up to 0.16 BAC are consistent with the Ref. 6 trends and support the same conclusions. Further, the observed relative insensitivity of phase lags near ω_c and decreased control coherency are consistent with the simple compensatory tracking data of Ref. 11 at BAC < 0.08.

Taken as a whole our results, for discrete-plus-control tasks which crudely simulate driving on rural roads at night in stormy weather, show

---

*Indifference Threshold ≡ thresholds in a perceptual motor control loop which are not specifically sensory or proprioceptive thresholds, e.g., control inaction while the error is within some tolerance zone (Ref. 14).

†Attentional Intermittency ≡ switching of control attention frequently, and usually asynchronously, from task to task (or loop to loop), often (but not always) evidenced by eye-point-of-regard or control inactivity (e.g., Ref. 15).

reliably increasing impairment of driving performance and skill as alcohol levels reach and exceed typical legal limits, near 0.11 BAC. Heavy drinkers show less sensitivity than Moderate drinkers at legal limits but are more impaired than Moderates when compared near each group's cusomary drinking habits.

SUMMARY AND CONCLUSIONS

Summary

A simplified laboratory driving simulator was developed to test both types of tasks used in driving a car on the open road: a continuous compensatory "steering task" to regulate against heading and path deviations; and an intermittent "discrete response task" requiring detection, scanning, recognition, and response (e.g., horn and brake operations). The description of this simple simulator, with an investigation of the basic effects of alcohol up to 0.11 BAC for 18 subjects under different task loadings (steering task alone, discrete task alone, and combined tasks requiring divided attention), is given in a companion paper (Ref. 6).

The objective of the present experiment, which formed the main facet of the overall investigation, was to determine if there is a difference in driving performance (and the underlying behavior) on the basis of an individual's drinking habits. This objective was successfully met, using a typical cross section of 20 licensed drivers who drink either moderately or heavily. They were divided into two drinking habit groups of 10 each (balanced as well as feasible for representative IQ and wide age range): Moderate drinkers (usually exceeding 0.05 BAC and occasionally reaching 0.10+ BAC); and Heavy drinkers (usually exceeding 0.10 BAC and occasionally exceeding 0.15+ BAC). Light drinkers (rarely exceeding 0.05 BAC) could not be tested at the desirable legal limit level of 0.10+ BAC due to excessive nausea. The main experiment compared Moderate vs. Heavy drinkers at BAC = 0, 0.06, and 0.11; the maximum just exceeds a common legal limit of BAC, and was very near the maximum limit for most of the Moderate drinkers due to nausea or other reasons. A separate session took the Heavy drinkers to 0, 0.11, and 0.16 BAC, the maximum being near their customary limit. (Serious problem drinkers or alcoholics were not tested.) Two subjects could not complete their runs.

The combined (divided attention) task analyzed herein included steering control against random disturbances, plus discrete commands (to tap the horn or brake) appearing randomly on small peripheral signs at locations corresponding to the road edges (±20 deg) and rear view mirror (±45 deg). The scenario was driving a rural road on a stormy night. Several parameters were measured including: heading, path, and steering deviations; driver's describing function and coherency; and discrete task detection index, recognition index, and response time. Discrete response and steering signals were recorded for all runs, plus eye-point-of-regard signals for selected subjects. As a target of opportunity, clinical ratings and tests of sobriety were also logged, but these have not yet been analyzed. Generally speaking, the data are quite repeatable (e.g., same group on separate sessions), are self-consistent (e.g., within tasks and drinking-habit groups), and show some effects very sensitive to BAC and to type of drinker.

Conclusions

The major conclusions from this experiment are as follows:

- At sober conditions (including one set of placebo runs during each session) there were no significant differences between the Moderate and Heavy drinkers. The chance of lane exceedance by some part of the car is less than 0.0001 for both groups when sober.

- Alcohol levels above common legal limits (0.11 to 0.16 BAC) cause very appreciable and statistically reliable **impairments** of the driving performance of both Moderate and Heavy drinkers, in particular to: path and heading deviations; driver's sensitivity to errors in path and heading; steering remnant; and discrete task misses and response times. Driver control loop stability margins, discrete task recognition accuracy, and steering wheel reversal rate are <u>not</u> changed significantly.

- Compared at legal limit alcohol levels (0.11 BAC), Heavy drinkers tend to be less impaired in the above measures than Moderate drinkers (probability of lane exceedance of 0.01 vs. 0.05); but compared near their customary drinking limits (0.11 BAC for Moderate vs. 0.16 BAC for Heavy drinkers) the Heavy drinkers are usually <u>more</u> impaired than Moderate drinkers (chance of lane exceedance of 0.10 vs. 0.05).

- The above effects could be explained by alcohol-induced increases in the driver's "indifference threshold" and/or more "attentional intermittency," plus some reduction in neuromuscular bandwidth at higher BAC.

- Eye-point-of-regard measurements showed that, in these reasonably stressful, combined steering and discrete tasks, the driver does not search (scan) for discrete events; rather he fixates primarily on the road ahead and detects "interesting" events peripherally, then fixates the event, recognizes it (usually perfectly), then makes the required response (sometimes late or ignored at high BAC).

- Peripheral discrete task data at ±45 deg were usually within 10 percent of those at ±20 deg at BAC = 0.11, partly because the outer sign brightness was increased for equal just-detectable levels when sober.

- The rate of steering wheel reversals corresponds roughly to the car/driver's closed heading loop frequency and follows a similar small decrease at higher BAC.

- The response time and describing function data tie in well with other investigators' results on similar setups.

REFERENCES

1. Driving Performance Impairment in Heavy Versus Light Drinkers, National Highway Traffic Safety Admin., Dept. of Transport., RFP NHTSA-2-B640, 17 Feb. 1972.

2. Borkenstein, R. F., R. F. Crowther, R. P. Shumate, W. B. Ziel, and R. Zylman, The Role of the Drinking Driver in Traffic Accidents, Dept. of Police Admin., Indiana Univ., 1964.

3. Perrine, M. W., Julian A. Waller, and Lawrence S. Harris, Alcohol and Highway Safety: Behavioral and Medical Aspects, Univ. of Vermont, Dept. of Psychology, Sept. 1971.

4. Alcohol and the Impaired Driver: A Manual on the Medicolegal Aspects of Chemical Tests for Intoxication, A.M.A., Chicago, Ill., 1970.

5. Hurst, P. M., "Estimating the Effectiveness of Blood Alcohol Limits," Behav. Res. in Highway Safety, Vol. 1, Summer (1970), pp. 87-99.

P-151

6. Allen, R. Wade, Henry R. Jex, Duane T. McRuer, and Richard J. DiMarco, "Alcohol Effects on Driving Behavior and Performance in a Car Simulation," presented at the Tenth Annual Conference on Manual Control, AFIT, Wright-Patterson AFB, Ohio, April 1974.

7. Klein, Richard H., and Henry R. Jex, Effects of Alcohol on a Critical-Tracking Task Using Unstable Controlled Element Dynamics, Systems Technology, Inc., P-143, Nov. 1973.

8. McRuer, Duane T., David H. Weir, Henry R. Jex, Raymond E. Magdaleno, and R. Wade Allen, "Measurement of Driver/Vehicle Multiloop Response Properties with a Single Disturbance Input," Ninth Annual Conference on Manual Control, Mass. Inst. of Tech., Cambridge, Mass., May 23-25, 1973.

9. Moskowitz, H., The Effects of Alcohol on Performance in a Driving Simulator of Alcoholics and Social Drinkers, UCLA, Inst. of Transport. and Traffic Engrg., Rept. 7205, Dec. 1971.

10. Platt, Fletcher N., and Bruce D. Greenshields, Objective Measurements of Driver Behavior, SAE Paper 809A, Jan. 1954.

11. Reid, L. D., M. K. F. Ibrahim, R. D. Miller, and R. W. Hansteen, The Influence of Alcohol and Marijuana on a Manual Tracking Task, SAE Paper No. 730092, Jan. 1973.

12. Haines, Richard F., "Dimensions of the Apparent Pupil When Viewed at Oblique Angles," Amer. J. of Ophthamology, Vol. 68, 1969, pp. 649-656.

13. Klein, Richard H., and Henry R. Jex, "An Eye-Point-of-Regard System for Use in Scanning and Display Research," 15th Annual Tech. Symposium of the Society of Photo-Optical Instrumentation Engrs., Aug. 1970.

14. McRuer, Duane T., and Ezra Krendel, Dynamic Response of Human Operators, WADC TR 56-524, Oct. 1957.

15. Allen, R. W., W. F. Clement, and H. R. Jex, Research on Display Scanning, Sampling, and Reconstruction Using Separate Main and Secondary Tracking Tasks, NASA CR-1569, July 1970.

AN EVALUATION OF A PREDICTOR USED WITH TWO DIFFERENT AIRCRAFT MAP DISPLAY ORIENTATIONS

D. L. Baty

Ames Research Center, NASA

ABSTRACT

Six airline pilots participated in a fixed base simulator experiment designed to study the advantages and disadvantages of incorporating a simple horizontal flight path predictor on both fixed and rotating electronic CRT map displays.

The pilots were asked to fly a modified "figure eight" ground track (similar to right and left procedure turns in sequence) while attempting to maintain constant altitude. The dynamics were representative of a transport aircraft. All flight information was displayed on one 17-in. (43-cm) CRT monitor. The controlled variables were: (1) map orientation; (2) pilots; (3) presence or absence of crosswinds; (4) presence or absence of wind gusts; (5) presence or absence of predictor. Error scores were recorded as deviations from the commanded ground track and altitude.

Pilot comments and ratings were also obtained. No interaction in performance scores was found between the predictor and the two different map display orientations. It was found that the predictor reduced deviations from the commanded ground track, narrowed performance differences among pilots, narrowed the error differences found with and without crosswinds, and decreased pilot workload.

INTRODUCTION

This study is a continuation of research directed toward establishing the role(s) of a pictorial map display in the commercial aircraft cockpit of the 1980s. Whether the map display is to be used as a primary flight instrument, or as a status apprisement/monitoring display, or both, depends in large part upon the compatibility of the various possible map display modes with the rest of the cockpit displays. The pilot must be able easily to assimilate the information on the map with the information from his other displays. Also, the method of map presentation should not introduce any perceptual conflicts that could lead to a blunder. A series of part-task studies was planned to investigate this compatibility and to obtain data and experience from which recommendations can be made concerning certain map display options for evaluation in a full mission simulation.

The first experiment in the series measured the effect of horizontal situation (ground path) predictor information on manual piloting performance while executing a standard instrument procedure turn.[1] The second experiment studied the effect of two other variables on manual piloting performance.[2] These variables were: (1) the position of the map display relative to the Vertical Situation Display (VSD) and, (2) the orientation and motion characteristics of the map displayed. The present experiment combined elements of

these two experiments, incorporating a predictor element into the simulation environment of the map position/orientation experiment with its choice of map displays and a more realistic aircraft simulation.

The primary purposes of this experiment were to further assess the positive utility, as well as any possible negative effects, of incorporating a flight path predictor on two different map displays. Specifically there were five major hypotheses:

1. The use of the predictor would improve overall task performance. Counter to this hypothesis was subjective opinion that the predictor could be sufficiently demanding of attention that, with certain conditions, measured performance could be poorer.

2. There would be no predictor/map orientation interaction. This hypothesis was based on the finding of no significant difference among three different map orientations in a prior experiment.[2] However, the importance that would be attached to any positive finding of interaction made this check a major objective of the experiment.

3. The use of the predictor would reduce the differences in performance among pilots. Possible homogeneity of performance among pilots could be another factor leading to justification for specifying more narrow flight corridors.

4. The use of the predictor would reduce the differences in tracking performance normally found between significant crosswind conditions and no wind conditions.

5. The presence of simulated wind gusts would not significantly affect performance for any condition. Wind gusts were included primarily to assess any annoyance factor related to the predictor element. (Possible interactions with other predictor types were not investigated.)

In addition to these major hypotheses there was interest in assessing the effect of the predictor on two other items. The first was to determine whether the predictor element had any effect on pilot workload. The second was to determine whether the tendency toward blunders (control reversals in this case) would be affected. The strength of the check on these two items was not as high as for the formal hypotheses, relying more on observation and pilot comment.

TASK AND PROCEDURES

Task and Displays

The task was to fly from point A to point B, as in Fig. 1, following the 360°, 315°, 135°, 180°, 225°, 045° and 360° legs in that sequence while maintaining constant 960 ft (292 m) altitude. The dynamics were representative of a transport aircraft. Throttle setting remained constant with a nominal airspeed of 160 knots. In the absence of crosswinds, a nominal 25° bank angle was required in the turns. All flight information was displayed on a 17-in. (43-cm) CRT monitor. The display was generated by an Evans & Sutherland LDS-2 graphics display computer using an SEL 840 as the main computer.

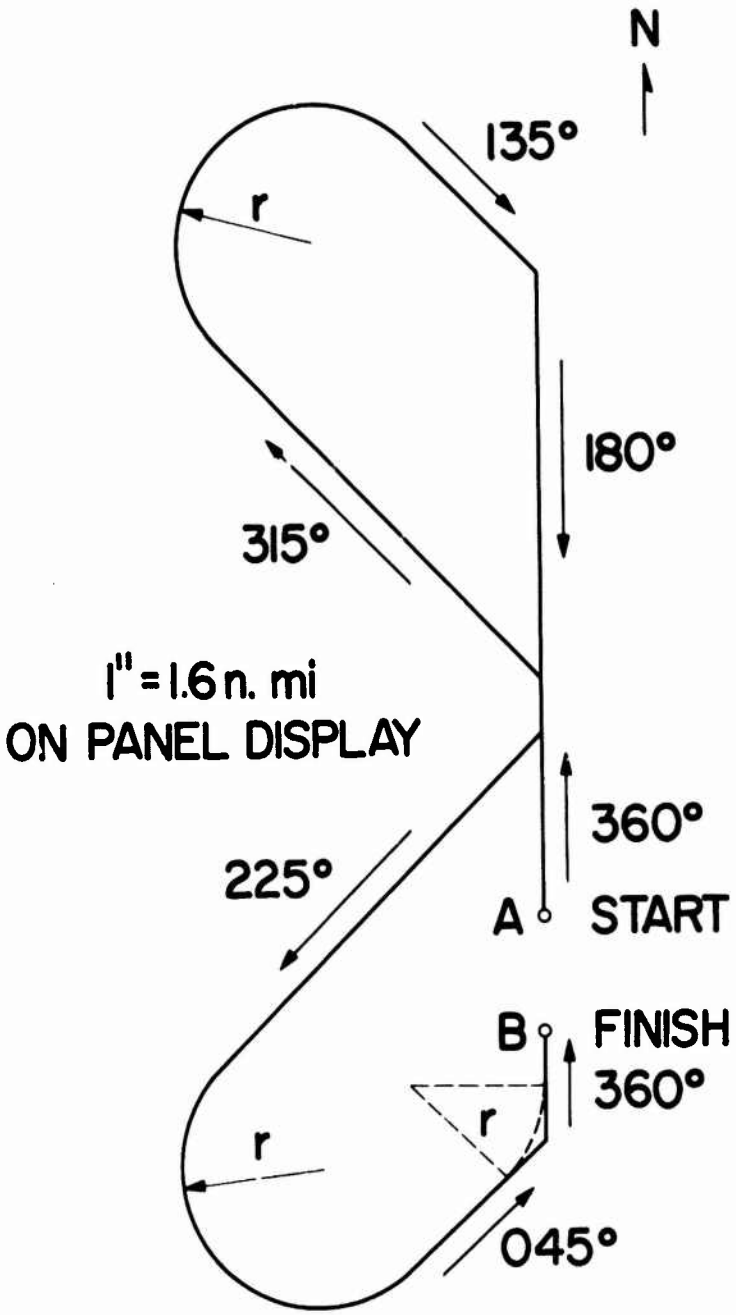

Fig. 1. Reference ground trajectory

Aircraft dynamics and scoring procedures were also generated by the SEL 840. Appropriate force-feel characteristics were provided by a hydraulic control loader system. Figure 2 is a photograph of the simulator interior.

Both the Vertical Situation Display (VSD) and the Horizontal Situation Display (HSD) were contained within 5-in. (12.7-cm) squares. Figure 3 is a photograph of the VSD with labels describing the display elements. The number at the top left corner of the display shows airspeed in knots. The center number is aircraft heading in degrees. The top right number is altitude in feet, and the number just below altitude is the vertical speed readout in feet per minute. The aircraft symbol remained fixed in the center of the display with pitch and roll indicated by movement of the horizon, ground plane lines, and pitch lines. The altitude error bar moved across the scope in the vertical direction only. A zero altitude error was indicated when the error bar was centered over the center square of the aircraft symbol. Motion from the center position to the end of the bar in either direction indicated a 100-ft (30.5-m) error. The aircraft was 100 ft (30.5 m) too high when the top end of the bar was just touching the square (i.e., the bar below the aircraft symbol) and 100 ft. (30.5 m) too low when the bottom end of the bar was touching the square, a sensitivity of approximately 250 ft/in. (30 m/cm). The rectangle of the turn rate indicator moved horizontally. Center position indicated zero turn rate and a 3°/sec turn was indicated with the rectangle centered over the right or left bar.

Figure 4 is a photograph of the HSD with labels describing the display elements. The primary display elements were the reference ground trajectory, the aircraft symbol, and the predictor element. The aircraft symbol gave both heading and position information. The aircraft position was the junction point of the wings and body. The other symbols were present to provide a touch of realism and to provide background display motion, which was considered particularly important for the condition when the aircraft remained in the center of the display during flight. For this condition, the map translated and additional symbols, not shown here, would come into view at different points along the flight. The map scale is 1.6 n.mi./in. (1170 m/cm). The predictor will be explained in more detail under "Experimental Variables."

One additional feature was shown on both the VSD and HSD to aid in timing the start of the turns. Approximately 5 sec before the transition point from a straight-line section of the reference ground trajectory to a circular section, the center square of the VSD aircraft symbol and the aircraft symbol on the HSD both began to flash at a 2-Hz rate. Figure 1 shows that there are two turns of 180° and four turns of 45°. For the 45° turns, the flashing began 5 sec before the tangent point of a circle with the same radius as the 180° turns. This is illustrated on Fig. 1 at the 045° to 360° heading transition.

Experimental Variables

Map orientation:

1. North up, fixed map (0_1). With this condition, all elements were fixed, the only moving symbols being the aircraft, which moved around the course to indicate present position and heading, and the predictor element (when used).

Fig. 2. Simulator interior

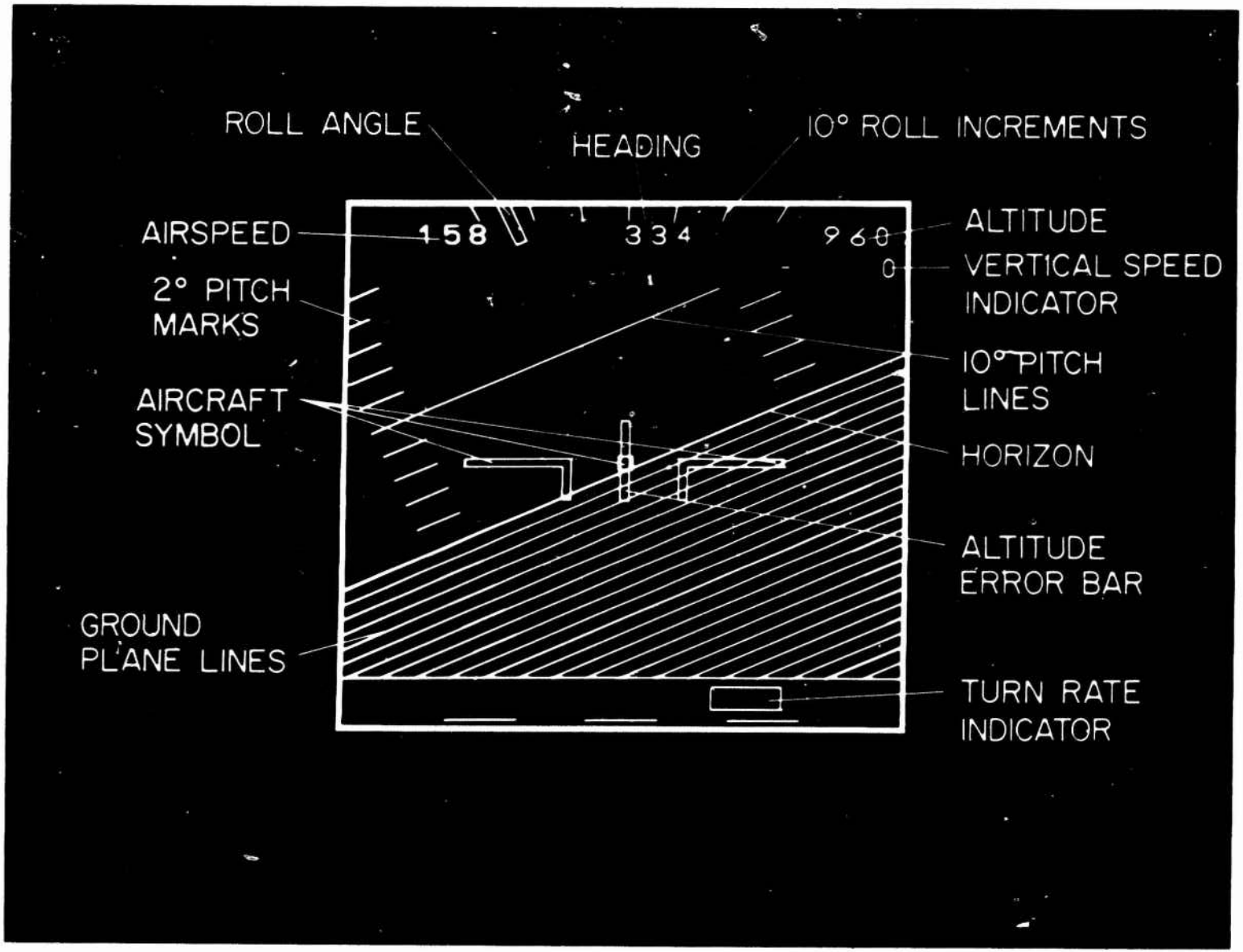

Fig. 3. Elements of the Vertical Situation Display

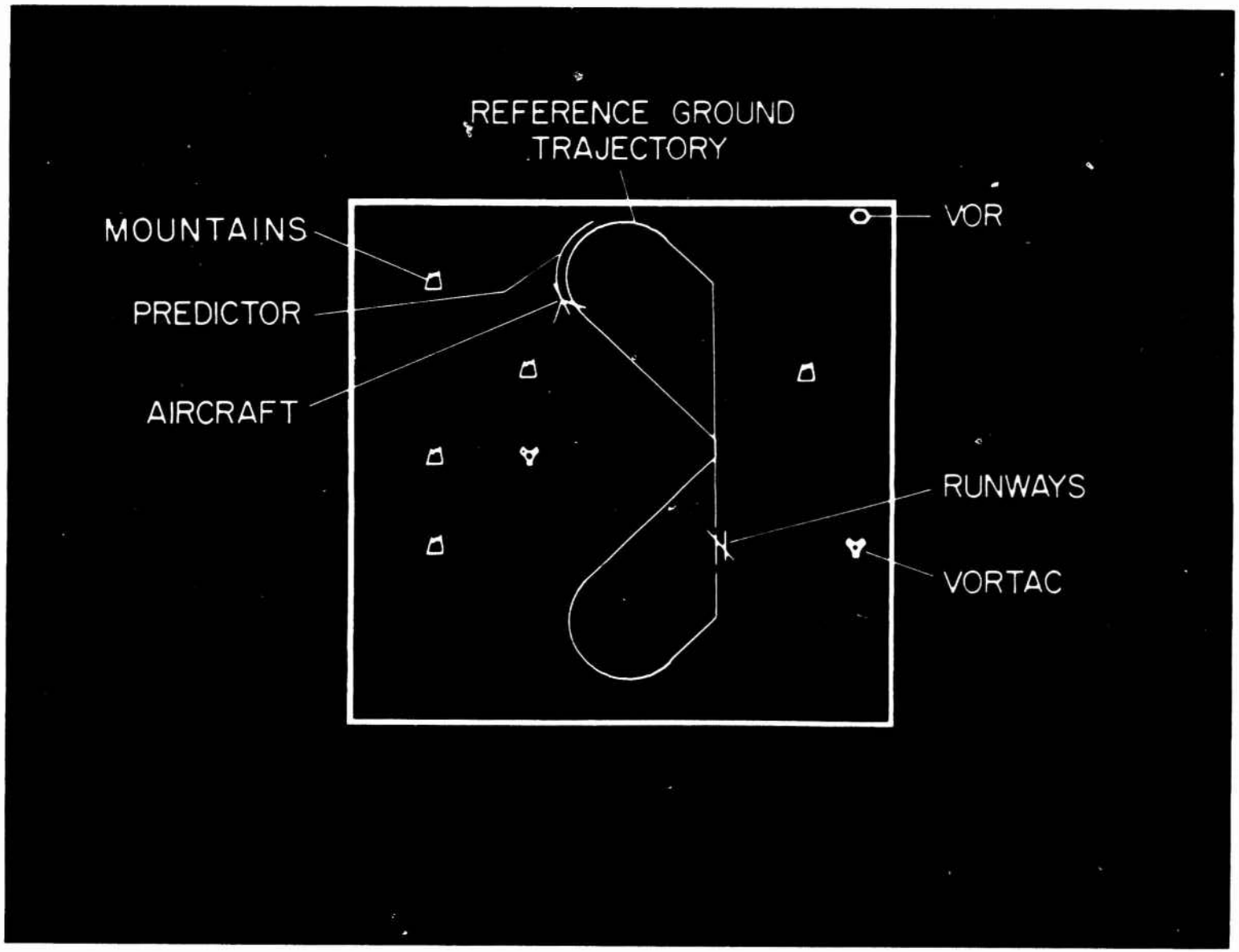

Fig. 4. Elements of the Horizontal Situation Display with predictor

2. Aircraft heading up, rotating map (O_2). The aircraft symbol always remained fixed in the center of the display, heading up. The predictor maintained the same relationship with the aircraft symbol as for O_1.

Steady-state winds:

1. Wind present (W_1). Always 32 knots and randomly selected from four directions, blowing from either 068°, 143°, 233°, or 338°.

2. No wind (W_0).

Wind gusts:

1. Gusts present (G_1). RMS lateral components of 5 ft/sec with a zero mean. At 1000 ft (305 m) altitude this gust level is equalled or exceeded 10 percent of the time.[3] The vertical component had an RMS value of 1 ft/sec.

2. No gusts (G_0).

Pilots: The pilot participants for this study were the same six airline pilots that had previously participated in an earlier study in this series.[2] The six pilots represented four airlines. One was a captain and five were copilots, of whom two were currently flying as second officers due to "bumping" procedures. The average age was 40, average total flight time about 9500 hr, and all had military experience with an average of 3,000 hr.

Predictor:

1. Predictor present (P_1).

2. No predictor (P_0).

The predicted path, corrected for steady-state wind, consisted of a solid line extending forward from the aircraft symbol to a length representing 30 sec of flight time. The measured length (on the face of the scope) of this line depended upon aircraft heading and velocity, and the strength and direction of the crosswinds relative to the aircraft heading. The coordinates for the predicted aircraft path were computed for every 3-sec interval into the future so the predictor path was actually a series of ten straight lines (Fig. 4). This predictor length was chosen as reasonable for this experiment after first trying both longer and shorter predictors. The 30-sec interval was also used in the prior experiment.[1]

The intent of this experiment was to evaluate the use of the predictor element for the map application, rather than to pursue an evaluation of various predictor parameters. With this in mind, the predictor equation integrated the following expression (plus compensation for steady-winds):

$$\dot{\psi} = \frac{g}{V} \tan \phi \qquad (1)$$

where

$\dot{\psi}$ = yaw rate

g = gravitational constant

V = aircraft velocity

ϕ = angle of bank

Another, more complete expression for the yaw rate was also programmed and tested but not used for the experiment:

$$\dot{\psi} = r\left(\frac{\cos \phi}{\cos \theta}\right) + q\left(\frac{\sin \phi}{\cos \theta}\right) \qquad (2)$$

where r and q are the instantaneous angular velocities about the aircraft inertial yaw and pitch axes, respectively, and θ is the pitch angle. As the experiment was originally conceived, a predictor using Eq. (2) was to have been the "best case"; performance with the simpler Eq. (1) was to be compared with it to see if there was any detectable performance difference between the two. However, the predictor using Eq. (2) was "too good" in that it was too sensitive, reflected changes in the aircraft states too accurately, and made a predictor that was too active, especially with the simulated turbulence. Based on the negative comments from two "in-house" pilots, that predictor was omitted from the formal experiment.

Procedure

Instructions: The purpose of the experiment, the details of the displays, the aircraft dynamics, and the experimental conditions were all explained the first day. The stated task was, "Stay as close to the reference ground trajectory as possible at all times while still maintaining altitude." The pilots were instructed to set up approximately the same turn rate for the 45° turns as for the 180° turns, using the blinking of the aircraft symbols to aid in timing the beginning of the turns. They were informed of all the conditions before each run, including wind direction. They were instructed that "Once we start a run for data, I want you to complete that run unless something unplanned happens, e.g., something obviously wrong with the simulation." They had a separate printed chart on a clipboard similar to Fig. 1, with headings and wind directions for handy reference.

At the end of each flight, a dashed line appeared on the map, showing the pilot the ground track of his entire flight path relative to the reference ground trajectory, as shown in Fig. 5. Also shown are the mean-square errors for both lateral and altitude track (digits in upper left).

Performance measures: (1) RMS error values for both lateral and altitude errors; (2) elevator and aileron control activities recorded as RMS deflections; (3) pilot questionnaire given to each pilot at the end of the experiment.

Training and experimental design: After one day of additional training, each pilot flew six days. The pilots were randomly separated into two groups, one group being given one map orientation for the first three days and the

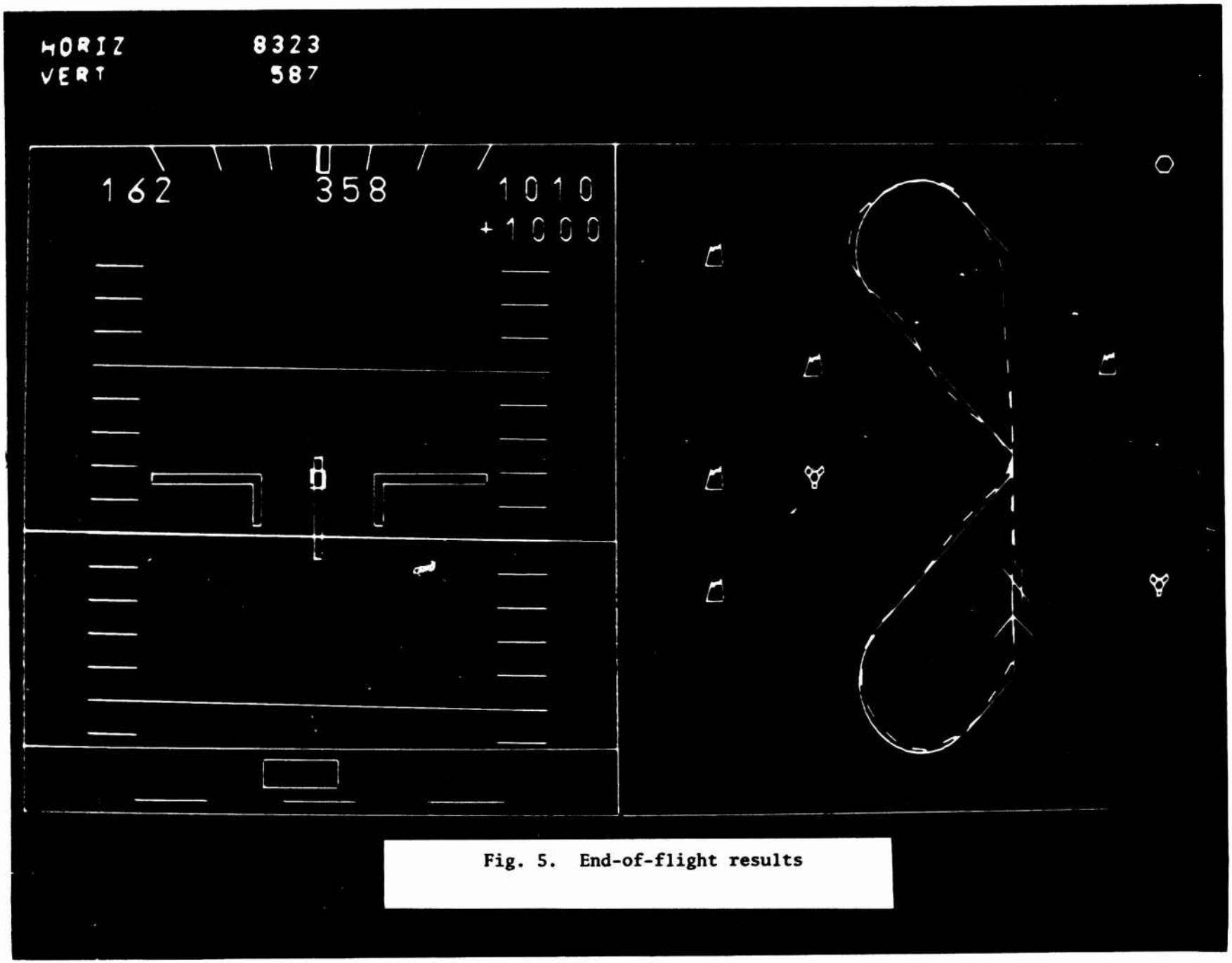

Fig. 5. End-of-flight results

other orientation for the last three days. The other group received the map orientations in reverse order.

The combination of two map orientations, two crosswind categories, two gust conditions, and two predictor conditions made a total of sixteen experimental conditions per pilot. After two warmup runs each day, each pilot made one flight with each of the possible eight conditions of crosswinds, gusts, and predictors using the map orientation chosen for that day. Thus, in the course of six days, each pilot flew three replications of each of the sixteen conditions. Each flight took approximately 6-1/2 minutes. There were at least 3 minutes between each flight with a break of 10-15 minutes about halfway through the session. Where practical, each pilot flew one or two sessions each week.

RESULTS AND DISCUSSION

Performance Data

Horizontal and vertical RMS errors: The left half of Table I tabulates the RMS error scores for the five controlled sources of variation for this experiment. The orientation of the map, i.e., fixed or rotating, had essentially no effect on the error scores. The presence of the predictor element reduced the overall lateral error score to 63 percent of the error obtained without the predictor. This was significant at the 0.01 level (see analysis of variance, Table II). The predictor had no significant effect on the altitude error scores. The presence of crosswinds significantly increased the scores for both the lateral and altitude error scores. The gusts had no effect on the error scores. The difference in performance among the pilots was significant at the 0.01 level for both error scores.

Since the same six pilots participated in this experiment and a similar prior experiment,[2] it is of interest to compare performance between the two experiments for those conditions that were identical. Figure 6 compares both lateral and altitude errors, showing wide differences as to how the pilots performed relative to their first experiment. Generally, the overall performance was slightly better for this experiment, with two notable exceptions. Pilot S clearly did much poorer the second time on the altitude task when there was a crosswind. Pilot X clearly did much better on both the lateral and altitude tasks the second time.

Another of the major results can be seen in Fig. 7, which compares the error scores with and without the predictor, and with and without crosswinds. Five results are apparent:

1. The lateral errors are lower with the predictor, both with and without crosswinds.

2. There is crosswind-predictor interaction in the lateral error scores, i.e., there is less difference between the "wind — no wind" conditions with a predictor than there is between the "wind — no wind" conditions without a predictor. This is significant at the 0.01 level (Table II).

3. There is little difference in mean altitude error performance with or without the predictor.

TABLE I. Means and standard deviations of the dependent variables

Source	RMS lateral error		RMS altitude error		RMS aileron stick activity		RMS elevator stick activity	
	Mean, m	Std dev	Mean, m	Std dev	Mean arbitrary units	Std dev	Mean arbitrary units	Std dev
Fixed Map (O_1)	69.96	34.60	7.54	3.12	63.04	19.55	6.24	1.93
Rotating Map (O_2)	67.19	32.18	9.10	5.98	63.84	21.93	6.01	2.18
Predictor OFF (P_o)	84.03 **	39.02	8.69	5.60	71.87 **	19.15	6.65 *	2.20
Predictor ON (P_1)	53.12	15.35	7.95	3.89	55.00	18.82	5.60	1.76
Crosswind OFF (W_o)	51.52 **	14.36	7.01 *	3.30	60.42 *	16.94	5.40 **	1.14
Crosswind ON (W_i)	85.63	38.06	9.64	5.69	66.46	23.62	6.86	2.48
Gusts OFF (G_o)	69.71	33.49	7.73	4.68	56.53 **	17.84	5.68 **	1.87
Gusts ON (G_1)	67.44	33.35	8.91	4.91	70.35	21.21	6.58	2.14
Pilot S	71.72	27.04	14.08	7.99	42.92	17.26	4.84	1.56
Pilot T	81.64	36.59	9.31	3.48	72.69	23.52	7.62	2.53
Pilot U	78.18 **	47.19	5.32 **	1.46	76.44 **	18.81	5.55 **	1.66
Pilot X	57.25	18.91	6.50	1.33	66.71	14.41	7.19	1.71
Pilot Y	54.45	18.64	8.53	1.67	67.94	15.27	5.89	1.66
Pilot Z	68.22	33.26	6.19	2.52	53.93	12.11	5.68	1.61

*Difference significant at 0.05 level
**Difference significant at 0.01 level
} See Table II

TABLE II. Analysis of Variance

Source	Deg. of freedom	RMS lateral error		RMS altitude error		RMS aileron stick activity		RMS elevator stick activity	
		Mean square	F ratio	Mean square	F ratio	Mean square	F ratio	Mean square	F ratio
Map Orientation (O)	1	555	<1	175	<1	46	<1	4	<1
Predictor (P)	1	68,776	36.2**	40	1.3	20,491	17.8**	80	11.7*
Crosswind (W)	1	83,728	40.0**	498	9.6*	2,631	9.6*	153	39.1**
Gust (G)	1	369	<1	101	5.8	13,741	47.4**	58	177.6**
Pilots (S)	5	5,766	16.5**	490	61.5**	7,652	64.6**	54	23.0**
O×P	1	940	3.0	28	3.0	6	<1	2	2.7
O×W	1	68	<1	21	1.5	6	<1	<1	<1
P×W	1	25,903	54.5**	26	<1	1,924	4.0	17	3.8
O×G	1	134	1.1	<1	<1	<1	<1	3	2.8
P×G	1	175	<1	<1	<1	70	<1	2	1.4
W×G	1	96	2.1	6	2.1	107	1.5	<1	<1
O×S	5	1,806	5.2*	184	23.1**	1,240	10.5*	5	2.3
P×S	5	1,902	5.4*	30	3.8	1,151	9.7*	7	2.9
W×S	5	2,093	6.0*	52	6.5*	274	2.3	4	1.7
G×S	5	462	1.3	18	2.2	290	2.4	<1	<1
All higher-order interactions		3,468		99		2,406		27	
Within Error		349		8		118		2	

*Significant at 0.05 level
**Significant at 0.01 level

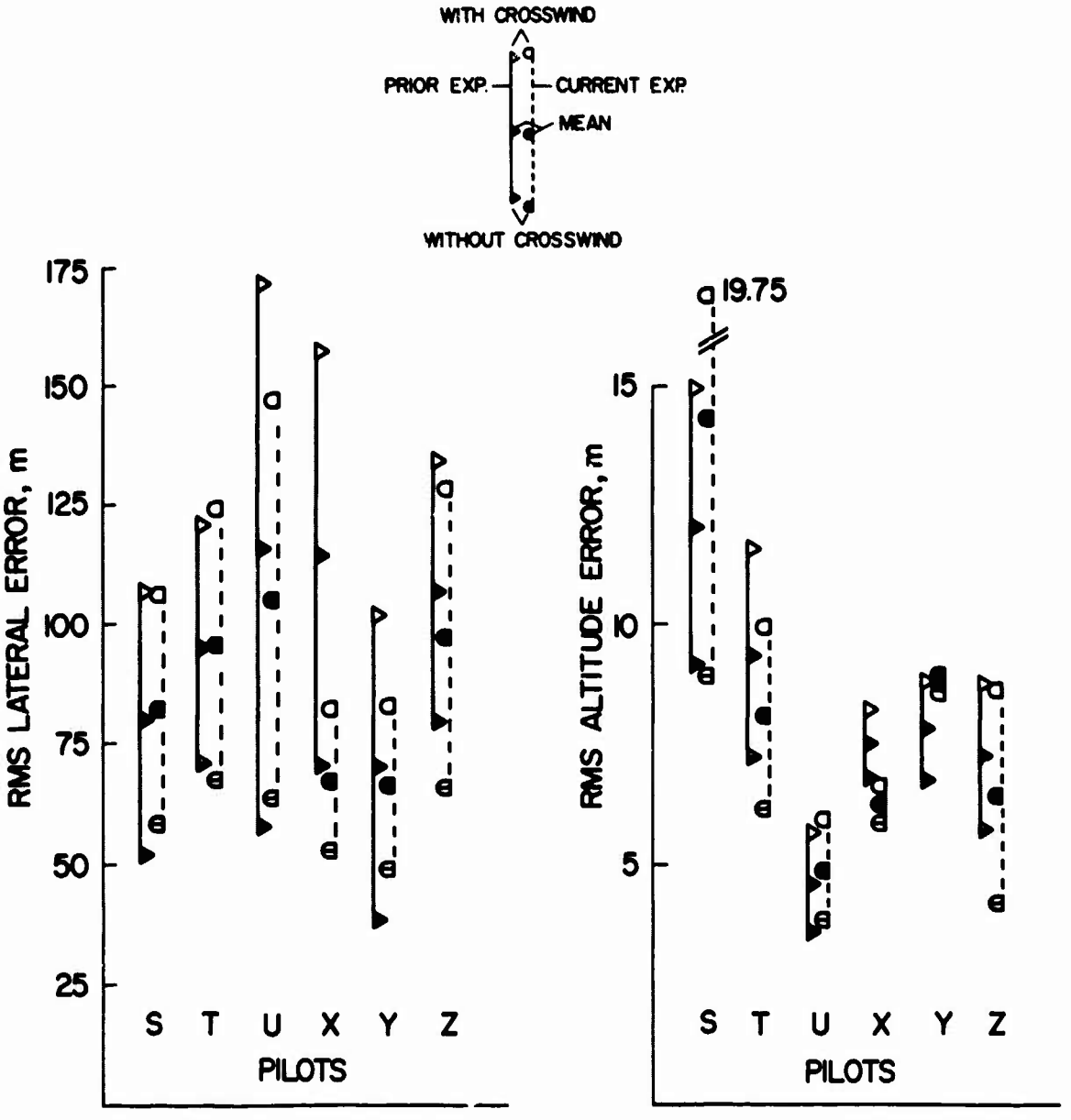

Fig. 6. Comparing the results of this experiment (excluding predictor and gust conditions) with the results of prior experiment

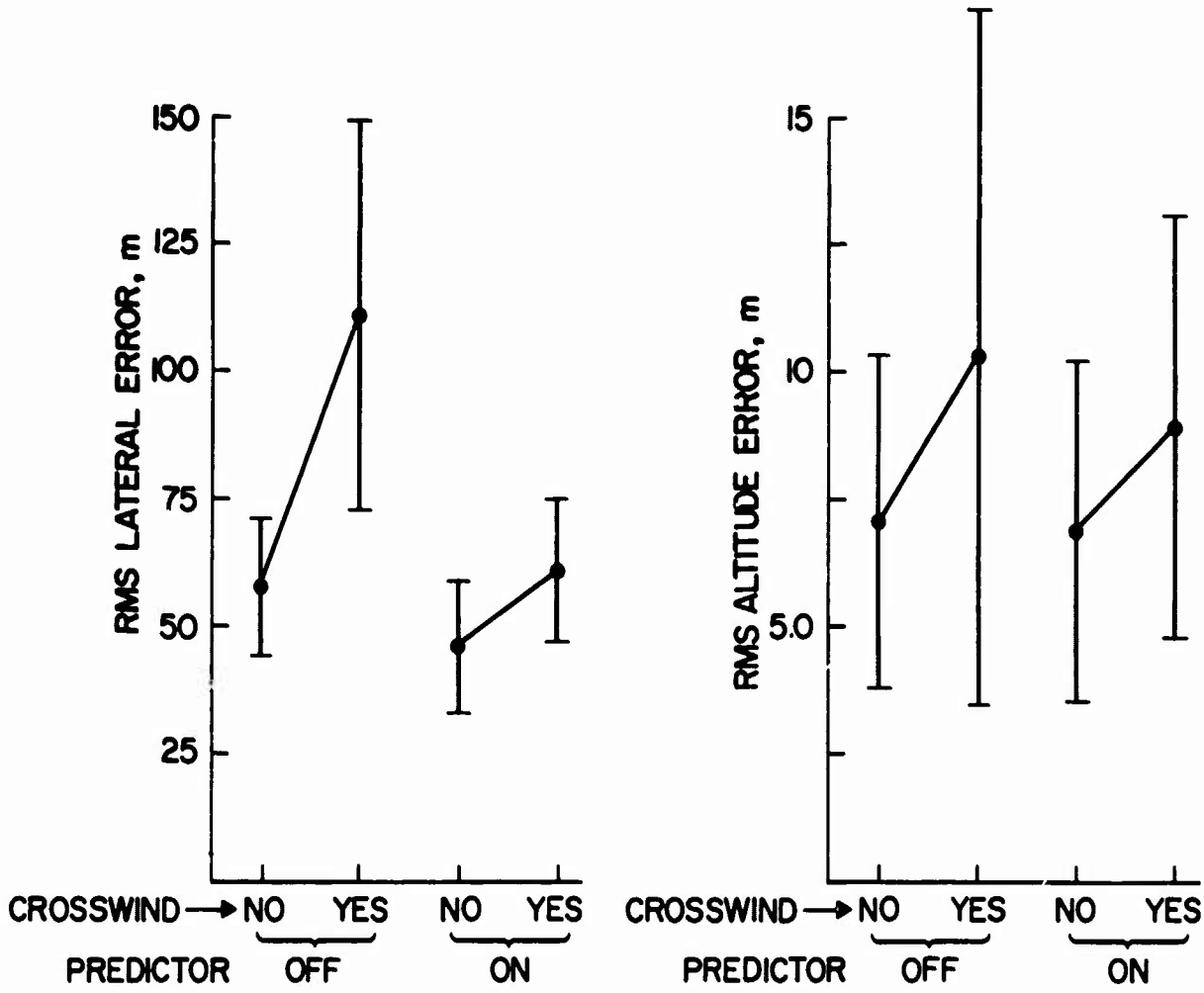

Fig. 7. Pilot error performance — with and without predictor; with and without crosswinds

4. Variability (standard deviation) of the error scores was nearly the same for the "no wind" conditions, with or without the predictor. This was true for both lateral and altitude error scores.

5. Variability of the error scores for the crosswind conditions was less when the predictor was used. Specifically, this variability was nearly the same as for the "no wind" conditions. The information presented by the predictor apparently enabled the pilots to cope better with the crosswinds so that their overall performance approached that of the "no wind" conditions.

The only other interactions of any significance (Table II) involved pilot interactions with map orientation, predictor, and crosswinds. As stated in the Procedure, each pilot first flew all flights with one map orientation, then with the other. To balance sequence effects, three of the pilots made all flights on one orientation first, and the other three flew the other orientation first. Even with the experience of the prior experiment and with the full session of training before starting this experiment (during which it appeared that there had been very little loss in skill) all of the pilots performed as well or better during the second half of the experiment than they did during the first half, regardless of the starting orientation. This would account for the pilot-map orientation interaction found for both the horizontal and vertical scores.

Figure 8 shows the other two pilot interactions, i.e., pilot-predictor (lateral scores only) and pilot-crosswind. Inspection will reveal two general features. First, the use of the predictor brought the lateral error scores, both with and without crosswinds, into the general region of each pilot's performance without predictor and without crosswinds. The wide range of scores on the "no predictor – with crosswind" condition points up the differences in ability among the pilots in coping with the crosswinds without a predictor. Mean RMS error scores with standard deviations are listed in Table III. The differences on this (no predictor – with crosswind) condition when compared with the general grouping of scores on the other conditions account for the majority of the pilot-predictor and pilot-crosswind interactions.

Aileron and elevator control activity: The right half of Table I shows a significant effect on the RMS aileron and elevator activities for four of the five controlled sources of variation. All except the map orientation showed a significant difference.

The presence of the predictor reduced aileron activity 24 percent. The presence of a crosswind increased both aileron and elevator control activities. The presence of the gusts increased the level of aileron activity more than the presence of crosswinds. Gusts affected neither the lateral nor altitude error scores. The significant differences among pilots reflected their difference in approach to the task. For example, pilot S, who had the largest average altitude error score (Fig. 8), also had the lowest average amount of elevator activity (Fig. 9). Pilot U, however, who had the lowest average altitude error score, had the next to lowest amount of elevator activity.

There were only two interactions of any significance (aileron activity only) and those were both pilot interactions. The first, pilot-orientation interaction, is accounted for in the same manner as previously described in the section on horizontal and vertical errors.

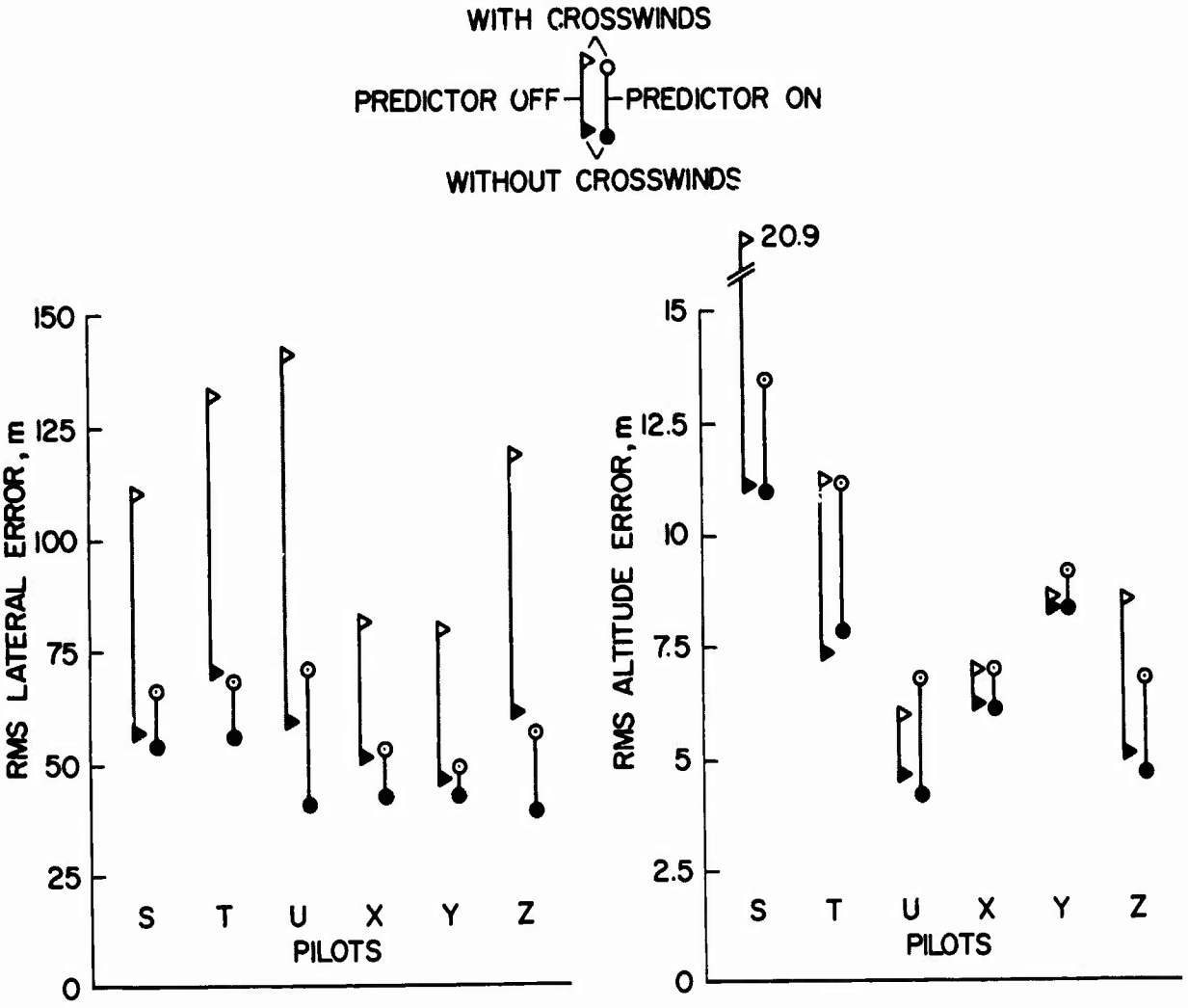

Fig. 8. Individual pilot error performance — with and without predictor; with and without crosswinds

TABLE III. Individual pilot performance — RMS error and standard deviation (σ)

			Pilot											
			S		T		U		X		Y		Z	
			Mean	σ	Mean	σ	Mean	σ	Mean	σ	Mean	σ	Mean	σ
Predictor OFF	Without crosswind	RMS lateral error	56.7	11.2	70.9	10.5	59.4	16.1	51.3	9.4	46.2	8.8	60.5	9.1
		RMS altitude error	11.1	4.9	7.3	1.9	4.6	0.8	6.2	1.4	8.3	1.8	5.0	1.4
	With crosswind	RMS lateral error	110.1	24.2	132.1	36.6	141.3	49.8	81.8	17.4	79.8	16.5	118.3	22.4
		RMS altitude error	20.9	10.6	11.2	2.5	5.9	0.6	6.9	1.1	8.5	1.2	8.5	3.1
Predictor ON	Without crosswind	RMS lateral error	53.9	9.2	55.6	17.9	40.9	6.7	42.5	8.9	42.4	7.3	38.1	9.7
		RMS altitude error	10.9	4.7	7.8	2.7	4.1	0.9	6.0	1.2	8.3	1.1	4.6	1.3
	With rosswind	RMS lateral error	66.3	9.0	68.0	7.6	71.1	18.6	53.4	9.6	49.5	10.2	55.9	11.2
		RMS altitude error	13.4	5.7	11.1	4.3	6.7	1.6	6.9	1.5	9.1	2.3	6.7	1.8

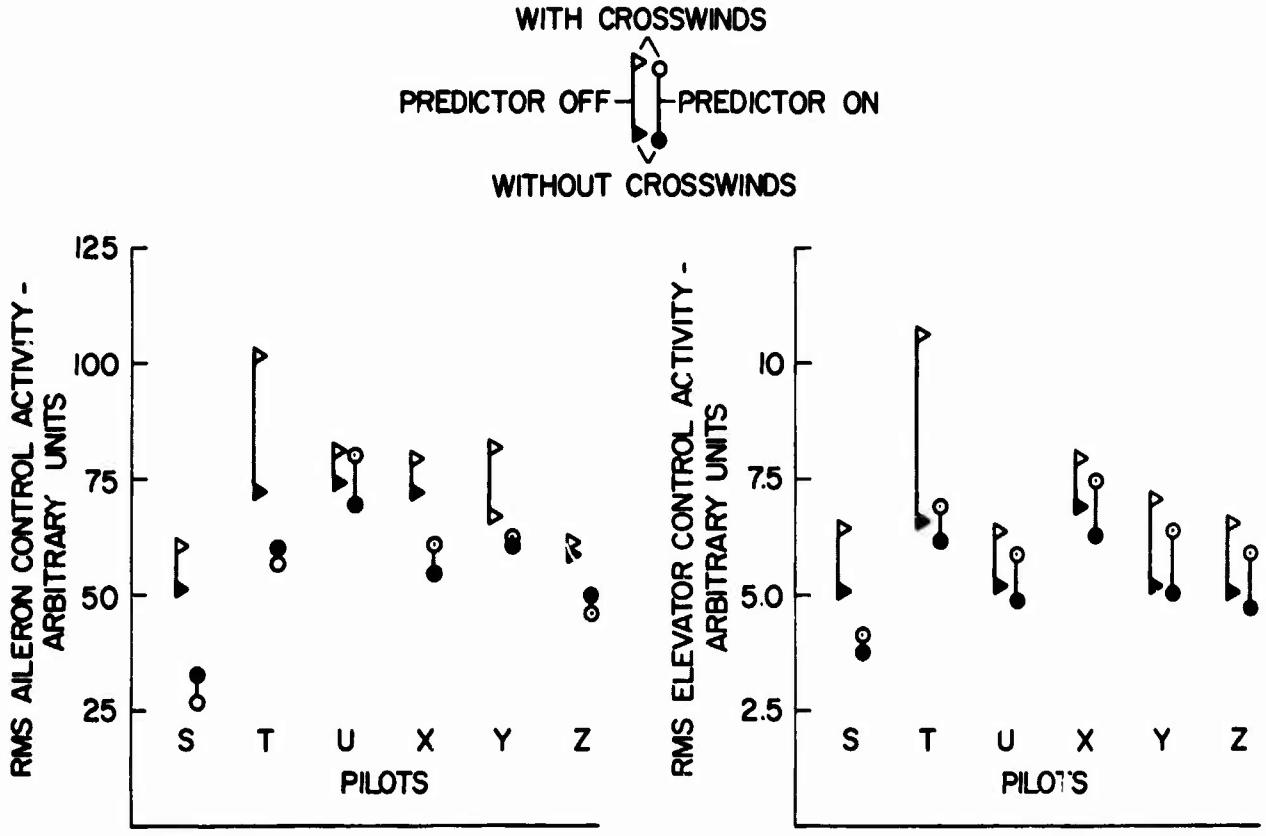

Fig. 9. Individual pilot control activity levels – with and without predictor; with and without crosswinds

Figure 9 shows that the predictor had a different effect on the pilots regarding aileron activity. For example, with the predictor, pilot S reduced control activity much more than did pilot U. The mean RMS control activity values with standard deviations are listed in Table IV.

Figure 10 is a companion to Fig. 7. Shown are the previously mentioned significant differences in aileron activity due to the predictor and due to the crosswinds. Figure 10 does not show a reduction in variability of the scores with the predictor that was found in the error terms.

Before ending this section, the behavior of one pilot on one flight (out of 288 scored flights for the entire experiment) is worthy of mention. Pilot Y, flying the condition of "predictor off, no wind, no gusts, fixed map" on the third from the last flight of his last day, reversed lateral control when attempting entry into the 180° turn to go from a 225° heading to a 045° heading. By the time he recognized his error and recovered, he had built up an error more than 10 times his usual lateral deviation for the course. This same pilot exhibited this same behavior on two flights in the prior experiment[2] on exactly the same experimental conditions. The rationale for the behavior was discussed in some detail, and will not be discussed here. Note, however, that this pilot never did adapt and feel comfortable with the fixed map. He is the only one that made a strong report against it. In this instance, as in the prior experiment, when he "quit thinking," he ran into trouble. For now, it must be assumed that some proportion of the pilot population will have trouble adapting to the fixed map. In such cases, control reversal blunders could occur. The impact of this assumption on a choice of map orientation is to be balanced with the potential perceptual problems of the rotating map. This will be discussed further in the next two sections.

Pilot Comments and Questionnaire Data

The most obvious new factor to the pilots in this experiment was the presence of the predictor element. Without exception, all pilots made some sort of spontaneous comment during the first training flight with the predictor such as, "That's neat," or "I like it," or "That's weird." As the experiment progressed, their acceptance of the predictor was expressed by other comments. "You sure can get used to it (predictor)." "Once you learn how to use it you get to depend on it." "The predictor is a good school master; it teaches you what to do for the cases with no predictor." (This last statement, made by pilot X, may explain his spectacular improvement from the prior experiment, as shown in Fig. 6.)

After completing the experiment, the pilots were asked to answer 26 questions. Some questions were quite complex, some were straightforward, and some were probing efforts, designed to see just what kind of information might be meaningfully derived from direct questions about the task. The procedure used was that of a structured interview. Some questions turned out to be useful and some did not, so only the most relevant and interesting results are presented here.

First, the pilots were asked to rank the four display conditions (predictor on or off for both O_1 and O_2) in order of preference. Table V summarizes these results. All except one pilot chose the "predictor on" conditions

TABLE IV. Individual pilot performance — RMS stick activity and standard deviation (σ)

			Pilot											
			S		T		U		X		Y		Z	
			Mean	σ	Mean	σ	Mean	σ	Mean	σ	Mean	σ	Mean	σ
Predictor OFF	Without crosswind	RMS aileron activity	52.2	12.2	73.5	14.4	74.6	18.0	72.3	8.9	66.2	14.2	58.8	11.7
		RMS elevator activity	5.1	0.7	6.6	0.9	5.2	0.6	6.9	0.9	5.2	0.5	5.1	0.6
	With crosswind	RMS aileron activity	60.7	11.7	100.6	26.0	81.3	15.5	79.0	7.7	81.5	13.8	61.7	10.4
		RMS elevator activity	6.5	1.7	10.7	2.8	6.4	2.3	8.0	2.2	7.1	1.8	7.1	1.8
Predictor ON	Without crosswind	RMS aileron activity	32.5	8.7	59.9	6.4	69.1	17.9	54.5	9.2	61.9	10.5	49.4	9.2
		RMS elevator activity	3.7	0.4	6.2	1.0	4.8	0.5	6.3	0.7	4.9	0.8	4.7	0.6
	With crosswind	RMS aileron activity	26.3	6.7	56.7	9.5	80.7	20.7	61.0	15.5	62.2	13.1	45.7	9.3
		RMS elevator activity	4.1	1.3	6.9	1.7	5.8	2.0	7.5	2.0	6.4	1.9	5.8	1.77

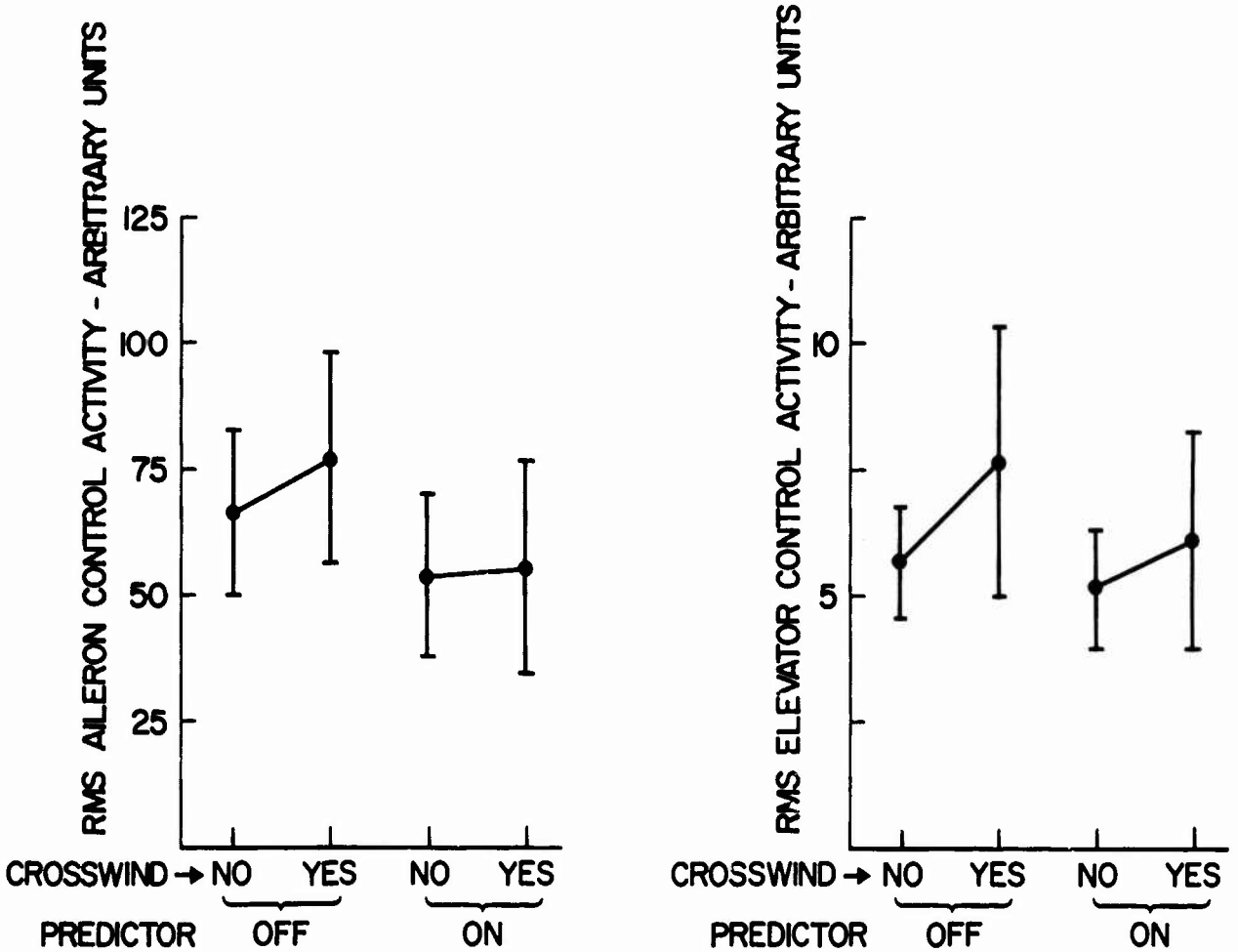

Fig. 10. Pilot control activity — with and without predictor; with and without crosswinds

as the first and second choices. (Pilot Y chose the heading up map orientation as his second choice in preference to the other "predictor on" choice, although his error scores were consistently better with the predictor.) Regarding the preferences for map orientation, it appears that there was an even split between the fixed and moving map conditions. This was the same as for the prior experiment,[2] except for one change: the pilots had changed categories, i.e., five of the six had apparently changed preference from one map orientation to the other.

On close inspection of pilot comments and taking into account differences between the two experiments, two of these changes can be explained. Yet, half of the pilots switched their preference when exposed a second time to these two map orientations. All pilots had definite reasons for their preference both times. Paraphrasing all comments during and after the experiment, the pros and cons for both map display orientations can be stated as follows:

Fixed map (O_1)

Pro: Visually stable—very important to some pilots.

Con: Potential control reversal problems (pilot Y as discussed in preceding section).

Rotating map (O_2)

Pro: With the aircraft heading always toward the top of the display, the direction of control is always obvious.

Con: The continual motion is objectionable to some. One pilot reported slight vertigo at times. Another pilot occasionally experienced a momentary feeling of being in a spin during a high rate turn.

The pilots were asked to rank the relative advantage of having the predictor for each of the four environmental conditions shown in Table VI. Generally, the more outside disturbance present, the more they felt it was an advantage to have the predictor. They had also been asked to rate the degree of the advantage of having the predictor for each of the conditions of Table VI over not having one on a four-point scale of: (1) decided advantage; (2) slight advantage; (3) no advantage; and (4) detrimental. All responded with "decided advantage" for their first two rankings and "slight advantage" for their fourth or last ranking. They were evenly split between "decided advantage" and "slight advantage" for their third ranking.

Another question was designed to see how well the pilots could rate their level of effort on the various tasks. They were asked to estimate their effort on each of the eight conditions shown in Table VII. They were asked to do this as a multiple of the reference task, which was taken to be the "predictor off, without crosswind, without gust" condition. They were told to rate a task which was half as hard as 0.5, twice as hard as 2.0, etc., that is, they were to construct a ratio scale. Table VII shows the results for each pilot. Two pilots indicated that the answers would be slightly different if a comparison were made between the two map orientations but these two were in opposite

TABLE V. Pilot ratings[a] of the four display conditions

Pilot	Predictor on		Predictor off	
	O_1*	O_2	O_1	O_2
S	1	2	3	4
T	2	1	4	3
U	1	2	3	4
X	1	2	3	4
Y	3	1	4	2
Z	2	1	3	4

[a]Most preferred = 1; least preferred = 4

*Map orientations:
O_1 = North up, fixed map
O_2 = Aircraft heading up, rotating map

TABLE VI. Pilot ratings[a] of the relative utility of the predictor for the four environmental conditions

Pilot	With crosswind		Without crosswind	
	With gusts	Without gusts	With gusts	Without gusts
S	1	2	3	4
T	1	2	3	4
U	1	2	3	4
X	1	2	4	3
Y	1	2	4	3
Z	1	2	3	4

[a]Most advantage = 1; least = 4

directions and would have cancelled out in the averaged score. Comparing the mean results with the control activity levels in Table I shows some validity in using control activity levels as a gross measure of relative workload (e.g., ref. 1). With the predictor on, the mean estimate of pilot workload was as low or lower than with it off. The control activities were also lower. A similar comparison with and without crosswinds showed similar results. Worthy of special attention are the results with and without gusts. The error scores showed no difference, yet the differences in control activity levels were both significant at the 0.01 level. This corresponds with the pilot estimates of task workload which definitely reflect a feeling of increased workload when coping with the gusts. Figure 11 is a plot of aileron and elevator control activity versus the mean value of the pilot estimates of workload for the eight experimental conditions shown in Table VII. The correlation between pilot workload ratings and aileron activity was 0.82 (significant at the 0.05 level). The correlation between workload ratings and elevator activity was 0.92 (significant at the 0.01 level). The correlation between aileron and elevator control activity was 0.90 (significant at the 0.01 level). Although not yet validated by other workload measures these results lend some credence to future use of both pilot ratings and control activity levels as means of comparing relative workload levels.

Although there was no actual eye scan data against which to compare, each pilot was asked to estimate the proportion of time they spent looking at the VSD and map displays for each of the four display conditions shown. Wide differences were given (Table VIII) and the reasons for their estimates were as interesting as the numbers themselves. The small difference between the average score for fixed map and moving map conditions would be expected from the lack of any significant differences in any of the performance scores. Five of the six pilots did, however, comment as follows on why they made changes in estimates between the map orientation:

Pilot S – The movement (of O_2) seemed to attract (attention) more.

Pilots U & X – The motion (of O_2) was bothersome (a strain) so went to the map to get what was needed and then "got away from it."

Pilot Y – Required less time to get information from the moving map (O_2) so less time was spent on it.

Pilot Z – The slight increased time on O_2 was due to the attraction caused by the extra motion with gusts.

There was general agreement that more time was spent on the map when the predictor was on, because, as one pilot put it, "There is more information there. In order to use it you have to look at it."

Generally, the pilots felt that the predictor provided a "fine tuning" capability that cannot be presented any other way. They all agreed that it particularly helped in coping with the crosswind. The only complaint with the predictor was its constant motion with gusts present. They were asked to rate how much this bothered them on a 4-point scale of: (1) very bothersome, (2) fairly bothersome, (3) slightly bothersome, and (4) no bother. Five rated it as "slightly bothersome," and one as "fairly bothersome."

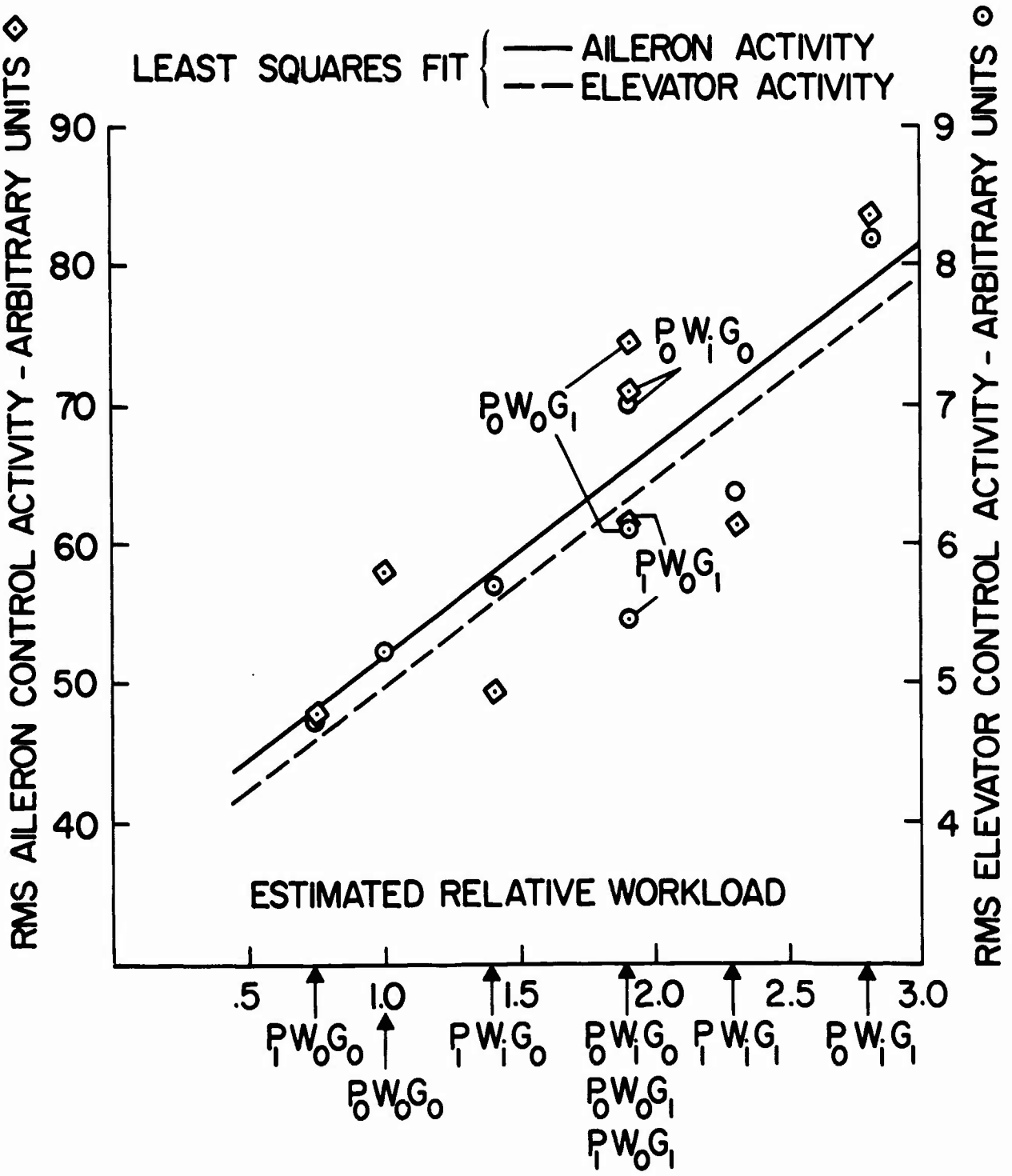

Fig. 11. Pilot estimates of their relative workload

TABLE VII. Pilot estimates of their relative workload

Pilot	Predictor	Without gusts (G_o)		With gusts (G_1)	
		Without (W_o) crosswind	With (W_i) crosswind	Without (W_o) crosswind	With (W_i) crosswind
S	Off (P_o)	1.0	1.4	2.0	2.5
T		1.0	2.5	2.0	3.0
U		1.0	2.0	3.5	4.0
X		1.0	2.1	1.5	2.5
Y		1.0	2.0	1.2(5)	2.5
Z		1.0	1.5	1.2	2.0
Mean		1.0	1.9	1.9	2.8
S	On (P_1)	0.5	0.8	1.5	1.8
T		0.5	1.5	1.5	2.0
U		1.5	3.0	4.5	5.0
X		0.7	0.9	1.1	1.7
Y		0.7(5)	1.5	1.5	2.0
Z		0.5	0.5	1.1	1.2
Mean		0.7(4)	1.4	1.9	2.3

TABLE VIII. Pilot estimates of their division of attention between the VSD and map displays

		North up – fixed map		Heading up – rotating map	
Pilot	Predictor	VSD	MAP	VSD	MAP
S	Off	50%	50%	45%	55%
T		60	40	60	40
U		75	25	80	20
X		60	40	80	20
Y		30	70	60	40
Z		80	20	80	20
Mean		65	35	69	31
S	On	40	60	40	60
T		50	50	50	50
U		70	30	75	25
X		55	45	70	30
Y		40	60	50	50
Z		75	25	70	30
Mean		58	42	61	39

Also, they generally felt that the predictor was all right the way it was presented. There was no desire to lengthen or shorten it. As one pilot put it, "It's already simple – keep it that way." Some way to better differentiate it from the rest of the display would probably be the biggest help. Two pilots suggested making it a different color if possible. One pilot suggested a predictor on-off button. Another pilot jokingly said he could sum up his opinion of the experiment thusly: "Give me my predictor back." The other pilots were not as outspoken but generally made favorable comments.

CONCLUDING REMARKS

There is sufficient information from the analysis of these data to address the five hypotheses stated in the Introduction.

1. The use of the predictor did improve the overall task performance to a significant degree as measured by lateral error. The mean RMS lateral error with the predictor for the entire experiment was 63 percent of the mean scores without the predictor. In addition, the standard deviation of the lateral scores with the predictor was 39 percent of the standard deviation of the scores without the predictor. The RMS altitude errors were also in favor of the predictor but not to a significant degree.

2. There was no predictor-map orientation interaction. This, therefore, eliminates any concern that the presence of the predictor could have an adverse effect with either of the display orientations. In fact, pilot reports indicate that the predictor helps eliminate problems inherent in both map orientations. It helps reduce the effect of a possible control reversal with the fixed map by making an incorrect control input immediately obvious before the error has a chance to build up. One pilot indicated that the predictor helped remove much of the adverse effect of the gusts with the rotating map by showing what part of the rotating motion was due to the gusts.

3. and 4. The use of the predictor generally resulted in more homogeneous performance for all conditions. This included the significant reduction in performance difference among pilots and the significant reduction in errors between the crosswind and no-crosswind conditions. This finding of a general decrease in variability due to the information presented by the predictor could be important in assigning future terminal area corridor widths.

5. The presence of the wind gusts did not significantly affect performance as measured by RMS error scores. Their presence did, however, increase pilot workload as measured by control activity levels and by pilot reporting.

Whether or not the predictor reduced pilot workload could not be as directly determined as the above five hypotheses. Control activity levels were measured but were an unproved measure of workload. The fact that pilot ratings of workload correlated highly with the control activity levels lent support to both as measures of relative workload. Neither would have stood strongly on its own merits. On the basis of this supporting evidence, it is concluded that the predictor does generally reduce pilot workload.

The last experimental question concerned blunders due to control reversals. Only one pilot (Y) experienced reversal problems throughout this

experiment with the fixed map orientation. This problem was mostly overcome by continuously "thinking ahead" regarding which direction the next control motion was to be made. The result of a lapse in this planning has already been described in the Results and Discussion section. The problem was essentially eliminated, however, when the predictor was present, because the predictor quickly alerted him to any control motion made in the wrong direction.

Based on the results of this experiment, the predictor appears to be a valuable addition to electronic map displays. A simple wind-compensated predictor similar to the one used in this study should not impose a significant additional load on a modern airborne computer. The motion of the predictor should be relatively smooth, it should be free of flicker, and it should be coded in some way (e.g., color or intensity) to make it stand out over other lines on the display.

BIBLIOGRAPHY

[1]J. G. Kreifeldt and T. Wempe, "Pilot performance during a simulated standard instrument procedure turn with and without a predictor display." NASA TM X-62,201, January 1973.

[2]D. Baty, T. Wempe, and E. Huff, "A study on aircraft map display location and orientation." NASA TM X-62,198, January,1973.

[3]C. R. Chalk, T. D. Neal, T. M. Harris, F. E. Pritchard, and R. J. Woodcock, "Background information and user guide for MIL-F-8785B(ASG), Military specifications—flying qualities of piloted airplanes." Technical report AFFDL-TR-69-72, August 1969.

ON INFORMATION PRESENTATION VIA DUAL KINESTHETIC-TACTUAL DISPLAYS

Robert E. Fenton
Dept. of Electrical Engineering

Richard D. Gilson
Dept. of Aviation

Ronald W. Ventola
Dept. of Electrical Engineering
The Ohio State University
Columbus, Ohio 43210

Previous inflight studies, in which a single control with a built-in kinesthetic-tactual display was employed, prompted further experimental work with two such control-display arrangements for simultaneously presenting independent information. Here, three different compensatory tasks were performed in a ground-based simulator under four display conditions:

I. Visual displays only;
II. Two visual and one tactual display;
III. Two visual and the other tactual display; and
IV. One visual and two tactual displays.

The tasks were chosen to simulate typical inflight informational inputs. Performance was assessed by comparing the results from the tactual-display conditions and with those from the visual task conditions.

Preliminary findings are as follows: First, the simultaneous use of two tactual displays of the type described herein does not result in performance degradation over the commonly used visual displays; Second, after training little relative interference existed between simultaneously performed tactual tasks; and Third, there was no appreciable cross-modality interference between the tactual- and visual tasks which were performed simultaneously.

I. INTRODUCTION

The manual control of a vehicle under high visual loading conditions can be an exacting task, especially when an operator must frequently shift his attention from panel instruments to the external environment. Various investigators have suggested that his task could be greatly eased if some control information were presented via nonvisual modalities. One of these, the auditory modality, has long been considered for use in a number of tasks ranging from flying by auditory reference (the 1945 FLYBAR study)[1] to the use of aural glide slope cues in a 1968 study.[2]

The cutaneous modality has also been used for many years (e.g., stick shakers for aircraft stall warning), and has been the subject of a number of other interesting approaches for information transfer. These include a two-way vibrotactile communication system,[3] a stomach-chest "cross" of stimulators for information transfer,[4] and an airjet stimulator moving across the forehead.[5] (An excellent overview of such efforts is contained in both Reference 6 and in a special issue of IEEE Man-Machine Transactions[7] which was devoted to tactual displays).

Until now, the efforts undertaken primarily have been laboratory studies; whereas, few effective and practically implementable displays have been reported. One of the few is a kinesthetic-tactile display evaluated by Fenton and others[8-10] in a series of both simulated and full-scale vehicular control situations. This has involved the presentation of unidirectional control information in close headway, car-following situations and in two difficult aircraft control situations. In the former, significant reductions in headway variation were obtained using this display as compared to visual tracking of a lead vehicle-- +0.6 ft versus +3.3 ft with a target headway of 33 ft at 40 mph. In the latter, inflight investigations were conducted to assess kinesthetic-tactual presentations of angle-of-attack information via a display built into an aircraft's yoke. Significant improvements in pilot's performance were obtained when visual attention was diverted outside the cockpit particularly during a series of turns about a point. The tactual display as compared with a visual display of the same information showed a 55% reduction in angle-of-attack tracking error ($P < .01$) and a reduction in the maximum altitude variation and speed variation by 51% and 33%, respectively.

The present study is focused on the presentation of independent information via two kinesthetic-tactual displays, and it has three goals:

a) The efficacy of such displays as compared to visual displays which are typical of inflight cockpit presentations;
b) The determination of the relative interference between simultaneously performed tactual tasks; and
c) The determination of any cross-modality interference between tactual and visual tasks performed simultaneously.

II. DISPLAY DESCRIPTION

A kinesthetic-tactile display, which is described in greater detail in Reference 8, consists of a rectangular metal slide mounted in the head of a

control stick such as is shown in Fig. 1. A forward protrusion of the slide corresponds to a "positive" error, and the corrective response is movement of the stick forward so as to decrease the error and return the slide to its neutral or flush position. An aft protrusion, such as is shown in Fig. 1, would require an aft corrective motion of the control stick. In essence, a subject follows the displayed tactual signal with the control to reduce the displayed error to zero. The slide is controlled by a servo with a natural frequency of some 32 rad/sec and a damping ratio of 0.5; thus the display dynamics are negligible in comparison with those of the subject and plant.

This presentation differs markedly from vibrotactile and airjet stimulation, in that it involves active feedback as opposed to a purely passive conveyance of somesthetic information.* It may be viewed as analogous to braille in that it is characterized by "embossed" features, and thus the subjects manipulations engender the stimulus patterns. This greatly enhances tactual acuity and allows alterations in the resulting spatio-temporal patterns for desired discriminability.** However, this analogy is only partially complete since the rectangular slide provides, in effect, a large "dot" with variable positive and negative height, thus allowing a continuous dimension for informational transmission -- e.g., magnitude and direction.

The constant handling of the control with its attendant displayed error creates a close stimulus-response site of action. Subjects frequently referred to the compelling nature of the presentation and how quickly the required control actions were performed without conscious thought.

III. EXPERIMENTAL APPARATUS

The experiment was conducted using the moving-base simulator shown in Fig. 2. The enclosed single-seat cockpit was mounted on a steel structure so that it could both be tilted fore-and-aft and rolled from side-to-side to provide motion cues. A front-mounted instrument panel contained two visual displays -- an airspeed indicator and a conventional localizer-glideslope (cross-pointer) display. The first of these presented airspeed values in proportion to the cab pitch, and the second presented was information analogous to glideslope deviation and lateral deviation from a desired path.

Two control sticks, each of which contained a built-in kinesthetic-tactual display were installed. One was located directly in front of a subject and corresponded to an aircraft yoke.*** Fore-and-aft motions

---

* The active feedback employed here is reminescent of Gibson's thesis[11] on the active nature of perceptual information. For touch, Gibson used the term haptic perception.

** Compare this with the generally ineffective sensation of braille characters when a reader simply presses his finger onto the one-to-six dot matrix without movement. The purely spatial passive pattern created is difficult to recognize.

*** This control was used in previous inflight studies wherein it replaced the yoke in a Cessna 172.[10]

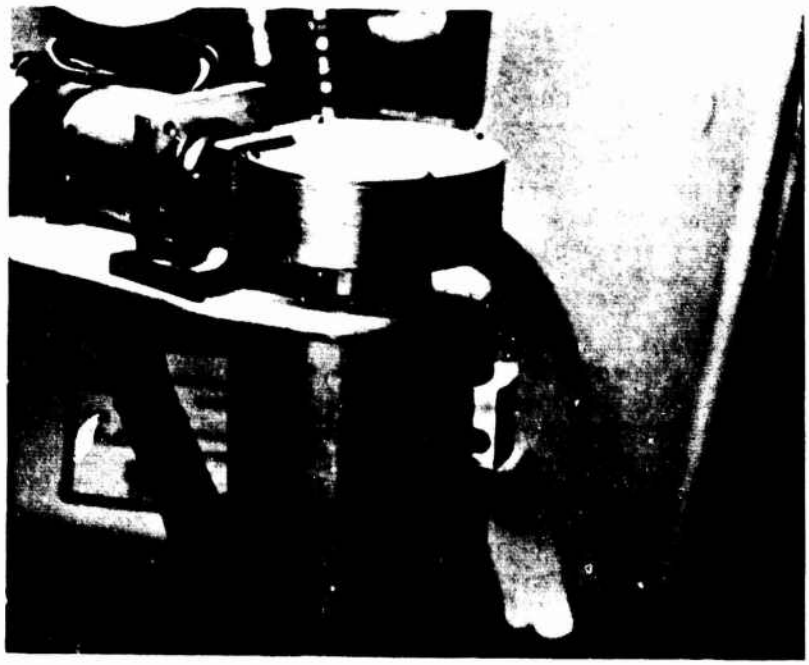

Figure 1. Control stick with built-in tactual display.

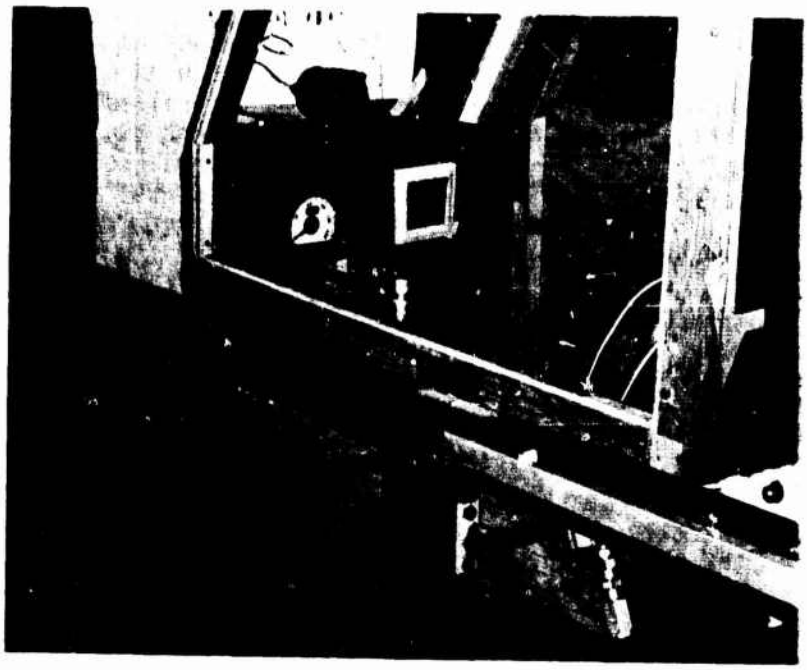

Figure 2. Simulator with two tactual display/control devises.

controlled cab pitch, and hence airspeed, while rotary motions controlled both cab roll and lateral deviations from the "localizer". The second stick was located to the right of the subject, and was analogous to an aircraft throttle controlling the glideslope.

The cab was enclosed to prevent a subject from directly observing pitch or roll. Therefore, all control was either based on displayed information--visual or tactual-- or obtained with the assistance of these motion cues.

IV. EXPERIMENTAL DESCRIPTION

A complex control problem was posed by using three random and independent forcing functions to vary the airspeed about an average value, and to cause both localizer and glideslope deviations. A subject's task was thus:

a) To maintain a constant airspeed;
b) To maintain his centered localizer course; and
c) To maintain the proper glideslope.

These tasks are depicted in the block diagram of Fig. 3 which shows the three control loops of interest. The airspeed or pitch loop contains the dynamics which are associated with the pitching of the cockpit as well as a first-order lag which is intended to account for the delay between changes in an aircrafts angle of attack and a corresponding change in the airspeed indicator. Similarly, the localizer control loop contains the simulator roll dynamics. The glideslope control loop contains only a first-order lag and was not coupled to cab motion.

Performance was assessed on the basis of absolute integrated error for each measured variable -- airspeed, lateral deviation and glideslope deviation.

Three preliminary tests, in which four display conditions were utilized, were conducted. The conditions were numbered in order of decreasing visual demand. Thus, in Condition I all information was presented visually on two displays; in Condition II localizer and airspeed information were presented visually on two displays (the glideslope movement was deactiviated) and glideslope information was presented tactually; in Condition III, both localizer and glideslope information were presented on a single visual display and airspeed was presented tactually; and in Condition IV, there was a single visual display of localizer information and a tactual display of airspeed deviation in the lefthand control and glideslope deviation in the righthand one.

Prior to testing, each subject underwent approximately 45 minutes of trial runs under all display conditions to familiarize him- or herself with the control task. The same conditions were present here as during the subsequent data-collecting phase.

Five subjects participated in each of 3 tests--hereafter referred to as tests 1, 2, and 3. In Test 1, Conditions I, III, and IV were considered with each subject making 6 3-minute runs per condition. Appropriate counterbalancing procedures were employed to minimize any secondary learning effects.

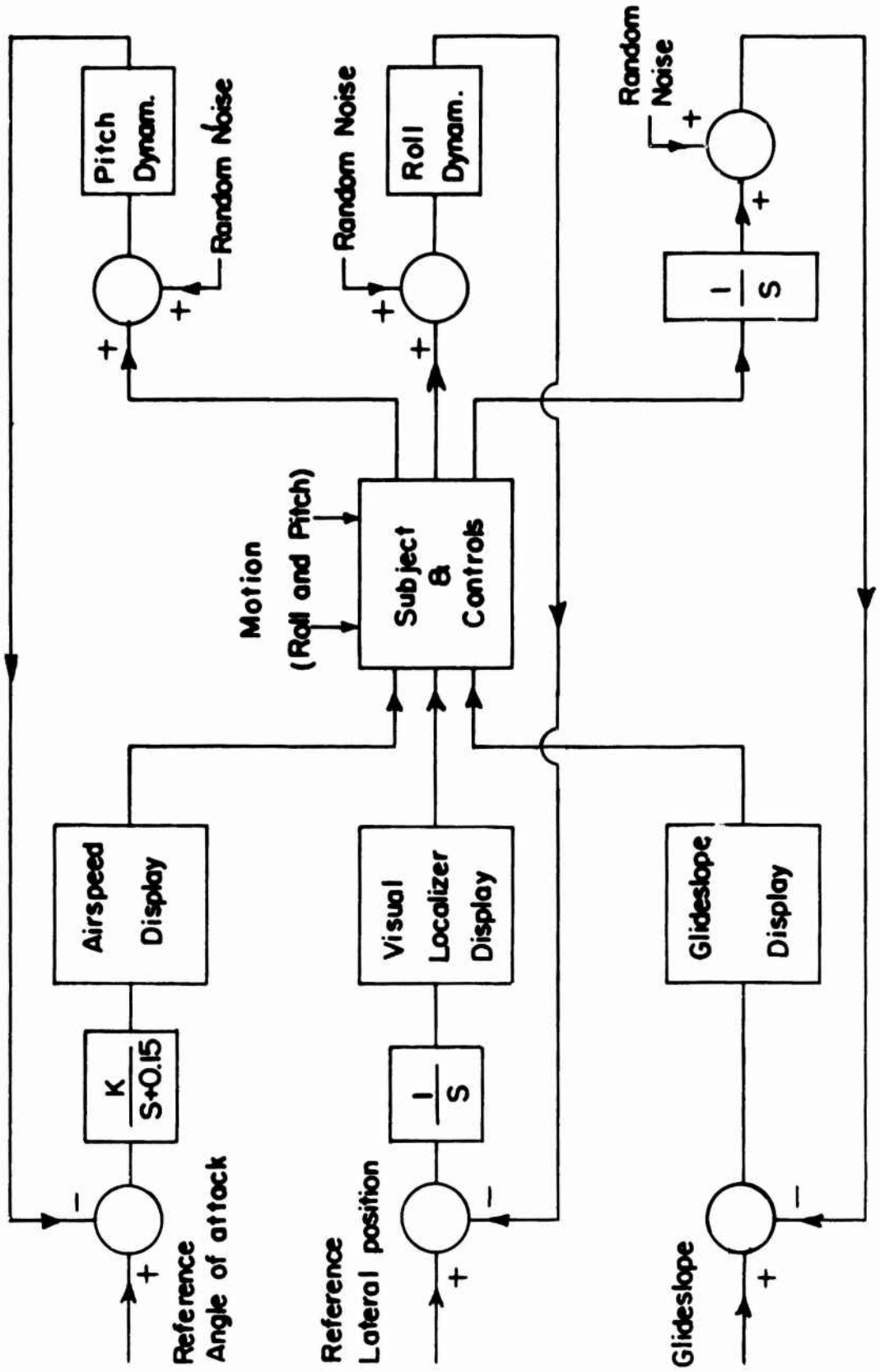

Figure 3. Block diagram of control tasks.

Following this, Test 2 which consisted of Conditions I, II and IV and 1 run/subject/condition, was conducted. Learning effects were considered minimal and counterbalancing was not employed.

After comparing the results from Tests 1 and 2, it was decided to change the glideslope control stiffness and the tactual display sensitivity. These modifications were utilized in Test 3, in which Conditions II, III and IV were considered, and 1 run/subject/display condition was obtained.*

V. RESULTS AND DISCUSSION

An analysis of variance was performed for each of the three test sets with both task and display condition taken as fixed effects and subjects as a random one. The results are shown in Table I-III.

Two effects were significant in Test 1: Airspeed deviations indicating an improvement in airspeed control for the tactual over the visual condition; and glideslope deviations indicating degraded performance for the tactual versus the visual condition. The former is clearly shown in Fig. 4 where the average results for each task have been plotted versus condition. Note from 4(b) that a substantial reduction in the averaged airspeed deviations was obtained for both tactual display conditions (III and IV) as compared to the visual display condition (I). An examination of the glideslope deviations (Fig. 4(c)) reveals a detrimental effect with the simultaneous use of a tactual display in each hand (Condition IV).

In Test 2, airspeed deviations were significant at the .05 level -- a significance which is again clearly evident in Fig. 4(b). Per Fig. 4(c), there is again a slight detrimental effect with Condition IV; however, this was not significant.

Either some interference existed between the simultaneously performed tactual tasks or some other problem was present. Evidence contrary to an interference hypothesis are:

a) The lack of interference in the airspeed task in Test 1 when Condition IV introduced a second tactual task;
b) The essentially invariant localizer task performance where there appeared to be little cross-modality interference between visual- and tactual task performance; and
c) Visual task performance was unaffected regardless of whether 1 or 2 visual displays (Conditions II and III) were used to present two sources of information (i.e., required shifts in gaze had little effect on task performance). (See Fig. 4).

The relative lack of intra- and inter-modality interference, combined with the failure to obtain the expected improvement in single tactual tracking with glideslope information (Condition II, Test 2), suggests that the apparent decrement in Condition IV was the result of a less than satisfactory

---

* This effort is currently in progress and additional data are being collected.

TABLE I

ANOVA Summary Table for Test 1 with Conditions I, III and IV (Note: replication and interaction terms were not significant ($p > .10$) and were not included)

Variable	Source	Error Term	Sum of Squares	df	Mean Squares	F Ratio
Localizer	A	SA	26.266	2	13.133	1.126
	SA		93.330	8	11.666	
Airspeed	A	SA	1540.071	2	770.035	7.305*
	SA		843.356	8	105.419	
Glideslope	A	SA	65.803	2	32.902	6.428*
	SA		40.946	8	5.118	

TABLE II

ANOVA Summary Table for Test 2 with Conditions I, II and IV (Note: Interaction terms were not significant ($p > .10$) and were not included)

Variable	Source	Error Term	Sum of Squares	df	Mean Squares	F Ratio
Localizer	A	SA	7.755	2	3.878	1.794
	SA		17.294	8	2.162	
Airspeed	A	SA	194.940	2	97.470	17.599*
	SA		44.306	8	5.538	
Glideslope	A	SA	14.536	2	7.268	1.562
	SA		37.222	8	4.653	

A = conditions
S = subjects
* = significance beyond the 0.05 level

TABLE III

ANOVA Summary Table for Test 3 with Conditions II, III and IV (Note: interaction terms were not significant ($p > .10$) and were not included)

Variable	Source	Error Term	Sum of Squares	df	Mean Squares	F Ratio
Localizer	A	SA	8.801	2	4.401	1.002
	SA		35.147	8	4.393	
Airspeed	A	SA	266.049	2	133.024	1.811
	SA		587.482	8	73.435	
Glideslope	A	SA	33.109	2	16.555	8.327*
	SA		15.904	8	1.988	

A = conditions
S = subjects
* = significance beyond the 0.05 level

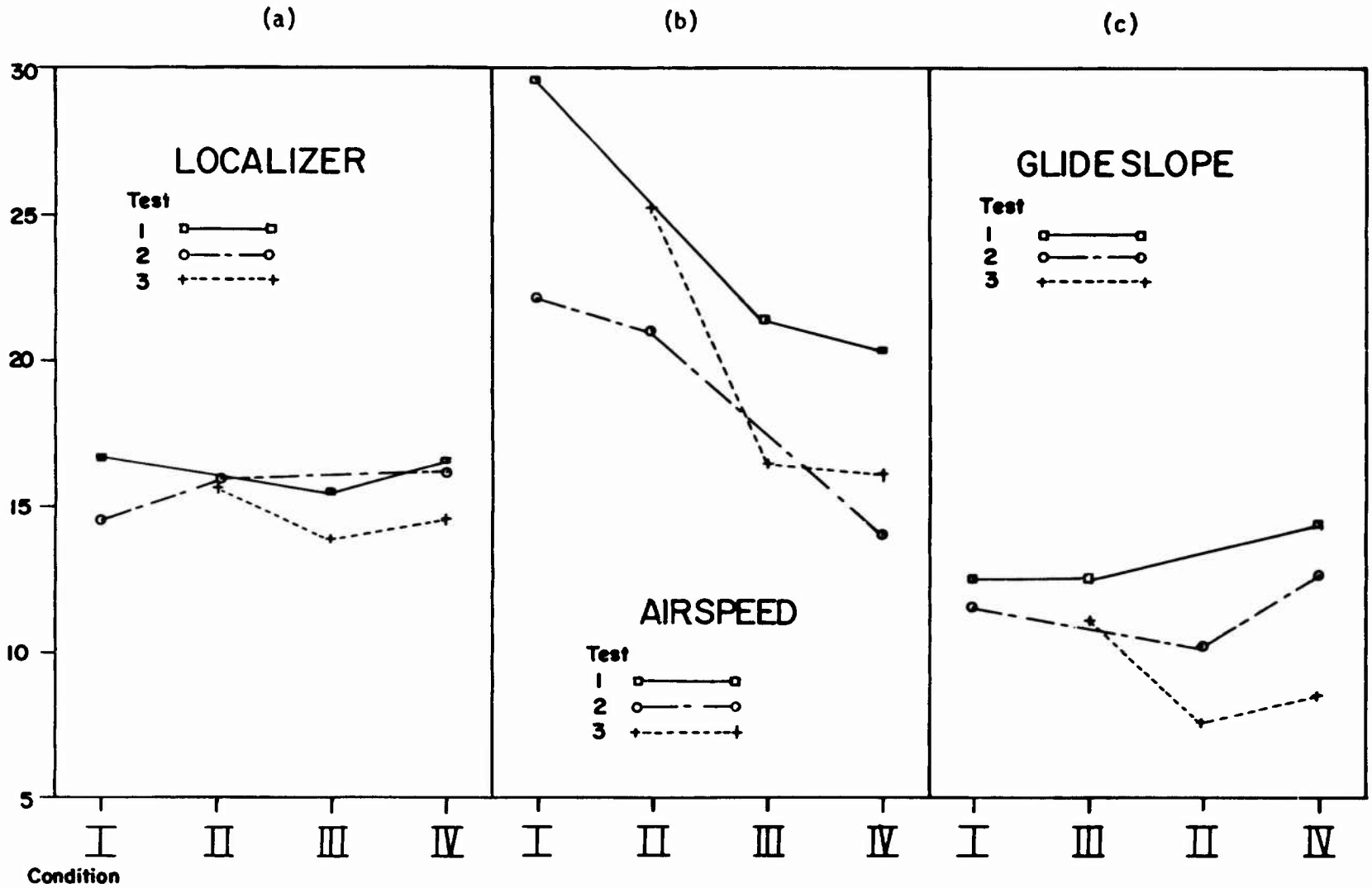

Figure 4. Averaged data for Tests 1, 2, and 3.

control/tactual display combination. This, together with subject comments, led to Test 3. This test was run after the glideslope control stiffness was reduced and the display sensitivity was increased.

These changes were clearly useful, as per Table III, glideslope deviations were significantly reduced (.05 level). This is also evident from an examination of Fig. 4(c).

The results from the other tasks are similar to the previous findings. For airspeed data (Fig. 4(b)), it is seen that a substantial decrease in airspeed deviations was again obtained for the two conditions (II and III); strangely enough, these were not significant. Once again the localizer deviations, which were not significant, tended to be invariant with condition (See Fig. 4(a)).

VI. CONCLUSIONS

The preliminary and incomplete results presented here suggest that, at least in the confines of a laboratory, the simultaneous use of two tactual displays of the type described herein does not result in performance degradation over the commonly used visual displays and may possibly result in some improvement. Further, in practice visual attention must be frequently directed away from the monitoring of instruments. It is probable, in light of previous evidence,[10] that visual performance would be significantly degraded compared to tactual performance, both in the laboratory simulator and inflight. It would seem appropriate to extend the tests described here to encompass such situations.

It also seems clear, that after training, little relative interference exists between simultaneously performed tactual tasks, nor was there any appreciable cross-modality interference between the tactual- and visual tasks which were performed simultaneously.

Subsequent studies should be performed to investigate the potential extent of information presented in this fashion to the cutaneous modality. For example, investigations could be undertaken to study the use of two tactual displays in a single control handle. Further, whether two control handles, both with multiple displays installed, can be effectively used.

These studies should focus on similar goals to those suggested in this paper. That is, the efficacy of such displays as compared to visual displays which are typical of present-day cockpit presentations; the determination of relative interference between simultaneously performed tactual tasks; and the determination of any cross-modality interference between tactual and visual tasks performed simultaneously.

REFERENCES

1. Forbes, T.W., Garner, W.R., and Howard, J.G., "Flying by Auditory Reference," PsychoAcoustic Laboratory, Harvard University, OSRD Rpt. No. 5123, 1945.

2. Hasbrook, A.H., and Rasmussen, P.G., "Aural Glide Slope Cues: Their Effect on Pilot Performance During In-Flight Simulated ILS Instrument Approaches," Federal Aviation Administration, Office of Aviation Medicien, Oklahoma City, Oklahoma, Report Number FAA-AM-11-24, May 1971.

3. Hirsch, J., Shafer, J.H., and Eitan, A., "Experiments in Tactile Communication," 6th Annual Conference on Aviation and Astronautics, Haifa, Israel, 1964.

4. Levison, W.H., Tanner, R.B., and Triggs, T.J., "Evaluation of Tactual Displays for Flight Control," Proceedings of the 9th Annual Conference on Manual Control, M.I.T., Cambridge, Mass., (In press).

5. Bliss, J.C., Lind, S.W., Mansfield, P.K., "Tactual Perception: Experiment and Models," Quarterly Report 1, Contract NAS2-3649, Stanford Research Institute, Menlo Park, California, Sept. 1966.

6. Geldard, F.A., Ed., "Conference on Cutaneous Systems and Devices," Psychonomic Monograph Supplement, (In press), 1973.

7. Bliss, J.C., Ed. "Special Issue -- Tactile Displays Conference," IEEE Transactions on Man-Machine Systems, Vol MMS-11, No. 1, March 1970.

8. Fenton, R.E., and Montano, W.B., "An Intervehicular Spacing Display for Improved Car-Following Performance," IEEE Transactions on Man-Machine Systems, Vol. MMS-9, No. 2, June 1968, pp. 29-35.

9. Rule, R.G., and Fenton, R.E., "On the Effects of State Information on Driver-Vehicle Performance in Car Following," IEEE Transactions SMC, Vol. SMC-2, No. 5, November 1972, pp. 630-637.

10. Gilson, R.D., and Fenton, R.E., "Kinesthetic-Tactual Information Presentations -- Inflight Studies," IEEE Transactions SMC, In press.

11. Gibson, J.J., The Senses Considered as Perceptual Systems, Houghton Miflin: Boston, 1966.

SIMULATOR EVALUATION OF THREE SITUATION AND GUIDANCE DISPLAYS FOR V/STOL ZERO-ZERO LANDINGS

M. R. Murphy, L. A. McGee, E. A. Palmer, C. H. Paulk, and T. E. Wempe

Ames Research Center, NASA, Moffett Field, Calif. 94035

ABSTRACT

Six helicopter pilots participated in a simulator study to compare and evaluate design features of three electronic displays for potential application to V/STOL zero-zero landings: the RAE proposed combined transition display, the SAAB perspective display, and the TELDIX hover display.

The experimental task was flown in a fixed-based simulation of the Bell UH-1 helicopter, without stability augmentation, and consisted of a straight-in approach with a commanded constant speed segment and a deceleration segment. Approaches were made down to approximately 20 knots indicated airspeed. The hover mode was not evaluated since the SAAB perspective display did not provide a hover capability. The six pilots flew data runs on each of the three displays with 6° and 15° flight-path angles, with and without wind conditions. The three displays were presented on a stroke-written, multifunction CRT and were slightly modified from original concepts.

Objective measures were obtained of tracking performance, attitude variability, and control activity and were analyzed by an analysis of variance. Pilot opinion was also obtained. It was concluded that (1) the RAE display is less effective than the SAAB or TELDIX displays for localizer tracking; (2) pilot workload, as indicated by RMS variability measures, was lowest with the SAAB display and highest with the TELDIX display; (3) time to capture was shortest with the TELDIX display and longest with the RAE display; (4) extensive central clutter on the TELDIX display probably resulted in its being given the lowest pilot opinion rating; and (5) pilot opinion favoring the RAE display over the SAAB display was at variance with objective performance measures.

INTRODUCTION

Ames Research Center has initiated a series of simulation and flight studies using a stroke-written, multifunction CRT to develop display concepts for application to vertical/short takeoff and landing (V/STOL) zero-zero landings. The resultant display concepts are expected to enhance both general V/STOL and tilt-rotor technology.

A requirement for an increased capability of V/STOL aircraft to operate in low-visibility and zero-zero visibility environments and the need for new displays to realize this increased capability have been substantiated in

references 1 and 2, with reference to military operations. Similar requirements exist for commercial operations.

Manual piloting of V/STOL aircraft during approach and landing is assumed to be required for an indefinite period for two reasons. First, V/STOL technology is at an early stage of development. Reference 2 states that: "At the present stage of development, reliability and cost of systems for guidance, control and stabilization for V/STOL aircraft, operational blind landings, with or without pilot control, are not to be expected in the near future." Secondly, the capability that should be provided for manual emergency takeover during operational blind landings has not been resolved.

The commercial V/STOL approach and landing problem differs from that for conventional takeoff and landing aircraft in that the following requirements are assumed: steep and/or curved approaches at low and/or decelerating speeds; transition to hover; highly precise energy management; and high-density, time-constrained flight environments. The latter requirement is assumed necessary from an economic standpoint.

In consideration of aspects of these requirements, and after a review of related research on separated vertical and horizontal situation displays, reference 2 concluded that: "The mass of information to be absorbed by the pilot, usually in different axes, poses peculiar problems in the integration of information and implies the use of combined displays." They further concluded that: "Due to their limited versatility, conventional electro-mechanical instruments do not have suitable characteristics for the V/STOL approach and landing case. Existing electronic displays and the advanced techniques being tested in laboratories and simulators hold more promise."

The objective of this initial study was to compare and evaluate design features of three electronic displays selected from reference 2: the RAE proposed combined transition display, the SAAB perspective display, and the TELDIX hover display. The study conditions purposely included a simulated vehicle without stability augmentation, with approaches to hover in a speed range above 20 knots indicated airspeed. No attempt was made to evaluate the displays in hover since the SAAB display did not provide a hover capability.

DESCRIPTION OF EXPERIMENTAL DISPLAYS

The three selected displays were slightly modified, primarily by adding digital information before the comparative study. Figures 1, 2, and 3 present these modified displays; the driving functions for the display elements are described and scale factors indicated. A heading tape and window were added to all displays for presentation of digital heading; the compass rose was eliminated from the RAE and TELDIX displays. Only heading error was presented on the SAAB display before this addition.

Two step changes in scale factor were provided for the RAE and TELDIX displays. The outer range mark for each display represents 20,000 ft initially.

When ground range becomes less than 4,000 ft, the outer range mark represents 4,000 ft. When ground range becomes less than 800 ft, the outer range mark represents 800 ft. Other modifications are discussed below for individual displays.

Modified RAE Proposed Combined Transition Display

The RAE display (Fig. 1) combines horizontal and vertical situation information in a single diagram and presents ground speed as a vector. The scaling of the velocity vector is such that the appropriate ground velocity rate is attained whenever the endpoint of the velocity vector is superimposed on the landing pad and along the appropriate approach direction. Both nominal and actual rates of descent are displayed. A horizon bar was added to the display to obtain pitch and roll information. A display of glide-slope deviation was also added. Angle of attack was removed from the display since it was not required with a helicopter simulation.

Modified SAAB Perspective Display

The SAAB display (Fig. 2) indicates height error by the position of the horizon line relative to the upper end of perspective "poles." Flight-path angle and course are displayed by the relationship of the velocity vector to the aiming dot in a "fly-from" implementation. Height error and roll information are presented in conventional "fly-to" implementations. A reference height pole is provided for use in determining absolute altitude. Airspeed error is indicated by the distance of the airspeed error indicator (line) from the periphery of the velocity vector symbol. Altitude rate was added to the display for standardization. Digital displays of altitude, airspeed, and distance to go were also added.

Modified TELDIX Hover Display

The TELDIX display (Fig. 3) differs from the RAE display mainly in that less prominence is given to the velocity vector; ground speed is displayed as length of the velocity vector with reference to range marks; glide slope and course deviation are displayed by cross pointers (horizontal and vertical lines); and the nominal rate of descent is not presented. Altitude rate was added to the display for standardization.

METHOD

Simulation Facility and Task

The experimental task was flown in a fixed-based, digital simulation of the Bell UH-1B, single lifting rotor helicopter with conventional tail rotor. Figure 4 is a diagram of the simulation facility and figure 5 is a photograph

of the simulation chair cab. The three experimental displays were presented to the pilots on a Sperry flight system, stroke-written multifunction display (MFD) located in the chair cab.

The UH-1B chair cab was fitted with conventional helicopter collective and cyclic controls and tail rotor pedals. A UH-1-type force-feel system was provided on the cyclic control and tail rotor pedals which could be disengaged by a switch on the instrument panel or by a pushbutton on the cyclic control. Rotor speed was assumed to be under governor control and was fixed at 323 rpm.

The MFD unit was located on the instrument panel 6-1/2 in. to the right of the pilot centerline. Conventional instruments (also located on the instrument panel) and the out-the-window display were covered during the experiment. Display symbology was updated 20 times per second. The usable display area was 6.5 in. wide by 7.0 in. high. Figures 6 through 9 are photographs of the RAE, SAAB, and TELDIX displays which generally present error conditions. Figure 7 shows the SAAB display without error for comparison.

The task was to fly a straight-in landing approach at the commanded speed: initial constant speed during the first segment of the approach path and commanded deceleration thereafter. Capture of approach localizer and glide slope from initial offset conditions (table 1) was also required. The localizer and glide-slope displays were processed to represent constant widths of ±400 and ±50 ft, respectively. Guidance equations for the deceleration profiles are given in table 2.

Experimental Design

Table 3 shows the modified Latin square design selected for use in this experiment. The wind sequences W_h through W_k and W_ℓ through W_o were randomly selected without replacement for each cell of the matrix from four wind conditions: (1) +24°, 18 knots; (2) -24°, 18 knots; (3) no wind; and (4) no wind. The second wind condition and the second no-wind condition were treated as repeated measures.

Pilots: Six pilots participated in the experiment. Pilots 1 through 3 were experimental test pilots. Pilots 4 and 6 were commercial airline helicopter pilots. Pilot 5 was a commercial airline fixed-wing pilot with military helicopter experience. Table 4 summarizes the flying experience of the six pilots.

Displays: The three displays were described previously.

Sequence: Each pilot flew each experimental condition twice on each of two days.

Glide slope: A 6° and a 15° glide slope were used. Since initial-condition airspeed is a function of glide slope, some confounding of glide-slope effects with airspeed effects are inherent in the experimental design.

Wind: Wind and no-wind conditions were randomly presented. Wind velocity was 18 knots and wind directions were randomly presented as ±24° with reference to the the localizer course.

Performance Measures: Fifty-five objective performance measures were taken. Table 5 defines these measures as follows:

Measure 1 is time-to-capture, where capture is defined arbitrarily to occur when the vehicle remains within 30% inner bounds of both localizer and glide-slope beams for a minimum of 10 sec.

Measures 2 through 17 are measures of absolute glide slope, localizer, ground speed, and sink-rate error at four points along the glide path, P1 through P4 (see definitions at bottom of table 5).

Measures 18 through 41 are measures of mean position, RMS error and RMS variability; for glide slope, localizer, ground speed, and sink rate; along the constant speed segment (Const) and the decelerating segment (Decel) (defined at bottom of table 4).

Measures 42 through 47 are measures of yaw, pitch, and roll RMS variability along the constant speed and decelerating segments.

Measures 48 through 55 are measures of RMS error for cyclic and collective controls and rudder pedal movement along the constant speed and decelerating segments.

Pilot Opinion: Pilot opinion and ratings were obtained from the 17 questions in table 6.

Procedure

Training: The three commercial pilots did not have UH-1 experience and were therefore given 2 hours of training on the UH-1 simulator before training on the experimental displays. This training consisted of flying with an out-the-window visual scene and with conventional cross-pointer presentations of localizer and glide-slope information. All pilots received training on the experimental displays consisting of a pictorial briefing to ensure knowledge of display element functions and an arbitrary 45 min of simulator flight experience with each display. Pilots were not trained to a criterion level.

Instructions: The purpose of the experiment and the experimental conditions were explained before the first experimental session. Initial conditions, aircraft dynamics, display descriptions, and task information were reviewed as required before each experimental session and were available to the pilots on briefing sheets at all times. The stated task was to "fly the vehicle from the initial conditions and capture the localizer and glide-slope. Fly down the approach path at commanded speed (initial constant speed during the first segment of the approach path, and commanded deceleration thereafter)."

The stated task performance criteria were (1) "minimum glide-path, localizer and speed errors" and (2) "low glide-path and localizer capture times."

Pilots were informed before the first experimental session that they could decide whether the force-feel system provided on the cyclic stick and tail rotor pedals was activated during their data runs. The three airline pilots chose to disengage the force-feel system and the three experimental test

pilots chose to engage the system. Their choices were apparently based on previous experience.

Data Sessions: During each of two data sessions for each pilot, eight data runs were made for each of three displays.

Data Handling and Analysis: Performance data were recorded on magnetic tape at a rate of 20 points/sec. An analysis of variance (ANOVA) was performed on the data by using the UCLA Biomedical Computer Program for Factorial Design (BMD08V). Table 7 shows a sample analysis for one of the 55 dependent measures.

RESULTS

Objective Measures

The results of the analysis of variance indicate large variability in pilot performance. Effects were accepted as significant for this study if $p \leq 0.05$. Forty-three of the 55 performance measures were significant for the pilot factor. The detailed analysis was confined to display main effects and display-glide slope, display-wind, and display-sequence interactions. Higher-order interactions were generally not significant and were not further analyzed.

Display Main Effects: All significant display main effects are shown in table 8. The patterning of significant effects is shown in table 9. For localizer tracking, four of the six measures of error are seen to be significant: absolute error at P2, P3, and P4; and RMS error over the constant speed segment. Table 9 also shows that these measures consistently order display effectiveness. Furthermore, figure 10 indicates that the two nonsignificant measures do not indicate contrary trends. The RAE display is clearly less effective than the SAAB and TELDIX displays for localizer tracking. The SAAB display appears to be more effective than the TELDIX display for localizer tracking.

The second consistent pattern indicated in table 9 is in measures of RMS variability. All six significant measures order the displays in effectiveness as follows: SAAB, RAE, and TELDIX. Localizer and roll variability measures are significant for both the constant speed and decelerating segments, while sink rate and yaw measures are significant only over the constant speed segment. Performance sampled by these RMS variability measures reflects display effectiveness from a workload and/or systems stability standpoint rather than from a systems accuracy standpoint.

The TELDIX display was most effective on time to capture, measure 1 with 64 sec as opposed to 76 sec for the SAAB display and 103 sec for the RAE display (see cell means in table 8). This effect is discussed further under Interactions.

Measure 53, collective stick RMS activity over the decelerating segment, indicates an effectiveness order of RAE, TELDIX, and SAAB. It is speculated that the lesser effectiveness of the SAAB display results from the lack of an artificial horizon indication for pitch cues.

No other consistent patterns were observed in the main effects.

Interactions: Display-sequence interactions were generally not significant and were not further analyzed. Significant display-glide slope and display-wind interactions are plotted in figure 11.

Time to capture is seen to have a display-wind interaction due almost entirely to the adverse effect of wind on performance with the RAE display. Wind is also seen to affect the localizer mean position over the constant speed segment much more for the RAE display than for the other two displays (measure 24). Localizer mean position over the decelerating segment is also affected by glide-slope angle (measure 25).

The large localizer tracking errors, the long time to capture, and the adverse effects of wind or steep glide slope all imply deficiencies in presenting of lateral guidance information in the RAE display. Although the SAAB display permitted the best localizer tracking of the three presentations, time to capture was shortest with the TELDIX display, possibly because of the relatively conventional cross-pointer presentation used in the capture process.

Other display-glide slope and display-wind interactions plotted in figure 11 provide little additional information.

Pilot Opinion

Cooper-Harper ratings assigned to the three displays and responses to the questionnaire in table 6 indicate a preference for the RAE display. The TELDIX display was least favorably regarded. Tables 10 and 11 summarize the favorable and unfavorable comments elicited by the questionnaire on the RAE and SAAB displays. All ratings and comments on the TELDIX display were unfavorable except for the presentation of horizontal position information. Negative responses were almost invariably stated to result from clutter associated with too many nearly indistinguishable straight-line symbols clustered at the center of the display. The average Cooper-Harper ratings assigned to the displays by the six pilots were: RAE, 3.2; SAAB, 3.9; and TELDIX, 6.5.

CONCLUDING STATEMENTS

The RAE display is less effective than the SAAB or TELDIX displa, for localizer tracking. RMS variability measures for localizer, roll, sink rate, and yaw tracking imply lower pilot workload and/or better systems stability associated with the SAAB display, followed (in order) by the RAE and TELDIX displays. Time to capture was shortest with the TELDIX display and longest with the RAE display. Cooper Harper ratings and pilot comments favor the RAE display over the SAAB display; this ordering is at variance with the objective performance data. Cooper-Harper ratings and pilot comments ranked the TELDIX display below both the RAE and SAAB displays; this ranking is supported in part by RMS variability measures. The pilots attributed the poor performance with the TELDIX display to extensive central clutter.

REFERENCES

1. V/STOL Approach and Landing Systems, Advisory Group for Aerospace Research and Development, AGARD Rept. 560, 1967.

2. V/STOL Displays for Approach and Landing, Advisory Group for Aerospace Research and Development, AGARD Rept. 594, 1972.

TABLE 1. INITIAL CONDITIONS

Dimension	6° Glide slope	15° Glide slope
Y-offset (from localizer), ft	600	600
Heading (to localizer), deg	45	45
X-range, ft	10,500	9,000
Altitude, ft	900	2,000
Airspeed, knots	60	45

TABLE 2. GUIDANCE EQUATIONS FOR DECELERATING PROFILES

Parameter	Equation*
Range to start deceleration	$X_o = \frac{V_{g_o}^2}{2a \cos \gamma}$
Altitude at start of deceleration	$h_o = X_o \tan \gamma$
Commanded ground speed	$V_{g_c} = (2a \times \cos \gamma)^{1/2}$
Ground-speed error displayed	$V_e = V_g = V_{g_c}$

*a is constant deceleration (0.025g); γ, desired glide slope; V_{g_o}, ground speed at start of deceleration; and X, range to go.

TABLE 3. EXPERIMENTAL DESIGN

Pilot	Display		
	RAE	SAAB	TELDIX
1	6° 15° W_h W_ℓ W_i W_m W_j W_n W_k W_o } Typical		
2	SAAB	TELDIX	RAE
3	TELDIX	RAE	SAAB
4	TELDIX	SAAB	RAE
5	RAE	TELDIX	SAAB
6	SAAB	RAE	TELDIX

TABLE 4. PILOT EXPERIENCE

Pilot	Total flying hours		Instrument hours		UH-1 hours
	Fixed wing	Helicopter	Fixed wing	Helicopter	
1	5100	500	600	15	70
2	1300	1600	196	98	350
3	2100	1150	287	33	600
4	1100	11850	140	20	0
5	1100	600	375	100	0
6	450+	5500+	90	10	0

TABLE 5. 55 PERFORMANCE MEASURES

Parameter	Time	Absolute Error				Mean Position		RMS Error		RMS Variability		Units
		P1	P2	P3	P4	Const	Decel	Const	Decel	Const	Decel	
Capture	1											sec
Glide slope		2*	3	4	5	18	19	20	21	22	23	ft
Localizer		6	7	8	9	24	25	26	27	28	29	ft
Ground speed		10	11	12	13	30	31	32	33	34	35	ft/sec
Sink rate		14	15	16	17	36	37	38	39	40	41	ft/sec
Yaw										42	43	rad
Pitch										44	45	rad
Roll										46	47	rad
Cyclic B-F								48	49			in.
Cyclic L-R								50	51			in.
Collective								52	53			in.
Rudder								54	55			in.

Coordinates:

Glide slope	P1	P2,$\overline{W}$	P2,W	P3	P4
6°	X = 8,500 ft	X = 6,374 ft	3,400 ft	X = 1119 ft GSp = 25 knots	Z = 66 ft GSp = 20 knots
15°	X = 7,000 ft	X = 3,482 ft	1,382 ft	X = 1152 ft GSp = 25 knots	Z = 163 ft GSp = 20 knots

*Numbers in table are nominal.

NOTE: B-F, back and forth movement; L-R, left and right movement; P1, start of constant speed data segment; P2, end of constant speed data segment, start of decelerating data segment; P3, end of decelerating data segment; P4, last point measured (low speed, near hover); Const, constant speed data segment; and Decel, decelerating data segment.

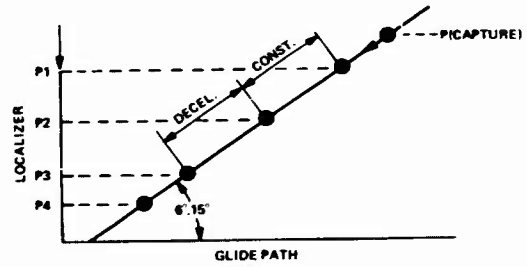

TABLE 6. DISPLAYS EVALUATION QUESTIONNAIRE

1. Did display give a feeling of realism? (Yes or No)
2. The task was (easy, a little difficult, difficult) to learn.
3. The workload was (low, medium, high) after learning the task.
4. Did you use any special strategies?
5. Information not displayed that would have been useful:_____.
6. Information displayed that was not needed:_____.
7. Were you able to satisfactorily distinguish vertical situation information from horizontal situation information? (Yes or no; explain if no)
8. Was attitude information adequate (Yes or no; explain if no)
9. Was horizontal position information adequately presented? (Yes or no; explain if no)
10. Was vertical position information adequately presented? (Yes or no; explain if no)
11. Was vertical speed information adequately presented? (Yes or no; explain if no)
12. Did the display use any confusing symbology? (Yes or no; explain if yes)
13. Was the display overly cluttered (busy)? (Yes or no; explain if yes)
14. Did the display have unsatisfactory distracting features (movements, rotations, etc.)? (Yes or no; explain if yes)
15. Did display adequately handle wind conditions? (Yes or no; explain if no)
16. Please comment on any other "good" or "poor" features of the displays.
17. Please use the attached, modified Cooper-Harper rating scale to assign each display a rating between 1 and 10.

TABLE 7. ANALYSIS OF VARIANCE FOR DEPENDENT VARIABLE 1 (TIME TO CAPTURE)

Source	Error term	F	Degree of Freedom	Mean square
1 Mean	P	172.1530	1	1898091
2 P (Pilot)	R(PDSGW)	9.0886	5	11025.60
3 D (Display)	PD	4.1381	2	37864.69
4 S (Sequence)	PS	.8950	1	2457.502
5 G (Glide slope)	PG	29.5995	1	96332.75
6 W (Wind)	PW	60.4438	1	68951.31
7 PD	R(PDSGW)	7.5427	10	9150.199
8 PS	R(PDSGW)	2.2633	5	2745.695
9 DS	PDS	.2286	2	440.7803
10 PG	R(PDSGW)	2.6828	5	3254.537
11 DG	PDG	1.8487	2	3435.844
12 SG	PSG	.2483	1	187.3125
13 PW	R(PDSGW)	.9403	5	1140.750
14 DW	PDW	5.3269	2	10342.50
15 SW	PSW	.1771	1	214.7500
16 GW	PGW	2.5796	1	486.2500
17 PDS	R(PDSGW)	1.5896	10	1928.365
18 PDG	R(PDSGW)	1.5320	10	1858.506
19 PSG	R(PDSGW)	.6218	5	754.2671
20 DSG	PDSG	1.9620	2	580.7188
21 PDW	R(PDSGW)	1.6005	10	1941.563
22 PSW	R(PDSGW)	.9993	5	1212.280
23 DSW	PDSW	1.6872	2	1329.219
24 PGW	R(PDSGW)	.1554	5	188.5000
25 DGW	PDGW	3.3288	2	3478.875
26 SGW	PSGW	.3501	1	691.5000
27 PDSG	R(PDSGW)	.2440	10	295.9827
28 PDSW	R(PDSGW)	.6494	10	787.8076
29 PDGW	R(PDSGW)	.8615	10	1045.069
30 PSGW	R(PDSGW)	1.6282	5	1975.208
31 DSGW	PDSGW	.9962	2	1666.344
32 PDSGW	R(PDSGW)	1.3788	10	1672.641
33 R(PDSGW)			144	1213.120

TABLE 8. SIGNIFICANT DISPLAY MAIN EFFECTS ($p \leq 0.05$)

No.	Parameter	Measure	Rank Order*	Cell means**		
1	Capture	Time, sec	TSR	64	76	103
7	Localizer	Absolute error at P2, ft	STR	86	132	218
8	Localizer	Absolute error at P3, ft	STR	76	112	235
9	Localizer	Absolute error at P4, ft	STR	71	110	235
10	Ground speed	Absolute error at P1, ft/sec	RTS	12	13	15
16	Sink rate	Absolute error at P3, ft/sec	RTS	5.4	5.5	6.9
27	Localizer	RMS error over Decel, ft	STR	80	128	238
28	Localizer	RMS variability over Const, ft	SRT	25	45	80
29	Localizer	RMS variability over Decel, ft	SRT	16	35	61
31	Ground speed	Mean position over Decel, ft/sec	STR	-1.8	3.9	6.9
36	Sink rate	Mean Position over Const, ft/sec	STR	1.4	2.6	3.1
37	Sink Rate	Mean position over Decel, ft/sec	STR	.1	.9	1.4
38	Sink rate	RMS error over Const, ft/sec	STR	3.8	4.7	4.9
40	Sink rate	RMS variability over Const, ft/sec	SRT	1.9	2.2	2.4
42	Yaw	RMS variability over Const, rad	SRT	.03	.05	.10
46	Roll	RMS variability over Const, rad	SRT	.02	.04	.07
47	Roll	RMS variability over Decel, rad	SRT	.02	.04	.07
53	Collective	RMS error over Decel, in.	RTS	5.0	5.2	5.4

*R = RAE, S = SAAB, T = TELDIX.

**Cell means are ordered by rank order of displays.

TABLE 9. SIGNIFICANT DISPLAY EFFECT PATTERNS AND EFFECTIVENESS ORDERS

Parameter	Time	Absolute Error				Mean Position		RMS error		RMS variability	
		P1	P2	P3	P4	Const.	Decel.	Const.	Decel.	Const.	Decel.
Capture	1 TSR										
Glide slope											
Localizer			7 STR	8 STR	9 STR				27 STR	28 SRT	29 SRT
Ground speed		10 RTS					31 STR				
Sink rate				16 RTS		36 STR	37 STR		38 STR	40 SRT	
Yaw										42 SRT	
Pitch											
Roll										46 SRT	47 SRT
Cyclic B-F											
Cyclic L-R											
Collective									53 RTS		
Rudder											

Note: R = RAE, S = SAAB, T = TELDIX.

TABLE 10. PILOT OPINION OF RAE DISPLAY

Favorable	Unfavorable
• Feeling of realism (4 pilots, Q1*) • Task easy to learn (4 pilots, Q2) • Low to medium workload (6 pilots, Q3) • No confusing symbology (6 pilots, Q12) • No clutter problem (6 pilots, Q13) • Excellent lead information in pitch and roll (1 pilot, Q16) • Excellent airspeed management display (1 pilot, Q16) • Modified Cooper-Harper rating: 3.2 (average: 6 pilots, Q17)	• Ineffective method of localizer tracking (1 pilot, Q9)

*Indicates response by four pilots to question 1 in table 6.

TABLE 11. PILOT OPINION OF SAAB DISPLAY

Favorable	Unfavorable
• Feeling of realism (6 pilots, Q1*) • Task easy to learn (4 pilots, Q2) • Low to medium workload (5 pilots, Q3) • No clutter problem (6 pilots, Q13) • Modified Cooper-Harper rating: 3.9 (average: 6 pilots, Q17)	• Ground-speed track error not readily determinable (1 pilot, Q7) • Pitch attitude information inadequate (2 pilots, Q8) • Vertical position (glide slope and/or altitude information) inadequately presented (3 pilots, Q10) • Reference height poles confusing (2 pilots, Q12) • Airspeed error indicator confusing (2 pilots, Q12 • Outside-in implementation of velocity vector confusing (1 pilot, Q12) • Vertical response of velocity vector to pitch attitude too sensitive when close in (1 pilot, Q12) • Ground speed and/or localizer tracking adversely affected by wind (3 pilots, Q15)

*Indicates response by six pilots to question 1 in table 6.

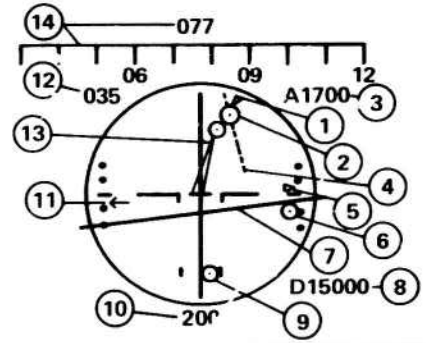

DISPLAY ELEMENT		DRIVING FUNCTIONS		SCALE/UNITS
NO.	NAME	SITUATION	GUIDANCE	
1	WIND SYMBOL	WIND DIRECTION		
2	LANDING PAD		RELATIVE POSITION OF LANDING SITE	
3	DIGITS	ALTITUDE		FT.
4	DOTTED LINE		REQUIRED APPROACH DIRECTION	
5	CURSOR	ALTITUDE RATE		600 FT./MIN./DOT
6	CIRCLE	REQUIRED ALT. RATE		600 FT./MIN./DOT
7	HORIZON BAR	ROLL & PITCH		ROLL = 20 DEG./IN. PITCH = 20 DEG./IN.
8	DIGITS	DISTANCE TO GO		
9	CIRCLE	SIDE FORCE		+2 FT./SEC.^{2}
10	DIGITS	RANGE MARK		20,000 FT. INITIALLY. CHANGES TO 4000 FT. AND TO 800 FT. WHEN GROUND RANGE $<$ 4000 FT. AND $<$ 800 FT. RESPECTIVELY.
11	CURSOR	GLIDE SLOPE DEVIATION		25 FT./DOT
12	DIGITS	GROUND SPEED		KT.
13	VELOCITY VECTOR	SPEED ERROR		(ORIGIN TO PAD DISTANCE) $\times$ $(1 + \frac{\text{SPEED ERROR}}{\text{COMMANDED ERROR}})$
14	HEADING TAPE + WINDOW	HEADING		

Fig. 1. Modified RAE proposed combined transition display.

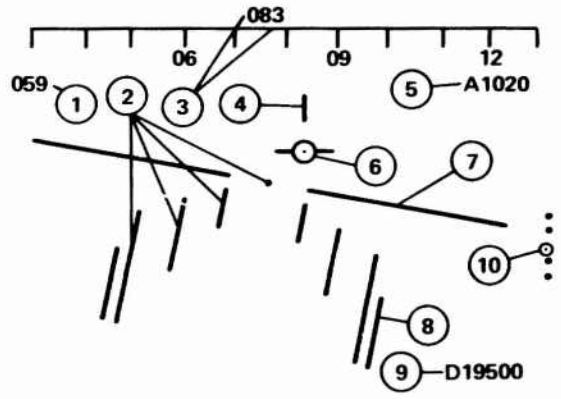

DISPLAY ELEMENT		DRIVING FUNCTIONS		SCALE/UNITS
NO.	NAME	SITUATION	GUIDANCE	
1	DIGITS	AIRSPEED		KT.
2	POLE TRACK & AIMING DOT		ALTITUDE ERROR (AE) & CROSSTRACK ERROR (CE)	AE = +160 FT./IN. CE = f(RANGE)
3	HEADING TAPE & WINDOW	HEADING		
4	AIRSPEED ERROR INDICATOR		AIRSPEED ERROR	33 KT./IN.
5	DIGITS	ALTITUDE		FT.
6	VELOCITY VECTOR SYMBOL		FLIGHT–PATH ANGLE ERROR & COURSE ERROR	20 DEG./IN.
7	HORIZON LINE	ROLL		
8	REFERENCE HEIGHT POLE	ALTITUDE		LENGTH = 300 FT.
9	DIGITS	DISTANCE TO GO		FT.
10	CIRCLE	ALTITUDE RATE		600 FT./MIN./DOT

Fig. 2. Modified SAAB perspective display.

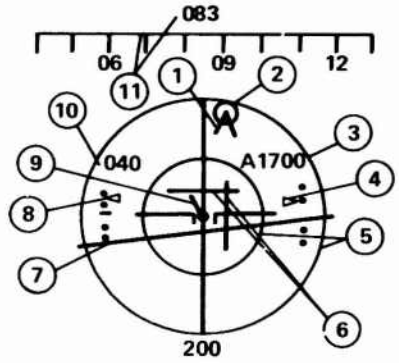

DISPLAY ELEMENT		DRIVING FUNCTIONS		SCALE/UNITS
NO.	NAME	SITUATION	GUIDANCE	
1	SECTOR		APPROACH SECTOR	
2	LANDING SITE		RANGE & BEARING TO LANDING SITE	
3	DIGITS	ALTITUDE		FT.
4	CURSOR	ALTITUDE RATE		600 FT./MIN./DOT
5	RANGE CIRCLES	RANGE		20,000 FT. INITIALLY. CHANGES TO 4000 FT. AND TO 800 FT. WHEN GROUND RANGE <4000 FT. AND <800 FT. RESPECTIVELY. INNER CIRCLE = 1/2 OUTER.
6	HORIZONTAL & VERTICAL LINES		GLIDE SLOPE, LOCALIZER	FULL SCALE: ±50 FT. GLIDE SLOPE, ±400 FT. LOCALIZER.
7	HORIZON BAR	PITCH & ROLL ATTITUDE		PITCH = 20 DEG./IN.
8	CURSOR	AIRSPEED DEVIATION		5 KT./DOT
9	VECTOR	GROUND SPEED		60 KT.=INNER CIRCLE
10	DIGITS	AIRSPEED		
11	HEADING TAPE + WINDOW	HEADING		

Fig. 3. Modified TELDIX hover display.

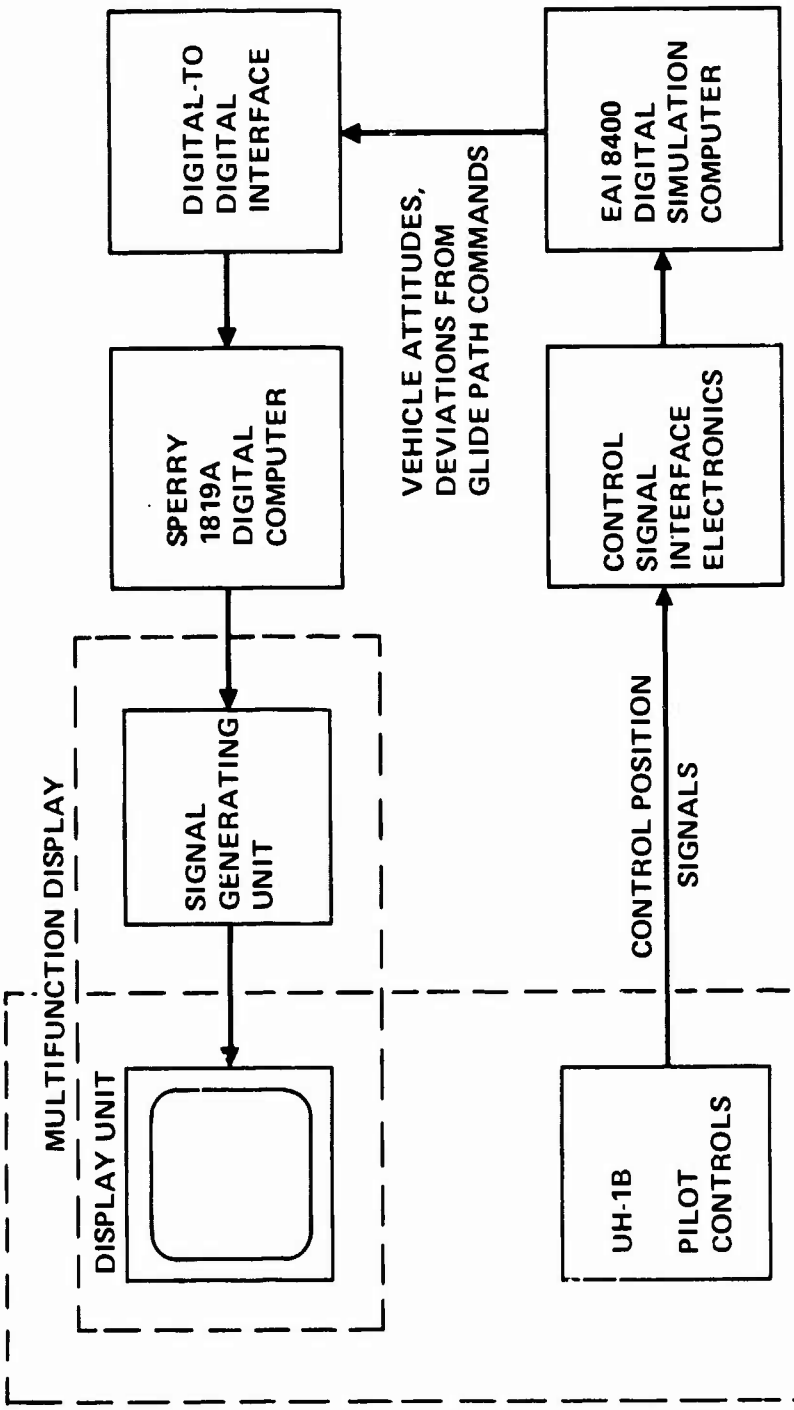

Fig. 4. Simulation facility.

Fig. 5. Simulation chair cab.

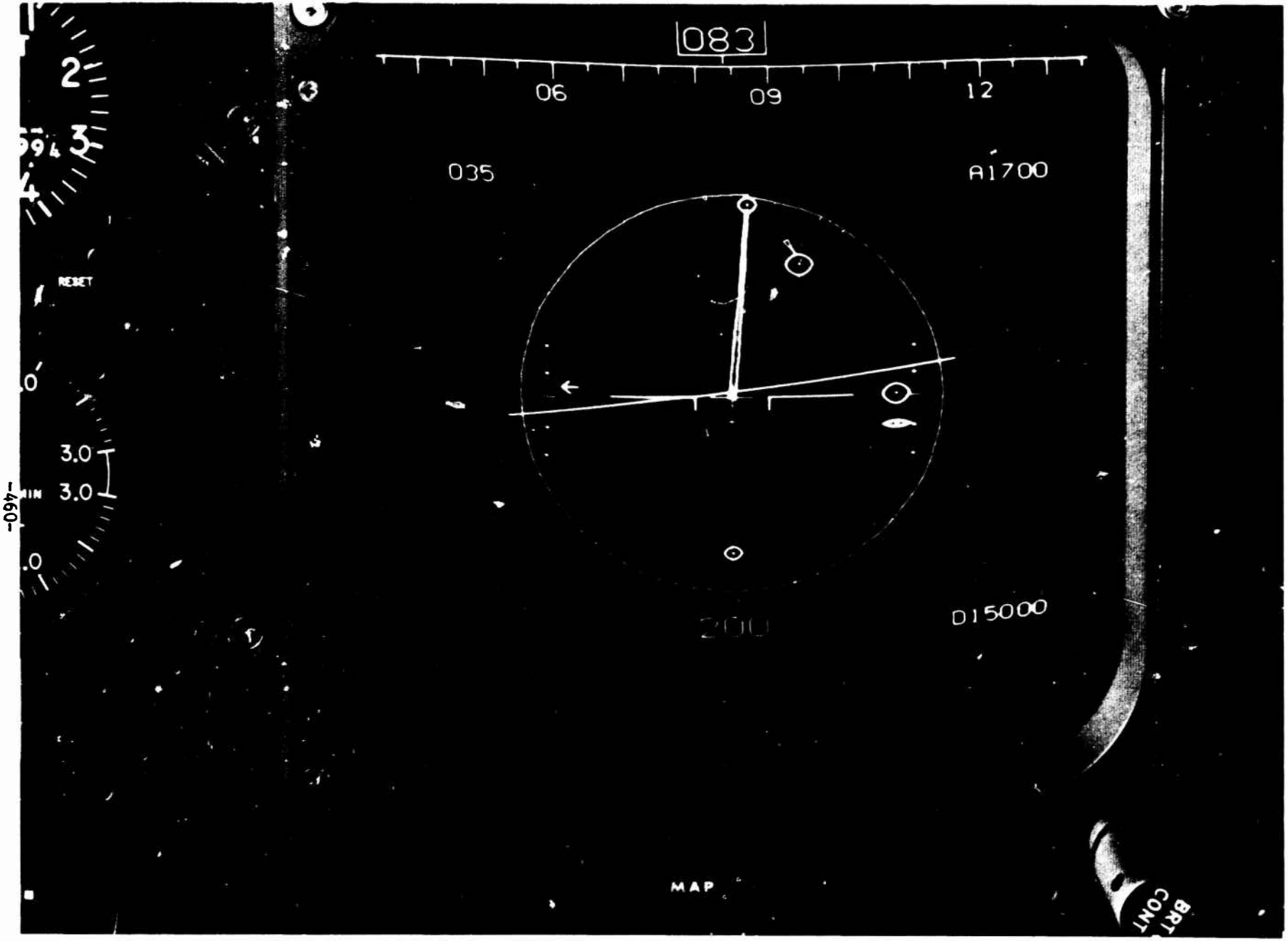

Fig. 6. Modified RAE display — showing errors.

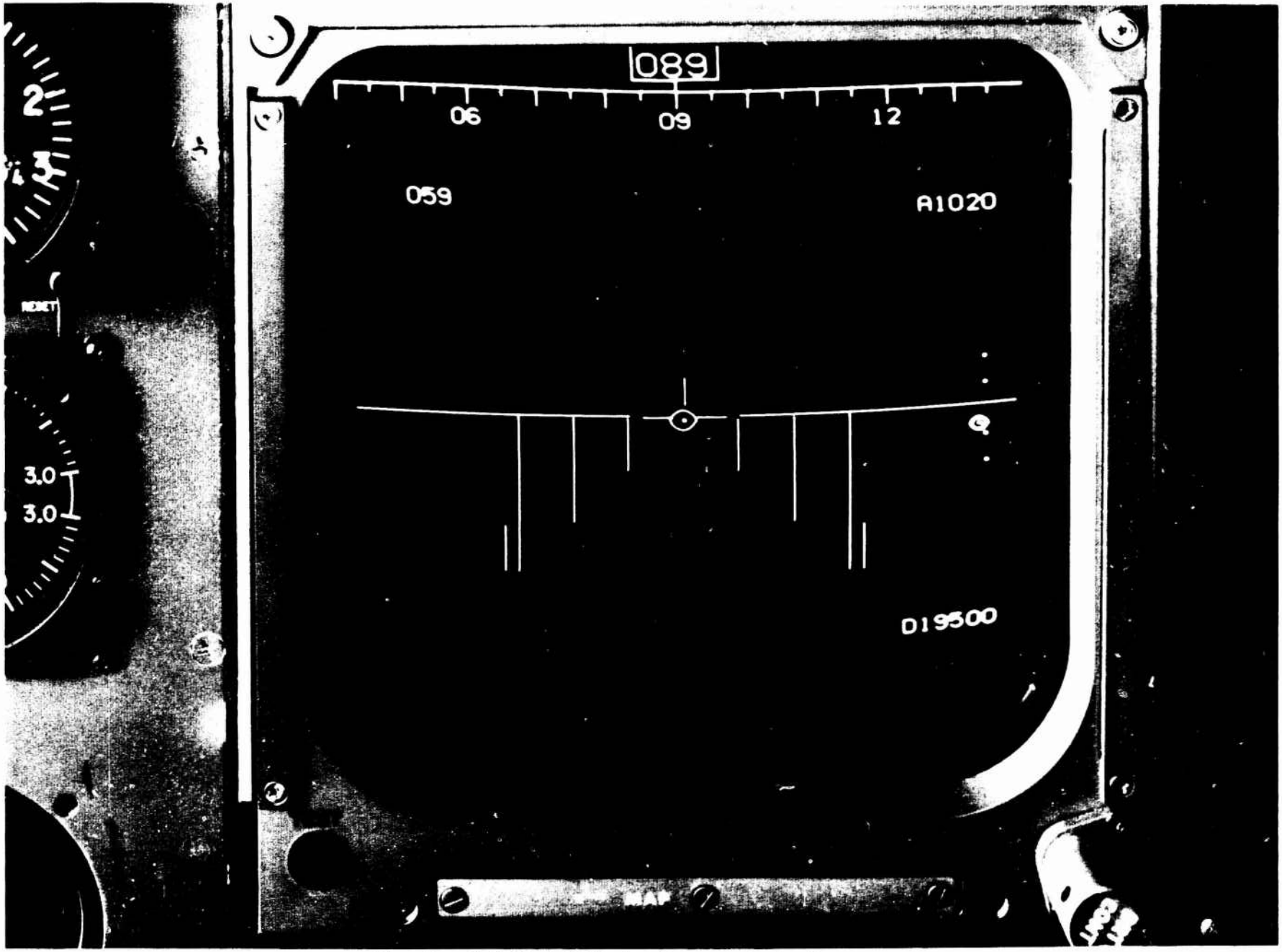

Fig. 7. Modified SAAB display — not showing errors.

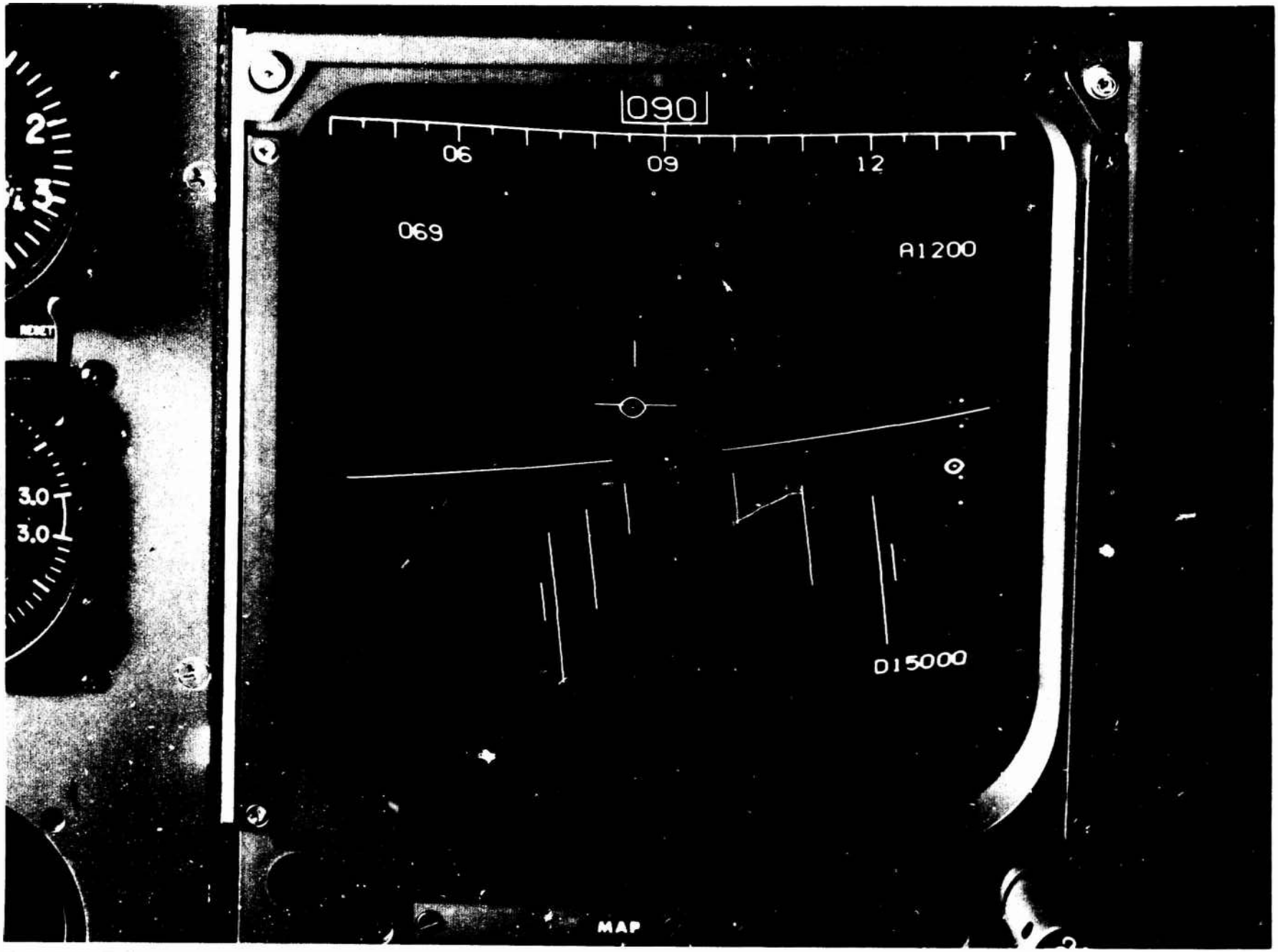

Fig. 8. Modified SAAB display — showing errors.

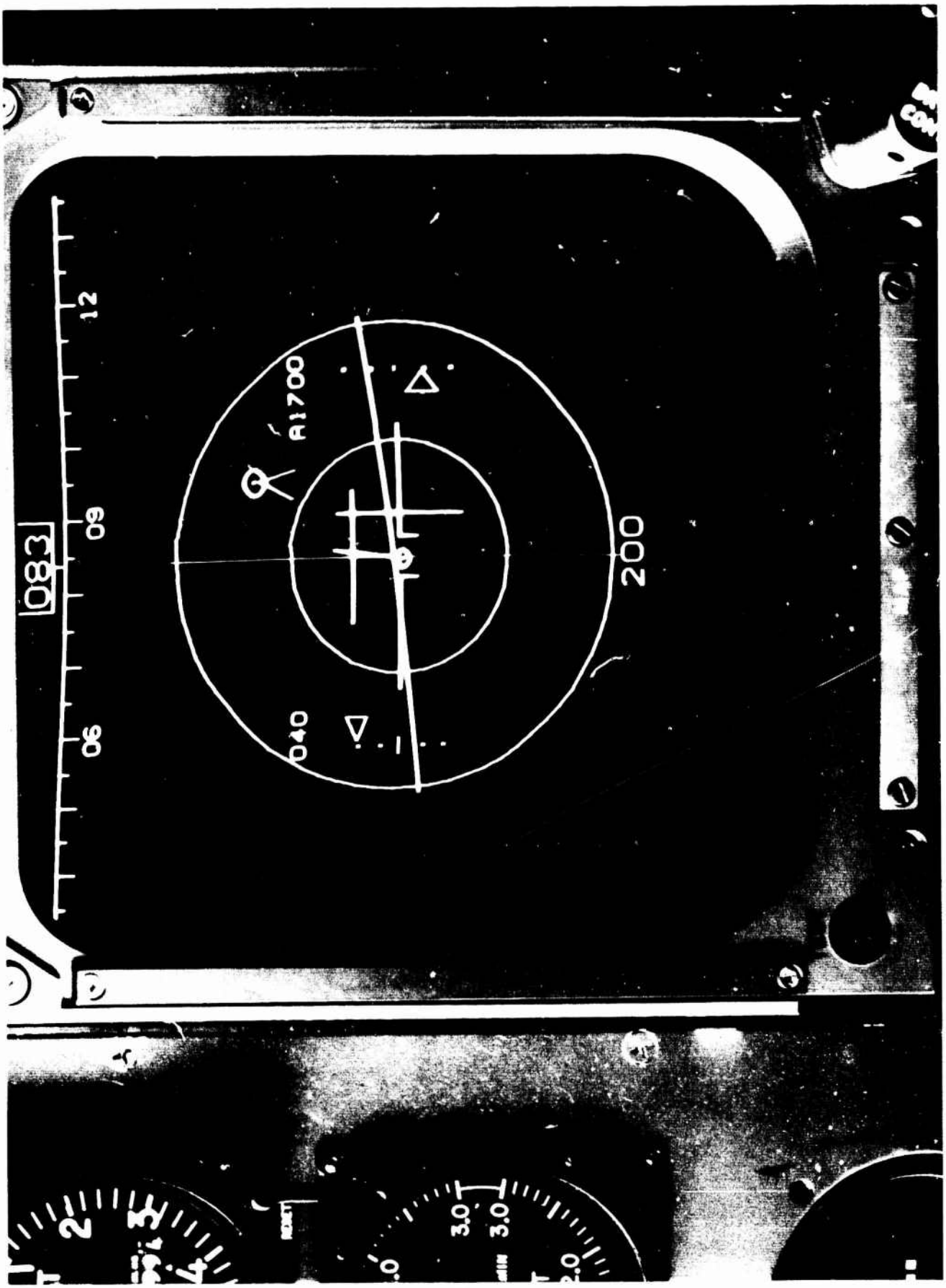

Fig. 9. Modified TELDIX display — showing errors.

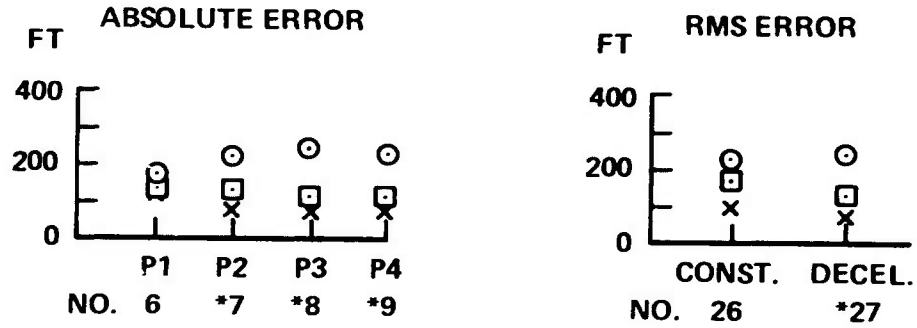

CODE: ⊙ = RAE, × = SAAB, ⊡ = TELDIX
* = SIGNIFICANT MEASURE
SEE TABLE 5 FOR CLARIFICATION OF MEASURES

Fig. 10. Localizer errors — display main effects.

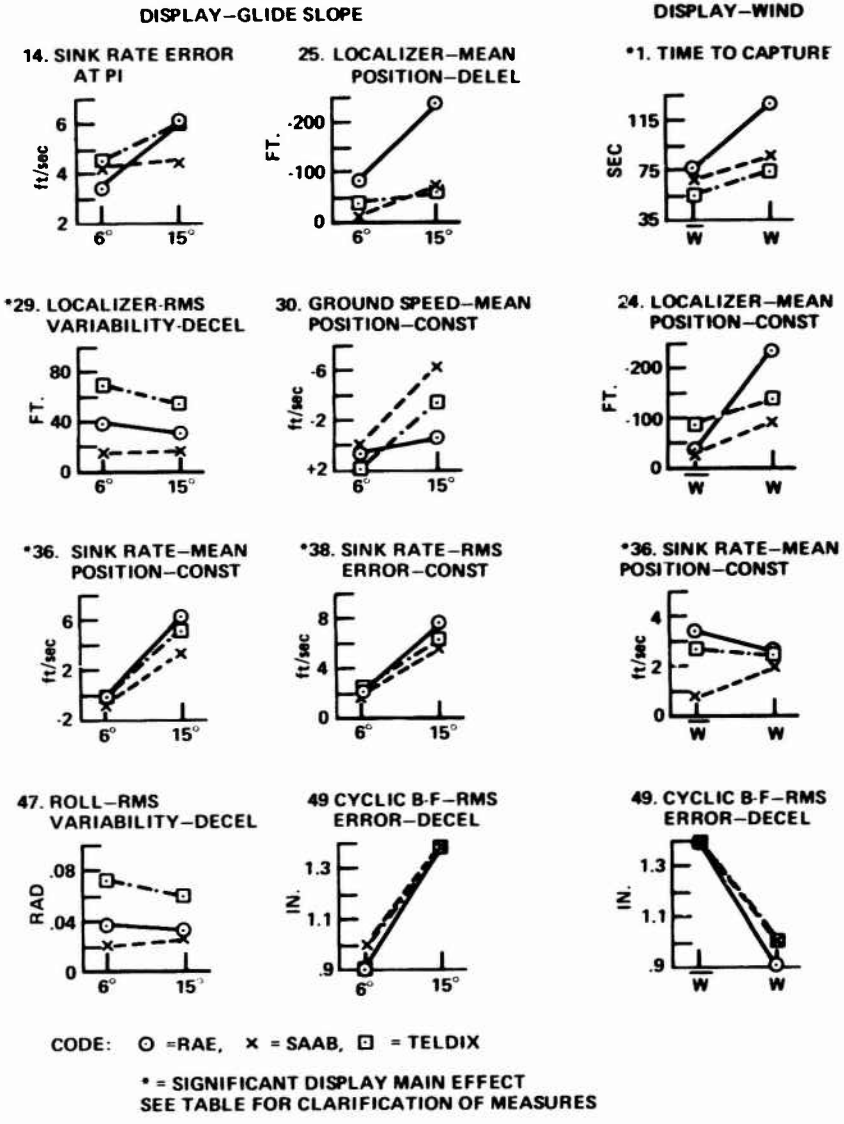

Fig. 11. Significant display-glide slope and display-wind interactions.

THE EFFECT OF DISPLAY FORMAT ON HUMAN PERCEPTION OF STATISTICS

William B. Rouse
University of Illinois at Urbana-Champaign
Urbana, Illinois

ABSTRACT

Three methods of displaying a discrete time series are compared. One display has a list format and two have graphical formats. An experiment where subjects estimated the mean and standard deviation of a time series is discussed. In the sense of average estimation error, it is shown that the display with the list format yields significantly better estimates of the mean while one of the graphically formatted displays yields significantly better estimates of the standard deviation. The other graphical display is shown to inherently distort the standard deviation of a time series. A third graphical display format is proposed and shown, in theory, to provide a reasonable compromise between the advantages and disadvantages of the other two graphical display formats.

INTRODUCTION

Data are often measured at discrete points in time rather than continuously. The time between measurements may be governed by the sampling rate of the measuring device, the cost of measurements, or the existence of some natural sampling period. A computer's cycle time is finite, and thus, it cannot sample continuously. The cost of a national census prohibits frequent measurements. Stock market quotations are referred to once per day by the nonprofessional invester because that is the natural period of his sampling of news.

Regardless of the reason, the human is frequently faced with discrete time series. Based on the information in the time series, he may make a decision to request a more detailed analysis of the computer's output, perform a check on the data collection methods, or sell his shares of IBM and buy those of Dome Mines. While the information that he perceives in the time series is usually not the only data on which he bases his decision, it certainly is often a motivating force. The point is that the human is, in some way, affected by his perception of various characteristics of the time series.

There are a variety of ways in which to display a discrete time series. A very elementary display is a simple list of numbers as shown in Fig. 1. A graphical display of a time series is shown in Fig. 2. Figure 3 illustrates a display similar to that in Fig. 2 except that the dots have been connected by straight lines. The question addressed by this paper is how these displays affect human performance.

The task chosen was that of estimating the mean and standard deviation

of a discrete time series. A knowledge of these statistics is important to various data manipulation and decision making techniques, and it is of interest to see how different forms of presentation affect human perception.

Peterson and Beach [1]* have summarized the literature on human perception of statistics. They conclude that the human is a good estimator of means. Beach and Swenson [2] asked subjects to estimate the mean of lists of two digit numbers. Subjects did very well, and similarly to statistical formulas, the quality of their estimates improved with sample size and degraded with increasing sample variance.

The data on human estimates of variability are less conclusive with some data indicating over-estimation and other data indicating underestimation depending on the emphasis of the instructions to the subjects [1]. Lathrop [3] has found human estimates of variability to be related to the actual mean, standard deviation, and sequence effects.

The results to be discussed in this paper have implications for the design of display systems. Figures 2 and 3 represent two very common display formats. The lines between the dots are usually added to give the user a better feeling for patterns, derivatives, etc. However, it will be shown that such a display inherently distorts the statistical nature of the time series and that this distortion is transmitted by the human in his estimates of the statistics of the time series.

THE EXPERIMENT

There were two experimental variables. One variable was display type, T_D. The displays illustrated in Figs. 1 through 3 will be termed List, Dot, and Line, respectively.

The second variable was the "true" standard deviation σ_T of the time series. Three values of σ_T were used for each display type. Each time series was 60 units in length and represented the sum of three periods of a sine wave and white noise where the signal-to-noise ratio equalled one.

Three replications of each T_D-σ_T combination were performed making for a total of 27 trials. Replications within a T_D-σ_T combination had statistically similar σ_T's but were different time series.

The displays were generated by a PDP-10 computer and output on 377 by 279 mm computer paper. A 56-page "book" of displays was generated for each subject. The first page of the book briefly described the experiment. The second page was blank and the remaining 54 pages presented the 27 trials, in a different random order in each book, with a blank page between each trial.

Eleven students in a senior/first-year graduate level course in Operations Research served as subjects. The experiment was performed following a two-week

*Numbers in brackets refer to entries in REFERENCES.

review of probability and statistics. Thus, the subjects were well aware of the concepts of mean and standard deviation.

The subjects all sat at classroom tables with their "books" in front of them. On the first page they read the following:

"The experiment that you are about to participate in has been designed to test your visual perception of statistics. You will look at three types of displays.

1. A list of numbers.
2. A series of dots.
3. A series of dots connected by lines.

Your task is to estimate the mean (average) and standard deviation (plus and minus one std. dev. about the mean includes 68% of the points). For a type 1 display, you should write down the numerical value of the mean and standard deviation. However, for display types 2 and 3, you need only make marks on the page indicating where you think the mean and plus and minus one std. dev. are".

The experimenter then explained each type of display on the blackboard. He discussed how one might find the distribution of a time series by drawing equally-spaced lines parallel to the time axis and counting the number of dots falling in each interval.

Based on questions from the subjects, the procedure was changed somewhat from that described above. For a Type 1 (List) display, the subjects wrote down the mean and those numbers which they felt represented plus- and minus-one standard deviation. They did not actually estimate the standard deviation.

It was explained to the subjects that they would have 20 seconds per trial to make their estimates. They were told to estimate the mean first and then the standard deviation with respect to the mean. The experiment started with the experimenter saying "turn" whereupon each subject turned the page of his book to look at the first trial. After 15 seconds, the experimenter said "write" and each subject indicated his estimates on the page. After five seconds, the experimenter again said "turn" and the subjects went to the next trial. This 20-second turn/write cycle repeated until all 27 trials were complete.

The experiment was forced-paced in this nature to avoid having subjects agonize over the decisions or attempt to actually calculate the statistics. In realistic tasks, estimation of statistics is often a minor, subconscious activity leading to some larger goal. Thus, the subjects had to be constrained from giving more attention to their estimates than they would in such realistic tasks.

RESULTS

The subjects' estimates are compared with the "true" statistics in Tables I and II. The true statistics were calculated using:

$$\bar{x} = \frac{1}{60} \sum_{i=1}^{60} x_i, \tag{1}$$

$$\sigma_x = \left\{ \left(\sum_{i=1}^{60} x_i^2 - 60\bar{x}^2 \right) \Big/ 59 \right\}^{1/2} \tag{2}$$

Table I Estimates of the Mean

	σ_T		
Display	1	2	3
LIST	3.08/16.61mm*	-1.62/18.77	4.46/22.39
	0.38/ 1.03**	-0.30/ 2.22	0.16/ 2.46
DOT	.2/ 7.36	7.95/ 8.93	10.17/13.00
	99/ 2.56	0.20/ 0.98	1.04/ 4.34
LINE	8.27/ 5.65	6.62/10.89	5.89/12.36
	-0.03/ 2.03	-2.41/ 1.64	-2.86/ 0.86

Mean/Standard Deviation of Estimate

Table II Estimates of the Standard Deviation

	σ_T		
	1	2	3
LIST	19.26/8.81mm*	35.94/14.64	38.14/23.34
	25.45/0.93**	40.23/ 1.81	52.66/ 1.38
DOT	22.55/6.24	36.88/ 7.14	49.78/13.54
	24.31/1.79	38.07/ 2.80	53.46/ 0.66
LINE	20.84/5.54	32.30/ 9.88	42.26/12.36
	24.68/0.77	39.02/ 2.07	50.24/ 6.17

Mean/Standard Deviation of Estimate

*Eleven subjects times three replications

**True statistics, three replications.

A complete analysis of variance of the estimation errors showed that σ_T was not a statistically significant factor in estimating means. However, the display-subject interaction in the mean estimates and the σ_T-display-subject interaction in the standard deviation estimates precluded further conclusions from the complete analysis.

Thus, a breakdown analysis by subjects was performed. This analysis showed that display effects were statistically significant for about one-half of the subjects. σ_T-display interaction was significant for about one-fourth of the subjects.

Looking at the estimation error distribution across subjects, it was found that List displays yielded significantly better estimates of the mean than Dot and Line displays. The errors with Dot and Line displays were not significantly different for estimates of the mean. However, while the average errors with the List displays were significantly better, the standard deviations of the errors were large. Perhaps this is due to subjects differing greatly. A reason for this might be that some subjects quickly calculated the average of a few elements of the time series to make their estimates of the mean while other subjects did (as they were told) and simply put down the estimate they perceived without any explicit calculating.

The consistently positive average errors and low variance (relative to List) of errors when estimating the mean with Dot and Line displays may have resulted because 9 of [illegible] subjects were right-handed. However, the data are too limited to support this conclusion.

Dot displays yielded significantly better estimates of the standard deviation than List or Line displays. The errors with List and Line displays were not significantly different for estimates of the standard deviation.

While Dot and Line did not yield significantly different results for estimates of the means, they did yield significantly different results for estimates of standard deviation. This motivated the calculation of the mean and standard deviation for each of these displays. For the Dot display, Eqs. (1) and (2) were used. For the Line display, the statistics were calculated by integrating the piecewise continuous functions as follows:

$$\bar{x} = \frac{1}{59} \int_1^{60} x(t)\, dt \tag{3}$$

$$\sigma_x = \left\{ \frac{1}{59} \int_1^{60} x^2(t)\, dt - \bar{x}^2 \right\}^{1/2} \tag{4}$$

Calculating these statistics for the 27 time series that were used, it was found that mean was not significantly different between display types but that the standard deviation with the Line display was significantly lower than that with the Dot display. Thus, the Line display distorts the standard deviation of a discrete time series.

If the subjects' Line display estimates of standard deviation are adjusted by adding the average amount that the statistics are distorted by connecting the dots, it is found that the estimates with Dot and Line displays are no longer significantly different. This leads one to conclude that humans perform equally well (in this task) with either display, but that the Line display is inferior because of an inherent defect in the format.

In an Appendix of this paper, the expected values of statistics calculated from connected dot displays are derived. The cases of linear and quadratic interpolation are considered. It is shown that either type of interpolation yields unbiased estimates of the mean. However, the dots connected with straight lines yielded

$$E[\overline{x^2(t)}] = E(x^2) + \frac{\sigma_x^2}{3}\left(\rho_{x_i\, x_{i+1}} - 1\right) \tag{5}$$

and the dots connected with parabolas yielded

$$E[\overline{x^2(t)}] = E(x^2) + \frac{\sigma_x^2}{15}\left(4\rho_{x_i\, x_{i+1}} - \rho_{x_i\, x_{i+2}} - 3\right) \tag{6}$$

where

$$\rho_{x_i\, x_j} = \frac{\overline{x_i\, x_j} - \overline{x_i}\;\overline{x_j}}{\sigma_{x_i}\,\sigma_{x_j}} \tag{7}$$

Interpreting Eqs. (5) and (6), ρ equals one yields unbiased statistics, but such a value for ρ is not very realistic. As ρ decreases to zero, the bias increases unitl, at ρ equals zero, the bias of Eq. (5) is almost 70 percent greater than that of Eq. (6). The actual bias in the standard deviation is dependent on the value of the mean. Equations (5) and (6) give lower bounds on the bias.

Higher order interpolations, perhaps $\frac{\sin x}{x}$ for a large number of points, will yield progressively better estimates of statistics. However, the law of diminishing returns will certainly come into play as the number of points increases and one should consider whether or not the savings will be worth the programming and execution time included in generating such a display.

The subjects' average error in estimating the standard deviation with the Dot display was 5.7 percent while, with the Line display, the average was 16.2 percent. Based on the calculations in the Appendix, it can be shown that, for the zero-mean time series in this experiment, Eq. (5) yields, at most, an 18.4 percent average error in estimating the standard deviation. This is not significantly different from 16.2 percent. Equation (6) yields, at most, a 10.5 percent average error in estimating the standard deviation.

If it is assumed that the human would make a corresponding improvement, and it is further assumed that the human estimation error will asymptotically approach 5.7 percent as the number of points used in the interpolation increases to infinity, then it could be claimed that a display incorporating a three-point interpolation scheme removes approximately 43 percent of the error that it is possible to remove and still retain the advantages of a connected dot display.

It is impressive that such a small change yields such a significant result. However, the designer of display schemes has several factors to consider. He would have to be willing to accept the assumptions of the previous paragraph and feel that the experimental task used here closely resembles the expected use for the display that he is designing. Also, he would have to determine whether or not estimation of statistics will be a significant component of that task.

As a final note on the types of displays considered in this paper, the List display caused much more variability than the other displays for both types of estimation. Before adopting such a display (perhaps for estimating means) one should consider the cost of the variability of error as well as the average error.

CONCLUSIONS

Three displays have been compared--one with a list format and two with graphical formats. Experimental data have been used to show that subjects estimate the mean of a time series better with the list format and estimate the standard deviation better with one of the graphical formats (Dot). The other graphically formatted display (Line) was shown to be inferior because it inherently distorted statistics and not because of a human limitation. It was shown, in theory, that quadratic interpolation will remove approximately 40 percent of the estimation error that it is possible to remove and still retain the advantages of a connected dot display.

Whenever a human is performing a task where estimation of statistics is a significant part of the task (even if only implicitly), the results presented in this paper should be taken into account. The format of the display may be as important as the statistics of the time series and the researcher or designer should try to avoid choosing a format that unnecessarily degrades performance.

ACKNOWLEDGEMENT

The author is grateful to Sandra H. Rouse for programming the compilation of the experimental data.

REFERENCES

1. Peterson, C. R. and L. R. Beach, "Man as an Intuitive Statistician," Psychological Bulletin, Vol. 68, No. 1, 1967, p. 29-96.

2. Beach. L. R. and R. G. Swensson, "Intuitive Estimation of Means," Psychonomic Science, Vol. 5, 1966, p. 161-162.

3. Lathrop, R. G., "Perceived Variability," J. Experimental Psychology, Vol. 73, No. 4, 1967, p. 498-502.

APPENDIX

The Statistics of Connected Dots

A. Straight Lines

The equation of a straight line between the points (x_1,t_1) and (x_2,t_2) is

$$x(t) = x_1 + \frac{(x_2 - x_1)}{(t_2 - t_1)}(t - t_1) \qquad t_1 \leq t \leq t_2 \qquad \text{(A1)}$$

If the process x(t) is stationary and ergodic, then the mean and mean-square are given by

$$\overline{x}(t) = \lim_{T \to \infty} \frac{1}{T} \int_0^T x(t)\, dt \qquad \text{(A2)}$$

$$\overline{x^2}(t) = \lim_{T \to \infty} \frac{1}{T} \int_0^T x^2(t)\, dt \qquad \text{(A3)}$$

For the piecewise continuous function defined by N - 1 straight lines connecting N points $x_1,x_2,\cdots,x_n$, assuming $t_{i+1} - t_i = 1$, $\overline{x}(t)$ and $\overline{x^2}(t)$ can be shown to be

$$\overline{x}(t) = \frac{1}{N-1}\left\{\frac{(x_1 + x_2)}{2} + \cdots + \frac{(x_{N-1} + x_N)}{2}\right\}, \qquad \text{(A4)}$$

$$\overline{x^2}(t) = \frac{1}{N-1}\left\{\frac{(x_1^2 + x_1 x_2 + x_2^2)}{3} + \cdots + \frac{(x_{N-1}^2 + x_{N-1} x_N + x_N^2)}{3}\right\}. \qquad \text{(A5)}$$

Taking the expected values of Eqs. (A4) and (A5),

$$E[\overline{x}(t)] = E(x), \qquad \text{(A6)}$$

$$E[\overline{x^2}(t)] = \frac{2}{3} E(x^2) + \frac{1}{3} \overline{x_i\, x_{i+1}} \qquad \text{(A7)}$$

Define the correlation function ρ_{ij} as

$$\rho_{x_i x_j} = \frac{\overline{x_i\, x_j} - \overline{x_i}\;\overline{x_j}}{\sigma_{x_i}\, \sigma_{x_j}}. \qquad \text{(A8)}$$

Since x(t) is stationary

$$\rho_{x_i x_j} = \frac{\overline{x_i\, x_j} - \overline{x}^2}{\sigma_x^2} \tag{A9}$$

Substituting (A9) into (A7),

$$E[\overline{x^2}(t)] = E(x^2) + \frac{\sigma_x^2}{3}\,(\rho_{x_i\, x_{i+1}} - 1). \tag{A10}$$

Thus, connecting the dots with straight lines yields an unbiased estimate of the mean and a biased estimate of the standard deviation.

B. Quadratic Lines

The equation of a parabola that goes through the three points (x_1,t_1), (x_2,t_2), and (x_3,t_3) is

$$x(t) = x_2 + \frac{(x_3 - x_1)}{2}\,(t - t_2) + \frac{(x_3 - 2x_2 + x_1)}{4}\,(t - t_2)^2 \quad t_1 \le t \le t_3. \tag{A11}$$

where it is again assumed that $t_{i+1} - t_i = 1$. For the piecewise continuous function defined by $(N - 1)/2$ parabolas connecting N points, where N is odd, (A2) and (A3) can be shown to yield

$$\overline{x}(t) = \frac{1}{N-1}\left\{\frac{x_1 + 4x_2 + x_3}{3} + \cdots + \frac{x_{N-2} + 4x_{N-1} + x_N}{3}\right\}, \tag{A12}$$

$$\overline{x^2}(t) = \frac{1}{N-1}\left\{\frac{2}{15}\,(2x_1^2 + 2x_1 x_2 + 8x_2^2 - x_1 x_3 + 2x_2 x_3 + 2x_3^2) + \cdots \right.$$

$$\left. + \frac{2}{15}\,(2x_{N-2}^2 + 2x_{N-2}\, x_{N-1} + 8x_{N-1}^2 - x_{N-2}\, x_n + 2x_{N-1}\, x_n + 2x_N^2)\right\}. \tag{A13}$$

Taking the expected values of (A12) and (A13),

$$E[\overline{x}(t)] = E(x), \tag{A14}$$

$$E[\overline{x^2}(t)] = \frac{4}{5}\,E(x^2) + \frac{4}{15}\,(\overline{x_i\, x_{i+1}} - \frac{1}{4}\,\overline{x_i\, x_{i+2}}). \tag{A15}$$

Substituting (A9) into (A15)

$$E[\overline{x^2}(t)] = E(x^2) + \frac{\sigma_x^2}{15}\,(4\rho_{x_i\, x_{i+1}} - \rho_{x_i\, x_{i+2}} - 3). \tag{A16}$$

Thus, connecting dots with parabolas yields an unbiased estimate of the mean and a biased estimate of the standard deviation.

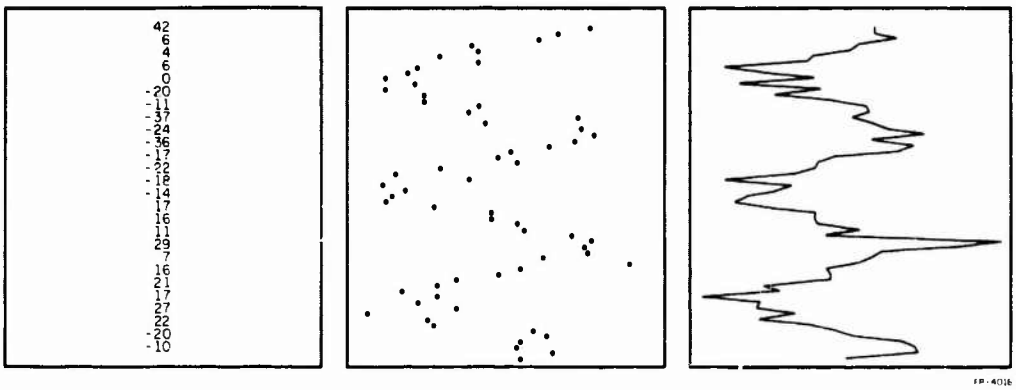

Figure 1 Figure 2 Figure 3

DISPLAY FORMATS

FUTURE TERMINAL AIR TRAFFIC MANAGEMENT CONCEPTS

John G. Kreifeldt
Department of Engineering Design
Tufts University, Medford, Mass. 02155

Thomas E. Wempe
Man/Machine Integration Branch
NASA Ames Research Center
Moffett Field, Calif. 94035

ABSTRACT

Simulation experiments are being conducted to investigate realistic alternatives to the centralized, ground-based ATC system with nearly complete computerization of human decision making projected for 1985 and beyond. The experiments involve three pilots flying simulated STOL craft and two professional approach controllers simultaneously managing a terminal traffic problem of a total of five A/C (including two 747's) all within 10 nm of touchdown at the problem start. The problem requires the 3 STOL A/C to merge between the two 747's and all five A/C to cross an approach point 1-1/2 nm away from the runway at 30 sec spacing. Seven variations of distributed-centralized control are being investigated based on three levels of ground responsibility (vectoring, sequencing only, advisory only) and four levels of pilot CRT information which combines traffic situation displays and 30 sec tactical path predictors.

A number of measures are used to compare the safety, expeditiousness, orderliness and workloads of the flights such as; average crossing rate, minimum spacing, stick and throttle activity, verbal communication etc. Except for the vectoring case, the pilots fly in an "electronic VFR" environment because of the traffic displays in the cockpits.

This report presents several initial findings. Specifically - spacing was maintained closer to a specified value and with less variance in non vectoring modes, and in general, vectoring did not produce better performance than the non vectoring modes. Predictors did not produce any large improvement in the measures so far analyzed although their presence was clearly preferred by pilots. Pilots favored vectoring least while controllers preferred it most. The group (pilots and controllers) preferred a moderate division of responsibility (sequencing) in which predictors were displayed on the traffic situation displays.

The suggestion is made that with a moderate division of responsibility, controllers could handle units of aircraft while the pilots manage the individual aircraft of a unit in a distributed responsibility management mode.

INTRODUCTION

The "Alexander Report"[1] is now fairly familiar to those interested in air traffic control systems. That report outlined the state of "crisis" in aviation in terms of present and projected future demand loads on the system (considering that several present airports such as JFK, LGA already experience heavy congestion and delays during weather conditions and peak hours), new aircraft types and the human work force in the system. Projections were made for a four-fold increase in aviation traffic and a ten-fold increase in demand for ATC service by 1995. While environmental and financial factors have reduced these projections, it would obviously be unsafe to count on them as solutions to the problem of providing the ATC systems necessary for the future.

The terminal ATC system (as of 1973) is still essentially a manual operation which provides separation service, sequencing, spacing, navigation-approach guidance and information service by employing controllers, radio communications radar and navigation aids. Increased demand on the system produces increased workloads for the controllers and requires increased controller workforce. However, attempting to solve the growing demand problem by utilizing a growing controller workforce is inherently self-limiting with the present highly-centralized philosophy for terminal ATC. As more sectors are added to the terminal airspace to keep a low aircraft density (and, therefore, low responsibility load) in each sector, the controller's workload due to aircraft hand-offs at each sector boundary increases because of the decreasing amount of time spent in a sector by an aircraft. In addition, as aircraft density increases so do the collision opportunities.

Ingredients for future ATC systems which can accommodate the projected demands and minimize controller/pilot workloads have centered heavily about improved instrumentation and automation (particularly computer automation). For example, the Third Generation ATC System (1960-1980) is semi-automated in relieving the controller of much clerical work by printing flight progress strips automatically, etc. and generally improving coordination of activities while still leaving basic decision-making to the human controller. New information display systems (ARTS III, ARTS II) for controllers are also being introduced as part of this generation.

An upgraded third generation system (1975-1995) was begun in 1969 to improve the 3rd generation system and these two should merge in the early 1980's. The upgraded third generation is a fairly radical departure in at least two ways. Much of the present human decision-making and planning are to be automated, and introduction of onboard CRTS and computers (specifically area navigation equipment-RNAV[2]) could allow the pilot to assume a greater responsibility in total air traffic control.

Even with the introduction of these two possibilities it is clear that the upgraded third generation system[3] in 1980 will still be man-intensive and ground-centralized with the controller continuing radar vectoring in medium and high density traffic.

Automation will assist the controller in metering and spacing aircraft and perhaps in conflict prediction and resolution. There will be a shift to data-link communication (isolating pilots from the general picture on "party line" where ATC system errors are often caught) and to airborne area navigation with self-contained airborne navigation systems of improved accuracy.

Some research has already been directed to the human factors aspects of the upgraded third generation system. For example, Air Traffic Situation Displays (ATSD) which were proposed several decades ago have recently been tested in simulations for their value as a pilot assurance device[4] to offset the potential hazards due to pilot isolation via data link communications. With an ATSD the pilot is assured of normal/abnormal sequence of events, his landing slot and adequate safety margins with respect to other aircraft. It was found that an ATSD did contribute to traffic awareness and did decrease controller workload. The simulated ATC system remained ground (controller) centered.

Division of Responsibility - Distributed Management

The upgraded third generation system is assumed to be completed by the end of the century at which time the fourth (or "advanced") generation system will have been in development since approximately 1985. This advanced generation system has not yet been fully detailed although implementation is expected to begin in the early 1980's. Although again a highly automated system (including human planning and decision making) is a basic assumption for the advanced system there is a great concern regarding the actual implementation of automation of the human intellectual and executive components of the system. Quotes from a recent publication may suggest some of this concern:[5]

"The fundamental issue is whether we pursue automation programs with the goal of removing the pilot (and the controller) from the command-response circuit, or with the goal of providing him with information on his aircraft's performance, its position, both geographical and in relation to other traffic, and the status of on-board and ground-based systems important to the conduct and safety of his flight. The airline pilots strongly support the latter view."

And with regard to automating aircraft guidance and control by (e.g.) coupling information directly from ground to the autopilot[6], the same writer continues:

"Transferring this responsibility to government personnel on the ground will never be acceptable to pilots and I strongly doubt that the government is ready to assume (the) liability that accompanies this responsibility."

The question of controller/pilot responsibility in future ATC system is a pivotal one[7]:

"Perhaps the single most decisive conceptual question to be answered is the extent to which traffic management in the system should be distributed between

the pilot and controller. Should the pilot be able to play an active part in the traffic management process or just a passive role?

"The number one human-factor problem in moving forward into future Air Traffic Control System design is that of controller/pilot responsibility. Behavior of the Man in the system must be given high priority."

"Human factor considerations, such as those relating to controller and pilot responsibility, may comprise the basis for the most difficult problems to solve in the development of an advanced air traffic management system."

There has been several recent examinations of this issue of pilot/controller division of responsibility. Litchford[8] suggests that there be an appropriate balance of cockpit and ground control emphasizing perhaps a greater future share of track and schedule keeping for the pilot. He points out that instrumentation in the cockpit could allow the pilot to completely execute a flight track and schedule non-conflicting tracks so that the ground need only monitor execution of the preplanned track and schedule. He cautions, as have others, that the pilots should not become controllers. It is not clear now even what the division of responsibility is to be. Litchford also suggests the use of air-to-air and air-to-ground signalling to balance controller/pilot responsibilities along with precision RNAV in the cockpit.

Anderson, et al,[9] performed a simulation experiment using a pilot and an ATC "system manager." Basically, a computer generated a sequence schedule for several aircraft and a 4-dimensional (space-time) flight path which was uplinked to a graphical aircraft situation display for the pilot. The display contained actual and desired aircraft positions and alphanumeric data. The pilot's primary role was to execute the (computer-generated) 4-D flight path, verify the data and monitor other aircraft in their flight paths. The ground controller (relieved of the major workload of radar vectoring) would insure correctness of the computer generated flight paths, monitor execution, participate during emergencies by direct communication and control over the computer. In this experiment, perfect conditions were simulated and the pilot had to maintain his 4-D position to touchdown. No other requirement was placed on him or investigated. The test was primarily one of computer sequencing, path generation and pilot execution. No pilot-ground interaction was reported so that the controller's (verbal) workload was small or non existent. No pilot-pilot interaction was possible. The pilot did in fact execute the preplanned flight path correctly.

The above experiment suggests that the pilot could be replaced by an autopilot following up-linked 4-D computer generated flight paths. This concept is being investigated by several workers[10][11] and it seems superficially capable of implementation. At present this concept demands a very highly centralized ground-based system and the earlier quotations may be recalled.

Interactive Traffic Management

The basic problem and question of interest as mentioned previously is the extent to which traffic management can be partitioned between ground and air using the capabilities offered by present and future cockpit resources such as CRT for rapidly displayed and assimilated visual information; on board computers for selected data processing and storage; air-borne sensors for inputting environmental conditions; air-to-air data exchange of information such as strategic (long range e.g. flight paths) and tactical (short range - e.g. path predictors) predictions; air-to-ground and air-to-air exchange of qualitative and quantitative information; air-to-ground data exchange channels.

These as well as future advances in cockpit capabilities coupled with the natural human decision making abilities present in the highly motivated and skilled aircraft crew define a collective resource for alternative approaches to traffic management which should be considered.

The traffic situation display forms the nucleus for thinking related to division of responsibility. Anderson, Curry et al[12] suggest that the rule structure for instrument flight rules (IFR) flying could be modified by utilizing the ATSD as a type of electronic VFR (visual flight rules) since the pilot has potentially complete information on the location of surrounding aircraft. In this use, the ATSD could also increase the number of aircraft landed per unit time by reducing the present IFR separation standards (3nm at present except for a light aircraft following a "heavy" at the same or lower altitude in which case 4 or 5 nm is required for the following aircraft) by having the pilot act as a monitor and control agent. The pilot for instance could simply be requested to trail at a commanded distance the aircraft ahead of him (visible on the ATSD). This suggestion allows the possibility of interactive traffic management between the human element in the aircraft and that on the ground. They did not, however, give any precise details. In fact no clear details exist as to how an interactive traffic management would operate. The United States Aviation Advisory Commission defined "distributed air traffic management" as "a system in which the ground controller is responsible for overall traffic flow, routing and monitoring, while the individual pilot is responsible for navigation, station keeping and collision avoidance in conformance with an approved flight plan."

Because of the lack of definite experiments in the area of interactive traffic management on which to base further conjectures and because of the need to examine alternatives to the strongly (ground) centralized highly-automated proposals for future ATC systems the experiments described here were begun at NASA-Ames Research Center in the Man-Machine Integration Branch during 1973.

EXPERIMENTS IN INTERACTIVE TRAFFIC MANAGEMENT

Research Objectives

The objectives of the research were to determine the extent to which individual

aircraft as a group in conjunction with ground based control could participate in managing their local traffic situation in the terminal area. This management involved sequencing, flight path planning and execution and spacing to insure a safe, orderly and expeditious operation of terminal traffic. Because there was little practical experimental information in this particular area of interactive ATC, the initial research was to be in the nature of probes to uncover sensitive areas and delimit potential applications. Specific research items included:

1) Measurement criteria for successful traffic management.
2) Type of visual displays and verbal communication networks most conducive to interactive management.
3) Role of prediction (anticipatory) elements in the traffic management concept.
4) Rule structures required.
5) Group decision making capabilities.

Research Purpose

The purpose of the research was primarily to investigate realistic alternatives to the highly centralized ground based ATC and computerization of high level human decision functions now being projected for future terminal air traffic management. Specific objections to proposed plans are:

1) Highly centralized, ground-based control does not seem to utilize effectively a large portion of the resources existing in the system - specifically the human decision making capabilities in the cockpit enhanced by the onboard computers, CRT displays and information exchange possibilities present or planned for future aircraft. In addition, crew members are both capable and desirous of increased traffic management participation.
2) Centralized structures suffer from difficulties in responding rapidly in an efficient adaptive manner to meet unexpected changes. Large amounts of data are required by centralized controls to deal with local perturbations.
3) It is extremely difficult to automate higher human decision processes or functions. This is particularly true when vague criteria are operative. The future controller force size is based upon projected traffic density and effective computerization of their decision making ability. The work force must be increased past projections if the software realizations do not materialize.
4) There is no guarantee that the projected automation software algorithms can be achieved.

Requirements of all future systems are that they be safe, orderly and expeditious.

Task Description

The task used to compare alternative concepts was arrived at following initial testing of several problems such as following in trail over a considerable distance, merging at an initial approach fix and trailing, etc. These were rejected basically because of a too specific nature. The adopted task incorporates a number of aspects which can be studied such as form-up, sequencing, spacing, orderliness, etc.

The basic task required that three aircraft, flown in simulated flight by professional pilots, be inserted between two scheduled aircraft on a 3^{o} glide slope initially separated at 5 nm. (The two scheduled aircraft flights are computer generated.) A map defining the task as projected onto the ground path is shown in Figure 1.

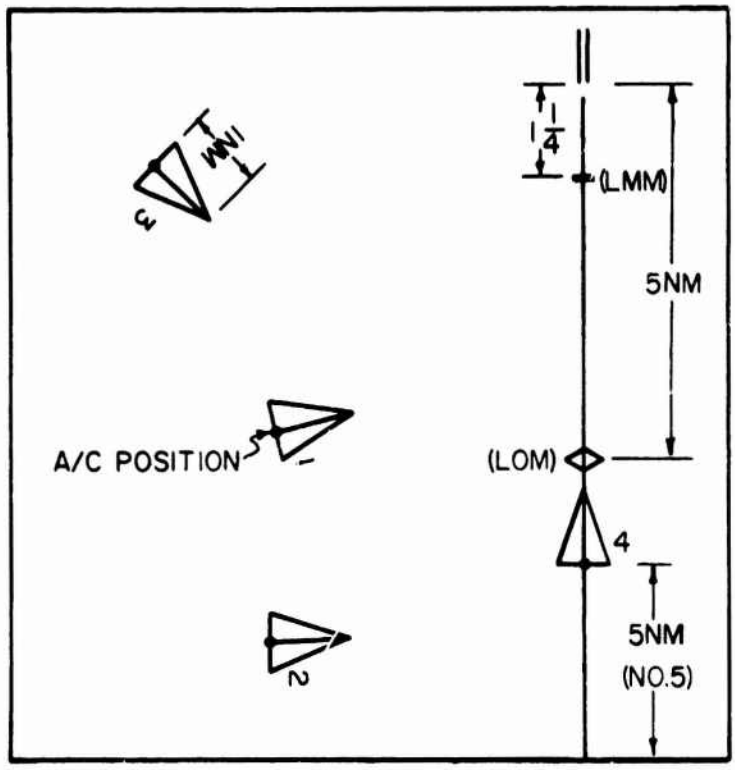

Figure 1 Ground Projection of the Task Layout

The task is terminated for each aircraft when it crosses the middle marker because adequate visual displays for the descent to touchdown were not incorporated into this simulation. Initial headings and X, Y positions and velocities of the three piloted aircraft were randomly assigned at the start of each run. Initial altitude for the three was always 3000 ft. Eighteen initial positions (and matching speeds) were possible. Positions were precalculated ensuring that the task could in fact be done within the capabilities of the simulated craft. The controllers could issue

only speed commands to the two computer aircraft via a TTY (INFOTON) keyboard operational throughout the experiment.

The task was a fairly reasonable problem in which the three piloted aircraft could be considered of a STOL type while the two (CTOL) independent computer aircraft were considered as 747. The two independent craft provided beginning and ending time constraints which required group interaction to solve the insertion problem. Each run required approximately 5 minutes to complete.

Division of Responsibility and Display Information

Three different divisions of responsibility for executing the task and four different information displays were investigated as shown in the paradigm in Figure 2.

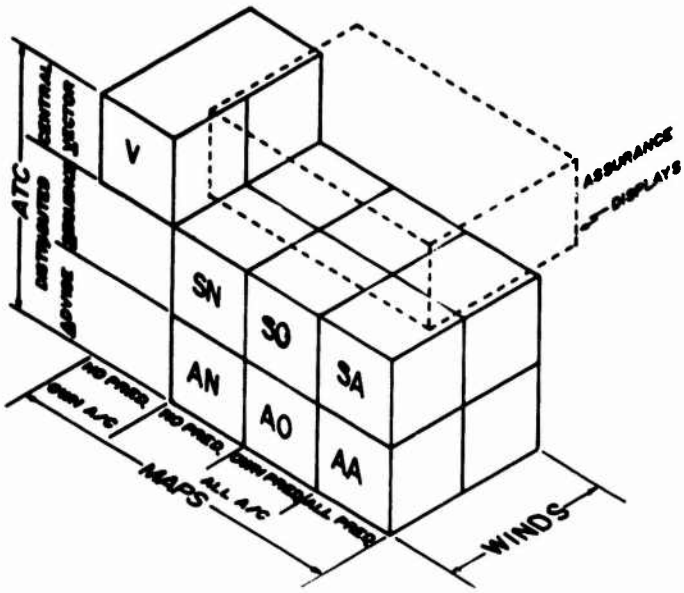

Figure 2 The Seven Alternatives Investigated in the Experiment. Assurance Displays were not Investigated.

The MAPS displays differ first in the presence or absence of other aircraft in addition to the pilot's own and secondarily in the presence of 30 sec. path predictors on "own" or on all aircraft. The ATC responsibility is either central (represented by usual radar vectoring of the piloted STOLS) as one extreme or distributed in which either an air-centered concept is used as the other extreme where the controller may only advise the STOLS) or a moderate division in which ground is responsible for issuing sequencing (order) instructions (e.g. "number 3 follow number 1") and advisorys. More definite rules for each of the three ATC possibilities were supplied to the subjects in an initial briefing and during practice. (Appendix)

The area of assurance displays was not investigated because of previous research [4] already reported. Thus a total of seven different conditions were investigated.

Pilots always saw their own aircraft on the map and controllers were aware of this and acted accordingly. For instance a pilot could be requested to "intercept the ILS." An eighteen knot north wind always blew horizontally and straight down the ILS approach line.

Task Objectives

Task objectives were defined for the subjects. Several of these are outlined here.

1) Aircraft (A/C) 4 must cross the middle marker first. A/C 5 should cross last. (4 & 5 are "747's" on a 3^{o} approach). Both should cross at 120 KTS.

2) A/C 1, 2, 3 (piloted) should be on a 6^{o} glide slope, 120 KTS, 0^{o} heading, on the ILS when crossing the middle marker.

3) Desired spacing of all A/C crossing the middle marker is 30 sec. (or 1 nm - ground projection at 120 KTS ground speed). Avoid spacing less than 30 sec.

4) Piloted A/C (1, 2, 3) must not descend below 4^{o} glide slope.

5) Minimize throttle changes, maneuvering etc.

Subjects were instructed to treat the problem as realistically as possible.

Because the "STOLS" were on a 6^{o} glide slope once on the ILS approach line and hence well above the "747's", no wake turbulence spacing was required for them although the "heavies" (A/C 4 & 5) remained approximately 5 nm apart on their 3^{o} glide slope.

Measures

A number of measures were defined which would give information relative to assessing alternatives on the three global concerns of safety, orderliness and expeditiousness and local concerns such as pilot and controller workloads, passenger comfort, fuel economy, etc. Data points were stored on each run so that the measures could be derived after the experiment. At the present time five measures are available for making comparisons, throttle movements, final lateral error, final heading error, final glide slope error and temporal spacing crossing the middle marker. In addition, questionnaires were distributed to the subjects after the experiment asking them to rank order alternatives on their own preference scales. Some of this reduced information is given in this report.

Tape recordings were made of voice communications for analysis which will be given in later reports.

Subjects were also requested to fill out sheets after each run for their qualitative assessments of workload and other factors.

Displays

Figure 3 shows a CRT display for one of the piloted A/C. The glide slope indicator assumes a conical 6^{o} cone centered on the touchdown point and thus curved approaches could be flown. The glide slope information is computed from altitude and range from touchdown. The upper lefthand numerics indicate per cent of thrust from 30%(stall at 60 KTS) to 100%(200 KTS). Altitude in feet and sinkrate in ft/min are given by the upper right hand numerics. Center numerics show heading in degrees. The map display can be selected by each pilot to show either a translating map (A/C centered, map north up) or a rotating map (A/C centered, A/C north up). The map scale could be selected by each pilot as 1" = 1.5 nm or 1" = 1/2 nm. Figure 3 shows the translating map and the 1.5 nm/inch scale.

The controller's traffic display was essentially the same as the map shown in Figure 2. The controller's display covered a 10" x 10" area, while the pilot's was a 5" x 10" display. The 2 nm radius range rings were generally dimmed by pilots and controllers until they were just visible. No predictors were ever shown on the controller's display since they are of limited or no[13][14] use.

All graphic displays were made by an Evans and Sutherland Line Drawing Systems in conjunction with an SEL 840 digital computer.

The controllers used an additional CRT display which showed flight information for the 5 aircraft displayed in the format below:

X	IDEN	A/C	ALT	HDG	SP
5		747		000	
1	FLIGHT NUMBERS	STOL CODES	ALTITUDE IN 100 ft	COMMANDED HEADING	SPEED IN 10'S KNOTS
2					
3					
4		747		000	

[SCRATCH AREA]

The aircraft list order always remained the same and only altitude, heading and speed changed. Commanded (not necessarily actual) heading appeared under HDG. This information was entered by one controller following a verbal request to a particular aircraft by the traffic controller. Heading on A/C 4 and 5 could not be changed. The speed of 4 and 5 was under direct controller control and the speed of these craft gradually approached commanded speed. Thus they could not be speeded up or slowed down instantaneously. Any commands (altitude, heading, speed) to aircraft 1, 2, 3 had to be carried out by the pilots. As an aircraft

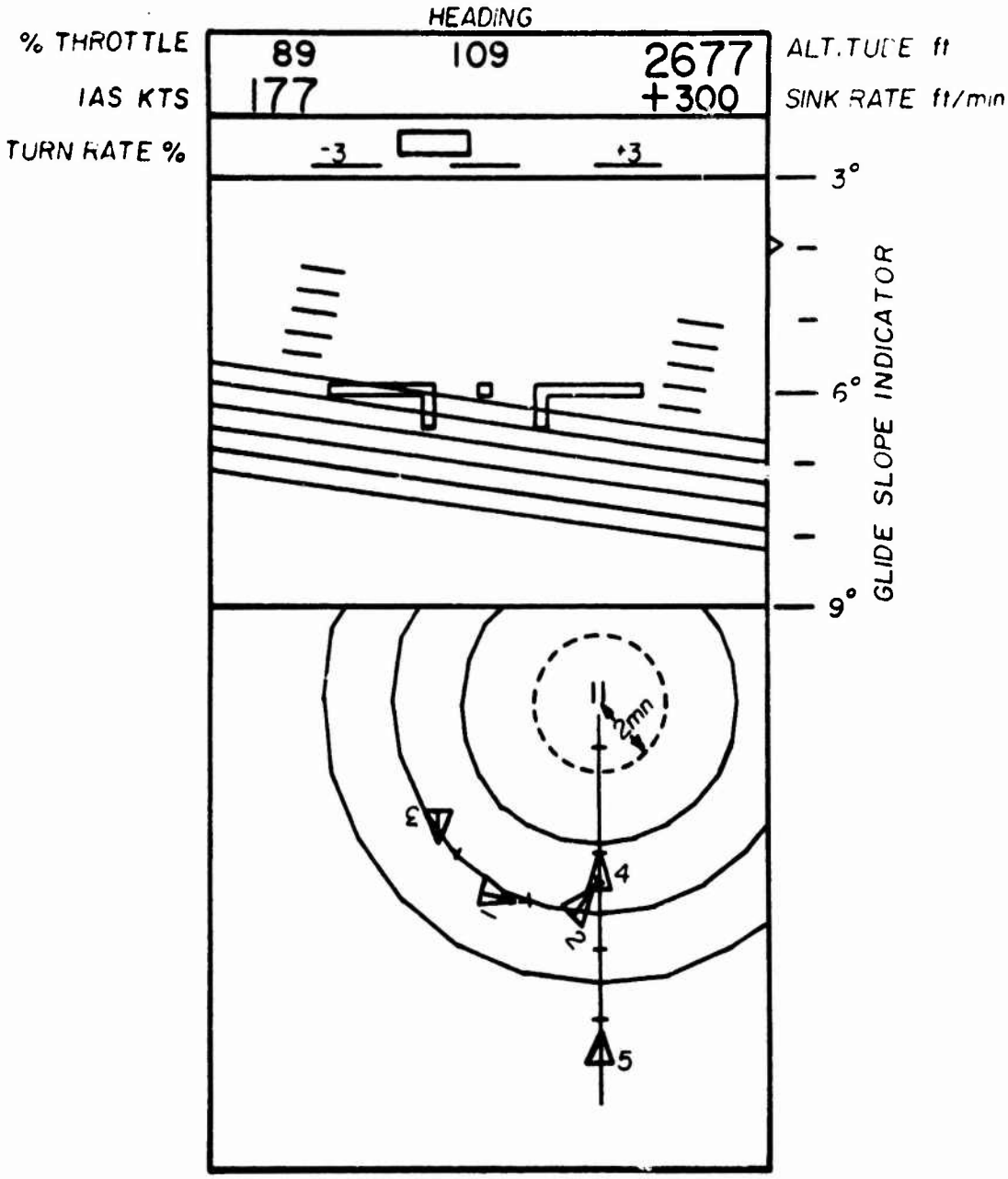

Figure 3 A CRT Display for one of the Piloted A/C. All A/C with All Predictors is shown. This is either an Advisory or Sequencing Condition.

crossed the middle marker its flight information would vanish from the display and when it crossed the farthest end of the runway lines, its symbol would vanish from all traffic displays. Controller entered information would first appear in the scratch area of the display and, if acceptable, it was entered by an appropriate key. A very rigid and simple entry format was used. Aircraft number (1-5) followed by A or H or S followed by the appropriate numerics. If a syntatical error were made, the scratch area blinked and ERROR appeared requiring re-entry from the keyboard. Controllers were generally satisfied with this display and data entry format.

Subjects, Instructions, Protocol

Figure 4 is a montage of the three pilots and two controllers who together formed a team throughout the experiment. Three separate teams have been evaluated to date with professional commercial airline pilots and practicing professional approach controllers serving as subjects.

Prior to a team's participation, each member received a six page set of instructions, objectives etc. describing the experiment. (These pages are reproduced in the Appendix.) The sheets were distributed during the first briefing period and any questions answered. A one page questionnaire directed toward the written information was then filled out by each subject to test his understanding of the material. The correct answers were read aloud and any mistakes noted and discussed. Pilots and controllers were then taken to their stations and given individual explanations of the equipment. The practice day was then started and twenty-one runs covering the seven conditions were given with intervening rest periods. A briefing was held following the practice period and the test questionnaire again distributed. Answers were read and any mistakes noted and discussed.

The experiment was then completed on two days. One trial and two test runs of the vectoring condition were given to start the first test day and to end the second test day. Three different conditions were tested on each day. One trial and four test runs of each condition were made. Thus, each condition received one trial and four test runs except vectoring. Pilots and controllers assumed the same stations throughout practice and test days.

Preliminary Results

At the present time five measures have been analyzed from the seven different conditions tested on three separate subject teams. These are reported below.

Quantitative Data

Table I shows the mean values and standard deviations for five measures - final lateral error, final heading error, final glide slope error (these were measured when the aircraft crossed the middle marker temporal spacing crossing

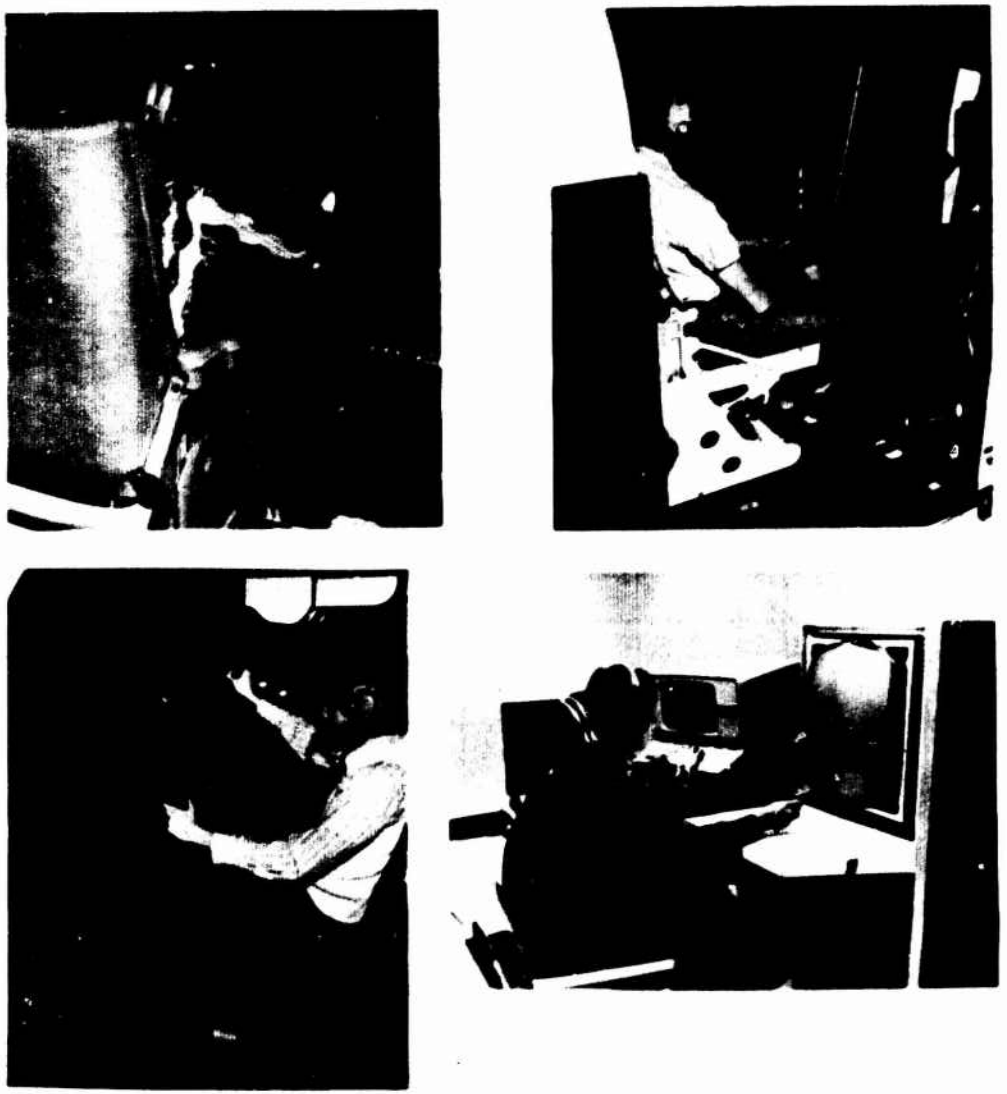

Figure 4 Montage Showing Three Pilots and Two Traffic Controllers Participating as a Team in the Interactive Traffic Management Experiments.

the marker and total number of throttle movements.

TABLE I

MEANS AND STANDARD DEVIATIONS FOR FIVE MEASURES TAKEN DURING THE DISTRIBUTED RESPONSIBILITY EXPERIMENTS

		FINAL ERROR									
		LATERAL (meters)		HEADING (degrees)		GLIDE SLOPE (deg)		THROTTLE MOVEMENT		SPACING (sec)	
		M	SD	M	SD	M	SD	M	SD	M	SD
ATC x MAPS	V	23.49	14.24	.713	.342	.139	.09	12.50	3.69	39.43	6.32
	SN	23.80	8.20	.557	.430	.153	.078	12.72	3.63	36.34	3.33
	SO	23.86	18.16	.487	.182	.181	.114	13.64	7.36	35.89	3.76
	SA	26.53	12.19	.642	.320	.172	.09	11.94	3.30	35.84	5.60
	AN	22.50	10.52	.787	.515	.133	.07	12.86	1.76	36.69	1.97
	AO	23.28	7.58	.703	.380	.167	.114	12.69	7.71	34.98	2.94
	AA	30.03	12.08	.660	.340	.216	.110	13.42	5.37	35.10	3.96
ATC	V	23.49	14.24	.713	.342	.139	.09	12.50	3.69	39.43	6.32
	VS	26.40	13.68	.508	.327	.162	.10	12.77	5.11	36.06	4.23
	A	25.17	10.23	.716	.418	.172	.10	12.99	5.52	35.59	2.96
	AVG.	25.40		.65		.166		12.8			
PRED.	N	23.0	9.35	.67	.47	.144	.07	12.8	2.68	36.52	2.65
	O	26.1	13.10	.59	.30	.174	.114	13.1	7.53	35.44	3.35
	A	28.3	12.13	.65	.33	.194	.10	12.7	4.46	35.47	4.78
	NP	23.0	9.35	.67	.47	.144	.07	12.8	2.68	36.5	2.65
	P	27.2	13.21	.62	.31	.184	.11	12.9	6.19	35.5	4.17

The measures were taken only on the three piloted simulators. Spacing was measured by the times between the crossing aircraft and the one preceding it. The task of inserting three aircraft between the two scheduled ones was completed successfully in all test runs. The data in Table I are organized to compare the seven separate conditions (ATC x MAPS); the ATC conditions separately (Vector, Sequence, Advise); the three MAPS used under Sequence and Advise (No Predictor, Own Predictor, All Predictors) and finally predictors (No predictor, Predictor). Table II shows the results of a statistical analysis [15] to test the

effects of predictors - vs- no predictors and the three ATC conditions (V-S-A) on mean values of the five measures. F-rations and degrees of freedom are given in the table.

TABLE II

F-RATIOS PREDICTOR-NO PREDICTOR
VECTOR-SEQUENCE-ADVISE

	LATERAL ERROR	HEADING ERROR	GLIDE SLOPE ERROR	THROTTLE MOVEMENT	SPACING
P-NP	3.40 (1,8)	NS (1,8)	9.33* (1,8)	1.36 (1,8)	NS (1,2)
V-S-A	NS (2,16)	1.95 (2,16)	NS (2,16)	NS (2,16)	17.86* (2,4)

NS=F<1.0 *P<0.05

Table II shows that there is a significant difference ($p < .05$) in spacing between vectoring, Sequencing and Advisory ATC conditions. Figure 5 is a plot of the spacings which indicates the vectoring condition resulted in a greater average spacing (39.4 sec.) (requested spacing was 30 sec.).

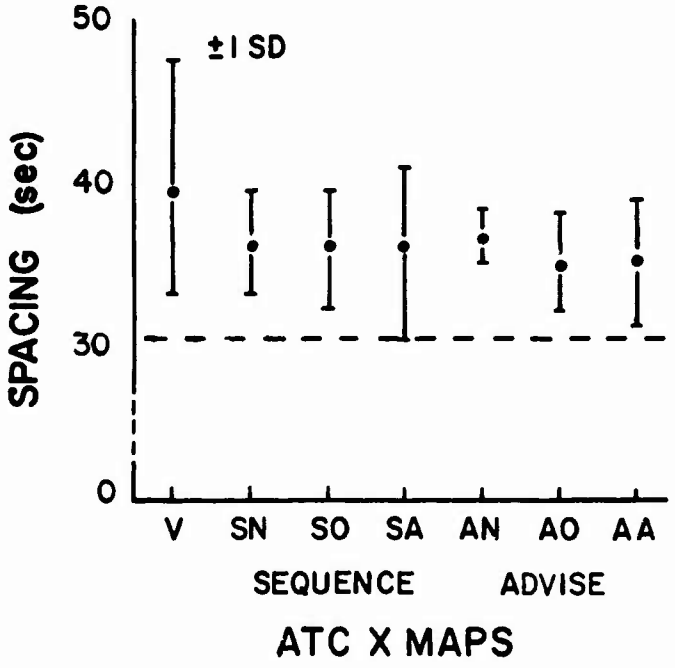

Figure 5 Means and Standard Deviations for Spacing Crossing the Middle Marker. Requested Spacing was 30 sec.

Sequencing and Advisory conditions had essentially the same spacings (36 sec.) The standard deviation of the spacings in Vectoring (6.3 sec.) also appears greater than for the non-vectoring conditions (3.76 sec.) and this difference is statistically significant ($p < .01$). Table I also suggests that the standard deviation of the spacing for Sequence is greater than for Advisory which is also confirmed ($p < .05$) as are those differences for predictors- no predictors (in Sequence and Advisory) ($p < .01$).

There were no significant differences in average number of throttle movements (12.8) although the standard deviations of the movements for no predictors-predictors were significant ($p < .01$). Throttle movements were defined as a 5 knot or greater change in throttle setting.

Lateral errors (grand average of 25.4 meters) were not significantly different nor were heading errors (grand average of 0.65 degrees). However, the standard deviations of lateral error were different when predictor-no predictor values were compared ($p < .05$).

When vectoring, Sequencing and Advisory ATC conditions were compared regarding final glide slope errors, no significant differences were found in the mean values (0.166 degrees), but use of the predictors resulted in a slightly larger glide slope error than not using predictors in Sequence and Advisory ($p < .05$). Likewise, the slide slope error variance was greater with predictors ($p < .01$) than without.

Heading error variance was slightly smaller when using predictors in Sequence and Advisory ($p < .01$).

Qualitative Data - Pilot, Controller Replies

The subjects were requested to rank order each of the seven conditions after the experiment was completed by their team. Responses from nine pilots and four (out of six) controllers were gathered and the average rank for each alternative was computed. Figure 6 shows the average rank for each basic condition, for the three ATC conditions, and for the predictor conditions in Sequence and Advise. These rankings are shown for pilots and controllers separately and both together.

The pilots preferred vectoring least and Sequencing most with Advisory close to vectoring. Controllers preferred Vectoring most and Advisory least. Sequencing is clearly preferred to Advisory by both pilots and controllers. Of the seven conditions, Advisory with no predictors was least preferred by both pilots and controllers. Sequencing with predictors would be the group preference. Sequencing with predictors and Advisory with predictors were preferred essentially equally by both pilots and controllers. Predictors were clearly preferred to no predictors by both pilots and controllers with only a slight preference for predictors on all aircraft as opposed to on own aircraft only. Statistical analyses of this preference data will be given in later reports.

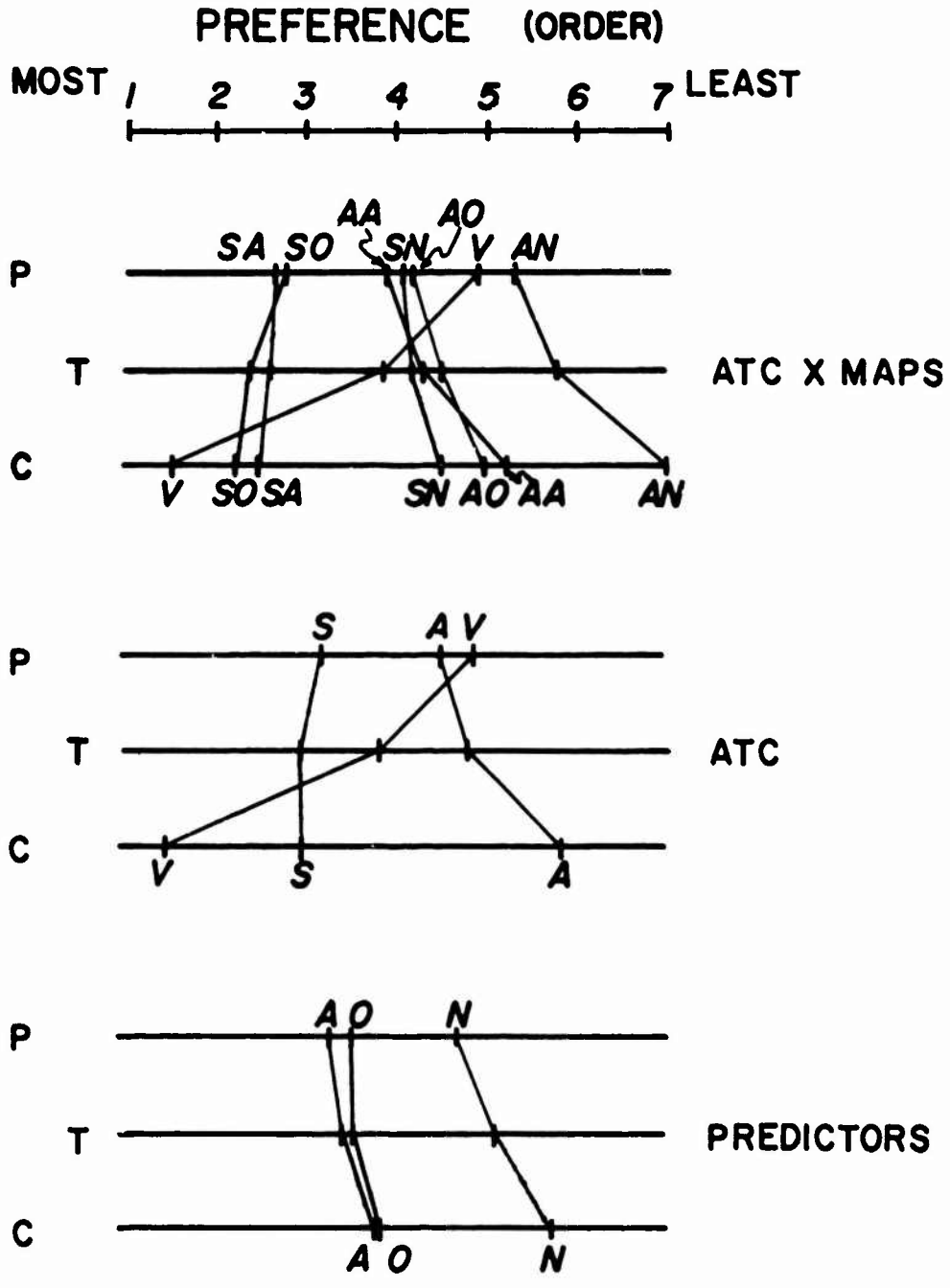

Figure 6 Average Rank Order Preference for each of the Seven Conditions (ATC x MAPS) expressed by Pilots (P), Controllers (C), and the Total Group (T).

Although analysis of the verbal data has not begun yet, anecdotal results suggest that the Controllers' verbal workload was much higher in Vectoring than in Sequencing or Advisory. Pilots' verbal workload in Sequence and Advisory did not seem comparable to that of the controllers in Vectoring. Typically in Sequence there was an initial amount of verbal instructions to the pilots followed by little or no exchange from then on. In Advisory, some controller teams kept up a constant stream of advisory information (e.g. "traffic at 2 o'clock, 2500 feet") Actual management verbal activity was low by both pilots and controllers in Sequence and Advisory.

DISCUSSIONS & CONCLUSIONS

The most obvious finding of this initial analysis is that the controllers' preferences for the three divisions of responsibility directly reflect their increasing responsibility in management. The pilots on the other hand appear to prefer least a highly air centered and a highly ground centered division (about equally) while preferring the more moderate division in which controllers issue initial sequence (i.e. order) for the aircraft leaving the pilots the remainder of responsibility for flight path planning, spacing etc. The pilots prefer a predictor, at least on their own aircraft in this mode.

Spacing, which is a global (system) concern, seems to be done better in either the Sequencing or Advisory mode. Not only is the mean spacing closer to the requested value of thirty seconds but the variance is smaller as well. From queuing theory it is known that the variance as well as the mean value of "service time" determines the average queue length such that the smaller the variance, the smaller the "stack-up". The spacing variance in the Vector condition was twice as large as for Sequencing and four times as large as for Advisory. However, while the average spacing was smaller (but not significant) using predictors, the variance was larger. This is somewhat counter to previous studies[16] which show that predictors tend to reduce variances particularly among subjects.

Table I suggests that as spacing becomes more accurately controlled (smaller mean and variance) the number of throttle movements increase slightly which would be reasonable.

There was no difference between Vectoring, Sequencing and Advisory on any of the measures except spacing from which one can conclude that for this particular task, Sequencing (a moderate division of responsibility) could be an acceptable alternative to Vectoring based on pilot and group preferences, improved spacing accuracy and (potentially) reduced spacing variability, and lack of evidence that Vectoring produced any superior performances.

There was some confounding in the experiment in that the Vectoring condition never displayed other aircraft to the pilots (assurance displays). This could change the preference (subjective) ratings but it is unlikely it could change the spacing (objective) results.

Predictors on "own" or all aircraft were clearly preferred even by the controllers who could not see them on their display but were aware of their characteristics from initial explanations and watching the pilots' displays during briefing sessions. Paradoxically, the only clear evidence of a predictor related average performance difference was a slight but statistically significant (.04 degrees) increase in glider slope error. Likewise, the error and spacing variances seemed to increase with predictors. Since the predictor-no predictor comparisons were made only in the non vectoring conditions, it is difficult to attribute these performance decrements to the increased responsibility (workload). It is expected that throttle movements would increase with predictors displayed since they provided tactical feedback on which adjustment could readily be made and assessed. It is not clear, however, why spacing variance should be larger with predictors. A possible explanation is that predictors added a certain amount of "clutter" to the display such that tendencies toward more accurate spacing possible with predictors were somewhat offset by display confusion. The "clutter" possibility is suggested by the smaller standard deviation of "own" predictor compared to all predictors in the Sequencing and Advisory modes. This difference is significant at the 5% level while the difference in average spacing is not significant.

Since there was a strong preference for having predictors displayed, it must be assumed that the pilots have some need for them even though the measures analyzed so far do not reflect this. It could be conjectured that predictors displayed on other aircraft provide tactical information as to their intentions and thus act at least as assurance elements to a pilot while the pilot's own predictor is useful in spacing and timing functions. Controllers may also feel assured of the pilots' ability to manage some of the traffic situations knowing that they have this tactical information and can respond to it. Clearly tactical information of this short range (30 sec.) is not useful directly to controllers as demonstrated by other work[13] and previous trials to this set of experiments.

The experimental results thus far suggest that a fairly expeditious flow of traffic can be managed without unrealistic workloads for controllers or pilots by allowing the pilots a considerable participation in the overall management.

Other measures such as closest spacing, trail stability, amount of maneuvering, aircraft roll and pitch accelerations etc. are being analyzed in order to continue comparisons between the experimental conditions. An attempt will be made to compare objectively the alternatives on the overall (subjective) criterion of orderliness by using fast time playbacks of recorded ground tracks and multidimensional scaling techniques based on the subjective evaluations. It is possible for example that the presence or absence of predictors may have an effect on the perceived orderliness of the flights.

POSSIBILITIES FOR IMPLEMENTATION

None of the experimental alternatives assumed anything more than existing or slightly state-of-the-art engineering. CRT's and onboard computers are presently available. Suitable air-air or air-ground data links are already in the planning phases at least. For example, the predictors were based on present bank angle

and air speed. An onboard computer is clearly capable of computing and displaying one's own predictor. A predictor from another aircraft could also be computed and displayed from similar information broadcast in a suitable code from that aircraft. If a high (several times/sec) data rate is not anticipated it is possible that state parameters from which an efficient model of the other aircraft could be made and the predictions "filled in" between transmissions could also be sent.

In a mode such a Sequencing with either "own" or all predictors displayed and with sufficient experience such that controllers are in fact assured of airborne human decision making and execution functioning, the total management strategy could be markedly different. High volumes of traffic could be managed safely, expeditiously and in an orderly manner with acceptable controller workloads by having a controller handle several aircraft organized as a unit rather than individual aircraft. He would rely upon the elements of the group to manage their local traffic situation with minimal controller input. Thus future concepts would revolve around ground-based centralized control of the units with a distributed management within each unit. The size of a unit would be variable from one (an individual aircraft) to several depending upon aircraft capability and intentions. Future experiments should be addressed to this concept and its ramifications.

SUMMARY

Preliminary results were reported from an experiment in three alternatives for pilot/controller division of responsibility in managing terminal approach air traffic. The problem required that three piloted simulator aircraft be inserted onto a 6^{o} glide slope between 2 computer aircraft on a 3^{o} glide slope such that the aircraft cross a middle marker on an ILS every thirty seconds. Three divisions of responsibility were defined: Vectoring, Sequencing (controller issues order, instructions and advisories only) and Advisory (controller issues advisories only). Pilots had Air Traffic Situation Display (ATSD) with or without predictors except in the Vectoring mode in which only their own aircraft was visible on the ATSD. No difference in mean performance could be found for five measures analyzed so far except for temporal spacing in which the two non-vectoring modes were superior both in average spacing and in reduced spacing variability. Vectoring was preferred first by the controllers and last by the pilots who preferred Sequencing first and Advisory second. Pilots (and controllers) preferred predictor displays to no predictor displays in Sequencing and Advisory.

A suggestion was made that, by using a distributed responsibility such as Sequencing, future terminal traffic management could be based upon units of aircraft handled as entities rather than individual aircraft.

REFERENCES

(1) Report of Department of Transportation Air Traffic Control Advisory Committee. U.S. DOT, December 1969.

(2) "RNAV Seen As Basis For Future ATC" AOPA Pilot. June 1973 pp. 42-43

(3) Gilbert, G. A. "Historical Development of the Air Traffic Control System". IEEE Trans. Communications, VOL. COM-21, No. 5, May 1973.

(4) Howell, J. D. Simulator Evaluation of Pilot Assurance Derived from an Airborne Traffic Situation Display. FAA Report No. FAA-EM-72-3. Final Report February 1972.

(5) Cotton, W. B. "Automation Issue". Letters to the Editor. AV Week & Space Tech. November 19, 1973 p. 20

See also

Cotton, W. B., "Formulation of the Air Traffic System as a Management Problem". IEEE Trans. Communications. VOL. COM-21, NOV. 5 May 1973.

(6) Erzberger, H., Pecsvaradi, T. "4-D Guidance System Design With Application to STOL Air Traffic Control" Paper 14-1. Proc. 1972 Joint Automatic Control Conference of the American Automatic Control Council. Stanford Univ., Stanford, Calif. August 1972.

(7) Gilbert, G. A. Air Traffic Control, The Uncrowded Sky Smithsonian Institution Press. City of Washington 1973. pages 104, 106, 107.

(8) Litchford, G. B. Aeronautics and Air Traffic Control NASA CR-1833 August 1971.

(9) Anderson, W. W., Will, R. W., Grantham, C. "Study of Aircraft-Centered Navigation, Guidance and Traffic Situation System Concept for Terminal-Area Operation". NASA TN D-6992 November 1972.

(10) Lee, H.Q., McLean, J.D., Erzberger, H., "Guidance and Control Techniques for Automated Air Traffic Control" Journal Aircraft, Vol. 9., No. 7, July 1972.

(11) McLean, J.D., Tobias, L., "An Interactive Real Time Simulation for Scheduling and Monitoring of STOL Aircraft in the Terminal Area". Journal Aircraft, Vol. 10, No. 6, June 1973.

(12) Anderson, R.E., Curry R.E., et al., "Considerations for the Design of an Onboard Air Traffic Situation Display" paper No. 8. 7th Annual Conference on Manual Control. Univ. of S. Cal., Los Angeles, Calif. June 2-4, 1971.

(13) Rouse, W.B. An Application of Predictor Displays to Air Traffic Control Problems. MIT Engr. Projects Lab. Report 70283-15, September 1970.

(14) Comment: We tried predictors on the Controller's Display and found them a definite hindrance due to their added clutter. Also the controllers could not effectively utilize this essentially tactical information. The controllers apparently obtained sufficient "predictor" information from heading which was displayed as part of the A/C symbols on the traffic display.

(15) Winer, B.J. Statistical Principles in Experimental Design 2nd ed. McGraw-Hill 1971.

(16) Kreifeldt, J.G., Wempe, T.E. Pilot Perfo ance During a Simulated Standard Instrument Procedure Turn With and Without a Predictor Display. NASA TMX-62, 2-1. January 1973.

ACKNOWLEDGEMENT

The first author would like to express his gratitude to the NASA-Ames Research Center (Man/Machine Integration Branch) and to the National Research Council for providing the opportunity to pursue this area of research. The help of many persons was received during the research year spent at Ames. In particular, the authors would like to thank Bernie Pardo for helping run the experiment and for doing much of the statistical analysis. The help of the local Professional Air Traffic Control Organization (PATCO) is also gratefully acknowledged.

INTERACTIVE TRAFFIC MANAGEMENT

Instructions to Subjects

This is an experiment to explore different techniques in air traffic management in terminal areas. These experiments are undertaken in order to examine the relationships that exist between equipment, people, rules, etc. that make up complex systems such as air traffic control. The experiment investigates three simplified air traffic management possibilities. Hopefully, insight can be gained into the design of future systems which optimize the human's participation in air traffic management.

You are asked to participate in the spirit of as much realism as is possible. A brief description of the experiment follows. Feel free to ask any questions as desired for clarification.

I. TASK DESCRIPTION

The basic task is outlined here. Refer to the figure below for a picture of the ground markings.

1. Aircraft (A/C) 4 must cross the Marker first. A/C 5 should cross the Marker last. The primary task is to try to get A/C 1, 2, and 3 between A/C 4 and 5 in the landing sequence.
2. Piloted A/C (1, 2, and 3) should be on a 6° glide slope, 120 kts., and a 0° heading when crossing the Marker.
3. Desired expeditious spacing of all A/C crossing the Marker is 30 sec. or 1 nm (at 120 kts.). Avoid spacing less than 30 sec. (Otherwise use "VFR" spacing or follow controller's instructions.)
4. Piloted A/C (1, 2, and 3) must not descend below a 4° glide slope (because of wake turbulence) within 4 nm. of end of runway; for sequencing and advisory conditions this is the only altitude rule.
5. The task is completed (i.e. data recording stops) for each A/C as it crosses the Marker. Continue at altitude and fly over the runway. A/C will vanish at the end of the runway.
6. The task will be scored on such variables (as the A/C cross the Marker) as deviation from the 6° glide slope, deviation from 120 kts., and deviation from 0° heading and glide path.
7. The task will also be evaluated in terms of performance measures such as safety, expeditiousness, and orderliness.
8. Initial conditions are such that A/C 1, 2, and 3 are at an elevation of 3000 ft. with various airspeeds and headings, A/C 4 and 5 are 5 nm apart, and are on a 3° glide slope with a speed of 130 kts.
9. For the Vectoring condition only: maintain a 3000 ft altitude for A/C 1, 2, & 3 until told to descend by controller's direction or told to descend by controller in response to a pilot request to descend.

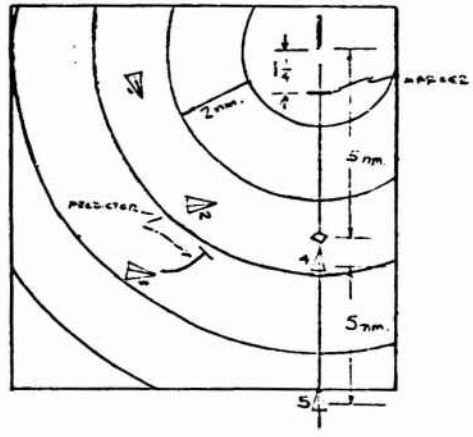

II. AIRCRAFT TYPES

1. A/C 4 and 5 are 747's on a 3° approach, nominal 130 kts. Their speeds are under controller command and are simulated by computer. Speed changes can be +30 kts and -10 kts (120 to 160 kts.).
2. Aircraft 1, 2 and 3 (piloted) are STOL type. Speed range 60 kts. (stall) to 200 kts.
3. Pilot CRT displays are shown in the figure below.

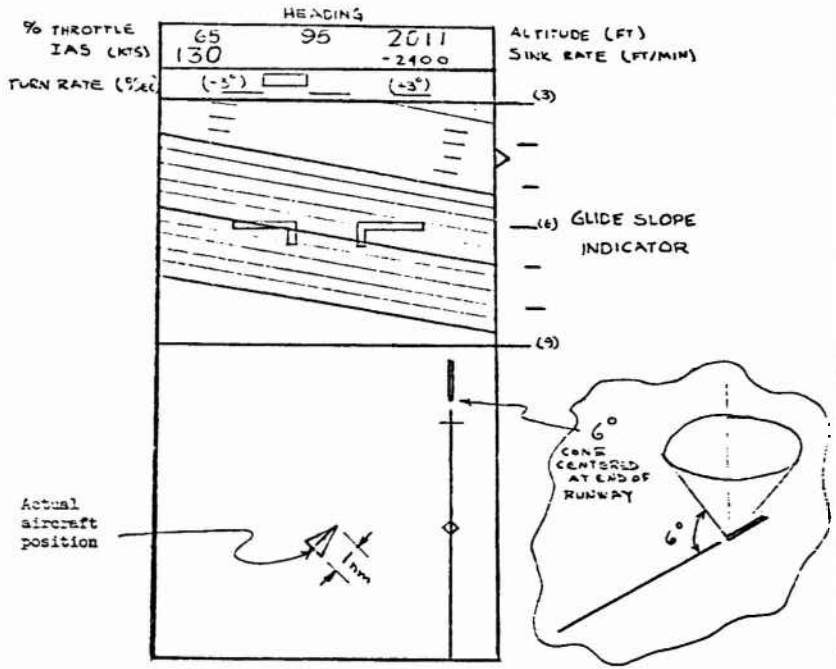

III. EXPERIMENTAL CONDITIONS

There are three different ATC conditions and four different levels of map information presented to the pilots to be explored in this experiment. There are seven clearly separated system possibilities as shown in the Table. Each possibility will be explained in more detail later.

ATC GROUND RESPONSIBILITY	MAP INFORMATION			
	own A/C visible only	all A/C visible		
	no predictor	no predictor	own predictor	all predictor
vectoring	X			
sequencing		X	X	X
advisory		X	X	X

Predictors are 30 sec. path extrapolations based on current bank angle and speed projecting from the aircraft present position at the center of the A/C symbol. The predictor originates from the center of the aircraft symbol. The controller always sees all aircraft without predictors. Pilots always see at least their own aircraft on the map.

Four trials will be made under each of the seven possibilities. All trials will be made with a headwind of 18 kts, 0°.

IV. SYSTEM RULES

There are several basic rules which apply under each of the seven conditions. Generally they are to be regarded as adding to realism and/or trying possible rules.

pilots: In performing the task, try to minimize the amount of maneuvering and throttle activity. Fly reasonable maneuvers assuming that you are carrying passengers and have the usual company concerns of fuel economy, schedule, etc. Computer records will be kept of such things as stick activity, throttle activity, etc. for later analysis.

controllers: For A/C 4 and 5, controllers have control over speed only. A/C 4 and 5 are on a 3° approach. Speed commands may be issued to help accomplish the task. Maintain a 5 nm separation between A/C 4 and 5 during approach. A/C 1, 2, and 3 (piloted) should always be above A/C 4 and 5.

pilots and controllers: Use the intercom system as usual and as desired. Pilots identify yourself when communicating. Pilots can communicate with each other (and the controller) under all conditions.

1. Vectoring

controllers: Vector A/C 1, 2 and 3 as necessary to accomplish the task subject to the task constraints. Spacing of A/C 1, 2 and 3 is at your discretion. Pilot can always see his own A/C relative to the fixed ground markings on the CRT but does not see the other A/C.

pilots: Follow vectors, subject to pilot acceptability. Verbal communication with controller or other A/C as required or desired.

2a. Sequencing - no predictors

controllers: Only control over A/C 1, 2, 3 is sequencing. This is issued at the beginning and may be changed at the controller's discretion. Pilots responsible for their own spacing as in VFR. Controller may also issue advisories.

pilots: Carry out sequencing. Use safe VFR spacing. 1 nm minimum spacing crossing the marker for all A/C. Verbal communication with controller or other A/C as required or desired.

2b. Sequencing - predictors (own or all)

controllers: Same procedure as in 2a.

pilots: Same procedure as in 2a except 30 sec. spacing crossing marker.

3a. Advisory - no predictors

controllers: May issue only advisories to A/C 1, 2, 3. Pilots are responsible for their own sequencing and safe spacing.

pilots: Work out own sequencing. Use safe VFR spacing. 1 nm spacing crossing marker. Communication with controller and other A/C as required or desired.

3b. Advisory - predictors (own or all)

controllers: Same procedure as in 3a. Spacing crossing marker is 30 sec.

pilots: Same procedure as in 3a except 30 sec. spacing crossing marker.

PLEASE DO NOT TALK DURING THE TIME BETWEEN THE RUNS except if you have questions which you should direct to the experimenter.

74-28,209 #22

PILOT VEHICLE DESCRIBING FUNCTION MEASURES IN HIGH α, LATERAL-LONGITUDINAL COUPLED FLIGHT*

Donald E. Johnston and Raymond E. Magdaleno†
Systems Technology, Inc.
Hawthorne, California

ABSTRACT

Pilot/vehicle describing function measures were obtained for a five-degree-of-freedom simulated air-to-air tracking task at high angle of attack and zero and non-zero sideslip. The task is representative of a situation in which the aircraft is near stall yet the pilot is attempting to maintain track without inducing aircraft departure. Non-zero sideslip is quite common for such flight situations and results in a controlled element having highly coupled lateral-longitudinal dynamics.

Highly skilled experimental flight test pilots were thoroughly trained in the stall/departure/recovery aspects of the simulation. Describing function measures were then obtained for multiloop, pitch, roll, and heading tracking tasks at selected pre-departure frozen conditions. The crossover model was found to be valid for each loop closure. The precision pilot model provided an excellent fit to the data except that in pitch the crossover was close to the longitudinal short-period mode and required the pilot to adopt a second-order lead equalization approximately the inverse of the longitudinal short period. The gain and low-frequency lag-lead equalization employed in the roll loop closure was found to differ depending upon whether the roll loop was an outer (roll tracking) or inner (heading tracking) loop. Coupling between the airframe lateral and longitudinal dynamics was found to increase the pilot workload but did not appreciably affect the equalization employed.

SIMULATION

The fixed-base simulation approximated an air-to-air tracking tail-chase as depicted in Fig. 1. A head-up display was employed with a symbol representative of own-aircraft (boresight) centerline fixed at the center of a TV screen. The target and horizon moved with respect to this own-aircraft boresight. The head-up field of view was ±24 deg azimuth and ±18 deg elevation.

---

*This work was accomplished under Contract F33615-73-C-3101 for the Air Force Flight Dynamics Laboratory, Wright-Patterson AFB, Ohio.

†Principal Research Engineer and Senior Research Engineer, respectively.

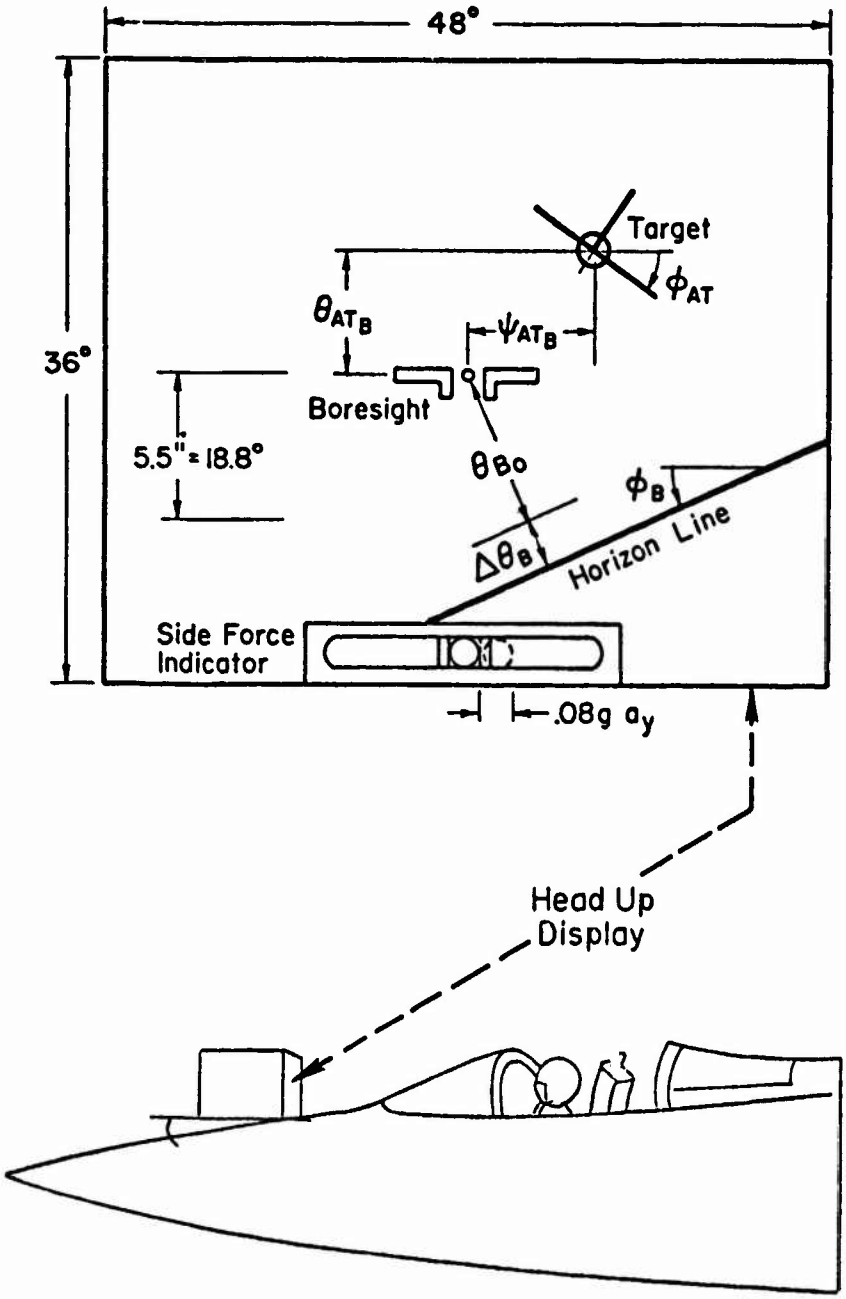

Figure 1. Pilot/Cockpit/Display Configuration

The subject aircraft could be maneuvered in bank, pitch, and heading relative to the target (φ_{AT}, θ_{AT}, ψ_{AT}) and sustained deviations would result in lateral or vertical displacement with respect to the target. Only range to target remained fixed at 2000 ft. The subject aircraft pitch and roll attitude could be discerned with respect to the horizon (φ_B, $\Delta\theta_B$). To partly compensate for the lack of lateral acceleration cue, a replica of the ball of the turn and slip indicator was also displayed on the TV screen.

The subject aircraft was modeled by a nonlinear, five-degree-of-freedom, coupled lateral-longitudinal representation as indicated by the equation flow diagram of Fig. 2. In addition to inertial terms, the equations included kinematic and aerodynamic coupling terms which result from sideslip. Thus, for the handling quality portion of the investigation, the aircraft dynamics varied with α and β, and realistic stall and nose slice departure characteristics were obtained.

The measurement of pilot describing functions with the DFA requires a linear, stationary control process. Therefore, the airframe dynamics were "frozen" for the data runs. This was accomplished by fixing all airframe stability derivatives at the value appropriate for the given trim condition and aircraft configuration (i.e., the derivatives were not allowed to vary with α and β). Three trim configurations representative of impending stall and departure were employed (Table 1). The base configuration (A) assumed symmetric flight ($\beta = 0$) and hence had uncoupled lateral-longitudinal dynamics. The other two (B and C) reflected coupled lateral-longitudinal dynamics.

TABLE 1

"FROZEN" CONFIGURATIONS

CONFIGURATION	α_o	β_o	COUPLING
A	17.3	0	None
B	18.8	3	Moderate
C	18.8	3	Strong

P-154

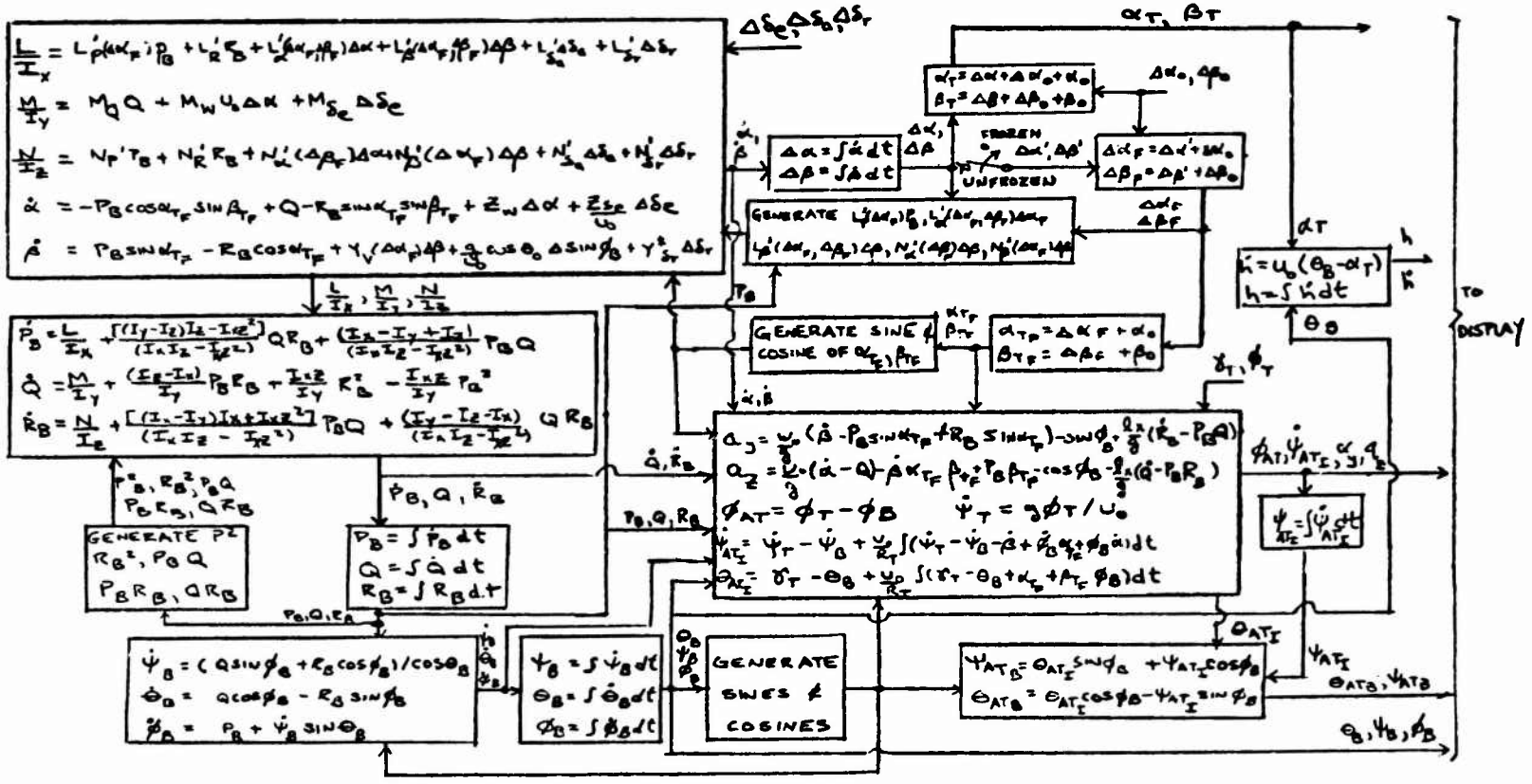

Figure 2. Aircraft and Display System Equation Flow Diagram

PILOT PARAMETER MEASUREMENTS

Measurement of pilot dynamic parameters was accomplished through use of the STI Describing Function Analyzer (DFA) described in detail in Refs. 1 and 2. Briefly, the DFA is a device for making on-line dynamic response measurements of manual control systems. It generates a sum-of-sinusoids input forcing function that is used to excite the dynamic system under consideration; and computes, on-line, the finite Fourier transform of a given system signal at each of the forcing function frequencies.

To obtain pilot describing functions in multiaxis tracking situations, past laboratory procedures have involved simultaneous introduction of separate, uncorrelated, forcing functions in each axis. This permits direct determination of describing functions for each axis as well as for crosstalk or noise between axes. Unfortunately, this does not provide a realistic forcing function for simulation of air-to-air tracking where between-axis target motion is correlated. That is, there are certain basic relationships between target bank, pitch and heading for any useful aircraft maneuver. It is not likely, for example, that a target will bank into a turn and then pitch away from the turn (i.e., negative g turn). Such apparent target motions are rejected by a skilled pilot as sight noise due to buffet, pipper wander, etc. Thus, to provide a realistic input which experienced fighter pilots would track, it was necessary to introduce the forcing function input to one axis at a time and depend upon stationary run-to-run performance.

The forcing function was employed to drive the target aircraft in pitch (θ_{AT}) or roll (φ_{AT}). The task was to track (match) target motion with the boresight symbol. Coupling within the airframe dynamics provided inter-axis disturbance. Three control loop structures were employed (Fig. 3). Two were pitch-roll tracking tasks with the heading degree of freedom not displayed to prevent inadvertent yaw error from biasing the pilot's tracking of roll attitude (i.e., temporary lapses in roll tracking in order to reduce heading error). In the third task heading error was displayed, and the pilot was specifically instructed to track heading. To test the concept that pilots use target bank angle as a primary cue, several heading tracking runs were made with the target wings and tail removed from the display. Pilot commentary indicated that all tasks were essentially compensatory tracking tasks.

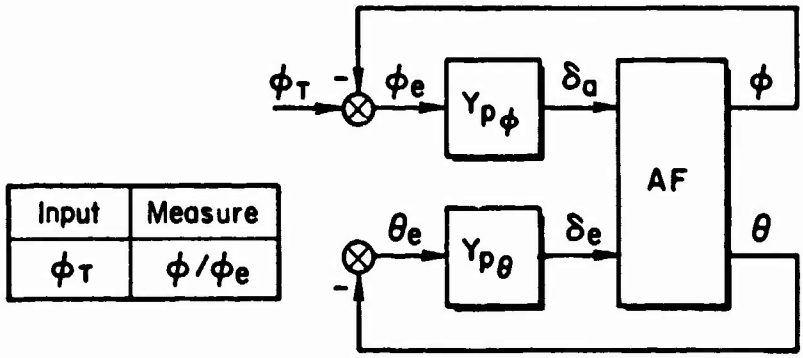

a) Roll Tracking Task

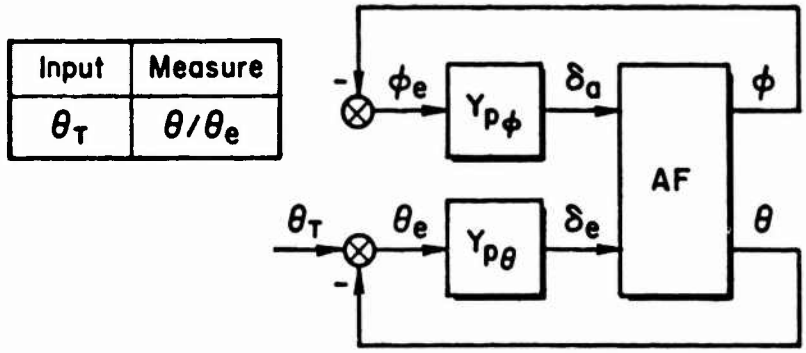

b) Pitch Tracking Task

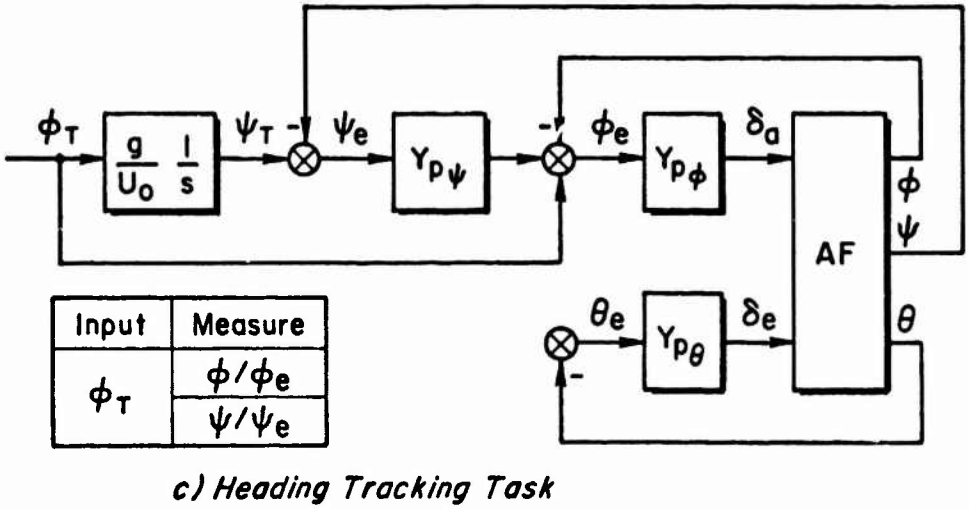

c) Heading Tracking Task

Figure 3. Control Task Block Diagrams

P-154

FORCING FUNCTION

The amplitude and frequency of the five sinusoids employed in the forcing functions are shown in Fig. 4. In general, the amplitude was decreased 6 dB per octave with increasing frequency. However, the lowest frequency sinusoid in the pitch forcing function had to be reduced in amplitude because the principal inter-axis coupling was from longitudinal into lateral motion in the frequency band of 0.1 to 0.5 rad/sec. The coupling was so severe that the pilots could not maintain control of the aircraft for the desired 100 sec run time without this decrease in forcing function amplitude.

SUBJECTS

Two pilot subjects were employed. Both are USAF experimental test pilots. Each participated in one week of stall/departure/recovery handling quality research runs before the describing function measurements were made. In addition, each pilot was allowed two training sessions, one-half day each, to learn to track the random target motion for 100 sec without inducing a departure. During all training sessions the complete nonlinear [$f(\alpha,\beta)$] airframe model was used and departures were possible. For the final data runs the airframe dynamics were frozen as indicated previously (Table 1).

ROLL PILOT MEASURES AND MODEL

The open-loop roll attitude dynamics for aileron control for each of the three configurations are shown in Fig. 5. The root locus and Bode for the uncoupled Configuration A case is shown at the top of Fig. 5 and that for the coupled Configuration B is shown in the middle. The bottom plots represent Configuration C. The relative magnitude of coupling from roll (or roll rate) control into longitudinal motion is reflected by the separation of the complex pole-zero dipole identified as ω_{sp}. The closeness of this pair indicates little coupling or excitation of longitudinal motion by aileron for all configurations. The only other difference in the dynamics of these configurations lies in Configuration B which has a low-frequency complex pole (ω_{SR}) in place of two real poles ($1/T_R$ and $1/T_S$).

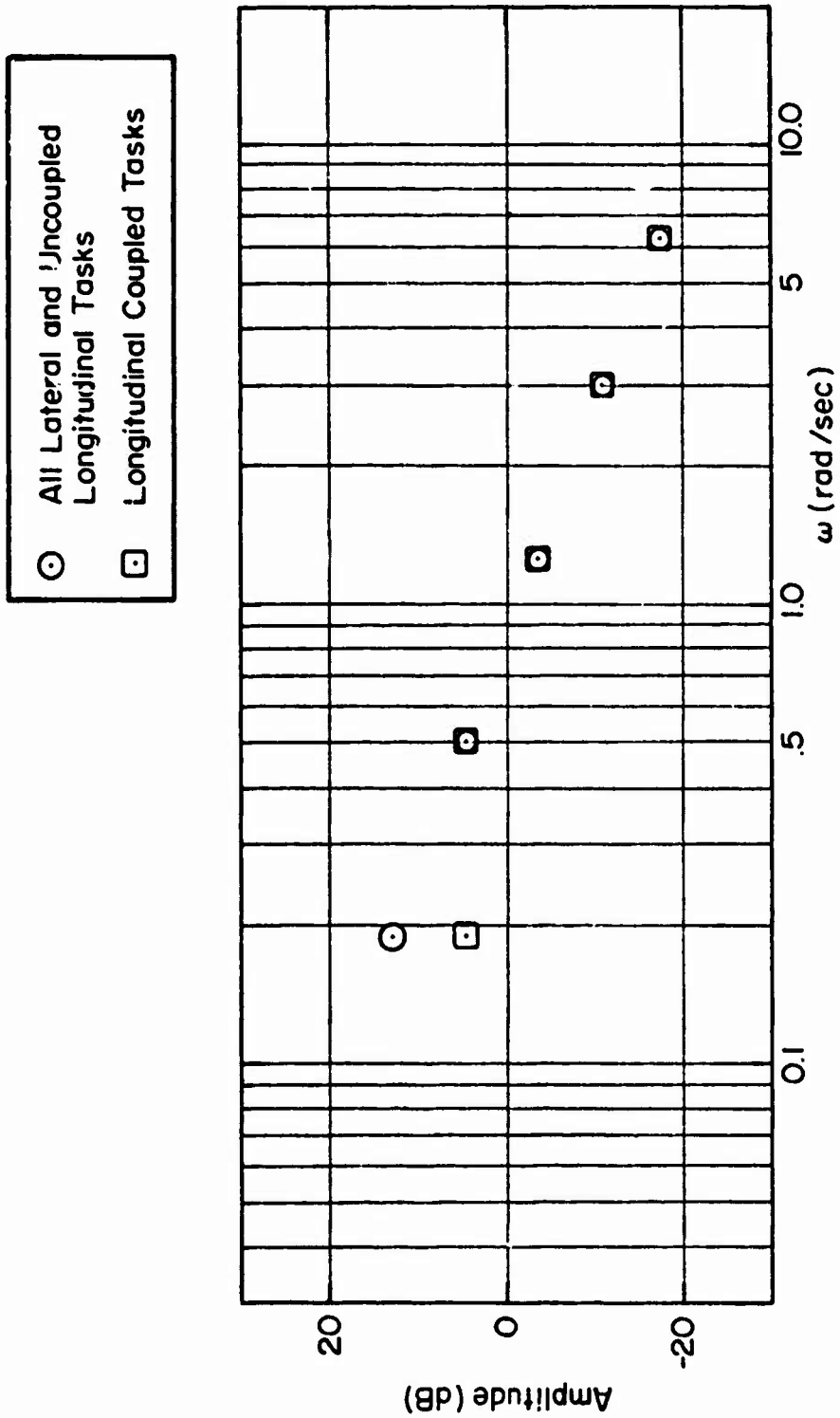

Figure 4. Forcing Function Spectrum

P-154

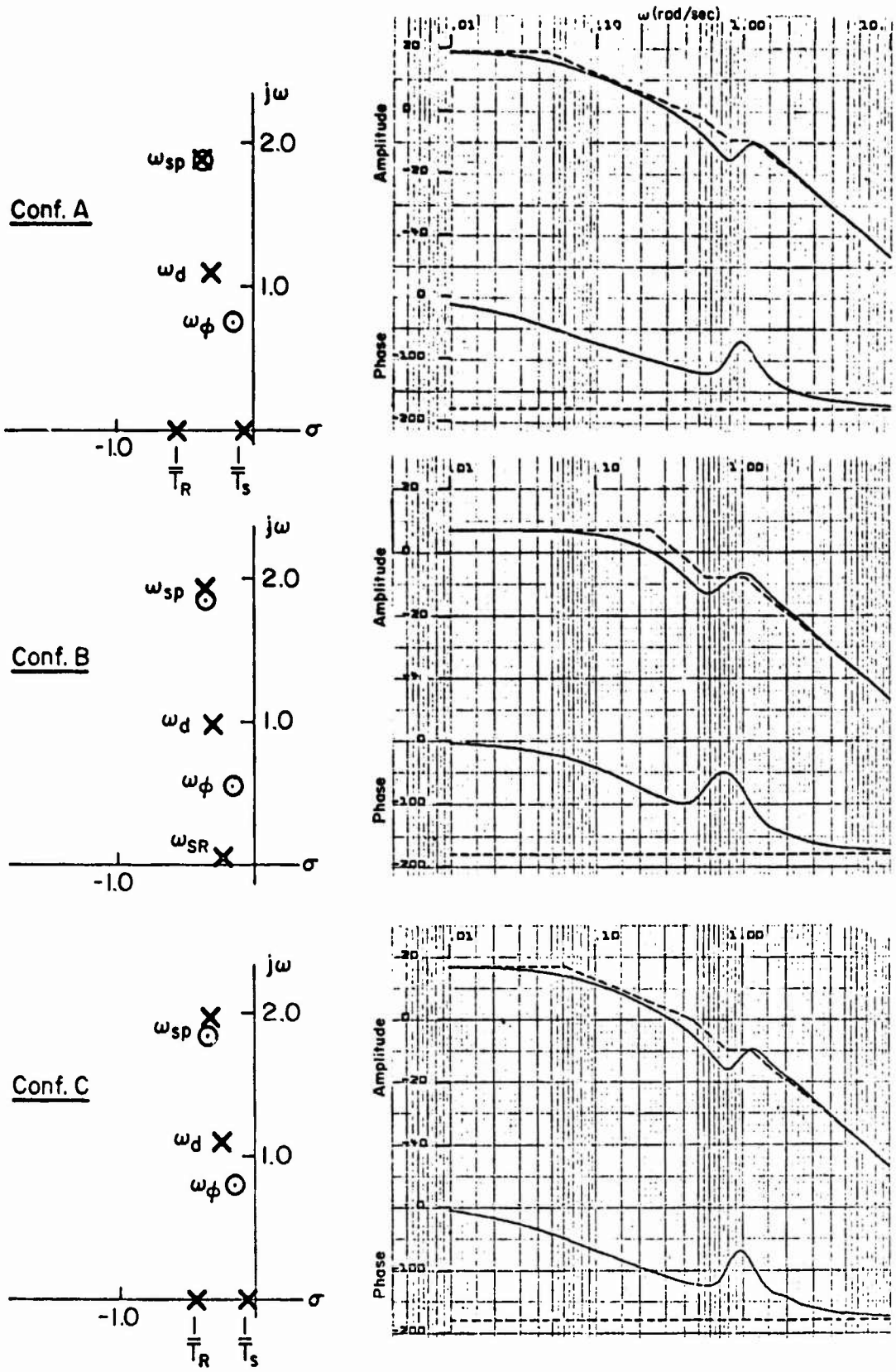

Figure 5. Open Loop Roll-to-Aileron Bode and Root Plots

Figure 6a presents a direct comparison of the open-loop $Y_{p_\varphi}Y_c$ data points obtained for the three configurations and Fig. 6b presents the Y_{p_φ} data points. Also shown is a reference 20 dB/decade slope line. It may be observed that the data exhibit less scatter than often is obtained for multiple runs of a single configuration. In each case the crossover is about 1.5 rad/sec and the phase margin about 35-40 deg. It is apparent the pilot has adopted first-order lead equalization in the vicinity of 1 rad/sec so that $Y_{p_\varphi}Y_c$ approximates the crossover model (Ref. 3). The only significant difference between the configurations is in the low-frequency region where it appears the coupled airframe dynamics cause the pilot to use somewhat higher gain and have considerably greater phase lag, i.e., a low-frequency lag-lead equalization. This difference in pilot low-frequency equalization is somewhat surprising because of the similarity in the Bode-root locus plots for Configurations A and C in Fig. 5. However, in the next section it will be shown that longitudinal control considerations significantly affect the pilot's low-frequency equalization in roll tracking.

The pilot model is shown in Ref. 4 to be of the form:

$$Y_{p_\varphi} \doteq K_{p_\varphi} \underbrace{\left(\frac{T_1}{T_2}\right)}_{\substack{\text{Low Frequency} \\ \text{Lag-Lead}}} \underbrace{\left(\frac{1.2}{1}\right)}_{\substack{\text{Series} \\ \text{Equali-} \\ \text{zation}}} \underbrace{\frac{1}{[.3,\ 10\ (15)]}}_{\substack{\text{Neuromuscular} \\ \text{System Lag}}} \times \underbrace{e^{-.5s}}_{\substack{\text{Time} \\ \text{Delay}}} \qquad (1)$$

PITCH PILOT MEASURES AND MODEL

The open-loop pitch dynamics for the three controlled element configurations are shown in Fig. 7. Again, the uppermost Bode and root locus plots represent the uncoupled case, the middle plots the nominal Configuration B coupled dynamics, and the lower plots the Configuration C case with increased coupling. It may be noted that the two coupled configurations have a right half plane zero. Pilot closure of the pitch attitude loop drives the pole from the origin into this zero and thus results in a first-order divergence. It is shown in Ref. 4 that this is related to the nose slice divergence. There is also considerable difference in low-frequency amplitude ratio for the most highly coupled configuration (C).

P-154

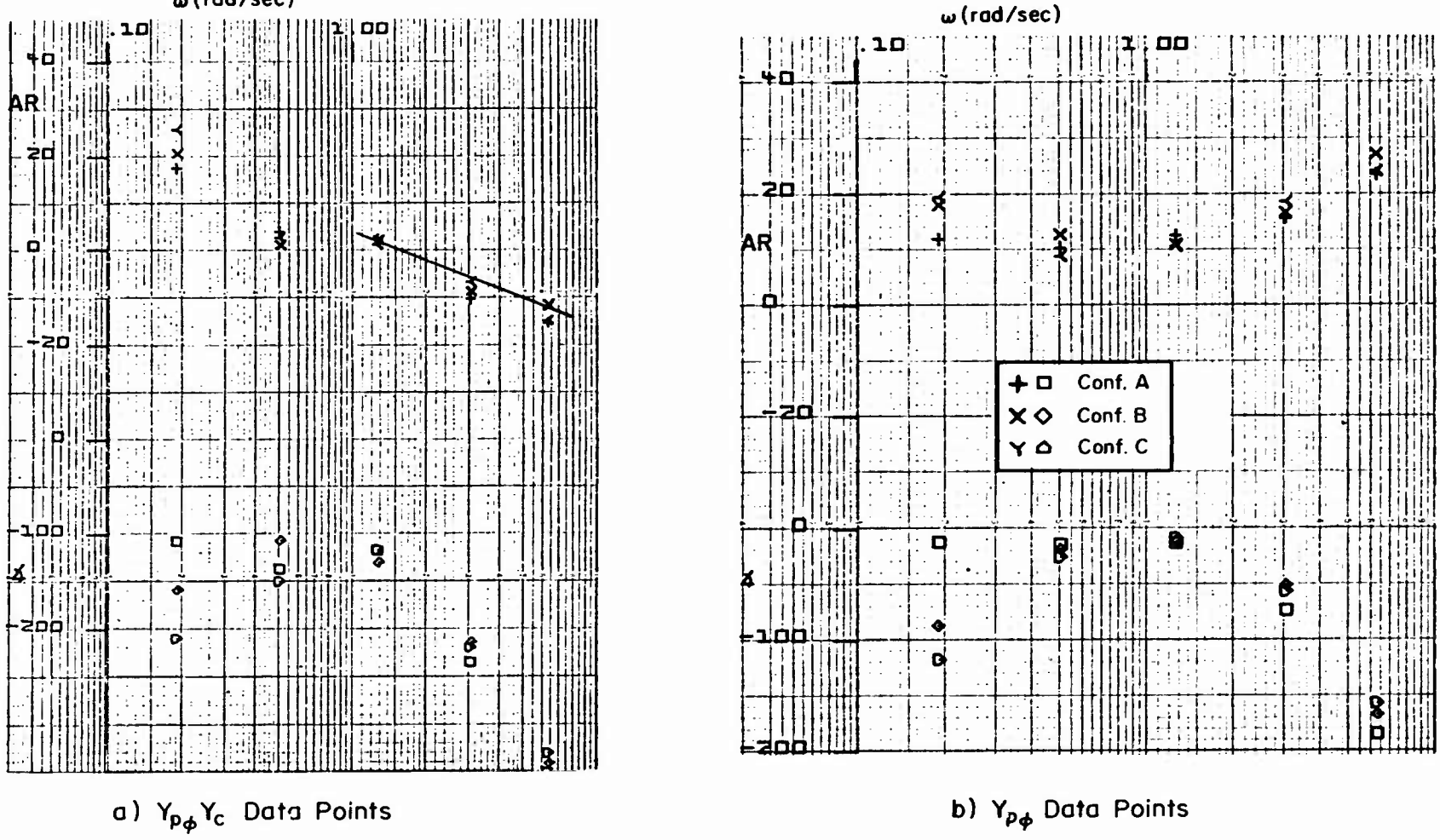

a) $Y_{p_\phi} Y_c$ Data Points

b) Y_{p_ϕ} Data Points

Figure 6. Roll Pilot Measures

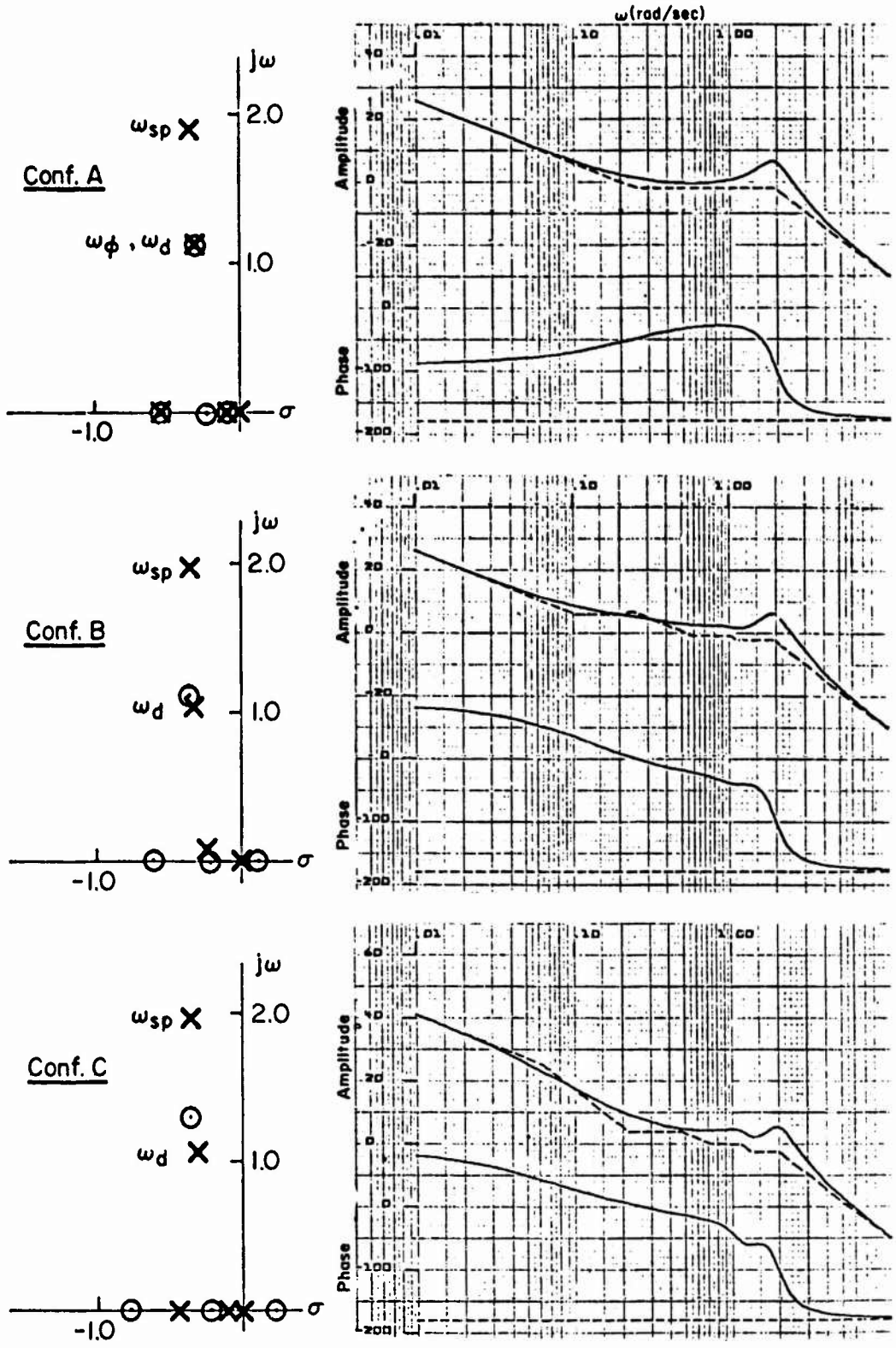

Figure 7. Open Loop Pitch-to-Elevator Bode and Root Plots

P-154

In the following, despite the coupled airframe dynamics, the data obtained will be analyzed neglecting the contribution of the roll loop closure and assuming the controlled element is described by the single open-loop Y_c shown in Fig. 7. This is an approximation only for the two cases having lateral-longitudinal coupling. But, more important, it is shown in Ref. 4 that pilot closure of the roll loop effectively decouples the lateral-longitudinal dynamics to the point that a pilot model derived from the assumed uncoupled case provides a good approximation.

Configuration A

The $Y_{p_\theta}Y_c$ data were fitted for one set of measurements for Pilot ML and are presented in Fig. 8a identified by the ✚ and □ symbols. These points represent an average of two runs having a maximum of ±2 dB and ±10 deg phase from the data point plotted. The data spread for two runs by Pilot JS is indicated by the ⊙ on Fig. 8a. These data points were not fitted; they are presented here to show the consistency between the two pilots. Pilot JS obviously was closing the loop with a lower gain and therefore had a crossover somewhat below 0.5 rad/sec, whereas Pilot ML achieved a crossover near 2 rad/sec. From the 20 dB per decade reference slope line shown on Fig. 8a it is apparent that both pilots closely approximate the crossover model. Pilot JS would appear to be placing a first-order lag on top of $1/T_{\theta_2}$ and a lead near ω_{sp} as might be expected (see Fig. 7). However, the transfer function fit to the Pilot ML data indicate he is using somewhat more complex equalization. This may be observed by subtracting the known single-loop Y_c amplitude and phase from the $Y_{p_\theta}Y_c$ data points and fitting them as shown in Fig. 8b. The Y_{p_θ} transfer function is shown in Eq. 2:

$$Y_{p_\theta} = \underbrace{584.}_{\text{Gain}} \times \underbrace{\frac{(.565)}{(-.08)}}_{\substack{\text{Low Frequency} \\ \text{Lag-Lead}}} \times \underbrace{\frac{[.226,\ 2.1]}{(1.69)}}_{\substack{\text{Series} \\ \text{Equali-} \\ \text{zation}}} \times \underbrace{\frac{1}{[.5,\ 10](10)}}_{\substack{\text{Neuromuscular} \\ \text{System Lag}}} \times \underbrace{e^{-.25s}}_{\substack{\text{Time} \\ \text{Delay}}} \qquad (2)$$

P-154

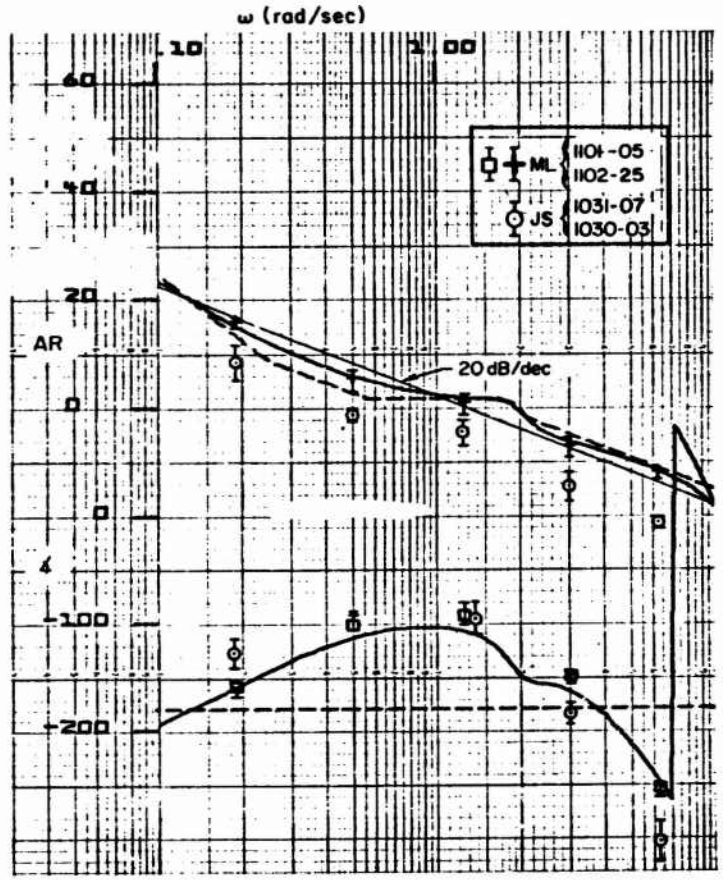

a) Open Loop $Y_{p\theta}Y_c$

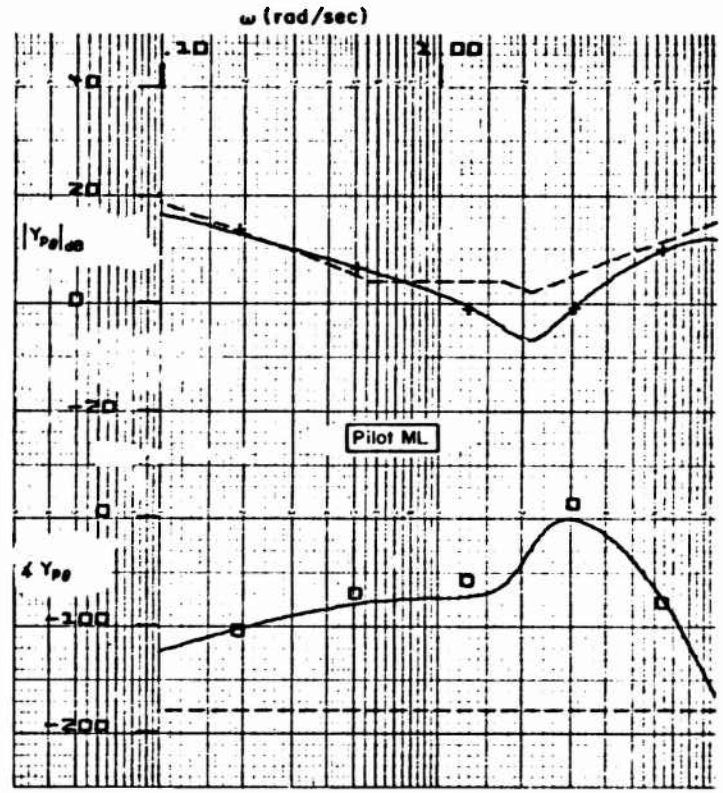

b) $Y_{p\theta}$ Data Point Fit

Figure 8. Single-Loop Pitch Attitude Command Input (Configuration A)

The results provide an excellent curve fit and are consistent with the precision pilot model (Ref. 5) at low and high frequencies. A low-frequency lag-lead is employed to match the low-frequency amplitude rise and phase droop and a third-order neuromuscular system was assumed at 10 rad/sec.

The main difference is the more complicated midband series equalization which consists of a second-order lead over a first-order lag. From the amplitude asymptotes of Fig. 8b it appears that this complex equalization might be approximated as a simple first-order lead; however, in order for the inflections of the fitted curve to closely match the actual amplitude ratio and phase data points a lowly damped second-order lead is required. It is apparent that the pilot is precisely inverting the short-period characteristics. The current precision model does not contain a second-order lead since it was based on data obtained with Y_c's having much more ideal dynamic characteristics than those for the high-angle-of-attack case employed here. That is, they did not have second-order dynamics in the crossover region and in our case the pilot is achieving crossover right at the short-period mode [.18, 1.9]. Thus, the series equalization might be expected to be more complex.

There is other evidence to support the existence of second-order lead equalization. A root plot of the early Hall data (Ref. 6) is shown in Fig. 9. Two data points at roughly 1.5 rad/sec and low damping ratio are shown to lie in a region in which double lead was employed. These have ratings of 7 and 10. A third data point is at roughly 2.5 rad/sec and also achieved a rating of 10. It may be noted from Fig. 7 that the short-period for all three configurations investigated here would lie in approximately the center of the double lead area shown in Fig. 9. The Cooper-Harper ratings of 8-9 obtained for the three configurations in this simulation are also consistent with the Hall data.

The Shirley data (Ref. 7) also resulted in pilot models with second-order lead. For example, the transfer functions shown in Table 2 indicate the pilot partially cancels second-order modes of the controlled element.

The precise reason for the Hall and Shirley data to result in second-order leads is not known. For the task employed in our simulation the cancellation is more complete than is Shirley's. It is suspected that the pilot learned to completely suppress the short-period dynamics in order to prevent departure, since during the task learning period with the unfrozen aerodynamics relatively

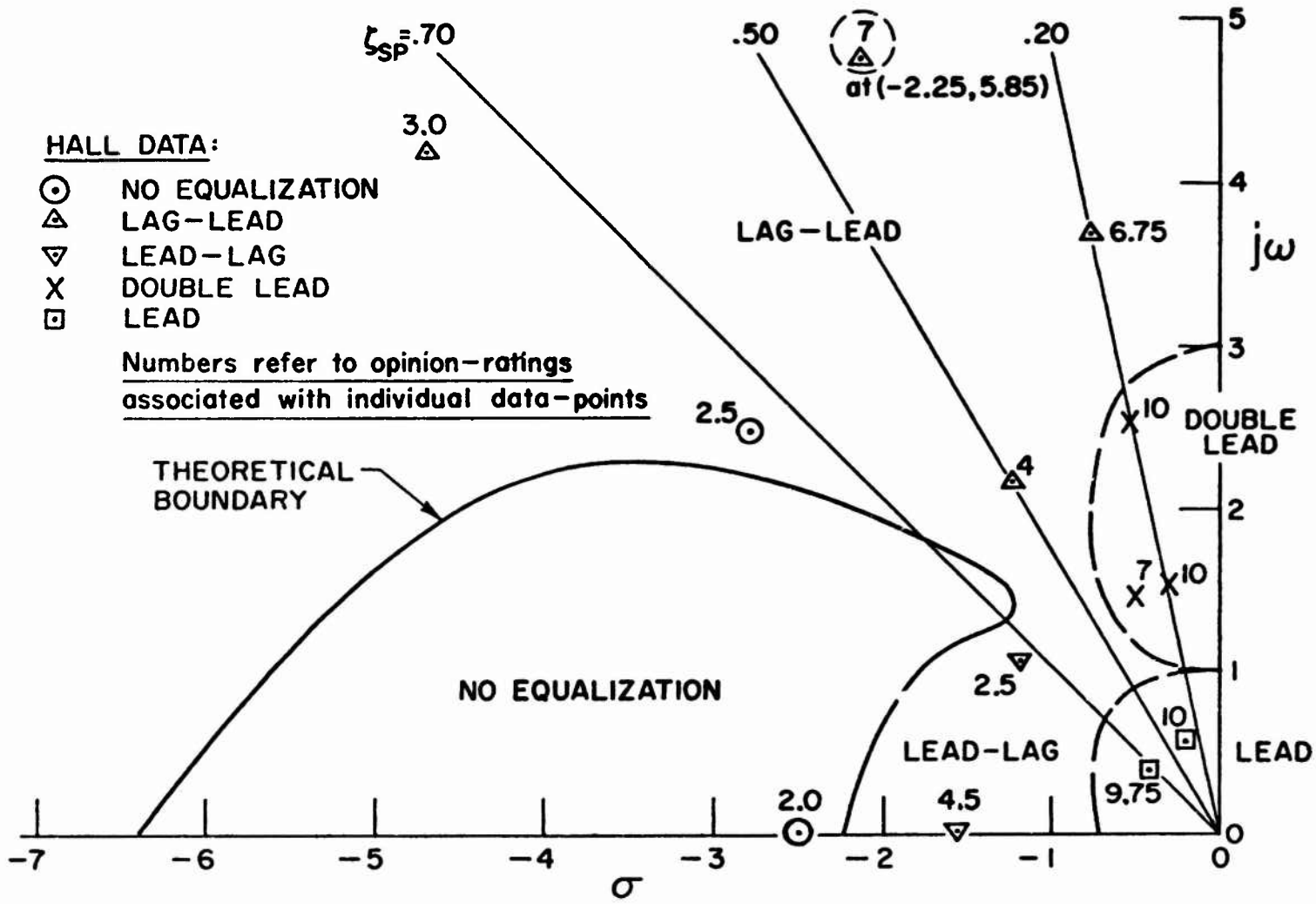

Figure 9. Comparison of Theoretical Non-Equalized Boundary with Hall Measured Data (From Ref. 6)

TABLE 2

EXAMPLE PILOT TRANSFER FUNCTIONS
FROM SHIRLEY (REF. 11)

Y_c	Y_p
$\frac{5e^{-.1s}}{[s^2 + s + 5]}$	$\frac{1.16e^{-.25s}(s + .5)[s^2 + 4s + 5]}{(s + .13)(s + 2)}$
$\frac{10e^{-.1s}}{[s^2 + 2s + 10]}$	$\frac{11e^{-.3s}(s + .4)[s^2 + 3s + 10]}{(s + .1)(s + 2.32)}$

small increases in angle of attack could result in departure. Since the short-period mode is predominantly α and θ motion, the pilot was forced to control α and θ quite tightly to suppress overshoots. Such complete suppression of the short-period mode would then require the complex equalization shown in Fig. 8b. However, the use of such equalization would not be suspected from the open-loop controlled element dynamics alone (Fig. 7). There are also no known pilot rating functionals for second-order lead equalization. Thus, it would be difficult indeed to predict both the pilot model and pilot rating for pitch attitude control at this Configuration A case in the absence of the departure-prone context of the unfrozen aerodynamics.

Configuration B

The $Y_{p_\theta}Y_c$ amplitude and phase data points for this case are shown in Fig. 10. Only the data points for Pilot ML have been fitted (the lowest-frequency phase point was given zero weight in the data fit for economy of computation).

For this case the crossover model seems better suited to the lower gain pilot (JS). Pilot ML adopted a slope somewhat less than 6 dB per octave. This decreased slope has been observed previously (Ref. 3) on subcritical tasks where the controlled element has a right half plane pole. Referring back to Fig. 7, it will be noted that this configuration does have a right half plane zero at 0.1 rad/sec. Closing the $\theta \rightarrow \delta_e$ loop drives the open-loop pole from the origin

P-154

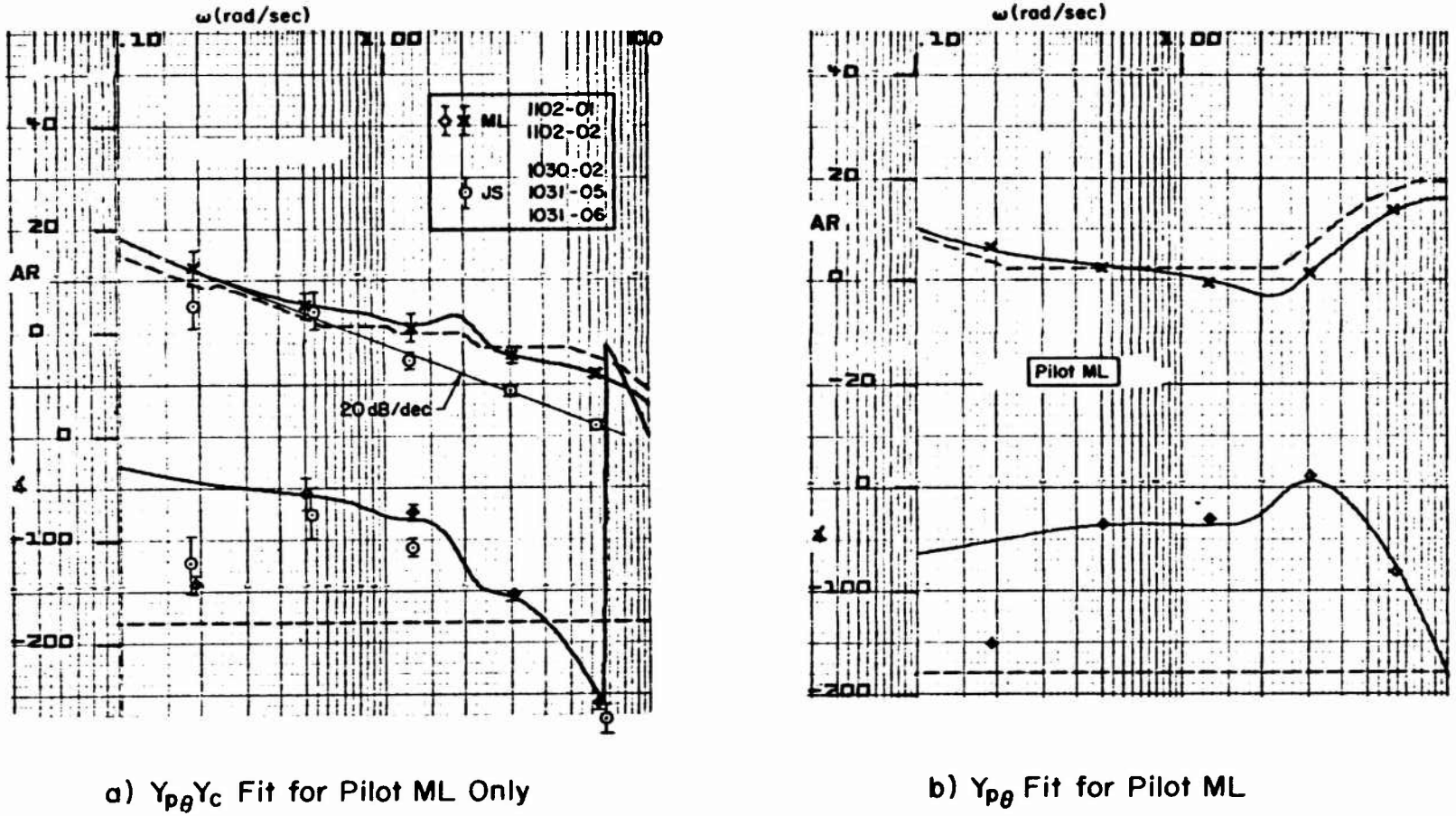

a) $Y_{p_\theta} Y_c$ Fit for Pilot ML Only

b) Y_{p_θ} Fit for Pilot ML

Figure 10. Pitch Tracking Data Points for Configuration B

into this zero and therefore results in a right half plane closed-loop pole. Therefore, we might expect the slope in the region of crossover to be less than 6 dB per octave.

The closed-loop right half plane pole would normally be expected to result in a pitch attitude instability that would prevent obtaining describing function data. However, if the pitch attitude loop is closed tightly, the closed-loop pole is essentially driven into the open-loop zero and there is very little pitch modal response. The small pitch modal response together with the low frequency provides a very long, slow pitch divergence which would not be observable. But, the instability will show up in another mode. The situation is analogous to tight attitude regulation for precise path control with an aircraft on the backside of the power required curve. The path numerator has a right half plane zero which gives rise to an unstable closed-loop mode. With tight attitude regulation, stable path control is obtained initially and the instability shows up as a speed divergence. However, after prolonged speed decay the path will also diverge. For our high α case, the right half plane zero arises due to an aerodynamic coupling stability derivative, N_α. From the Ref. 4 analysis we found that the closed-loop instability shows up in a lateral mode (nose slice) and the pilot must close a $\varphi \rightarrow \delta_a$ loop to restabilize it. The end result is that the pitch attitude control task is similar to the uncoupled Configuration A case except the pilot is now required to close a $\varphi \rightarrow \delta_a$ loop to decouple the lateral-longitudinal motion and hence is working harder. Furthermore, the longitudinally induced instability lies in the low-frequency region and accounts for the previously noted lag-lead equalization in the roll pilot model.

The pitch pilot describing function is again obtained by subtracting the Y_c from the $Y_{p_\theta} Y_c$ data of Fig. 10a and curve fitting the resulting data points. As indicated previously the effective Y_c is adequately described (Ref. 4) by the open-loop $\theta \rightarrow \delta_e$ transfer function of Fig. 7. The resulting data points and their curve fit are presented in Fig. 10b. The pilot model for the fit is given in Eq. 3:

$$Y_{p_\theta} = \frac{930.8(.22)[.3,\ 2.3]}{(.006)(5.1)(7.6)[.5,\ 10]}\, e^{-.306s} \qquad (3)$$

P-154

Again, the pilot model has the form of the precision model with a series equalization consisting of a second-order lead over a first-order lag. From Fig. 10b it is apparent that the pilot is acting as a pure gain in the region just below crossover and is applying the second-order lead to cancel the vehicle short-period mode. In this case the effect of the second-order lead is more pronounced because of the greater separation between it and the associated lag break point.

Configuration C

The $Y_{p_\theta}Y_c$ data points and curve fit for Pilot ML are shown in Fig. 11a. Also shown are the raw data points for Pilot JS. Again, the slope in the region of the crossover is less than that which would be obtained with the crossover model and again the pitch numerator has a right half plane zero. In this case it is at 0.25 rad/sec and provides a significant increase in the airframe low-frequency amplitude. Also, upon closure of the pitch attitude loop, the unstable root is driven further into the right half plane and thus the mode divergence is more rapid. The unstable mode should be more apparent to the pilots and hence constrain the gain and equalization necessary to achieve satisfactory performance. This is probably the reason why the describing function data points for both pilots are in closer agreement for this configuration than for the previous two.

Again, subtracting the open-loop $\theta \rightarrow \delta_e$ airframe amplitude and phase from $Y_{p_\theta}Y_c$ gives the data points and curve shown in Fig. 11b. The pilot model transfer function is presented in Eq. 4:

$$Y_{p_\theta} = \frac{491\,[.37,\ 2.11]}{(3.4)(8.7)\,[.5,\ 10]}\, e^{-.286s} \qquad (4)$$

Here, the low-frequency lag-lead apparently is not required because of the higher gain of the Y_c. The pilot essentially adopts a pure gain out to the short-period frequency and then assumes a second-order lead to cancel the short-period resonance peak.

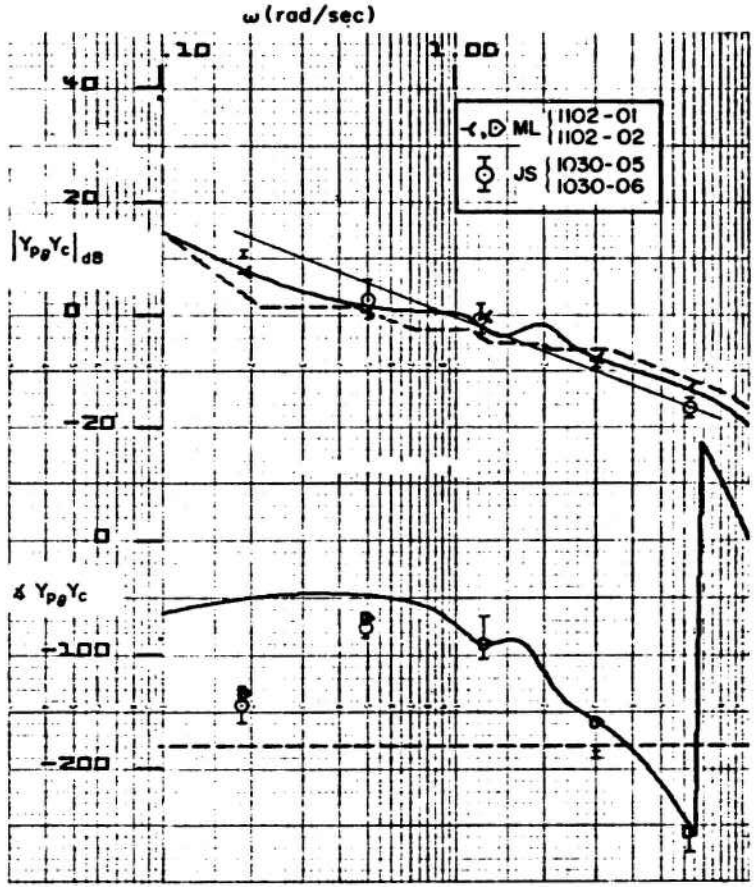

a) Open-Loop $Y_{p_\theta}Y_c$ Fit for ML Only

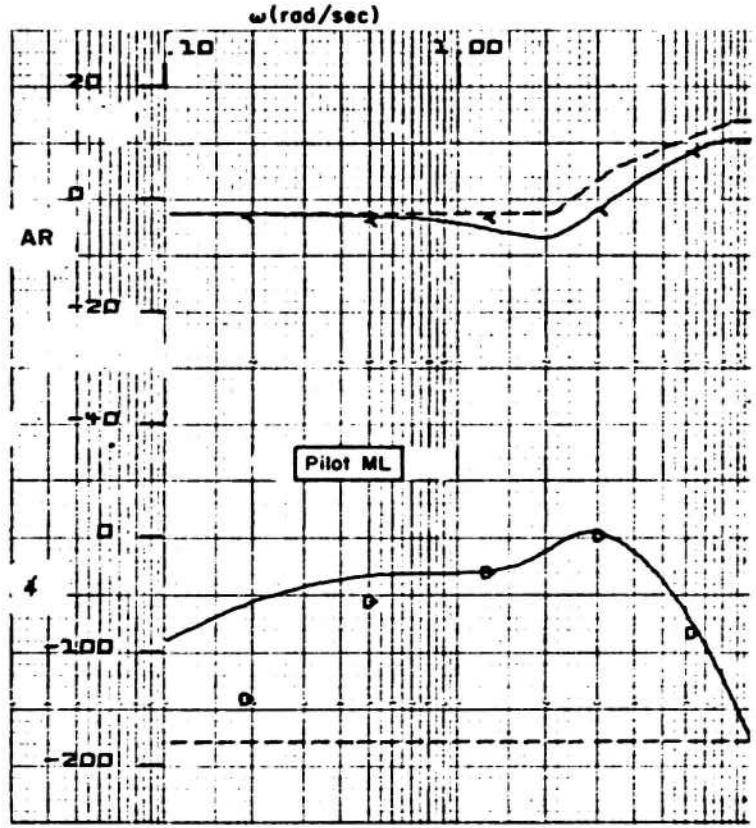

b) Y_p Data Fit for Pilot ML

Figure 11. Pitch Attitude Command, Configuration C

Summary

Figure 12a presents a direct comparison of the $Y_{p_\theta}Y_c$ data points from the three configurations for Pilot ML. These demonstrate the uniformity the pilot was achieving in the pitch task — coupled versus uncoupled.

Figure 12b presents a direct comparison of the Y_{p_θ} data points after removing the controlled element amplitude and phase. As with the roll closure these show remarkable similarity in the region of crossover and above and could readily be fit by a single model. Again, the major difference is in the low-frequency band but in this instance with the greater coupling conditions showing the lower pilot amplitude contribution.

This is precisely the opposite of the trend shown in Fig. 6 where the lateral Y_{p_φ} for the coupled case showed increased low-frequency gain. It appears that the pilot is achieving a tradeoff between the two axes — possibly to effect a decoupling of the motions. The major coupling is from longitudinal to lateral via N_α. Therefore, as coupling increases (N_α increased), the pilot reduces his longitudinal gain and increases the lateral gain.

In all cases, whether coupled or uncoupled, the pilot is closing the pitch loop essentially at the short period and is nearly canceling the short-period peak through generation of a second-order lead. This unusual equalization has apparently been adopted through the necessity to avoid excessive angle of attack and subsequent nose slice divergence. A clue to the possible tension of the pilot in pitch control is the quite small time delay ($0.25 < \tau < 0.3$ sec) obtained in this task as compared to that ($0.5 < \tau < 0.56$ sec) obtained in roll (Ref. 4). This might also signal that the pilot closes the pitch loop as the inner loop and roll as the outer loop.

The $Y_{p_\theta}Y_c$ amplitude and phase did not fit the crossover model for the two coupled cases. These exhibited considerably flatter amplitude through the crossover region and are consistent with previous data obtained with a controlled element having unstable modes.

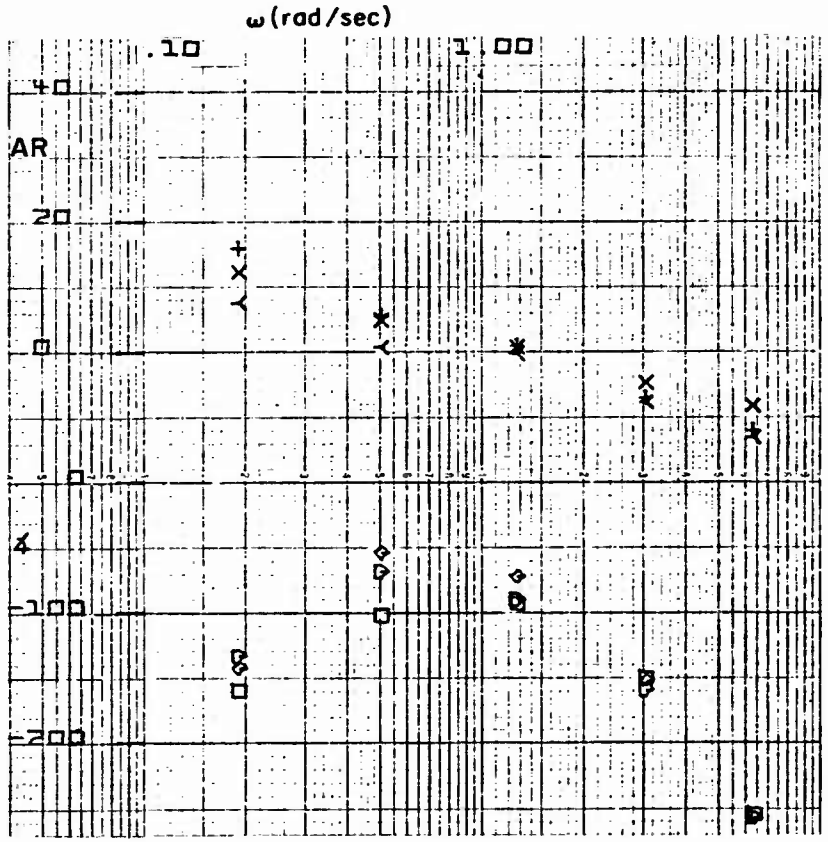

a) $Y_{p_\theta} Y_c$ Data Point Comparison

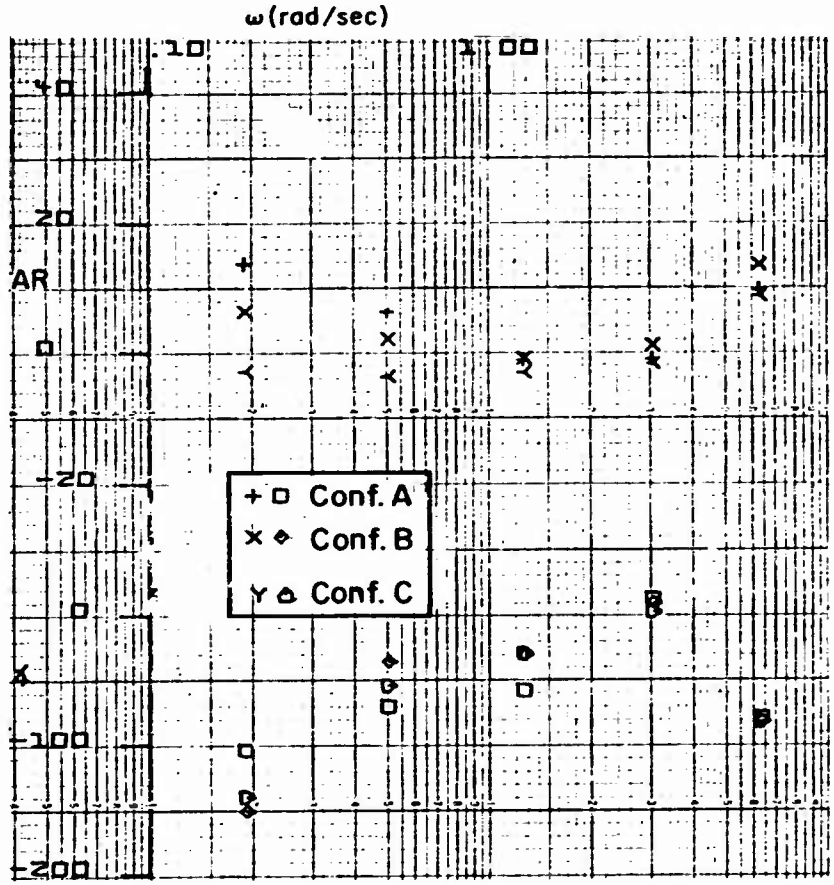

b) Y_{p_θ} Data Point Comparison

Figure 12. Summary of Pitch Pilot Data Points

HEADING PILOT MEASURES AND MODEL

The heading pilot measures were obtained by inserting the forcing function command as target bank angle but with the target free to displace in heading [i.e., $\psi_T = (g/U_o s)\varphi_T$, see Fig. 3c]. Repeat runs were made recording ψ_e and φ_e separately to facilitate modeling the dynamics of each loop. The heading and roll pilot models are thus subject to the following assumptions:

1. The run-to-run process is stationary.
2. The roll loop is closed as an inner loop to heading.
3. Coupling from lateral to longitudinal motion is sufficiently slight that the pitch closure does not alter the lateral dynamics appreciably.

The $Y_{p_\psi} Y'_{c_\psi}$ data points obtained from the ψ_e measures for five runs with Configuration B airframe dynamics are plotted in Fig. 13. It should be noted from the legend that these data reflect two different piloting techniques. In two runs they were allowed to use rudder if they desired. Rudder was not considered beneficial in this task and was used sparingly, if at all. However, this appears partially responsible for the considerably greater scatter than was obtained in the previous pitch and roll measurements.

The rather surprising aspect of these results is the heading crossover above 1 rad/sec. The data are quite consistent in this factor. Past measures of heading control in landing or similar tasks have generally indicated crossovers considerably below 1 rad/sec. With the exception of three amplitude points at 3 rad/sec the data also are in good agreement with the crossover model (slope 20 dB/decade).

The effective airframe Y'_{c_ψ} of Fig. 13 is dependent upon the inner roll loop closure. As previously indicated, the feedforward φ_c path of Fig. 3c was purposely opened to determine the effect of this path on overall loop dynamics as measured by ψ_e. The data points for Run 1102-18 of Fig. 13 reflect the absence of this bank angle cue and it is apparent that the removal has little effect on the heading describing function data. It is therefore concluded that the pilot pays little attention to target bank angle during close-in heading tracking. This is supported further by comparing the $Y_{p_\varphi} Y_c$ data points obtained from the φ_e/φ measures for the three loop (ψ, φ, θ) tracking

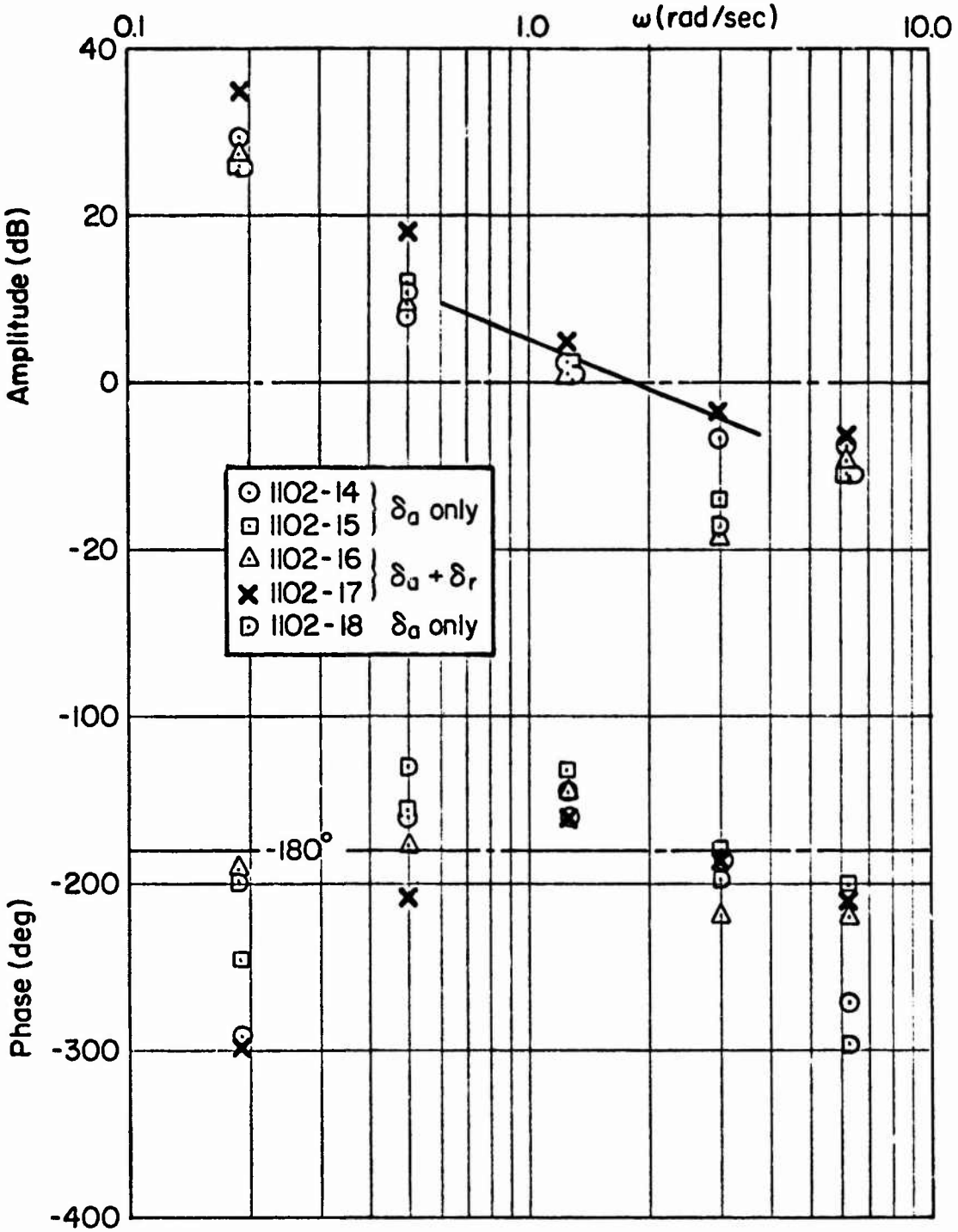

Figure 13. Measured $Y_{p_\psi} Y'_{c_\psi}$ with Inner φ Loop Closed

P-154

task (Fig. 3c) with those for the two (ϕ, θ) loop task (Fig. 3a). The describing function data for these two cases, two runs each, are plotted in Fig. 14. The three-loop data indicate considerably less amplitude ratio at the lowest frequency and much less phase lag at the two lower frequencies. This is consistent with the pilot not tracking in roll when this is the inner loop. Therefore, it is not necessary to adopt the low-frequency lag-lead equalization which was central to the roll tracking task.

Based upon the comparison of data in Fig. 14, a simplified inner-loop roll pilot model was selected as shown in Eq. 5:

$$Y_{p_\phi} = \frac{960(.6)}{[.3, 10](15)} e^{-.4s} \qquad (5)$$

This reflects the first-order lead and third-order neuromuscular lags identified in Eq. 1 but the low-frequency lag-lead is eliminated and the gain is reduced by roughly a factor of four. The time delay has also been reduced slightly on the basis that it would be necessary for the pilot to reduce his high-frequency lags if the outer (ψ) loop is to be stable with a closure above 1 rad/sec. The resulting multiloop structure and dynamics are shown in Fig. 15. The open-loop, ψ/ψ_e, amplitude and phase plot for this loop structure is shown in Fig. 16. Also shown in Fig. 16 are the describing function data points of Fig. 13 shifted in amplitude to correspond to an outer loop $K_{p_\psi} = 0.625$. The derived model is considered to provide an excellent fit* to the data points measured during the simulation.

Again, this multiloop model reflects a minimum equalization, minimum effort, approach on the part of the pilot. Apparently, he is using the inner loop primarily to damp the dutch roll nuisance mode. For example, the open-loop ζ_d is 0.296 whereas the closed inner-loop $\zeta_d' = 0.38$. This decreases the amplitude peak at dutch roll sufficiently that the outer ψ loop can be closed tightly (above 1 rad/sec) without the necessity for additional equalization. The ψ loop with its high dc gain then provides good flight path control.

*It is to be reemphasized that no attempt has been made here to model the low-frequency phase droop due to the "α effect."

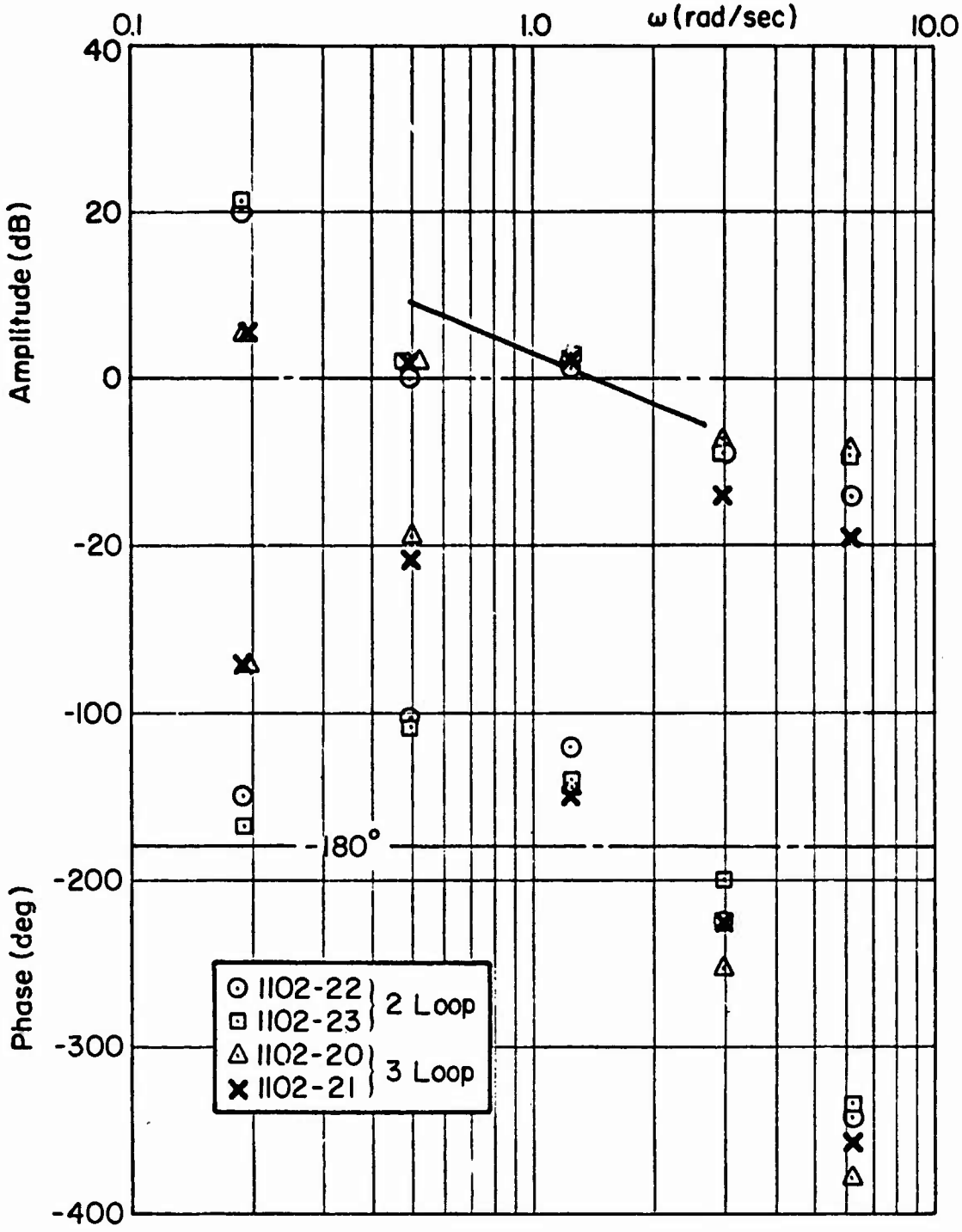

Figure 14. $Y_{p_\varphi} Y_{c_\varphi}$ Obtained from Describing Function Analyzer

P-154

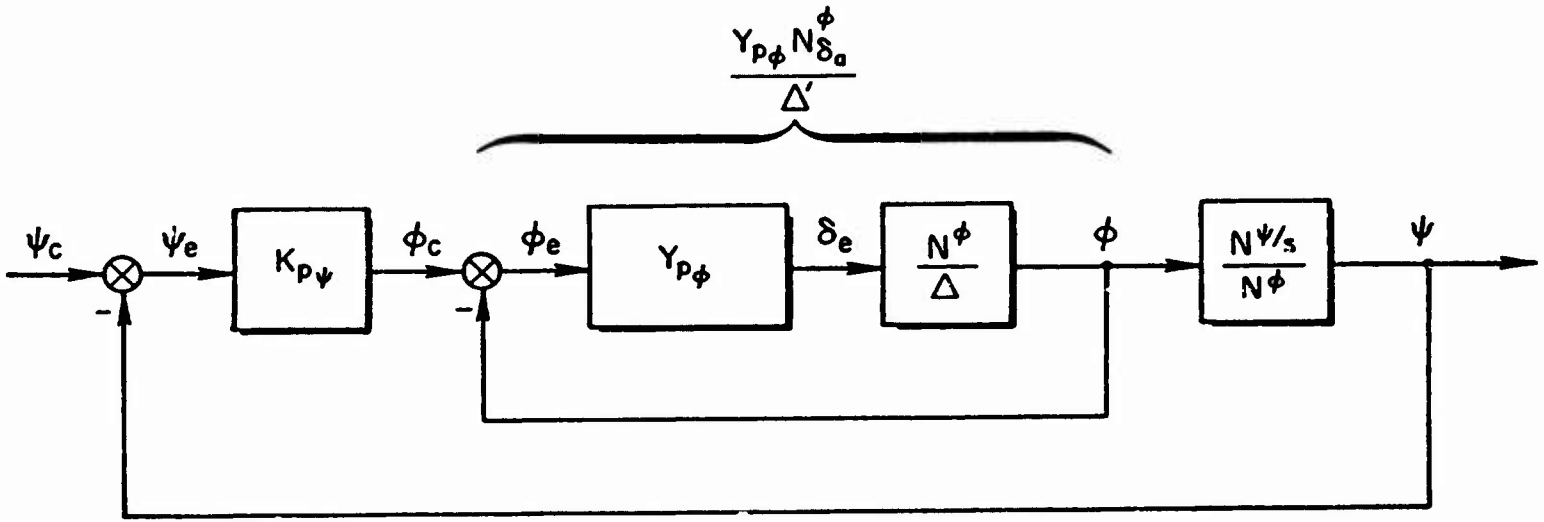

INNER LOOP

$$Y_{p\phi} = \frac{960(s+.6)e^{-As}}{\left[s^2 + 2(.3)(10)s + (10)^2\right](s+15)}$$

OUTER LOOP

$$Y_{p\psi} = 0.625$$

Figure 15. Multiloop Roll/Heading Pilot Model

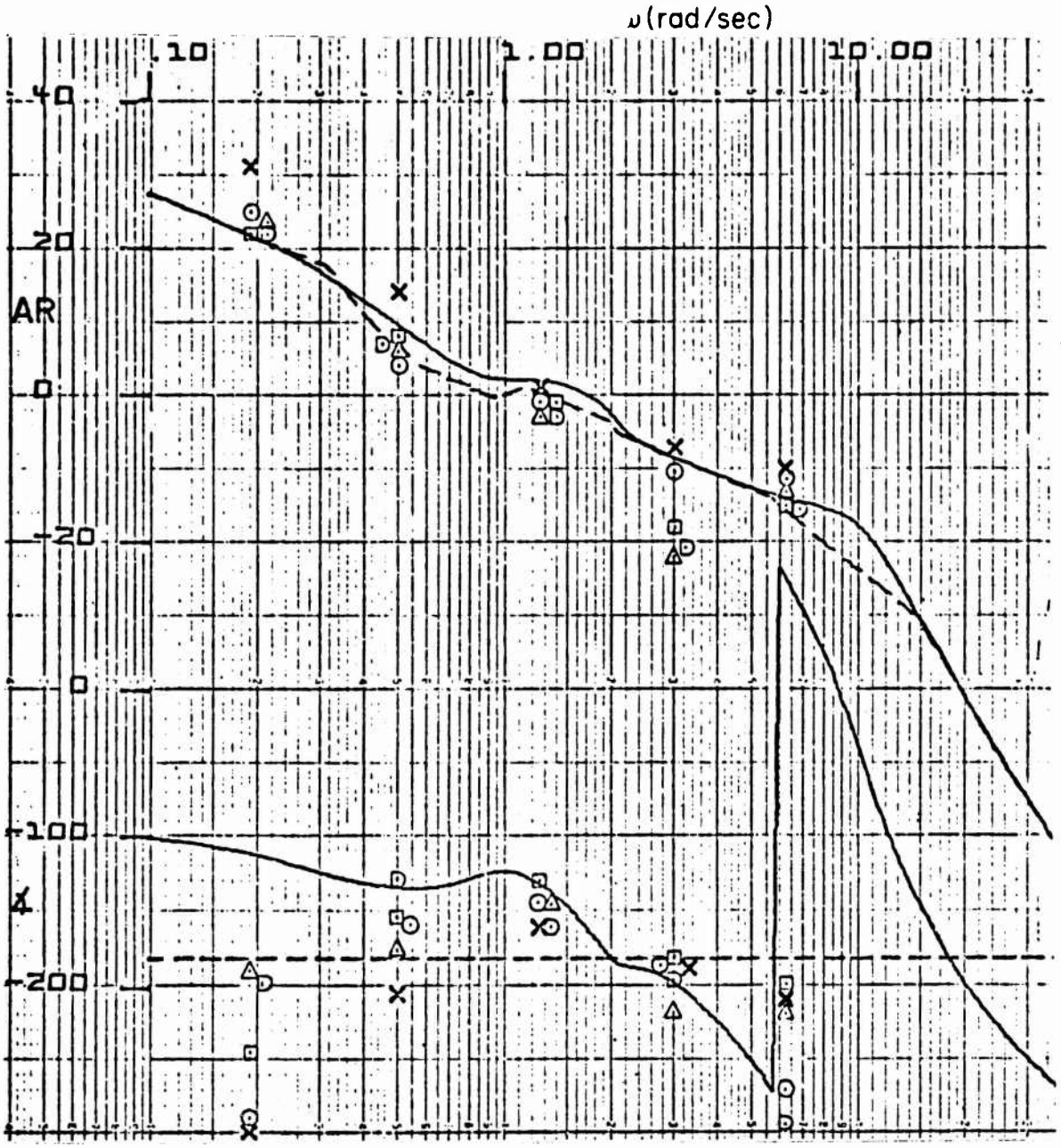

Figure 16. Open-Loop ψ/ψ_e with Inner Loop Closed

P-154

SUMMARY AND CONCLUSIONS

Multiloop, multi-input, multi-output pilot measurements have been made for an air-to-air tracking task with aircraft dynamics representative of impending stall/departure. These measures have allowed identification of the effect of impending stall/departure on pitch control, coupled versus uncoupled lateral-longitudinal airframe dynamics, and inner versus outer loop applications on pilot dynamic parameters.

The crossover model was found to apply in all loop closures, including multiloop situations, except when the controlled element exhibits a right half plane pole. In the latter case the crossover is achieved at an amplitude ratio slope somewhat less than 20 dB/decade.

The detailed pilot models obtained for the two-loop, coupled lateral-longitudinal airframe tracking task reflect the precision pilot model form except for the adoption of a second-order series lead in the pitch task. The presence (and degree) of coupling principally influences the low-frequency lag-lead equalization adopted by the pilot. This is adjusted within and between axes to effectively decouple the airframe motion with the least pilot effort (equalization).

Based only upon the open-loop pitch airframe dynamics used here we would not expect the pilot to adopt second-order lead equalization for either coupled or uncoupled cases. This apprently is a result of the requirement to prevent pitch (θ or α) overshoot which would trigger a departure. Thus, the pilot adopts equalization based on crossover, phase, and penalty criteria. While there are some previous pilot parameter measurement data which also reflect generation of second-order lead, these are insufficient to generate pilot rating functionals or to even predict the adoption of such equalization in the absence of the departure-prone context of the unfrozen aerodynamics.

Considerably more data must be obtained before a paper-pilot-type model can be devised for the pre-departure flight regime. Most past effort has been devoted to tasks and controlled elements where the airframe has relatively good dynamics, i.e., operation well within the nominal flight envelope, and concern is related to identification of the 3.5 boundary. This high-angle-of-attack task has involved operation at (if not beyond) the permissible

flight envelope boundary with attendant airframe dynamics which have been shown in the previous sections to rate in the 6 to 9 region at best.

It was found in the heading tracking task that the pilot was not making use of target bank angle information in the manner usually professed by fighter pilots, i.e., match target bank. One possible explanation is that this technique is used mainly for gross maneuvers and that once in a precise tracking position the pilot switches to a "pointing" mode — which this simulation has shown can accomplish a heading crossover of greater than 1 rad/sec even with relatively poor lateral airframe dynamics. If the target were to make a sudden large bank angle change it is likely the pilot would immediately switch to a "match bank angle" mode to minimize either error or reacquisition time.

REFERENCES

1. McRuer, Duane, "The Development of Pilot-in-the-Loop Analysis," J. Aircraft, Vol. 10, No. 9, Sept. 1973, pp. 515-524.

2. Peters, Richard A., and R. Wade Allen, Operation Manual. Describing Function Analyzer. Model 1003 Serial 1001, Systems Technology, Inc., Working Paper No. 406-2, Oct. 1970.

3. McRuer, Duane, Dunstan Graham, Ezra Krendel, and William Reisener, Jr., Human Pilot Dynamics in Compensatory Systems — Theory, Models, and Experiments with Controlled Element and Forcing Function Variations, AFFDL-TR-65-15, July 1965.

4. Johnston, Donald E., Irving L. Ashkenas, and Jeffrey R. Hogge, Investigation of Flying Qualities of Military Aircraft at High Angles of Attack, Systems Technology, Inc., Tech. Rept. No. 1033-1, Mar. 1974.

5. McRuer, D. T., and E. S. Krendel, Mathematical Models of Human Pilot Behavior, AGARDograph No. 188, Jan. 1974.

6. McRuer, Duane T., Irving L. Ashkenas, and C. L. Guerre, A Systems Analysis Analysis View of Longitudinal Flying Qualities, WADD-TR-60-43, Jan. 1960.

7. Shirley, Richard S., Motion Cues in Man-Vehicle Control, Ph.D. Thesis, MIT, Man-Vehicle Lab. MVT-68-1, Jan. 1968.

MANUAL CONTROL OF A TIME-VARYING VEHICLE

by

Thomas E. Moriarty
Department of Electrical Engineering
Air Force Institute of Technology
Wright-Patterson AFB, Ohio 45433

ABSTRACT

Manual control of a simulated task representing the regulation of angle of attack in a lifting re-entry vehicle has been studied as the plant characteristics gradually change from a pure inertia to a dampened second-order system. The characteristics change rapidly enough to prevent analysis by time averaging. Using ensemble averaging, the bandwidth of the pseudo spectra of the tracking error is estimated for several transition speeds, and several input disturbance bandwidths. The average power in the tracking error signals is also estimated. These results are compared to time-stationary vehicle analyses to show that point-by-point stationary analysis appears valid for transitions as rapid as 30 seconds. The inability of subjects to consciously detect transitions although they were changing their control techniques is discussed.

1. INTRODUCTION

In recent years there has been an increasing interest in analyzing the behavior of human operators as controllers. The control of time-varying vehicles is important since most physical vehicles change with time, at least to some extent. Many manual control analyses can be performed using time-invariant methodology because the vehicles change so slowly that point-by-point stationary analysis is valid. Manual control during abrupt or instantaneous changes has been studied since the mid-1960's, and various models for the human operator's actions have been formulated. [1][2][3]

This paper concerns itself with the study of transitions which are neither abrupt, nor so slow that the variation is unimportant. Although some work has been done in this area [4], the difficulties associated with describing non-stationary phenomona have limited most efforts to the methods of time domain analysis and optimal control theory [5]. The information presented here is a summary of an investigation into the description of a time-varying manual control problem using frequency domain parameters [6].

The investigation consisted of three main phases, the first being the design and performance of an experiment to generate and record the necessary data on a time-varying control task. The second phase of the investigation was the development of methodologies which were needed to analyse the time-varying data. The final phase was then the data reduction and interpretation of the results.

2. EXPERIMENTAL TASK

Two subjects were asked to control the longitudinal dynamics of a simulated vehicle whose characteristics varied from those of a pure inertia to those of a damped second-order system. Given an instrument similar to an artificial horizon, each subject tried to maintain an angle of attack of zero, while the vehicle was being disturbed in a random fashion. The vehicle characteristics, as shown in Figures 1 and 2, varied as the parameter ϕ; and ϕ varied linearly from zero to one in time intervals of 0,30,75 and 120 seconds An analog computer with logic capability was used for the simulation.

Figure 3 presents a block diagram of the simulation and indicates the various elements. In order to have a system with a known input and an observable output, the block diagram can be rearranged so that the input is the disturbance and the output is the error signal. It is this system, the pilot-vehicle combination in a regulator task as indicated in Figure 4, that was analyzed.

The input disturbance consisted of zero-mean, Gaussian, band-limited white noise with a filter break-frequency of 0.8, 1.4, or 2.0 rad/sec. Thus, there was a twelve-entry condition matrix to which each subject was exposed. Each entry was replicated 10 times to provide a statistical sample for each subject at each condition. Each run consisted of a 60 second initial static phase, followed by the time variation, and ending with a final static phase with the length adjusted so that each run lasted 240 seconds.

The data signals shown on Figure 3 (attack angle, error, input disturbance, and control stick deflection), were all recorded along with a timing signal to identify the time points at which the variations began and ended. The recording was done in digital form after passing the signals through an A to D converter that sampled 10 times a second.

3. ANALYSIS METHODS

The time-varying character of the data signals precluded the use of conventional time-averaging methods. Thus, ensemble averaging was used to provide time-varying statistics for the measured quantities. The statistical quantities utilized were:

mean:
$$\bar{y}(t_0) = \frac{1}{10} \sum_{i=1}^{10} y_i(t_0)$$

standard deviation:
$$\sigma_y(t_0) = \sqrt{\frac{1}{10} \sum_{i=1}^{10} [y_i(t_0) - \bar{y}(t_0)]^2}$$

and

autocovariance:
$$C_y(t_1, t_0) = \frac{\frac{1}{10} \sum_{i=1}^{10} [y_i(t_0) - \bar{y}(t_0)][y_i(t_1) - \bar{y}(t_1)]}{\sigma_y(t_1)\, \sigma_y(t_0)}$$

Although the problem was time-varying, the speeds of variation were well known. This allowed the use of a quasi-stationary assumption, that is that there is some relatively short period of time during which the characterists of the data signals do not vary appreciably. The assumption then provides a link between a slowly time-varying signal and a series of different spectral representations. This series of spectral representations is called the pseudo-spectral representation of the quasi-stationary signal, and the pseudo spectra are in general time-varying quantities.

It is possible to utilize the concept of quasi-stationarity in conjunction with ensemble averaging in order to decrease the statistical variation associated with a statistical quantity. This is accomplished by taking ensemble arranged statistics and time averaging them within regions of quasi-stationarity. The effect of this process is to increase the effective number of replicates, the amount of increase depending upon the correlation between the values being averaged.

Figure 5 shows the standard deviation of the stick deflection, attack angle, and error signals versus time for one subject and one condition. The data shown represents the 10 replicate ensemble averages, averaged over 1.5 second intervals. The square of the standard deviation, or variance, is an estimate of the power in the psuedo-spectral density; thus, Figure 5 is an indication of the manner in which the power in the various signals changes with time.

Figure 6 is a set of plots of the autocovariance function of the error signal for one of the subjects during one of the time varying intervals. Direct application of the Fourier Transform to these functions would result in imaginary spectral components and non-unique representations. In order to obtain an estimate of the character of the pseudo spectrum, the lowest value of the time interval from the origin to the first relative minimum of the autocovariance function was used to estimate the bandwidth of the pseudo spectral density. Reference 6 provides a detailed discussion of the character and validity of the bandwidth estimate which is actually the bandwidth of a low-pass rectangular spectrum whose transform or autocorrelation exhibits a first relative minimum at the same distance from the origin as that of the autocovariance for the unknown spectrum.

Applying this estimate to the autocovariances of the error signal taken at various points during the transition gives and indication of how the signal bandwidth changes with time.

4. RESULTS

The standard deviation of the output of the Pilot-Vehicle-Regulator combination, the error signal, was computed for each subject at each of the twelve conditions. A three-way Analysis of Variance in conjunction with the Newman-Keuls Test indicated that the actual transition speed was not a significant variable; whereas the input filter frequency and the value of ϕ were significant variables at $P < .001$. Figure 7 shows the standard deviation during the transitions after averaging out the transition speed. These results indicate that for the transitions studied here the power in the output signal is not a function of the transition speed, but is clearly a function of the input bandwidth and the vehicle configuration. Figure 7 also indicates that the transitions in power level of output occur only during a portion of the vehicle's transition, depending upon the input bandwidth.

Figure 8, a comparison of the transition with a set of static runs corresponding to various points in the transition, indicates that the time-varying and the data from static analyses are in general agreement.

The estimate of the bandwidth, called the bandwidth parameter, of the error signal was computed for each subject in each condition. Figures 9 through 14 show the effects of averaging out first the filter frequency (ω_f) variable, then the transition speed variable, and finally the percent of variation (100 ϕ) variable. An analysis of variance for subject B showed that the shapes of all the curves were essentially the same. Subject A appeared to exhibit an inconsistency relative to the 75 second variation speed which caused the analysis of variance to show an interaction between input bandwidth and transition speed. In both subjects, the confounding effect of experiencing the instantaneous switch and the 75 second variation during the same session tended to make the middle speed (75 second variation) data stand out from the high and low speed data sets. Although the statistics show the variables of transtition speed and input bandwidth to be significant, it is the opinion of the author that the significance may be due to confounding effects and also that the variance due to these factors may be of low practical importance. The lack of interaction, and the significance of the percent of variation (100 ϕ) were certainly of prime importance.

Figure 15 shows that the time-varying value of the bandwidth parameter for one particular condition compares fairly well with those values given by analysis of time-invariant data sets representing various points in that same transition.

All the results seem to indicate that for the tasks encompassed by this experiment, the pilot's performance in controlling the time-varying system is essentially equivalent to his performance in controlling time-invariant systems which correspond to various points in the transition.

It was noted in informal conversations with the subjects, that they were not consciously able to detect the system changes until well into the variation, i.e., around the 30-40% point, and yet they are changing their characteristics almost immediately.

REFERENCES

1. Young, et al, "Adaptive Dynamic Response Characteristics of the Human Operator in Simple Manual Control," Transactions on Human Factors in Electronics, Vol HFE5, No.1, September 1964, pp 6-13.

2. Elkind, J.I. and Miller, D.C., "The Process of Adaption by the Human Controller, "Second Annual NASA University Conference on Manual Control, NASA-SP-128, 1966, pp 47-63

3. Young. L.R., "On Adaptive Manual Control," Ergonomics, Vol 12, No.4, July 1969, pp. 635-674.

4. Ince, F., and Williges, R.C., "Detecting Slow Changes in System Dynamics," Aviaton Research Laboratory, Institute of Aviation, University of Illinois, Technical Report ARL-72-4/AFOSR-72-2, April 1972.

5. Baron, S., et al, "Application of Optimal Control Theory to the Prediction of Human Performance in a Complex Task." Air Force Flight Dynamics Laboratory, AFFDL-TR-69-81, March 1970

6. Moriarty, T.E., "The Manual Control of Vehicles Undergoing Slow Transitions in Dynamic Characteristics," Ph.D. dissertation, University of Michigan, Ann Arbor, 1973.

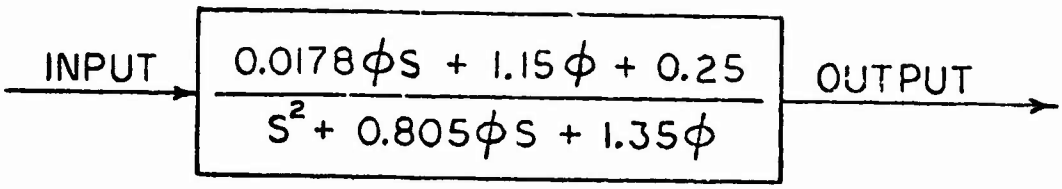

Figure 1. Time-Varying Vehicle Transfer Function

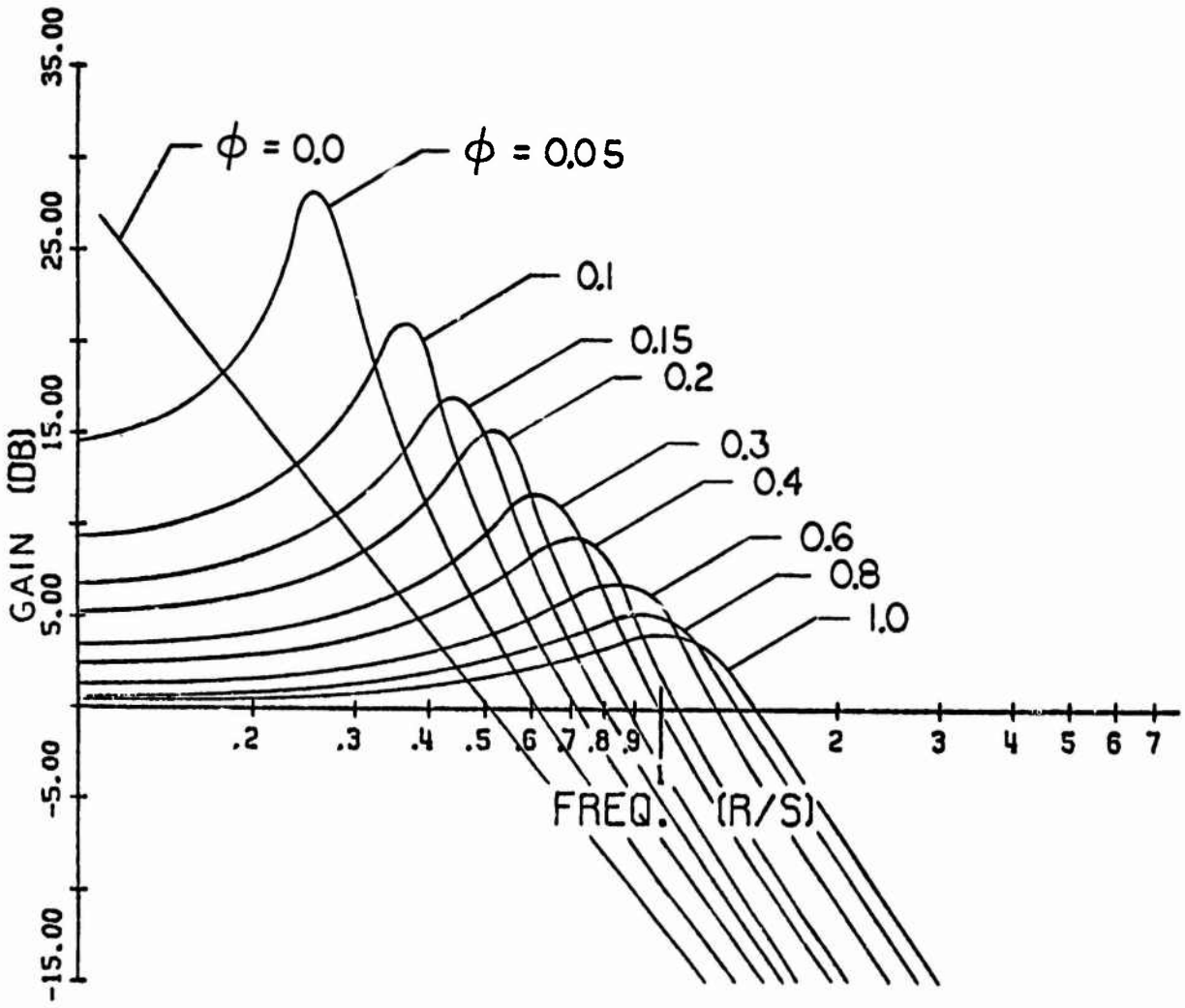

Figure 2. Bode Magnitude Plot for Vehicle

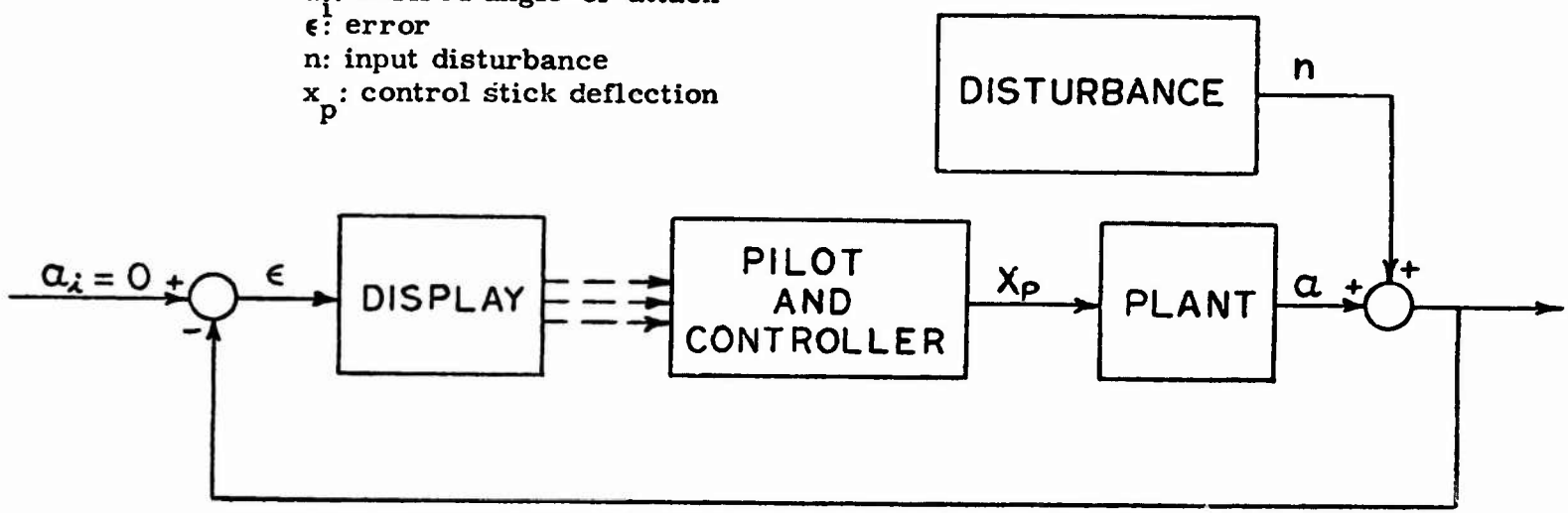

Figure 3. Simulation Block Diagram

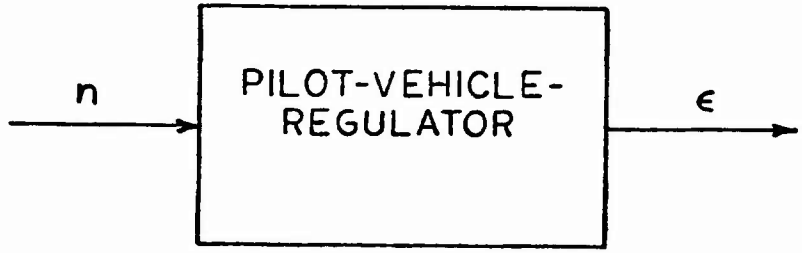

Figure 4. Pilot-Vehicle-Regulator

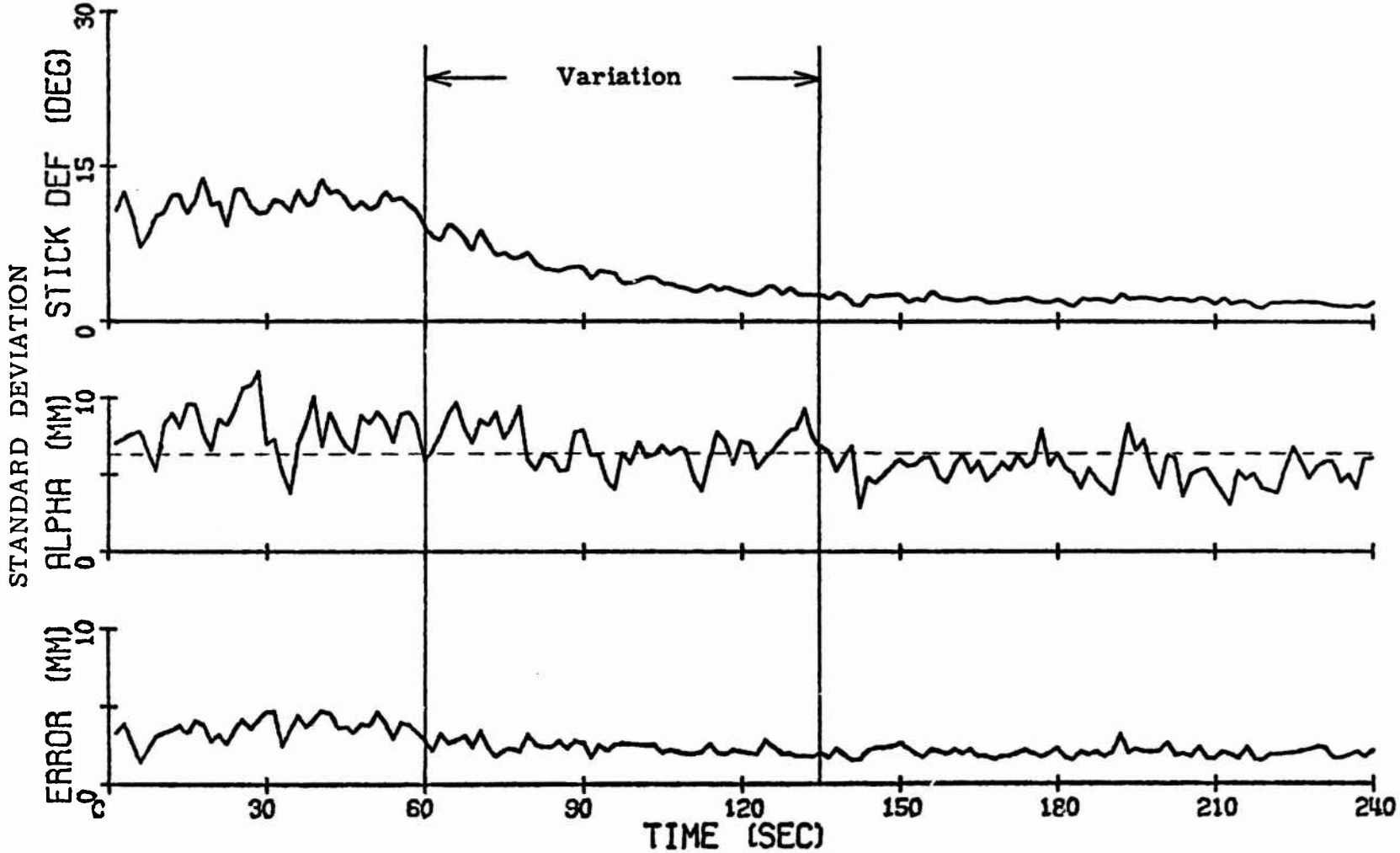

Figure 5. Standard Deviation of Recorded Data for Subject B, Input Filter Frequency = 1.4 r/s, Transition in 75 seconds.

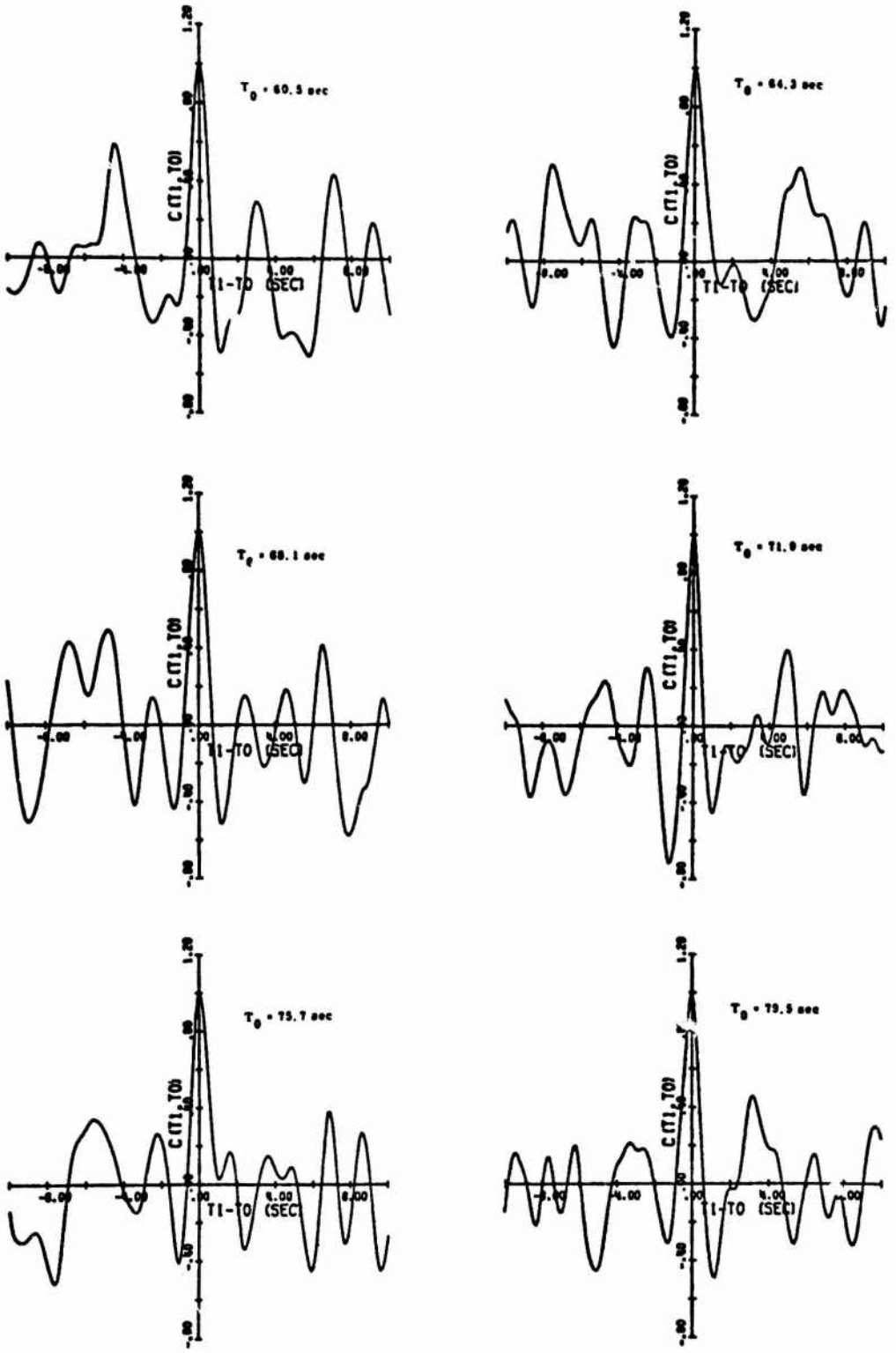

Figure 6. Error Signal Average Autocovariance Functions for Subject B, Input Filter Frequency = 1.4 r/s, Transition in 75 sec.

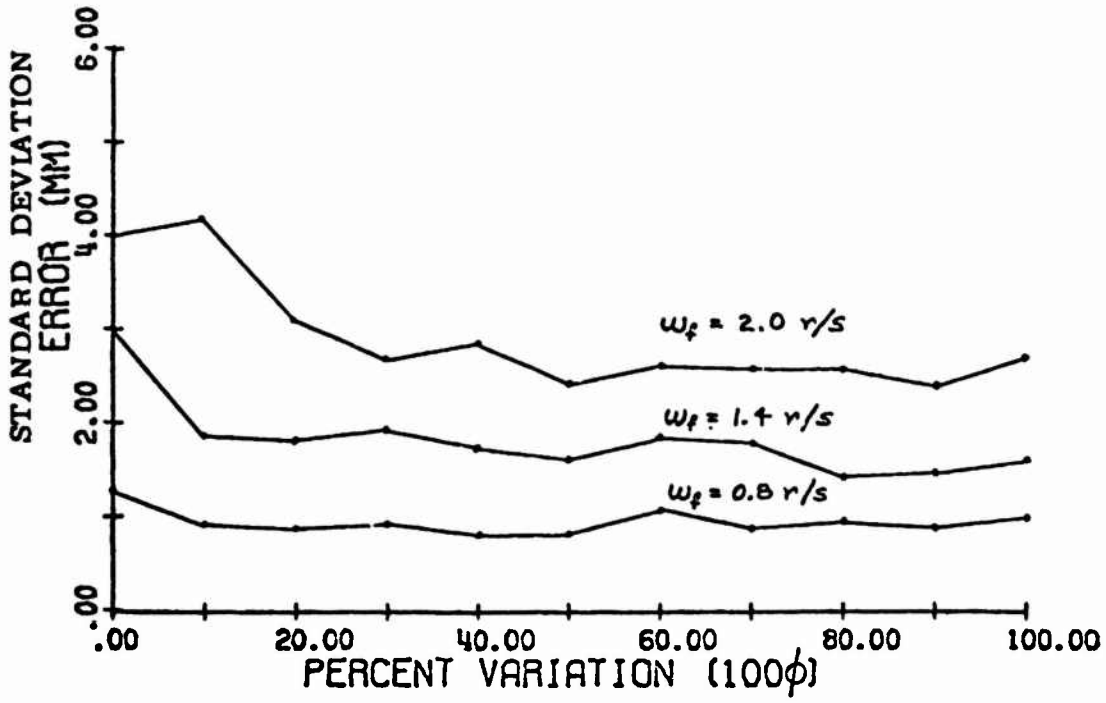

σ_ϵ Versus Percent Variation for 3 Input Filter Frequencies, Subject A

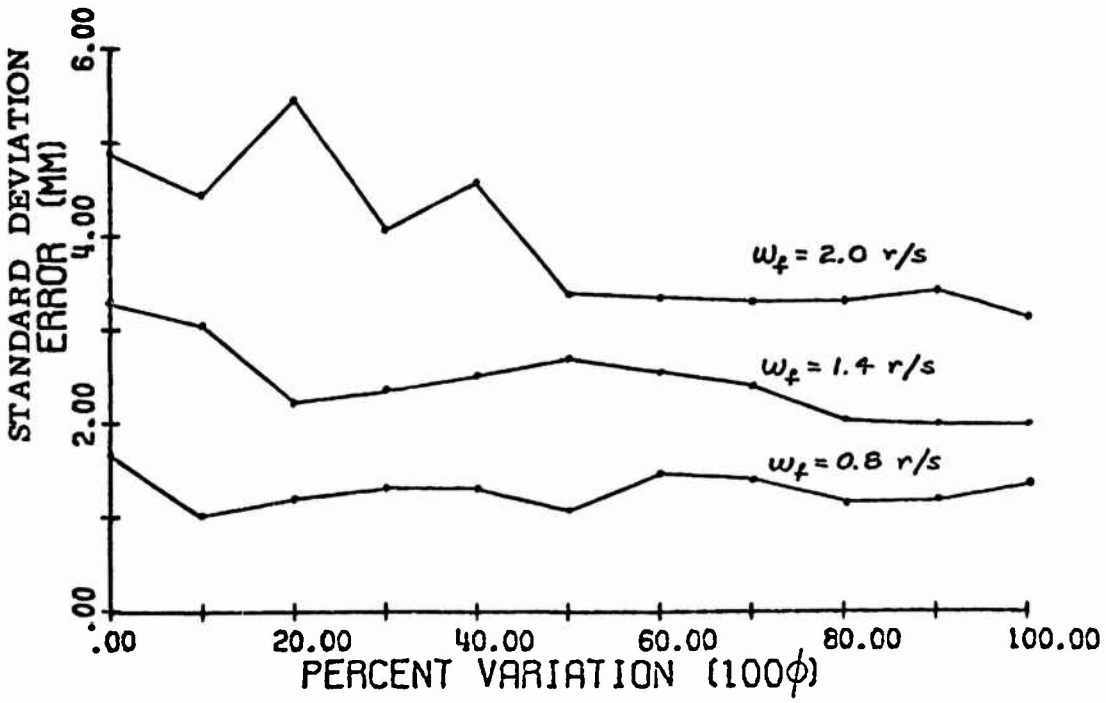

Figure 7. σ_ϵ Versus Percent Variation for 3 Input Filter Frequencies.

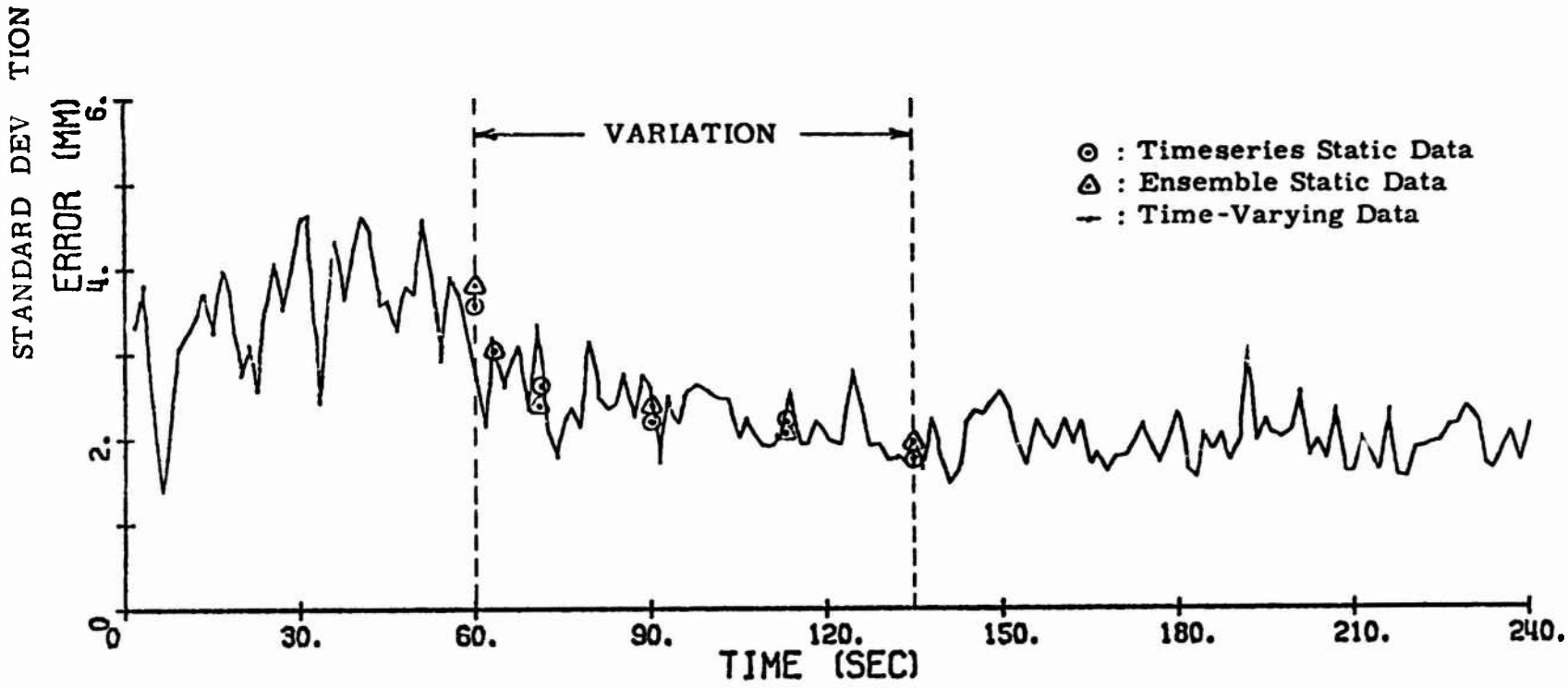

Figure 8. Comparison of Static and Time-Varying σ_ε Data for Subject B, Input Filter Frequency = 1.4 r/s, Transition in 75 sec.

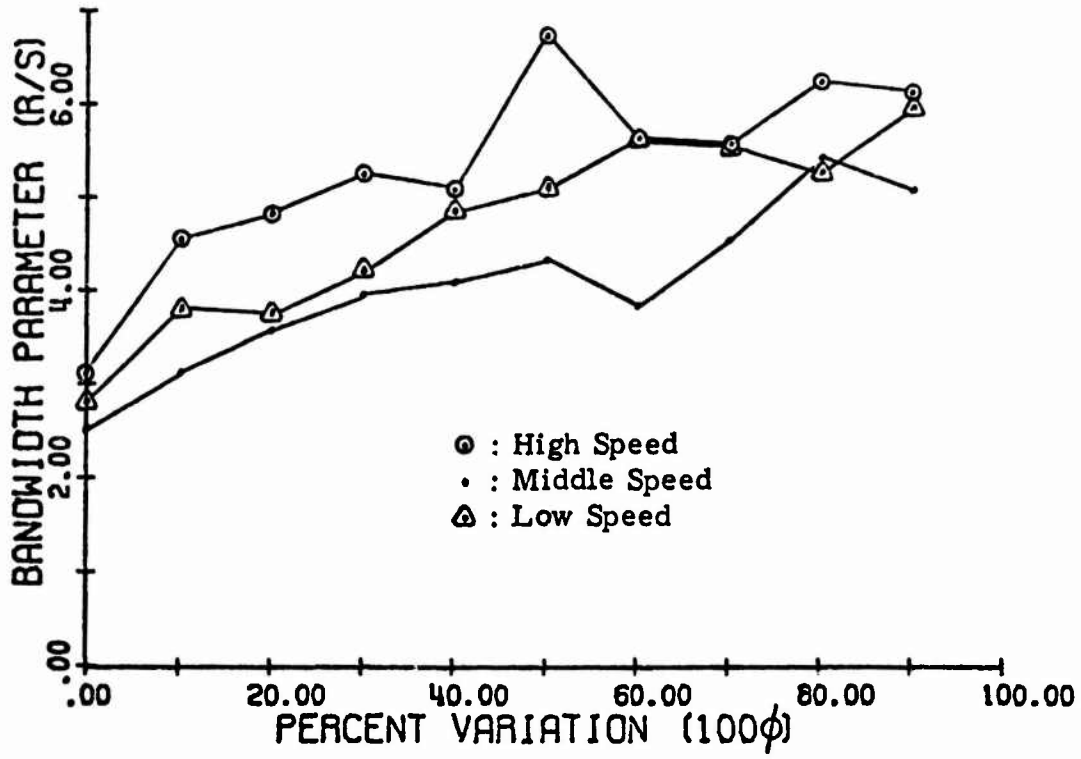

Figure 9. Bandwidth Parameter Averaged over Filter Frequency, Subject A.

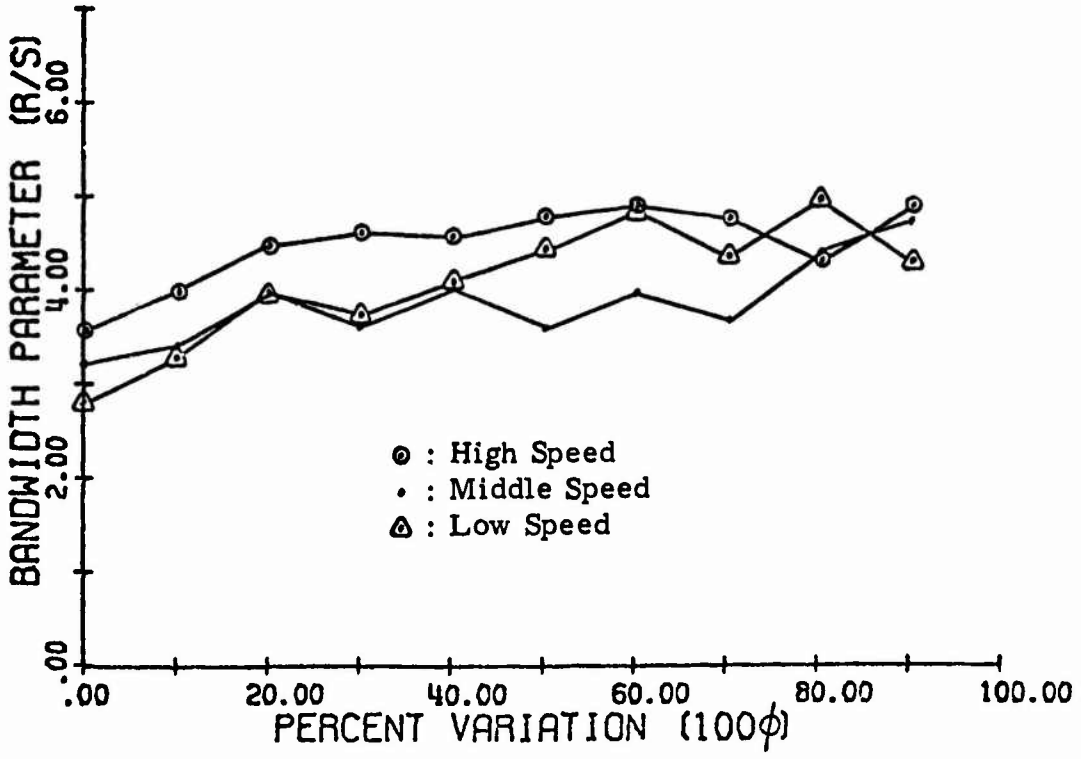

Figure 10. Bandwidth Parameter Averaged over Filter Frequency, Subject B.

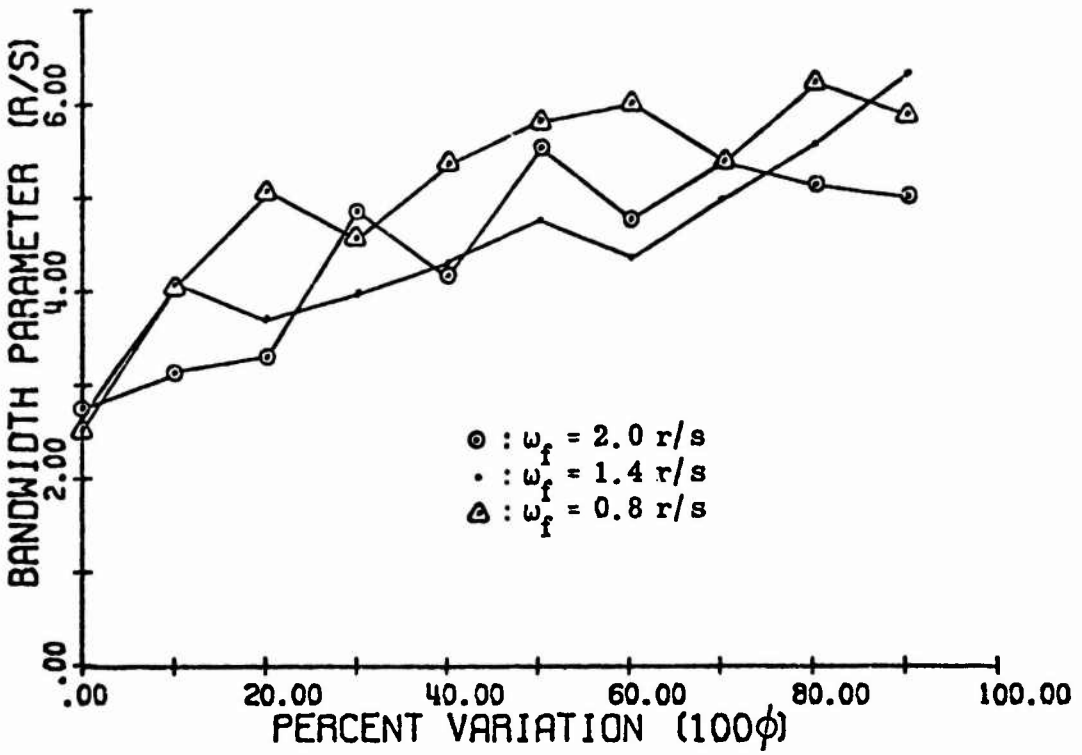

Figure 11. Bandwidth Parameter Averaged over Speed, Subject A.

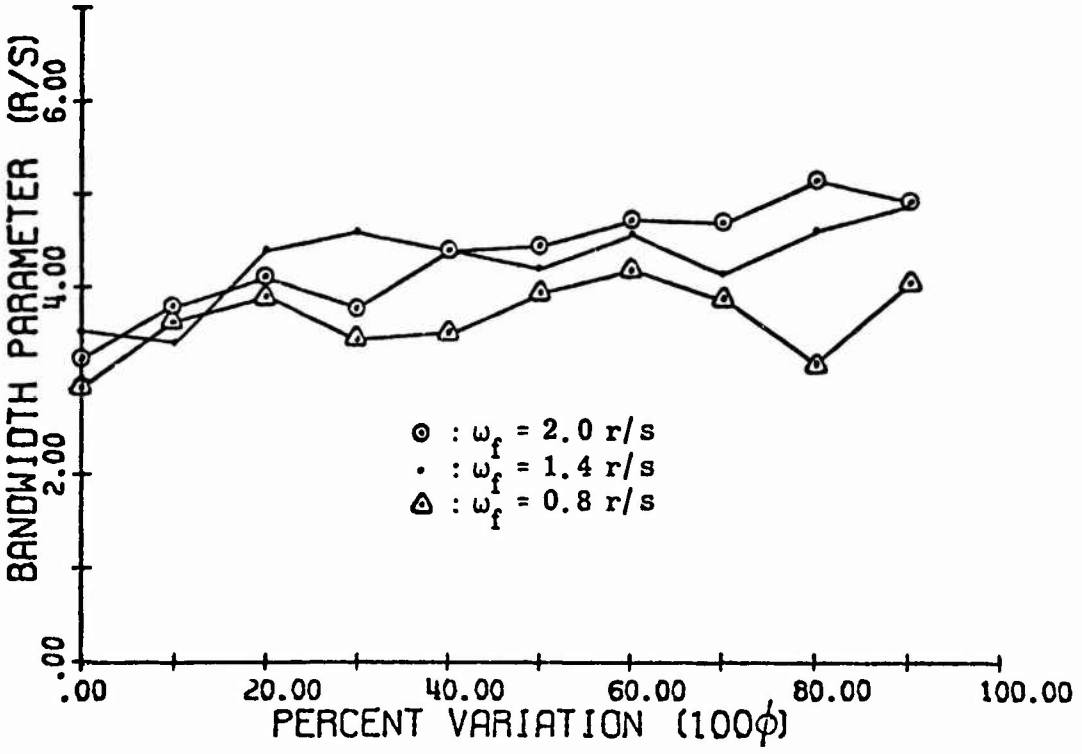

Figure 12. Bandwidth Parameter Averaged over Speed, Subject B

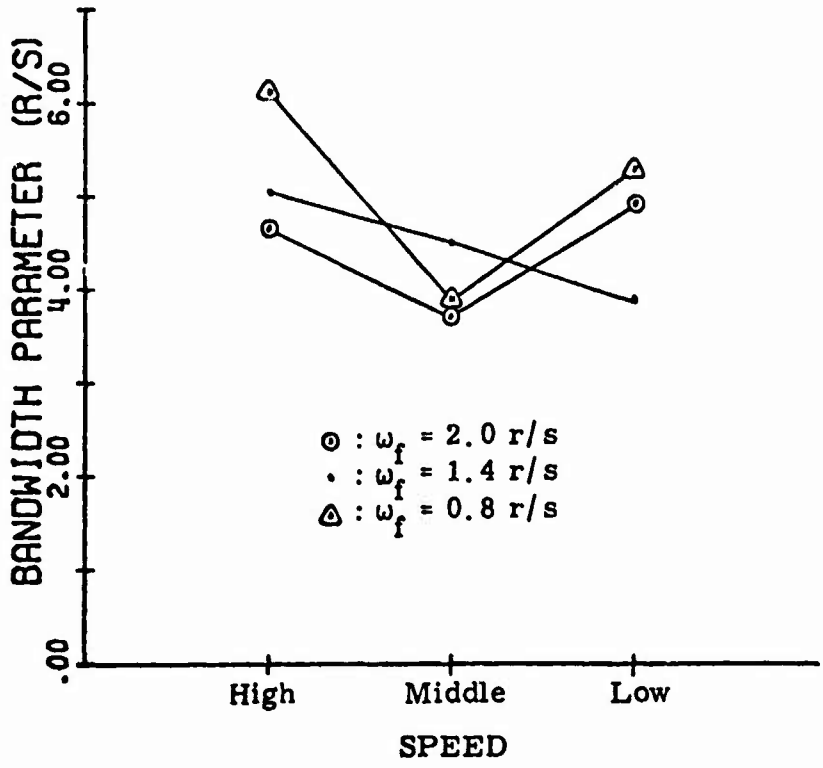

Figure 13. Bandwidth Parameter Averaged over Percent, Subject A

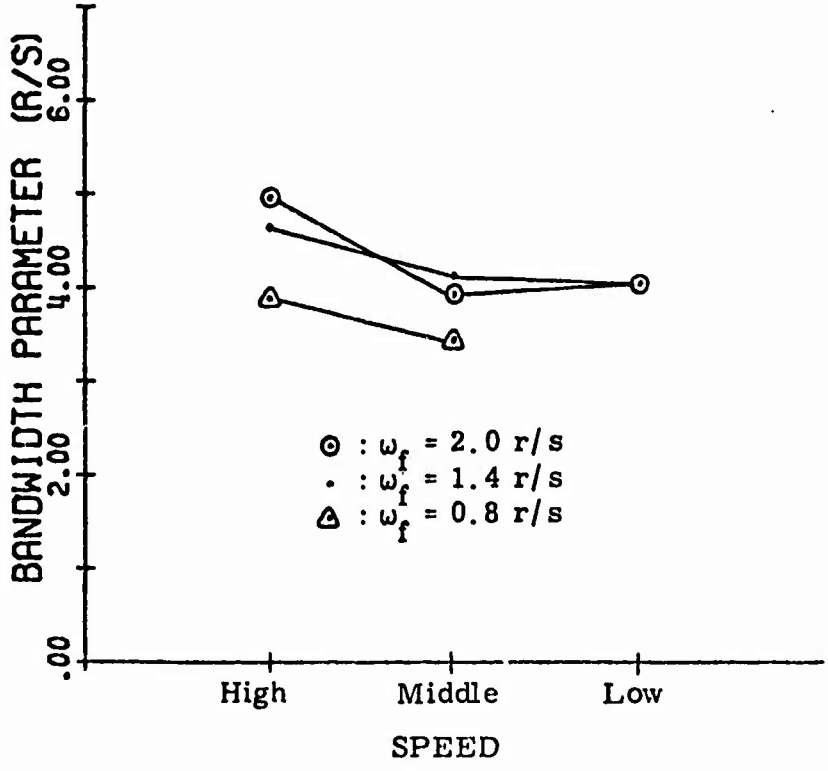

Figure 14. Bandwidth Parameter Averaged over Percent, Subject B

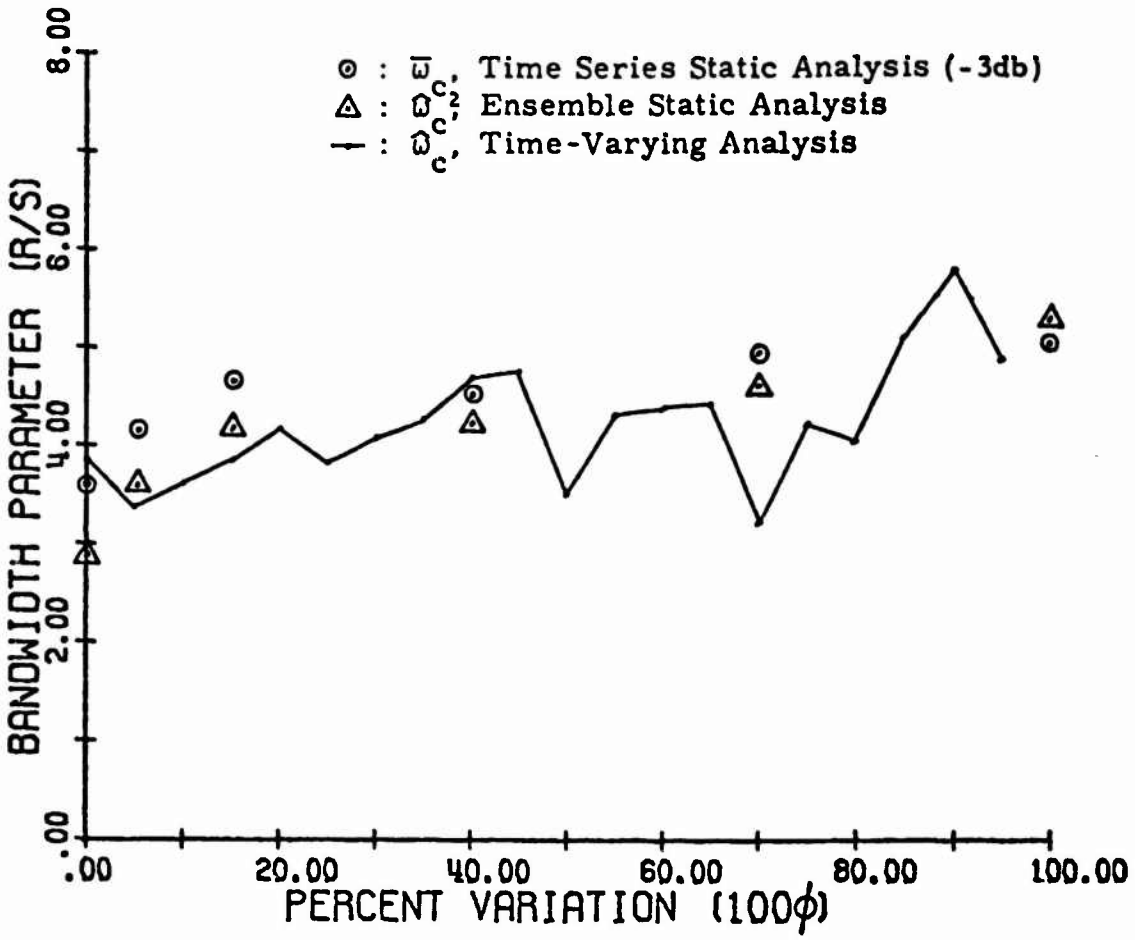

Figure 15. Comparison of Static and Time-Varying Bandwidth parameter for Subject B, Input Filter Frequency = 1.4 r/s, Transition in 75 sec.

14-28,209 #24

A PRELIMINARY LOOK AT FLIGHT DIRECTOR DESIGN PHILOSOPHIES FOR APPLICATION TO A VTOL LANDING APPROACH FLIGHT EXPERIMENT*

R.T.N. Chen, J.V. Lebacqz, and E.W. Aiken

Calspan Corporation
Buffalo, New York 14221

ABSTRACT

A flight program using the variable stability X-22A aircraft is being conducted to investigate the interactive effect of control augmentation complexity and display sophistication on pilot rating and performance for VTOL instrument landings employing a decelerating transition during a steep approach. This paper provides a general review of the scope of the program, and discusses in detail one aspect of flight director design philosophy that has been investigated. The paper demonstrates with a simple example that using optimal control theory to design flight director gains, assuming the pilot to be a simple gain, leads to a less stable closed-loop system than the "classical" STI K/s design for a given level of pilot gain, and that the closed-loop characteristics are also more sensitive to pilot gain. An analog synthesis procedure using a pure gain pilot model with a time delay is then developed which both compensates the optimal control gains and defines a passive compensation network; this system is shown to exhibit good closed-loop dynamics. Piloted ground simulator evaluations verify the fact that the uncompensated optimal design is undesirable; few noticeable differences between the compensated optimal and "K/s" designs were found.

INTRODUCTION

It is clear that the capability of V/STOL aircraft to operate into small areas can provide significant advantages for both commercial and military users, and in fact these advantages have been demonstrated under visual flight conditions. The extension of this capability under instrument conditions, however, has proved to be much more difficult than the same extension for CTOL aircraft. This increased difficulty is a result of the fact that the landing approach now involves not only control of the spatial position of the aircraft but also precise control of a non-constant total velocity; this task requires active use of at least one additional controller,

*The experiment described here is being performed under Contract No. N00019-73-C-0504 for the United States Naval Air Systems Command and the National Aeronautics and Space Administration, Langley Research Center.

and furthermore requires additional information to the pilot concerning the increased dimensions of his task. The pilot's control problem is exacerbated by the generally degraded flying qualities encountered as the dependence on powered lift increases, and, in VTOL configurations different than the helicopter, by an additional control requirement related to the conversion from forward flight to powered lift (e.g. wing tilt, rotor tilt, jet thrust vectoring).

Accordingly, a flight research program using the variable stability X-22A V/STOL aircraft has been undertaken to investigate the control, display, and guidance requirements for VTOL instrument landings. The primary purpose of the experiment is to provide meaningful data related to the interaction of aircraft control system and pilot display characteristics on pilot rating and performance during a steep decelerating descending transition from a representative forward velocity ($\sim$ 110 kt) to a hover and vertical landing under instrument conditions. The experiment is therefore designed to investigate combinations of several types of control system characteristics with display presentations of varying sophistication, the most sophisticated of which includes three-axis continuous flight director information plus a fourth discontinuous "configuration" director. As part of the flight director design process, the "classical" K/s approach pioneered by STI (References 1, 2) was compared to "modern" approaches using optimal control theory (Reference 3), with some interesting results.

This paper therefore has the following two objectives:

- To provide a general description of the scope of this flight program
- To discuss in detail, using a simple example, one aspect of flight director design.

The organization of the paper is as follows. The first two sections review briefly the X-22A research facility and the current research experiment. The following sections discuss in detail a hypothesized design procedure for flight director gains, compare the resulting design with "classical" and "modern" approaches for a simple example, and review preliminary piloted simulator results of testing the hypothesized design. The final section presents some concluding remarks.

X-22A RESEARCH FACILITY

The X-22A research facility consists of: (1) the X-22A aircraft itself, with associated response-feedback variable stability system, onboard analog computer, and onboard programmable analog symbol generator for an electronic display; (2) a mobile ground station, which receives all flight data via telemetry, acts as a processor for digital data analyses, and provides the computational capability for the ground simulator; and (3) the X-22A

ground simulator, which consists of an X-22A cockpit and variable stability system identical to that of the aircraft. This total facility is described in detail in References 4, 5, and 6, and is therefore only summarized here.

As is shown in Figure 1, the X-22A aircraft has four ducted propellers and four engines. The engines are connected to a common system of rotating shafts which distribute propulsive power to the four propellers. Changes in the direction of the thrust vector are accomplished by rotating the ducts, which are interconnected so that they all rotate through the same angle. Thrust magnitude is determined by a collective pitch lever, similar to a helicopter; a recent expansion of the capability is the alternative of a fore-and-aft thrust magnitude controller. Normal-looking pitch, roll, and yaw controls in the cockpit provide the desired control moments by differentially positioning the appropriate control elements (propeller pitch or elevon deflection) in each duct.

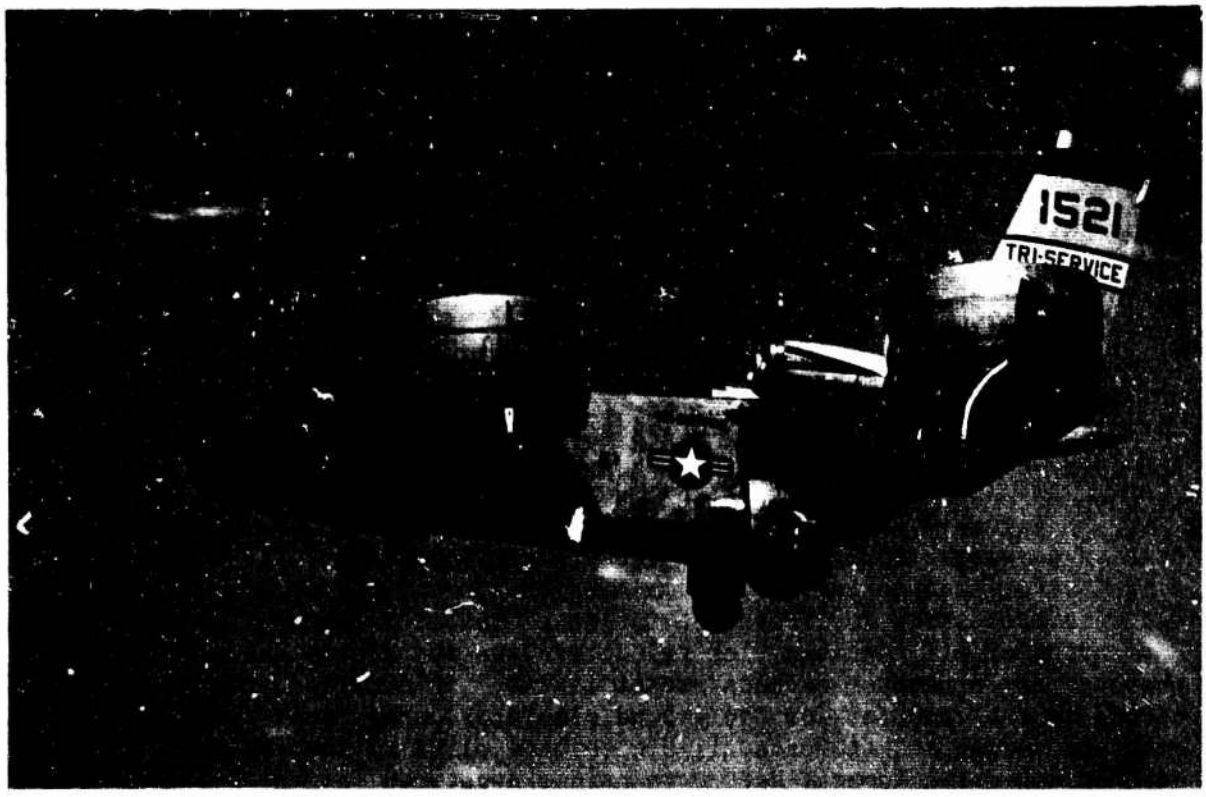

Figure 1 VARIABLE STABILITY X-22A AIRCRAFT

There are four variable stability system (VSS) controllers - thrust, pitch, roll and yaw - and three artificial feel servos for the evaluation pilot cockpit controls, each employing electrohydraulic servos. When rigged for VSS flight, the left hand flight controls are mechanically disconnected from the right hand flight controls and connected to the set of VSS pitch, roll and yaw feel servos. The VSS thrust servo operates the boost servo for the collective pitch system. VSS pitch, roll and yaw servos operate the right hand flight controls, moving the same linkages which are moved manually by the right hand pilot in normal non-VSS flight. (In fact, these same actuators serve a dual role by providing artificial feel for the primary flight control system when the VSS is not engaged.) Phasing of these control motions to the blades and elevons is accomplished by the mechanical mixer as for normal flight.

During VSS operation, the evaluation pilot occupies the left hand seat in the cockpit. The system operator, who also serves as the safety pilot, occupies the right hand seat The evaluation pilot's inputs, in the form of electrical signals, operate the appropriate right hand flight controls through the electrohydraulic servos. In addition to the evaluation pilot's inputs, signals proportional to aircraft motion and relative wind variables (for example, angle of attack or pitch rate) are fed back to move the right hand controls in the required manner and thus modify the aircraft's response characteristics as desired. The response-feedback and input gain controls are located beside the safety pilot and are used to set up the simulation configuration in flight. Note that the evaluation pilot cannot feel the basic X-22A control motions caused by the variable stability system.

Recent additions to the aircraft systems include an on board analog computer and a programmable symbol generator for an electronic display. The analog computer provides the capability to compute flight director gains, generate additional control variations (e.g., command pre-filtering) and perform guidance data transformations and smoothing. The symbol generator provides up to 32 different symbols for display on a cathode ray tube, and the capability to vary the symbols presented during a flight is provided by switches on a separate console.

Figure 2 summarizes schematically the functions of the mobile ground station developed for the X-22A. The primary purposes of the equipment include flight safety monitoring, real-time data monitoring and experiment control, and data processing for flight operations. The mini-computer provides on-line monitoring of all the down-link telemetry data and alerts the ground crew whenever any parameter exceeds preset limits. In addition, the mini-computer serves as the computer for the ground simulator. Paramount among the digital data processing techniques available to be applied to the recorded flight data is a digital identification technique developed for the X-22A and successfully applied to over 300 data records to date (References 7 and 8); an example is shown in Figure 3.

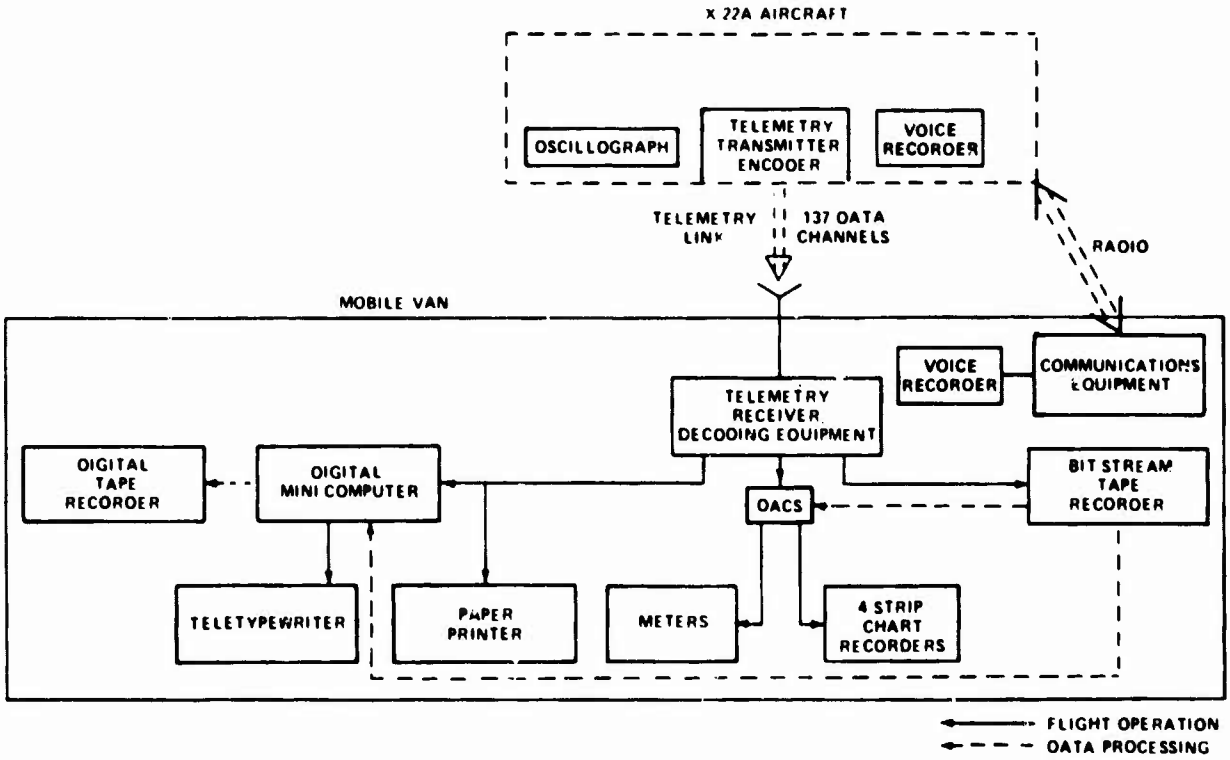

Figure 2 SCHEMATIC DIAGRAM OF DIGITAL DATA ACQUISITION SYSTEM

The fixed-base X-22A ground simulator (Figure 4) is designed to supplement the X-22A aircraft operation in the following manner:

- Perform preliminary tests of experimental programs prior to flight tests in the actual aircraft.
- Develop new experimental hardware and systems, such as control systems and displays, prior to installation in the actual aircraft.
- Ground test new equipment and check experimental setups in the aircraft prior to actual flight test.
- Provide pilot training as required.

The first of these capabilities was used to perform preliminary evaluations of the flight director designs to be discussed shortly.

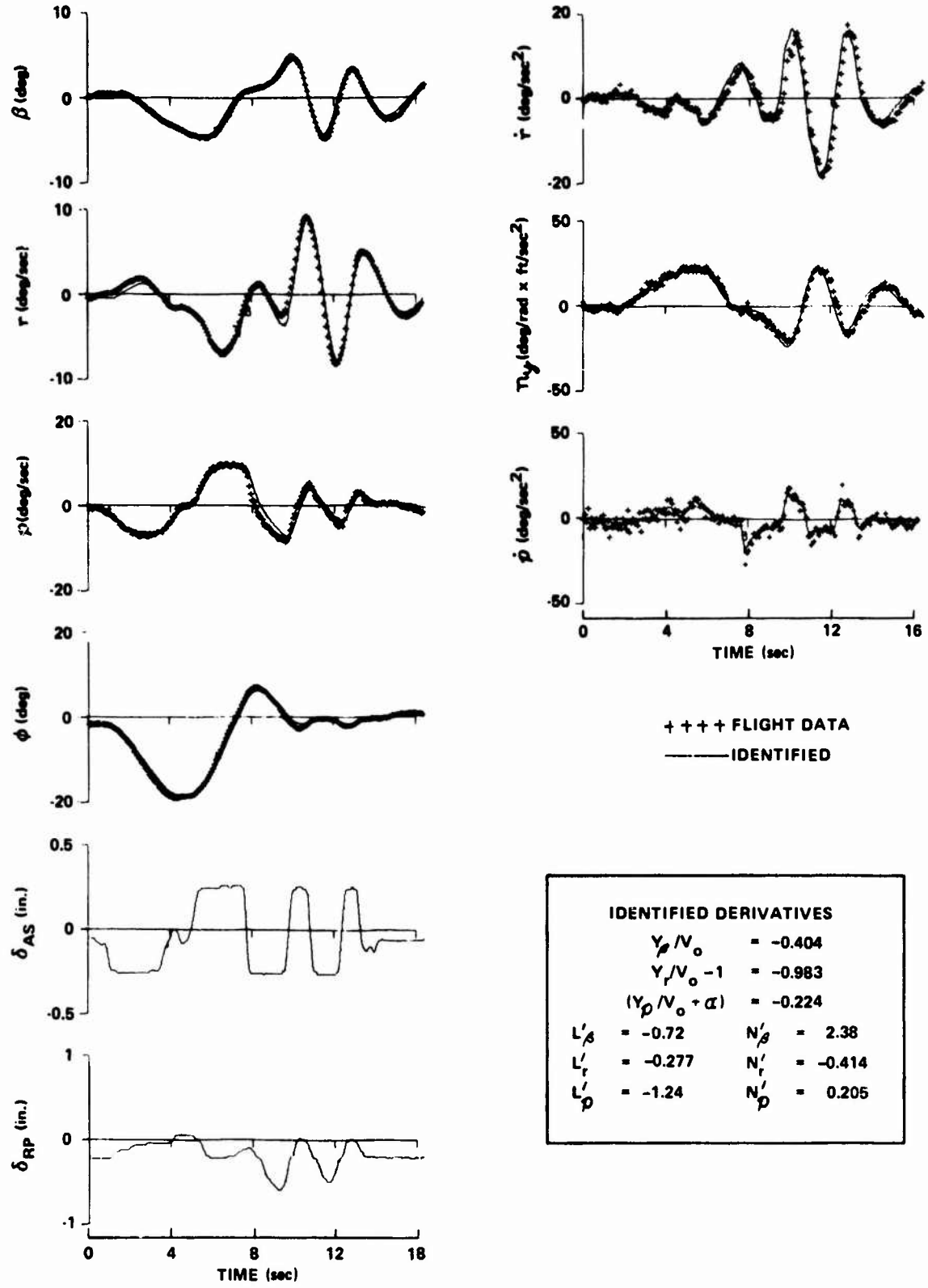

IDENTIFIED DERIVATIVES

Y_β/V_o	= −0.404		
$Y_r/V_o - 1$	= −0.983		
$(Y_p/V_o + \alpha)$	= −0.224		
L'_β	= −0.72	N'_β	= 2.38
L'_r	= −0.277	N'_r	= −0.414
L'_p	= −1.24	N'_p	= 0.205

Figure 3 IDENTIFICATION OF CONFIGURATION 4

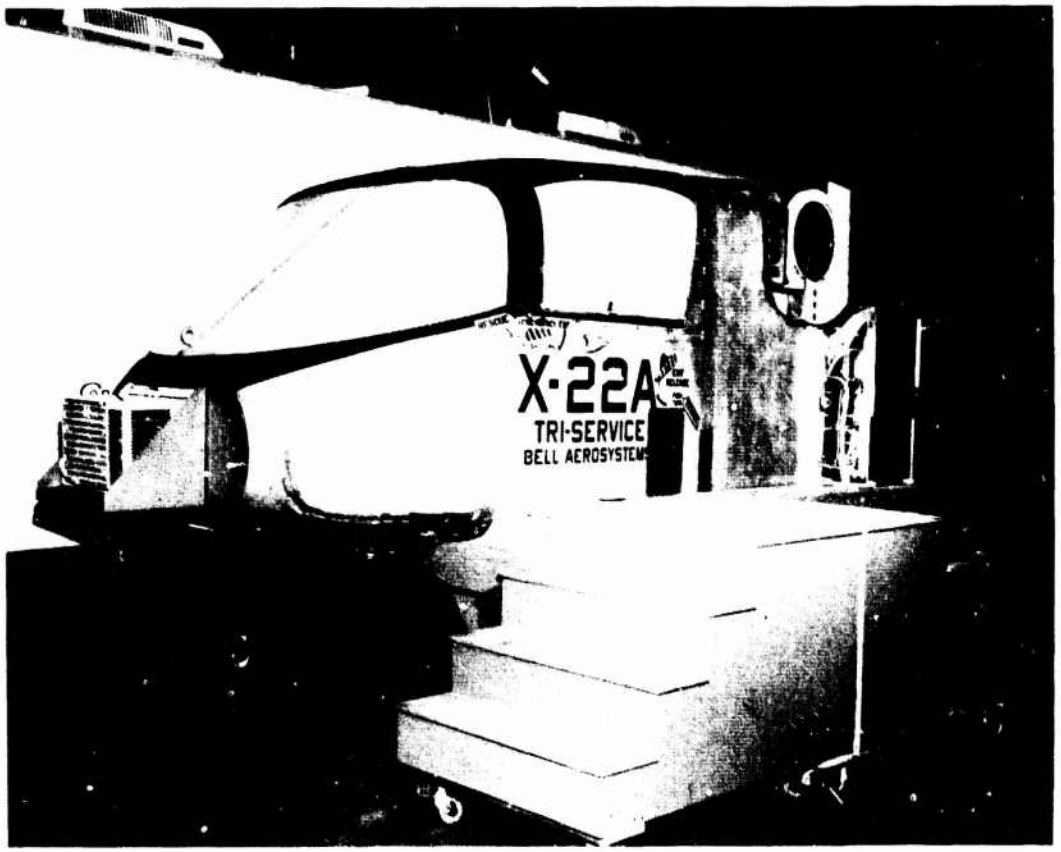

Figure 4 X22A GROUND SIMULATOR

CURRENT X-22A RESEARCH PROGRAM

The first two X-22A programs investigated STOL flying qualities and demonstrated the usefulness of the X-22A aircraft as a viable experimental tool (References 9, 10, 11, and 12). In addition, as is discussed in Reference 4, the second program also performed preliminary flight work relevant to the VTOL decelerating landing problem. In a general sense, the conclusions of these two programs most relevant to the current program might be summarized as follows:

- For a simple but steep approach trajectory (constant speed and descent angle), if longitudinal and lateral-directional stability and control characteristics are such as to provide satisfactory flying qualities (PR < 3.5), then instrument approaches could be performed using only standard aircraft electromechanical instrument displays and raw ILS information with an ease and precision similar to steep visual approaches.

- For a more complex approach (constant steep descent angle but decelerating along the glide path), instrument approaches could not be successfully performed using the same instrumentation and guidance display.

The current flight program is therefore a logical outgrowth of the first two. As was discussed at the beginning of this paper, the purpose of the experiment is to attempt to define satisfactory control-display system combinations to perform decelerating descending approaches. The general concept guiding the experiment design was based on attempting to quantify the control-display interplay on pilot rating and performance; this quantification was given the highest priority for future research by the AGARD Advisory Report on V/STOL display requirements (Reference 13), and is shown schematically in Figure 5. The configuration matrix was developed on the basis of work done by NASA Langley (References 14, 15) and extensive ground simulation on the X-22A ground simulator; the base matrix is shown in Figure 6. Brief descriptions of the elements of each axis are given below.

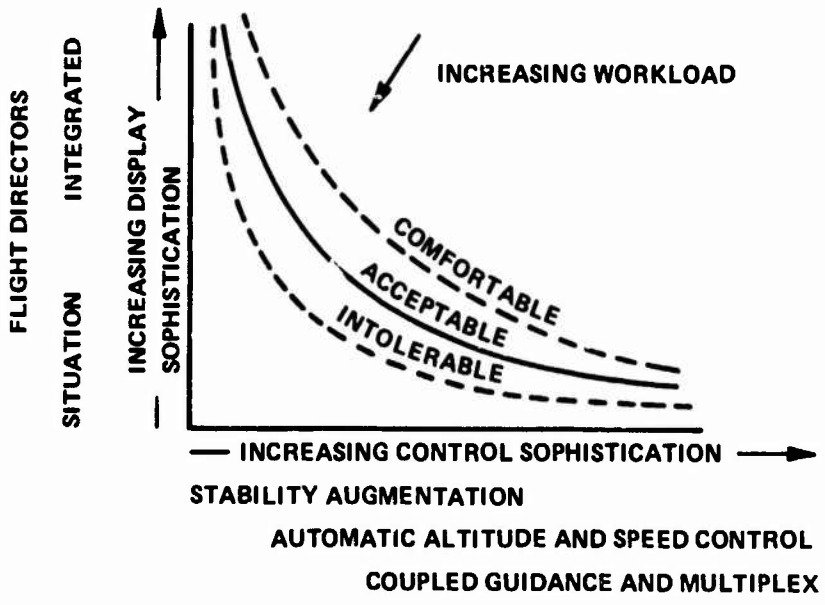

Figure 5 TRADE OFF BETWEEN DISPLAY AND CONTROL SOPHISTICATION (FROM REFERENCE 13)

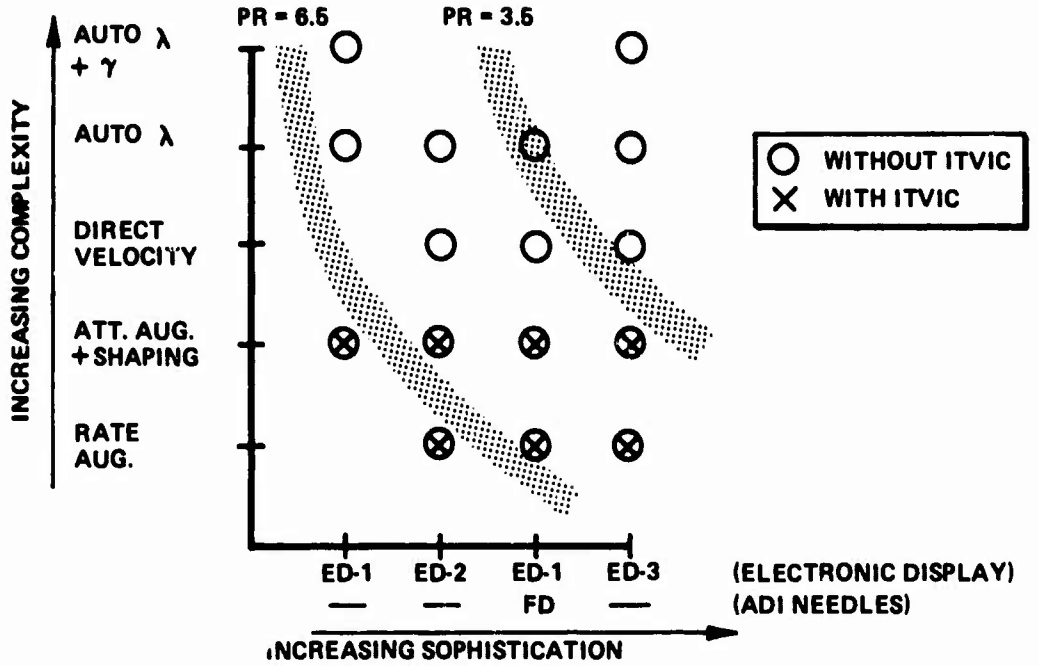

Figure 6 BASE CONFIGURATION MATRIX (25 CONFIGURATIONS)

(1) Control Systems

- Rate Augmentation. This control system represents the minimum control and stability augmentation system complexity considered for this program. In particular, the system is mechanized as rate SAS only instead of the more complex rate-command, attitude-hold type of system. Pitch, roll, and yaw rate stabilization approximately equal to the basic X-22A SAS is used as a level representative of V/STOL aircraft.

- Attitude Augmentation and Control Shaping. This system represents the most complex angular augmentation investigated, and is essentially equivalent in concept to that used in Reference 15. The pitch and roll axes are attitude stabilized through high feedbacks and the control inputs to these axes are shaped through a second order prefilter or model to provide satisfactory responses to the stick commands.

- Direct Velocity Control. The purpose of this control system is to give the pilot decoupled control of the two longitudinal velocity components (with respect to the ground) by using control crossfeeds and response feedback including duct angle.

- Automatic Duct Angle Control. This system represents a minimal automation complexity by removing the necessity for the pilot to change aircraft configuration (i.e., duct angle). The implementation of this system uses the same logic as the ITVIC light to be discussed shortly, with the signal now driving the ducts instead of the light.

- Automatic Duct Angle and Glide Slope Tracking Control. This system represents the maximum automation complexity which maintains the pilot-in-the-loop as essentially an attitude regulator only. The mechanization of this system uses the thrust magnitude flight director logic to feed signals directly to the thrust controller (i.e., collective stick) and the automatic duct angle control discussed above.

(2) Displays

- Electronic Display. The electronic display integrates vertical and horizontal information plus command information in one unit to minimize scanning problems. Much of the symbology, as well as the analog symbol generator, is based on work done by Dukes (References 16, 17). Three formats are being investigated in this experiment:
  (a) ED-1: position and commanded position information
  (b) ED-2: position, commanded position, ground velocity, and commanded ground velocity information
  (c) ED-3: position, commanded position, ground velocity, and pitch, roll, thrust magnitude control directors.

These formats and the symbology are shown in Figure 7 in an earth-referenced axis system for ED-3.

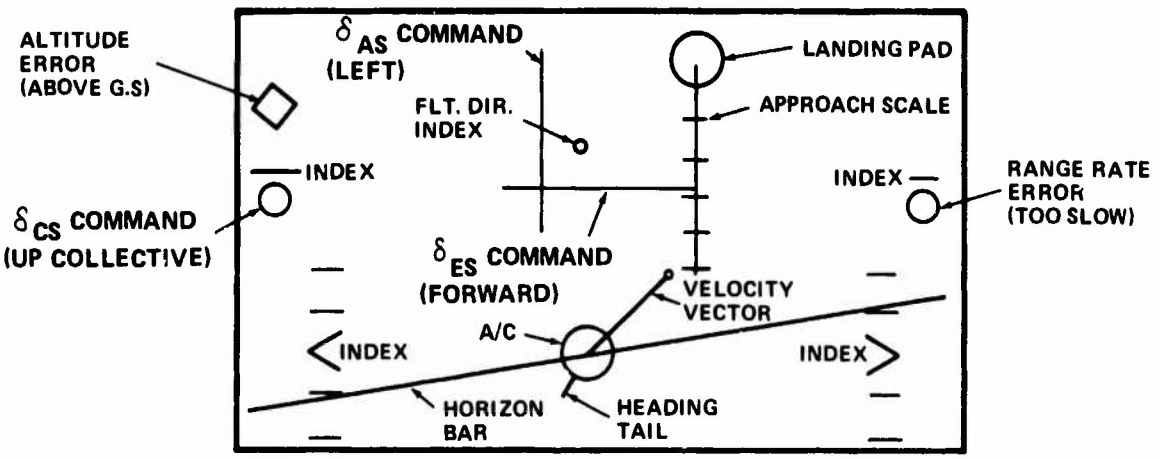

Figure 7 ELECTRONIC DISPLAY SYMBOLOGY (EARTH-REFERENCED)

- ADI and Integrated Cross Pointers/Tab. An electromechanical attitude indicator with integrated pointers is used as an auxiliary vertical display. The pointers and tab either present flight director information (with ED-1) or are not active.

- Independent Thrust Vector Inclination Command (ITVIC) Light. V/STOL aircraft that require configuration changes to convert from forward flight to hover may need to be provided with command information to effect these changes. For the X-22A, the duct rotation control is an "ON-OFF" rotation rate controller, and hence the rotation command should be an "ON-OFF" signal. In the ground simulation investigation it was found that using a light, which came on when the commanded duct angle exceeded the duct angle by a specified amount, provided significant improvements in pilot opinion of control-display combinations which required duct angle changes independently (i.e., rate augmentation, attitude augmentation). Therefore, most of the display combinations for the two least complex control systems will be evaluated with and without the ITVIC director to ascertain possible benefits in performance.

At the time of the writing of this paper, the flight program is not sufficiently complete to ascertain whether or not the results expected from this experiment design will materialize. By virtue of the ground simulation capability, however, it has been possible to investigate the configuration matrix in a general sense; in addition, the design process itself has resulted in hypotheses that have led to some interesting discoveries. The remainder of this paper discusses the generation, theoretical verification, and experimental investigation of one of these hypotheses in the design of the flight director signals.

DEVELOPMENT OF A "COMPENSATED OPTIMAL" FLIGHT DIRECTOR DESIGN PHILOSOPHY

The flight director signals used in the initial X-22A ground simulator study, which was preliminary to the current experiment (Reference 6), were based on the well-known manual control theory result of attempting to have the open loop controlled element frequency response be K/s in the region of pilot crossover (References 1, 2). It is not clear, however, that this approach leads to the best closed-loop automatic system if the pilot is replaced by a zero-delay black box of gains. Since optimal control theory provides a useful tool for designing zero-delay automatic systems in multiloop multichannel situations, a preferable flight director design might be based on compensating such an optimal design for the pilot to act in it. Reference 3 is an example of a study with a similar aim, but in that case the pilot model used neglected

the inherent effective time delay of the pilot, which is an assumption of dubious validity. The design philosophy developed during the program described in this paper is therefore an attempt to ensure that:

1. the pilot does not need to do any compensation; i.e., he acts as a proportional control with an inherent delay

$$G_p(s) = K_p e^{-\tau s}$$

with τ = 0.3 sec (0.2 to 0.4 is a usual range of values)

2. the closed-loop performance (some function of the trajectory error) is comparable with that of using a zero-delay automatic landing system designed using optimal control theory, for a reasonable loop gain, as well as with that of a K/s design.

With these two criteria, the man-vehicle closed-loop system, will, theoretically, have good mission performance and the pilot will be comfortable flying the mission.

The design problem is solved in two steps. First, uncompensated optimal control gains are found for an automatic system. These gains are then compensated for the pilot's time delay in an approximate, analog fashion for implementation in a flight director. The symbology is shown in Figure 8, and the problem solution outlined below.

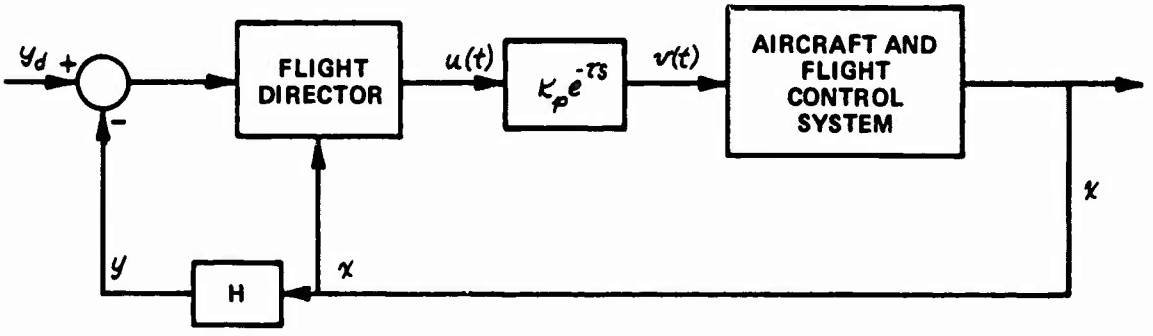

Figure 8 FLIGHT DIRECTOR DESIGN PROBLEM

Given

$\dot{x}(t) = Fx(t) + Gv(t)$	aircraft dynamics
$y(t) = Hx(t)$	kinematics
$u(t) = v(t+\tau)$	pilot time delay
$\dot{z}(t) = D_o z(t),\ z(0) = z_o$	description of desired output
$y_d(t) = Cz(t)$	(conversion from servo to regulator problem)

Index of Performance: $$J = \int_0^\infty \left\{ (y_d - y)^T Q (y_d - y) + v(t)^T R v(t) \right\} dt$$

Solution:

a) Optimal (Automatic) Control Law

$$v(t) = K_0 z(t) - K x(t)$$

where
$$K_0 = -R^{-1} G^T P_2$$
$$K = R^{-1} G^T P_1$$

and
$$P_1 F + F^T P_1 - P_1 G R^{-1} G^T P_1 = -H^T Q H$$
$$P_2 D + \left(F^T - P_1 G R^{-1} G^T\right) P_2 = H^T Q C$$

b) Flight Director Signal

$$u(t) = v(t+\tau) = K_0 z(t+\tau) - K x(t+\tau)$$
$$= K_0 e^{D\tau} z(t) - K \left\{ e^{F\tau} x(t) + \int_t^{t+\tau} e^{F(t+\tau-\theta)} G u(\theta-\tau) d\theta \right\}$$

Since $e^{D\tau}$ and $e^{F\tau}$ represent constant gain adjustments, the remaining problem is an approximation to the convolution integral for analog mechanization. Making a linear assumption for $u(t)$ between $t-\tau$ and t, we have*:

$$\int_t^{t+\tau} e^{F(t+\tau-\theta)} G u(\theta-\tau) d\theta \cong K_3 u(t) + K_4 u(t-\tau)$$

where
$$K_3 = \frac{F^{-2}}{\tau} \left[e^{F\tau} - I - F\tau \right] G$$
$$K_4 = \frac{F^{-2}}{\tau} \left[I + e^{F\tau}(F\tau - I) \right] G$$

Hence, the flight director signal becomes:

$$u(t) = (I + KK_3)^{-1} \left\{ K_0 e^{D\tau} z(t) - K e^{F\tau} x(t) - KK_4 u(t-\tau) \right\}$$

or transforming to the "s" domain:

$$u(s) = \left[I + KK_3 + KK_4 e^{-\tau s} \right]^{-1} \left\{ K_0 e^{D\tau} z(s) - K e^{F\tau} x(s) \right\}$$

---

*Invertability of F is not required, since $e^{F\tau} = I + F\tau + \frac{\tau^2}{2} F^2 + \ldots$.

The resulting flight director is shown in Figure 9. The following important points should be noted:

(1) The design is directly applicable to a multivariable multicontroller situation.

(2) The initial term of the equation is a delay compensator which is always physically realizable (poles and zeros in the left-hand plane).

(3) The design has the advantages associated with quadratic synthesis of providing a complete procedure which ensures a stable closed-loop system with good performance characteristics.

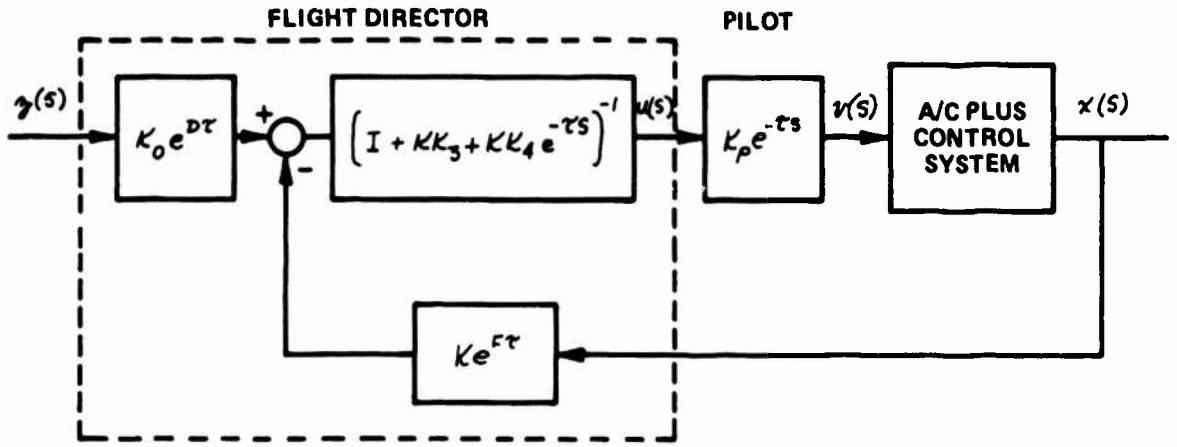

Figure 9 COMPENSATED OPTIMAL CONTROL FLIGHT DIRECTOR

For implementation simplicity, a first-order Pade' approximation might be used for $e^{-\tau s}$; the initial term (delay compensator) then becomes:

$$\left[I + KK_3 + KK_4 e^{-\tau s}\right]^{-1} \cong \left(s + \frac{2}{\tau}\right)\left[sI + \frac{2}{\tau}\left(I + KK_3 - KK_4\right)^{-1}\left(I + KK_3 + KK_4\right)\right]^{-1} \cdot \left(I + KK_3 - KK_4\right)^{-1}$$

For example, a single controller problem reduces to the scalar expression:

$$\frac{1}{1 + KK_3 + KK_4 e^{-\tau s}} \cong \frac{1}{1 - K(K_4 - K_3)} \quad \frac{s + \frac{2}{\tau}}{s + \frac{2}{\tau}\,\frac{1 + K(K_3 + K_4)}{1 - K(K_3 - K_4)}}$$

As can be seen, this approximation for a single controller leads to a delay compensator which is a simple lead-lag circuit.

APPLICATION OF HYPOTHESIS TO EXAMPLE

To test the hypothesized design against both a typical K/s design and a zero-delay optimal control design as in Reference 3, the plunge mode of the X-22A in hover was considered. For this example, considering a constant commanded altitude (z_c = 10 ft):

$$F = \begin{pmatrix} 0 & 1 \\ 0 & -.2 \end{pmatrix}, \quad G = \begin{pmatrix} 0 \\ -2 \end{pmatrix}, \quad H = (1, 0), \quad D = 0, \quad C = 1$$

Designing the automatic system to have closed-loop characteristics of ζ = .7, ω_n = 2.5 rad/sec yields the uncompensated gains:

$$K = (-3.16, -1.68), \quad K_o = -3.16$$

For the uncompensated case, then, the displayed quantity is:

$$u(s)_{UC} = K_d \left\{ -3.16 \left(z_c - z(s) \right) + 1.68 s\, z(s) \right\}$$

where K_d is a variable "sensitivity" scalar.

Assuming a time delay of 0.3 seconds, the compensator gains are:

$$K_z = \begin{pmatrix} 0 \\ -.3 \end{pmatrix}, \quad K_y = \begin{pmatrix} -.090 \\ -.282 \end{pmatrix}$$

Hence, the compensated displayed signal is (in the frequency domain):

$$u(s)_C = K_d \frac{s + 6.67}{s + 20.23} \left\{ -4.24 \left(z_c - z(s) \right) + 3.35 s\, z(s) \right\}$$

For comparison with the above, a K/s design for this example valid over all frequencies would be:

$$u(s)_{K/s} = K_d \left\{ (s + 0.2) \left(z_d(s) - z(s) \right) \right\}$$

Root loci sketches for each of these cases with a pilot model $G(s) = -K_p \left(\frac{s - 6.67}{s + 6.67} \right)$ are shown in Figure 10.

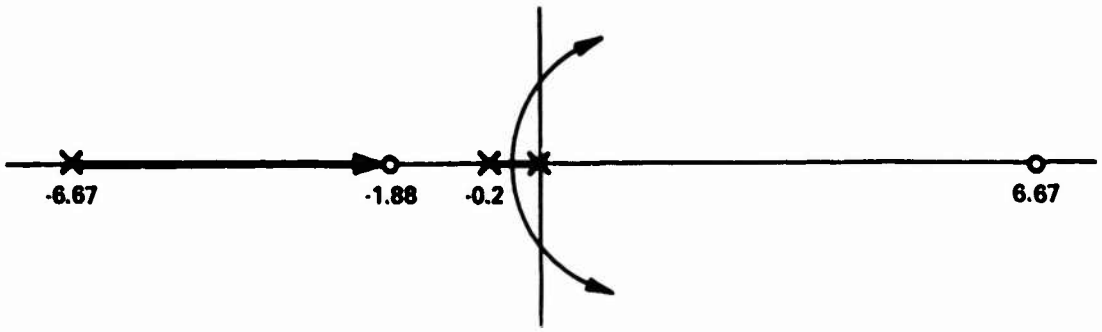

a) OPTIMAL CONTROL DESIGN WITHOUT DELAY COMPENSATION

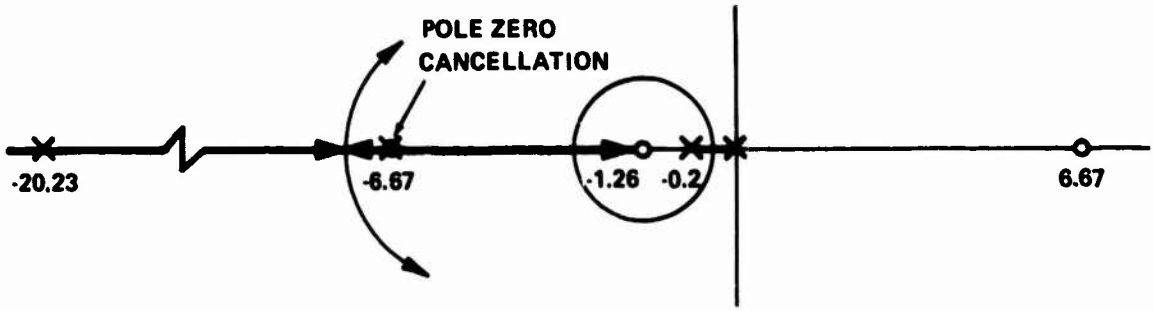

b) OPTIMAL CONTROL DESIGN WITH DELAY COMPENSATION

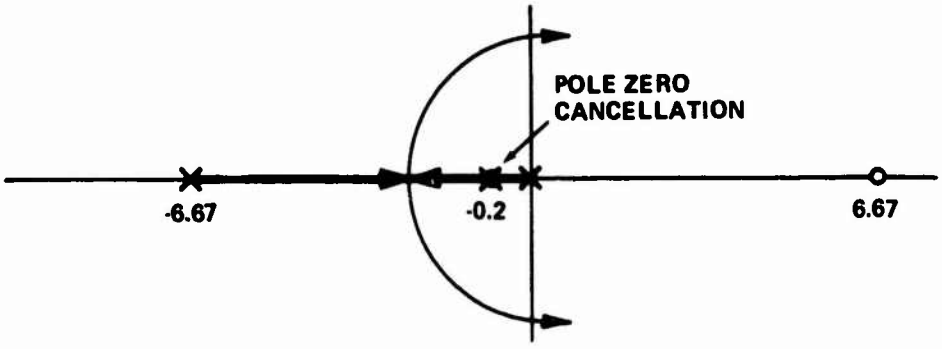

c) K/s DESIGN

Figure 10 ROOT LOCI FOR FLIGHT DIRECTOR DESIGN EXAMPLE

Time histories are shown in Figure 11 for these designs and various values of pilot-display ($K_p K_{\dot{z}}$) gain. On the basis of these time histories, the following results would be expected in a piloted simulation:

- The uncompensated (zero-delay) optimal design would be unacceptable due to closed-loop lightly damped oscillations for a relatively low value of pilot gain
- The compensated optimal design would yield closed-loop performance that is similar to that of the zero-delay optimal design for the same loop gain.
- The compensated optimal and K/s designs should have similar sensitivities to changes in pilot gain, and would provide similar closed-loop performance.

The following section reviews the results that actually were obtained in a piloted simulation.

EXPERIMENTAL INVESTIGATION OF DISPLAY PHILOSOPHY

To obtain a preliminary estimate of the efficacy of the new flight director design philosophy, the compensated and the uncompensated optimal design was implemented for the δ_{CS} command on the ED-3 display discussed earlier and evaluated on the X-22A ground simulator against the conventional K/s design. For completeness, an additional design which added a delay compensator (based on the same theory) to the K/s design was also investigated. Since the implementations were only on the δ_{CS} command (collective stick), which is used for altitude control, the primary differences among the designs appear in tracking errors both for the δ_{CS} command and for the δ_{ES} command, workload (collective and longitudinal stick motions), and pilot commentary and rating. Three pilots performed qualitative relative evaluations of the four designs; in addition, two engineers familiar with the designs but not the specific one being evaluated also performed "quick look" studies. The task included glide slope acquisition and tracking during deceleration to a precision hover; the pilots were instructed to attempt to make step altitude changes after the precision hover had been achieved to aid in their evaluation of the δ_{CS} director. The qualitative results are summarized below:

(1) Performance: δ_{CS} command tracking was best (in the sense of mean square error) with the compensated K/s design, followed by the uncompensated K/s design and then the compensated optimal design; no large differences among those three were found, however. The uncompensated optimal design gave significantly worse δ_{CS} command tracking performance. The tracking performance of the δ_{ES} (longitudinal stick) command was also checked as an indication of the amount of attention the pilots needed to devote to tracking the δ_{CS} command; this performance measure was best

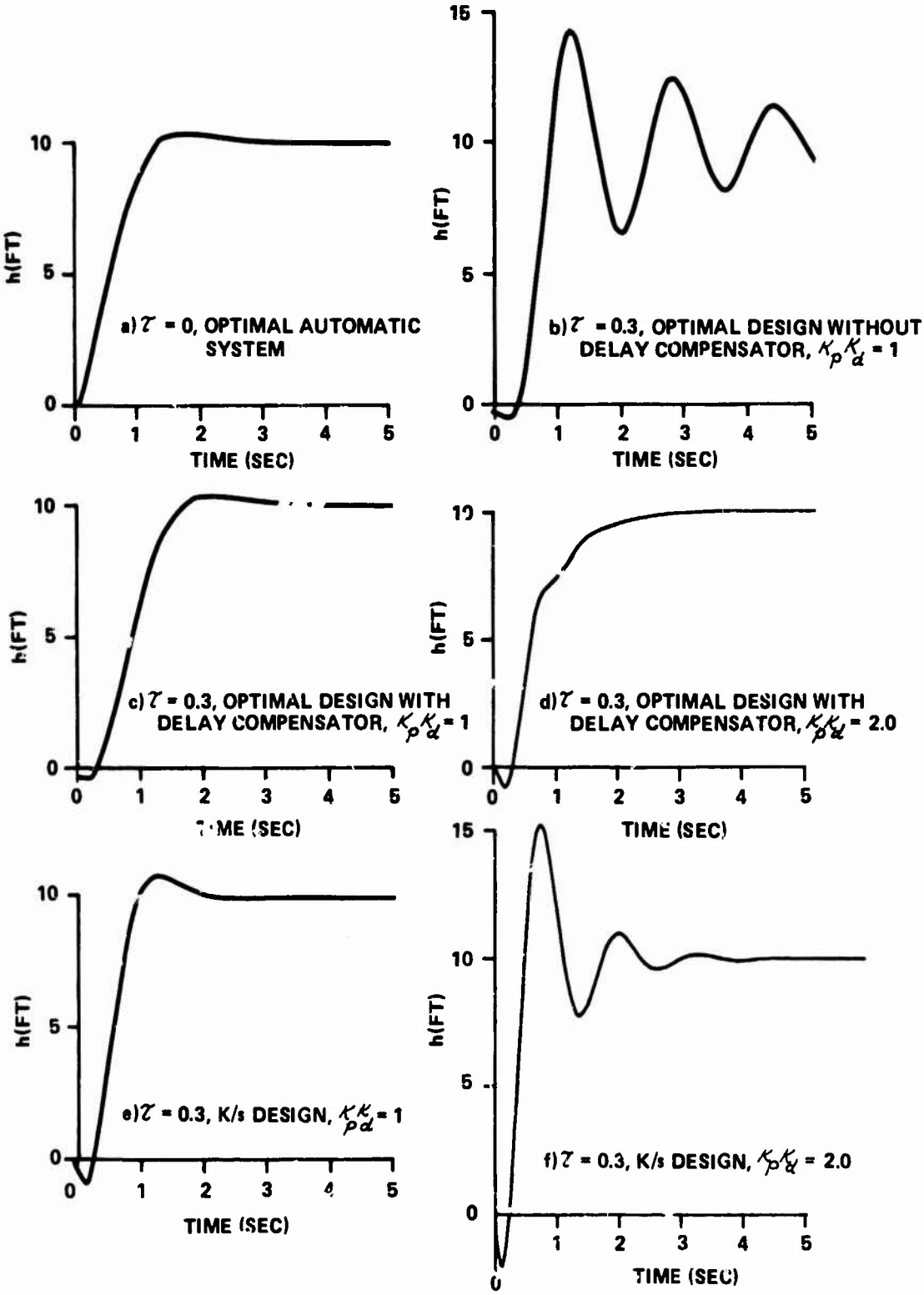

Figure 11 EXAMPLE TIME HISTORIES OF FLIGHT DIRECTOR DESIGNS

with the new compensated optimal design, followed by the compensated K/s design and then the uncompensated K/s design, with no large differences among these three. Again, the performance was the worst for the uncompensated optimal design.

(2) Control Activities: Collective stick (δ_{cs}) motion was least with the new compensated optimal design, followed by the compensated K/s design. Longitudinal stick (δ_{es}) motion was least for the compensated K/s design, followed by the compensated optimal design. For both sticks, the most motion (highest workload) occurred with the uncompensated optimal design.

(3) Pilot Opinion: The pilots were unanimous in disliking the uncompensated optimal director the most. In all cases, they found it "sloppy" and overcontrolled it, with tendencies toward a PIO. In general, the pilots preferred both the compensated and the uncompensated K/s designs to the compensated optimal design, although no significant differences were noted.

These results verify the hypothesis that the uncompensated optimal control flight director design results in poor system performance and pilot rating. The pilots generally preferred the K/s design to the compensated optimal design, although measurable differences were not significant. It is interesting to note that the compensated optimal design might have been degraded somewhat relative to the K/s system by the following factors:

- System noise is considerably amplified in the compensated optimal control design, both because of the higher feedback gains and also because of the lead term in the compensator. This noise on the director needle was disconcerting to all of the pilots.

- Pilots tended to describe the compensated optimal system as exhibiting a "predictable final response but sluggish initial response" to control inputs. This situation is illustrated in Figure 12. In this figure, the dominant branch root loci of the K/s design and the "compensated optimal" design are compared. It is evident that, with decreasing pilot gain, the "compensated optimal" system undergoes a reduction in bandwidth accompanied by a slight undamping of the lower frequency closed-loop root. With increasing pilot gain, the system bandwidth increases, but the damping of the higher frequency closed-loop root is reduced. The system becomes unstable at approximately the same value of pilot gain at which the K/s design system does. If the optimal control design had been

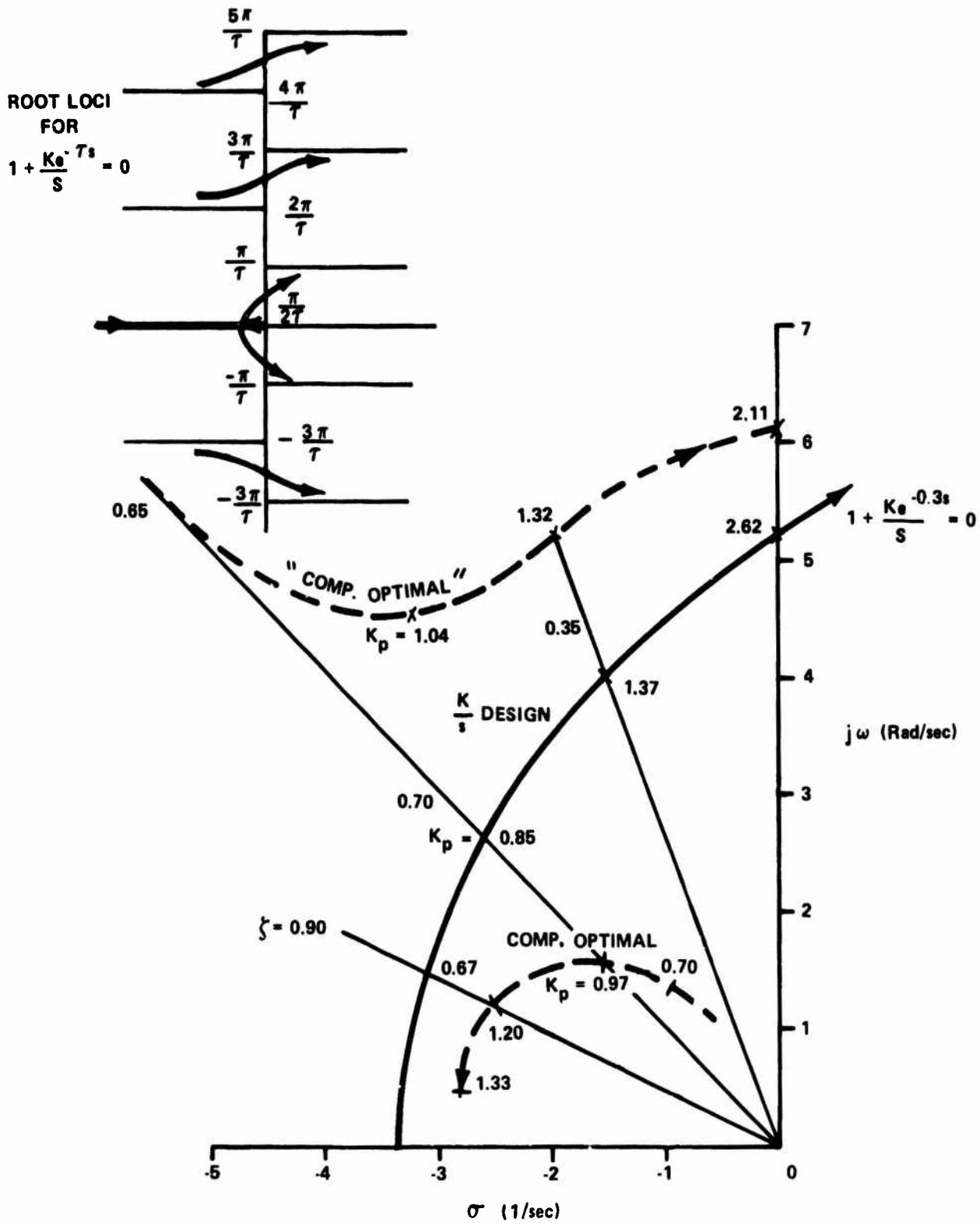

Figure 12 DOMINANT BRANCH ROOT LOCI OF K/S DESIGN AND "COMPENSATED OPTIMAL" DESIGN

for a closed-loop system of 3.5 rad/sec rather than 2.5 rad/sec, the system bandwidth would have approached that of the K/s system at the design point. This design change should result in a more acceptable response to control inputs.

- The example design considered a step command in altitude. It is possible that applying this design to the glide slope acquisition and tracking task was not proper, and instead it should have been redesigned to follow a step plus ramp.

CONCLUDING REMARKS

The interaction of aircraft control system complexity, guidance requirements, display sophistication, and aircraft flying qualities presents a multidimensional research problem whose solution is not yet well understood. The current X-22A experiment will make an initial contribution to understanding this problem for V/STOL instrument landings, and the research facility provides an unmatched capability for performing research in this area; possible examples include guidance, display, and control requirements to permit zero-zero shipboard VTOL landings, or similar requirements for VTOL, STOL or conventional aircraft using projected microwave landing systems (MLS). The X-22A's combinations of variable stability/control dynamics and variable display capabilities, coupled with the increased efficiency of flight time usage afforded by the ground simulator capability and the digital data processing system, results in a versatile and extremely useful research tool for these investigations.

This paper has reviewed the current experiment and these capabilities in a general fashion, and has also discussed in more detail one aspect of flight director design philosophy that has been investigated in the preliminary phase of the program. A design philosophy was formulated which uses quadratic synthesis to design an automatic control system; the characteristics of the automatic system are then rationally compensated to allow for a human controller. Based on both analytic and experimental investigation of this hypothesized design, the following general remarks are in order:

- A flight director design which uses optimal control theory without explicitly accounting for the pilot delay term resulted in unsatisfactory pilot-vehicle closed-loop dynamic characteristics. The pilot delay term must be included to provide a viable design.

- Using a pilot model consisting of a gain and a pure time delay, a synthesis procedure was developed to: a) compensate the optimal gains, and b) provide a physically realizable delay compensator circuit. This procedure results in a closed-loop system including the pilot whose performance is the same as the optimal automatic (no time delay) system for similar loop gains.

- Both analytic and ground simulator investigations demonstrated that the compensated optimal design was similar to the classic "K/s" system in performance and pilot rating, although the K/s design was generally preferred by the pilots.

- The design approach developed in this paper has the advantage of providing a uniform approach to both automatic control and manual display design for multiloop, multichannel situations.

REFERENCES

1. Klein, R.H., McRuer, D.T., and Weir, D.H.: "A Pilot-Vehicle Systems Approach to Longitudinal Flight Director Design," paper presented at the Sixth Annual Conference on Manual Control, 7-9 April, 1970.

2. Hoh, R.H., Klein, R.H., and Johnson, W.A.: "Design of a Flight Director/Configuration Management System for Piloted STOL Approaches," NASA CR-114688 (STI TR 1015-3), September 1973.

3. Seitz, W.R., and Goodson, R.E.: "Flight Director Design for a STOL Aircraft," Journal of Aircraft, Vol. 10, No. 8, August 1973.

4. Lebacqz, J.V., Smith, R.E., and Radford, R.C.: "A Review of the X-22A Variable Stability Aircraft and Research Facility," Calspan Report No. AK-5130-F-2, February 1974.

5. Beilman, J.L.: "An Integrated System of Airborne and Ground-Based Instrumentation for Flying Qualities Research with the X-22A Airplane," paper presented at the 28th Annual National Forum of the American Helicopter Society, May 1972.

6. Aiken, E.W., and Schuler, J.M.: "A Fixed-Base Ground Simulator Study of Control and Display Requirements for VTOL Instrument Landings With a Decelerating Approach to a Hover," Calspan Report No. AK-5113-F-2, February 1974.

7. Chen, R.T.N., Eulrich, B.J., and Lebacqz, J.V.: "Development of Advanced Techniques for the Identification of V/STOL Aircraft Stability and Control Parameters," Calspan Report No. BM-2820-F-1, August 1971.

8. Lebacqz, J.V.: "Application of a Kalman Filter Identification Technique to Flight Data from the X-22A Variable Stability V/STOL Aircraft," paper presented at NASA Symposium on Parameter Estimation, April 24-25, 1973.

9. Smith, R.E., Lebacqz, J.V., and Schuler, J.M.: "Flight Investigation of Various Longitudinal Short-Term Dynamics for STOL Landing Approach Using the X-22A Variable Stability Aircraft," Calspan Report No. TB-3011-F-2, January 1973.

10. Schuler, J.M., Smith, R.E., and Lebacqz, J.V.: "An Experimental Investigation of STOL Longitudinal Flying Qualities in the Landing Approach Using the Variable Stability X-22A Aircraft," paper presented at the 28th Annual National Forum of the American Helicopter Society, Map 1972.

11. Smith, R.E., Lebacqz, J.V., and Radford, R.C.: "Flight Investigation of Lateral-Directional Flying Qualities and Control Power Requirements for STOL Landing Approach Using the X-22A Aircraft," Calspan Report No. AK-5130-F-1 (Vols. I and II), February 1974.

12. Lebacqz, J.V., Radford, R.C., and Smith, R.E.: "An Experimental Investigation of STOL Lateral-Directional Flying Qualities and Roll Control Power Requirements Using the Variable Stability X-22A Aircraft." paper to be presented at the 30th Annual Forum of the American Helicopter Society, May 1974.

13. Anon.: "Displays for Approach and Landing of V/STOL Aircraft." AGARD Advisory Report No. 51, November 1972.

14. Kelly, J.R., Niessen, F.R., Garren, J.F., Jr.: "A Manual Control Approach to Development of VTOL Automatic Landing Technology." 29th Annual National Forum of the American Helicopter Society, Washington, D.C., May 1973.

15. Garren, J.F., Jr., et. al.: "Flight Investigation of VTOL Control and Display Concept for Performing Decelerating Approaches to an Instrument Hover." NASA TN D-6109, February 1971.

16. Dukes, T.A.: "An Integrated Display Concept for Helicopter and VTOL Aircraft." 25th Annual National Forum Proceedings of the American Helicopter Society, Washington, D.C., May 1969.

17. Dukes, T.A., Keane, W.P., and Tsoubanos, C.M.: "Image and Superimposed Symbology - an Integrated Display for Helicopters." 29th Annual National Forum of the American Helicopter Society, May 1973.

74-28,209#25

VERTICAL VIBRATION INTERFERENCE ON A PITCH ATTITUDE CONTROL TASK*

Raymond E. Magdaleno, R. Wade Allen,
and Henry R. Jex†
Systems Technology, Inc., Hawthorne, California

ABSTRACT

The basic mechanisms for vibration interference with manual control tasks have been explored in a series of studies sponsored by the USAF Aeromedical Research Laboratories, and the general approach and early findings have been previously published at this conference. This paper presents a summary of some new results on the effects of sinusoidal and quasi-random vertical vibration.

Performance and cross-power spectra measurements are presented which show vibration-induced effects in the visual-motor dynamics and remnant. Describing function measurements of head motion and subjective comments on visual blur show large effects in the region of 7 Hz which correlate with the performance data. Measurements under different stick gains also provide strong evidence of a motor remnant source. Overall, these results generally indicate that vibration interference is related to relative motions of eye, head, and limbs with respect to platform motion; and several component biodynamic and control theory models are suggested which should be capable of predicting the performance manifestations of these effects.

INTRODUCTION

The reliable performance of manual control tasks is important to the aerospace mission, but often times these tasks must be performed under adverse environmental stresses. Vibration is one of the more common stresses which degrades manual control performance (Ref. 1), and it is desirable to determine the underlying causes of interference so that performance effects can be extrapolated to new situations.

---

*Performed in part under Contract F33615-73-C-4003 for the 6570th Aerospace Medical Research Laboratory with Lt. Phil Houck as Contract Monitor, with additional work supported by the Air Force Office of Scientific Research, under the cognizance of Col. W. Wisecup of the Life Sciences Division.

†Senior Research Engineer, Senior Research Engineer, and Principal Research Engineer, respectively.

Vibration effects are time dependent. Short-term exposures lead mainly to biomechanical interference with task performance; fatigue and behavioral accommodation factors become important for longer exposures; while chronic exposures can lead to physiological accommodation or deterioration as in some occupational diseases. The direct biomechanical interference of vibration will always underlie longer term effects, however, and the purpose of the research reported here was to determine the basic interference mechanisms affecting manual control, develop component models for the various phenomena involved, and eventually to put together overall task performance models which explain the short-term effects of vibration on manual control performance. The explanation of the short-term vibration effects will then provide a theoretical construct from which to evaluate longer-term effects.

APPROACH AND METHODS

Control theory based measurement and modeling techniques are used in this research to describe both the detailed dynamic response manifestations of vibration interference and the resulting performance effects. This approach has been described previously (Ref. 2) and is summarized in Fig. 1. The manual control system has two external inputs, the traditional tracking input command (i) and a mechanical (vibration) disturbance which enters through the body and control stick (v). Inputs internal to the operator (remnant) are also generated at his perceptual input (n_e) and motor output (n_c) which are a function of task variables and vibration interference.

Given the above inputs the composition of the error and control stick signals are then determined by the operator's visual-motor response (Y_p), the machine dynamics he is controlling (Y_c), the vibration feedthrough dynamics (Y_v), and the two remnant sources (Φ_{nn_e} and Φ_{nn_c}). For simplicity, the dynamics and motor remnant are shown as separate blocks in Fig. 1; as will be shown subsequently, each process is highly coupled, however, both biomechanically and in a signal processing sense.

For measurement purposes the approach of Fig. 1 allows the error and stick signals to be partitioned into a linear sum of spectral components as shown in the bottom of Fig. 1 and, consequently, the variances of these

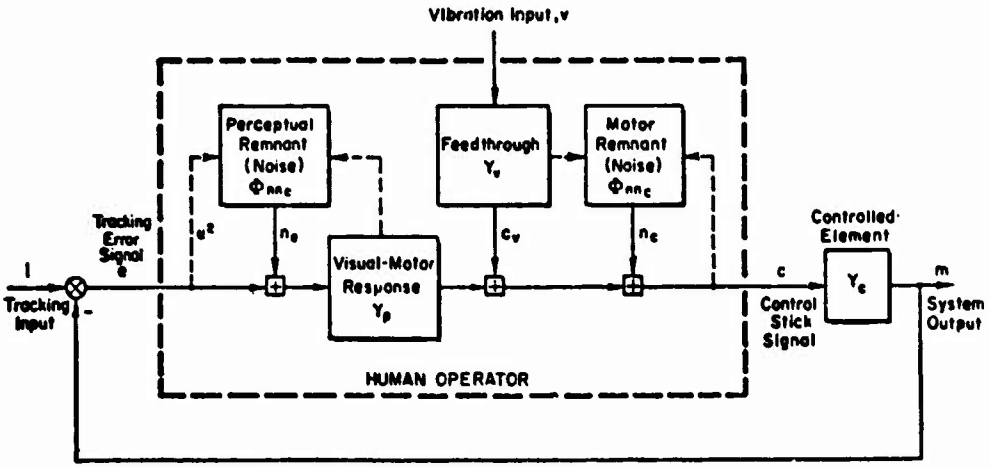

Transfer Function Forms

$$Y_c(s) = \text{Vehicle Transfer Function} = \frac{K_c(s + 1.42)}{s[s^2 + 2(.56)(1.71)s + 1.71^2]}$$

$$Y_p(s) = \frac{K_\pi(T_L s + 1)e^{-\tau s}}{(T_I s + 1)(s + 1/T_N)[s^2 + 2\zeta_N\omega_N^2 s + \omega_N^2]}$$

$$Y_v(s) = f(\text{Vibration, Stick/Arm/Body Biomechanics})$$

Remnant Spectra Forms

$$\Phi_{nn_e}(\omega) = \sigma_e^2 \cdot \frac{R_E'}{1 + (\omega/\omega_{RE})^2} \quad ; \quad R_E', \omega_{RE} = f(\text{Task, Vibration, Biomechanical Configuration})$$

$$\Phi_{nn_c}(\omega) = f(\text{Task, Vibration, Biomechanical Configuration})$$

Closed-Loop Signal Spectra from All Sources

$$\Phi_{ee}(\omega) = \underbrace{\left|\frac{1}{1 + Y_pY_c}\right|^2\Phi_{ii}}_{\text{Due to input}} + \underbrace{\left|\frac{Y_vY_c}{1 + Y_pY_c}\right|^2\Phi_{vv}}_{\text{Due to Feedthrough}} + \underbrace{\left|\frac{Y_pY_c}{1 + Y_pY_c}\right|^2\Phi_{nn_e} + \left|\frac{Y_c}{1 + Y_pY_c}\right|^2\Phi_{nn_c}}_{\text{Remnant}}$$

$$\Phi_{cc}(\omega) = \left|\frac{Y_p}{1 + Y_pY_c}\right|^2\Phi_{ii} + \left|\frac{Y_v}{1 + Y_pY_c}\right|^2\Phi_{vv} + \left|\frac{Y_p}{1 + Y_pY_c}\right|^2\Phi_{nn_e} + \left|\frac{1}{1 + Y_pY_c}\right|^2\Phi_{nn_c}$$

Figure 1. Operator Model Structure, Forms, and Closed-Loop Signal Relationships for Measurements Under Vibration Stress

P-152

signals can be partitioned in the same manner. Thus, in experiments we can consider vibration effects on the various signal components, and for modeling separate component models can be set up which when summed together give overall performance measures of vibration effects on the manual control system.

The data considered in this paper cover two experiments, one involving sinusoidal vibration at frequencies 2, 3.3, 5, 7, and 10 Hz, the other involving quasi-random vibration composed of a sum of these five frequencies with four different amplitude envelopes (Ref. 4). The range of frequencies included is typical of aircraft buffet and structural mode excitation and also brackets the human operator's whole-body resonance mode.

In the research reported here subjects performed a pitch attitude control task with a CRT-displayed artificial horizon and a center stick control. The stick force gradient turns out to be an important variable, influencing both motor remnant and vibration feedthrough; and in the sinusoidal study two extremes of stick restraint were used: minimal ("spring" stick) and near rigid ("stiff" stick). Only the stiff stick was used in the random experiment. The controlled element dynamics were equivalent to the short-period response of a large aircraft and are given in Fig. 1. The dynamics had appreciable lag requiring significant lead generation by the human operator so that this aspect of the human operator's visual-motor response could be checked under vibration.

A substantial subject population was used in each experiment (8 in the sinusoidal study, 6 in the random), and the subjects were well trained before the formal data sessions. Suitable precautions were taken to avoid procedural bias in the results, including random ordering and counterbalancing, and the final results were statistically analyzed to determine the reliability of the data.

Performance and human operator describing functions were measured on-line during the tests with analog computing equipment (Ref. 2). During the sinusoidal study biomechanical response measurements were also obtained on-line. For the random study cross-spectral measurements were obtained off-line using a General Radio TD 1923 spectral analyzer.

OVERALL PERFORMANCE EFFECTS

Partitioned Performance for Sinusoidal Vibration

Partitioned error and control variances averaged over 8 subjects under sinusoidal vibration are given in Fig. 2. For tne spring stick control errors are generally elevated over static levels for all frequencies with a slight peaking in the region of 7 Hz. Fcr the stiff stick errors are increased only at higher frequencies (7 and 10 Hz) which is the region in which reports of visual blurring were received. Thus, increase in remnant in this region is felt to be due to a visual source.

Control variance is increased at low frequencies for the spring stick and at high frequencies for the stiff stick. These effects are mainly due to remnant, as noted in Fig. 2, and the magnitude of remnant seems to correlate with the amount of vibration feedthrough in the control stick output. Although there is not a great deal of absolute feedthrough in the case of the spring stick, there is evidence of considerable vibration-correlated limb motion, and it will subsequently be explained how this may lead to proprioceptive induced motor remnant (pp. 18-21).

Overall, the results in Fig. 2 indicate that spring stick errors are influenced by motor remnant at low frequencies (2-5 Hz) and visual remnant at higher frequencies (7-10 Hz), whereas the stiff stick is affected by both types of remnant at high frequencies. Input correlated errors determined by the operator's visual-motor response, Y_p, increase slightly at high frequencies. This is most likely due to the operator's awareness of visual remnant (blurring) and probably represents an adaptive response to a lower closed-loop bandwidth in order to minimize the effect of internal noise as will be shown subsequently (pg. 23). Finally, no vibration feedthrough shows up in the error variance as it is filtered out by Y_c before it reaches the error point.

Stick Electrical Gain Effects Under Random Vibration

In the sinusoidal experiment, stick gain was purposely set at a level on the low side of optimum (based on subjective opinion) in order to avoid any undue sensitivity to vibration interference. Ordinarily, tracking

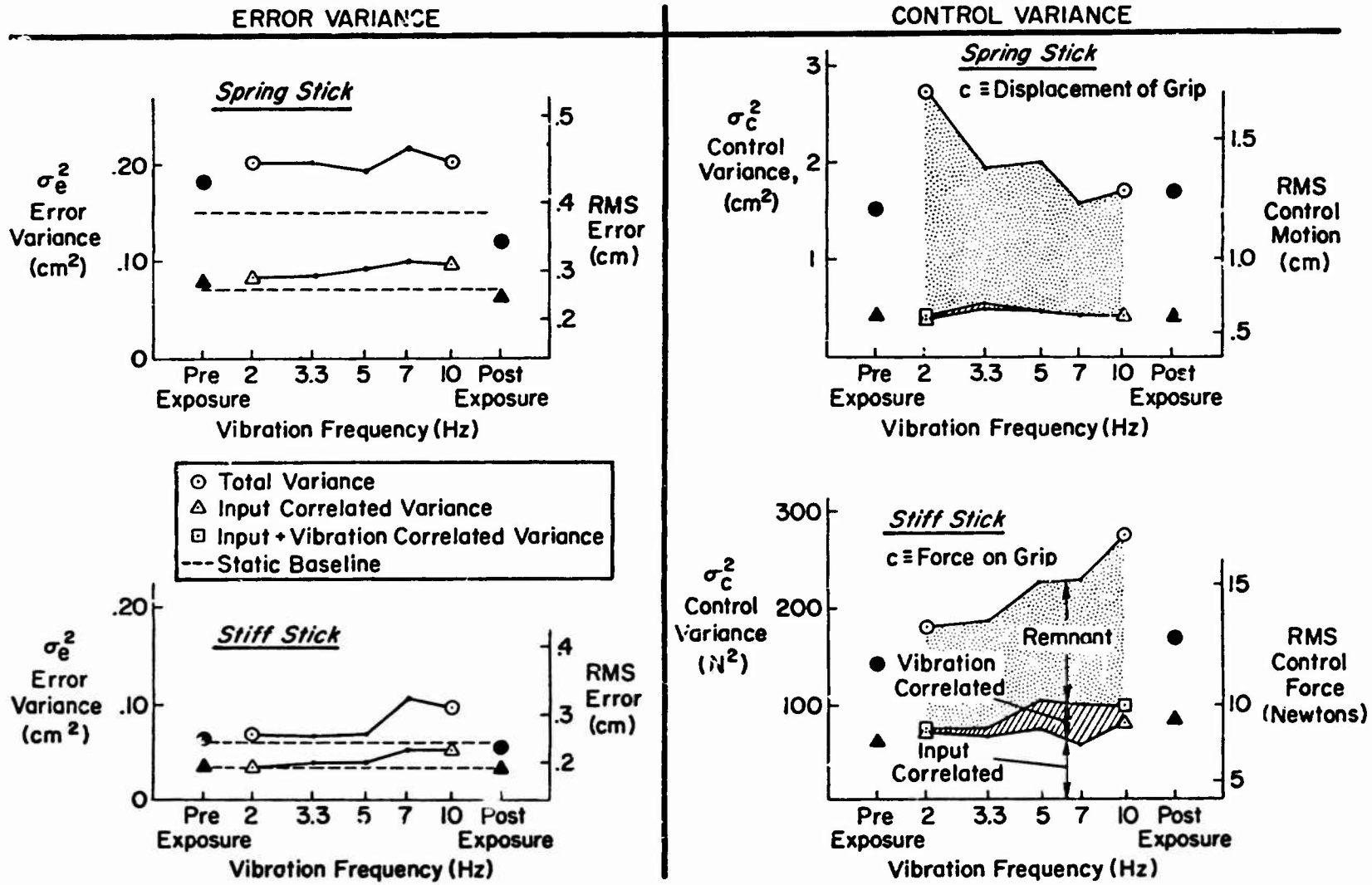

Figure 2. Partitioned Error and Control Variance for Sinusoidal Vibrations (Spring and Stiff Sticks)

performance is optimum over a very broad range of stick gains (Ref. 5). This situation changes radically under vibration, however, as demonstrated by results from the random experiment given in Fig. 3. Under static conditions performance stays relatively constant over a gain increase of 10 times; however, under bandpass vibration centered at 5 Hz, the error remnant increases radically. An example of partitioned control spectral density for one run is shown in Fig. 4. The vibration feedthrough is essentially the same for either electrical stick gain. For the high stick gain the operator must lower his gain (force output) by a factor of 10 times to maintain an equivalent loop closure, and this shows up in the lowered input correlated components. The remnant goes down for the higher stick gain although not as much as the input correlated components. However, remnant has at least two sources as indicated in Fig. 1 where the expression for Φ_{cc} shows that the part of the remnant dependent on Φ_{nn_e} also depends directly on Y_p. The middle part of Fig. 1 indicates that Φ_{nn_e} varies directly with σ_e^2 and since this increases (see Fig. 3 for 0.28 g rms) for the high stick gain we would expect this to counteract part of the remnant decrease due to the Y_p reduction. The analysis of the data base (ongoing at the time of this writing) provides the first direct evidence of vibration-induced motor remnant as the remnant level is influenced by mechanical forces at the control stick, rather than depending totally on visual remnant sources.

COMPONENT EFFECTS AND MODELS

Visual-Motor Response

The visual-motor response properties of the human operator have been well established and modeled under static conditions (Refs. 5 and 6), and in this research we have used a "precision model" form to fit describing function data and to describe vibration effects. For every run taken in both the sinusoidal and random vibration experiments a model curve fit was made as a part of the data reduction.

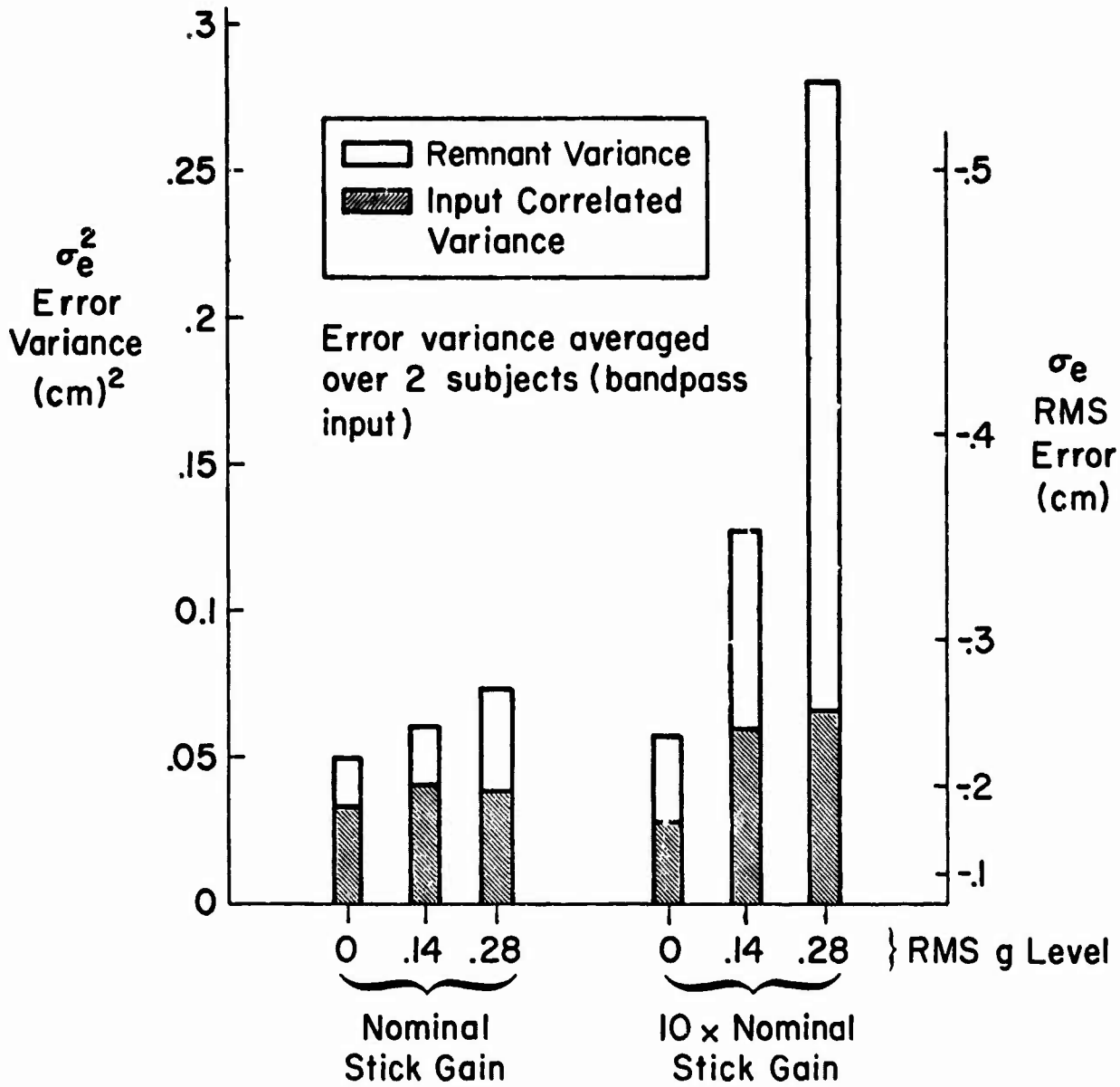

Figure 3. Effect of Stick Electrical Gain on Error Variance

P-152

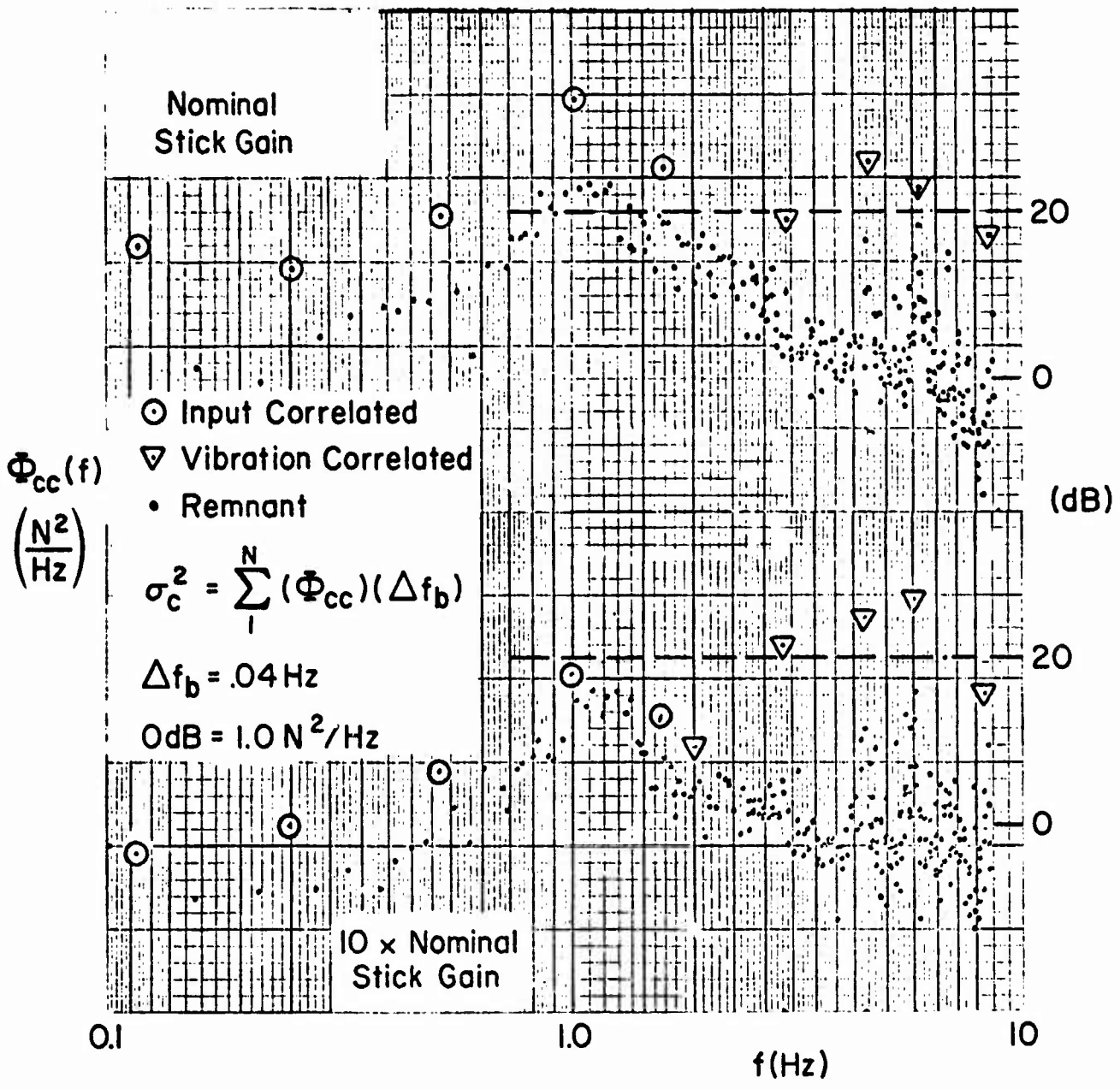

Figure 4. Effect of Stick Electrical Gain on Control Spectral Density for 0.28 g rms Vibration

For the stiff stick control Fig. 5 shows an example of the effect of vibration on the pilot's describing function data (averaged over 7 subjects by 2 repetitions). Also shown are the curve fits that result from using the averaged precision model parameters. Basically, the human operator's midband gain, K_π, decreases under vibration, which probably represents an adaptive response to minimize the effect of closed-loop remnant by lowering the bandwidth of the tracking loop. The neuromusuclar system natural frequency, ω_N, also decreases, although this effect has much less influence on performance since the frequency of this mode is well past the closed-loop bandwidth of the tracking loop.

Statistical analysis of the model parameters showed that only the human operator midband gain, K_π, and neuromuscular system natural frequency, ω_N, were significantly affected. Surprisingly enough, vibration did not affect the operator's lead, T_L, generating capability, which depends on perceiving error rates, even though visual blurring was reported at 7 and 10 Hz (which might be expected to degrade error rate estimates). Statistical analysis of the model parameters obtained in the random experiment also showed that only K_π and ω_N were significantly affected (Ref. 4).

Biomechanical Response

The mechanical interference of vibration on manual control is determined in large part by the operator's biomechanical response. This is a factor in the vibration feedthrough dynamics, Y_V (Fig. 1), as well as a factor in the generation of remnant which will be discussed subsequently.

The structural elements of a biomechanical model pertinent to a seated pilot performing a pitch control task under vertical vibration are illustrated in Fig. 6. The general seating position, lap and shoulder belts, and nominal arm angles are shown on the left. On the right the arm segments are shown for positive values of their nominal position angles, θ_1, and θ_a. The arm segments are assumed to have pin joints at the shoulder, elbow, and wrist and to be restrained by neuromuscular systems (a passive system at the elbow and an active system at the shoulder that respond to central commands as well as force or displacement feedback). The details of the active neuromuscular system will be discussed subsequently. The passive neuromuscular restraint

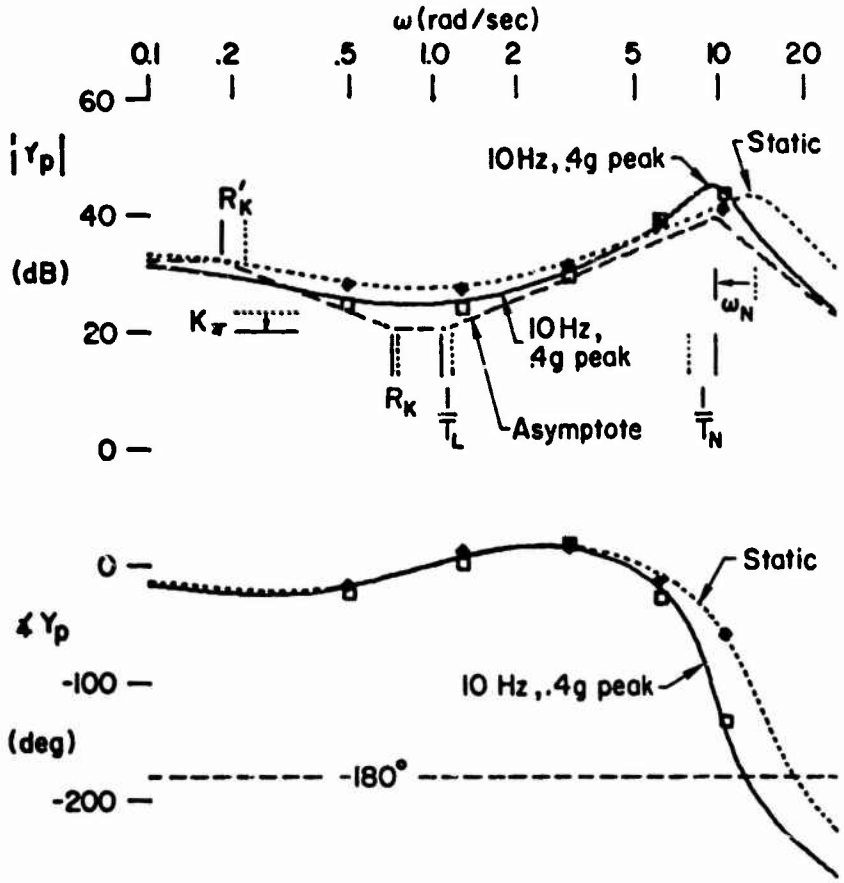

Y_p Data Averaged Over 7Ss and 2 Repetitions	Z Axis Vibration Condition	Averaged Precision Model Parameters									Averaged Y_pY_C	
			K_T	R_K	R'_K	T_L	ζ_N	ω_N	T_N	τ_d	Crossover Frequency ω_c	Phase Crossover ω_u
◇	Static	------	15	.76	.22	.84	.29	13.9	.13	.071	3.6	5.5
□	10 Hz .4g peak	——	10.6	.72	.18	.92	.19	9.7	0.1	.12	3.1	4.85

$$Y_p = \frac{K_T(s+R_K)(T_Ls+1)e^{-\tau_d s}}{(s+R'_K)(T_Ns+1)\left(\frac{s^2}{\omega_N^2}+\frac{2\zeta_N}{\omega_N}s+1\right)}$$

$$Y_C = \frac{.273(s+1.42)}{s\left[s^2+2(.56)(1.71)s+(1.71)^2\right]}$$

Figure 5. Effect of Sinusoidal Vibration on Pilot Describing Function (Stiff Stick Averaged Data and Averaged Precision Model Curve Fit)

P-152

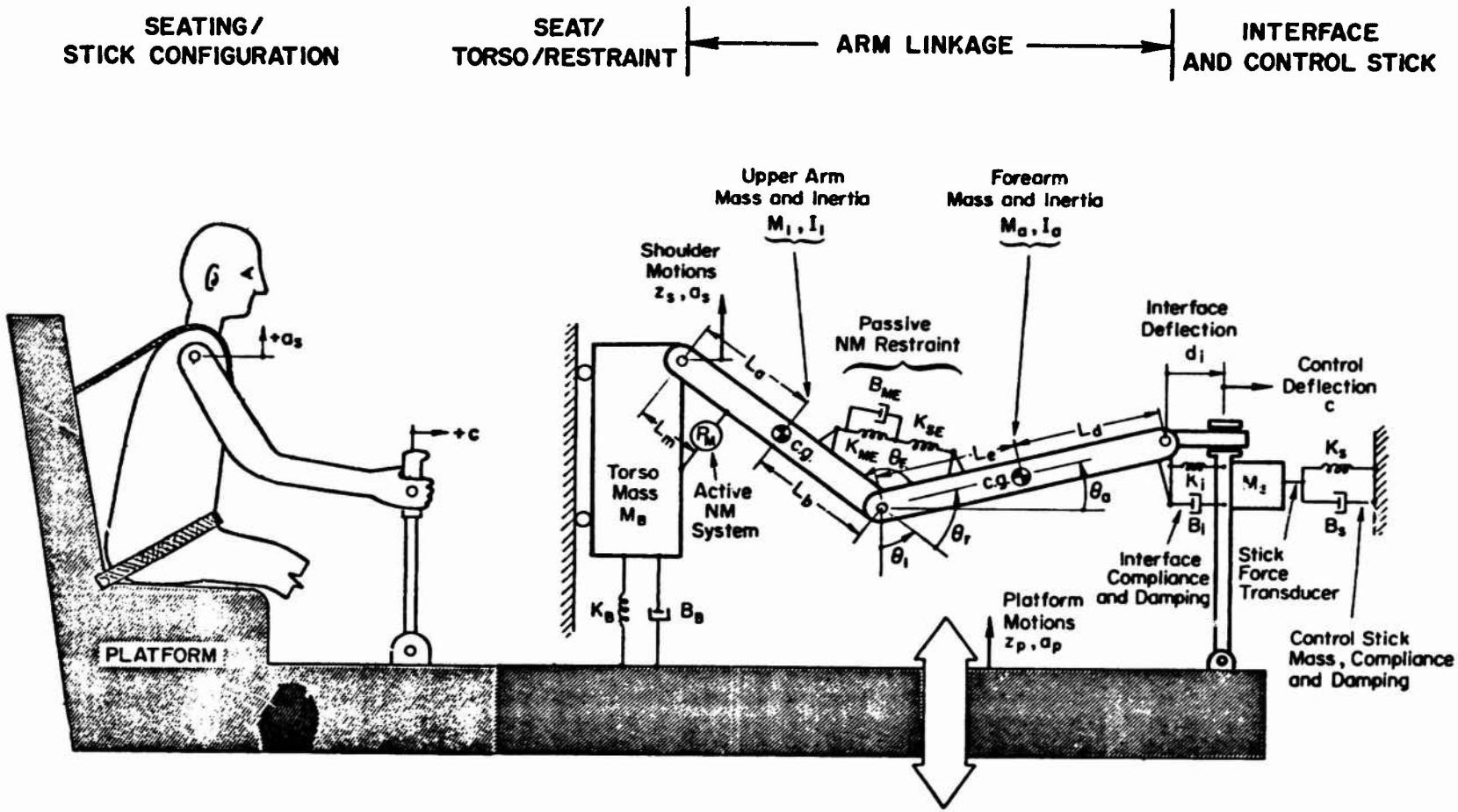

Figure 6. G_z Torso/Arm Linkage/Stick Biomechanical Model

reflects the small signal perturbation elements for an agonist/antagonist muscle pair as developed in Ref. 7. For the wrist/hand/stick system there is provision for equivalent lumped interface compliance and damping, and the control stick has the usual force feel characteristics of mass, compliance, and damping restraining fore-aft stick motion. Torso motions are modeled by a mass (constrained to vertical motions only based on movies of subjects under vibration) restrained by a simple spring and damper. Reference 11 found that this simplest possible model gave an adequate description of shoulder response to platform acceleration.

Assuming all arm segments are in planar motion the small perturbation equations of motion were written and put on a timesharing computer program that writes a set of simultaneous equations from a file of raw parameter values (measured stick restraints, muscle descriptors, Refs. 7 and 8, and arm/torso masses and inertias from cadaver data, Ref. 9). A systems analysis library program (USAM, Ref. 10) is then used to solve for the various transmissibilities and feedthroughs of interest.

Before examining some preliminary results, note that as the platform accelerates upwards vibration feedthrough to the stick results from two sources:

- Shoulder motion downward relative to the platform which tends to push the stick forward.
- Inertial reaction of the arm segments which tends to pull the stick back.

These effects will be illustrated in the next three figures.

Figure 7 shows vertical shoulder acceleration averaged over eight subjects in response to 0.4 g peak sinusoidal vibration for both spring and stiff sticks. The small transmissibility differences between stick types indicate that the different control stick forces (~15 N for stiff stick vs. 2.46N* for spring stick) have not affected shoulder transmissibility.*

*From Fig. 2 compare 15 N for stiff stick with (1.5 cm) × (0.64 N/cm) = 2.46 N for the spring stick rms force levels.

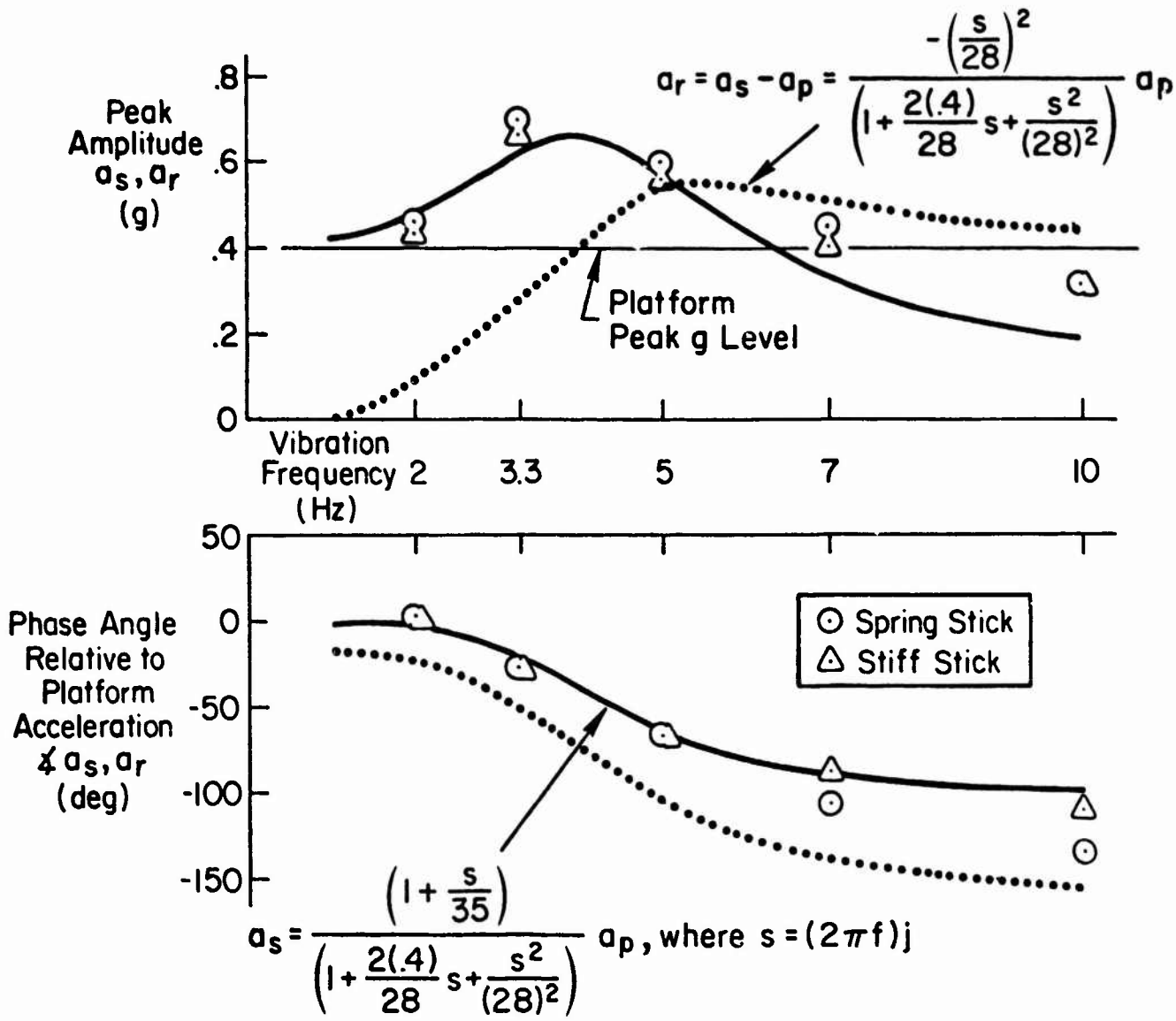

Figure 7. Vertical Shoulder Acceleration Averaged Over Eight Subjects (Sinusoidal Vibration, 0.4 g Peak)

P-152

Also shown in Fig. 7 is a curve fit to the peak shoulder transmissibility which indicates a body resonance at 28 rad/sec = 4.5 Hz, very close to the Ref. 11 results. In Fig. 7 we have also shown the shoulder motion relative to the platform ($a_s - a_p$) which is an important factor in vibration feedthrough. This indicates very little relative motion at 2 Hz but rapidly increases above that to a peak at whole body resonance with a remaining high level thereafter.

Figure 8 illustrates typical spectral and cross-spectral measurements under a quasi-random sum of 5 sine waves vibration. The 5 input components were set by oscillators rather than precision equipment, thus the acceleration spectrum appears to have power near each component rather than appearing "clean" as does the 5 Hz component which evidently fell exactly on 5 Hz. The shoulder shoulder acceleration spectrum reveals no significant nonlinearities, the coherence is near unity at the 5 frequencies, and, finally, the shoulder transmissibility magnitude and phase are consistent with the curve fit from the sine wave experiment (Fig. 7) where each frequency was presented in a separate run.

The single run shown in Fig. 8 indicates that superposition holds between the sinusoidal and random vibration data in the major data trends. We are in process of examining and interpreting further random data over a range of subjects and vibration input spectral shapes so as to evaluate the degree of consistency in torso transmissibility measurements.

Figure 9 shows stick response to platform acceleration measurements from the sinusoidal experiment averaged over seven subjects for spring and stiff sticks. The feedthrough amplitude with the stiff stick is highest at high frequencies, whereas it is highest at lower frequencies with the spring stick. Also shown in Fig. 9 are oversimplified biomechanical model (Fig. 6) responses (using each stick's spring gradient) for the following conditions:

- The same level of muscle stiffness used in each case.
- Interface locked up ($K_i = \infty$).
- No passive neuromuscular restraint at the elbow.
- Active neuromuscular system replaced by a passive system.

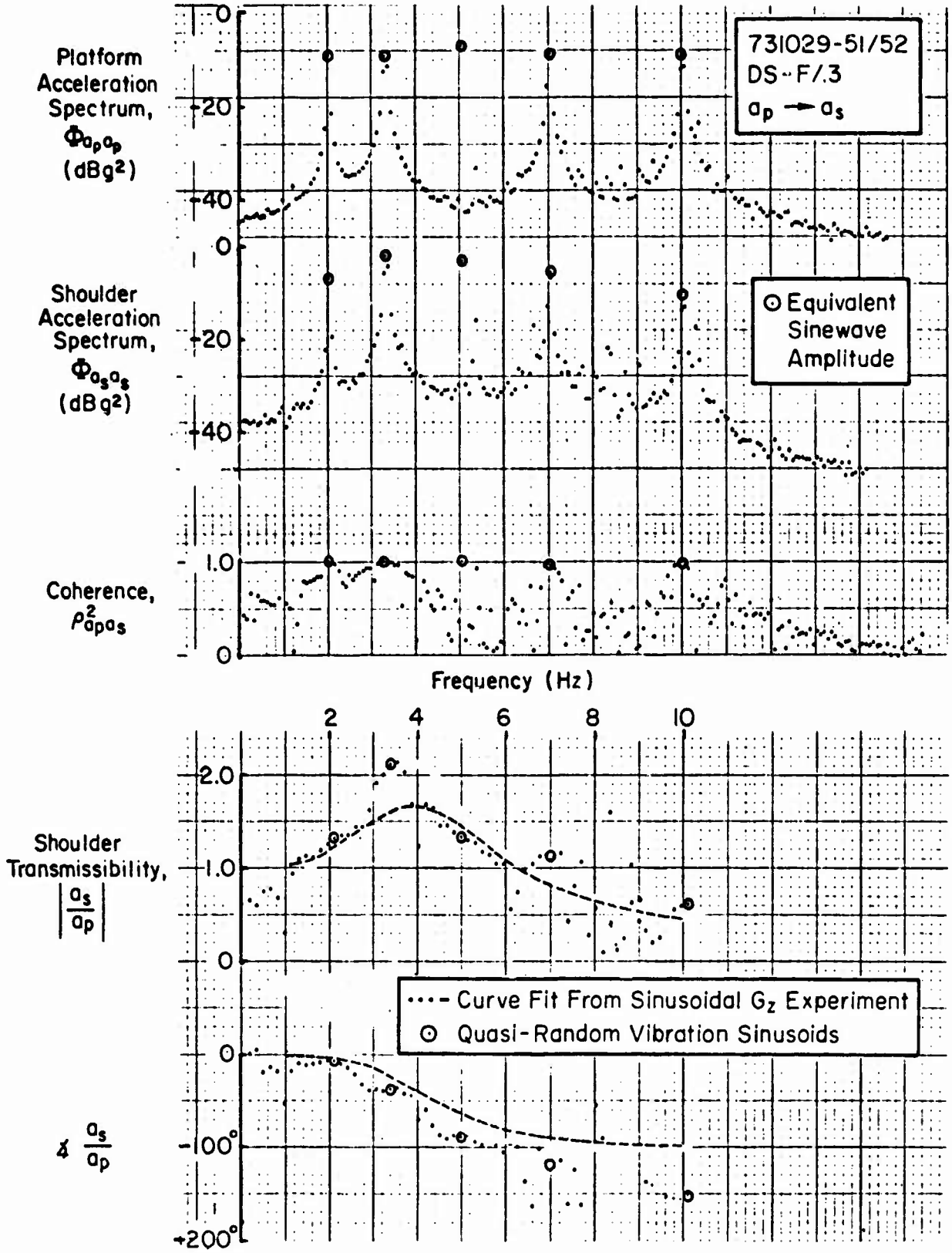

Figure 8. Transmissibility Measurements Under Quasi-Random Vibration

P-152

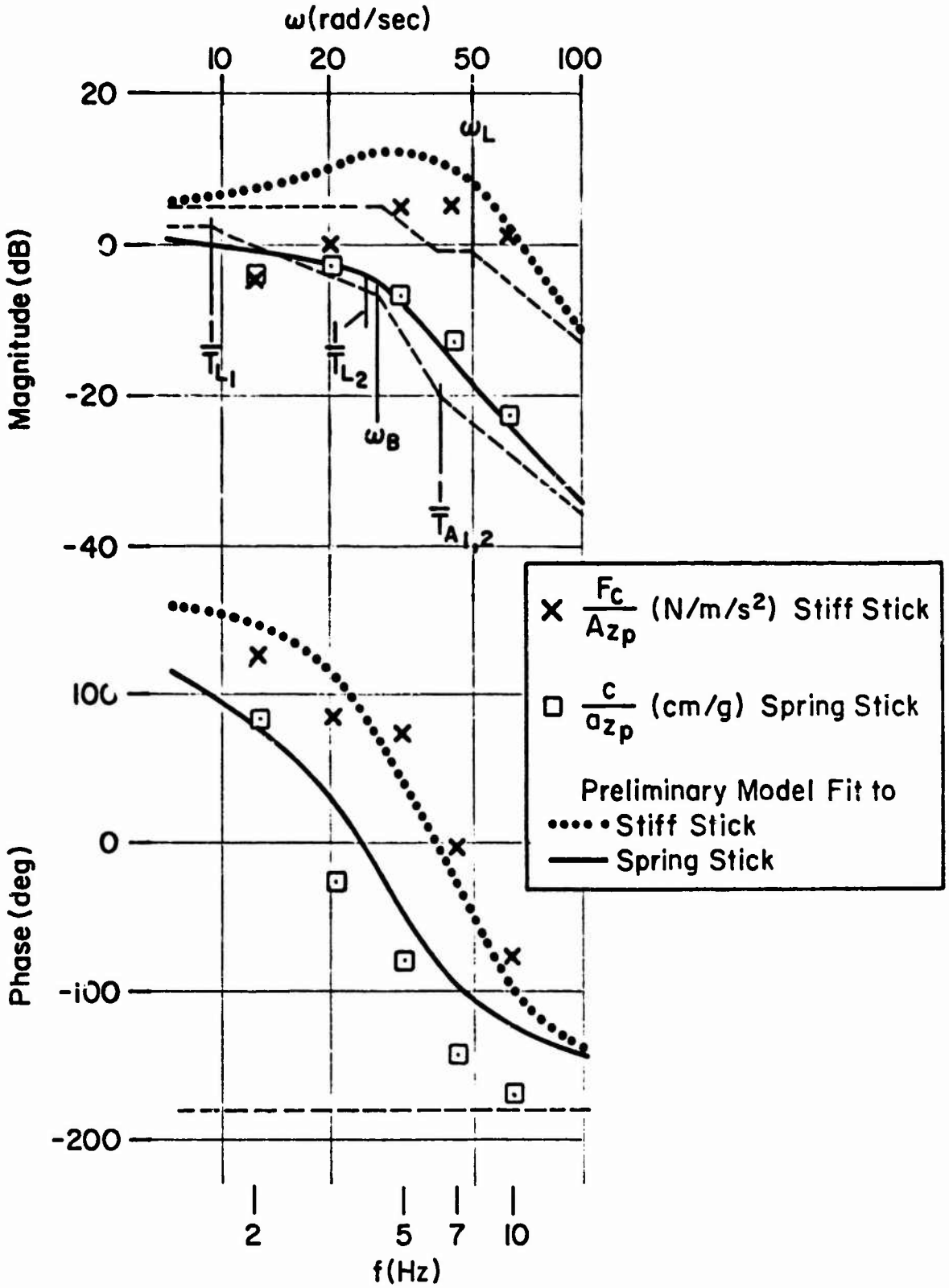

Figure 9. Stick Response to Platform Acceleration
(Sinusoidal Input Data Averaged Over 7 Subjects)

P-152

- Shoulder motions not loaded down by arm linkage forces, i.e., shoulder motion is a pure position input.
- $\theta_a = -15^o$, $\theta_1 = 45^o$ (Fig. 6)

Both curves exhibit the shoulder transmissibility mode (ω_B) as well as the limb reaction effect which shows up as one right and one left half plane zero ($1/T_{A_1}$, $1/T_{A_2}$) near 40 rad/sec. The non-minimum phase zero is the cause of both phase curves starting at +180 deg at low frequency.

The curve fit to the spring stick data is quite good whereas the fit to the force stick data is fine in phase but not in amplitude. This is probably due partly to the interface being assumed locked which should be reasonable for the weak spring stick gradient (K_s = 164 N/m) but not for the stiff stick gradient (K_s = 13900 N/m). An interface gradient much larger than that of the spring stick but less than that of the stiff stick along with interface damping will tend to decouple the stiff stick results, producing less feedthrough at lower frequencies. Other factors not included in the preliminary fits in Fig. 9 are the effects of the active neuromuscular system, possible anthropometric differences, and possible differences between results from single sine wave vibrations and quasi-random sums of sine waves results. At this point in time we are examining the large data bank of spectral and cross-spectral results to evaluate the above effects.

Visual-Motor Biodynamic Model

The details of the "active neuromuscular system" used in Fig. 6 are given in Fig. 10, the visual-motor biodynamic model. At the far right is the muscle insertion into upper arm (Fig. 6). Tendon compliance connects the bone to the equivalent muscle model for the agonist/antagonist muscle pair involved in torquing the upper arm (Ref. 7). New features are the series elastic damping, B_e (Ref. 12), and the force activation dynamics (to be discussed in a later paragraph).

The spinal cord receives feedbacks as well as central commands arising from visual inputs. The processed visual inputs have noise ("processing remnant," Refs. 5 and 6), much of which scales with the variance of the perceived signal and is sometimes referred to as observation noise (Refs. 13-15).

The spindle feedback models reflect our interpretations of Refs. 7, 8, 22-29. The intrafusal fibers have dynamics similar to the extrafusal fibers of the muscle model. The γ_o bias also serves to set the lead/lag (Z_{sp}, P_{sp}) values as well as provide a bias to keep the muscles under an average tension which helps set some of its parameters (this path is not shown in Fig. 10). The spindle sensor lead appears to be at rather high frequency (40-50 rad/sec, Ref. 22) but may saturate for anything but small perturbations. The Golgi feedback reflects a describing function interpretation of some transient responses found in Ref. 17.

In Fig. 10 we have postulated three "motor" remnant sources each injected at the input to a specific box (much as the processing remnant is injected at the front end of the pilot). The spindle/muscle noise source reflects possible gamma bias time variations as well as intrafusal muscle fiber noise. The spindle sensor noise reflects possible sensor variations due to spindle tension variations as well as saturation effects for the larger amplitudes that are induced by vibration. Similarly, a possible force sensing noise is shown referred to the input to the Golgi feedback.

The force activation dynamics (Fig. 10) were first proposed in Ref. 16 to explain the describing function measurements for the forward path of the neuromuscular system dynamics, G_M, between α_a (Fig. 10) and, c, the stick response (Fig. 6). These results (Fig. 11) were reported in Refs. 8 and 6. For the cross-spectral ratios shown in Fig. 11 the i signal is the tracking input (Fig. 1) and the x signal* corresponds to the α_a signal of Fig. 10. Note that the results from the cross-spectral ratios taken with respect to the sum of sine waves input, i, give the same results as those with respect to the x signal which is within the closed loop system and contains remnant that is circulating around the loop. This implies that there are no signficant remnant sources between the alpha motorneuron signals, α_a, and the stick response. Further, note that essentially the same dynamics result for both rudder pedals and hand manipulator despite the large difference in limb size.

---

*Obtained from processing EMG signals by bandpass filtering, then full wave rectifying, and then low pass filtering, to obtain the effective muscle driving signal. The difference between agonist and antagonist muscle processed EMG signals then forms x.

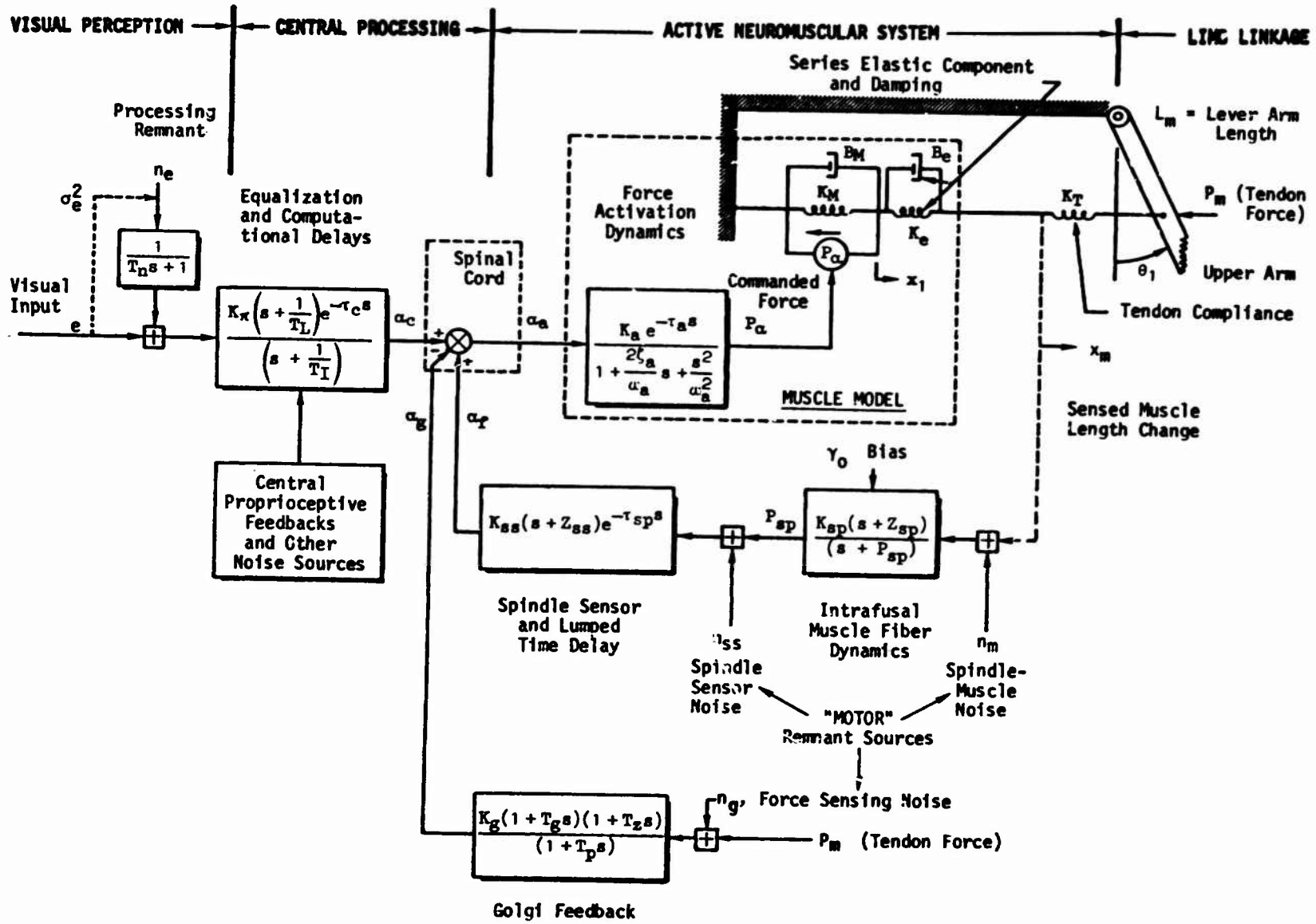

Figure 10. Visual-Motor Biodynamic Model

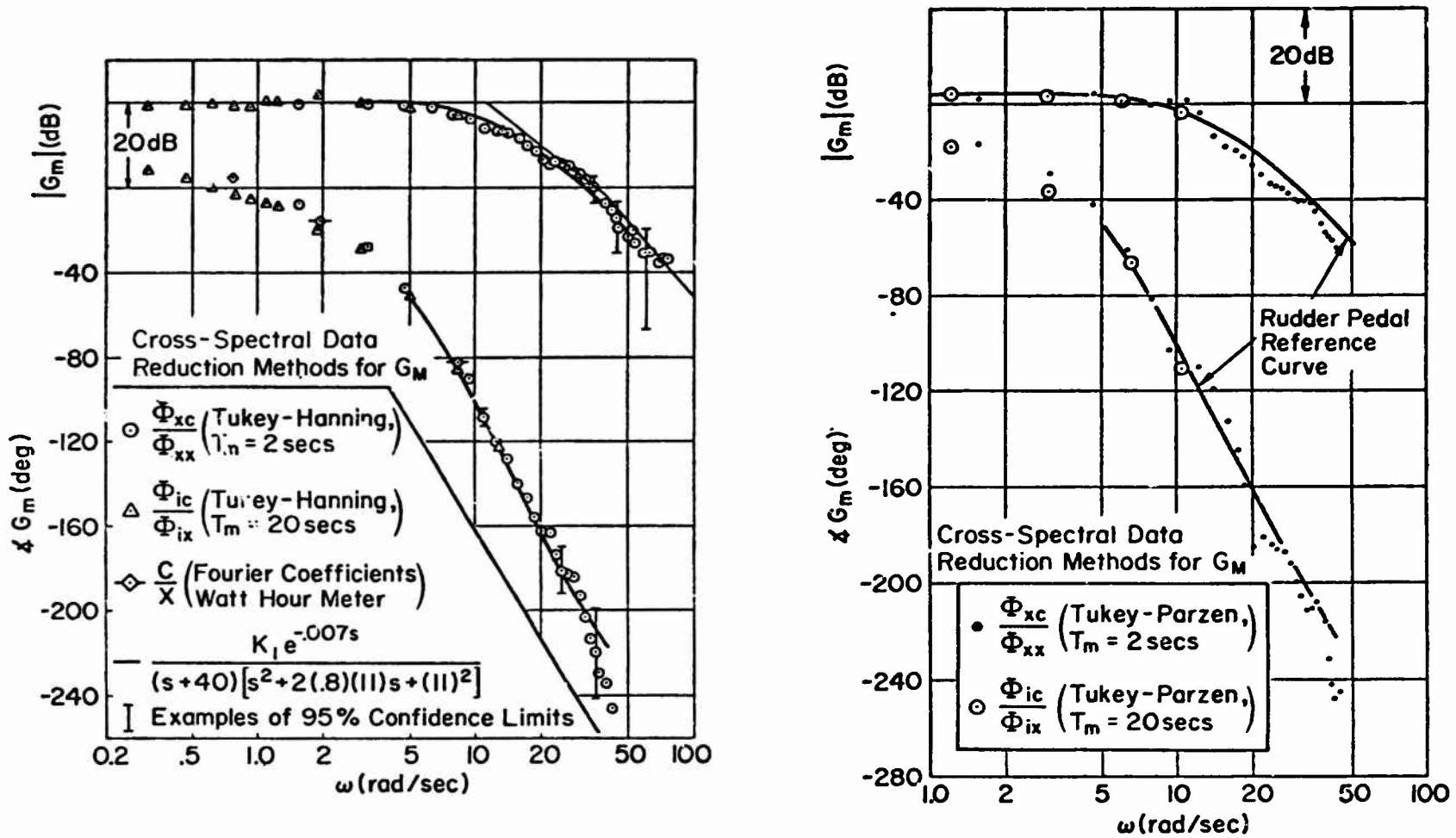

a) Rudder Pedal *b) Hand Manipulator*

Figure 11. Comparison of the Forward Path for the Muscle/Manipulator Describing Function, G_M, for Leg and Hand Actuators

That the major portion of the muscle/manipulator rolloff must be force activation dynamics rather than just the effect of limb mass on stick spring gradient, was verified by applying the biomechanical model (Fig. 6) to the rudder pedal geometry of Ref. 8. The resulting natural frequency was >45 rad/sec for any degree of muscle stiffness and damping. Since the break frequencies in Fig. 11 (and other configurations in Ref. 8) are on the order of 10 rad/sec for both rudder pedals and hand manipulators, these breaks cannot be biomechanical in nature. Hence we have postulated the presence of force activation dynamics (which is consistent with the active state interpretation in Ref. 21).

Under static conditions there has been little need for a "motor" remnant source (Refs. 6, 15, 19, 20) as shown on the upper left side of Fig. 12. For the control spectrum the precision model fits the correlated components and processing remnant fits essentially all the remnant. Under vibration (upper right) the precision model also fits the correlated components but the processing remnant model only fits up to about 1.4 Hz as the actual remnant has less rolloff at high frequency. The processing remnant model comparison (lower left of Fig. 12) shows the effects of vibration on the processing remnant pathway. From Fig. 5 vibration causes a reduction in the pilot's midband gain and neuromuscular system natural frequency. The closed visual loop consequence of the gain reduction is a lower ω_{CL} with larger damping. The closed visual loop consequence of the neuromuscular system natural frequency reduction is a drop in the pass band of the processing remnant pathway.

We are not at this time concluding anything about the degree to which the processing remnant scales with the variance of the error (Figs. 1 and 10) as we are still in the process of untangling effects across the data base. In particular, we will be examining the motor remnant sources (Fig. 10) especially the consequences of spindle sensors and spindle muscle noise sources, as these go through one and two lead terms, respectively, before they get to the spinal cord. Hence they are likely to have less high frequency rolloff, thus providing a possible explanation of the high frequency remnant when vibration is present.

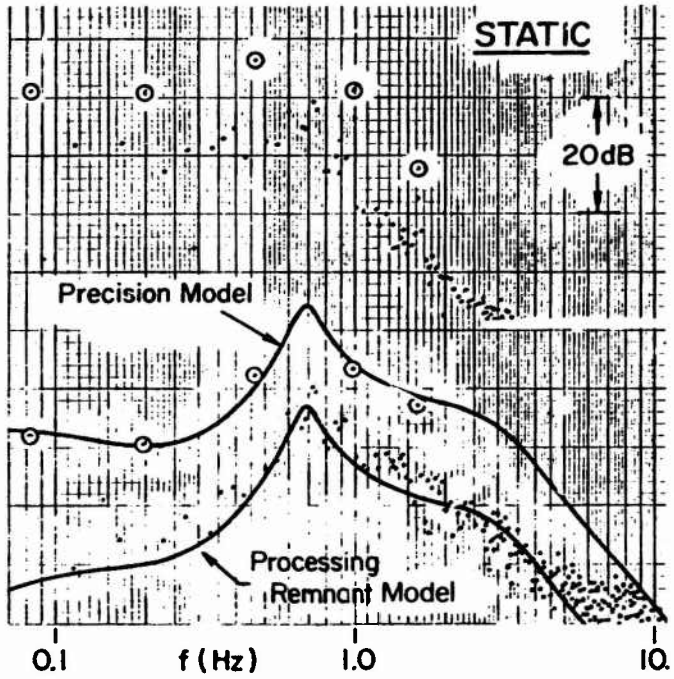

Φ_{ee} Error Spectrum

Φ_{cc} Control Spectrum

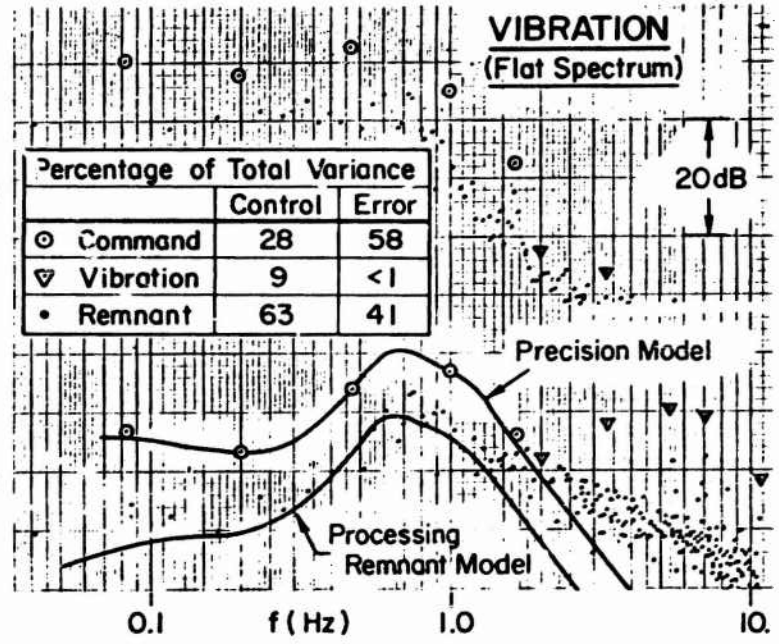

Percentage of Total Variance

	Control	Error
⊙ Command	28	58
▽ Vibration	9	<1
• Remnant	63	41

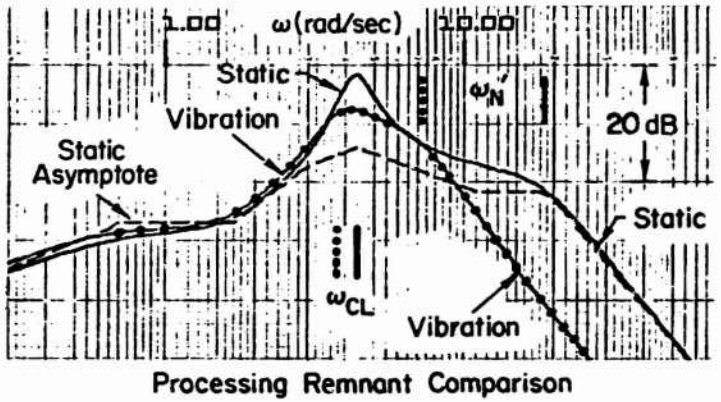

Processing Remnant Comparison

- Spectrum points from a General Radio 1923-C Time Series Analyzer
- f_b = .04 Hz averaged over four fundamental time frames
- Remnant points not corrected for correlated power via $\Phi_{cc_n} = \Phi_{cc}(1 - \rho^2_{ic} - \rho^2_{vc})$

Figure 12. Typical Effects of Vibration in Error and Control Spectrum

Visual Remnant: Head Motion Model and Measures

As indicated previously (pg. 5) both performance measurements and subjective reports suggest vibration interference with vision out in the region of 7-10 Hz, which at these frequencies is probably due to head motions rather than any direct effect on the eyeball itself (e.g., resonance, distortion, etc.). A block diagram model indicating the influence of head motions on retinal image motion is given in Fig. 13a. At low frequencies (<4 Hz) feedbacks to the occulomotor system tend to stabilize the eye line of sight (Ref. 18) such that a constant eye point of regard can be maintained during normal head motions (such as caused by walking, gesturing, etc.). Beyond the occulomotor bandwidth the eye no longer compensates for head motion, however, at which point the eye-point-of-regard follows head motions. Thus head motions beyond 4 Hz tend to disturb vision.

During the sinusoidal experiment, measurements on both head rotation and translation were obtained (with two accelerometers mounted on a simple bite bar clenched in the teeth) in order to determine their correlation with other data on visual disturbance. As shown in Fig. 13b both head translation (measured near the eye) and head rotation accelerations peak in the region of 7 Hz. These data were also computationally projected out to the display plane to determine the apparent relative motion of display images caused by relative head/display motion. As shown at the bottom of Fig. 13b head rotation caused the major contribution to apparent display image motion.

Given vibration induced retinal image motions, there are still many perceptual factors (such as perceptual blanking, displacement vs. velocity of motion, etc.) that combine to determine visual interference. However, as suggested by the present data, head motions are certainly a key factor, and development of a biomechanical head motion model will be pursued as a key factor in describing vibration interference with vision.

CONCLUDING REMARKS

In recent years we have explored the basic mechanisms of vertical vibration interference with manual control performance using the combined approach of experimental studies and model development. Preliminary models

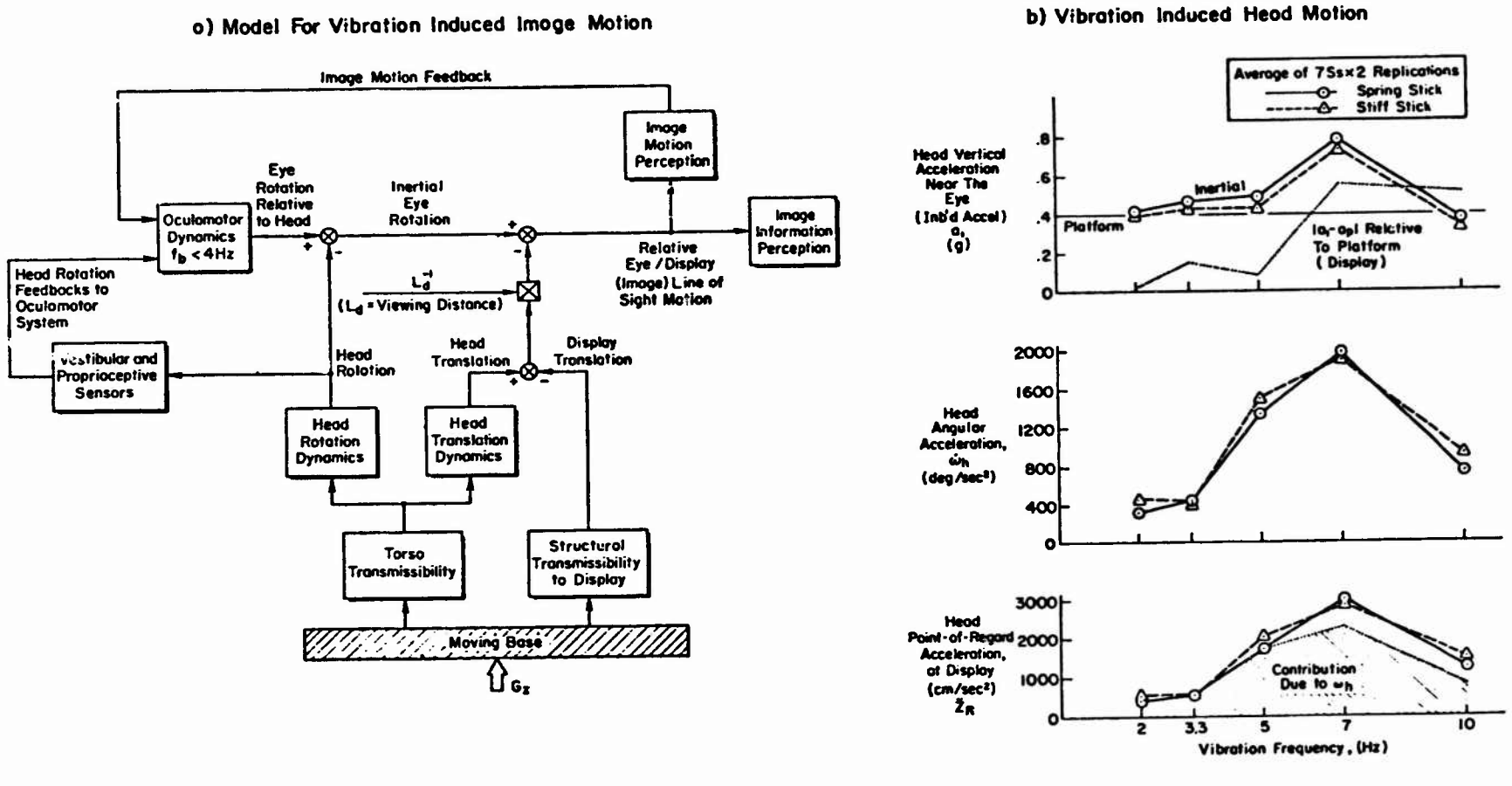

Figure 13. Head Motion Model and Measurements

were used to suggest appropriate experimental measurements, and based on these measurements the models are now in the process of further refinement. Model developments thus far have indicated that most vibration effects arise from the relative motions of various body parts with respect to the seat, stick and display. The modeling effort has also shown how complicated the interaction is between body, arm and stick motions.

Evidence is presented for the presence of motor noise, and appropriate structural models for the limb/neuromuscular system are suggested which should allow modeling the sources of motor noise. Motor remnant is an important factor at high control stick gains, and this connection will be studied further. Ultimately we hope to have a complete performance model, explaining feedthrough, remnant, and adaptive visual-motor covariations as affected by vibration. This effort will be greatly aided by our use of structurally related models which contain the natural covariations of vibration induced effects.

While the models presented here are structurally complete, they are also more complicated than may be required in specific design and analysis situations. Once the important aspects of the models are uncovered, however, they can be greatly simplified for various applications. Part of the ongoing modeling effort will be devoted to developing simplified model forms.

Some potential applications of biodynamic models are shown in Fig. 14 which include both analysis and design situations involving the visual, control and seat interfaces with the human operator.

Eye/Head/Helmet Dynamics:

- Analyze vibration interference with vision
- Biodynamic design of helmet-mounted displays under high G_z and buffet

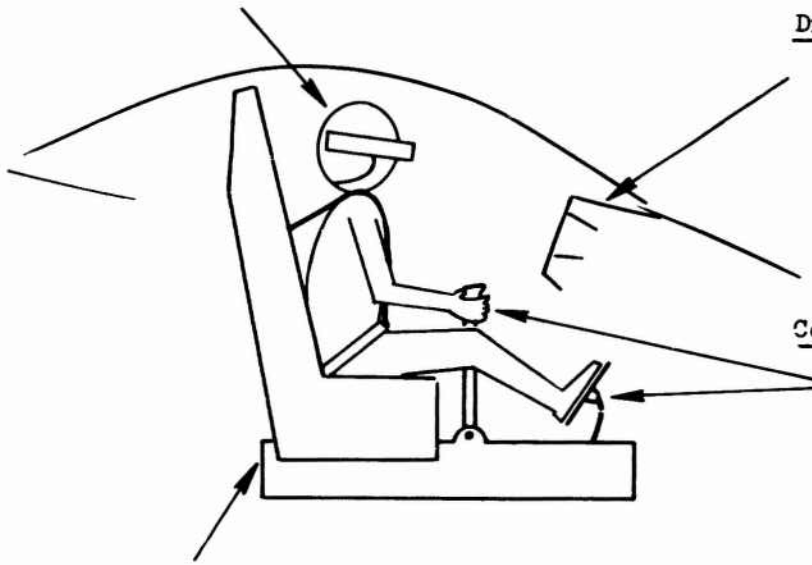

Displays:

- Analyze display mounting, isolation, stabilization concepts
- Analyze effects of size, viewing distance, orientation, etc.

Controls/Motor Coordination:

- Analyze competing control configurations (e.g., fly-by-wire vs. center stick) for (a) effects of rough air excited bending modes for large aircraft, or (b) high g buffet for fighters
- Design vibration resistant controls

Restraint/Seating and Isolation Systems:

- Analyze performance consequences of competing restraints and cushions
- Design new restraint and isolation systems
- Analyze performance effects of various postural situations (i.e., supine seating)
- Ride quality implications on various tasks and locations in aircraft

Overall

- Optimize among various tradeoffs prior to testing, also simulations to operational situations
- Predict pilot control/vehicle motion interactions (e.g., pilot induced oscillations)

Figure 14. Potential Applications for Biodynamic Models of Manual Control Behavior

REFERENCES

1. Shoenberger, Richard W., "Human Response to Whole-Body Vibration," Perceptual and Motor Skills, Monograph Supplement 1-V34, 1972, pp. 127-160.

2. Allen, R. Wade, Henry R. Jex, and Raymond E. Magdaleno, Manual Control Performance and Dynamic Response During Sinusoidal Vibration, AMRL-TR-73-78, Oct. 1973.

3. Allen, R. Wade, Raymond E. Magdaleno, and Henry R. Jex, Effects of Vertical Sinusoidal Vibration on Manual Control Behavior, Performance and Biodynamic Response, Systems Technology, Inc., ITR 1027-2, Oct. 1973

4. Allen, R. Wade, Raymond E. Magdaleno, and Henry R. Jex, Random G_z Study Preliminary Data Analysis, Systems Technology, Inc., ITR 1027-3, Nov. 1973.

5. McRuer, Duane, Dunstan Graham, Ezra Krendel, and William Reisener, Jr., Human Pilot Dynamics in Compensatory Systems – Theory, Models, and Experiments with Controlled Element and Forcing Function Variations, AFFDL-TR-65-15, July 1965.

6. McRuer, D. T., and E. S. Krendel, Mathematical Models of Human Pilot Behavior, AGARDograph No. 188, Jan. 1974.

7. Magdaleno, R. E., D. T. McRuer, and G. P. Moore, Small Perturbation Dynamics of the Neuromuscular System in Tracking Tasks, NASA CR-1212, Dec. 1968 (also "A Neuromuscular Actuation System Model," IEEE Trans., Vol. MMS-9, No. 3, Sept. 1968, pp. 61-71).

8. Magdaleno, R. E., and D. T. McRuer, Experimental Validation and Analytical Elaboration for Models of the Pilot's Neuromuscular Subsystem in Tracking Tasks, NASA CR-1757, April 1971.

9. Braune, W., O. Fischer, J. Amar, and W. T. Dempster, Human Mechanics: Four Monographs Abridged, AMRL-TDR-63-123, Dec. 1963.

10. Stapleford, R. L., Users' Manual for STI Control System Design Programs, Systems Technology, Inc., TR-407-1, July 1970.

11. Coermann, Rolf R., The Mechanical Impedance of the Human Body in Sitting and Standing Position at Low Frequencies, ASD TR-61-492, Sept. 1961.

12. Wells, J. B., "Comparison of Mechanical Properties Between Slow and Fast Mammalian Muscles," J. Physiol., Vol. 178, 1965, pp. 252-269.

13. Levison, W. H., S. Baron, and D. L. Kleinman, "A Model for Controller Remnant," IEEE Trans., Vol. MMS-10, No. 4, Dec. 1969, pp. 101-108 (also Bolt, Beranek and Newman, Inc., Rept. 1731, 15 Oct. 1968).

14. Jex, H. R., and R. E. Magdaleno, "Corroborative Data on Normalization of Human Operator Remnant," IEEE Trans., Vol. MMS-10, No. 4, Dec. 1969, pp. 137-140.

15. Jex, H. R., R. W. Allen, and R. E. Magdaleno, Display Format Effects on Precision Tracking Performance, AMRL-TR-71-63, Aug. 1971.

16. Magdaleno, R. E., H. R. Jex, and R. W. Allen, "Modelling and Measuring Limb Fine-motor Unsteadiness," Proceedings of the Ninth Annual Conference on Manual Control, MIT, Cambridge, Mass., May 23-25, 1973, pp. 335-350.

17. Houk, J., and E. Henneman, "Responses of Golgi Tendon Organs to Active Contractions of the Soleus Muscle of the Cat," J. Neurophysiol., Vol. 30, 1967, pp. 466-481.

18. Meiry, Jacob L., "Vestibular and Proprioceptive Stabilization of Eye Movements," in Paul Bach-Y-Rita, Carter C. Collins, and Jane E. Hyde (eds.), The Control of Eye Movements, Academic Press, N. Y., 1971, pp. 483-496.

19. Levison, W. H., The Effects of Display Gain and Signal Bandwidth on Human Controller Remnant, Bolt, Beranek and Newman, Inc., Rept. 1968, 15 Aug. 1970.

20. Levison, W. H., Analysis of Vibration-Induced Pilot Remnant, Bolt, Beranek and Newman, Inc., Rept. 2608, Aug. 1973.

21. Jewell, B. R., and D. R. Wilkie, "An Analysis of the Mechanical Components in Frog's Striated Muscle," J. Physiol., Vol. 143, No. 3, 1958, pp. 515-540.

22. Terzuolo, C. A. and C. K. Knox "Linear Systems Analysis of Mechanoreceptor," Systems Analysis Approach to Neurophysiological Problems, A Conference held at the University of Minn., Brainerd, Minn., 22-28 June 1969, pp. 121-127.

Poppele, R. E., and R. J. Bowman, "Linear Analysis of Muscle Spindles," Systems Analysis Approach to Neurophysiological Problems, A Conference held at the University of Minn., Brainerd, Minn., 22-28 June 1969, pp. 128-140.

23. Terzuolo, C. A., "Data Transmission by Spike Trains," The Neurosciences: Second Study Program, F. O Smith, Editor-in-Chief, The Rockefeller University Press, N Y., 1970, pp. 661-671.

24. McKean, T. A., R. E. Poppele, N. P. Rosenthal and C. A. Terzuolo, "The Biologically Relevant Parameter in Nerve Impulse Trains," Kybernetik, Vol. 6, 1970, pp. 168-170.

25. Terzuolo, C. A., T. McKean, W. Roberts and P. Rosenthal, "Gain of the Stretch Reflex in Extensor Muscles of the Decerebrate Cat," Synaptic Processes, 1970, pp. 327-332.

26. Poppele, R. E., "The System Approach to the Function of the Nervous System," Synaptic Processes, 1970, pp. 259-268.

27. Poppele, R. E., and R. J. Bowman, "Quantitative Description of Linear Behavior of Mammalian Muscle Spindles," J. Neurophysiology, Vol. XXXIII, No. 1, 1970, pp. 59-72.

28. Roberts, W. J., N. P. Rosenthal, and C. A. Terzuolc, "A Control Model of Stretch Reflex," J. Neurophysiology, Vol. XXXIV, No. 4, 1971, pp. 620-634.

29. Berthoz, A., W. J. Roberts, and N. P. Rosenthal, "Dynamic Characteristics of Stretch Reflex Using Force Inputs," J. Neurophysiology, Vol. XXXIV, No. 4. 1971, pp. 612-619.

ANALYSIS OF VIBRATION-INDUCED PILOT REMNANT

William H. Levison
Bolt Beranek and Newman Inc.
Cambridge, Massachusetts

Presented at the Tenth Annual Conference
on Manual Control, April 9-11, 1974,
Wright-Patterson Air Force Base, Ohio

ABSTRACT

The effects of whole-body sinusoidal vibration on pilot remnant are analyzed. Data for one test subject, five vibration conditions, and one control configuration are considered. The primary effect of vibration on the remnant spectrum is to increase the overall remnant level; no important changes in spectral shape are ascertained. Vibration-induced remnant can be modeled as an injected wide-band motor noise process that, for the most part, varies proportionally with stick variance. A model structure for relating pilot performance to vibration parameters is suggested.

INTRODUCTION AND SUMMARY

Objectives

The effects of sinusoidal whole-body vibration on manual tracking performance have recently been reported by Allen et al. in [1]. As tracking performance in vibration environments has not heretofore been analyzed to the level of detail reported by these investigators, this effort must be regarded as a considerable advance towards understanding the effects of vibration on manual control behavior.

The ultimate objective of studying laboratory tracking performance in vibration environments is to develop a body of knowledge that will allow one to minimize and/or compensate for the effects of vibration in operational situations requiring manual control. This objective would be materially aided by the development of analytic models to describe the interrelationships between vibration parameters, physical characteristics of the pilot/vehicle interface, vehicle dynamic response properties, pilot response strategy, and overall system performance. Although the study reported in [1] provides a good step in this direction, a number of gaps in our understanding remain. Specifically, the published data do not show in a quantitative fashion

why the vibration disturbances affect tracking performance the way they do. That is, cause and effect are not well defined. Rather, the results are more of a descriptive nature in the sense that a "catalog" of vibration parameters and changes in certain system performance measures and pilot response parameters is developed. Nevertheless, these results, plus the bio-mechanical models developed in the same study, provide a solid basis for further model development.

Additional analysis of the data obtained by Allen et al. was performed by Levison to obtain a more detailed description of the interaction between vibration and tracking performance. The results of Levison's study are summarized in this paper and are reported in greater detail in [2]. Some of the specific goals of the latter study were to (a) determine pilot describing functions and remnant spectra for various vibration conditions, (b) ascertain the sources of vibration-induced remnant via model analysis, and (c) suggest a means for quantitative prediction of pilot remnant and system performance in vibration environments.

Background

Tracking performance for a variety of tracking situations and vibration conditions was observed in the study performed by Allen et al. The results of the experiments with lateral vibration inputs are reviewed here, as these provided the data examined subsequently by Levison.

Sinusoidal whole-body vibration at six frequencies (applied singly) was explored, along with the static (i.e., no-vibration) condition. Zero-to-peak acceleration was 0.4g for each vibration test signal. A single set of controlled-element dynamics, simulating aircraft roll response, was used.

Two variations of control-stick properties were studied in this experimental program. A "stiff stick" configuration was designed to provide essentially an isometric control device, and a "spring stick" was provided with a very light spring gradient.

Various tracking performance measures were obtained, including (a) variance scores for tracking error and control activity, (b) measures of "coherence" to indicate the fraction of total error and control power correlated with the tracking input signal, and (c) pilot describing functions were analyzed to yield various descriptions of the pilots' tracking strategy such as "gain-crossover" and "phase-crossover" frequencies. Remnant spectra were not obtained, however; hence the need for further analysis of the experimental data.

The correlation between the pilot's control input and the vibration input was computed in order to determine the extent of difect mechanical feedthrough from vibration to tracking error. In addition, motions of the head, shoulder, and elbow were recorded so that a model for the mechanical coupling could be developed.

The results of the data analysis reported in [1] regarding the lateral vibration experiments may be summarized as follows:

1. Vibration had a much greater effect on tracking error when the relatively free-moving spring stick was used.

2. Performance degraded increasingly with decreasing vibration frequency. Maximum increase in error coincided with maximum body response to the vibration input.

3. The increase in tracking error was apparently due primarily to increased pilot remnant. Changes in describing function parameters were relatively small.

4. Pilot commentary, as well as consideration of the above results, suggested that motor-related sources of remnant were dominant in the lateral-vibration experiments.

5. Mechanical transmission between vibration input and various parts of the body was studied, and relatively simple models were constructed to describe the mechanical coupling between vibration input and control.

Data-Base

The analytical study reported in this paper was intended to be a small-scale effort to explore the nature of vibration-induced remnant and to suggest some tentative modeling approaches. Accordingly, only a limited portion of the data obtained in the experimental study of Allen et al. was explored in this regard.

Analysis was confined to data obtained from a single test subject using the spring stick. Analysis of error and stick variances reported in [1] was performed to find the subject whose performance was most representative of the four subjects that had participated in the experiments. Data for the static condition and for vibration frequencies of 1.3, 2, 3, and 4.5 Hz were analyzed.

Conclusions

The major conclusions of the study summarized in this paper are as follows:

1. The findings reported by Allen et al. regarding the effects of lateral vibration on tracking performance are confirmed.

2. The primary effect of vibration on the closed-loop stick remnant spectrum is to increase the overall level of remnant. Consistent changes in spectral shape are not observed.

3. The effect of vibration on pilot behavior and system performance can be largely accounted for by an increase in wide-band motor-related pilot "noise" for the spring-stick experiments. For all but the most severe vibration condition, the variance of the injected noise process can be considered to vary proportionally with stick variance.

4. A combination of existing models for pilot/vehicle performance and vibration feedthrough would appear to provide a powerful tool for predicting pilot behavior and system performance in vibration environments.

PRIMARY DATA ANALYSIS

The data analyzed in this study have been reduced to provide signal variances and standard deviations, pilot describing functions, and spectral density functions of tracking error and control stick signals. Computations were made over 50-second intervals for each experimental trial. The measurement intervals used in this study coincide to within one or two seconds with the measurement intervals used in the original study by Allen et al.

Performance Scores

Variance and standard deviation (SD) scores for input, error, and stick displacements are given in Table 1 for the five vibration conditions (including the static condition). Each entry represents the average of three replications and includes the effects of the tracking input, the vibration input, and pilot remnant.* Since the average SD scores were obtained by averaging the individual SD scores, the SD scores shown in Table 1 are not necessarily equal to the square root of the average variance score.

*"Remnant" is defined in this study as signal power at other than input frequencies.

EFFECT OF VIBRATION CONDITION ON PERFORMANCE SCORE

Average of 3 Replications

Vibration Condition	Variance			Standard Deviation (SD)		
	Input	Error	Stick	Input	Error	Stick
Static	4.24	1.65	2.06	2.06	1.28	1.42
4.5 Hz	4.23	1.67	1.91	2.06	1.29	1.38
3.0 Hz	4.21	1.92	9.71	2.05	1.38	3.10
2.0 Hz	4.23	3.76	19.7	2.06	1.93	4.48
1.3 Hz	4.23	10.0	34.1	2.06	3.15	5.83

Both the stick and error scores increase progressively with decreasing vibration frequency. The percentage changes in stick and error scores from one frequency condition to the next appear to agree quite well with the performance scores shown for the test subject (Subject BC) in Figures 25a and 26a of [1].

Stick Remnant Spectra

Closed-loop stick remnant spectra are shown in Figure 1 for the static condition, the most severe vibration condition (1.3 Hz), and an intermediate vibration condition (3 Hz). Each datum point presented in this figure reflects the average of remnant estimates obtained at up to four adjacent measurement frequencies. These frequency-smoothed estimates have been averaged across three replications for each condition. The data shown in this figure (and in all subsequent figures in this paper) have been normalized to represent continuous spectra as described in [2].

The primary effect of vibration on the remnant spectrum is to increase the overall level, rather than to distort the frequency-dependency. All three curves show a peak at around 4-5 rad/sec with a fall-off of about 40 dB/decade at frequencies above the peak. At frequencies below the peak, the remnant spectrum appears to increase with frequency by roughly 20 dB/decade. Since the location of the spectral peak appears to be independent of the vibration frequency, the peaking effect is most likely a consequence of the closed-loop system characteristics rather than a reflection of non-linear feedthrough of the vibration input.

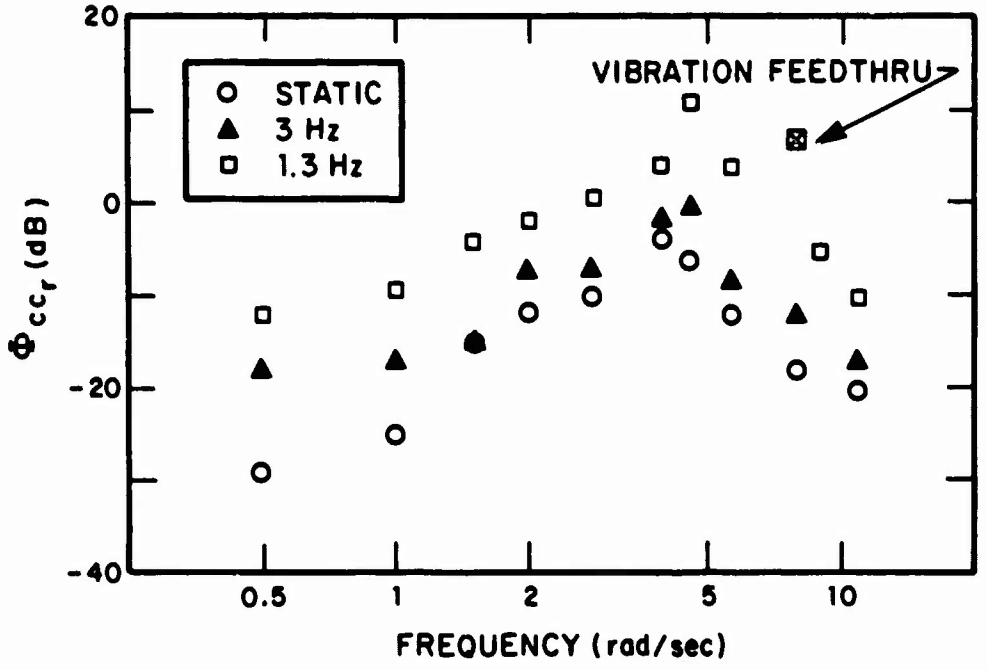

FIGURE 1. Effect of Vibration on Stick Remnant Spectrum
Average of 3 Replications

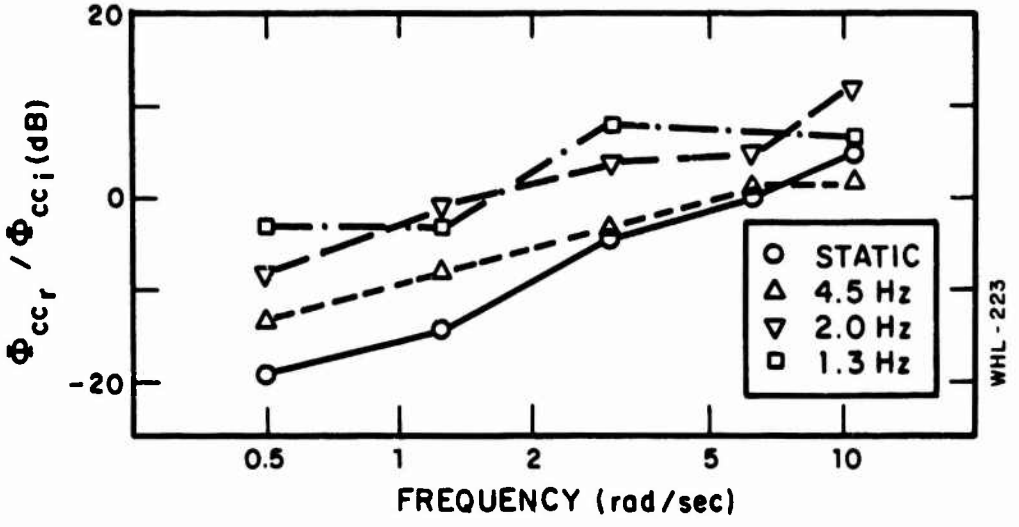

FIGURE 2. Effect of Vibration on Stick Remnant Ratio
Average of 3 Replications

The cross-hatched point associated with the 1.3 Hz curve at about 8 rad/sec reflects the direct feedthrough of the vibration signal. Otherwise, the shape of the 1.3 Hz curve is similar to that of the other remnant spectra shown in Figure 1.

"Remnant ratios" for four of the five conditions explored are shown in Figure 2.* To compute each of these curves, remnant measurements were averaged over ± 1/8 octave about each input frequency and normalized with respect to the spectral estimate at the corresponding input frequency. As expected, the overall level of the remnant ratio increases with the severity of the vibration condition. Except for a somewhat greater rate-of-change of remnant ratio with frequency for the static condition, there appears to be no consistent effect of vibration on the shape of this curve.

Pilot Describing Functions

Pilot describing functions for four conditions are presented in Figure 3. Although the slope of the amplitude-ratio curve in the region of gain crossover appears to increase with increasing severity of vibration, no consistent effects of vibration on phase-shift characteristics are observed. Gain-crossover frequencies are essentially the same (about 2.6 rad/sec) for all four conditions, which suggests that the presence of vibration inputs did not appreciably affect the efficiency of the pilot/vehicle system with respect to minimizing the effects of the tracking input.

MODEL ANALYSIS

Model analysis was performed to help identify the source of vibration-induced remnant and to determine whether or not a straightforward procedure could be found for predicting the effects of vibration on tracking error.

The Pilot/Vehicle Model

This analysis was performed with the state-variable (or "optimal-control") model for pilot/vehicle systems developed at Bolt Beranek and Newman Inc. The model is based on the assumption that the well-motivated and well-trained human operator behaves in a near optimal manner subject to his inherent constraints and

*Data for the 3 Hz condition were omitted from this figure to maintain readability. The shape of this curve was similar to that of the 4.5 Hz condition, with a somewhat higher overall level. The estimate of the remnant ratio for the 1.3 Hz condition at 6.3 rad/sec has been omitted because the estimate of input-correlated power at this frequency did not meet the test or reliability defined in [2].

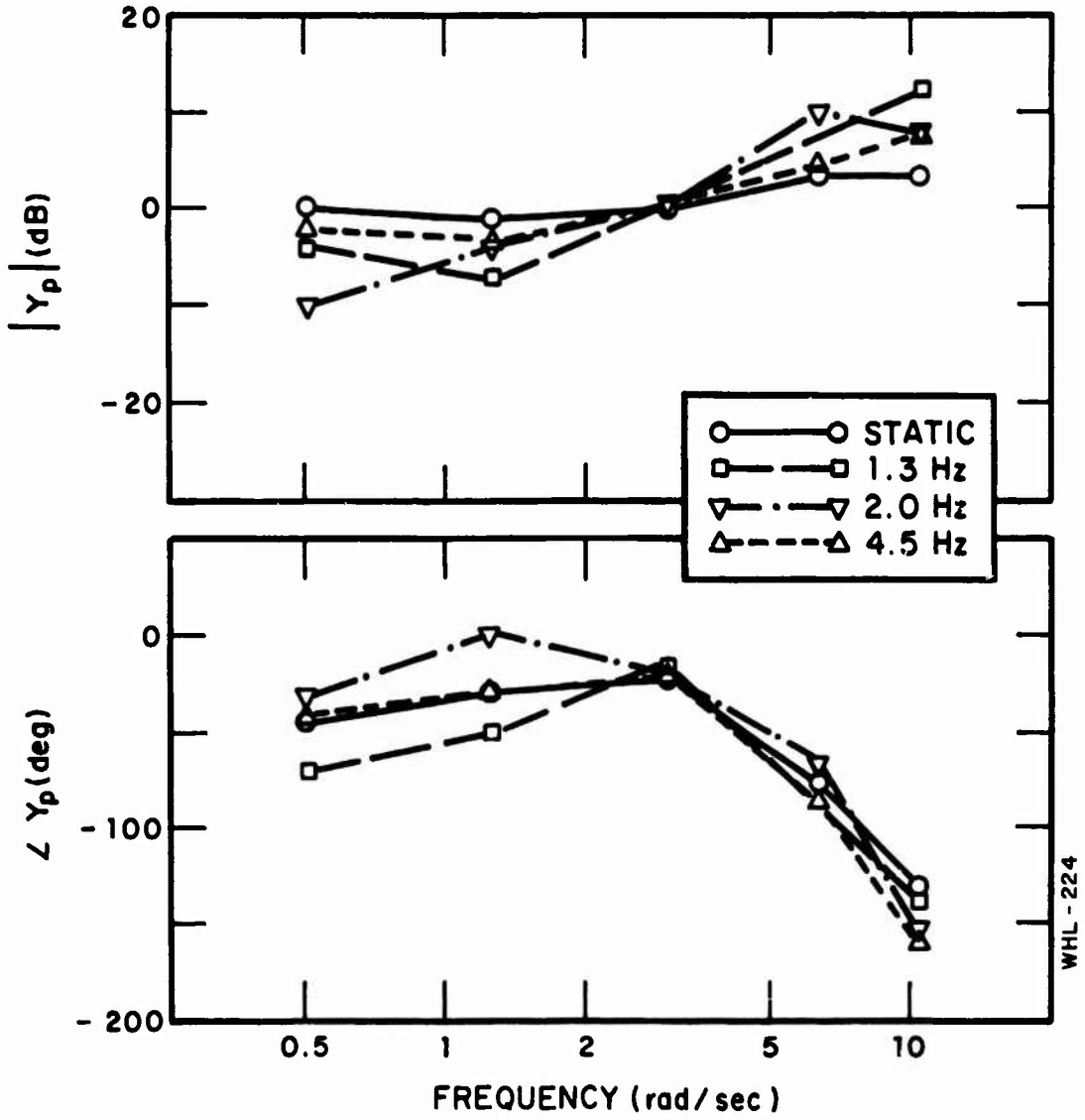

FIGURE 3. Effect of Vibration on Pilot Describing Function
Average of 3 Replications

limitations. Thus, once control system dynamics, performance requirements, and inherent pilot limitations have been specified, pilot behavior and overall system performance can be predicted.

Readers unfamiliar with this model are referred to the literature for a mathematical description of the model and for supporting experimental data [3-5]. Because of the importance of pilot remnant in accounting for the effects of vibration on tracking performance, however, we shall discuss here our representation of pilot randomness.

Remnant is modelled partly as a set of observation (i.e., perceptual) noise processes and partly as a motor noise process. Each display variable used by the pilot is assumed to be perturbed by a white noise process that is linearly uncorrelated with other signals circulating through the tracking system. Similarly, the pilot's control input is assumed to be perturbed by an additional independent white noise process. For situations in which the control and display gains are essentially optimized, the covariances of these noise processes scale proportionally with the variances of the signals they perturb. Thus, in the case of a single-variable tracking task, the noise covariances are given as

$$V_y = \sigma_y^2 P_y$$

$$V_{\dot{y}} = \sigma_{\dot{y}}^2 P_{\dot{y}}$$

$$V_u = \sigma_u^2 P_u$$

where the subscripts y, $\dot{y}$, and u denote tracking error, tracking error rate, and control displacement, respectively. (We assume that the pilot extracts both position and velocity information from his display indicator.) The quantities P_y, $P_{\dot{y}}$, and P_u are the "noise/signal ratios" that relate injected noise covariance to signal variance. Typical values for laboratory tracking tasks are -20 dB for perceptual noise processes and -25 dB for motor noise.

Other pilot-related model parameters that are important in representing single-variable tracking behavior are the effective time delay (to account for transmission and processing delays of sensory inputs) and the "motor time constant" (to reflect bandwidth limitations). Typical values for these variables are 0.2 seconds for the delay and 0.1 second for the time constant.

Modeling Procedures

In order to derive a state-variable representation of the tracking task, it was necessary to represent the sums-of-sinusoids disturbance used in the experiments by an equivalent filtered noise process. Accordingly, the input signal was approximated by a second-order Butterworth filter driven by white noise. A critical filter frequency of 1.0 rad/sec was chosen to provide an analytical input signal of the same rms displacement and velocity (and, presumably, of similar tracking difficulty) as the experimental input. The vehicle dynamics were $10.5/s(s+3)$ as measured from the experimental data. No attempt was made to model the effect of linear vibration feedthrough on tracking performance.

The following modeling strategy was adopted. First, the data obtained from the static condition were matched so that the full set of pilot-related model parameters could be quantified. Next, data from the 2 Hz vibration condition were compared with model results to determine which source of remnant best accounted for the effects of vibration. A simple relationship between injected noise and tracking behavior was determined from these results and tested by comparing experimental and model results for the remaining vibration conditions.

Additional details regarding the modeling procedure are given in [2].

Comparison of Experimental and Model Results

Static Condition

The following model parameter values were found to provide the best overall visual match to measured frequency-domain parameters and performance scores:

Time delay = 0.15 second

Motor time constant = 0.095 second

Observation noise/signal ratio for visual variables = -20 dB

Motor noise/signal rate = -30 dB

Values for time delay, motor time constant, and observation noise/signal ratios are similar to those that have been found in previous laboratory tracking studies; the motor noise/signal ratio, however, is lower than that generally found in the past. The low motor noise/signal ratio may have arisen in part from the somewhat different representation of the pilot-control interface adopted in this analysis (see [2]. Also, it should be noted that remnant was accounted for primarily by equivalent perceptual noise in the static case; consequently, the goodness of the model match was relatively insensitive to the selection of a motor noise level.

A comparison of experimental and model frequency-domain measures is given in Figure 4. Amplitude ratio and phase shift are shown in the upper two curves; the lower curve indicates the remnant ratio at each input frequency. Except for the remnant ratio at 0.5 rad/sec, a reasonably good fit is obtained to the experimental measurements. The model error and stick SD scores are within 10% and 20%, respectively, of the measured SD scores.

The 2 Hz Vibration Condition

The 2 Hz vibration condition was selected for exploring the effects of vibration on pilot performance because this was the most severe vibration condition that provided reliable measurements at all five input frequencies. Since it was apparent from preceding analysis that the primary effect of vibration was to increase pilot remnant, model parameters related to perceptual and motor sources of remnant were varied alternately to determine which of these two sets of variables best accounted for the effects of vibration on pilot/vehicle performance.

Two variations in model parameters were explored. With all remaining model parameters kept at values appropriate to the static condition, the injected motor noise was increased until the predicted error SD score was within 10% of the score obtained experimentally for this vibration condition. The motor noise was then reset to the value appropriate to the static condition, and the observation noise/signal ratios for error displacement and rate perception were jointly incremented until the error SD score was again matched to within 10%.

Comparisons of the two sets of model results with experimental frequency-domain measures are given in Figures 5 and 6. The motor-noise model appears to provide a better match to the high-frequency portion of the pilot describing function (Figure 5), whereas the observation-noise model provides a better match at low frequencies. If we consider the predictions of the two models in the region of gain crossover, however, we find that the motor-noise model provides a superior match. The gain crossover predicted by this model configuration is about 2.8 rad/sec (versus an estimated 2.6 rad/sec for the experimental data), whereas the large observation noise leads to a gain-crossover frequency of about 2.0 rad/sec. Thus, the high motor noise configuration provides a better prediction of the effects of vibration on tracking effectiveness.

Although the two high-noise model configurations appear to reproduce the remnant-ratio curve equally well (Figure 5), differences are apparent when we consider individually the input-correlated

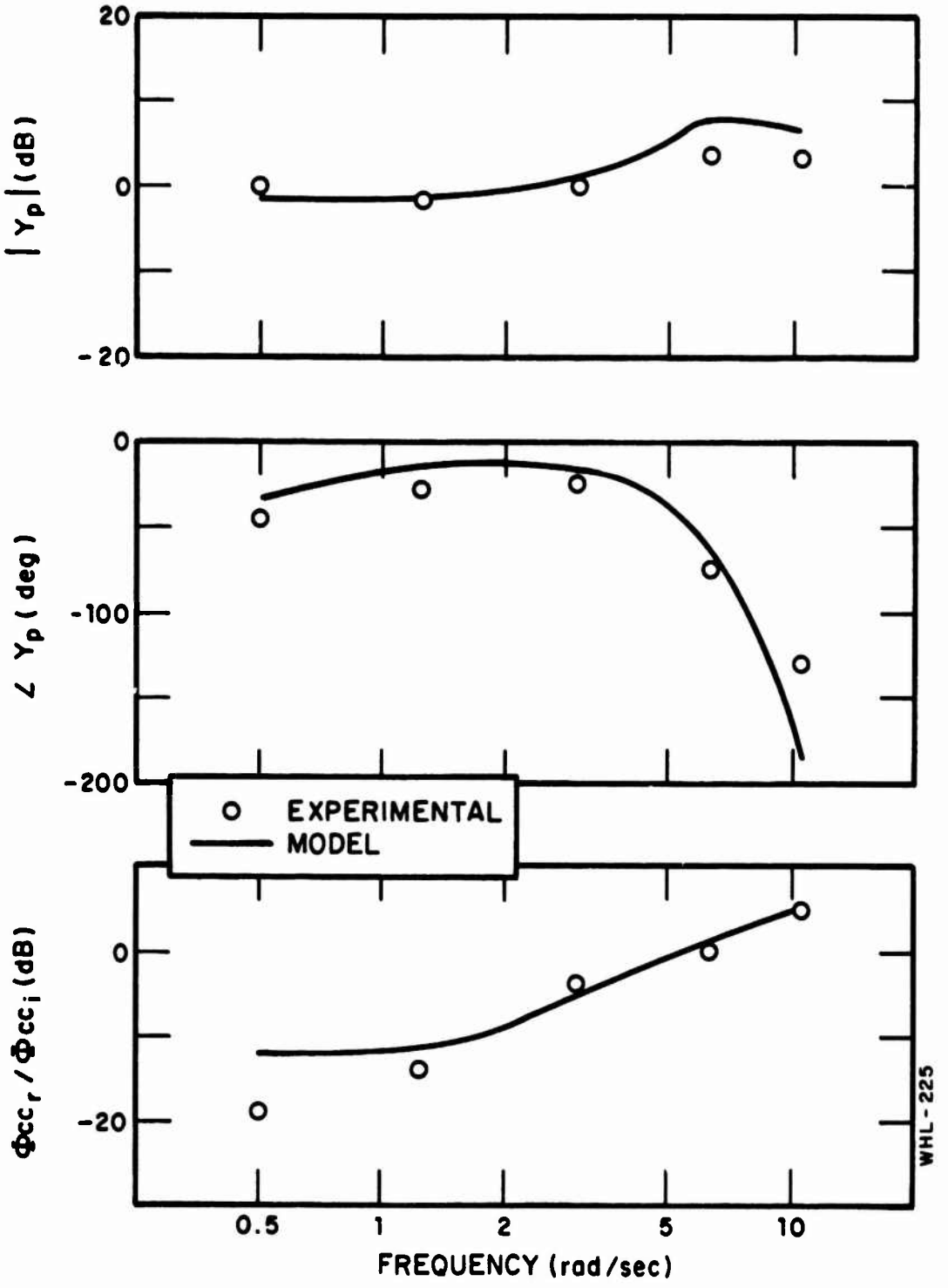

FIGURE 4. Comparison of Experimental and Predicted Frequency-Domain Measures, Static Condition Average of 3 Replications

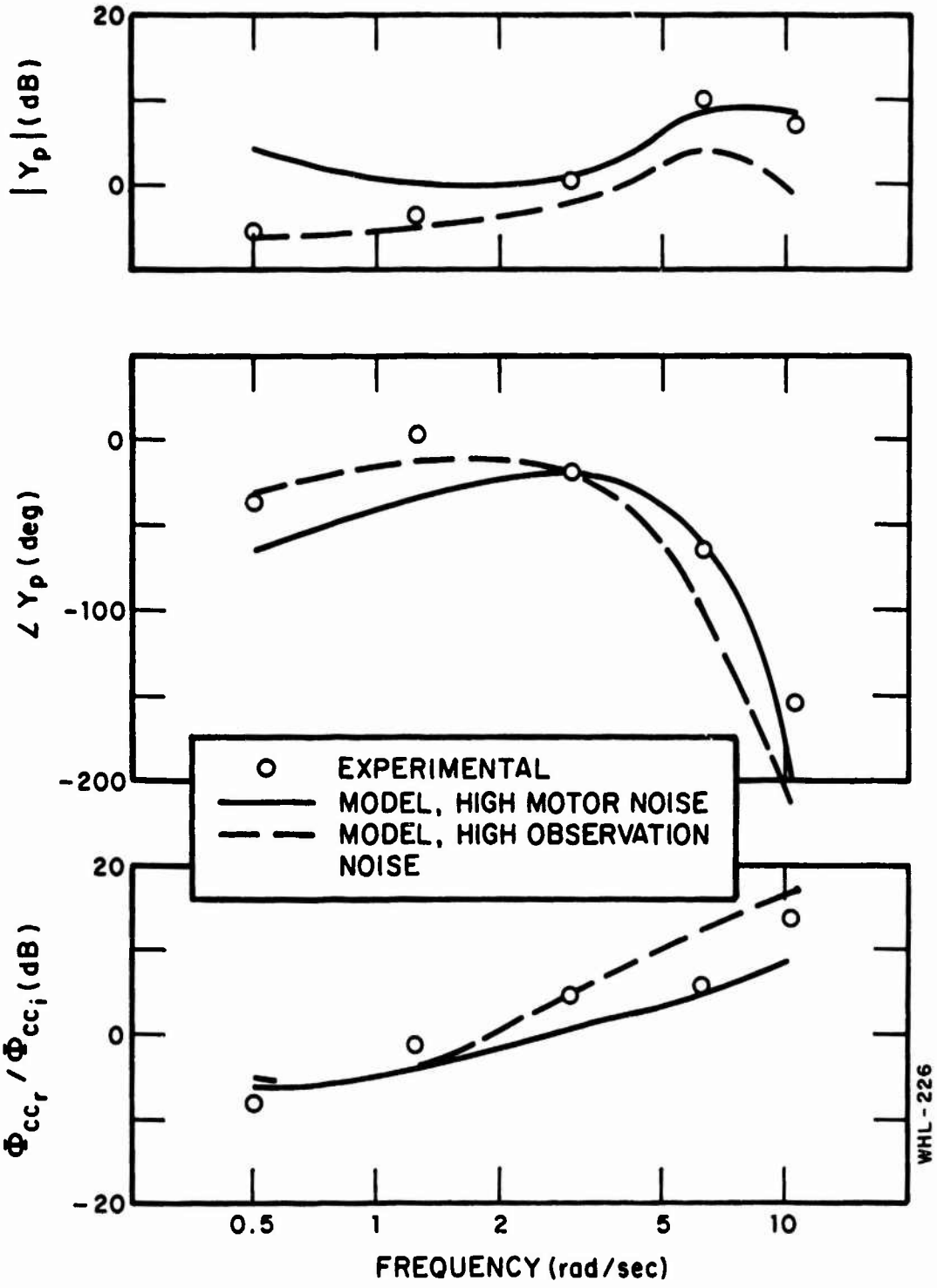

FIGURE 5. Comparison of Experimental and Predicted Frequency-Domain Measures, 2 Hz Vibration
Average of 3 Replications

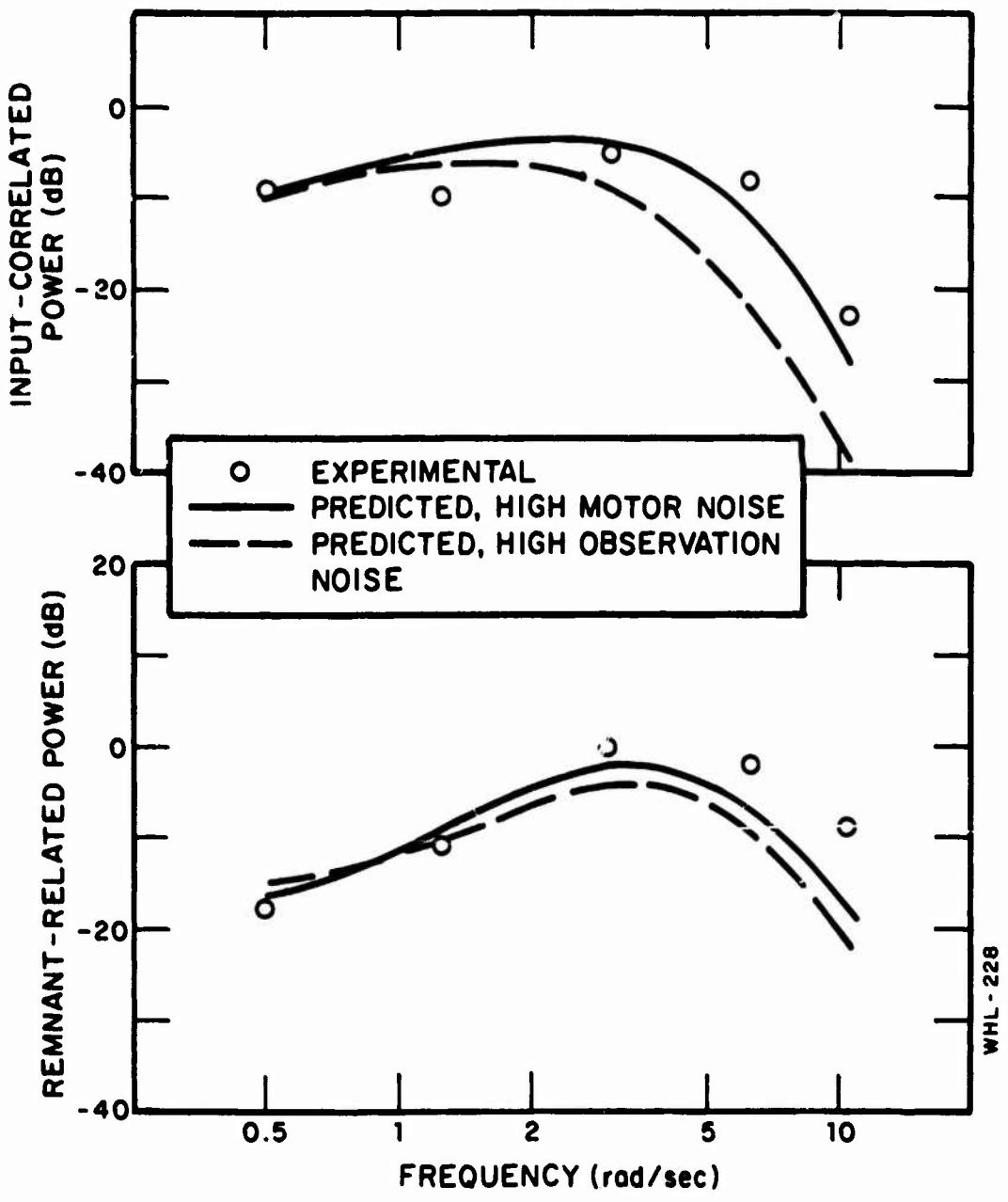

FIGURE 6. Comparison of Experimental and Predicted Stick Spectra, 2 Hz Vibration Average of 3 Replications

and remnant-related portions of the stick spectrum (Figure 6). An appreciably better match to experimental data is obtained at mid and high frequencies by the high motor noise model, especially for the input-correlated spectrum.*

In summary, the effects of vibration on tracking performance, at least for the 2 Hz vibration input, can be reasonably well accounted for by an increase in the injected wide-band motor noise process. Given the current formulation of the model, an increase in motor noise represents both an increase in noise injected into the system as well as degradation in motor-related perceptual feedbacks. Thus, we cannot at present use the state-variable model to discriminate between a degradation in kinesthetic feedback and wide-band driving noise arising from nonlinear or time-varying feedthrough of the vibration input. We can, however, consider the combined contribution of motor-related disturbances.

Remaining Vibration Conditions

The results of the preceding analysis were extrapolated to yield predictions of error scores and frequency-domain measures for the remaining vibration conditions. The injected motor noise was assumed to be proportional to stick variance,** and a scale factor of 0.081 was obtained by dividing the motor noise variance used in matching the 2 Hz data by the stick variance measured in that experiment. This scale factor was used in conjunction with experimental stick variance scores to compute the motor noise levels to be used in predicting performance for the remaining conditions.

The motivation for testing a simple proportional relationship of this type is that it provides a parsimonious scheme for predicting the effects of vibration on pilot remnant and, hence, system performance. Once the transmissibility between the vibration source and the pilot's control member has been determined, prediction of pilot remnant is straightforward. The rationale for a proportional motor noise process stems from extensive previous experience in analyzing manual control data. In situations where threshold and saturation effects have been unimportant, the various perceptual and motor noise processes have been found to scale in proportion to corresponding signal variances [3-5].

Figure 7 provides a comparison of the measured error variances with the variances predicted by the model for the four

*Simultaneous variations of *both* motor and perceptual noise processes did not produce a noticeably better overall match than obtained by an increase in motor noise alone.

**Including the effects of vibration feedthrough as well as the tracking input.

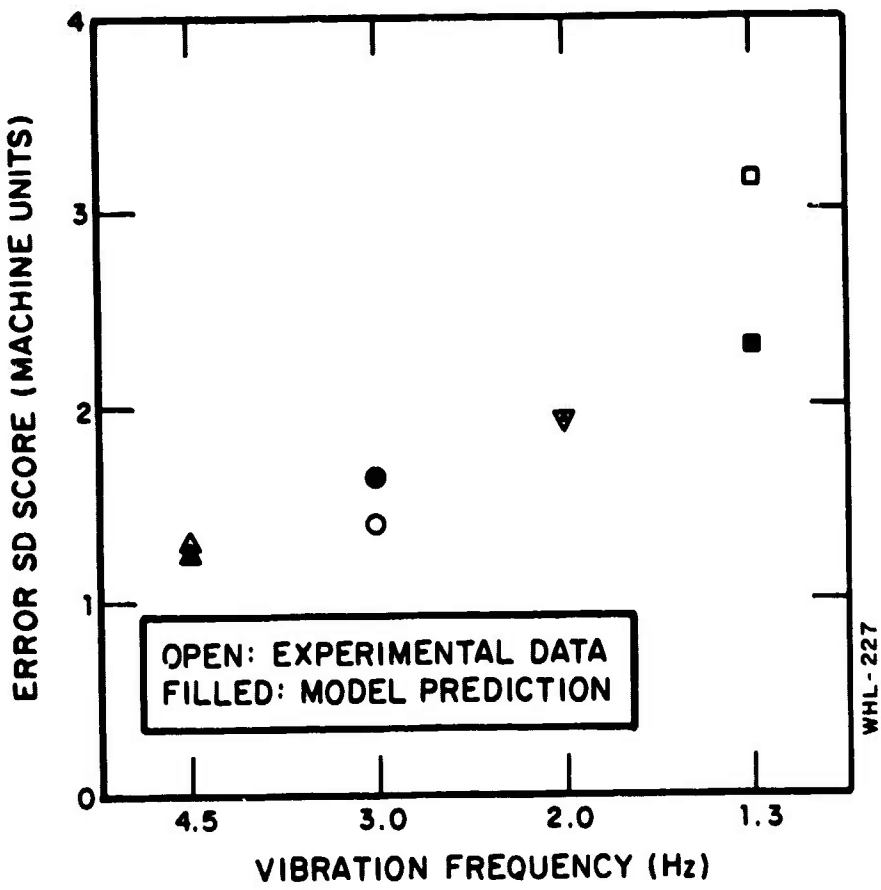

FIGURE 7. Comparison of Experimental and Predicted Error SD Scores Average of 3 Replications

vibration conditions (including the matched 2 Hz case); comparisons of measured and predicted frequency-domain measures may be found in [2].

Error SD scores for the 4.5 and 3 Hz conditions were predicted to within 20%, and reasonably good predictions were obtained for the frequency-domain measures. (Qualitatively, the match between measured and model results was similar to that shown in Figure 4 for the static case.) The error score for the 1.3 Hz condition was predicted less accurately (about a 30% error), and the qualitative match between predicted and measured frequency-domain measures was considerably less good than that obtained for the other vibration conditions. Accordingly, both motor and observation noise variables were re-adjusted in an attempt to obtain a better match to the 1.3 Hz data. Although the measured error SD score could be matched exactly by increasing motor and/or perceptual noise levels, correspondence between model and measured frequency-domain measures was not materially improved.

It should be noted that the frequency-domain measures for the 1.3 Hz condition were not as reliable as those that have been presented for the other experimental conditions. Because of the large amount of remnant, reliable measures at the 6.3 rad/sec input frequency could not be obtained, and only one of the three replications of this condition provided reliable measures at the lowest and highest input frequencies. Thus, the data available to this study were not sufficiently reliable to determine whether or not the assumptions underlying the pilot/vehicle model were violated in the 1.3 Hz situations.

SUGGESTED MODEL EXTENSIONS

The pilot/vehicle model used in this study can be combined with models for mechanical vibration feedthrough to provide a tentative overall model for relating vibration parameters to pilot and system performance. This overall model consists of three basic elements: (a) a model relating vibration parameters and various physical properties of the pilot/vehicle interface to hand and eye motions, (b) a mathematical expression relating vibration-induced motions to perceptual and motor sources of "pilot noise", and (c) a model for relating pilot noise and other pilot- and system-related considerations to pilot control strategy and system performance.

Models for mechanical feedthrough have been proposed in [1], and continuing studies are underway to further validate and refine these models. The state-variable model for predicting the effects of pilot remnant on system performance has been well-documented in the literature, as noted earlier. The second stage of the overall model – the relation of vibration-induced motions to injected pilot noise – is new and is outlined below.

We draw upon the results of previous analysis, as well as the analysis documented in this paper, to postulate the following tentative model for the effects of vibration on injected remnant. Each perceptual noise source is to be represented as a white noise process having a variance

$$V_y = (\sigma_y^2 + \sigma_o^2) \cdot P_y \qquad (1)$$

where σ_y^2 is the variance of the displayed variable, σ_o^2 is an increment to the variance due to relative motions between the eye and the display induced by vibration, and P_y is the observation noise/signal ratio.

A similar relationship is postulated for motor noise:

$$V_u = (\sigma_{u_T}^2 + \sigma_{u_v}^2)\, P_u \qquad (2)$$

where $\sigma_{u_T}^2$ is the component of control variance due to the tracking input and to pilot remnant, $\sigma_{u_v}^2$ is the component due to direct coupling of the vibration disturbance, and P_u is the motor noise/signal ratio. The observation and motor noise/signal ratios are considered to reflect central-processing sources of pilot randomness and, for the present, are assumed to be relatively invariant with respect to system and environmental variables.

The three-stage model would be applied in an iterative fashion. First, the feedthrough models would be used to predict variances for relative eye-display motions as well as for vibration-induced control disturbances. These variances would be used to obtain initial estimates of injected perceptual and motor noise levels as shown in equations (1) and (2). The state-variable pilot/vehicle model would then be applied to predict system performance scores, with P_y, P_u, and other pilot-related model parameters being assigned values typical of those found in the literature. The values of σ_y^2 and $\sigma_{u_T}^2$ predicted by the model would be used with the vibration-related variances to re-adjust the injected noise variances, and new model predictions would be obtained. This process would be repeated until the relationships shown in equations (1) and (2) were satisfied to within acceptable tolerances.

The model expressed by the relationships of equations (1) and (2) is perhaps the most parsimonious representation of the effects of vibration on remnant that can be justified by existing knowledge. Use of this model in the manner outlined above allows a highly simplified treatment of vibration. Consider some of the implications:

a. Injected remnant levels depend only on total control variance and total effective display variance. The spectral shape of the vibration signal is unimportant.

b. The injected noise spectra are white (i.e., wide-band with respect to the signals in the tracking loop). Consequently, the shape of the closed-loop remnant spectrum depends only on the closed-loop pilot/vehicle dynamics (which can be predicted by the state-variable model) and not on the vibration spectrum.

c. Results of the sinusoidal vibration experiments can readily be extrapolated to complex vibration inputs.

Obviously, the model structure suggested here could be expected to apply at best over a limited range of vibration environments, since one would expect assumptions of linearity to be invalid in situations of extreme vibration. Consequently, further experimentation and analysis is suggested to determine the range of applicability of the model and to identify model refinements that might extend this range.

REFERENCES

1. Allen, R. W., H. R. Jex, and R. E. Magdaleno, "Manual Control Performance and Dynamic Response During Sinusoidal Vibration", AMRL-TR-73-78, Wright-Patterson Air Force Base, Ohio, October 1973.

2. Levison, W. H., "Analysis of Vibration-Induced Pilot Remnant", BBN Report No. 2608, Bolt Beranek and Newman Inc., Cambridge, Massachusetts, August 1973.

3. Kleinman, D. L., S. Baron, and W. H. Levison, "An Optimal Control Model of Human Response Part I: Theory and Validation", Automatica, Vol. 6, pp. 357-369, Pergamon Press, 1970.

4. Kleinman, D. L., S. Baron, and W. H. Levison, "A Control Theoretic Approach to Manned-Vehicle Systems Analysis", IEEE Transactions on Automatic Control, Vol. AC-16, No. 6, December 1971.

5. Levison, W. H., "The Effects of Display Gain and Signal Bandwidth on Human Controller Remnant", Wright-Patterson Air Force Base, Ohio, AMRL-TR-70-03, March 1971.

6. Cooley, J. W., J. W. Tukey, "An Algorithm for the Machine Calculation of Complex Fourier Series", Mathematics of Computation 10, No. 90, pp. 297-301, April 1965.

74-28,209#27

FLY AND FIGHT: PREDICTING PILOTED PERFORMANCE IN AIR-TO-AIR COMBAT

Thomas R. Harvey* and James D. Dillow
Air Force Institute of Technology
Wright-Patterson Air Force Base
Ohio

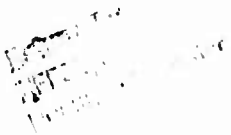

ABSTRACT

The two dimensional, longitudinal dynamics of an air-to-air combat tracking task with a lead computing optical sight system were simulated on an analog computer. Three pilots flew three different aircraft configurations in a fixed base simulator. The target motion was simulated by zero mean, filtered, gaussian noise with rms amplitudes corresponding to 3.5 g and 5.0 g. Range to target was constant and 3000 ft and 1000 ft ranges were simulated. Averaged rms data for attacker's elevator deflection, pitch rate, lead angle, line of sight to the target, and tracking error was taken for each case.

A closed loop model for the air-to-air combat task is developed using an optimal model for the pilot. The optimal model accounts for inherent human limitations such as neuromuscular dynamics, reaction time delay, and visual acuity. The pilot model is optimal in the sense that feedback gains in the model are selected to minimize a quadratic function of tracking error, error rate, lead angle rate, and elevator deflection rate.

The rms values of the attacker's elevator deflection, pitch rate, lead angle, line of sight to the target, and tracking error for the model are compared to the simulation data. The analytic values of rms pitch rate tended to be slightly higher than the values from the simulation; however, the trends agree quite well. The analytic values of rms tracking error are in general agreement with the simulation results and in every case the difference between the analytic value and simulation value is less than the visual threshold of the pilot. The analytic values of rms elevator deflection, lead angle, and line of sight agree quite precisely with the measured values. It is concluded that the model can be used to predict pilot-vehicle performance in the air-to-air combat task simulated.

---

*Currently assigned to the Air Force Systems Command, Satellite Control Facility, Sunnyvale, California.

INTRODUCTION

The task of accurately tracking a maneuvering target for the purpose of obtaining a kill with airborne cannon fire is one of the most difficult required of a fighter pilot. As is the case when firing any projectile at a moving target, lead for target motion must be computed and the aiming direction adjusted to compensate accordingly. Further complicating the air-to-air problem, trajectory adjustments must be made to account for projectile drag, velocity jump, and gravity drop, as well as other more minor effects. In most modern fighter aircraft, the required lead compensation is continuously computed using air data information and displayed on a heads up display. The lead information is normally presented to the pilot of the attacking aircraft in the form of a pipper that is two mils in diameter and is surrounded by a larger circle called the reticle. The pipper is depressed from the weapon line by the amount of the computed lead angle as shown in Fig. 1. When the pilot maneuvers his aircraft in such a manner as to place the pipper on the target, he has achieved the proper aiming direction to insure a kill provided the target maneuver remains constant. A sight of this type is called a lead computing optical sight (LCOS).

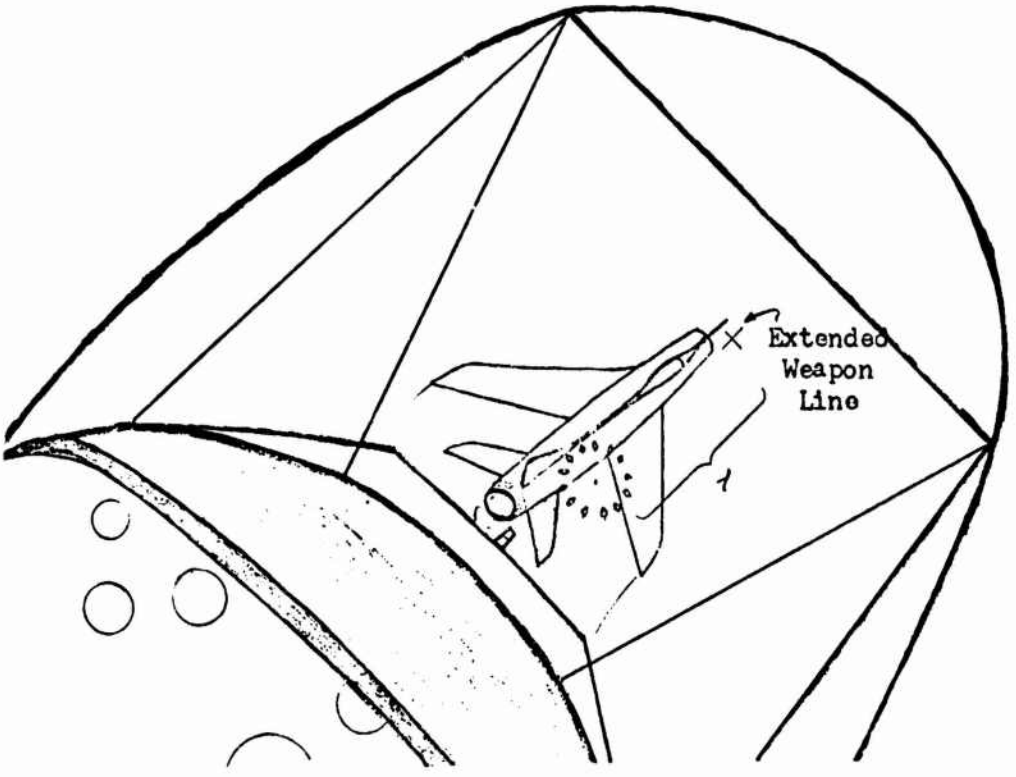

Fig. 1. Air-To-Air Tracking as Seen by Pursuing Pilot at Close Range (Approximately 1000 Feet).

Two practical problems are encountered with the sight design. First, the lead computation is an approximation and there is usually a trade off between the accuracy of the computed lead and the time lag introduced by the computation time. Secondly, the continuous lead computation creates sight dynamics or motio. of the pipper that may be confusing or unsuitable to the pilot. For example if the sight dynamics are lightly damped, the pilot may have to exercise special care to avoid pilot induced oscillations (PIO). The overall effect of adverse sight dynamics can be a reduction in the aiming accuracy despite the fact that the lead computation is reasonably accurate.

It would be extremely desirable to have a reliable method for analytically predicting piloted performance in an air-to-air combat situation. In this way, the trade offs involved in computing lead could be evaluated using the closed loop dynamics of the pilot-vehicle system. The sight parameters could be optimized and the suitability of the sight dynamics in the closed loop tracking task could be evaluated. Furthermore, this could be done without resorting to extensive simulation or flight tests.

A simplified model for the closed loop air-to-air combat task has been developed and validated by experimental data. This work is described in this paper. First the piloted simulation study that was used to collect data for an air-to-air combat task is described. The equations are given and the assumptions delineated. A control theoretic optimal pilot model is used to develop an analytic model for the task. This model is briefly described and the representation of human limitations used in the model are given. A comparison of the experimental and analytic results are given as a demonstration of the model's validity.

SIMULATION

The two dimensional, longitudinal dynamics of an air-to-air combat tracking task with a lead computing optical sight were simulated. The in plane geometry for the air-to-air tracking situation is shown in Fig. 2. The following notation is used in Fig. 2:

V_A - velocity of attacker (ft/sec)

V_T - velocity of target (ft/sec)

γ_A - attacker flight path angle (radians)

γ_T - target flight path angle (radians)

α - attacker angle of attack (radians)

θ - attacker pitch angle (radians)

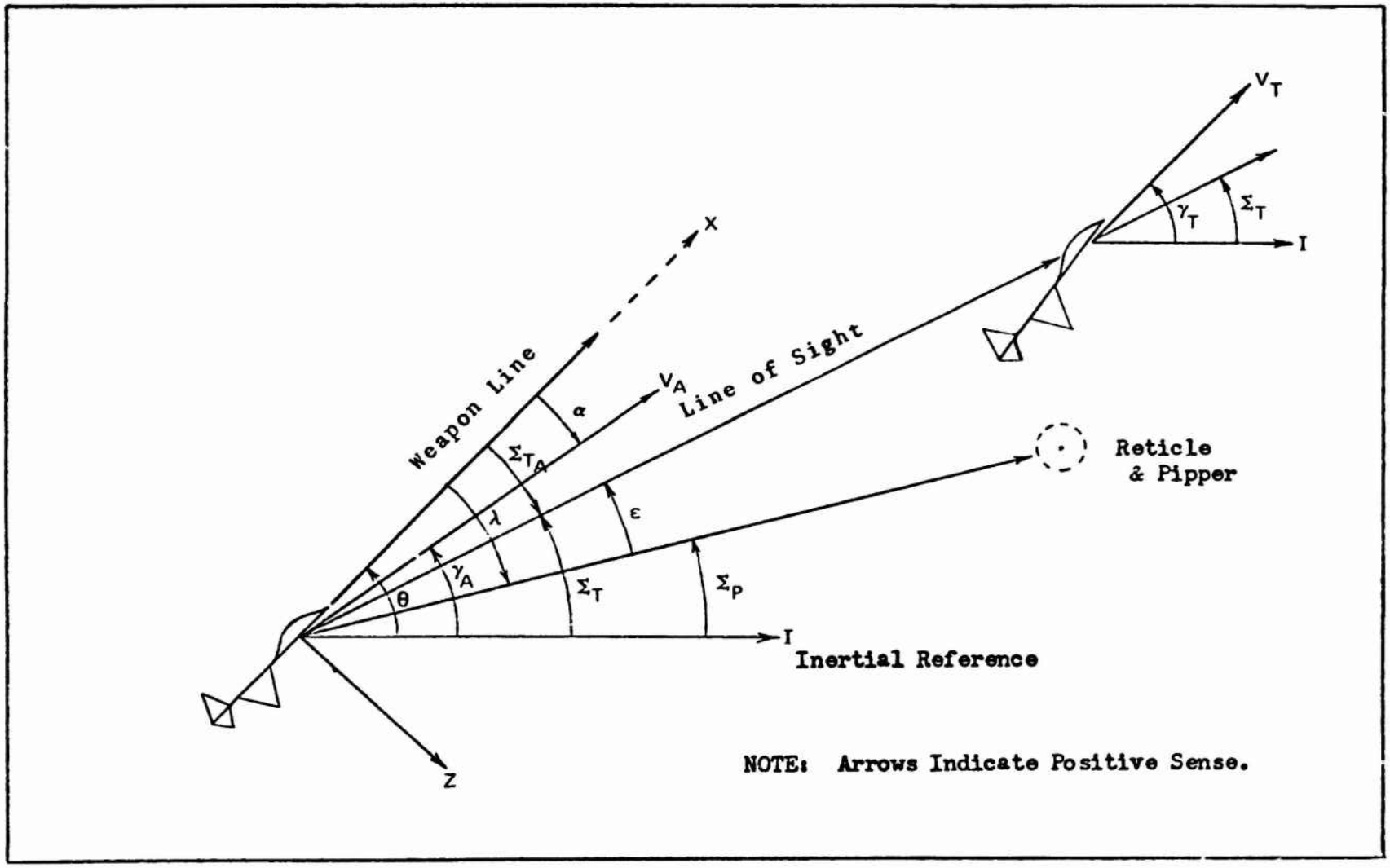

Figure 2. Air-To-Air Tracking Geometry.

Σ_{T_A} - relative line of sight angle (radians)

λ - lead angle (radians)

ϵ - error (radians)

Σ_T - inertial line of sight angle (radians)

Attacking Aircraft Equations

The equations of motion of the attacking aircraft are approximated by the linearized longitudinal short period equations of motion. These are

$$\dot{\alpha} = q + Z_\alpha \alpha + Z_\delta \delta$$

$$\dot{q} = M_q q + M_\alpha \alpha + M_{\dot{\alpha}} \dot{\alpha} + M_\delta \delta$$

$$\dot{\theta} = q$$

where

q - pitch rate (radians/sec)
δ - elevator deflection (radians)

The constants Z_α, Z_δ, M_q, etc., are stability derivatives associated with a given aircraft and flight condition.

Elevator actuator dynamics are modeled by a first order lag,

$$\dot{\delta} = -20\delta + 20K_L\delta_c$$

where δ_c is commanded elevator position and K_L is the control linkage gain. A force stick was used in the simulation and $-\delta_c = K_f F_s$ where F_s is force applied by the pilot and K_f is the force stick sensitivity. K_f was adjusted to insure the pilot had as much control authority as he wanted.

Target Equations

The target was assumed to be a fighter aircraft and the target's normal acceleration, A_{nT}, was modeled by driving a second order filter with zero mean, gaussian white noise. The equations are

$$\dot{y} = -\frac{1}{\tau_T} y + \xi$$

$$\dot{A}_{nT} = -\frac{1}{\tau_T} A_{nT} + y$$

$$\dot{\gamma}_T = -.01\gamma_T - \frac{1}{V_T} A_{nT}$$

The dummy variable y is used to put the equations in first order form and ξ is the white noise input. The $-.01\gamma_T$ term in the target flight path differential equation is an artificial feedback used to keep the steady state variance of γ_T finite. A value of $\tau_T = 3$ sec was used because it resulted in a target motion that looked good.

The inertial line of sight from the attacker to the target is given by (Ref 1)

$$\dot{\Sigma}_T = \frac{1}{D} [\vec{s} \times \vec{V}_T - \vec{s} \times \vec{V}_A]$$

where $\vec{s}$ is a unit vector along the line of sight and D is the distance between the attacker and the target. Assuming motion only in the plane,

$$\dot{\Sigma}_T = \frac{V_T}{D} \sin (\gamma_T - \Sigma_T) - \frac{V_A}{D} \sin (\theta - \Sigma_T - \alpha)$$

Assuming that the velocity vectors of the attacker and the target are closely aligned with the line of sight, small angle approximations can be used to arrive at

$$\dot{\Sigma}_T = \frac{V_A}{D} \alpha + \frac{V_A - V_T}{D} \Sigma_T + \frac{V_T}{D} \gamma_T - \frac{V_A}{D} \theta$$

In the simulation, the closing velocity, $V_A - V_T$, was taken to be zero and D was assumed to be constant. This restriction was made so that the simulation equations would not be time varying.

Sight Equations

The sight equation is taken from Ref 1 and a more detailed derivation is contained in Ref 2. The differential equation for lead that was used is

$$\dot{\lambda} = -\frac{1}{T_f} \lambda + q - \frac{V_A}{V_f} \frac{Z_\alpha}{2} + \frac{J_V}{T_f} \alpha$$

where

T_f - time of flight of projectile (sec)

V_f - muzzle velocity of projectile (ft/sec)

J_V - velocity jump correction angle (radians)

The velocity jump correction angle is used to compensate for the misalignment of the velocity vector of the attacker and the projectile muzzle velocity vector. The lead correction

for gravity drop is a function of roll angle. Based on the assumption that the plane of flight is not rotating, the gravity drop term will only introduce a fixed bias in the equations and not affect the rms values of the states. For this reason it was not considered in the simulation.

Display

A dual beam oscilloscope was used to display the target and the sight. The display is shown in Fig. 3. The center of the oscilloscope was taken to be the extension of the aircrafts weapon line. The target was an inverted T positioned relative to the weapon line by Σ_{TA}. The sight is positioned relative to the weapon line by λ. Only the reticle portion of sight was displayed due to the limitations of the oscilloscope. In order to accomodate the large lead angles, the display was scaled for 13° per cm. The scope was positioned 20 inches in front of the pilot.

Cases Simulated

Twelve cases were considered by considering all combinations of three aircraft dynamics, two ranges, and two rms normal accelerations for the target.

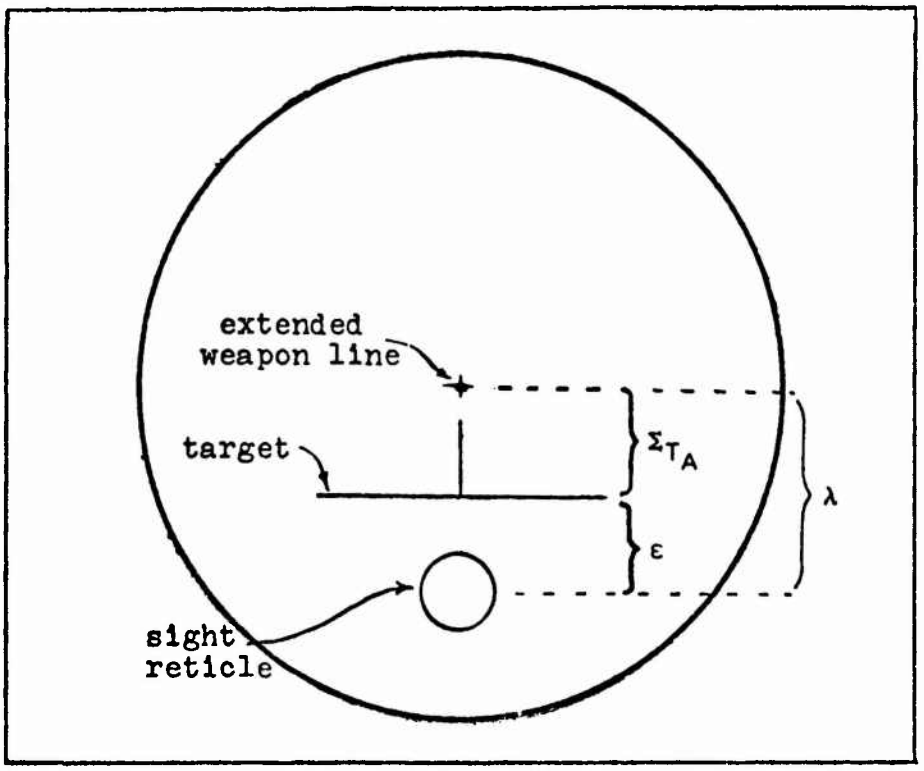

Fig. 3. Simulation Display.

The three aircraft considered were F-4E, F-5, and A-7. The aircraft and corresponding flight conditions were picked to give a range of aircraft dynamics from good to bad for the air-to-air combat tracking task.

The two ranges simulated were 1000 ft and 3000 ft. In retrospect, the 3000 ft range was not very realistic as a firing range. However, the choice was fortunate in that the sight dynamics for that range were highly oscillatory and the results were useful in developing the analytic model.

The two rms acceleration levels for the target were 3.5g's and 5.0 g's.

Test Conduct

Three military pilots were used in the simulation. All three pilots had air-to-air combat experience. Each pilot was thoroughly trained on each of the twelve cases prior to taking data. Each pilot made three data runs for each case. Different target time histories were used to keep the pilot from learning the target motion. The simulation was conducted so that data was taken only during steady state tracking over a 100 second interval. The mean and the variance of the following variables were determined: elevator deflection, pitch rate, lead angle, relative line of sight to the target, and tracking error.

PILOT MODEL

An analytic model was developed for the closed loop air-to-air combat tracking task that was simulated. The pilot was modeled by an optimal pilot model, the form of which was developed by Kelinman, Baron, and Levison (Ref 3). This model has been successfully applied to a number of other tasks including VTOL hover, landing approach, and anti-aircraft gun tracking (Refs 3 through 7). A block diagram of the optimal pilot model is shown in Fig. 4. The displayed variables, y, are observed by the pilot. Visual errors are accounted for by additive gaussian white noice, v_y. The noisy observation is delayed by time τ, which represents a perceptual time delay. The best estimate of the current state, $\hat{x}$, is reconstructed using an optimal estimator and predictor. The control is generated by multiplying the optimal estimate of the state by a set of optimal feedback gains. The feedback gains are optimal for the cost function

$$J(\delta_c) = \lim_{T\to\infty} E\{[M_\varepsilon \varepsilon(T)]^2 + [M_{\dot\varepsilon}\dot\varepsilon(T)]^2 + [M_{\dot\lambda}\dot\lambda(T)]^2 + [M_{\dot\delta_c}\dot\delta_e(T)]^2\}$$

Gaussian white noise, v_n, is added to the control output, δ'. This noise accounts for neuromuscular noise and control errors.

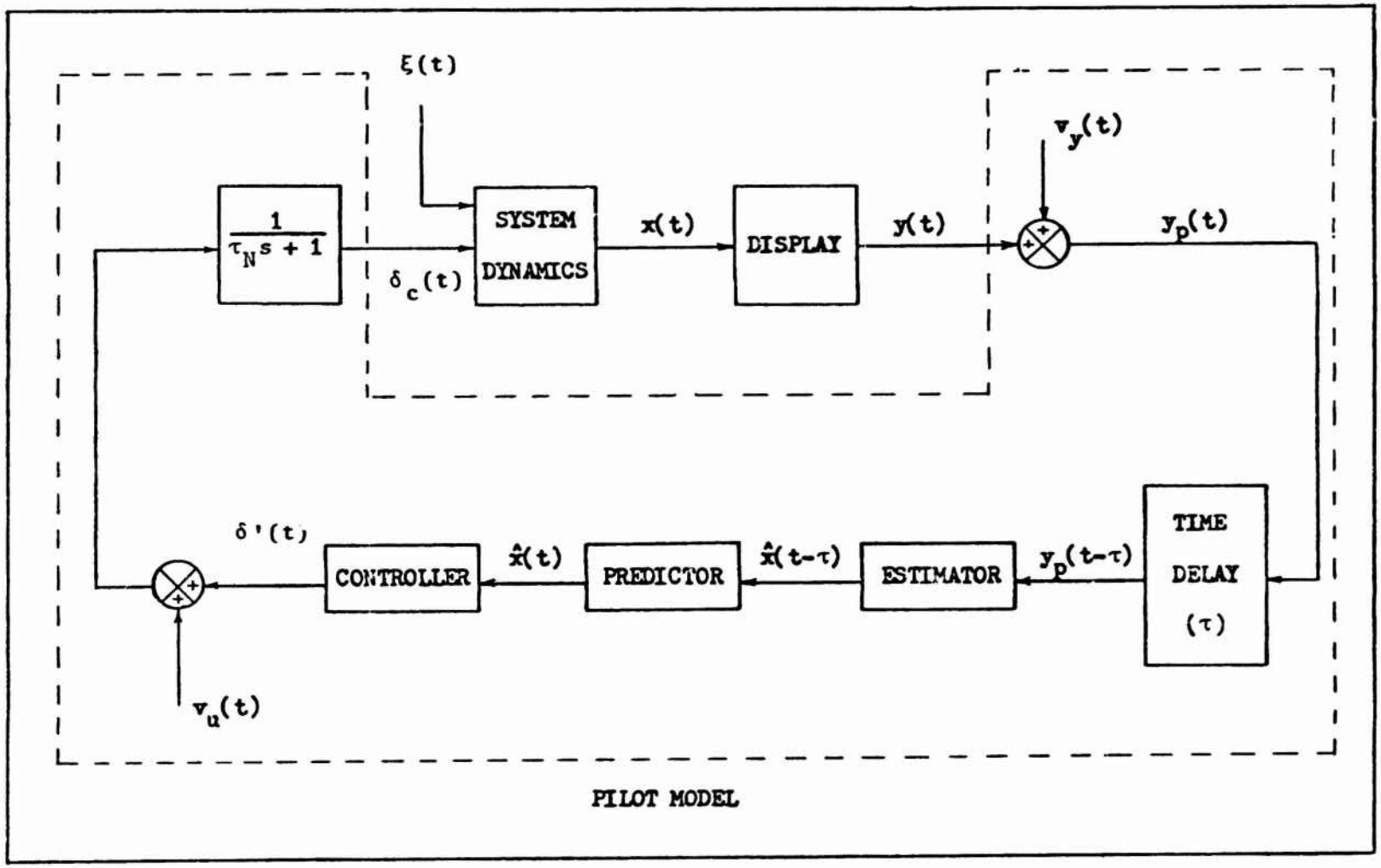

Figure 4. Functional Schematic of the Optimal Pilot Model in the Control Loop.

The pilot output, δ_c, is obtained by passing $\delta + v_n$ through a first order lag with time constant τ_N. Mathematically, the lag is a part of the optimal solution for the cost function $J(\delta_c)$ since it includes a weighting on control rate, $\dot{\delta}_c$. Physically, can be considered as a model of the lag in the neuromuscular system. The parameters that are used to define the specific model are described next.

Cost Functional Weightings

The weightings in the cost function are defined by the pilot's objective and subjective measures of goodness for the task. The primary objective in the air-to-air combat task is to minimize the error. The pilot will also avoid excessive error rate since it induces undesirable oscillations in the error. The first WAG that was tried was $M_\varepsilon = M_{\dot{\varepsilon}}$, $M_\lambda = 0$. This worked well for the 1000 ft cases, but the analytic values of rms error for the 3000 ft cases were way too low. The pilots were asked what they did different at 3000 ft than at 1000 ft. It turned out that the sight was extremely oscillatory at the 3000 ft range and the pilots had to be very careful not to cause the sight to oscillate. This subjective consideration is treated by weighting lead rate. The values used are related by

$$M_{\dot{\varepsilon}} = \frac{1}{4} M_\varepsilon$$

$$M_{\dot{\lambda}} = \frac{1}{2} M_\varepsilon$$

The value of M_ε is arbitrary.

The weighting on control rate, $M_{\dot{\delta}_c}$, is set to a value that yields $\tau_N = .1$ sec. This value of τ_N is consistent with prior applications of the optimal pilot model (Refs 3 through 7).

Observation Noise

Error and lead are observed by the pilot. In accordance with the model ground rules, it is assumed that the first derivative of the displayed variable are perceived by the pilot (Ref 3). Thus the output vector is

$$y_1 = \varepsilon$$

$$y_2 = \dot{\varepsilon}$$

$$y_3 = \lambda$$

$$y_4 = \dot{\lambda}$$

Denoting

$$E\{v_{yi}(t)v_{yi}(s)'\} = V_{yi}\delta(t-s), i=1,\ldots,4$$

the observation noise is scaled to the rms magnitude of the observation by

$$V_{yi} = \pi\rho_v\sigma_{yi}^2$$

A value of $\rho_v = .01$ was used and is consistent with the value used in Refs 3 through 7. (This corresponds to a -20dB white noise power spectral density level.)

Threshold Effects

Threshold effects associated with visual acuity and the ability to percieve motion were considered in the model. These effects turn out to be significant for this simulation because of the way the display was scaled. To account for the visual thresholds, the percieved output, y_{pi}, is expressed as

$$y_{pi}(t) = f_i[y_i(t)] + v_{yi}(t)$$

where

$$f_i(y) = \begin{cases} y-a_i, & y \geq a_i \\ 0, & -a_i \leq y \leq a_i \\ y+a_i, & y \leq -a_i \end{cases}$$

and a_i is the threshold level. Describing function theory (Ref 8) is used to determine a scale factor k_i as a function of a_i so that the effect of the nonlinearity can be approximated by an increase in the observation noise as follows:

$$y_{pi}(t) = y_i(t) + k_i v_{yi}(t)$$

A typical value for the human threshold for position is .05° of visual arc (Refs 5 and 7). For the position of the pilot and the display scale factor in the simulation, this gives theshold levels of

$$a_\varepsilon = a_\lambda = .65°$$

A threshold for human rate perception of .05-.1° visual arc/sec is suggested in Ref 5; however, no specific value was used. In Ref 7, a value of .18° visual arc/sec was used. In this study a value of .15° visual arc/sec for the rate threshold was used. It was found that lower values did not result in as good agreement between the simulated and analytic values of rms error. The value of .15° visual arc/sec results in rate thresholds of

$$a_\varepsilon^* = a_\lambda^* = 1.95°/sec$$

Time Delay

The pilot time delay was taken to be $\tau = .2$ sec. This value is consistent with Refs 3 through 7.

Neuromuscular Noise

Denoting

$$E\{v_u(t)v_u(s)\} = V_u\delta(t-s)$$

The neuromuscular noise is scaled to the rms magnitude of the pilot output by

$$V_u = \pi\rho_u\sigma_{\delta_c}^2$$

Values for ρ_u of from .003 to .01 are suggested in Refs 3 through 7. It was found that better agreement between the simulation and analytic rms values of error was obtained with $\rho_u = .002$. This corresponds to a white noise power density level of -27dB. There are two possible reasons that the neuromuscular noise had to be relatively small in the pilot model. First, a force stick was used in the simulation. The force stick is a very linear transducer and any errors due to stick nonlinearities are virtually eliminated. Secondly, the pilots selected stick sensitivites that were optimal and control errors should therefore be minimized.

RESULTS

The rms values of the attacker's elevator deflection, pitch rate, lead angle, line of sight to the target, and tracking error for the model are compared to the simulation data in Figs. 5 through 9. The comparisons are made via scatter diagrams. It can be seen from Fig. 6 that the analytic values of rms pitch rate are slightly higher than the simulation values. The trend is excellent, however. The analytic values of rms tracking error are in general agreement with the simulation results (Fig. 9). It may be noted that in every case, the difference between the analytic values and simulation values of rms error is less than the error threshold value of .65 degrees. The agreement between analytic values and simulation values of rms elevator deflection, lead angle, and line of sight is excellent.

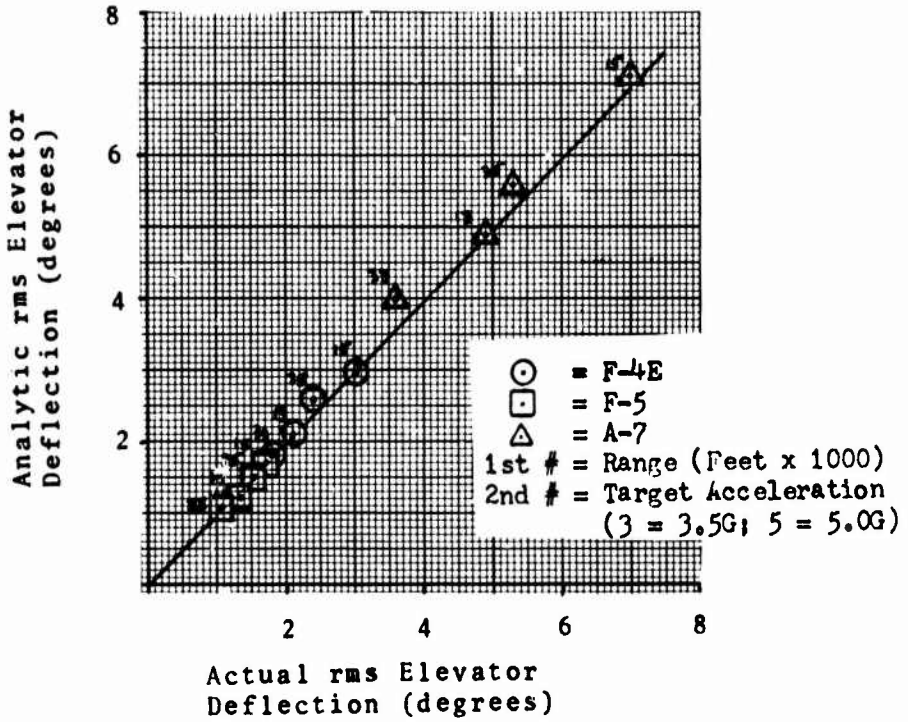

Fig. 5. Comparison of Actual and Analytic Values of rms Attacker's Elevator Deflection, δ.

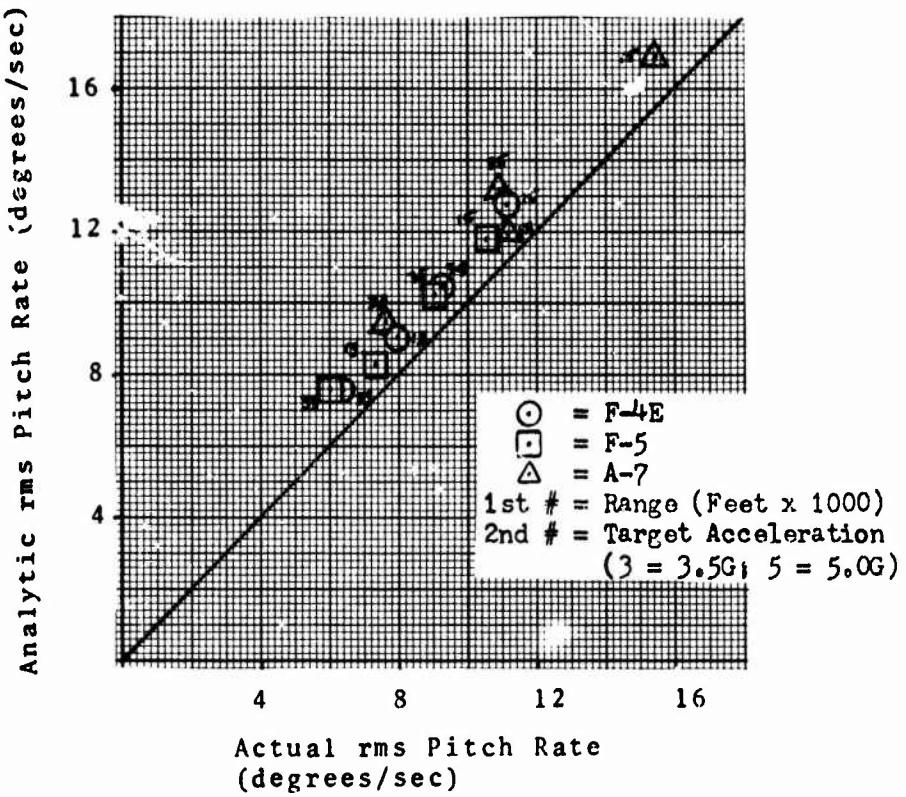

Fig. 6. Comparison of Actual and Analytic Values of rms Pitch Rate, q.

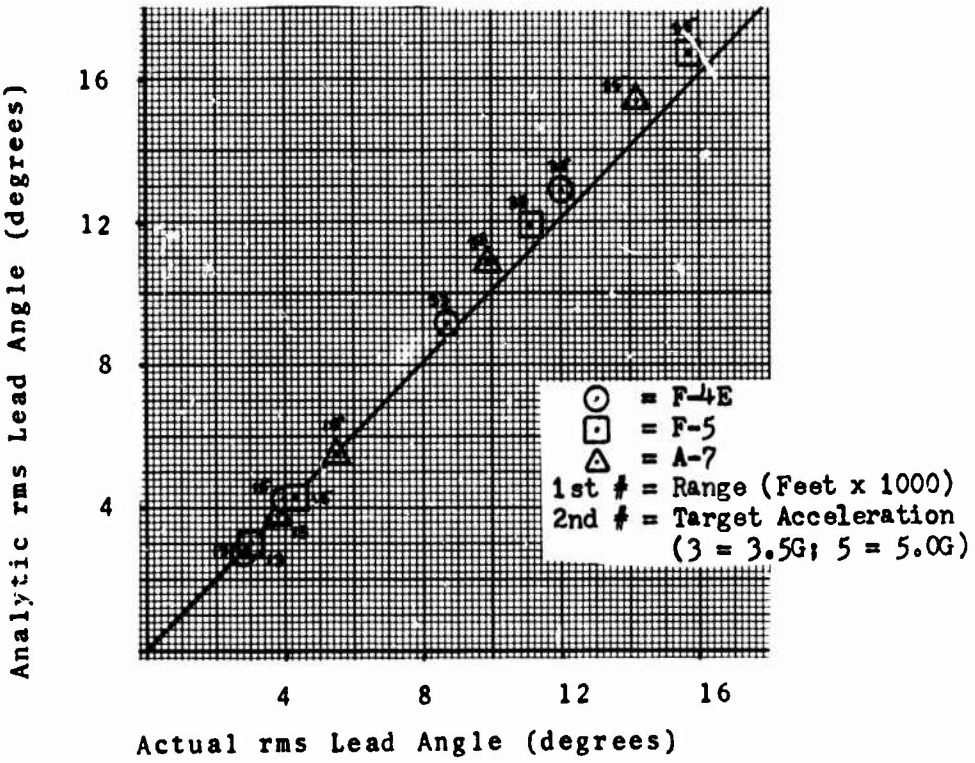

Fig. 7. Comparison of Actual and Analytic Values of rms Lead Angle, λ.

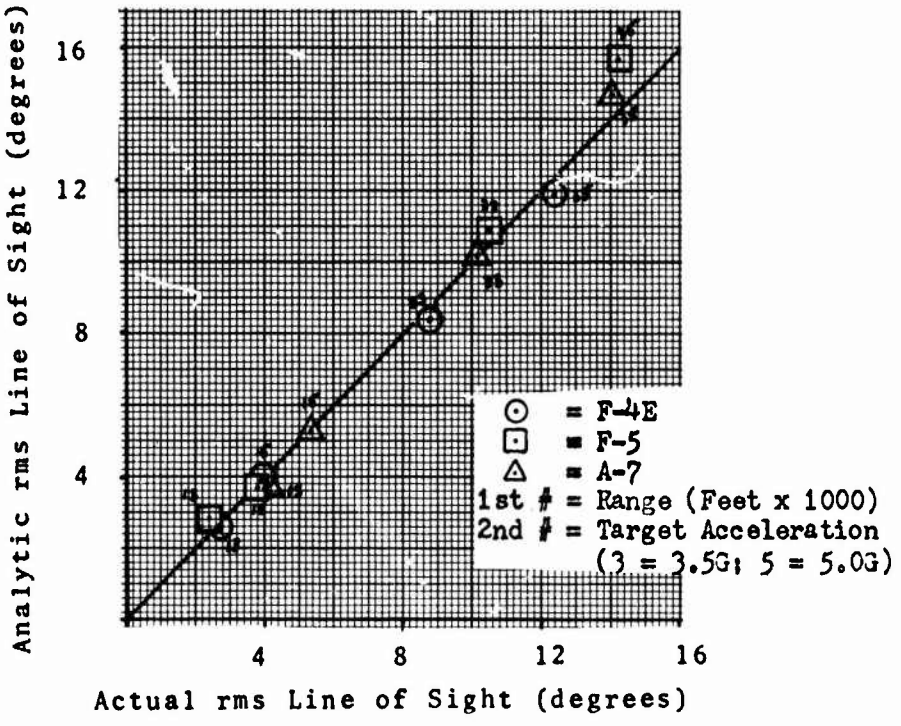

Fig. 8. Comparison of Actual and Analytic Values of rms Line of Sight, Σ_{TA}.

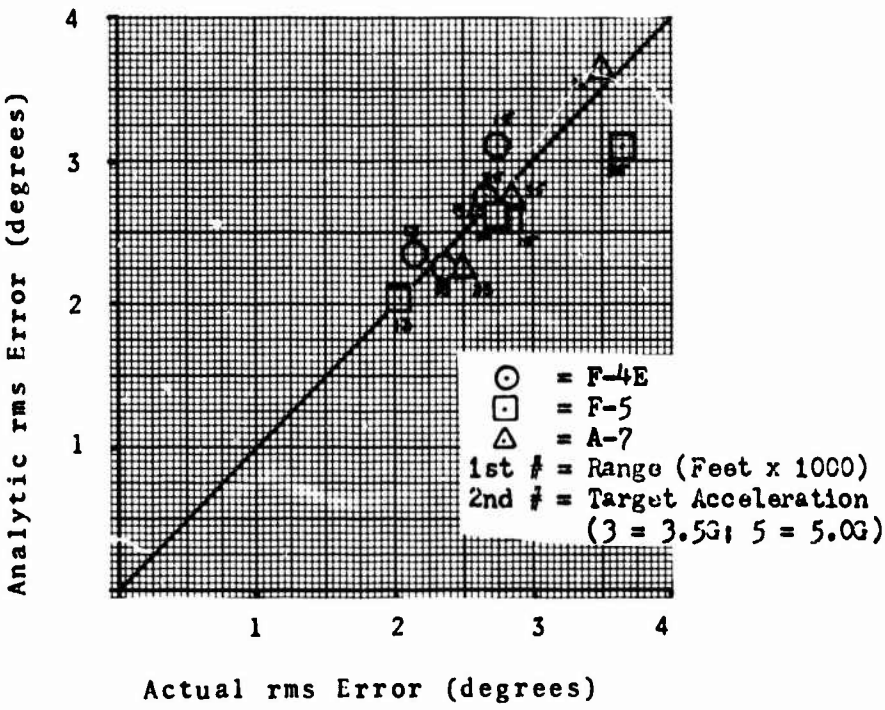

Fig. 9. Comparison of Actual and Analytic Values of rms Error, ε.

CONCLUSIONS

The major conclusion is that the model worked! The model provided a faithful reproduction of those results that were measured in the simulation. The model was reasonably simple to develop. The analytic values of rms error and pitch rate are senstivie to the choice of weightings on state in the cost function, i.e., M_{ε}, $M_{\dot{\varepsilon}}$, and $M_{\dot{\lambda}}$. The values used were established after three trials and were picked so the data matched. It may have been possible to pick the values a priori by judicious questioning of the pilots. The rms value of error was also sensitive to the neuromuscular noise level. The lower value of ρ_u, corresponding to -27dB white noise power density level for the neuromuscular noise, is probably reasonable for an ideal linear control input device. A value of -25dB was used in Ref 6 and the control device was nonlinear. All other parameters used in the pilot model were basically taken from previous applications of the optimal pilot model.

It is not definite at this point if the simulation described, and hence the analytic model, is a suitable representation of the actual air-to-air combat tracking task. The pilots indicated that the dynamics in the simulation were representative of actual aircraft and sight dynamics. However,

there are some way out assumptions (linear equations, time invariance, in plane motions, etc.) which can not be justified in an off handed manner. The next order of business is to determine if the simple model described in this paper can be used to predict performance in the actual air-to-air combat tracking task. If not, the model can be extended to include lateral dynamics and three dimensional kinematics. If it is necessary the time varying dynamics can be included in the model as in Ref 7 and even nonlinearities can be accounted for in the model as in Ref 6.

REFERENCES

1. Quinlivan, R. P. Multimode Flight Control Definition Study for Precision Weapon Delivery. AFFDL-TR-71-39. Wright-Patterson Air Force Base, Ohio: Air Force Flight Dynamics Laboratory, June, 1971.

2. Harvey, Thomas R. Application of an Optimal Control Pilot Model to Air-to-Air Combat. AFIT Thesis, GA/MA/74M-1. Wright-Patterson Air Force Institute of Technology, March 1974.

3. Baron, S., et al. Application of Optimal Control Theory to the Prediction of Human Performance in a Complex Task. AFFDL-TR-69-81. Wright-Patterson Air Force Base, Ohio: Air Force Flight Dynamics Laboratory, March, 1970.

4. Kleinman, D. L., S. Baron, and W. H. Levison. "An Optimal Control Model of Human Response, Part 1," Automatica, 6:357-363 (May 1970).

5. Kleinman, D. L. and S. Baron. Analytic Evaluation of Display Requirements for Approach to Landing. NASA CR-1952. Washington: National Aeronautics and Space Administration, November, 1971.

6. Kleinman, D. L. and R. Perkins. "Modelling the Human in a Time-Varying Anti-Aircraft Tracking Loop." Submitted for publication in IEEE Transactions on Automatic Control, May 1973.

7. Levison, W. H. and D. L. Kleinman. Analysis of Pilot/System Performance in Carrier Approach. Cambridge, Massachusetts: Bolt Beranek and Newman, Inc., September, 1971.

8. Graham, Dunstan, and Duane McRuer. Analysis of Nonlinear Control Systems. New York: Dover Publications, Inc., 1971.

74-28,209 #28

DESIGN OF A MANUAL CONTROL SYSTEM FOR A STOL AIRCRAFT ON MICROWAVE LANDING SYSTEM CURVED APPROACHES

Dr. Thomas B. Cunningham
Honeywell, Inc.
Minneapolis, Minnesota

Dr. Robert L. Swaim
Associate Professor of Aeronautics and Astronautics
Purdue University
West Lafayette, Indiana

Abstract

Potentially more complex and demanding maneuvers during instrument landing approaches may be fostered by microwave landing guidance systems of the future. A flight control system is designed for a STOL aircraft (Breguet 941) which would allow a pilot to follow curved approach paths while subjected to turbulence and initial approach position errors. The performance index is the expected value of a weighted integral quadratic sum of state and control variables.

The pilot-in-the-loop design results in a closed-loop system which sends an optimal sum of aircraft and pilot states to the display command. It takes into account pilot response limitations and makes use of pilot model parameter values known to evoke good pilot ratings.

The system model includes aircraft, pilot, and control dynamic models, as well as gust disturbance and measurement noise models. Noise is also inserted to account for the pilot's multi-axis workload.

Limited state feedback theory is used to produce a control structure which does not include certain prespecified state variables. A unique algorithm for calculating the limited state feedback gain matrix is developed.

Frequency response techniques are used to test the designed system for evaluation of handling qualities. A nonlinear digital simulation is performed to test the total system design. Results acceptable for Category II-B landing approach were obtained.

This paper is a condensed version of work reported in greater detail in Reference 17.

Research sponsored in part under NASA Engineering Systems Design Traineeship Grant NGT-15-005-61.

INTRODUCTION

Congestion in the airport terminal area has resulted in much research related to improving approach accuracy and increasing aircraft landing rates. One new landing aid is the scanning beam microwave instrument landing system (MLS) [1,2] which will replace the current ILS. The MLS has a number of interesting properties which have fostered research into ways of employing the system to its utmost capabilities. The scanning property enables design of curved and broken trajectories which add new possibilities for separation investigations and noise abatement approaches.

Curved trajectories are particularly interesting as they afford an extra separation dimension, i.e., lateral spacing for different speed classes [3]. This situation has been investigated [4] as a minimum time to landing for a two and a three aircraft optimization problem.

Given a specified trajectory, the problem becomes one of following the approach track. An aircraft is faced with numerous inputs which tend to force it off the desired path. These are steady winds and shears, wind gusts, collision avoidance possibilities, piloting technique, and errors in measurements. In addition, the assurance of a fast tract capture for initial position and attitude errors is an important consideration.

Cherry, et. al., [23] investigated attitude commands to compensate for steady winds. Although there are numerous published works on collision avoidance, the task of collision prevention or strategic avoidance is best served by insuring the most accurate path following in the face of the other inputs.

Trajectory path following requires a closed-loop design which commands reasonable control effort and produces minimum path deviation. The design must yield acceptable pilot responses and opinions, while retaining passenger comfort. The problem can be viewed as a feedback regulator design. There are two types of regulator problems: one is recovery from initial track errors, and the other is regulation in the face of stochastic inputs. It can be assumed, however, that initial errors can be sufficiently eliminated sometime soon after beam capture just by designing a reasonably stable system. The assumption is that the closer one gets to the critical part of the path sequence, i.e., closer to the ground, the less likely that an initial path error will still aggravate the situation. The stochastic inputs, such as wind gust and measurement noise being constantly applied throughout the trajectory, provide a much greater design challenge for regulation.

The design criterion of a control system of this type is appropriate path error achievement in relation to the FAA Category II window. Pilot acceptance, in terms of a good pilot rating, is also important. The first criterion will be investigated by examining the three-sigma standard deviation position response, i.e., 99.74% probability of never exceeding. The pilot acceptance requirement will be checked by comparing the designed systems parameters with those associated with a given pilot rating [5]. One can also get a qualitative feel for passenger comfort by examining the aircraft attitude responses.

Another important aspect of the problem is the dynamic coupling of the longitudinal and lateral modes of flight during high bank maneuvers. Conventional control design techniques make use of the convenient de-coupling of the plant dynamics under zero bank flight. For the new curved trajectories one must account for the steady state bank commands given, if not by appropriate compensation, then by verification of designed feedback gains, i.e., those designed with uncoupled dynamics.

PROBLEM FORMULATION

Since visual displays can prescribe the control commands for a pilot to operate on, the idea of using a pilot model in the synthesis process, rather than just the evaluation process, gains validity. Conventional displays, i.e., using predetermined display variables, have been designed in this fashion [6,7]. The pilot model used most often is the McRuer Crossover model. It has been discovered that, like the consistency of plant model parameter variation versus pilot rating, there is a correlation between pilot rating and pilot model parameters [8,9,10,11].

The objective of this work is to determine a display variable set which best achieves the design goals stated earlier. These display variables would be presented as control commands on a display screen, but no attempt is made in the present work to specify how these commands are presented. William Seitz [12] did much work on this aspect of the problem through the comparison of the flight director mode versus a control director design.

Also assumed at the outset is that each display command will not be a function of just one variable, e.g., pitch error to command the elevator, but the commands will be a linear function of many states, e.g., position, velocity, pitch angle, pitch rate, etc. entering into the elevator command. This idea is called a quickening display and was originated by Muckler and Obermayer [11]. Seitz employed this idea in designing a display setup. He used optimal feedback to specify the quantity of each state used in a control command. The optimal control idea spurred this current effort.

The use of optimal control theory requires that the number of measurements or unique combinations of states equals the order of the controllable system. There is, however, theory [13,14] developed allowing the designer to choose a smaller set of output variables for feedback which allows one to eliminate states which are inconvenient to measure. Perhaps more importantly, limited state feedback allows insertion of the pilot into the overall design plant without requiring that his state variables be measured for use in the control commands.

Because the output signals are optimally combined for display, the position of the pilot in the feedback loop is between the aircraft dynamic plant and the feedback control gain matrix as shown in Figure 1. The appearance of a remnant term, exponentially correlated noise, accounts for the pilot's additional workload, i.e., multiaxis task with instrument scanning.

It has been shown that for a human tracking task, the pilot response is rated proportionally to his perception of how well he is doing [9]. The idea, however, is implicit in that once designed it is hoped that the real pilot will perform similar to the design model and give the rating commensurate with these dynamics. The design verification used is an examination of the open-loop frequency response of the aircraft and pilot using the designed control commands. This is done because the open-loop system response indicates possible pilot rating trends [8,5].

The aircraft which served as the design vehicle was the Breguet 941 STOL airplane. The possibility of a high approach flight path angle and slow speed provides one with a good challenge for stochastic regulation.

MODEL DEVELOPMENT

The use of optimal quadratic control theory allows the designer to specify the goals of the tracking mission in the performance index. The one used here is

$$J = E\{\lim_{t_f \to \infty} \frac{1}{t_f} \int_0^{t_f} [x^T(t)Qx(t) + u^T(t)Ru(t)]dt\} \tag{1}$$

where x(t) is the n dimensional state vector subject to the differential constraint

$$\dot{x}(t) = Ax(t) + Bu(t) + G\eta \tag{2}$$

u(t) is the control vector. η is a random input noise (gaussian-white) vector. The matrices A, B, and G contain the plant parameters and may be functions of time.

Many physical situations can be included in the plant matrices A, B and G. The system to be controlled can also contain many subsystems. The plant for this problem is composed for four subsystems: the aircraft and control dynamics, pilot dynamic model, gust dynamic model, and models of measurement noise and filter dynamics.

The aircraft vector has twelve states for this work. This is the continuous perturbation approach which represents both the translational and rotational dynamics of the aircraft. In state-matrix form this is

$$\dot{x}_a = A_a x_a + B_a x_c + G_a x_g \tag{3}$$

x_c is the control input state vector, x_g is the gust input vector, and x_a is the aircraft state vector.

$$x_a = \begin{bmatrix} x, \text{ position perturbation in forward direction} \\ y, \text{ position perturbation in lateral direction} \\ z, \text{ position perturbation in vertical direction} \\ \dot{x}, \text{ velocity perturbation in forward direction} \\ \dot{y}, \text{ velocity perturbation in lateral direction} \\ \dot{z}, \text{ velocity perturbation in vertical direction} \\ p, \text{ perturbated roll rate} \\ q, \text{ perturbated pitch rate} \\ r, \text{ perturbated yaw rate} \\ \phi, \text{ perturbated roll angle} \\ \theta, \text{ perturbated pitch angle} \\ \psi, \text{ perturbated yaw angle} \end{bmatrix} \tag{4}$$

Although this dynamic description is not an explicit function of time, the theory allows changes in steady-state roll angle ϕ_o and yaw rate ψ_o as they are assumed to be functions of time. This will be important for investigations of curved approaches. A detailed description of this plant for the Breguet aircraft is given elsewhere [17].

The pilot model used is both simple and demanding. A survey of past and current literature [8,9,10,15,5] reveals that a pilot will behave in a predictable manner under certain conditions. Given a continuous control task requiring human responses within predetermined physical limitations, a pilot will perform in a single axis according to the following transfer function [9]:

$$\text{P.T.F.} = \frac{K_p(T_D s+1)}{(T_L s+1)} e^{-T_N s} \tag{5}$$

To use this transfer function in the linear system form proposed, one must approximate the pure delay term with the Padé [16] first order form.

$$e^{-T_N s} = \frac{(\frac{2}{T_N} - s)}{(\frac{2}{T_N} + s)} \tag{6}$$

The T_D term is a lead corresponding to the pilot's anticipation of commands and is set to zero in the design as lead tends to degrade the pilot rating. A value of $T_N = 0.3$ sec allows ample margin for cerebral computation and muscular reaction time, while a value of $T_L = 0.1$ sec allows for a little "laziness" in control movements.

The gain K_p is adjusted by the pilot to set the control task frequency demands into a desirable range for his manipulation. This parameter varies somewhat with the individual pilot and can be adjusted independently of the design phase for best ratings. A unit value will be used here.

Putting this into state-matrix form yields the following vector-matrix differential equation:

$$\dot{x}_{pi} = A_{pi}x_{pi} + B_{pi}u \tag{7}$$

where

$$x_{pi} = \begin{bmatrix} p_{\delta e1}, \text{ pilot stick deflection to elevator} \\ p_{\delta e2}, \text{ second pilot elevator deflection state} \\ p_{\delta a1}, \text{ pilot stick deflection to aileron} \\ p_{\delta a2}, \text{ second pilot aileron deflection state} \\ p_{\delta r1}, \text{ pilot control deflection to rudder} \\ p_{\delta r2}, \text{ second pilot rudder deflection state} \end{bmatrix} \tag{8}$$

Since the pilot is asked to perform a tracking task in three axes, the pilot model must somehow account for this increased workload and the coupling of the tasks. Significant work in this area, [9,10,6], has been done, and it has been demonstrated that one can account for multi-axis tasks by employing a pilot remnant, i.e., extra noise input to simulate a human's input to a given task which is uncorrelated to any direct command given to him.

The development of the remnant model is detailed by Graham, et. al., [6] with the specific parameters chosen for this work outlined elsewhere [17]. The remnant allows for display observation in three axes while the crossover model only accounts for each one independently. The parameter values chosen for this work also allow for approximately 22% for scanning time of the other instruments.

This correlated noise can be written in vector-matrix form.

$$\dot{x}_r = A_r x_r + G_r \eta_r \tag{9}$$

where

$$x_r = \begin{bmatrix} P_{er}, \text{ elevator input remnant} \\ P_{ar}, \text{ aileron input remnant} \\ P_{rr}, \text{ rudder input remnant} \end{bmatrix} \tag{10}$$

$$E[\eta_r] = 0, \; E[\eta_r \eta_r^T] = I$$

The use of these pilot and remnant models is contingent upon the single most critical assumption of this work: a system design using a well-behaved, somewhat contented, human operator model will evoke similar responses from pilots in actual application of the designed system.

The necessity of accurate control of aircraft on landing approach demands adequate compensation for all inputs into the system. Because wind gusts provide an intense stochastic disturbance, the treatment of this input requires most careful consideration.

Gusts are inserted into the plant as gaussian random variables which are added to their respective state variables forming the total plant input. This is illustrated with the angle of attack state

$$\alpha = \alpha_a + \alpha_g \tag{11}$$

The Dryden spectral form [18] provides the appropriate representation for linear analysis. This form is recommended by the FAA [19] and military [18] for use in control systems design and analysis.

Table 1 contains the gust response levels used for this investigation.

Standard Deviation (direction)	Value
σ_u(forward)	10 ft/sec
σ_v(lateral)	10 ft/sec
σ_w(vertical)	6.5 ft/sec

Table 1. Gust Parameters

Again, for this linear analysis the state variable approach can be used.

$$\dot{x}_g = A_g x_g + G_g \eta_g \tag{12}$$

x_g is an eighth order vector containing one forward velocity state, two lateral, two vertical, and a state for each of the three rotational gusts.

The control surfaces, as well as the throttle, cannot respond instantaneously to commands. The dynamic models used were first order lags representing the approximate delays. For all control surfaces, elevator, aileron and rudder, the time constants were chosen to be 0.1 second. For the throttle delay a time constant of one second was used. In vector-matrix form these dynamics become

$$\dot{x}_c = A_c x_c + B_{th} u_{th} + B_c x_{pi} + G_c x_r \tag{13}$$

u_{th} is the throttle command and x_c is defined as

$$x_c = \begin{bmatrix} \delta_{el} \\ \delta_{th} \\ \delta_{al} \\ \delta_{rd} \end{bmatrix} \tag{14}$$

One can now write an overall state-vector differential equation (2) for the entire system.

$$\dot{x}_s = A_s x_s + B_s u_s + G_s \eta_s \tag{15}$$

where

$$A_s = \begin{bmatrix} A_a & B_a & 0 & G_a & 0 \\ 0 & A_c & B_c & 0 & G_c \\ 0 & 0 & A_{pi} & 0 & 0 \\ 0 & 0 & 0 & A_g & 0 \\ 0 & 0 & 0 & 0 & A_r \end{bmatrix} \tag{16}$$

$$B_s = \begin{bmatrix} 0 \\ B_{th} \\ B_{pi} \\ 0 \\ 0 \end{bmatrix} \tag{17}$$

$$G_s = \begin{bmatrix} 0 & 0 \\ 0 & 0 \\ 0 & 0 \\ G_g & 0 \\ 0 & G_r \end{bmatrix} \tag{18}$$

$$x_s = \begin{bmatrix} x_a \\ x_c \\ x_{pi} \\ x_g \\ x_r \end{bmatrix} \tag{19}$$

$$u_s = \begin{bmatrix} u_{el} \\ u_{th} \\ u_{al} \\ u_{rd} \end{bmatrix} \tag{20}$$

$$\eta_s = \begin{bmatrix} \eta_g \\ \eta_r \end{bmatrix} \tag{21}$$

MEASUREMENTS AND FILTERING

The use of feedback control in any system requires measurement of a number of observed output variables. This may or may not pose a problem for a given system. The established engineering developments in attitude control of aircraft has led to experienced use of measuring devices for sensing the attitude states, i.e., p, q, r, ϕ, θ and ψ. For the present work these measurements are assumed to be available and shall be used.

The translational states, x, y, z, $\dot{x}$, $\dot{y}$, and $\dot{z}$, must gain more attention as these are rarely measured directly. The position states are supplied by the scanning beam microwave landing system. The MLS azimuth scanner provides horizontal angular position, while a vertically swept microwave unit would a allow an aircraft to derive elevation angular position. The addition of distance measurement equipment (DME) completes the three dimensional position set. The measurement noise model for the azimuth and elevation angular measurements is exponential correlated noise [6]. The total measurement noise model can be expressed in the vector-matrix form.

$$\dot{x}_{mw} = A_{mw} x_{mw} + G_{mw} \eta_{mw} \tag{22}$$

where

$$x_{mw} = \begin{bmatrix} a_y, \text{ azimuth measurement perturbation} \\ a_z, \text{ elevation measurement perturbation} \end{bmatrix} \tag{23}$$

$$\eta_{nw} = \begin{bmatrix} \eta_y \\ \eta_z \end{bmatrix} \quad , \quad E\left[\eta_{nw}\right] = 0 \quad , \quad E\left[\eta_{mw} \eta_{mw}^T\right] = I \tag{24}$$

$$A_{mw} = \begin{bmatrix} \frac{-2.8}{T_o} & 0 \\ 0 & \frac{-2.8}{T_o} \end{bmatrix} \tag{25}$$

$$G_{mw} = \begin{bmatrix} \sqrt{\frac{5.6}{T_o}}\,\sigma_y & 0 \\ 0 & \sqrt{\frac{5.6}{T_o}}\,\sigma_z \end{bmatrix} \tag{26}$$

Parameter	Description	Value
T_o	Sample interval	0.2
σ_z	Elevation angular noise standard deviation	0.66 mrad.
σ_y	Azimuth angular noise standard deviation	0.50 mrad.

Table 2. Microwave Disturbance Model Parameters

The range measurement disturbance model is generally represented as Gaussian white noise. The RTCA signal format team report recommendation [1] is σDME = 20 ft.

The approach phase prior to the straight-in final is where curved maneuvers take place. It has been suggested that first-order, low-pass filters are sufficient for signal smoothing [1,23,6]. The modeling of the measurement process for this work, therefore, consists of passing each of the position measurements through a first-order filter with a time constant of 0.08 seconds.

LIMITED STATE FEEDBACK

Using the performance index (1) with the differential constraint (2), m measurements are taken y(t) and these are related to x(t) through H (an mxn matrix with rank m).

$$y(t) = H\,x(t) \tag{27}$$

The plant matrix A is modified by assuming a feedback control law with an unknown gain matrix F (rxm matrix).

$$u(t) = -Fy(t) \tag{28}$$

This defines the controlled plant as

$$A_u = A - BFH \tag{29}$$

with the differential state equation (2) becoming

$$\dot{x} = A_u x + G\eta \tag{30}$$

The covariance matrix is defined as

$$X(t) = E[x(t)x(t)^T] \quad (n \times n \text{ matrix}) \tag{31}$$

and has the following differential equation

$$\dot{X} = XA_u^T + A_u X + GG^T, \quad E[\eta(t)\eta(\tau)^T] = I\delta(t-\tau) \tag{32}$$

For our purposes the steady state case, i.e., $\dot{X} = 0$, is sufficient.
The performance index can be restated in terms of this covariance matrix.

$$J = \text{trace } \{(Q + H^T F^T RFH)X\} \tag{33}$$

The problem is now a parameter optimization with an algebraic constraint (32). Augmenting J with a multiplier term results in a new performance index, one without an algebraic constraint.

$$J' = \text{trace } \{(Q + H^T F^T RFH) \cdot X + P(XA_u^T + A_u X + GG^T)\} \tag{34}$$

P is a constant multiplier (nxn matrix).

Differentiating (34) with respect to X, P, and F, respectively, yields the necessary conditions for an extremum for J. (* indicates the optimum for each matrix).

$$\frac{\partial J'}{\partial X} = A_u^{*T} P^* + P^* A_u^* + Q + H^T F^{*T} RF^* H = 0 \tag{35}$$

$$\frac{\partial J'}{\partial P} = X^* A_u^{*T} + A_u^* X^* + GG^T = 0 \tag{36}$$

$$\frac{\partial J'}{\partial F} = 2(RF^*H - B^T P^*)X^* H^T = 0 \tag{37}$$

These equations take certain familiar forms. Equation (35) is the Matrix Riccati condition used in full state optimal feedback control. Equation (36) is the steady-state covariance matrix definition (32). If one solves Equation (37) for F*, the result is

$$F^* = R^{-1}B^T P^* X^* H^T (HX^* H^T)^{-1} \tag{38}$$

These necessary conditions prove very difficult to solve for, and while there are algorithms proposed [13,14], these are very slow. The one used here has near second order convergence [17] and is summarized as follows:

1. Guess $F^{(K)}$ with the increment parameter, K, set to zero.
2. Solve (36) and (35) with $A_u^{(K)}$ defined by (29) for $X^{(K)}$ and $P^{(K)}$.
3. Use (38) to define a stepping direction, i.e.,

$$F^{(K+1)} = R^{-1}B^T P^{(K)} X^{(K)} H (H X^{(K)} H^T)^{-1} \tag{39}$$

4. Use cubic interpolation [20] or some other unidirectional search technique to find the directional minimum.
5. Employ some convergent stopping condition to decide if the process can be terminated.
6. If a new iteration is necessary, set K = K + 1 and go back to 2.

The problem of making an initial guess to achieve a global optimum is rarely easy for any iterative scheme. Here the difficulty is compounded as the limited feedback problem is not only multimodal, but a guess which stabilizes* the system is mandatory before the procedure can be initiated. One is tempted to make the initial guess be the feedback gains from the full state measurement optimal solution after the appropriate elements of F corresponding to the unmeasured states are set to zero. This not only fails to guarantee a guess in the lowest valley of J but possibly will not even stabilize the initial augmented plant. Methods for systematically phasing out unwanted gain elements are described in detail elsewhere [17,21].

OPTIMAL FEEDBACK TECHNIQUES

The use of limited feedback optimal control allows unconstrained model building as the extra state variables need not be accounted for in the output vector. A number of simplifications can be employed that help provide a better initial guess for the limited state feedback algorithm from the full state feedback solution and more efficient use of the limited feedback computer scheme.

*Stability in this sense means all negative real parts to eigenvalues of A-BFH.

In an effort to make the design procedure self-contained, the insertion of control, measurement and filter dynamics, along with the appropriate noise inputs, is necessary. To reduce the number of feedback states from that for the full state design procedure, the simplest possible dynamics were used for the feedback design and the complete system dynamics were inserted for the covariance matrix calculation. This idea is somewhat justified by the separation theorem, but the intuitive justifications and practical reasons are even more appealing.

An example of this idea is the elevator control input. Modeled as a first-order lag in this research, the feedback design was performed by by-passing the control dynamics. After the gains were calculated, the feedback was applied to the control dynamic's input and the covariance matrix was calculated. This procedure resulted in eliminating the unwanted f edback gains corresponding to the elevator state but fully taking the elevator lag into account for the covariance test.

This idea proved so successful for the full state feedback calculations, in terms of the satisfactory results obtained, that it was also used for the limited feedback program, but for another reason. Using the theory of limited state control fully takes into account the desire to eliminate the unwanted states while retaining their respective dynamics. The high-order dynamics, however, require correspondingly more computer time. Since the calculations are mostly matrix multiplications, the required computer time increase is proportional to the cube of the system order. Using these simplifications does remove the more accurate situation of using complete system dynamics in the design phase, but all dynamics are still included in the covariance test.

Figure 2 illustrates the idea of adding dynamics for testing the gains. The figure is descriptive of both the limited and full state design except that the gust dynamics are not necessary for the full state feedback design phase. The limited feedback design is still needed to eliminate some states, i.e., pilot, gust, and velocity.

RESULTS

The landing approach task for the Breguet aircraft is composed of two somewhat distinct phases. The portion of the approach of interest here takes place between approximately 4 miles from the runway to approximately 2000 ft. from touchdown [4]. The three dimensional nature of the coverage allows curved maneuvers along the initial approach phase. This is in contrast to the final approach where the necessity of allowing a final trim up of the aircraft for landing precludes dynamic maneuvers inside the 2000 ft. point.

All the dynamic states described previously are summarized in Table 3. Of all the longitudinal and lateral states, the twelve chosen for measurement represent a balance between the ease of measurement, the importance of contribution, and filtering necessary. As mentioned, the attitude states, ϕ, θ, ψ, p, q and r are easily measured and useful for attitude control. The position states, x, y and z are necessary for path control and are provided by the MLS and filtered to produce x_m, y_m and z_m. The velocity states $\dot{x}$, $\dot{y}$, and $\dot{z}$ provided the

Longitudinal State	Description	Lateral State	Description
$x^{*,**}$	forward position	y^{*}	lateral position
$z^{*,**}$	vertical position	$p^{*,**}$	roll rate
$q^{*,**}$	pitch rate	$\phi^{*,**}$	roll angle
$\theta^{*,**}$	pitch angle	$r^{*,**}$	yaw rate
$p_{\delta el}^{*,**}$	pilot elevator 1	$\psi^{*,**}$	yaw angle
$p_{\delta e2}^{*}$	pilot elevator 2	$p_{\delta a1}^{*,**}$	pilot aileron 1
$\dot{x}^{*}$	forward velocity	$p_{\delta r1}^{*,**}$	pilot rudder 1
$\dot{z}^{*}$	vertical velocity	$p_{\delta a2}^{*}$	pilot aileron 2
δ_{el}	elevator	$p_{\delta r2}^{*}$	pilot rudder 2
δ_{th}	throttle	$\dot{y}^{*}$	lateral velocity
x_m	forward measurement	δ_{al}	aileron
z_m	vertical measurement	δ_{rd}	rudder
u_{as}	airspeed	y_m	lateral measurement
a_y	m-w azimuth noise	a_y	m-w azimuth angle
a_z	m-w elevation noise	$p_{\delta_{a,rem}}$	pilot aileron remnant
$p_{\delta_{e,\ rem}}$	pilot elevator remnant	$p_{\delta_{r,\ rem}}$	pilot rudder remnant
u_g	forward gust	v_{gl}	lateral gust 1
w_{gl}	vertical gust 1	v_{g2}	lateral gust 2
w_{g2}	vertical gust 2	p_g	roll gust
q_g	pitch gust	r_g	yaw gust

*full state gains required

**limited state gains required

Table 3. Total System State Vector

limited state feedback algorithm with the most difficult elimination task. These states would be very helpful for path and attitude control, but as they require acceleration integration or reconstruction which is most difficult, the possibility of leaving them out of the design was pursued. The pilot output states, $P_{\delta el}$, $P_{\delta al}$, $P_{\delta rd}$, were chosen for their accessibility and their effect on overall performance.

As mentioned previously, banked maneuvers along the initial approach path require that the pilot handle those maneuvers with the same ease as level flight. Table 4 shows the stochastic responses for the Breguet aircraft flying at steady state bank angles, but using the compensation separately designed for the uncoupled longitudinal and lateral dynamics. In most cases the responses increase with bank angle, but the changes, up to 30° banking, are quite small. In addition it can be speculated that gains for coupled dynamics, if calculated, would be small and demonstrate little improvement over the observed results.

The design to this point has been predicated on the notion that the pilot would actually adopt the behavior represented by the pilot model. It has been demonstrated that with this performance index and a given system [9], the pilot will adopt a behavior which minimizes his tracking error. An appropriate rating can then be assigned to the pilot dynamics.

At this point it might be useful to examine a pilot evaluation technique seemingly independent of the pilot-in-the-loop design philosophy. The frequency domain investigations into pilot model and rating techniques [8,10, 15,5] have been in use longer than the more modern control approach [9]. Numerous system parameter guidelines and pilot model parameters have been set down as a result. The pilot model used in this research was developed using such techniques.

For such analysis, one must restrict the evaluation to single input-single output transfer functions. Breaking B and F into vectors

$$F = \begin{bmatrix} f_{el}^T \\ f_{al}^T \\ f_{rd}^T \\ f_{th}^T \end{bmatrix} \tag{40}$$

$$B = [b_{el}, b_{al}, b_{rd}, b_{th}] \tag{41}$$

State	Units	3σ Responses ϕ_o=0°	10°	20°	30°
x	ft	184.5	184.6	185.6	189.2
y	ft	310.0	315.7	329.1	348.2
z	ft	57.5	58.8	62.7	68.9
$\dot{x}$	ft/sec	15.57	15.65	15.95	16.56
$\dot{y}$	ft/sec	19.51	20.31	22.52	26.19
$\dot{z}$	ft/sec	20.41	20.52	20.86	21.40
p	deg/sec	19.99	20.00	20.05	20.15
ϕ	deg	8.40	8.41	8.45	8.50
q	deg/sec	11.95	11.73	11.18	10.54
θ	deg	6.94	6.96	7.04	7.29
r	deg/sec	4.89	5.45	6.74	8.41
ψ	deg	6.23	6.49	7.18	8.34
δ_e	deg	12.32	12.24	12.08	12.00
δ_a	deg	18.64	18.64	18.66	18.71
δ_r	deg	9.94	10.23	10.76	11.59
δ_{th}	h.p.	670.44	672.04	679.26	697.87
δ_{ec}	--	0.2980	0.2970	0.2940	0.2915
δ_{ac}	--	0.4119	0.4118	0.4119	0.4127
δ_{rc}	--	0.1726	0.1711	0.1869	0.2023

Table 4. Stochastic Response Results for 45° Flaps and 177 ft/sec Airspeed on Initial Approach Phase

The pilot transfer function can now be inserted to result in the total open-loop function for each pilot control axis.

$$M_i(j\omega) = f_i^T(j\omega I - A)^{-1}b_i \frac{e^{-T_N j\omega}}{(T_L j\omega + 1)} \qquad (42)$$

$$i = el, al, \text{ and } rd$$

The published guidelines (8, 10, 15, 5) for the frequency response of $M_i(j\omega)$ can be summarized as follows:

1. For best ratings the pilot adjusts his gain to place a good stretch of -1 slope rolloff of log magnitude of M_i versus log frequency in the region of the crossover frequency, i.e., where the magnitude of $M_i(j\omega)$ equals unity.

2. The crossover frequency should be between approximately 2 rad/sec and 7 rad/sec.

3. The pilot rating is degraded with poor phase margin.

One important guideline is pilot gain versus rating, but, as outlined earlier, the gain of the display variables can be adjusted to accommodate this.

Of the three axes examined only the aileron and elevator results are displayed. The rudder task easily satisfied all of the criteria mentioned. The aileron and elevator tasks have much more interesting interpretations.

Figure 3 shows the aileron open-loop frequency characteristics. The magnitude plot demonstrates the good characteristics at the crossover region. The phase plot, however, reveals a problem. Using the design delay time constant, $T_N = 0.3$ seconds, results in a low phase margin. If one uses a lower value, say $T_N = 0.2$ instead, this problem is cleared up.

The question that arises is does this compromise the design for minimum tracking task? The answer is no. It was never assumed that the pilot would adopt the exact behavior used in the design. The $T_N = 0.3$ value was chosen to provide an upper bound or worst case design challenge with the intent of influencing the feedback structure with the pilot's ultimate limitations. A trained pilot can easily adopt a T_N of 0.2 seconds and other, more rating degrading, compensation, such as that represented by the lead term in equation (15) is still unnecessary. A question now arises about the overall performance with this parameter. Table 5 shows the output responses for the same feedback gains calculated earlier but with both pilot delay constants being used. Without exception the system responses improved with the greater pilot concentration.

By designing the feedback gains with somewhat lazy pilot dynamics, it was hoped that the pilot characteristics would have a greater influence

State	Units	3σ Responses, Φ_o = 0° T_N = 0.3	T_N = 0.2
y	ft	310.0	262.9
$\dot{y}$	ft/sec	19.51	16.74
p	deg/sec	19.99	10.85
ϕ	deg	8.40	5.58
r	deg/sec	4.89	4.33
ψ	deg	6.23	5.72
$p_{\delta a1}$	--	0.3918	0.2275
$p_{\delta a2}$	--	0.3734	0.2275
$p_{\delta r1}$	--	0.1683	0.1517
$p_{\delta r2}$	--	0.1658	0.1498
δ_a	deg	18.64	10.25
δ_r	deg	9.94	8.95
δ_{ac}	--	0.4119	0.2369**
δ_{rc}	--	0.1726	0.1552**

** The pilot remnant input values are -

$3\sigma_{ac}$ = 0.31, $3\sigma_{rc}$ = .17

Table 5. System Response for Different T_N's (45° flaps and 177 ft/sec airspeed)

in the final structure than a more demanding pilot model. These results indicated that the pilot now has a certain range of parameter variation which yields good task performance.

The second frequency response curve, Figure 4, describes the elevator control task. The interpretation here is far more difficult than the previous two cases. The magnitude slope at the crossover point approaches -2 which indicates that pilot differentiation is necessary to raise this to an overall system crossover slope of -1. This is, however, somewhat compromised by the fact that the crossover frequency itself is lower than normal, $\omega_c = 2.6$, allowing slower pilot compensation.

Discarding the temptation to add further compensation, e.g., lead-lag compensator or stability augmentation, a look at the limitations of the feedback structure perhaps can help explain the result. Given that all the compensation passes through the pilot, via the display signals, and no loop closing is performed otherwise, then the system poles are not changed by the feedback structure in the open-loop sense. The feedback structure, therefore, constrains the performance to allow only zero changes which could leave the design process powerless to compensate for certain pole characteristics.

SUMMARY, CONCLUSIONS AND RECOMMENDATIONS

The use of optimal feedback control theory for this work provides the control designer with a precise design objective. The regulation of a command flight path in the face of stochastic inputs is a natural application for the performance index chosen.

The use of the pilot-in-the-loop analysis influenced the control design in favor of the pilot's dynamic limitations. The results indicate that designing for worst case pilot response and testing using a more demanding pilot model did demonstrate improved response.

The pilot remnant disturbance model is perhaps the newest and most untested portion of the pilot modeling process. Its use here was not intended to lump the entire pilot input not dictated by the crossover model into a single quantity. As yet there is no mathematical way of doing this. It has been demonstrated in the past, however, that this quantity somewhat simulates the pilot's performance in a multitask environment. After using this disturbance model in a design effort, one can better understand its influence. The remnant does provide an input into the problem which is at least intuitively justified. The crossover model suffers from the mathematical fact that the more one requires of it at input the more one achieves as an output. The remnant was useful in dictating a point of diminishing returns for the command inputs. This, more than any other design criterion, kept the pilot control activity at a low level.

Limited state feedback control theory plays a large part in this design effort. The algorithm developed represents a major portion of the overall design effort. Its greatest utility comes in eliminating states which cannot be reasonably deleted from the design phase. The paper by Mendel [22] brings

this entire area into better focus. His work dealt with the need for accounting for all stochastic inputs, disturbance and measurement noises into the full state feedback design. Although explicitly removed from the design process by the separation theorem, these noises must be observed and compensation adjusted accordingly. This idea leads to the combination of dynamic by-pass for this design work with the reinsertion into the final covariance check.

The results of this work have led to a number of conclusions about the landing approach problem for manual control and stochastic regulation in general. An excessive vertical acceleration, $\ddot{z}$, was observed which shows the need for special compensation. The performance index weightings were adjusted to bring this down with no success. A vertical accelerometer could help alleviate this problem but it is doubtful that feeding an accelerometer state to a pilot is feasible as he could not respond fast enough to the situation. A feedback ahead of the pilot (stability augmentation) is necessary here.

The pilot-in-the-loop design idea has been used with increasing regularity in the past couple of years. The usage here was unique in that the feedback structure was completely unconstrained, i.e., any state could contribute to any command. The design stops with the display set. The actual implementation can take many forms: compensatory, pursuit, or combinations of the two. It is believed that this does not preclude other visual cues, e.g., runway pictoral or projected glidepath. The design phase here does represent a logical break point between design and analysis and investigations of implementation procedures.

Although the design techniques employed produced results generally acceptable for the initial approach phase, to obtain even better results, the need for all compensation to go through the pilot must be removed. Allowing the attitude states, i.e., ϕ, θ, ψ, p, q, r and perhaps accelerometer states, to be fed into the system ahead of the pilot should remove much of the attitude regulation task from the pilot's attention. This can be performed by classical stability augmentation design procedures or an optimal control design identical to this one employed without the microwave measured path states or pilot model in the design loop. One control task already mentioned for this type of augmentation is the vertical acceleration excursion problem. The complete path is then closed with a pilot-in-the loop design as employed here. The attitude states are still allowed to be used but, in this case, they would serve only the path control. This later design idea could perhaps be combined into a single synthesis procedure by allowing use of attitude states for both ahead-of-the-pilot and through-the-pilot compensation.

The increased use of high speed digital computers doing state variable control analysis allows larger dynamic model size representing more complete descriptions of the physical situations in the design loop. Many dynamic situations within the entire model can be validly argued to be insignificant. The use of modern algorithms for evaluating Lyapunov equations, such as the covariance matrix definition, however, makes total system dynamic testing for steady state stochastic response efficient and complete.

Finally, the use of pilot states for feedback in the design was accomplished with output states of the pilot, i.e., input to control deflections, in

the feedback structure. These states were used for two reasons. They were easily accessible as one needs to merely attach appropriate measuring devices to the control stick and rudder pedals. The second reason is that they improve the performance of the pilot in the control task. Supplying the operator with an adjustment for his own dynamic behavior had a more explicit influence in the feedback design than just including the pilot as an unattainable filter. The testing of the design gains over more than one set of pilot parameters removes the fear that these gains are only valid for the pilot time constants used in the design, yet it is believed that using the second pilot states, the derivatives, would assume too much of the model. The use of pilot states in the feedback structure with larger pilot model parameter variations is an area for future research.

REFERENCES

1. Anonymous, "Signal Format Development Team Report to RTCA SC-117, Microwave Scanning Landing Guidance System (LGS)," Sept. 5, 1971, Radio Technical Commission for Aeronautics, Washington, D.C.

2. Poritzky, S. B., "Seeking a New Precision Approach and Landing System--A Test of Maturity," Journal of Aircraft, Vol. 8, No. 7, July 1971, pp. 538-542.

3. Cunningham, T. B., "A Study of Aircraft Separation Using a Scanning Beam Microwave ILS," Purdue University, 1971.

4. Schmidt, D. K., and Swaim, R. L., "An Optimal Control Approach to Terminal Area Air Traffic Control," Journal of Aircraft, Vol. 10, No. 3, Mar. 1973, pp. 181-188.

5. McDonnell, J. D., "Pilot Rating Techniques for the Estimation and Evaluation of Handling Qualities," AFFDL-TR-68-76, Dec. 1968, AF Flight Dynamics Lab, Wright-Patterson AFB, Ohio.

6. Graham, D., Clement, W. F., and Hofmann, "Investigations of Measuring System Requirements for Instrument Low Visibility Approach," AFFDL-TR-70-102, Feb. 1971, AF Flight Dynamics Lab, Wright-Patterson AFB, Ohio.

7. Stapleford, R. L. and McRuer, D. T., "A Practical Optimization Design Procedure for Stability Augmentation Systems," AFFDL-TR-70-11, Oct. 1970, AF Flight Dynamics Lab, Wright-Patterson AFB, Ohio.

8. McRuer, D. T. and Jex, H. R., "A Review of Quasi-Linear Pilot Models," IEEE Transactions on Human Factors in Electronics, Vol. HFE-8, No. 3, Sept. 1967, pp. 231-249.

9. Baron, S. and Kleinman, D. L., "Application of Optimal Controls Theory to the Prediction of Human Performance in a Complex Task," AFFDL-TR-69-81, Mar. 1970, AF Flight Dynamics Lab, Wright-Patterson AFB, Ohio.

10. Adams, J. J. and Hatch, H. G., "An Approach to the Determination of Handling Qualities by Using Pilot Transfer Functions," TN D-6104, Jan. 1971, NASA.

11. Muckler, F. A. and Obermayer, R. W., "Manual Control System Performance with Quickened Display, State Variable Display, and Display Gains," Third Annual NASA University Conference on Manual Control, SP-144, Mar. 1967, NASA.

12. Seitz, W. R. and Goodson, R. E., "Flight Director Design for a STOL Aircraft," Journal of Aircraft, Vol. 10, No. 8, Aug. 1973, pp. 491-494.

13. Levine, W. S. and Athans, M., "On the Determination of the Optimal Constant Output Feedback Gains for Linear Multivariable Systems," IEEE Transactions on Automatic Control, Vol. AC-15, No. 1, Feb. 1970, pp. 44-48.

14. Axsater, S., "Sub-optimal Time-variable Feedback Control of Linear Dynamic Systems with Random Inputs," International Journal on Control, Vol. 4, No. 6, 1966, pp. 549-566.

15. Wasicko, R. L. and McRuer, D. T., "Human Pilot Dynamic Response in Single-Loop Systems with Compensatory and Pursuit Displays," AFFDL-TR-66-137, Dec. 1966, AF Flight Dynamics Lab, Wright-Patterson AFB, Ohio.

16. Truxal, J. G., Control System Synthesis, McGraw Hill, New York, 1955, p. 550.

17. Cunningham, T. B., "The Design of a Pilot Augmented Landing Approach Control System." Ph.D. Thesis, Purdue University, 1973.

18. Chalk, T. P. and Harris, T. M., "Background Information and User Guide for MIL-F 8785B (ASG), 'Military Specification-Flying Qualities of Piloted Airplanes,'" AFFDL-TR-69-72, Aug. 1969, AF Flight Dynamics Lab, Wright-Patterson AFB, Ohio.

19. Anonymous, "Automatic Landing Systems," FAA Advisory Circular 20-57A, Jan. 1971.

20. Fletcher, R. and Powell, M. D. D., "A Rapid Descent Method for Minimization," British Computer Journal, Vol. 6, 1968, pp. 163-168.

21. Vandierendonck, A. E., "Design Method for Fully Augmented Systems for Variable Flight Conditions," AFFDL-TR-72-52, Jan. 1972, AF Flight Dynamics Lab, Wright-Patterson AFB, Ohio.

22. Mendel, J. M., "On the Need for and Use of a Measure of State Estimation Errors in the Design of Quadratic-Optimal Control Gains," Joint Automatic Control Conference Proceedings, Aug. 1971.

23. Cherry, G. W., De Wolf, B. and MacKinnon, D., "Increasing Airport Capacity and Terminal Area Safety by Means of the Scanning Beam Instrument Landing System," AIAA Paper 70-1033, Santa Barbara, Calif., 1970.

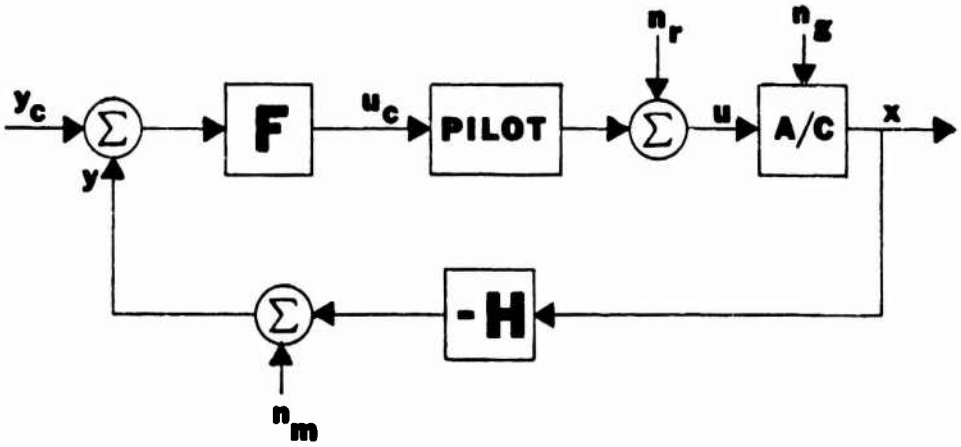

x is the state vector
y is the output vector
u is the control vector
$\mathbf{y_c}$ is the command output vector
$\mathbf{u_c}$ is the command control vector displayed to pilot
n is the random noise vector
r remnant noise
g wind gust
m measurement noise

Figure 1. Pilot-in-Loop Control Schematic

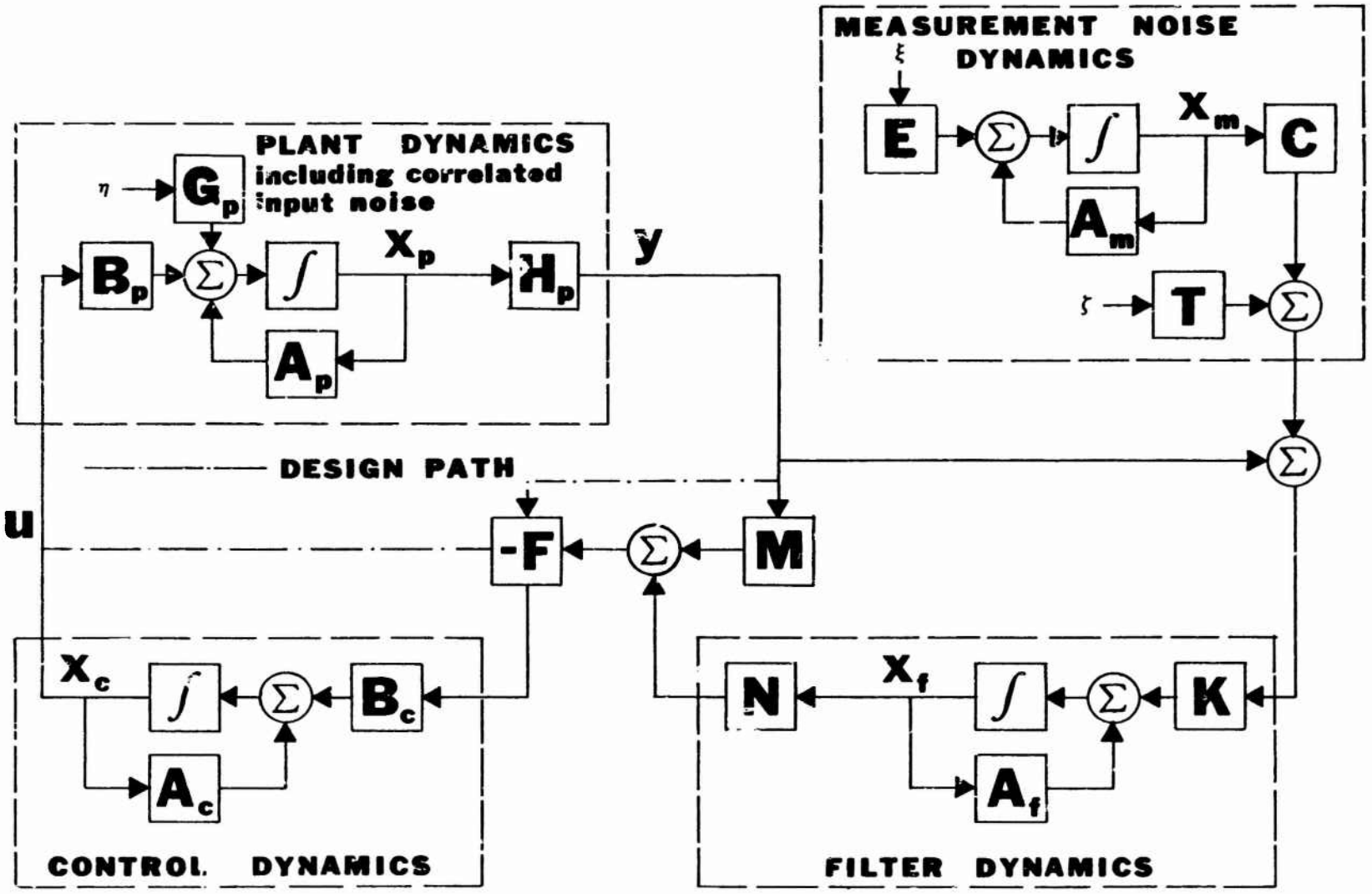

Figure 2. Complete System Dynamics

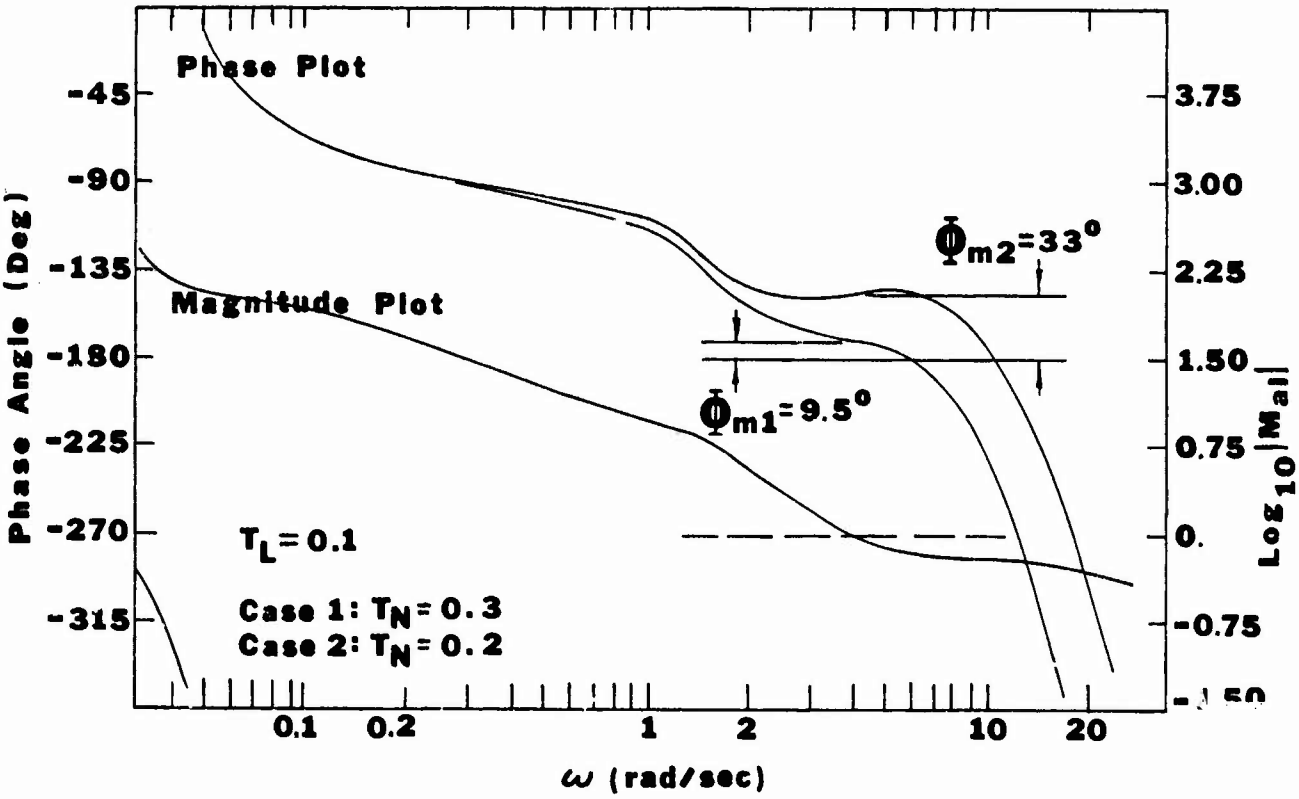

Figure 3. Aileron Task Open-Loop Frequency Response

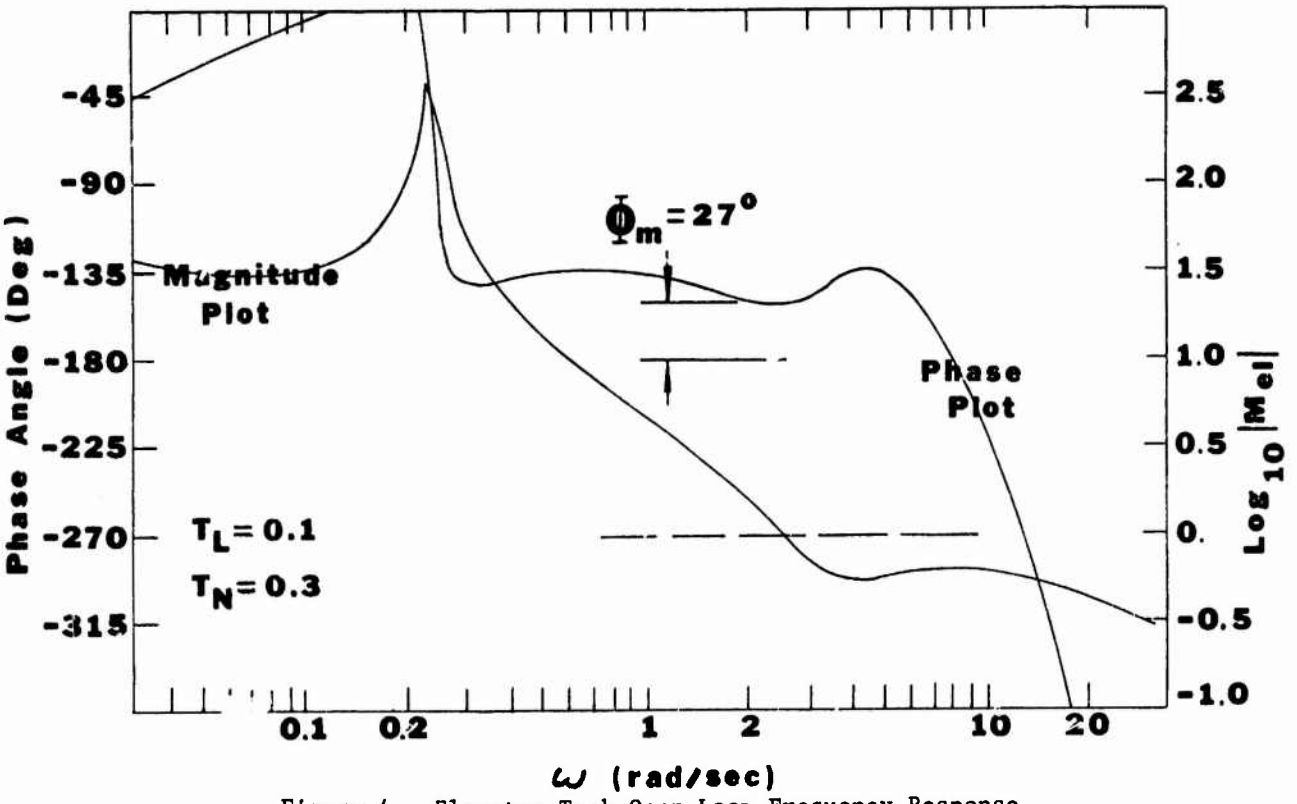

Figure 4. Elevator Task Open-Loop Frequency Response

A CONTROL AUGMENTATION CONCEPT FOR IMPROVED MANUAL CONTROL

Captain K. W. McElreath
Air Force Flight Dynamics Laboratory

ABSTRACT

The types of tasks involved in many Air Force missions dictate that the pilot must be an active control element in order to exercise maximum flight path flexibility. As a control element, however, the human pilot has two limitations. One is the frequency response required for short term stabilization, and the other is the ability to concentrate on many demanding tasks at the same time.

The V/STOL IFR Control/Display Technology Program conducted by the Air Force Flight Dynamics Laboratory has developed a control system to overcome the pilot limitations while enhancing his performance and decision-making flexibility as an active control element. This system includes a highly flexible V/STOL aircraft flight director which feeds only the high-frequency control inputs to a simple, limited-authority automatic stability augmentation system. The low-frequency control commands are displayed to the pilot to be executed manually.

Using the techniques of analysis, simulation, and flight testing, this concept has been verified to improve performance and decrease workload while retaining the natural pilot flexibility. Pilot control inputs required to fly any given profile are reduced in number and quickness of response. Through the elimination of high-frequency control inputs, the aircraft is more flyable and the pilot can devote more attention to analyzing his situation and the progress of the mission.

Such a control system has been implemented and flight tested in the dynamic maneuvering control of cyclic pitch on a CH-3E helicopter. Future work is recommended to optimize the complementing of manual and automatic functions, to evaluate the effectiveness of the control concept under operational conditions, and to extend the concept to other control applications.

NOTATION

s = Laplace operator

T_1 = time constant, pilot model

T_2 = time constant, pilot model

T_3 = time constant, pilot model

ζ = damping ratio, 2nd order system

θ_c = basic cyclic pitch command

INTRODUCTION

The problem of interfacing a human pilot and a dynamic aircraft, particularly under instrument weather conditions, has been the focus of many development programs. This problem is now appearing again with the advent of STOL and V/STOL instrument (IFR) operations, such as with the AMST or the Army's new helicopters. The deficiencies which prevent effective IFR utilization of these vehicles lie in the areas of stabilization and control systems, pilot displays, flight path sensors, and appropriate guidance sources.

The best solution to these deficiencies is one which integrates developments in each of these areas into a total compatible system.[1] V/STOL mission requirements define four criteria that will guide the design of such a system, to ensure maximum operational effectiveness: (1) flight path flexibility, (2) precision, (3) low pilot workload, and (4) simplicity at low cost. However, these requirements are somewhat interrelated.[2]

The Air Force Flight Dynamics Laboratory is conducting a development program that has made significant progress in defining an operational V/STOL control/display system, aimed at meeting these four requirements. The approach taken during this development program to arrive at a workable solution includes four steps. First, the task or problem is defined in terms of the results desired. Then analysis, simulation, and flight testing are employed to develop the solution and verify the results. The systems integration and flight evaluations are accomplished on a CH-3E helicopter.

OVERALL CONTROL CONCEPT

Extensive effort was expended in determining the optimum overall control/display concept, keeping in mind the four constraints listed above.

The first trade off, and the one reported herein, concerned the degree of manual control vs automatic control. Pilot frequency response limitations dictate that some automaticity in the form of stability augmentation be employed, if only for aircraft attitude stabilization. Beyond automatic stability augmentation, however, the choice is less clear. Automatic control systems can remove some of the pilot workload and give repeatable, good performance, when the task is well defined. They do, however, require extensive failure monitoring by the pilot in critical

flight conditions. This distracts him from the primary mission. Also, since the pilot is not directly flying the aircraft, he must step in and re-establish positive control of the vehicle when a partial or total failure occurs.

Another important consideration is that the pilot alone can make decisions and choose alternatives when faced with difficult or unforeseen conditions. On the other hand, a pilot who is burdened with many tasks cannot afford the time or attention to exercise his authority or options. For these reasons, the best system is one in which the pilot is an active element and not just a monitor of automatic performance.

The solution that has been adopted for the AFFDL control/display system is one where the pilot is included as a primary control element in the design of the overall system. This means that there are certain tasks which are directly assigned to him, some that are shared with automatic controls, and some that are completely automatic under normal conditions.

Among the tasks selected for the pilot to do are those which offer the greatest benefits in flexibility and performance under human control. In this area are the dynamic maneuvering controls of cyclic pitch and roll and the selection or modification of the flight profile to satisfy the mission requirements. The role of the automatic control system is threefold: Uncoupling of the pilot's control inputs, elimination of the manual coordinating functions, and a simplifying of his primary control tasks.

The primary element of the control/display system is a 3-cue flight director, which is mechanized to directly control the aircraft velocity vector through airspeed, flight path angle, and heading/course control. The cyclic pitch and roll commands of the flight director are integrated in the center of the attitude director indicator (ADI). The collective stick command is on the left of the ADI, superimposed over a flight path angle tape. The experimental instrument panel layout is shown in Figure 1.

MECHANIZATION OF THE BLENDED SYSTEM

In the CH-3E test vehicle, cyclic pitch is the primary airspeed control. When flying the experimental flight control/display system, the pilot selects a reference airspeed indicator using a thumb slew switch located on the cyclic grip. Thus he can change the reference without removing his hand from the stick or diverting his attention. The flight director then computes the proper control inputs to null the airspeed error. The short-term commands are fed directly into the automatic pitch stabilization system, and the longer-term commands are displayed to the pilot to be executed manually. Thus the vehicle assumes not only an attitude stability, but a short-term airspeed stability against longitudinal gusts, assisting the pilot in his control task. The block diagram of the flight director mechanization is shown in Figure 2. Note that a

failure of the automatic system means that the pilot will have to follow the high-frequency commands as well as the low-frequency ones. However, his piloting technique and instrument scan are as before; that is, the control task is intensified but not changed.

Referring to Figure 2, the basic cyclic pitch computation (θ_c) is airspeed error damped with washed-out pitch. For the noncoupled, manual operation, filtered cyclic stick position is summed with θ_c to provide anticipatory damping. With appropriate filtering, cyclic stick position can be made to approximate pitch rate. This approximate pitch rate signal does not contain the effects of external gusts; it contains only the pilot inputs. When used as a damping signal, therefore, it will cause less unnecessary command activity on the ADI than an actual pitch rate signal.

When the system is coupled to form a blended system, the basic cyclic pitch computation, θ_c, is slowed down with a 2-second lag before it is displayed on the ADI. At the same time, θ_c is hi-passed and fed into the servo so the automatic system can pick up the high-frequency commands. A pitch command that is lagged by two seconds and then fed to the ADI would not result in a stable, flyable command. Therefore, the lagged command is augmented by cyclic pitch stick position filtered to approximate short term pitch. This signal is used because, as mentioned above, it does not contain the external gust effects. The signal fed to the automatic system is damped with derived pitch rate. The frequency response of the servo is fast enough to respond to and help damp pitch rate disturbances.

The automatic system used in this instance is the normal CH-3E Sikorsky stability augmentation system (SAS), with a series servo and 10% control authority. The high-frequency flight director airspeed command is added to the normal SAS command.

In normal operations it was desired that the pilot not be aware of the automatic inputs. Preliminary analysis showed that for this constraint the best frequency split between automatic and manual execution would occur about 0.5 radian/second, meaning that the automatic input has a 2-second washout and the displayed manual command appears with a 2-second lag.

The rationale for using the 0.5 radian/second frequency crossover split can be visualized by looking at the assumed, simplified pilot model in Figure 3. With the uncertainties of modeling the display/pilot combination, this project did not devote a great effort to modeling it. Instead, a simple analytical model was used and the results verified on a simulator by studies using a good spectrum of actual pilots[3]. The linear model that was assumed is:

$$\frac{\text{Control Action}}{\text{Display Movement}} = \frac{(T_1 s + 1)(T_2 s + 1)}{s(T_3^2 s^2 + 2\xi s + 1)}$$

A plot of this pilot model is given in Figure 3.

The gain parameter is dependent on the display gain and on the control column ratio to the aircraft surface.

The lead corner frequency, $1/T_1$, is dependent on how much rate information the pilot derives from the background attitude data of the attitude display indicator, but is somewhere in the range of 1 to 3 radians/second. The integration rollout corner frequency, $1/T_2$, is again very display dependent, but usually occurs between 0.1 and 0.5 radian/second. The quadratic rolloff frequency, $1/T_3$, which occurs at the point where the pilot is no longer able or willing to track the display, is usually modeled at approximately 8 radians/second.

By assigning to the automatic system the execution of all inputs of frequencies greater than 0.5 radian/second, the control inputs required of the pilot are those which he can integrate and thus perform most easily and effectively. These types of responses can be accomplished as a result of his normal instrument scan without requiring constant attention. He can then devote more time to other mission and flight management tasks.

EXPERIMENTAL DATA

The simulator used in the program is a fixed-base simulator with three degrees of freedom at a time. The three degree-of-freedom limitation is imposed because of analog computer capacity.

In the pitch/collective study, the three degrees of freedom were airspeed, pitch attitude, and vertical rate. CH-3E dynamics were simulated with the SAS, and the system was perturbed by 2-sigma longitudinal and vertical gusts. The flight director was mechanized as in the aircraft, and the pilot's task was to maintain a reference airspeed and altitude by following the cyclic pitch and collective stick commands. The performance and workloads were compared using the flight director commands alone vs the blended system with pitch coupling.

Examples of the improvement in performance and workload may be seen in the data illustrated in Figures 4 and 5 which was taken on the fixed-base simulator. Figure 4 shows data taken with a manually flown (flight director only) system, and Figure 5 shows data taken using the blended (coupled) control system. Cyclic stick activity may be considered to be an indicator of pilot workload in that axis. Note the reduction of about 60% in the high-frequency cyclic pitch activity with the blended system.

Figures 4 and 5 were taken with a project pilot flying the simulator. His task only required attention to two items, cyclic and collective pitch commands. Under higher stress conditions, such as during terminal area navigation and communications, his cyclic pitch performance would have been worse with the flight director only system because he would not have had

the luxury of devoting so much of his attention to that particular task. Even with only two tasks to perform, however, his workload in cyclic pitch was reduced with the blended system.

As a result of the encouraging simulation results, the blended control concept was included in the flight director mechanization in the CH-3E test aircraft. An extensive pilot evaluation of the overall system with the blended control concept for airspeed control is being conducted. The results obtained to date confirm that the pilot and the control/display system combination do produce superior performance and improved workload and flexibility. Low-speed, steep letdowns can be flown with precision and relative ease.

As a result of blending the automatic and manual control of airspeed through cyclic pitch in the manner described above, several benefits are gained. First, the absence of high-frequency manual control responses allows him to spend his time more profitably by assessing his situation and planning his flight profile than by exercising short-term airspeed control. Second, the pitch control task itself becomes less demanding and more comfortable for the pilot than it is under purely manual control. Thirdly, the automatic controls, by washing out with a 2-second time constant, do not interfere with the normal aircraft handling qualities or the pilot's control feel or authority.

CONCLUSIONS AND RECOMMENDATIONS

From the results to date in the Air Force Flight Dynamics Laboratory development program, it is apparent that much can be gained by including the pilot as an active element in the control/display system design. Flexibility is enhanced because the pilot is exercising continuous authority and can react quickly and positively. Precision and workload are improved because the automatic system can respond to high-frequency perturbations, improve vehicle flight path stability, and remove unnecessary pilot inputs which are only coordinating functions. Finally, the system concept minimizes the cost and complexity associated with automatic control systems. The degree of required redundancy is reduced by using the pilot as the primary full-authority control as well as the backup to the automatics, and by limiting the control authority of the automatic servos.

The system concept has been developed and flight validated to a fair degree of confidence. Further work will apply this concept to bank attitude control, where wind shears and close-range captures of a final approach course increase the pilot's workload to an unmanageable level. Other applications may be considered for control applications which have similar requirements to those discussed here.

REFERENCES

1. Litchford, G. B., "Low-Visibility Landing, Part 2: The Systems Challenge," Astronautics and Aeronautics, Vol 6, No. 12, December 1968, pp 44-56.

2. Levison, W. H., and Elkind, J. I., "Studies of Multivariable Manual Control Systems: Two-Axis Compensatory Systems With Separated Displays and Controls," NASA CR-875, October 1967.

3. McRuer, D. T., and Jex, H. R., "A Review of Quasi-Linear Pilot Models," I.F.E.E. Transactions on Human Factors in Electronics, Vol HFE 8, No. 3, September 1967, pp 231-249.

Figure 1. Experimental Instrument Panel.

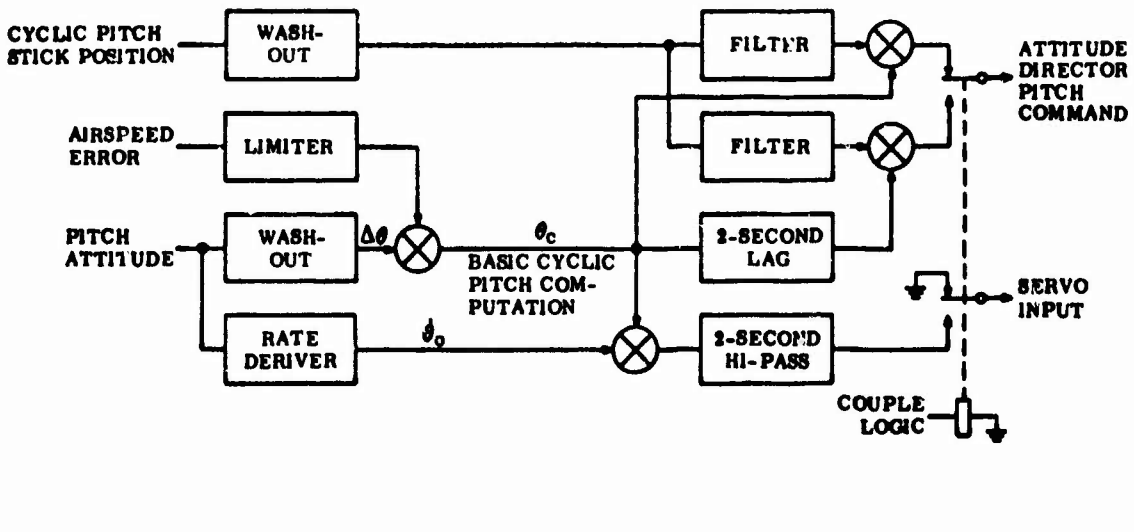

Figure 2. System Block Diagram.

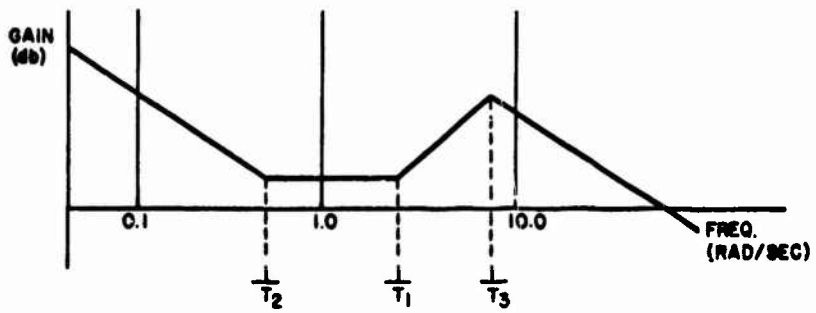

Figure 3. Simulation Pilot Model.

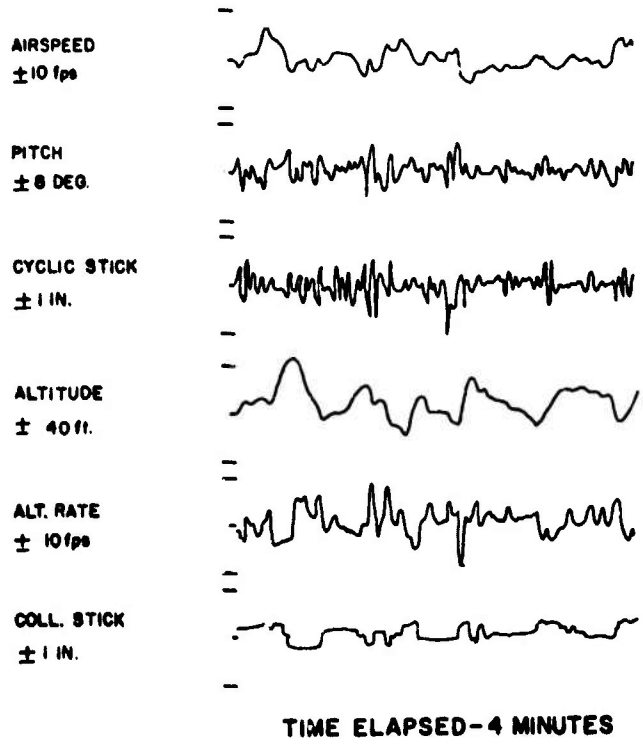

Figure 4. Actual Pilot Flying Flight Director (SAS On).

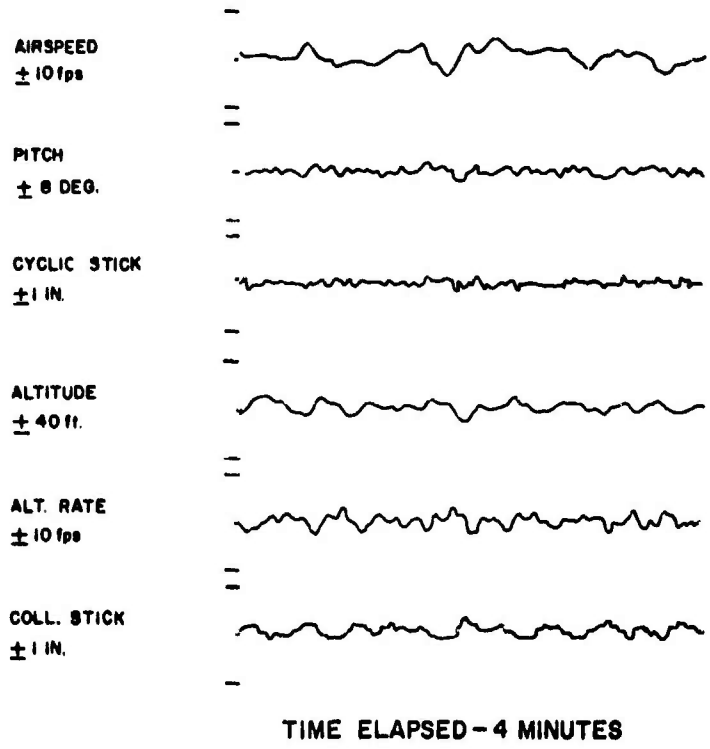

Figure 5. Actual Pilot Flying Blended System.

APPLICATION OF DESCRIBING FUNCTIONS FOR EVALUATION OF SPACE SHUTTLE LANDING AID DISPLAY CONCEPTS

by

Wendell D. Chase
Ames Research Center, NASA
Moffett Field, California 94035

ABSTRACT

The task of development and evaluation of airborne flight displays to support approach management and flight path control has had a slowly evolving history. A recent display concept to provide a more direct outside world pictorial runway representation and aiding symbology has been identified to enhance the management of the shuttle recovery for manual flight control operations. Of present interest is the application of human operator describing function measurements to help evaluate this display in either a head-down, panel-mounted or head-up windscreen position. The advantages of this method for more effective man-vehicle display evaluation are discussed, and utilize the supporting describing function-analytical performance measure techniques obtained from four participating pilots.

INTRODUCTION

The display concepts that would provide a more direct pictorial representation of key flight situation parameters have only recently been attempted through various types and stages of head-up displays (references 1, 2). This approach was conceived to provide the pilot better monitoring or manual takeover features rather than the more abstract and symbolic representations provided by conventional attitude – directors and flight situation instruments. A preliminary analysis of pilot task requirements and display requirements during the unpowered terminal area maneuvering and final approach sequences for the Space Shuttle reentry vehicle, indicate that flight information based on an outside world perspective display concept of the runway and aiding symbology would enhance the pilot's management of the vehicle for both automatic and manual flight control (reference 3).

An experimental display was derived and constructed for evaluation in simulated space Shuttle approach and landings. It was intended that data obtained would support the contention that pilots require display support not currently available in conventional flight instrumentation for more accurate approach management. In the present study, the focus of display aid to manual flight path regulation begins with a simplified head-up display and advances to a higher degree of display aid represented by a more sophisticated head-up and head-down version. The inherent display evaluation problem, when it comes to attempt to distinguish advantages of one display over another display, is one of performance measurement techniques. Many times, the results are limited, inconclusive, insensitive or even contradictory. Therefore, in order to help preclude any potential conflicts arising from interpreting insensitive data and its use to justify the advantages or merits for any of the above display concepts, an attempt was made to supplement the usual landing performance data with human operator describing function measurements.

The technique to be described was an attempt to measure a single longitudinal outer loop of the Space Shuttle vehicle during terminal area maneuvers. It represents and extension of human operator describing functions to a demanding and realistic task. Previous attempts have been made to measure multiloop pilot describing functions during instrument approaches in a simulation of a large subsonic aircraft (reference 5); however, after a lengthy computational analysis, the results showed inconclusive multiloop describing function variations between two dissimilar pilot techniques. For this reason the present attempt was limited to measuring a single outer loop describing function. The objectives of this experiment were: (1) to test the validity and emphasize the feasibility of generating describing functions for on-line display evaluation while the pilot was seated in the simulator, (2) plot the describing function data and other terminal performance measures for similar trends among pilots and test for repeatable display effects, and (3) use the results to indicate where display improvement would be desirable.

System Simulation

Vehicle Simulation. A sophisticated six degree-of-freedom simulation of the North American Rockwell 134-C High Cross Range Orbiter

was programmed on a hybrid analog-digital computer facility with options for either manual or automatic control (reference 6). A stability augmentation system (SAS) was also incorporated. A block diagram of the longitudinal airframe including SAS compensation functions is depicted in figure 1. The basic airframe equations without SAS are complicated by the unpowered deceleration descent schedule which continually bleeds-off the final approach velocity. Following are two representative closed loop transfer functions with SAS augmentation of flight path angle (γ) to control column (δ_c) taken at altitudes of (1) 10,000 and (2) 300 feet, respectively, and are plotted in figure 2. Selection of the transfer function γ/δ_c was based upon the nature of the flight path regulation task features incorporated into the display and is to be used later for calculating the open loop describing functions.

$$Y_c = \frac{\gamma(S)}{-\delta_c(S)} = \frac{55.48\ (S + .245)}{S\ (S + .53)\ (S + 2)\ (S + 7.9)} \qquad (1)$$

$$Y_c = \frac{\gamma(S)}{-\delta_c(S)} = \frac{45.22\ (S + .097)}{S\ (S + .3)\ (S + 2)\ (S + 6.9)} \qquad (2)$$

The SAS augmentation (reference 5) coupled around the basic airframe transfer function, requires pitch feedback and control column feed forward commands which are necessary to generate a satisfying responding vehicle. As can be seen from figure 2, the response is almost identical over the high and low altitudes.

Disturbance Input. The disturbance input (γ_d) was the sum of seven sinusoids with a -20 db high frequency shelf at 3.927 rad/sec and applied as shown in figure 1. The spectral input frequencies were located at .078, .393, .785, 1.257, 1.963, 3.927, 7.854 rad/sec and the respective amplitudes at each frequency were 1., -1., .6, -.38, .17, -.1, .1 degrees. The composite sum had a root mean square (RMS) amplitude of 1.78 degrees.

Describing Function Loop Selection. Selection of the inner loop pitch was not considered for analysis because this parameter was highly non-stationary in view of a constantly changing angle of attack

attributed to a decreasing velocity profile peculiar to an unpowered approach. Because of the nature of the flight path regulation display task, a middle loop or flight path loop was selected. A modified version of the Fast Fourier Transform (FFT) was used to compute pilot (Y_Y) describing functions, including remnant spectra (reference 7) by measurements of the ratio of control column (δ_c) to flight path error (γ_e). This particular version allowed the computations to proceed at a greatly reduced time than that normally required to calculate the truncated Fourier transform of the sampled control column output (δ_c). Based upon the computed pilot describing function (Y_Y), the open loop describing function (Y_{OL}) was defined and calculated as:

$$Y_{OL} = Y_Y \cdot Y_c$$

Display Simulation. Experimental display configurations were generated by an Evans & Sutherland Line Drawing System (LDS-2) and displayed on the cathode ray tube (CRT) installed and collimated at the pilot's station. Analog signals generated by the vehicle simulation were sampled 30 times per second by the Systems Engineering Laboratories digital computer (SEL 840) and transferred to the LDS-2 under control of the display generation program. The basic perspective computations for the runway image and ground reference display elements were executed in the LDS-2. The experimental display configurations are shown in figure 3 (a and b). A photograph of the full display complement is seen in figure 4. The entire head-up scene was later presented on the head-down panel positioned CRT. For the head-down presentation, a closed circuit TV runway image, obtained from the Ames General Precision System Visual Flight Attachment, was phased in from an in-cloud condition through the windscreen as the vehicle descended below 300 feet altitude.

Experimental Plan

Ten participating pilots were briefed on the project activities and experimental task and completed the necessary training, experimental run series including a debriefing session in a single 6-8 hour visit to Ames Research Center. This was a collaborative effort between Ames and Biotechnology, Inc. to conduct off nominal approach sequences

(reference 4). Figure 5 shows five display modes and approach profiles presented for a total of 160 flights, or 16 flights per pilot. The above main study, which utilized all ten participating pilots, was aimed at an examination of the subject display concept for different flight profiles and wind configurations outside the nominal 10 degree flight path approach. For purposes of the describing function measurements, only display modes C-1, C-4 and C-5 were retained for a nominal 10 degree flight path profile. Mode C-5 was presented head-down and contained identical display information. Consequently for the purposes of this paper C-5 will be referred to as C-4 head-down. Typically, C-1 is the display illustrated in figure 3-a, and C-4 and C-4 head-down illustrated in figure 3-b. Both C-1 and C-4 were head-up display presentations viewed through the windscreen.

Four of the ten pilots also participated in the present experiment to measure their describing functions. Each of the four pilots completed his training and 16 required display mode-approach profile flights for the main study before attempting the disturbance input flights. Injection of the disturbance input as shown in figure 1 was interpreted to resemble gust inputs. For these flights, each of the four pilots was given two final flights; the first was a training effort, and the second for best effort. Both flights, however, had describing functions calculated to investigate similarities, strategies or trend effects among pilots and display modes. Each flight was segmented as indicated in figure 6 because it was anticipated that the pilots might adopt different strategies or techniques when transitioning from a steep 10 degree to shallow 2-1/2 degree glide slope. Each segment, the pre-transitional and transitional span, was divided into 100 seconds. Describing function data was calculated on 80 seconds of each respective segment. A preview period of about one minute transpired with the disturbance input before entering the first transitional segment. Actual transition from 10 to 2-1/2 degree glide slope took about 4 seconds and occurred about midway through segment 2. Completion of segment 2 occurred at about 200 feet altitude.

Results & Discussion

The first of the experimental series involved an interpretation of the displays by the pilots for the ground oriented perspective features, and the techniques used to adjust the glide path. Since the displays

contained glide slope reference symbology, it was expected that the pilots would adjust the ground referenced aiming point by regulating flight path angle.

Landing Performance Measure Results. The experimental displays were developed to support flight control during the approach to the landing site, but not the final landing maneuver and touchdown on the runway. Figure 7 shows the overall RMS glide slope error (ξ_{gs}) values with the disturbance input applied over both approach segments 1 & 2. The only real obvious differences occur in glide slope tracking accuracy for the second segment ($p < .05$). A significantly tighter standard deviation between the head-down and head-up glide slope error can be observed in figure 7 for the second segment. The means of these displays are also observed to be about equal. It appears from this data that the C-4 display was considerably better than the C-1 display. Providing that these results would hold up for more pilots it would be useful for making display evaluations that C-4 indeed was better than C-1. This data will be correlated with describing function results later in the paper. Evidence thus far based on the above RMS performance measure is not sufficient to make sound engineering display evaluations.

Describing Function Results. In referring back to figure 1, there were two measurements taken on both the pilots control column output (δ_c) and the pilots display. These measurements were used to generate the pilot transfer function (Y_γ). As pointed out earlier, the inner loop pitch was considered to become highly non-stationary and hence more difficult to examine; whereas, the flight path loop would remain more consistent throughout the approach maneuver and would also be associated closer to the flight path regulation tasks. It must be emphasized that these results were an attempt to analyze data obtained from a complex unpowered and manually controlled vehicle. The environment is that essentially of a demanding and realistic task in a non-linear and non-stationary final approach maneuver from a steep to shallow glide path.

Pilot Describing Functions (Y_γ). Figure 8 shows the effect of increasing display aid (C-1 to C-4) for the same pilot pair (7 and 8). It can be observed for C-4 that a gain advantage of about 10 db throughout both segments is predominate in the mid-high frequency regions. The phase over the first segment appears to have a higher phase lead with

C-4 at the low frequency spectrum. The phase over the second segment has consistently higher phase lead over most of the spectrum. In general, the first segment shows a substantial phase lead for both displays, but more uniform for C-4.

As a comparison, figure 9 shows that the second pilot pair (9 and 10), who flew the same C-4 display, maintained very good gain and phase relationship as well as good behavioral correlation to the first pilot pair (7 and 8) results. Definite phase peaking consistently appears throughout each second segment display mode at about .78 rad/sec.

Figure 9 also shows the results of the head-down panel mounted C-4 display mode. Although the pilots reacted in a manner very similar to the previous C-4 head-up display there is some evidence of higher gain and phase lead over the low frequency spectrum for both segments of the head-down display application.

Open Loop Describing Function (Y_{OL}). The open loop describing function was determined analytically based upon the measured pilot describing function and the results of the Y/δ_c transfer function presented in figure 2. As can be seen from figure 2, Y/δ_c or Y_c varies very little from the high altitude segment 1 to low altitude segment 2 because of the stability augmentation system (SAS) compensation. Therefore, the results of the open loop describing function and their respective crossover frequencies are considered valid estimates. Figure 10 shows the effect of increasing display aid (C-1 to C-4) for the same pilot pair (7 & 8). For the first and second segments it is observed that the C-4 display has higher gain and more phase lead. The crossover frequencies are about .6 to .7 rad/sec for both C-1 display segments, but move to around 1.75 rad/sec for each of the C-4 segments. Phase margin for the C-1 display is about 20 degrees lower over segment 2 than that obtained for the C-4 display.

Also of interest and comparison, figure 11 shows the results of the same C-4 display for the second pilot pair (9 & 10). Their crossover frequencies seem to be higher over the first segment (1.1 - 2 rad/sec) compared to the range (.82 - 1.5 rad/sec) over the second segment. Also the pilots appear to be operating at a lower gain over the first segment. Good behavioral correlation between these pilots can also be observed. As seen with the other pilots and display configurations, there is a noticeable difference in phase angle between segment 1 and 2.

Probably one of the most important comparisons is that between head-up and head-down displays. Figure 11 also shows the open loop describing function for the head-down display mode for the same pilot pair (9 & 10), and should be compared with the C-4 head-up version results seen in the same figure. For C-4 head-down the first segment gain was higher by about 10 db around .39 rad/sec. This should be considered potentially important because pilots like to fly low gain when possible. Such is the case for the C-4 head-up display segment 1 where the gain appears to be low. The higher gain observed over the first segment for C-4 head-down is not too unlike that obtained over the second segment and indicates that about equal efforts are applied. Other than this, the only remaining feature is a slight higher shift in crossover frequency for the second segment C-4 head-down display. Phase and phase margin are about equal.

Pilot Workload Estimates

For the first segment, figure 12a shows that pilots who flew C-1 and progressed to fly C-4, showed an increase in crossover frequency. Over the same segment, pilots who flew C-4 head-down and progressed to fly C-4 head-up likewise increased their crossover frequency. An average estimate of crossover frequency appears to be about 1.4 rad/sec.

For the second segment, figure 12b shows that pilots who flew the C-1 display and progressed to fly C-4, showed an increase in crossover frequency. Pilots who flew C-4 head-down and progressed to C-4 head-up experienced a decrease in crossover frequency. Across the second segment, an overall average estimate of crossover frequency also appears to be around 1.4 rad/sec and similar to the first segment.

As another measure of how hard the pilots worked, figure 13 shows the ratio of control column (δ_c^2) output to the input distrubance (γ_d^2) across both segments for each of the three display configurations. It can be observed that the pilot's output for the first segment was substantially less than that for the second segment by about a factor of two. In either case, however, there appears to be an obvious difference in display aid between the C-1 and C-4 head-up displays, but with little evidence to support major differences between head-up or head-down displays. Further examination shows a 10-15% decrease in the pilot's control column spectral output to input ratio for the second segment C-4 head-down version compared to C-4 head-up which is the only

obvious trend. This trend toward the lower control column spectral output to input ratio for the C-4 head-down display may also be associated with the smaller glide slope deviation, which is half that observed for C-4, although the mean errors are essentially equal. Because changes in control column output ultimately result in glide path variations, a correlation with the effect upon glide slope error and their association with crossover frequency is suggested. Therefore, from figures 7 and 13, it can be seen that pilots who flew the C-4 displays had about equal glide slope errors and control column input/output spectral ratios. Further examination suggests investigating a tripartite correlation between normalized crossover frequency, glide slope error, and control column to input disturbance spectral ratio as seen in figures 14 and 15. This data was normalized from figures 7 and 13 for both segments. It appears that the higher crossover frequencies are related to more accurate glide slope tracking as reflected by an increase in the pilot's output power through his control column. This appears generally across both segments for pilots transitioning from low display aid (C-1) to increased display aid (C-4). Figure 15 shows that pilots transitioning from head-down to head-up display aid for the second segment, crossover frequency decreases and flight path error and control column output power increases. The exception occurred for pilot 9 over the first segment where crossover frequency increased rather than decreased. Because the second segment encompasses the transition from high to low approach glide slope, more emphasis should be placed on the second segment as the more critical maneuver area. It should be emphasized at this point that all the pilot describing functions over the second segment (figures 8 & 9) show more dramatic phase changes whereas the gain was more uniform for either segment. Therefore, considering the second segment, it appears that the pilots were more consistent and performed better with the C-4 head-down display. There is an explanation why the pilots verbally expressed a preference and more confidence with the C-4 head-up display, even though this conflicted with the measured data. One explanation stands out. That for displays presented in true or in real world perspective and viewed through the windscreens, the pilot is allowed to identify and orient himself subconsciously in space, whereas when compressing the display for head-down operations, the pilot may loose his ability to identify his true position relative to real world space. Consequently, he tries to compensate through inflated work efforts as reflected through his control column output strategies and the resultant effect upon glide slope errors.

Conclusions

The literature of describing function measurements aimed toward the evaluation of complex flight displays is very limited. Of current interest is the development of landing aid displays to assist the pilot for an unpowered Space Shuttle final approach maneuver. Conventional landing performance data taken during the approach and landing, generally need more powerful measurement techniques in order to make a responsible decision in terms of assessing display aid to the pilot. Describing function measurements can be used to provide a support measure for other performance data. Use of a modified Fast Fourier transform was integrated into the display program to investigate the pictorial display concepts designed for increasing display aid to the pilot. Three displays were evaluated by four pilots for either a head-up or head-down display operating throughout a simulated unpowered final approach maneuver.

Among the display features were accentuated ground referenced pre-flare and runway positioned aiming point references and velocity vector information for flight path alignment. The primary task was one of flight path regulation. As determined from performance criteria and both pilot and open loop describing functions, the pilots' ability or strategies varied between the pre-transitional and transitional segmental phases of the flight maneuver. Marked differences occurred between the simplified and the more sophisticated display aid through both segments. According to the pilot describing function analysis, the more sophisticated display aid was favored. For the open loop describing function analysis, the crossover frequencies tend to increase for the more advanced display aid over both approach segments. Comparing head-up to head-down displays, the crossover frequencies are equal over the first segment and tend to increase slightly for the head-down display over the second segment.

Larger glide-slope errors occurred over the first pre-transitional segment and were reduced over the second segment. A tripartite correlation between crossover frequency, glide-slope error, and ratio of control column power to input disturbance indicates that lower glide slope errors are related to higher crossover frequencies and higher control column activity. The pilots tended to relax more and preferred the head-up displays. The performance relative to crossover frequency, glide slope error and control column power over the first pre-transitional

segment was about evenly divided between the head-up and head-down displays. During the second more critical transitional segment it appears that the pilot's performance was better for the head-down operations. One possible explanation is that the pilots tend to loose their space orientation and true world perspective when the entire head-up version is compressed to a small panel representation. The reaction among the pilots was that the head-down display required more concerted efforts to achieve satisfactory performance compared to the head-up display. From the results of the measured pilot transfer function and the technique of analyzing a flight path loop, the data obtained appear to be consistent and repeatable. These results are obtained in a very complex environment whereby the describing function approach can be applied to a complex time varying task such as that demonstrated by the Space Shuttle final approach maneuver. Although one cannot easily surmise the psychological impact of pilot display preference or confidence and its possible conflict with other types of performance data, it is felt that the above extrapolation of these data obtained through describing function measurements lend more support in predicting display evaluation for Space Shuttle operations. A thorough and sound engineering evaluation of other advanced display concepts could be approached by this technique providing that a good experimental design with sufficient replications and pilots are included.

REFERENCES

1. Naish, J. M., "Head-Up Display for the Visual Approach," 8th Annual Conference on Manual Control, University of Michigan, May 1972.

2. Naish, J. M., "Combination of Information in Superimposed Visual Fields," Nature, Vol. 202, May 1964, pp. 641-646.

3. Gartner, W. B. & Jenny, L. L., "Display Requirements and Concepts for Space Shuttle Recovery and Landing," prospective NASA Contractor Report NASW-1987, NASA Headquarters, July 1971.

4. Garner, W. B. & Baldwin, K. M., "Simulator Evaluation of Display Concepts for Pilot Monitoring and Control of Space Shuttle Approach and Landing," prospective Contractor Report NAS2-6460, NASA-Ames January 1973.

5. Weir, D. H. & McRuer, D. T., "Pilot Dynamics for Instrument Approach Tasks: Full Panel Multiloop and Flight Director Operations," NASA CR-2019, May 1972.

6. Osder, S. & Keller, R., "Study of Automatic and Manual Terminal Guidance and Control Systems for Space Shuttle Vehicles." Sperry Flight Systems Division Final Report No. 71-0225-01-00, August 1971.

7. Shirley, R. S., "Application of a Modified Fast Fourier Transform to Calculate Human Operator Describing Functions," NASA TM X-1762, March 1969.

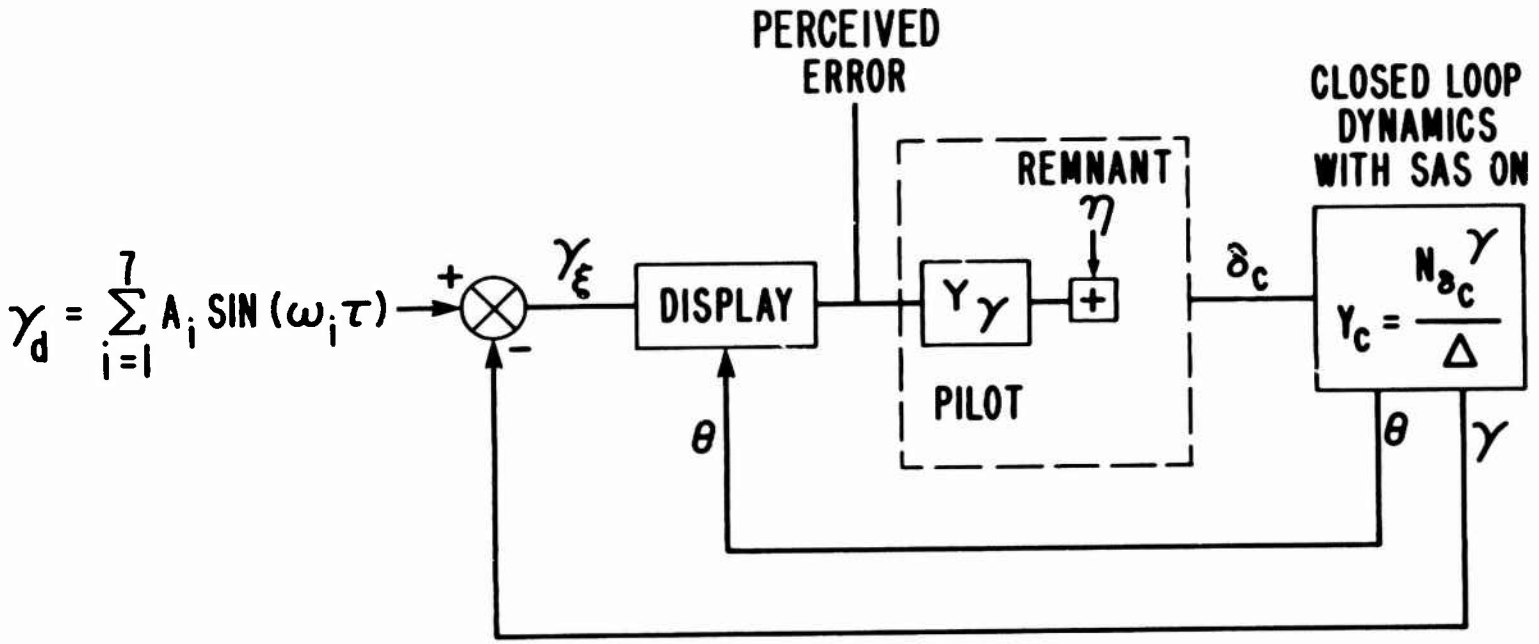

Figure 1.- Block Diagram of Longitudinal Airframe with Manual Stability Augmentation System (SAS) on and Disturbance Input.

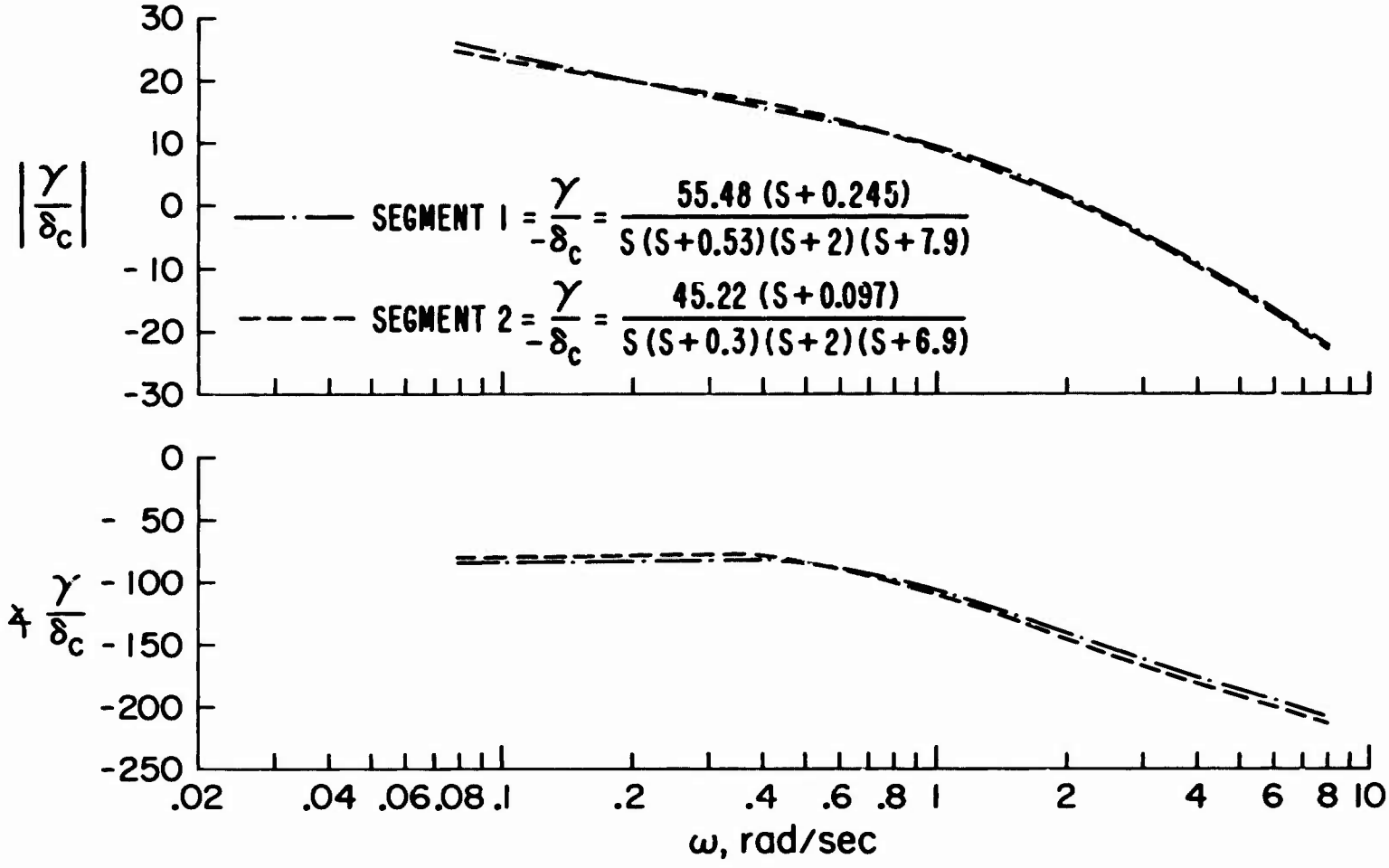

Figure 2.- Closed Loop Vehicle Dynamics with SAS on, Manual Mode, Over Segments 1 and 2.

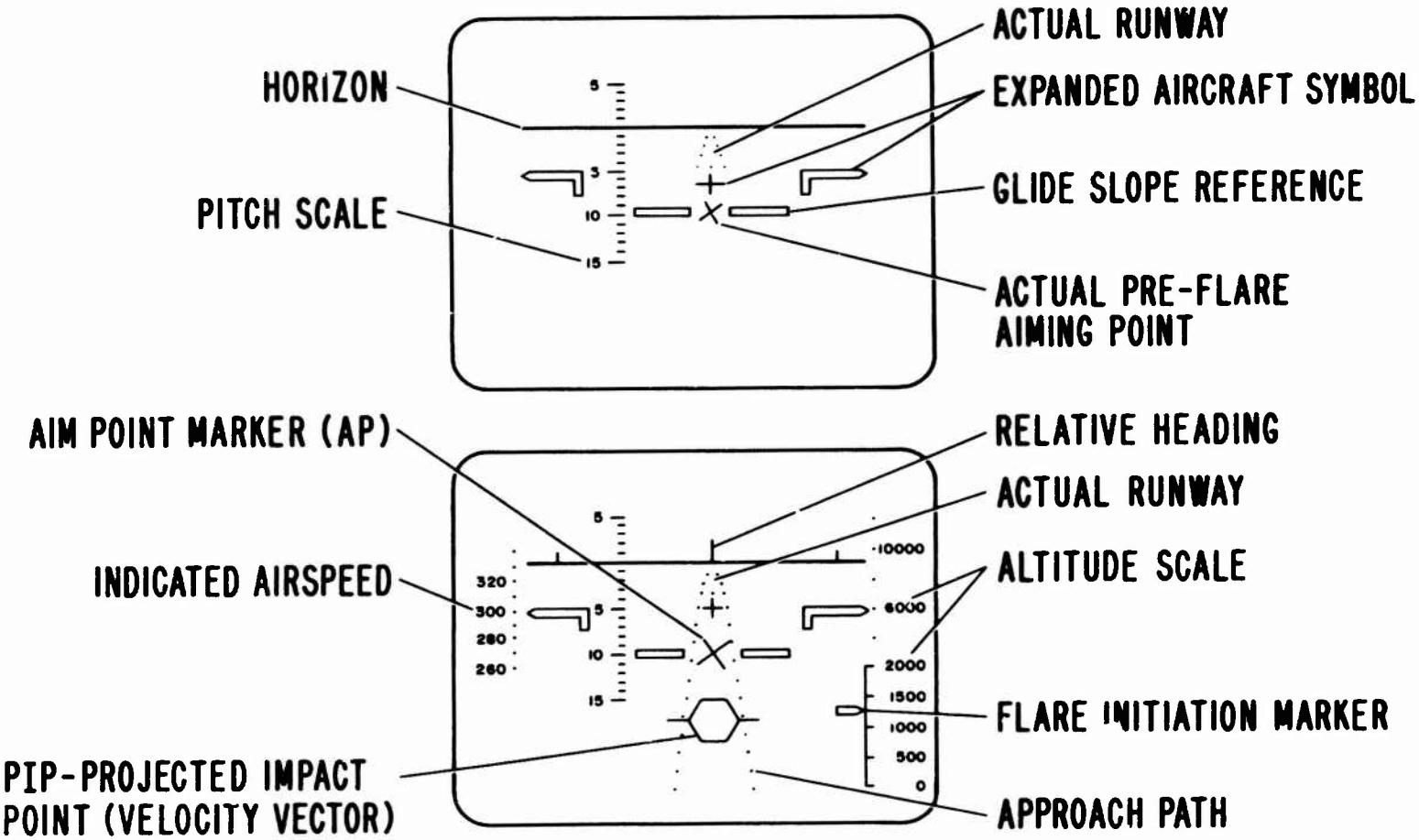

Figure 3.- Illustration of Simplified and Full Complement Display Elements.

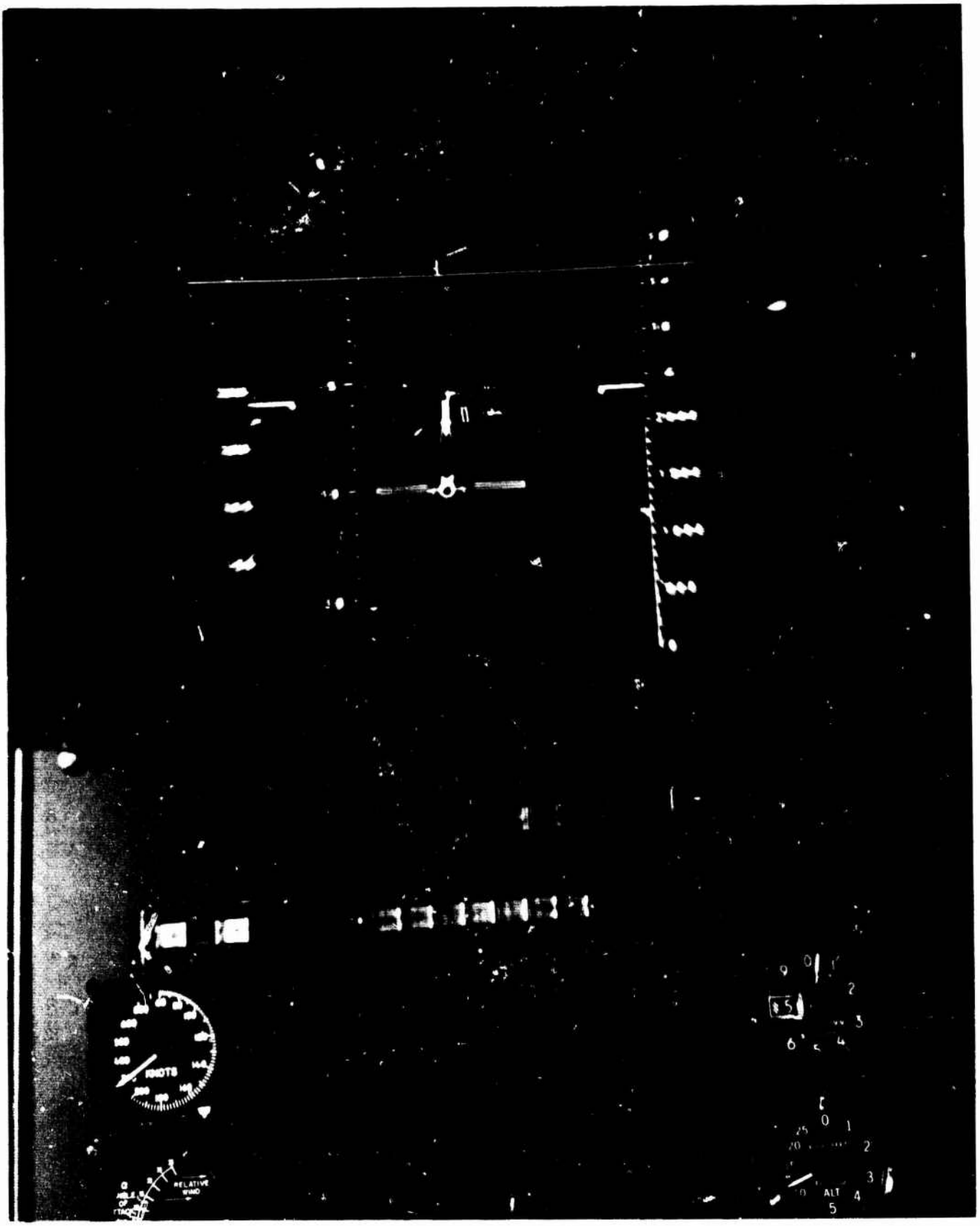

Figure 4.- Full Display Complement in Head-up Viewing Position and Panel CRT for Head-down Operations. -692-

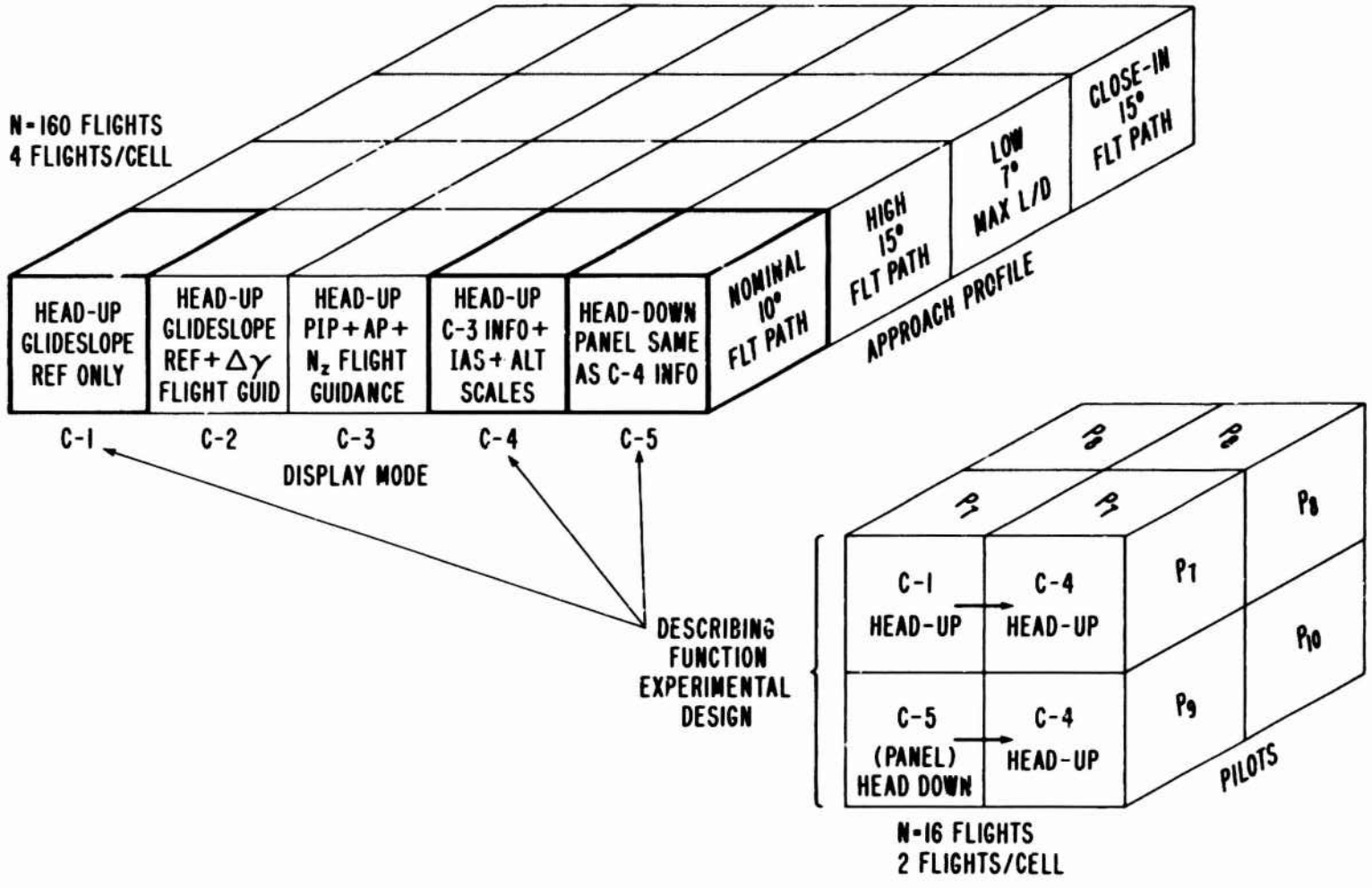

Figure 5.- Experimental Design for Describing Function Measurements.

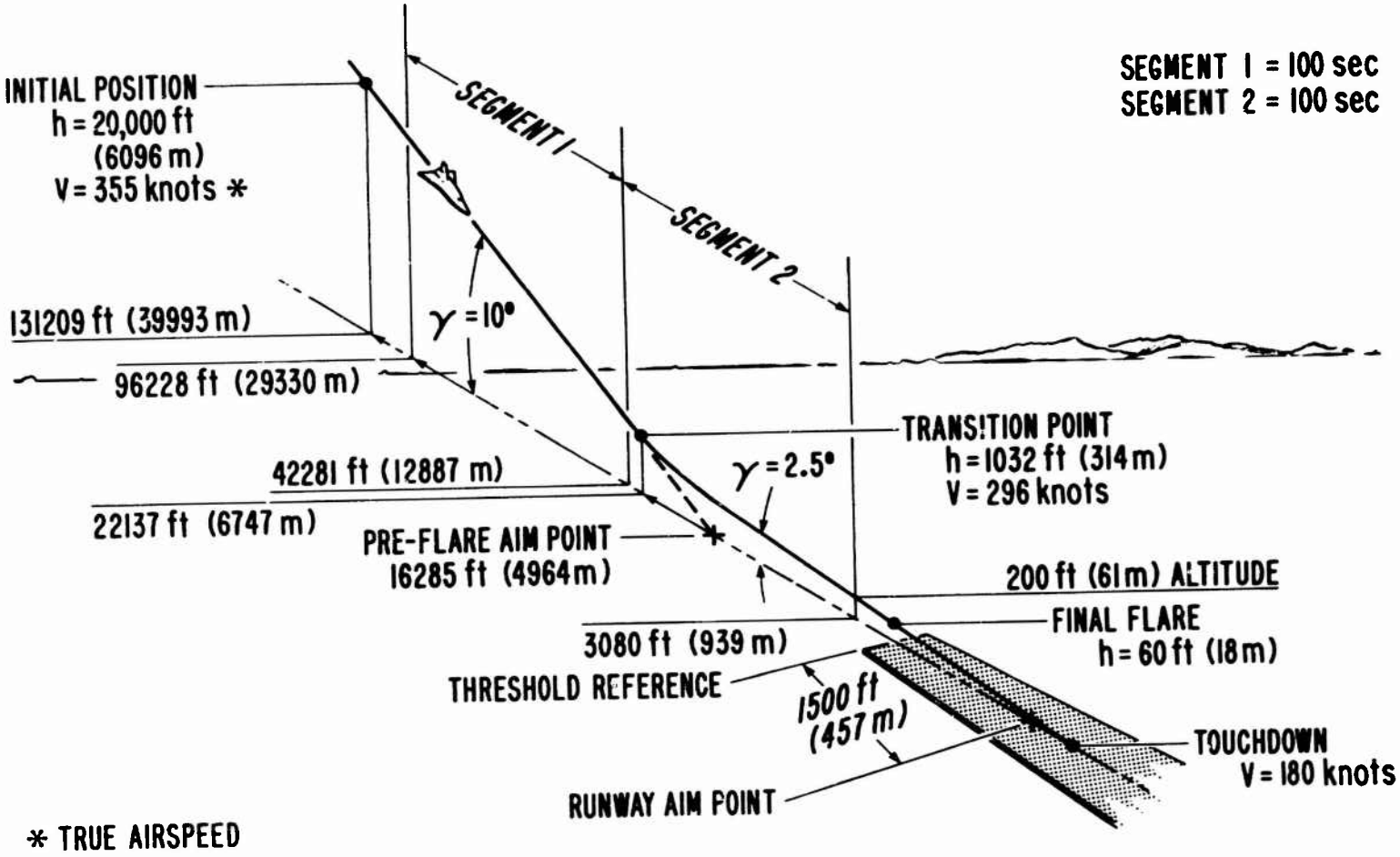

Figure 6.- Final Approach Geometry with Pre-flare and Runway Aiming Point Symbology.

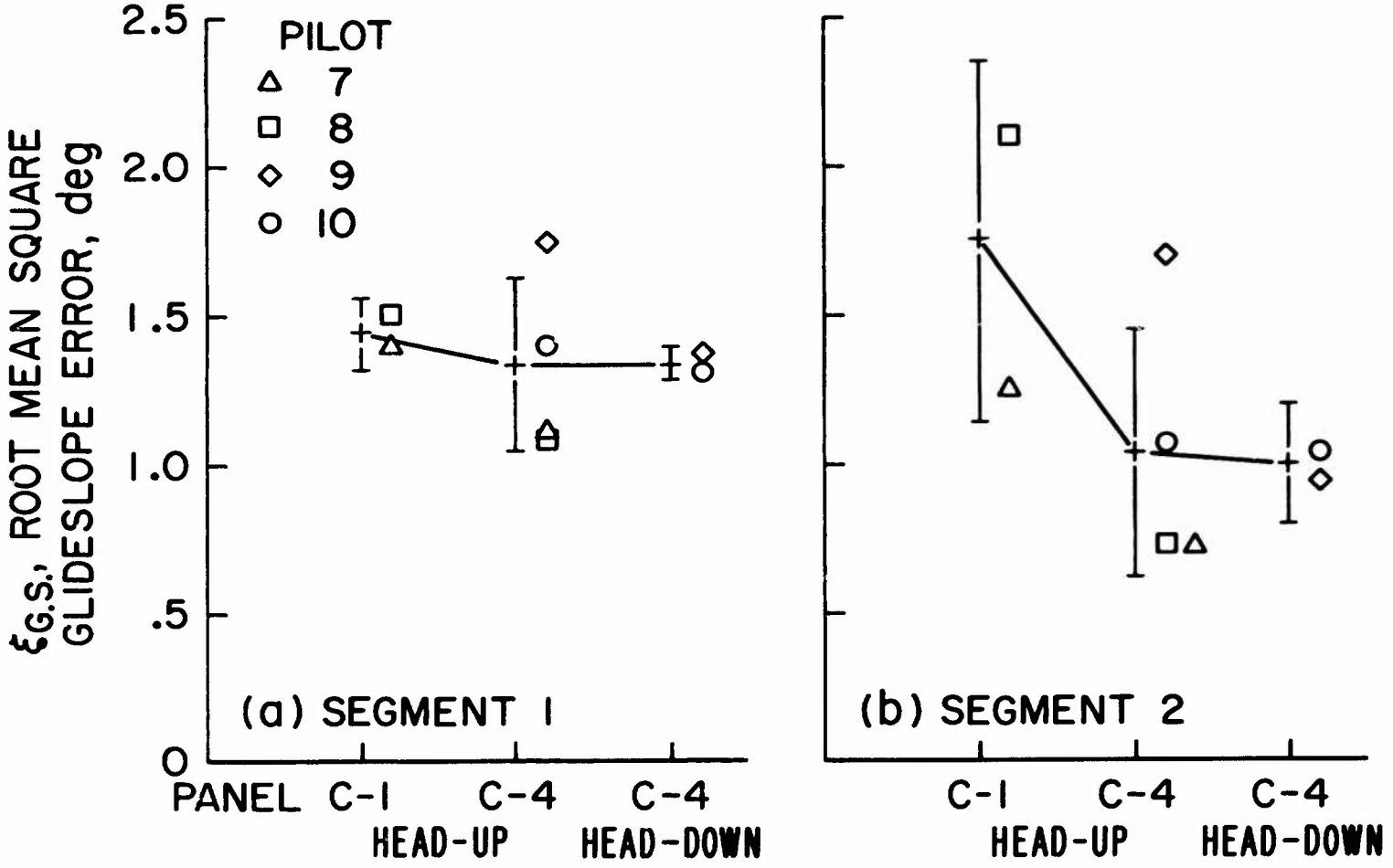

Figure 7.- Glideslope (Root Mean Square) Tracking Accuracy on First and Second Segments Obtained with Disturbance Input.

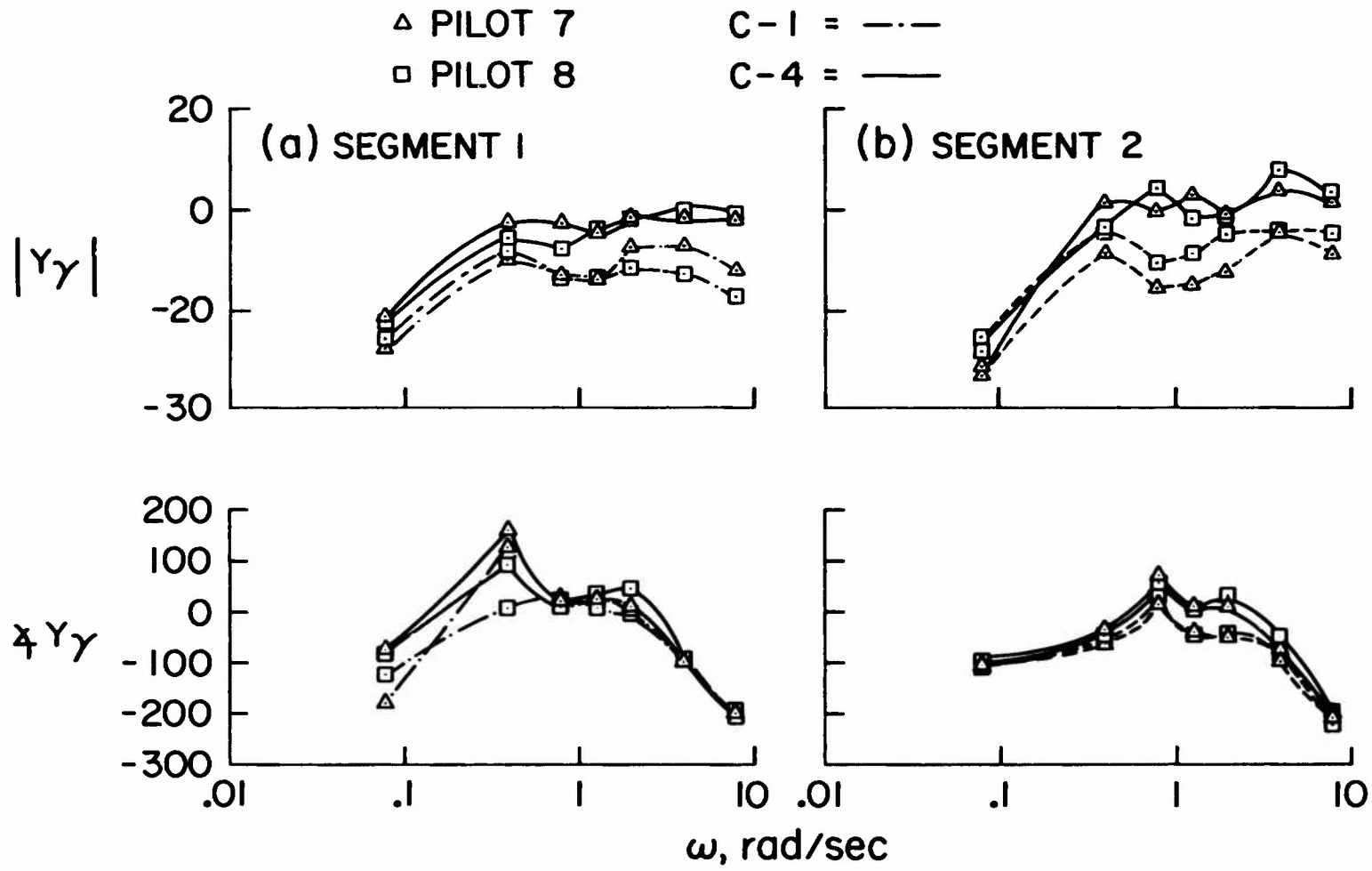

Figure 8.- Pilot Describing Function for C-1 and C-4 Display Mode.

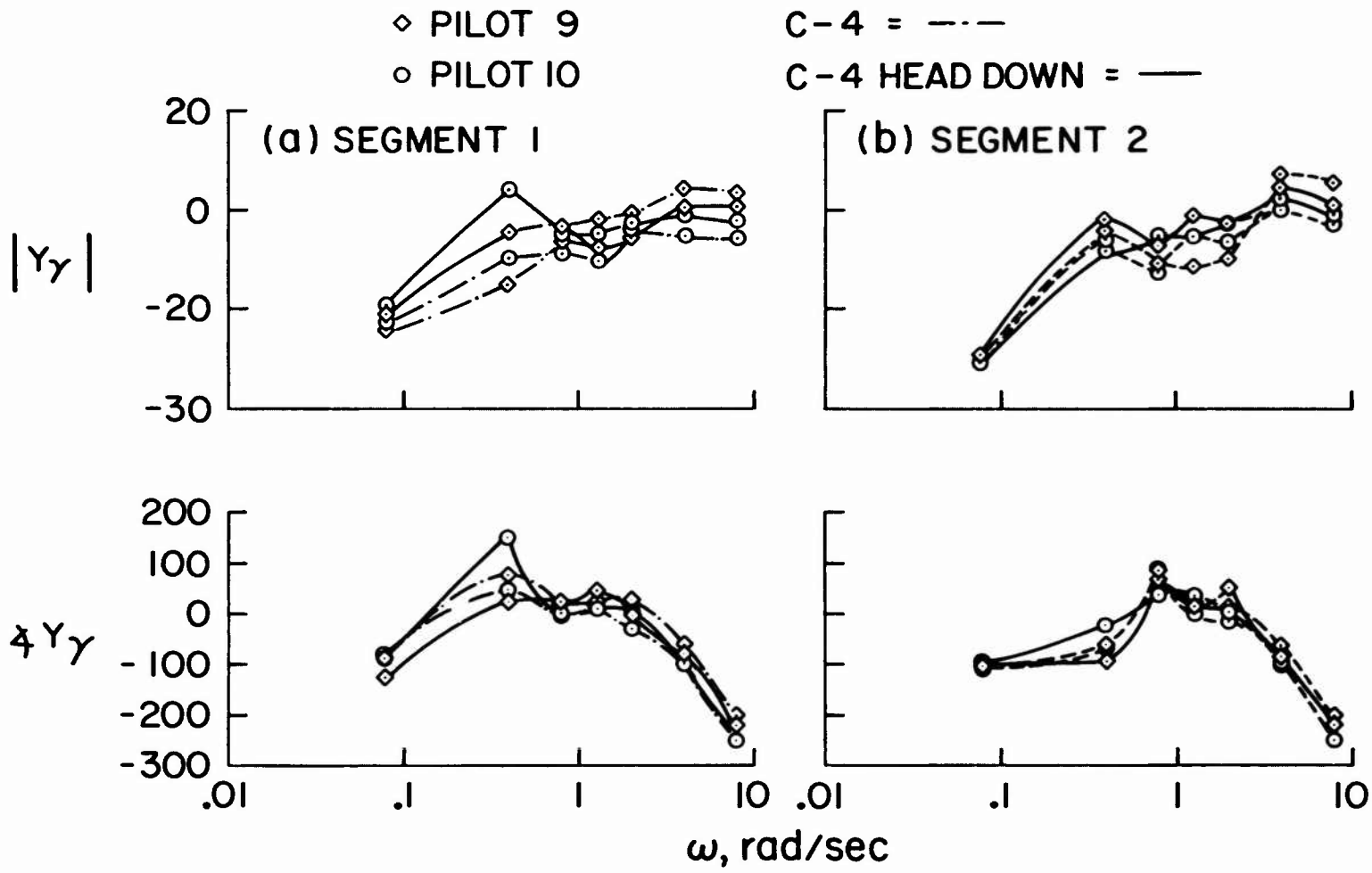

Figure 9.- Pilot Describing Function for C-4 and C-4 Head-down Display Mode.

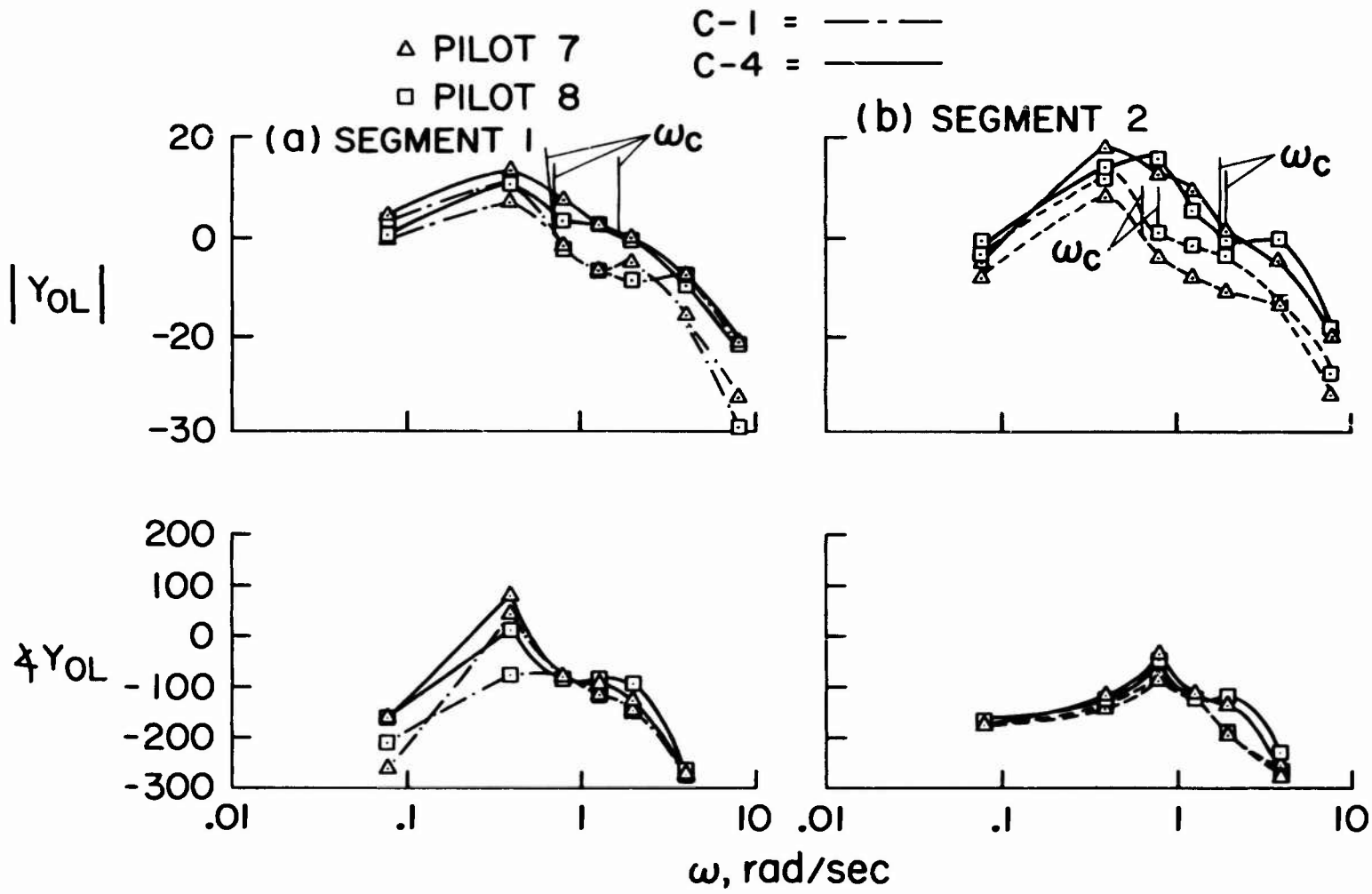

Figure 10.- Open Loop Describing Function for C-1 and C-4 Display Mode.

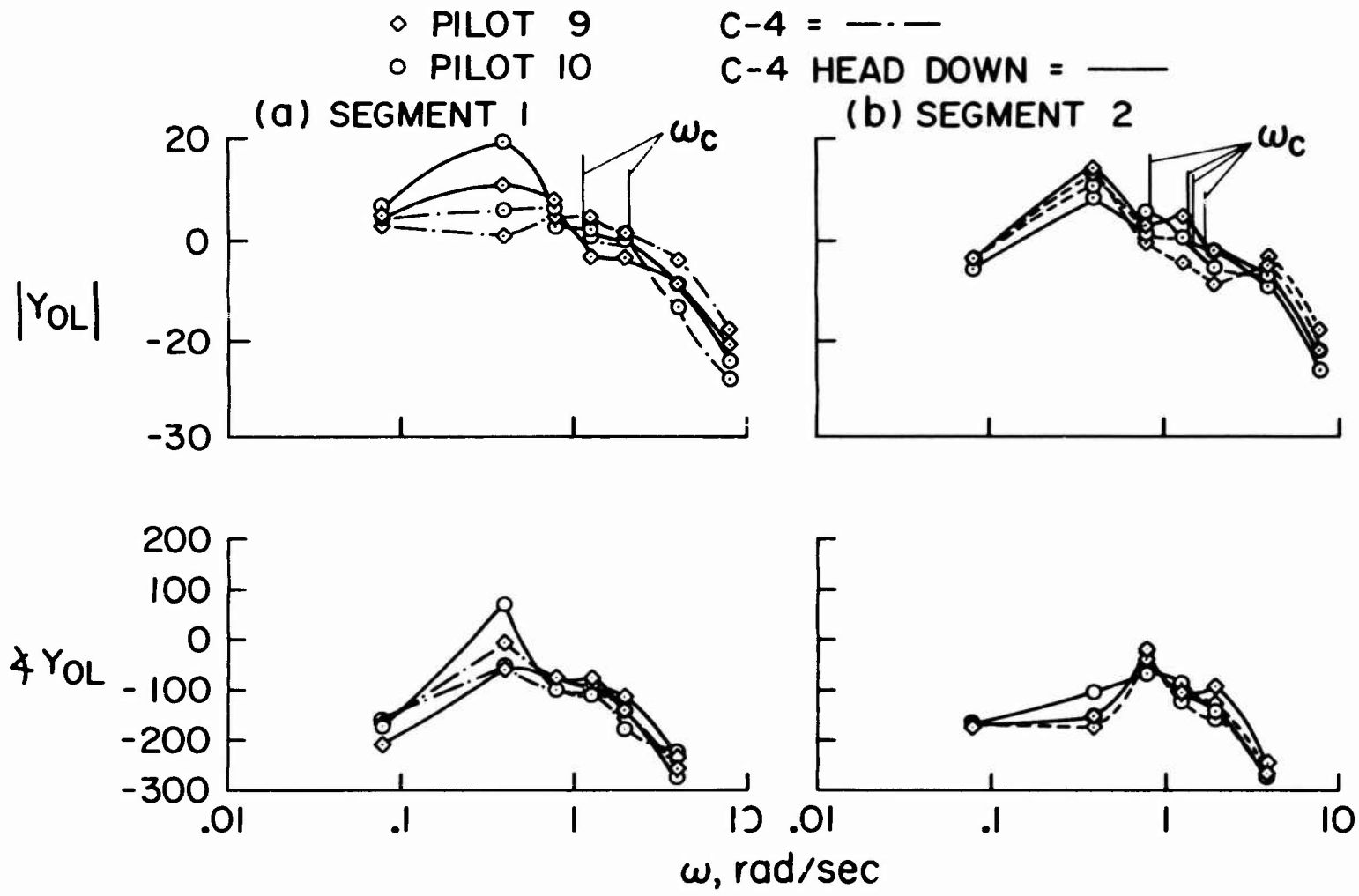

Figure 11.- Open Loop Describing Function for C-4 and C-4 Head-down Display Mode.

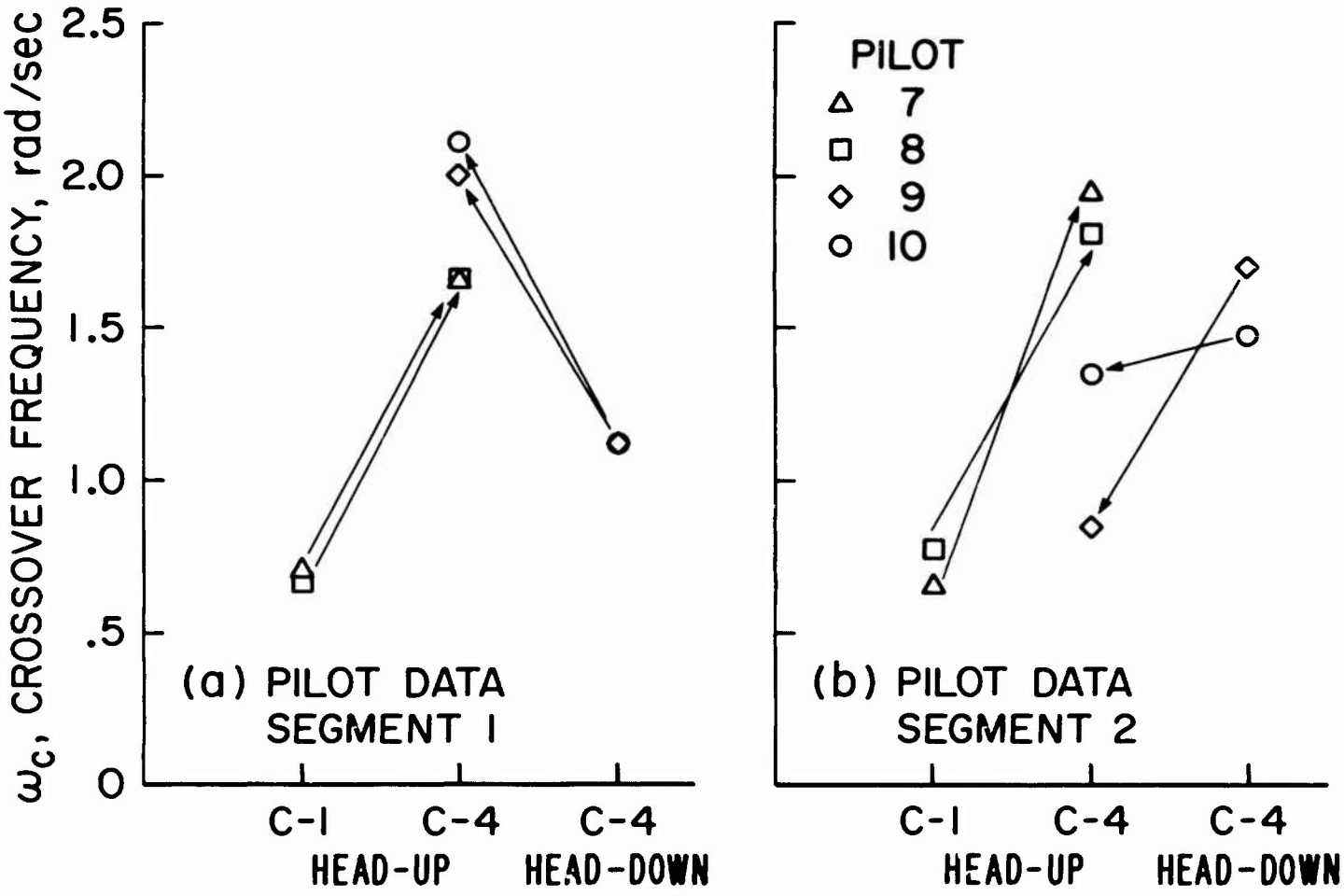

NOTE: ARROWS REFRESENT ORDER OF DISPLAY PRESENTATION

Figure 12.- Relationship of Crossover Frequency to Displays.

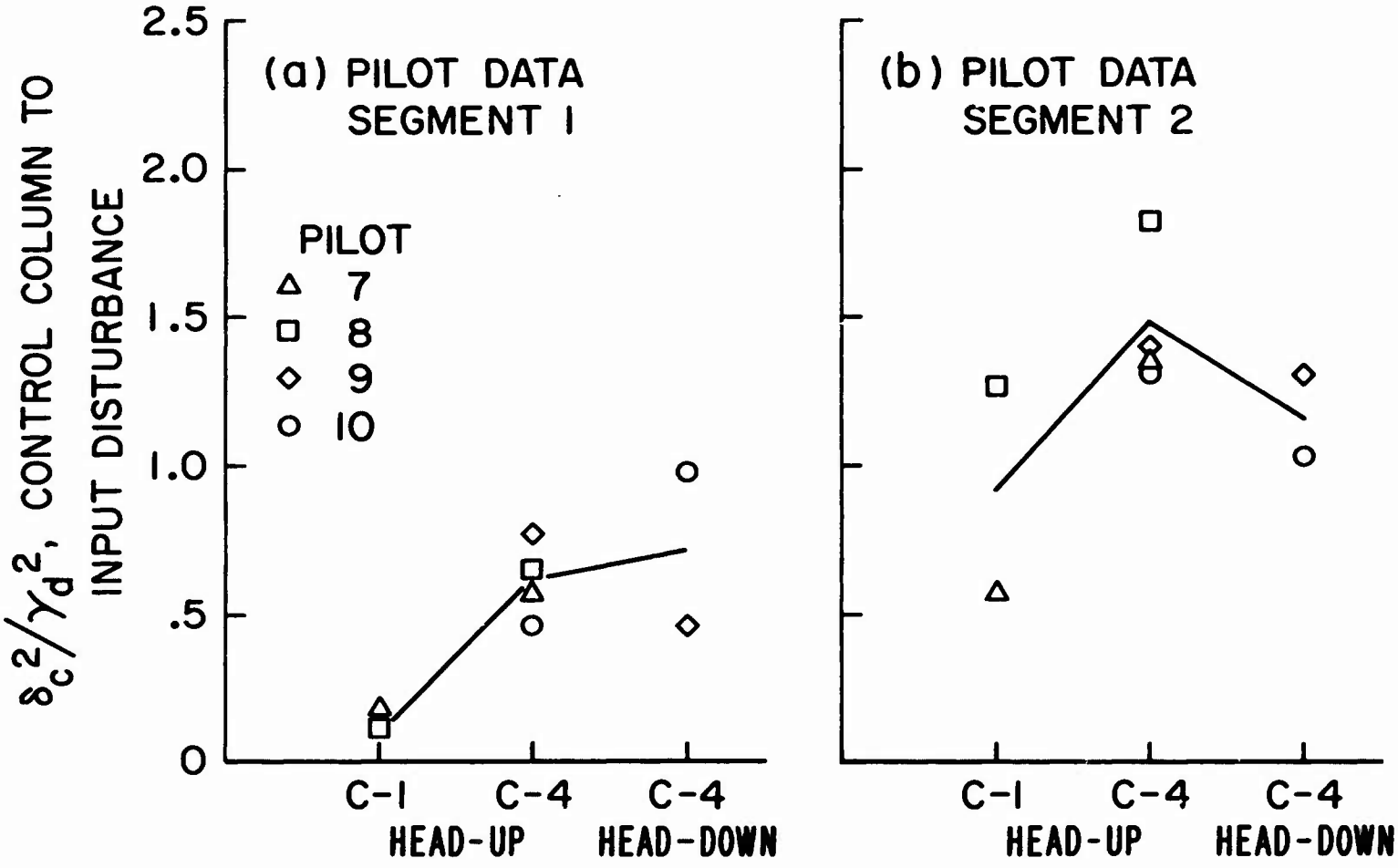

Figure 13.- Relationship of Pilot's Control Column Output to Input Disturbance as a Function of Displays.

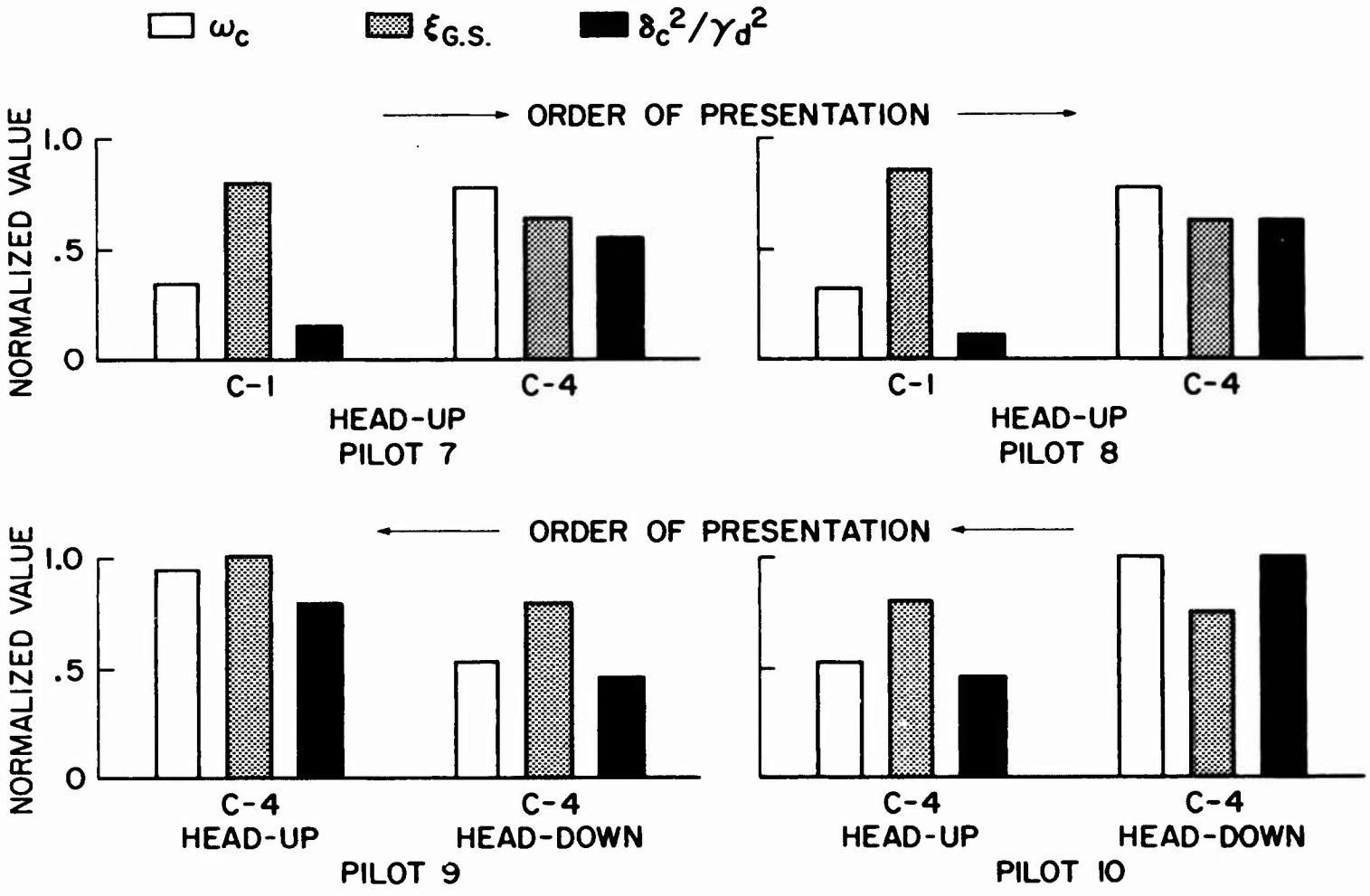

Figure 14.- First Segment Total Correlated Crossover Frequency, Glide Slope Error and Ratio of Control Column to Input Disturbance Versus Displays.

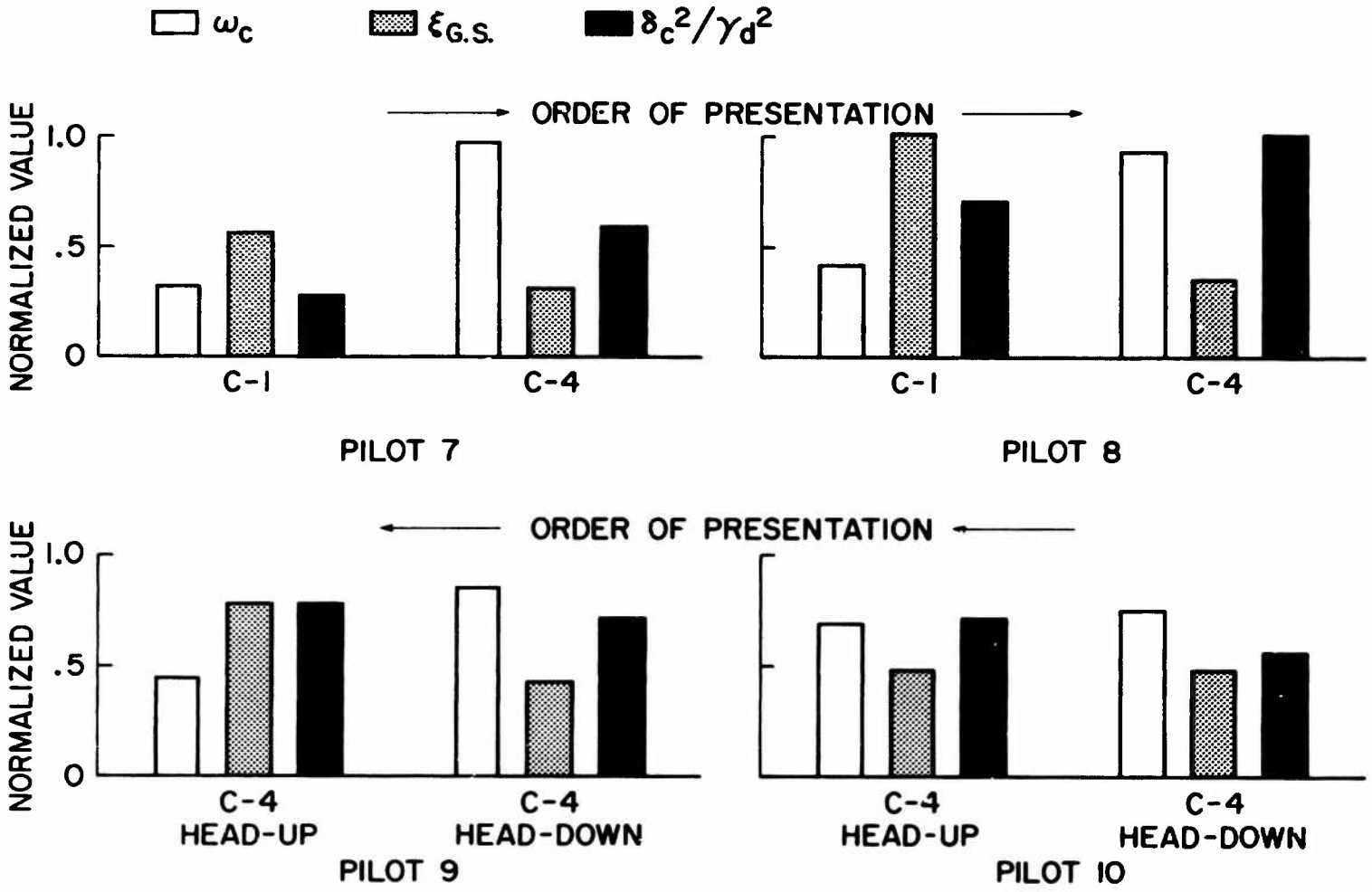

Figure 15.- Second Segment Total Correlated Crossover Frequency, Glide Slope Error and Ratio of Control Column to Input Disturbance Versus Displays.

PAPER PILOT HOVERS LATERALLY

David L. Nolting*, James D. Dillow, Russell A. Hannen

SUMMARY

Data was obtained from a fixed base simulation of VTOL aircraft in the lateral hover mode and used to develope a technique for predicting lateral hover flying qualities. The task for the simulation was to maintain position in the presence of lateral gusts. Root-mean-square aircraft state and pilot input data were obtained and correlated with Cooper-Harper Pilot Ratings. A mathematical model for predicting the pilot rating of VTOL aircraft in lateral hover is developed. This model includes: (1) the lateral hover aircraft equations of motion; (2) a stochastic gust model; (3) a linear pilot model; and (4) a pilot rating expression that is a function of rms position error, rms lateral velocity, rms roll rate, and pilot lead terms. Pilot gains and lead time constants are chosen to minimize the pilot rating. Predicted and actual pilot ratings and performance are compared for the fixed base simulation data. The differences between predicted and actual pilot ratings have a mean of 0.11 rating units and a standard deviation of 0.24 rating units on a 10 point scale. Predicted and actual pilot ratings are compared for 131 additional aircraft configurations with differences less than ± 1.0 rating unit for 82.4% of the cases.

INTRODUCTION

The paper pilot concept for predicting aircraft handling qualities in a specified piloted task is based on the following hypothesis.

1. For a well defined task, the pilot rating is a function of the closed loop performance and the pilot workload. This function is called the pilot rating expression.

2. The predicted pilot rating can be obtained by minimizing the pilot rating expression with respect to free pilot parameters in the closed loop pilot-vehicle model. (The lower the rating--the better the handling qualities.) The minimal value of the pilot rating expression corresponds to the pilot rating for the task.

The paper pilot concept has been demonstrated in the past for various tasks including longitudinal hover, pitch tracking, roll attitude, and heading tasks (Refs 1 through 5). In this study the paper pilot concept is applied to the task of maintaining a fixed position over the ground in a vertical take off

---

*Currently assigned to the 6585 Test Group, Holloman AFB, New Mexico.

and landing (VTOL) type aircraft. Lateral disturbances are introduced in the form of a side turbulence. Longitudinal motion was not considered.

In this paper the simulation study used to collect performance data and pilot ratings is briefly described. This data was used to develop a pilot rating expression which is a function of the rms lateral hover error, rms roll rate, rms side slip, and two pilot leads in the pilot model. Predicted pilot ratings are computed by selecting four free parameters in the pilot model so as to minimize the pilot rating expression. These results are compared to the actual pilot ratings obtained from the simulation. This method of predicting pilot rating was also used for 15? other configurations for which pilot rating data was available. The predicted pilot ratings are compared to actual ratings for these cases. Details of this paper are contained in Ref 6.

SIMULATION

A fixed base simulation was used to collect data on the lateral hover task. The simulation was conducted at the Flight Control Division of the Air Force Flight Dynamics Laboratory, Wright-Patterson Air Force Base, Ohio.

The equations of motion for roll and lateral displacement for hover are taken from Ref 7. These equations assume small perturbations from hovering flight. The general form of the linearized lateral equations, assuming lateral translations can be affected only through roll, are

$$\dot{y} = v$$

$$\dot{v} = Y_v v + \frac{g}{57.3}\phi + Y_v v_g$$

$$\dot{\phi} = p$$

$$\dot{p} = 57.3\, L_v v + L_\phi \phi + L_p p + L_{\delta_a}\delta_a + 57.3\, L_v v_g$$

$$\dot{\delta}_a = -\frac{1}{\tau_a}\delta_a + \frac{1}{\tau_a}\delta$$

where y is lateral displacement, v is lateral velocity, ϕ is roll angle, p is roll rate, δ_a is effective control input, δ is commanded control input, τ_a is the control lag time constant, and v_g is turbulence velocity in the v direction. All angles are in degrees. Displacement, y, is in ft and v and v_g are in ft/sec.

The turbulence was simulated by passing a white Gaussian random process through a first order filter with a break frequency of 0.314 rad/sec. This is a first order approximation to the Dryden gust model (Ref 8) and is the gust model used in Ref 7. An rms turbulence level of 5.1 ft/sec was used, consistent with Ref 7.

The task in this experiment was to maintain a fixed position relative to a reference line in the presence of turbulence. This task is similar to the lateral hover experiment in Ref 7, except that no longitudinal motion was simulated for this study. A side force stick with a USAF fighter-type grip was used for pilot inputs to the system. The stick sensitivity was selected by each pilot to give the preferred roll acceleration per pound input for a given configuration. Aircraft roll altitude and lateral displacement were displayed on a dual beam oscilloscope. The scope was placed level with and approximately 20 inches from the pilots eyes. The scope display is shown in Fig. 1. A vertical line indicated actual position. As

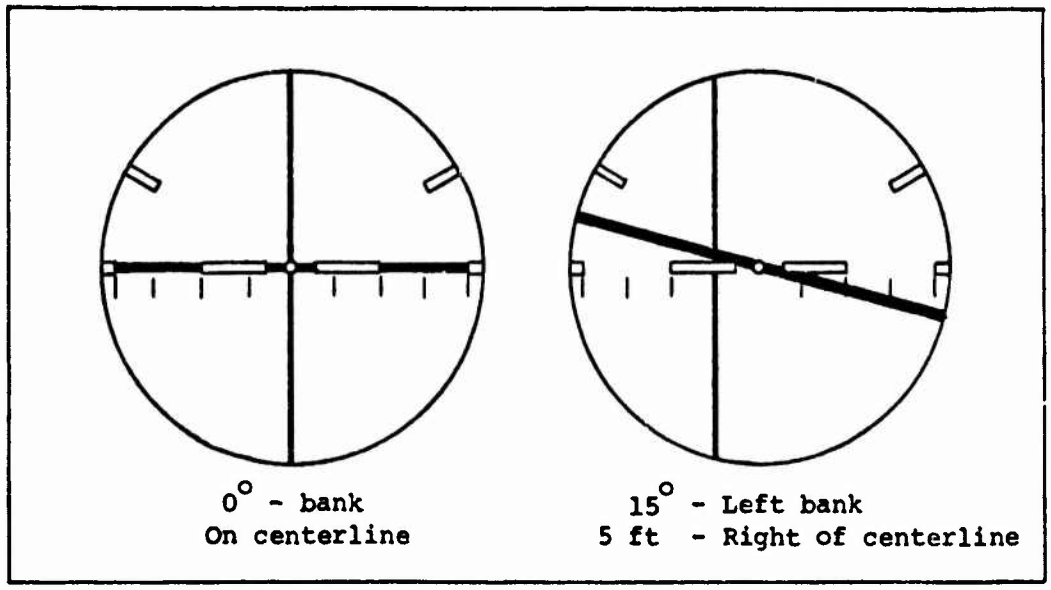

Fig. 1. Roll and Lateral Position Display with Desired Position and Disturbed Position.

viewed by the pilot, the movement of the vertical line corresponded to the apparent movement of a vertical pole located approximately 200 feet in front of the pilot. Roll angle was displayed by a rotating "horizon" line. This line rotated about the center of the display. One degree of indicated roll equaled one degree of simulated aircraft roll. Fifteen cases were selected from Ref 7 for the simulation. The cases were selected to give a wide range of pilot rating with 8 cases between 3.0 to 4.0. An attempt was also made to include a

wide range of different stability derivatives which are indicative of a diverse set of flight conditions.

Four military pilots participated in the experiment. Two of the pilots had helicopter experience; however, helicopter experience was not a significant factor in this task. Each pilot was thoroughly trained with each configuration before data was taken. The Cooper-Harper rating scale was used to obtain numerical pilot ratings (Ref 8).

The pilot ratings from this simulation are compared with those obtained from Ref 7 in Fig. 2. The most important differences in pilot rating come basically from two sources. First, Miller and Vinje used the Harper scale (Ref 7) and this simulation used the revised Cooper-Harper scale (Ref 8). Second, Miller and Vinje used a sophisticated contact analog display system to indicate aircraft position and altitude. The display sensitivity provided information comparable to actual low altitude hovering flight. The oscilloscope display used in this experiment provided information comparable to hovering on instruments. This is a much more difficult task.

The data indicated that different pilot techniques do not significantly change the pilot ratings. Pilot DB worked harder and maintained smaller hover error in most cases than did pilot EL. Pilot EL did not work as hard and accepted larger hover error. However, their pilot ratings do not differ significantly

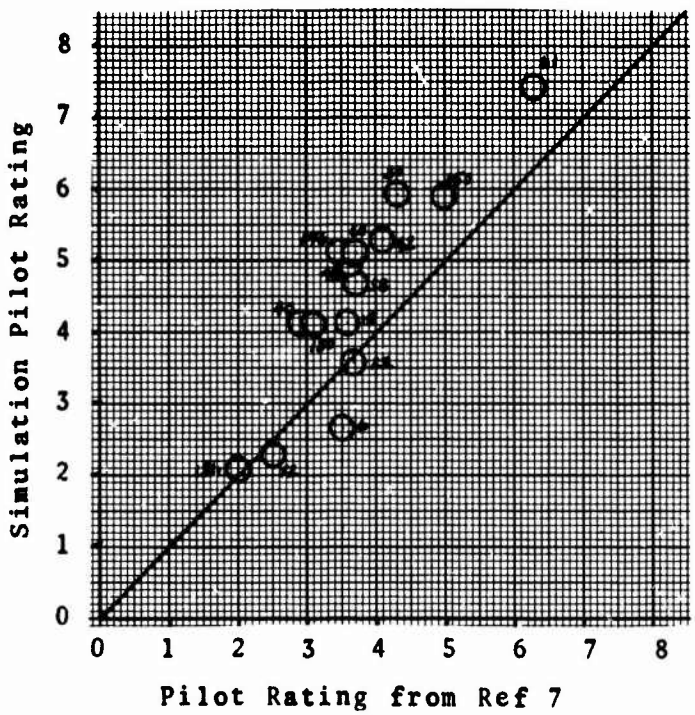

Fig. 2. Comparison of Simulation and Miller-Vinje Pilot Ratings.

for the 15 cases flown. This tends to support the theory that pilot rating is a sum of a measure of workload and a measure of performance as postulated by Anderson (Ref 1).

PAPER PILOT

An analytic model of the closed loop pilot vehicle system was used to predict pilot rating and system performance.

The pilot model used is the fixed form model shown in Fig. 3. K_{p_y} and K_{p_ϕ} are pilot gains, T_{L_y} and T_{L_ϕ} are pilot leads, T_{I_y} and T_{I_ϕ} are pilot lags, and $e^{-\tau s}$ is a pure time

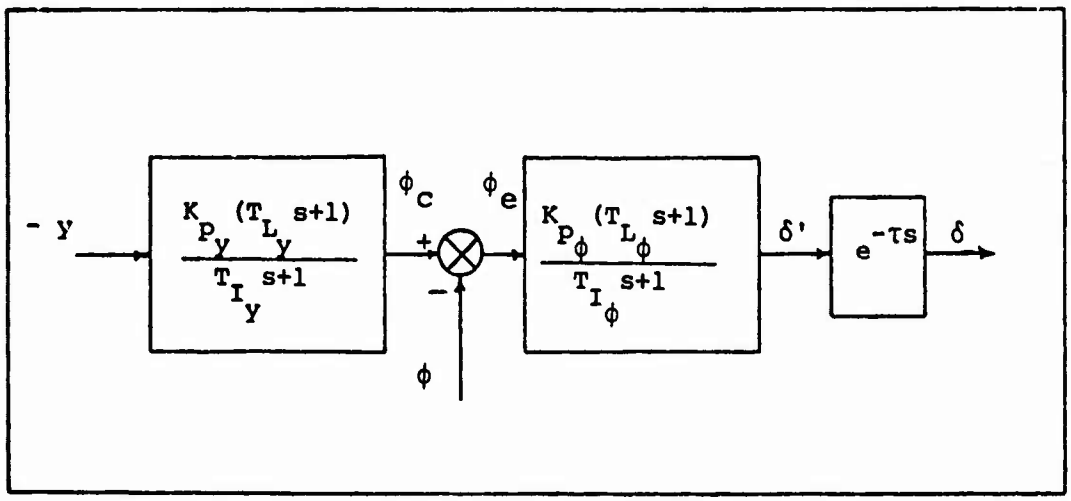

Fig. 3. Fixed Form Pilot Model.

delay. The y and ϕ subscripts indicate the position and roll loops respectively. Various values for the lag and time delay terms were examined. The final values selected give the best performance match between the simulation and digital computer results. These values are $\tau = 0.4$ sec, $T_{I_y} = 0.05$ sec, and $T_{I_\phi} = 0.15$ sec. K_{p_y}, K_{p_ϕ}, T_{L_y}, and T_{L_ϕ} are considered as free parameters in the optimization procedure described below.

The predicted pilot rating and performance is obtained in the following manner. The four free pilot parameters are selected to minimize the pilot rating expression given by

$$PR = PERF + .26\, T_{L_y} + 1.25\, T_{L_\theta} + 1.0$$

where

$$PERF = \begin{cases} TPERF & , TPERF \leq 5.0 \\ \frac{1}{2}(TPERF + 5.0) & , TPERF > 5.0 \end{cases}$$

and

$$TPERF = .3\,\sigma_y + .34\,\sigma_v + .48\,\sigma_p$$

As in the simulation, a rms gust disturbance velocity, σ_{v_g}, of 5.1 ft/sec was used. The resulting minimum value of PR is the paper pilot rating.

The expression for PERF in the pilot rating expression reflects the assumption that once rms performance exceeds a certain level, any further degradation in performance is not rated as heavily by the pilot. The weightings on the pilot lead terms and the weightings on the rms values of y, p, and ϕ in the pilot rating expression were determined by an iterative procedure described in Ref 6. This iterative procedure uses the data obtained in the simulation to derive the set of weightings. The predicted values for pilot rating and performance agree well with the data from the simulation. The scatter diagrams comparing predicted and simulated pilot rating and performance are shown in Figs. 4 through 9. The difference between pilot ratings from the minimization technique and the simulation is less than 0.5 in all but one case.

The predicted rms performance values also compare quite well with the results from the simulation. There is a tendency for predicted rms performance to be lower than actual rms performance values. This is especially true for pilot input, δ_a. Roll and roll rate are also somewhat low. This could possibly be explained by the absence of pilot remnant in the pilot model. Since pilot remnant adds uncertainty, it would tend to increase the predicted rms performance. Thus the addition of remnant in the pilot model would cause a closer match between the predicted and simulation rms performance values.

TESTING PAPER PILOT

If the "paper pilot" concept is valid, the minimization routine should accurately predict pilot ratings for configurations that were not used in the development of the pilot rating expression. Miller and Vinje (Ref 7) tested 166 lateral hover configurations. Fifteen of these cases were used in this study to develop the pilot rating expression. Of the remaining cases, 20 could not be used because they were tested in Ref 7 without a gust input. The remaining 131 cases were used to test the ability of the paper pilot scheme to accurately predicted pilot ratings.

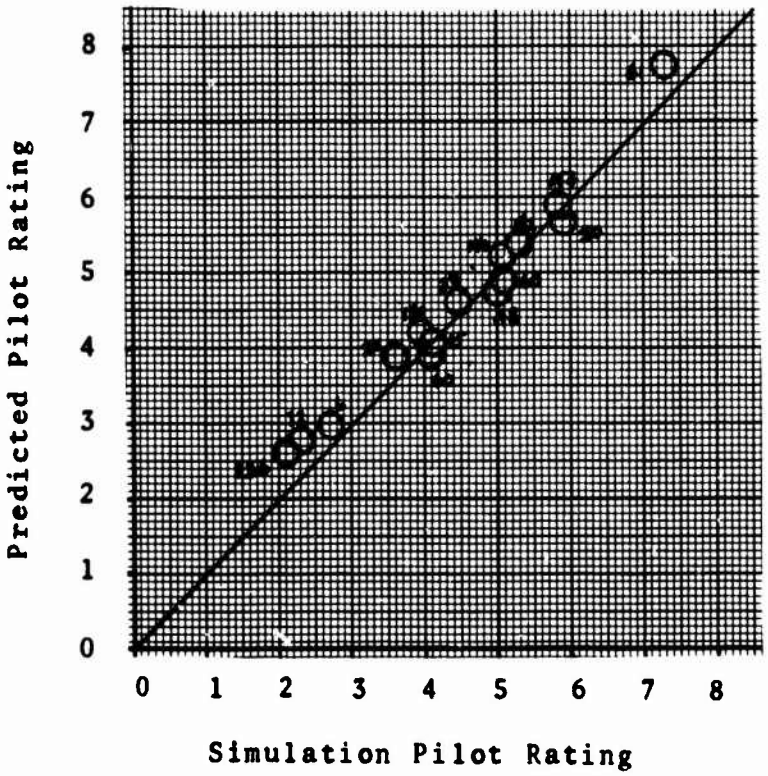

Fig. 4. Predicted Pilot Rating vs. Simulation Pilot Rating.

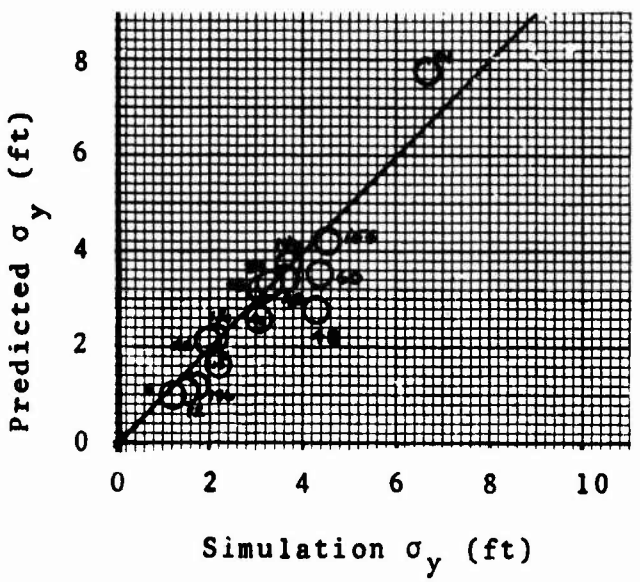

Fig. 5. Predicted vs. Simulation σ_y.

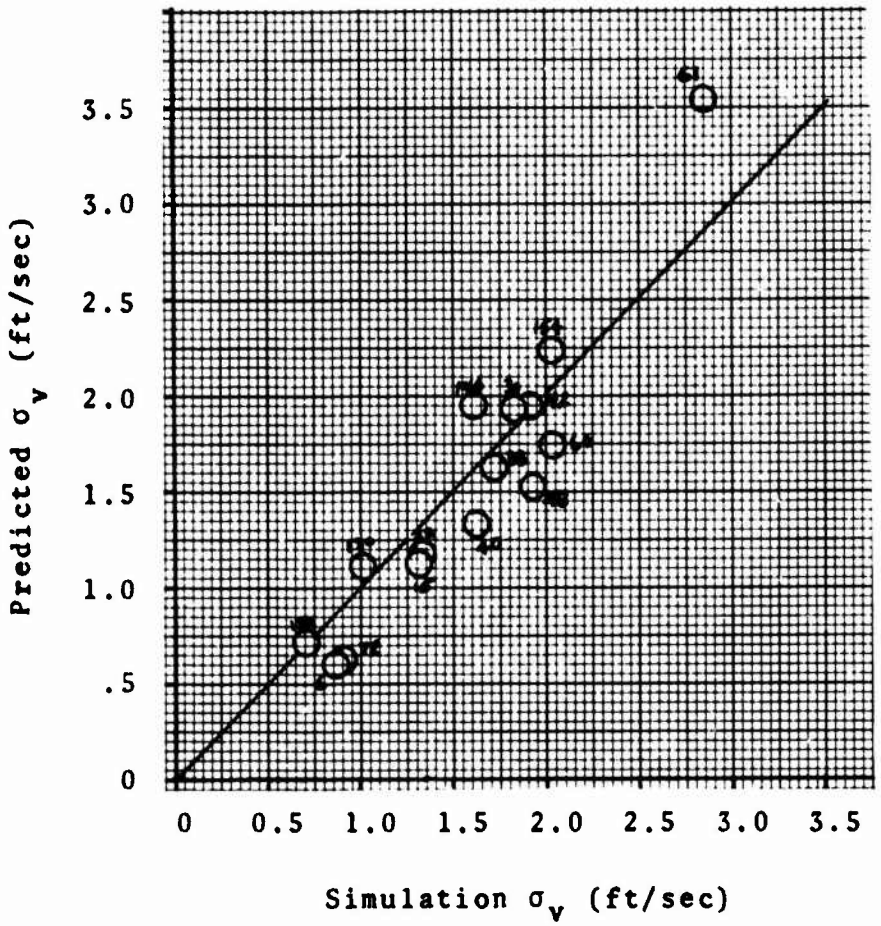

Fig. 6. Predicted vs. Simulation σ_v.

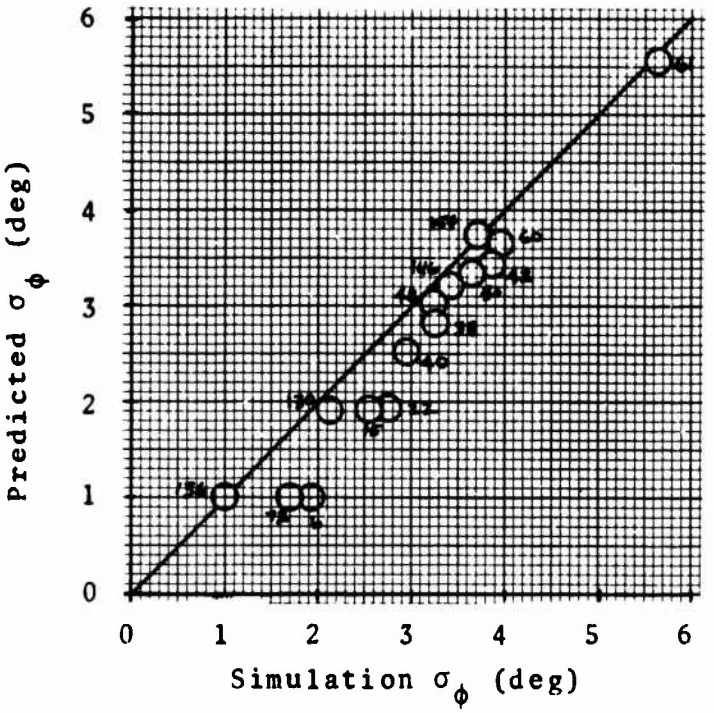

Fig. 7. Predicted vs. Simulation σ_ϕ.

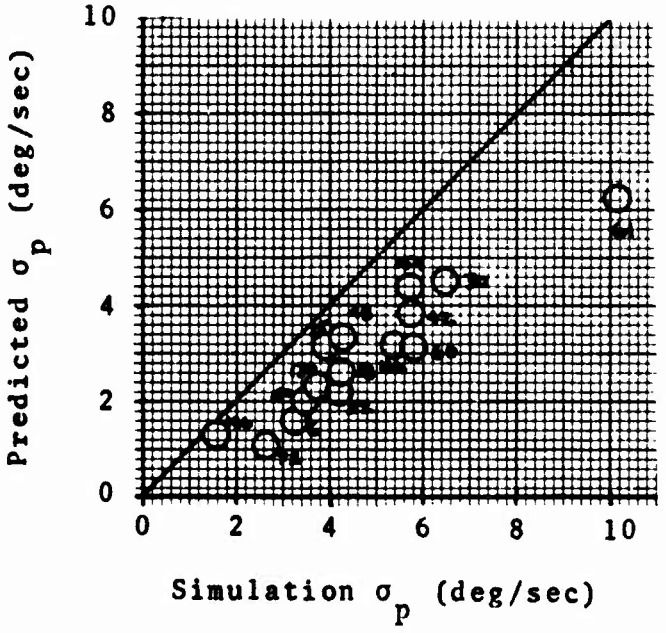

Fig. 8. Predicted vs. Simulation σ_p.

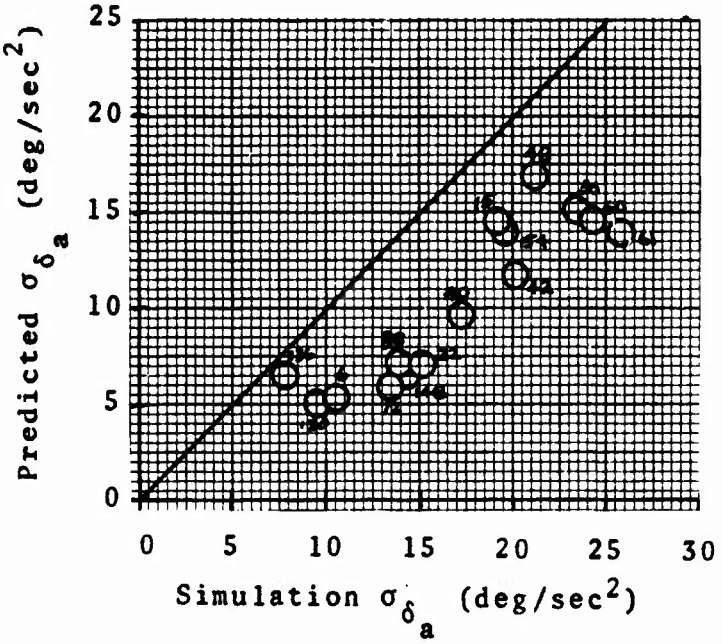

Fig. 9. Predicted vs. Simulation σ_{δ_a}.

In Fig. 2, the pilot ratings from Ref 7 are compared with those taken from the simulation described in this report. There is not exact agreement and the actual pilot ratings from this simulation are generally higher than those from Ref 7. As was mentioned, the visual display used in the simulation of Ref 7 was superior to the one used in this simulation and different rating scales were used. An aircraft rated on a Cooper-Harper scale would tend to have a higher rating than if it were rated on a Cooper scale. There are also other instances where configurations from Ref 7 have been used in an independent simulation and the pilot ratings have tended to be higher than those given in Ref 7 (Refs 9, 10). Thus it was decided to modify the pilot rating of Ref 7 to give paper pilot a fair shake.

The data shown in Fig. 2 was used to determine the best linear fit (in a least squares sense) between the actual pilot ratings of this simulation and those of Ref 7. It was found that multiplying the pilot ratings from Ref 7 by a factor of 1.23 resulted in the closest match between the two sets of actual ratings for these 15 cases.

The predicted pilot ratings are compared with the Ref 7 pilot ratings multiplied by this factor for the remaining 131 cases. The results of the 131 cases are shown in Fig. 10.

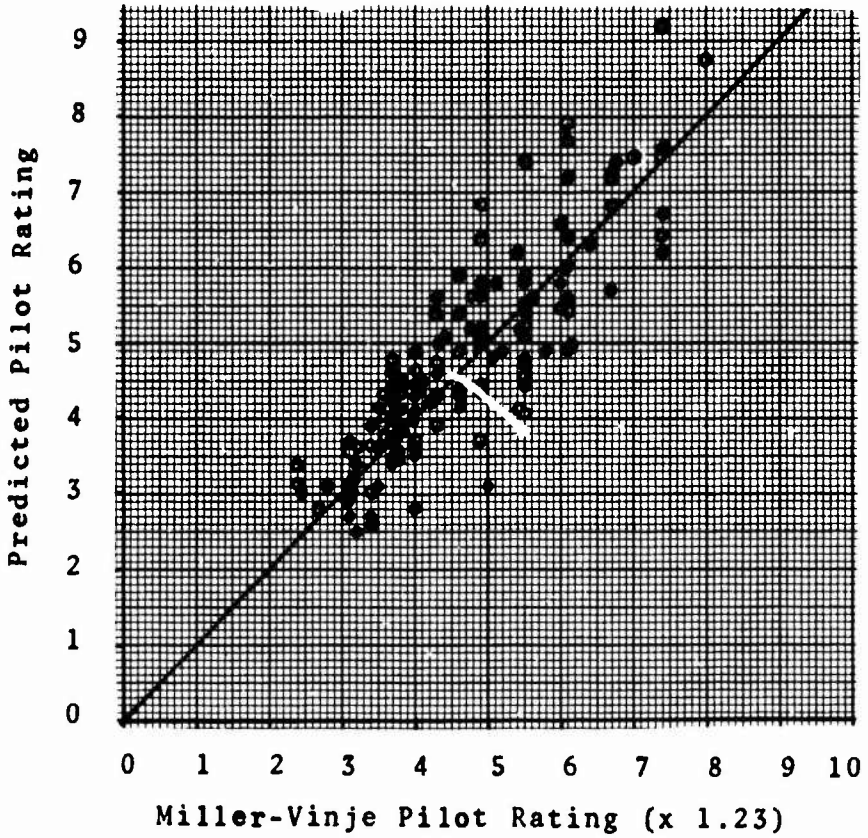

Fig. 10. Predicted Pilot Rating vs. Miller-Vinje Pilot Ratings (x 1.23).

The predicted pilot rating is within ± 1.0 of the actual for 82.4% of the cases. It is within ± 1.5 for 97.7% of the cases and is always within ± 2.0. This is excellent agreement considering both the differences in the simulations and the fact that different pilot rating scales were used.

The accuracy of the predicted pilot ratings compares favorably with the accuracy of the actual pilot rating given by a pilot on a single flight. An analysis of the simulation data indicates that single run pilot ratings are within ± 1.0 of the case average for only 81.4% of the runs.

YOU DONE GOOD, PAPER PILOT!

REFERENCES

1. Anderson, Ronald O. A New Approach to the Specification and Evaluation of Flying Qualities. AFFDL-TR-69-120. Wright-Patterson Air Force Base, Ohio: Air Force Flight Dynamics Laboratory, June 1970.

2. Dillow, James D. The "Paper Pilot" - A Digital Computer Program to Predict Pilot Rating for the Hover Task. AFFDL-TR-70-40. Wright-Patterson Air Force Base, Ohio: Air Force Flight Dynamics Laboratory, March 1971.

3. Naylor, Flynoy R. Predicting Roll Task Flying Qualities with "Paper Pilot". AFIT Thesis GAM/MA/73-1. Wright-Patterson Air Force Base, Ohio: Air Force Institute of Technology, September 1972.

4. Arnold, J. D. An Improved Method of Predicting Aircraft Longitudinal Handling Qualities Based on the Minimum Pilot Rating Concept. AFIT Thesis GGC/MA/73-1. Wright-Patterson Air Force Base, Ohio: Air Force Institute of Technology, June 1973.

5. Taylor, C. R. Predicting Heading Task Flying Qualities with Paper Pilot. AFIT Thesis GE/MA/73-1, Wright-Patterson Air Force Base, Ohio: Air Force Institute of Technology, June 1973.

6. Nolting, D. L. Predicting Lateral Hover Flying Qualities with Paper Pilot. AFIT Thesis GA/MA/73A-2. Wright-Patterson Air Force Base, Ohio: Air Force Institute of Technology, December 1973.

7. Miller, D. P. and E. W. Vinje. Fixed-Base Simulator Studies of VTOL Aircraft Handling Qualities in Hovering and Low Speed Flight. AFFDL-TR-67-152. Wright-Patterson Air Force Base, Ohio: Air Force Flight Dynamics Laboratory, January 1968.

8. Chalk, C. R., et al. Background Information and User Guide for MIL-F-8785B(ASG), "Military Specification - Flying Qualities of Piloted Airplanes". AFFDL-TR-69-72. Wright-Patterson Air Force Base, Ohio: Air Force Flight Dynamics Laboratory, August 1969.

9. Teper, G. L. An Assessment of the "Paper Pilot" - An Analytical Approach to the Specification and Evaluation of Flying Qualities. AFFDL-TR-71-174, Systems Technology, Inc., June 1972.

10. Vinje, E. W. and D. P. Miller. Flight Simulator Experiments and Analysis in Support of Further Development of MIL-F-83300-V/STOL Flying Qualities Specification. AFFDL-TR-73-34. Wright-Patterson Air Force Base, Ohio: Air Force Flight Dynamics Laboratory, June 1973.

SOME APPLICATIONS OF OPTIMAL CONTROL THEORY TO MANUAL CONTROL

by

K.W. ANDERSON
Department of Electrical Engineering
University of Queensland
St. Lucia Q 4067
Australia

ABSTRACT

The model of Miller and Vinje is arranged as a state-feedback model with the adjustable pilot parameters represented by adjustable feedback gains. The system is then regarded as a sub-optimal control system to permit rapid derivation of unknown parameters. Results for the inverse optimal control problem are presented, and the model is used to design and compare compensators for the complete man-machine system.

1. THE PILOT-VTOL AIRCRAFT SYSTEM

The modelling of human response in controlling a hovering V.T.O.L. aircraft, has received considerable attention in recent years. In the true engineering sense, the human controls a vehicle of basically unstable dynamics in the presence of some disturbance. His control actions are based upon observations of the various states of the vehicle.

The model and results of Miller and Vinje [1] are often quoted, and have been used in the project described herein. Applicable to the longitudinal control of a simulated Sikorsky S-61 helicopter, their model is shown in Figure 1. The models for the aircraft and pilot are given in equations (1) and (2) respectively.

$$\begin{bmatrix} \dot{U}g \\ \dot{U} \\ \dot{x} \\ \dot{q} \\ \dot{\theta} \end{bmatrix} = \begin{bmatrix} -\omega_1 & 0 & 0 & 0 & 0 \\ Xu & Xu & 0 & 0 & -g/c \\ 0 & 1 & 0 & 0 & 0 \\ cMu & cMu & 0 & Mq & 0 \\ 0 & 0 & 0 & 1 & 0 \end{bmatrix} \begin{bmatrix} Ug \\ U \\ x \\ q \\ \theta \end{bmatrix} + \begin{bmatrix} 0 \\ 0 \\ 0 \\ cM\delta \\ 0 \end{bmatrix} \delta + \begin{bmatrix} 1 \\ 0 \\ 0 \\ 0 \\ 0 \end{bmatrix} \omega \quad \ldots(1)$$

$$Y_{Px} = K_{Px} (T_{Lx} S + 1)$$
$$Y_{P\theta} = K_{P\theta} (T_{L\theta} S + 1) \frac{e^{-\tau s}}{(T_N S + 1)} \quad \ldots(2)$$

Regarding T_N and τ as fixed pilot parameters, Miller and Vinje sought to adjust the other pilot parameters (gains and leads) to match the measured performance for each set of vehicle parameters.

2. STATE FEEDBACK REPRESENTATION

In order to arrange the model as a linear state-feedback system, it is necessary to split the pilot model into two parts. One for the fixed-lag and delay terms, and one for the adjustable terms. The intermediate pilot state thus formed is called U_c, and may be regarded as the pilots intended or

controlled output. Thus,

$$Uc(s) = K_{P\Theta}(T_{L\Theta}s + 1)[-\Theta(s) + K_{Px}(T_{Lx}s + 1)(-x(s))]$$

$$= -Ko\, s^2 x(s) - K_1 s\, x(s) - K_2 x(s) - K_3 s\, \Theta(s) - K_4 \Theta(s)$$

where: $Ko = K_{P\Theta} K_{Px} T_{L\Theta} T_{Lx}$

$K_1 = K_{P\Theta} K_{Px} (T_{L\Theta} + T_{Lx})$

$K_2 = K_{P\Theta} K_{Px}$

$K_3 = K_{P\Theta} T_{L\Theta}$

$K_4 = K_{P\Theta}$

In the time domain, we therefore have

$$Uc(t) = -Ko\, \ddot{x}(t) - K_1 \dot{x}(t) - K_2 x(t) - K_3 \dot{\Theta}(t) - K_4 \Theta(t) \qquad ...(3)$$

which is a linear combination of some vehicle states. The pilot actually observes x and Θ only, but the rate terms are regarded as being available since the differentiation process is readily performed by human operators. The remaining term, $\ddot{x}$, is implicit in $\dot{x}$ and Θ as seen from the vehicle equation:

$$\ddot{x} = \dot{U} = -g/c\, \Theta + Xu\, U + Xu\, Ug$$

when the latter (disturbance) term is deleted as outside the closed loop. Thus we have:

$$Uc(t) = \left[-K_1 + Ko\, Xu \quad K_2 \quad K_3 \quad K_4 - \frac{g\, Ko}{c}\right] \begin{bmatrix} u \\ x \\ q \\ \Theta \end{bmatrix}$$

$$= \ell_p \; Y_p \qquad ...(4)$$

where Y_p is vector of available states and ℓ_p is vector of feedback gains. The actual pilots output is thus found

$$\frac{\mu(s)}{U_c(s)} = \frac{e^{-\tau s}}{(T_N s + 1)}$$

which is a fixed dynamic element. For computational purposes, it is proposed to include this with the vehicle dynamics, to form the total "plant". The non-linear delay term may be modelled as a Pade lead/lag or lag, or included with the neuromuscular lag T_N, in order to make a suitable linear approximation.

The latter course was taken in the work following this. Thus we have

$$\frac{\mu(s)}{U_c(s)} = \frac{1}{(T_N s + 1)} \qquad \ldots(5)$$

The composite model is illustrated in Figure 2. This form is suitable for analysis as a limited-state-feedback control system.

3. THE HUMAN PILOT AS A SUB-OPTIMAL CONTROLLER

In Physiology and Psychology, it has long been held that the human's adaptive capabilities are used to optimize some criterion. In Control engineering, the work of Roig [12] was first to recognize the strategy of optimality, albeit constrained. More recently, and directly relevant to VTOL tasks, the works of Kleinman [3] and Dillow [2] reinforce the hypothesis that the human controller has some subjective cost function which he seeks to minimize by adapting his own parameters.

It is therefore proposed to use the results of Levine et. al. [7] to predict the adjustable feedback terms for a given set of vehicle parameters. Computationally, this is very attractive, as the problem can be solved rapidly by the method of successive approximations. This contrasts with the work of Dillow [2], Hollis [10], and Stapleford [11], where the optimal parameters were sought by function minimization methods [8] with varying speeds and reliability.

Use of the optimal, limited state feedback model of Levine, requires that the cost function be quadratic in system states and inputs. In our application, this may be

$$J_p = \int_0^\infty (q_1 u^2 + q_2 x^2 + q_3 q^2 + q_4 \Theta^2 + r\, U_c^2)\, dt \qquad \ldots(6)$$

where q_1, q_2, q_3, q_4 and r are weighting coefficients. The latter may be normalized to unity. Cross product terms are also permissible.

4. APPLICATION OF THE MODEL

Use of the model demands an estimation of the weighting term, q_i. This then becomes the model fitting or identification stage, and records of pilot's behaviour for the particular task must be examined.

One arbitrary method is to choose weightings such that each element contributes approximately equally to the cost J_p, when typical values of u, x, q and Θ are inserted.

However, if the optimality thesis, and the above format of J_p (6) are accepted, a more rigorous approach is to analyse the system as an inverse problem in optimal control [9].

Various procedures to solve this problem are discussed in [5] and were used to analyse the data of Miller and Vinje. For each vehicle configuration (PH1 etc.), the feedback vector was calculated and the inverse program then determined the values of q_1, q_2, q_3, q_4 which would produce the same vector as the sub-optimal (in a limited-state feedback sense) control. The results are presented in table I. It must be noted that a single, universal, cost function does not exist, and minor variations in q_i values do occur for different sets of vehicle parameters. The mean values and standard deviations are given below

	Mean	Standard Deviation
q_1	-2.846	1.1
q_2	1.189	0.5
q_3	-0.114	0.03
q_4	.728	0.25

The negative values are of some concern, as most literature in optimal control theory refers to positive definite cost functions. There is, however,

VEHICLE DESIGNATION	COMPUTED PARAMETERS FOR J_P $J_P = \int_0^\infty (q_1 u^2 + q_2 x^2 + q_3 q^2 + q_4 \theta^2 + u_c^2)\, dt$			
	q_1	q_2	q_3	q_4
PH1	-2.26	1.2	-0.16	0.65
PH3	-3.82	1.79	-0.14	0.83
PH4	-4.19	1.69	-0.14	1.05
PH5	-2.54	0.86	-0.10	0.70
PH7	-1.95	0.71	-0.14	0.57
PH8	-2.59	1.13	-0.12	0.65
PH9	-2.75	1.27	-0.10	0.67
PH10	-2.61	1.24	-0.09	0.63
PH12	-2.49	1.10	-0.14	0.63
PH17	-1.95	1.25	-0.06	0.36
PH18	-3.38	1.75	-0.09	0.73
PH19	-4.40	2.27	-0.08	0.89
PH21	-4.80	2.40	-0.08	0.96
PH28	-4.64	1.60	-0.14	1.30
PH30	-3.52	1.34	-0.14	0.94
PH31	-2.52	0.84	-0.14	0.83
PH32	-2.16	0.98	-0.05	0.49
PH34	-1.98	0.59	-0.11	0.66
PH35	-3.13	1.44	-0.15	0.86
PH36	-2.06	0.67	-0.14	0.75

TABLE I RESULTS OF INVERSE OPTIMAL CONTROL ANALYSIS OF PILOT-VTOL SYSTEMS. (DATA FROM MILLER AND VINJE, PILOT B)

no reason why an optimal control cannot exist for such a cost function. Molinari [13] and Kalman [9] indicate the existence of such possibilities. Physically, it would seem that the cost function encourages rate terms to be large. They cannot, however, be very large for very long without causing large values of x and θ which is penalised by the cost. The negative weightings on the rate terms are therefore regarded as a characteristic of a low damping system. Obermayer and Muckler [4] found negative cost values for their manual control systems, although a different model was used.

Using the above mean values, several systems were analysed to predict pilot parameters using the forward, sub-optimal control analysis. These results are presented in Table II together with the values fitted by Miller and Vinje.

The agreement between the two sets of values is not sufficient to claim the method as a successful pilot parameter estimator. This is to be expected from the consideration of:

(i) the Miller and Vinje results were based upon "fitting" the model to observed system data. Another combination of parameters may yield similar performance.

(ii) the nature of this method is to estimate overall performance rather than any individual parameter. All are found simultaneously and considering the influence of the others.

(iii) the form of J_p chosen in (6) was chosen arbitrarily. Other possibilities with many more parameters, exist. A more complex cost matrix may give a better fit.

It would appear that the model is useful for comparing the performance of different systems, by looking at the pilot parameters and overall cost functions. In particular, it may enable a best set of compensation parameters to be determined.

VEHICLE DESIG-NATION	COMPUTED PARAMETERS				FITTED PARAMETERS			
	$K_{P\Theta}$	$T_{L\Theta}$	K_{Px}	T_{Lx}	$K_{P\Theta}$	$T_{L\Theta}$	K_{Px}	T_{Lx}
PH1	0.70	0.37	-1.2	0.69	0.69	0.27	-1.3	0.91
PH3	0.67	0.28	-1.3	0.52	0.73	0.18	-1.5	0.39
PH4	0.69	0.17	-1.4	0.41	0.80	0.16	-1.4	0.35
PH7	0.67	0.31	-1.3	0.57	0.67	0.10	-1.2	0.53
PH8	0.67	0.23	-1.3	0.50	0.66	0.16	-1.4	0.49
PH9	0.69	0.15	-1.3	0.45	0.64	0.20	-1.4	0.50
PH12	0.75	0.22	-1.2	0.59	0.76	0.05	-1.3	0.56
PH30	0.68	0.21	-1.4	0.36	0.76	0.20	-1.3	0.31
PH34	0.68	0.17	-1.3	0.60	0.68	0.13	-0.95	0.60

TABLE II COMPUTED AND FITTED PILOT PARAMETERS FOR THE VTOL HOVER TASK. THE COMPUTED VALUES USED A SINGLE COST FUNCTION J_p. THE FITTED VALUES ARE FOR MILLER AND VINJE'S PILOT B.

5. COMPENSATOR DESIGN

Compensation in manual control systems, has two purposes:

(i) To improve performance of the total system according tc some criterion of the designer.

(ii) To "unload" the pilot, or enable him to achieve the same level of performance with less effort.

The compensator may take the form of a dynamic element somewhere in the loop, or augmented feedback. Different configurations may be arranged into a dual controller model as shown in Figure 3, where the feedback gains are free to be chosen by the designer. If these are to be chosen to be optimal, a designer's cost function, J_D, must be defined.

A typical and appropriate quadratic cost function is

$$J_D = \int_0^\infty (A_1 U^2 + A_2 x^2 + A_3 q^2 + A_4 \Theta^2 + \delta_c^2)\, dt \qquad ...(7)$$

where A_1, A_2, A_3 and A_4 are weighting coefficients, and δ_c is the control signal from the compensator. δ_c must be weighted so that it does not become too large and dominate μ.

The choice of A_i values will reflect the designer's experience, and in work which follows, the values

$$A_1 = A_3 = 0$$

$$A_2 = A_4 = 1$$

were used.

The optimal values for the dual controller are found rapidly using the method described in Anderson [6]. The essence of the model is that there are two controllers with two (different) cost functions. Both sets are optimized simultaneously.

Different configurations can be handled by choosing the plant dynamics

to model the problem. Different states available for feedback are selected by the choice of the observation matrix.

Various configurations based on the PH8 vehicle were analysed with different feedback permitted. The optimal costs J_D and J_P, as well as the computed pilot parameters, are shown in Table III.

It should be noted that the improvement in performance is accompanied by a large decrease in the inner loop gain and lead terms, $K_{P\Theta}$ and $T_{L\Theta}$. The increase in the outer loop terms is not unreasonable, as the model is a series loop model, and the actual pilot feedback gains on x and u are also decreased. This is interpreted as a decrease in the pilot's load or effort required to achieve satisfactory performance.

Further, the same technique may be used to establish the design potential of a particular dynamic element placed somewhere in the loop. By way of illustration, a control lag or lead/lag was placed in the loop immediately after the pilots output, as shown in Figure 4, such that

$$\frac{\delta_p(s)}{\mu(s)} = \frac{T_E\ s + 1}{T_A\ s + 1}$$

For computational purposes, all dynamic elements are considered as part of the total plant. As before, the signals U_c and δ_c are regarded as feedback controls to be optimized. Table IV presents the results. It is observed that there is no significant change in the pilots optimal cost J_P, while the designer's cost deteriorates somewhat for the time constants shown. A smaller inner loop gain ($K_{P\Theta}$) is evidenced for the lag controls, but this is accompanied by an increase in the inner loop lead ($T_{L\Theta}$). This is evidently generated by the pilot in the presence of the control lag. A higher outer loop gain (K_{Px}) is also required, except where the lead/lag element is used.

AUGMENTED FEEDBACK VECTOR Y_c^T	J_D	J_p	COMPUTED PILOT PARAMETERS			
			$K_{P\Theta}$	$T_{L\Theta}$	K_{Px}	T_{Lx}
NONE	15.42	2.34	0.67	0.23	-1.3	0.50
[u x q Θ]	7.43	2.04	0.26	-0.03	-2.03	0.66
[μ u x q Θ]	7.07	1.96	0.09	-0.004	-1.93	0.69

TABLE III PILOT PARAMETERS AND PERFORMANCE COSTS FOR VARIOUS FEEDBACK CONFIGURATIONS, BASED ON VEHICLE PH8.

T_A	T_E/T_A	J_D	J_p	COMPUTED PILOT PARAMETERS			
				$K_{P\Theta}$	$T_{L\Theta}$	K_{Px}	T_{Lx}
0	0	7.43	2.04	0.26	-0.03	-2.03	0.66
0.5	0	7.51	2.03	0.13	0.14	-2.79	0.56
1.0	0	7.7	2.06	0.10	0.20	-2.83	0.67
0.5	2.0	8.15	2.07	0.28	-0.14	-1.96	0.61

TABLE IV PILOT PARAMETERS AND PERFORMANCE COSTS FOR VARIOUS CONTROL LEAD/LAG CONFIGURATIONS, BASED ON VEHICLE PH8 WITH AUGMENTED FEEDBACK [u x q Θ]

The consequence of other dynamic elements may be estimated in the same way.

6. CONCLUSION

With some simplifications and approximations, the above technique can be used to model many design configurations which may be considered appropriate for man-machine systems. The well established results of modern control theory can then be used to predict the best set of parameters (both pilots and augmented feedback gains). The principal advantage of the method is that small amounts of computer time are required to produce an estimation of the potential of any such configuration, and some of the costs and parameters which may result.

It must be recognized that the technique is not accurate for the prediction of pilot parameters alone. Kleinman's model provides good accuracy, but is not useful here as the order of the total system (pilot plus vehicle) is too large for the numerical treatment described in this paper.

The results quoted in the paper provide a basis for comparing different design configurations, including feedback and control lead/lag elements. These are submitted as further evidence of the value of optimal control theory to the analysis and understanding of the man-machine systems.

REFERENCES

[1] E.W. Vinje and D.P. Miller, *"An Analysis of Pilot Adaptation in a Simulated Multiloop VTOL Hovering Task"*, Proc. Fourth Annual Conference on Manual Control, March 1968, pp. 95-118.

[2] J.D. Dillow, *"Paper Pilot - A Digital Computer Program to predict Pilot Rating for the Hover Task"*, AFFDL-TR-70-40 March 1971.

[3] D.L. Kleinman, S. Baron and W.H. Levison, *"A Control Theoretic Approach to Manned Vehicle Systems Analysis"*, IEEE Trans Auto Control, Vol. AC-16, Dec. 1971, pp. 824-832.

[4] R.W. Obermayer and F.A. Muckler, *"On the Inverse Optimal Control Problem in Manual Control Systems"*, IEEE International Convention Record, 1965, Part 6, pp. 153-165.

[5] K.W. Anderson, *"Computational Methods for the Inverse Problem of Sub-Optimal (Limited State Feedback) Control Theory"*, Report CGR73/4, Dept. Elec. Engineering, University of Queensland, Australia, November 1973.

[6] K.W. Anderson, *"A New Approach to the Design of Optimal Compensators for Manual Control Systems, Using the Dual-Sub Optimal Controller"*, Report C6R73/], Dept. Elec. Eng., University of Queensland, May 1973.

[7] W.S. Levine and M. Athans, *"On the Determination of the Optimal Constant Output Feedback Gains for Linear Multivariable Theory"*, IEEE Trans Auto. Control, Vol. AC-15, February 1970, pp. 40-48.

[8] J.L. Keuster and J.H. Mize, *"Optimization Techniques with FORTRAN"*, McGraw-Hill, 1973.

[9] R.E. Kalman, *"When is a Linear Control System Optimal?"*, Trans. ASME, Series D, J. Basic Engineering, Vol. 86, pp. 51-60, March 1964.

[10] T.L. Hollis, *"Optimal Selection of Stability Augmentation Parameters to Reduce Pilot Ratings for the Pitch Tracking Task"*, MSc Thesis, Air Force Institute of Technology, June 1971.

[11] R.L. Stapleford et. al. *"A Practical Optimization Design Procedure for Stability Augmentation Systems"*, AFFDL-TR-70-11, October 1970.

[12] R.W. Roig, *"A Comparison between Human Operator and Optimal Linear Controller RMS-Error Performance"*, IEEE Trans Human Factors in Electronics, Vol. HFE-3, March 1962.

[13] B.P. Molinari, *"The Stable Regulator Problem and its Inverse"*, IEEE Trans. Auto. Control, Vol. AC-18, No. 5, October 1973, pp. 454-459.

TABLE OF SYMBOLS

c	constant to convert radians to degrees, 57.3
g	gravitational constant, 32.2 ft. sec $^{-2}$.
J_P	pilot's subjective cost function
J_D	designer's objective cost function
K_{Px}	pilot gain in displacement, deg. (ft.)$^{-1}$
$K_{P\theta}$	pilot gain in pitch, in.(degree)$^{-1}$
M_q	pitch rate damping, (sec.)$^{-1}$
Mu	speed stability parameter, rad (ft. sec)$^{-1}$
Mg	Control sensitivity, rad (sec^2 in)$^{-1}$
$q = \dot{\theta}$	pitch rate, deg (sec)$^{-1}$
s	Laplace Operator
$T_{L\dot{x}}$	Pilot lead time in longitudinal displacement, sec
$T_{L\theta}$	Pilot lead time in pitch, sec.
T_N	Pilot neuromuscular lag, sec.
$u = \dot{x}$	Longitudinal Aircraft Velocity, ft (sec)$^{-1}$
u_c	Pilot't control output, in.
Ug	Longitudinal wind gust velocity, ft.(sec)$^{-1}$
ω	white noise
x	longitudinal displacement, ft.
Xu	Longitudinal drag parameter, (sec)$^{-1}$
Y_{Px}	Pilot Transfer Function in displacement (outer or x) loop
$Y_{P\theta}$	Pilot Transfer Function in pitch (inner or θ) loop
δ	Control input to vehicle, in.
θ	pitch attitude, deg.$^{-1}$
μ	Net output from pilot, in
τ	Pilot Reaction Time delay
ωi	Wind gust break frequency, .314 rad (sec)$^{-1}$

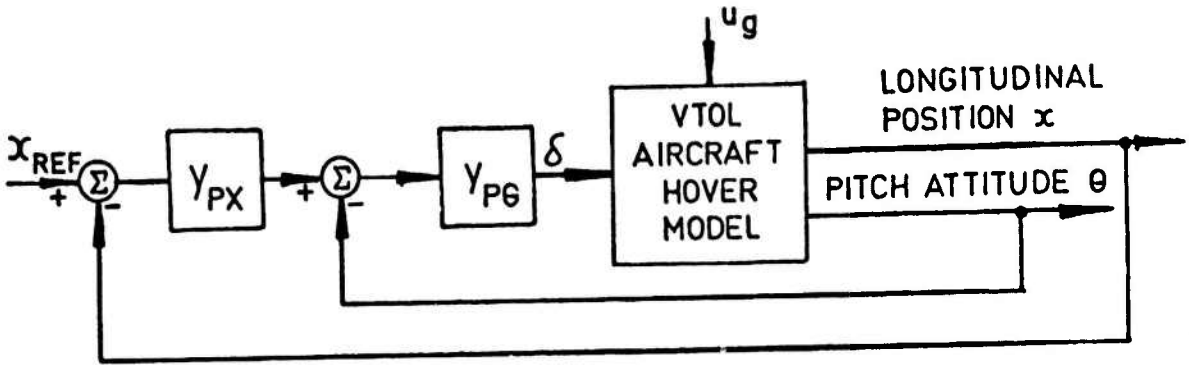

FIGURE 1 SERIES LOOP MODEL FOR PILOT LONGITUDINAL CONTROL IN HOVER (MILLER AND VINJE)

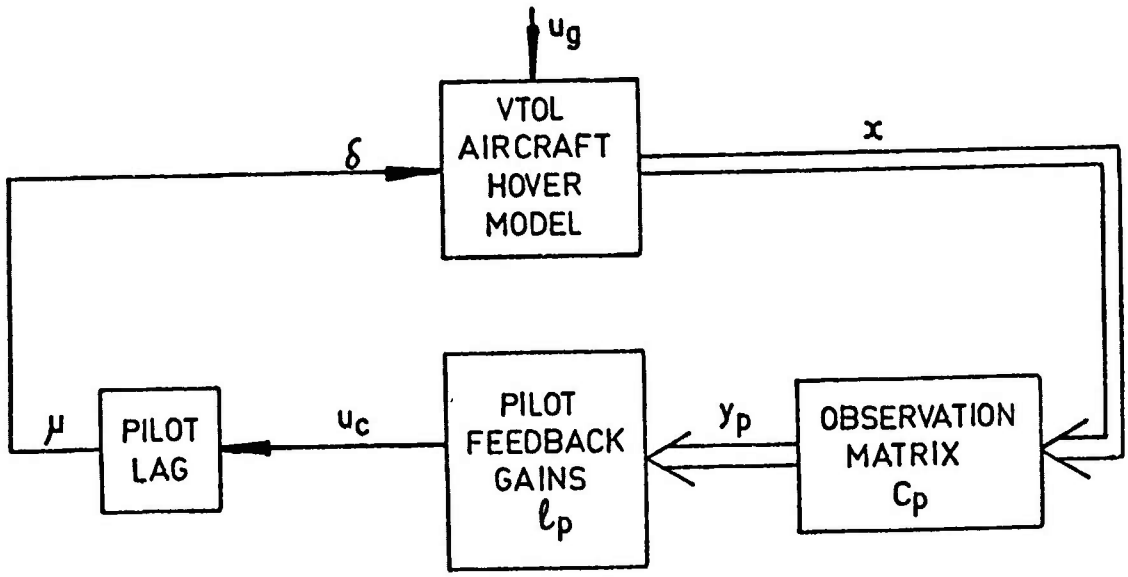

FIGURE 2 STATE FEEDBACK REPRESENTATION OF THE SERIES LOOP MODEL

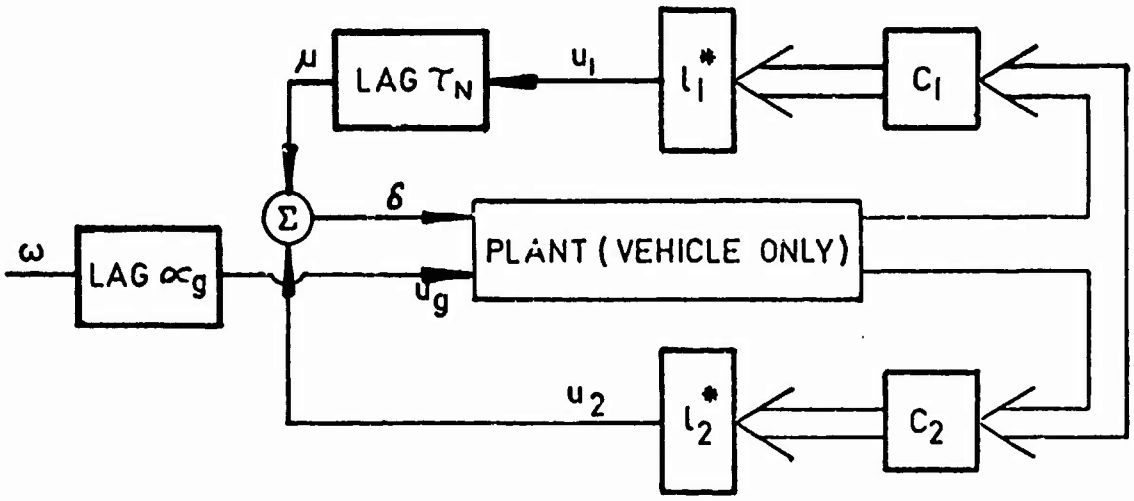

FIGURE 3 THE MANUAL CONTROL SYSTEM AS A DUAL SUB-OPTIMAL CONTROLLER

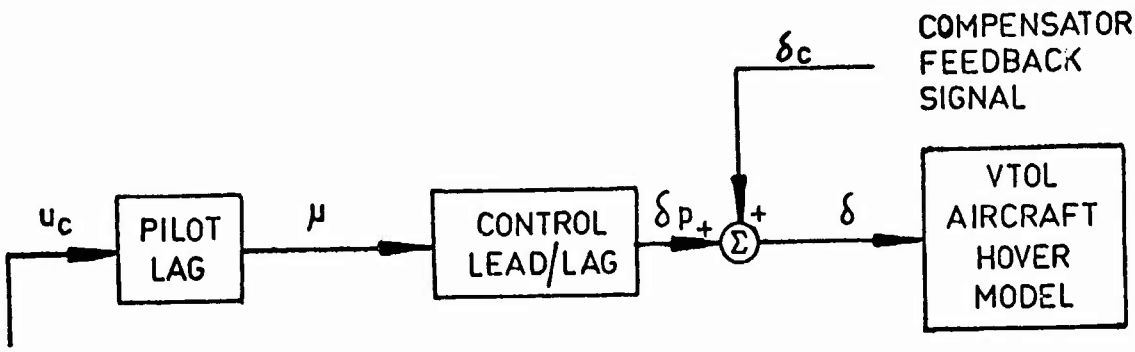

FIGURE 4 LOCATION OF THE CONTROL LEAD/LAG COMPENSATORY ELEMENT.

74-28,209 #33

PAPER PILOT MAKES A BLIND LANDING

Daniel J. Biezad*, James D. Dillow, Douglas G. Picha
Air Force Institute of Technology
Wright-Patterson AFB
Ohio

ABSTRACT

A mathematical prediction scheme was developed to predict the pilot rating for the longitudinal handling qualities of aircraft flown on the glide slope in turbulence. Actual pilot ratings and rms performance data were obtained from a fixed-base simulation of various aircraft configurations represented by the longitudinal short-period equations of motion. A linear equation was developed which expressed pilot ratings from the fixed-base simulation as a linear function of rms pitch angle, rms pitch rate, and rms glide-path deviation.

The pilot-vehicle system was mathematically modeled by a closed-loop feedback system. Certain parameters of the pilot model used in the system were selected to minimize the linear rating expression developed from the fixed-base simulation. Since pilot rating was expressed as a linear blend of rms performances, predicted ratings were analytically obtained for each configuration.

All pilot ratings obtained from the mathematical prediction scheme were within ± 1.05 rating units of the actual rating from the fixed-base simulation. The closed-loop rms pitch angle and rms pitch rate also agreed fairly well, but predicted rms glideslope deviation did not correlate with the actual rms tracking deviation.

The mathematical prediction scheme was applied to an independent flight data source for aircraft being flown in turbulent approach conditions. In 94% of the configurations tested, the predicted evaluation was within ± 1.5 rating units of the actual pilot rating. The maximum difference was 2.07 rating units.

INTRODUCTION

The paper pilot concept for predicting aircraft handling qualities in a specified piloted task is based on the following hypothesis.

1. For a well defined task, the pilot rating is a function of the closed loop performance and the pilot workload. This function is called the pilot rating expression.

---

*Currently assigned to the 6585 Test Group, Holloman AFB, New Mexico.

2. The predicted pilot rating can be obtained by minimizing the pilot rating expression with respect to free pilot parameters in the closed loop pilot-vehicle model. (The lower the rating--the better the handling qualities.) The minimal value of the pilot rating expression corresponds to the pilot rating for the task.

The paper pilot concept has been demonstrated in the past for various tasks including longitudinal hover, pitch tracking, roll attitude, and heading tasks (Refs 1 through 5). In this study the paper pilot concept is applied to the task of tracking glideslope in a turbulent environment and a method for predicting handling qualities is described.

In this paper the simulation study used to collect performance data and pilot ratings is briefly described. For the cases simulated, the pilot rating tends to correlate linearly with rms pitch angle, pitch rate and glideslope deviation. The formula that describes this correlation is the pilot rating expression. A fixed form pilot model is described and predicted (or paper pilot) ratings are computed by minimizing the pilot rating expression with respect to four free parameters in the pilot model. These results are compared to the actual pilot ratings from the simulation. This method of predicting pilot rating was also used for a set of aircraft configurations which had been evaluated for longitudinal handling in a simulation conducted by North American Aviation (Ref 6). The paper pilot ratings are compared to the actual pilot ratings for this independent data base.

Details of this paper can be found in Ref 7.

SIMULATION

The object of the simulation was to obtain the "data base" for aircraft flying the glideslope and to use this information in formulating a pilot rating expression. The system variables, or states, chosen to represent aircraft performance are aircraft pitch angle, pitch rate, angle of attack, and deviation from desired glide path. The overall simulation is represented by the functional representation of Fig. 1.

The aircraft dynamics were represented by short period equations of motion. That is, the phugoid mode (longitudinal velocity perturbations) was neglected. It was assumed that the pilot would be predominantly sensitive to the short period states--pitch, pitch rate, vertical velocity--in an evaluation of the longitudinal handling qualities.

The glide path geometry is shown in Fig. 2. The quantity displayed to the pilot is angular deviation, Γ, from the nominal glide path. During an actual ILS approach, as the

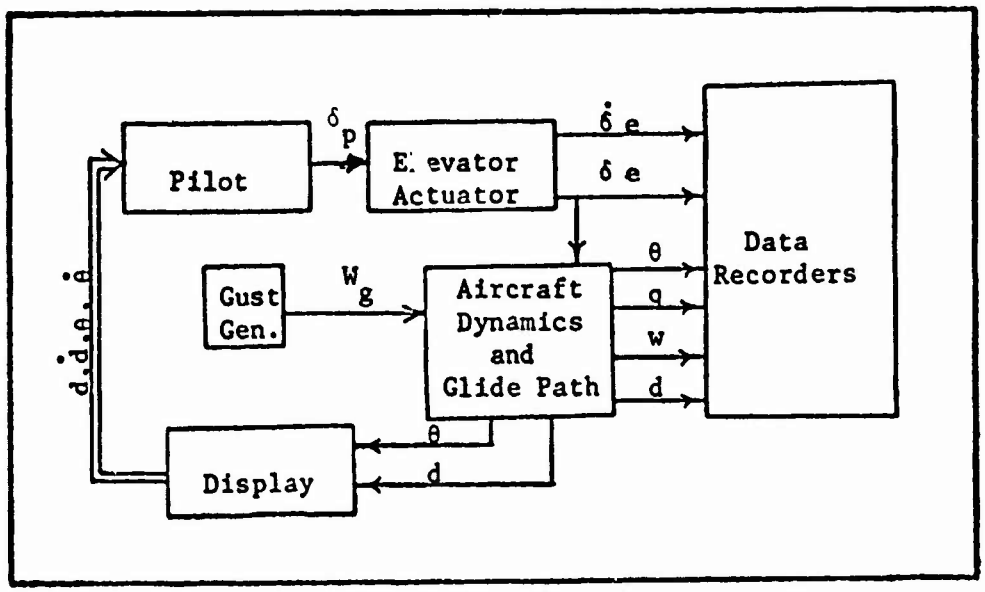

Fig. 1. Functional Representation of Analog Simulation.

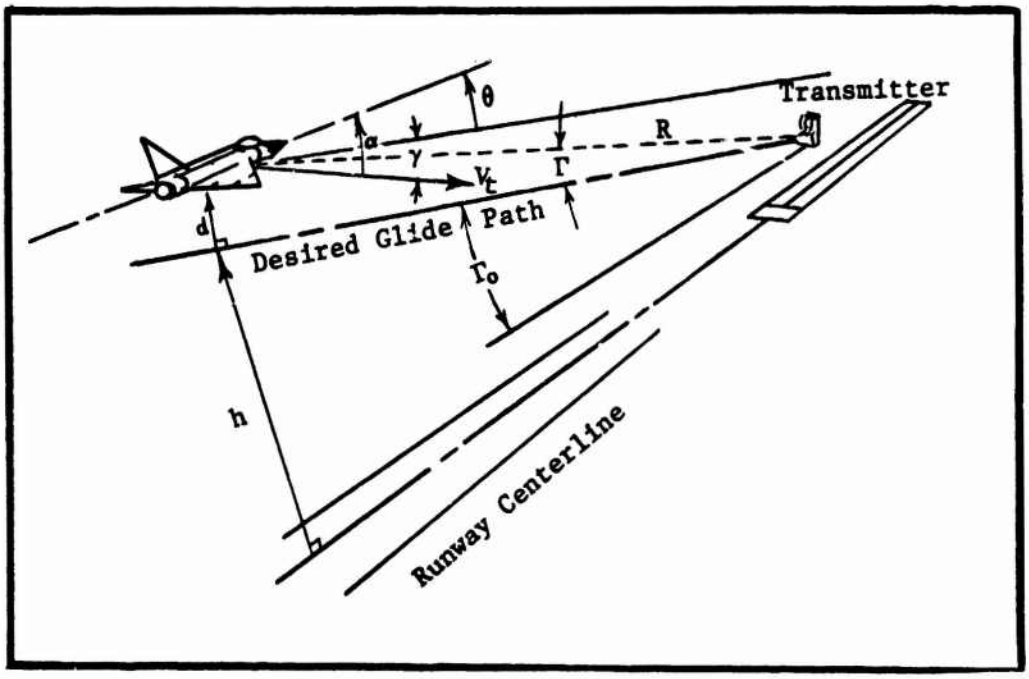

Fig. 2. Glideslope Approach.

runway is approached, the angular deviation from nominal glide path angle becomes increasingly sensitive to both angle of attack changes and pilot inputs. The relationship between glide path deviation, d, and angular deviation from nominal glide path is

$$\frac{d}{R} = \tan \Gamma \approx \Gamma \quad \text{(radians)}$$

where R is the distance to the glideslope transmitter in feet.

In order to maintain a time-invariant and linear problem, it is necessary for R to be constant. This constraint can be justified by considering the pilot's behavior as the aircraft approaches a decision height. Decision height is the absolute altitude, normally between 100 feet and 300 feet, where the pilot decides either to land visually or to execute an instrument "missed approach". It is chosen by considering a number of factors which include aircraft maneuverability, weight, and forward airspeed. Since the most critical portion of the instrument approach occurs as the aircraft nears decision height, it is assumed that the overall pilot rating is decided at this time. The range R is selected for each aircraft configuration so that the aircraft is being flown near this height.

A force stick was used by the pilot to command elevator input. The pilot was allowed to adjust the stick sensitivity to a preferred value. In this way, the pilot rating is not influenced by an adverse stick sensitivity.

Elevator dynamics were modeled by a first order lag with a relatively high band width.

Only vertical gusts were considered in the simulation. An approximation to the Dryden gust model (Ref 8) was used. The gust is generated by passing white Gaussian noise through a first order filter. A rms gust intensity of 10 ft/sec was used in the simulation.

Pitch attitude and deviation from glide path were displayed to the pilot using a dual-beam oscilloscope mounted at eye level. The relative scaling of these quantities is illustrated in Fig. 3. This display provides implicit information concerning pitch rate and rate of deviation from glide path. Vertical velocity and aircraft "g" loading were displayed on separate instruments.

A hodge podge of twelve configurations were simulated. Five of the aircraft configurations were based on cases studied in a flight test (Ref 9), four of the configurations were based on B-1 Bomber data, two of the configurations were conjured up to give bad pilot ratings, and the last case is a DC-8.

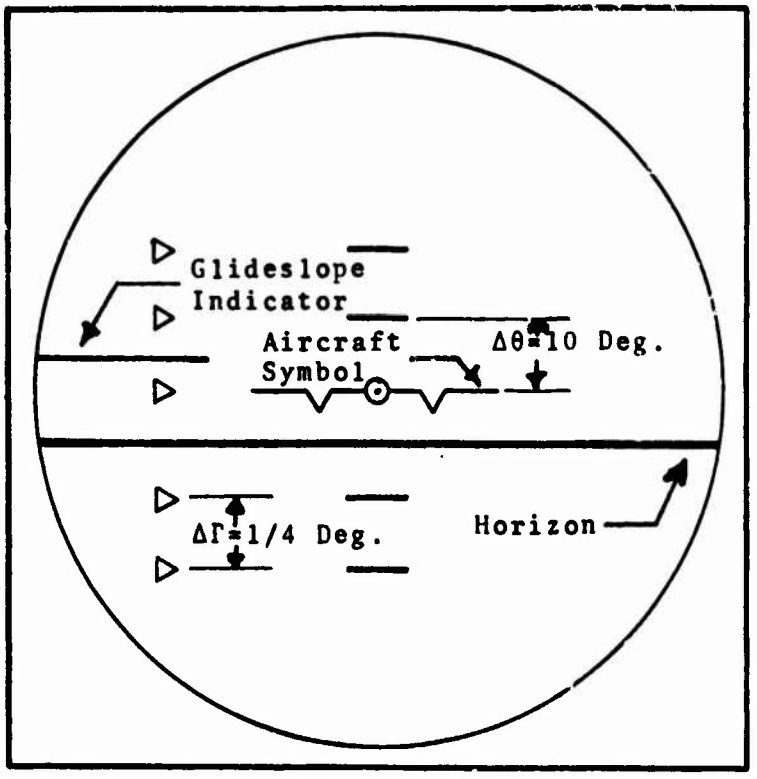

Fig. 3. Oscilloscope Display.

Four military pilots participated in the simulation. Each pilot was convinced that any attempt to model their behavior was ludicrous and they were anxious to debunk the paper pilot theory with solid data. Each pilot was thoroughly trained with each configuration before data was taken. The Cooper-Harper rating scale was used for numerical pilot ratings (Ref 8).

PILOT RATING EXPRESSION

The data taken from the simulation was used to derive a linear correlation between rms values of the states and pilot rating. The possibility of an additive constant or bias was considered and a formula with negative coefficients was not considered. The answer was not unique and the five bes. formulas are as follows:

$$PR = .86\sigma_q + .12\sigma_d + .047\sigma_{\delta e}$$

$$PR = 1.06\sigma_\theta + .70\sigma_q + .0095\sigma_{\dot{\delta}e}$$

$$PR = 1.11\sigma_\theta + .67\sigma_q + .004\sigma_{\delta e}$$

$$PR = 1.14\sigma_q + .12\sigma_{\dot{\delta}e}$$

$$\boxed{PR = .36\sigma_\theta + .96\sigma_q + .11\sigma_d}$$

where σ_θ and $\sigma_{\delta e}$ are in degrees, σ_q and $\sigma_{\dot{\delta} e}$ are in degrees/second, and σ_d is in feet.

The last formula was used as the pilot rating expression for a couple of reasons. First of all, it includes a term involving the rms glideslope deviation which represents the primary task. If σ_d doesn't appear in the pilot rating expression, the subsequent method for determining the pilot model would result in a pilot-vehicle model that would not track glideslope. The second reason for using the last formula is because it doesn't include a term involving $\sigma_{\delta e}$ or $\sigma_{\dot{\delta} e}$. This was because of a limitation in the computer program that existed at the time.

PAPER PILOT

An analytic model of the closed loop pilot-vehicle system was used to predict pilot rating and system performance.

The pilot model is shown in Fig. 4. The model includes an outer loop transfer function,

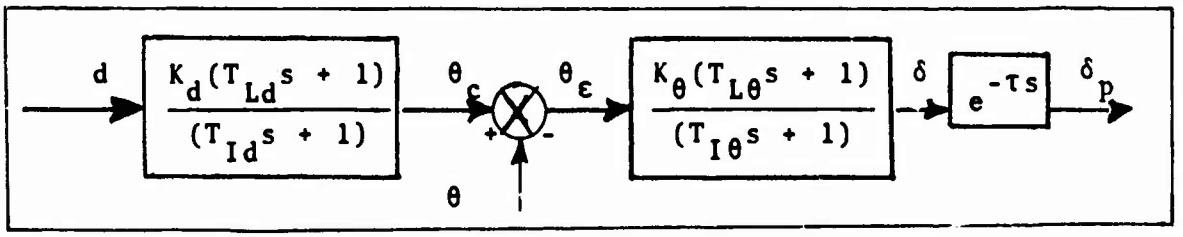

Fig. 4. Pilot Model.

$$\frac{\theta_c}{d} = \frac{K_d(T_{Ld}s + 1)}{T_{Id}s + 1}$$

an inner loop transfer function,

$$\frac{\delta}{\theta_\varepsilon} = \frac{K_\theta(T_{L\theta}s + 1)}{T_{I\theta}s + 1}$$

and a pure time delay, $e^{-\tau s}$. The following parameter values are used.

$$\tau = .3 \text{ sec}$$

$$T_{Id} = .01 \text{ sec}$$

$$T_{I\theta} = .1 \text{ sec.}$$

The other pilot parameters, K_d, T_{Ld}, K_θ and $T_{L\theta}$, are free parameters in the minimization scheme.

The predicted pilot rating and performance is obtained in the following manner. The free pilot parameters are selected to minimize

$$J = .36\sigma_\theta + .96\sigma_q + .11\sigma_d$$

for the closed loop pilot-vehicle system. The disturbance is a vertical gust with an rms intensity of 10 ft/sec. The paper pilot rating, PR, is given by

$$PR = \begin{cases} 1 & , J < 1 \\ J & , 1 \leq J \leq 5.5 \\ 1/2\ (5.5+J) & , J > 5.5 \\ 10 & , J > 14.5 \end{cases}$$

This final fudge to arrive at the paper pilot rating reflects two additional considerations. First, the pilot rating can never be less than one or greater than 10. Secondly, the form for PR is also based on the assumption that once the performance deteriorates beyond a certain point, a further deterioration of performance is not as consequential in the pilot rating.

A comparison of the paper pilot ratings and those obtained in the simulation is shown in Fig. 5. The paper pilot ratings are within $\pm$ 1.05 rating units of the actual pilot ratings in all cases.

Scatter diagrams relating actual and predicted values for σ_θ, σ_q, and σ_d are shown in Figs. 6 through 8. Paper pilot accurately predicts the actual rms value of pitch rate, σ_q, but it is slightly high in predicting σ_θ. There is no apparent correlation between predicted and actual values for σ_d!

TESTING PAPER PILOT

The paper pilot scheme was tested against an independent data base developed by North American Aviation, Inc. (Ref 7). In the study by North American Aviation, various aircraft configurations were pilot evaluated for the carrier approach-to-landing task. A visual flight simulator was flown by experienced pilots to determine the overall rating. A large number of control and configuration parameters were varied during the carrier approach simulation. Because of this, care was exercised to select only those configurations for test which manipulated th short period dynamics and which were flown with

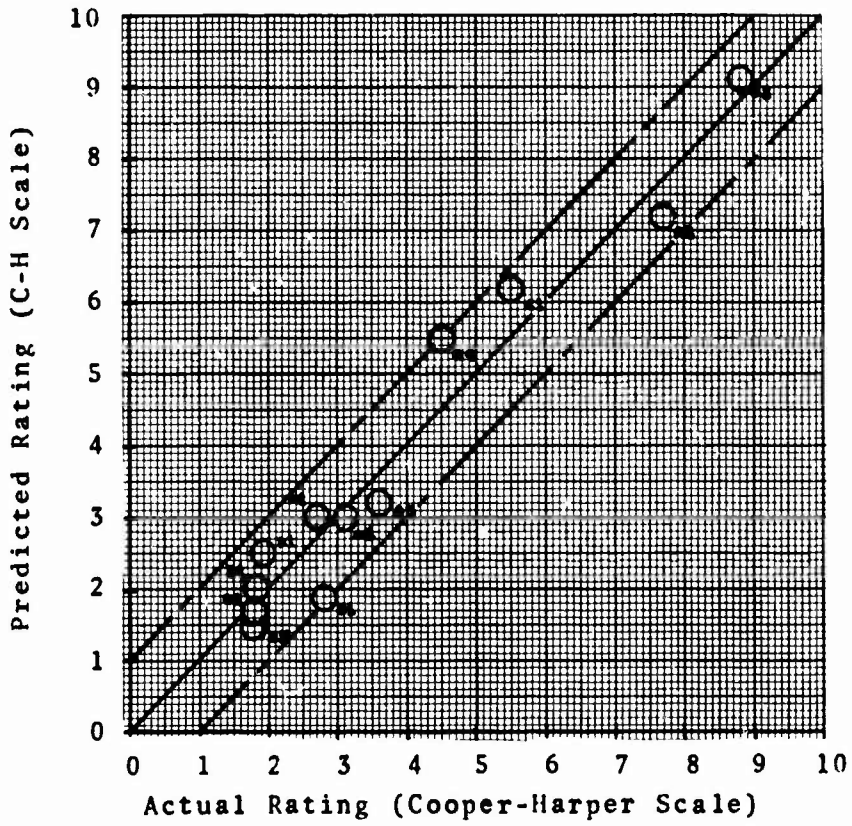

Fig. 5. Predicted Pilot Ratings vs. Pilot Ratings from Analog Simulation.

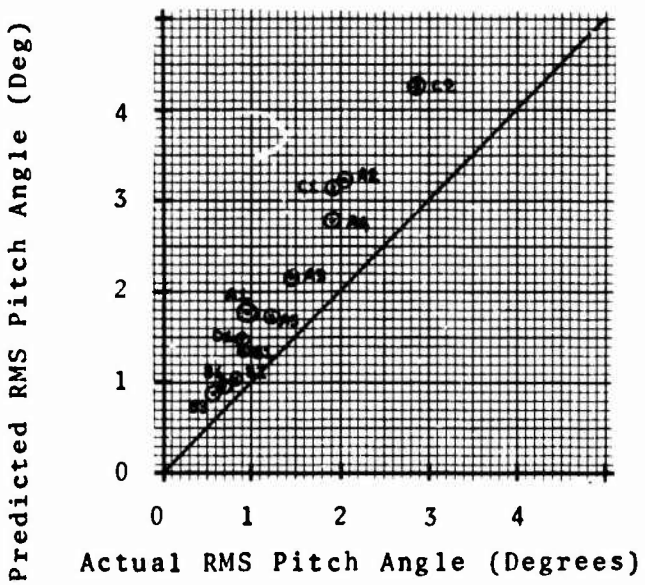

Fig. 6. Predicted RMS Pitch Angle vs. RMS Pitch Angle from Analog Simulation.

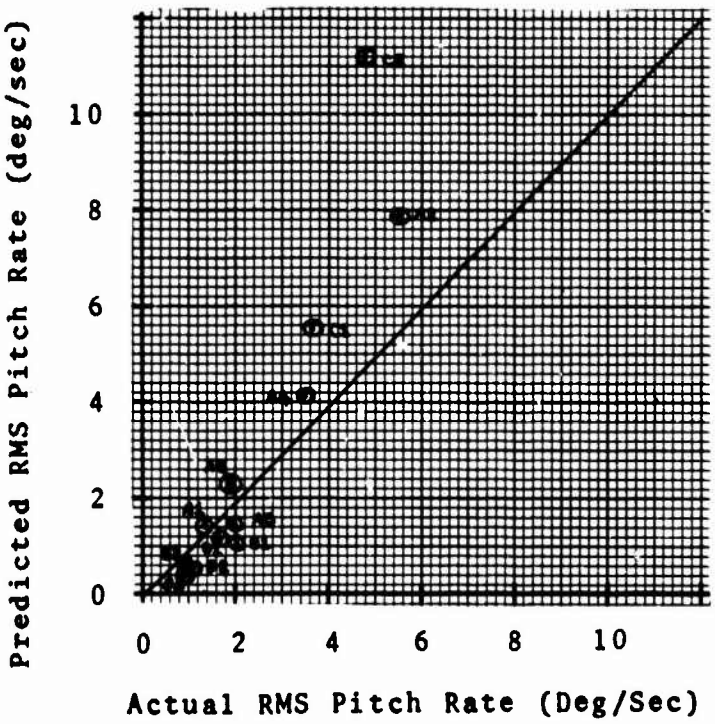

Fig. 7. Predicted RMS Pitch Rate vs. RMS Pitch Rate from Analog Simulation.

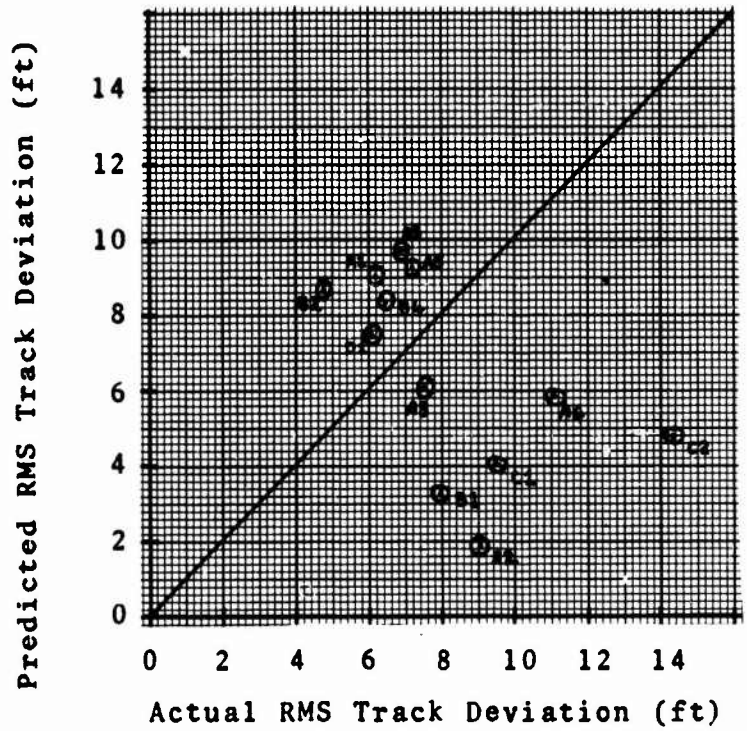

Fig. 8. Predicted RMS Glid Path Deviation vs. RMS Deviation from Analog Simulation.

optimum stick sensitivity. Using this criteria, the linearized equations of motion were determined for 17 different configurations.

The gust variance was difficult to determine since a three-dimensional turbulence model was used by North American Aviation. In addition to this stochastic gust input, the longitudinal and vertical axes were subject to gust inputs that were a function of distance. From the results of trial solutions for two of the configurations, it was decided that the equivalent rms disturbance should be 5.5 feet per second. This value of σ_{w_g} was constant for all of the test configurations.

The accuracy of the paper pilot ratings is depicted by the scatter diagram of Fig. 9. For 97% of the test configurations, the paper pilot ratings are within $\pm$ 1.5 rating units of the actual evaluation. The maximum rating difference was 2.07 units.

CONCLUSIONS

The paper pilot scheme was applied to the task of tracking glideslope in turbulence. The pilot rating tends to correlate linearly with rms pitch attitude, rms pitch rate, and rms glideslope deviation. The pilot ratings predicted by paper pilot

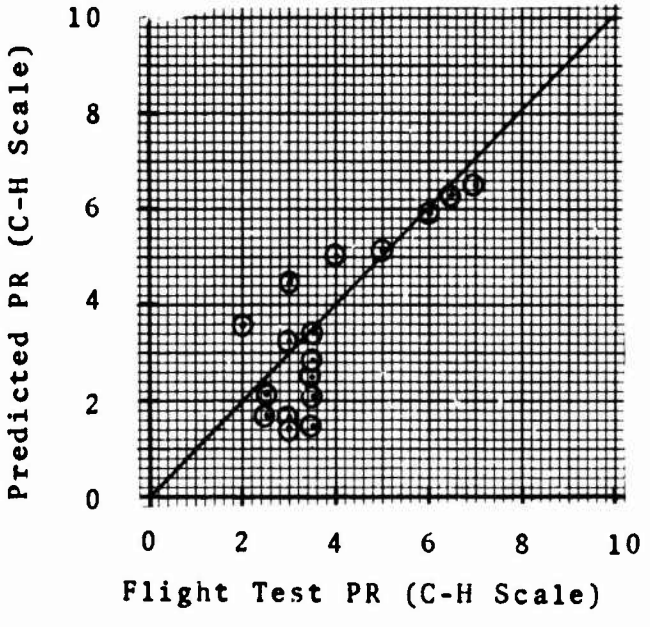

Fig. 9. Predicted Pilot Ratings vs. Actual Pilot Ratings for North American Test Configurations.

agree reasonably well with actual ratings. Even when applied to a data set other than the one used to develop the pilot rating expression, the paper pilot ratings agree reasonably well with actual rating. The analytic values of rms pitch and rms pitch rate agree well with actual data. However, there is no correlation between the analytic values of glideslope deviation and those measured in the simulation.

An examination of the simulation data revealed that the pilot rating tended to correlate with $\sigma_{\delta e}$ and $\sigma_{\dot{\delta} e}$. Although these possibilities were not pursued in this study, it is conjectured that these terms relate to the pilot work load. In previous paper pilot studied, work load was related to the values of pilot lead (T_L) that were used to minimize the pilot rating expression. The use of rms control rate in the pilot rating expressions is well suited to the use of an optimal pilot model developed by Kleinman, Baron, and Levison (Ref 10). This may be worth further study.

YOU DONE GOOD, PAPER PILOT!

REFERENCES

1. Anderson, R. O. and J. D. Dillow. "Paper Pilot"--An Application of Pilot Models to Predict VTOL Flying Qualities in Precision Hover. Proceedings of the Sixth Annual Conference on Manual Control: pp 349-364. Wright-Patterson Air Force Base, Ohio: April 1970.

2. Naylor, Flynoy R. Predicting Roll Task Flying Qualities with "Paper Pilot". AFIT Thesis GAM/MA/73-1. Wright-Patterson Air Force Base, Ohio: Air Force Institute of Technology, September 1972.

3. Arnold, John D. An Improved Method of Predicting Aircraft Longitudinal Handling Qualities Based on the Minimum Pilot Rating Concept. AFIT Thesis GGC/MA/73-1. Wright-Patterson Air Force Base, Ohio: Air Force Institute of Technology, October 1972.

4. Johnson, Robert B. Predicting Pitch Task Flying Qualities Using Paper Pilot. AFIT Thesis GGC/MA/73-2. Wright-Patterson Air Force Base, Ohio: Air Force Institute of Technology, June 1973.

5. Taylor, C. R. Predicting Heading Task Flying Qualities with Paper Pilot. AFIT Thesis GE/MA/73-1, Wright-Patterson Air Force Base, Ohio: Air Force Institute of Technology, June 1973.

6. Shooter, K. L., J. L. Lockenour, and J. D. Richardson. Advanced Vehicle Flying Qualities Studies Task 0001-Carrier Approach Characteristics Status Report. NA67H-791/North American Aviation, Inc., Columbus, Ohio: March 1969.

7. Biezad, Daniel J. A Method of Predicting Pilot Rating for the Pitch Handling Qualities of Aircraft Flown on the Glide Slope. AFIT Thesis GA/MA/73A-1. Wright-Patterson Air Force Base, Ohio: Air Force Institute of Technology, December 1973.

8. Chalk, C. R., T. P. Neal, T. M. Harris, F. E. Pritchard, and R. J. Woodcock. Background Information and Users Guide for MIL-F-8786B (ASG), Military Specification - Flying Qualities of Piloted Airplanes. AFFDL-TR-69-72. Wright-Patterson Air Force Base, Ohio: Air Force Flight Dynamics Laboratory, August 1969.

9. Franklin, James A. Turbulence and Longitudinal Flying Qualities. NASA CR-1821. Princeton, New Jersey: Princeton University, July 1971.

10. Kleinman, D. L., Baron S, et al. Application of Optimal Control Theory to the Prediction of Human Performance in a Complex Task. AFFDL-TR-69-81. Wright-Patterson Air Force Base, Ohio: Air Force Flight Dynamics Laboratory, March 1970.